

Ali Sayigh *Editor*

Mediterranean Green Buildings & Renewable Energy

Selected Papers from the World
Renewable Energy Network's Med Green
Forum



 Springer

Mediterranean Green Buildings & Renewable Energy

Ali Sayigh

Editor

Mediterranean Green Buildings & Renewable Energy

Selected Papers from the World
Renewable Energy Network's
Med Green Forum



Springer

Editor
Ali Sayigh
Flat 3
World Renewable Energy Congress
Brighton, UK

ISBN 978-3-319-30745-9 ISBN 978-3-319-30746-6 (eBook)
DOI 10.1007/978-3-319-30746-6

Library of Congress Control Number: 2016956858

© Springer International Publishing Switzerland 2017, corrected publication 2020

This work is subject to copyright. All rights are reserved by the Publisher, whether the whole or part of the material is concerned, specifically the rights of translation, reprinting, reuse of illustrations, recitation, broadcasting, reproduction on microfilms or in any other physical way, and transmission or information storage and retrieval, electronic adaptation, computer software, or by similar or dissimilar methodology now known or hereafter developed.

The use of general descriptive names, registered names, trademarks, service marks, etc. in this publication does not imply, even in the absence of a specific statement, that such names are exempt from the relevant protective laws and regulations and therefore free for general use.

The publisher, the authors and the editors are safe to assume that the advice and information in this book are believed to be true and accurate at the date of publication. Neither the publisher nor the authors or the editors give a warranty, express or implied, with respect to the material contained herein or for any errors or omissions that may have been made.

Printed on acid-free paper

This Springer imprint is published by Springer Nature
The registered company is Springer International Publishing AG
The registered company address is: Gewerbestrasse 11, 6330 Cham, Switzerland

PROCEEDINGS OF MED GREEN FORUM – III

MEDITERRANEAN GREEN BUILDINGS AND RENEWABLE ENERGY FORUM – 2015



WREC- WREN
ABITA



etaflorence
renewableenergies

August 26 -28, 2015,
School of Architecture,
University of Florence,
Florence, Italy.

A large, multi-faceted graphic poster for the Med Green Forum. The central graphic is a 3D cube-like structure composed of various images related to green buildings and renewable energy, including solar panels, a cityscape, and the Florence Cathedral dome. Text on the poster includes:

THE WORLD RENEWABLE ENERGY CONGRESS FORUM
ORGANIZED BY:
WREC-WREN ABITA
etaflorence @ renewableenergies

UNIVERSITÀ DEGLI STUDI DI FIRENZE
DIDA
26-28 AUGUST 2015
UNIVERSITY OF FLORENCE
DEPARTMENT OF ARCHITECTURE
FLORENCE, ITALY

AMONG THE MAIN SPONSORS:
Springer
UNIVERSITY OF BARI
UNIVERSITY OF TRIESTE

MED GREEN FORUM
MEDITERRANEAN GREEN BUILDINGS AND RENEWABLE ENERGY FORUM 2015

Edited by:
Professor Ali Sayigh, Chairman of WREC and Director General of WREN
(A World Renewable Energy Congress Event)

Mission Statement

This World Renewable Energy Congress and Network Forum is aimed at the international community and Mediterranean countries. The first forum was held in 2010 in France, followed by one in Morocco in 2012. This volume represents the best paper submissions from the third forum, which took place in Florence, Italy, from 25 to 28 August 2015.

The forum was arranged to highlight the importance of growing renewable energy applications in two main sectors: electricity generation and sustainable building. The Mediterranean region was chosen to illustrate the viability of using renewable energy to satisfy all its energy needs. We hope to demonstrate the effectiveness of renewable energy in these countries to act as a beacon of light for the rest of the world to follow. Renewables are the cornerstone and foundation of a truly *sustainable energy future*. The World Renewable Energy Network's mission is to promote enabling policies and to further develop a broad range of renewable energy technologies and applications in all sectors – for electricity production, heating and cooling, agricultural applications, water desalination, and industrial applications, as well as for the transport sectors, leading to A BETTER, CLEANER, AND SAFER WORLD.

Chairman's Message



In this third Med Green Forum, I was lucky to have as my co-chair Professor Marco Sala, Head of ABITA, Florence. The head of administration was Ms. Angela Grassi, Director of ETA Renewable Energy-Florence. We also had an excellent team representing the Technical Committee.

We received more than 150 abstracts from 51 countries covering the 9 topics of the forum. We achieved our aim: to learn from each other's experiences and to highlight best practices. The Mediterranean region is poised to be the first in the world where all energy demands are met through renewable energy sources. During the last 25 years, the World Renewable Energy Congress and Network has held outstanding events in more than 50 countries. It is fitting that this, our fifth meeting, took place in Florence, the city of culture, art, and knowledge. Our thanks to all the sponsors, including ISESCO, the Italian Foreign Ministry, and Springer Science+Business Media.

Technical Committee



Mr Rainer Hinrichs-Rahlwes
- Germany



Prof Arch Fernando Recalde
- Italy



Dr Neveen Hamza – UK



Prof Bahram Moshfegh
– Sweden



Prof Federico Butera – Italy



Prof Runming Yao -UK

Contents

1	Energy-Saving Solutions for Five Hospitals in Europe	1
	Marco Sala, Giuseppina Alcamo, and Lucia Ceccherini Nelli	
2	Climate Adapted in NZEB Retrofitting for Residential Buildings	19
	Marco Sala and Lucia Ceccherini Nelli	
3	Sustainable Strategies for Protecting and Managing Cultural Heritages: The Case Study of Gonfienti in the Tuscany Region of Italy	33
	Marco Sala, Giuseppina Alcamo, and Lucia Ceccherini Nelli	
4	Buildings' Energy Flexibility: A Bottom-Up, Multiagent, User-Based Approach to System Integration of Energy Infrastructures to Support the Smart Grid	47
	Wim Zeiler, Timilehin Labeodan, Kennedy Aduda, and Gert Boxem	
5	Influence Effect of Energy Roof on PV Efficiency: A Case Study	61
	Paul Kemme and Wim Zeiler	
6	Retracted Chapter: Green Buildings and Renewable Energy Application Based on Life Cycle Performance Costing	73
	Wim Zeiler, Anna Vanderveen, Wim Maassen, and Rik Maaijen	
7	A Comparative Study Between Photovoltaic Pumping Systems Using a Permanent Magnet DC Motor and an Induction Motor	89
	S. Abdourraziq and R. El Bachtiri	

8	Development of a Design of a Drop-In Hydrogen Fueling Station to Support the Early Market Buildout of Hydrogen Infrastructure: Topic-9	103
	Abdulahkim Agll, Tarek Hamad, Sushrut G. Bapat, Yousif Hamad, and John W. Sheffield	
9	Sustainability of Higher Educational Buildings: Retrofitting Measures to Enhance Energy Performance—The Case of AASTMT Business Management School Building, Egypt	117
	Mohsen Aboulnaga, Ayman Wanas, Mohamed Hammad, and Mohamed Hussein	
10	Effectiveness of Thermal Inertia in South Mediterranean Climate: Residential Houses	151
	Giuseppina Alcamo	
11	Thermal Habitability Monitoring in Housing for Low-Income Families in Extreme Warm, Dry Weather	165
	R.A. Romero-Moreno, G. Bojórquez-Morales, A. Luna, M. Corral, and T. Gutiérrez-García	
12	Multidisciplinary Energy-Efficiency Think Tank for Supporting a Multilevel Governance Model in Energy Policies and Measures: MEETHINK Energy Project: Topic-6	177
	Antonella Trombadore	
13	An Integrated Building Energy Management System	191
	Carlos Henggeler Antunes, Ana Soares, and Álvaro Gomes	
14	The Normal: Minimising Energy Use; The Abnormal: Changing Habits	201
	Anwar El Hadi, Ingi A. El-Hadi, and Mohammed A.I. Alameer	
15	Semi-Empirical Models for the Estimation of Global Solar Irradiance Measurements in Morocco	213
	N. Laaroussi, M. Garoum, A. Hajji, M. Tajayouti, and A. Feiz	
16	Assessing PV Module Degradation and the Potential of Using Greenhouse Roofs for Supplemental PV Power Generation in Malta	223
	Kristy Bartolo and Charles Yousif	
17	Revitalization and Refurbishment of Minor Historical Centers in the Mediterranean	235
	Alessandra Battisti	
18	Building Envelope–Systems Integrated Models: Topic 4	245
	Fabio Conato	

19 Lessons for Future Cities and Architecture: Ecology, Culture, Sustainability 259
 Derya Oktay

20 Thermal Performance of Vacuum Glazing with Tempered Glass Panes 275
 Yueping Fang, Trevor J. Hyde, Farid Arya, and Neil Hewitt

21 Energy Refurbishment Towards Nearly Zero-Energy Terrace Houses in the Mediterranean Region 293
 D.K. Serghides, M. Michaelidou, Stella Demetriou, and M.C. Katafygiotou

22 Geo-Climatic Applicability of Direct Evaporative Cooling in Italy 311
 Giacomo Chiesa, Fabio Acquiletti, and Mario Grosso

23 Integrating Deep Offshore Wind with Pumped Hydro Storage in a Central Mediterranean Archipelago’s Electricity Generation System 325
 Robert N. Farrugia, Tonio Sant, and Cedric Caruana

24 Energy Choice to Support Carbon Dioxide Reduction in Indonesia 341
 Herliyani Suharta, Arnold Soetrisnanto, and Unggul Priyanto

25 A Study of Space Syntax and Sustainable Design in Chinese Vocational Education Parks: Three Case Studies 355
 Qiushi Hao, Benchen Fu, and Teng Fei

26 Micro-Aeolic in Residential Districts: A Case Study in Sant’Arsenio (South-western Italy) 369
 Dora Francese, Emanuela Adamo, and Shoaib Khanmohammadi

27 Effect of Shadows on the Performance of Solar Photovoltaic 379
 Hussein A. Kazem, Miqdam T. Chaichan, Ali H. Alwaeli, and Kavish Mani

28 Study of Landform-Reconstruction Method Applied to Architectural Forms in Cold Areas 387
 Chen Shuo and Mei Hongyuan

29 Building-Integrated Renewable Energy Systems, or Rediscovering Forgotten Principles 399
 Ana-Maria Dabija

30 The Possible Shift Between Heating and Cooling Demand of Buildings Under Climate Change Conditions: Are Some Mitigation Policies Wrongly Understood? 417
 Massimo Palme

31	Robustness of Residential Houses in Ecuador in the Face of Global Warming: Prototyping and Simulation Studies in the Amazon, Coastal and Andes Macroclicmatic Regions	423
	Massimo Palme and Andrea Lobato	
32	Performance Analysis and Parametric Studies of a Bi-fluid Type Photovoltaic/Thermal (PV/T) Solar Collector in Simultaneous Mode under Tropical Climate Conditions	429
	Hasila Jarimi, Mohd Nazari Abu Bakar, Mahmud Othman, and Mahadzir Din	
33	Bi-fluid Photovoltaic/Thermal PV/T Solar Collector with Three Modes of Operation: Experimental Validation of a Theoretical Model	445
	Hasila Jarimi, Mohd Nazari Abu Bakar, Mahmud Othman, and Mahadzir Din	
34	High Quality of Calibration Accuracy for Smart Building Energy-Efficiency Opportunities	465
	G. Mustafaraj	
35	Liquid and Gas Biofuels from the Catalytic Re-forming of Pyrolysis Bio-Oil in Supercritical Water: Effects of Operating Conditions on the Process	479
	Javier Remón, Pedro Arcelus-Arrillaga, Jesús Arauzo, Lucía García, and Marcos Millan-Agorio	
36	Pyrolysis Bio-Oil Upgrading to Renewable Liquid Fuels by Catalytic Hydrocracking: Effect of Operating Conditions on the Process	491
	Javier Remón, Pedro Arcelus-Arrillaga, Jesús Arauzo, Lucía García, and Marcos Millan-Agorio	
37	Supporting Electromobility in Smart Cities Using Solar Electric Vehicle Charging Stations	501
	J.K. Kaldellis, G. Spyropoulos, and St. Liaros	
38	Exploitation of Wave Energy Potential in Aegean Sea: Greece	515
	F. Xanthaki, Chr. Giannaraki, E.F. Zafeiraki, and J.K. Kaldellis	
39	Energy Performance of a Renovated Multi-Family Building in Sweden	531
	Lina La Fleur, Bahram Moshfegh, and Patrik Rohdin	
40	Building Thermal Exergy Analysis	541
	Lorenzo Leoncini and Marta Giulia Baldi	
41	Light and Shadow: Mediterranean Visual Scenes	553
	Judit Lopez-Besora and Helena Coch	

42 Potential of Solar Electricity for Grid-Connected Systems in Algeria 561
 L. Hassaine and A. Mraoui

43 Thermal Energy Recovery System for Upgrading Waste Heat by an Absorption Heat Pump 575
 Yoshinori Itaya

44 Mathematical Model for System Planning on Campus: A Case Study in Harbin Institute of Technology in China 589
 Rong Guo and Tong Wu

45 Urban Sustainable Development in the Mediterranean Area: The Case of Sestri Ponente, Genoa 599
 Katia Perini and Adriano Magliocco

46 Development of Energy Devices Based on Photovoltaic Panels with Extra Consumer Properties 609
 L. Mikhailov, S. Mikhailova, G. Ismailova, G. Yar-Muhamedova, and S. Sokolov

47 Assessment of Airflows in a School Building with Mechanical Ventilation Using Passive Tracer Gas Method 619
 Jessica Steen Englund, Jan Akander, Mikael Björling, and Bahram Moshfegh

48 Energetic and Functional Upgrading of School Buildings 633
 Paolo Giordani, Alessandro Righi, Tiziano Dalla Mora, Mauro Frate, Fabio Peron, and Piercarlo Romagnoni

49 Evaluation of Thermal Performance, Environmental Impact, and Cost Effectiveness of an XLam Component for Retrofitting in Existing Buildings 643
 Tiziano Dalla Mora, Alessandro Righi, Fabio Peron, and Piercarlo Romagnoni

50 Self-Awareness Tool for Renewable Energy Production in Mixed-Use Urban Tissues: Incubators European Project for the Mediterranean Region 657
 Luca Caneparo, Federica Bonaverò, and Barbara Melis

51 Renewable Energy in South of Morocco and Prospects 667
 Hassan Nfaoui and Ali Sayigh

52 Analysis of Energy Performance of a High-Performance Building in a Local Mediterranean Climatic Context 681
 Maria Teresa Lucarelli and Caterina Claudia Musarella

53 Skylight Optimization Design Based on the Interior Ventilation in the Office Building in Cold Region 691
 Tiantian Du and Jianfei Chen

54	An Environmental Technological Approach to Architectural Programming for School Facilities	701
	Giacomo Chiesa and Mario Grosso	
55	Green, Smart, Sustainable Building Aspects and Innovations	717
	Abdul Salam Darwish	
56	Soilless Urban Temporary Agriculture as a Strategy for Brownfield Site Renewal	729
	Leonardo Boganini and Chiara Casazza	
57	Solar Building Systems for the Mediterranean Region: Research Outputs Between Italy and France	741
	Christian Cristofari, Andrea Giachetta, and Chiara Piccardo	
58	Spectral Variation of Energy-Efficient Room Lighting	755
	Helmut F.O. Müller	
59	The Housing Retrofit Market in Italy: Constraints and Barriers to Development	765
	Riccardo Pollo	
60	Passive Cooling in Mediterranean Area for a Bioclimatic and Zero Energy Architecture	773
	Fabrizio Tucci	
61	First-Year Performance of a PV Plant in Jordan Compared to PV Plants in the Region	785
	Ali Hamzeh, Sadiq Hamid, Abbas Sandouk, Zakaria Al-Omari, and Ghada Aldahim	
62	Gauging the Effectiveness of a Resource Management Awareness Campaign on a Central Mediterranean Island	799
	Paul Refalo, Robert N. Farrugia, Luciano Mulè Stagno, Charles Yousif, Tonio Sant, Nora Jakkel, Anthony Zammit, and Joseph Portelli	
63	The ‘Reduce and Save’ Project: An Island-Wide Resource Management Awareness Initiative	811
	Paul Refalo, Luciano Mulè Stagno, Robert N. Farrugia, Charles Yousif, Tonio Sant, Nora Jakkel, Anthony Zammit, and Joseph Portelli	
64	Heat and Light Intensity Influence on (I–V) Characterization of Cu₂S Film/p-Si Heterojunction	821
	M. Saadeldin, M.M. El-Nahass, and K. Sawaby	
65	Using Renewable Energy to Process Seaweed	835
	A. Kamaruddin, Aep Saepul Uyun, Herman Noer Rahman, Eri Suherman, and Salnida Y. Lumbessi	

66 New Environmentally Friendly Chlorine-Free Solar-Grade Silicon Production Technologies 845
 Sergey Karabanov, Victor Yasevich, Dmitriy Suvorov, Evgeniy Slivkin, and Andrey Karabanov

67 Some Physical Properties of Pure and Fluorine-Doped Tin Oxide Films Used as Transparent Conducting Oxide 857
 Kamil M. Yousif and Sayran A. Abdulgafar

68 Socioeconomic, Environmental, and Social Impacts of a Concentrated Solar Power Energy Project in Northern Chile 865
 Irene Rodríguez, Natalia Caldés, Alberto Garrido, Cristina De La Rúa, and Yolanda Lechón

69 Learning Sustainability from Arab Gulf Vernacular Architecture 885
 Khaled A. Al-Sallal

70 Transparent Conducting Oxides for Solar Cell Applications 899
 Shadia J. Ikhmayies

71 Solar-Driven Cold Storage Units to Reduce Food Waste 909
 Sraisth

72 An Adaptive Thermal Comfort Model for the Romanian Climate 921
 Ioana Udrea, Cristiana Croitoru, Ilinca Nastase, Ruxandra Crutescu, and Viorel Badescu

73 A Whole-Building, Integrated Approach for Designing a High-Performance, Net-Zero-Energy and Net-Zero-Water Building 931
 Richard V. Piacentini

74 Dynamic Simulation for Increasing the Efficiency of Solar Cooling Systems in Northern Latitudes 941
 Peteris Shipkovs, Janis Shipkovs, Andrejs Snegirjovs, Galina Kashkarova, Kristina Lebedeva, and Lana Migla

75 Investigation of Urban Microclimate Parameters of City Square in Harbin 949
 Hong Jin, Peng Cui, and Meng Huang

Retraction Note to: Green Buildings and Renewable Energy Application Based on Life Cycle Performance Costing E1

Correction to: Investigation of Urban Microclimate Parameters of City Square in Harbin E3

Correction to: Integrating Deep Offshore Wind with Pumped Hydro Storage in a Central Mediterranean Archipelago’s Electricity Generation System C1

Contributors

S. Abdourraziq LESSI Lab FSDM, REEPER Group, EST, Sidi Mohammed Ben Abdellah University, Fez, Morocco

Sayran A. Abdulgafar Department of Physics, Faculty of Science, Dohuk University, Dohuk, Iraq

Mohsen Aboulnaga Department of Architectural Engineering, Cairo University, Cairo, Egypt

Fabio Acquiletti Department of Architecture and Design–DAD, Politecnico di Torino, Turin, Italy

Emanuela Adamo Department of Architecture, “Federico II” University, Naples, Italy

Kennedy Aduda Faculty of the Built Environment, University of Technology Eindhoven, Eindhoven, The Netherlands

Abdulhakim Agll Department of Mechanical and Aerospace Engineering, Missouri University of Science and Technology, Rolla, MO, USA

Jan Akander Division of Building, Energy and Environment Technology, Department of Technology and Environment, University of Gävle, Gävle, Sweden

Mohammed Abdalwahid Ibrahim Alameer College of Engineering and Architecture, Bahri University, Khartoum, Sudan

Giuseppina Alcamo Department of Architecture DIDA, Centro ABITA, University of Florence, San Niccolò 93, Florence 50125, Italy

Ghada Aldahim FMEE Department of Electrical Engineering, Damascus University, Damascus, Syria

Zakaria Al-Omari Department of Electrical Engineering, Al-Ahliyya Amman University, Amman, Jordan

Khaled A. Al-Sallal UAE University, Al-Ain, United Arab Emirates

Ali H. Alwaeli Sohar University, Sohar, Oman

Carlos Henggeler Antunes Department of Electrical and Computer Engineering,
University of Coimbra, Coimbra, Portugal

INESC Coimbra, DEEC - University of Coimbra, Coimbra, Portugal

Jesús Arauzo Thermochemical Processes Group (GPT), Aragon Institute for
Engineering Research (I3A), Universidad Zaragoza, Zaragoza, Spain

Pedro Arcelus-Arrillaga Department of Chemical Engineering, Imperial College
London, London, UK

Farid Arya School of the Built Environment, Ulster University, Northern
Ireland, UK

R. El Bachtiri LESSI Lab FSDM, REEPER Group, EST, Sidi Mohammed Ben
Abdellah University, Fez, Morocco

Viorel Badescu Faculty of Mechanical Engineering and Mechatronics,
Thermodynamics Department, Polytechnic University of Bucharest, Bucharest,
Romania

Mohd Nazari Abu Bakar Universiti Teknologi Mara Perlis, Perlis, Malaysia

Marta Giulia Baldi Department of Industrial Engineering, University of
Florence, Florence, Italy

Sushrut G. Bapat Department of Mechanical and Aerospace Engineering,
Missouri University of Science and Technology, Rolla, MO, USA

Kristy Bartolo Institute of Earth Systems, University of Malta, Msida, Malta

Alessandra Battisti PDTA Planning Design Technology of Architecture
Department, La Sapienza Rome, Rome, Italy

Mikael Björling Division of Building, Energy and Environment Technology,
Department of Technology and Environment, University of Gävle, Gävle, Sweden

Leonardo Boganini Dipartimento di Architettura DIDA, Centro ABITA,
Università degli Studi di Firenze, Florence, Italy

G. Bojórquez-Morales Faculty of Architecture and Design, Autonomous
University of Baja California, Mexicali, Mexico

F. Bonavero DAD—Department of Architecture and Design, Politecnico di
Torino, Turin, Italy

Gert Boxem Faculty of the Built Environment, University of Technology
Eindhoven, Eindhoven, The Netherlands

Natalia Caldés Energy Department, Energy Systems Analysis Unit, Madrid, Spain

L. Caneparo Department of Architecture and Design, Politecnico di Torino, Turin, Italy

Cedric Caruana Department of Industrial Electrical Power Conversion, University of Malta, Msida, Malta

Chiara Casazza Dipartimento di Architettura DIDA, Centro ABITA, Università degli Studi di Firenze, Florence, Italy

Miqdam T. Chaichan University of Technology, Baghdad, Iraq

Jianfei Chen School of Architecture, Harbin Institute of Technology, Harbin, China

Giacomo Chiesa Department of Architecture and Design—DAD, Politecnico di Torino, Turin, Italy

Helena Coch Architecture and Energy, School of Architecture of Barcelona, UPC, Barcelona, Spain

Fabio Conato Department of Architecture, University of Ferrara, Ferrara, Italy

M. Corral Faculty of Architecture and Design, Autonomous University of Baja California, Mexicali, Mexico

Christian Cristofari University of Corsica Pascal Paoli—IUT UMR CNRS 6134, Corte, France

Cristiana Croitoru Building Services Department, Technical University of Civil Engineering in Bucharest, Bucharest, Romania

Ruxandra Crutescu Spiru Haret University, Bucharest, Romania

Ana-Maria Dabija “Ion Mincu” University of Architecture and Urbanism, Bucharest, Romania

Abdul Salam Darwish Phoenix Renewable Energy Centre, Manchester, UK

Stella Demetriou Department of Environmental Science and Technology, Cyprus University of Technology, Limassol, Cyprus

Mahadzir Din Universiti Teknologi Mara Perlis, Perlis, Malaysia

Tiantian Du School of Architecture, Harbin Institute of Technology, Harbin, China

H.H. El-Ghetany Solar Energy Department, National Research Centre, Giza, Egypt

Ingi A. El-Hadi University of Khartoum, Khartoum, Sudan

Anwar El-Hadi College of Engineering and Architecture, Bahri University, Khartoum, Sudan

M.M. El-Nahass Physics Department, Ain-Shams University, Cairo, Egypt

Jessika Steen Englund Division of Building, Energy and Environment Technology, Department of Technology and Environment, University of Gävle, Gävle, Sweden

Yueping Fang School of the Built Environment, Ulster University, Northern Ireland, UK

Robert N. Farrugia Institute for Sustainable Energy, University of Malta, Marsaxlokk, Malta

Department of Mechanical Engineering, University of Malta, Msida, Malta

Teng Fei Department of Architecture, Harbin Institute of Technology, Harbin, China

A. Feiz Laboratoire de Mécanique et d’Energétique d’Evry (LMEE), Equipe Mécanique des Fluides et Environnement (MFE), Université d’Evry Val-d’Essonne, Evry, France

Lina La Fleur Division of Energy Systems, Linköping University, Linköping, Sweden

Dora Francese CITTAM, Naples, Italy

Mauro Frate Università IUAV di Venezia, Venice, Italy

Benchen Fu Department of Architecture, Harbin Institute of Technology, Harbin, China

Lucía García Thermochemical Processes Group (GPT), Aragon Institute for Engineering Research (I3A), Universidad Zaragoza, Zaragoza, Spain

M. Garoum EST de Salé, Laboratoire d’Energétique, Matériaux et Environnement (LEME), Université Mohammed V Rabat, Maroc, Rabat, Morocco

Alberto Garrido CEIGRAM, Research Centre for the Management of Agricultural and Environmental Risks, Madrid, Spain

Andrea Giachetta Department of Sciences for Architecture, University of Genoa, Genoa, Italy

Chr. Giannaraki Soft Energy Applications and Environmental Protection Laboratory, Piraeus University of Applied Sciences, Athens, Greece

Paolo Giordani Università IUAV di Venezia, Venice, Italy

Gennadiy Gololobov Ryazan State Radio Engineering University, Ryazan, Russia

Álvaro Gomes Department of Electrical and Computer Engineering, University of Coimbra, Coimbra, Portugal

INESC Coimbra, DEEC - University of Coimbra, Coimbra, Portugal

Mario Grosso Department of Architecture and Design—DAD, Politecnico di Torino, Turin, Italy

Rong Guo School of Architecture, Harbin Institute of Technology, Harbin, China

T. Gutiérrez-García Faculty of Architecture and Design, Autonomous University of Baja California, Mexicali, Mexico

A. Hajji EST de Salé, Laboratoire d’Énergétique, Matériaux et Environnement (LEME), Université Mohammed V Rabat, Maroc, Rabat, Morocco

Tarek Hamad Department of Mechanical and Aerospace Engineering, Missouri University of Science and Technology, Rolla, MO, USA

Yousif Hamad Department of Mechanical and Aerospace Engineering, Missouri University of Science and Technology, Rolla, MO, USA

Sadiq Hamid Department of Electrical Engineering, Al-Ahliyya Amman University, Amman, Jordan

Mohamed Hammad Department of Architectural Engineering, Cairo University, Cairo, Egypt

Ali Hamzeh Department of Electrical Engineering, Al-Ahliyya Amman University, Amman, Jordan

Qiushi Hao Department of Architecture, Harbin Institute of Technology, Harbin, China

L. Hassaine Centre de Développement des Energies Renouvelables (CDER), Algiers, Algeria

Neil Hewitt School of the Built Environment, Ulster University, Northern Ireland, UK

Mei Hongyuan Heilongjiang, China

H.M.S. Hussein Solar Energy Department, National Research Centre, Giza, Egypt

Mohamed Hussein Department of Architecture and Environmental Design, AASTMT, Cairo, Egypt

Trevor J. Hyde School of the Built Environment, Ulster University, Northern Ireland, UK

Shadia J. Ikhmayies Physics Department, Al-Isra University, Amman, Jordan

G. Ismailova Al-Farabi Kazakh National University, Almaty, Kazakhstan

Yoshinori Itaya Environmental and Renewable Energy Systems Division, Graduate School of Engineering, Gifu University, Gifu, Japan

Nora Jakkel Institute for Sustainable Energy, Marsaxlokk, Malta

Hasila Jarimi Universiti Teknologi Mara Perlis, Perlis, Malaysia
Universiti Teknologi Mara Shah Alam, Selangor, Malaysia

J.K. Kaldellis Soft Energy Applications and Environmental Protection Laboratory, Piraeus University of Applied Sciences, Athens, Greece

A. Kamaruddin Graduate School/Renewable Energy, DarmaPersada University, East Jakarta, Indonesia

Sergey Karabanov Ryazan State Radio Engineering University, Ryazan, Russia

Andrey Karabanov Ryazan State Radio Engineering University, Ryazan, Russia

Galina Kashkarova Institute of Physical Energetics, Riga, Latvia

M.C. Katafygiotou Department of Environmental Science and Technology, Cyprus University of Technology, Limassol, Cyprus

Hussein A. Kazem Sohar University, Sohar, Oman

Paul Kemme Faculty of the Built Environment, University of Technology Eindhoven, Eindhoven, The Netherlands

Shoab Khanmohammadi Department of Mechanical Engineering, Guilan University, Rasht, Iran

N. Laaroussi EST de Salé, Laboratoire d'Energétique, Matériaux et Environnement (LEME), Université Mohammed V Rabat, Maroc, Rabat, Morocco

Timilehin Labeodan Faculty of the Built Environment, University of Technology Eindhoven, Eindhoven, The Netherlands

Kristina Lebedeva Institute of Physical Energetics, Riga, Latvia

Yolanda Lechón Energy Department, Energy Systems Analysis Unit, CIEMAT, Madrid, Spain

Lorenzo Leoncini Department of Industrial Engineering, University of Florence, Florence, Italy

St. Liaros Soft Energy Applications and Environmental Protection Laboratory, Piraeus University of Applied Sciences, Athens, Greece

Andrea Lobato Instituto Nacional de Eficiencia Energética y Energías Renovables (INER), Quito, Ecuador

Judit López-Besora Architecture and Energy, School of Architecture of Barcelona, Barcelona, Spain

Maria Teresa Lucarelli dArTe Department, Mediterranean University of Reggio Calabria, Reggio Calabria, Italy

Salnida Y. Lumbessi Mataram University, Mataram, Indonesia

A. Luna Faculty of Architecture and Design, Autonomous University of Baja California, Mexicali, Mexico

Rik Maaijen Royal Haskoning DHV, Building Services Rotterdam, Rotterdam, The Netherlands

Wim Maassen Faculty of the Built Environment, University of Technology Eindhoven, Eindhoven, The Netherlands

Royal Haskoning DHV, Building Services Rotterdam, Rotterdam, The Netherlands

Adriano Magliocco Dipartimento di Scienze per l'Architettura, Università degli Studi di Genova, Genoa, Italy

Kavish Mani Sohar University, Sohar, Oman

B. Melis Department of Architecture and Design, Politecnico di Torino, Turin, Italy

M. Michaelidou Department of Environmental Science and Technology, Cyprus University of Technology, Limassol, Cyprus

Lana Migla Institute of Physical Energetics, Riga, Latvia

L. Mikhailov Al-Farabi Kazakh National University, Almaty, Kazakhstan

S. Mikhailova Al-Farabi Kazakh National University, Almaty, Kazakhstan

Marcos Millan-Agorio Department of Chemical Engineering, Imperial College London, London, UK

Tiziano Dalla Mora Università IUAV di Venezia, Venice, Italy

Bahram Moshfegh Division of Building, Energy and Environment Technology, Department of Technology and Environment, University of Gävle, Gävle, Sweden

Division of Energy Systems, Department of Management and Engineering, Linköping University, Linköping, Sweden

A. Mraoui, Centre de Développement des Energies Renouvelables (CDER), Algiers, Algeria

Helmut F.O. Müller Green Building R&D GmbH, Düsseldorf, Germany

Caterina Claudia Musarella dArTe Department, Mediterranean University of Reggio Calabria, Reggio Calabria, Italy

G. Mustafaraj International Energy Research Centre IERC, Tyndall Institute, University College of Cork, Cork, Ireland

Ilinca Nastase Building Services Department, Technical University of Civil Engineering in Bucharest, Bucharest, Romania

Lucia Ceccherini Nelli DIDA Department, ABITA Interuniversity Centre, University of Florence, Florence, Italy

Hassan Nfaoui Solar Energy and Environment Laboratory, Mohammed-V University, Rabat, Morocco

Derya Oktay Ondokuz Mayıs University, Samsun, Turkey

Mahmod Othman Universiti Teknologi Mara Perlis, Perlis, Malaysia

Massimo Palme School of Architecture, Catholic University of the North, Antofagasta, Chile

Escuela de Arquitectura, Universidad Católica del Norte, Antofagasta, Chile

Instituto Nacional de Eficiencia Energética y Energías Renovables (INER), Quito, Ecuador

Katia Perini Dipartimento di Scienze per l'Architettura, Università degli Studi di Genova, Genoa, Italy

Fabio Peron Università IUAV di Venezia, Venice, Italy

Richard V. Piacentini Phipps Conservatory and Botanical Gardens, Pittsburgh, PA, USA

Chiara Piccardo Department of Sciences for Architecture, University of Genoa, Genoa, Italy

Riccardo Pollo Department of Architecture and Design—DAD, Politecnico di Torino, Torino, Italy

Joseph Portelli Ministry for Gozo, Pjazza San Frangisk, Gozo, Malta

Unggul Priyanto The Agency for the Assessment and Application of Technology (BPPT), Jakarta, Indonesia

Herman Noer Rahman The Graduate School/Renewable Energy, DarmaPersada University, East Jakarta, Indonesia

Paul Refalo Institute for Sustainable Energy, Marsaxlokk, Malta

Javier Remón Thermochemical Processes Group (GPT), Aragon Institute for Engineering Research (I3A), Universidad Zaragoza, Zaragoza, Spain

Department of Chemical Engineering, Imperial College London, London, UK

Alessandro Righi Università I.U.A.V., Venice, Italy

Irene Rodríguez Energy Department, Energy Systems Analysis Unit, CIEMAT, Madrid, Spain

Patrik Rohdin Division of Energy Systems, Linköping University, Linköping, Sweden

Piercarlo Romagnoni Università IUAV di Venezia, Venice, Italy

R.A. Romero-Moreno Faculty of Architecture and Design, Autonomous University of Baja California, Mexicali, Mexico

Cristina De La Rúa Energy Department, Energy Systems Analysis Unit, CIEMAT, Madrid, Spain

M. Saadeldin Physics Department, Cairo University, Giza, Egypt

Marco Sala DIDA Department, ABITA Interuniversity Centre, University of Florence, Florence, Italy

Abbas Sandouk FMEE Department of Electrical Engineering, Damascus University, Damascus, Syria

Tonio Sant Institute for Sustainable Energy, University of Malta, Marsaxlokk, Malta

Department of Mechanical Engineering, University of Malta, Msida, Malta

K. Sawaby Physics Department, Cairo University, Giza, Egypt

Ali Sayigh WREC, WREN, IEI, Brighton, UK

D.K. Serghides Department of Environmental Science and Technology, Cyprus University of Technology, Limassol, Cyprus

John W. Sheffield Department of Mechanical and Aerospace Engineering, Missouri University of Science and Technology, Rolla, MO, USA

Peteris Shipkovs Institute of Physical Energetics, Riga, Latvia

Janis Shipkovs Institute of Physical Energetics, Riga, Latvia

Riga Technical University, Riga, Latvia

Chen Shuo Heilongjiang, China

Evgeniy Slivkin Ryazan State Radio Engineering University, Ryazan, Russia

Andrejs Snegirjovs Institute of Physical Energetics, Riga, Latvia

Riga Technical University, Riga, Latvia

Ana Soares Department of Electrical and Computer Engineering, University of Coimbra, Coimbra, Portugal

INESC Coimbra, DEEC - University of Coimbra, Coimbra, Portugal

Arnold Soetrisnanto National Research Council, Jakarta, Republic of Indonesia

- S. Sokolov** Al-Farabi Kazakh National University, Almaty, Kazakhstan
- G. Spyropoulos** Soft Energy Applications and Environmental Protection Laboratory, Piraeus University of Applied Sciences, Athens, Greece
- Sraisth** Global Production Engineering in Solar Technology, Berlin, Germany
- Luciano Mule' Stagno** Institute for Sustainable Energy, Marsaxlokk, Malta
- Herliyani Suharta** The Center of Energy Conversion Technology, BPPT, Kawasan PUSPIPTEK, Serpong, Tangerang Selatan, Republic of Indonesia
- Eri Suherman** Graduate School/Renewable Energy, DarmaPersada University, East Jakarta, Indonesia
- Dmitriy Suvorov** Ryazan State Radio Engineering University, Ryazan, Russia
- M. Tajayouti** EST de Salé, Laboratoire d'Energétique, Matériaux et Environnement (LEME), Université Mohammed V Rabat, Maroc, Rabat, Morocco
- Antonella Trombadore** DIDA Department of Architecture, Università degli Studi di Firenze, Florence, Italy
- Fabrizio Tucci** Department Planning Design Technology, University di Architecture, Rome, Italy
- Ioana Udrea** Thermodynamics Department, Polytechnic University of Bucharest, Bucharest, Romania
- AepSaepul Uyun** Graduate School/Renewable Energy, DarmaPersada University, East Jakarta, Indonesia
- Anna Vanderveen** Faculty of the Built Environment, University of Technology Eindhoven, Eindhoven, The Netherlands
- Ayman Wanas** Arab Academy for Science, Technology and Maritime Transport, AASTMT, Cairo, Egypt
- Tong Wu** School of Architecture, Harbin Institute of Technology, Harbin, China
- F. Xanthaki** Soft Energy Applications and Environmental Protection Laboratory, Piraeus University of Applied Sciences, Athens, Greece
- G. Yar-Muhammedova** Al-Farabi Kazakh National University, Almaty, Kazakhstan
- Victor Yasevich** Ryazan State Radio Engineering University, Ryazan, Russia
- Charles Yousif** Institute for Sustainable Energy, University of Malta, Msida, Malta
- Kamil M. Yousif** Department of Environmental Science, Zakho University, Zakho, Iraq

E.F. Zafeiraki Soft Energy Applications and Environmental Protection Laboratory, Piraeus University of Applied Sciences, Athens, Greece

Anthony Zammit Ministry for Gozo, Pjazza San Frangisk, Gozo, Malta

Wim Zeiler Faculty of the Built Environment, University of Technology Eindhoven, Eindhoven, The Netherlands

Chapter 1

Energy-Saving Solutions for Five Hospitals in Europe

Marco Sala, Giuseppina Alcamo, and Lucia Ceccherini Nelli

Abstract This chapter is the result of a European research project developed by the University of Florence – Centro ABITA on adopting energy-saving strategies to reduce the annual energy demand in new and retrofitted hospital buildings. The research project, which is funded by the European Union, aims to apply energy-saving strategies, advanced technologies and plant solutions in five case studies in different climatic areas of Europe: Meyer Children’s Hospital in Italy, Fachkrankenhaus Nordfriesland Hospital in Germany, Torun City Hospital in Poland, Deventer Hospital in the Netherlands, and Aabenraa Hospital in Denmark. The research aims to demonstrate the significant opportunity to reduce energy demand in the European hospital sector, thereby contributing to a substantial reduction in CO₂ emissions. The main goal is the integration of strategies for energy efficiency in the hospital sector, in compliance with current regulations, improving environmental quality and ecosystems and promoting sustainable management of natural resources. Innovative strategies for the integration of renewable energies in buildings are combined with bioclimatic design to improve building control and management, upgrading energy efficiency, thermal control and comfort, natural ventilation, and daylighting. Moreover, the use of photovoltaic modules, high-efficiency heat pumps, integration with surrounding green areas, and the use of vegetation inside buildings are explored as opportunities to both reduce energy demand and improve patient comfort. At the end of the project, the researchers provide an overview of the results achieved on indoor comfort, energy savings, and CO₂ not emitted through the energy solutions adopted.

Keywords Energy • Environment • Daylighting • Energy savings • Renewable energies • Natural ventilation • Green roof

M. Sala (✉) • G. Alcamo • L.C. Nelli
DIDA Department—ABITA Interuniversity Centre, University of Florence,
Via San Niccolò 93, Florence 50125, Italy
e-mail: marco.sala@unifi.it; giuseppina.alcamo@unifi.it; luca.ceccherininelli@unifi.it

1 Introduction

Hospitals are energy- and resource-intensive buildings that contribute to climate change and to respiratory and other illnesses. The proper adoption of energy-saving strategies in the health sector can demonstrate a reasonable response to climate change, playing a leading role and supporting a healthy and sustainable future.

The implementation of sustainable energy systems is one of the principal objectives of the European Union's (EU) energy policy, which aims to promote secure energy supplies with high-quality services and high environmental comfort. Moreover, Europe intends to build zero-energy buildings in the near future, and experiences in the hospital sector can be very useful for reaching these goals.

Research demonstrates that technological and plant strategies plus renewable energy technologies may be used with very positive results in the European healthcare building sector and in this way encourage the integration of renewable energies. This chapter aims to illustrate the reduction in energy consumption and the comfort achieved from the adoption of energy-saving and bioclimatic-design solutions, as well as the resulting reduction in CO₂ emissions quantified in five case studies.

2 Objective

Energy efficiency reduces hospital energy consumption and costs. Hospitals designed on the principles of green building are responsive to local climate conditions and optimized to reduce energy and resource demands. Alternative energy generation produces or consumes clean, renewable energy on site to ensure reliable and resilient operation. Transportation involves the use of alternative hospital vehicles (such as electric vehicles). In addition, energy efficiency encourages walking and biking, promotes the use of public transport by staff, patients, and the community, and minimizes the need for staff and patients to use transportation by optimizing hospital routes, and encourages people to reduce, reuse, recycle, compost, use alternatives to waste incineration, and conserve water.

Standard operating procedures for most hospitals require significant energy use, such as for heating water, regulating temperature and humidity for indoor air, and controlling lighting, ventilation, and numerous clinical processes, all of which entails significant greenhouse gas emissions. Hospitals can implement many measures to improve energy efficiency while satisfying the energy requirements of these important energy-consuming end uses.

Using combined heat and power (CHP) technology, for example, facilities can generate onsite electricity and capture waste heat from the generation process as thermal energy. This can double energy efficiency by eliminating losses associated with the grid delivery of electricity. For artificial lighting LED light bulb can reduce energy consumption. Two principal objectives adopted in the case studies are:

- Conservation, reduction, and control of solar radiation;
- Provision of natural ventilation and natural cooling of external building surfaces by evaporative cooling.

3 Methodology

The adopted bioclimatic and technological design approach covers a range of strategies to save energy in buildings. What follows are some strategies adopted in accordance with local climatic conditions and with specific patient requirements:

-
- Building orientation and form
-
- Green building design
-
- Building envelope and materials: glazing and double-skin façade
-
- Envelope insulation
-
- Integration of renewable energy photovoltaic (PV)
-
- Green roofs
-
- Rational use of water
-
- Daylight strategies
-
- Appropriate shading devices
-
- Innovative bore holes
-

The five case studies examined here, with specific applied strategies, are as follows:

Italy: Meyer Children’s Hospital, Florence. The designed hospital creates a healing environment for patients and landscape as well. The hospital has abundant open spaces that are airy and bright and have high ceilings, which creates a comfortable place and peaceful setting for young patients and their families. The hospital is well integrated with the surroundings by a greenhouse, landscaped roofs, skylights, open buffer spaces, and an energy-efficient hybrid ventilation system. To monitor and conserve energy, the hospital design also includes a building energy management system and light tubes that create natural light throughout the building. The hospital consumes 40 % less energy for heating and cooling and electricity than a standard newly built Italian hospital (Figs. 1.1 and 1.2).

3.1 Technical Solutions

Envelope insulation: external façades and roofs have an adequate U-value ($0.32 \text{ W/m}^2 \text{ K}$ for external walls and $0.26 \text{ W/m}^2 \text{ K}$ for the roof) that is low enough to reduce as much as possible energy losses; they also have an adequate thermal mass (thermal lag is approximately 10 h) to reduce summer overheating on exposed surfaces (southern, western, and eastern exposure) (Figs. 1.3, 1.4, and 1.5).



Fig. 1.1 Aerial view of green roof of Meyer Children's Hospital



Fig. 1.2 South façade of new part of building

Windows and shading: The windows are constructed with wooden frames. Patient rooms are protected from direct sunlight by an overhanging structure externally covered with copper plates to reduce the visual impact of the building in the park, with the internal surface covered in wood. The greenhouse is shaded by internal white blinds that are adjusted by an automatic control system.

Fig. 1.3 Northern corridors and greenhouse



Fig. 1.4 Solar pipes and skylights

Fig. 1.5 PV façade



Sun pipes and light ducts: To improve patients' well-being, an important aspect is to provide daylight and positive surroundings, with plenty of sunshine and high thermal comfort levels. Sun pipes are installed to achieve a good illuminance value in patient rooms. Each room accommodates two patients and has two windows, one facing outside (surroundings) and receiving daylight, the other illuminated by sun pipes. Solar tubes and roof lights in hallways provide a good amount of daylight.

Heating: Heat pumps are used to generate heating and cooling. These are appropriate where both summer cooling and winter heating are required. Radiant panels and high-efficiency boilers are used for the heating system. Radiant floor heating panels are installed in patient rooms, where a decent level of thermal comfort is achieved at low energy cost. For winter heating and domestic hot water (DHW) generation there are two boilers, condensing combi boilers with an efficiency of approximately 106%. The boilers use gas, not electricity. Another conventional type of boiler kicks in only when necessary.

Cooling: For summer cooling there are two electric chillers. A third chiller is of the water/water type: the heat generated from this last machine is used for DHW.

Ventilation: Ventilation is guaranteed by windows that move up and down and open manually. A combination of shading and ventilation systems can keep indoor temperature to within 10 °C under outside temperature. To save on cooling energy, passive cooling and ventilation techniques are used as much as possible with air conditioning only where necessary. Glazing adopted for the greenhouse has a very low U-value, 0.78 W/m² K. This type of glazing reduces transmission losses and the greenhouse effect.

Photovoltaic: Meyer Children's Hospital's PV greenhouse is a structure with southern exposure and unobstructed solar access to the main solar glazing of the

greenhouse to maximize winter sunshine; it is not only a particular type of structure but also, and more importantly, a particular kind of space. The design considered not only energy and environmental aspects but also social impact: the primary objective was to create a pleasant and “socializing” space that could be used for semi-outdoor activities throughout most of the year with no extra energy space, a social space well integrated into the adjacent green park. The PV system is 30 kWp and realized with glass/glass PV modules.

Cogeneration: The design of the cogeneration plant is formed by a gas turbine, with an electrical power of 7.5 MWe (ISO), which allows the use of self-produced energy in the hospital complex.

Energy performance: The performance criterion was to achieve a 40 % reduction in consumed energy. The results of energy consumption are presented in this section and derived from simulation, calculation, and monitoring. Specific energy consumption targets were as follows: lighting sun pipes and roof lights in corridors and halls should provide a good level of daylight, and all installed lamps should be high efficiency.

The total annual electricity demand is 12.3 kWh/m². Compared with the energy demand in which all these features are not applied, the energy saving is 35 %. As for heating and cooling, the internal temperature and relative humidity measured during the monitoring phase are in accordance with simulations. The insulation used in walls and the roof gives energy savings of 35 % for heating and cooling. The annual heating demand is 73.4 kWh/m², and the annual cooling demand is 87.3 kWh/m². Regarding DHW, during the summer period, two chiller machines are used to cool the hospital. The heat produced is used for DHW. The annual heating for DHW demand is 13 % less than in a conventional Italian hospital. A cogeneration plant was not considered for energy performance because it must be completed. Project by: CSPE Architects, ABITA Unifi for technological strategies and renewable-energy strategies. Fachkrankenhaus Nordfriesland Pichiastric Hospital, Germany. The hospital is located near the North Sea and specializes in psychiatry and psychosomatic disorders.

Achieving superior indoor air quality is a priority in this psychiatric hospital. The designers’ emphasis on healthy, low-emission materials was a response to the hospital administration’s belief that indoor air quality improvements would markedly improve the treatment of patients with environmentally related illnesses.

Innovative strategies were adopted primarily to improve comfort, daylight conditions, and indoor climate for users of the buildings and secondarily to reduce energy consumption and CO₂ emissions. River- and rain-water-capture techniques, a solar mass wall with transparent insulation, a double-skin façade, and emission reduction are key performance indicators. Innovative and natural sources are used to minimize the use of metal in living rooms. Moreover, by improving daylight conditions, the need for electricity in the living rooms is consequently reduced, and the use of transparent insulation on the outer wall increases comfort inside the building. In parallel, energy consumption is reduced. Moreover, environmentally sensitive patients receive 100 % organic foods. Special attention is given to windows, which are treated as multifunctional building components with respect to all



Fig. 1.6 Main entrance in Fachkrankenhaus Nordfriesland Hospital

Fig. 1.7



the different parameters affecting indoor climate and energy consumption with a double-skin façade.

Double-skin façades with integrated natural ventilation and passive cooling are used in the glass façades facing east and west. The system was created to be used in different ways depending on the time of year and the weather. During summer the glass can reflect solar radiation and work jointly with a system of lamellas to provide shade from the sun. During winter the system is closed, thereby keeping hot air inside the buildings. The double-skin façades improve the daylight conditions and lead to reduced electricity use (Figs. 1.6 and 1.7). The hospital's renovation was guided primarily by energy conservation concerns, innovations in material selection, and careful attention to ventilation.

Energy description: emission reductions are as follows: CO₂: 261,740 kg CO₂/year, SO_x: 230 kg SO_x/year, NO_x: 2 kg NO_x/year. Project by: Architect S&I Arkitekter A/S.

4 Deventer Hospital, Overijssel, The Netherlands

Deventer Hospital is a 380-bed hospital with specialty clinics for psychiatry and radiation therapy. The energy savings in the new hospital are 47 % on heating and 13 % on electricity compared to a standard hospital. This reduction in energy use is equal to 1299 tons of CO₂ per year and is accompanied by an important reduction in related emissions like SO_x and NO_x. The project design focuses on energy efficiency, with energy-efficiency measures that result in annual emission reductions of 1.943 tons of CO₂, 8.71 tons of SO_x, and 3.35 tons NO_x. This is a reduction of 69 % compared with the average Dutch hospital. Patient comfort is guaranteed by the location of single-, double-, and triple-patient rooms away from public waiting rooms and high-traffic circulation areas and by improving patient access to daylight and views.

The roofs are partly covered with vegetation. Window frames are made of hard wood. Heat and cold storage is applied using a heat pump and concrete core activation for low-temperature heating. Heat is also recovered from ventilation air. Outside, rainwater is transported more slowly to open-surface water using cascades. The integral design has an energy-performance coefficient of 0.67. The environmental index of the building, according to the Greencalc method, attains a score of 212. The so-called hard facilities are located in the main part of the building. On the ground floor are less flexible polyclinics, on the first floor the perinatology center, intensive care unit, operating room, and daycare, on the second floor are patient rooms, and on the third floor laboratories and a pharmacy (Figs. 1.8 and 1.9).

The three energy principles of the hospital are:

1. Good insulation and natural ventilation;
2. Heat recovery techniques like energy wheels, which recover heat, cold, and latent energy;



Fig. 1.8 Deventer Hospital building entrance and pond



Fig. 1.9 Internal view of Deventer Hospital

3. Alternative renewable energy sources, heat–cool storage, and heat pumps and heat recovery applications in exhaust ventilation.

The ground is surrounded by a village and a natural reservoir, so groundwater-level fluctuations are not allowed. Since the conventional techniques could not be used in Deventer for heat–cool storage, a revolutionary new energy concept was designed with better performance, lower costs, and higher flexibility, and by implementing sufficient redundancy the failure risks are also minimized, which is important for the operation budget of a hospital. For this technique, 95 % of the effects will occur on the projects ground. In addition, the effects on the environment will be positive instead of negative. For a dry winter they send only based on the heat requirements of the building, whereas for a wet winter they send also based on environmental requirements in the, such that the groundwater level fluctuates very little.

5 Aabenraa Hospital, Denmark

The renovation being undertaken at this hospital includes covering three courtyards with glass and a well-insulated opaque roof, changing the courtyards from outdoor areas to real indoor areas. For the Aabenraa Hospital, optimization of the use of daylighting has been given special priority since optimum daylighting conditions had to be provided not only in the glazed courtyards themselves but also in the rooms surrounding the glazed courtyards. For the hybrid ventilation – natural fan-assisted ventilation – careful planning of the system controls was necessary to



Fig. 1.10 Aabenraa Hospital aerial view



Fig. 1.11 Internal view of Aabenraa Hospital

ensure that the patients would have optimum thermal comfort during summer, when there is a risk of overheating, and in winter, when the cold outdoor air needs to be preheated to provide draft-free fresh air to the building (Figs. 1.10 and 1.11).

The ventilation system in the glazed courtyards was designed as a displacement ventilation system. Fresh air is provided through external fresh air inlets and passed through the basement, assuring a constant air temperature around 16 °C. Fresh air then passes through a filter and a convector element. Exhaust is ensured via roof-integrated wind cowls, utilizing the wind load to create sufficient air under pressure in the glass-covered courtyard to ensure the required air change of approximately 1.0–1.5 h⁻¹. The roof-integrated wind cowls are equipped with assisting fans to ensure a satisfactory ventilation level when the



Fig. 1.12 Skylight

wind load is not sufficient. The hybrid ventilation system is controlled with a new building management system (BMS), including the necessary control points. For each building section, the BMS controls a number of throttle motors, valve motors, sensors for fresh air temperature, and combined room air temperature and CO₂ sensors. All sensors are placed 1.6 m above floor level. District heating is used for space heating and hot water. The generation of hot water is supported by a 150 m² thermal solar collector, which provides an annual yield of about 540 kWh/(m²a), meeting approximately 60 % of the annual need for DHW (Figs. 1.12, 1.13, and 1.14).

6 City Hospital, Torun, Poland

The Polish city of Torun is a member of the World Health Organization (WHO)'s "Healthy Cities" project, so when the city hospital needed renovation and expansion, authorities included environmental sustainability criteria in the plans. Both new and renovated buildings in this 249-bed hospital have upgraded insulation, room temperature controls, modern heaters, and advanced valves, among other measures. Energy savings are approximately 30 % in the renovated buildings, and new buildings use 54 % less energy than standard newly built hospitals.

In the Torun hospital, district heating from a CHP is used for space heating and hot water. A cooling system is not necessary because the hospital is located in a cool climatic zone.



Fig. 1.13 Ventilation chimneys



Fig. 1.14 Courtyard of Aabenraa Hospital

A natural ventilation system is used. Fresh air enters rooms through gaps at tops of window frames. The warm air is conducted outward via a central duct system (Figs. 1.15 and 1.16, Table 1.1).

Fig. 1.15 Torun Hospital
100 mm exterior insulation



Fig. 1.16 Torun Hospital 100 mm exterior insulation

7 Results

The following table summarizes the results achieved for indoor comfort, energy consumption reduction due to the installation of an advanced plant, CO₂ reduction achieved through the energy solutions adopted, and the behavior achieved by implementing sustainable strategies.

Table 1.1 Primary energy before and after renovation/new construction[5]

Case study	Energy solutions adopted	Energy consumption	CO ₂ emission reduction
Italy: Meyer Children's Hospital, Florence, Italy	• Green roof	The hospital consumes 40 % less energy for heating and cooling and electricity than a standard newly built Italian hospital Total annual electricity demand is 12.3 kWh/m ²	Annual 899 tons CO ₂ , 0.77 tons SO _x , 7.91 tons NO _x ; this is 36 % from the average Italian
	• PV façade		
	• Solar ducts		
	• Thermal insulation		
	• Greenhouses		
	• Shading devices		
	• Green building design		
	• Lighting strategies		
	• Natural ventilation		
Germany: Fachkrankenhaus Nordfriesland,	• Double-skin façade	Energy savings are approximately 46 % in the renovated buildings, and new buildings use 30 % less energy than standard newly built hospitals	Annual 262 tons CO ₂ , 0.23 tons SO _x , 0.002 tons NO _x ; this is 46 % from average German hospital
	• River- and rain-water-capture techniques		
	• Solar mass wall with transparent insulation		
Denmark: Aabenraa Hospital	• Daylighting	Energy savings are approximately 36 % in renovated buildings, and new buildings use 7 % less energy than standard newly built hospitals	Annual 974 tons CO ₂ , 0.18 tons SO _x , 1.59 tons NO _x ; this is 60 % from average Danish hospital
	• Hybrid ventilation – natural fan-assisted ventilation		
	• Glazed courtyard		
	• Control systems		
	• Preheating		
Netherlands: Deventer Hospital	• Green roof	Energy savings in new hospital are 47 % on heating and 13 % on electricity compared to a standard hospital. This reduction of energy equals a reduction of 1.943 tons of CO ₂ per year, as well as a significant reduction in related emissions, e.g., 8.71 tons of SO _x and 3.35 tons of NO _x	Annual 1.943 tons CO ₂ , 8.71 tons SO _x , 3.35 tons NO _x ; this is 69 % from average Dutch hospital
	• Heat recover		
	• Good insulation		
	• Natural ventilation		
	• Alternative renewable energy sources		
	• Heat-cool storage and heat pumps and application of heat recovery in ventilation exhaust		
Poland: City Hospital Torun	• Upgraded insulation room temperature controls	Energy savings are approximately 30 % in renovated buildings, and new buildings use 54 % less energy than standard newly built hospitals	Annual 3.537 tons of CO ₂ , 116 tons of SO _x , 9 tons of NO _x ; this is 50 % from average Polish hospital
	• Modern heaters		
	• Advanced valves		

8 Conclusions

It was demonstrated through pilot projects that energy-efficient and sustainable hospital buildings can fully meet all architectural, functional, comfort, control, and safety features through the application of innovative and intelligent design and integrated design.

A very high insulation level, with a U-value for the walls between 0.2 and 0.3 W/m² K, for the roof between 0.12 and 0.8 W/m² K, and for the windows between 1.3 and 1.8 W/m² K (except Meyer Children's Hospital, which had a U-value of 3.2 W/m² K), ensured low energy demand.

As a result of the planning for the hospital projects, it can be asserted that they comply with the requirements of the project, the reduction of primary energy consumption by approximately 30 % on average.

Between 46 and 170 kWh/(m²a) primary energy can be saved. The primary energy savings for heating is between 26 and 170 kWh/(m²a). The average reduction in air pollution is approximately 26 % for CO₂ and 23 % for SO₂ and NO_x.

Acknowledgements Aabenraa Hospital was part of the EU-HOSPITALS. The project's technical coordinator, Esbensen Consulting Engineers, applied Integrated Energy Design (IED).

In the Meyer Children's Hospital project, under a TESIS/ABITA experimental research program, the European Community financed the incremental cost of the innovative technological and environmental solutions that were implemented in the project, monitoring the effectiveness of the results retrospectively. In particular, the experiments involved a bioclimatic greenhouse, a PV system integrated into the translucent wall of the greenhouse, solar tube systems to capture and transfer sunlight to functional environments so as to reduce electricity consumption, innovative solutions of a green roof, and the environmental insertion of the complex into the landscape.

References

1. Sala M (2005) Design Report Meyer Children's Hospital—report highlighting initial ideas and concepts + design drawing, technical drawings and picture of the completed solutions. Hospital Brochure
2. Sala M (2006) Monitoring plans including occupants survey—Meyer Children's Hospital. Hospital Brochure
3. Boonstra CH (2013) Design Report Deventer Hospital—plans, details, features with specifications energy performance, simulation results and results regarding thermal and visual comfort conditions, Hospital Brochure 2005 [1] Del Nord R (2013) The teaching and research hospital: an inpatient design experience in Hospital planning and building. TESIS Unifi Edition, Firenze
4. <http://www.ics.ele.tue.nl/~akash/maartje/getExampleDetail.php?ID=5>
5. Data taken from: Christel Russ, Fraunhofer Institute for Solar Energy Systems Freiburg, Final Report WP 3 Monitoring, Hospitals—Exemplary Energy-Conscious European Hospitals and Health Care Buildings. Project Number: NNE5-2001-00295

Chapter 2

Climate Adapted in NZEB Retrofitting for Residential Buildings

Marco Sala and Lucia Ceccherini Nelli

Abstract The climate-adapted residential nearly zero-energy building (NZEB) retrofitting project aims to update and upgrade the knowledge and competence of building designers (architects, civil engineers) as well as the specific skills of experienced building workers (site managers, craftsmen, and construction supervisors) who already have a decent background in sustainable energy solutions for the building sector gained by attending national Build Up Skills initiatives or related training. The overall objective is to increase the energy performance of European building stock as envisioned in EU Energy Efficiency Directive 2012/27/EU by supporting specific professional development through a broad roll-out of an integrated training model targeting both designers in the building sector and higher-level building workers, especially of SMEs. The training model will address, among the others, the management of the construction process and the active promotion of market uptake of cost-efficient, climate adapted Smart Retrofitting Solutions in order to reach NZEB standards in existing residential buildings.

Keywords Energy • Environment • Energy savings • Smart retrofitting • Sustainable energy solutions • Training model

1 Introduction

For a successful refurbishment towards nearly zero-energy building (NZEB), there is an urgent need for an efficient building retrofitting process. Innovative approaches should ensure practical on-site implementation of competitive, state-of-the-art retrofitting technologies using intelligent and smart “packages” for representative examples of actual building types and climate conditions. Thus, a holistic vision of the retrofitting process towards NZEB standards demonstrates the need to improve the skills and competencies of all actors involved in the retrofitting process; NZEB standards in existing buildings can only be attained if both

M. Sala (✉) • L.C. Nelli

DIDA Department—ABITA Interuniversity Centre, University of Florence,
Via San Niccolò 93, Florence 50125, Italy
e-mail: marco.sala@unifi.it; lucia.ceccherininelli@unifi.it

designers and the workforce are efficiently upskilled and brought up to date on new technical and operative approaches.

2 Research Objectives

The main objective of climate-adapted residential NZEB retrofitting is to implement a large-scale, multilevel and integrated training model for the NZEB renovation of existing residential buildings based on climate-adapted energy solutions, targeting the main actors of the building sector: designers *and* higher-level on-site building workers. The project aims to fill the knowledge gap between the design phase and the on-site operational level through the improvement of NZEB retrofitting methodologies in planning and operative management practices to enable the creation of a “common language” between designers and higher-level workers at construction companies. The overall aim of the integrated training activities is to train a large number of building designers and building workers in several partner countries, targeting a high level of participation of women. Taking into account specific work constraints of the trainees, such as working hours, balancing career and family commitments (especially for women), a flexible user-friendly training solution will allow for dedicated e-learning sections through the *Adaptive ICT e-Teaching Portal*.

3 Methodology

The goals of the project must be combined with the economic competitiveness of smart, clean and non-invasive retrofitting technologies, through excellence in operational on-site management practices and a strong value added in terms of specific, climate-appropriate solutions, partially based on dry-building technologies, guaranteeing a low carbon footprint and high energy efficiency combined with good all-season indoor comfort. The building actors should thus be trained not only on technical and organizational issues but also on the financial mechanisms that can trigger market uptake of NZEB retrofitting.

Based on this concept, the overall approach of the project will be as follows:

- Integrated training model aimed at NZEB renovation of existing residential buildings, capable of creating a “common language” between designers and workers at construction companies
- Implementation of three rolling cycles of integrated training courses, including planning and development and a periodic review of the training model, targeting both designers and building professionals

- The development of an integrated training model with specific teaching modules for continuous professional training for designers and on-site building workers will include the following items:
 - Theory lessons (some delivered by dedicated e-learning tools)
 - Common practical applications
 - Common project workshop
 - Market orientation events aimed at involving all stakeholders of the building process “triggering empowerment of the supply/value chain
- Flexible and adaptive training will facilitate the involvement of professionals/women: family-friendly scheduling and dedicated e-learning modules through the ICT-based adaptive teaching platform
- The introduction of smart retrofitting solutions in the training model, such as innovative dry technologies aimed at fast and cost-effective retrofitting methodologies for existing residential buildings, will promote competitive, new work practices that will also be suitable for the integration of women into the building sector

3.1 Best Practice NZEB Retrofitting Construction Management: Hands-on Manual for Designers and Construction Workers

To reduce the on-site mismatch and aim at a more synergic workflow between the planning activities and the on-site works, the elaboration of a hands-on manual highlights the main technical basis for the correct execution of the works, explaining different technical solutions using a common language for the successful implementation of retrofitting technology from planning to on-site management.

The *Best Practice Hands-On Manual* outlines general planning strategies for climate-adapted solutions. The manual is geared toward higher-level construction workers and designers in the building sector, including local administrators who are actively involved in the promotion and implementation of the Energy Performance of Buildings Directive (EPBD) goals.

The *Best Practice Hands-On Manual* will contain at least the following three sections.

1. Retrofitting methodology, where the main technical issues are explained by building information modeling (BIMS) for designers with intuitive tools/outputs that will also be understandable for on-site workers, such as a graphical user interface for computer-based virtual 3D modelling;
2. Catalogue of smart NZEB retrofitting solution, including a step-by-step construction guide for smart retrofitting solutions dedicated to the construction workforce;

3. Smart retrofitting packages with construction time scheduling, estimation of degree of invasiveness, average costs and pay-back period of investment;
4. Adaptive teaching portal with dedicated e-Learning section;
5. Management of technical platform: case studies, *Best Practice Hands-On Manual*, catalogue of smart retrofitting solutions;

3.2 Definition of a Climate-Oriented Approach to NZEB Retrofitting of Residential Buildings

The project focuses on a critical evaluation of the three main climatic contexts for residential NZEB retrofitting, including the more appropriate and innovative and specific technical solutions for the integration of building technologies and systems in existing buildings; the partnership will identify climate-specific approaches regarding a highly energy-efficient retrofitting methodology, including knowledge transfer from already implemented research, assessments and monitored case studies, in order to establish a catalogue of competitive, cost-efficient technical solutions and financial models aimed at a concrete and instant applicability of NZEB retrofitting in residential buildings.

The general indicators for climate-related retrofitting potential in existing residential buildings will be divided into three significant climate areas: north-west (France/UK/Belgium), central-east (Bulgaria/Hungary/Croatia), and south Mediterranean (Italy/Spain/Greece). This evaluation grid defines the profile of climate-specific energy demands for heating, cooling and electricity of the existing European residential sector, based on the aforementioned three climatic areas, including the year of construction (“old” before 1961, “modern” 1961–1991 and “recent” after 1991) and the two building types (single houses/multiple-apartment blocks), which together represent 75 % of the gross building surface in the EU. The research project highlights the climate-related criticalities, the actual mental and economic barriers and behavioural resistances of end users. The project will investigate the actual technical mismatch between designers and builders and elaborate a common approach to the implementation of successful NZEB retrofitting within the three different climate areas (Figs. 2.1 and 2.2).

3.3 Climate-Adapted Smart Retrofitting Solutions

Considering innovative highly energy-efficient building models, first developed by countries from northern Europe, the Passivhaus Model has earned international recognition and approval, representing today a model with a large number of completed and monitored examples of new buildings and retrofitted existing buildings. Clearly, the Passivhaus Model is not automatically and completely




		CLIMATE ZONE					
YEAR OF CONSTRUCTION	NORTH-WEST		CENTRAL-EAST		SOUTH-MEDITERRANEAN		
	SINGLE	MULTIPLE	SINGLE	MULTIPLE	SINGLE	MULTIPLE	
							
HISTORICAL CONTEXT DIFFICULTIES IN APPLYING EXTERNAL INSULATION							
BEFORE 1945- MAIN CLIMATE RELATED ISSUES	<ul style="list-style-type: none"> - INTERNAL/EXTERNAL INSULATION, -HIGH PERFORMANCE WINDOWS -INSTALLATION OF HVAC, HEAT RECOVERY, -PV AND SOLAR PANEL FOR HOT WATER ON ROOF -MAIN CLIMATE RELATED ISSUES -PASSIVE SOLAR WINTERGARTEN -BOWINDOWS RETROFIT -GREENHOUSE -PASSIVE SOLAR HEATING 		<ul style="list-style-type: none"> - INTERNAL/EXTERNAL INSULATION, -HIGH PERFORMANCE WINDOWS -INSTALLATION OF HVAC, HEAT RECOVERY, -PASSIVE SOLAR WINTERGARTEN -BOWINDOWS RETROFIT -LOW THERMAL MASS 		<ul style="list-style-type: none"> - INTERNAL INSULATION - INTERNAL / EXTERNAL SHADING DEVICES - VENTILATED ROOFS - DOUBLE GLAZING - PASSIVE COOLING 		
			<ul style="list-style-type: none"> - CENTRAL HVAC, HEAT RECOVERY, - PV AND SOLAR PANEL FOR HOT WATER ON ROOF 		<ul style="list-style-type: none"> - CENTRAL HEATING - PV AND SOLAR PANEL FOR HOT WATER ON ROOF 		<ul style="list-style-type: none"> - CENTRAL HEATING - PV AND SOLAR PANEL FOR HOT WATER ON ROOF
1945-1980	<ul style="list-style-type: none"> - INTERNAL/EXTERNAL INSULATION - INNOVATIVE SOLUTIONS WITH PCM -HIGH PERFORMANCE WINDOWS -INSTALLATION OF HVAC, HEAT RECOVERY, -PV AND SOLAR PANEL FOR HOT WATER ON ROOF -MAIN CLIMATE RELATED ISSUES -PASSIVE SOLAR WINTERGARTEN -BOWINDOWS RETROFIT - THERMAL BRIDGES -GREENHOUSE -PASSIVE SOLAR HEATING -PV AND SOLAR PANEL FOR HOT WATER ON ROOF 		<ul style="list-style-type: none"> - INTERNAL/EXTERNAL INSULATION - INNOVATIVE SOLUTIONS WITH PCM -HIGH PERFORMANCE WINDOWS -INSTALLATION OF HVAC, HEAT RECOVERY, -PV AND SOLAR PANEL FOR HOT WATER ON ROOF -MAIN CLIMATE RELATED ISSUES -PASSIVE SOLAR WINTERGARTEN -BOWINDOWS RETROFIT - THERMAL BRIDGES -GREENHOUSE -PV AND SOLAR PANEL FOR HOT WATER ON ROOF 		<ul style="list-style-type: none"> - INCREASE THERMAL MASS FOR SUMMER COMFORT - INCREASE AIR EXCHANGES - NIGHT VENTILATION -HIGH PERFORMANCE WINDOWS -PV AND SOLAR PANEL FOR HOT WATER ON ROOF 		
		-AUTOMATION		-AUTOMATION		-AUTOMATION	
AFTER 1980	<ul style="list-style-type: none"> - INTERNAL/EXTERNAL INSULATION - INNOVATIVE SOLUTIONS WITH PCM -HIGH PERFORMANCE WINDOWS -INSTALLATION OF HVAC, HEAT 		<ul style="list-style-type: none"> - INTERNAL/EXTERNAL INSULATION - INNOVATIVE SOLUTIONS WITH PCM -HIGH PERFORMANCE WINDOWS 		<ul style="list-style-type: none"> - INCREASE THERMAL MASS FOR SUMMER COMFORT - INCREASE AIR EXCHANGES - NIGHT VENTILATION -HIGH PERFORMANCE WINDOWS - LOW THERMAL MASS FOR 		

Fig. 2.1 Table of climate contextualization of existing EU residential building stock divided into three climate areas and three historical construction periods for both single houses and multiple-apartment blocks



Fig. 2.2 Environmental building, Netherlands

transferrable to other climate areas without specific adaptation. Taking into account the previously mentioned assessment efforts and considering the significant case studies, we will focus on the knowledge transfer of residential Passivhaus experiences to residential NZEB retrofitting in different climatic areas. Climate-adapted retrofitting solutions are based on smart retrofitting solutions; the articulation of knowledge transfer is based on three main factors:

- Upgrading of building envelope performance;
- Integrated HVAC technology fostering a high percentage of renewable energy use (building integrated energy production through PV and solar hot water provision and advanced building envelope performances are becoming necessary in order to match NZEB standards;)
- Integration of passive technology (e.g., passive cooling, cool roofs and natural lighting systems)

A. Retrofitting Building Envelopes

- Highly energy-efficient building envelopes, dry technological packages for thermal insulation with PCM phase-change materials;
- Combining the outer shells of energy-efficient buildings with state-of-the art, building-integrated, energy-generating technology, architectural photovoltaic integration and solar panels for hot water;
- Highly energy-efficient windows and doors with high wind and airtightness guaranteed by high-performance fixing and taping systems, representing crucial problematical aspects in NZEB building;
- Dry-building and partial prefab technologies for indoor insulation, including an emphasis on taping and airtightness;
- Ventilated *façade* systems especially for hot climates;
- Green roofs and *façades*.



Fig. 2.3 Funen Blok, Amsterdam, NL Architecten

B. Innovative, integrated HVAC systems for NZEB retrofitting

- Integrated renewable energy applications for buildings: solar energy and geothermal heat pumps for synergic integration of technology and building design, on the other;
- Geothermic heat pumps for innovative energy efficiency;
- HVAC calibrated specifically to the Mediterranean;
- Climate conditions (visiting building sites where this technology is applied, distributor of renewable energy technology, where possible) (Figs. 2.3, 2.4, and 2.5).

C. Integration of passive technologies

- The use of passive technologies and bioclimatic principles, integrated HVAC systems and heat recovery to guarantee, in addition to low energy demand, also good comfort in winter and summer, following specific end user needs in each climate area.
- Innovative passive cooling technology, combined with mechanical ventilation systems and air-to-air heat exchangers in retrofit (existing walls) and new building contexts (visit of building site where this technology is applied, where possible, thermodynamic simulation of passive cooling technology with dedicated software, demonstration by expert);



Fig. 2.4 Bardini Museum refurbishment (EULEB)

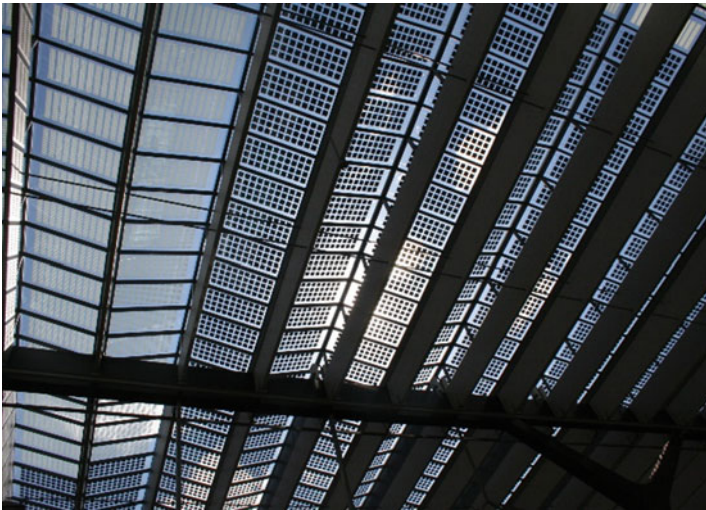


Fig. 2.5 Rotterdam central railway station

- Innovative highly energy-efficient heating systems suitable for retrofitting (radiant floor or ceiling based on low-temperature systems capable of ensuring heating *and* cooling, guaranteeing high indoor comfort levels);
- Use of innovative internal elements using PCM, especially for cooling in hot climates;
- Integration of sun shading systems to avoid overheating of opaque and transparent building envelopes;
- Management and control with automation systems. Systems for plant energy control cover all subsystems related to energy regulation, responding to the



Fig. 2.6 PV integration in Amersfoort, Newland, Netherlands. Photovoltaic roof integration, Foster & Partners



Fig. 2.7 Solar decathlon winner, 2015, Rubner [RhOME](#)

effective ambient temperature required by the occupants in single zones. In retrofitting actions, the adoption of a building automation and control system (BACS) or a home and building electronic system (HBES) is strongly recommended. These systems can be installed in housing with four different performance class levels, in relation to the energy efficiency their adoption ensures adoption (Figs. 2.6 and 2.7):

- Level 0 (no energy efficiency): this level is related to the traditional heating-and-cooling plant, without automation;
- Level I (standard): this level corresponds to standard automatic systems (i.e., one thermostatic control system that regulates the on-off of the central heat, as a function of the temperature inside the zone);

- Level II (advanced): this is related to controller plant systems with a bus automatic control (BACS/HBES) and with a centralized management of single plant systems (TBM);
- Level III (high energy performance): an advanced precision level of automatic control that can guarantee high energy performance for plant systems.

3.4 Environmental Impact

- A life-cycle assessment is made for the use of sustainable materials: renewable materials and low-carbon-footprint materials and technologies (e.g., structural material, plaster, moisture brakes, ventilated roof).

Based on these main themes, the project elaborates a catalogue of appropriate climatic technical solutions which will investigate highly energy-efficient retrofitting from so-called deep renovations (60–90 % less consumption), such as Passivhaus standards with respect to NZEB thresholds (over 90 % less consumption).

Renovating is an ideal time to make your house healthier for you, the community and the environment. When upgrading your mechanical systems to increase their efficiency, be sure to consider the following aspects (Figs. 2.8, 2.9, and 2.10):

- Occupant health – venting strategy for combustion appliances, adequate ventilation for occupants, addition of air filtration;



Fig. 2.8 Virtual environments and ICT Centre, Marco Sala Associati

Fig. 2.9 Virtual Environments and ICT Centre, Lucca



- Energy efficiency – energy-efficient appliances, high-efficiency motors for fans and furnaces;
- Resource efficiency – upgraded insulation and draft proofing to reduce heating needs and allow installation of a smaller heating system;
- Environmental responsibility – energy-efficient appliances to reduce a home’s environmental impact;
- Affordability – energy-efficient fixtures to reduce ongoing operating costs.

4 Results

The climate-adapted residential NZEB retrofitting project expects to support innovation and sustainable energy use in building renovation, reducing technical mismatch and increasing the management skills of building designers (engineers/architects) and on-site construction workers. The project will use an integrated training model for NZEB renovation of existing residential buildings, aiming to develop a common language as a starting point for a more efficient on-site implementation of NZEB thresholds in retrofitting. The implementation of climate-oriented retrofitting using advanced bioclimatic technology and applying renewable energy management and the implementation of so-called smart and green supply chains, based on innovative materials (and taking into account LCA evaluation of the building process as a whole), will effectively open up new market opportunities. Moreover, the implementation of innovative technologies should launch a new practice of non-invasive retrofitting (where inhabitants would be able to stay while work is going on) and less expensive retrofitting solutions oriented toward specific climate contexts. The involvement of financial institutions could increase investments in innovative sustainable energy technologies.

5 Conclusions

The climate-adapted smart retrofitting solutions promoted within the project discussed in this chapter aim at a high level of economic competitiveness through the use of innovative and cost-effective dry technology. Moreover, the number of trained workers will make it possible to calculate the potential annual energy savings in the construction sector as well as the annual production of renewable energy, representing impacts derived from training activities (starting in 2015).

Potential NZEB energy consumption is calculated in each residential building category: energy savings over the course of the project's lifetime of 50 GWh/year and renewable energy production over the project's lifetime of 4 GWh/year.

In particular, the developed tool makes it possible to calculate the realistic impacts from two types of trainees for the renovation of residential buildings:

- Designers
- On-site workers of construction companies subdivided into three different types of professional (builders, thermo-hydraulic technicians, and electrical technicians)

6 Future Implementation

Climate-adapted residential NZEB retrofitting projects will ensure a positive long-term impact on the European construction sector focusing on the added value of *integrated training* in order to fill the gap between planning and on-site construction management, promoting competitive, climate-adapted NZEB retrofitting technology.

Of particular importance will be the development of a strategy for using and rolling out projects and supporting innovation in the construction sector with dedicated training programs beyond project lifetimes; also important will be the stimulation of other stakeholders to trigger top-level training courses based on the climate-adapted residential NZEB retrofitting training model (using the *Best Practices Hands-On Manual* and the guidelines developed by the project).

Acknowledgements The authors would like to acknowledge Prof. Marco Sala, Centro Abita-Unifi research group leader, and Architect Rainer Toshikazu Winter, LUCENSE research group, Lucca, Italy, who organised the Didactical Training Centre in Lucca, Abitare Mediterraneo, www.abitaremediterraneo.eu, a 700-square-meter continuous exposition of about 60 building mock-ups representing state-of-the-art building technology for the Mediterranean climate. The Didactical Training Centre has dedicated part of it to analysis tools, such as a thermo camera, that will help to control the performance of existing building envelopes.

References

1. Kurnitski J (2013) Cost optimal and nearly zero-energy buildings (NZEB): definitions, calculation principles and case studies (green energy and technology). Springer, London
2. Piano R, Piano C, AA VV (2012) Almanacco dell'Architetto, Costruire L'architettura, Bologna, Proctor Edizioni Spa
3. Ceccherini Nelli L (2012) European project for training on renewable energy solutions and energy efficiency in retrofitting (REE_TROFIT). In: 2nd World Sustainability Forum, Web, 1–30 Nov 2012, MDPI, ISBN:390698028 Editor ONLINE Access

Chapter 3

Sustainable Strategies for Protecting and Managing Cultural Heritages: The Case Study of Gonfienti in the Tuscany Region of Italy

Marco Sala, Giuseppina Alcamo, and Lucia Ceccherini Nelli

Abstract Global warming has caused an unprecedented rise in sea levels as well as increased storm intensity. Both phenomena are responsible for an increase in flooding and erosion of many archaeological sites located on the coast, which constitute a weak interface between the hydrosphere, atmosphere, anthroposphere, and lithosphere. The present research project aims to develop a sustainable model for safeguarding archaeological sites from the adverse effects of climate change and environmental degradation. In addition, by implementing site-specific planning and design based on ecological, bioclimatic, and energy-efficient strategies and techniques, sustainable preservation and enhancement of cultural heritage sites can be achieved to increase sitings and accessibility to sites.

The main objectives of the project are as follows:

- Investigate the impact and damage inflicted on archaeological sites by climate change and the risks and hazards of further deterioration;
- Analyze local climatic conditions and evaluate and use free energy systems available at archaeological sites while at the same time respecting the cultural character of locations.
- Improve visitors' experience by creating a pleasant and comfortable sightseeing environment.
- Rehabilitate select archaeological sites in a holistic approach by protecting, defining, and upgrading sites through advanced planning and design solutions.

The project will establish a comprehensive state of the art of archaeological sites and spaces in the Mediterranean region. It will select three pilot site studies, one in each participating country—Italy, Cyprus, and France—for the ultimate aim of establishing sustainable preservation and cultural enhancement of the archaeological sites to the benefit of society.

M. Sala (✉) • G. Alcamo • L.C. Nelli

Department of Architecture DIDA, Centro ABITA, University of Florence,
San Niccolò 93, Florence 50125, Italy

e-mail: marco.sala@unifi.it; giuseppina.alcamo@unifi.it; lucia.ceccherininelli@unifi.it

Keywords Archaeological spaces • Sustainability • Protection • Rehabilitation • Accessibility • Shading devices • Renewable energies

1 Introduction

The preservation of cultural heritage is strongly linked to the study, safeguarding, and evaluation of the barriers, risks, and vulnerabilities surrounding the sustainability of archaeological sites and spaces. The rich cultural heritage of countries is under threat also due to the effects of climate change, adverse climatic conditions, and especially the impact of extreme weather events on historic and archaeological sites, as well as on tourism. To preserve archaeological heritage sites, an efficient, long-term management plan is needed to protect, enhance, and revitalize culturally significant places for future generations. Moreover, a sustainable approach to tourism at archaeological sites will encourage a structured and managed tourism with economic benefits for all parties responsible for site management. In addition, the planning of sustainable transport to archaeological sites, the integration of existing renewable components with temporary information points, and the use of renewable energy for displaying information about a site on a screen should be adequately investigated.

The project will endeavor to uncover the underlying principles that shaped the archaeological sites. Exploiting local resources, responding to local climate, vegetation, and topography and guided by local cultural traditions, the ancients used sophisticated tools over the ages to establish and build a precious harmony between structures and setting. These are the very tools that will be used in this project to protect both ecosystems that took millions of years to evolve to their present states and the richly ordered historic human constructions that took thousands of years of sensitive accretion. In this way, this project will aim to contribute to the birth of a viable European culture, valued by tourists, in which networks of communication and trade will no longer just be homogenizing and distracting agents. It will have an abundant capacity to allow for specific local and regional features inherent in historic sites to survive and be enjoyed, enhancing the specifics of culture, climate, and topography.

The project will emphasize the significance of archaeological sites to help communities remember as well the role we have in helping preserve forgotten pasts and promote sustainable heritage tourism. The project will aim to redefine selected pilot archaeological sites in three Mediterranean countries: Italy, Cyprus, and France. It will also aim to identify the most appropriate planning and designs based on ecological, bioclimatic, and energy-efficient design strategies and techniques to achieve sustainable preservation and enhancement of the cultural heritage of the areas to increase sightings and accessibility. The tourism industry should benefit from the proposed transition. It will be based on a holistic, regional approach and will aim to combine the instrumental values of civilization with human concerns of heritage and local culture.

Three main goals have been defined:

- Create a potentially threatened-site corpus aimed at the sites' social integration, environmental adaptation, and economic development;
- Create a protocol study for preventive intervention if no material or other means of protection is applicable.

Create documents to:

- Orient national archaeological scheduling to study coastal or other sites threatened primarily by climate change, but other dangers as well;
- Encourage organizations in charge of general and coastal administration to implement concerted programs for site protection, using means adapted to local contexts;
- Increase awareness among decision makers in Mediterranean countries on these issues.

2 Objectives

A significant aspect of the project is to establish national advisory committees, a collaborative network among relevant scientific centers, professional associations, and public and private bodies, with the aim of effectively disseminating information to stimulate engagement by local communities.

The research project objectives are based on the following considerations:

- The investigation of the impact of climate change on archaeological sites and on related tourism activities, with proposed guidelines for the mitigation of its effects;
- The most appropriate utilization of climatically damaging factors that provoke the deterioration of a site, using, for example, direct solar radiation to negate their effects [e.g., renewable energy production systems on tents, such as photovoltaic (PV) panels; solar screening with green water collection systems, wind power, geothermic]; in particular, clean rainwater collection is needed by archaeologists to clean their findings;
- Create a pleasant sightseeing environment for visitors by improving their comfort level during their visit to sites and installing interactive local info-point at archaeological sites connected to a renewable energy structure (e.g., PV umbrella, creative use of water, sustainable mobility at sites, pleasant seating along walkways);
- Analyze the potential of the proposed tools and solutions in the context of archaeological site management practices.

3 Methodology

The protection of archaeological sites requires an aggressive long-term management program that includes thorough documentation of site characteristics and conditions, stabilization, security, maintenance, monitoring, compatibility, and research employing analysis techniques to define the context of the problems faced by participant countries at their archaeological heritage site (e.g., risks, hazards, damage, and degradation factors).

For this reason, information obtained using both satellite and ground remote sensing techniques will be fed into a geographical information system (GIS) to investigate the impact of climate change and destructive agents at the sites. The use of archive satellite data sets along with in situ observations using sun photometers and LiDar technology will assist in better understanding the impact of these agents on cultural heritage monuments. The integration of the previously mentioned state-of-the-art technologies will lead to the production of climate change vulnerability maps for each participating country. In addition, Global Positioning Systems and archived stereo-pair aerial images will be used to reconstruct historic landscapes from the last century.

Three archeological sites were chosen, one from each country, as pilot cases; the local resources, climatic conditions, and beneficial aspects of the archaeological sites will be used to evaluate and enhance the special character of each site. The strategies to be adopted for the Italian archeological site, Gonfienti, near Prato and Florence, will be described in detail.

Advanced design techniques, including the implementation of a renewable energy production system, in combination with the application of local ecological materials that will be linked to the surrounding landscape and specific constructions made to protect the location and visitors, are proposed to protect archaeological landscapes from the impacts of climate change, in particular, to protect these places from extreme weather events such as, for example, extreme rainfall, extreme temperatures, extreme wind speeds, and extreme natural phenomena such as earthquakes, and volcanic eruptions. These method form the core of the strategy to be used to formulate the plans and designs geared toward preserving the sites and adapting to climate change. Comparative evaluation studies are carried out using relevant strategies applied at archaeological sites in other locations in the Mediterranean region (Fig. 3.1).

4 Planning and Design of Spaces for the Ecological Preservation and Enhancement of Each Pilot Archaeological Site

Schematic designs are formulated for each of the selected historic locations, using software for simulations, in order to protect the archeological sites from damage and deterioration while at the same time acknowledging and respecting the specific



Fig. 3.1 Gonfienti archaeological site near Prato, Italy

symbolisms of the sites that make visiting them enjoyable. An in-depth analysis of possible alternatives to include the production of renewable energy on site will be considered so that the archaeological sites can become self-sufficient or even contribute to the energy needs of the region without altering the character of the sites.

The designs will also be oriented toward the comfort of visitors and tourists. Improvements to the way people experience the sites (e.g., accessibility, comfort during the visit) are indispensable in assessing the spaces and increasing visitor traffic.

Urban, territorial, and landscape designs, including small structures, will be developed to exploit and enhance the local topography and climate, just as the archaeological sites and constructions did, and with a similar accentuation on the regional flavor. The designs will aim at achieving variety, continuity, and coherence by making connections with and enhancing the specifics of culture, climate,

and location in sensitive, disciplined, and willful acts and imaginative designs. Comparative evaluation studies will be carried out using relevant designs applied at other Mediterranean region archaeological sites.

5 Archaeological Site of Gonfienti (PO) in Tuscany, Italy

The Etruscan population to which Tuscany is closely tied is mysterious in many ways, starting with its name: the area between the Arno and the Tevere Rivers in the pre-Roman period belonged to the Etruscans, or Tuschi. In that period they were called Etruria or Tuscia. Subsequently from Tuscia the name became Tuscany. A disastrous famine drove the Tuscans to this sport from the Middle East in the first millennium BC. This population already had a strong commerce, were used to traveling by sea, had a strong army, and with no trace of a prince or a leader.

The structure of Tuscan society was based on clans, organized into *luchums*. There were no more than 12 in all of Italy. When the settlement was consolidated, the federated city-state formed a powerful economic, religious, and military alliance: the Etruscan League. The following important cities of modern Tuscany were part of it: Roselle, Vetulonia, Populonia, Arezzo, and Volterra, and later on Cortona and Fiesole. The oldest one is surrounded by walls built during times of danger. The cities were built on grid plans with *decumanus* doors.

The last discovery destined to mark a turning point in the history of the study of the Etruscans dates from 1996. A large Etruscan acropolis dating back to the sixth to fifth centuries BC came to light by chance in the eastern outskirts of Prato (in the area of Gonfienti). This area, at the edge of the plain of Prato, in the shadow of the Apennines, along the Sole highway that today connects northern Italy with southern, was settled by the Etruscans thousands of years ago. Following archaeological analysis, Gonfienti appeared to be one of the greatest acropolises ever discovered, connected to its sister city the ancient Misa (currently known as Marzabotto, in the region of Bologna). For the last 200 years it has been an important trade center of Etruria, and some experts even believe that it may have been the mythical city where King Porsenna was buried. The exquisitely beautiful bronze religious statue called *l'Offerente* (now at the British Museum in London), discovered in 1735 less than 1 km from the settlement, was not found there just by chance; the site is not yet open to the public (Fig. 3.2).

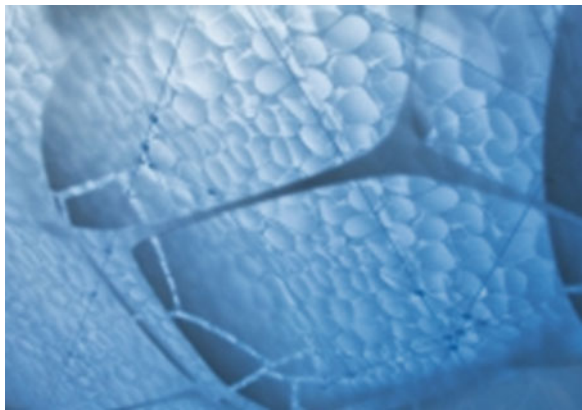
Ventilation strategies using membrane roofs should be adopted to protect the Gonfienti area, a very developed location, applying the following systems:

- PV roof, open air, with semitransparent panels;
- Translucent materials with EFTE membrane;
- PTFE glass;
- PVC/PES;
- Tensotherm insulated tension membranes;
- TO₂.



Fig. 3.2 View of Gonfienti area

Fig. 3.3 Example of ETFE membrane; the airtight cushion offers shelter while allowing light to pass through its transparent form (photo by Niklaus Spoerri)



To protect archaeological sites we chose different light roofs, one of which is a fabric roofing membrane. It has the advantage of being lightweight, strong, and durable and can be cut into different shapes that can be joined together in a cost-efficient way. Roofing membrane fabrics use tension structures, either by stretching the material or “prestressing” the membrane between structural supports or, alternatively, by supporting the material pneumatically in inflated structures. The use of fabric membranes in prestressed roofs seems to be a very useful technology for the most common application of inflatable fabric roofs (Figs. 3.3, 3.4, 3.5, and 3.6).

Another system considered for placement above archaeological sites is a semi-transparent roof made of a transparent part composed of ETFE cushions so as to optimize the light weight of the support structure. Each cushion is made with white

Fig. 3.4 Example of ETFE membrane, the airtight cushion offers shelter while allow light to pass through its transparent form (photo by Niklaus Spoerri)



Fig. 3.5 Example of ETFE membrane; the airtight cushion offers shelter while allowing light to pass through its transparent form (photo by Niklaus Spoerri)



Fig. 3.6 Example of ETFE membrane; the airtight cushion offers shelter while allowing light to pass through its transparent form (photo by Niklaus Spoerri)

and transparent ETFE panels that are staggered to create shadow effects and to reduce the solar factor (Figs. 3.7, 3.8, 3.9, 3.10, and 3.11).



Fig. 3.7 ETFE semitransparent roof

Fig. 3.8 Section of half an ETFE membrane

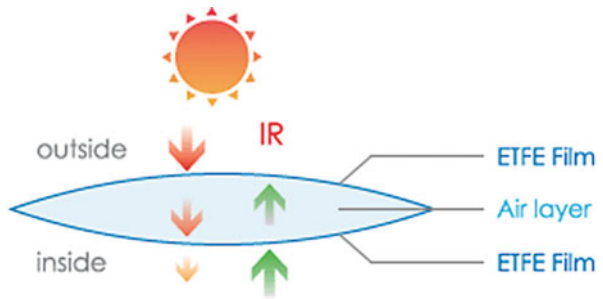


Fig. 3.9 This cover is realized in a stretchable water tight fabric, ensuring easy protection against sun and rain. The stretchable fabric bends and strains under tension. It is ultralight (only 3 kg) and easily washed. The corner fixation hooks are automatically loosened in case of strong gusts or excessive tension



Fig. 3.10 Fully transparent and open in the central part to maximize natural ventilation of the site

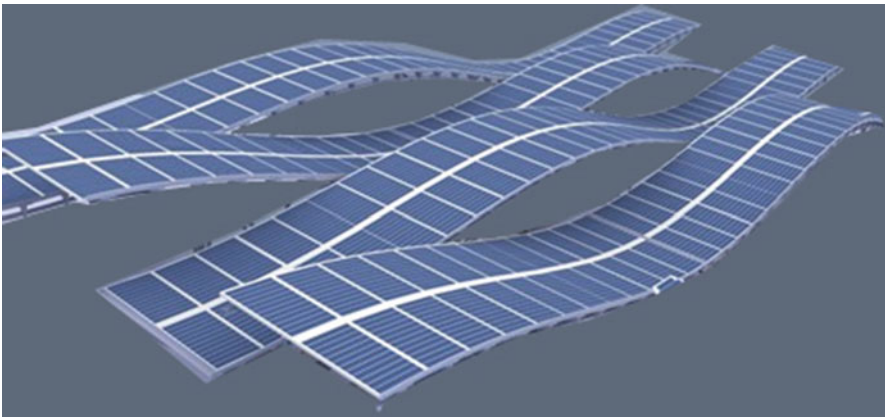


Fig. 3.11 Roof integrated BIPV allow the entry of natural light, provide both thermal and sound insulation, filter out harmful radiation, and produce clean free energy

The environmentally sensitive design includes tourism facilities built in the archaeological architecture in the following ways:

- *Rainwater catchment*: Rainwater is collected from roofs in the rainy season, passed through a natural filter, and stored in underground cisterns to be reused in green areas.
- *Solar water heating*: Rainwater is pumped up from cisterns through a solar-powered heating system into hot- and cold-water containers for toilets and showers (Fig. 3.12).



Fig. 3.12 Another solution for PV shelter roof



Fig. 3.13 Different solutions for translucent PV roof and PV shelter

- *Graywater recycling*: Water from showers is recycled through plant beds so that no polluted water seeps into the area. Beds are planted with species with high water and nutrient requirements, appropriate for the shower water rich in nitrates and phosphates.
- *Natural ventilation*: Roofs have natural ventilation, from the top and both sides.
- *Composting toilets*: Toilets economize on water. They also prevent sewage from seeping through the porous ground into the area. Human waste quickly decomposes into natural fertilizer when mixed with compost (aerobic composting) in a compost chamber.
- *Photovoltaic power*: Lights are powered by PV panels on the roof, which provide enough energy for average use (Figs. 3.13, 3.14, and 3.15).



Fig. 3.14 Different solutions for translucent PV roof and PV shelter



Fig. 3.15 Different solutions for translucent PV roof and PV shelter

6 Results

The project, through a Web site, is creating a national advisory committee to guarantee a permanent exchange of information, research results, development of technological solutions, experiences and dissemination of results, applied incentive schemes, and governance models of adapted transition.

Expand the collaboration to other European and universal bodies, such as International Union of Architects–Architecture and Renewable Energy Sources (UIA-ARES).

The principal goal is to share experiences in the field of archaeological heritage preservation in European countries.

The milestones focus on the following objectives:

- Provide a legal framework and national strategies for preserving archaeological heritages;



Fig. 3.16 One of the analyzed solutions for Gonfienti archaeological site with a PV roof

- Understand the meanings that cultural heritage holds for people and how they perceive, use, and interpret it;
- Develop an archaeological heritage management and sustainable development system;
- Investigate the impact of climate change and the possible mitigation measures concerning archaeological sites;
- Develop methodological tools and designs for so-called integrated landscapes;
- Promote cultural tourism and archaeological heritage preservation;
- increase accessibility and visitor traffic and frequency at archaeological sites.

The project is generating new, research-based knowledge to promote the sustainable use of cultural heritage in order to meet societal challenges and contribute to development at the local, national, and international levels (Fig. 3.16).

7 Conclusions

The project achieved significant results due to the nature of the project itself and to the expertise of the consortium; moreover, the results are due to the type of heritage archaeological sites chosen.

The ideas and knowledge, which will be transferred to the public and private sector, will include the main aims and most significant results of the project:

- The proposal aims to redefine the notion of what an archaeological site can mean to society.
- The imminent risk of destruction of important cultural heritage sites should be prevented. This can be achieved using a holistic design that permits the adoption of new techniques and technologies.

- Through this study new and innovative ways of dealing with the protection of an archaeological site will be listed in guidelines that can be used by all archaeological sites in Europe and abroad.
- The public and private sectors can benefit from the outputs of the presented research in a positive way, given the utilization of the sites as power-generating spots. The interest in investments aimed at the protection of sites would increase.
- An interactive relation among the local people, visitors, and staff will be promoted by the use of questionnaires eliciting responses about people's perceptions before and after rehabilitation.

The outline plans for dissemination aims to increase synergies among researchers and nonacademic stakeholders, including SMEs, heritage site owners, public administrators, research partners, and local communities. The tasks will include the development of informational material (e.g., logo, Web site, videos, photos), as well as inputs to European portals and databases in the quality and form specified. Dissemination events such as workshops, conferences, briefing days, and exhibitions will also take place over the lifetime of the project. Moreover, national advisory committees will be developed in order to guarantee a permanent exchange of information, results, technological solutions, and experiences.

Sustainable tourism as an approach to preserving archaeological sites reflects a new vision and the new idea of this project, and the impact of this vision will include increased funding to support the site itself.

Consequently, the results of the project will be invaluable, not just for researchers but for nonacademic stakeholders, including SMEs, heritage site owners, public administrators, and local communities.

Acknowledgements We acknowledge the contributions of research team leader ABITA Interuniversity Research Centre (DIDA Department of the University of Florence, Italy). ABITA is a large interuniversity research center focused on sustainable issues in architectural technology and environmental design.

Thanks also go to Cyprus University of Technology (CUT). The CUT has as its strategic goal the design and development of research activities both within the university and in cooperation with other research institutes in Cyprus and abroad.

The Cyprus Institute (CYI, www.cyi.ac.cy) is a nonprofit, technology-oriented, interdisciplinary research and educational institution that upholds world-class standards of excellence. Finally, we would like to thank the Laboratoire d'Archéologie Médiévale et Moderne en Méditerranée.

References

1. Giuffrè R, Mazzeo A (2005) Rethinking PV technology: an innovative system for archaeological sites. In: 20th European photovoltaic solar energy conference proceedings
2. Scognamiglio A, Cancro C, Formisano F, Graditi G, Privato C (2006) A landscape integrated PV component suitable for valuable sites. In: XXXIV IAHS World Congress on housing sustainable housing designemphasizing urban housing September 20-23, Naples, Italy

Chapter 4

Buildings' Energy Flexibility: A Bottom-Up, Multiagent, User-Based Approach to System Integration of Energy Infrastructures to Support the Smart Grid

Wim Zeiler, Timilehin Labeodan, Kennedy Aduda, and Gert Boxem

Abstract Using the flexibility within energy generation, distribution infrastructure, renewable energy sources, and the built environment is the ultimate sustainable strategy within the built environment. However, at the moment this flexibility on the building level has yet to be defined. The new IEA Annex 67 is just starting to define this specific flexibility. Our research is aimed at developing, implementing, and evaluating new process control strategies for improving the energy interaction within a building, its environment, and the energy infrastructure by effectively incorporating occupant needs for health (ventilation) and comfort heating/cooling. An integral approach based on general systems theory is used that divides the whole system into different layers from user up to centralized power generation. A bottom-up approach, starting from the user up to the smart grid, offers new possibilities for buildings' energy flexibility. To make use of the dynamic possibilities offered by the flexibility, new intelligent process control concepts are necessary. Multiagent systems, in combination with building energy management systems, can offer the required additional functionalities. The approach is tested in a case-study building.

Keywords Energy flexibility • User • Smart grid

1 Introduction

Energy infrastructures form the backbone of modern society since energy is needed for nearly all necessary services [1]. The built environment is currently a major consumer of fossil energy, at nearly 40% [2], but it also has huge potential to contribute to the supply and management of renewable energy. The built

W. Zeiler (✉) • T. Labeodan • K. Aduda • G. Boxem
Faculty of the Built Environment, University of Technology Eindhoven, Eindhoven,
The Netherlands
e-mail: w.zeiler@bwk.tue.nl

environment is the most complex distributed technical system with its energy infrastructures for electricity, gas, heating, and cooling at the utility level, as well as all the ducts, pipes, and cables within buildings. As concerns grow about the environmental cost and limited supply of fossil energy resources, so too does the importance to society of carefully managing the availability of energy resources and developing and implementing renewable energy sources such as wind turbines, geothermal heat pumps, and photovoltaic systems. Traditionally top-down organized energy supplies in electricity and gas networks have had to cope with decentralized renewable energy production. Energy consumption is quite predictable on the macro level, and large power plants preschedule their power generation based on such predictions.

Coping with complex and unpredictable factors related to decentralized renewable energy sources (DRESs) and the grid requires a more flexible approach to process control that is increasingly bottom-up rather than top-down. As a result, the influence of a building's design and its users' interactions becomes more important. Buildings, building service systems, and energy infrastructure must be designed to be more flexible. It is widely recognized that increasing flexibility is key for the reliable operation of future power systems with very high penetration levels of DRESs [3]. Using the flexibility within energy generation, distribution infrastructure, renewable energy sources, and the built environment is the ultimate sustainable strategy. However, at the moment this flexibility at the building level has yet to be defined. The new IEA Annex 67 is just starting to define this specific flexibility. Clearly the energy demand characteristics of buildings, available from building energy management systems (BEMSs), constitute very valuable information for grid optimization. Smart control of energy consumption and generation inside (nanogrid) and around buildings (microgrid) can make major contributions to addressing imminent energy problems within the total energy infrastructure, the smart grid. However, a working definition of the IEA Annex 67 Energy Flexible Buildings is its ability to manage energy demand and generation according to local climatic conditions, occupant needs, and energy grid requirements [2]. There is a need to take a more holistic approach to system flexibility, which looks at the potential interactions between new and traditional sources of flexibility and how these sources are used by different parties [4]. New integral approaches are needed to increase buildings' flexibility in relation to the smart grid.

2 Methodology

To optimize the energy infrastructure in the built environment, an integral approach based on general systems theory developed by von Bertalanffy [5] is proposed [6, 7]. To cope with the complexity of the energy infrastructure of the built environment, this system-engineering-like method uses functional decomposition and different levels of abstraction (Fig. 4.1) as follows:

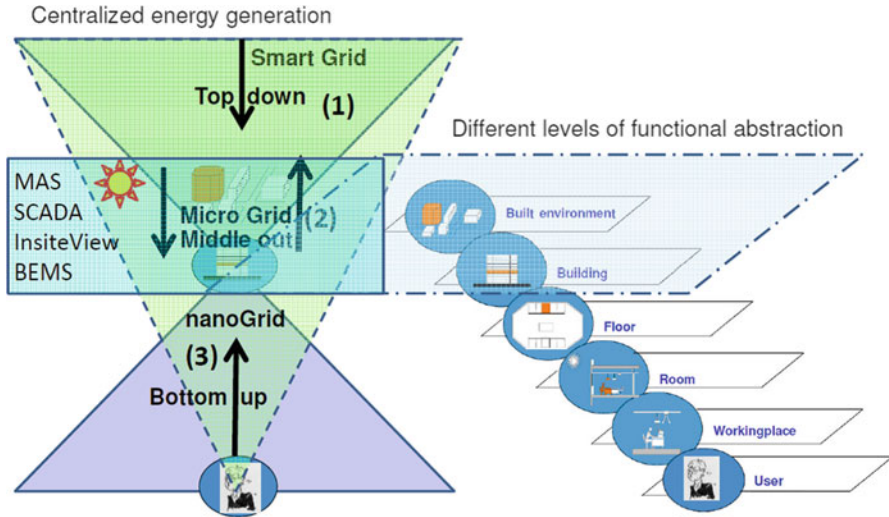


Fig. 4.1 Representation of building interaction with smart grid

- Built environment (possible energy supply from the smart grid, large renewable energy sources);
- Building level (possible energy supply from microgrid, nanogrid; Small renewable energy sources, storage, and other buildings);
- Floor level (distribution of occupancy and the necessary energy flows);
- Room level (energy needs depend on outside environmental conditions and internal heat load);
- Workplace level (workplace conditions and energy needs from appliances); and
- User level (different comfort needs of individuals).

Applying the principles of systems engineering to the optimization of the energy infrastructure of a building makes it possible to integrate in a flexible way the energy flows connected to heating, cooling, ventilation, lighting, and power demand within a building and between buildings and the built environment. This leads to a flexibility of energy exchange between different energy requirements and sustainable energy supply on the different levels of abstraction in the built environment. Traditionally, the energy approach to the built environment is top-down (centralized energy generation/distribution through the smart grid). We want to use instead a middle-out (control at the building level by the BEMSs) as well as a bottom-up approach (demand driven by human needs for energy/comfort) (Fig. 4.1).

An energy infrastructure's functionalities boil down to energy management, making use of the flexibilities of all grid-connected systems, which will lead to a more balanced and controlled network at all levels [8–11]. In general, two kinds of flexibility can be distinguished in energy infrastructures [1]:

- Architectural flexibility makes it possible to modify the configurations of a system based on future uncertainty;
- Operational flexibility allows energy modification of operating strategies without major changes.

The energy demand characteristics of buildings available in building automation systems represent crucial information for grid optimization [12] to activate participation of buildings in the grid. For an optimal smart grid from a system-of-systems point of view, the BEMS must be coupled with the management platform of the grid [9].

3 Multiagent System

The concept of intelligent agent technology is at an intriguing stage in its development as commercial-strength agent applications are increasingly being developed in domains as diverse as manufacturing and defense systems as well as in the operation and management of the smart grid [13, 14]. In artificial intelligence, agents are physical or virtual entities that intelligently interact in an environment by both perceiving and affecting it. Consequently, an agent can be described as a computational system with a high degree of autonomy performing actions based on the information received from the environment. Within a multiagent system (MAS), agents interact to achieve cooperative (e.g., distributed problem solving) or competitive (e.g., coalition formation, auction) group behavior. Agents achieve this by sharing a minimum amount of information between modules and asynchronous operation implemented via message exchanges. The agent paradigm promotes the use of independent, loosely coupled software entities that encapsulate some specific functionality and interaction with each other to solve tasks [15].

The proposed framework is based on the MAS paradigm owing to its easier manageability and distributed and robust properties. As depicted in Table 4.1, distinct levels of hierarchy that include the user, room, zone, building, neighborhood aggregators, low-voltage aggregators, medium-voltage aggregators, distribution service operator (DSO), and transmission service operator (TSO) are notable.

Because the primary goal is to ensure that occupants' comfort is not compromised in the process of attaining the maximum possible peak-load reduction for use in Demand Response (DR), information on building occupancy as depicted in Fig. 4.3 is obtained using embedded chair sensors [16]. The availability and use of fine-grained building occupancy information, in addition to contributing to improving the energy performance of buildings through demand-driven control, can also contribute to the improvement of building responsiveness to Demand Response (DR).

Table 4.1 Hierarchy levels in distributed approach

Actor/hierarchy level	Role
User	Registers comprehensive user preference, associated comfort, and energy profile
Room	Aggregate comfort and energy profile inside room
Zone	Aggregate comfort and energy profile for all spaces associated with a zone
Building	Aggregate energy use and available power flexibility for whole building dynamically
Neighborhood aggregator	Dynamically aggregates available power flexibility for buildings in a neighborhood
Low-voltage aggregator	Dynamically aggregates available power flexibility for a number of neighborhoods at low voltage level of network
Medium-voltage aggregator	Dynamically aggregates available power flexibility of connections at medium-voltage level of network
DSO	Ensures network reliability and integrity of power distribution network
TSO	1. Operates and manages market
	2. Ensures network reliability and integrity of power transmission network

Leveraging on the distributed but cooperative properties of MASs, the agent architecture (Fig. 4.2) is composed of the following agents: user, room, zone, building, services, and admin agents.

User agent: The user agent represents each room occupant. It communicates with its environment via installed sensors to ensure that information on building occupancy and individual user preferences is readily available.

Room agent: The room level is critical for striking a balance between user comfort and energy efficiency because this is where both goals have contradictory requirements [17]. In addition, the orientation, occupancy use pattern, appliance, and equipment type, as well as room function, are contributory factors that determine the amount of flexibility available for participation in a DR event. The concept of utility function and the available service table (AST) are introduced at the room level. A utility function is a very useful decision-making mechanism that is often used in MASs, particularly in situations where there are conflicting goals (e.g., comfort and energy consumption). The utility function is used in describing the appropriate tradeoff [18]. The AST, on the other hand, is a concept derived from networking protocols [19] and information push strategy [20]. Table-driven routing protocols attempt to maintain consistent, up-to-date routing information from each node to every other node in a network. These protocols require that each node maintain one or more tables to store routing information, and they respond to changes in network topology by propagating updates throughout the network in order to maintain a consistent network view.

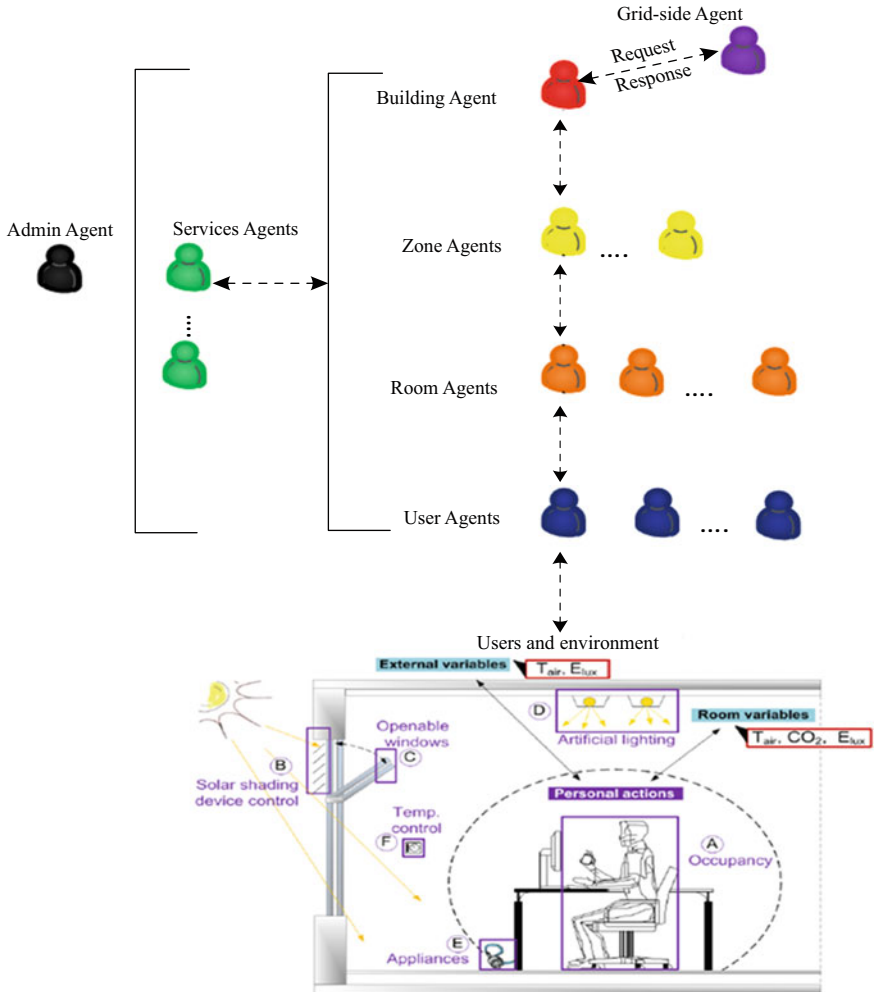


Fig. 4.2 MAS structure

Within this framework, information on available services that can be used in a DR event is pushed up from the room level and aggregated on the building level in the building's AST (Table 4.2).

The basic information pushed to the AST is the available energy in kilowatts (kW) and the duration of availability. The room agent, in addition to ensuring that the room is running optimally in terms of energy efficiency, also continuously updates the AST with the available electrical power in kilowatts (kW) that can be used during a DR event without causing disruptions to occupants' activities or deterioration in the comfort index of occupants. This approach, in addition to ensuring that buildings are constantly operating at optimal performance, also

Table 4.2 AST

	S[8–9] kW	S[9–10] kW	S[10–11] kW	S[11–12] kW	S [12–13] kW	S[13–14] kW	S[14–15] kW	S[15–16] kW	S[16–17] kW
Zone agent	0–24				0–24			0–24	
Building agent			14		14		14		
Available service	0–24	0	14	0	14–24	0	14	0–24	0

ensures that building occupants will not have to experience disruptions or tolerate discomfort for an extended period of time.

Zone agent: In the design of buildings, spaces with identical or similar comfort requirements, such as solar shading, heating, cooling, and ventilation requirements, are often grouped together. The zone agent is hence an aggregator, as identified earlier in Table 4.1. It computes the sum of services available for its zone using the information provided by the room agents in the zone.

Building agent: The building agent is the contact point between the grid and the building. The building agent receives a DR request from the grid and responds appropriately to the request. In most typical MAS coordinated DR events [21], the building agent is often responsible for making decisions on both comfort and a building's participation in a DR event. However, within this framework, the building agent is mainly tasked with negotiating a building's participation using available information in the AST as depicted in Fig. 7.

Services agent: The services agent introduces more task distribution in the agent structure. Because it is in daily human interactions where specialized tasks are often assigned to specialists, the services agent offers specialized services to the agents within the system. Within this framework, the services agent performs a data-mining function that could be utilized by any of the agents in the system.

Admin agent: The MAS design paradigm provides a flexible framework in which agents can be included and removed at any time without causing disruption in the system's operation. It is, however, necessary to have up-to-date information about the state of agents operating in the system. The task of the admin agent is thus to monitor all agents (active, passive, dead, or alive) operating in the system.

4 Multiagent Platform

An agent platform is an execution environment for agents. It supplies the agents with various functionalities, such as agent intercommunication, autonomy, and mobility [22]. In selecting a suitable agent design platform, it is essential that the chosen design platform be easily accessible, supported, compatible with standards, and interoperable with other technologies. The agents are designed using an open-source Web-based agent design platform called EVE [23]. The EVE agent design platform is a fully decentralized and Web-based agent design platform that promotes distributed problem solving. It is also a very scalable and robust agent design platform.

5 Resulting Concept

There is a different focus on the processes that occur in a building, which also depends on the leading strategy: bottom-up (user oriented), middle-out (building services systems oriented), and top-down (smart grid). A top-down approach gives mainly the boundaries for energy consumption related to occupancy behavior [24]. A bottom-up approach is able to estimate the individual energy consumption and then aggregate it to predict the total building energy demand, based on end-user behaviors in time and space. Based on each of these approaches, the results and insights are used to specify specific functionalities for the level below and the level above. In this way, flexibility enables developers to gain from upside opportunities and minimize downside risks [1, 25]. Taking our cue from the required dynamism and flexible operations, we adapt the framework of Kofler et al. [15] as ideal for realization of the pervasive control envisioned by Kolokotsa et al. [26], with a central role for BEMS and MAS (Fig. 4.3).

6 Case Study

This chapter uses an office building in the Netherlands to illustrate typical building-centered electrical flexibility. The case-study building has three floors with an approximate total floor area of 1500 m² and average occupancy count of 35 when busy. Electrical installation in the case-study building is as illustrated in Fig. 4.4; the key electrical system load groups in the building are cooling, humidifier, ventilation, lighting, and office appliances. The installed cooling system in the building has a maximum power consumption rating of 25 kW; the ventilation system is consumption rated at 9.5 kW, with 6 kW of the demand dedicated to the fan system. Cooling is effected by cold-air circulation dedicated to serving the three main cooling zones. Total ventilation fan capacity is 15,000 m³/h.

During periods when the air is cold and dry (normally during winter and specifically when the ambient temperature is less than 15 °C and the ambient relative humidity is less than 30%), the humidifier is activated. At a 30 kW power consumption rating the humidifier is the single biggest load in the building. The lighting system in the building accounts for 16 kW demand. Lighting is provided by florescent tubes (T5 type). The scope of this chapter is the summertime operation of building processes; in what follows, flexibility will only be discussed with respect to the cooling and ventilation processes.

Building service control in the case-study building is effected by a Web-based building management system that is operated based on optimal rules on set-point manipulation. Based on temperature and relative humidity readings from installed sensors, feedback is given for switching on or off or upwards or downwards adjustments of settings for optimal operation of the building. Cooling can be achieved in two ways: night ventilation or chiller use. The night ventilation setting

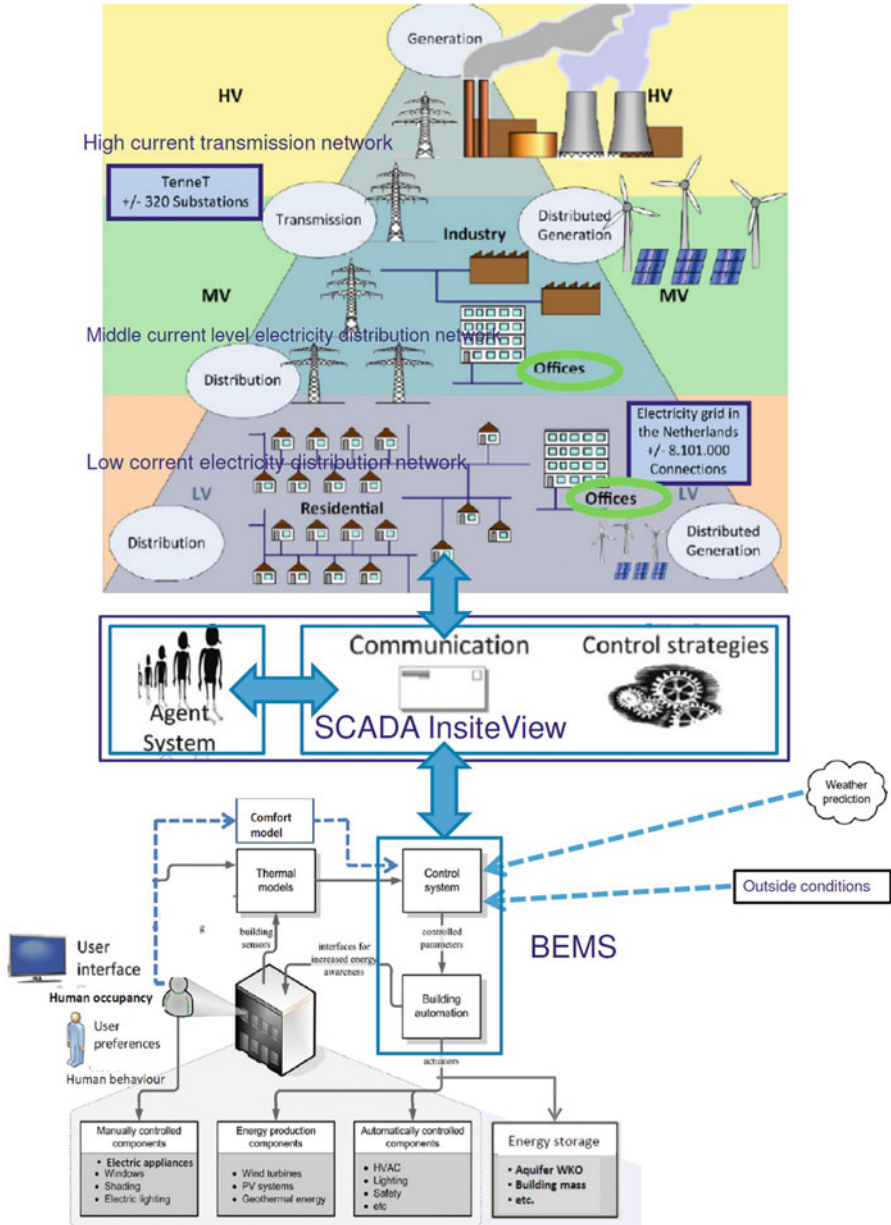


Fig. 4.3 Smart grid and user interaction, based on Kolokotsa et al. [26] and Kofler et al. [15]

cools the building with outside air (free cooling) during the night or early morning (between 10:00 p.m. and 5:00 a.m.) whenever the average room temperature exceeds

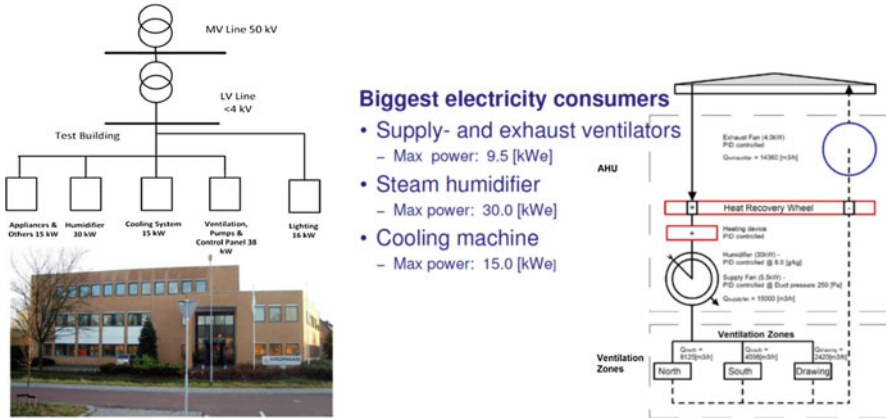


Fig. 4.4 Electrical connections from mid-voltage grid to building and its major electricity consumers

23 °C and outside/ambient temperature is below 12 °C. Night ventilation is stopped when the room temperature has dropped to 21 °C or when the end time is reached. The chiller system is switched on whenever the following preconditions are satisfied:

1. For stage 1 operations, the outside/ambient temperature should have been above 18 °C for over 1 h and the circulation pump for the chiller is also at an operational position. For stage 2 operation, the outdoor temperature should be above 26 °C for 30 min.
2. In stage 2, the chiller is switched off again when the outside temperature continues for 30 min under 24 °C. The chiller is switched off again when the outside temperature is below 16 °C for an hour or if there is no more cooling demand from the coolers.

If no differential pressure is present on the chiller, the chiller is switched off and a fault message is generated. Also, the ventilation system remains on whenever night ventilation is required and when the building is occupied. The building is occupied during weekdays between 7:00 a.m. and 5:00 p.m.

7 The Concept

In the case study, energy-related performance and comfort profiles were captured at 100 % nominal operational capacity for the cooling and ventilation systems. Thereafter, cooling and ventilation systems were operated outside the nominal range or at varied sequences with the aim of harvesting demand-side flexibility. For the ventilation system, performance was monitored at 100, 80, 70, and 60 % nominal settings; for the cooling system, performance was monitored for operations under

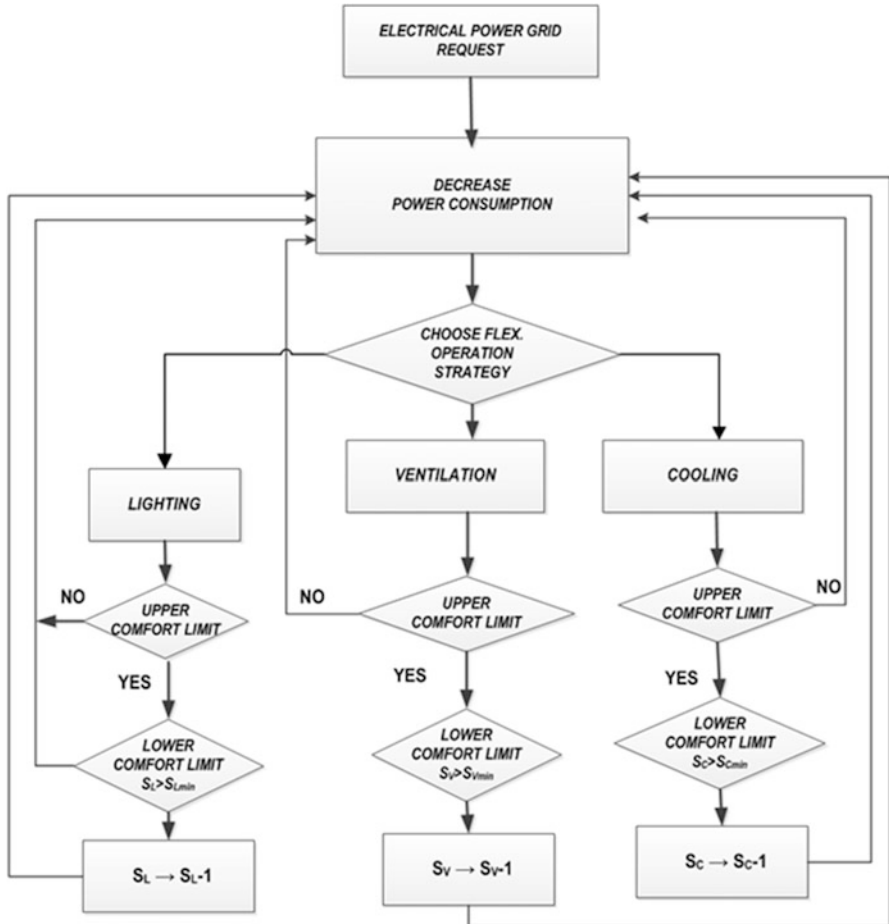


Fig. 4.5 Deployment of building service processes as ramp-up of flexibility resources for power grid support activities

normal settings and operations with zonal cooling set-point temperature reset of 2 °C higher than normal. The conceptual basis of the case study entails the intelligent manipulation of visual, ventilation, and thermal comfort bandwidths (Table 4.2) to yield building-centered electrical power flexibility. Figure 4.5 outlines the operational sequence in realizing this concept. During the whole period of experiments, the monitored parameters included (1) load category power consumption; (2) space comfort parameters, including duct airflow rate, room temperature, radiant temperature, carbon dioxide concentration, relative humidity, and occupant feedback on satisfaction with the thermal comfort and indoor air quality; and (3) ambient weather data, specifically relative humidity, solar irradiation, and air temperature.

8 Discussion and Conclusion

The problems of the smart grid are partly caused by the use of DRESSs. Break-throughs need to be made in the field of process control of heat, cold and electricity storage, demand, and distribution.

New process control strategies are needed for improving energy interactions within buildings, their environment, and the energy infrastructure by effectively incorporating occupant behavior. Energy system integration is a key issue; however, most research is aimed at the high system level of existing energy infrastructures, whereas in a building the different energy systems are already integrated to supply the necessary comfort of the occupants. Starting from this bottom-up insight, an integral approach was used to divide the whole system into different layers from the user up to centralized power generation. On different scale levels, from individuals to the building level, possibilities are being investigated both within laboratory conditions as well as in a real office building as case studies. Specific control strategies were applied on the existing HVAC systems. The initial results showed that in the process of developing the optimal interaction between the smart grid and the nanogrid of a building, more than just a contribution to optimizing smart grid control is possible. The next step is to define neighborhood energy management systems and to look for the possibilities of a virtual coupling with the SCADA systems of the grid operators. Grouping the energy demand of end users and local renewable producers in neighborhoods will enforce end-user involvement and automated load shifting, which greatly improves the efficiency of advanced energy management. This allows for maximizing the utilization of flexible demand resources within neighborhoods and forms a bottom-up approach to system integration of energy infrastructures, starting from the user, to support the smart grid.

The responsiveness of the smart grid to changing uncertainties and requirements can be realized through the intrinsic flexibility measures embedded in the energy infrastructures of buildings. A systems engineering approach presents an opportunity to systematically integrate architectural and operational flexibility early on in the conceptual design phase of energy infrastructures of the built environment. This hierarchical framework aims at providing support for integrating the flexibility of the infrastructure systems to build MAS structures based on it. The manner of description of a system influences the identification of the possible changes that may take place and the interpretation of their demands for flexibility. In this paper the focus was on operational flexibility for which the integration of the end user through a bottom-up approach is essential for supporting the smart grid.

References

1. Melese YG, Heijnen PW, Stikkelman RM (2014) Designing networked energy infrastructure with architectural flexibility. *Procedia Comput Sci* 28:179–186
2. IEA (2015) International energy agency, energy in buildings and communities programme. EBC annual report 2014

3. Papaefthymiou G, Grave K, Dragoon K (2014) Flexibility options in electricity systems. Project number: POWDE14426, Ecofys 2014 by order of European Copper Institute
4. Frerk M (2015) Open letter: facilitating efficient use of flexibility sources in the GB electricity system. OFGEM, The Office of Gas and Electricity Markets, 28 Jan 2015
5. Blanchard BS, Fabrycky WJ (2005) Systems engineering and analysis, 4th edn. Prentice Hall, Upper Saddle River
6. Savanović P (2009) Integral design method in the context of sustainable building design. PhD thesis, Technische Universiteit Eindhoven
7. Zeiler W, Savanović P (2009) General systems theory based integral design method. Proceedings ICED'09, Stanford, USA
8. Lo C, Ansari N (2011) The progressive smart grid system from both power and communications aspects. *IEEE Commun Surv Tutor* 14(99):1–23
9. Dave S, Sooriyabandara M, Yearworth M (2011) A systems approach to the smart grid. In: The first international conference on smart grids, Green Communications and IT Energy-aware Technologies
10. Lopes AJ, Lezama R, Pineda R (2011) Model based systems engineering for smart grids as systems of systems. *Procedia Comput Sci* 6:441–450
11. Acevedo S, Molinas M (2012) Identifying unstable region of operation in a micro-grid system. *Energy Procedia* 20:237–246
12. Wang S (2013) Intelligent building electricity demand management and interactions with smart grid. In: Proceedings Clima, Prague, 2013
13. Jarvis D, Jarvis J, Rönquist R, Jain L (2013) Multiagent systems and applications. *Intell Syst Ref Libr* 46:1–12
14. Basso G, Gaud N, Gechter F, Hilaire V, Lauri F (2013) A framework for qualifying and evaluating smart grids approaches: focus on multi-agent technologies. *Smart Grid Renew Energy* 4(4):333–347
15. Kofler MJ, Reinisch C, Kastner W (2012) A semantic representation of energy-related information in future smart homes. *Energy Build* 47:169–179
16. Timilehin L, Zeiler W, Boxem G, Yang Z (2015) Occupancy measurement in commercial office buildings for demand-driven control applications—a survey and detection system evaluation. *Energy Build* 93:303–314
17. Clarke JA, Janak M, Ruysssevelt P (1998) Assessing the overall performance of advanced glazing systems. *Sol Energy* 63(4):231–241
18. Dounis AI (2010) Artificial intelligence for energy conservation in buildings. *Adv Build Energy Res* 4(1):267–299
19. Royer EM, Toh C-K (1999) A review of current routing protocols for ad hoc mobile wireless networks. *IEEE Pers Commun* 6(2):46–55
20. Kim JJ (2014) Automated demand response technologies and demonstration in New York city using OpenADR, Sep 2014
21. Hurtado LA, Nguyen PH, Kling WL (2015) Smart grid and smart building inter-operation using agent-based particle swarm optimization. *Sustain Energy Grids Netw* 2:32–40
22. Leszczyna R (2008) Evaluation of agent platforms
23. de Jong J, Stellingwerff L, Paziienza GE (2013) Eve: a novel open-source web-based agent platform. In: Proceedings of the 2013 I.E. international conference on systems, man, and cybernetics, 2013
24. Bloem JJ, Strachan P (2012) Evaluating and modelling near-zero energy buildings; are we ready for 2018? Expert meeting 30-31 January 2012 Glasgow, JRC Technical report
25. de Neufville R, Scholtes S (2011) Flexibility in engineering design. MIT Press, Cambridge
26. Kolokotsa D, Rovas D, Kosmatopoulos E, Kalaitzakis K (2011) A roadmap towards intelligent net zero- and positive-energy buildings. *Sol Energy* 85:3067–3084

Chapter 5

Influence Effect of Energy Roof on PV Efficiency: A Case Study

Paul Kemme and Wim Zeiler

Abstract Increasingly there is a need for high-performance (sustainable) buildings. Even in a country with as little solar radiation as the Netherlands, the application of so-called solar energy roofs is becoming more popular. Already some different concepts exist, and one of the latest developments is the use of the roof as combined solar thermal collector and photovoltaic (PV) laminate. This chapter presents the results of research on the energy roof of a school in the Netherlands. The school was designed as an energy-plus school, and the energy roof, in combination with the PV laminate, plays a significant role in this project. The aim of this research was to determine the added value of the combined concept of PV and thermal collector in the total performance of the energy roof. It was expected that cooling of the PV laminate would have a positive effect on the electrical efficiency of this PV as the thermal collector absorbed heat from the overlying PV laminate. The producers of the PV laminate claim it has higher efficiencies. This claim was examined by studying the correlation of efficiency and the thermal gain of the roof in three different situations. The results showed no clear positive effect of the energy roof on the average efficiency of the PV laminate.

1 Introduction

Growing populations and economic development are leading to a constant rise in the use of fossil fuels, resulting in ever higher levels of CO₂ emissions, a significant cause of global warming. If no policy changes are enacted and no new technological designs implemented regarding the use of energy sources, greenhouse gas emissions are expected to double by the year 2050. Thus, it is crucial that alternative energy technologies be developed and utilised before the problem grows out of hand. The Sun is the source of all energy on Earth, and incoming solar irradiance

P. Kemme • W. Zeiler (✉)

Faculty of the Built Environment, University of Technology Eindhoven, Eindhoven,
The Netherlands

e-mail: w.zeiler@bwk.tue.nl

amounts to 174 PW (1 Petawatt = 10^{15} W) [1], of which approximately 1,069,444 PW of energy is absorbed by the Earth's atmosphere, oceans and land masses over the course of a year [2]. The energy absorbed from the Sun by Earth corresponds to nearly 7500 times more than what the whole world needs in a year (143 PW). Therefore, efficient and economic conversion of clean solar power could make a very significant contribution toward fulfilling today's growing energy needs and alleviating climate concerns [3]. One of the most promising renewable options is solar, with photovoltaic (PV) cells to generate electricity and solar collectors for heat generation being the two main examples.

The study of photovoltaic/thermal (PV/T) systems started in the mid-1970s. It was initiated when PV modules faced a drop in efficiency when the temperature of the surface panel increased. Martin Wolf was the first known researcher to work on flat-plate PV/T liquid-based systems [4, 5]. A detailed review of the research and development in PV/T systems is presented in [5–11]. Various PV/T systems exist, and they depend on the type of PV module as well as its design, type of heat removal fluid (water/glycol or air) and the concentration of the incoming radiation. Therefore, PV/T products can be classified as liquid PV/T collectors, air PV/T collectors and PV/T concentrators.

The most common working fluids in liquid-based PV/T collectors are water, water/air and, most recently, refrigerants. The water type PV/T collectors are the most widely system studied. A classification scheme for PV/T liquid collectors is given in Fig. 5.1 [9].

In particular, liquid PV/T collectors, which use a water heating system similar to that of a flat plate collector, are used for various building and industrial applications. A schematic diagram of different types of PV/T water collectors is shown in Fig. 5.2 [12, 13].

Aesthetics, uniformity, functionality, lifetime, roof protection capability, watertightness, ethics, autonomy and prestige are some of the noneconomic factors considered when making a decision to invest in solar energy [6, 14]. Solar PV/T systems have the advantages of providing efficient solar technology, a single warranty, space reduction and cost reduction versus separate solar PV and solar thermal systems [6, 17].

One of the newer energy conversion methods is called the energy roof, which is a PVT system. The elements of the energy roof serve as one device that converts sunlight into electricity and heat at the same time. Basically, the technique combines solar cells and a solar collector. Consequently, this system has higher energy output per unit surface area than a PV cell and a solar collector placed in side-by-side configuration [15]. Both PV cells and solar collectors are known technologies, and the combination of both of them dates back to the 1970s [4]. The idea behind this technology is to extract the heat generated by unconverted absorbed solar radiation from PV cells. Storing this heat should result in greater efficiency, and the lowered temperature of the PV cells should also increase their efficiency.

The basis of the energy roof are the integrated thermal roof collector pipes, which contain a mixture of 70 % water and 30 % glycol to prevent freezing of the medium. A pump circulates the medium through the roof to absorb heat from solar

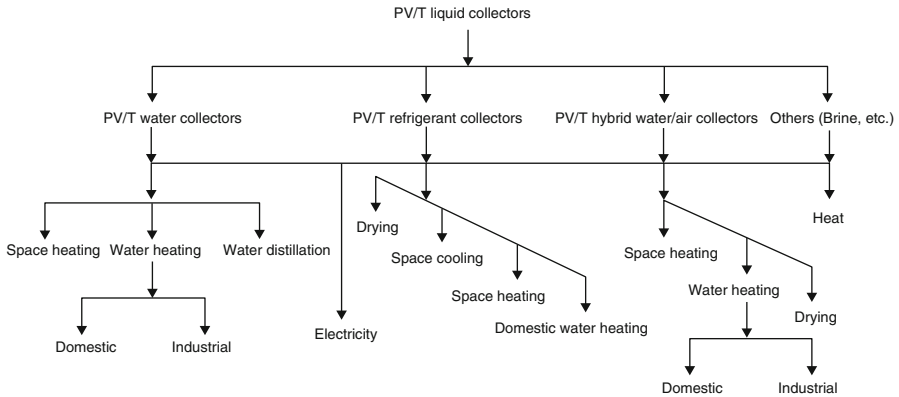


Fig. 5.1 Classification of PV/T liquid-based collectors [9]

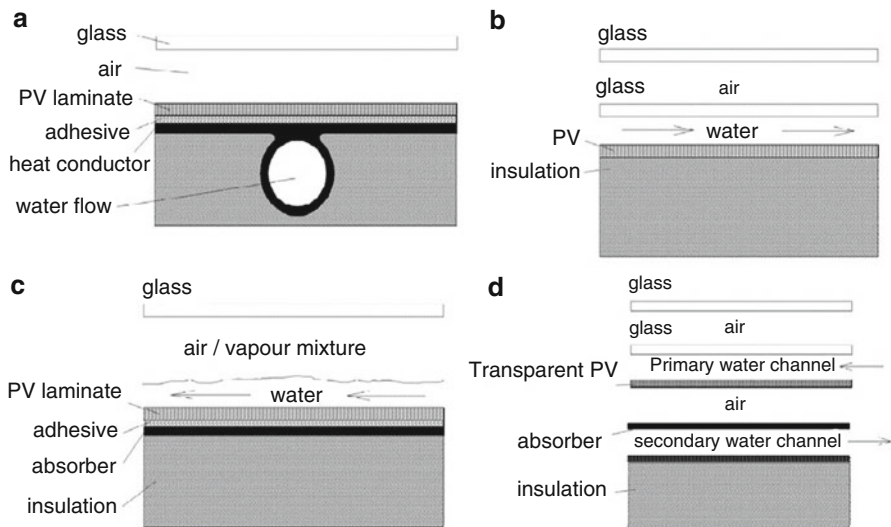


Fig. 5.2 Groups of PV/T collectors: (a) sheet-and-tube PV/T, (b) channel PV/T, (c) free-flow PV/T and (d) two-absorber PV/T [12]

radiation. The tube collector is covered in synthetic roofing material with an integrated layer of amorphous PV laminate cells that generate electricity (Fig. 5.3).

The aim of this research is to investigate the claim of the producers of the energy roof of a positive effect of heat transfer from PV cells to the roof on the efficiency of the PV cells. As shown by previous studies, a high temperature of PV cells negatively affects their efficiency, so chilled PV laminate should perform better.

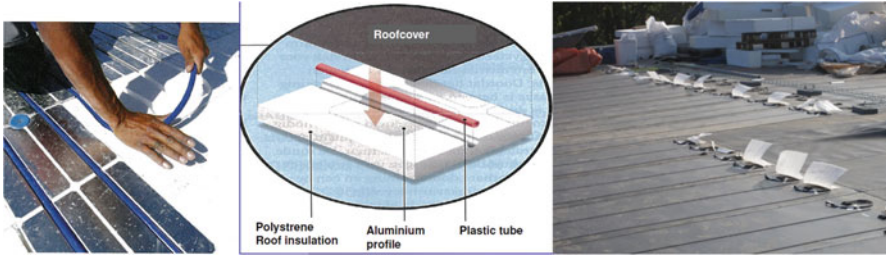


Fig. 5.3 Energy roof construction

2 Methodology: A Field Case

In early 2011, Christian Huygens College opened a new location in western Eindhoven. The school is designed for up to 850 students and contains 3 stories with a total of 7800 m² of floor area. Thanks in part to the energy roof (Fig. 5.1), the school building, designed by architect RAU, generates more energy than it needs for its own use. That surplus is stored in an underground aquifer storage system. In winter, this energy can be used to heat the building. A heat pump increases the temperature before usage for heating the school; see Fig. 5.4 for the total energy concept of the building.

The objective of this research is to investigate the effect of heat removal by the thermal tube collector integrated within the energy roof on the efficiency of the PV laminate. To this end, a comparison was made between two operational situations that are similar, but with the roof working in one case and not working in the other. PV laminate efficiency is dependent on a variety of weather conditions, and the combination of these conditions is never the same over a long period of time. Therefore, a set of measured data of two periods of 4 days was selected in which weather conditions were comparable and in which in one situation the hydraulic circuit of the energy roof's thermal collector was working and in the other was not.

3 Measurements and Data Processing

Using sensors and measuring devices, the inflow (101TE03) and outflow temperatures (101TE04) of the medium in the energy roof system and mass flow were monitored through pump activity percentage (101CP01) (Fig. 5.5). An insulation layer is placed on the roof construction to avoid heat transmission to the interior environment. In this layer, channels are cut out in which polyethylene pipes are placed. Around these pipes aluminium sheets are bent, and the sheets also form fins on both sides of the tube and on top of the insulation layer (Fig. 5.6).

A local weather station provides data on the ambient temperature, solar radiation and wind speed. For measurements of global radiation at the roof a CaTec GSM 3.3

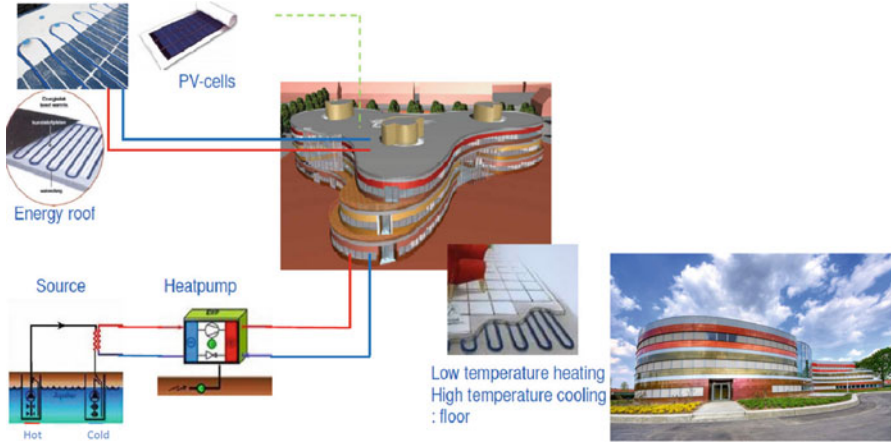


Fig. 5.4 Total energy concept of Christian Huygens College, Eindhoven

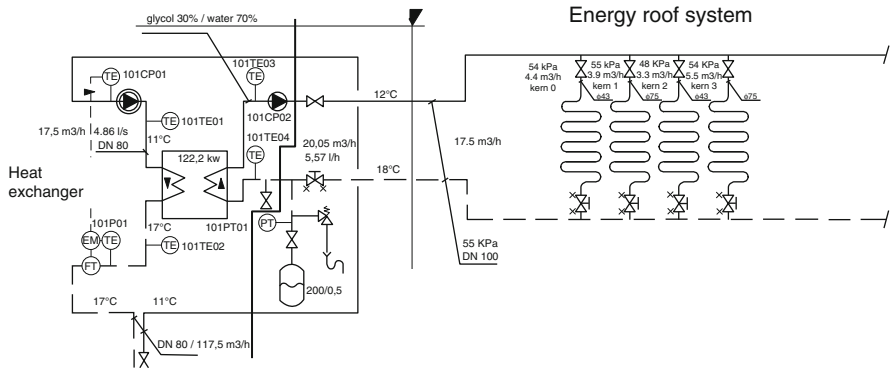


Fig. 5.5 Schematics of energy roof, including location of measurement instruments

pyranometer (G) was used. This instrument has an absolute error of less than 10 %. For ambient temperature and wind velocity, a CaTeC Clima Sensor 2000 was used with a cup star for measuring wind speed and a platinum Pt 100 sensor for temperature measurements. The accuracy of the wind speed measurements is less than or equal to 0.5 m/s. For the ambient temperature the accuracy is 0.15 °C at 0 °C. The temperatures of the inflow and outflow of the roof system were measured with a Kamstrup MULTICAL 601. Again, Pt 100 sensors were used, with an accuracy of around 0.5 %. Data sets were measured as momentous values with an interval of 8 min. Temperatures were measured in degrees Celsius (°C), solar radiation in watts per square meter (W/m^2), wind velocity in meters per second (m/s), and mass flow indirectly in kilograms per second (kg/s). The measurement results for electrical gains of the PV laminate were measured in kilowatts (kW), with a 15 min interval, so these values are not momentous but the total for 15 min.



Fig. 5.6 Detail of different layers of energy roof

First of all, the data needed to be synchronised. Therefore, data were recalculated to obtain hourly values. For temperatures, mass flow and wind velocity, the average value for all measurements within 1 h were used. For electrical gain the hourly total was found by adding the totals of the four measurements and dividing the results by the number of measurements per hour.

Using the measured data, certain variables could be determined to carry out the study. PV temperature is known to have a significant effect on the efficiency of the system. This temperature was not measured but approximated using the following equation [16]:

$$T_{PV} = T_a + \frac{(\text{NOCT} - 20)}{800} \cdot G, \quad (5.1)$$

where T_a and G are measured by the weather station integrated into the roof, and NOCT is provided by the manufacturer of the PV laminate.

The electrical efficiency of the PV is calculated by dividing the electrical yield of the PV laminate as measured by the system by the global radiation as measured by the weather station integrated into the roof:

$$\eta_{PV} \frac{E_{PV}}{G}. \quad (5.2)$$

Q_{tot} is defined as the amount of energy absorbed by the energy roof. When the roof is active, this can be calculated using the following equation:

$$Q_{\text{tot}} = \dot{m} \cdot C_p \cdot (T_{\text{out}} - T_{\text{in}}), \quad (5.3)$$

where C_p is the heat capacity of the medium in the roof (70 % water, 30 % glycol), m the mass flow as provided by the system data and T_{out} and T_{in} are also measured by the system.

When the roof is inactive, energy can still be absorbed because of the differences between ambient temperature, PV temperature, and the temperature of the roof medium. The amount of energy absorbed can be found by

$$Q_{\text{tot}}(t) - \rho \cdot C_p \cdot (T_m(t) - T_m(t-1)), \quad (5.4)$$

where ρ is the density of the roof medium and V the total volume of the medium in the roof. T_m is the mean temperature of the medium calculated by

$$T_m = \frac{(T_{\text{out}} + T_{\text{in}})}{2}. \quad (5.5)$$

4 Measurement Periods and Results

The objective of this research was to investigate the effect of heat absorption by an energy roof on the efficiency of a PV laminate. To this end, a comparison must be made between two situations that are similar, but with the roof working in one case and not working in the other. Because PV efficiency is dependent on a variety of weather conditions and the combination of these conditions is never the same over a long period of time, another method must be found. Manually switching the system on and off is not realistic for this research, and obviously weather conditions cannot be manipulated. Out of a large set of measured data, two periods of 4 days were found in February and March in which weather conditions were comparable. However, for the second period, temperature and solar radiation were higher, causing the system to be active during parts of these days. During the first period the system was not active. Therefore, these two sets of data are suitable for the current research (Table 5.1).

Figure 5.7 shows the measured data for the first period, from midnight on 23 February 2014 to midnight on 27 February 2014. The maximum temperature was around 15 °C, and the maximum solar radiation was 464 W/m². Mass flow was constant at zero, indicating that the energy roof was not active during this period. Figure 5.8 shows the measured data for the second period, from midnight on 28 March 2014 to midnight on 1 April 2014. The maximum temperature was around 22 °C, and the maximum solar radiation was 683 W/m². The set-point temperature of the roof was exceeded for a couple of hours per day, so the roof system was active during these hours, as indicated by the mass flow line.

Table 5.1 Mean values for the three parameters of weather conditions for the two measuring periods

		Mean	Minimum	Maximum
T_a [°C]	February	9.05	4.00	15.00
	March	15.21	7.07	23.00
I [W/m ²]	February	106	0	464
	March	183	0	683
V [m/s]	February	2.96	0.76	5.79
	March	2.21	0.50	4.51

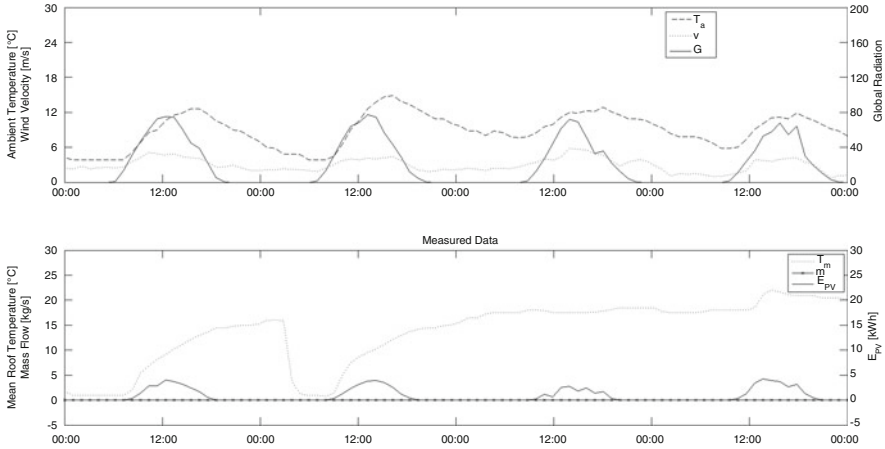


Fig. 5.7 Measured data from first period, late February 2014

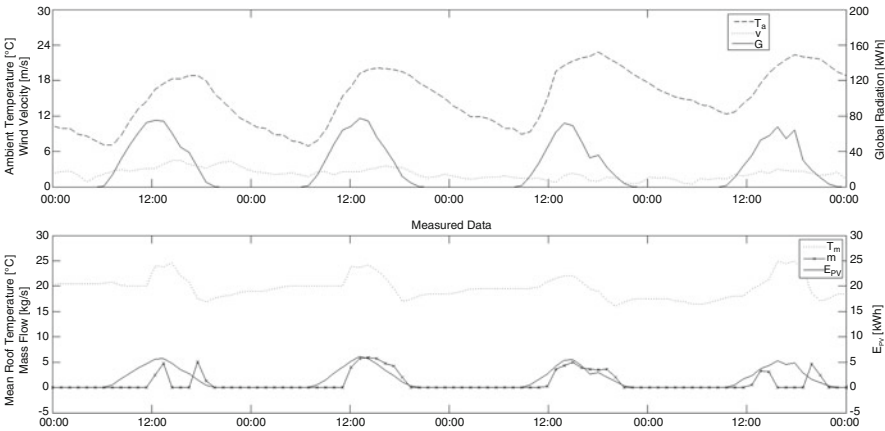


Fig. 5.8 Measured data from second period, late March 2014

5 Data Analyses

To test whether the removal of heat absorption by the energy roof led to an increased PV efficiency, three operational scenarios were presented:

1. The energy roof is inactive, and no sunlight falls on the PV laminate (night situation). This scenario is of no interest for this research.
2. The energy roof is inactive, and light falls on the PV laminate (daytime situation, minimum conditions for activity are not met). The energy roof is only profitable when certain weather conditions are present. The PV laminate is generating electricity, but it is not actively cooled by the energy roof. For this scenario, two situations can be distinguished:
 - (a) Mean roof temperature exceeds PV temperature; heat flow occurs from roof to PV and PV is 'heated' (passively).
 - (b) PV temperature exceeds mean roof temperature; heat flow occurs from PV to roof, and PV is 'cooled' (passively).
3. The energy roof is active and sunlight falls on the PV laminate. The PV temperature exceeds the mean roof temperature, heat is absorbed by the roof medium, and the PV is actively cooled.
 - Scenario 3 could be extended to a situation with an active roof, illuminated PV and roof temperature exceeding the PV temperature. However, no data are available for this scenario in the current data set. Moreover, owing to the material properties of the PV laminate and the roof, the PV laminate heats up more quickly than the roof medium. Therefore, this situation is very rare and not really relevant for this research.
 - There is no night-time scenario in which nightly weather conditions meet the minimum conditions for activation of the energy roof. This research focuses on electrical efficiency, but in the night-time scenario the PV laminate is not illuminated and no electricity is generated, and so this scenario is not relevant for the present research. Moreover, this situation does not occur in the current set of measurement results.

For this research, Scenarios 2a, 2b and 3 are taken into consideration. For that purpose, the measured data are divided into Situation 1 (Scenario 2a), Situation 2 (Scenario 2b) and Situation 3 (Scenario 3). Criteria for these situations are as follows:

Situation 1: $m = 0$, T_{pv} and $G > 4$ kW,

Situation 2: $m = 0$, T_{pv} and $G > 4$ kW,

Situation 3: $m = 0$, T_{pv} and $G > 4$ kW,

m : mass flow (kg/s),

T_{pv} : PV temperature ($^{\circ}$ C),

T_m : mean roof temperature ($^{\circ}$ C),

G : solar radiation (kW).

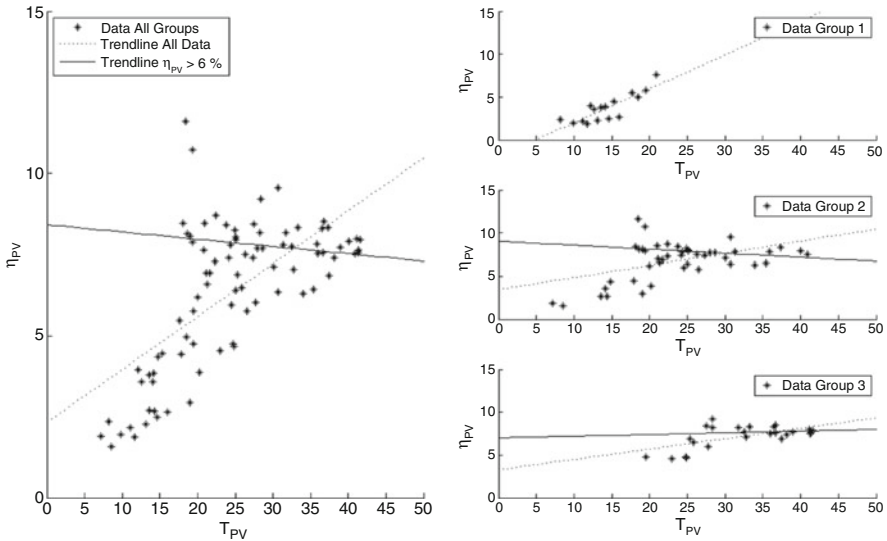


Fig. 5.9 Correlation between PV temperature and electrical efficiency for all data in Situations 1–3 (*left*) and for the situations separately (*right*)

Measuring moments for which electrical efficiency was under 6% were filtered out, and again a linear fitted line was calculated. Figure 5.9 shows the expected effect of PV temperature on PV efficiency. On the right side of Fig. 5.8, the situations are presented separately. Situation 2, in which the roof is inactive, shows the expected decline for the efficiency of PV is greater than 6%. When the roof is active, Situation 3, the efficiency is almost constant for a PV efficiency greater than 6%. Note that in Situation 3, PV temperature is not necessarily lower than in Situation 2, even though the roof is active in Situation 3. Although trend lines were found for these sets of data, the deviations are significant in numerous cases.

6 Results

The results (Table 5.2) show that the mean efficiency is lowest in Situation 1. For Situation 1, the roof is inactive and the PV laminate temperature is lower than the temperature of the medium in the roof thermal collector, the water-glycol mix. Moreover, the total solar energy reaching the roof (G) is higher than 4 kW. However, analysis of this situation shows that those measurements all occur around dusk or dawn, so global radiation was relatively low. Of the three situations, Situation 1 is the least interesting for the current research.

For this research, the focus is on Situations 2 and 3. Both situations contain measurements in broad daylight, and the mutual differences are in the activity of the

Table 5.2 Mean, minimum, and maximum electrical efficiencies for the three operating situations

		Mean (%)	Minimum (%)	Maximum (%)
η^{PV} [%]	Situation 1	3.70	1.89	7.63
	Situation 2	5.79	1.59	11.60
	Situation 3	7.21	4.55	9.22

energy roof. The mean efficiency is slightly higher for Situation 3, in accordance with the hypothesis. However, peaks are found to be higher for Situation 2, and the efficiencies in Situation 3 do not seem to be significantly higher compared with Situation 3. This can be explained by the set point for activation of the roof; the roof is activated only when T_{out} (entering the heat exchanger) exceeds 35 °C for more than 5 min and shut down when the temperature measured for the medium leaving the heat exchanger drops under 17 °C for more than 10 min. Therefore, peak moments for the generation of electricity can occur when the roof is not active. Looking at the numbers in Table 5.2, it is not possible to conclude that the roof has a significant positive effect on PV efficiency. Although the mean electrical efficiency for this Situation 3 is higher, the difference is small, and the fact that peaks occur in Situation 2 indicates that other factors might be play a role.

7 Discussion and Conclusions

The current study was carried out as experimental research using measurements provided by instruments integrated into a roof system. Measurements were carried out under exposure to numerous outside factors, and conditions were far from those of standardised tests. Therefore, it was impossible to isolate all factors of influence. The PV laminate temperature was not measured, but the literature provided a method to approximate this temperature. This method uses global radiation and ambient temperature for the calculations. Results showed that in this case, wind velocity had a significant effect on the PV laminate temperature but was not taken into account in the calculation method. A more accurate method for determining PV laminate temperature could improve the results and conclusions of this research.

Comparison of situations where the roof was either inactive or active showed no significant difference in the mean efficiency of the PV laminate. Also, looking at the situation with an active roof system, no positive effect was found on electrical efficiency for higher values of heat absorption or mass flow within the roof. Thermal yield varied between 40 and 170 kW without a significant difference in electrical efficiency. Although mean efficiency was slightly higher when the roof was active, numerous peak measurements were found when the roof was off that exceeded all measured values for the active roof. These values were balanced by low efficiency values, resulting in a slightly lower mean efficiency. On average, in real outdoor conditions, there is no significant positive effect of the energy roof concept on the efficiency of a PV laminate.

We agree with Michael et al. [6] that additional, proper standards, regulations and continuous field testing are required to promote solar PV/T technology. This would allow installers and clients to make more suitable comparisons of the various alternatives from different manufacturers. The integration of this system in buildings offers several additional benefits combined with faster payback periods. The combined production of electrical and thermal energy in a limited area allows for maximum usage of solar energy and provides a path toward near zero-energy buildings.

References

1. Smil V (1991) General energetics energy in the biosphere and civilization. Wiley, New York
2. Smil V (2006) Energy at the crossroads. In: OECD global science forum conference, Paris
3. Kaya M (2013) Thermal and electrical performance evaluation of PV/T collectors in UAE. Master of Science Thesis EGI 2013:037MSC, KTH Stockholm, Sweden
4. Wolf M (1976) Performance analysis of combined heating and photovoltaic power systems for residences. *Energy Convers* 16(1–2):79–90
5. Mamid SA, Othman MY, Sopian K, Zaidi SH (2014) An overview of photovoltaic thermal combination (PV/T combi) technology. *Renew Sustain Energy Rev* 38:212–222
6. Michael JJ, Iniyan S, Goic R (2015) Flat platesolarphotovoltaic–thermal (PV/T) systems: a reference guide. *Renew Sustain Energy Rev* 51:62–88
7. Chow TT, Tiwari GN, Menezo C (2012) Hybrid solar: a review on photovoltaic and thermal power integration. *Int J Photoenergy*. <http://dx.doi.org/10.1155/2012/307287>
8. Chow TT (2010) A review on photovoltaic/thermal hybrid solar technology. *Appl Energy* 87:365–379
9. Daghigh R, Ruslan MH, Sopian K (2011) Advances in liquid based photovoltaic/thermal (PV/T) collectors. *Renew Sustain Energy Rev* 15:4156–4170
10. Kumar A, Baredar P, Qureshi U (2015) Historical and recent development of photovoltaic thermal (PVT) technologies. *Renew Sustain Energy Rev* 42:1428–1436
11. Ibrahim A, Othman MY, Ruslan MH, Mat S, Sopian K (2011) Recent advances in flat plate photovoltaic/thermal (PV/T) solar collectors. *Renew Sustain Energy Rev* 15:352–365
12. Vries DW de (1998) Design of a PV/thermal combi panel. Ph.D. thesis, Eindhoven University of Technology, Eindhoven
13. Tyagi VV, Kaushik SC, Tyagi SK (2012) Advancement in solar photovoltaic/thermal (PV/T) hybrid collector technology. *Renew Sustain Energy Rev* 16:1383–1398
14. Zondag HA, van Helden WGJ, Bakker M, Affolter P, Eisenmann W, Fechner H, Rommel M, Schaap A, Sørensen H, Tripanagnostopoulos Y (2005) Roadmap—a European guide for the development and market introduction of PV–thermal technology. In: Proceedings of the 20th European photovoltaic solar energy conference, Barcelona, Spain, 6–10 June 2005
15. van Helden WGJ, van Zolingen RJC, Zondag HA (2004) PV thermal systems PV panels supplying renewable electricity and heat. *Prog Photovolt* 12:415–426
16. Ciulla G, Lo Brano V, Moreci E (2013) Forecasting the cell temperature of PV module with an adaptive system. *Int J Photoenergy* 2013:10p (Article ID: 192854)
17. Kalogirou S (2006) Hybrid PV/T solar systems for domestic hot water and electricity production. *Energy Convers Manag* 47:3368–3382

Retracted Chapter:

Chapter 6

Green Buildings and Renewable Energy

Application Based on Life Cycle

Performance Costing



Wim Zeiler, Anna Vanderveen, Wim Maassen, and Rik Maaijen

Abstract There is a clear need for more sustainable, more productive solutions within the built environment. However, at the moment, the initial investment costs for applying new renewable energy sources and solutions to green buildings with better indoor air quality are higher than for traditional solutions. Because there is often a fixation on primary investment costs, it is important to use life cycle costing models to show clients which alternative is ultimately the best choice. Unfortunately, currently there are no good and simple tools available to use in the early stage of the design process. A life cycle performance costing decision support tool was developed to assess conceptual design decision making. The tool shows the value of more sustainable, healthier, and more productive solutions over the long term and so stimulates the application of these solutions. Because investment costs are important but profits are even more so for organizations, performance/productivity was added as a key element to the Life cycle value costing approach. An example of a design project is presented to demonstrate the added value of comparing alternative solutions based on the life cycle value costing outcomes of different building service designs for green buildings and the application of renewable energy.

An erratum of the original chapter can be found under DOI [10.1007/978-3-319-30746-6_76](https://doi.org/10.1007/978-3-319-30746-6_76)

W. Zeiler (✉) • A. Vanderveen
Faculty of the Built Environment, University of Technology Eindhoven, Eindhoven,
The Netherlands
e-mail: w.zeiler@bwk.tue.nl

W. Maassen
Faculty of the Built Environment, University of Technology Eindhoven, Eindhoven,
The Netherlands

Royal Haskoning DHV, Building Services Rotterdam, Rotterdam, The Netherlands

R. Maaijen
Royal Haskoning DHV, Building Services Rotterdam, Rotterdam, The Netherlands

1 Introduction

The early planning phases (programming and predesign) play a crucial role in future performance in terms of resource and energy consumption of a building; it is here that the optimization potential can be most effectively used –and at a rather low cost. Bogenstätter [2] already pointed out that early design stages determine up to 80 % of building operational costs [7] and of environmental impacts. In the later planning phases, the potential for change rapidly decreases with simultaneously increasing costs ([10] in [1]) (Fig. 6.1).

A decision-making framework for investors allowing assessment not only of costs but also of life-cycle savings and value (sustainability and productivity) is necessary to shift the focus of decision-making from almost exclusively construction costs toward life cycle costs and value [9, 11, 12]. Sustainable development revolving around environmental, economic, and social aspects [15] led to concepts for life cycle thinking: taking into account impacts of a product over its entire life cycle [13]. This formed the basis for life cycle sustainability assessment (LCSA) described by the United Nations Environment Programme and the Society for Environmental Toxicology and Chemistry [13]. LCSA aims at combining stand-alone life cycle assessment techniques to start a holistic assessment and to complementarily address the three sustainability dimensions [13]:

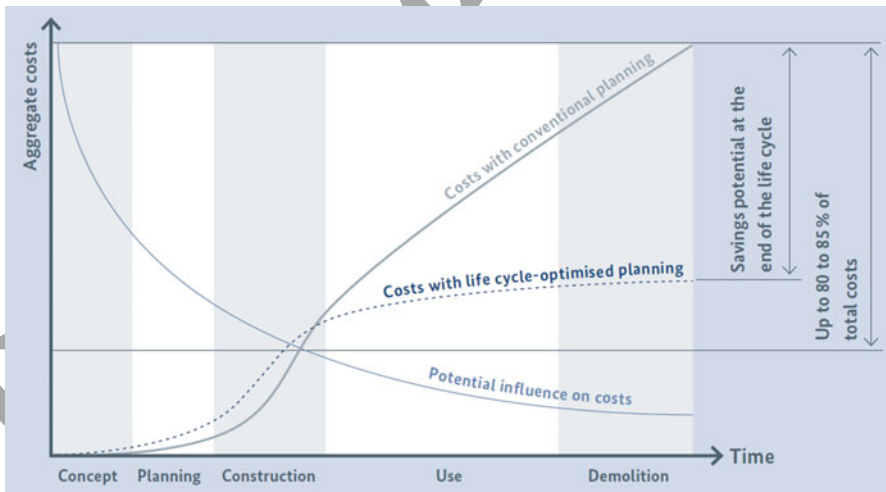


Fig. 6.1 Cost development vs. change potential over building life cycle ([10] in [1])

1.1 Economic Sustainability: Life Cycle Costing

Life cycle costing (LCC) is used to assess the cost implications of the life cycle of a product or system and therewith address the economic dimension of sustainability. However, the implications of LCC for the building sector have not been fully explored because of uncertainties in predicting future costs [8]. A framework is needed to systemically gather data to improve the reliability and decrease the uncertainty of results.

1.2 Environmental Sustainability: Life Cycle Assessment

An (environmental) life cycle assessment (e-LCA) looks at impacts on the environment as a result of the extraction of resources, transportation, production, use, recycling, and discarding of products [13]. The method has been standardized in ISO 14040 and 14044 and is applied by practitioners globally.

1.3 Social Sustainability

In contrast to environmental and economic aspects of sustainability assessment, social assessment still lacks a broad consensus on a standardized method or adequate indicators [5, 6]. The latter may, for example, regard working conditions or health and safety [5, 6]. In the case of the built environment, this may concern either the makers of building materials and products or the people who will be working and living in the building.

Assessing the environmental impact and cost of a whole building over its lifetime is a complex exercise because it requires assessing all its elements and life cycle stages [8]. Most studies focus on either the e-LCA or LCC of whole buildings or life cycle stages in building assembly design; relatively few integrate them [8]. To bring about sustainable development, we need life cycle, systems-oriented thinking frameworks, tools, and methods to support policy and regulation formulation as well as for decision making [6]. Furthermore, such studies are typically performed after crucial design decisions have already been made or even after construction. The research presented here therefore presents a methodology and a tool for integrated economic (LCC) and environmental (e-LCA) assessment of whole-building design variants in an early stage of the design process, with a focus on newly built or largely renovated office buildings. Also, a first attempt is made to integrate social aspects of sustainability, but further research in this area is still required. The aim of the method and tool is to provide guidance and to support multiobjective decision making in the early stages of design

processes to design buildings with a high life cycle value, to achieve the lofty goals for the built environment set for the near future, and to accelerate the application of sustainable combinations of products and systems.

2 Methodology: Life Cycle Value Engineering

Life cycle costing is part of whole-life costing. This approach means that insight is provided in all costs and benefits of a scenario over its entire life cycle, while LCC only includes direct costs (Fig. 6.2) and led to the development of Sustainable Building Accelerator 2.0.

3 Sustainable Building Accelerator 2.0

The name *Sustainable Building Accelerator* indicates both a method and a tool. It was a strategic commercial choice to explicitly call it a method, to transcend the level of tools and spreadsheets. The method involves the generation of design variants based on scenarios and evaluating these variants. For the latter, the tool is used. The question is how it is possible, right from the early design phases, to accelerate the adaptation of new techniques to increase energy performance and, consequently, reduce CO₂ emissions maintaining or increasing indoor comfort levels. This intended acceleration is shown in Fig. 6.3.

Sustainable Building Accelerator 2.0 enables designers to compile variants from building blocks. Because the tool is easy to use, it is suitable for early stages of design processes. Thus, important design decisions can be made quicker, so the design process will be faster, more effective, and less costly. To illustrate and

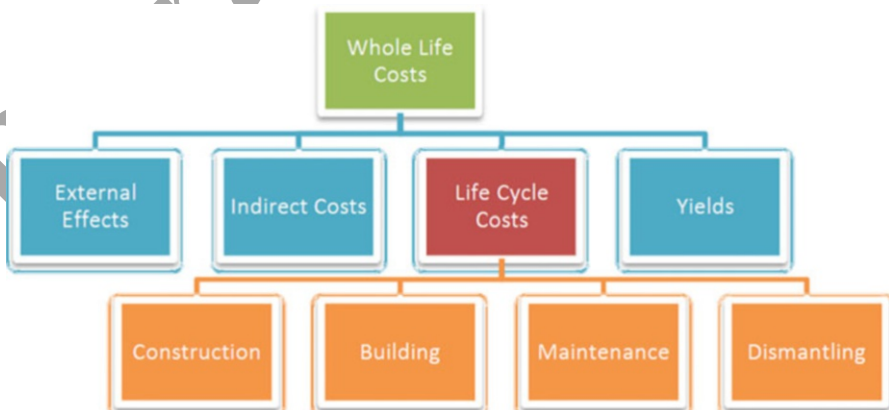


Fig. 6.2 Schematic representation of costs and benefits over buildings' entire life span

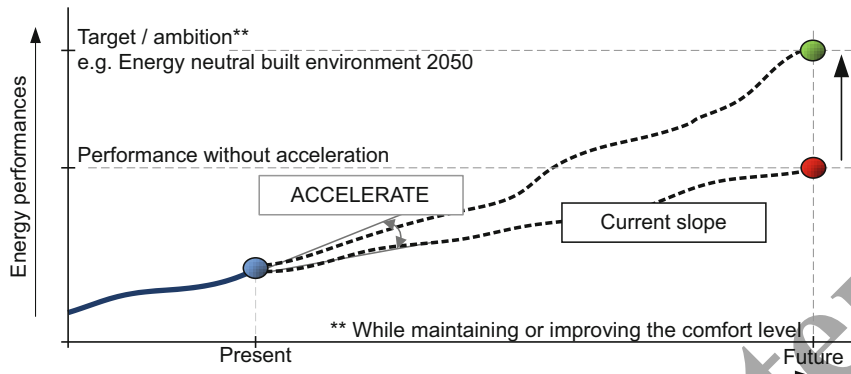


Fig. 6.3 Acceleration of performances is required to meet increasing demand

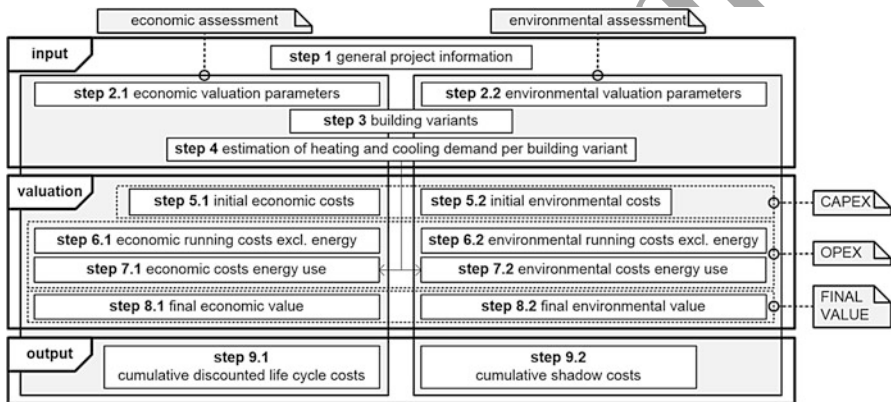


Fig. 6.4 Flowchart of different stages of method

validate the functioning of the tool, several blocks were developed based on a case study project [14]. The first block in this flowchart concerns user input, the second block covers the steps taken for the valuation of building variants, and the third block shows the final results. This section presents the methodology developed for combined economic and environmental assessment of whole (office) building variants using the methods described earlier. The method is presented in a flowchart in Fig. 6.4.

The nine steps are discussed in the following subsections. For a more detailed description, including all equations and resulting assessment variables, see [14]. The word *costs* should always be seen in the context of either economic costs or environmental costs. Environmental costs are expressed as so-called shadow prices, which are the result of extensive research in conformity with the environmental life cycle assessment method.



Fig. 6.5 Case study building

The valuation (second block in Fig. 6.4) of both the economic and environmental costs is divided into initial costs (CAPEX, step 4) and running costs (OPEX, steps 6 and 7), and in both cases the final value (step 8) is subtracted from the costs. The case study project under consideration has to do with Eurojust. This is a newly built office building for an agency of the European Union dealing with judicial cooperation in criminal matters (Fig. 6.5).

Step 1. General project information: The parameters handled in this first step are uniform for all design variants under consideration, such as the building dimensions, its gross floor area, the starting year (reference year), and the duration of the calculation period. In the tool, the shape of the building is simplified to allow for easy assessment: as seen in Fig. 6.6, the buildings' width, depth, height, and number of stories are taken into account.

Step 2. Valuation parameters: All evaluation parameters are assumed constant over time. The valuation parameters relate to both economic and environmental assumptions about prices and price rate developments regarding energy, salaries, and products. Prices and price developments can be set by the tool user since they depend to a large extent on the type of company involved (prices) and their view on how the market will develop (price developments). The material bounded shadow costs are captured in the system blocks. The ecological costs due to energy use are preset. For the environmental impact of energy use (shadow price per kilowatt hour or megajoule), a distinction is made between *green* and *regular* energy (Table 6.1).

Step 3. Building variants: In this step, building variants are compiled. Each building variant consists of building components related to the structure, skin, and

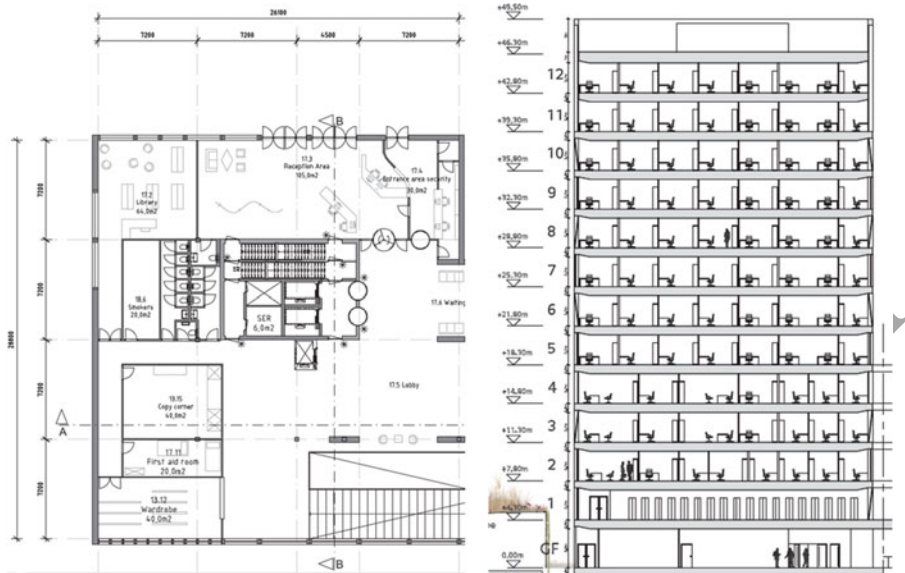


Fig. 6.6 Dimensions of building tower: (a) plan and (b) section valuation parameters

Table 6.1 Shadow prices for energy use (1 MJ gas ≈ 1/3.6 kWh)

		Shadow price
Electricity	Average	€ 0.064025/kWh
	Green electricity	€ 0.008013/kWh
Gas	Natural gas	€ 0.005529/MJ
	Green gas	€ 0.004816/MJ

These values are provided by Nederlands Instituut voor Bouwbiologie en Ecologie bv (NIBE: <http://www.nibe.info>)

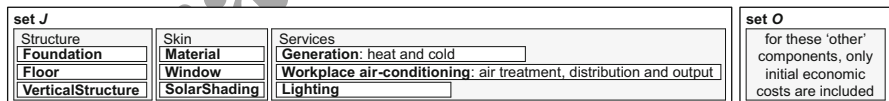


Fig. 6.7 Sets J and O, together representing whole building

services. To give a representative indication of the total economic initial investment, initial costs for other building components are also taken into account (Fig. 6.7).

The building variants are compiled by selecting building blocks. The blocks included in the tool are currently restricted to those assumed to be most influential on the concept of the design: they have to do with strategic choices in an early stage of the design process. For later stages, more components and a more detailed assessment will be required. Furthermore, the mutual influence between the building blocks is currently limited. This implies that the user should ensure correct use

of the method or tool: it is not meant to replace experienced consultants but to support them with insight in the performances of their design solutions. The building blocks used are based on the analysis already performed for the BREEAM-NL application of the case study project Eurojust. However, most of this quantitative data needed for the assessment were not yet widely accessible: the method served as a framework to systematically gather data, and a separate database was developed. All data currently still contain a large degree of uncertainty, and substantial assumptions have been made. The environmental data were obtained from the Dutch National Environmental Database for building materials, a leading initiative in Europe to unify data used for environmental assessment. The economic data are based on a limited amount of projects.

Step 4. Energy consumption calculation: This step involves estimating the secondary heating demand and cooling demand of each building variant. Many methods and tools are available to make this calculation. The estimation of the secondary heating demand and cooling demand of each building variant is made using CASanova, a freely available, easy-to-use tool meant for use in the early design phase to calculate heating and cooling demand.

Step 5. Initial costs: Each component (building block) represents initial costs, economic and environmental. The valuation steps 5–8 are not visualized in the tool because they relate to calculations only. For example, three concepts for workplace climatization are presented in Fig. 6.8. These concepts are represented by both a heating and a cooling table. The output table additionally has an *efficiency* and a *productivity increase* column. These specifications regard the combination of the three components (air treatment, distribution, and output system together). The efficiency affects the primary energy demand resulting from the secondary energy demand, which is estimated in step 4. The productivity increase column is used to determine the benefits for the operational costs (reduction in salary costs, step 6). All components in this section are assumed to have a life span of 20 years (Tables 6.2, 6.3, and 6.4).

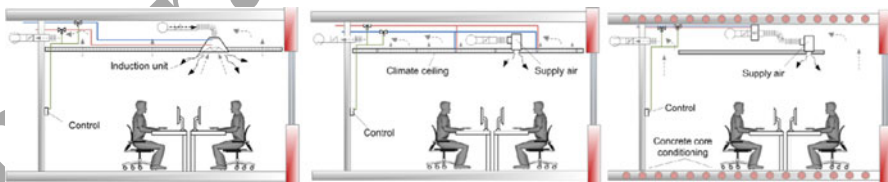


Fig. 6.8 Active ceiling induction units, climate ceiling, and concrete core activation

Table 6.2 Air treatment (functional unit: gross floor area)

TABLE AirTreatment		Search	Show All	Add	Duplicate	Edit	Delete		
rowid	name	lifespan [yr]	CLCC _f	CLCC _m	assembly time [...]	CLCA _f	CLCA _m	code DGBC-dat...	comments
1	Concrete core ...	20	118.06	0	0	0	0	-	-
2	Climate ceiling	20	80.42	0	0	0	0	-	-
3	Active ceiling in...	20	71.71	0	0	0	0	-	-

Table 6.3 Distribution (functional unit: gross floor area)

TABLE Distribution		Search	Show All	Add	Duplicate	Edit	Delete		
rowid	name	lifespan [yr]	CLCC _c	CLCC _m	assembly time [...]	CLCA _c	CLCA _m	code DIBC-dat...	comments
1	Concrete core ...	20	76.26	0	0	0	0	-	-
2	Climate ceiling	20	172.87	0	0	0	0	-	-
3	Active ceiling in...	20	81.52	0	0	0	0	-	-

Table 6.4 Output system (functional unit: gross floor area)

TABLE Output		Search	Show All	Add	Duplicate	Edit	Delete				
rowid	name	lifespan [yr]	CLCC _c	CLCC _m	assembly ti...	CLCA _c	CLCA _m	efficiency [%]	code DIBC-...	comments	productivity ...
1	Concrete co...	20	50.15	0	0	0	0	60	-	-	0
2	Climate ceiling	20	49.36	0	0	0	0	80	-	-	0.5
3	Active ceiling...	20	56.6	0	0	0	0	90	-	-	0.25

- *Active ceiling induction units:* This all-air concept is used as the reference situation. The room is conditioned by the supplied air (Fig. 6.8). This combination of components is assumed to have an efficiency of 90 % and to result in a productivity increase of 0 %.
- *Climate ceiling:* The rooms are heated and cooled by the climate ceilings (Fig. 6.8). This combination of components is assumed to have an efficiency of 80 % and to result in a productivity increase of 0.5 %.
- *Concrete core activation (VAVI met NV):* This combination of components is assumed to have an efficiency of 60 % and to result in a productivity increase of 0.25 % (Fig. 6.8).

Step 6. Running costs excluding energy: The economic running costs excluding energy relate to maintenance costs, costs for periodic replacements, and operational costs. The latter are influenced by the indoor climate: a comfortable climate will result in a higher productivity of staff and will thus yield savings in labor (salary) costs.

Step 7. Energy costs: The energy costs are assumed to be dependent on the energy consumption for workplace air-conditioning (heating, cooling, and ventilation) and lighting. The annual primary energy demand for workplace air-conditioning is dependent on the heating and cooling demand per square meter, the building’s gross floor area, the coefficient of performance of heat and cold generation, and the efficiency of the workplace air-conditioning concept.

Step 8. Final value: The final value of each component is the value that this component has at the end of the calculation period. This value is determined by straight-line depreciation of the last replacement costs until the end of the calculation period [4].

Step 9. Results: Table 6.5 presents the assessment variables at each step, and Fig. 6.9 presents all the results visually.

Table 6.5 Nomenclature of all assessment variables, presented per method stage step

Symbol	Description	Unit	Symbol	Description	Unit
Step 1					
W	Building width (length of north + south façade)	[m]	GFA	Gross floor area	[m ²]
d	Building depth (length of east + west façade)	[mL]	τ_0	Starting year	[–]
h	Building height	[m]	τ	Calculation period	[Year]
n	Number of stories	[–]	H_{wk}	Hours in use per week (52 weeks a year)	[Hour]
Step 2					
$R_{LCC,e,e}$	Price development rate for electricity	[%]	$P_{LCC,e,e}$	Economic price for electricity	[€/kWh]
$R_{LCC,e,g}$	Price development rate for gas	[%]	$P_{LCC,e,g}$	Economic price for gas	[€/kWh]
$R_{LCC,s}$	Price development rate for salary	[%]	$P_{LCC,s}$	Economic salary price	[/m ² × year]
$R_{LCC,p}$	Price development rate for products	[%]	$P_{LCA,e,e}$	Environmental price for electricity	[€/kWh]
R_{in}	Inflation rate	[%]	P_{LCA}	Environmental price for gas	[€/kWh]
R	Market interest rate	[%]	$R_d(t)$	Discount rate as a function of time	[–]
R_r	Real interest rate	[%]			
Step 3					
All components (Fig. 6.2)					
t_n^j	Lifespan	[Year]	R_c^j	Additional for floors, skin materials, and windows	
$C_{LCC,i}^j$	Economic initial costs	[€]		Thermal resistance	[m ² × K/W]
$C_{LCC,m}^j$	Economic costs, maintenance	[€/year]		Additional for heat ($x = h$) and cold ($x = c$) generation	
$C_{LCC,r,p}^j$	Economic costs, replacements (products)	[€/n _r]	COP_x	Coefficient of performance	[–]
$C_{LCC,r,h}^j$	Economic costs, replacements (labor)	[€/n _r]	$F_{x,e}$	Fraction electricity	[%]
$C_{LCA,i}^j$	Environmental initial costs	[€]	$F_{x,g}$	Fraction gas	[%]
				Additional for workplace air-conditioning concept	

$C_{LCA,m}^j$	Environmental costs, maintenance	[€/year]	η	Efficiency	[%]
$C_{LCA,r,p}^j$	Environmental costs, replacements (products)	[€/n _r]	pro/ncr	Expected productivity increase	[%]
$C_{LCC,i}^0$	Other components only (Fig. 6.2)			Additional for lighting	
	Initial economic costs, other components	[€]	W_l	Power (work)	[kWh/(m ² × h)]
Step 4					
$C_{LCC,i}^B$	Total economic initial costs	[€]	$C_{LCA,i}^B$	Total environmental initial costs	[€]
Step 5					
$C_{LCC,o}^B$	Total economic operational costs	[€]	n_t^j	Number of replacements of component j	[-]
$C_{LCC,m}^B$	Total economic running costs	[€]	$C_{LCA,m}^B$	Total environmental running costs	[€]
Step 6					
$E_{s,h}^B$	Secondary heating energy demand	[kWh/(m ² × year)]	$E_{s,c}^B$	Secondary cooling energy demand	[kWh/(m ² × year)]
Step 7					
$E_{p,h}^B$	Primary heating energy demand	[kWh/year]	$E_{p,c}^B$	Primary cooling energy demand	[kWh/year]
$C_{LCC,e}^B$	Total economic costs, energy	[€/year]	$C_{LCA,e}^B$	Total environmental costs energy	[€/year]
Step 8					
$V_{LCC,f}^B$	Total final economic value	[€]	$V_{LCA,f}^B$	Total final environmental value	[€]
Step 9					
C_{LCC}^B	Total economic costs	[€]	C_{LCA}^B	Total environmental costs	[€]

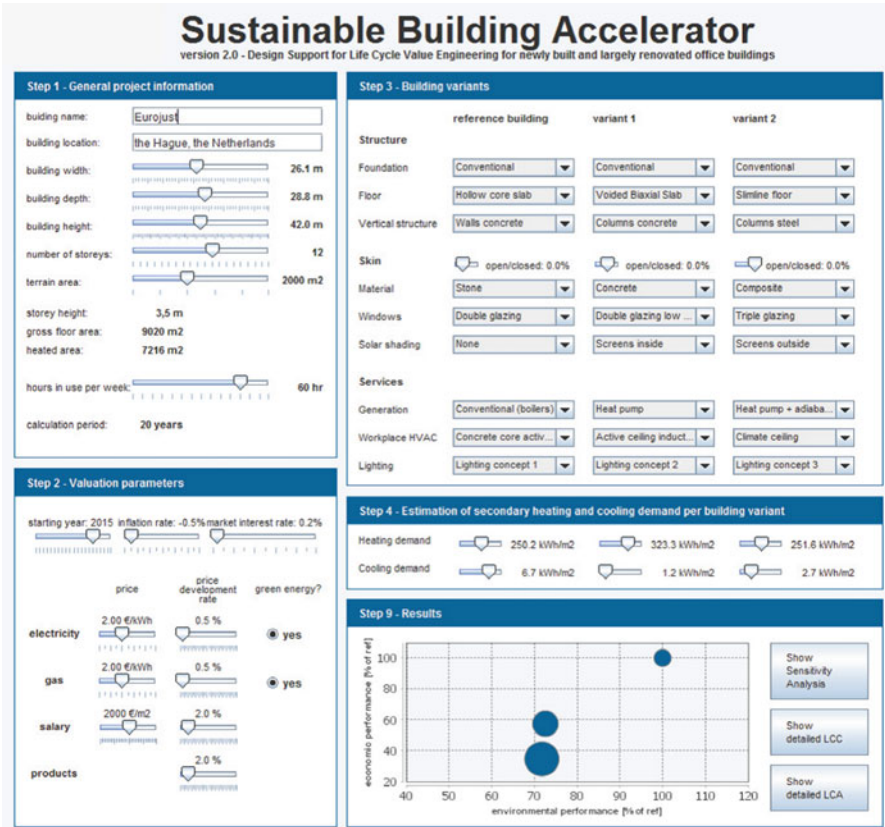


Fig. 6.9 Screen presentation of all results from sustainable building accelerator

The total costs are found by adding the initial costs, the running costs, and the energy costs. The final value of the building under consideration is subtracted from these costs. Final results are presented graphically: economic and environmental performances are indicated on the y- and x-axes, respectively. The size of the bubble gives an indication of user comfort as a first attempt to integrate social aspects of sustainability. For the latter, the expected productivity increase in staff is used because it gives an indication of the extent to which a healthy and comfortable indoor environment is created. Since the absolute cumulative economic and environmental costs are hard to interpret, they are presented as a percentage of the first building compiled, which is the reference building. These (relative) results serve as a basis to compare variants: the tradeoff is up to the designer. Both the method and the tool therewith support multiobjective decision making in an early stage of the design process with the goal of engineering buildings with a high life cycle value. They provide guidance in the design of newly built or largely renovated office buildings by giving insight into the (relative) life cycle economic and

environmental performances of whole-building design variants. A first attempt is made to integrate aspects of social sustainability to complementarily address the three dimensions of sustainable development and therewith move toward holistic LCSA.

4 Detailed LCC and LCA Results

Finally, the tool provides the option of showing more detailed results of both the economic and environmental assessment (per component and as a function of time). The detailed LCC results can be used for an application for BREEAM-NL credit MAN 12 [3] for the early stages of the design process as variants for the structure, skin, and services are assessed (Fig. 6.10).

5 Sensitivity Analysis

Furthermore, the tool provide insight into the sensitivity of the results to variations in the input parameters. Currently, the sensitivity analysis is performed symmetrically around the value assumed for the parameter under consideration. This could also be set differently if the expected range of a parameter is not symmetrical (Fig. 6.11).

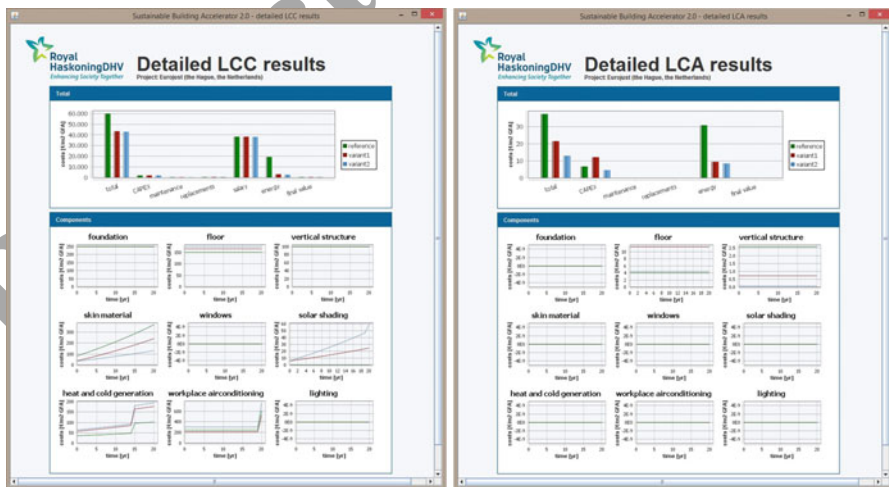


Fig. 6.10 Tool to show detailed results of (a) economic and (b) environmental assessment

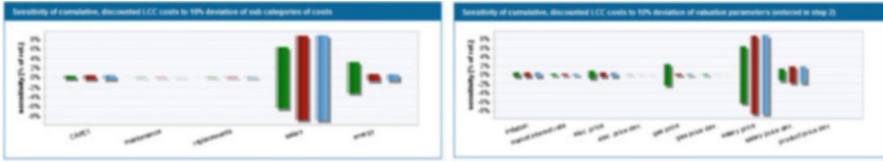


Fig. 6.11 Tool to give insight into the sensitivity of results for variations in input parameters

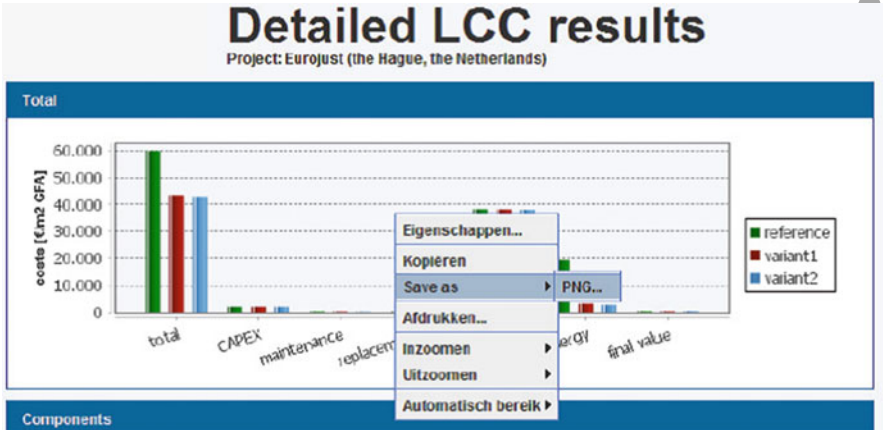


Fig. 6.12 Right clicking on a graph enables copying or storing figure

6 Using the Results

All results presented in a graph (Fig. 6.12) can easily be saved or copied to include them in, for example, a LCC report. For most graphs it is also possible to zoom in and out.

7 Discussion and Future Work

The components included in the tool are currently restricted to those assumed to be most influential on the concept of the design: they relate to strategic choices in an early stage of the design process. For later stages, more components and a more detailed assessment will be required. Furthermore, the mutual influence between building blocks is currently limited. This implies that the user should ensure correct use of the method or tool; it is not meant to replace experienced consultants but to support them with insight into the quantitative performances of their design solutions. Since the result of the assessment is highly dependent on the reliability of input variables and most of the data needed for this assessment are often not yet available, the method serves as a framework for systematic data gathering to improve the reliability of results in the near future.

8 Conclusions

The novel approach introduced in this chapter entails building design-oriented life cycle value costing analysis in the earliest, crucial design stages for future life cycle building performance, when only low-resolution design information is available on which to base decision making. The presented tool supports multiobjective decision making in an early stage of the building design process with the goal of developing buildings with a high life cycle value. They provide guidance in the design of buildings by giving insight into the life cycle economic and environmental performances of whole-building design variants.

References

1. BMUB (2014) Guideline for sustainable building. Federal Ministry for the environment, nature conservation, building and nuclear safety, 11055 Berlin
2. Bogenstätter U (2000) Prediction and optimization of life-cycle costs in early design. *Build Res Inform* 28(5&6):376–386
3. DGBC (2014) Dutch Green Building Council, BREEAM.NL, BRE Global Ltd. 2012, Rotterdam
4. ECS (2007) European committee for standardization. EN 15459 Energy performance of buildings—economic evaluation procedure for energy systems in buildings. CEN, Brussels
5. Geibler J, Walbaum H, Liedke C (2006) Development of sustainable bioprocesses: modelling and assessment. Wiley, Chichester, pp 82–113
6. Halog A, Manik Y (2011) Advancing integrated systems modelling framework for life cycle sustainability assessment. *Sustainability* 3(2):469–499
7. Hofer G, Grim M, Herzog B (2011) Calculating life cycle cost in the early design phase to encourage energy efficient and sustainable buildings. In: Proceedings ECEEE 2011 SUMMER STUDY, Energy efficiency first: the foundation of a low-carbon society
8. Islam H, Jollands M, Setunge S (2014) Life cycle assessment and life cycle cost implication of residential buildings—a review. *Renew Sustain Energy Rev* 42:29–140
9. Jakob M (2006) Marginal costs and co-benefits of energy efficiency investments: the case of the Swiss residential sector. *Energy Policy* 34(2):172–187
10. Jones Lang LaSalle (2008) Green Building, Nachhaltigkeit und Bestanderhalt in der Immobilienwirtschaft [in German]
11. Kneifel J (2010) Life-cycle carbon and cost analysis of energy efficiency measures in new commercial buildings. *Energy Build* 42(3):333–340
12. Kovacic I, Zoller V (2015) Building life cycle optimization tools for early design phases. *Energy* 92: 409–419. <http://dx.doi.org/10.1016/j.energy.2015.03.027>
13. Valdivia S, Sonnemann G (2011) Towards a life cycle sustainability assessment: making informed choices on products, UNEP/SETAC: life cycle initiative
14. Vanderveen A (2015) Design support for life cycle value engineering. Sustainable building accelerator 2.0. Towards life cycle sustainable assessment and application for whole building design. Master report TU/e, 19 March 2015
15. WCED (1987) World commission on environment and development, our common future. Oxford University Press, Oxford

Chapter 7

A Comparative Study Between Photovoltaic Pumping Systems Using a Permanent Magnet DC Motor and an Induction Motor

S. Abdourraziq and R. El Bachtiri

Abstract The solar power source for pumping water is one of the most promising areas in photovoltaic (PV) applications. This chapter presents a comparative study of a PV pumping system driven by a permanent magnet DC motor and one driven by an AC motor. The studied system consists of a PV array, a DC–DC boost converter, an inverter, a motor–pump set, and a storage tank. In addition, we use a maximum power point tracking algorithm to improve the efficiency of the PV system. The comparison was carried out to define the characteristics and the performance of each system. Each subsystem is modeled to simulate the whole system in MATLAB/Simulink. The results obtained from the simulation of the system are satisfactory.

Keywords Photovoltaic pumping system • Permanent magnet DC motor pump • AC motor pump • DC–DC boost converter

1 Introduction

Renewable energy sources are being increasingly implemented in many applications owing to growing concerns over environmental pollution. The photovoltaic (PV) pumping system has become one of the most promising areas for PV applications. To achieve the most reliable and economical operation, more attention is being paid to their design and optimal use [1]. Depending on the state of the location, pumped water can be used in many applications such as domestic use, irrigation, and village water supplies [2, 3]. Several types of pumps and motors are available on the PV pumping market. Various studies have been done on the choice of drive system, which relates to the PV source, type of pump to use, and ways to control and optimize the whole system.

S. Abdourraziq (✉) • R. El Bachtiri
LESSI Lab FSDM, REEPER Group, EST, Sidi Mohammed Ben Abdellah University,
Fez, Morocco
e-mail: sarah.abdourraziq@usmba.ac.ma; rachdi.elbachtiri@usmba.ac.ma

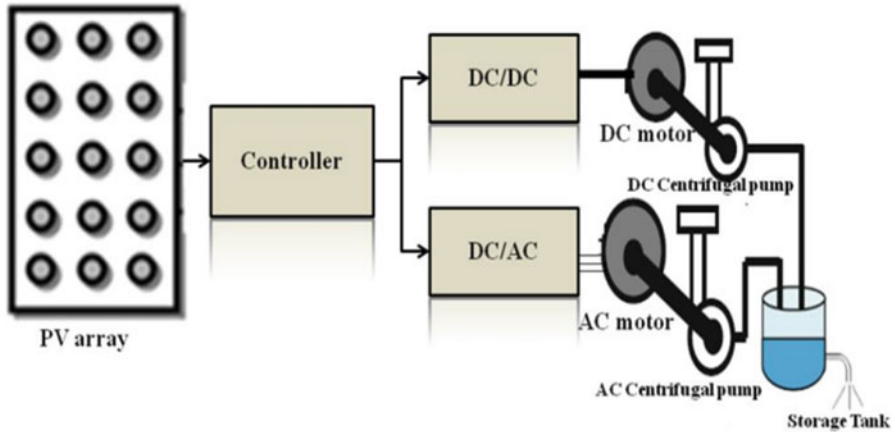


Fig. 7.1 General configuration of a PV pumping system

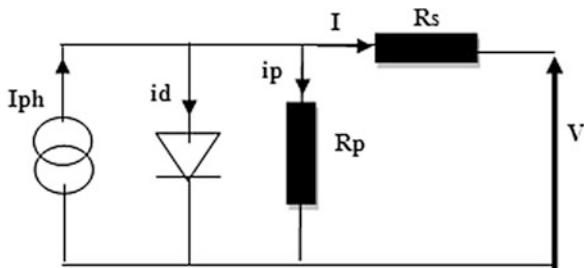
The most commonly employed pump type is the centrifugal pump. Single-stage centrifugal pumps are frequently used in PV shallow water pumping for low head applications. For PV subterranean water pumping and surface water pumping with higher heads, multistage centrifugal pumps are more suitable. Other pump types, such as progressive cavity pumps [4] and piston pumps [3], have also been used. Power conditioning plays a role in optimizing the transfer of energy between the PV array and the motor-pump set. Power conditioning can be a DC/AC inverter for an AC electric motor or a DC/DC inverter for a DC electric motor. The motor used in the PV pumping systems is one of two main types, either induction motor or DC motor [5–7].

In this chapter, we propose a model of two different configurations of a photovoltaic pumping system (PVPS), the first one driven by a DC motor, the second one entrained by an induction motor. The performance of each system is analyzed. The studied systems were tested in a MATLAB/Simulink environment to define the characteristics and efficiency of each subsystem. A block diagram of the PVPS studied is shown in Fig. 7.1.

2 PV Panel Model

A PV cell is a $p-n$ junction semiconductor that converts light into electricity. In the literature, several mathematical models describe the $I-V$ characteristic [8, 9]. The difference between each model is the procedure for the calculation, the intervening number of parameters to compute the $I-V$ characteristic, and the accuracy of the results. The equivalent circuit of a PV cell is shown in Fig. 7.2.

Fig. 7.2 Equivalent circuit of PV cell



The behavior of a PV array may be described by the following equations:

$$I = I_{ph} - I_d - I_p, \tag{7.1}$$

with

$$I_d = I_o \left(\exp \left(\frac{V_j \cdot q}{K_o \cdot T} \right) - 1 \right) \tag{7.2}$$

and

$$I_p = \frac{V + R_s \cdot I}{R_p}, \tag{7.3}$$

$$I = I_{ph} - I_o \left(\exp \left(\frac{V_j q}{K_o T} \right) - 1 \right) - \frac{V + R_s \cdot I}{R_p}, \tag{7.4}$$

where V is the PV output voltage, I the PV output current, I_{ph} the photocurrent, I_o the saturation current, R_s the series resistance, R_p the shunt resistance, q the electronic charge, n the diode factor, K Boltzmann's constant, and T the junction temperature.

The output characteristics of the voltage power and voltage current of a PV panel called SES96M, under different values of radiation at $T = 25 \text{ }^\circ\text{C}$, are presented in Fig. 7.3.

3 PV Pumping Subsystem Models

The PVPS entrained by a motor-pump group consists of a PV panel, a DC-DC boost converter, an inverter (for the AC motor), and a motor-pump set. The modeling of each component is described in the following paragraphs.

3.1 DC-DC Boost Converter Model

The DC-DC boost converter is inserted between the solar generator and the motor-pump set and used as an adapter between the PV generator and the load. Its purpose

Fig. 7.3 Output characteristics of PV array at $T = 25\text{ }^{\circ}\text{C}$. (a) $V-P$, (b) $V-I$

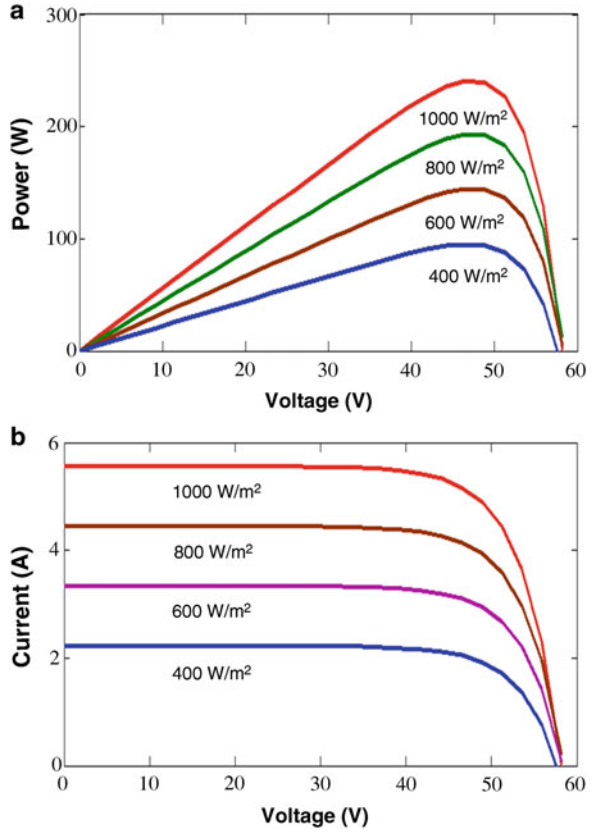
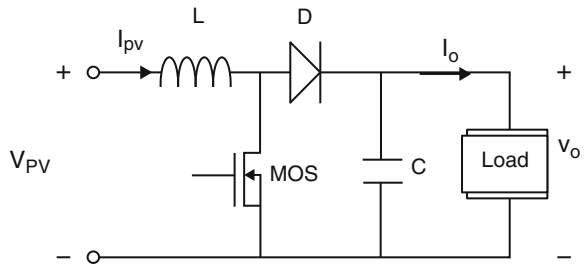


Fig. 7.4 DC-DC boost converter



is to make the solar array operate at an operating point corresponding to the maximum output power by adjusting the duty cycle α . A circuit diagram of a boost converter is shown in Fig. 7.4.

The equation of the output voltage depending on the input voltage and the duty cycle α can be expressed as

$$V_o = \frac{1}{1 - \alpha} V_{pv}. \tag{7.5}$$

3.2 Maximum Power Point Tracking Algorithm

The DC–DC boost converter is used as an adapter between the PV panels and motor–pump set to force the panels to operate at their maximum power point. In the literature, a variety of maximum power point tracking (MPPT) techniques have been proposed, including fractional open-circuit voltage [10], fractional short-circuit current [10], perturb and observe (P&O) [11–13], incremental conductance [14], and fuzzy logic control command [15]. These algorithms vary in their complexity, efficiency, cost, and potential applications. In this chapter we use the P&O MPPT method; it is the most commonly used algorithm for PV systems. Its principle is simple (a flowchart of the traditional P&O algorithm is shown in Fig. 7.5):

$$\frac{dP}{dV}(n) = \frac{P(n) - P(n - 1)}{V(n) - V(n - 1)}, \tag{7.6}$$

$$P(n) = V(n).I(n). \tag{7.7}$$

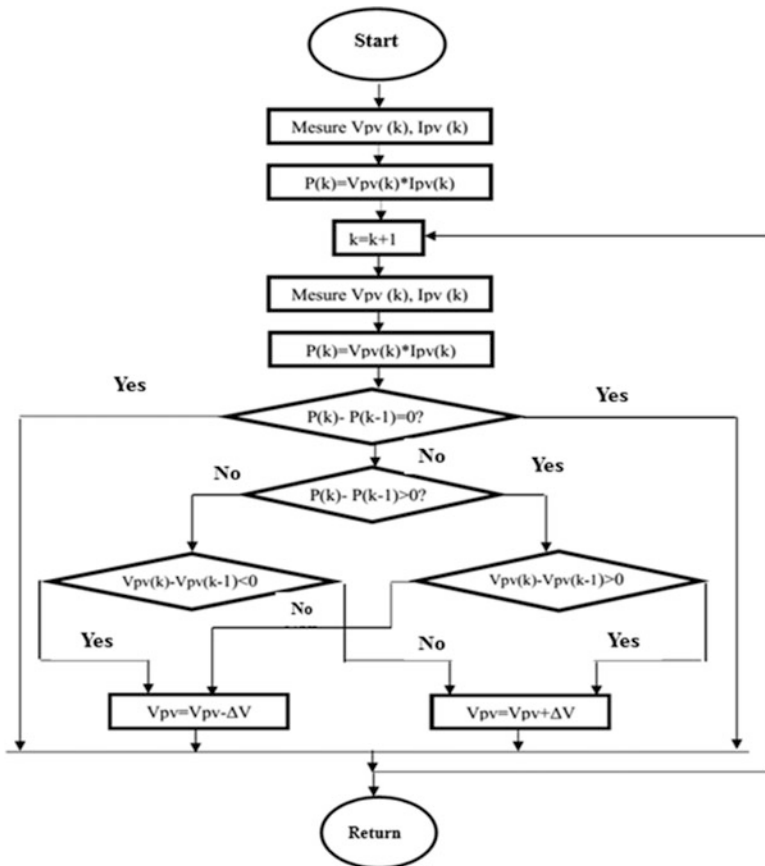


Fig. 7.5 General flowchart of perturb and observe method

3.3 Inverter

The DC–AC inverter provides a three-phase system of voltages that vary in amplitude and frequency according to the solar radiation. They vary from 0.1 up to 1 times the rated voltage and frequency [16], depending on the loads and climatic conditions:

$$\begin{bmatrix} V_{as} \\ V_{bs} \\ V_{cs} \end{bmatrix} = \frac{\alpha V_{pv}}{3} \begin{bmatrix} 2 & -1 & -1 \\ -1 & 2 & -1 \\ -1 & -1 & 2 \end{bmatrix} \begin{bmatrix} f_{ca} \\ f_{cb} \\ f_{cc} \end{bmatrix}, \quad (7.8)$$

where αV_{pv} is the input voltage, and f_{ca} , f_{cb} , and f_{cc} are the pulse width modulation (PWM) control signals.

3.4 PMDC Motor Model

Many PVPSs use DC motors because they can be directly coupled to PV panels, making for a very simple system. The direct coupling of series, shunts, and separately excited DC motor PVPSs was studied in [2–17]. Permanent magnet DC (PMDC) motors are most commonly used in PVPSs. The mathematical relation that describes the dynamic model of a DC motor with constant magnetic flux can be expressed as follows:

$$V = E + IR + V_b \quad \text{Terminal voltage of armature,} \quad (7.9)$$

$$E = K\Phi\omega \quad \text{Electromotive force,} \quad (7.10)$$

$$T_e = K'\Phi I \quad \text{Electromagnetic torque,} \quad (7.11)$$

where K' is the constant torque, Φ the magnetic flux through the turns, K the constant of electromotive force, R the armature resistance, V_b the brush voltage drop, and ω the angular speed of the rotor.

3.5 Induction Motor Model

The mathematical dynamic model of a three-phase, connected induction motor is described by the following equation set [18]:

- Stator voltage equations:

$$\left\{ \begin{array}{l} V_{ds} = R_s I_{ds} \frac{d\theta_{ds}}{dt}, \\ \end{array} \right. \quad (7.12)$$

$$V_{qs} = R_s I_{qs} \frac{d\Phi_{qs}}{dt}, \quad (7.13)$$

where (I_{ds}, I_{qs}) , (V_{ds}, V_{qs}) , and (Φ_{ds}, Φ_{qs}) are the (d, q) components of the stator current, voltage, and flux, and R_s is the stator resistance.

- Rotor voltage equations:

$$\left\{ \begin{array}{l} 0 = V_{dr} = R_r I_{dr} \frac{d\Phi_{dr}}{dt} + p \omega_{rAC} \Phi_{qr}, \\ 0 = V_{qr} = R_r I_{qr} \frac{d\Phi_{qr}}{dt} + p \omega_{rAC} \Phi_{dr}, \end{array} \right. \quad (7.14)$$

$$\left\{ \begin{array}{l} 0 = V_{dr} = R_r I_{dr} \frac{d\Phi_{dr}}{dt} + p \omega_{rAC} \Phi_{qr}, \\ 0 = V_{qr} = R_r I_{qr} \frac{d\Phi_{qr}}{dt} + p \omega_{rAC} \Phi_{dr}, \end{array} \right. \quad (7.15)$$

where I_{dr} and I_{qr} are the (d, q) rotor currents, Φ_{qr} and Φ_{dr} are the (d, q) rotor fluxes, and R_r is the rotor resistance.

3.6 Centrifugal Pump

Depending on the application and the water sources (e.g., wells, drilling, pumping river), different types of pumps are used. In a PV pump, centrifugal and volumetric pumps are the most widely used [16]. The centrifugal pump considered in this study applies a torque proportional to the square of the rotational speed of the motor [19]:

$$T_r = K_c * \omega^2 \quad (7.16)$$

where K_c is the proportionality constant [(Nm/rad/s)²] and ω is the rotational speed of the motor (rad/s).

Any pump is characterized by its absorptive power, which is obviously a mechanical power on the shaft coupled to the pump, which is given by

$$P = \frac{\rho g H Q}{\eta}, \quad (7.17)$$

where η is the overall performance, ρ the fluid density (kg/m³), g the gravity acceleration (m²/s); H the height of the rise (m), and Q the water flow (m³/s).

4 Simulation of PMDC Motor–Pump System

The overall simulation model of the DC pumping system fed by solar array is shown in Fig. 7.6.

The output performance characteristics of the DC–DC boost converter and DC motor are shown in Figs. 7.7 and 7.8.

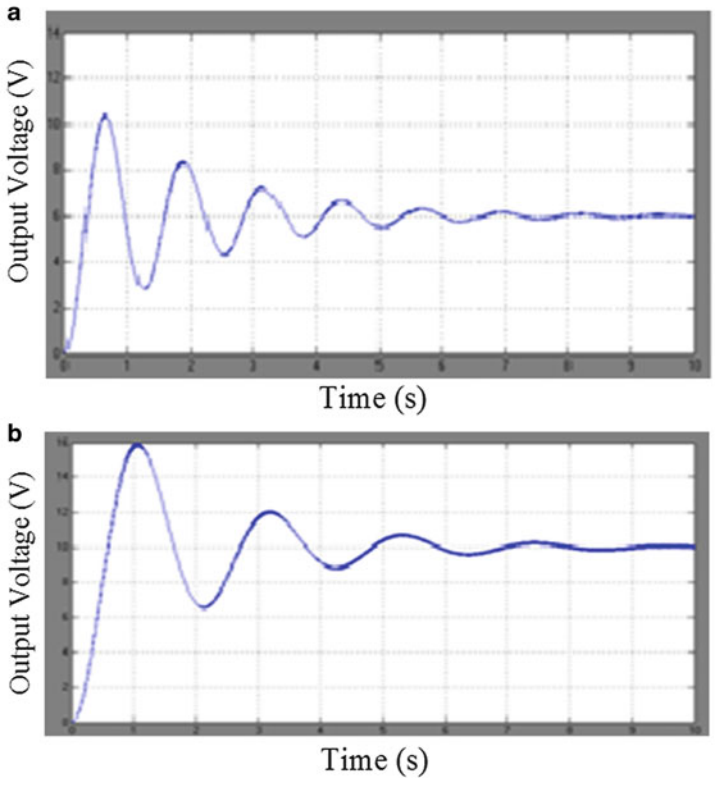
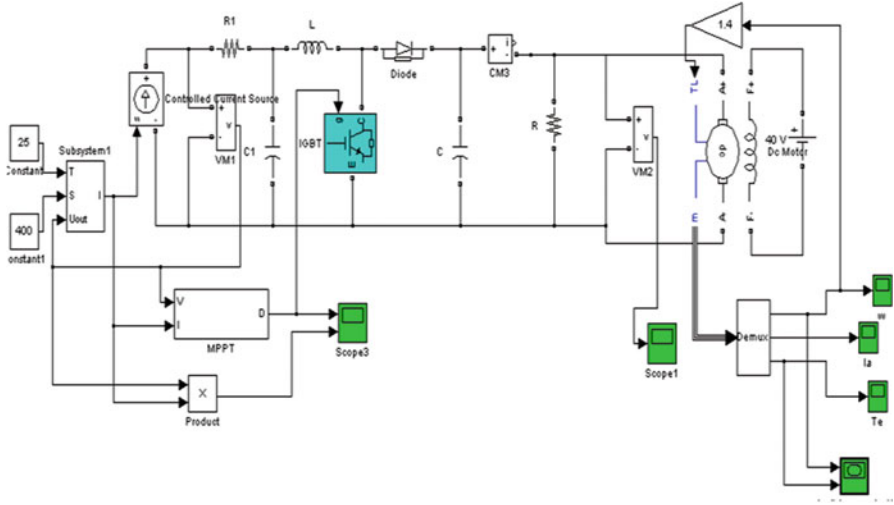


Fig. 7.6 Simulink diagram of PV-based DC motor system. (a) Output voltage of DC–DC boost converter for $V_{pv} = 3$ V and $\alpha = 0.5$. (b) Output voltage of DC–DC boost converter for $V_{pv} = 3$ V and $\alpha = 0.7$

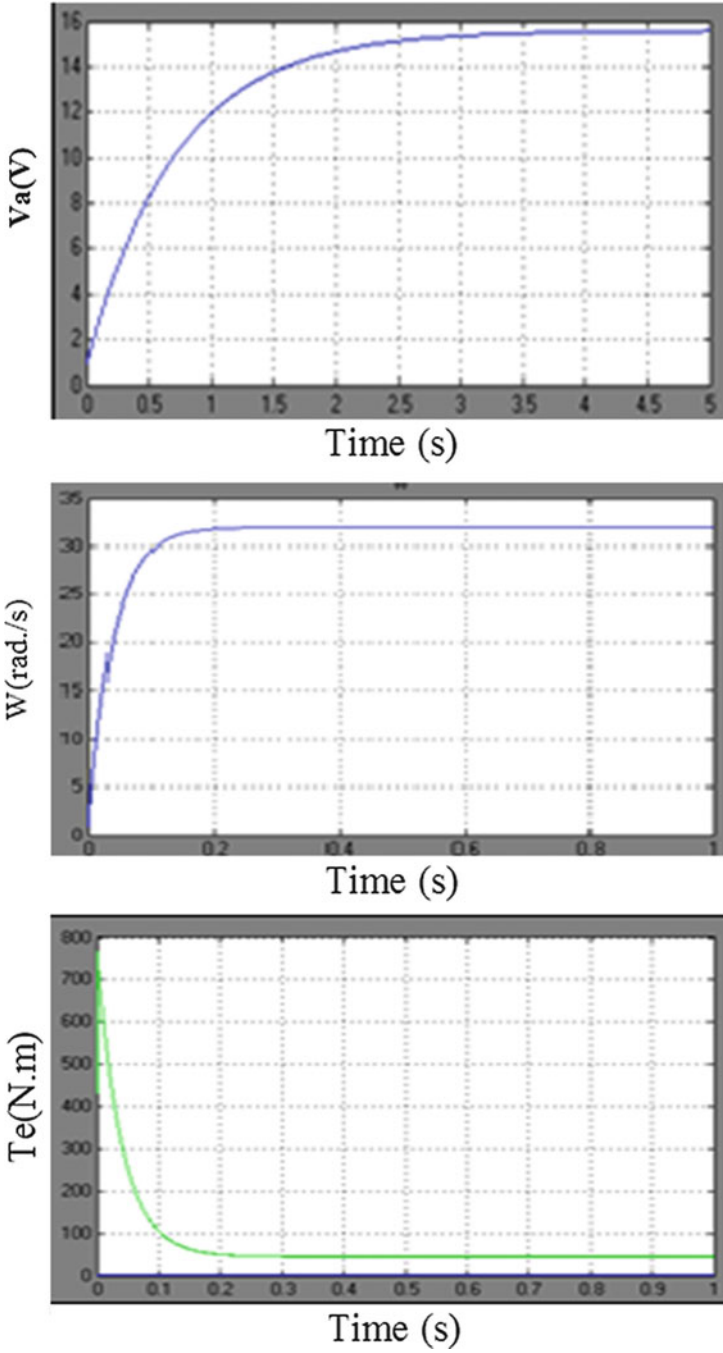


Fig. 7.7 Simulink output of PMDC motor characteristics

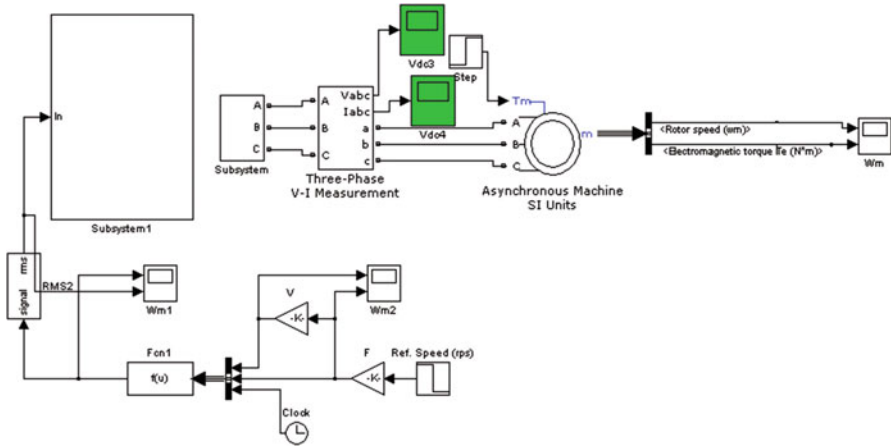


Fig. 7.8 Simulink diagram of PV-based induction motor system

5 Simulation of Induction Motor–Pump System

AC induction motors are being used increasingly for PV pumping systems. The simulation results of a PVPS driven by an AC motor system are shown in the figures (Fig. 7.9).

6 Conclusion

This work has presented the performance of two different configurations of PVPSs; it lays the foundation for the modeling and simulation of PV drive systems using MATLAB/Simulink. The various components, like PV panels, boost regulator, and motor–pump driving system, were modeled and validated using MATLAB. A comparison was made to show the advantages and drawbacks of each method so as to determine the more efficient method, and a comparison was made to show the advantages and drawbacks of each type of motor. The results obtained from the simulation of the system are satisfactory and will make it possible to provide a very high speed of rotation in an AC motor compared to a PMDC motor (Fig. 7.10), which is an important source of power for driving a pump.

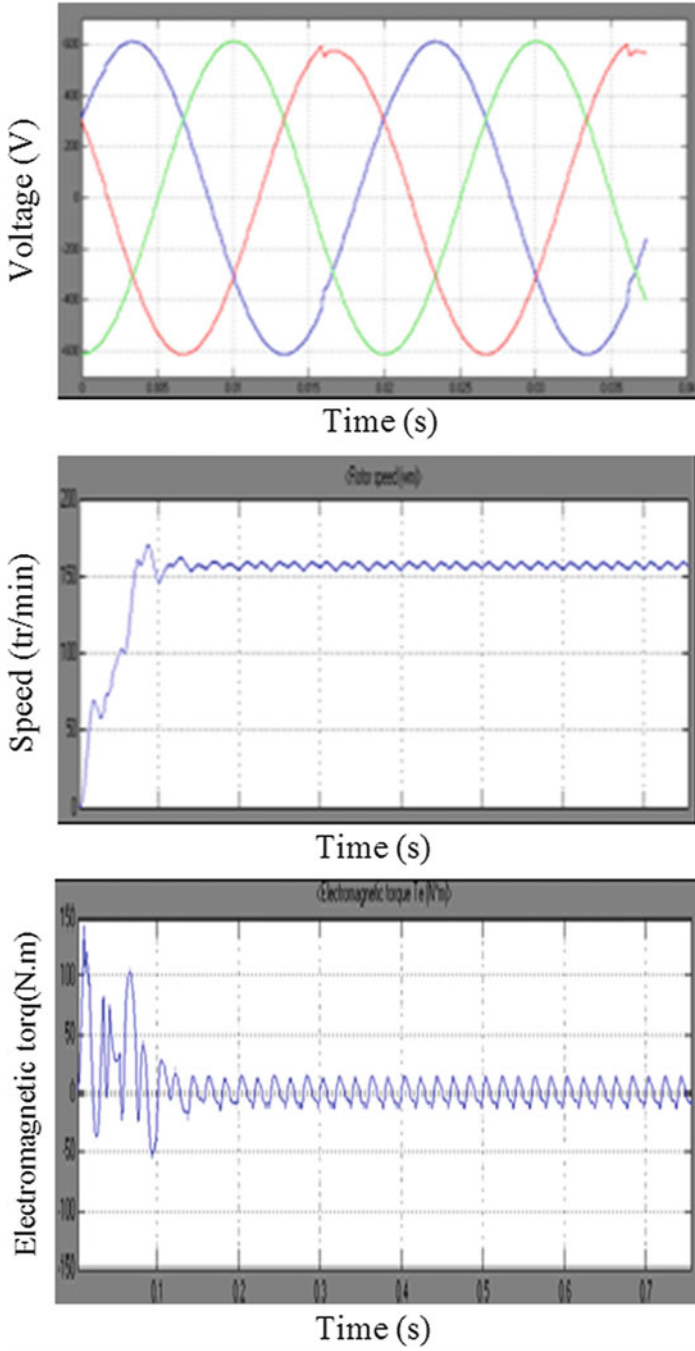


Fig. 7.9 Simulink output of induction motor characteristics

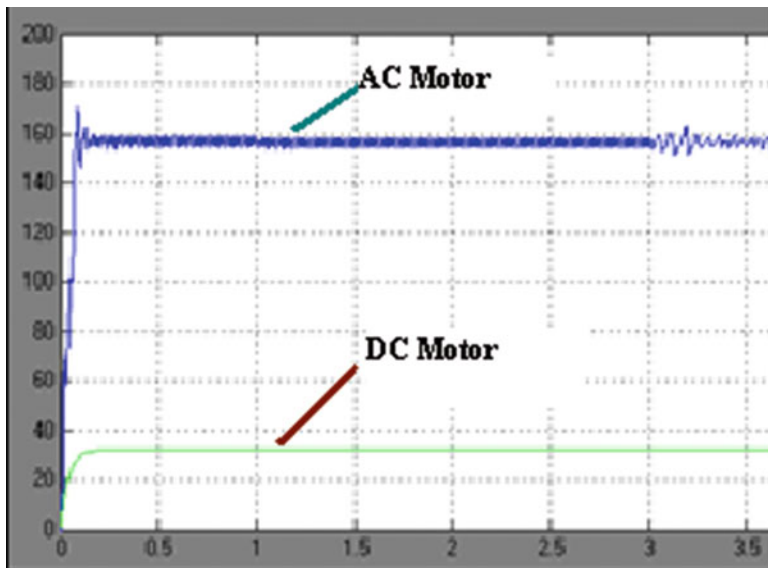


Fig. 7.10 Comparison between speed of PMDC motor and that of an induction motor

References

1. Abdourraziq S, El Bachtiri R (2013) Modeling of a photovoltaic pumping system using centrifugal pump and DC motor. *Sustain Energy Buildings* 2:1–6, mgf13s-002. Mediterranean Green Energy Forum 2013 (MGEF-13)
2. Moussi AT (2002) An improved efficiency permanent magnet brushless DC motor PV pumping system. *Larhyss J* No. 01, Mai 2002. <http://dx.doi.org/10.1115/isec2005-76253>
3. Betka A, Attal A (2010) Optimization of a photovoltaic pumping system based on the optimal control theory. *Solar Energy* 84:1273–1283
4. Nejib H, Moncef J (2009) Theoretical and experimental analysis of the behaviour of a photovoltaic pumping system. *Solar Energy* 83:1335–1344
5. Elgendy MA, Zahawi B (2010) Comparison of directly connected and constant voltage controlled photovoltaic pumping systems. *IEEE Trans Sustain Energy* 1(3):184–192
6. Corrêa TP, Seleme SI Jr (2012) Efficiency optimization in stand-alone photovoltaic pumping system. *Renew Energy* 41:220–226
7. Davies JL, Malengret M (1992) Application of induction motor for solar water pumping, 0-7803-0835-2/92. In: AFRICON '92 Proceedings, Third AFRICON Conference, Ezulwini Valley
8. Badia A, Abderrezak G (2012) A simple behavioural model for solar module electric characteristics based on the first order system step response for MPPT study and comparison. *Appl Energy* 91:395–404
9. Kadri R, Andrei H (2012) Modeling of the photovoltaic cell circuit parameters for optimum connection model and real-time emulator with partial shadow conditions. *Energy* 42:57–67
10. de Brito MAG, Luigi G (2013) Evaluation of the main MPPT techniques for photovoltaic applications. *IEEE Trans Indus Electron* 60(3):1156–1166
11. Elgendy MA, Zahawi B (2012) Assessment of perturb and observe MPPT algorithm implementation techniques for PV pumping applications. *IEEE Trans Sustain Energy* 3(1):21–33

12. Sarah A, Rachid EB (2012) A perturb and observe method using fuzzy logic control for PV pumping system. In: IEEE multimedia computing and systems (ICMCS'14), pp 1608–1612
13. Abdourraziq S, Bachtiri R (2014) A perturb and observe method using dual fuzzy logic control for resistive load. In: Recent advances in environmental science and biomedicine, ISBN: 978-960-474-391-9, pp 107–112
14. Elgendy MA, Zahawi B (2013) Assessment of the incremental conductance maximum power point tracking algorithm. IEEE Trans Sustain Energy 4(1):108–117
15. Abdourraziq S, El Bachtiri R (2014) A novel MPPT dual fuzzy logic applied to resistive load and PV pumping system. Int Rev Automat Control 7(4):446–452
16. Jraidi M, Hamrouni N, Cherif A, Dhoub A (2004) Modélisation et Simulation des Systèmes de Pompage Photovoltaïque avec de nouvelles stratégies de commande. JTEA, Hammamet, Tunisie
17. Benlarb K, Mokrani L (2004) A fuzzy global efficiency optimization of a photovoltaic water pumping system. Solar Energy 77:203–216
18. Rekioua D, Rekioua T, Laporte B, Benmahammed K (2001) Design of a position sensor for torque ripple minimization of VSI fed self synchronous machine. Int J Electron 88(7):158
19. Arrouf M, Ghabrou S (2007) Modelling and simulation of a pumping system fed by photovoltaic generator within the Matlab/Simulink programming environment. ScienceDirect 209:23–30

Chapter 8

Development of a Design of a Drop-In Hydrogen Fueling Station to Support the Early Market Buildout of Hydrogen Infrastructure: Topic-9

Abdulkhkim Agll, Tarek Hamad, Sushrut G. Bapat, Yousif Hamad,
and John W. Sheffield

Abstract This chapter provides a design of a drop-in hydrogen fueling station. Drop-in stations are expected to be an important factor in the introduction of hydrogen fueling infrastructure. The stations not only allow a streamlined introduction of hydrogen in the vehicle fueling infrastructure but also act as mini pilot plants that can allow for detailed control studies. The effect of the location and availability of utilities, the closeness of stations to residential areas, safety concerns, general attitudes toward hydrogen, and others are some of the issues that arise with such drop-in stations. The proposed design of a drop-in station mainly considers off-the-shelf items and is conceptualized to be implemented at the Missouri University of Science and Technology. The modular design approach, with the off-the-shelf items, allows for a design with the capacity for mass production and an ease in transport and integration.

1 Introduction

According to International Energy Outlook 2013, released by the U.S. Energy Information Administration, worldwide energy-related carbon dioxide emissions will rise from about 31 billion metric tons in 2010 to 36 billion metric tons in 2020. These emissions will further grow to 45 billion metric tons by 2040, resulting in a 46 % total increase [1]. One of the major contributors to the emissions will be exhaust gases released from vehicles. Therefore, it can be stated that by employing zero-carbon-footprint vehicle fuel, we would see a significant change in the carbon

A. Agll (✉) • T. Hamad • S.G. Bapat • Y. Hamad • J.W. Sheffield
Department of Mechanical and Aerospace Engineering, Missouri University of Science
and Technology, Rolla, MO, USA
e-mail: aaa7w2@mst.edu

dioxide emission levels. Research in the area of alternative fuels, renewable and nonrenewable, has demonstrated their applicability in the vehicle powertrain sector; however, this was in a laboratory environment. With the available research findings, and considering the time needed, steps must be taken toward the development of a fueling infrastructure. Of the available alternative fuels, hydrogen has shown the greatest potential. Hydrogen not only provides cleaner energy but is also easy to transport, allowing centralized production, mimicking a gasoline fueling infrastructure [2]. To prove the market potential of hydrogen and test the business case, mobile drop-in units have been an ideal mode of introducing a hydrogen fueling infrastructure. This chapter presents the design of such a drop-in hydrogen fueling station that can be utilized to develop the required experience in the technical and business aspects of a hydrogen energy infrastructure. The design utilizes available technology and off-the-shelf equipment and represents a modular setup for a hydrogen fueling station. The station requires a steady supply of methane, water, and electricity. These utilities can be obtained either from nearby locations or through the installation of a CHHP system, as described in Hamad et al. [3]. The station design consists of equipment, security and safety interlock details, and the final installation layout. The drop-in station is conceptualized for use at the Missouri University of Science and Technology (Missouri S&T).

1.1 Site Plan and Location

The drop-in hydrogen fueling station is conceptualized to be located on the Missouri S&T campus. Figure 8.1 shows the master plan of Missouri S&T, along with the proposed site of the drop-in hydrogen fueling station marked on it. The station will be located west of the Algood-Bailey Stadium, near the tennis courts. The location has a sufficient supply of natural gas, water, and electricity for the operation of the drop-in hydrogen fueling station design presented in this chapter.

2 Drop-In Hydrogen Fueling Station Design

Figure 8.2 shows a schematic of the drop-in hydrogen fuel station design. The station is designed for the production of 100 kg/day. The design utilizes an off-the-shelf hydrogen production unit that produces hydrogen using steam methane re-forming technology. An integral part of this unit is a hydrogen compression and storage station. Hydrogen is compressed to 5000 psig and stored for delivery. To take advantage of this feature, the design has a hydrogen dispenser that is capable of dispensing hydrogen at 5000 psig and at 10,000 psig. A three-way valve is used to direct the hydrogen from the fuel cell to either the dispenser or the compressor. The positive displacement compressor in the fuel station will compress hydrogen



Fig. 8.1 Site location for proposed drop-in hydrogen fueling station [4]

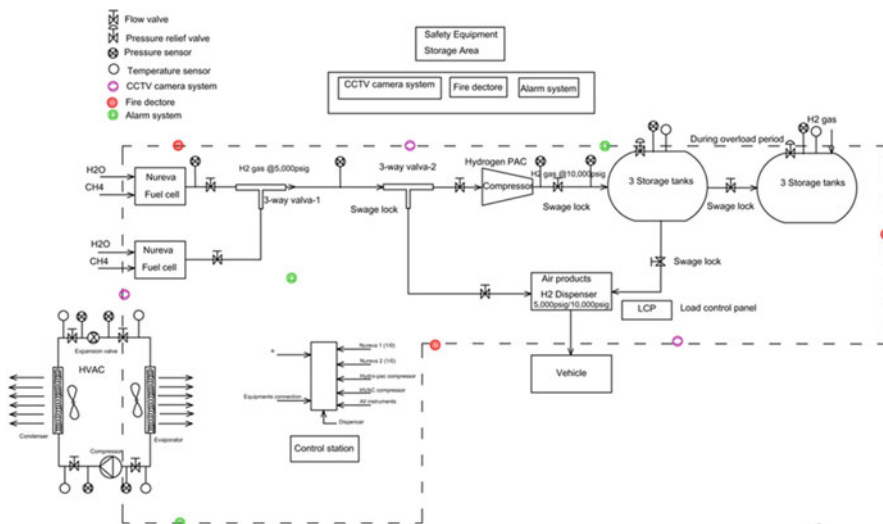


Fig. 8.2 Schematic of drop-in hydrogen fuel station design

to 10,000 psig. A local control panel near the dispenser will allow an operator to manipulate the three-way valve. The station houses a HVAC unit, which helps in maintaining the surrounding temperature. Hydrogen's density is dependent on the temperature, and therefore the HVAC unit is a very important part of the design. In addition to these basic components, the station contains adequate safety hardware. Control stations required for major components are supplied with the unit itself.

2.1 Hydrogen Production Evaluation

Holladay et al. [5] and Bicakova and Straka [6] provided an extensive list of hydrogen production technologies. Although hydrogen can be produced using many approaches, steam methane re-forming is still the most suitable mode of hydrogen production at the commercial scale. Natural gas required for steam methane re-forming is readily available in the USA. Additionally, recent advancements have shown that methane, a key component of natural gas, can be produced on site by performing anaerobic digestion of biomass [3]. Therefore, considering future expansion of the station and transformation to a renewable feedstock, steam methane re-forming was considered here by the authors for hydrogen production.

With this background, the authors performed an extensive search for modular steam methane reformers (SMRs) and selected the Nuvera PowerTap (NPT) for hydrogen production. In addition to the SMR, this unit also houses preprocessing, compressing, and hydrogen storage stations. The unit requires a supply of natural gas and water to provide 50 kg hydrogen/day at 5000 psig. The selected NPT and Table 8.1 provide its specifications. The unit is easy to install and is supplied on a skid.

2.2 Hydrogen Compression

The NPT hydrogen production unit houses a compression and hydrogen storage station, which allows hydrogen output at 5000 psig. Hydrogen gas has a much lower energy density by volume than fossil-fuel-based sources of energy. As a

Table 8.1 Specifications for Nuvera PowerTap [7]

Item	Specification
Hydrogen generation capacity	50 kg/day
Dispensing pressure	5000 psig
Natural gas requirements	7–14 in. water column pressure
Environment	Outdoor or indoor

Table 8.2 Specifications for C15-60FX-H2/SS-EXT [7]

Item	Specification
Inlet pressure and temperature	5000 psig and 80°F
Discharge pressure	10,000 psig
Flow rate	400 scfm
Motor power	60 HP
Electricity requirements	460 V, 60 Hz, 3 phase
Electric protection	Class I Div. 2
Control power	120 V, 60 Hz, 1 phase
Operating temperature	50–100 °F
Cooling water requirement	15 gpm at 60–80°F
Installation	Indoors
Dimensions	122 in. long, 37 in. wide, 66 in. high
Weight	8000 lb.

result, compression of the gas to improve its energy density is a commonplace practice. Therefore, the design incorporates a Hydro-PAC high-pressure positive displacement unit (Model C15-60FX-H2/SS-EXT FLEXI-POWER) to compress hydrogen to 10,000 psig [8]. The compressor is also capable of supplying hydrogen at 13,000 psig, as required for some higher-pressure hydrogen fuel cell vehicles. Table 8.2 shows the specifications of the selected compressor.

The compressor is a hydraulically driven, nonlubricated piston intensifier type machine equipped with a hydraulic power unit and a high-pressure gas intensifier. Also equipped on the compressor are full-length isolation spacers to prevent hydraulic oil carryover into the process gas and stainless steel wet ends to prevent hydrogen embrittlement at high pressures. The compressor also includes a control system, explosion-proof reciprocating circuit, and full-length distance pieces to prevent hydraulic oil carryover. The controls and piping system for the compressor provide automatic or manual on/off operation. If an alarm is detected, the controller automatically shuts off the unit and displays an alarm fault condition. Items included are as follows:

1. NEMA 4 (IP66) electrical enclosure with motor starter, Allen Bradley PLC (Micro 820/Micrologix 1100 or equivalent), Allen Bradley C400 interface, and necessary I/O;
2. Valves and piping for manual isolation, air-operated isolation manual vent, and safety relief;
3. Gas after cooler;
4. Inlet and discharge pressure transducers;
5. Discharge thermocouple;
6. Inlet and discharge pressure gauges;
7. Cooling water isolation valves, flow switch, and sight meter.

2.3 Hydrogen Storage Pressure Vessel

Hydrogen discharge from the compressor at 10,000 psig is stored in three pressure vessels. The vessels are designed as per ASME Section VIII, Division 3. The current design incorporates three storage pressure vessels from FIBA Technologies, Inc. Each vessel has a design pressure of 15,000 psig and is 29 ft. long and 1.33 ft. in diameter [9]. Each vessel can hold 34 kg hydrogen. To meet the set demand of 100 kg/day, three such hydrogen storage vessels are considered. To minimize the footprint, these three vessels are arranged one above the other.

2.4 Hydrogen Dispensers

The Air Products SmartFuel H70/H35 retail hydrogen dispenser [10] was selected for the customer end of the drop-in hydrogen fueling station. The dispenser provides features similar to those of an existing gasoline dispenser, e.g., same look, feel, and payment options, and is in compliance with SAE J2601. The dispensing equipment includes SAE-certified nozzles, gas piping, and valves and includes adequate safety features required to fuel high-pressure hydrogen gas at 10,000 psig; Table 8.3 provides a description of various parts, and Table 8.4

Table 8.3 Description of various parts [10]

Part number	Description
1	Valence with gas detection sensors for immediate leak detection
2	Enclosed and shrouded breakaway connectors
3	Reinforced polycarbonate upper door with ergonomic design to provide simple, customer-friendly user interface
4	Energy-efficient display panel with LED backlighting for clear visibility of display in all lighting conditions; all displays equipped with clear, hard-coated sacrificial lenses for increased durability and extended life
5	Debit payment system and 5.7" color LED display with on-screen training instructions for first-time users
6	Durable encrypting PIN pad/TDS keypad
7	Credit card reader
8	Emergency stop button and operating instructions
9	H70 and H35 unit price displays
10	Unique fueling pressure selection buttons with no moving parts for unmatched durability
11	Lower door assembly
12	Radio frequency identification detector (RFID) reader for vehicle identification and communications
13	Universal metal nozzle boot (the industry's most durable)
14	Protective jackets over hoses

Table 8.4 SmartFuel H70/H35 retail hydrogen dispenser [10]

Item	Specification
Dispensing pressure	5000 and 10,000 psig
Compliance with SAE standards	J2600, J2601, J2719, and J2799
Nominal fill quantity	1–10 kg/fill
Complete fill accuracy	98 %
Other features	Credit card and RFID payment options with store point of sale (POS) interface

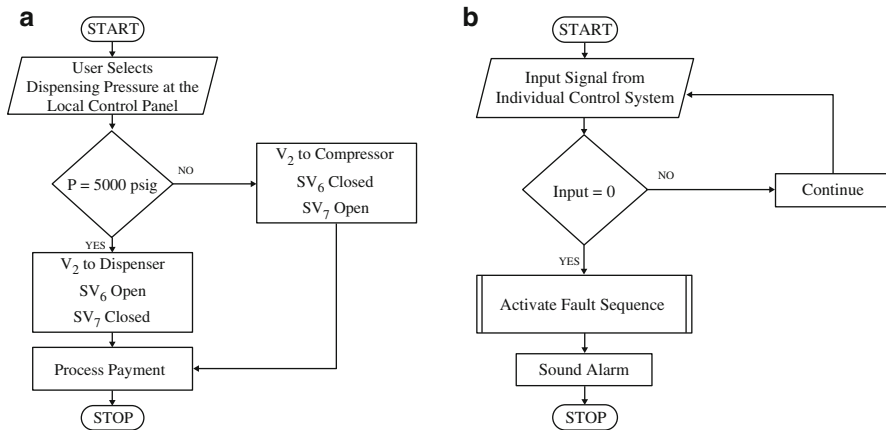


Fig. 8.3 (a) Control logic in local control panel. (b) Control logic for drop-in fuel station control system

presents the specifications of the dispenser. The dispenser complies with all of the industry regulations, codes, and standards. Specifically, the dispenser design is in compliance with ASME B31.3, NFPA 70, NFPA496, NFPA 497 M, International Fire Code, NFPA 55, and NFPA 2.

The dispenser control panel allows the user to select the dispensing pressure. Based on the selection, the control sequence shown in Fig. 8.3a will be executed. In case of any faults in the subsystems, the dispenser will be cut off, all the shut-off valves will be closed, and the alarm will be activated, as shown in Fig. 8.3b.

2.5 Piping Valves and Fittings

Piping, valves, and fittings form a very important group of hardware in the drop-in fuel station. SS316L is selected as the material of construction for all the components that are in contact with hydrogen. In addition, the components are selected for a design pressure of 10,000 psi. The design will utilize the piping, valves, and

fittings from Parker Hannifin Corporation. The three-way valve and shut-off valves will also be purchased from Parker Hannifin Corporation.

2.6 Safety Equipment

Safety is of utmost importance in interactions with humans. With the hydrogen-based stigma, safety becomes even more important. The design considers the following safety equipment, as shown in Fig. 8.4.

1. Camera at hydrogen dispensing island,
2. Hydrogen detectors within station and at hydrogen dispensing islands,
3. Appropriate number of pressure relief valves within station,
4. Appropriate number of shut-off valves to isolate system in case of accident,
5. A safety switch that will shut off all equipment when door of drop-in station is opened,
6. Fire detectors,
7. Fire suppression systems,
8. Hydrogen detection alarm and fire detection alarm.

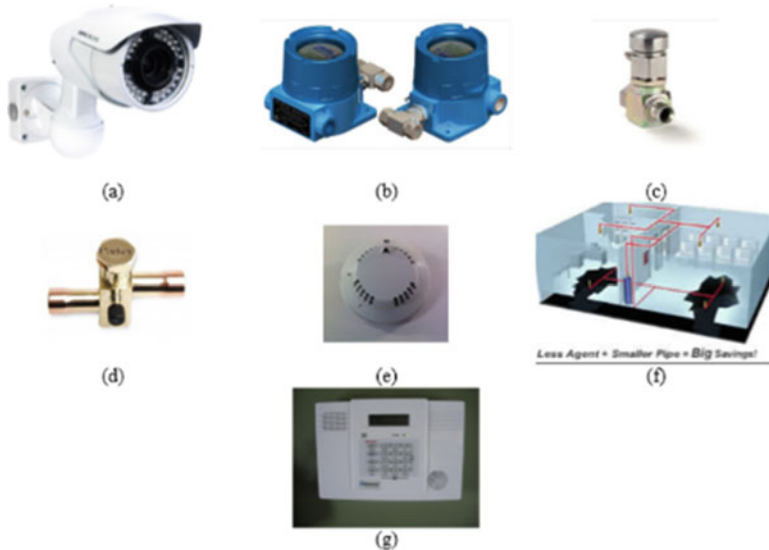


Fig. 8.4 Safety equipment selected for drop-in hydrogen fueling station: (a) CCTV camera systems by Super Circuits [11], (b) hydrogen detector from H2 Scan [12], (c) pressure relief valves from Parker Hannifin Corp. [13], (d) shut-off valves by Parker Hannifin Corp. [13], (e) fire detector from Bosch [14], (f) fire suppression systems from Fire Suppression Systems Inc. [15], and (g) alarm systems from Honeywell [16]

2.7 Structural Components

Because all of the subsystems will be skid-mounted, the drop-in fuel station just needs a supporting structural frame. The suppliers will provide all the necessary mounting hardware, along with the designs for the supporting structure. Structural steel A36 will be utilized as the primary material for the structure.

3 Energy-Saving and Environmental Analysis

The energy-saving and environmental analysis for the system architecture is performed using the procedure provided in [17]. The analysis highlights the energy savings following the use of natural gas.

3.1 Energy-Saving Analysis

The total energy savings can be estimated by the following equation:

$$F_s = F_H - F_{NPT} - F_C - F_{HVAC} - F_{DIS} - F_{GL}, \quad (8.1)$$

where F_s , F_H , F_{NPT} , F_C , F_{HVAC} , F_{DIS} and F_{GL} represent the total fuel savings, fuel use from avoided energy services provided by hydrogen, fuel use by the NPT system, electrical consumption for the compressor, electrical consumption for the heating, ventilation, and air-conditioning system, electrical consumption for the dispenser, and electrical consumption for general lighting.

3.1.1 Fuel Consumption by NPT System

As mentioned in the technical design section, Missouri S&T has decided to use two NPT units, each of which requires natural gas of 16.978 m³/h and delivery 50 kg of hydrogen daily. Based on the NPT product specifications, on-site generation of electricity per kilogram H₂ is 12 kWh and natural gas consumption per kilogram H₂ is less than 0.192 MMBTU. Since each PowerTap unit can generate 50 kg hydrogen, it is easy to find the F_{NPT} s

$$F_{NPT} = F_G + F_E, \quad (8.2)$$

where F_G and F_E represent the natural gas consumption and electrical consumption for one NPT, respectively.

$$F_G = \text{mass of hydrogen per unit} \times \text{natural gas consumption/kg hydrogen} \quad (8.3)$$

$$F_G = 101,363,52;$$

$$F_E = \text{mass of hydrogen per unit} \times \text{electrical consumption/kg hydrogen} \quad (8.4)$$

$$F_E = 50 \times 12 = 600 \text{ kWh} = 3600.5167 \text{ kJ}.$$

From Eq. (8.2) we obtain

$$F_{\text{NPT}} = 10136352 + 3600.5167 = 10.14 \times 10^6 \text{ kJ}.$$

Thus, this is the consumption for one unit.

$$\text{The total } F_{\text{NPT}} = 10.14 \times 10^6 \times 2 = 20.28 \times 10^6 \text{ kJ},$$

$$F_{\text{NPT}} = 7.4 \times 10^9 \text{ kJ/year}.$$

3.1.2 Fuel Consumption by Compressor

Missouri S&T has decided to use high-pressure hydrogen Flexi-Power compressors, which require hydrogen gas flow rate 24.4904 m³/h at 350 barg and a delivery rate of 1 kg/min hydrogen at 700 barg. Based on the Flexi-Power compressors Product as:

$$\text{FLOE} = \text{TAOS} / \text{CS}_{\text{max}} = 8760 \text{ h/year}, \quad (8.5)$$

where FLO_E, TAOS, CS_{max} and FI_R represent the equivalent full-load operating hours, total annual output by the system, maximum capacity of the system, and fuel input rate, respectively. The fuel consumption for the compressor system can be estimated as

$$F_C = \text{FI}_R \times \text{FLO}_E = 0.0101 \times 10^9 \text{ kJ/year}. \quad (8.6)$$

3.1.3 Fuel Consumption by HVAC System

Missouri S&T has decided to use two GREE DC inverters, premium-efficiency and ductless mini split systems; each unit has 1 RT (3.52 kW) cooling load capacity. Based on the GREE Product as

From Eq. (8.5), FLO_E = 8760 h/year”

$$F_{\text{HVAC}} = \text{MCFI}_R \times \text{FLO}_E = 0.97 \times 10^9 \text{ kJ/year}, \quad (8.7)$$

where MCFI_R denotes the maximum capacity of the system and the fuel input rate.

3.1.4 Fuel Consumption by Dispenser

The hydrogen dispenser program is currently focused on providing both 350 and 700 bar (5000 and 10,000 psig) dispensing technologies and components to the continually evolving hydrogen market. Based on the Kraus global product we have

From Eq. (8.5), $FLO_E = 8760$ h/year:

$$F_{DIS} = MCOFI_R \times FLO_E = 0.5 \times 10^9 \text{ kJ/year}, \quad (8.8)$$

where $MCOFI_R$ denotes the maximum capacity of the system and the fuel input rate.

3.1.5 Fuel Consumption by General Lighting System

As mentioned in the previous section, the station plane area is 80×20 ft (148.72 m^2). Missouri S&T has decided to make light intensity 3.4 w/ft^2 . The energy services provided by the lighting can be calculated using the following equation:

From Eq. (8.5), $FLO_E = 8760$ h/year:

$$F_{GL} = MFI_R \times FLO_E = 0.477 \times 10^9 \text{ kJ/year}, \quad (8.9)$$

where MFI_R denotes the maximum capacity of the system and the fuel input rate.

3.1.6 NPT System Hydrogen Output and Fuel Savings

As mentioned in the previous section, 100 kg hydrogen will be used per day to displace conventional fuel. The energy services provided by the hydrogen involve a savings in the fuel saved. The conventional fuel saved for the application due to the hydrogen used can be calculated using the following equation:

$$AF_H = NPT_{HC} \times HCR \times HCOCF / DCFCR, \quad (8.10)$$

where AF_H , NPT_{HC} , HCR , $HCOCF$, and $DCFCR$ are the avoided fuel hydrogen, NPT hydrogen consumption, hydrogen consumption rate, heat content of conventional fuel, and displaced conventional fuel consumption rate, respectively.

Therefore, the fuel savings due to hydrogen usage is

$$AF_H = F_H = 1.3 \times 10^{12} \text{ kJ/year}.$$

Using Eq. (8.1) the total energy savings will be

$$\begin{aligned}
 F_s &= F_H - F_{NPT} - F_C - F_{HVAC} - F_{DIS} - F_{GL}, \\
 F_s &= 1.3 \times 10^{12} - 7.4 \times 10^9 - 3.0 \times 10^9 - 0.97 \times 10^9 \\
 &\quad - 0.5 \times 10^9 - 0.477 \times 10^9 = 1.288 \times 10^{12} \text{ kJ/year}.
 \end{aligned}$$

3.2 Environmental Analysis

The environmental impact of the proposed design is investigated through the savings in the carbon dioxide emissions, which can be estimated by the following relationship:

$$OR_{CO_2} = \left(\sum k \right) \times (AF_H) \times (ER_{net_{CO_2}}), \quad (8.11)$$

where OR_{CO_2} and $ER_{net_{CO_2}}$ are the overall CO_2 reduction and net CO_2 emissions rate. Also, $k = -1$ for fuel consumed and 1 for fuel saved, which includes the CHHP fuel consumption, fuel consumption for feed stock transport, saved central station fuel, saved thermal fuel, and saved fuel due to hydrogen. Thus, the overall CO_2 reduction is 66,319 t/year.

4 Conclusion

This chapter provided a design for a drop-in hydrogen fueling station. The design utilizes off-the-shelf components and is conceptualized to be implemented at the Missouri University of Science and Technology. The design develops a SMR, a positive displacement compressor, and a two-pressure hydrogen dispenser. The design provides necessary sensors, isolation valves, and redundancies, in line with current standards and regulations. A detailed analysis of failure modes and effects demonstrated the feasibility of the proposed design. The drop-in hydrogen fueling station will facilitate a variety of control studies, including on an economic model of hydrogen fueling infrastructure, customer outlook, and the determination and implementation of technical procedures and their impact on the hydrogen fueling infrastructure.

Acknowledgments The authors wish to thank the Hydrogen Design Solutions Team at the Missouri University of Science and Technology.

References

1. The U.S. Energy Information Administration (EIA) (2013) International energy outlook 2013: July 2013: DOE/EIA-0484
2. Hamad Y, Agli A, Hamad T, Bapat SG, Bauer C, Clum A, Shivaprasad N, Thomas M, Sheffield JW (2014) A design for hydrogen production and dispensing for northeastern United States, along with its infrastructural development timeline. *Int J Hydrogen Energy* 39:9943–9961
3. Holladay JD, Hu J, King DL, Wang Y (2009) An overview of hydrogen production technologies. *Catal Today* 139:244–260
4. Bicakova O, Straka P (2012) Production of hydrogen from renewable resources and its effectiveness. *Int J Hydrogen Energy* 37:11563–11578
5. Nuvera (2014) PowerTap™ specification sheet <http://www.nuvera.com/images/PDFs/PowerTap-PTS001-RevA.pdf>. Accessed 8 Nov 2014
6. Ali DM, Salman SK (2006) A comprehensive review of the fuel cells technology and hydrogen economy. In: Paper presented at the 41st international universities power engineering conference, conference proceedings UPEC 2006:1 98-102
7. Adapted from Missouri S&T Master Plan (2014) <http://www.phyfac-eb.mst.edu/dcm/pdf/masterplan.pdf>
8. Hydro-Pac Proposal EST14-0263
9. Email proposal from FIBA Technologies, Inc.
10. Air Products SmartFuel™ H70/H35 retail hydrogen dispenser specification sheet
11. Affordable Home Electronics specification sheet <http://www.affordablehomeelectronics.com/supercircuits-pc508ir-3-ultralongrange450feetvandalproofinfraredsecuritycamera.aspx>. Accessed 8 Nov 2014
12. Direct Industry specification sheet <http://www.directindustry.com/prod/h2scan/hydrogen-detectors-40428-1354771.html>. Accessed 8 Nov 2014
13. Parker specification sheet <http://ph.parker.com/us/en/pressure-relief-valve>. Accessed 8 Nov 2014
14. Buy Fire Alarm Part specification sheet https://www.buyfirealarmparts.com/shop/index.php/catalog/product/view/id/5049/s/bosch-d273thc/?gclid=CKSijNHv_cMCFQqDaQod40oAVw. Accessed 8 Nov 2014
15. SSI Fire & Explosion Protection specification sheet http://www.suppressionsystems.com/fire_supp.html. Accessed 8 Nov 2014
16. Mansion House specification sheet <http://mansionhouse.info/honeywell-home-alarm-systems/>. Accessed 8 Nov 2014
17. Hydrogen Student Design Contest Official Rules and Guidelines (2014) <http://hydrogencontest.org/pdf/2014%20Official%20Rules%20and%20Guidelines%20v1.1.pdf>

Chapter 9

Sustainability of Higher Educational Buildings: Retrofitting Measures to Enhance Energy Performance—The Case of AASTMT Business Management School Building, Egypt

Mohsen Aboulnaga, Ayman Wanas, Mohamed Hammad,
and Mohamed Hussein

Abstract Buildings compose the highest portion of global CO₂ emissions from different sectors (approximately 5.5 Gt CO₂-eq.). According to the Intergovernmental Panel on Climate Change, Egypt is among those nations that will be heavily affected by the impact of climate change, even though its greenhouse gas (GHG) emissions represent only 1 % of the world's GHG emissions. Electricity consumption in public buildings, including administrative, educational, and healthcare-related buildings, is 9 % – the second largest category after residential buildings at 40 %. Enhancing energy performance in higher education and residential buildings will have a significant impact on the reduction of electrical energy consumption, resource efficiency, and the nation's energy footprint. Energy consumption in educational buildings depends on activities, time of use, and influx of visitors, students, and academic staff, as well as the academic term, that is, winter or summer. Retrofitting measures are important for reducing energy consumption in higher educational buildings and cooling requirements in a hot climate. The most important measures in the retrofitting process of the building envelope, including its roof, are mainly the glazing type and characteristics and the thermal insulation of walls. This chapter focuses on sustainability measures of the Business Management School building at the Arab Academy of Science, Technology & Maritime Transport campus in Cairo, Egypt. The objective is to set a baseline assessment of the building's energy use and compare it with energy performance after retrofitting

M. Aboulnaga (✉) • M. Hammad
Department of Architectural Engineering, Cairo University, Cairo, Egypt
e-mail: mohsen_aboulnaga@yahoo.com; mohsen_aboulnaga@cu.edu.eg

A. Wanas
Arab Academy for Science, Technology & Maritime Transport, AASTMT, Cairo, Egypt

M. Hussein
Department of Architecture and Environmental Design, AASTMT, Cairo, Egypt

measures and simulations. This includes upgrading the glazing with a shading coefficient from 0.81 to 0.35, a wall thermal insulation of the building's envelope from 4.8 to 1.15 W/Km², and a green roof. Results show that applying these retrofitting measures led to a reduction in energy use by 27 % from the baseline average energy use of 14.6 kWh/m² yearly and was further reduced to 495 kWh when a green roof with a U-value of 0.14 W/m² K was applied.

Keywords Sustainability • Retrofitting • Energy use • Energy conservation • Higher education building • CO₂ emission

1 Introduction

Cities are associated with 67 to 76 % of global energy use and 71 to 76 % of global energy-related greenhouse gas (GHG) emissions [1]. According to C40 Cities Climate Leadership Group and Local Governments for Sustainability, their members have collectively agreed to emission reductions equivalent to 0.4 Gt CO₂ per year by 2030 [2]. The largest 500 cities by population, including Cairo, Egypt, could contribute 1.65 Gt CO₂e by 2030, nearly half the identified urban mitigation potential [3]. Most of these emissions come from the combustion of fossil fuels to provide electrical energy in buildings for cooling/heating, lighting, appliances and electrical equipment, as well as heating water. Accelerating energy efficiency in new buildings is therefore of huge significance. Many cities are accordingly establishing municipal green building (GB) codes that far exceed national standards, for example Pune in India, San Francisco in the USA and Shanghai in China [4]. In accordance with a study on GB standards in Recife, Brazil, conducted by the University of Leeds, such standards would pay for themselves quickly if, in meeting so-called passive cooling standards, which entails incremental investment needs of 3 %, investors could recover their costs through energy savings in 6, 7 and 18 years in commercial, public and residential buildings respectively, where a smaller share of total electricity consumption is for cooling purposes [4]. Table 9.1 shows the benefits from complying with GB standards.

In Singapore, such a programme has already been implemented; it aims to have 80 % of its buildings achieve the Green Mark standard by 2030 [5]. This could potentially reduce building electricity use by approximately 22 %, with net economic savings of over US\$400 million [6]. Nonetheless, this result suggests that innovative GB design can yield much broader benefits, including expanding green space, reducing heat island effects, filtering air pollution and capturing rainwater to reduce demand for piped water [6].

Table 9.1 Significant value of green building standards in Recife, Brazil, 2030

	Energy savings (GWh/% of BAU sector electricity consumption) (%)	Emission reductions (1000 t CO ₂ /% of BAU sector emissions) (%)	Economic savings in 2030 with a 2 % real energy price increase (USD millions)	Payback period with a 5 % interest rate (years)
Commercial	404.5/13.7	45.5/16.4	64.92	6
Public	119.7/4.0	13.5/16.5	16.55	7
Residential	58.0/2.54	6.5/1.5	10.78	18

Source: Analysis by the University of Leeds [1]

1.1 Existing Buildings

In comparison to new buildings, existing buildings contribute to high energy consumption owing to their inefficiency as reflected in their envelope insulation and almost complete absence of application of sustainability and energy-saving measures. In Cairo, Egypt, existing buildings are the main consumers of electrical energy, which is almost 86 %. Hence, improving existing buildings is as vital to urban climate action as improving energy efficiency in new buildings. Several cities have initiated large-scale retrofit schemes to realise the multiple benefits of more efficient buildings. Because the direct energy savings are vital, unlocking the wider benefits is equally crucial [7]. Despite the fact that the incremental costs of retrofitting can create a major barrier to deployment, financing mechanisms can help surmount these barriers to unlock both the direct economic savings and the wider benefits [7]. Investing in energy efficiency is considered a key promising solution; nevertheless, recent work on the Leeds City Region in the UK considered the potential of a revolving fund to finance domestic building retrofits. Similar models include the Thai Energy Efficiency Revolving Fund and the New York State Drinking Water Revolving Fund, where analyses considered funds of three different types [7]. Analysis of the first type (profit-led fund) results in cumulative mitigation by 2050 of 6.5 Mt CO₂ – only around half that of the Public and private partnership (PPP) or not-for-profit scheme – but the profit-led fund would recoup initial investments in less than 20 years, while the PPP scenario would take an estimated 37 years and the not-for-profit scheme would suffer a financial loss [5, 6]. Even when the wider economic benefits of a retrofit programme are considered, both the PPP and the not-for-profit schemes become more economically attractive. In the UK, it is estimated that every UK£1 spent on reducing fuel poverty can save the National Health Service £0.42 in health costs [5, 6]. For Leeds City Region in the UK, if investments targeted the 10 % of households in fuel poverty, the PPP and non-profit schemes would lead to health care savings of £80–100 million. Accordingly, a retrofitting scheme for a building becomes a very economically attractive option for the public sector when taking into account the significant wider social and economic benefits [6, 7].

Energy consumption in buildings comprises almost 40 % of total energy consumption worldwide, and buildings are responsible for 30 % of the CO₂ emissions in the world [8]. Educational buildings are among the building types that are of great importance when it comes to energy consumption because of their pattern of occupancy and activities throughout the year. In contrast, building energy use associated with non-domestic buildings in the UK accounts for approximately 19 % of the total UK CO₂ emissions [9, 10]. In Egypt, public (educational, administrative and hospitals) and commercial buildings are responsible for more than 13 % of the total electrical energy, whereas industrial and residential buildings account for 37 and 40 % respectively [5]. Existing buildings account for 34 % of the 40 % of energy consumption in residential buildings [11].

Energy consumption in a non-domestic building is complex owing to a wide variety of uses and energy services. Therefore, the energy demand of educational buildings needs to be understood. The carbon trust in the UK stated that a carbon reduction of 70 to 75 % could be achieved in non-domestic buildings at no net cost [12]. In the UK, educational building, mainly universities, consume significant amounts of energy [2, 13]. In accordance with new legislation [14], most of the UK's colleges and universities are required to report on their energy use and improve their efficiency. This is not the case in Egypt; nonetheless, Energy consumption and user patterns in university buildings were reported more than other non-domestic buildings, including schools and offices, but were not analyzed in terms of energy use (cooling, lighting, and hot water, etc.) [5, 6, 15]. In Turkey, 36 % of the total energy is consumed for heating, cooling and lighting in buildings [16]. Government statistics issued in 2009 indicated that there are total of 59,539 school buildings in Turkey [16]. In this context, educational buildings should be high-performance buildings.

1.2 Policies for Improving Existing Buildings

In the building sector, most energy consumption happens in existing buildings [17]. Nevertheless, the rate of replacement of existing buildings by new ones is relatively small, around 1 to 3 % yearly [17]. Thus, retrofitting of existing buildings is vital to reducing energy consumption. Measures towards enhancing existing buildings, mainly energy efficiency, have been adopted by many governments around the world. In the USA, the federal government offered financial assistance to support retrofitting existing buildings [18, 19], whereas in Australia, the Commercial Buildings Disclosure Programme asked owners of large commercial office buildings to furnish information on energy efficiency to buyers and occupants [20, 21]. The UK government issued a major commitment in 2010 to upgrade seven million British homes to be energy efficient by 2020 with the intent to reduce CO₂ emission by about 30 % [22].

1.3 Educational Buildings

In 2013, Mehreen Gul et al. conducted a study on reducing energy use in an educational building and stated that it was impossible without good data on which to make management and investment decisions [23]. A pilot study was pursued to understand the energy consumption and occupancy of a multi-purpose postgraduate centre at the School of the Built Environment at Heriot-Watt University, Edinburgh, Scotland, UK [23]. The study analysed the relationship between electrical energy demand profiles and user activities. The shape and magnitude of energy demand profiles showed a significant trend which does not seem to be strongly connected to occupancy patterns, but it indicated that detailed information on the occupancy patterns could help in controlling energy use [23]. Another study by Fulvio Ardente et al. presented the results of an energy and environmental assessment of a set of retrofit actions implemented in the framework of the European Union (EU) Project “BRITA in PuBs” (Bringing Retrofit Innovation to Application in Public Buildings [24]). The assessment outcomes showed that the most significant benefits were mainly related to improvements in envelope thermal insulations, lighting and glazing [24]. It also highlighted the role of the life cycle approach in selecting the most effective options during the design and implementation of retrofit actions [25].

In International Energy Agency (IEA) member countries, educational buildings, such as kindergartens, schools, training centres and universities, exhibit various similarities in their design, operation and maintenance features [26]. Many of these buildings have identical structures, often need to be retrofitted and have high energy consumption. Also, the IEA’s Energy in Buildings and Communities Programme (EBCP) published a report by Richard Barton on Annex 36 – Retrofitting in Educational Buildings – Energy Concept Adviser for Technical Retrofit Measures (Faber Maunsell Ltd, UK, 2007), which indicated two significant similarities amongst these types of educational buildings [26]:

- (a) High energy consumption,
- (b) Necessity to retrofit many buildings within this sector.

The design tools used included tools ranging from simple spreadsheets to advanced computer programs that took into account the impact of light, heat and cooling in buildings. The results of this extensive study were summarised in [26].

Approximately 60 % of all public building floor surfaces in the EU are schools; one third of all EU citizens spend their days in these buildings. The EU 2020 targets will be unattainable if the only measure taken is to build new, energy-efficient schools. Retrofitting these schools in a conventional method would also mean moving entire school populations for the duration of the process, which would be costly and educationally very negative [27]. Marc van Praet indicated that 60,000 school buildings in the EU could be retrofitted to EU 2020 standards without closing them down in the process [27]. Thus, the main road to a sustainable school building stock in the EU will be one which uses a high-performance retrofit of

existing school buildings. According to the study, this would also maximise energy efficiency Passive house system (PHS) or Near zero energy system (NZEB) and the return on investment, minimise disruptions to school life, and provide overall superior comfort and adaptability to future changes in use [27].

Bahar Basarir et al.'s study on energy-efficient retrofit methods on school building envelopes revealed that energy-efficient retrofit methods were beneficial. It was proposed that an energy-efficient retrofit be done on a nearly 60-year-old elementary school building by improving the thermal properties of the building envelope. Results showed that financial gain would take place in 8 years. If a retrofit were applied, the annual fuel costs would be reduced by approximately 33 % of current costs [16].

Retrofitting in Egypt, especially from energy saving and energy efficiency, is a new concept which started to gain momentum in mid-2014 as a result of the electrical power shortage in the summer and frequent power cuts due to load sharing. The retrofitting actions taken at the time focused mainly on changing inefficient bulbs with CFLs or LEDs, and in some government buildings, photovoltaic (PV) arrays were installed to generate electrical energy during working hours. In general, this is not a holistic approach.

There is a potential link between building performance and energy use. In educational buildings, students spend long hours in lecture halls and classrooms, labs and libraries. The relationship between indoor environmental conditions (e.g. temperature, relative humidity and air speed) in general and student performance is well established [29]. Improving energy performance in educational buildings will have a significant impact on reducing electrical energy use and enhance resource efficiency and, above all, the nation's footprint. Energy-efficient retrofitting means ensuring the protection of cities with innovative technologies and systems with the aim of reducing energy consumption and CO₂ emissions associated with the built environment [16]. The work presented here is intended to assess existing buildings to understand the energy performance pattern in educational buildings with the intent of saving energy and making buildings energy efficient using retrofitting strategies to address Egypt's energy challenges.

2 Objectives

This chapter aims at retrofitting an educational building – the Business Management School (BMS) building at the Arab Academy of Science, Technology & Maritime Transport (AASTMT) in Heliopolis, Cairo, Egypt. The project's goals are threefold: (a) simulate retrofitting of the BMS building as a higher education building; (b) conduct an energy audit of the BMS building; and (c) pursue a baseline assessment of the building's energy use and compare it with its energy performance after retrofitting measures and simulation.

3 Methodology

Retrofitting of existing buildings faces enormous challenges. Two challenges are uncertainties such as climate change and variation in government policies; hence, these may affect the retrofitting process and adaptive technologies. The main elements impacting building retrofitting include main issues such as policies and regulations, client and resource expectations, building-specific information, energy data, human factors and retrofitting technologies. Key phases in a sustainable building retrofit programme are outlined by Zhenjun Ma et al. [17]. There are five phases involved in building retrofit, as shown in Fig. 9.1. One of these phases is the energy audit (EA). An EA is used to analyse building energy data, understand building energy consumption, and identify areas with excessive energy use and areas with energy waste in order to arrive at a solution and inexpensive approaches to reducing energy consumption and implement the appropriate retrofitting measures [17]. An EA is an investigation of energy use in a defined space, a floor in a building, or the building as whole. It helps in identifying energy use and costs on the basis of which energy cost and consumption control measures can be executed and reviewed [30]. EAs vary in range and depth (ASHRAE Handbook and Australia/New Zealand standards). EAs are classified into three levels: (1) walk-through assessment; (2) energy survey and analysis; and (3) detailed energy analysis [28, 29, 30–32].

Energy consumption in educational buildings depends mainly on the building activities, time of use and influx of students, academic staff and visitors, as well as the academic term, whether winter or summer. The retrofitting methodology and strategy are based on two main components: (1) types of activities and frequency and (2) energy services. Detailed elements for each component in relation to daily and monthly energy consumption are shown in Fig. 9.2. In this study, a theoretical approach was adopted based on available data. Design Builder energy simulation software was used to assess several parameters of the building, including cooling and heating loads, energy consumption (kWh/m²) and daylight distribution, so that appropriate measures could be taken. The applied measures were simulated and results were compared with the baseline energy use to assess and determine the savings from the enhancement. To carry out the simulation, the process includes the following sequences.

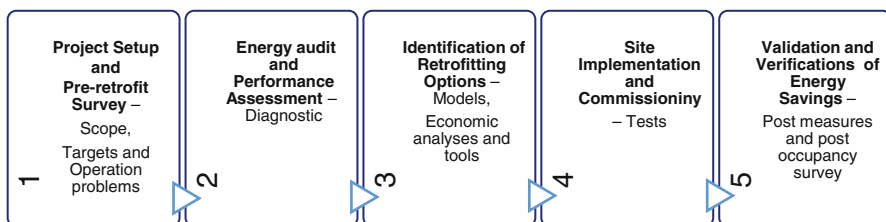


Fig. 9.1 Major phases used in a sustainable retrofitting of buildings

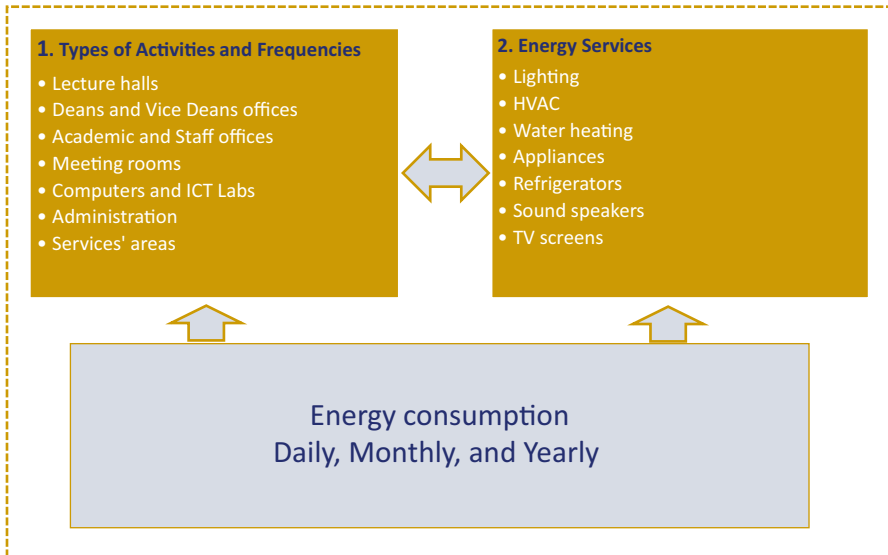


Fig. 9.2 Energy audit methodology and components

3.1 Campus Land-Use Distribution

Although the BMS building at the AASTMT campus in Heliopolis, Cairo, is an educational building, the campus is surrounded by residential low-rise buildings (Figs. 9.2 and 9.3). The BMS building is part of a complex known as Building No. 1175, which has three wings: A, B and C. Wing B was chosen as the case study for analysis and EA because accessibility permission was obtained. The site of the building is surrounded by streets (black), i.e. very low solar reflective index.

3.2 Data Gathering: Case Study

The School of Business Management building at the AASTMT was selected for study. The building is surrounded by low- to medium-rise residential blocks. It consists of six storeys: a ground floor and five floors; each floor is 3.2 m high. The building was commissioned and began operation in 1990 (Figs. 9.3, 9.4 and 9.5). In summer the building is surrounded by hot air. The highest monthly average high temperature is 35.7 °C in June, July and August, with a maximum of 48 °C, and the lowest monthly average low temperature is 13.3 °C in January and February. There is an average of 3451 h of sunlight per year, with an average of 9.5 h of sunlight/day, making heat gain higher in summer and, hence, increasing energy demand for cooling [26]. A thermal imaging type e6 infrared camera was used to measure the temperature of external surfaces on 12 August 2015 at 3:00 p.m. The surface

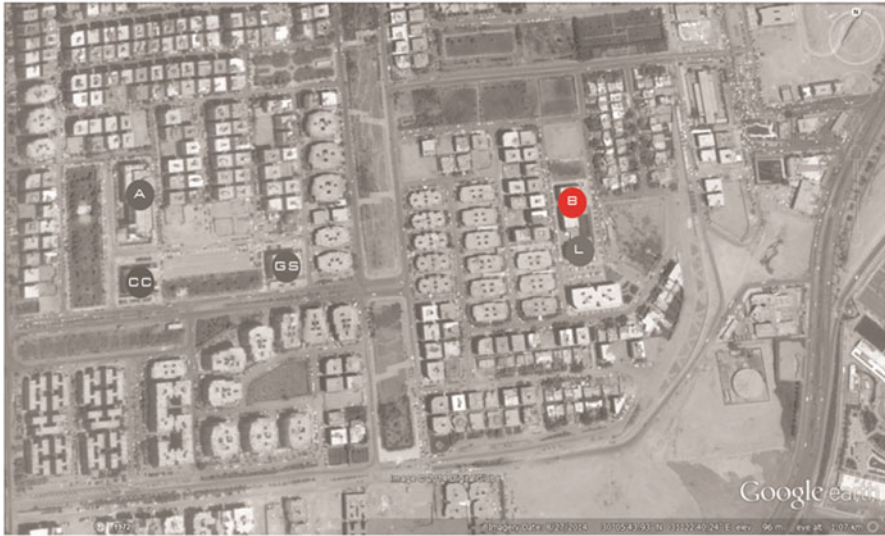


Fig. 9.3 Layout of Business Management School (BMS)

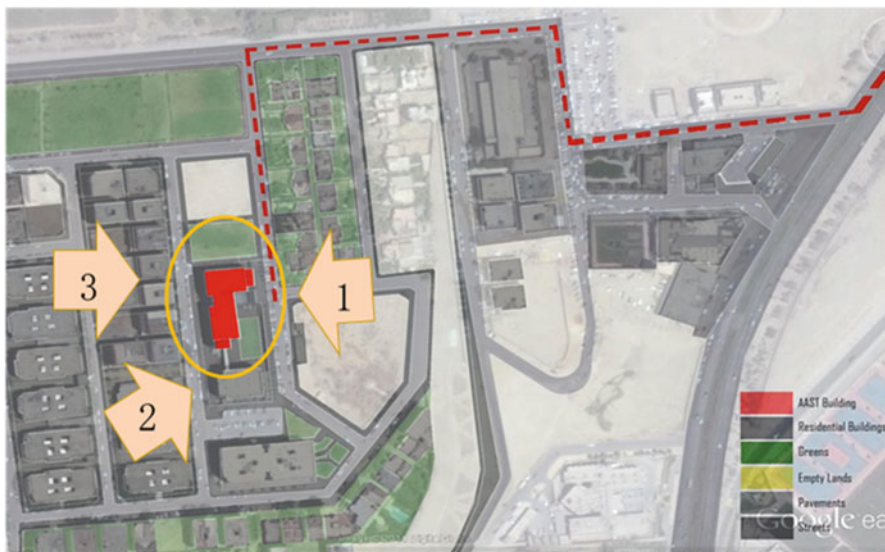


Fig. 9.4 BMS Campus, AASTMT

temperature on the western *façade* of the building under investigation was recorded at 55–56 °C.

No record of energy performance of the BMS building was conducted. Hence, electricity bills that reflect consumption were gathered for the academic year 2014–2015. Data on consumption were in Egyptian pounds. They were analysed



Fig. 9.5 Facades of BMS building, AASTMT Campus, Cairo, Egypt

to obtain the actual electrical energy consumption in terms of cost (EGP) of electrical energy use/month and electrical energy consumption/month (kWh) as shown in Fig. 9.6. An EA of all air-conditioning (AC) equipment, office apparatus and appliances, as well lighting, was also conducted for all floors of the building in terms of members and electrical power (in watts), as shown in Table 9.2.

3.3 *Retrofitting Process and Measures*

Studies show that energy-saving measures have rarely been applied [27]. This is mainly attributed to a lack of knowledge by decision makers regarding required investments and the efficiency of potential energy-saving measures. Due to the lack of information in many cases, decisions made did not accurately take into account energy-saving aspects. There are no so-called rules of thumb to enable a quick and easy estimation of the levels of required investment before a detailed analysis of the building structure and energy performance. For better retrofitting, there are three considerations to focus on [27]:

- (a) Developing simple prediction tools for retrofit concepts which allow the decision maker to evaluate integrated construction, installation and lighting measures;
- (b) Developing a so-called concept adviser to analyse existing buildings and their economic efficiency and to supplement this by simple methods for testing the efficiency of the applied measures;
- (c) Promoting energy and cost-efficient retrofit measures and to support decision makers in evaluating the efficiency and acceptability of available concepts.

This study revealed that the development of an energy concept adviser for economical retrofit measures was useful during the planning and realisation phase. It was recommended that the adviser be available during the entire retrofitting phase to ensure that both the calculated energy savings and economic success would be achieved after retrofitting [27]. Accordingly, the selection and analysis of existing information were made across all IEA member countries. One of the case studies (2000–2002) included schools and institutional and laboratory

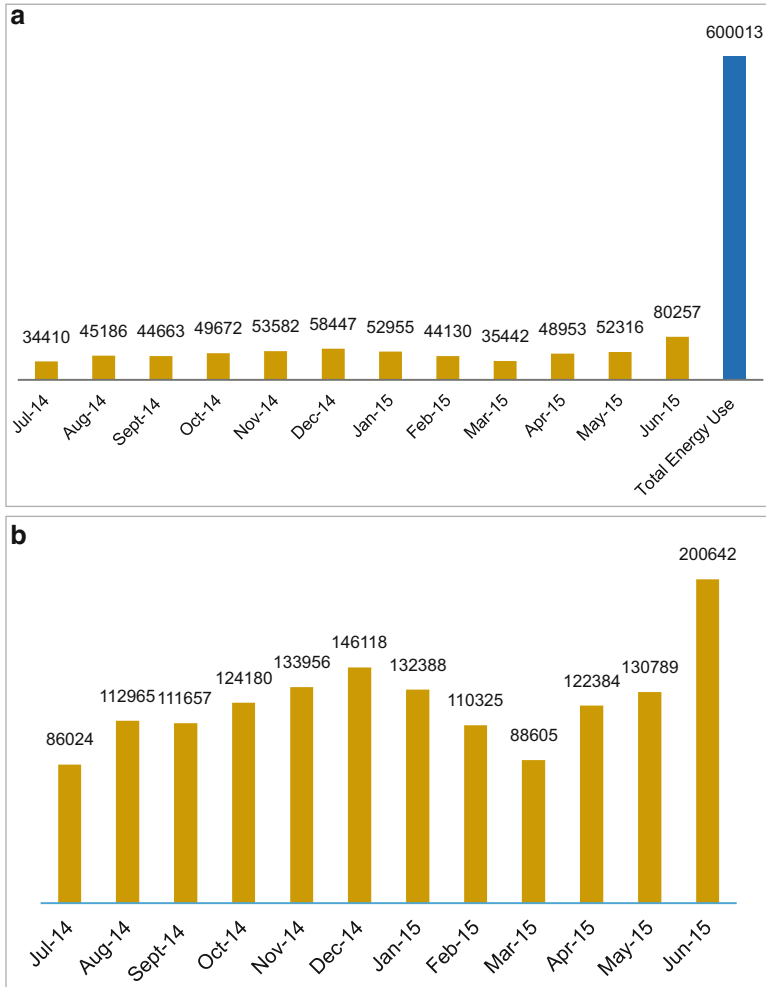


Fig. 9.6 Actual electrical energy consumption of BMS building. (a) Cost of electrical energy use/month (EGP). (b) Electrical energy consumption/month (kWh)

buildings, where innovative energy-saving measures, daylighting and artificial lighting systems were implemented along with advanced control systems. Measured performance data covered temperature, illuminance and other comfort criteria of the interior space, heating, cooling and electrical lighting consumption, the power consumption of the installations and control systems, the total building energy consumption and the indoor air quality [27].

For the retrofitting process of the BMS building on the AASTMT campus, the aforementioned measures, mainly energy saving, including artificial lighting systems will be applied. Also measured performance data covering air temperatures,

Table 9.2 Electrical appliance audit – all floors of BMS building

Appliance	Type	Number	Watts
Air conditioner	5 t	1	3895
Air conditioner	2.25 t	1	2200
Computer lab	–	1	100
Switcher in rack		1	100
Computer lab projector	Epson	1	450
Lecture room projector	Epson	1	450
Speaker (sound system)		1	30
Laptop		1	75
Fluorescent lamp	120 cm	1	36
CFL (spot light)	60 cm	1	18
Personal computer		1	100
Scanner		1	25
Laser jet printer (hewlett-packard)		1	75
Photocopying machine		1	1450
Kettles (water heating)		1	1800
LCD screen	50 in.	1	300
Fan (pantry)		1	75
Water boiler (pantry)		1	3600
Blender (pantry)		1	350
Electrical cooker (pantry)		1	750
Fridge (pantry)		1	1200
Hand dryer (WC)		1	180

cooling and electrical lighting consumption, total energy use and CO₂ emissions were considered in the assessment.

3.3.1 Building Envelope Components

The building envelope consists of all elements of the outer shell that maintain a dry, heated or cooled indoor environment and facilitate its climate control. For the case study, the envelope components are the exterior walls, fenestration, roof and ground floor (Fig. 9.7). The building *façades* are almost modularly designed; taking a section in one of the *façades* can determine its components. It is a medium colour (peach) that absorbs solar radiation and the glass windows are low-efficiency panes with a shading coefficient of 0.77 that highly absorb the solar radiation.

3.3.2 Occupancy Patterns

Energy consumption in educational buildings depends mainly on the building's activities, time of use and influx of students, academic staff, and visitors, as well as the academic term, whether winter or summer. So these occupancy pattern data

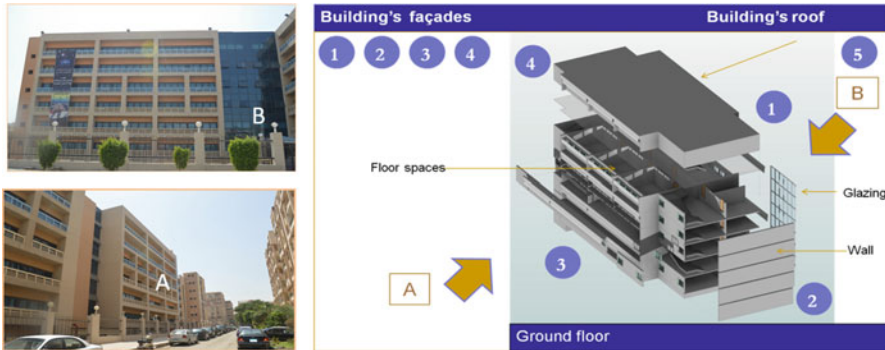


Fig. 9.7 Building envelope components

were collected and used as a base and added to the Design Builder energy simulation software. Descriptions of each floor and its energy consumption by space use and energy consumption by service are shown in Table 9.3.

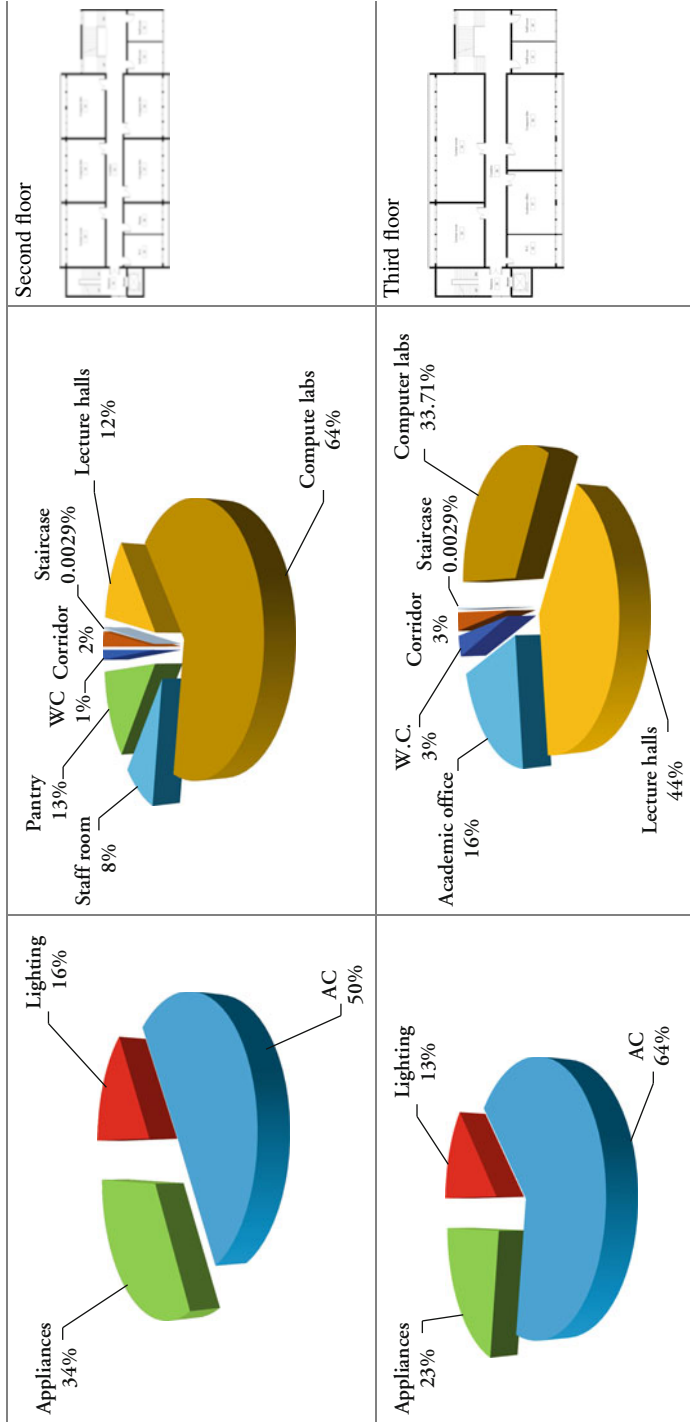
3.4 The BIM Model

Building information modelling (BIM) can be used to predict the energy performance of retrofit measures by developing models of existing buildings, proposing alternatives, analysing and comparing building performance for these and modelling improvements [13]. A BIM model was constructed for the whole building in REVIT with the thermal properties gathered and assigned to the different building components (walls, fenestration, floor and roof); then the generated model was exported to Design Builder, where climatic data assigned from the US Department of Energy weather files and occupancy patterns were added (Figs. 9.8 and 9.9).

The electrical energy consumption based on an EA of the energy services of the building's ground floor and five floors, with a floor area of 606.60 m² each, is illustrated in Fig. 9.10. It is clear that AC is the highest at 57%, followed by appliances (24%) and electrical lighting (15%). Also, the monthly electrical energy consumption per service (kWh)/floor is illustrated in Fig. 9.11. Total electrical energy use based on occupancy patterns without external lighting and elevator and with external lighting and elevator are 70,221 kWh/month (116 kWh/m²) and 73,467 kWh/month (121 kWh/m²) respectively. The energy consumption by space use and by service as well as floor plans (each floor occupies an area of 606.6 m²) as well all spaces' functions and uses based on the EA are shown in Table 9.3. It is seen from Table 9.3 that for energy use by service on all floors, AC is the highest (59–64%) followed by office appliances (23–34%) and lighting (13–16%), whereas energy consumption per space use is as follows: lecture halls and computer labs (second, third and fifth floors) are the highest. The lecture halls vary from 12 to 70%, whereas the computer labs from 34 to 64%, followed by

Table 9.3 Description of building's floors, energy use by space use and services (audit)

Energy consumption by service	Energy consumption by space use	Floor plans
<p>Appliances 20%</p> <p>Lighting 15%</p> <p>AC 64%</p>	<p>WC 2%</p> <p>Corridor 4%</p> <p>Staircase 0.24%</p> <p>Academic offices 24%</p> <p>Lecture halls 70%</p>	<p>Floor area: 606.6 m²</p> <p>Ground floor</p>
<p>Appliances 23%</p> <p>Lighting 16%</p> <p>AC 61%</p>	<p>Pantry 18%</p> <p>WC 2%</p> <p>Staircase 0.01%</p> <p>Corridor 1%</p> <p>Academic Offices and Dean's Office 20%</p> <p>Lecture halls 59%</p>	<p>First floor</p>



(continued)

Table 9.3 (continued)

	Energy consumption by service	Energy consumption by space use	Floor plans
<p>Appliances 24%</p> <p>Lighting 16%</p> <p>AC 60%</p>	<p>Computer labs 21%</p> <p>W.C. 3%</p> <p>Corridor 3%</p> <p>Staircase 0.0029%</p> <p>Vice Dean, Staff & Academic offices 34%</p> <p>Lecture halls 39%</p>	<p>Floor area: 606.6 m²</p> <p>Fourth floor</p>	
<p>Appliances 26%</p> <p>Lighting 15%</p> <p>AC 59%</p>	<p>Academic and Staff offices 20%</p> <p>W.C. 2%</p> <p>Corridor 2%</p> <p>Staircase 0.0029%</p> <p>Lecture halls 22%</p> <p>Computer labs 54%</p>	<p>Fifth floor</p>	

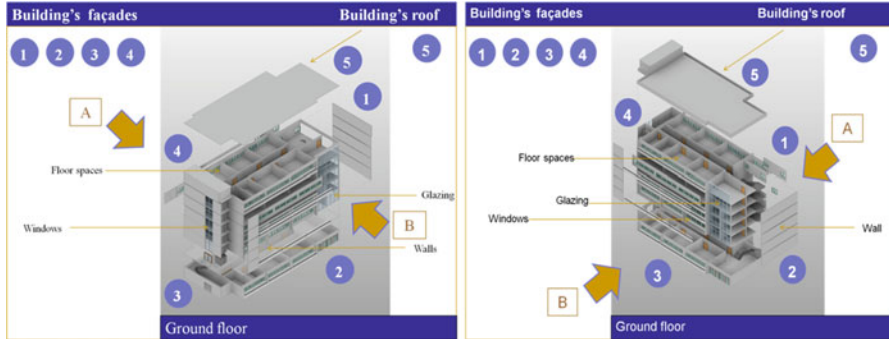


Fig. 9.8 Building information modelling (BIM) of case study



Fig. 9.9 Details of BIM of case study

academic and staff offices (8–34 %) and pantries on the first and second floors, which are 18 and 13 % respectively. The lowest energy use was that of corridors (1–4 %), WC (1–3 %) and staircases (0.003–0.24 %).

3.4.1 Building Description and Activities

An EA was conducted for all floors. It started with a walk-through assessment. The findings of the EA for all floors are shown in the appendix. Each table represents a floor in terms of space (type and area), occupancy (hourly, daily and total monthly hours), and energy use (lamps, AC and appliances in kilowatt-hours).

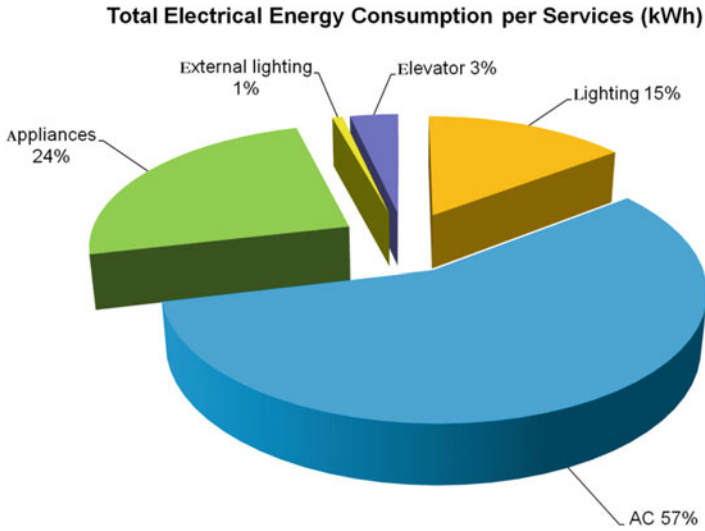


Fig. 9.10 Electrical energy audit per month (kWh) – whole building

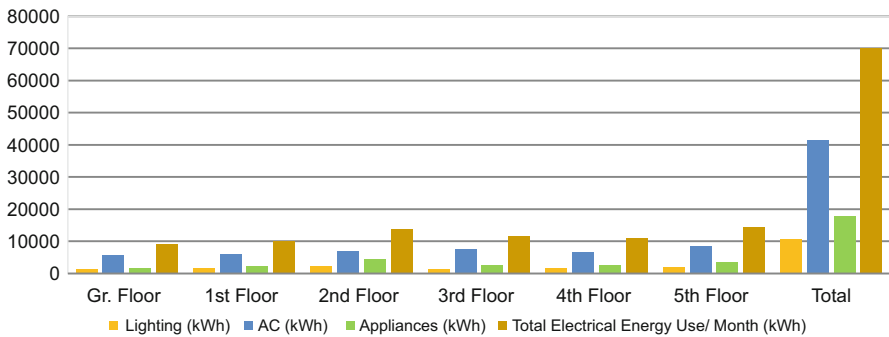


Fig. 9.11 Monthly electrical energy consumption per services (kWh/floor)

4 Energy Audit and Baseline Electrical Energy Consumption

Baseline energy consumption was determined using several methods, including the following:

- Electrical energy consumption/month and electrical energy consumption/month/m² are 86.63 kWh and 11.44 kWh/m² respectively (Figs. 9.12 and 9.13);
- Manually calculated electrical energy consumption based on occupancy patterns on each floor (e.g. 17,134.04 kWh/month and 7.60 kWh/m²);
- Simulated results of energy consumption using Design Builder (e.g. 15.36 kWh/m²);

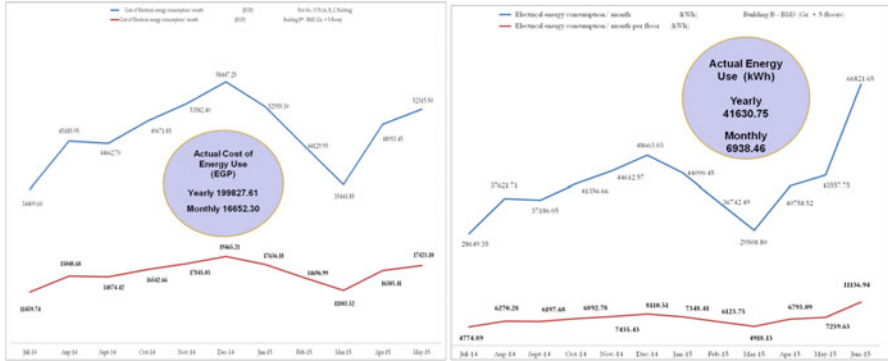


Fig. 9.12 Actual cost (EGP) and electrical energy use per month (kWh) – academic year 2014–2015

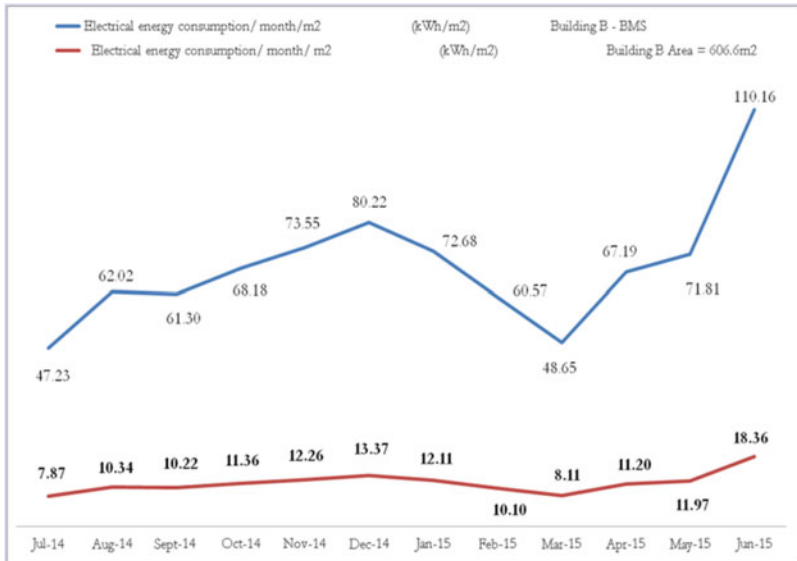


Fig. 9.13 Actual electrical energy use per square metre (kWh) – academic year 2014–2015

- Valid results for simulated baseline model and comparison of its results with calculated energy bills; this process requires knowledge of the time of use of all spaces (Table 9.4).

Table 9.4 Time of use of all floors' spaces, BMS building (Number 1175)

Space type	Working hours		Total hours
Lecture halls	8:30 a.m.	9:30 p.m.	13
Administrative staff	8:30 a.m.	6:30 p.m.	10
Academic staff	8:30 a.m.	6:30 p.m.	10
Assistant staff	8:30 a.m.	6:30 p.m.	10
Computer labs	8:30 a.m.	6:30 p.m.	10
Library	8:30 a.m.	6:30 p.m.	10
Elevators	8:00 a.m.	9:30 p.m.	13.5
WC	8:30 a.m.	9:30 p.m.	13
Corridors	8:30 a.m.	9:30 p.m.	13
Staircases	8:30 a.m.	9:30 p.m.	13

5 Sustainability and Retrofit Measures

Several retrofit measures were applied to retrofit the various floors of the building. These measures were used in the simulation of cases A and B. In the baseline assessment, cases A and B were chosen to be applied to all floors. The applied retrofitting measures are described in what follows.

5.1 Envelope Assessment

The building envelope has an effect on the amount of daylight in interior spaces. Analysing the lighting levels in the selected floor plans showed that daylight levels were not at their recommended levels throughout the spaces. For educational spaces, 400–500 lx is the optimum level that must be achieved in classes and lecture halls [33].

5.2 Glazing

Single glazing with a high solar heat gain coefficient (SHGC) of 0.81 and a high U-value of $4.8 \text{ W/m}^2 \text{ K}$ that was replaced by a double glazing low-E glazing and resimulation was done to determine the effectiveness of the change, as shown in Table 9.5. The window area is 2.257 m^2 ($1.85 \times 1.22 \text{ m}$) and made of a well-fitted aluminium frame with a thermal resistance of $0.61 \text{ m}^2 \text{ K/W}$ and the glazing visible light transmission of 89 %.

Table 9.5 Glazing characteristic of baseline, cases A and B

Scenario	Baseline	Case A	Case B
	Single glazing	Low-E double glazing filled with argon (13 mm)	Low-E double solar control glazing filled with argon ^a
U-value (W/m ² K)	4.80	1.514	1.484
Solar heat gain coefficient (SHGC)	0.81	0.595	0.33
Shading coefficient (SC)	0.76	0.48	0.37
Visible light transmission (VLT)	0.89	0.769	0.38

^aST 450 Reflecta-Sol glass produced by Saint Gobain Glass, Egypt

5.3 External Wall Thermal Insulation

Thermal insulation for the building envelope was added to change its section from the baseline of a U-value of 1.64 W/m² K to a compound wall area of 7.312 m² (cases A and B) of an overall U-value of 0.250 W/m² K. This wall layer includes 2.00 mm external paint on plaster applied on a brick wall (25 cm), an air gap of 13.00 mm and a 12.00 mm Gibson board covered with caulk and internal paint. The slab U-value is 1.359 W/m² K based on a resistance of 0.736 m² K/W.

5.4 Green Roof

The original roof was made of a traditional finish that included a noninsulated roof with a U-value of 1.89 W/m² K. The roof section was composed of 2 cm tiles, 3 cm gravel, a 2 cm waterproof membrane, 5 cm screed and a 20 cm reinforced concrete roof slab. A green roof (GR) was applied on the roof of the fifth floor to act as a heat insulator and to take advantage of its ability to lower air temperatures and minimise the heat island effect. An extensive GR type was used (U-value of 0.14 W/m² K), which requires low maintenance and which is supported by the current roof structure.

6 Results and Discussion

Electrical energy consumption was determined using Design Builder computer simulation software. The patterns of total electrical energy consumption/month for the ground, first, second, third, fourth and fifth floors are shown in Figs. 9.14, 9.15 and 9.16. The CO₂ emissions and reductions are illustrated in Figs. 9.17, 9.18 and 9.19. Figure 9.14 represents the baseline assessment before retrofitting, whereas

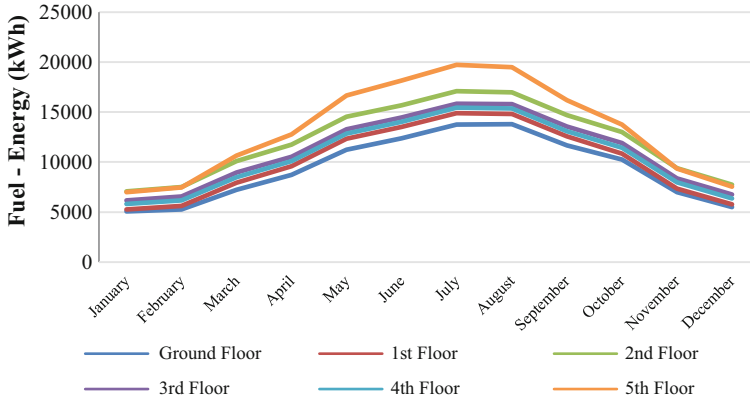


Fig. 9.14 Energy consumption breakdown/month (simulated) – baseline case

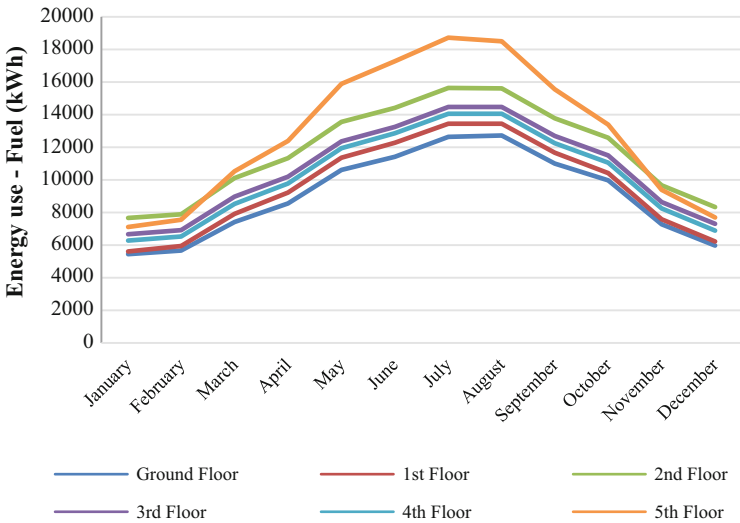


Fig. 9.15 Energy consumption breakdown/month (simulated) after improvements – case A

Figs. 9.15 and 9.16 represent cases A and B, taking into account the measures applied for the retrofitting, including the changing of glazing characteristics to case B (Table 9.6). In addition, a GR (U-value of 0.14 W/m² K) was applied above the fifth floor. This resulted in a reduction of electrical energy consumption of 7.6 % and actual savings of 9997 kWh/month compared to the original roof. The results of retrofitting measures applied in cases A and B for all floors resulted in a reduction of electric energy consumption of 50 % and total monthly energy savings in the building of 5558.4 kWh. The CO₂ emissions reduction/month in cases A and Case B compared with the baseline case (simulated) are shown in Fig. 9.20,

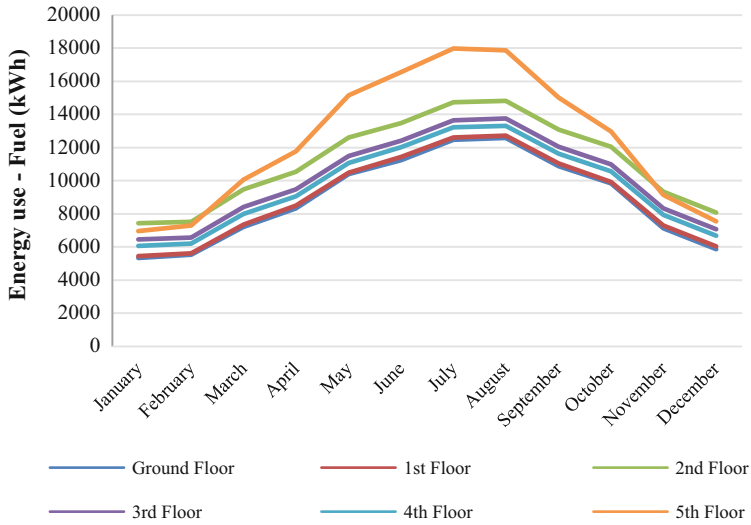


Fig. 9.16 Energy consumption breakdown/month (simulated) after improvements – case B

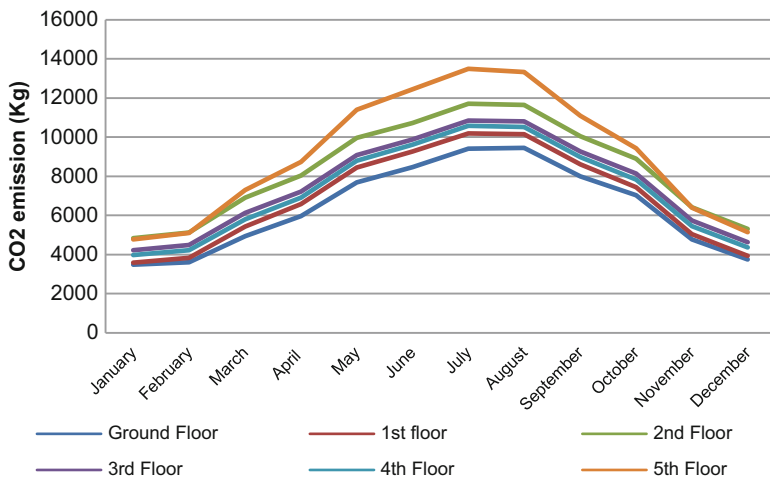


Fig. 9.17 CO₂ emissions/month (simulated) – baseline case

whereas the comparison of CO₂ reduction on all floors and with a GR (case B) is shown in Fig. 9.21.

It is clear from Fig. 9.21 that CO₂ emissions were reduced from 101,596.3 to 100,479.93 kg when the GR was installed on the fifth floor. Figure 9.22 illustrates a comparison between the baseline of the retrofitted building and improvements when retrofitting measures were applied in cases A and B on the ground floor and first floor as a pilot. The Electrical energy consumption of the ground floor was

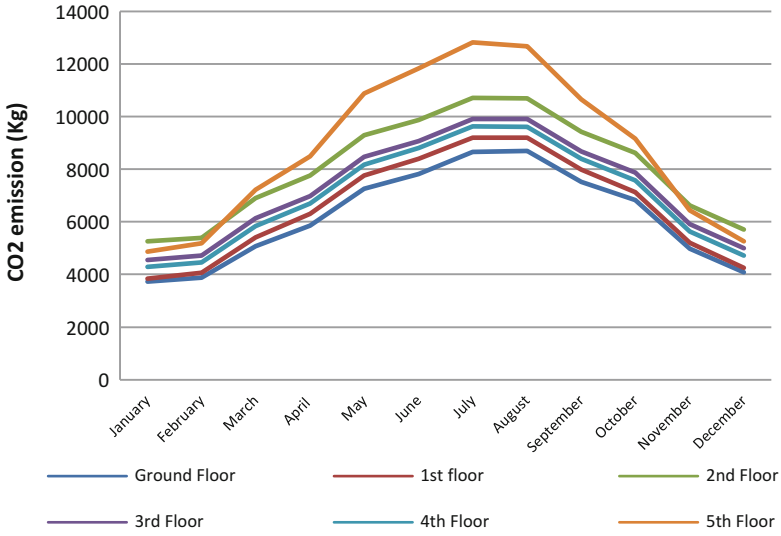


Fig. 9.18 CO₂ emission reduction/month after improvements – case A (simulated)

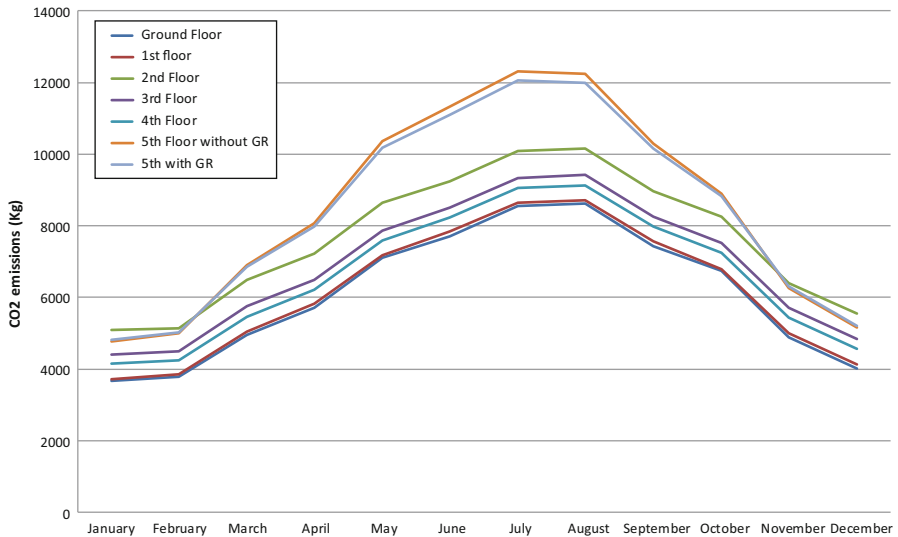


Fig. 9.19 CO₂ emission reduction/month after improvements – case B (simulated)

reduced from 9316.30 kWh (baseline) to 9045.41 kWh (Case A) and was further reduced to 8824.3 kWh for Case B, i.e. case A savings were 271 kWh (2.91 %) and case B savings reached 492 kWh (5.28 %), as shown in Fig. 9.22a. Savings per square meter (kWh/m²) are illustrated in Fig. 9.22b.

Figure 9.23 shows the savings in electrical energy when applying improvements to cases A and B, ground floor, whereas Fig. 9.24 depicts these savings for the fifth

Table 9.6 Results in energy savings in case B

Floor	Saving of electrical energy consumption (%)	Actual savings (kWh/month)
Ground	5.30	492.00
1	10.01	1005.18
2	8.48	1028.05
3	8.72	960.16
4	9.00	940.41
5	1.10	136.00
5 with GR	7.54	996.60

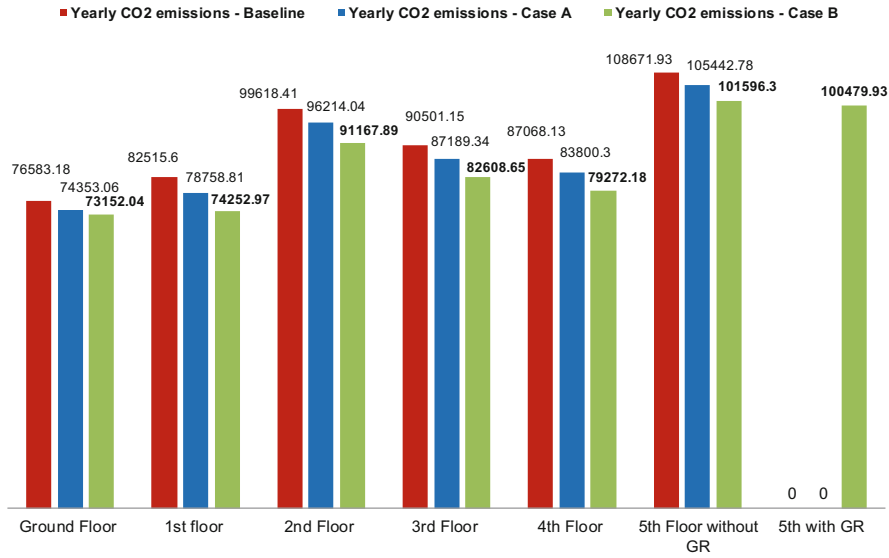


Fig. 9.20 CO₂ emission reduction/month in case A and case B vs. baseline (simulated)

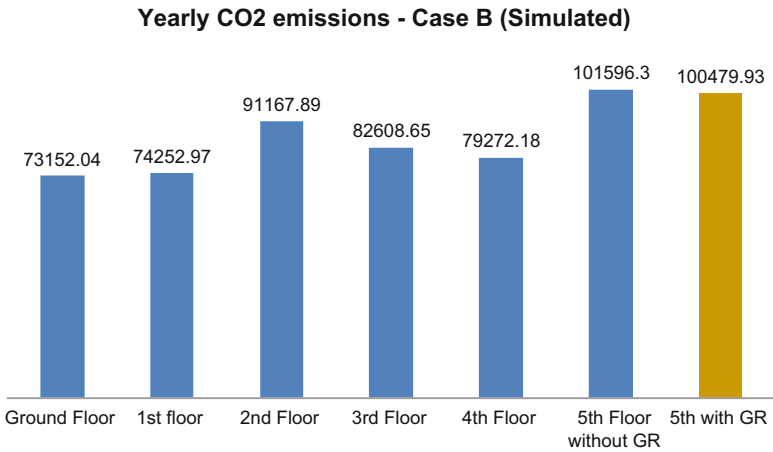


Fig. 9.21 Comparison of CO₂ reduction in all floors after improvements – case B

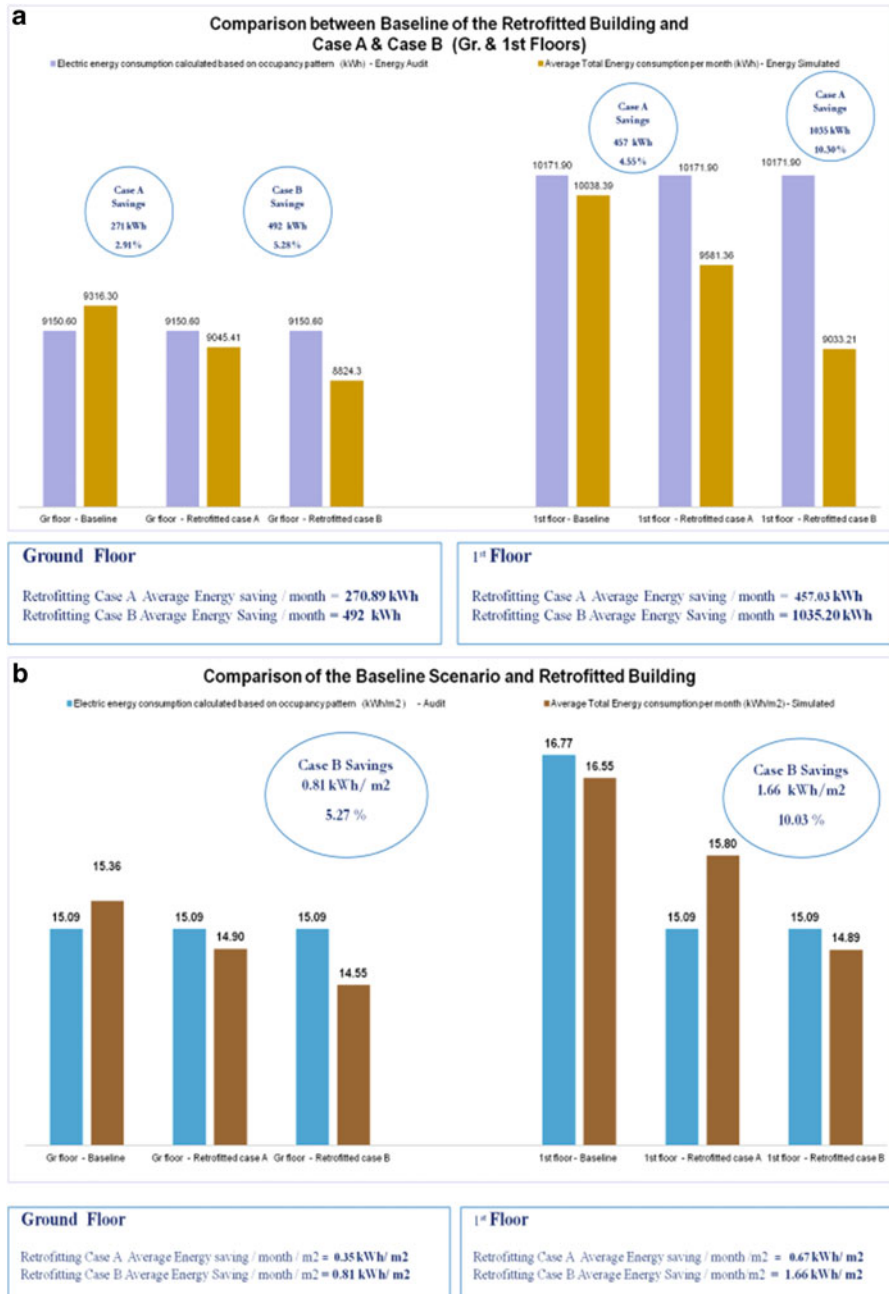


Fig. 9.22 Comparison between baseline of retrofitted building and cases A and B. (a) Electrical energy savings (kWh/month). (b) Electrical energy saving (kWh/m²)

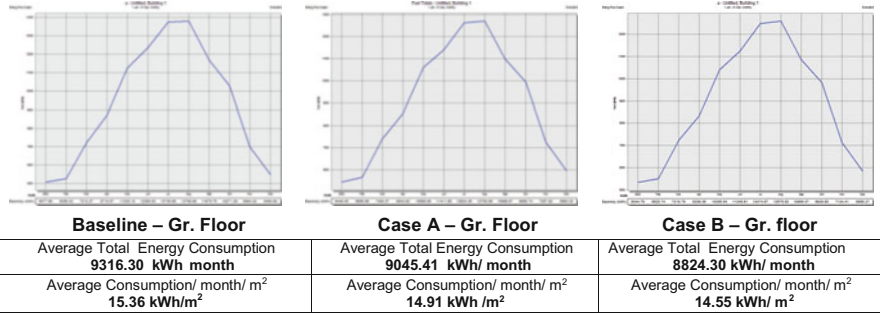


Fig. 9.23 Savings in electrical energy when applying improvements to cases A and B – ground floor

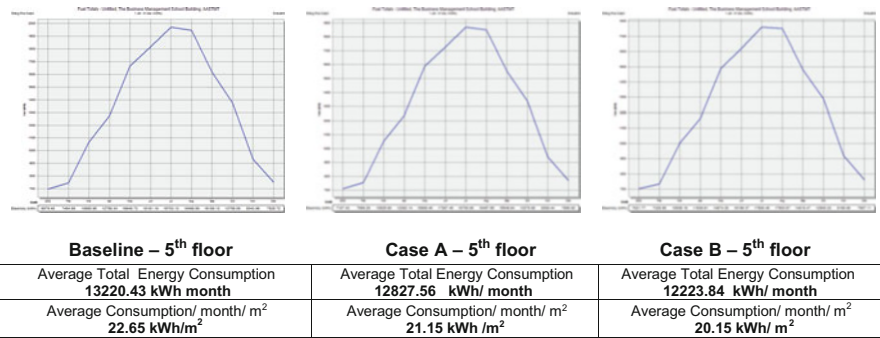


Fig. 9.24 Savings in electrical energy when applying improvements to cases A and B – fifth floor

floor after retrofitting. It is clear from Fig. 9.23 that average total energy consumption for the baseline, cases A and B are 9316.30, 9045.41 and 8824.30 kWh/month respectively, whereas the average consumption/month/m² is 15.36, 14.91 and 14.55 kWh/m² respectively. It has been reduced by 492 kWh/ month from 9316.30 kWh/month (Baseline) to 8824.30 kWh/ month (Case B), i.e., by 5.28 %. On the fifth floor, consumption was reduced 437 from 13,220.43 kWh/ month (baseline) to 12,223.84 kWh/ month in case B (22.65–20.15 kWh/m²), a reduction in electrical consumption of 7.54 % (Fig. 9.24).

Figure 9.25 shows the reduction in the building total cooling when improvements are applied in cases A and B on all floors. Figure 9.26 presents details on the total savings in energy use for all floors as a result of the retrofitting scenarios in reference to the baseline. The analysis of the energy consumption for each floor and the total building is depicted in Figs. 9.27 9.28, and 9.29. As seen, case A’s improvement from the baseline resulted in an energy consumption reduction of 26.79% (all floors) and the improvements of case B resulted in a reduction of 48.99 % as shown in (Fig. 9.29).

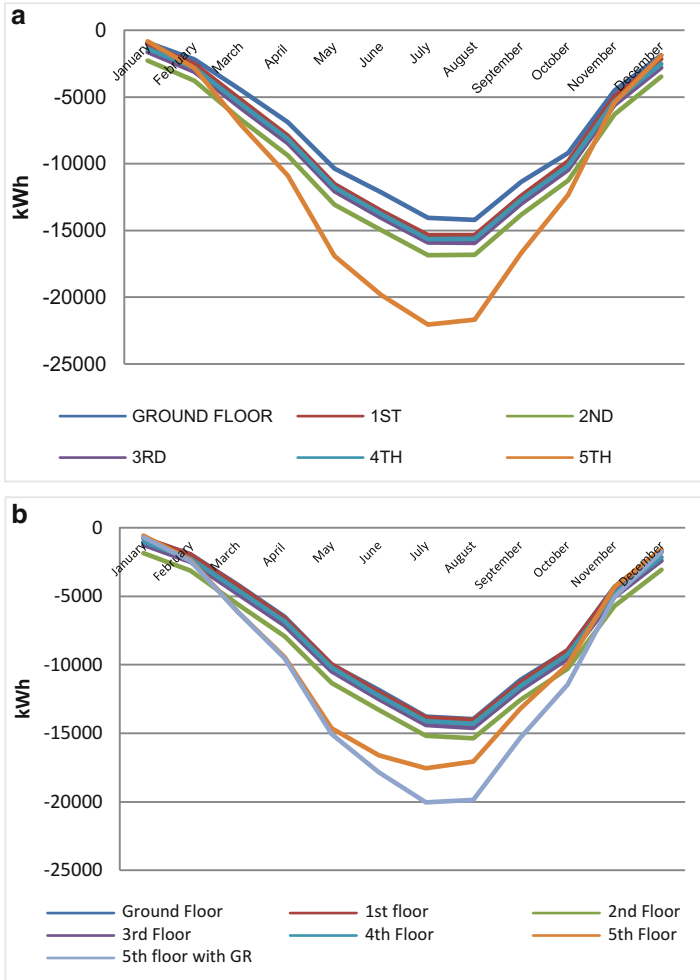


Fig. 9.25 Saving in total cooling when applying improvements to cases A and B—all floors. (a) Without green roof. (b) With green roof

7 Conclusions

The retrofitting of existing buildings is vital for saving energy and reducing CO₂ emissions. The results of the retrofitting project discussed in this chapter indicated that in case B, on all floors, the reduction in energy consumption was much greater than in case A. Despite the changes in floor energy use due to activities, the overall reduction was approximately 27% from the baseline energy consumption in case A and 49% in case B. Changing the glazing to a low-E double glazing, with a U-value of 1.514 W/m² K, SHGC of 0.595 and light transmission of 0.77, led to actual

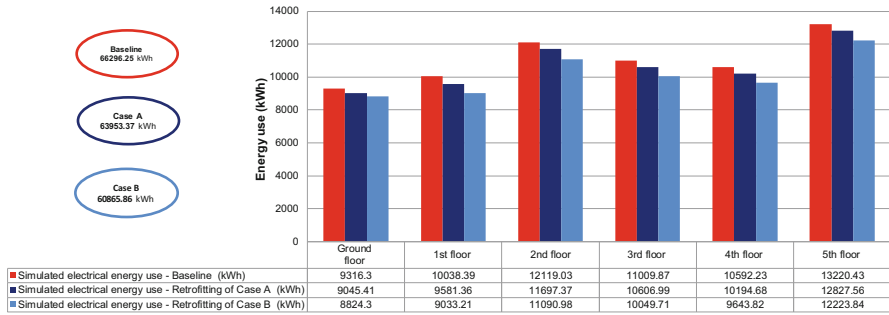


Fig. 9.26 Savings in energy use on all floors as a result of retrofitting scenarios

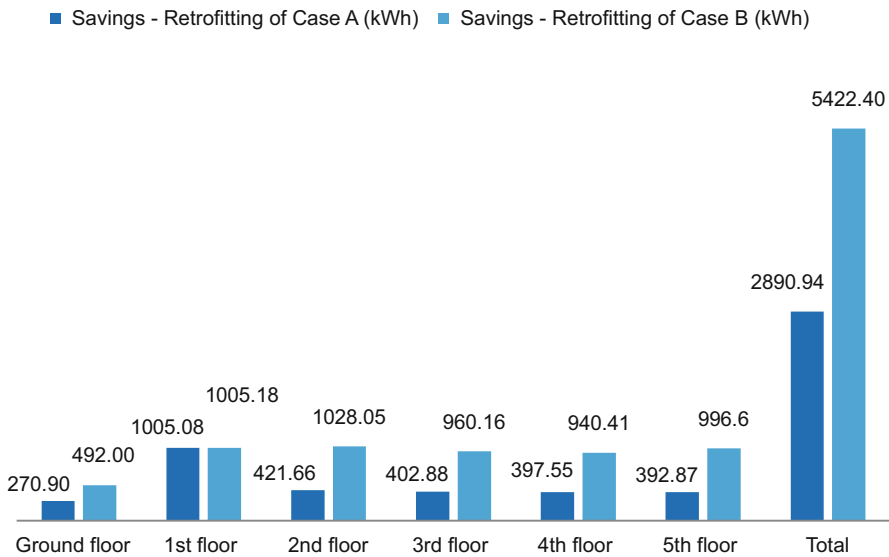


Fig. 9.27 Details of savings for each floor and total

savings of 2891 kWh/month from the baseline. The maximum savings were due to improvements in the envelope’s thermal insulation, 27 % in case A and and 49 % in case B. This was due to the integration of three retrofitting measures – glazing efficiency, wall thermal insulation (whole envelope) and green roof on the fifth floor. Changing the glazing to a low-E double glazing (Solar Control-Saint Gobain Glass, Egypt, ST450—Reflecta-Sol glass) with a U-value of 1.50 W/m² K, SHGC of 0.33, light transmission of 0.38, wall U-value of 0.25 W/m² K and roof improvements resulting from the installation of an extensive green roof (U-value 0.14 W/m² K) led to savings of 5422 kWh/month from the baseline. It is clear that improving glass efficiency is vital in the retrofitting of existing buildings.

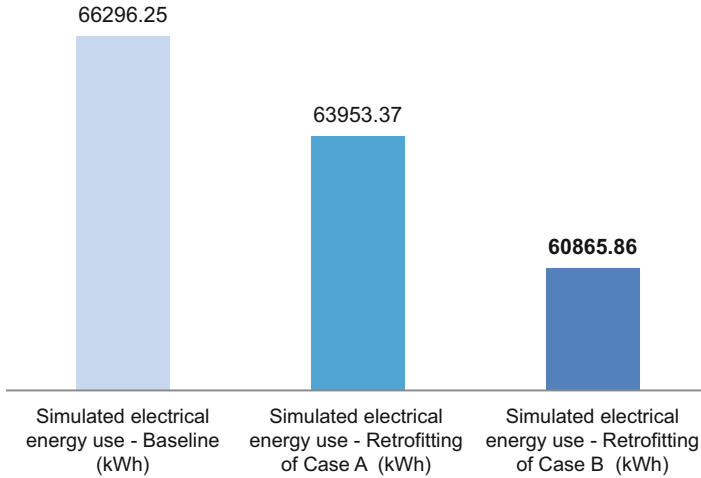


Fig. 9.28 Total building energy consumption based on retrofitting scenarios

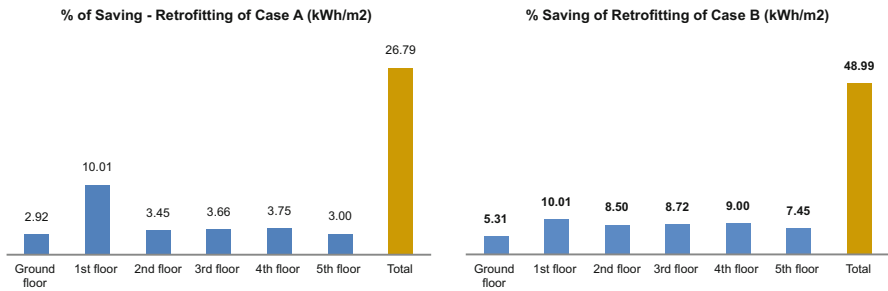


Fig. 9.29 Savings in energy consumption of two retrofitting scenarios (cases A and B)

Acknowledgments The authors would like to thank to Prof Tarek Abdin, Dean of the Business School, for his support and providing access to building information and spaces. Thanks go to the administrative staff for providing the walk-through and technical data. Finally, I thank research students Mohamed Hassan and Heba Sarag for their assistance during data gathering in connection with the energy audit. Last but not least, I sincerely express my gratitude to Architect Mohamed Hammad for running the simulations.

Appendix

Ground floor

No.	Space		Occupancy patterns				Energy Consumption								
	Name	Area (m ²)	Hours/day	Days/week	Total hours (week)	Total Hours (Month)	Lamps (36, 32 & 18 Watts)			Air conditioning (3895 & 2200 Watts)			Appliances (PC, LT, Sc, Ptn, Pj, Ke, Sw, Fnd, Co, Bl, Fw, LCD)		
							Nos.	Power kW	Energy kWh	Nos.	Power kW	Energy kWh	Nos.	Power kW	Energy kWh
1	Lecture room	58 m ²	12	6	72	288	24	0.768	221.2	1	3.9	1123.2	8 (3 Lt + 1 Pro + 4 Sp)	0.795	228.96
2	Lecture room	57 m ²	12	6	72	288	24	0.768	221.2	1	3.9	1123.2	8 (3 Lt + 1 Pro + 4 Sp)	0.795	228.96
3	Lecture room	58 m ²	12	6	72	288	24	0.768	221.2	1	3.9	1123.2	8 (3 Lt + 1 Pro + 4 Sp)	0.795	228.96
4	Lecture room	57 m ²	12	6	72	288	24	0.768	221.2	1	3.9	1123.2	8 (3 Lt + 1 Pro + 4 Sp)	0.795	228.96
5	Academic office	28 m ²	10	5	50	200	16	0.288	57.6	1	2.2	440	11 (3 Pc + 1 Ke + 2 Pm + 1 Sc + 4 Sw)	2.68	536
6	Academic office	30 m ²	10	5	50	200	16	0.288	57.6	1	2.2	440	5 (1 Pc + 1 Ke + 1 Pr + 1 Sc + 1 Sw)	0.375	75
7	Academic office	28 m ²	10	5	50	200	16	0.288	57.6	1	2.2	440	5 (1 Pc + 1 Ke + 1 Pr + 1 Sc + 1 Sw)	0.375	75
8	W.C.	30 m ²	13	6	78	312	16	0.288	89.9	0	0	0	3 (1 Hd + 2 Fa)	0.33	102.96
9	Staircase	50 m ²	13	6	78	312	4	0.128	39.9	0	0	0	0	0	0
10	Lobby	77 m ²	13	6	78	312	20	0.64	199.7	0	0	0	1 (1 LCD)	0.3	93.6
11	Entrance	118 m ²	13	6	78	312	16	0.288	89.9	0	0	0	2 (2 Pj)	0.2	62.4
Total Electrical Energy Consumption														9150.600	kWh/month

- Appliances*
- Pc Computer
 - Lt Laptop
 - Sp Speakers
 - Sc Scanner
 - Pm Printer
 - Ke Keyboard
 - Sw Switch
 - Pr Projector
 - Hd Head-ayer
 - Fa Fan
 - Pj Pj
 - LCD LCD screen
 - Ke Ke

First floor

No.	Space		Occupancy patterns				Energy Consumption								
	Name	Area (m ²)	Hours/day	Days/week	Total hours (week)	Total Hours (Month)	Lamps (36, 32 & 18 Watts)			Air conditioning (3895 & 2200 Watts)			Appliances (PC, LT, Sc, Ptn, Pj, Ke, Sw, Fnd, Co, Bl, Fw, LCD)		
							Nos.	Power kW	Energy kWh	Nos.	Power kW	Energy kWh	Nos.	Power kW	Energy kWh
12	Academic office	26 m ²	10	5	50	200	16	0.288	57.6	1	2.2	440	9 (2 Pc + 1 Ke + 1 Pm + 1 Sc + 4 Sw)	0.25	50
13	Academic office	26 m ²	10	5	50	200	16	0.288	57.6	1	2.2	440	8 (4 Pc + 1 Ke + 2 Pm + 2 Sc + 1 Sw)	0.25	50
14	Desk's office	58 m ²	10	5	50	200	24	0.768	153.6	1	3.9	780	7 (2 Pc + 1 Ke + 2 Pm + 1 Sc + 1 Sw)	0.225	45
15	Lecture room	37 m ²	12	6	72	288	24	0.768	221.2	1	3.9	1123.2	8 (3 Lt + 1 Pro + 4 Sp)	0.795	228.96
16	Putry	28 m ²	10	5	50	200	24	0.768	153.6	1	0	0	4 (1 Pfd + 1 Bl + 1 Co + 1 Fa)	3.625	1125
17	W.C.	30 m ²	13	6	78	312	16	0.288	89.9	0	0	0	3 (1 Hd + 2 Fa)	0.33	102.96
18	Staircase	50 m ²	13	6	78	312	4	0.128	39.9	0	0	0	0	0	0
19	Corridor	143 m ²	13	6	78	312	20	0.64	199.7	0	0	0	1 (1 LCD)	0.30	93.6
20	Lecture room	58 m ²	12	6	72	288	24	0.768	221.2	1	3.9	1123.2	8 (3 Lt + 1 Pro + 4 Sp)	0.795	228.96
21	Lecture room	37 m ²	12	6	72	288	24	0.768	221.2	1	3.9	1123.2	8 (3 Lt + 1 Pro + 4 Sp)	0.795	228.96
22	Lecture room	58 m ²	12	6	72	288	24	0.768	221.2	1	3.9	1123.2	8 (3 Lt + 1 Pro + 4 Sp)	0.795	228.96
Total Electrical Energy Consumption														10171.900	kWh/month

- Appliances*
- Pc Computer
 - Lt Laptop
 - Sp Speakers
 - Sc Scanner
 - Pm Printer
 - Ke Keyboard
 - Sw Switch
 - Pr Projector
 - Hd Head-ayer
 - Fa Fan
 - Pj Pj
 - LCD LCD screen
 - Ke Ke

Second floor

No.	Space		Occupancy patterns				Energy Consumption								
	Name	Area (m ²)	Hours/day	Days/week	Total hours (week)	Total Hours (Month)	Lamps (36, 32 & 18 Watts)			Air conditioning (3895 & 2200 Watts)			Appliances (PC, LT, Sc, Ptn, Pj, Ke, Sw, Fnd, Co, Bl, Fw, LCD)		
							Nos.	Power kW	Energy kWh	Nos.	Power kW	Energy kWh	Nos.	Power kW	Energy kWh
23	Lecture room	58 m ²	12	6	72	288	24	0.768	221.2	1	3.9	1123.2	8 (3 Lt + 1 Pro + 4 Sp)	0.795	228.96
24	Computer labs	57 m ²	12	6	72	288	32	1.152	331.8	1	3.9	1123.2	23 (20 Pc + 1 Pro + 2 Sw)	2.550	734.40
25	Computer labs	57 m ²	12	6	72	288	32	1.152	331.8	1	3.9	1123.2	23 (20 Pc + 1 Pro + 2 Sw)	2.550	734.40
26	Computer labs	57 m ²	12	6	72	288	32	1.152	331.8	1	3.9	1123.2	23 (20 Pc + 1 Pro + 2 Sw)	2.550	734.40
27	Computer labs	57 m ²	12	6	72	288	32	1.152	331.8	1	3.9	1123.2	23 (20 Pc + 1 Pro + 2 Sw)	2.550	734.40
28	Putry	28 m ²	10	5	50	200	24	0.664	172.8	1	2.2	440	4 (1 Pfd + 1 Bl + 1 Co + 1 Fa)	3.625	1125
29	W.C.	30 m ²	13	6	78	312	16	0.288	89.9	0	0	0	3 (1 Hd + 2 Fa)	0.33	102.96
30	Staircase	50 m ²	13	6	78	312	4	0.128	39.9	0	0	0	0	0	0
31	Staff room	26 m ²	10	5	50	200	16	0.288	57.6	1	2.2	440	6 (4 Pc + 1 Ke + 1 Sw)	0.24	75
32	Staff room	26 m ²	10	5	50	200	16	0.288	57.6	1	2.2	440	8 (6 Pc + 1 Ke + 1 Sw)	0.25	75
33	Corridor	143 m ²	13	6	78	312	20	0.64	199.7	0	0	0	1 (1 LCD)	0.30	93.6
Total Consumption														13740.02	kWh/month

- Appliances*
- Pc Computer
 - Lt Laptop
 - Sp Speakers
 - Sc Scanner
 - Pm Printer
 - Ke Keyboard
 - Sw Switch
 - Pr Projector
 - Hd Head-ayer
 - Fa Fan
 - Pj Pj
 - LCD LCD screen
 - Ke Ke

Third floor

No.	Space		Occupancy patterns			Total Hours (Month)	Energy Consumption								
	Name	Area (m ²)	Hours/day	Days/week	Total hours (week)		Lamps (36, 32 & 18 Watts)			Air conditioning (3095 & 2200 Watts)			Appliances (Pc, Lt, Sc, Pm, Pk, Ke, Sw, LCD, Hd, Fa, Hd)		
							Nos.	Power kW	Energy kWh	Nos.	Power kW	Energy kWh	Nos.	Power kW	Energy kWh
34	Lecture room	115 m ²	12	6	72	288	32	1.152	331.8	4	8.8	2534.4	8 (3 Lt + 1 Pro + 4 Sp)	0.795	238.96
35	Lecture room	38 m ²	12	6	72	288	24	0.768	221.2	1	3.9	1123.2	8 (3 Lt + 1 Pro + 4 Sp)	0.795	238.96
36	Computer labs	86 m ²	12	6	72	288	46	1.656	476.9	2	7.8	2246.4	23 (18 Pc + 4 Sp + 1 Pro)	2.40	691.20
37	Academic office	27 m ²	10	5	50	200	14	0.144	28.8	1	3.9	780	6 (2 Pc + 1 Ke + 1 Pm + 1 Sc + 1 Sw)	2.20	440
38	Corridor	143 m ²	13	6	78	312	20	0.64	199.7	0	0	0	0	0	0
39	Staircase	50 m ²	13	6	78	312	4	0.128	39.9	0	0	0	0	0	0
40	Staff room	26 m ²	10	5	50	200	16	0.288	57.6	1	2.2	440	6 (4 Pc + 1 Ke + 1 Sw)	2.30	460
41	Staff room	26 m ²	10	5	50	200	16	0.288	57.6	1	2.2	440	8 (6 Pc + 1 Ke + 1 Sw)	2.30	500
42	W.C.	30 m ²	13	6	78	312	16	0.288	89.9	0	0	0	3 (1 Hd + 2 Fa)	0.33	102.96
Total Consumption														11719.48	kWh/month

- Appliances
- Pc Computer
 - Lt Laptop
 - Sp Speakers
 - Sc Scanner
 - Pm Printer
 - Pk Projector
 - Ke Kettle
 - Hd Hand dryer
 - Fa Fan
 - LCD LCD screen
 - Sw Switcher

Fourth floor

No.	Space		Occupancy patterns			Total Hours (Month)	Energy Consumption								
	Name	Area (m ²)	Hours/day	Days/week	Total hours (week)		Lamps (36, 32 & 18 Watts)			Air conditioning (3095 & 2200 Watts)			Appliances (Pc, Lt, Sc, Pm, Pk, Ke, Sw, LCD, Hd, Fa)		
							Nos.	Power kW	Energy kWh	Nos.	Power kW	Energy kWh	Nos.	Power kW	Energy kWh
43	Staff room	52 m ²	10	5	50	200	16	0.288	57.6	1	3.895	779	7 (5 Pc + 1 Ke + 1 Sw)	2.4	480
44	Lecture room	58 m ²	12	6	72	288	24	0.768	221.2	1	3.895	1123.2	8 (3 Lt + 1 Pro + 4 Sp)	0.795	113.76
45	Lecture room	37 m ²	12	6	72	288	24	0.768	221.2	1	3.895	1123.2	8 (3 Lt + 1 Pro + 4 Sp)	0.795	113.76
46	Visi-Dial's office	29 m ²	10	5	50	200	16	0.512	102.4	2	4.4	880	2 (2 Pc + 1 Pm)	0.175	35
47	Academic office	28 m ²	10	5	50	200	14	0.144	28.8	1	2.2	440	5 (1 Pc + 1 Ke + 1 Pm + 1 Sc + 1 Sw)	4.55	910
48	Computer labs	58 m ²	12	6	72	288	46	1.656	476.9	1	3.895	1123.2	22 (20 Pc + 1 Pro + 1 Sw)	2.55	734.4
49	Staff room	57 m ²	12	6	72	288	24	0.768	221.2	1	3.895	1123.2	8 (3 Lt + 1 Pro + 4 Sp)	0.795	113.76
50	W.C.	58 m ²	13	6	78	312	20	0.72	224.6	0	0	0	3 (1 Hd + 2 Fa)	0.33	102.96
51	Corridor	143 m ²	13	6	78	312	20	0.64	199.7	0	0	0	1 (1 LCD)	0.20	93.6
52	Staircase	50 m ²	13	6	78	312	4	0.128	39.9	0	0	0	0	0	0
Total Electrical Energy Consumption														11082.540	kWh/month

- Appliances
- Pc Computer
 - Lt Laptop
 - Sp Speakers
 - Sc Scanner
 - Pm Printer
 - Pk Projector
 - Ke Kettle
 - Hd Hand dryer
 - Fa Fan
 - LCD LCD screen
 - Sw Switcher

Fifth floor

No.	Space		Occupancy patterns			Total Hours (Month)	Energy Consumption								
	Name	Area (m ²)	Hours/day	Days/week	Total hours (week)		Lamps (36, 32 & 18 Watts)			Air conditioning (3095 & 2200 Watts)			Appliances (Pc, Lt, Sc, Pm, Pk, Ke, Sw, LCD, Hd, Fa)		
							Nos.	Power kW	Energy kWh	Nos.	Power kW	Energy kWh	Nos.	Power kW	Energy kWh
53	Lecture room	58 m ²	12	6	72	288	24	0.768	221.2	1	3.9	1123.2	8 (3 Lt + 1 Pro + 4 Sp)	0.795	238.96
54	Lecture room	57 m ²	12	6	72	288	24	0.768	221.2	1	3.9	1123.2	8 (3 Lt + 1 Pro + 4 Sp)	0.795	238.96
55	Computer labs	58 m ²	12	6	72	288	32	1.152	331.8	2	7.8	2346.4	22 (20 Pc + 1 Pro + 1 Sw)	2.55	734.4
56	Computer labs	57 m ²	12	6	72	288	32	1.152	331.8	2	7.8	2346.4	22 (20 Pc + 1 Pro + 1 Sw)	2.55	734.4
58	Staff room	32 m ²	10	5	50	200	32	1.024	204.8	2	4.4	880	19 (15 Pc + 1 Ke + 1 Pm + 1 Sc + 1 Sw)	3.5	700
59	Academic office	29 m ²	10	5	50	200	14	0.144	28.8	2	4.4	880	3 (2 Pc + 1 Pm + 1 Sc)	0.375	75
60	W.C.	29 m ²	13	6	78	312	20	0.72	224.6	0	0	0	3 (1 Hd + 2 Fa)	0.33	102.96
61	Staircase	50 m ²	13	6	78	312	4	0.128	39.9	0	0	0	0	0	0
62	Corridor	143 m ²	13	6	78	312	20	0.64	199.7	0	0	0	1 (1 LCD)	0.3	93.6
63	Computer labs	58 m ²	13	6	78	312	32	1.152	339.4	0	0	0	22 (20 Pc + 1 Pro + 1 Sw)	2.55	765.6
Total Electrical Energy Consumption														14356.28	kWh/month

- Appliances
- Pc Computer
 - Lt Laptop
 - Sp Speakers
 - Sc Scanner
 - Pm Printer
 - Pk Projector
 - Ke Kettle
 - Hd Hand dryer
 - Fa Fan
 - LCD LCD screen
 - Sw Switcher

References

1. Gouldson A, Colenbrander S, Sudmant A, Godfrey N, Millward-Hopkins J, Fang W, Zhao X (2015) Accelerating low-carbon development in the world's cities. In: Contributing paper for seizing the global opportunity: partnerships for better growth and a better climate—new climate economy, London and Washington, DC. <http://newclimateeconomy.report/misc/working-papers>
2. Zhang T, Siebers P, Aickelin U (2011) Modelling electricity consumption in office buildings: an agent based approach. *Energy Build* 43:2882–2892
3. Research Councils UK. <http://www.rcukenergy.org.uk/.../research-councils-energy-program.html/>. Accessed 16 May 2015
4. European Commission Joint Research Centre http://re.jrc.ec.europa.eu/energyefficiency/html/standby_initiative_data_centers.htm. Accessed 16 May 2015
5. Gallachoir BPO, Keane M, Morrissey E, O'Donnell J (2007) Using indicators to profile energy consumption & to inform energy policy in a university: a case study in Ireland. *Energy Build* 39:913–922
6. Yao R, Steemers K (2005) A method of formulating energy load profile for domestic buildings in the UK. *Energy Build* 37(6):663–671
7. Ma Z, Cooper P, Daly D, Ledo L (2012) Existing building retrofits: methodology and state-of-the-art. *Energy Build* 55:889–902. <http://www.sciencedirect.com/science/article/pii/S0378778812004227>. Accessed 15 May 2015
8. Ozdil OS (2010) Sürdürülebilir Yapılaşma Sorunu ve Celik. Turk Yapısal Celik Derneği <http://www.tucsa.org/images/yayinlar/makaleler/Surdurulebilir-Yapilasma-Sorunu-ve-Celik.pdf>. Accessed May 2015
9. UKGBC UK Green Building Council (2011) Carbon reductions in existing non-domestic buildings. UK Green Building Council, London
10. DECC (Department of Energy and Climate Change) <https://www.gov.uk/government/policies/improving-the-energy-efficiency-of-buildings-and-using-planning-to-protect-the-environment/supporting-pages/energy-performance-of-buildings>. Accessed 15 May 2015
11. Egyptian German High Level Joint Committee for cooperation on renewable energy and energy efficiency and environmental protection (JCEE). <http://www.jcee-eg.net/>. Accessed May 2015
12. Liddiard R, Taylor S, Rylat M (2010) Characterising space use and electricity consumption in non-domestic buildings. In: Proceedings of conference: IESD PhD conference: energy and sustainable development, 2010. Institute of energy and sustainable development, De Montfort University
13. Research Councils UK. <http://www.rcukenergy.org.uk/.../research-councils-energy-program.html>. Accessed 15 May 2015
14. European Commission Joint Research Centre. http://re.jrc.ec.europa.eu/energyefficiency/html/standby_initiative_data_centers.htm/. Accessed 16 May 2015
15. Bordass B, Cohen R, Standeven M, Leaman A (2001) Assessing building performance in use 3: energy performance of probe buildings. *Build Res Inform* 29(2):114–128
16. Bahar B, Berrin SD, Cüneyt D (2009) Energy efficient retrofit methods at the building envelopes of the school buildings. http://www.salford.ac.uk/_data/assets/pdf_file/0015/142422/063-Basarir.pdf. Accessed 18 May 2015
17. Ma Z, Cooper P, Daly D, Ledo L (2012) Existing building retrofits: methodology and state-of-the-art. *Energy Build* 55: 889–902. <http://www.sciencedirect.com/science/article/pii/S0378778812004227>. Accessed 15 May 2015
18. DOR, DOE to fund up to \$454 million for retrofit ramp-ups in energy efficiency. <http://energy.gov/articles/doe-fund-454-million-retrofit-ramp-ups-energy-efficiency>. Accessed 21 May 2015
19. HUD, U.S. <http://portal.hud.gov/hudportal/HUD>. Accessed 11 May 2015

20. Australian Building Codes Board (2011) Energy efficiency general information <http://www.abcb.gov.au/index.cfm?objectid=7384D70A-28B9-11DE-835E001B2FB900AA>
21. Department of Climate Change and Energy Efficiency, Australian Government (2010) Building code of Australia. <http://www.climatechange.gov.au/en/what-you-need-to-know/buildings/commercial/building-code.aspx/>. Accessed 5 May 2015
22. DECC, Warmer homes, greener homes: a strategy for household energy management, UK. Department of Energy and Climate Change. <http://www.decc.gov.uk>. Accessed 7 May 2015
23. Gul MS, Patidar S (2015) Understanding the energy consumption and occupancy of a multi-purpose academic building. *Energy Build* 87:155–165
24. Ardenne F, Beccali M, Cellura M, Mistretta M (2011) Energy and environmental benefits in public buildings as a result of retrofit actions. *Renew Sustain Energy Rev* 15(1):460–470
25. <http://www.ecbcs.org/annexes/annex36.htm>. Accessed 26 May 2015
26. de Boer J (2003) IEA ECBCS Annex 36: retrofitting of educational buildings—REDUCE, energy concept adviser for technical retrofit measures. International energy agency, Energy conservation in building & community, December 2003. http://www.annex36.com/eca/uk/06util/pdf/A36SubtaskC_Report_AuditProcedures.pdf. Accessed 26 May 2015
27. <https://eu-smartcities.eu/content/60000-school-buildings-eu-can-be-retrofitted-eu-2020-standards-without-closing-down-school-1>. Accessed 27 May 2015
28. Syed A (2012) *Advanced building technologies for sustainability*. Wiley, New York, p 115
29. Standards Australia, Australia/New Zealand standard: Energy audits: (AS/NZ 3598:2000), Standards Australia International Ltd., and Standards New Zealand 2000, ISBN: 0733735762
30. Standards Australia, Australia/New Zealand standard: energy audits: part 1—commercial buildings (AS/NZ 3598.1:2014), Standards Australia International Ltd., and Standards New Zealand 2000, ISBN: 9781775514992. [http://shop.standards.co.nz/catalog/3598.1:2014\(AS%7CNZS\)/scope?](http://shop.standards.co.nz/catalog/3598.1:2014(AS%7CNZS)/scope?)
31. ASHREA (2011) *ASHRAE handbook, HVAC application*, Atlanta 2011
32. Climate consultant software based on Cairo weather files of US Department of energy
33. Richman EE Requirements for lighting levels. Pacific Northwest National Laboratory, https://www.wbdg.org/pdfs/usace_lightinglevels.pdf. Accessed 8 Apr 2015

Chapter 10

Effectiveness of Thermal Inertia in South Mediterranean Climate: Residential Houses

Giuseppina Alcamo

Abstract This research focuses on annual energy demand, indoor comfort during the summer period and indoor temperature in residential family houses. Buildings in a South Mediterranean climate differ only with respect to building technology: one house may be ‘massive’, the other ‘light’. Simulation has been done using the well-known building simulation program ESP-r from the University of Strathclyde in Glasgow, UK.

The research is organised into three stages. In the first stage of the research, models are compared during the summer period assuming residential houses are naturally ventilated and have no cooling system. An investigation searches for a sufficient ventilation strategy able to avoid overheating during occupancy hours. The results of this stage are related to the internal dry-bulb temperature, resultant temperature, temperatures of inside surfaces, air changes per hour, Predicted Mean Vote values and Predicted Percentage of Dissatisfied values. In the second part of the research, the annual energy demand is investigated assuming the utilisation of a cooling system in summer and a heating system during winter. In the third part, two similar insulation materials with different density values are compared.

Keywords Indoor comfort • Thermal inertia • Energy demand

1 Introduction

The purpose of this research is to evaluate thermal behaviour simulating and comparing two models under dynamic climatic conditions; to reproduce the most realistic and variable thermo-physical conditions, internal gains due to occupancy conditions in southern Italy are studied and integrated in simulations to globally compare the performance of *massive* vs. *light* residential buildings in a Mediterranean climate.

G. Alcamo (✉)

Department of Architecture DIDA, Centro ABITA, University of Florence,
San Niccolò 93, Florence 50125, Italy
e-mail: giuseppina.alcamo@unifi.it

2 Model Description

2.1 Model Geometry

The studied case is a residential house located in Rome, Italy. It is a one-bedroom flat with a total gross area of 67.2 m². The analysed building typology is a terraced house with only two external *façades*, oriented towards the north and south. The model was built in ESP-r [1], zone by zone. Each zone is characterised by a geometry (.geo files), construction materials (.con files) and internal gains (.opr files) (Fig. 10.1).

2.2 Model Construction Materials

Three building models were built in ESP-r: a *base case*, a *massive model* and a *light model*. The *base case* is a model without control or internal gains and is used to check and control that the simulation is running as expected.

The *massive* and *light* models are identical except for the construction materials: they have the same U values for external opaque and transparent surfaces but different thermal capacities and different densities. The ground floor constructions is the same in both models. All the characteristics related to the dynamic thermal behaviour of a complete building component and the methods for their calculation are provided by the international standard UNI EN ISO 13786.

Massive and *light* relate to the specific building components used for the simulation and are described in Table 10.1. The terms *massive* and *light* need not be generalised or used improperly (Fig. 10.2).

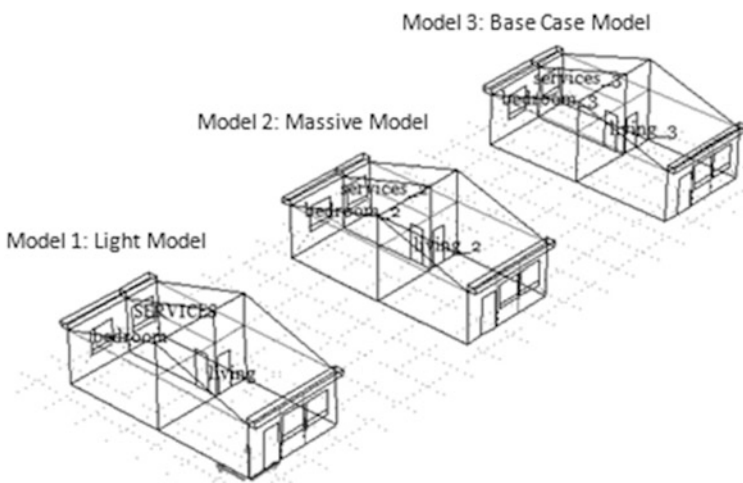
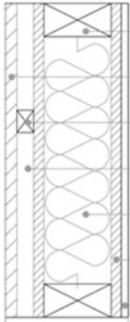
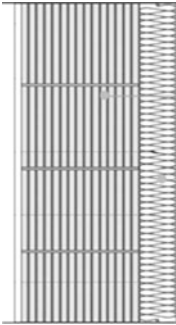
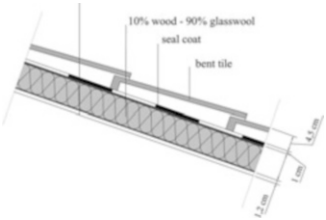



Fig. 10.1 Three models modelled in ESP-r

Table 10.1 Component characteristics with indication of U-value, thickness, areal heat capacity, time shift and decrement factor

	U-value (W/m ² K)	Thickness (mm)	Areal heat capacity (kJ/m ² K)	Time shift (h)	Decrement factor
<p>Light wall</p> 	0.296	220	32.547	5.12	0.81
<p>Massive wall</p> 	0.30	505	58.356	19.74	0.03
<p>Light roof</p> 	0.291	207	37.289	4.48	0.83
<p>Massive roof</p> 	0.30	405	35.029	7.45	0.47

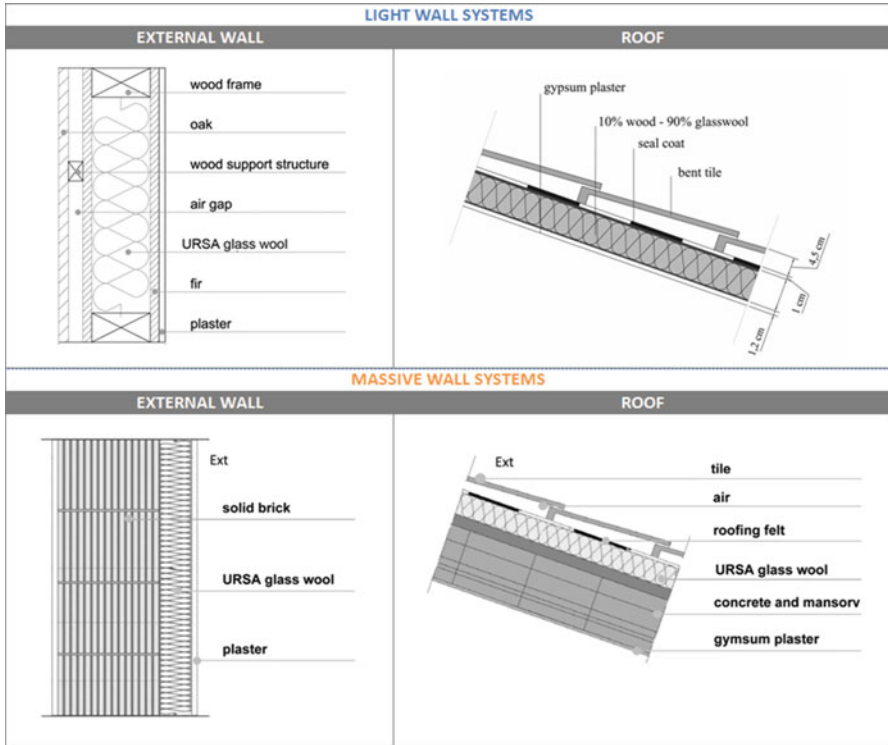


Fig. 10.2 Layer descriptions of *light* and *massive* model components

2.3 Internal Gains

Internal gains were considered during the simulation and represent the energy dissipated inside the heated space by people – body heat – and appliances – for example, lighting and a cooker. Internal gains due to occupants, lights and equipment are very important for a correct simulation [2] in terms of internal temperature and thermal comfort because of the proportion of this energy to energy heating requirements (kWh). Operations are listed as follows (Table 10.2).

3 First Stage of Research

In the first stage of the research, models are compared during the summer period assuming residential houses without a cooling system. An investigation is conducted in search of a sufficient ventilation strategy [3] able to avoid as far as possible overheating during occupancy hours. The results of this phase are related to the internal maximum temperature, air changes per hour (ac/h), Predicted Mean

Table 10.2 Description of internal gains used in each thermal zone

Type	Start	Stop	Sensible (W)	Latent (W)	Radiant fraction	Convective fraction
Internal gains – living area and kitchen (2 adults)						
Equipment (refrigerator)	0	24	30	–	0.5	0.5
Equipment (cooking for breakfast)	7	9	100	–	0.5	0.5
Equipment (cooking for lunch)	12	14	100	–	0.5	0.5
Equipment (cooking for dinner)	19	21	200		0.5	0.5
Light	7	8	70	–0.8	0.2	
Light	19	21	70	–	0.8	0.2
Occupant	7	9	114	76	0.2	0.800
Occupant	12	14	114	76	0.200	0.800
Occupant	19	21	114	76	0.200	0.800
Internal gains – bedroom (2 adults)						
Light	22	24	70	–	0.8	0.2
Occupant (sleeping)	0	7	48	32	0.2	0.8
Occupant (sleeping)	22	24	48	32	0.2	0.8
Internal gains – services (2 adults)						
Light	6	7	30	–	0.8	0.2
Occupant	6	7	24	16	0.2	0.8

It was assumed that 1-day-a-week occupants were out for dinner

Vote (PMV), and Predicted Percentage of Dissatisfied (PPD). The evaluations are made from 1 June to 30 September, or 2928 h.

3.1 Results of First Stage of Research

3.1.1 Number of Hours with Dry-Bulb Temperature Above 26 °C

Regarding the number of hours with a dry-bulb temperature above 26 °C, the simulation demonstrates that during the summer period, the *light* model has more hours during which the temperature exceeds 26 °C because of the low heat capacity of roof and *façade* constructions compared to the *massive* model (Table 10.3).

3.1.2 Number of Hours with Resultant Temperature Above 26 °C

In the case of number of hours with resultant temperature above 26 °C, during the summer period, the difference between the *light* and *massive* models is higher than the results given in the previous table owing to the influence of the inside surface temperature, as shown in the following results (Table 10.4).

Table 10.3 Number of hours with dry-bulb temperature above 26 °C in *light* model and in *massive* model

	Number of hours with dry-bulb temperature above 26 °C		
	Zone	Number of hours	Percentage
Light model	living_L	571.25	19.5
	bedroom_L	322	11
	services_L	409.5	14
Massive model	living_M	499.5	17.1
	bedroom_M	277.25	9.5
	services_M	352	12

Table 10.4 Number of hours with resultant temperature above 26 °C in *light* model and in *massive* model

	Number of hours with resultant temperature above 26 °C		
	Zone	Number of hours above	Percentage
Light model	living_L	529	18.1
	bedroom_L	208	7.1
	services_L	325	11.1
Massive model	living_M	412	14.1
	bedroom_M	159	5.4
	services_M	246	8.4

3.1.3 Number of Hours Below 3 ac/h

Concerning the number of hours below 3 ac/h during the hot seasons, an identical ventilation strategy is used in models 1 and 2 so they achieve very similar results and differences are, as expected, not significant.

3.1.4 Comfort Analysis

The PMV and PPD values are calculated supposing a sedentary activity of occupants in living rooms and service zones of -1.2 MET and a sleeping activity in bedroom zones -0.8 MET, summer clothing value of 0.5 clo and an air velocity of 0.15 m/s.

A small number of hours for PMV above 0.5 expresses the optimal situation in rooms during the summer period.

It is shown that a *PMV above 0.5* also expresses the *Predicted Percentage of Dissatisfied below 10 % (PPD10) for the warm and hot hours* in the analysed period. In fact, the value for PPD10 for warm and hot hours is the number of total hours in the analysed hot period (2928 h) minus the number of hours in which the value for PMV is above 0.5.

Table 10.5 PPD below 10 %

	Number of hours with PPD below 10 %		
	Zone	No. of hours	%
Light model	living_L	2500	85
	bedroom_L	2754	94
	services_L	2670	91
Massive model	living_M	2616	89
	bedroom_M	2811	96
	services_M	2738	94

The predicted percentage of dissatisfied below 10 % demonstrates that in the living and kitchen zones, in the summer period, the *massive* model had 116 h of more comfort compared with the *light* model. However, in bedroom zones the difference is 57 h and in service zones 68 h (Table 10.5).

4 Second Stage of Research: Annual Energy Demand

In the second part of the research, the annual energy demand is evaluated for the *light* and *massive* models considering the use of a cooling system in the hot season and a heating system during the cold season.

4.1 Winter Heating Regime

The heating period is analysed following Italian regulation *DRP n. 412/1993-art.9*, which specifies the following issues: according to *regulations*, the heat cannot be running for more than 12 h per day in Rome, from 5:00 to 23:00. The heating season starts on 1 November and goes till 15 April.

The active heating regime is defined by the following periods within a 24 h day:

- 0:00 to 5:00 – free floating
- 5:00 to 8:00 – basic control: 21 °C
- 8:00 to 11:00 – free floating
- 11:00 to 14:00 – basic control: 21 °C
- 14:00 to 17:00 – free floating
- 17:00 to 23:00 – basic control: 21 °C
- 23:00 to 0:00 – free floating

An additional simulation is run without a time step, with a basic heating control setting at 21 °C. The annual energy demand increases in both models, but differences between the *light* and *massive* models are reduced.

4.2 Summer Cooling Regime

The energy demand for cooling systems is calculated for the following period: from 1st June until 30th September.

The active cooling regime is defined by the following periods within a 24 h day:

- 0:00 to 11:00 – free floating
- 11:00 to 14:00 – basic control: 27 °C
- 14:00 to 17:00 – free floating
- 17:00 to 23:00 – basic control: 27 °C
- 23:00 to 0:00 – free floating

An additional simulation is run without a time step, with a basic cooling control setting of 27 °C. The annual energy demand increases slightly in both models, but differences with the model simulated using set periods are irrelevant.

4.3 Results of Total Annual Energy Demand

According to the simulations, if the house has an active control on its heating and cooling system, the *light* model global energy demand is 40.24 kWh/m², whereas the *massive* model requires 39.89 kWh/m², which is 0.36 kWh/m² less than *light* model. The histogram shows that the *light* model achieves a lower energy demand value than the *massive* model during the cold period. In contrast, during the summer, energy demands in the *light* model are higher than in the *massive* model.

4.3.1 Winter Period

During the winter period, in the studied specific case – a terraced house with south and north *façades* exposed – the *light* model requires 37.62 kWh/m², whereas the *massive* model requires 38.11 kWh/m², which is 0.49 kWh/m² more than the *light* model.

4.3.2 Cooling Period

For the summer period, the *light* model consumes 2.62 kWh/m² and the *massive* model consumes 1.78 kWh/m², so the *light* model requires 0.84 kWh/m² more than the *massive* model.

As in the case of the heating system, the results demonstrate that the *light* model is affected by solar irradiation because of its lower decrement factor and lower time delay capacity. Zones with a *façade* facing south, in which the external wall is affected by daily solar radiation, reaches high internal temperatures, and consequently the *light* construction requires more energy for cooling.

Table 10.6 Annual energy demand by month in kilowatt-hours (kWh)

	Annual energy demand (kWh)												
	Jan.	Feb.	Mar.	Apr.	May	Jun.	Jul.	Aug.	Sep.	Oct.	Nov.	Dec.	Total
Light model	609.96	477.52	419.62	156.76	–	6.97	46.82	89.90	32.58	–	331.01	532.94	2704.08
Massive model	627.62	486.27	425.00	155.50	–	0.00	28.03	71.69	19.90	–	335.07	531.34	2680.42

Table 10.7 Annual energy demand by month in kilowatt-hours per square meter (kWh/m^2)

	Total annual energy demand (kWh/m^2)												
	Jan.	Feb.	Mar.	Apr.	May	Jun.	Jul.	Aug.	Sep.	Oct.	Nov.	Dec.	Total
Light model	9.08	7.11	6.24	2.33	–	0.10	0.70	1.34	0.48	–	4.93	7.93	40.24
Massive model	9.34	7.24	6.32	2.31	–	0.00	0.42	1.07	0.30	–	4.99	7.91	39.89

In the case of a northward orientation, the internal surface temperature of the *light* model is a few degrees lower than that of the *massive* model. Therefore, the *light* model is significantly influenced by the orientation, while the *massive* model tends to retain an almost constant internal temperature.

5 Third Stage of Research

In this stage, the influence of high-density insulation materials on the *light* model is analysed. The calculations were undertaken to reveal the incidence of the insulation material's thermal capacity.

In the study, URSA glasswool insulation material (GW) was replaced by wood fibre (WF) insulation in each construction element of the *light* model to obtain a new model called the *light model WF*, and then a comparison of the two *light models* was made.

The main differences between the URSA glasswool insulation material and the WF insulation relate to density, specific heat and conductivity (Table 10.8).

The following results are for:

- Models simulated with a natural ventilation strategy,
- Models simulated with a cooling system,
- Models simulated with a heating system.

5.1 Results of Third Stage of Research

5.1.1 Natural Ventilation Strategy

The analysis here takes into account inside surfaces' temperature, dry-bulb temperature in zones and resultant temperature in zones. Results are related to the hottest month – August (Fig. 10.3).

5.1.2 Energy Demand

The same heating control and cooling control introduced in the second stage of the research was considered for this analysis.

Table 10.8 Differences between two different insulation materials

Description	Conductivity (W/m °C)	Density (kg/m ³)	Specific heat (J/kg °C)	IR emissivity	Solar absorption	Diffusion resistance
Ursa glasswool	0.035	20	1030	0.90	0.30	5
Wood fibre	0.039	55	2000	0.99	0.30	5

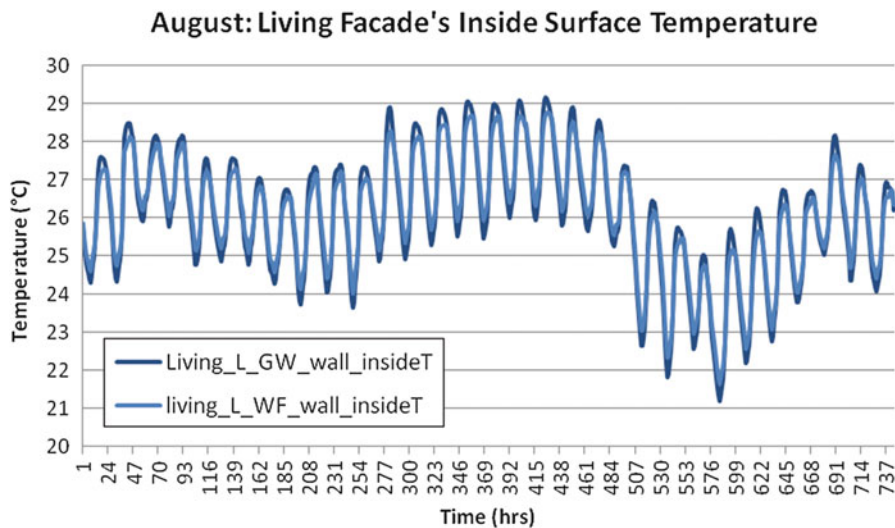


Fig. 10.3 Internal surface temperatures. The comparison of the *light* models using different insulation materials (*dark blue*: glasswool, *light blue*: wood fibre) shows that *differences are slight*. There are some differences in the extreme temperature values; in fact, the model with glasswool insulation reaches higher and lower temperatures than the model with WF insulation

According to simulations, during the winter period, energy demand for the *light* model with glasswool insulation is 37.67 kWh/m^2 , while with WF insulation it requires 38.12 kWh/m^2 , so the *light* model with WF insulation requires 0.5 kWh/m^2 more energy for heating than the *light* model with glasswool insulation owing to the slight differences in building construction U values between the two models.

For the summer period, the energy demand in both models has the same value of energy needs (2.62 kWh/m^2).

With regard to the total energy demand, the *light* model with glasswool insulation requires 40.24 kWh/m^2 , while the *light* model with WF insulation requires 40.74 kWh/m^2 , that is, 0.5 kWh/m^2 more than glasswool insulation.

6 Conclusions

6.1 Non-Cooled Buildings (Summer Comfort)

During the hot season, without a cooling system, *Light* and *Massive* residential buildings in Rome reach similar extreme internal dry-bulb temperatures. The different thermal capacities in these two models is reflected in the inside surface temperatures, resultant temperatures, frequency in hours of temperature above $26 \text{ }^\circ\text{C}$ and, consequently, in comfort parameter values. A PMV above 0.5 occurs 4% more in zones of the *light* model exposed to a southern orientation, 2% more in

zones of the *light* model exposed to the north. In conclusion, the *massive* model provides slightly better internal comfort, especially in southward-oriented zones. The *Light* system is strongly dependent on internal gains, external temperature and solar irradiation; consequently, follow-up research in offices or schools with different internal gains, in different orientations and with extreme climatic conditions could yield different results.

Finally, in the specific analysed case of a terraced house with only southward and northward oriented external façades there are:

- *No significant differences between the models regarding the minimum, maximum and average dry-bulb temperature;*
- *Slight differences on inside surface temperature oscillations; the massive model is more stable;*
- *A slight difference in comfort indicators owing to the greater stability of surface temperatures in the massive model*

6.2 Fully Air-Conditioned Buildings (Energy Demand)

In the second stage of the research, the annual energy demand was evaluated for the *light* and *massive* models, considering the utilisation of a cooling regime in the hot season and a heating regime during the cold season.

Recall that the results concern a specific building typology and specific orientation: the models' typology is a terraced house in which living rooms are oriented southward, bedroom and services zones are oriented to the north and finally east and west walls are adjacent to neighbouring houses. Infiltration is fixed and imposed; shutters are considered fully opened.

In conclusion, in Rome, in representative parts of the Mediterranean area:

- *Heating energy demand is significantly higher than cooling energy demand;*
- *The massive model is more energy demanding during the cold season but less energy demanding during the hot season;*
- *The difference in terms of annual energy demand between the models is very slight.*

6.3 Different Insulation Materials

In the third stage of the research, the influence of high-density insulation material on the *light* model was analysed. The calculations were undertaken to reveal the insulation material's thermal capacity.

In the study, URSA glasswool insulation material was replaced with (WF) insulation in each construction element of the *light* model in order to obtain a new model; then a comparison of the two *Light* models was made.

Simulations demonstrated that the insulation material's thermal capacity was more negligible than that of the building's envelope.

Acknowledgment The research presented here was supported by URSA Insulation-spain, S.A.

References

1. ESRU Manual (1997) The ESP-r system for building energy simulation. User Guide Version 9, ESRU, University of Strathclyde, Glasgow
2. Jiménez MJ, Madsen H (2008) Models for describing the thermal characteristics of building components. *Science* 43:152–162
3. Alcamo G, Murgia S, Sala M (2007) The impact of different window configurations, natural ventilation and solar shading strategies on the indoor comfort level in simple rooms. In: Mediterranean area, 2nd PALENC conference and 28th AIVC conference on building low energy cooling and advanced ventilation technologies in the 21st century, September 2007, Crete island, Greece, pp 22–25

Chapter 11

Thermal Habitability Monitoring in Housing for Low-Income Families in Extreme Warm, Dry Weather

R.A. Romero-Moreno, G. Bojórquez-Morales, A. Luna, M. Corral, and T. Gutiérrez-García

Abstract As of 2002, government policies regarding housing promoted mass construction and focused on housing for low-income families. In cities with hot-dry weather extremes, such as Mexicali, Baja California, Mexico, these types of houses cause problems related to the housing's physical dimensions, architectural design, and lack of adaptation to climate building systems that did not provide adequate thermal comfort conditions. The aim of this chapter is to present a comparative study of thermal performance of a bioclimatic model of affordable housing and a commercial housing model. The study was made through a longitudinal monitoring of the external and internal conditions of the two models. With the database obtained, regression analyses were performed. Based on measured data, predictive models for both homes were created. The results obtained support the construction of homes with better thermal conditions and present the possibility of improving inhabitants' quality of life.

Keywords Thermal monitoring • Housing for low-income families • Extreme warm-dry weather

1 Introduction

In Mexico, housing built in series for low-income families is called *affordable housing*; such homes have basic services such as pavement, electricity, water, and storm drains. The National Affordable Housing Program established that the cost should be 117.6 times the minimum wage (TMW) and it was destined for families with incomes up to 3.9 TMW [1], a cost that was accessible to the families' ability to pay.

R.A. Romero-Moreno (✉) • G. Bojórquez-Morales • A. Luna • M. Corral • T. Gutiérrez-García
Faculty of Architecture and Design, Autonomous University of Baja California,
Mexicali, Mexico
e-mail: ramonaromero@uabc.edu.mx

In the city of Mexicali, Baja California, located in the northwest of the country, subdivisions with affordable housing were built on the outskirts of the city in late 2002 and had their greatest growth from 2006 to 2008. The single-unit houses, built on lots measuring an average of 120 m² and having a building surface area of 32 m², which later increased to 38 m², have a common space (living room–dining room–kitchen) and one or two bedrooms on one floor. The construction system used was concrete-block walls, beam and vault ceilings, and concrete floors.

The local climate is an extreme, warm, dry one, with strong daily and seasonal variations, predominantly sunny days, and intense solar radiation. The city is located at 32°N, 115°W latitude at an elevation of 3 m above sea level. It has a maximum annual average temperature of 31.4 °C, an annual average of 23.7 °C, and a minimum annual average of 16.1 °C. In July, the average maximum temperature is 42.9 °C, with maximum monthly temperatures of 45.0 °C and maximum daily temperatures up to 52 °C. In August, the average maximum temperature is 42.0 °C, with maximum monthly temperatures of 44.2 °C and maximum daily temperatures up to 49.4 °C, while the average minimum temperature is 6.8 °C in December and 7.1 °C in January, with minimum monthly temperatures of 3.4 °C. The annual rainfall is 73.3 mm in the months of December and January [2]. Its warm period is from May to October, while its cold period runs from November to April. The months with the highest intensity of solar radiation are from June to August, with peaks in July of 1100 W/m².

The described weather conditions affect the way the houses' envelope generates internal environments with temperatures above the thermal comfort levels in the warm season and sometimes below the minimum range for the cold period. According to a thermal comfort analysis based on Docherty and Szokolay and processed by Luna [3], the neutral temperature (T_n) for the annual period is 24.4 °C; however, for the summer it is 26.8 °C. According to the evidence from fieldwork among affordable-housing inhabitants, $T_n = 26.4$ °C; however, values such as $T_n = 29.4$ °C were also found, demonstrating the adaptation process the inhabitants undergo with weather conditions [4]. Table 11.1 shows the different thermal comfort ranges, obtained through fieldwork and estimated for the local affordable-housing user.

The house presents thermal comfort problems, forcing the unselective use of artificial air conditioning in the summer. In addition, living condition deterioration is present in the home owing both to spatial dimensions and thermal conditions, as well as social repercussions (such as overcrowding) and economic effects (because of higher electricity consumption during the summer, which has an impact on the household economy), especially in low-income families.

For quantitative evidence of affordable housing's thermal performance in adverse climatic contexts, such as in Mexicali, a bioclimatic model of affordable housing was built and compared with a conventional house model; a longitudinal monitoring of the external and internal ambient conditions of both houses was made as part of the interagency investigation "Thermal comfort and energy savings in economic housing in Mexico: regions of hot-dry weather and humid. Second stage" [6].

Table 11.1 Thermal comfort ranges, Mexicali

Author	Focus	Model	Average temperature (°C)	Neutral temperature (°C)	Thermal comfort range	
					Lower limit	Upper limit
Auliciems	Predictive	$T_n = 17.6 + 0.31 T_m$	23.71	24.95	22.95	26.95
Luna, from Docherty Szocolay	Predictive	$T_n = 17.6 + 0.31 T_m$	26.8	25.91	23.91	27.91
De Dear [5]	Adaptive	$T_n = 17.8 + 0.31 T_m$	23.71	25.15	23.15	27.15
Fieldwork Mexicali	Adaptive	$T_n = 15.6 + 0.545 T_m$		26.40	24.40	28.40

Internationally, there have been different researches based on thermal monitoring processes – longitudinal or transversal – in housing, including Kruger and Givoni’s work [7], where models were obtained to predict maximum internal temperatures from the maximum daily temperatures. Singh et al. conducted longitudinal monitoring in vernacular inhabited houses, obtained prediction models based on the maximum, average, and minimum daily temperatures, and considered the effect that they had 2–3 days before [8]. Gonzalez and Givoni also used Kruger and Givoni’s indicators for monitoring conducted on an experimental prototype of a bioclimatic house for a moist, warm climate in Venezuela [9].

Nationally, investigations have been conducted based on monitoring processes, both in test modules and built homes, including modules with different bioclimatic techniques in a hot-dry climate [10, 11], subhumid climate, and humid climate. There is also research on bioclimatic models of affordable housing in Hermosillo, La Paz, Colima, and Merida [6].

2 Method

The thermal monitoring took place in two case studies: (1) Model A: prototype with bioclimatic techniques and (2) Model B: conventional housing and one of the most representative in the region.

2.1 Case Studies

Study homes are located in a subdivision for low-income families, located in the southeast part of the city of Mexicali. They are contiguously located on lots measuring 6.86×17.50 m (an area of 120 m^2), with the main façade facing north and each house having a construction area of 38 m^2 .



Fig. 11.1 Bioclimatic affordable housing model: Model A

2.1.1 Bioclimatic Affordable Housing Model (Model A)

This house has bioclimatic design on its walls and ceilings; it has a common living room–dining room–kitchen area, a bedroom, and a bathroom. Its distribution allows for the flexible use of space according to the needs of its inhabitants; its space can grow, and the position of the doors and windows allows natural ventilation within the spaces. The house’s roofing construction system is based on the traditional houses in the region – wooden ceilings with a ventilated attic [12]. The house has a longitudinal opening of 0.15 m tall on the west façade and a longitudinal grid on the east façade, in addition to thermal resistance on the inside. A common concrete-block system was used for the walls, which integrates heat resistance and management of optical properties (color and texture) of the materials’ surface (Fig. 11.1).

2.1.2 Model B

This property corresponds to a conventional model in the local housing market. On its eastern side, it is next to Model A, while on its western and southern sides it is near a model similar to Model B. The house has an area of 38 m², distributed in a common area of living room–dining room–kitchen, two bedrooms, and a bathroom (Fig. 11.2). Table 11.2 shows the building methods’ specifications used in Models A and B.



Fig. 11.2 Models A and B of houses for low-income families in Mexicali

Table 11.2 Building systems’ technical specifications and overall heat-transfer coefficient (U), Models A and B, Mexicali

Element	Model A	U (W/m ² °C)	Model B	U (W/m ² °C)
Ceilings	Wooden structure on studs measuring 0.0508 m × 0.15 m (2 × 6 in.), coated with 5/8 in. plywood, 26-gauge galvanized sheet exterior finish; on the interior, 0.0508 m (2 in.) polystyrene insulation and 3/8 in. interior plaster finish	0.313	0.15 m beam with polystyrene 0.10 m vault, with a layer of 0.05 m compressed concrete	1.257
North and south walls	0.12 m common concrete block with cement–sand mortar	3.460	0.12 m common concrete block with cement–sand mortar, 0.0254 m (1 in.) polystyrene insulation	0.980
East and west walls	0.12 m common concrete block, cement–sand mortar, 0.0254 m (1 in.) polystyrene insulation and cement bond coating	0.980	0.12 m common concrete block with cement–sand mortar	3.460
Floors	0.10 m reinforced concrete slab, $f'_c = 240 \text{ kg/cm}^2$	3.18	0.10 m reinforced concrete slab, $f'_c = 240 \text{ kg/cm}^2$	3.18
Windows	Single-pane 3 mm glass with aluminum frame	7.24	Single-pane 3 mm glass with aluminum frame	7.24
Doors	Hollow-core wooden door	2.78	Hollow-core wooden door	2.78

2.2 Thermal Monitoring

Longitudinal monitoring of Models A and B was carried out with the houses' doors and windows closed; they were only opened once a month when data from the records were downloaded. The houses were not occupied; no internal thermal loads of any kind were made. To reduce the effects of infiltration and exfiltration, all visible cracks were sealed.

The external dry-bulb temperature and relative humidity were recorded; a sensor on a tripod was installed between the two houses in the front room where it was out of thermal or electric sources that could cause errors. Inside each house, dry bulb temperature, relative humidity and black globe temperatures were recorded. The sensors were placed at the geometric center of the space, at a height of 1.30 m above the finished floor, as specified by the ISO 7726 standard for monitoring comfort in thermal environments [13]. The measuring equipment consisted of HOBO U12-013 transducers, dry-bulb temperature and relative humidity were recorded in a temperature measurement range of -20 to 70 °C and relative humidity of 5–95 %; an accuracy of ± 0.35 °C in a range of 0–50 °C for temperature and ± 2.5 % (10–90 %) to ± 3.5 % maximum for relative humidity was achieved.

For this article, records from 29 September to 30 November (first period) and 1 December 2012 to 4 February 2013 (second period) were grouped together; the first period included warm conditions – high temperatures similar to those in the months of July and August were observed – and in the second period cold conditions prevailed. All the variables were frequently measured every 5 min. The consistency of the records was checked in order to compare and determine hourly averages of all variables.

The processing of the data helped demonstrate the average scheduled behavior of exterior air temperature and relative humidity, the interaction of external temperature and internal temperature in each of the houses and between the indoor air temperature and black globe temperature. Furthermore, thermal performance results of the houses' different envelopes, along with buffer quantities and delay times are included.

3 Results

The external environment's behavior, the interior–exterior relationship, and the interior of both houses in the study periods are illustrated. Emphasis is placed on the everyday behavior of the critical warm day.

The study period helped demonstrate the behavior of high-temperature climatic conditions, ranging from extreme maximum of 42.4 °C to minimum of 1 °C.

The exterior environment's variations in temperature (T_o) showed a different behavior in the internal temperatures of both houses; in the first period, the average maximum exterior temperature (T_{o_max}) was 31.9 °C (14 h), and

the maximum internal temperature (T_{i_max}) was 27.7 °C (13 h) in Model A and 25.6 °C (17 h) in Model B (Table 11.3). Outdoor temperature fluctuations during the warm period, where the outdoor temperature hovered around 17 °C, ranged from 3.4 °C in Model A to 3.7 °C in Model B on the inside. In the cold period, the outdoor temperature oscillation was 13.3 °C, and the indoor temperature oscillation was 5.75 °C in Model A and 3.09 °C in Model B.

Based on the resulting buffer between T_{o_max} and $T_{i_max A}$ and between T_{o_max} and $T_{i_max B}$, during the warm season a buffer zone of 4.20 °C in Model A and 6.32 °C in Model B were presented; there was a 1 hour thermal lag in Model A and 3 hours in Model B; in the cold period, $T_{i_max B}$ was greater than T_{o_max} and $T_{i_max B}$ was 2.79 °C less than T_{o_max} . This proved that Model A, in both periods, presented a greater T_i than Model B, which is favorable in the winter nevertheless but unfavorable in the summer.

On warm days, from 1:00 to 9:00, T_{i_A} and T_{i_B} (indoor temperature) is higher than T_o , so both houses release heat to the environment; however, from 10:00 until 18:00 h both houses gain heat and indoor temperatures increase. The envelope's thermal inertia maintains an almost stable indoor temperature (in Model A there is a fluctuation of 3.4 and in Model B 3.7 °C) (Fig. 11.3).

For a critical day's condition (high temperature), the average maximum outdoor temperature (T_{o_max}) was 42.4 °C (14 h), while the maximum indoor temperature (T_{i_max}) was 35.7 (16 h) in Model A and 35.34 °C in Model B, with a 6.75 and 7.10 °C buffer and a thermal delay of 3 h in both houses. Based on the preceding information, it was observed that Model A presented an average temperature difference of 0.36 °C over Model B, which proves that for warm days both houses have relatively similar behavior. Figure 11.4 shows the average schedule behavior on a critical day during the summer.

Depending on the living conditions that a house presents, it was observed that on days with maximum temperatures higher than 40 °C, neither the conventional house (Model B) nor the bioclimatic house (Model A) had comfortable environmental conditions for its inhabitants at any time of day, which makes the use of different mechanical and environmental conditioning equipment a necessity.

The differences between the indoor air temperature (T_{i_max}) and black globe maximum temperature (BGT_{max}) Show that in Model A, the BGT is bigger than inner temperature, this because the isolation of the walls and roofs does not help in the loss of heat through the envelope. While in Model B, BGT is lower than inner temperature. This shows that Model A was impacted by the effects of the existing insulation in the walls and ceilings. Regarding the predictive models of indoor temperature and globe, they were mostly favorable in Model B (Fig. 11.5).

Table 11.3 Comparative average temperature schedule, bioclimatic model (Model A) and conventional model (Model B), 29 September 2012 to 4 February 2013, Mexicali

	29 September–30 November 2012						1 December 2012–4 February 2013					
	Outdoor temperature (T_o) °C			Indoor temperature (T_i) °C			Outdoor temperature (T_o)			Indoor temperature (T_i)		
	Max.	Min.	Oscill.	Max.	Min.	Oscill.	Max.	Min.	Oscill.	Max.	Min.	Oscill.
Model A	31.95	14.73	17.22	27.71	24.31	3.4	20.46	7.16	13.3	21.32	15.57	5.75
Model B				25.61	21.91	3.7				17.67	14.58	3.09

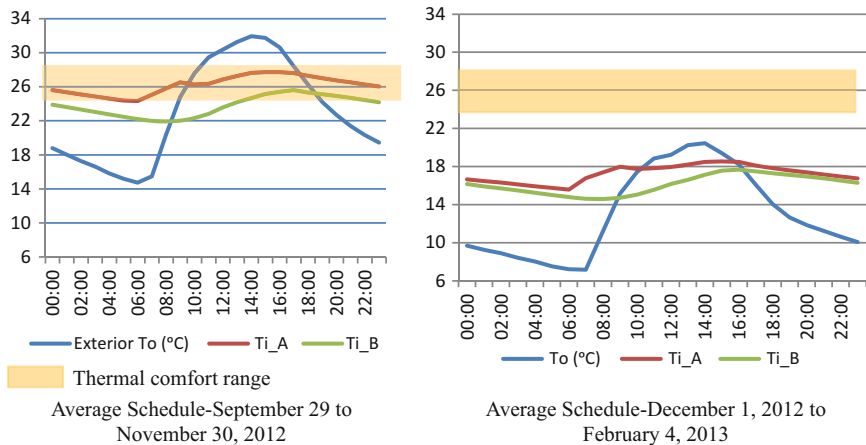


Fig. 11.3 Comparative ambient temperature (outdoor) and indoor temperature of Houses A and B, 29 September 2012 to 4 February 2013, Mexicali

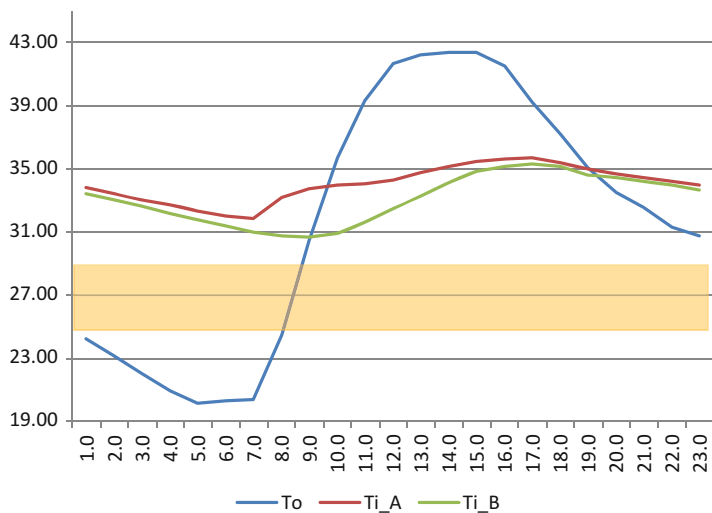


Fig. 11.4 Comparative outdoor temperature and indoor temperature of Houses A and B, critically warm day (3 October 2012), Mexicali

4 Conclusions

During both the summer and winter, the envelope’s thermal performance in conventional houses for low-income families does not present favorable, thermally comfortable living conditions. On average, the bioclimatic model remained within

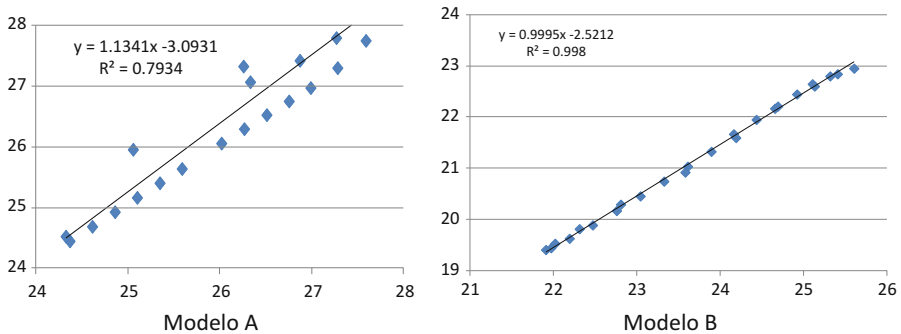


Fig. 11.5 Regression models, indoor and black globe temperature, Models A and B, Mexicali

the range of comfortable conditions, whereas the conventional model did not; in the winter it showed better thermal performance, although not enough to provide thermal comfort. The bioclimatic model of affordable housing did not experience a shading effect from the adjacent construction compared with the conventional house, which did have a shading effect from neighboring constructions; however, it offered slightly better thermal conditions than the conventional model. The buffer presented in both cases was not sufficient to mitigate the effects of the high temperatures of Mexicali.

Acknowledgments The authors would like to thank the National Council for Housing and the National Council for Science and Technology for the financial support provided for the “Thermal Comfort and Energy Savings in Low-income Dwellings in Hot Regions of Mexico” research project, in addition to the “Environmental habitability in housing built to cities in Mexico” PRODEP program. We also thank the Ruba Construction Company.

References

1. INFONAVIT (2002) Programa Nacional de Vivienda Económica. <http://www.infonavit.org.mx>, Mexico
2. National Weather Service (2014) Standard climatological 1981–2010. <http://smn.cna.gob.mx>, Mexico
3. Luna A (2008) Climatic analysis. Mexico
4. Gómez G, Bojórquez G, Ruiz P, Romero R (2009) Thermal comfort monitoring. Final Technical Report CONAVI 2004-01-20: Product 3, Mexico
5. ANSI-ASHRAE (2010) Standard 55-2010 thermal environmental conditions for human occupancy, Atlanta
6. Autonomous University of Baja California, Autonomous University of Baja California Sur, Autonomous University of Yucatan, University of Colima, University of Sonora (2013) Thermal comfort and energy savings in low-income dwelling in Mexico, Second Part Final Technical Report, Mexico
7. Kruger E, Givoni B (2008) Thermal monitoring and indoor temperature predictions in a passive solar building in an arid environment. *Build Environ* 43:1792–1804

8. Sing M, Mahapatra S, Atreya S, Givoni B (2010) Thermal monitoring and indoor temperature modeling in vernacular buildings of North-East India. *Energy Build* 42:1610–1618
9. González E, Givoni B (2005) Testing and modeling an evaporative passive cooling system in a hot humid climate—Maracaibo. In: *Proceedings of ISES 2005 Solar World Congress, Florida*
10. Vázquez JE, González EM, Elizondo Mata MF (2008) Cubiertas y estanques para optimizar el sistema pasivo de techo estanque metálico en clima cálido seco extremo: estudio experimental. *Palapa* 3:43–54
11. Corral M, Romero R, Gallegos R (2008) Comportamiento térmico experimental de un sistema constructivo industrializado de alta resistencia y uno tradicional de alta masa térmica: ladrillo y tridipanel. In: *Proceedings of 14 Convención Científica de Ingeniería y Arquitectura, Cuba*, pp 285–294
12. Robles C (2010) *La Arquitectura de Mexicali, 1900–1920*, Orígenes edn. UABC, México, p 89
13. International Organization for Standardization (1998) *Standard 7726: ergonomics of the thermal environment—instruments for measuring physical quantities*, Geneva

Chapter 12

Multidisciplinary Energy-Efficiency Think Tank for Supporting a Multilevel Governance Model in Energy Policies and Measures: MEETHINK Energy Project: Topic-6

Antonella Trombadore

Abstract MEETHINK Energy is a European research project headed by the Tuscany Region under the Horizon 2020 call for proposals involving 30 municipalities in 6 European countries (Albania, Greece, Italy, Serbia, Slovenia and Spain). The project will stimulate a multilevel governance model by joining regional and local authorities and involving policymakers, technicians and stakeholders in a bottom-up integrated approach. The core of the project focuses on the definition of a common protocol and on the identification of common criteria and energy-efficiency performance indicators, as well as on a pilot phase during which the multilevel governance model will be tested in collaboration with small and medium-sized city partners. Several potential scenarios will be evaluated, and the multilevel governance model will make it possible to improve the quality and effectiveness of energy policies and measures as well as establish or strengthen connections among different key actors and levels of government. A common information and communications technology (ICT) platform, supported by a peer-to-peer methodology, will be structured with three different access levels (free access, policymakers, technicians) and will include a data-sharing tool, open data repositories, a decision support system and a communication Web site. This platform will support public authorities in monitoring and evaluating the current situation with the aim of identifying its strengths, weaknesses and opportunities in order to determine the most suitable policies and measures. The platform will allow for the involvement of public/private stakeholders and promote a multidisciplinary think tank network across the European Union. With a focus on three thematic priority areas (energy efficiency in buildings and districts, in particular public buildings; renewable energy sources and distributed energy generation; and energy

A. Trombadore (✉)
DIDA Department of Architecture, Università degli Studi di Firenze,
San Niccolò 93
Florence 50125, Italy
e-mail: antonella.trombadore@unifi.it

in urban mobility), the aim of the project will be achieved by sharing activities through large-scale networking, peer-to-peer learning and best practices, assessing the training gaps and needs of the participating municipalities in reference to energy-efficiency planning and implementation and developing a detailed capacity building strategy for public authorities at different levels of government.

Keywords Smart cities • Smart governance • Think tank network • Renewable energy management • Low-energy building • Energy efficiency in buildings and districts • Renewable energy sources • Distributed energy generation

1 Why MEETHINK Energy Project

The European Union (EU) Directive 2012/27/EU establishes a set of binding measures to help the EU in reaching its 20 % EE (EE) target by 2020.¹ Under the directive, all EU member countries are required to use energy more efficiently at all stages of the energy chain from production to final consumption and to incorporate the directive's provisions into their national laws by 5 June 2014.

On the one hand, public authorities play a key role in the reduction of EU energy consumption and an increase in renewable energy capacity.² Member states (MSs) must produce and implement National Energy Efficiency Action Plans (NEEAPs) and National Renewable Energy Action Plans. Furthermore, they are obligated to produce detailed action plans in specific sectors, such as the renovation of buildings or the application of high-efficiency cogeneration and efficient district heating and cooling systems. Local and regional authorities are also developing plans at their own levels, and other public authorities also play an important role. National energy regulatory authorities should provide incentives for grid operators (heat, cold and electricity) to enable network users to produce renewable energy and implement EE measures.

¹ To reach the EU's EE targets, individual EU countries have set their own indicative national EE targets. New national measures must ensure major energy savings for consumers and industry alike. Some of them are directly related to buildings, and Article 7 of the Energy Efficiency Directive can be implemented by having in place or establishing one or a combination of the following policy measures: energy efficiency obligation schemes (EEOs) or alternative policy measures.

² Energy efficiency must be increased at all stages of the energy chain from generation to final consumption. At the same time, the benefits of EE must outweigh the costs, for instance those involved in renovations. EU measures therefore focus on sectors where the potential for savings is greatest, such as in buildings.

The EU has set itself a 20 % energy-savings target by 2020 against the projected use of energy in 2020. At an EU summit in October 2014, EU countries agreed on a new EE target of 27 % or greater by 2030, and the European Commission proposed 30% in its Energy Efficiency Communication.

The EU has adopted a number of measures to improve EE in Europe. They include (among others) the preparation of National Energy Efficiency Action Plans every 3 years by EU countries.

Secondly, the Covenant of Mayors (CoM) plays a pivotal role in achieving the targets for Europe set by the EU Climate Action and Energy Package. Nevertheless, owing to a number of barriers, municipalities in many countries are hesitant to adhere to the CoM or to prepare and implement the necessary Sustainable Energy Action Plan (SEAP); very often these plans are set up as individual actions, not interconnected with regional EE policies and measures and without a well-defined governance framework. In addition, the implementation phase is often very complex owing to a lack of funds to carry out actions, as well as a lack of proper links among the various decision makers and actors.

Energy-efficiency planning requires a multidisciplinary approach, involving different actors (at local, regional and national scales), a large number of stakeholders and different types of energy contracts. In addition, very often local authorities and municipalities do not have enough expertise or appropriate staff to manage this complex area.

- How can governments at the regional level support local strategic energy planning to facilitate the transition from a centralized model to a distributed model?
- What organizational structure of the public sector would allow it to play a proactive role at the local level in terms of planning for EE?
- What indicators should be monitored to verify the effectiveness of the actions under the SEAP, according to social, cultural and urban/architectonic contexts and climatic conditions?
- What type of relationship among the different levels of government (national/regional/local levels) would enable the realization of effective and rapid actions in connection with energy planning?
- What tools are most suitable for supporting an integrated planning approach and monitoring its results and effects at the local level?
- What new social patterns, economic models and experts networks facilitate sharing of knowledge, experience and best practices?

2 Aim of MEETHINK Energy Project

The main aim of the MEETHINK Energy project is to stimulate a multilevel governance model by joining regional with local authorities and involving policymakers, technicians and stakeholders (e.g. energy suppliers, utilities, infrastructure providers and developers, research and innovation centres) in a bottom-up integrated approach.

The core of the project focuses on the definition of a common protocol and the identification of common criteria and EE performance indicators, as well as on a pilot phase during which the multilevel governance model will be tested in collaboration with city partners. Several scenarios will be evaluated, and the multilevel

governance model will make it possible to improve the quality and effectiveness of EE policies and the connection among different actors and levels of government.

With a focus on three thematic priority areas (EE in buildings and districts, in particular public bodies buildings; renewable energy sources and distributed energy generation; energy in urban mobility), the aim of the project will be achieved by sharing activities through large-scale networking, peer-to-peer learning and best practices, by assessing the training gaps and needs of the participating municipalities in reference to EE planning and implementation and by developing a detailed capacity building strategy for public authorities at different levels of governments.

At the same time, a common information and communications technology (ICT) platform will be integrated with existing networks (e.g. PLEEC, Europeansmartcities 3.0). The platform, supported by a *peer-to-peer methodology*, will be structured with three different access levels (free access, policymakers, technicians) and it will be made up of a data-sharing tool, open data repositories, a decision support system and a communication Web site. The platform will support public authorities in monitoring and evaluating their current situation with the aim of identifying strengths, weaknesses and opportunities as a baseline for evaluating the next EE policies and measures. The platform will make it possible to involve public/private stakeholders and promote a multidisciplinary think tank network across the EU.

Moreover, the project will support MS public authorities to implement Article 7 of the energy efficiency directive (EED) by setting up, revising and implementing robust energy-efficiency obligation schemes (EEOSs) or alternative policy measures while providing appropriate information and tools and to strengthen the capacity of EU regions and municipalities in institutionalizing sustainable energy policies in their operations and committing and fulfilling their CoM obligations.

3 Added Value of Multilevel Governance Approach

While many initiatives focus on the local level only, the MEETHINK Energy project will also highlight the regional dimension of EE efforts. This aspect assumes a great relevance, for example, in the field of mobility, where a big share of transport energy use is related to commuting, which is usually not confined to municipality boundaries but subject to a functional region. Also, other important aspects, such as renewable energy production, management or land-use planning, will be characterized by a considerable regional dimension.

The regional dimension will foster the multilevel governance approach in three specific ways:

- The regional dimension will drive the indicator framework, the database structure and the monitoring tool;
- The regional structural and cohesion funds managing authorities will be involved in the selection of energy-saving packages during the development

and evaluation phase of local action plan scenarios to reduce the governance gap among regional and local planning and to achieve synergies and effectiveness of integrated actions;

- Through the engagement of several municipalities in the same region in the project, MEETHINK Energy will set up regional groups to foster debates on regional issues, supplementing the local agenda.

Moreover, the regional groups will allow a fast exchange of ideas and approaches to implementing EE measures in similar policy contexts, while the cross-national exchange between partner cities will promote new thinking and critical perspectives on local practices.

The MEETHINK Energy project wants to make real contributions to achieving European targets by improving legislation through knowledge dissemination of best practices on sustainable building and knowledge transfer. Special attention will be dedicated to the building sector (improving energy saving–EE in existing buildings) (Fig. 12.1).

The general objective of MEETHINK is to test innovative approaches to empowering public authorities to develop, finance and implement ambitious sustainable energy policies and plans on the basis of reliable data and analyses in sectors with high energy-saving potential such as buildings, industry and urban mobility with geographical coverage of clear European value added and considering capacity building as an integral part of project proposals, including Energy Efficiency Directive (EED) implementing bodies, joining regional with local authorities and involving policymakers, stakeholders and technicians in a bottom-up integrated approach. This general objective will be pursued by implementing a new multilevel governance model/methodology (from motivation, planning, and implementation to monitoring and evaluating) and identifying a set of common

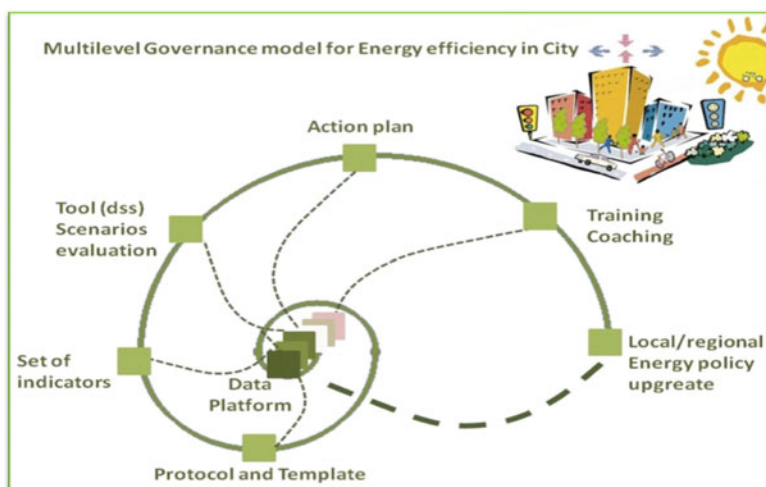


Fig. 12.1 Multilevel governance model for EE in cities

criteria and multidisciplinary performance indicators to drive ambitious integrated regional or local SEAPs to reduce policy gaps among several levels of government. The model will be supported by an international network and tools (platform, database, software) to engage vertical and horizontal cooperation, generating synergies and economies of scale on the defined priority areas (Table 12.1; Fig. 12.2).

4 Target Groups

MEETHINK Energy targets regional/local administrations of 30 small and medium-sized European cities: under 5000 (small) and 30,000 to 300,000 (medium) inhabitants. More than 1500 public agents/trainees/trainers should benefit and move forward with project results in the short and long terms, according to the stage of local planning activity. The participating municipalities might very likely be involved in very different stages of actions. Some might consider joining the CoM, while others might have already submitted an action plan and be working on its implementation or even be close to the evaluation stage and might have to follow up on its results. It would make sense to support municipalities at the specific stage they are in. There are two main groups:

1. Municipalities which need to get started and need help on mapping stakeholders, identifying energy problems (data), or developing an action plan, for example.
2. Municipalities which are in process and need help prioritizing their existing action plan and, probably, critically reviewing it, monitoring its implementation and evaluating its impacts.

Again, as a unique selling point for MEETHINK, the project places more emphasis on the second point, with a focus on the evaluation of the CoM efforts in the different municipalities. This is really an added value of the project. All cities in the Tuscany and Sardinia regions, along with a couple in Greece and Slovenia, are already in the CoM. Membership in the CoM shows that members are already working on the next step in certain municipalities (Covenant of Mayors 2.0).

MEETHINK Energy will involve local experts and technicians from public authorities (as trainees/trainers) with experience in building and city planning and in formulating Energy Efficiency Action Plans, as well as having the capability as trainers to conduct activities at the European level, to consolidate the MEETHINK peer-to-peer methodology network, a network in which a group of agents/experts from different cities working on similar issues evaluates local policies, programmes and practices being implemented in a particular city and gives recommendations on possible action areas or improvements (Fig. 12.3).

Table 12.1 Multilevel integrated approach: four levels – policies, measures, tools, people

Level approach	Objectives	Main results	Field	Project concept MEETHINK energy suite
<i>Policy</i>	Integrated approach – multilevel – regional scale	New integrated management model	<i>Governance</i>	<i>Think</i>
	Definition of EE performance indicators to assess potential scenarios and integrated solutions for comprehensive city planning			
	Stimulation of interactions between stakeholders/officers/administrators and citizens/final users to ensure opinions and views of interested parties are heard			
<i>Measures</i>	Project level where project definition takes place, in terms of scenarios, integrated technological solutions and socioeconomic measures	Scenarios	<i>Planning</i>	
	Development of a strategic plan and creation of scenarios, consolidating foundations to properly support an action plan; valuation and analysis of SEAP results to keep track of gap between achieved results and achieved goals, in reference to EU 2020 targets	Action plan		
	And to compare others' position with respect to EU targets and other SEAP achievements	SEAPs evaluation and monitoring		
<i>Tool</i>	One component of MEETHINK suite multilevel governance model and tool, <i>as support decision system</i> , to close distances between policy choices, planning at regional/local scale, fostering building capacity on EE governance integrated approach, data management, monitoring, and results analysis of SEAPs with respect to EU 2020 targets	Data base	<i>DATA</i>	<i>Tank</i>
		Protocol	<i>Platform</i>	
		Decision support system software	<i>Suite</i>	
<i>People</i>	Think tank network – knowledge exchange	Local chapter	<i>Skills and knowledge</i>	<i>Network</i>
	New level of “advanced municipality”	Cross-departmental task unit		
	Skills and policy capacity building to define new energy-saving target and visions			

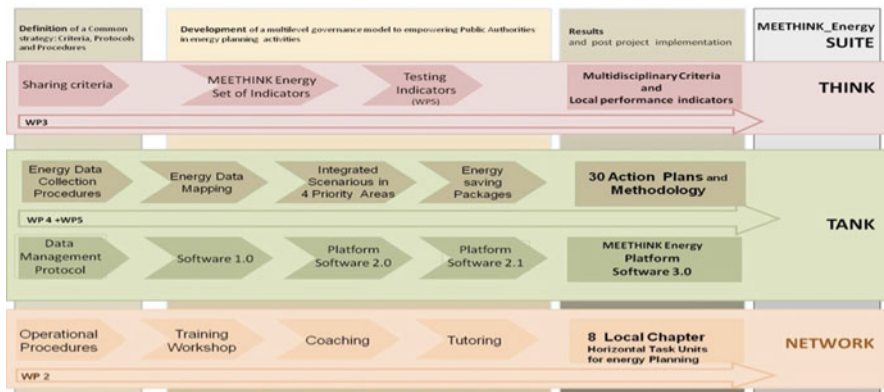


Fig. 12.2 MEETHINK Energy integrated approach

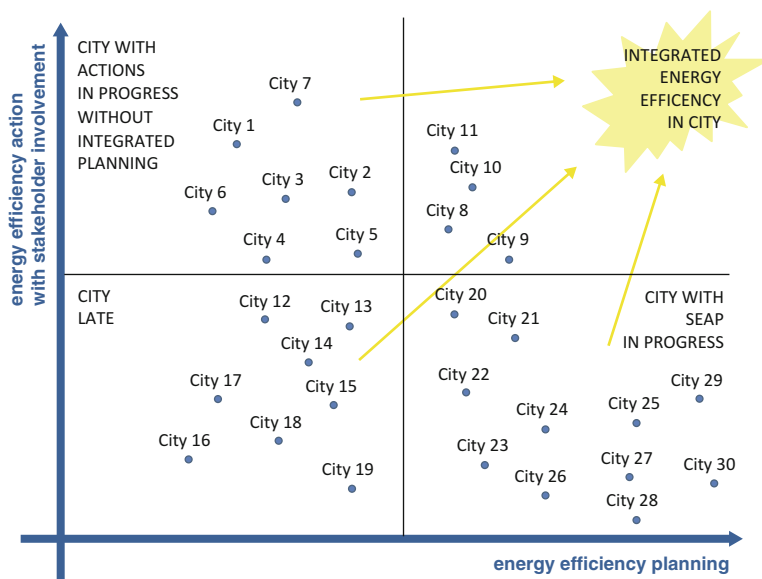


Fig. 12.3 City placement according to developed action in field of EE planning and stakeholder involvement

5 Impact

Impacts are expected on the accuracy and efficacy of the New Energy/City Action plans and the calibration of existing ones, specifically in reference to three priority areas (EE in buildings and districts; renewable energy sources and distributed energy generation; and energy in urban mobility), a time/cost reduction during planning development and recalibration processes, the possibility of accessing

qualified and highly qualified personnel, especially in the case of small and medium-sized cities, and a smartness/experience exchange container, not just a database but a knowledge and experience open-source library. MEETHINK_Energy project wants to make a real input in the achievement of a better EE, promoting renewable energy and reducing GHG emissions, by creating an international platform and improving legislation through action of learning and dissemination of Best Practices on sustainable building and knowledge transfer.

The following chart defines the three thematic priority areas (EE in buildings and districts; renewable energy sources and distributed energy generation; and energy in urban mobility) of action plans in which to intervene in order to achieve the highest EE. In each area, three action levels (low, medium, high) will be considered; they are conditioned by municipalities' vision, needs, priorities, stakeholder involvement and budget (Fig. 12.4).

The objective in each area of action is to attain the highest level of integration. The level of each action is, as described earlier, determined by external factors, and for each action, the level of action could be different, as represented in the

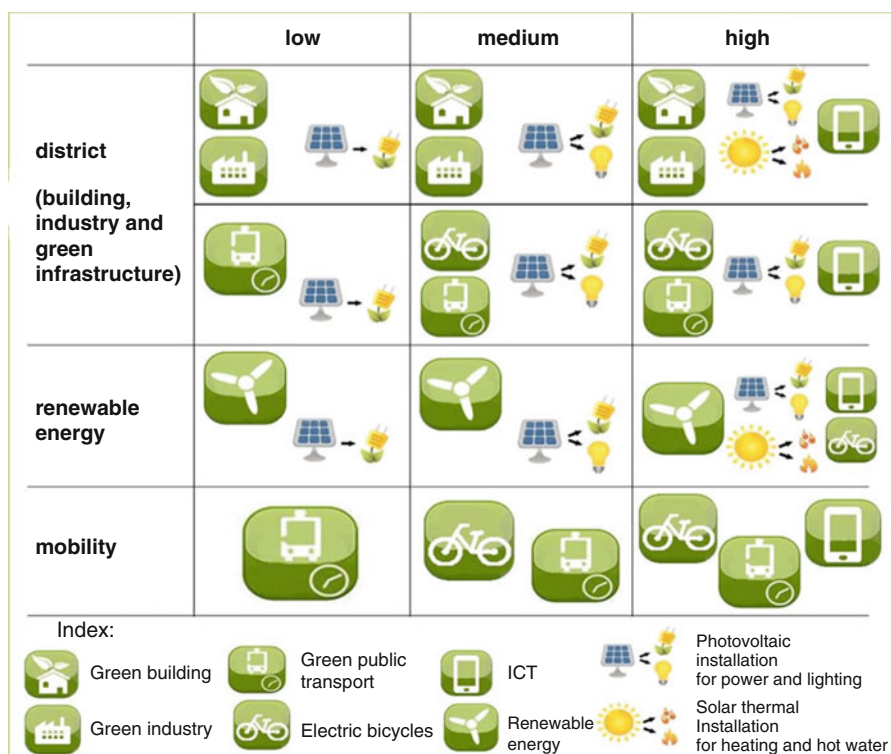


Fig. 12.4 Chart defining actions and strategies to combine three thematic priority areas (EE in buildings and districts; renewable energy sources and distributed energy generation; and energy in urban mobility)

following images (e.g. Scenarios 1, 2 and 3). In any case, it is important to highlight that all the impact areas have their own characteristics, needs for solutions, methodologies and tools.

Example: *Scenario 1*

	low	medium	high
district (building and green infrastructure)			
industry			
mobility			

In this case the intervention at the district level (building, industry and green infrastructure) is low and involves the installation of photovoltaic systems to satisfy a percentage of the consumption of energy and for the electrical supply for public vehicles, excluding illumination

On renewable energy, the level of action is medium, for a proposed action for the installation of renewable systems to cover a range of energy devoted to energy management of green infrastructure and public lighting

On mobility, the action level is medium, where the proposed action is to strengthen the public transportation system, integrating it with a bicycle mobility infrastructure

In the end, the outcomes will reveal what remains to be done for each city to meet EU 2020 objectives on EE and gas emissions

Example: *Scenarios 2*

	low	medium	high
district (building and green infrastructure)			
industry			
mobility			

In this case, the intervention at the district level (building, industry and green infrastructure) is medium and involves the installation of a photovoltaic system to satisfy a percentage of energy needs, green infrastructure and public illumination

On renewable energy action, the level is medium and involves the installation of renewable systems for energy and public lighting management

On mobility, the action level is high, and the proposed action is to strengthen the public transportation system, integrating it with a bicycle mobility infrastructure supported by an ICT management model

(continued)

	In the end, the outcomes will reveal what remains to be done for each city to meet EU 2020 objectives on EE and gas emissions
--	---

Example *Scenarios 3*

	low	medium	high
district (building and green infrastructure)			
industry			
mobility			

In this case, the intervention at the district level (building, industry and green infrastructure) is high and involves the installation of a photo-voltaic system to meet a percentage of energy consumption and public illumination needs, plus a solar thermal system for hot water production supported by the installation of a building automation system

On renewable energy, the action level is high and involves the installation of a renewable system to fully cover public illumination and green infrastructure management supported by an ICT model

On mobility, the action level is high and the proposed action is to strengthen the public transportation system, integrating it with a bicycle mobility infrastructure supported by an ICT management model

The expected impact will reflect the multilevel approach of the project:

- *Policy/governance*: New multilevel integrated management model;
- *Measures*: Criteria, set of indicators, scenarios, SEAP evaluation and monitoring;
- *Tools*: Database, protocol, decision support system software;
- *People/skills and knowledge/network*: Implement technical skills as well as policy awareness to define new cross-sector strategies in energy planning; structure local chapters (at national level) as support and training expert group of think tank network; cross-departmental task unit (at municipality level).

In the long term, MEETHINK Energy will support the fulfillment of EU long-term 2030 and 2050 energy-saving targets and GHG reduction goals outlined by the ‘Roadmap for moving to a competitive low-carbon economy in 2050’ the EU ‘Energy Roadmap 2050’³ and in the ‘EU policy framework for climate and energy in the period from 2020 to 2030’.

³ Communication from the Commission to the European Parliament, the Council, the European Economic and Social Committee, and the Committee of the Regions: Energy Roadmap 2050—COM/2011/0885 final.

In the short term, it will have a direct impact on a number of EU directives where real energy performance is crucial to effective implementation.

By focusing on real municipalities' energy data, collection, analysis and monitoring of SEAP data, MEETHINK Energy addresses one of the main barriers *to enhancing the capacity of public authorities to plan and implement sustainable energy policies and measures*.

The project will contribute to raising awareness implementing capacity building in the multidisciplinary field of EE planning involving more than 1500 public officials (policymakers, fund managers, technicians, urban/energy planners, decision makers and administrators) of 30 municipalities in 6 European countries (Albania, Greece, Italy, Serbia, Slovenia and Spain). Thanks to common experimentation activities, they will be able to apply locally a *set of common criteria and multidisciplinary performance indicators in order to drive ambitious integrated regional or local SEAPs*. The think tank mission, in the short to medium term, is to train other officers in their respective countries/regions/municipalities to diffuse MEETHINK Energy methodology and integrated solution capabilities on EE and urban planning. At the same time they will be the first members of a peer-to-peer information-exchange network (e.g. energy consumption/savings data, know-how, experiences, failures, best practices), sharing concepts and helping officials from other municipalities in building up robust and accurate energy/urban plans.

6 Project Partners

Tuscany Region (RT), *Coordinator*, Italy

University of Copenhagen (UCPH), Denmark

Except Integrated Sustainability, Netherlands

Tecopy Sa, Spain

National Association of Italian Communities Tuscany (Associazione Nazionale Comuni Italiani Toscana, ANCI Toscana), Italy

Centre for Renewable Energy Sources and Saving (CRES), Greece

Autonomous Region of Sardinia (Regione Autonoma della Sardegna, RAS), Italy

Association of Spanish Agencies for Energy Management (Asociación de Agencias Españolas de Gestión de la Energía, ENERAGEN), Spain

Local Energy Agency Pomurje (LEA Promurje), Slovenija

Vojvodina, Provincial Secretariat for Energy and Mineral Resources, Serbia

Albania Energy Association (AEA), Albania

References

1. AA.VV (2001) *Costruire sostenibile—Il Mediterraneo*. Alinea Editrice, Firenze
2. AA.VV (2001) *Verso un architettura nel Mediterraneo*. Ed. L'Epos, Palermo

3. Bradbury D (2006) *Mediterranean modern*. Thames & Hudson, London
4. Sala M, Ceccherini Nelli L, D'Audino E, Trombadore A (2007) *Schermature Solari*. Alinea Editrice srl, Firenze
5. Santamouris M, Wouters P (2006) *Building ventilation. The state of the art*. Earthscan, London
6. Santamouris M (2001) *Energy and climate in the urban built environment*. Earthscan, London
7. Trombadore A (2009) *Processi di trasformazione Urbana e qualità architettonica ambientale: il progetto Med Indo Cities*. In: Sala M (a cura di) *100 tesi....sostenibili*. Alinea Firenze, pp 47–52
8. Trombadore A, Gallo P, Lusardi AP (2001) *Potenzialità e prestazioni dell'organismo edilizio esistente*. In: Sala M (Ed.), *Recupero Edilizio e Bioclimatica*. Sistemi Editoriali—Gruppo editoriale Esselibri—Simone, Napoli, pp 59–96
9. Yannas S, Erell E, Molina JL (2005) *Roof cooling techniques: a design handbook*. Earthscan, London

Antonella Trombadore Professor at the University of Florence, Senior Researcher, Ph.D., M. Sc., architect since 1999, works at ABITA Interuniversity Research Centre. Ph.D. in Architectural Technology at University of Florence, M.Sc. in Energy Management, senior expert in fields of project management, integrated projects, sustainable urban design, energy-conscious design, low-energy buildings, communication and dissemination strategies; specialized in sustainable architecture and bioclimatic design; team leader/collaborator for management of European master course “ABITA – Sustainable Design and Technologies for the Built Environment” and post-graduate courses in bioclimatic architecture and energy conservation in buildings at the University of Florence.

Chapter 13

An Integrated Building Energy Management System

Carlos Henggeler Antunes, Ana Soares, and Álvaro Gomes

Abstract Environmental concerns and the need to reduce the dependency on imported fossil fuels have fostered several policy and economic mechanisms to incentivize the deployment of renewable generation plants, namely based on wind and photovoltaics, including microgeneration at the residential level. However, these sources are inherently intermittent, and consequently actions should be taken to mitigate the potential undesirable impacts that a large share of renewable generation may have on supply reliability and power quality. Moreover, the promotion of electric mobility requires the consideration of a new significant load, and electric vehicles would be expected to impose further challenges on power systems, in both grid-to-vehicle and vehicle-to-grid modes. Additionally, storage systems suitable for residential use are being announced. Therefore, a paradigm change is emerging in power systems involving a shift from a supply-follows-demand to a load-follows-supply strategy, making the most of the evolution toward smart grids.

Residential demand may play a key role in this transition because of the flexibility that these consumers generally have in the operation of their loads, and this may also positively affect electricity bills, i.e., shifting in time the operation cycle of some loads and modifying the (e.g., temperature) settings of other loads is easily accommodated by residential consumption patterns without compromising the quality of the energy services provided. The adequate control and coordination of residential demand should take into account operational aspects such as the integrated monitoring of electricity consumption at the household level, the evolution of dynamic tariff schemes with energy prices varying in short periods of time possibly with significant differences, and the characteristics of multiple energy resources (manageable loads, microgeneration, storage systems).

However, the continuous monitoring of demand and load control is too demanding for residential end users because of the diversity of decisions to be made (e.g., scheduling cycling loads, thermostat settings) and their time availability to implement management actions. Therefore, the deployment of automated energy

C.H. Antunes (✉) • A. Soares • Á. Gomes
Department of Electrical and Computer Engineering, University of Coimbra,
Coimbra 3030-290, Portugal

INESC Coimbra, DEEC - University of Coimbra, Coimbra 3030-290, Portugal
e-mail: ch@deec.uc.pt; argsoares@inescc.pt; agomes@deec.uc.pt

management systems (EMSs) is essential to optimizing the integrated management of energy resources. These EMSs should be able to design optimal energy decisions to reduce electricity bills without impacting the quality of the energy services provided (e.g., room temperature below/above a prespecified comfort threshold, completion of the washing machine cycle before a given time, electric vehicle battery in a given state of charge by a required deadline). These decisions are strongly influenced by energy costs, end-user preferences and requirements, potential dissatisfaction of end user when the operation cycle of loads is changed, technical constraints, weather forecasts, and the existence of local microgeneration and storage.

This chapter presents an evolutionary algorithm to optimize the integrated use of residential energy resources and provides an analysis of simulation results under different scenarios. Two objective functions are considered to assess the merit of solutions: minimizing the electricity bill and minimizing the dissatisfaction felt by the end user resulting from the control actions. Results show that significant savings can be achieved, though they will depend on end users' willingness to accept a certain degree of automated control, the characteristics of managed loads, the pricing structure, and end-user preferences.

1 Introduction

The emergence of smart grids as a highly efficient low-carbon energy system requires a paradigm change that involves shifting from a supply-follows-demand to a load-follows-supply strategy [1–3]. In this context, end-user engagement will play a crucial role in assuring high levels of operational efficiency and contributing to the security of the energy system through the flexibility in the operation of their loads. Information and communication technologies already provide the technological basis of the deployment of smart meters and bidirectional communication between end users and the utility, which will allow the adoption of dynamic pricing schemes as opposed to traditional flat tariffs that do not reflect the costs of generation during the day. On the other hand, end users can profit by responding to dynamic tariffs through an optimized use of their energy resources.

Evolutionary algorithms (EAs) [4, 5] have been used in several problems in the energy sector owing to their ability to cope with the combinatorial characteristics of mathematical models, large and irregular search spaces, and multiple objectives of various natures, such as economic, environmental, quality of service, and technical aspects [6].

In our approach, an EA was designed to optimize the use of energy resources from a residential end user's perspective, aiming at simultaneously minimizing electricity bills and the dissatisfaction felt by end users when the operation cycle of loads is changed through demand response actions. The loads that will be the target

of control actions may include shiftable loads, thermostatically controlled loads and storage systems, as either stationary or electric vehicles (EVs) batteries. Based on end-user preferences and the regulatory framework at stake, an EV may be used only in the grid-to-vehicle (G2V) mode or in the vehicle-to-grid (V2G) mode [7]. Management decisions include the allocation in time of shiftable loads, the modification of temperature settings in thermostatically controlled loads, and the control of storage systems in order to trade off the minimization of electricity bills and the quality of energy services provided (through a surrogate dissatisfaction objective function).

The planning period considered for the optimization process is one and a half days, and the time step is 1 min. The planning period may be easily changed by simply inserting the desired number of minutes for optimization scheduling as long as the input data, namely, the buying and selling of energy tariff information, are consistent with the new planning period.

The chapter begins with a brief overview of the methodology used, and some simulation results under different scenarios are then presented. Conclusions are drawn in the final section, including the identification of further research areas and issues to resolve.

2 Methodology

The analogy underlying EAs is Darwin's evolutionary theory of natural selection (or the survival of the fittest in Herbert Spencer's words) in the realm of search and optimisation processes. In general, in EAs a potential group of solutions (population) to a problem evolves over several generations through the use of specific operators inspired by genetic mechanisms offering the strongest individuals, according to a fitness function, a higher chance of survival. However, the preservation of diversity is a concern to avoid premature convergence and having the search process being trapped in local optima. This evolution leads to the identification of the fittest individual in single objective optimization or a Pareto optimal frontier in multiobjective optimization. The operators usually employed are as follows:

- Selection – to select individuals, either to generate offspring or to be included in the next-generation population;
- Crossover – to transfer characteristics from parent solutions to offspring;
- Mutation – to insert changes and consequently promote diversity in the population.

The transmission and improvement of some characteristics of the solutions from one generation to the next can be perceived as a form of memory that allows the population to evolve to regions in the search space where better solutions reside [8].

In our approach the EA is based on an elitist strategy and uses a population of candidate solutions to the problem that is suited for this multiobjective optimization

in the sense that solution encoding (representation) and genetic operators are designed to take into account the physical characteristics of solutions representing demand response actions [9]. The initial population consists of random individuals representing the allowable management actions defined based on problem domain expertise. The parent solutions for the next generation are chosen using a selection procedure based on a tournament. The fitness function is used to evaluate solutions and is composed of two objective functions: minimization of electricity bills and minimization of dissatisfaction felt by end users when the normal operation cycle of loads is changed. The consideration of a multiobjective model makes it possible to study the tradeoffs between the competing objective functions and then select a compromise solution more in accordance with the end-user profile (e.g., more cost oriented or more quality-of-service oriented). The crossover operator is then used over the previously selected parent solutions to generate offspring by combining the parents' characteristics. The mutation operator is used at that point to introduce new features in some solutions, thereby promoting the diversification of the search process. The selection, crossover, and mutation operators make it possible to choose, combine, and modify possible solutions iteratively until a good approximation of the Pareto optimal front to the multiobjective optimization model is found after a maximum number of generations is completed.

This nature-inspired technique is able to cope with the combinatorial characteristics of this multiobjective problem with two conflicting objectives: electricity bill vs. consumer dissatisfaction. The minimization of electricity bills includes possible revenues from selling electricity to the grid when using a stationary storage system or the EV in the V2G mode. The minimization of the dissatisfaction felt by the end user takes into account the potential undesired impact of management actions over comfort and the proximity of power peaks to the contracted power, which could lead to the interruption of the energy supply [10].

The potential undesired impacts of management actions depend on the load being managed, and so the end user is asked to assign preference penalties to time slots for scheduling shiftable loads during the planning period [10]. Concerning thermostatically controlled loads, an allowable temperature range modification is defined and the dissatisfaction is computed considering the difference between the expected temperature if the regular working cycle of that load had not been modified and the actual temperature due to the implementation of the management action. The dissatisfaction is cumulative during the planning period, with different coefficients for different thermostatically controlled loads. Considering the example displayed in Fig. 13.1 of the dissatisfaction penalties for solutions that individually optimize each objective function, it can be seen that management actions over an electric water heater (EWH) are the ones that are most responsible for causing dissatisfaction in the end user. Of course, hot water consumption also contributes to that situation, since using hot water implies that new water coming from the water distribution network will enter the EWH at a lower temperature and cause a decrease in the overall temperature.

Some simulation results obtained using this EA according to three different scenarios are presented in the next section. The tariff structure (Fig. 13.2) and the

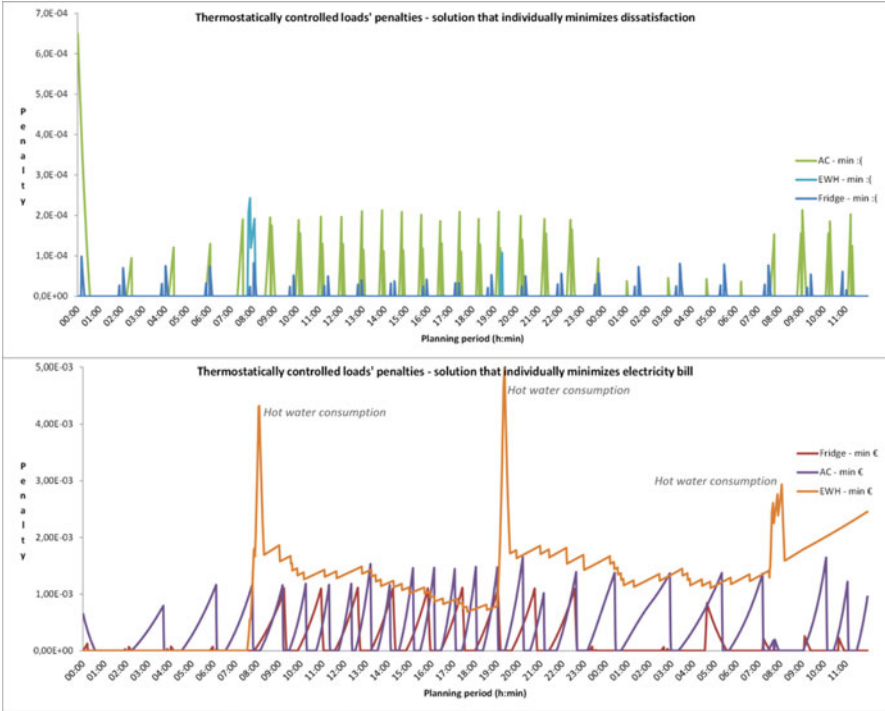


Fig. 13.1 Example of penalties associated with thermostatically controlled loads for solutions that individually optimize each objective function

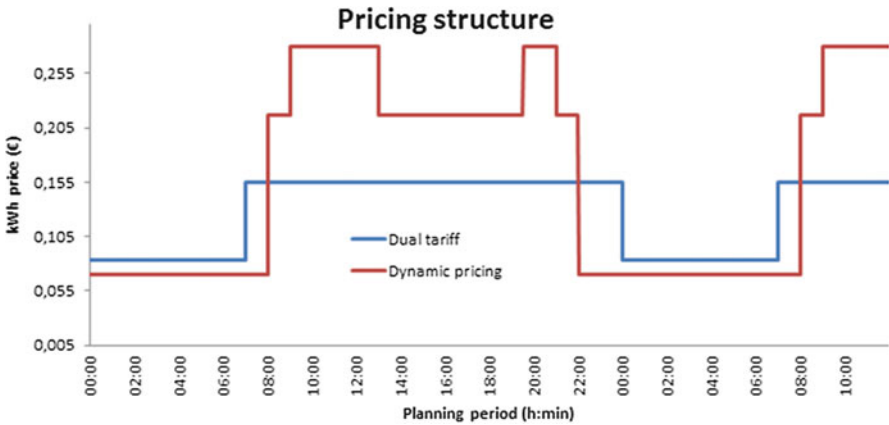


Fig. 13.2 Pricing structure

loads managed display some differences for the distinct case studies. The allowable management actions are the same, although they are dependent on end users' willingness to accept an automated EMS to control the loads, aimed at simultaneously minimizing electricity bills and minimizing the dissatisfaction felt by end users owing to the implementation of those management actions in the planning period.

3 Simulation Analysis

The management actions to be implemented over shiftable and thermostatically controlled loads are determined by the optimization strategy based on an EA presented in the previous section and depend on several factors, such as the loads being managed, their technical characteristics, pricing scheme, and end users' preferences and requirements. The aim of this section is to present some solutions obtained for three different case studies:

- Case study 1: using a dual tariff for managing typical residential loads (shiftable loads and thermostatically controlled loads – no EV and no stationary storage system);
- Case study 2: using a dynamic pricing structure for managing typical domestic loads (shiftable loads and thermostatically controlled loads – no EV and no stationary storage system);
- Case study 3: using the previous dynamic pricing structure for managing the loads of case study 1 plus storage systems.

To allow a comparison of the simulation results, three reference cases are used:

- Reference case 1: dual tariff and no use of EVs or storage systems;
- Reference case 2: dynamic tariff scheme and no use of EVs or storage systems;
- Reference case 3: dynamic tariff scheme and use of an EV and a storage system.

The reference cases are characterized by the aim of representing typical consumer behavior associated with the use of multiple energy resources without the help of an EMS, i.e., without the use of an EA to optimize load and storage system usage, while respecting time slot preferences specified by the end user (Fig. 13.3).

In reference case 1, the electricity bill for the planning period is 2.30 € while in the optimized situation these costs vary from 1.93 to 2.16 €, according to the level admitted for the dissatisfaction objective function. This represents savings within the range 6–16 %, mainly due to the control of thermostatically controlled loads, without jeopardizing the quality of the energy services provided by these loads.

Reference case 2 differs from the previous one in the tariff structure, which has a significantly higher average kilowatt-hour cost. Thus an electricity bill corresponding to the use of the same loads comes to 2.71 €. The methodology proposed is able to reduce costs to the range [2.24; 2.5] €, representing [7; 17] % savings. Therefore, the strategy presented in the previous section is able to achieve

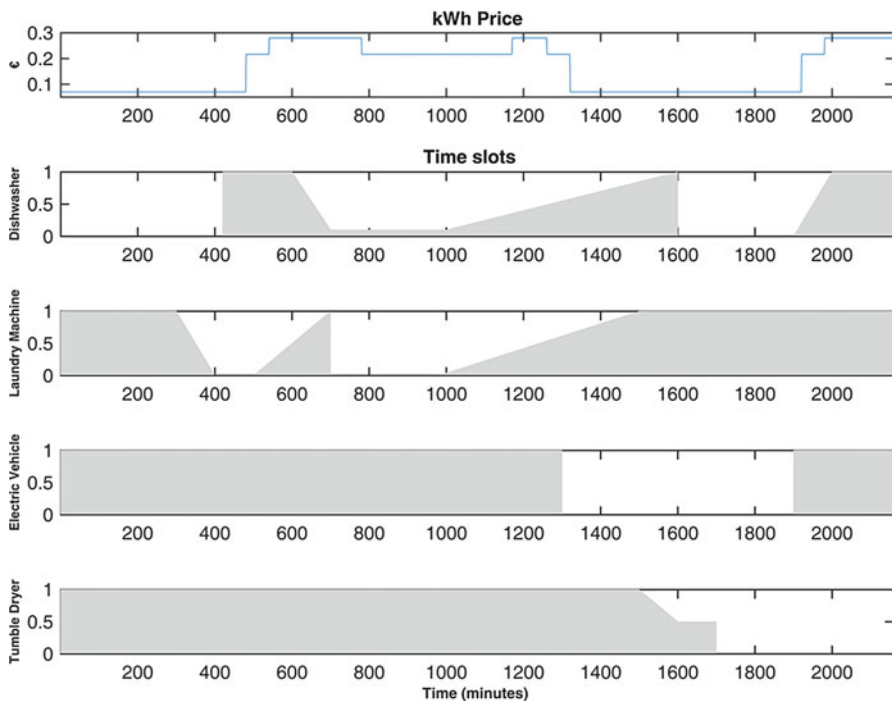


Fig. 13.3 Time slot preferences

slightly higher savings with tariffs, with more regular variation and higher fluctuation between the minimum and maximum kilowatt-hour price, although it is strongly dependent on end-user preferences and requirements.

Reference case 3 profits from the existence of a stationary storage system that is used to store energy when the kilowatt-hour price is low and uses it later on when the kilowatt-hour price is more expensive. The excess energy is sold to the grid, even though the selling price is 20 % lower than the buying price. The electricity bill for reference case 3 is 3.83 € since it includes, in addition to the stationary storage system, the charging of the EV. The degradation of the battery and the initial investment needed in this system are not considered in the optimization process. The optimization strategy can achieve around 6 % savings, which is not as high as in the previous case studies. The allocation of the EV in the preferred time slot with lower kilowatt-hour price has an energy cost of 1.26 €. In the corresponding reference case, decisions taken by the end user concerning when to store, use, or inject back into the grid energy from the battery are made based on a set of rules guided by the kilowatt-hour price. In case study 3, these decisions are not influenced by the end user but made by the optimization strategy based on the EA. It was possible to conclude through experimentation that trying to influence battery decisions, in the same way as an end user would do, would mislead the

Table 13.1 Summary of some results

	Reference case			Case study		
	#1	#2	#3	#1	#2	#3
Electricity bill	2.30	2.71	3.83	[1.93;2.16]	[2.24;2.50]	[3.57;3.59]

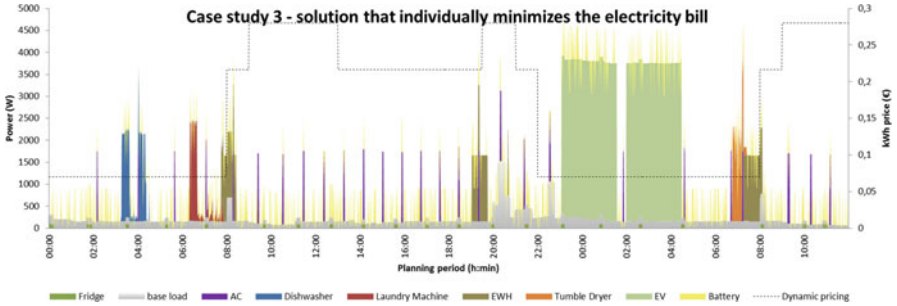


Fig. 13.4 Case study 3 – solution that individually minimizes electricity bills

optimization strategy and negatively influence it, leading to situations in which the electricity bill would be even higher than in the reference case.

Comparing the results summarized in Table 13.1, it is possible to conclude that the EA is able to compute management actions leading to a lower electricity bill when compared to the corresponding reference cases while simultaneously minimizing the dissatisfaction felt by the end user. Since the aim of the strategy is to solve a multiobjective problem and explore the tradeoffs between the objective functions, several solutions, as well as the corresponding range of the electricity bill objective function, are presented. The choice of the final solution is strongly linked to the end user’s profile [9].

An example of a solution is displayed in Fig. 13.4. This solution individually optimizes the electricity bill and complies with the end user’s preferences, allocating shiftable loads to time slots with no associated penalty and interrupting the EV charging cycle to allow the air conditioning system to lower the room temperature without having to increase the contracted power.

4 Conclusion

The EA proposed in this chapter uses solution encoding and genetic operators customized to the physical and combinatorial characteristics of the model, enabling the exploration of the tradeoffs between electricity bills and end-user dissatisfaction objective functions. Input data, such as electricity tariff costs, end-user preferences and requirements, technical constraints, weather forecasts, and the existence of

stationary and EV storage are considered from a perspective of integrated optimization of all energy resources.

Future work is under way on the implementation of this optimization approach in a hardware prototype to control energy resources and its extension to encompass the aggregation of end-user clusters to offer ancillary services to the grid.

Acknowledgments This work was partially supported by the projects SusCity: Urban data driven models for creative and resourceful urban transitions (MITP-TB/CS/0026/2013), UID/MULTI/00308/2013, and Grant SFRH/BD/ 241 88127/2012.

References

1. IEA (International Energy Agency) (2012) World Energy Outlook 2012. doi:[10.1787/weo-2012-en](https://doi.org/10.1787/weo-2012-en)
2. Katz RH, Culler DE, Sanders S, Alspaugh S, Chen Y, Dawson-Haggerty S, Dutta P, He M, Jiang X, Keys L, Krioukov A, Lutz K, Ortiz J, Mohan P, Reutzel E, Taneja J, Hsu J, Shankar S (2011) An information-centric energy infrastructure: the Berkeley view. *Sustain Comput Informatics Syst* 1:7–22. doi:[10.1016/j.suscom.2010.10.001](https://doi.org/10.1016/j.suscom.2010.10.001)
3. Parag Y (2015) Beyond energy efficiency: a “prosumer market” as an integrated platform for consumer engagement with the energy system. ECEEE 2015 summer study energy efficiency. Belambra Presqu’île de Giens, France, pp 15–23
4. Deb K, Pratap A, Agarwal S, Meyarivan T (2002) A fast and elitist multiobjective genetic algorithm: NSGA-II. *IEEE Trans Evol Comput* 6:182–197. doi:[10.1109/4235.996017](https://doi.org/10.1109/4235.996017)
5. Eiben AE, Smith JEE (2003) Introduction to evolutionary computing. Springer, Berlin
6. Soares A, Gomes Á, Antunes CH (2015) Soft computing applications for renewable energy and energy efficiency. *Soft Comput Appl Renew Energy Energy Effic*. doi:[10.4018/978-1-4666-6631-3](https://doi.org/10.4018/978-1-4666-6631-3)
7. Yilmaz M, Krein PT (2013) Review of the impact of vehicle-to-grid technologies on distribution systems and utility interfaces. *IEEE Trans Power Electron* 28:5673–5689. doi:[10.1109/TPEL.2012.2227500](https://doi.org/10.1109/TPEL.2012.2227500)
8. Dréo J, Pétrowski A, Siarry P, Taillard E (2006) Metaheuristics for hard optimization. Springer, Berlin. doi:[10.1007/3-540-30966-7](https://doi.org/10.1007/3-540-30966-7)
9. Soares A, Oliveira C, Gomes A, Antunes CH (2015) Integrated optimization of energy resources in a residential setting—development of an energy management system. ECEEE 2015 summer study energy efficiency
10. Soares A, Antunes CH, Oliveira C, Gomes Á (2014) A multi-objective genetic approach to domestic load scheduling in an energy management system. *Energy* 77:144–152. doi:[10.1016/j.energy.2014.05.101](https://doi.org/10.1016/j.energy.2014.05.101)

Chapter 14

The Normal: Minimising Energy Use; The Abnormal: Changing Habits

Anwar El-Hadi, Ingi A. El-Hadi, and Mohammed A.I. Alameer

Abstract Homes and shelters with their diversified structures, are designed to cater for a controlled inside environment. Air conditioning, in heating or cooling, and refrigeration are known to use 75 % of the total electrical power generated in the world. Their thermal load is a function of the heat transferred through the boundaries of the building in addition to internal sources. Hence insulation is regarded a priori. Reducing this percentage to 50 % and increasing the energy efficiency of machinery by 5 % results in petroleum reserves lasting for 500 years instead of 190, with additional merits involved. A very simple study of the effects of the geometry and the geographic orientation of the building on the thermal load are investigated. The amount of heat transgressing the boundaries is a direct function of the heat transfer area. Single story model buildings of same material, equal areas, internal heat sources and occupancy is investigated. They are a square, rectangle and a dome (hemisphere). The calculations followed ASHRAE standard procedures. The Finite Element method is used in calculations for the hemispherical dome segmented surface area. The dome building gives the least calculated external thermal load. It is 58–68 % of that calculated for the other models, depending on variation in building materials. Heat ingress at 43.33 °C (110 °F) is double the heat ingress at 32.22 °C (80 °F) for all the models. But the average heat ingress of the other models is 29–67 % higher than that of the dome, depending on type of building materials. At high temperatures it is emphasised to use dome structures. A NASA Spinoff product, NSP, with its insulating properties is used on the surfaces of the models to further investigate reductions in the amount of heat ingress. The NSP is very effective in buildings with poor thermal resistivity and the heat ingress to the building is reduced to 47 %. Its effect is considerable in dome shaped buildings. The dome geometric structure gives the least heat ingress in addition to its benefits of friendly and cozy interior. As dome buildings contribute to the green

MED GREEN FORUM 2015—Florence, Italy, 26–28 August 2015. www.wrenuk.co.uk

A. El-Hadi • M.A.I. Alameer

College of Engineering and Architecture, Bahri University, Khartoum, Sudan

e-mail: anwarelhadi1@gmail.com; birdmail1982@gmail.com; alsada100@yahoo.co.uk

I.A. El-Hadi (✉)

University of Khartoum, Khartoum, Sudan

e-mail: ingielhadi@live.co.uk

environment, it is recommended to build more domes in residential compounds, especially when high-rise buildings are restricted. As the normal lies in minimising energy use, the abnormal lies, temporarily, in the attitudes during the process of acceptance and acclimatisation as some of us must change some of their habits. However, architects are very capable to re-introduce the dome and the dome habitat. As decisions in energy and town planning are inseparable from political decisions, it is recommended to encourage more building of domes by calling the year 2015 of Med Green Forum by the Year of the Dome and/or by the Florence Dome Declaration, with the Cathedral's Dome as a logo.

Keywords Minimizing energy • Dome and hemisphere thermal load • Building geometry and heat transfer • NASA spinoff: Insuladd • Florence Dome Declaration • Year of the Dome

1 Introduction

This work was initiated when the author was looking into the effects of geographical orientations of buildings on their total thermal load. The author wondered what would happen if the geometry were changed. If a certain geometric design were found to be thermally favorable, would it be feasible structurally?

Historically, throughout the world, humans have tried to secure shelter and protect themselves from elements. The basic local designs were imposed by the direct environmental conditions, which are globally diversified; hence we see igloos in frigid regions, tents in Arabia, yurts in Mongolia, quottiyas in the sub-Saharan regions, and even stilts in swampy areas as well as along the coasts.

Development and growth in all aspects of life are reflected in the development of today's habitats. Shelters have developed and taken on a more unified appearance. Their interiors are controlled environments; with respect to temperature, relative humidity, air quality, and freedom from pollutants, they are conditioned spaces. It is an established fact that 75 % of electricity generated globally goes to air conditioning and refrigeration. Air conditioning includes heating, cooling and ventilation.

All these processes lead to global warming, ozone depletion, and acid rain and, hence, climate change. Climate change will definitely lead to changes in the ways we shelter ourselves in every locality and in general in terms of buildings and infrastructures. It is our choice whether the changes we face will be sudden or gradual or whether we will prepare ourselves for them well in advance so as to minimize damages and expenses. If the power used in air conditioning and refrigeration is reduced from 75 % to just 50 %, and the energy efficiency of appliances used is increased by 5 %, this may lead to an increase in the life expectancy of petroleum reserves from 190 years to 500 years [1]. The direct benefits are greater political stability, enhanced security, and more space for advancements in technology and energy research to further improve the global environment. All this is in

addition to the utilization of petroleum for other novel, intelligent uses. Such a reduction in use in this respect will lead to commensurate improvements in the environment.

The cooling or heating load will be referred to here as the thermal load. This is the total heat transferred through the boundaries of a building and due to internal sources. Heat ingress through boundaries is a function of outside environmental conditions – temperature differences, wind velocity, solar radiation, and relative humidity coupled with the outside total area of the walls and roofs and their structure and materials. These affect the insulating capacities and as such thermal insulation is always given priority.

The heat transfer area is often overlooked in the design of buildings. It is presented as a given in the calculation of the thermal load; it is decided by the building designer who governed by concepts for the particular project. In the design of heat exchangers, by contrast, the designer enhances the thermal energy exchange by increasing the heat transfer surface area several fold by adding fins to the tubes of the heat exchangers.

Reducing the thermal load by reducing the heat transfer area will reduce the power requirements. The need for insulation and its production will be reduced. A very simple study of the effects of the heat transfer surface area and buildings' geometry on heat loads is conducted. Three examples of single-story buildings are considered. They are in the shapes of a square, rectangle (length = 1.5 times the width), and a dome (hemisphere). The models are similar in area, internal heat source, and occupancy. Similar materials were considered. Materials used in current practice were also included.

The models were further investigated. Because the ultimate goal is to reduce energy use, and following the principle of benchmarking as in Total Quality management (TQM), effective low-cost insulation materials were sought from NASA spinoff products [2], referred to here as NSPs. The NSP is a powder additive that can be mixed with ordinary interior or exterior paint, causing the paint to act as a layer of insulation. The powder is formed of microscopic inert gas-filled ceramic microspheres that comprise the NSP. It forms a radiant heat barrier by reflecting heat away from the painted surface and hence reduces heat transfer into the building. It does not add an insulation thickness. The effect of this material on the models was investigated.

2 Procedure

The external thermal load, heat ingress to the building, is calculated following the standard procedures of the American Society for Heating, Refrigerating and Air-Conditioning Engineers (ASHRAE).

The overall heat transfer coefficient for each part of the structures is calculated as shown in Fig. 14.1.

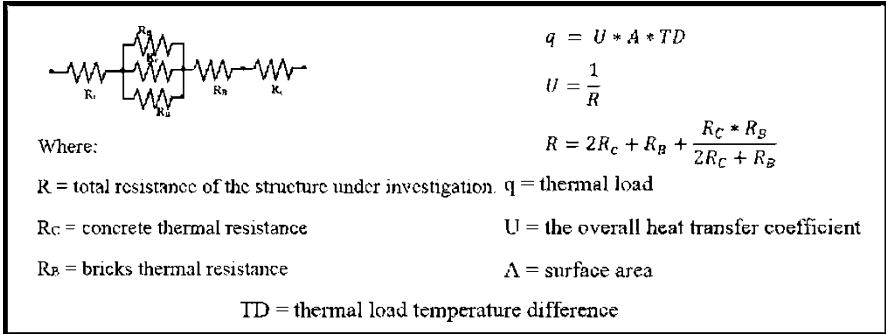


Fig. 14.1 Overall heat transfer coefficient

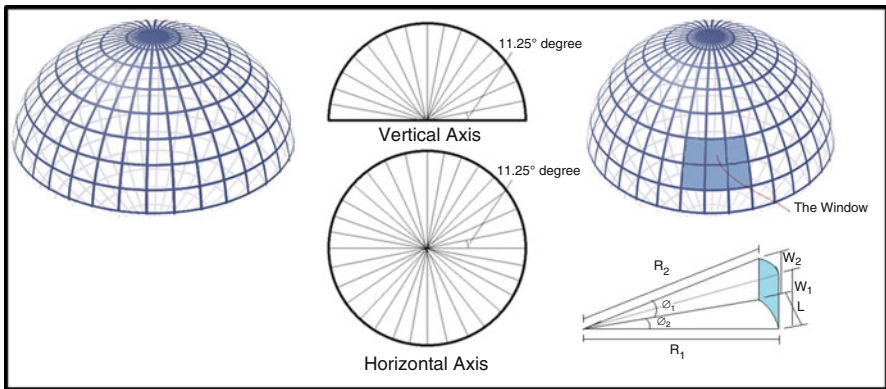


Fig. 14.2 Dome surface area elements

The dome structure is Lotus with the same wall thickness from base to top. To generate finite surface areas for the sake of calculations, the dome surface was segmented into areas small enough to represent a flat surface area with the representative temperature at the center.

Using a finite-element method each segment’s contribution to the external thermal load was calculated (Fig. 14.2).

Calculations for the heat ingress through the boundaries of the models were performed with different materials (Table 14.1) and with different geometric orientations (Fig. 14.3).

The total thermal resistance after adding the insulation NSP is shown in Fig. 14.4.

Table 14.1 Building materials used

Item	Material
Walls	Brick, fired clay with thermal resistance $0.12\text{--}0.10 \frac{^{\circ}\text{F}\cdot\text{ft}^2}{\text{Btu}\cdot\text{h}}$, density 150 lb./ft.^3
Roof	(A) Brick, fired clay with thermal resistance $0.12\text{--}0.10 \frac{^{\circ}\text{F}\cdot\text{ft}^2}{\text{Btu}\cdot\text{h}}$, density 150 lb./ft.^3 or (B) Sand and gravel or stone aggregate concretes (concretes with more than 50% quartz or quartzite sand have conductivities at the higher end of the range) Thickness 0.492 ft. , with thermal resistance $0.10\text{--}0.05 \frac{^{\circ}\text{F}\cdot\text{ft}^2}{\text{Btu}\cdot\text{h}}$, density 150 lb./ft.^3
Window	Regular single glass, draperies, venetian blinds, translucent roller shades, fully drawn
Door	Southern pine, with thermal resistance $1.00\text{--}0.89 \frac{^{\circ}\text{F}\cdot\text{ft}^2}{\text{Btu}\cdot\text{h}}$, density $35.6\text{--}41.2 \text{ lb./ft.}^3$
NSP	$R_{\text{NSB}} = 6 \text{ h. ft.}^2 \text{ }^{\circ}\text{F/Btu}$

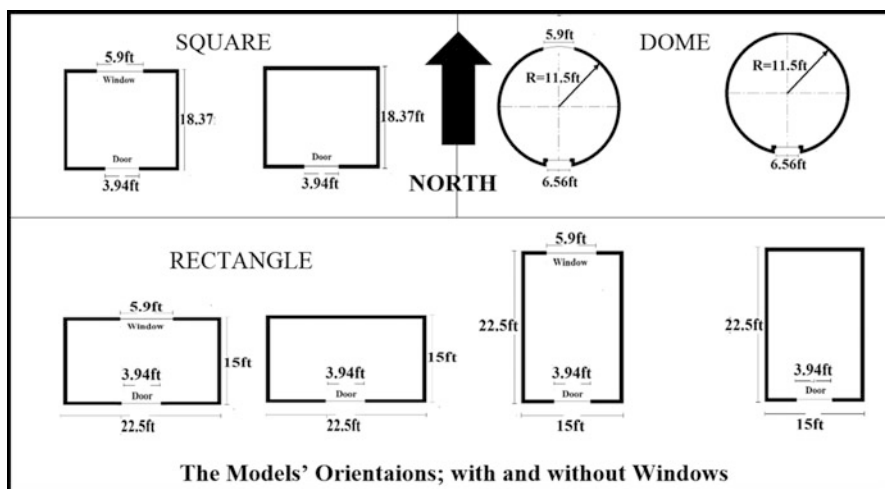


Fig. 14.3 Orientations and geometries of models

3 Results

Results for the calculations of the external thermal loads for the three models of equal internal load, same building materials, and equivalent areas are displayed in Table 14.2. The building materials for all models include brick fired clay according to Table 14.1 (A).

Table 14.3 displays the results of calculations for the same three models but using material B for the square and rectangular models in the roofing.

Table 14.4 shows the results of calculations for the same three models in Table 14.2 after adding the insulation NSP. The same thermal resistance of the NSP as was used by the researchers in [3], who conducted experimental and theoretical investigations on it, was used.

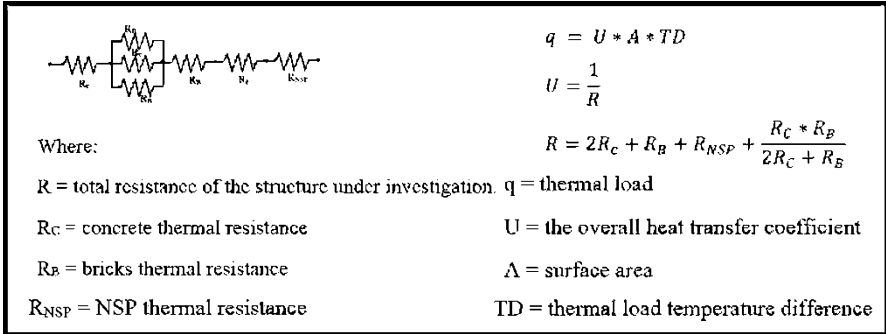


Fig. 14.4 Structure with NSP thermal resistance

Table 14.2 External thermal load on buildings using Type A material in Table 14.1

External load in Btu/h						
Building shape (orientation)	With window			Without window		
	90°F	100°F	110°F	90°F	100°F	110°F
Square	12,699.96	19,997.63	26,069.47	12,569.06	20,505.55	26,090.90
Rectangle (North–South)	13,358.66	20,867.99	26,938.36	12,870.41	20,743.68	26,217.61
Rectangle (East–West)	13,147.62	20,883.06	27,166.69	12,659.37	20,758.76	26,445.94
Dome	10,473.38	18,456.37	21,348.07	10,716.89	18,594.72	20,932.18

Table 14.3 External thermal load on buildings using Type B material in Table 14.1

External load in Btu/h						
Building shape (orientation)	With window			Without window		
	90°F	100°F	110°F	90°F	100°F	110°F
Square	16,735.85	26,275.68	34,589.68	16,604.95	26,783.61	34,611.11
Rectangle (North–South)	17,395.07	27,146.84	35,459.66	16,906.82	27,022.54	34,738.91
Rectangle (East–West)	17,184.03	27,161.92	35,687.99	16,695.78	27,037.61	34,967.24
Dome	10,473.38	18,456.37	21,348.07	10,350.89	18,594.72	20,932.18

The results of calculations after adding the thermal resistance NSP to the models of Table 14.3 are presented in Table 14.5.

Since the calculations follow a standard procedure, they are edited in tables, constituting 80 pages, given separately as reference [4] in appendix form. The novelty is the use of the infinite-element method for the dome’s heat transfer area. The appendix is made to assist, as an example, those who are interested in bridging the gap between disciplines.

Table 14.4 External thermal load to buildings using Type A material in Table 14.1 + NSP

The external load when adding NSP in Btu/h						
Building shape (orientation)	With window			Without window		
	90°F	100°F	110°F	90°F	100°F	110°F
Square	7921.70	12,370.33	16,291.46	7479.28	11,881.62	15,733.94
Rectangle (North– South)	8034.38	12,562.65	16,483.78	7546.13	11,934.90	15,763.03
Rectangle (East–West)	7987.97	12,565.96	16,534.00	7499.72	11,938.21	15,813.25
Dome	5918.57	11,459.79	12,166.96	7250.92	10,857.99	11,467.71

Table 14.5 External thermal load to buildings using Type B material in Table 14.1 + NSP

External load when adding NSP in Btu/h						
Building shape (orientation)	With window			Without window		
	90°F	100°F	110°F	90°F	100°F	110°F
Square	7930.66	12,384.27	16,310.38	7488.24	11,895.57	15,752.86
Rectangle (North– South)	8043.35	12,576.60	16,502.71	7555.10	11,948.85	15,781.96
Rectangle (East–West)	7996.94	12,579.91	16,552.93	7508.69	11,952.16	15,832.18
Dome	5918.57	11,459.79	12,166.96	7250.92	10,857.99	11,467.71

4 Discussion and Conclusions

4.1 Effect of Geometry

As can be seen from Tables 14.2 and 14.3, the dome building gives the lowest calculated external thermal load: 58–68 % of that calculated for the other models. The variation is due to the variation in building materials. It is low when the other models are roofed by concrete, which is the current practice. When the fired clay bricks are used, local traditional Libyan roofing, the rate is higher. This reflects the low resistance of the traditional materials. The effect of windows can be neglected with the right choice of glass index.

Heat ingress at 110 °F is double the heat ingress at 90 °F for all models. But the average heat ingress of the other models is 67 % higher than that of the dome when Type B materials are used and 29–30 % higher when Type A materials are used.

With higher temperatures dome structures are more recommended.

4.2 Effect of NSP

With the NSP insulation considered in the calculations, the external thermal load – the heat ingress – reduces to 59 % for the dome at 90 °F, and for the other models it

reduces to 62 % for Type A, the traditional Libyan brick roofing. On the other hand, for Type B material, common concrete, the heat ingress reduces to 47 %. This reflects the importance of the NSP for today's standard practices. These percentages are more or less maintained for the calculations at 110 °F. The NSP is most effective when the building materials have a low thermal resistance.

In all cases the dome geometric structure gives the lowest heat ingress through the boundaries. The dome building offers additional benefits:

- Smooth inside air circulation without stagnation at corners;
- More volume for inside air with less heat transfer surface areas;
- Unlike other construction designs, domes are strong and resistant enough under extreme conditions, such as in earthquakes or hurricanes.

The following recommendations are made:

More domes should be built, especially where high-rise buildings are restricted. The dome structure conserves the most energy and contribute the most to a green environment. The curved surfaces, even in walls, give the same effect of thermal resistivity to radiation;

Building designers should familiarize themselves with the details of the thermal load calculations of a given building prior to installation of the relevant equipment. The development of software, based on the standard procedure and the finite-element method used for the calculation of curved roofs and curved wall heat transfer segmented areas, will help greatly in bridging the relevant disciplines;

As the normal lies in minimizing energy use, the abnormal lies, temporarily, in people's attitudes during the process of acceptance and acclimatization, meaning some of us will have to change some of our habits. Frank Zappa [5] expressed it another way: "Without deviation from the norm, progress is not possible."

However, architects are fully capable of reintroducing the dome and dome habitats.

Domes have been found in Persian, Hellenistic Roman, and Chinese architecture. They dominated Islamic architecture. With the Renaissance their use spread from Italy, with Florence at the vanguard.

Since decisions in energy and town planning are inseparable from policy decisions, the building of more domes should be encouraged by calling 2015, in which Med Green Forum 2015 was held, the Year of the Dome or the Florence Dome Declaration, with the Cathedral Dome serving as the logo.

Many architects and homebuilders are encouraged to build residential compounds formed of dome houses (Fig. 14.5), in addition to sports domes and domes for public use.

The interiors of dome houses are friendly and cozy (Figs. 14.6 and 14.7).

The dome of the Florence Cathedral is proposed as the logo for the Florence Dome Declaration (Fig. 14.8).



Fig. 14.5 Dome houses, residential compounds



Fig. 14.6 Dome house interiors



Fig. 14.7 Dome house interiors



Fig. 14.8 Florence Cathedral Dome

Acknowledgements The authors are truly indebted to Ms. Randi EL-Hadi, whose efforts led to the final presentation of this text.

References

1. Abdel-Rahman AH (2012) Low initial capital and operating costs industrial air conditioning system design. In: Proceedings, world renewable energy forum (WREF) 2012, Including 41st ASES annual conference, 37th national passive solar conference, 7th renewable energy policy and marketing conference, world renewable energy congress XII, and Colorado Renewable Energy Society (CRES) annual conference, Denver, 13–17 May 2012
2. NASA Scientific and Technical Information (2007) Additive transforms paint into insulation. NASA Spinoff, Innovative Partnership Program, p 72
3. Poppendick HF (2003) A study of the energy savings that can occur when using insuladd solar reflective patent on irradiated building walls. R-value-geoscience-report, Geo Science, April 2003
4. Appendix for the Article. “The normal; minimising energy use, the abnormal: changing the habits ”, MED GREEN FORUM 2015—Florence, Italy, 26–28 August 2015, <http://www.wrenuk.co.uk>
5. Frank Z (1940–1993) Brainy quotes. Composer, musician, film director

Chapter 15

Semi-Empirical Models for the Estimation of Global Solar Irradiance Measurements in Morocco

N. Laaroussi, M. Garoum, A. Hajji, M. Tajayouti, and A. Feiz

Abstract This chapter presents semi-empirical models for estimating global horizontal irradiance (GHI) under specific sky conditions. We analysed the models to estimate GHI measurements in four regions of Morocco. The data consist of a 1-year period at four solar irradiance monitoring stations located in the south of the country, Missouri (32.86°N, -4.11°E), Erfoud (31.49°N, -4.22°E), Zagora (30.27°N, -5.85°E) and Tantan (28.50°N, -11.32°E). Several empirical clear sky models are considered for a Moroccan case study. These models are validated using GHI measurements from different stations over different time periods.

The disagreement between the various measurements of GHI and the semi-empirical models used for the estimation of radiation in atmospheric physics and radiative transfer modelling is sometimes significant, especially in the presence of clouds or large concentrations of aerosols. A good agreement is noticed between the measured values and those estimated by some models.

Keywords Solar irradiation • Global horizontal irradiance • Direct normal irradiance • Diffuse horizontal irradiance • Semi-empirical models

N. Laaroussi (✉) • M. Garoum • A. Hajji • M. Tajayouti
EST de Salé, Laboratoire d'Energétique, Matériaux et Environnement (LEME), Université Mohammed V Rabat, Avenue Prince Héritier, BP. 227 Salé Medina, Maroc, Rabat, Morocco
e-mail: n.laaroussi@est.um5a.ac.ma

A. Feiz
Laboratoire de Mécanique et d'Energétique d'Evry (LMEE), Equipe Mécanique des Fluides et Environnement (MFE), Université d'Evry Val-d'Essonne, 40 Rue du Pelvoux, Evry 91020, France

Nomenclature

I_0	Solar constant, 1367 W.m^{-2}
I_{sc}	Extraterrestrial solar irradiance
I_G	Global solar irradiance, W m^{-2}
I_{di}	Direct solar irradiance, W m^{-2}
I_{da}, I_{dm}	Diffuse solar irradiance, W m^{-2}
m_a	Air mass
ρ	Terrestrial albedo
$\theta_z(^{\circ})$	Zenith angle in degrees
α_0	Ozone absorption coefficient
α_w	Water vapour absorption
τ_{aa}	Transmittance of aerosol absorptance
$\tau_0 = (1 - \alpha_0)$	Transmittance of ozone absorptance
τ_r	Rayleigh scattering transmission
τ_a	Transmittance of aerosol absorptance and scattering

1 Introduction

Solar radiation or solar irradiance is the energy that reaches the Earth and is vitally important for plants and humans and in addition supplies a cheap source of renewable energy [1]. Several models are developed by the authors to predict the global, direct and diffuse solar irradiance needed by solar collectors or photovoltaic panels to produce the required energy. Thus, the knowledge of the clear sky global horizontal irradiance (GHI) reaching the ground represents the solar resource used by solar technologies and the important factor in the field of solar radiation modelling and system evaluation of energy efficiency for buildings [2]. Mesri et al. [3] studied some theoretical models to estimate the components of solar radiation received at ground level, and their models are based on the determination of transmission coefficients of atmospheric constituents. A comparison between the measured and estimated values using theoretical models at two Algerian sites is conducted by Koussa et al. [4]. The term of reference related to direct irradiance received on a plane normal to the Sun is called the direct normal irradiance (DNI), as specified by Blanc et al. [5]. The importance of circumsolar radiation in DNI is demonstrated, and its potential contribution is evaluated for typical atmospheric conditions. Singapore GHI measurements to estimate the clear sky in the equatorial region are analysed by Dazhi et al. [6] using several empirical clear sky models. The validation of models for computing solar radiation on inclined surfaces for building energy simulations is given in [7]. Bird and Hulstrom have compared several simple global radiation models with rigorous radiative transfer models and have described an improved global radiation model. They have formulated a simple clear sky model for direct and diffuse radiation [8].

2 Description of Used Models

Several methods exist in the literature for modelling solar radiation components. Parametric models, like those of Lacis and Hansen, Davies and Hay, Bird and Hulstrom and Atwater and Ball models [9], require detailed information on atmospheric conditions and meteorological parameters, including the type, amount and distribution of clouds, or other observations, such as the fractional sunshine, atmospheric turbidity and perceptible water content.

A description of the models employed in this study is presented here. The models are based on the reduction in the power of the solar radiation due to absorption, scattering and reflection in the atmosphere. Those models require more input parameters, such as column ozone, column precipitable water, aerosol optical depth and other atmospheric transmittances.

Figure 15.1 and Table 15.1 show the geographical location and coordinates of the four studied sites: Missouri, Erfoud, Zagora and Tantan.

To estimate the global and diffuse radiations at the site, measurements of sunshine hours, bright sunshine hours, maximum and minimum temperature, humidity, pressure, visibility, wind speed and direction, gust speed, water precipitation and air mass are very important parameters.

For this we have accurate measurements of the direct, diffuse and global solar radiation on a horizontal surface, temperature, relative humidity, wind speed and direction and atmospheric pressure in different Moroccan climates – Missouri

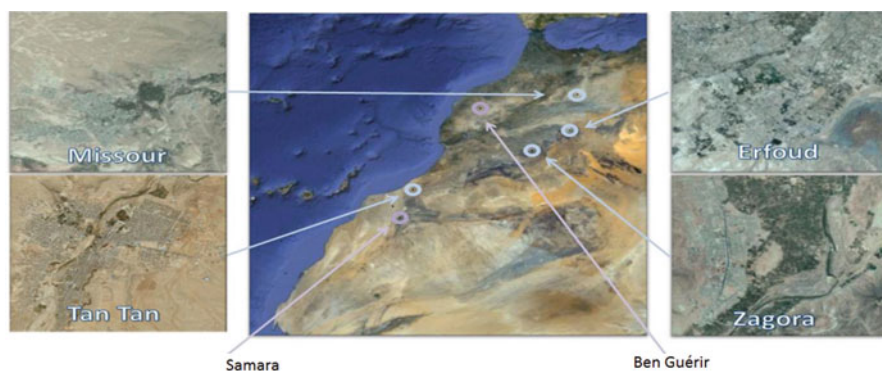


Fig. 15.1 Solar monitoring stations used in study on map of Morocco

Table 15.1 Geographical coordinates of the four sites

Site	Latitude (°)	Longitude (°)	Height (m)
Missour	-4.10725°N	32.68031°E	1107
Erfoud	-4.21801°E	31.49078°N	859
Zagora	-5.85161°E	30.27219°N	783
Tan-Tan	-11.32171°E	28.49828°N	75

(semi-arid), Erfoud (arid), Zagora (Sahara) and TanTan (coastal) –using two types of weather stations, MHP and MDI. The temporal resolutions of the used monitoring stations are 1 min and 10 min, and only 1 min data are used in this study showing more information.

Several authors propose a simplified clear sky model for direct and diffuse irradiance on horizontal surfaces. In this work, we compare several simple GHI models with measurements and describe the optimum simple global irradiance.

All used parameters, like the equations of transfer and the transmission functions for all irradiance models, are described in [3, 4].

The extraterrestrial irradiance I_{sc} outside the atmosphere on a plane perpendicular to the Sun's rays and the day of the year n_j are such that for 1 January, $n_j = 1$:

$$I_{sc}(n_j) = I_0 \times \left[1 + 0.033 \times \cos \left(\frac{360}{365}(n_j - 3) \right) \right]. \quad (15.1)$$

Most solar power calculations use I_{sc} as a starting point because, for any given day of the year, it is the maximum possible energy obtainable from the Sun at the edge of the Earth's atmosphere.

2.1 *Lacis and Hansen Model*

The model developed by Lacis and Hansen [9] gives the equation for total irradiance,

$$I_G = I_{sc}(n_j) \times \cos(\theta_z) \left[\frac{(0.647 - \rho'_s - \alpha_0)}{(1 - 0.0685\rho)} + 0.353 - \alpha_\omega \right], \quad (15.2)$$

with $\rho \approx 0.25$ the terrestrial albedo and $\rho'_s = \frac{0.28}{(1 + 6.43 \cos(\theta_z))}$, where $\theta_z = 90^\circ - h$ is the zenith angle measured between a line to the Sun and the local zenith and h is the elevation angle, measured up from the horizon.

2.2 *Davies and Hay Model*

A model for direct I_{di} and diffuse I_d solar radiation was proposed by Davies and Hay [9]. The equation used in this model is the result of comparing several existing models. The global solar irradiance I_G is described by

$$I_G = I_{di} + I_{da} + I_{dm}, \quad (15.3)$$

with

$$I_{di} = I_{sc} [\tau_0 \tau_r - \alpha_\omega] \times \tau_a \times \cos(\theta_z), \quad (15.4)$$

$$I_{da} = I_{sc} \cos(\theta_z) [(\tau_0 \tau_r - \alpha_\omega)(F_c \omega_0 (1 - \tau_a)) + 0.5 \times \tau_0 \tau_a (1 - \tau_r)], \quad (15.5)$$

$$I_{dm} = \frac{(I_{di} + I_{da}) \rho \times \rho_s}{(1 - \rho \times \rho_s)}. \quad (15.6)$$

The value $\omega_0 = 0.90$ is used for data generated here and is representative of a fraction of the light lost from an incident radiation of radiation that is due to scattering by albedo and ρ_s is the sky or atmospheric albedo. F_c is the ratio of the forward-scattered irradiance to the total scattered irradiance due to aerosol as calculated by Robinson [11]. The calculations of τ_a depend on the atmospheric turbidity based on 0.38 at a 0.8 μm wavelength and a ground albedo of 0.25 [4].

2.3 Bird and Hulstrom Model

A model has been constructed which is based on comparisons with other direct insolation models [12]. The adopted equations for this model are as follows:

$$I_G = I_{di} + I_{da} + I_{dm}, \quad (15.7)$$

$$I_{di} = 0.9662 I_{sc} \tau_g \tau_r \tau_0 \tau_w \tau_a \cos(\theta_z), \quad (15.8)$$

$$I_{da} = 0.79 I_{sc} \tau_g \tau_0 \tau_w \tau_{aa} \cos(\theta_z) \frac{[0.5(1 - \tau_r) + F_c(1 - \tau_{as})]}{(1 - m_a + m_a^{1.02})}, \quad \text{with } \tau_{as} = \frac{\tau_a}{\tau_{aa}}, \quad (15.9)$$

$$I_{dm} = \frac{(I_{da} + I_{di}) \rho \rho_s}{(1 - \rho_g \rho_s)}, \quad (15.10)$$

where ρ_g is the ground albedo and $F_c = 0.84$ is the value recommended for this model

2.4 Atwater and Ball Model

Direct and global radiation models were proposed by Atwater and Ball [9]. An equation for global solar irradiance I_G on a horizontal surface (W_m^{-2}) in this model is given by

$$I_G = I_{Sc} \times \cos(\theta_z) \times \left[\frac{(T_{M-w})\tau_a}{(1 - \rho_g \rho_s)} \right]. \tag{15.11}$$

The value of $\rho_s = 0.0685$ for a molecular atmosphere, as reported in [10], was used with this model.

T_M is the global transmittance of all molecular effects.

3 Results

This work is focused on estimating the values of global solar radiation on a horizontal surface, with models which use measured meteorological data and geographical and geometrical parameters for four cities of Morocco. Then the measured data of global solar radiation on a horizontal surface are compared with the obtained results from the four models described earlier.

Figure 15.2 shows the measuring intensity of global, direct and diffuse solar radiation coming through the atmosphere on a horizontal surface. The DNI is the diffuse radiation partially absorbed or reflected by constituents like aerosol particles. Therefore, the knowledge of diffuse radiation DNI on a horizontal surface is important in the design of various energy utilization systems.

To examine the magnitude of each component, we assume that the direct component (DHI) provides approximately 80 % of the total irradiance, whereas the diffuse ground sky component (DNI) is approximately 20 %.

Figures 15.3, 15.4 and 15.5 present comparisons of measured and modelled global irradiance from all of the clear sky models. The Lacis and Hansen, Davies and Hay, and Atwater and Ball models produce very similar results and

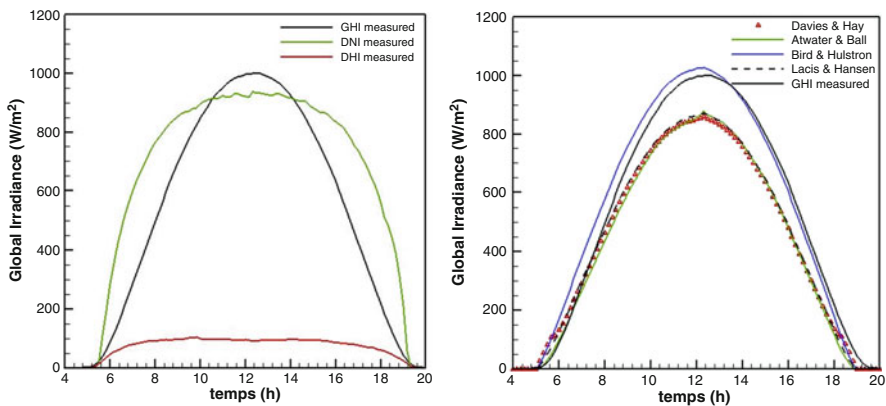


Fig. 15.2 Global, diffuse and direct irradiances on horizontal surface measured in city of Erfoud on 7 June 2013

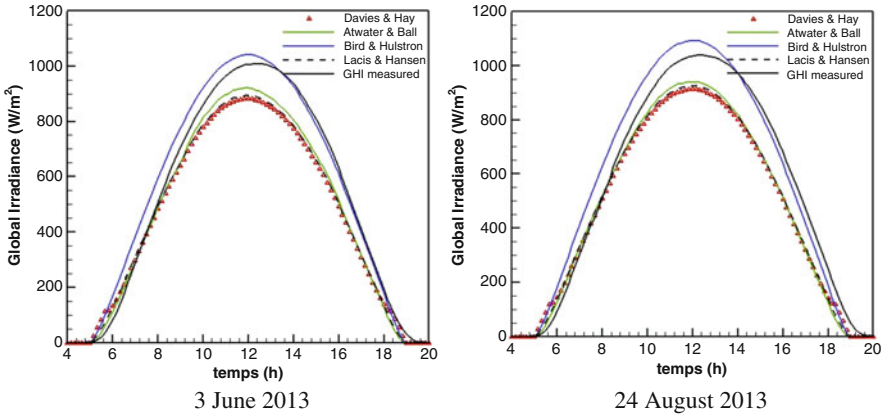


Fig. 15.3 Global horizontal irradiance measured in city of Erfoud on 7 June 2013 and comparison with models

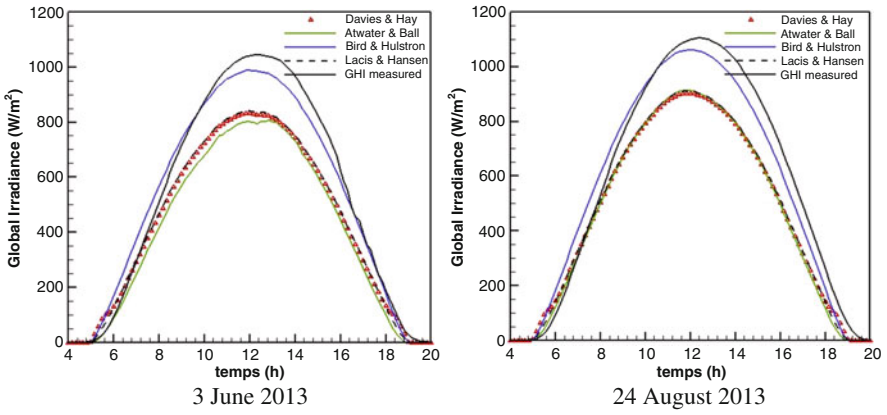


Fig. 15.4 Global horizontal irradiance measured in city of Missouri and comparison with models

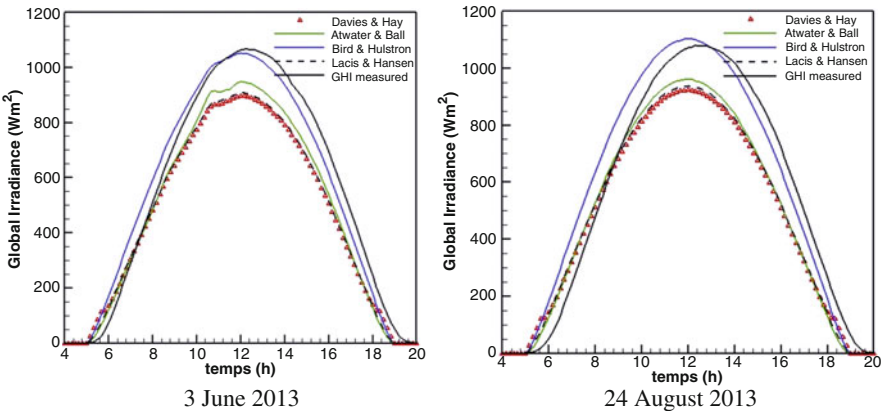


Fig. 15.5 Global horizontal irradiance measured in city of Zagora and comparison with models

underestimate the global sky irradiance. The model of Bird and Hulstrom is significantly close to the measured values.

The results of the Davies and Hay model would have shown much better agreement with measurement results if a greater value of the aerosol transmittance had been considered because the model does not have a good method for treating aerosol transmittance.

The Atwater and Ball model is applicable to extremely clear atmospheric conditions with an atmospheric turbidity near 0.1 at a 0.5 μm wavelength. This model is extremely simple but does not have a good method of treating aerosol transmittance.

It can be seen from Figs. 15.3, 15.4 and 15.5 that the Bird and Hulstrom model slightly overestimates the values of the total solar radiation during the early morning and sometimes during the middle part of the day. However, it slightly underestimates total solar radiation during the late afternoon hours and in the second half of the day. This discrepancy may be attributed to a local variation in aerosol synthesis and concentration, factors that cannot be simulated properly in the model with a single value of F_c for the whole day.

It is hoped that the accurate, simple models will provide results which will agree within 30 % of each other with quality experimental data on clear days. Cloudy days are more difficult to model accurately, and clouds can have the greatest effect on the total irradiance because the extra diffuse radiation produced under cloudy skies is still unknown for the various types of clouds.

Solar irradiance data at different sites were tested in the four proposed irradiance models. An indicator is employed including the relative error (R) given by the following equation:

$$R = \left| \frac{(GHI_{mod,i} - GHI_{exp,i})}{GHI_{exp,i}} \right| \times 100. \tag{15.12}$$

The best model for describing the solar radiation on site was selected as the lowest value of the coefficient (R), which gives quite satisfactory results, as shown in Table 15.2 (maximum error of around 31 %).

Table 15.2 Mean relative error (R) of four sites (%)

Dates	Missour	Erfoud	Zagora	Tan–Tan	Model
3 June 2013	14	13	15	12	Bird and Hulstrom
	25	22	21	20	Lacis and Hansen
	31	25	24	23	Davies and Hay
	29	17	18	17	Atwater and Ball
24 August 2013	12	14	13	12	Bird and Hulstrom
	30	22	29	20	Lacis and Hansen
	29	25	29	23	Davies and Hay
	27	21	28	17	Atwater and Ball

4 Conclusion

In this work, we presented a trend in solar energy modelling, which is of major interest to solar energy engineers, architects, building designers, and thermal device manufacturers for efficient utilization of this non-conventional energy resource.

We carried out a comparison study between measured and modelled global horizontal irradiance at sites located in Morocco. The simulations were obtained with four models using MATLAB software. The model input parameters, such as total ozone and aerosol optical depth, were taken into consideration and collected from the literature. A comparison between measured and modelled direct solar radiation was made, showing acceptable agreement, with differences below 30%. However, these differences were attributed to the effect of the underlying surface albedo owing to the frequent existence of a sea of clouds below the station altitude. The underlying surface albedo was varied throughout the day and was determined using different methods and having the influence of the considered models.

References

1. Hanif M, Ramzan M, Aamir M, Rahman M, Khan M, Amin M (2012) Studying power output of PV solar panels at different temperatures and tilt angles. *ISESCO J Sci Technol* 8(1):9–12
2. Ineichen P (2008) A broadband simplified version of the solis clear sky model. *Solar Energy* 82:758–762
3. Mesri-Merad M, Rougab I, Chekmane A, Bachari NI (2012) Estimation du rayonnement solaire au sol par des modèles semi-empiriques. *Revue des Energies Renouvelables* 15(3):451–463
4. Koussa M, Malek A, Haddadi M (2006) Validation de quelques modèles de reconstitution des éclaircissements dus au rayonnement solaire direct, diffuse et global par ciel clair. *Revue des Energies Renouvelables* 9(4):307–332
5. Blanc P, Espinar B, Geuder N, Gueymard C, Meyer R, Pitz-Paal R, Reinhardt B, Renne D, Sengupta M, Wald L, Wilbert S (2014) Direct normal irradiance related definitions and applications: the circumsolar issue. *Solar Energy* 110:561–577
6. Dazhi Y, Jirutitjaroen P, Walsh WM (2012) The estimation of clear sky global horizontal irradiance at the equator. *Energy Procedia* 25:141–148
7. Loutzenhiser PG, Manz H, Frlsmann C, Strachan PA, Frank T, Maxwell GM (2007) Empirical validation on models to compute solar irradiance on inclined surfaces for building energy simulation. *Solar Energy* 81(2):254–267
8. Bird RE, Hulstrom RL (1981) A simplified clear sky model for direct and diffuse insolation on horizontal surfaces, February 1981, *SERI/TR*, pp 642–761
9. Davies JA, Hay JE (1979) Calculation of the solar radiation incident on a horizontal surface. In: *Proceedings of first Canadian solar radiation data workshop, 17–19 April, 1978, Canadian Atmospheric Environment Service*
10. Lacis AL, Hansen JE (1974) A parameterization absorption of solar radiation in the earth's atmosphere. *J Atmos Sci* 31:118–133
11. Robinson GD (1962) Absorption of solar radiation by atmospheric aerosol as revealed by measurements from the ground. *Archivfür Meteorol Geophys Bioclimatol Ser B* 12(1):19–40
12. Bird RE, Hulstrom RL (1980) Direct insolation models. *Solar Energy Research Institute, Golden. SERI/TR*, pp 335–344

Chapter 16

Assessing PV Module Degradation and the Potential of Using Greenhouse Roofs for Supplemental PV Power Generation in Malta

Kristy Bartolo and Charles Yousif

Abstract This chapter presents work carried out on the evaluation of the added photovoltaic (PV) capacity that Malta might need to install to counter-balance the loss of energy production from installed solar PV systems caused by degradation in order to achieve the government's target of 5 % PV generation by 2020. The potential of using unconventional rooftops is investigated with a focus on greenhouses, which are normally found in rural areas. Such a possibility also has the capability of providing renewable energy to greenhouses, making it greener and self-sufficient. The study started by analysing the actual degradation experienced by a number of PV modules which have been in operation on the island of Malta for between 3 and 33 years. An average degradation of 1.2 % has been found. Visits to greenhouses were also made to categorize their construction materials, area and other technical characteristics to have a better and more hands-on understanding of their ability to take up the added load of PV modules. Two cases were found where new greenhouses were actually in the process of installing PV modules, one in Malta and one in Gozo. The results of this study can help the government to provide incentives for greenhouse owners to invest in PV modules while alleviating the drop in energy production due to the degradation of already installed PV systems to reach the set target.

Keywords Solar PV module degradation • 2020 EU targets • Malta • Solar greenhouses

K. Bartolo (✉)
Institute of Earth Systems, University of Malta, Msida, Malta
e-mail: kbartolo94@hotmail.com

C. Yousif
Institute for Sustainable Energy, University of Malta, Msida, Malta
e-mail: charles.yousif@um.edu.mt

1 Introduction

In the past few years, renewable energy (RE) technologies have gone mainstream all around the world since they are the most effective means by which countries are able to meet their RE policy goals. Moreover, they allow countries to have reliable, secure and affordable energy to promote development enhancements and expand electricity access [1].

Malta has been highly influenced by higher-level European Union (EU) energy policies since its accession to the EU in 2004. In 2007, the EU set a benchmark with the Renewable Energy Road Map, which proposed a mandatory target for the EU's member states to reach a 20 % RE share of overall energy consumption by the year 2020. Subsequently, this was adopted in the RE Directive 28/2009/EC [2]. Malta's contribution was set at 10 % RE of its overall energy consumption by 2020 [3]. The first Malta National Renewable Energy Action Plan (NREAP) of 2009 focused primarily on developing onshore and offshore wind farms [4]; however, a number of issues were identified which hindered the development of these projects. As a result, the newly elected government of 2013 has decided to shelve wind energy projects and replace them with a stronger drive towards PV installations. Under this policy, the PV share should reach 5 % of the total energy consumption by 2020 out of the total of 10 % RE that needs to be achieved [5].

Malta's geographical location and climate provide a high potential for obtaining RE from the sun since for most of the year it has an abundance of moderate temperatures and sunshine. In fact, on the horizontal plane, Malta has the highest annual solar irradiance amongst EU member states, reaching 1875 kWh/m² per year. It also has the least variation in solar energy from one year to the next, giving stability to the electrical energy production from this resource [6]. However, Malta faces certain obstacles due to its relatively small size (300 km²), small amount of available land and large population density (1536 persons/km²), as well as to a lack of other natural resources. PV modules have proven to be the most successful forms of RE technologies in Malta owing to their relatively low operating costs, reliability and ease of installation. Moreover, since 2006 a significant amount of EU funds has been used to provide capital grants to households to install PV systems on their roofs. This was also further encouraged by the introduction of feed-in tariffs, which currently stand at 16.5 euro cents/kWh [7].

Nonetheless, such PV systems greatly depend on high solar energy performance, so maximum sun exposure is necessary and large open spaces are required for multi-megawatt installations. In a country like Malta where land resources are so restricted, the RE capacity to which it is able to extend is limited and therefore such projects are not easily implemented since other activities may be competing for the same piece of land. An example of this is agriculture. Since agriculture takes up a lot of Malta's rural areas, it would be quite hard to find a way whereby both agriculture and alternative renewable sources of energy could be incorporated together. However, a solution may be possible.

In recent years, the industry of greenhouses has grown in Malta, and with it larger rural areas have been taken up for their installation. Interestingly, the technology of PV systems has also developed over the years, and today it is possible to integrate such systems in greenhouses, without losing on the production rate of the crops within the greenhouses.

The main questions that this chapter attempts to answer are the following:

1. How do PV modules degrade in performance when subjected to the Maltese local climate and solar radiation?
2. How much extra power capacity is needed every year to counterbalance the drop in electrical energy production due to this degradation and reach 5 % PV energy share by 2020?
3. Can greenhouses be used to install PV modules, and hence provide the necessary space for such installations, without having to take up any more land?

2 Methodology and Test Procedures

This study consisted of two parts. The first part was based on technical studies to determine the rate of drop in power generation by PV modules operating in Malta due to ageing. As a result, an estimate would be made to determine the additional power required every year to counterbalance this drop, so that by 2020 the energy produced from PV modules would be the same as when each of these systems was installed on its first day.

The second part of the study aimed at determining potential unconventional areas where added PV capacity could be installed. Consequently, two questionnaires were made, one for greenhouse owners who had no PV modules installed on their greenhouses in order to gauge their willingness to invest in PV installations. The first questionnaire helped to determine the total area available to support the extra solar modules needed and to determine potential sites where they could be installed, while the second questionnaire was for those planning to install PV systems on their greenhouses and to understand better the main reasons why they opted for such projects.

The standard I-V curve of a PV device is measured in the laboratory under standard test conditions, since otherwise it would not be possible to compare one module to another [8]. In this study, the I-V curve was tested in the field, so all readings were corrected to the appropriate standard conditions using appropriate equations and factors. This was done so as to compare the present situation of a PV module to its original technical specifications when produced from the factory and, hence, to determine the total degradation of each module in this study.

Later, calculations were carried out to determine the additional power required every year to counterbalance a PV's drop in efficiency, so that by 2020, the energy produced from PV modules would be the same as when each of these systems was installed on its first day. Statistical information regarding PV installations in Malta was acquired from reliable sources [9, 10]. This information was used to carry out

the necessary calculations to determine the total energy drop that would accumulate by 2020 and the total area of solar PV modules that would be needed to counter-balance this deficiency.

2.1 Determining the Efficiency of PV Modules

Testing was done on the premises of the Institute for Sustainable Energy in Marsaxlokk during the months of July and August. Measurements were taken between 11:30 a.m. and 12:30 p.m. (solar noon) on clear days in order to have as little solar energy variation as possible. Also, the sun's radiation would be close to 1000 W/m^2 as reported by the standard testing specifications. This also allowed multiple readings of different panels to be taken at practically the same solar radiation value and temperature conditions. The modules were also set to be perpendicular to the sun during testing.

To calculate the present efficiency of solar PV modules, the following measurements were taken:

- Open-circuit voltage (V_{oc}): found simply by measuring the voltage across the panel at no-load conditions;
- Short-circuit current (I_{sc}): found by measuring the current passing from the negative to the positive poles of the PV panel when it is short-circuited in the sun. A PV panel is the only electronic apparatus that is not damaged when short-circuited. This is because the electrons simply move from the negative to the positive part of PV cells and the generated energy is converted to heat. In other words, there are no other electronic components in this passage and, hence, no damage is done.
- Voltage at maximum power point (V_{mpp}): measured when a PV panel is connected to a partially discharged battery. The battery forces the PV module to operate very close to its maximum power point. The solar in-plane radiation and the module's temperature were also measured, using a solar pyranometer and an infrared camera.
- Current at maximum power point (I_{mpp}): measured when PV panel is connected to battery, immediately following measurement of V_{mpp} .

Conversion of the PV power results to standard testing conditions was carried out using the following steps:

1. Power correction due to solar radiation assumed linear, given that the difference between the actual solar radiation during the testing procedure and the standard testing condition of 1000 W/m^2 was very low, within $\pm 0.03\%$.
2. Power correction due to temperature, whereby the manufacturer's power coefficient was used for each type of PV module.

Hence, it was possible to calculate the percentage drop in power under standard conditions and, consequently, determine the average drop in power per year assuming a linear degradation curve.

2.2 Preparation of Questionnaires

The questionnaires were prepared with the following scope in mind:

1. To collect information on the type of greenhouses available (construction, area);
2. To determine whether greenhouse owners were aware of solar PV greenhouse projects
3. To gauge the level of interest among owners in utilising the roofs of greenhouses.

On this basis, several questions were devised. Since the questionnaires included categorical, metric and multiple-response questions, analysis was completed using IBM SPSS Statistics 22 (Statistical Package for the Social Sciences). This program allows users to statistically analyse data collected from surveys and questionnaires.

3 Results

3.1 Solar PV Module Efficiency

It was noted that the average percentage drop per annum for all solar modules under study was approximately 1.2 % (Table 16.1). Although the tests carried out are not statistically representative of the total installations in Malta (12 PV modules tested), it gives a good qualitative indication of the expected degradation, which is in line with several previous studies carried out worldwide [11–13]. This drop is quite significant since it has direct implications for the solar PV energy output over the lifetime of PV modules. This impact increases as the number of PV installations grows. Moreover, such a drop in efficiency should be considered when planning for any country's long-term RE targets. This is because once a PV module is installed, it will start to degrade, and therefore the decrease in the efficiency of solar PV modules would need to be considered when setting RE trajectories in future years.

With this value, it is possible to calculate the extra PV power needed to be installed in Malta to maintain the set target of 5 % contribution from PV systems for 2020, as shown in what follows.

Table 16.1 Overall annual average percentage drop of all solar modules tested

PV module age (years)	Sample size	Type of silicon cell	Country of origin	Average efficiency (% drop/year)
33	3	Mono-crystalline	USA	2.06
20	3	Poly-crystalline	USA	0.76
10	3	Mono-crystalline	Malta	1.4
3	3	Mono-crystalline	India	1.1
<i>Average efficiency (% drop/year)</i>				1.2

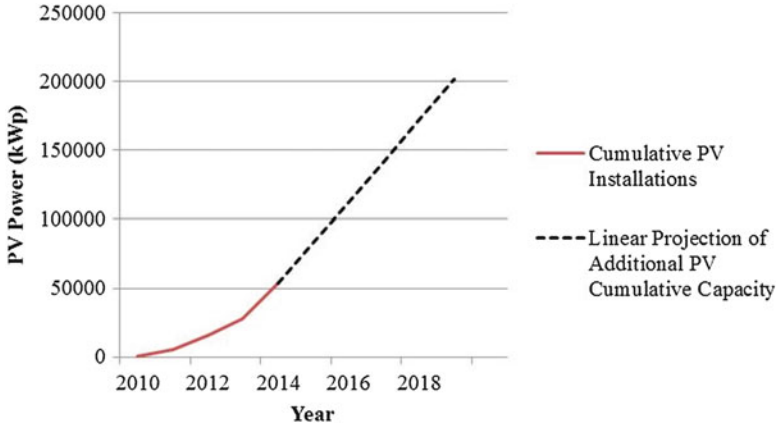


Fig. 16.1 Installed PV capacity in Malta by 2014 (*red brick solid line*) and estimated projection of installed PV capacity to reach 5 % RE contribution by 2020 (*black dotted line*)

Malta's NREAP shows a final energy consumption of 534,490 toe [14], which is equivalent to 6,216,118,700 kWh, of which 5 % (310,805,935 kWh) is planned to be generated by PV systems [5]. Calculations were made to determine the minimum kilowatt peak (kWp) needed each year from 2015 until 2020, taking into consideration a degradation factor of 1.2 % per annum for solar PV modules. Figure 16.1 shows the actual cumulative PV capacity installed through the end of 2014 and the projected installations through the end of 2019, in order to reach the required total installation of 201,458 kWp, equivalent to a 5 % RE contribution. According to these calculations, a minimum annual installation of 29,584 kWp should be realised between 2015 and the end of 2019 in order to reach the 5 % RE contribution from PV installations.

If all installations needed to reach the target of 5 % had been made in the last year, the total installed capacity would have been 194,254 kWp (Table 16.2). However, this is not practical, and therefore the resulting total installation based on the real installed and projected capacities would total 201,458 kWp, which implies that 7204 kWp are needed to account for the degradation of the PV modules, taking into consideration the assumed linear growth of PV installations between 2015 and 2020. This added capacity would cover an area of 47,980 m² or 8.1 % of the total area occupied by greenhouses [15].

Assumptions

- Each kilowatt peak of new PV modules produces 1600 kWh of energy per year when installed facing southwards and inclined at a 30° angle to the horizontal (this value is also the statistical average of newly installed PV systems in Malta).
- The area occupied by 1 kWp of PV modules is 6.66 m².
- The degradation of the already installed modules was taken into consideration year by year as of 2010.

Table 16.2 Results of calculations for additional PV power required until 2020 and corresponding area needed to install them

Year	2010–2020
Actual 2019 PV energy output required to achieve 5 % contribution (kWh)	310,806,797
Actual kilowatt peak needed to produce this energy, including effect of degradation (kWp)	201,458
Capacity required if all PV was installed by end of 2019 (kWp)	194,254
Extra kilowatt peak needed (kWp)	7204
Area occupied by extra kilowatt peak (m ²)	47,980

Table 16.3 Comparison between ‘Census of Greenhouses’ issued by NSO for 2001 and 2007 [15, 16]

Census year	2001	2007
Agricultural holdings	348	338
Total greenhouse structures	1023	1168
Total greenhouse area (m ²)	510,174	595,000

3.2 Questionnaire Analysis

In two consecutive censuses of greenhouses undertaken in 2001 and 2007 respectively, the National Statistics Office (NSO) published data with regard to greenhouses within Malta’s agricultural sector, including their structural and economic information. The information shown in Table 16.3 was taken from these published results [15, 16]. This information shows that in a period of 6 years, there was a substantial increase in the amount of greenhouses installed on the Maltese Islands, from 1023 greenhouse structures covering a total area of 510,174 m² in 2001 to 1168 structures covering a total of 595,000 m² in 2007—an increase of 14 % in number and 16 % in area.

The surveyed greenhouses together covered a total area of 40,498 m², which is equivalent to 6.8 % of the total greenhouse area in Malta as of the 2007 NSO ‘Census of Greenhouses’ (Table 16.3). The results show that 53.3 % of the greenhouse owners surveyed owned more than one greenhouse. Therefore, when considering multiple greenhouse ownership, the total area of the greenhouses surveyed amounted to approximately 67,498 m², equivalent to 11.3 % of the total greenhouse area on the Maltese Islands as of the 2007 NSO ‘Census of Greenhouses’. This gives an idea of the significantly large areas taken up by greenhouses in Malta and Gozo, further implying that such areas should be considered for solar PV greenhouse installations. Furthermore, it implies that this survey has an interesting coverage of the existing greenhouses. Responses to the questionnaires revealed that there is little awareness amongst greenhouse owners regarding such projects. However, the fact that there are currently two solar greenhouses being built, one in Malta and the other in Gozo, shows that gradually people are starting to realise such the potential of these systems.

From the questionnaires it was noted that 94 % of the greenhouses surveyed had a rounded top rather than a slanted one, whilst the materials used for their construction were mostly metal and polythene. In many countries in Europe, the



Fig. 16.2 Rounded-roof solar greenhouse (*left*) and slanted-roof solar greenhouse (*right*) [18, 19]

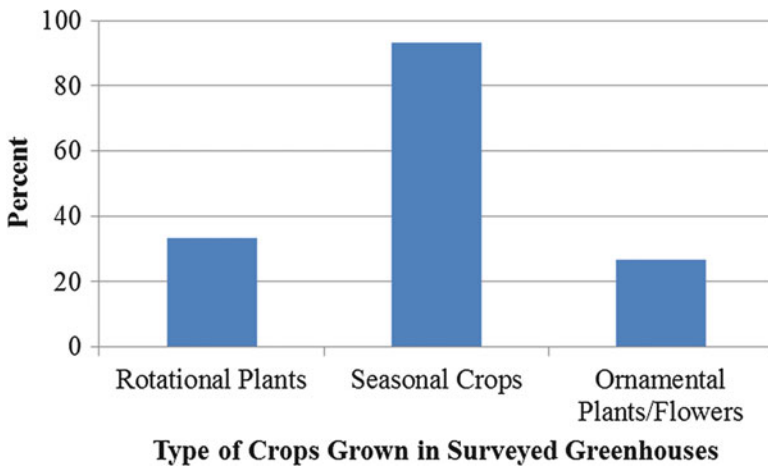


Fig. 16.3 Percentage of greenhouses growing different types of crops

majority of greenhouses have a slanted roof, most of which are constructed using metal and glass [17]. With regard to the installation of solar PV modules on greenhouses, having a rounded roof would not be an issue since solar greenhouse installations have been successful on both types of roofs, as shown in Fig. 16.2. Moreover, any necessary structural reinforcement to a greenhouse's roof would be easily and cheaply achieved.

The questionnaire also showed that 86.7% of greenhouses have a direct connection to the electrical grid, with 54% of them having a three-phase and the rest having a single-phase system, which makes grid-connected PV systems feasible.

It is important to know the type of crops grown in greenhouses so as to choose the right type of PV module to install as well as the mode of installation without causing undue shading, which might reduce crop productivity. The results showed that the most frequently grown crops in greenhouses were rotational, seasonal and ornamental plants. Around 94% of the greenhouses grow seasonal crops, but they also grow other types of crops, as shown in Fig. 16.3. Interestingly enough, almost

half of the growers do not believe that their crops require full sunshine. Studies show that certain types of crops may be severely damaged when exposed to excess solar radiation [20]. This is well known amongst local farmers since during periods of high-intensity solar radiation (mostly in the summer), most of the greenhouses in Malta have to be covered in order to protect the crops. Hence, the installation of solar PV modules is considered to be an advantage in this regard. Taking into account that the quality of light is crucial for plant growth, there is a wide range of crops which tolerate low light intensities, including tomatoes, lettuce, kale, peas, beans, spinach and root vegetables (potatoes, beetroots, carrots, turnips and radishes) [21]. This would also need to be taken into account when considering solar greenhouse installations.

With regard to new solar greenhouses currently being developed, it was clear that the Malta Environment and Planning Authority welcomes such developments as long as the PV modules are carefully integrated into the greenhouse structure, and as long as their appearance does not create an aesthetic distortion of rural areas.

4 Conclusions

This chapter has shown that solar PV modules degrade by approximately 1.2% per year, rather than the widespread assumption of 1% per year. When studying the effect of this degradation on the RE target that should be met by 2020 in Malta, it was established that with the present installed capacity of 54 MWp (end of 2014) and assuming a linear increase in annual installations between 2015 until 2020, to achieve the government's goal of 5% RE share from PV, a cumulative total installed capacity of 201.5 MWp is needed, of which 7.2 MWp will be required only to counterbalance the degradation of the installed solar PV modules. This is equivalent to 47,980 m² of PV module area, which would only require 8% of the total existing area covered by greenhouses in 2007. The total added costs of the 7.2 MWp would amount to €8.6 million to install. This will entail a greater investment in solar PV modules in Malta, which in turn would make up for the efficiency losses of the already installed solar PV modules.

The conducted surveys covered an equivalent of 11.3% of total greenhouse area registered in 2007. It was established that there are a sufficient number of greenhouses in Malta and Gozo which can potentially be equipped with solar PV installations. Also, at least 50% of them have the necessary infrastructure to install PV systems such as accessibility to the electricity grid. Such investments in solar greenhouses can also change how greenhouse owners construct new greenhouses. The results showed that there is a significant lack of knowledge pertaining to solar greenhouses in Malta. Nonetheless, most respondents were very interested in learning more about these projects; however, since this concept is still relatively new in the Maltese Islands, most respondents claimed that they would not consider such an investment. However, the fact that two solar greenhouses are currently being built in Malta and Gozo implies that there is a demand for such projects, and

therefore other greenhouse owners should be given the opportunity to learn more about such investments.

The Maltese Islands depend heavily on electrical power generation fuelled by 97 % oil imports. The fact that Malta's geographical location provides an excellent base for the use of solar PV systems makes it critical to invest further in these technologies. Since Malta is part of the European Union and has RE targets to meet by 2020 and beyond, it is imperative to consider the induced degradation of solar PV modules. This chapter has shown that the correct PV power capacity required to reach 5 % RE share from photovoltaics is 201.5 MWp and not, as reported, 190 MWp [5]. The extra capacity that needs to be installed can be easily accommodated within existing roofs of greenhouses rather than taking up new rural agricultural land.

Acknowledgments The authors would like to acknowledge the support of the technical staff of the Institute for Sustainable Energy, Mr. Emanuel Aquilina and Mr. Malcolm Farrugia, who have helped in setting the experimental tests. Additionally, our thanks go to Ing. Carl Fenech who has shared some of his test results with us and Mr. Mark Debono who has provided a lot of useful information with regards to his new solar greenhouse project. We would also like to thank all the participants in the greenhouse questionnaire, who have contributed by sharing their views and aspirations and the University of Malta for its support.

References

1. Sovacool BK (2009) The importance of comprehensiveness in renewable electricity and energy-efficiency policy. *Energy Policy* 37(4):1529–1541
2. Roe S (2013) Solar efficiency losses over time. <http://sroeco.com/solar/solar-efficiency-losses-over-time>
3. Klessmann C, Held A, Rathmann M, Ragwitz M (2011) Status and perspectives of renewable energy policy and deployment in the European Union—what is needed to reach the 2020 targets? *Energy Policy* 39(12):7637–7657
4. Kotzebue JR, Bressers HTA, Yousif C (2010) Spatial misfits in a multi-level renewable energy policy implementation process on the small island state of Malta. *Energy Policy* 38(10):5967–5976
5. Malta Today (2015) http://www.maltatoday.com.mt/news/national/47712/solar_farms_set_to_cater_for_half_of_maltas_2020_renewable_energy_targets#.VdcN8_IVikp
6. Farrugia R, Fsadni M, Yousif C, Mallia E (2005) The renewable energy potential of the Maltese Islands. *Xjenza* 10:32–42, <http://www.mcs.org.mt/index.php/xjenza/xjenza-archives/49-xjenza-vol-10-2005>
7. Malta Resources Authority (2015) <http://mra.org.mt/consumers/feed-in-tariffs/>
8. Honsberg C, Bowden S (2015) Electroluminescence. <http://www.pveducation.org/pvc/drom/characterisation/electroluminescence>
9. MRA (2015) The uptake of solar systems in the Maltese residential sector (status as of end of 2014). <http://mra.org.mt/wp-content/uploads/2012/07/216/Solar-RES-growth-in-residential-sector-Feb2015.pdf>
10. Yousif C (2010). Photovoltaic grid-connected systems in Malta. <http://staff.um.edu.mt/cisk1/pvsystems.htm>
11. Peter K, Preis P, Díaz-Pérez PE, Theobald J, Enebakk E, Soiland AK (2011) Light induced degradation in multicrystalline solar grade silicon solar cells evaluated using accelerated LID.

In: Proceedings of the 26th European photovoltaic solar energy conference and exhibition, pp 1856–1858

12. Yedidi K, Tatapudi S, Mallineni J, Knisely B, Kutiche J, TamizhMani G (2014) Failure and degradation modes and rates of PV modules in a hot-dry climate: results after 16 years of field exposure. In: 40th IEEE photovoltaic specialist conference (PVSC), Denver, 8–13 June 2014, 5–9 September 2011, Hamburg, pp 3245–3247
13. Saikku L, Rautiainen A, Kauppi PE (2008) The sustainability challenge of meeting carbon dioxide targets in Europe by 2020. *Energy Policy* 36(2):730–742
14. EC (2015). National action plans. <http://ec.europa.eu/energy/en/topics/renewable-energy/national-action-plans>
15. NSO (2007) Census of greenhouses. *Agriculture and Fisheries* (27/2008)
16. NSO (2002) Census of agriculture 2001: Greenhouses. *Agriculture* (99/2002)
17. Bellows B (2008) Solar greenhouse resources. <http://www.agrisk.umn.edu/cache/ar101480.htm>
18. HortiDaily (2015) Greenhouse with integrated solar panels. <http://www.hortidaily.com/photoalbum/PASearch.asp>
19. Promec (2012) Supporti per fotovoltaico promec TRIS. <http://www.promecpachino.it/index.php/struttureT/prodotto/supporti-per-fotovoltaico-promec-tris#>
20. Carpenter DO, Ayrapetyan S (1994) Biological effects of electric and magnetic fields: sources and mechanisms. Academic, San Diego
21. Liu J, Mahoney K, Sikkema P, Swanton C (2009) The importance of light quality in crop–weed competition. *Weed Res* 49(2):217–224

Chapter 17

Revitalization and Refurbishment of Minor Historical Centers in the Mediterranean

Alessandra Battisti

Abstract Minor historical centers are like living organisms that operate at a macro scale (historical center and urban fabric) and at a micro scale. It is possible to propose a methodological framework for transformation and upgrading, in a close relationship between history, culture, and technology, through development processes that are not only a series of measures aimed exclusively at increasing the financial value of land and buildings but that also pursue the broader goals of redevelopment and revitalization of the architectural, energy, social, economic, and cultural contexts of the city they refer to. In order for the process to be more than just real estate development, building restoration, or urban upgrading, not only must existing and potential resources be used to gain more leverage, but the shortcomings of the urban fabric and socioeconomic demands must also be met.

1 Rescue of Historical Heritage

Over the last decade, the redevelopment and renovation of minor historical centers have increasingly become a focus point within Europe in order to fight land take and the decline of cultural heritage. In financial programs and community policies comprising projects to protect cultural heritage, the focus is being increasingly placed on the energy upgrading of historical buildings and specifically of minor neighborhoods and historical centers. These projects represent the distinctive feature of a large number of European cities and play a key role in the revitalization of urban environments aimed at strengthening the sense of community and identity and improving the quality of life, representing a major opportunity to bring together

A. Battisti (✉)
PDTA Planning Design Technology of Architecture Department,
La Sapienza Rome, Rome, Italy
e-mail: alessandra.battisti@uniroma1.it

resources for energy upgrading in minor historical centers and neighborhoods¹ [3]. The projects provide confirmation that it is no longer sufficient to target individual buildings, but a virtuous critical mass of examples needs to be created, extending upgrading to whole neighborhoods and well-established entities such as minor centers and small towns. This involves reorganization of all residential area services from an eco-sustainable viewpoint, considering the historical buildings as a resource to be optimized in order to obtain quality accommodation and spaces with zero land take² [4].

Recent studies carried out by Legambiente and Confcommercio show that 72 % of Italy's more than 8000 municipalities have fewer than 5000 inhabitants, and 1560 are at "risk of extinction" in 2016, as confirmed by the "Riutilizziamo l'Italia" campaign [5]. This campaign highlights how these small towns, generally located in protected settings of great cultural and natural importance, are inhabited by 17.2 % of the national population.

In this context, the urban fabric of minor historical centers is to be looked upon as a living organism that operates at a macro scale (historical center and urban fabric) and at a micro scale (the structure in its process of conservation and refunctionalization). Thus minor historical centers are called upon to change their conformation and configuration, in a close relationship between history, culture, and technology, through development processes that are not merely a series of measures aimed exclusively at increasing the financial value of land and buildings but that pursue the broader goals of redevelopment and revitalization of the architectural, energy, social, economic, and cultural contexts of the city they refer to.

In order for the process to be more than just real estate development, building restoration, or urban upgrading, not only must existing and potential resources be used to gain more leverage, but the shortcomings of the urban fabric and socioeconomic demands must also be met [6].

Indeed, the European Commission singles out building renovation, and specifically upgrading of the existing infrastructure and residential heritage as regards energy, environment, seismic, and hydrogeological profiles and maintenance, as one of the favored areas for increases in investments in the construction sector. It also cites more extensive partnership of various interests within projects to be funded as being indispensable, especially for highly energy-efficient buildings, cultural heritage, cities, minor historical centers, and intelligent communities [7].

Moreover, in light of the possible reductions of energy consumption, abatement of harmful emissions into the atmosphere, and improvement in bioclimatic well-being, which can actually be achieved as part of architectural, energy, and environmental

¹ J Owen Lewis, Sadhbh NíHógáin, Antonio Borghi: "Given the evidence of very significant challenges, for this to be realised, we need to adopt and implement stable, integrated policies and legislation, which will provide certainty to the market and transform the buildings sector, at European, national and municipal levels".

² Bourdic, L. and Salat, S. (2012) 'Building energy models and assessment systems at the district and city scales: a review', in: *Building Research & Information* 40(4), 518–526.

upgrading of minor historical centers, there is a need to study transformation models in relation to the two aspects of problems affecting ancient urban buildings and that can be linked to two macro categories of project models. The first is more strictly linked to the so-called technological area, in other words to everything connected to the conservation of places or structures using innovative and environmentally sustainable rescue procedures and techniques. The second model concerns the transformation processes that attempt to reinterpret local historical and cultural contexts, revitalizing their functionality in order to attract new activities and interests [8].

To start this eco-efficient renovation process, all market operators need to be involved, from state bodies to construction firms and architects. However, a change is required not only in design and construction prospects, but also in working instruments. Changes will be necessary in areas such as the structuring of loans, public contracts, education, and marketing.

Upgrading in these contexts means integrating two types of actions, promoting access and improving the quality of life, in accordance with sustainable redevelopment strategies. This does not just mean straightforward protection and conservation of assets and resources but action based on a more general process of architectural, energy, social, and economic revitalization, revitalization in which the optimization of resources and their organization within the system – favoring criteria of accessibility and usability – may represent the keystone for generating new attractions and, hence, social and economic relaunch.

The actions in question form part of a working framework that singles out five thematic macro areas:

- Protection of territory;
- Relaunch of tourism, promotion of agriculture, and the local food farming industry;
- Design, management, and sustainable governance of infrastructure systems and transport;
- Use of renewable sources of energy and achievement of energy efficiency;
- Refunctionalization, management, and sustainable governance of existing building heritage.

In operational aspects that result – to put it simplistically – in the following strategies:

- Zero land take;
- Zero emissions;
- Zero energy consumption;
- Zero-kilometer agriculture.

Actions aimed at a change in direction that will turn around a regressive process, which means that minor historical centers in Italy and a large part of Europe will be characterized by an incipient abandonment on the one hand and by a difficulty in creating a new territorial role for themselves on the other.

In this type of project, technological input is in line with the principle of minimum intervention on important buildings. Correct use of the most recent

technologies for energy upgrading allows for the provision of noninvasive solutions that can be implemented with little or no significant impact on the general appearance of buildings or contexts, increasing energy efficiency and guaranteeing thermohygrometric, visual, and acoustic and psychophysical well-being. This represents an approach that promotes a low level of energy consumption, technological innovation, and implementation of passive systems in a way that is compatible with what already exists and can be reversed at any time.

1.1 I borghi della salute: Marmilla Pilot Project

The pilot research project presented involves the redevelopment and upgrading of small towns in the Marmilla area of Sardinia and was drawn up by the FO.CU.S research center.³

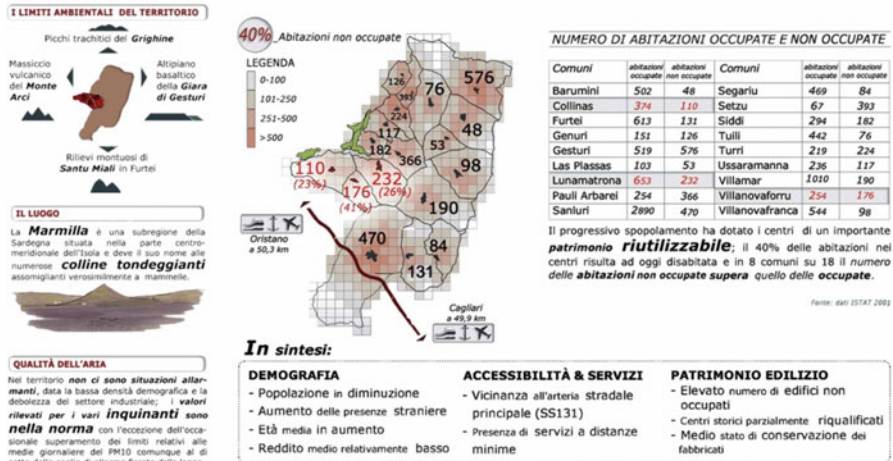
As regards the Marmilla area, Operation *Borghi della salute*⁴ involves three small towns – Lunamatrona, Villanovaforru, and Solinas – for a total of 2500 inhabitants, boasting a wealth of historical, natural, and production features, but experiencing a major decline from a socioeconomic viewpoint. The choice of the three municipalities and their aggregation, to form a network included in the regional project called “Integrated Health Program,” depends on the following factors: services offered, distance from ports and airports, main lines of communication, favorable weather conditions, and rural economy. Buildings have been singled out inside the historical center of each of the three towns that must be acquired by the municipal authorities and renovated and upgraded.

Project activities include:

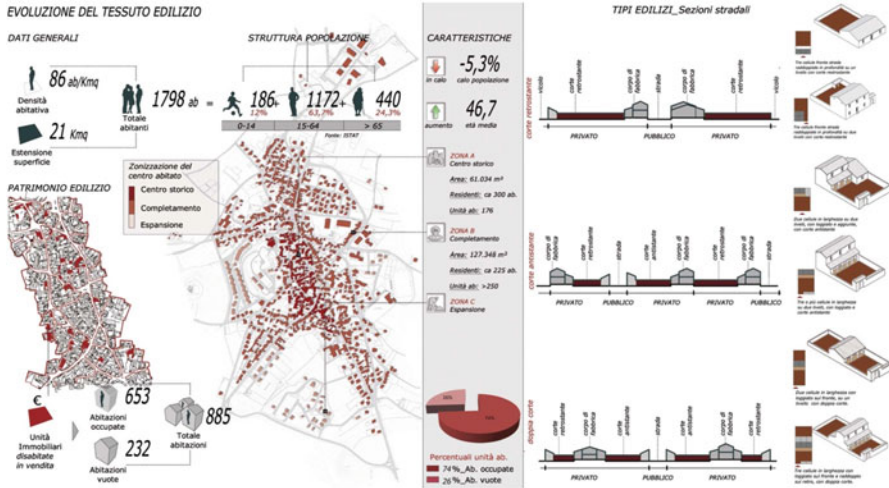
- Renovation of privately owned properties that will be purchased by the municipal authorities, located in three different small towns, to be used as tourism and social-healthcare residential accommodation with the possibility for guests to entertain visiting family members, friends, tourists, etc.; at present, three properties have been singled out, providing a total of 30 beds;
- Creation of shared spaces to be used by guests, which will be fitted out as gyms, a wellness center, therapy areas, restaurants, and small common rooms;
- Functional upgrading of public spaces and areas for healthcare accommodation.

³The “*Borghi della salute*” research project fits into this logical framework and has been conducted for some years by La Sapienza’s FO.CU.S. research center. The author of this chapter is one of the leading professors in the capacity of expert in energy efficiency and environmental and bioclimatic design.

⁴Collinas, Lunamatrona, and Villanovaforru are the three municipalities in the Marmilla area included in the 2007–2013 National Plan for the South’s list as “*Borghi della Salute*.” These are places where the environment is a therapeutic instrument, in the sense of feeling good about oneself, and not just a means of providing healthcare services. Seven million euros are available for psychophysical well-being achieved through healthy lifestyles in small towns not overrun with concrete, not stressed by deafening automobile traffic, and not polluted by industrial fumes.



Research has focused on the difficulties in optimizing the various performance targets required by the buildings subject to upgrading for bringing together said targets. The buildings will go from being traditional shared accommodations to buildings for use by citizens for healthcare, hospitality, educational, and therapeutic purposes. On the one hand, the environmental and technological upgrading project has focused on cutting primary energy consumption and implementing the use of renewable sources and increasing environmental quality parameters, while it has also concentrated on optimizing performance requirements linked to functions relocated within the small towns' changing urban fabric, comprising new expectations, including a predisposition toward the necessary capacity to be flexible and adaptable to changes in use. The research project attempted to obtain – or bring back to light and optimize, as is often the case for historical buildings – a so-called global quality of space. The latter, combined with users' thermohygrometric and psychoperceptive well-being, strives to harmonize buildings and architectural spaces with macro- and microclimatic characteristics, social and behavioral traditions, and environmental and biophysical factors of the specific local context. This is achieved through the correct use of energy and resources, recycling or reusing materials and generally reducing the release of harmful substances into the local and global ecosystem during their complete lifecycle, and by pursuing containment of energy consumption, the production of energy from renewable sources, and correct ecological governance of future management and maintenance processes.



2 Methodological Approach

From a methodological viewpoint, the research comprised a first phase containing the following elements:

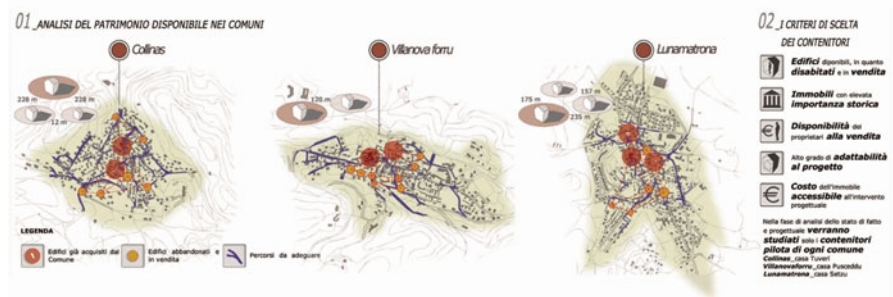
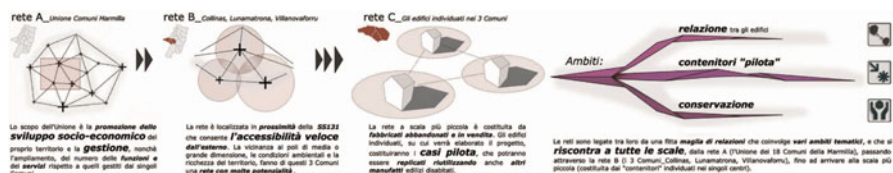
- Bioclimatic analyses with fluid dynamic, thermophysical, and lighting measurements and simulations; energy audit of buildings and measurement of microclimatic characteristics of external spaces within towns; survey and critical analysis of buildings’ original bioclimatic characteristics; checking of compatibility between functions depending on their position and orientation inside buildings;
- Technological analyses with studies of systems and parts characterizing the existing architectural structures to be transformed;
- Plant engineering analyses with energy measurements and assessment of level of building–plant interface.

In light of the bioclimatic and environmental analyses, the second phase involved the definition of a framework of rules for optimizing passive bioclimatic aspects, as well as the identification of renewable energy sources to be used in the small towns based on their intrinsic characteristics.

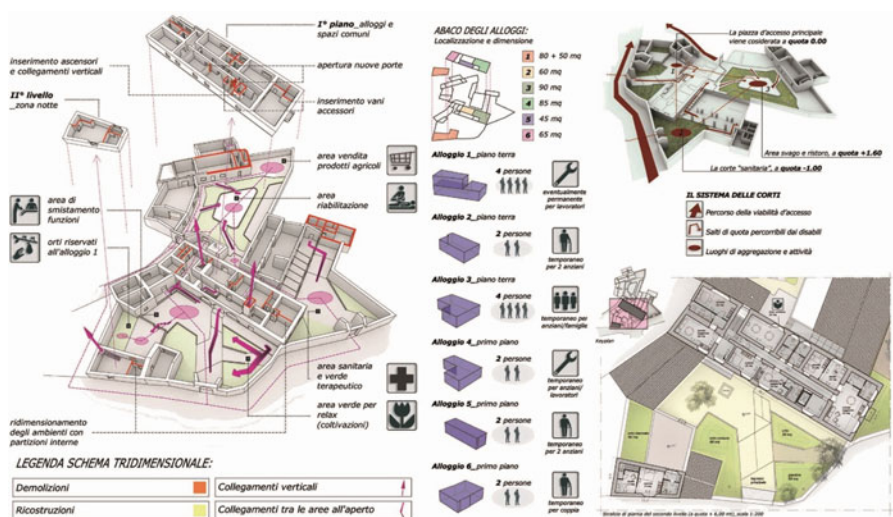
Strategic positioning of technological solutions for energy production from renewable sources was also decided on, together with devices to mitigate microclimatic effects and reduce energy consumption.

Lastly, the strategies singled out were systematized within a synergic framework in order to proceed with the third research phase following careful synthesis. This phase concerns proposed actions focusing on the question of redefining environmental energy–efficiency design choices through a process of choosing from among possible alternatives, also staggered over time. The aim is refunctionalization of the small towns for their new role of offering accommodations and well-being and

eliminating energy dispersion, cutting consumption, encouraging widespread and integrated use of renewable sources, improving overall level of eco-compatibility and achieving bioclimatic results as regards performance, and demonstrating the ability to ensure optimal thermohygrometric and psychophysical conditions inside buildings.



The vision is a multidisciplinary one taking into account various aspects linked to the specific performance requirements of a refunctionalized small town, construction techniques and procedures, management problems resulting from the specific characteristics of each individual assets, and economic and financial resources to be invested – hence the need for various alternative or staggered solutions – modeling them on resources that are actually available or can be funded.

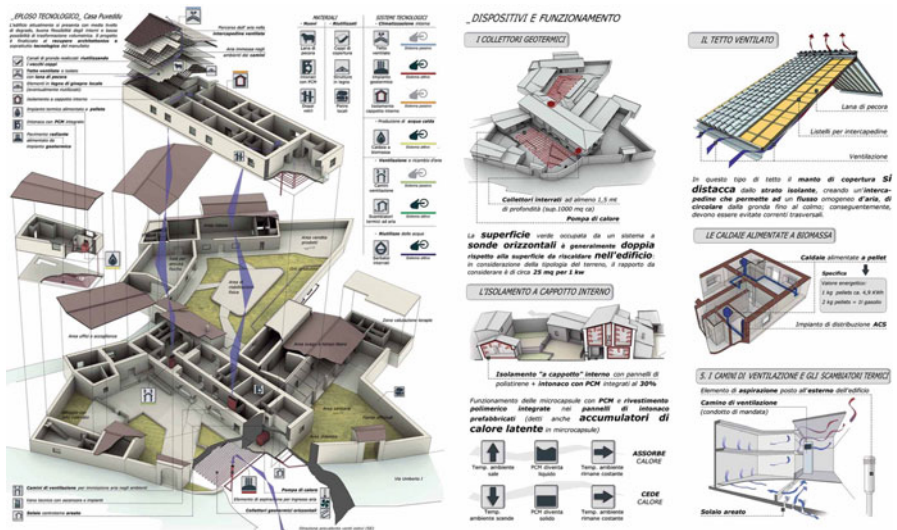


3 Technological Solutions

The project tackles the reticence and doubts often present among designers, construction firms, public administrations, and users when dealing with energy upgrading and refunctionalization of historical buildings.

The three basic principles of this technologically innovative research project model, in full compliance with the construction characteristics of historical buildings, aimed at major regeneration, architectural renovation, and energy efficiency, are as follows:

- The principle of minimum intervention, applied at all scales, from the single brick to works involving significant changes; all works are reduced to the minimum necessary in order to preserve the identity of the historical fabric;
- The principle of compatibility, according to which all changes, from the smallest to the largest, must be made using materials and techniques that are compatible with the historical fabric. Modern materials tend to be harder, less flexible, and less permeable than traditional materials and can significantly speed up decline and dereliction if combined directly with the historical fabric. Generally speaking, for all new works performed in the direct vicinity of the historical fabric, the tendency is to choose softer, more permeable technologies to ensure better coexistence with traditional technologies;
- The principle of reversibility, according to which transformation processes can prove damaging over time; so it is recommended they be completely reversible where possible. The adoption of this principle allows the historical fabric to be returned to its original state without any damage following removal of the transformation. This principle can be applied transversally to all levels of action, from individual localized actions on a building to large-scale operations.



Specifically, three main technological solutions have been singled out while aiming to comply with the aforementioned principles during performance of the *Borghi della salute* project:

1. Solutions for optimizing thermal insulation of historical buildings while avoiding thickening of the buildings' external envelope for aesthetic and historical reasons and at the same maintaining the benefit of thermal mass. Indeed, Marmilla is characterized by thick stone walls (40–60 cm) left bare on the outside or plastered with lime mortar.

The reduction of energy consumption for heating purposes largely depends on the envelope's performance as well as on the inhabitants' behavior and activities. The insulating layer can be positioned as follows:

From the outside in order to exploit the walls' thermal inertia (this option was preferred in the event of permanent residence, and aerogel insulation panels of limited thickness were used to reduce thickening of the walls) or from the inside. In the event of its being strictly necessary to maintain the external appearance, the wall mass is thermally separated from the internal environment. (This solution entails reducing the internal space by at least 8–10 cm.) Vacuum insulation panels (VIPs) were used to achieve limited thicknesses;

2. Solutions able to considerably mitigate the negative aspects of excessive solar radiation in summertime, in terms of overheating and excessive albedo, for passive cooling, aspects of specific importance on roofs and on south-west and west-facing external vertical walls (through the implementation of ventilated roofs and use of cool materials and pigments);
3. Solutions for the choice of heating and hot water production plants, devised by assessing the available renewable resources, existing networks, and community choices. The decision made was for noninvasive devices using renewable energy sources, compatible with the setting and whether or not they could be removed if necessary (geothermal plants).

4 Conclusions

The redevelopment and upgrading of the historical heritage of minor centers and small towns in the Mediterranean region offers opportunities for the design of new residences, tourist facilities, healthcare facilities, hostels, and energy facilities while renovating existing buildings, generating a process able to create important economic and employment activities within the territory, all with zero land take.

A heritage, in most cases, is characterized by great environmental, architectural, and landscape value and its renovation primarily requires knowledge and awareness of its identity. Given the opportunities and significant challenges outlined earlier, we need to adopt and implement stable integrated policies and legislation to carry out these projects, which will allow this process to become a flywheel for the construction and hospitality. In this sense, the "Covenant of Mayors" represents a

significant step forward with the drafting of plans of action for sustainable energy (PAES) and the introduction of urban-level policies aimed at reducing CO₂ emissions, increasing the energy efficiency of existing heritage buildings, and implementing renewable energy production plants. This is an operation that will provide for multilevel governance aimed at ensuring vertical subsidiarity between the various levels of government and horizontal cooperation between local actors from the private and public sectors and citizens.

References

1. European Union (2012) Cultural heritage research: survey and outcomes of projects within the environment theme: from 5th to 7th Framework programme. European Commission, Directorate-General for Research and Innovation. Luxembourg: EUR-OP
2. European Commission (2006) Thematic strategy on the urban environment. Office for Official Publications of the European Communities, Bruxelles
3. Lewis JO, NíHógáin S, Borghi A (2013) Cities of tomorrow—action today. URBACT II Capitalisation. Building energy efficiency in European cities. URBACT, Saint-Denis
4. Bourdic L, Salat S (2012) Building energy models and assessment systems at the district and city scales: a review. *Build Res Inform* 40(4):518–526
5. Geremia F, Zampilli M (2013) Il patrimonio culturale dismesso: i centri storici e gli edifici di valore storico architettonico. In: Filpa A, Lenzi S (a cura di) *Riutilizziamo l'Italia*. Report 2013. Dal censimento del dismesso scaturisce un patrimonio di idee per il futuro del Belpaese. WWF Italia, Roma, pp 137–150
6. Carta M (1999) *L'Armatura culturale del territorio: il patrimonio culturale come matrice di identità strumento di sviluppo*. FrancoAngeli, Milano
7. Boermans T, Bettgenhäuser K, Offermann M, Schimschar S (2012) *Renovation tracks for Europe up to 2050*. ECOFYS Germany for Eurima—European insulation manufacturers association
8. Ministry of Interior, Hungary & VÁTI Hungarian Nonprofit Ltd. for Regional Development and Town Planning (2011) *Climate-friendly cities—a handbook on the tasks and possibilities of European cities in relation to climate change*, Ministry of Interior, Hungary & VÁTI, Budapest

Chapter 18

Building Envelope–Systems Integrated Models: Topic 4

Fabio Conato

Abstract The need to design building envelopes as machines able to offer flexible behaviors due to the variability of the boundary conditions has led to study and develop a methodology for evaluating the correct relationship between casings' energy performances and production systems connected to technical implants. The result was the definition of an application model, able to indicate the most appropriate mix of renewable energies in synergy with the casing. The objective is to maximize the use of renewable energies in compliance with general and functional needs related to the balance of the system.

The study started from the identification and classification of types and families of building envelope, defining materials and operating principles. The simulations used in the assessment models were performed by integrating empirical data with predictive modeling.

The matrix produced was implemented starting from the scenario of the typical needs of each building typology and of every function of it, making possible to evaluate in a forecasting way the variation of primary energy use depending on the performances of each solutions of envelopes.

At the end of this consideration, the model produced was applied to two pilot projects, that constitute the most meaningful product of this research.

Keywords Building envelope • Renewable energies • Technological systems

1 Introduction

The Mediterranean context, and especially that of mainland Italy, is particularly complex from a climate point of view owing to extreme thermal fluctuations and other multiple factors.

All these so-called influential factors determine the constraints and conditions the building envelope needs to respond to in terms of performance.

F. Conato (✉)
Department of Architecture, University of Ferrara, Ferrara, Italy
e-mail: fabio.conato@unife.it

The influential factors are classified as fixed and variable, in terms of their degree of variability over time and in the specific context. A further division can be made by distinguishing between internal and external, depending on the spaces they refer to.

Some examples of *external fixed factors* are the external climatic area of a site, the morphology of the site and the relationship with the surrounding buildings and the orientation of the building in the lot. Some examples of *internal fixed factors* are the intrinsic design factors related to the building project, such as the building type, its intended use and its aspect ratio. The *variable external factors* are defined as the changing seasons and the daily irradiation conditions, the weather variations the general microclimate context the morphology of the site and the relationship with the surrounding buildings, while *internal variable factors* are the internal distribution system and activities inside the compartments.

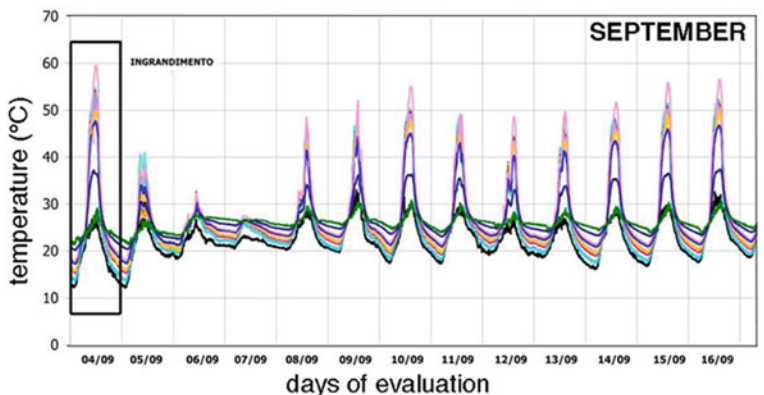
In this context, it is clear that the design of linear behavior building envelope systems presents limits that are sometimes insurmountable; despite the fact that technological research has developed materials and components with increasingly high static performance, the variability of the context in which we work often creates the need to make the same element assume opposing behaviors as a response to the fluctuations of the environmental conditions.

2 Research Completed by the Department of Architecture of the University of Ferrara on the Dynamic Behavior of a Double Skin Building – Envelope

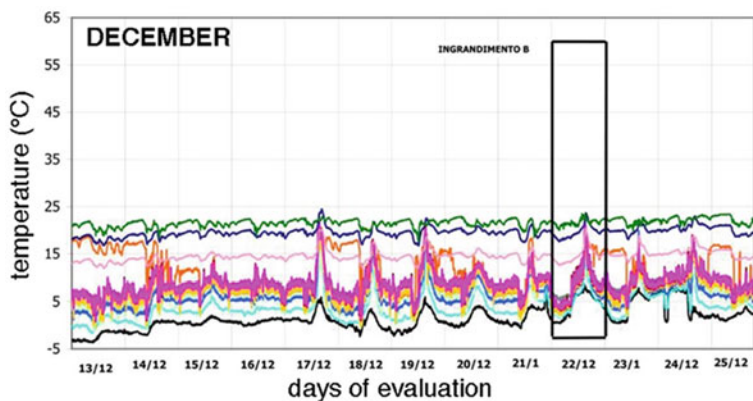
Research conducted by us within the Ferrara Department of Architecture, as early as the 2000s, has allowed us to test the application and operation of double layer building envelope systems, glass–glass, in a residential building in the Italian context (Imola, BO).

The study of these systems in operation – already widely used in the Nordic countries but still not widespread in the Italian context, although they are potentially more functional to its complexity – has allowed the understanding of their dynamic behavior. The experimental data obtained confirmed that, thanks to the triggering of physical phenomena – such as the greenhouse effect, the selective reflection and the air pressure control – generated by the combination of the two layers and maximized from the use of glass, it is possible to manage and monitor the effects of temperature peaks arising from daily and seasonal variability and the different climatic conditions between inside and outside spaces. During the winter season, for example, it is possible to accumulate heat inside the interspace, taking advantage of the so-called “tampon effect” arising from this buffer to create an intermediate weather condition between the inside and outside and therefore to obtain a reduction in energy needs; likewise, during the summer season it is possible to exploit the ventilation in the interspace to extract the excess heat,

bringing the temperature of the contained air close to the external conditions, thereby reducing the impact of the greenhouse effect. Finally, in the intermediate seasons, the air of the interspace can be managed in a selective manner inside the confined environments in order to obtain from it a positive contribution to the creation of the ideal microclimate.



- 1 - ARIA ESTERNA
- 2 - VETRO FACCIATA ESTERNA LATO ESTERNO
- 3 - VETRO FACCIATA ESTERNA LATO INTERCAPEDINE
- 4 - SUPPORTO TERMOCOPPIE INTERCAPEDINE
- 5 - SUPPORTO TERMOCOPPIE INTERCAPEDINE
- 6 - SUPPORTO TERMOCOPPIE INTERCAPEDINE
- 7 - SUPPORTO TERMOCOPPIE INTERCAPEDINE
- 8 - SUPPORTO TERMOCOPPIE INTERCAPEDINE
- 9 - SUPPORTO TERMOCOPPIE INTERCAPEDINE
- 10 - SUPPORTO TERMOCOPPIE INTERCAPEDINE
- 11 - SUPPORTO TERMOCOPPIE INTERCAPEDINE
- 12 - SUPPORTO TERMOCOPPIE INTERCAPEDINE
- 13 - VETRO FACCIATA INTERNA LATO INTERCAPEDINE
- 14 - INFISSO FACCIATA INTERNA LATO INTERCAPEDINE
- 15 - VETRO FACCIATA INTERNA - LATO VANO INTERNO
- 16 - VANO INTERNO



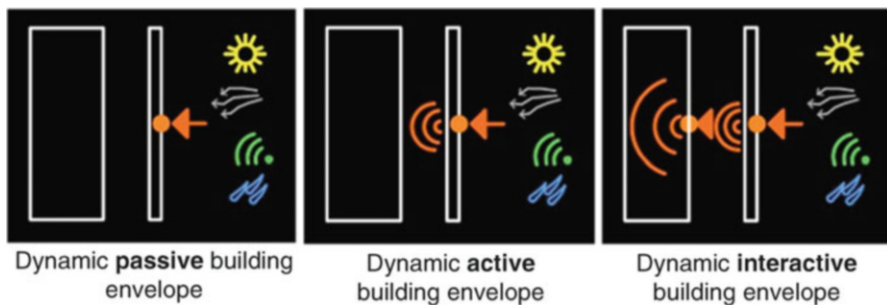
- 1 - ARIA ESTERNA
- 2 - VETRO FACCIATA ESTERNA - LATO ESTERNO
- 3 - SUPPORTO TERMOCOPPIE "I" ESTERNO
- 4 - SUPPORTO TERMOCOPPIE "I" CENTRO
- 5 - SUPPORTO TERMOCOPPIE "I" INTERNO
- 6 - VETRO FACCIATA ESTERNA - LATO INTERCAPEDINE
- 7 - SUPPORTO TERMOCOPPIE "H" ESTERNO
- 8 - SUPPORTO TERMOCOPPIE "H" CENTRO
- 9 - SUPPORTO TERMOCOPPIE "H" INTERNO
- 10 - VETRO FACCIATA INTERNA - LATO INTERCAPEDINE
- 11 - SUPPORTO TERMOCOPPIE "G" ESTERNO
- 12 - SUPPORTO TERMOCOPPIE "G" CENTRO
- 13 - SUPPORTO TERMOCOPPIE "G" INTERNO
- 14 - INFISSO FACCIATA INTERNA - LATO VANO
- 15 - VETRO FACCIATA INTERNA - LATO INTERNO
- 16 - VANO INTERNO

3 Extension and Adaptation of the Concept of Dynamic Behavior Building Envelope

The use of building envelope systems with a double glass–glass layer is a borderline case since this solution is difficult to apply in residential projects within the Mediterranean context. Therefore, in it is not possible to obtain similar performance answers using single building envelope solutions, but it is necessary to define more complex systems that can respond to the dynamic and changing nature of environmental conditions.

Thus, it was determined that in complex climatic environments like the Italian one, it is not feasible to assign the responsibility of managing the fluctuations of the environmental conditions to a single technological resource. It is necessary to refer to a combination of outputs from different solutions. Then the building envelope needs to be designed like a true machine, where the output of each individual element makes a positive contribution to improving the global performance of the system.

The building envelope must therefore be configured as a dynamic behavior system – able to address all the fixed and variable factors that influence the design – on which to the basic skin (made of one or more layers with appropriate static output to the conditions) are added elements of the second skin one by one (e.g., ventilated façades or fixed and mobile shielding systems), which then can interact with the base layer, passively, actively, or interactively, to meet the changing conditions of the environment. These elements can be evolved technological systems (like adjustable shading, nets, or fabrics) or common elements, an integral part of the distribution and technological system of the building (such as projections, balconies, window offsets or boxes).



Further research was completed on the development of empirical evaluation methodologies of the overall effects of different solutions. The outcome is the definition of evaluation grids that allocates a synthetic score to each solution. Then it was possible to obtain quantitative and qualitative estimates of the contribution of each technological solution to the global performance of the building envelope.

	North	South	East	West
<i>Opaque components</i>				
Heavy basic skin	2.5	3	2	3
Light basic skin	3	1	2	1
<i>Correctives</i>				
External layer with low thermal inertia	+0.50	+0.25	–	–
External layer with high thermal inertia	–	–	+0.50	+0.25
<i>Addition of elements of second skin</i>				
Addition of opaque ventilated façade	+0.50	+2	+1	+2
Addition of transparent ventilated façade	+0.50	+2.50	+1	+2.50
<i>Transparent components</i>				
Orientation	1.40	1.90	1.80	1.80
<i>Correctives</i>				
Oversizing of transparent openings (living room) – surface > 1/6	–0.80	+0.80	+0.50	–0.50
<i>Addition of elements of second skin</i>				
Summer shading corrective	–	+1	+0.50	+0.80
Winter shading corrective	–	–1	–0.20	–0.50
Presence of solution for energetic recovery (living room)	–	+0.80	+0.30	+0.50
Synthetic final score = $\frac{\sum_{\text{closure}} (\text{score} + \text{corrective})}{\text{number of closures}}$				

Note that such an approach based on a comparative assessment of the multiple performance effects involved brings together the effects of simple elements with those of complex elements in order to get as close as possible to situations of comfort in indoor spaces characterized by stationary conditions, with significant reduction of thermal peaks conditions.

The presence of a second layer of passive elements, for example, if correctly positioned in relation to openings below, can provide a significant contribution to the control of overheating, effectively shielding the building against incoming solar radiation during the summer season while at the same time allowing radiation through during the winter season in order to obtain a significant heat gain from direct irradiation of glass surfaces.

The experimental data in our possession in fact reveal that the gain obtained by irradiation of each square meter of the glass surface properly exposed represents an average increase in daytime during winter of 1 °C/20 m³ air. By increasing the portion of the glass surfaces in the living areas by 50 %, an average increase of around 0.7 °C can be obtained instantly, with peaks of up to 3°.

Indirect heat gains can be obtained through complex active systems, (such as ventilated facades, seasonal greenhouses or true double layers) and it is possible to decrease the thermal delta between inside and outside spaces with average temperature increases during the day in winter of around 2 °C/m³ air, with peaks that reach

as high as $5\text{--}6^\circ/\text{m}^3$. This results in a lower dispersion of the building envelope expressed in terms of *equivalent transmittance*, a parameter that expresses the instant variable value of transmittance resulting from the contribution of the average amount of sunshine on the façade throughout the day and from the mass and the heat storage capacity of the materials, placed in the background with respect to the glass surface, that make up the base layer.

If the material constituting the base layer has a good thermal capacity, then the rise in temperature of these layers will in fact result in a significant reduction of the heat flow between the inside and the outside. The increased heaviness of the inner layers results in an increase in the time during which such an effect is prolonged (over 3 h more than in light materials) with a significant increase of the average performance with respect to the latter by 20 %.

This also depends on the type of ventilated façade selected since its dynamic effect will vary depending on the coating material. Obviously this effect is maximized with glass, in which the energy captured from the glass surface for the greenhouse effect is total. In opaque façades, the contribution made by sunshine is exclusively a function of the thermal conductivity of the coating material, of the orientation to which a portion of the façade is exposed and of its ability to radiate heat toward the inside by reducing the thermal delta with the outside.

4 Identification of Building Envelope – Systems Integrated Models

Based on the foregoing premises, research activity was carried out within the Regional Programme for Industrial Research, Innovation and Technology Transfer (PRRIITT) from 2010, in collaboration with “Laboratorio Larco” (*Rete Alta Tecnologia Regione Emilia Romagna*) and several companies. The focus was on the definition of an integration model between the building envelope and the systems of residential buildings. The first phase of this research was aimed at defining costs, reduced consumption and energy-savings goals and determining the balance between building envelope performance and the use of renewable energy sources to meet such requirements.

There are some borderline context cases in which the trend is to maximize the use of renewable energy sources, neglecting the level of performance of the building envelope. This is the case of the Canadian urban residential sector, consisting largely of high-rise buildings in which mostly renewable energy (hydro-power) is used since it is available at very low cost in the Canadian territory. Attention is paid to the application of water and air control technology through the building envelope, while aspects related to the reduction of energy requirements are neglected. Another extreme is the design of the building envelope focusing on minimizing the primary energy consumption and then obtain the minimum residual

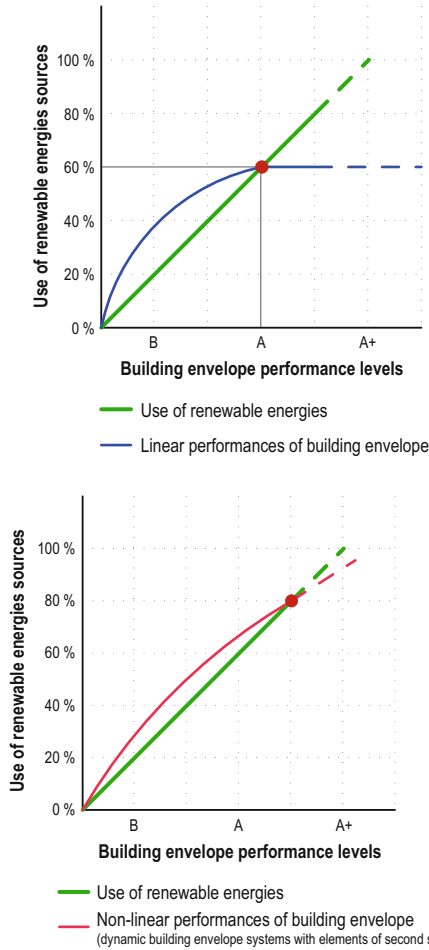
usage from fossil energy sources. This is the case of the so-called Passive House, in which the detailed and careful planning and design of the casing systems focus on maximizing the positive contributions of the environmental conditions and minimizing thermal dispersion, thereby making it possible to resort to almost negligible external energy sourcing for air conditioning and heating, making less relevant the adoption of nonrenewable energy sources for the containment of management and deployment costs.

However, in a climatic environment like that in Italy – with complex and articulated residential complexes - that have intrinsic challenges that don't allow the implementation of the approaches described earlier – it is critical to find the balance between the technological aspects of the building envelope and energy systems. This balance seeks to reduce the primary energy requirements and then make it compatible with the use of renewable energy sources through the correct design of building envelope systems while maintaining a positive economic outlook.

Once the usage of renewable energy was defined in relation to the effects on the energy systems that use a variety of renewable energy sources, the second phase of the research started. This was related to three scenarios of building envelope systems. The goal was to understand the threshold of convenience for the integration of technological and performance components linked to the casing with the internal systems.

Three types of building envelope were defined (*A – Energy Class B building, annual consumption under 40 kWh; B – Energy Class A building, annual consumption under 20 kWh, and C – Energy Class A+ building, annual consumption under 15 kWh*) and cross-referenced with the different facility scenarios available.

First, it was determined that in this specific context, the percentage of renewable energy supply should be between 60 and 70% of the total energy needs. Second, in those cases where the facility systems obtain more than 60% of their energy from renewable energy sources, the reduction in fossil fuels is not proportional to the level of linear response of the building envelope. The contribution of the latter, over the identified performance threshold, is significant only if it is designed correctly to interact with external environmental conditions, managing the effects of thermal peaks with the application of a second layer according to the scope. The application of a significant component of renewable energy installations, in fact, requires the most stable operating conditions to avoid inefficiencies or having to cope with peak conditions with the renewable component alone.



5 Planning Stage: Application of Models to Case Studies

The third phase was to support the technological and architectural design of two pilot projects, located in the Bologna province – mainly residential – of comparable size but with very different structural and functional characteristics. It is a mainly residential block within the new Bertalia-Lazzaretto implementation plan, and a complex situated in the municipality of Castel Maggiore (Bologna) consists of a 22-floor residential tower, a square, a shopping center and offices. After analyzing these interventions, the ideal percentages of renewable energy installations were determined and then applied to the corresponding building envelope performance characteristics, following the balance described earlier.

The selection of energy systems was made based on their compatibility – from both functional and architectural points of view – with the typological and climatic aspects of the context in which we operate. Therefore, a mix was selected combining geothermal energy, as the renewable energy source, and cogeneration, as a nonrenewable energy source, which provides functional and economic benefits.



Solar energy was excluded because it does not meet the functional requirements owing to the variability on the climatic context in which we operate. With regard to nonrenewable energy, a cogeneration plant system was selected because it is ideal for integration with geothermal systems since it generates electricity for power, allows both summer and winter regimes, and enjoys tax reduction benefits in the Italian legal framework, related to the tax reduction of methane gas.

In the two case studies, the facilities consist of geothermal probes connected to heat pumps and cogenerators. The percentages of use of renewable and nonrenewable energy are the same for both projects – 60 and 40 %, respectively.



In the Castel Maggiore tower, the system provides for a continuous operation owing to the expected high-volume consumption intended for commercial use. The cogeneration system, which has an absorption system and is powered by two 100 kW turbines, provides an on-call heating or cooling operation mainly associated with the use of hot water for the residential units and the summer and winter cooling of the commercial areas. In the Lazzaretto project, the cogeneration system, powered by two 100 kW turbines, operates intermittently. The heat is directed toward accumulators.

Therefore, the technological characteristics of both buildings were defined in order to achieve the expected performance effects through the design of the base layers and the elements of the second layer. The effects of the building envelope solutions were predicted using synthetic points. This made it possible to further refine the building envelope models in order to obtain the most effective stationary conditions inside the spaces.

In the tower of Castel Maggiore (Bologna), the defined building envelope model is made of two layers (opaque basecoat and second transparent layer) separated by a variable interspace. At the Lazzaretto project, it was not possible to adopt a single type of building envelope, but the sum of different contributions from elements of the second layer was resorted to. These were evaluated in relation to the specific needs. The building envelope model defined here therefore presents a second opaque layer with a summation of point and widespread features on the second layer.

Once the building envelope models were defined, the consumption of renewable energy was estimated in relation to each project as well as to the environmental impact of such integrated solutions, putting the integrated models thus obtained compared to traditional scenarios in compliance with local regulations.

6 Implementation Phase: The Yard

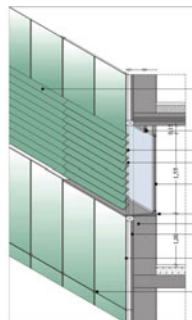
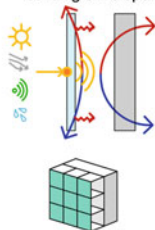
The implementation phase of the two projects included several verification and refining activities of the developed model, aimed on the one hand at verifying the effective behavior of the facility systems – through the selection of the most suitable and reliable components and equipment and soil testing to assess the exact efficiency of geothermal systems. On the other hand, it included the design of the building envelope system to achieve the performance expectations. In both case studies, the technological solutions adopted to maximize the positive effect of their implementation were studied in detail.

At the Castel Maggiore tower, the closure consists of a building envelope with a second active layer (transparent on opaque) and punctual solutions of interactive individual elements of the building envelope. The base layer (made of aerated concrete and masonry sealer coat) is applied along all the façades of the tower, meeting thermal and environmental standards required by law. The second layer – in active operation – is made of glass, with typology to individual elements (consisting of a curtain wall with structural fastening, with different surface finishings according to the orientation and the functional requirements of the individual rooms that overlook it).

The particular type of façade with ducted operation was chosen to inhibit the excessive chimney effect that would have occurred owing to the height of the building and that would have cancelled the positive contribution owing to radiation and the overheating of the air in the interspace. By using glass as a finishing material, this effect was increased, maximizing heat gain in winter and translating the incident solar energy into a significant reduction of the transmittance equivalent.

To control the incident solar radiation, at the openings that face outward, punctual interactive solutions were adopted (glass blades) that offer a different behavior in different seasons. During the winter season, the blades enable the management of sunshine directly on the base layer, with a consequent thermal gain for the greenhouse effect; in summer, these elements can control the entering luminous flow, keeping the blades upright, the frequency of incident infrared radiation on the glass surface is damped, becoming ultraviolet light, and the incoming heat then dissipates within the interspace between the two layers, allowing only light within the confined environment. Finally, the living areas are equipped with significant openings, using passive elements, generated by a correct dimensioning of the terrace–parapet system against the transparent base layer.

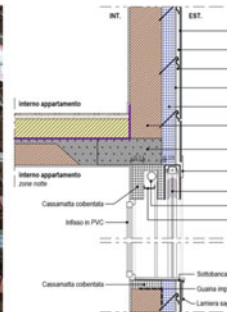
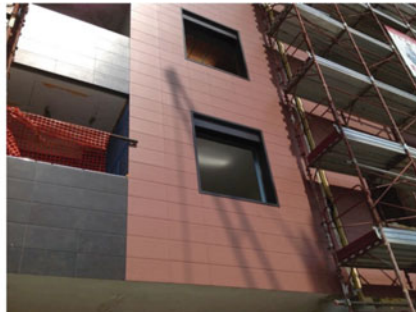
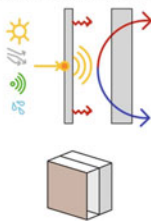
Castel Maggiore tower: building envelope with second active skin and punctual solutions of interactive building envelope



In the Lazzaretto project, instead, the closures have a second layer (opaque on opaque) with punctual solutions with passive second-layer individual discrete elements (opaque on transparent). The ventilated façade here is made with ceramic material (porcelain gres) chosen by virtue of its thinness associated with excellent thermal conductivity and therefore able to contribute fairly quickly to warming the interspace. The underlying masonry, built with blocks of very thick porous brick, is capable of prolonging this effect up to a maximum of 6 h from its onset. In this case, a difference in pressure is created inside the interspace, which is lower than inside the tower – the difference is due to the height of the building. To make the heat gain significant, it was necessary to adopt systems for mechanical ventilation at variable flow to make the most use of the positive effect created within the interspace.

The problems arising from direct sunlight during the summer season and the consequent overheating of the interior –corresponding to building envelope solutions where the base layer is made from simple transparent fixtures – are resolved by punctual elements on the second layer belonging to the distribution and technology systems of the building (such as jetties and terraces) and designed according to the orientation of the building, in order to impose an effective glare control and the resulting light flux entering the compartments.

Lazzaretto project: building envelope with second active skin and punctual solutions of second passive skin with single elements



7 Monitoring Phase

The implementation of the integrated models thus obtained presented some problems, as expected, mostly linked to the need to adjust such articulated and complex systems. To determine the most suitable regulation criteria for managing the computerized control of these systems, an analysis was completed on the first completed project (Isolato 2A – Bertalia-Lazzaretto). It was a manual compilation of changes linked to the adopted system typologies, based on 45 regulation points.

Next, thanks to the compilation of the operative regulations, it was possible to understand their relationship with the functionality of the building envelope system. This helped to refine the defined model further by incorporating corrections on the

functionality and the refining of the second-layer elements (for example, modifying the façade ventilation modalities or inserting adjustable sunshades).

Thanks to this activity, it was possible to determine 12 common scenarios that summarize the operation model of the facility systems (linked to the stationary and peak conditions of summer and winter, day and night, and the stationary condition of the intermediate seasons) that allow the balance in relation to the performance of the casing, the instant contribution of the different energy sources (both renewable and non) keeping the annual sourcing from renewable sources close to the forecasted estimate (60–70 %) and making the system able to adapt to the fluctuations of the detected conditions.

Finally, by analyzing data on the consumption of gas and electricity – in order to calculate the management costs of the buildings and ensure that they correspond to the initial objectives – it was confirmed that, on the one hand, the actual consumption data are in line with those of maximum forecasted projections and, on the other, the other system parts are basically oversized; the forecasted models were conservative, defining performances of the systems obtained between building envelope and systems higher than foreseen in the initial phase. This has therefore allowed a further refinement of the model thus defined, increasing the storage capacity of the heat produced by the systems while limiting their period of operation compared to the expected threshold, thereby reducing the stress on the ground caused by geothermal probes and limiting the operation of the components that exploit nonrenewable energies to daylight hours only. The redefined model has therefore allowed the development of an electronic and information system based on the scenarios described.

Types of scenarios (operation of systems)	Percentage of use of renewable energies in defined building envelope–systems integrated model	Appraised percentage of use of renewable energy in linear building envelope model (without elements of second skin)
1. Summer, stationary conditions – day	80	50
2. Summer, stationary conditions – night	55	30
3. Summer, peak conditions – day	50	30
4. Summer, peak conditions – night	30	5
5. Winter, stationary conditions – day	60	40
6. Winter, stationary conditions – night	50	30
7. Winter, peak conditions – day	30	5
8. Winter, peak conditions – night	20	0
9. Spring, stationary conditions – day	100	60
10. Spring, stationary conditions – night	70	40
11. Autumn, stationary conditions – day	100	60

Annual consumption: Bertalia-Lazzaretto block 2A – Bologna (Jan 2014–Jan 2015)

HSW	Heating	Cooling
2756,96 mc	238 365,30 kWh	35 820,80 kWh

(continued)

Annual consumption: Bertalia-Lazzaretto block 2A – Bologna (Jan 2014–Jan 2015)		
HSW	Heating	Cooling
€30 050,86	€18 706,91	€12 895,49
Approx. 2.40 €/sm	Approx. 1.50 €/sm	Approx. 1.10 €/sm
Total 5 € /sm as predicted		

Chapter 19

Lessons for Future Cities and Architecture: Ecology, Culture, Sustainability

Derya Oktay

Abstract In the era of globalisation, in which serious environmental problems are threatening cities and their inhabitants, as cultural integrity is constantly under attack and many cities lack socially inclusive and responsive environments, there is an urgent need for a radical shift towards a holistic strategy for sustainable urbanism combining ecological sustainability and sociocultural sustainability. This calls for sensitivity to traditional urbanism and impact of global ideas, practices and technologies on local social and cultural practices, both on the city scale and architectural scale. In line with these considerations, this chapter aims to establish an environmentally sound and human-friendly framework for sustainable urbanism in future cities. In this context, the study first provides a conceptual understanding of sustainable urbanism and a critical review of its philosophical and practical framework; secondly, it provides a critical assessment of contemporary approaches to sustainable urbanism and architecture; thirdly, the chapter analyses the traditional Turkish (Ottoman) city which provides valuable clues for sustainable development and discusses possible research directions that could help promote the concept of sustainability in the urban and architectural environments of future cities.

Keywords Cities • Ecology • Culture • Sustainability • Contemporary paradigms • Turkish (Ottoman) city • Future of cities

1 Introduction

Changes that have taken place in the world over the past 20 years, including ecological disturbances and radical changes in traditional settlements, have produced cities that are not just chaotic and monotonous in appearance but have serious environmental problems threatening their inhabitants. In this context, environmentally sensitive design approaches at the building scale have been understood better

D. Oktay (✉)
Ondokuz Mayıs University, Samsun, Turkey
e-mail: Derya.oktay@omu.edu.tr; de.oktay@gmail.com

in comparison with those at the urban scale (especially in northern European countries and the USA), and significant developments have occurred in the field, although contemporary architectural practice in developing countries still lacks many aspects of sustainable building design.

The efficient layout of our built environment presents an exceptional opportunity to enhance our quality of life while reducing our ecological footprint to protect the environment. On that basis, sustainable urbanism emerges as a sound framework that draws attention to the immense opportunity to redesign the built environment in a manner that supports a higher quality of life and human health.

When sustainable urbanism is characterised in many contexts, what is usually addressed as the main concern is the natural environment and, hence, ecological sustainability, a condition that could be explained by climate change, the ultimate environmental crisis. However, we should be aware of the fact that today's development practices do not only consume enormous amounts of land and natural resources, damage ecosystems, produce a wide variety of pollutants and toxic chemicals, create growing distances between different parts of the city owing to the urban sprawl and fuel global warming; they also create inequities between groups of people, undermining local community and social values, economies and quality of life. These incremental changes imply a more critical state in cities of traditional societies where transformations in the urban level are still visible.

2 A Critical Review of Sustainable Urbanism

2.1 Contemporary Paradigms and Sustainability

Sustainable urbanism grows out of three late-twentieth-century reform movements that transcend McHarg's antisocial environmentalism to highlight so-called sustainable development, a development that is non-damaging to the environment and that improves the long-term health of human and ecological systems: 'new urbanism', 'smart growth' and 'green architecture'.

Each of these movements, however, is associated with a certain narrow-mindedness. Within architecture and urban design, the movement known as the new urbanism, which appeared in the early 1990s and has become a strong force for re-evaluating the physical layout of communities, cannot be considered efficient and urban since its focus was better-designed *suburban* development. New urbanism cannot be considered new, either, because it revives many ideas about the city and planning that were mainstream before the modern movement. Another criticism of new urbanism is that it is elitist [1]. Indeed, the movement is open to criticism on a number of fronts – in particular for being focused on

better-designed suburban development, often for upper-income groups, rather than the creation of truly urban places, and for not incorporating green building design and landscaping.

Just a few years later, in the mid-1990s, so-called smart growth evolved as an effort to recast the policy debate over sprawl in a way that more directly linked the environment, the economy and daily life concerns in pursuit of a positive and sustainable urban growth as being essential to the quality of the city and urban life. The movement focused especially on mechanisms to promote more compact, walkable and economically efficient urban development. Compact cities are said to offer opportunities for reducing fuel consumption for travelling, as homes, work and leisure facilities are closer together. They are also favoured by many in the field of urbanism because urban land can be re-used, while rural land beyond the urban edge is protected. Economic benefits, owing to high concentrations of people supporting local economies and easier access to services and facilities, are also touted. Compact cities with higher densities may also mean that people are more likely to encounter each other on the street than in low-density areas, and people may have a stronger sense of attachment to place. Ultimately, a good quality of life should be sustained, with high concentrations of people providing social conditions conducive to vibrancy, vitality and cultural production and consumption.

On the other hand, anti-sprawl strategies, which have obvious consequences for green and open space, have frequently led to gridlock in planning, especially concerning green space [2]. Just as a city with high-quality and generous green spaces symbolises good planning and management, a healthy environment for humans, vegetation and wildlife populations, and bestows pride on its citizenry and government, it can be asserted that if green space is absent, a compact city may become the antithesis of a green city. Further, the compact city makes less sense for developing countries because the context is completely different from those of North American and European countries whose cities have experienced declining populations and deindustrialisation. Cities of developing countries have much higher densities than their counterparts in developed countries, and they are not becoming significantly less compact in spite of decelerating population growth and the beginnings of decentralisation. Most of these cities cannot be restructured into compact sustainable cities within the current planning framework, which is limited to two-dimensional thinking and private land-owning interests at the expense of long-term sustainability.

Because buildings are amongst the principal users of energy and materials and major causes of environmental degradation, new approaches are needed in the conception, theorisation and implementation of architectural practices that will generate architectural designs responsive to the new conception of the relations between nature and humans, where the latter are part of the former depending on and determining it in a dynamic and parametric relationship. In this context, so-called green architecture or sustainable building has emerged as the practice of creating structures and using processes that are environmentally responsible and resource-efficient throughout the life cycle of buildings. Although new

technologies are constantly being developed to complement current practices in creating greener structures, the common objective is to design green buildings in such a way that the overall impact of the built environment on human health and the natural environment is diminished by the efficient use of energy, water and other resources, safeguarding of inhabitants' health and improvements to worker productivity, and the reduction of waste, pollution and environmental degradation.

2.2 The Need to Focus on the Primacy of Settlement Patterns

There are very successful examples of green architecture or sustainable building. However, contemporary architecture in most cases is still lacking many aspects of sustainable building. The absence of an urban or neighbourhood scale in most of the environmental literature has been masked by the recent obsession with so-called green building. Based on these shortcomings, I would like to highlight here the primacy of settlement patterns, a necessity for sustainable urbanism.

The primacy of settlement patterns is demonstrated by what can happen when it is overlooked. Take the ecologically sited headquarters to which every employee must daily drive long distances, or the green mall that depends on a trade area of 50 km, or stylish houses with outlandishly expensive 'solar' glass walls and with no connection to a sociospatial context.

The facts that demonstrate an ignorance of the primacy of settlement patterns can be summarised as follows:

- developers believe that company executives are easily dazzled by iconic design.
- Architects, including most educators in many architectural schools, tend to visualise buildings as isolated objects, as if the city were a canvas and expectations were an artistic brushstroke.
- Many architecture magazines miss the important point of how design fits into human and environmental contexts.

2.3 The Need to Focus on Sociocultural Sustainability

What is disregarded in all these approaches is that cities also have sociocultural aspects. Most urban and suburban development during the past 50 years has been relatively generic, with little sense of place, history or cultural distinctiveness. Many critics condemn low-density, car-oriented, suburban-style development, which they label socially isolating, segregating and alienating, calling instead for the widespread use of higher-density, mixed-use planning principles that lessen reliance on the automobile and increase social interactions. All these factors have

led to a long-term decline in the extent to which citizens participate in community groups and social institutions, and this decline of community participation is at least partly related to the physical nature of our cities and towns [3, 4]. To this end, social sustainability has arisen as an important aspect of sustainable urbanism, a system of cultural relations in which the positive aspects of disparate cultures are valued and promoted and there is widespread participation of citizens not only politically but also socially in all areas of urban life.

3 Lessons from the Ottoman City

The Ottoman city, built collaboratively by various cultures in a geographical setting extending from Central Asia to Anatolia, from the Mediterranean to the Balkans, demonstrates a sensitivity to local topography, Islamic and Christian philosophies about the natural world, and local habits and traditions built from a multitude of human values over centuries [5].

From an urban and social point of view, the main characteristic of the Ottoman city was its compartmentalisation into *mahalles* (neighbourhoods), the outcome of ethnic particularities and religious differences (Fig. 19.1). The *mahalle* was a geographical entity as well as a homogeneous community providing social and economic cooperation among neighbours. Each *mahalle* had its own characteristics and provided a cohesive and unique social environment for its inhabitants. The *mahalle* was self-sufficient as well, made so by the presence of a variety of



Fig. 19.1 Traditional townscape in Safranbolu, Turkey

functions, including a religious-social centre, small local markets, fountains, *imarets* (open kitchens) and, sometimes, workshops [6]. As a result of the closed economy, every household produced its own foodstuffs, i.e. vegetables, fruits and a variety of seasonal produce, that could be preserved and stored.

The efforts of numerous private builders (masters) in residential areas were guided by only a few simple rules of civility, assuring individuality within the neighbourhood and community identity apart from the works of government. It is a remarkable lesson that every house in the Ottoman city was different, even though there was an overall unity and consistency in building technique, scale and character [7]. As such, despite the lack of an organising development plan at the governmental level, which is a must in today's development practices, the respect for local environmental and social values made the Ottoman city a sustainable settlement in many regards.

The space of the traditional (Ottoman) city was, at a functional level, clearly divided into public and private realms. The public realm, often in the town centre, contained all the collective activities of the town, such as trade and commerce, religion, education, administration and urban facilities, resulting in a fine-grain mixed-use character. The main public node and the representation of people's power were focused on the citadel, the Friday mosque and its courtyard, and the bazaar. One of these elements, the main – often covered – street or streets of the city, the bazaar or *arasta*, functioned also as a communication channel, connecting these to each other and to less important activities such as public baths, water storage, and educational centres, creating a vivid public realm in a spatial continuum (Fig. 19.2).

The street system, which was mostly pedestrian and had a hierarchical order, was achieved through a process of organic growth in which the street pattern was gradually adjusted and changed according to the peculiarities of the land and needs of the local people, where there was no need for wider streets and a low level of accessibility was required. Despite the criticism of the street system from the viewpoint of accessibility and vehicular traffic, a conservationist principle is said to have existed in this organic growth that concentrated on the minimum space required [8]. Moreover, the hierarchical pattern of streets with dead-end branches serving a group of houses created privacy for the dwellers (especially for women – a significant need at the time) and helped create a strong sense of belonging to their neighbourhood. From an urbanistic point of view, this organic character of the street, in a state of continuous becoming, produces an effect of great expressiveness and, therefore, enhances the character of the Ottoman city. The street also served as a venue where children could play and women could chat around street fountains whilst obtaining water mornings and evenings.

On the other hand, in regions with hot or mild climates, the *avlu*, the courtyard of a house, an isolated environment that is well defined and well protected, served a variety of uses, including for social gatherings, such as weddings and circumcision parties, joint winter food preparation by women or for simply spending time together, and helped create a more cohesive community in the *mahalle*.



Fig. 19.2 Representation of *arasta*

Because Ottoman urbanism was never based on the kind of strong formalism characteristic of Western cultures, a generally informal character was dominant in cities. In this context, there were no formal public open spaces, i.e. well-defined squares, or monumental axes to be found in the cityscape. However, despite having no planned squares and the lack of an active use of *meydan* by the people, there was a social and psychological tendency towards meeting and gathering in open spaces of a natural character (Fig. 19.3) [5, 7].

The Ottoman city possessed various attributes that generated an ecologically sustainable environment. Regional climatic characteristics were reflected in the patterns of settlements, and accordingly every region produced its own characteristic urban fabric and architecture. For instance, in Safranbolu, one of the most typical towns in the north-western Black Sea region of Anatolia (Turkey), hard winters forced people to settle in sheltered valleys [9, 10]. The pre-existing topographic character of the site was apparent at the urban scale, even in intensively built-up areas. Green gardens, i.e. vegetable gardens and patches (*bostan*), orchards and so forth, implied a green belt dividing the quarters (sometimes occupying a natural creek as observed in Antep, a city in the south-eastern region of Anatolia) and bounded the town [12], contributing to the general self-sufficiency. The small squares at the intersections of streets with trees created opportunities to access nature in the public realm as well. The streets, defined by the high walls of residential courtyards, provided a protected and comfortable space and, being



Fig. 19.3 *Meydan*, the main public space

divided in two by a typical medieval gutter in the centre for rain and wastewater, helped in watering gardens and prevented rainwater from flowing into the courtyards.

The presence of a variety of house plans reveals the fact that there was a natural relationship between such a layout and the Anatolian life-style (Kuban, 1983). With its fruit trees, flowers and small kitchen garden, the *avlu*, separated from the street by a wall, was the closest connection the house had to nature, and thus it also provided inhabitant with direct access to nature and enhanced both the building ecology and self-sufficiency of the house.

All these features, in contrast to many newly developed urban environments in Turkey and around the world, make the Ottoman city an ideal model for ecologically and socially sustainable cities despite its shortcomings in terms of the viability of certain aspects (i.e. women's limited use of the public realm) for today's cities and urban life. Since sustainability needs to be assessed considering the cultural codes and realities of the time, as discussed in the background section of this chapter, these shortcomings may be tolerated within a larger, holistic context provided that requirements for every aspect of life are satisfied in modern urban planning and urban design.

4 Redefining the Essentials for Sustainable Urbanism and Architecture in Future Cities

Based on our critical review of contemporary approaches to sustainable urbanism and our analysis of the Ottoman city as an ideal model for sustainable urbanism, I would advocate that new urban planning and design endeavours should comprise a human dimension and demonstrate respect for regional characteristics. In this context, the following aspects are considered essential: context-sensitive compactness and defragmentation; completeness: good mixed use; connectedness: integrated transportation and land use; ecological sensitivity; a focus on settlement patterns, place and public spaces; sociocultural sustainability and cohesive neighbourhoods; and sustainable lifestyle (Fig. 19.4).

Context-sensitive compactness and defragmentation. Assuming that urban sprawl is mostly a negative phenomenon characterised by a low-density development pattern and presenting many problems, such as traffic congestion, massive absorption of green space, inadequate infrastructures and services and low-quality developments, as well as bureaucratic dysfunction and lack of financial resources [13], a proactive management approach to urban growth containing sprawl can be considered essential. The design of compact cities can obviously contribute to a

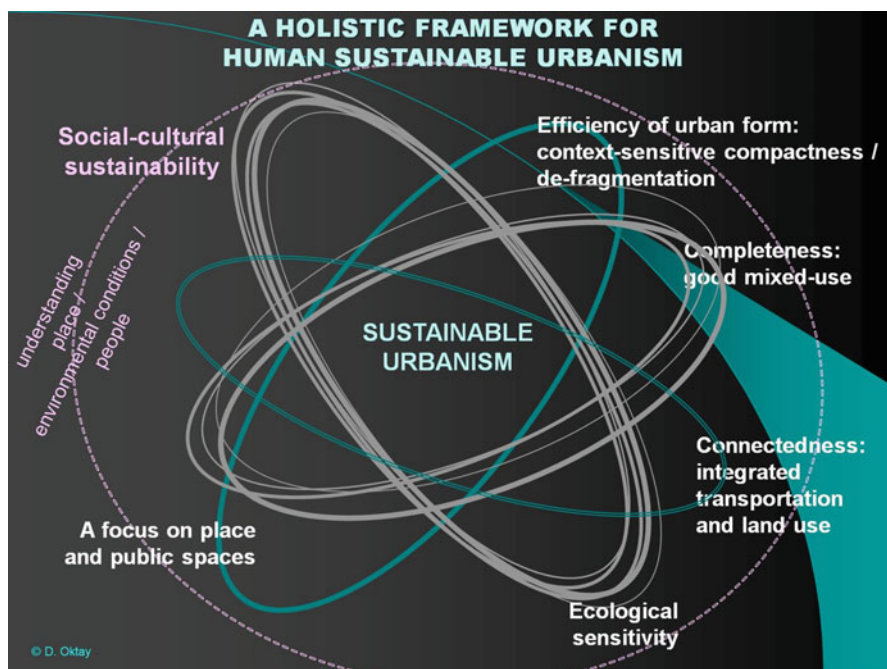


Fig. 19.4 Essentials for sustainable urbanism and architecture

more sustainable way of life, particularly in industrialised societies. However, as revealed through the ideas exemplified by the traditional Ottoman city that conform to regional characteristics, it cannot be expected that the same formula could be applied to all cities. What is needed is not a radical set of measures but a complete diagnosis of the territory, identifying local characteristics (i.e. climate, landscape, identity, culture and traditions), specificities, demands and dynamics and an estimation and evaluation of urban development processes by comparing the demand and supply for urban growth and considering the issues of where and how urban settlements should grow.

Inspired by the Ottoman city and *mahalle*, the contemporary city could be conceived as an entity made up of cohesive and identifiable districts, and smaller towns with functional diversity could be created near cities rather than growing to unacceptable levels of density and population. In this context, density should be related to design in such a way that its advantages and disadvantages are investigated by considering local social dynamics (the need for privacy, degree of privacy, neighbourly relations and so forth) and environmental values (e.g. green infrastructure, wetlands, forests, groundwater recharge zones), and new scenarios for 'defragmentation', where open growth may be encouraged.

Completeness: good mixed use. Fine-grain mixed-use is sought in urban expansion in order for those environments to be lively, safe, sensorily rich, choice-laden, economically and spatially efficient and ecologically diverse; it should be as sustainable as the built environment can credibly be. Looking at these objectives in light of what has been produced in contemporary expansion and future proposals, we see that we are nowhere near achieving them. This good mixed use was an important component of the public realm in the Ottoman city. Containing all the collective activities (i.e. trade and commerce, religion, education, administration and urban facilities), the central parts of the city revealed a fine-grained mixed-use character and helped the local people come together (despite the limited contact allowed to women owing to the cultural codes of the time) and have contact with the outside world. The main street and the bazaar, or *arasta*, in the Ottoman city, functioned as a communication channel, connecting the main activities to each other and to the less important activities (i.e. public baths, water storages and educational centres), and created a vibrant public realm in a spatial continuum. These characteristics can be re-interpreted as a model when planning or redesigning our cities whose central zones are deteriorating owing to a lack of diversity of main functions (business, commerce, housing, recreation) and the effects of privately owned, introverted spaces of modern urban commerce and design.

Connectedness: integrated transportation and land use. In a sustainable urban environment, people should have abundant opportunities to walk, ride in cars (if possible), bike and (if necessary) use wheelchairs in neighbourhoods, as well as have access to good public transport. These varied transportation options would increase access to services and facilities, help reduce car dependency and thus congestion and pollution, achieve a reduction in energy consumption and help maintain a high level of energy-efficient and environmentally friendly mobility

inside city limits or its environs. The findings of empirical surveys (i.e. [10, 14, 15]) suggest that the social and physical contexts of the walkable neighbourhood enhance casual interactions and social participation and are likely to contribute to a sense of community. The lesson for future cities, then, is to design city streets above all for people, taking into account their functional and aesthetic needs rather than catering for cars only.

Ecological sensitivity. As observed in the Ottoman settlements, which reveal an ideal integration with the natural environment and climate, sustainable urbanism seeks to connect people to nature and natural systems, even in dense urban environments. In this context, an attempt at integrating such features as edible landscapes of fruit trees and large vegetable patches (allotments) into a city would be beneficial for dwellers in terms of lower heating and cooling bills, lower food costs and reduced risk of flooding and landslide damage. Trees with canopies can be used for their shadowing effect and for the definition of spaces, in both streets and courtyards. When a more flexible design is possible, the traditional concept of courtyard can be reinterpreted and modified in the new housing developments, and walk-up type housing blocks can be arranged around a semi-private courtyard space in some areas in a diverse typological pattern. To address safety issues and to enhance the sense of place, the design of residential complexes should be based on the principles of responsive urban design by providing active edges (mixed use if possible) along streets and encouraging active use of courtyards by residents. At the building scale, other important aspects to ecological sensitivity are the use of local and regional materials of a natural character, conformity of buildings to their environs and in particular to climate, flexibility to adapt to changing conditions over time, and a rich variety of spaces extending from interior spaces to open spaces through various types of semi-open spaces.

Focus on settlement patterns, place and public spaces. Although public spaces form a crucial feature of sustainable and liveable cities, contemporary urban environments frequently do not have enough space set aside for them, and most of those spaces that are introduced as 'public spaces' lack spatial, ecological and social qualities and cannot be considered 'places for people'. Inspired by the Ottoman city, new urban areas could be planned and designed around a hierarchy of spaces for different purposes; the idea of a main shopping strip could be revived in order to prevent shopping malls becoming the norm, and the street pattern could be organised in such a way that each street has an identity through the continuity, design and functional layout of buildings.

Sociocultural sustainability. The success of sociocultural sustainability depends on the level of people's expectations, behaviour, value systems, transparency and accountability in both public and private decision-making. Since the most appealing aspect of sustainable urbanism is the sustainable neighbourhood, with its societal benefits, we must widen our definition of the sustainable urban neighbourhood to include social as well as environmental concerns, as reflected in

the *mahalle*, the cohesive neighbourhood unit in the Ottoman city. However, we should not ignore the great changes that occurred in the daily life of people, i.e. a significant increase in the percentage of working women, women's equal participation in almost all aspects of life and so forth.

Sustainable lifestyle. Everything we do as professionals and as human beings in the name of sustainability means very little if we do not actually change environmental behaviour of consumers, companies, communities and governments. Adopting sustainable lifestyles require incorporating a range of behavioural responses from energy saving and water conservation, to waste recycling and green consumption, and these would influence the urban quality of life without threatening the planet's future. In the Ottoman city, in the early Ottoman and Seljuk periods in particular, owing to the preferred simplicity in every aspect of life and self-sufficiency in many senses, people generally adopted a sustainable lifestyle, and it was a healthy and contented community. In today's cities, what is needed for a sustainable lifestyle is 'education for sustainable development' and, hence, ecological citizenship', which would enable urban residents to develop the knowledge, values and skills to participate in decisions about the ways they do things individually and collectively, both locally and globally.

5 Conclusion

Because we live in environments that have been very damaged, in ecological, social and cultural terms, there is an urgent need for a radical shift towards a holistic approach to sustainable urban planning/design, combining ecological and socio-cultural sustainability. This calls for sensitivity to traditional urbanism and the impact of global ideas, practices and technologies on local social and cultural practices. In that sense, the Ottoman city, in the early Ottoman and Seljuk periods in particular, possesses various characteristics that can inform modern planning and urban design.

The urban design of compact cities can obviously contribute to a more sustainable way of life, particularly in industrialised societies. However, since cities are all different in form and structure owing to a host of place-specific factors, it cannot be expected that the same formula could be applied to all of them when it comes to the question of a sustainable urban form. The degree of compactness or defragmentation should therefore be context-sensitive. Inspired by the Ottoman city and *mahalle* that comply with local environmental and sociocultural values of the time, the contemporary city could be reconsidered as an entity made up of cohesive districts, and smaller towns of functional diversity could be created near the city rather than grow to unacceptable levels of density and population.

A sustainable community endeavours to promote multi-functional rather than mono-functional settlement patterns by providing compact urban centres, with a broad range of services and amenities in close proximity. This reduces the need for vehicular and public transport, thereby decreasing demands on infrastructure and energy resources, while promoting pedestrian accessibility and community. The fine-grained mixed-use in the public realm of the Ottoman city can be reinterpreted as a model when planning or redesigning our cities whose central areas are deteriorating owing to a lack of diversity of primary functions and the negative effects of privately owned, introverted spaces of modern urban commerce and design.

In the course of an environmental transition, cities could attempt to retain as many environmentally sustainable ingredients as possible, including green spaces. In that sense, an attempt at integrating such features as edible landscapes and directing some of the efforts of greening towards streets would be beneficial.

What matters in terms of green architecture or sustainable buildings is that the concept of the relationship between nature and architecture as a design philosophy would be restored without resorting to superficial mimicry. It is worrying that so-called contemporary green buildings are often considered in isolation from their urban or regional contexts. It should be accepted that a city is not a simple collection of buildings, and green or so-called zero-energy buildings alone do not create a sustainable city. What is important to green architecture are the use of local and regional materials, the conformity of buildings to their environs and in particular to the local climate, the flexibility to adapt to changing conditions over time, and the rich variety of spaces extending from interior spaces to open spaces through a variety of semi-open spaces. High-tech innovation and new sustainable technologies undoubtedly have an important role to play, but in an energy-depleted world, cities that can de-link from their dependence on these technologies are likely to be more resilient.

We must widen our definition of sustainable urban neighbourhood to include social as well as environmental concerns as reflected in the *mahalle*, the social-spatial unit in the Ottoman city, without ignoring the great changes that occurred in people's daily lives. In the new settlements, there must be places that foster special rituals where all residents come together for their collective observance, as used to be done in streets and courtyards. There should be places that support multiple public activities, recreation and settings arranged to encourage safe and everyday personal exchanges among people who might otherwise remain strangers.

- To this end, we must ask ourselves what specific measures need to be taken to create sustainable urban environments, and how environmental and social concerns can be brought together into one convincing scenario in which everyone benefits. In this context, it is important to understand that the idea of sustainability is not new and traditional cities are excellent examples to learn from regarding various dimensions of sustainable urbanism.

- Developing countries like Turkey should give up copying the bad habits found in the Western world and return to their own regional practices and culture and develop them with innovative approaches.
- The newly developed paradigms that focus on how to achieve sustainable environments need to be understood in light of an understanding of local conditions and characteristics.
- Smart growth (compact city), new urbanism, urban renaissance and other terms reflect useful paradigms developed in temperate climates; they deal with expansion and growth, not decline. We should adapt them to our own conditions without generalising concepts and practices.
- Research in sustainable urban design recommends the increased use of the energies manifested in existing urban fabrics through the adaptive reuse of former industrial (brownfield) sites and upgrading the existing building stock.

Recent efforts towards more sustainable urban environments have revealed that, in order for sustainable urbanism to move forward and gain traction, it is essential that it be seen by citizens as playing an integral role in addressing the key issues of our times. The shift to a more sustainable lifestyle calls for the integration into everyday life of individual and private environmental actions and efforts to achieve resource savings in a more extensive context by using less water, less energy and less fuel for transportation, leading to lower CO₂ emission levels.

References

1. Kelbaugh DS (2002) *Repairing the American metropolis: common place revisited*. University of Washington Press, Seattle
2. Stähle A (2010) More green space in a denser city: critical relations between user experience and urban form. *Urban Des Int* 15(1):47–67
3. Ehrenhalt A (1995) *The lost city: the forgotten virtues of community in America*. Basic Books, New York
4. Moe R, Wilkie C (1997) *Changing places: rebuilding community in the age of sprawl*. Henry Holt, New York
5. Cerasi MM (1999) *Osmanli Kenti: Osmanli Kentinde 18. ve 19. Yüzyillarda Kent Uygarlığıve Mimarisi*. Yapi Kredi Yayinlari, Istanbul
6. Oktay D (2004) Urban design for sustainability: a study on the Turkish city. *Int J Sustain Dev World Ecol* 11(1):24–35
7. Eldem SH (1987) *Turkish houses, ottoman period, vol 3*. T.A.Ç, Istanbul
8. Madanipour A (1994) Urban public space in the middle east. In: *Proceedings of CARDO conference: people, place & development*. Awotona A. Newcastle upon Tyne
9. Günay R (2005) *Safranbolu houses*. Yapi Yayin, Istanbul
10. Kim J, Kaplan R (2004) Physical and psychological factors in sense of community. *Environ Behav* 36(X):313–340
11. Aru KA (1998) *Türk Kenti*. Building-Industry Center (YEM) Publications, Istanbul

12. Kuban D (1986) Turkish culture and arts. BBA, Istanbul
13. Downs A (1999) Some realities about sprawl and urban decline. *Housing policy debate*, 10/4
14. Khandokar F (2009) Briefing: user-perspectives on walkable neighbourhoods. In: *Proceedings of ICE: urban design and planning*, 162/DP4, p 155–158
15. Lund H (2002) Pedestrian environments and sense of community. *J Plan Educ Res* 21:301–312

Chapter 20

Thermal Performance of Vacuum Glazing with Tempered Glass Panes

Yueping Fang, Trevor J. Hyde, Farid Arya, and Neil Hewitt

Abstract The thermal performance (U -value) of 0.4×0.4 m and 1×1 m double vacuum glazing (DVG) and triple vacuum glazing (TVG) using annealed and tempered glass panes with pillar separations of 25 and 50 mm respectively was simulated. It was found that (1) for both dimensions of DVG with 0.03 emittance low-emittance (low-e) coatings, the U -values at the centre of the glazing area of the DVG made of annealed and tempered glass panes were 0.57 and $0.30 \text{ Wm}^{-2} \text{ K}^{-1}$, a reduction of 47.4%; (2) for both dimensions of TVG with 0.03 emittance low-e coating, the U -values at the centre of glazing area of the TVG with annealed and tempered glass panes were 0.28 and $0.11 \text{ Wm}^{-2} \text{ K}^{-1}$, a reduction of 60.7%. The reduction in U -values for both DVG and TVG results from the significant reduction in pillar number, leading to the large reduction in heat conduction through the pillar arrays. The reduction in U -values from using tempered glass panes instead of annealed glass panes for TVG is larger than that for DVG; this is because the radiative heat transfer of TVG with three glass panes is much lower than that in DVG with two glass panes; therefore, the heat conduction through the pillar array in TVG plays a larger role compared with that in DVG. The reduction in pillar number in TVG results in a larger reduction in U -value compared to DVG; thus, using tempered glass panes in TVG confers a greater advantage compared to DVG, given that DVG can also achieve a large reduction in U -value when switching from using annealed glass panes to tempered glass panes.

Keywords Annealed glass • Tempered glass • Vacuum glazing • U -value and pillar separation

Y. Fang (✉) • T.J. Hyde • F. Arya • N. Hewitt
School of the Built Environment, Ulster University, Londonderry BT37 0QB,
Northern Ireland, UK

Nomenclature

a	Radius of support pillar (m)
h	Surface heat transfer coefficient ($\text{Wm}^{-2} \text{K}^{-1}$)
k	Thermal conductivity ($\text{W m}^{-1} \text{K}^{-1}$)
p	Pillar separation (m)
R	Thermal resistance ($\text{m}^2 \text{K W}^{-1}$)
t	Thickness of glass pane (m)
T	Temperature ($^{\circ}\text{C}$)
U	Thermal transmission ($\text{Wm}^{-2} \text{K}^{-1}$)

Greek letters

ε	Hemispheric emittance of a surface
σ	Stefan-Boltzmann constant (5.67×10^{-8}) ($\text{Wm}^{-2} \text{K}^{-4}$)

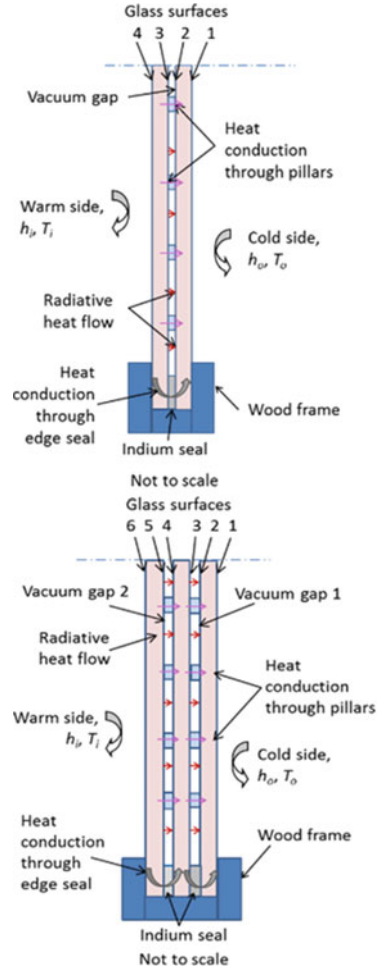
Subscripts

1–6	Surfaces of glass panes shown in Fig. 20.1
I, II, III	First, second and third glass panes
i, o	Refer to warm and cold ambient temperatures
g	Glass
m	Glass pane number of TVG
n	Vacuum gap number
p	Pillar
r	Radiation
tot	Total resistance of TVG

1 Introduction

Heat is lost through glazing by three mechanisms – conduction, convection and radiation. A single pane of glass is a poor insulator, with a thermal conductivity of $1 \text{ Wm}^{-1} \text{K}^{-1}$, leading to a total heat transmission U -value of $5.8 \text{ Wm}^{-2} \text{K}^{-1}$ for a 4-mm-thick uncoated glass pane. This results in a significant amount of heat loss or gain through a single glass pane window, leading to large heating and cooling loads for the building. Taking advantage of the low heat conductivity of air gaps, a typical double glazing with two parallel glass panes and an air-filled gap reduces the U -value to $2.8 \text{ Wm}^{-2} \text{K}^{-1}$. Replacing the air gap between the two glass panes with a narrow vacuum gap with a thickness of 0.2 mm results in double vacuum glazing (DVG). The narrow vacuum gap is maintained by an array of support pillars which resist the atmospheric pressure exerted on the external glass

Fig. 20.1 Schematics of DVG (a) and TVG (b)



surfaces. One or two low-emittance (low-e) coatings on the internal glass surfaces within the vacuum gap reduce the radiative heat transfer to a very low level. The vacuum eliminates gaseous heat conduction and convection between the two panes of glass. The heat transfer across the DVG is dramatically reduced to $0.8 \text{ Wm}^{-2} \text{ K}^{-1}$ if two panes with 0.16 emittance low-e coatings and a pillar array with a pillar diameter of 0.3 mm are used. The concept of DVG was first patented more than 100 years ago by Zoller [1]. However, it was only in the 1990s that the first successful DVG was reported by a team at Sydney University [2]. Since then, substantial developments have taken place, with significant findings published in scientific journals [3, 4]. The team at the University of Sydney used solder glass as a vacuum seal; however, other technologies have also been developed, for example low-temperature metal alloy [5], flexible edge seals and metal slip sealing methods [6].

The first successfully fabricated DVG used solder glass with a melting point of around 450 °C to seal the vacuum gap. A U -value of $0.8 \text{ Wm}^{-2} \text{ K}^{-1}$ for DVG has been achieved experimentally with a pillar separation of 25 mm and diameter of 0.3 mm [7]. Another type of DVG using indium alloy with a melting point of less than 200 °C of the vacuum gap sealant was successfully fabricated at Ulster University using a low-temperature fabrication method [5]. With fabrication temperatures of less than 200 °C, both soft and hard coatings can be used for vacuum glazing, while many soft low-e coatings cannot survive at fabrication temperatures of 450 °C for solder glass sealing. Another advantage of the low-temperature fabrication method is that tempered glass can be used for vacuum glazing, which would otherwise degrade under temperatures of 450 °C.

The design principle of vacuum glazing is to use the minimum number of support pillars with minimum diameter to minimise heat conduction through the pillar array, given that the radiative heat transfer across the glazing can be reduced to a very low level by low-e coatings. However, if the pillar diameter is too small, the glass panes will break owing to the high stress at the glass surfaces directly contacting the two ends of the support pillars. If there are too few pillars, the glass panes will also break because of the high tensile stress between two pillars. The optimal pillar diameter and separation have been determined using a finite-element model (FEM) [3]. It has been found that when using tempered glass panes, the pillar separation can be significantly increased because tempered glass panes are four times stronger than annealed glass panes. For instance, when using two 4-mm-thick tempered glass panes, instead of annealed glass panes, with the same pillar diameter, the pillar separation can be increased from 25 to 54 mm [8]. This will result in a significant reduction in the number of pillars in the pillar array and, thus, a significant reduction in heat conduction across the pillar array and in the U -value of the vacuum glazing. Motivated by this idea, this chapter investigates improvements in the U -values of DVG and triple vacuum glazing (TVG) with soft and hard coatings with emittances of 0.03 and 0.16. A DVG with tempered glass panes was fabricated and its U -value was experimentally characterised using a guarded hot box calorimeter (GHBC) and compared with the simulation results calculated using a finite-volume model (FVM). The two results are in very good agreement.

2 Methodology

The schematics and heat transfer mechanism of DVG and TVG (not to scale) are presented in Fig. 20.1. Figure 20.1a shows that the heat transfer across the DVG by (1) conduction, convection and radiation from the warm ambient air onto

the warm side of glass surface 4; (2) heat conduction through support pillars and edge seal; (3) radiation between surfaces 2 and 3 within the vacuum gap; (4) heat conduction, convection and radiation from glass surface 1 to the cold side ambient air; and (5) heat conduction from surface 4 to 3 and from surface 2 to 1 within the glass panes. Heat transfer across the TVG (Fig. 20.1b) is by (1) heat conduction, convection and radiation from the warm ambient onto glass surface 6; (2) radiation between surfaces 4 and 5, and between surfaces 2 and 3; (3) conduction through the pillar array within vacuum gaps 1 and 2; (4) heat conduction through the edge seal of vacuum gaps 1 and 2; (5) heat conduction from surface 6 to 5, from surface 4 to 3, and from surface 2 to 1; (6) conduction, convection and radiation from cold side surface 1 to cold ambient air. The analytic models for analysing the heat flow through the centre of glazing were established by Collins and Simko [3] for DVG and by Manz et al. [9] for TVG. The heat transmissions calculated by both analytic and FEM were in very good agreement [4].

2.1 Analytic Model Analysis for DVG

A quarter of the unit of cell with one pillar in the centre of the glazing is shown in Fig. 20.2a for DVG and in Fig. 20.2b for TVG. In Fig. 20.2a, since the thermal conductivity ($20 \text{ W m}^{-1} \text{ K}^{-1}$) of the stainless steel support pillar is much larger than that ($1 \text{ W m}^{-1} \text{ K}^{-1}$) of the glass panes, the temperature difference between the two ends of the pillar is only a very small proportion of the temperature difference between the two glass panes. If the glass is assumed to have a semi-infinite thickness and extent, the thermal resistance associated with the spreading heat flow in the glass has been found to be

$$R_{\text{spreading}} = 1/(2k_g a), \quad (20.1)$$

where a is the radius of the pillar [10]. The overall air-to-air thermal resistance is

$$R_{\text{air-to-air}} = \frac{1}{h_i A} + \left[\left(\frac{2t}{k_g A} + \frac{1}{h_r A} \right)^{-1} + 2k_g a \right]^{-1} + \frac{1}{h_o A}, \quad (20.2)$$

where A is the area of the unit cell, i.e. $A = p^2/4$. The radiative heat transfer $Q_{\text{radiative}}$ between glass surfaces 2 and 3 with an area of A , mean surface temperatures T_2 and T_3 , and hemispherical emittances ε_2 and ε_3 is calculated by [11]

$$Q_{\text{radiation}} = \varepsilon_{\text{effective}} \sigma A (T_2^4 - T_3^4), \quad (20.3)$$

$$Q_{\text{radiation}} = 4\varepsilon_{\text{effective}} \sigma A T_{\text{average}}^3 (T_2 - T_3), \quad (20.4)$$

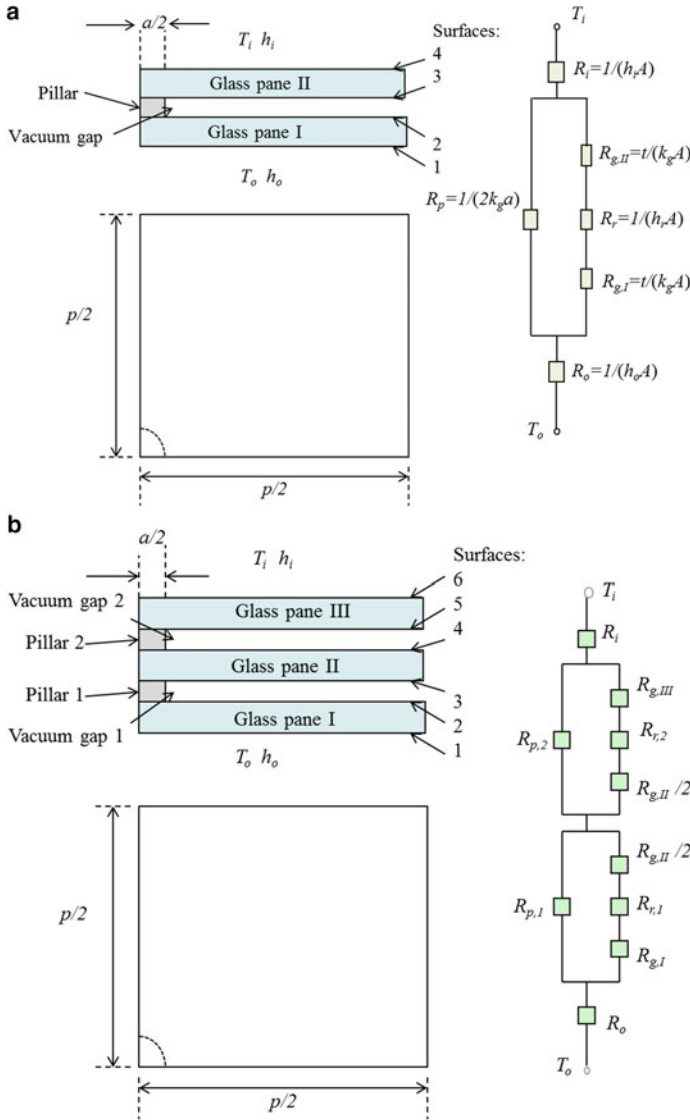


Fig. 20.2 Schematics and thermal network of a quarter of the unit cell within the DVG (a) and TVG (b)

where σ is the Stefan-Boltzmann constant, $T_{\text{average}2,3}$ is the average of temperatures T_2 and T_3 and the effective emittance, $\epsilon_{\text{effective}}$, is determined by

$$\frac{1}{\epsilon_{\text{effective}2,3}} = \frac{1}{\epsilon_2} + \frac{1}{\epsilon_3} - 1. \tag{20.5}$$

The emittance was approximated to be independent of the wavelength and angle of incident radiation. The error caused by this approximation is 4% [12].

2.2 Analytic Model for TVG

In Fig. 20.2b, the thermal resistance associated with the heat flow per square metre due to the heat conduction of each glass pane is given by

$$R_{g,m} = \frac{t_m}{k_g}, \quad (20.6)$$

where t_m is the thickness of glass pane m , where $m \in \{I, II, III\}$, k_g is the thermal conductivity of the glass.

The thermal resistance associated with radiative heat flow between the glass surfaces within each of the vacuum gaps is

$$R_{r,1} = \left(\frac{1}{\varepsilon_2} + \frac{1}{\varepsilon_3} - 1 \right) (4\sigma T_{2,3}^3)^{-1} = (4\varepsilon_{2,3}\sigma T_{2,3}^3)^{-1}, \quad (20.7)$$

$$R_{r,2} = \left(\frac{1}{\varepsilon_4} + \frac{1}{\varepsilon_5} - 1 \right) (4\sigma T_{4,5}^3)^{-1} = (4\varepsilon_{4,5}\sigma T_{4,5}^3)^{-1}, \quad (20.8)$$

where $\varepsilon_2, \varepsilon_3, \varepsilon_4$ and ε_5 are respectively the hemispheric emittances of glass surfaces 2, 3, 4 and 5 within vacuum gaps 1 and 2, as shown in Fig. 20.2b; $\varepsilon_{2,3}$ and $\varepsilon_{4,5}$ are combined effective emittances of surfaces in vacuum gaps 2 and 1; $T_{2,3}$ and $T_{4,5}$ are the mean temperatures of glass surfaces 2, 3 and 4, 5 respectively in vacuum gaps 1 and 2 in Kelvin. The thermal resistance associated with the heat conduction through the support pillars in vacuum gap n (1 or 2) is determined by (20.9) [9]

$$R_{p,n} = \frac{1}{2k_g a}, \quad (20.9)$$

where a is the radius of the cylindrical pillar. The thermal resistance of the middle glass pane is divided into two equal thermal resistances; therefore the total thermal resistance associated with the heat flow between surfaces 1 and 6 is determined by Eq. (20.10):

$$R_{\text{tot}} = \frac{R_{p,1}(R_{g,1} + R_{r,1} + \frac{1}{2}R_{g,II})}{R_{p,1} + R_{g,1} + R_{r,1} + \frac{1}{2}R_{g,II}} + \frac{R_{p,2}(R_{g,III} + R_{r,2} + \frac{1}{2}R_{g,II})}{R_{p,2} + R_{g,III} + R_{r,2} + \frac{1}{2}R_{g,II}}. \quad (20.10)$$

The thermal resistances associated with heat flows R_i and R_o at glazing surfaces 6 and 1 are the inverse of the surface heat transfer coefficients, i.e. $R_i = 1/h_i$

and $R_o = l/h_o$. The total heat transmission of the unit cell at the centre-of-glazing area is then given by

$$U_{\text{tot}} = \frac{1}{R_i + R_{\text{tot}} + R_o}. \quad (20.11)$$

The heat flow through the entire TVG is the sum of heat flow across the centre-of-glazing area and the heat flow through the edge area, including the heat conduction through the edge seal, whose analytic model is presented in the literature [3].

2.3 Finite-Volume Approach

The FVM used leads to a sparse, well-structured system of equations that can be efficiently solved [4]. This enables a large number of volumes to be used to represent the vacuum glazing geometry and allow the direct representation of the small pillars. The equation bandwidth using the FVM method is smaller than that obtained for the FEM method using 24 node brick elements and, consequently, requires fewer numeric operations and less CPU time to obtain a satisfactory solution. Because of the symmetry conditions, only one quarter of the vacuum glazing was simulated to represent the whole glazing system under ISO ambient conditions (ISO 2007). In the three-dimensional (3-D) FVM, the support pillars were integrated and modelled into the complete system for ease of computation in the simulation. The cylindrical pillars used in the fabricated systems were replaced by the same number of cubical pillars with the same areas of cross section since both pillar shapes conduct similar amounts of heat under the same boundary conditions [10]. The length of the square base of each cubical pillar is $\sqrt{\pi}a$, where a is the radius of the equivalent cylindrical pillar. A graded mesh is used with a high density of nodes in and around each pillar to provide adequate representation of the heat transfer. To test the accuracy of simulations with the specified mesh number, the thermal performance of a small central area (25×25 mm) with a single pillar in the centre was simulated using a mesh of $50 \times 50 \times 25$ nodes. The mesh was denser in the area close to the pillar. The 25 nodes were distributed in a graded mesh through the glazing thickness of 8.2 mm. The thermal conductance of this simulated unit with a pillar in the centre was in good agreement with the analytic prediction, with 1.5% variation, which is comparable to the result of Wilson et al. [11]. This level of agreement indicates that the density of nodes is sufficient to simulate a realistic level of heat flow with high accuracy in DVG. The detailed description for the FVM for DVG is presented in Fang et al. [4].

The FVM of Fang et al. [4] for DVG was adapted to suit the structure of TVG. The heat Manz et al. [9] and Fang et al. [4]. The simulated thermal transmission of a standard unit containing a pillar in the centre of a 25×25 mm centre-of-glazing area was in good agreement with the result calculated using the analytical model,

with a 1.8 % variation Fang et al. [4] which is comparable to the variation (2 %) of Manz et al. [9]. With the 85×85 nodes distributed on the y and z directions on the glazing surface and with 20 nodes on the x direction, the thermal transmission at the centre-of-glazing area for DVG with an emittance of 0.03 was determined to be $0.36 \text{ Wm}^{-2} \text{ K}^{-1}$ with a glass pane thickness of 6 mm. This is comparable to the findings of Griffiths et al. [13] and Fang et al. [4]. This level of agreement is satisfactory to simulate a practical heat flow with high accuracy in TVG.

3 Predicted Thermal Performance of DVG and TVG with Tempered Glass Panes

The thermal performances of DVG and TVG rebated by 10 mm within a solid wood frame were simulated with the following ambient conditions. The pillar diameter is 0.4 mm. The edge seal width of the DVG and TVG is 6 mm. The warm- and cold-side ambient temperatures are 20 and 0 °C respectively; the surface heat transfer coefficients h_i and h_o at the warm- and cold-side glass pane surfaces are $7.7 \text{ Wm}^{-2} \text{ K}^{-1}$ and $25 \text{ Wm}^{-2} \text{ K}^{-1}$ respectively [14].

3.1 Influence of Tempered Glass Panes on U-Value of DVG

The use of tempered glass panes for vacuum glazing enables the pillar separation to be significantly increased while keeping the stresses within the glass pane surfaces between two consecutive pillars and at the glass surfaces at either end of the support pillars under bearable levels. For instance, for annealed low-e coated float glass panes with a thickness of 4 mm, the typical pillar separation is 20–25 mm, while for tempered glass panes with the same thickness, the pillar separation can be increased to 54 mm [8]. In this work, 50 mm pillar separation is used for the DVG and TVG with 4 mm thick tempered glass panes. The temperature profiles along the central line of the DVG where the pillars are distributed with two annealed and two tempered glass panes with 0.03 emittance coatings were simulated (Fig. 20.3).

The temperature profiles in Fig. 20.3 show the periodic temperature variations against the distance from the sightline. These are caused by heat conduction across the support pillars. For the annealed glass panes, the variation in the periodic distance along the sightline is 25 mm; for the tempered glass panes, it is 50 mm, corresponding to the pillar separations within the DVG. The temperatures at the warm-side surface of the tempered glass pane are significantly higher than those of the annealed glass pane. For the cold-side glass panes, the trend is reversed; thus, the temperature difference between the tempered glass panes is significantly greater than that of the annealed glass panes. This results in a large difference in the U -values of the DVGs with annealed and tempered glass panes. The calculated

Fig. 20.3 Comparison of temperature profiles of 0.4×0.4 m DVG with annealed and tempered glass panes coated with 0.03 emittance coatings

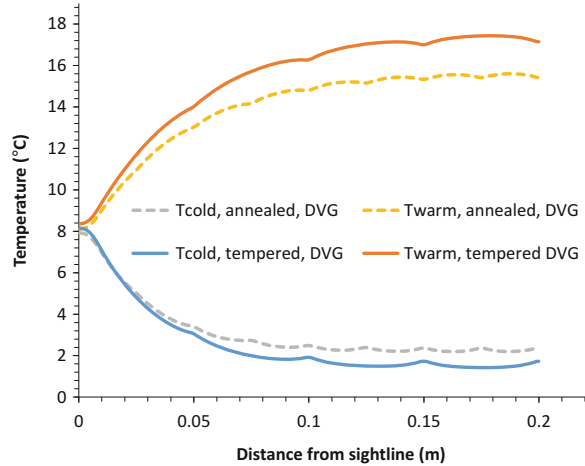


Table 20.1 U -values of 0.4×0.4 m (A_1) and 1×1 m (A_2) DVG with tempered and annealed glass panes

	ϵ	U -value central glazing ($Wm^{-2} K^{-1}$)		Improvement (%)	U -value total glazing ($Wm^{-2} K^{-1}$)		Improvement (%)
		$U_{T,c}$	$U_{A,c}$		$U_{T,t}$	$U_{A,t}$	
A_1	0.03	0.30	0.57	47.4	0.53	0.73	27.4
	0.16	0.63	0.81	22.2	0.78	0.97	19.6
A_2	0.03	0.30	0.57	47.4	0.48	0.69	30.4
	0.16	0.63	0.81	22.2	0.76	0.96	20.8

U -values at the centre-of-glazing area and total glazing area of the DVG with annealed and tempered glass panes with 0.03 and 0.16 emittance low-e coatings (typical soft and hard coating emittances respectively) are listed in Table 20.1, where $U_{T,c}$ and $U_{A,c}$ indicate the U -values at the centre-of-glazing area of the DVG with tempered and annealed glass panes; $U_{T,t}$ and $U_{A,t}$ indicate the U -values of the total glazing area of the DVG with tempered and annealed glass panes; *Imp.* stands for the improvement in U -value as a percentage.

Table 20.1 shows that (1) the percentage improvements in U -value at the centre-of-glazing and total glazing areas of the DVG with two tempered glass panes over two annealed glass panes with 0.03 emittance low-e coatings are larger than those with two 0.16 emittance low-e coatings. This is because when the number of pillars is reduced for the tempered glass, the ratio of heat conduction through the pillar array to the total heat transfer across the glazing is reduced, while the influence of the low-e coating on the total heat transfer across the glazing is increased; (2) the improvements in the U -value of the total glazing area of 1×1 m DVG are larger than those of the 0.4×0.4 m DVG. With the decrease in the influence of the pillar array on the total heat transfer across the glazing, the advantage of a larger DVG having a lower heat transfer compared to a smaller DVG becomes more significant.

3.2 Influence of Tempered Glass on U-Value of TVG

The temperature profiles along the central line of the TVG where the pillars are distributed with two annealed and tempered glass panes with 0.03 emittance coatings were simulated (Fig. 20.4). Figure 20.4 shows that the temperatures along the central line of the warm-side tempered glass pane are significantly higher than those of the annealed glass pane, whereas for the cold-side glass panes this trend is reversed. This means that the overall temperature difference between the warm- and cold-side glass panes of the TVG with tempered glass panes is larger than that with annealed glass panes. The U -values of 0.4×0.4 m and 1×1 m TVG using tempered and annealed glass panes were simulated and are listed in Table 20.2. The emittance of low-e coatings on the internal glass surfaces within the vacuum gaps of the TVG is 0.03 or 0.16.

Table 20.2 shows that (1) replacing three annealed glass panes and a pillar separation of 25 mm with three tempered glass panes and a pillar separation of 50 mm for TVG with 0.03 emittance coatings results in a larger percentage

Fig. 20.4 Comparison of temperature profiles of 0.4×0.4 m TVG with annealed and tempered glass panes

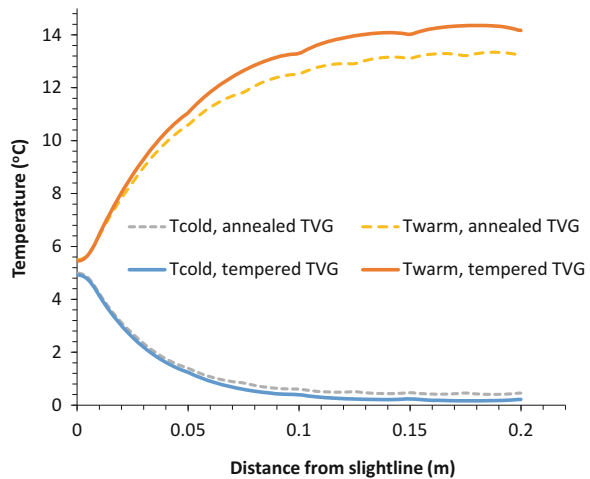


Table 20.2 U -values of 0.4×0.4 m (A_1) and 1×1 m (A_2) TVG with tempered and annealed glass panes

	ϵ	U -value central glazing ($Wm^{-2} K^{-1}$)		Improvement (%)	U -value total glazing ($Wm^{-2} K^{-1}$)		Improvement (%)
		$U_{T,c}$	$U_{A,c}$		$U_{T,t}$	$U_{A,t}$	
A_1	0.03	0.11	0.28	60.7	0.57	0.69	17.4
	0.16	0.29	0.43	33.3	0.72	0.82	12.2
A_2	0.03	0.11	0.28	60.7	0.40	0.52	23.1
	0.16	0.29	0.42	33.3	0.55	0.66	16.7

improvement in the U -value at the centre-of-glazing and total glazing areas over three annealed glass panes with 0.16 emittance coatings. This is because the radiative heat transfer within the TVG with 0.03 emittance coatings is significantly lower than that of the TVG with 0.16 emittance coatings; thus, heat conduction through the pillar array of the TVG with 0.03 emittance coatings plays a larger role in the total heat transfer across the glazing than that of the TVG with 0.16 emittance coatings; (2) since the edge effect within the 1×1 m TVG is less than that of the 0.4×0.4 m TVG, the improvements in the U -value of the total glazing area of 1×1 m TVG resulting from the replacement of the annealed glass panes with tempered glass panes is larger than that of the 0.4×0.4 m TVG.

3.3 Comparison of DVG and TVG with Tempered Glass Panes

The temperature profiles of the 0.4×0.4 m DVG and TVG with two and three tempered glass panes with 0.03 emittance coatings are compared in Fig. 20.5. Figure 20.5 shows that the temperatures of the warm- and cold-side glass panes of the DVG are higher than those of the TVG since the heat flow across the DVG is larger than that across the TVG. The U -values of both the 0.4×0.4 m (A_1) and 1×1 m (A_2) DVG and TVG with tempered and annealed glass panes with 0.03 emittance coatings are compared in Table 20.3.

Table 20.3 shows that (1) the improvements in the U -value at the centre-of-glazing area of the TVG using three annealed glass panes are greater than those of DVG using two annealed glass panes. Three glass panes with low-e coatings significantly reduces radiative heat transfer in TVG compared to the two glass panes in DVG; therefore, the heat conduction through the pillar array has a larger influence on the overall heat transfer across the TVG compared to DVG. When the

Fig. 20.5 Comparison of temperature profiles of DVG and TVG with tempered glass panes

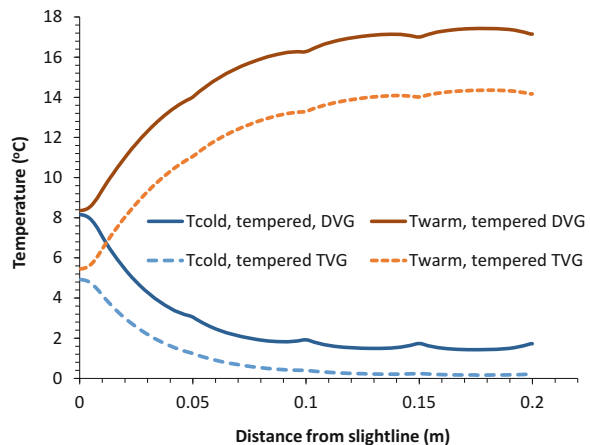


Table 20.3 Comparison of U -values of DVG and TVG with tempered and annealed glass panes with 0.03 emittance coatings

		U -value central glazing ($\text{Wm}^{-2} \text{K}^{-1}$)		Improvement (%)	U -value total glazing ($\text{Wm}^{-2} \text{K}^{-1}$)		Improvement (%)
		$U_{T,c}$	$U_{A,c}$		$U_{T,t}$	$U_{A,t}$	
A ₁	DVG	0.33	0.57	42.1	0.53	0.73	27.4
	TVG	0.11	0.27	59.2	0.57	0.69	17.4
A ₂	DVG	0.33	0.57	42.1	0.48	0.69	30.4
	TVG	0.11	0.27	59.2	0.40	0.52	23.1

pillar number is reduced, the reduction in heat transfer across the centre-of-glazing area of the TVG is larger than that across the DVG; (2) the improvement in the U -value of the total glazing area of the DVG using two annealed glass panes is greater than that of the TVG using three annealed glass panes. Because lateral heat conduction through the edge seal of TVG is greater than that of DVG, the influence of heat conduction through the pillar array on the U -value of the total glazing area for DVG is larger than that for TVG. Once the pillar number is reduced, the reduction in the U -value of the total glazing area for DVG is larger than that for TVG.

4 Experimental Validation of Thermal Performance of DVG Made with Tempered Glass Panes

A 0.4×0.4 m DVG was fabricated with two 0.16 emittance low-e tempered glass panes to validate the simulation results.

4.1 Fabrication of DVG with Tempered Glass Panes

The fabrication method using tempered glass panes was similar to that used for annealed panes [7]. The first step was to drill a pump-out hole at the corner of an annealed pane. The drilled and undrilled glass panels were then toughened in a conventional toughening furnace. During the toughening process, the glass panes experienced roller wave, leading to a deviation of around 0.5 mm in the flatness of the glass surface. Given the pillar height of 0.15 mm, this 0.5 mm deviation on the tempered glass surface presents a challenge for fabrication, as some pillars may not have contact with the tempered glass surfaces, leading to movement of the pillar within the vacuum gap. Experiments were conducted to check the probability of pillar movement. When the pillar separation was 25 mm, 50% of the pillars moved after the sample was fabricated; when the pillar separation was 40 mm,

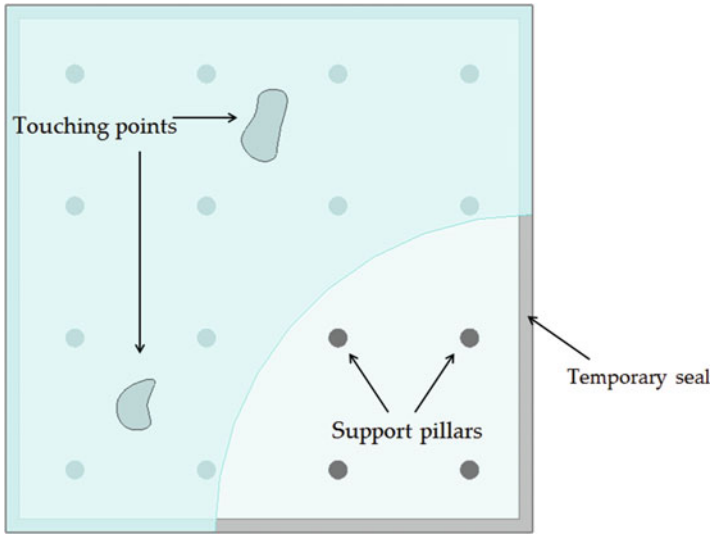


Fig. 20.6 Schematics of DVG fabricated using tempered glass panes with pillar separation of 50 mm

around 35% of the pillars moved; when the pillar separation was 50 mm, no pillars moved. However, with 50 mm pillar separation, the glass panes made contact with each other at random locations. Because of the irregular pattern of deviation of the tempered glass panes, it was difficult to predict the contact point of two glass panes.

To overcome this contact problem, a prefabrication process was carried out to establish the possible contact points within the vacuum gap. The pillar array was laid on the bottom glass pane and an indium wire 0.5 mm in diameter was set around the periphery of the bottom glass pane. The top glass pane was laid to match the bottom glass pane with the pillar array and indium wire temporary seal. Both glass panes were clamped together. A pump-out device was located over the pump-out hole, and the assembly was evacuated. The atmospheric pressure acting on the two glass surfaces caused the two glass panes to make contact with each other at specific areas, as shown in Fig. 20.6. These contact points were marked on the external glass surface; then the pumping process stopped and the upper glass pane was disassembled. To prevent the glass panes touching during the subsequent pump-out process, support pillars were set on the bottom glass pane at the marked locations. After removing the temporary edge seal and creating a soldered edge seal, the upper glass pane was laid onto the assembly to match the bottom glass pane. The glazing system then underwent the same fabrication process as the vacuum glazing with annealed glass panes [7].

Another challenge in the fabrication of the DVG was that when subjected to fabrication temperatures of 150 °C it was found that the epoxy resin seal around the periphery of the DVG was not able to create a strong bond with the two tempered glass panes, and so the sample failed. This was a result of the added stress within the tempered glass panes compared to the annealed glass panes where

the epoxy resin seal can form a strong bond. To overcome this problem, a new sealant was used that could withstand 340 °C and create a strong bond with not only annealed glass panes but also tempered glass panes. Following this, a DVG with tempered glass panes was successfully fabricated.

4.2 Thermal Performance Characterization of DVG with Tempered Glass Panes

The thermal performance U -value of the DVG made with tempered glass panes was characterised using a GHBC. A detailed descriptions of the GHBC appears elsewhere [15]. The sample was rebated within a solid wood frame and installed in the centre of the mask wall. The air temperatures at the hot and cold boxes were controlled at 19.2 and -0.3 °C; the surface heat transfer coefficients were 7 and $24.5 \text{ Wm}^{-2} \text{ K}^{-1}$ respectively. The experimentally determined U -value at the centre-of-glazing area was $0.69 \text{ Wm}^{-2} \text{ K}^{-1}$, which is in good agreement with the predicted result of $0.63 \text{ Wm}^{-2} \text{ K}^{-1}$. It was considered that the deviation might have resulted from the added support pillars to prevent the tempered glass panes making contact with each other.

5 Conclusions

Vacuum glazing has significant potential to reduce heat loss or gain through windows, which are traditionally seen as the weakest component of buildings in terms of thermal performance. With commercially available hard low-e coatings, a U -value for DVG of $0.8 \text{ Wm}^{-2} \text{ K}^{-1}$ was achieved experimentally with a pillar separation of 25 mm and diameter of 0.4 mm. The low-temperature (less than 200 °C) fabrication method for vacuum glazing developed at Ulster University makes it possible to apply a wide range of soft low-e coatings that have lower emittance values compared to hard coatings, thereby improving the glazing thermal performance. The low-temperature sealing method also enables the use of fully tempered glass panes in vacuum glazing, which would otherwise lose temper at higher sealing temperatures.

The use of tempered glass panes enables the pillar separation to be increased while the stress within the glass panes between the two pillars and at the glass surfaces immediately above and below the support pillars is kept under bearable levels. For instance, for annealed low-e coated glass panes with a thickness of 4 mm, the typical pillar separation is 20–25 mm, while for tempered glass panes with the same thickness, it was shown by previous research using a FEM that the pillar separation can be over 50 mm. In this work, U -values of $0.4 \times 0.4 \text{ m}$ and $1 \times 1 \text{ m}$ DVG and TVG using tempered and annealed glass panes with pillar

separations of 50 and 25 mm were simulated. It was found that the U -value at the centre-of-glazing area of the DVG with two glass panes of 0.03 emittance was reduced from $0.57 \text{ Wm}^{-2} \text{ K}^{-1}$ for annealed glass panes to $0.30 \text{ Wm}^{-2} \text{ K}^{-1}$ for tempered glass panes. The U -value at the centre-of-glazing area of the TVG with three glass panes of 0.03 emittance was reduced from $0.28 \text{ Wm}^{-2} \text{ K}^{-1}$ for annealed glass panes to $0.11 \text{ Wm}^{-2} \text{ K}^{-1}$ for tempered glass panes. When using a hard coating with an emittance of 0.16, the U -value at the centre-of-glazing area of the DVG was reduced from $0.81 \text{ Wm}^{-2} \text{ K}^{-1}$ for annealed glass panes to $0.63 \text{ Wm}^{-2} \text{ K}^{-1}$ for tempered glass panes; the U -value at the centre-of-glazing area of the TVG reduced from $0.43 \text{ Wm}^{-2} \text{ K}^{-1}$ for annealed glass panes to $0.29 \text{ Wm}^{-2} \text{ K}^{-1}$ for tempered glass panes. These numbers indicate that using tempered glass panes leads to significant improvements in U -values for both DVG and TVG, though the improvement for TVG was greater than that for DVG because the three low-e coated glass panes significantly reduced radiative heat transfer across the TVG compared to that across the DVG; therefore, the heat conduction through the pillar array has a greater influence on the total heat transfer across TVG than that across DVG. When the pillar number is reduced, the reduction in heat transfer across TVG is greater than that across DVG.

For $1 \times 1 \text{ m}$ DVG and TVG, the improvement in the U -value of the total glazing area as a result of the tempered glass panes is greater than that for the $0.4 \times 0.4 \text{ m}$ DVG and TVG. This is because the edge effects for the $1 \times 1 \text{ m}$ DVG and TVG are less than those of $0.4 \times 0.4 \text{ m}$ DVG and TVG, so the influence of heat conduction through the pillar array on the total heat transfer across the $1 \times 1 \text{ m}$ DVG and TVG is greater than that across the $0.4 \times 0.4 \text{ m}$ DVG and TVG.

The improvement in the U -value at both centre-of-glazing and total glazing areas of both DVG and TVG with 0.03 emittance low-e coatings over annealed glass panes is greater than those with 0.16 emittance coatings. This is because the 0.03 emittance coatings in both DVG and TVG more significantly reduce radiative heat transfer across the glazings than the 0.16 emittance coatings, so the influences of heat conduction through the pillar array of DVG and TVG with 0.03 emittance coatings on the total heat transfer across the DVG and TVG are greater than those with 0.16 emittance coating.

A DVG with two tempered glass panes with 0.16 emittance was fabricated and a U -value of $0.69 \text{ Wm}^{-2} \text{ K}^{-1}$ was experimentally determined using a GHBC, which is in good agreement with the simulated U -value of $0.63 \text{ Wm}^{-2} \text{ K}^{-1}$ with a deviation of 8.6%. The deviation may result from the additional support pillars, which prevent the contact of the tempered glass panes. The improvement in thermal performance from annealed glass to tempered glass for both DVG and TVG will further stimulate application of vacuum glazing in the near future.

References

1. Zoller F (1924) Hollow pane of glass. German Patent 387655
2. Collins RE, Robinson SJ (1991) Evacuated glazing. *Sol Energy* 47:27–38
3. Collins RE, Simko TM (1998) Current status of the science and technology of vacuum glazing. *Sol Energy* 62:189–213
4. Fang Y, Hyde TJ, Arya F, Hewitt N, Eames PC, Norton B (2014) Indium alloy-sealed vacuum glazing development and context. *Renew Sust Energy Rev* 37:480–501
5. Hyde TJ et al (2000) Development of a novel low temperature edge seal for evacuated glazing. In: *Proceedings of World Renewable Energy Congress VI (WREC2000)*. Brighton, UK, pp 271–274
6. Friedl W (2011) USB ultra sonic bond—proceeding of glass performance days (GPD) conference, 17–20 June. Tampere, Finland, pp 299–300
7. Zhao JF, Eames PC, Hyde TJ, Fang Y, Wang J (2007) A modified pump-out technique used for fabrication of low temperature metal sealed vacuum glazing. *Sol Energy* 81(9):1072–1077
8. Collins RE et al (1999) Paper presented at glass in buildings conference. Bath, UK
9. Manz H, Brunner S, Wullschleger L (2006) Triple vacuum glazing: heat transfer and basic mechanical design constraints. *Sol Energy* 80(12):1632–1642
10. Holm R (1967) *Electric contacts, theory and application*, 4th edn. Springer, Berlin, pp 9–16
11. Wilson CF, Simko TM, Collins RE (1998) Heat conduction through the support pillars in vacuum glazing. *Sol Energy* 63(6):393–406
12. Zhang Q-C, Simko TM, Dey CJ, Collins RE, Turner GM, Brunotte M et al (1996) The measurement and calculation of radiative heat transfer between uncoated and doped tin oxide coated glass surfaces. *Int J Heat Mass Transfer* 40(1):61–71
13. Griffiths PW et al (1998) Fabrication of evacuated glazing at low temperature. *Sol Energy* 63(4):243–249
14. EN ISO 1007-11 (2000) *Thermal performance of windows, door, and shutters—calculation of thermal transmittance—part 1: simplified method*. Brussels
15. Fang Y, Eames PC, Noton B, Hyde JT (2006) Experimental validation of a numerical model for heat transfer in vacuum glazing. *Sol Energy* 80:564–577

Chapter 21

Energy Refurbishment Towards Nearly Zero-Energy Terrace Houses in the Mediterranean Region

D.K. Serghides, M. Michaelidou, Stella Demetriou, and M.C. Katafygiotou

Abstract The building sector in Europe is responsible for an estimated 40 % of the total energy consumption and 10 % of total CO₂ emissions. Given an annual rate of 1 % of addition of new buildings in the existing building stock, the energy efficient renovation of the existing housing stock is imperative in order to reduce building energy consumption. It is for this reason that the European Union (EU) ranked the improvement of the energy performance of the old building stock as a high priority on its research agenda. Following Europe's 20:20:20 objective, this case study investigates refurbishment scenarios that will make it possible to achieve nearly zero-energy buildings (nZEBs) in Cyprus.

The research focuses on the terrace family house typology in Cyprus, as classified in the framework of the Intelligent Energy Europe, EU project EPISCOPE. The aim is to upgrade an old terrace building built before 1980. It into a nZEB with the implementation of national energy performance requirements, as drafted by the Ministry of Energy, Commerce, Industry and Tourism (MECIT). A representative terrace family building was chosen and modeled using the Simplified Building Energy Model iSBEMcy tool. This is the official government software in Cyprus used for issuing Energy Performance Certificates (EPCs) for the categorisation of the energy class of buildings and the calculation of CO₂ emissions according to European Directives 2002/91/EC and 2010/31/EC.

The study investigates whether it is possible for an old terrace family building to meet nZEB standards and identifies the lurking obstacles and challenges through building simulations. To this end, various refurbishment scenarios were developed, aimed at fulfilling the MECIT requirements. The efficiency of each strategy and technique employed towards minimising energy consumption and greenhouse gas emissions was evaluated, in terms also of its cost-effectiveness. Furthermore, the

D.K. Serghides (✉) • M. Michaelidou • S. Demetriou • M.C. Katafygiotou
Department of Environmental Science and Technology, Cyprus University
of Technology, Limassol, Cyprus
e-mail: despina.serghides@cut.ac.cy; archi.mmarilena@gmail.com;
demetriou_stella@yahoo.com; martha.katafygiotou@cut.ac.cy

results of the research were investigated to assess whether the nZEB requirements, as developed by MECIT, are appropriate for existing terrace family houses in Cyprus and whether alternative strategies may be employed to meet the target of nZEB and to effectively reduce energy consumption and CO₂ emissions.

Keywords Energy performance • Existing terrace housing typology • Old houses • Nearly zero-energy buildings

1 Introduction

The built environment is not only the largest industrial sector in economic terms; it is also the largest in terms of resource flow [1]. The increasing energy demand already threatens the future of the planet, as research has shown that 10 % of the world's population uses 90 % of its energy resources [2]. The European Union (EU) [3], the second largest economy worldwide, while consuming one-fifth of the energy produced in the world, has few stocks of energy resources. Under this threat, the EU aims to achieve a more sustainable future and therefore focuses on the existing building stock by identifying the potential for energy conservation in the building sector.

Residential buildings comprise the largest segment of the EU's building stock, with a floor space of 75 %, and are responsible for two-thirds of the sector's energy consumption [1]. While new constructions add at most 1 % a year to the existing stock, the other 99 % of buildings are already built and produce about 26 % of the energy-use-induced carbon emissions [4]. The oldest part of the building stock contributes greatly to the high energy consumption in the building sector. Older buildings tend to consume more owing to their low performance levels. Furthermore, old buildings' thermal performance and indoor comfort suffer from a variety of construction problems, many of which are related to the building envelope; these weaken its role as a regulator and as a moderator of external climatic fluctuations. Taking into account that the expectation for the structural life of a building often exceeds 60 years while the envelope shows signs of obsolescence after only 20 or 30 years [4], it is understandable that the residential stock needs serious refurbishment. Greater potential energy savings and further sustainable benefits can be achieved in existing residential buildings than in newly built constructions. Improvements to the energy performance of the existing residential stock in every country is essential since operational costs, energy consumption and carbon dioxide emissions are major issues and concerns in Europe with respect to achieving EU 2020 goals.

The Energy Performance Building Directive (EPBD) establishes the nearly zero-energy building (nZEB) as the building target from 2018 for all publicly owned buildings or buildings occupied by public authorities and from 2020 for all new buildings [5]. With these objectives set at the Europe-wide level, the nZEBs should be reality in just 5 years. The EU has set targets for 2020 which aim at a 20 % reduction in greenhouse gas emissions from 1990 levels. The intent is to raise the share of the European energy mix produced from renewable resources by 20 % and to improve energy efficiency by 20 %. To meet these targets, the EU emphasises the

need for national definitions of nZEB. Complying with EU targets [6], Cyprus [7] has published Directive 366/2014 referring to the minimum national requirements concerning nZEB. In addition to this, two major challenges need to be addressed before full integration of the nZEB concept into national building codes or international standards. This includes the adaptation of a common and unambiguous definition and the development of a supporting methodology for computing the energy balance [8]. Furthermore, it is necessary to investigate the effectiveness of refurbishment scenarios for existing residential buildings to set minimum national requirements and establish a definition of nZEB for renovation processes.

Sufficient thermal insulation of building envelopes is in fact essential for shielding the indoor environment of buildings from external adverse environmental conditions and, thus, minimising, through the envelope, thermal heat losses during winter and heating gains during summer. Many surveys have been carried out in search of nZEB standards concerning the optimisation of building envelopes, upgrading of electromechanical systems and utilisation of renewable energy sources (RESs). Regarding the optimisation of building envelopes, in a recent study, Serghides and Georgakis investigated the energy performance of a building envelope to identify the optimum relationship between cost-effectiveness and energy efficiency in the thermal performance of buildings in the Mediterranean region. This study concluded that the most effective solution for an improved building envelope's thermal performance was provided by the combination of external insulation on the building envelope and an increase in the internal mass, which in turn increases the thermal capacity of the structure [9].

The RES contribution to nZEB has proven vital for improvements in the energy performance of buildings [10] and may even result in positive-energy buildings [11]. A combination of upgrading electromechanical systems, refurbishing external envelopes and introducing RESs in buildings is the most effective approach. Furthermore, an individualised approach to each building, taking into consideration its own particularities, is necessary for finding an optimal solution [12].

Previous studies on the Cyprus housing stock investigated the impact of different refurbishment scenarios on the energy consumption of dwellings and the resulting savings [13–15]. The studies demonstrated the effectiveness of insulation on building envelopes and the high contribution of photovoltaic (PV) systems in the reduction of greenhouse gases.

This study focuses on the conversion of existing terrace family houses, representing one of the main residential typologies in Cyprus [16] (6.7% of the residential building stock), into nZEB houses and highlights the arising challenges.

2 Methodology

In accordance with the Intelligent Energy Europe (IEE) project TABULA (Typology Approach for BUiLding stock energy Assessment) and the ongoing IEE project

EPISCOPE [17], 12 residential building typologies were established as typical and representative of the national residential building stock in Cyprus [18]. These are classified according to their chronological period of construction and their architectural and constructional characteristics. The three building typologies are the multifamily houses, terrace family houses and single-family houses. These are divided into four different chronological periods, supported by the data collected from the Cyprus Statistical Service [16]. Each chronological division was defined based on the different constructional regulations and techniques applicable throughout the years during which the four distinctive chronological categories were formulated. These categories are as follows: (1) before 1980, (2) between 1981 and 2006, (3) between 2007 and 2013 and (4) after 2014. The divisions were also guided by the rapid growth of the construction industry in Cyprus, which occurred after 1980, by the adoption of European Directive 2002/91/EC in 2007 and the amendment of Directive 433/2013, which was enforced in early 2014. It is worth mentioning that before the entrance of Cyprus into the EU, there was no energy-related legislation for the building sector.

The dwellings under study were selected based on their space-related characteristics (e.g. floor area, number of bedrooms), which approach those of the typical terrace family house of the third chronological period. To perform the study, the total building area, the heated living volume and the constructional characteristics of the building envelope, as well as the type of electromechanical systems installed for heating, hot water and cooling, were collected. The constructional characteristics of the roof, the wall, the floor slab, the structure and the openings were recorded and their U -values as well as their thermal capacities calculated. The installed electromechanical systems were documented and their energy efficiency estimated. In this study, due to a lack of available data, mainly concerning the installed electromechanical systems, certain assumptions were made (length and type of pipes, condition of systems) [19].

Initially, the energy performance of the houses was found for their existing state and the corresponding levels of energy consumption were calculated. Subsequently, a standard nZEB refurbishment scenario was applied based on Directive 366/2014. The energy efficiency and cost viability for each refurbishment measure related to the building envelope elements' thermal performance were assessed separately. Additional measures, not included in the prerequisites of Directive 366/2014, were examined in terms of their energy efficiency and cost-effectiveness. Based on the findings, an optimized nZEB scenario was developed, oriented toward improving the energy efficiency and cost-effectiveness of the refurbishment. The investment cost associated with the nZEB refurbishment scenarios, as well as the payback period, was based on current market values. These were calculated using the official tool published by the Ministry of Energy, Commerce, Industry and Tourism of Cyprus [20] for the cost optimal energy conservation measures to include the purchase, installation and construction costs for all systems used for these retrofitting scenarios. The modelling tool used throughout this study for the energy performance calculation was the iSBEM-Cy, which is the government software for

the issuance of Energy Performance Certificates (EPCs) [21]. This is the official governmental software in Cyprus used for the categorisation of energy efficiency in buildings and the calculation of CO₂ emissions according to European Directive 2002/91/EC [21].

3 Case Study

The case study concerns three terrace family houses, part of a residential block, situated in Aglantzia, in the capital city of Nicosia, an inland area. The dwellings were constructed in 2004 and are representative of their typology for the chronological period 1981–2006. The dwellings were built before any energy-related legislation for the building sector was in force, so their energy performance is inevitably poor [19]. Thus, the impact of an effective deep energy refurbishment in these houses may be applied to all the old terrace family houses and result in high energy savings at the national level. It is one building with multiple houses/dwellings in Fig. 21.1.

3.1 Existing Condition of Dwellings

The dwellings are rectangular two-storey houses. The building is situated at an altitude of 156 m above sea level and has a south-west orientation. The common spaces of each dwelling are located on the ground floor (living room, kitchen, dining room, toilet), while the bedrooms (three bedrooms, one bathroom) are on the first floor.

The usable heated living area and volume of the three dwellings of the terrace block are presented in Table 21.1 and their layout in Fig. 21.2.

The external envelope of the three houses consists of conventional brick.

The load-bearing structure of the dwellings (beams and pillars) is made of reinforced concrete and the walls are of conventional brickwork, with plaster



Fig. 21.1 Terrace building under study: (a) south-west view; (b) north-east view

Table 21.1 Heated floor area and volume of terrace housing units

Dwelling	Ground floor (m ²)	First floor (m ²)	Total area (m ²)	Volume (m ³)
North-west	66.98	53.50	120.48	451.33
Middle	63.50	53.25	116.75	435.13
South-east	63.50	53.25	116.75	435.13

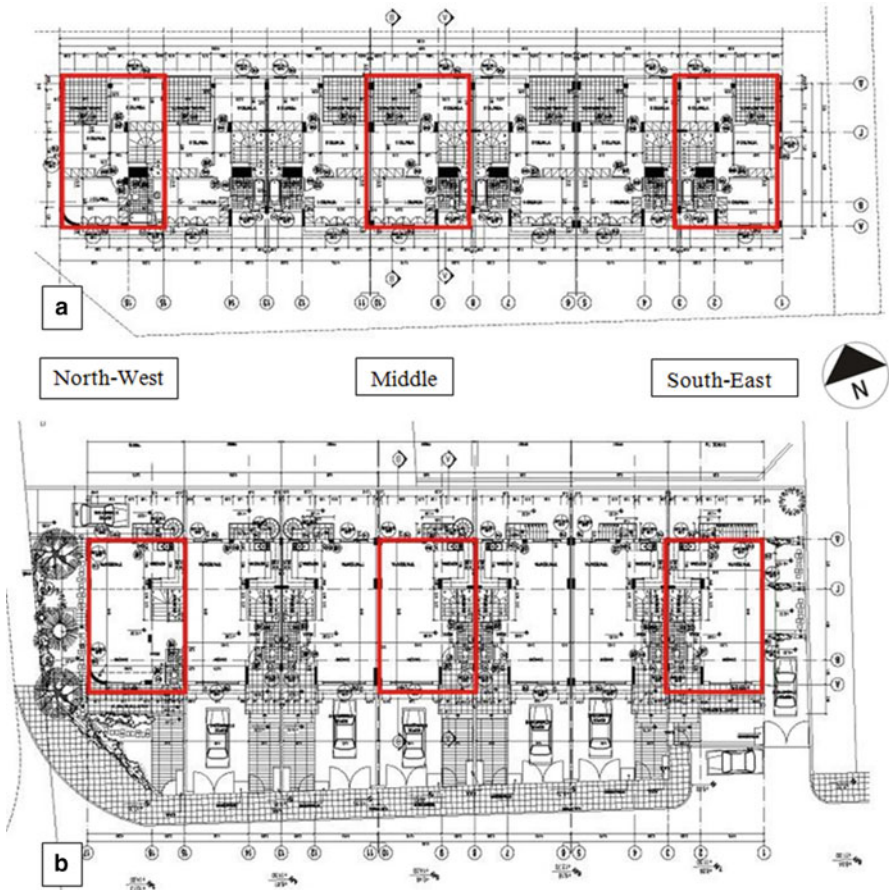


Fig. 21.2 Layout of dwellings under study. (a) First floor. (b) Ground floor

coating on both sides, resulting in a total thickness of 24 cm. The windows are double glazed with an aluminium frame. The glazing corresponds to 21.8 % of the north-west dwelling’s external wall area, 11.4 % of the middle and 24.1 % of the south-east. The roof is made of reinforced concrete and is partly pitched and partly horizontal. The inclined part is a non-insulated, ventilated, tiled pitched roof with

Table 21.2 Existing electromechanical equipment

Electromechanical system	Existing installation
Domestic hot water system	Single pipeline internal building envelope, well insulated + storage tank + stand-by immersion resistance
Renewable energy	Solar collectors
Cooling system	Split units
Heating system	Split units (north-west and south-east), storage electric heater (middle)

Table 21.3 *U*-values of building envelope elements

Construction element	<i>U</i> -value [W/(m ² K)]
Pitched roof with horizontal ceiling	3.42
External walls	1.40
Floor in contact with ground	0.91
Double glazed windows	3.70

horizontal ceiling of reinforced concrete. The floors of both floors are clad with ceramic tiles of 2 cm thickness.

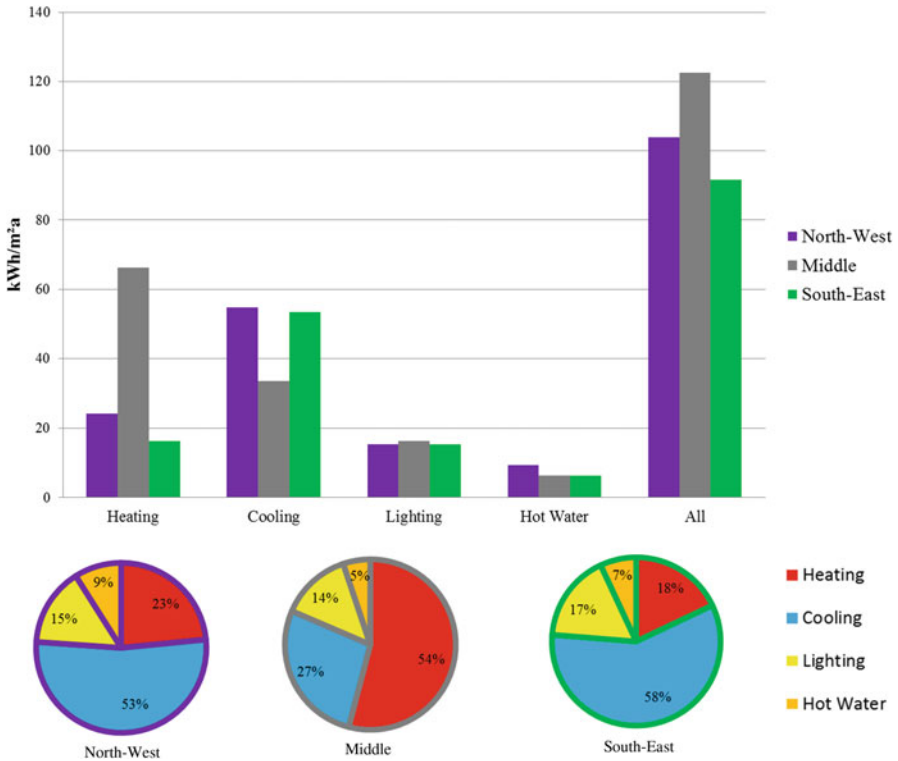
The houses are separated by double walls with a gap (air) 33 cm thick. For calculation purposes, each house is considered to be independent and the detached wall is treated as adjacent to a non-heated space.

The north-west and south-east dwellings use split units for heating and cooling. The middle one has a constant temperature electric storage heater, without thermal insulation. All three dwellings use solar thermal panels for domestic hot water (DHW), backed up by an electric element. The existing electromechanical equipment can be seen in Table 21.2.

The thermal characteristics (*U*-values) of the building's envelope are calculated and the resulting values are shown in Table 21.3.

After simulating the dwellings' energy performance using the iSBEM-cy tool, the calculated total primary energy consumption is 287 kWh/(m²a) for the north-west, 338 kWh/(m²a) for the middle and 254 kWh/(m²a) for the south-east dwelling. The primary energy consumption is higher for the middle dwelling compared with the corner ones owing to the use of storage electric heaters for heating instead of split units. The 7 kWh/(m²a) of the total primary energy consumption is produced from renewable energy sources (RESs) owing to the solar thermal panels on the roof for DHW consumption for all the dwellings. Therefore, the renewable energy contribution in the total primary energy consumption ranges from 2.07 % (middle) to 2.75 % (south-east).

The total energy consumption for the houses reaches 103.86 kWh/(m²a) for the north-west, 122.5 kWh/(m²a) for the middle and 91.57 kWh/(m²a) for the south-east dwelling. The corresponding energy consumption for heating is 24.35 kWh/(m²a), 66.26 kWh/(m²a) and 16.45 kWh/(m²a) and for cooling it is 54.71 kWh/(m²a), 33.52 kWh/(m²a) and 53.38 kWh/(m²a). The energy consumption for DHW is 9.31 kWh/(m²a) for the north-west, 6.31 kWh/(m²a) for the



Graph 21.1 Energy consumption of dwellings; existing situation

middle and 6.36 kWh/(m²a) for the south-east dwelling, and for lighting it is 15.49 kWh/(m²a), 16.42 kWh/(m²a) and 15.39 kWh/(m²a) respectively. The EPC categorisation reaches class C for both the north-west and south-east and D for the middle dwelling. The major energy consumption is connected with the high need for cooling for the north-west and middle dwellings, while for the south-east dwelling it is connected with heating because of the low efficiency of the storage electric heaters (Graph 21.1) used as the heating system. The line around the pies corresponds to the colour attributed to each dwelling in the bar graph.

3.2 Standard nZEB Refurbishment Scenario

Based on the Cyprus EPBD Directive 366/2014, specific *U*-values must be obtained and certain requirements fulfilled to define a building as being nearly zero-energy, according to the minimum energy performance requirements with respect to the *U*-values of the elements of the building envelope and the energy demand for

Table 21.4 nZEB requirements for dwellings in Cyprus according to Directive 366/2014

nZEB requirements for houses	
Technical specifications – construction element	U -value [W/(m ² K)]
Pitched roof with horizontal ceiling	0.40
External walls	0.40
Double glazed windows	2.25
Energy performance specifications	Minimum requirements
Energy Performance Certificate	A
Total primary energy consumption	100 kWh/(m ² a)
Energy demand for heating	15 kWh/(m ² a)
Renewable energy percentage of total primary energy consumption	25 %

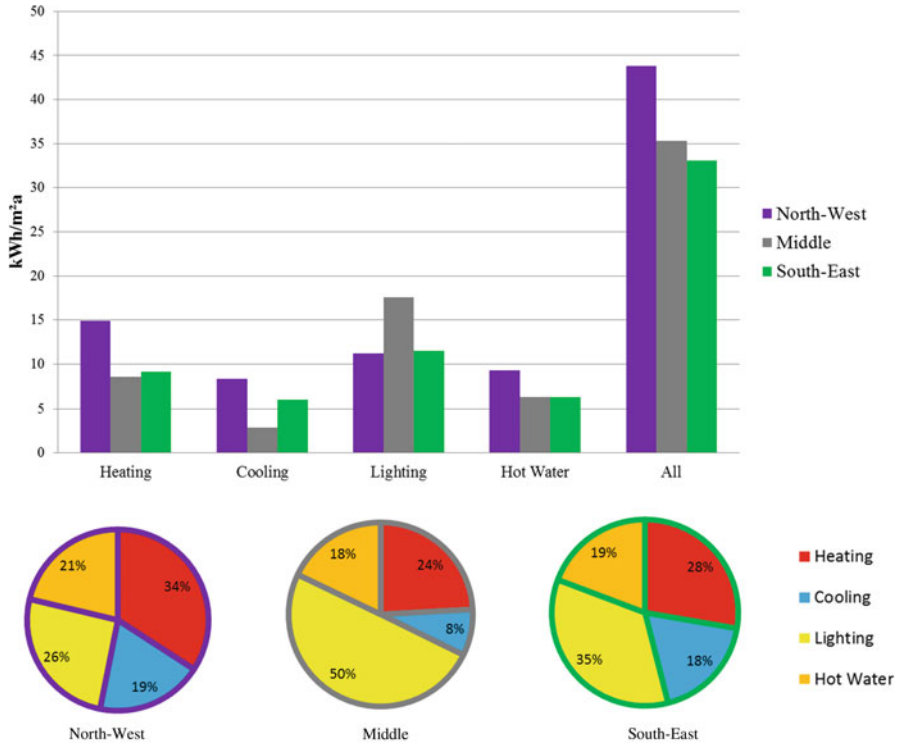
heating, as well as the total primary energy consumption and the share of RESs in total primary energy consumption. These requirements are shown in Table 21.4.

To meet the minimum requirements for the building envelope for a nZEB house, 70 mm of thermal insulation (expanded polystyrene) was added externally on the walls and 90 mm was installed externally on the roof; the windows were replaced with new, thermally improved ones with lower U -values. The thermal characteristics of the building envelope after the energy-conservation measures were implemented were calculated to reach the minimum technical specifications of the nZEB directive. The roof and walls have a U -value of 0.38 W/(m² K), whereas the selected windows have a U -value of 2.25 W/(m² K). Furthermore, three PV panels with a total area of 4.8 m² were placed on the roof of each dwelling at an inclination of 30° and the existing air-conditioning units were replaced by A+++ class units.

Using the aforementioned energy-conservation measures, the two corner dwellings were raised by two EPC categories, from C to A, and the middle one by three, from D to A, thereby meeting all the requirements of the nZEB definition for residential buildings under deep renovation [23].

The calculated total primary energy consumption for the nZEB refurbishment scenario is reduced to 125 kWh/(m²a) for the north-west, 102 kWh/(m²a) for the middle and 96 kWh/(m²a) for the south-east dwelling. The contribution of RESs, including solar thermal panels for DHW and PV panels on the roof, was 32 kWh/(m²a) for the north-west, 26 kWh/(m²a) for the middle and 33 kWh/(m²a) for the south-east dwelling, covering 25.60, 25.5, and 34.4 % respectively of the total primary energy consumption.

The total final energy consumption is reduced to 43.77 kWh/(m²a) for the north-west dwelling, of which the energy consumption for heating is 14.94 kWh/(m²a) and that for cooling is 8.32 kWh/(m²a). The lighting and DHW consumption levels are 11.19 kWh/(m²a) and 9.31 kWh/(m²a) respectively. The total final energy consumption for the middle dwelling is 35.3 kWh/(m²a), of which the energy consumption for heating is 8.52 kWh/(m²a) and that for cooling is 2.87 kWh/(m²a). The lighting and DHW consumption levels are 17.60 kWh/(m²a) and 6.31 kWh/(m²a) respectively. The total final energy consumption for the south-east dwelling is

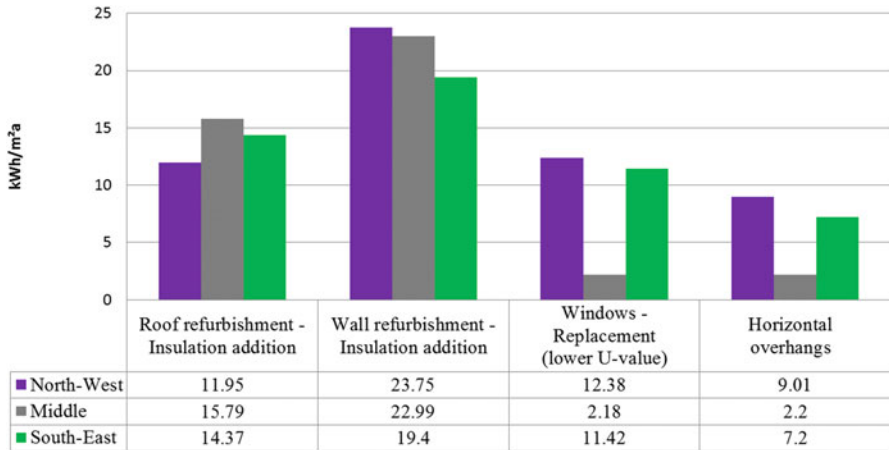


Graph 21.2 Energy consumption of dwellings after standard nZEB refurbishment

33.05 kWh/(m²a), the lowest of the three. Of that, the energy consumption for heating is 9.16 kWh/(m²a) and that for cooling is 6.05 kWh/(m²a). The lighting and DHW consumption levels are 11.48 kWh/(m²a) and 6.36 kWh/(m²a) respectively. The energy profile of the dwellings after the standard nZEB refurbishment is presented in Graph 21.2.

3.3 Impact of Energy-Conservation Measures and Their Cost-Effectiveness

The impact of each measure addressing the building’s envelope energy performance upgrade was separately investigated to detect the most energy-efficient and cost-optimal ones. The measures investigated were the placement of insulation on the roof and walls, the replacement of the windows and the installation of horizontal overhangs above the south-facing windows. Each measure was studied separately, and its energy savings for space heating and cooling were calculated.



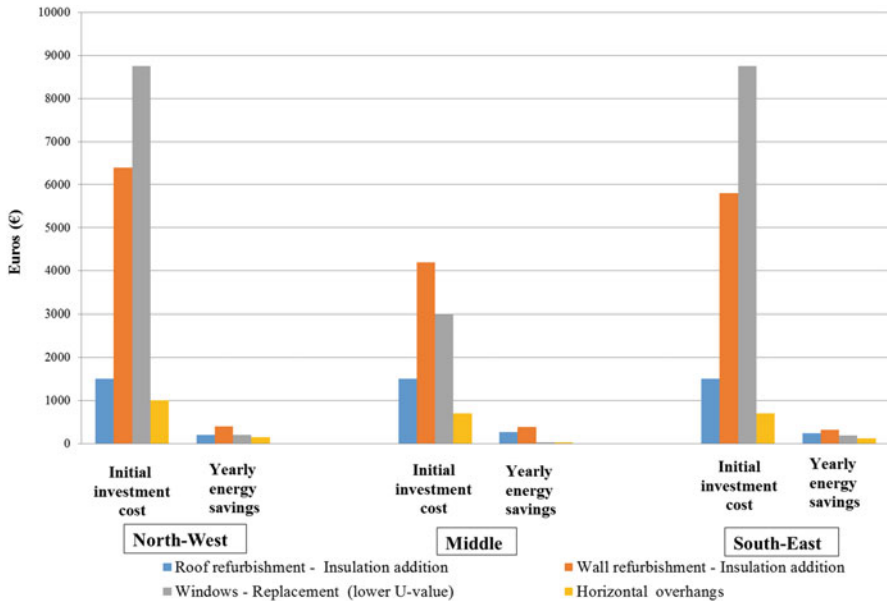
Graph 21.3 Energy savings after implementation of each energy-conservation measure

It was concluded that the most effective measure was the placement of thermal insulation [24] (Graph 21.3). The thermal insulation of the walls had the highest energy savings among the investigated measures. The thermal insulation when placed on the walls resulted in savings of 23.75 kWh/(m²a) for the north-west, 22.99 kWh/(m²a) for the middle and 19.40 kWh/(m²a) for the south-east dwelling. The corresponding savings for the roof insulation were 11.95 kWh/(m²a) for the north-west, 15.79 kWh/(m²a) for the middle and 14.37 kWh/(m²a) for the south-east dwelling. The placement of the insulation on the walls was more effective than the placement of the insulation on the roof owing to the difference in the exposed area of each component. The exposed area of the walls was twice that of the roof.

The replacement of the existing double glazed windows with new ones, of lower *U*-value, results in savings of 12 % for the two corner dwellings and 2 % for the middle one. The area of the windows for the corner dwellings is three times the area of the windows of the middle one, resulting in six times higher energy savings compared with the middle dwelling.

The placement of the 1 m length overhangs [25] above the windows with a southern orientation, complying with the maximum length permitted by the existing building regulations, reduces the energy consumption for the three dwellings, achieving saving percentages of 9 % for the north-west, 2 % for the middle and 8 % for the south-east dwelling. These results take into consideration that the device is manually or automatically operated, so as to benefit from solar radiation during winter. To this end, the direct results from the energy performance calculation tool (iSBEM-Cy), showing that the energy consumption for cooling decreases while the energy consumption for heating increases owing to the tool’s inability to perform dynamic simulations of the building, had to be adequately modified to obtain the highest possible energy savings.

From Graph 21.4 it is obvious that the two most cost-effective measures for the corner dwellings is the placement of horizontal overhangs and the roof insulation,



Graph 21.4 Cost-effectiveness of each energy-conservation measure

with expanded polystyrene 90 mm thick, with a 6 to 7.5 year payback period. The wall insulation, with expanded polystyrene of 70 mm, has proven to be less cost-effective with a 16 to 18 year payback period, whereas window replacements with windows having lower U -values require more than 40 years to amortize the initial investment. For the middle dwelling, the most cost-effective measure is the roof insulation, followed by the wall insulation and horizontal overhangs. Window replacement with thermally improved windows is also the least effective measure, needing up to 80 years to amortize the initial investment cost.

3.4 Optimised nZEB Refurbishment Scenario

From the evaluation of the energy and cost-effectiveness results of the different energy-conservation measures applied to the building envelope, it was considered necessary to develop an alternative nZEB scenario for the houses which aims at maximising the effectiveness of the refurbishment both in terms of energy savings and payback period. The scenario included installation of insulation on the roof and walls, achieving the same U -values as the standard nZEB scenario, and horizontal overhang [25] instalment in the south-facing windows. The replacement of windows with improved ones was not included in the optimized nZEB scenario owing to the economically non-viable investment cost related to them. The split units were replaced by ones of higher energy efficiency (A+++)

of PV panels was increased from the initial standard nZEB scenario from 3 to 12, amounting to 19.2 m^2 , which corresponds to the maximum permissible potential of 3 kW per dwelling [26].

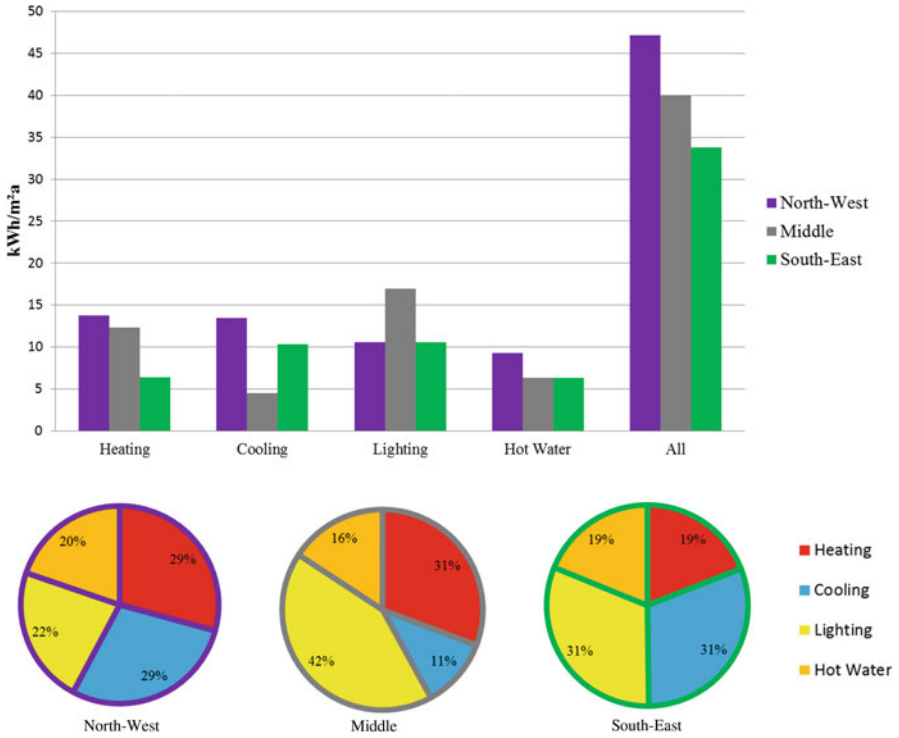
Using the aforementioned energy-conservation measures the dwellings were raised to A category. The calculated total primary energy consumption for the nZEB refurbishment scenario for the north-west dwelling was reduced to $135 \text{ kWh}/(\text{m}^2\text{a})$, for the middle dwelling to $115 \text{ kWh}/(\text{m}^2\text{a})$ and for the south-east dwelling to $99 \text{ kWh}/(\text{m}^2\text{a})$. The contribution of RESs, including solar thermal panels for DHW and PV panels on the roof, was $107 \text{ kWh}/(\text{m}^2\text{a})$ for the north-west, $80 \text{ kWh}/(\text{m}^2\text{a})$ for the middle and $113 \text{ kWh}/(\text{m}^2\text{a})$ for the south-east dwelling, covering 79.25, 70 and 114 % respectively of the total primary energy consumption. The south-east dwelling therefore was converted to one of positive energy.

The total final energy consumption was reduced to $47.13 \text{ kWh}/(\text{m}^2\text{a})$ for the north-west dwelling, of which the energy consumption for heating was $13.78 \text{ kWh}/(\text{m}^2\text{a})$ and that for cooling was $13.46 \text{ kWh}/(\text{m}^2\text{a})$. The energy consumption for lighting and DHW was $10.58 \text{ kWh}/(\text{m}^2\text{a})$ and $9.31 \text{ kWh}/(\text{m}^2\text{a})$ respectively. The total final energy consumption for the middle dwelling was $40.06 \text{ kWh}/(\text{m}^2\text{a})$, of which the energy consumption for heating was $12.32 \text{ kWh}/(\text{m}^2\text{a})$ and that for cooling was $4.51 \text{ kWh}/(\text{m}^2\text{a})$. The lighting and DHW energy consumption was $16.92 \text{ kWh}/(\text{m}^2\text{a})$ and $6.31 \text{ kWh}/(\text{m}^2\text{a})$ respectively. The total final energy consumption for the south-east house was $33.77 \text{ kWh}/(\text{m}^2\text{a})$, of which the energy consumption for heating was $6.43 \text{ kWh}/(\text{m}^2\text{a})$ and that cooling was $10.38 \text{ kWh}/(\text{m}^2\text{a})$. The lighting and DHW consumption was $10.60 \text{ kWh}/(\text{m}^2\text{a})$ and $6.36 \text{ kWh}/(\text{m}^2\text{a})$ respectively. The energy consumption of the dwellings after the optimized nZEB refurbishment is presented in Graph 21.5.

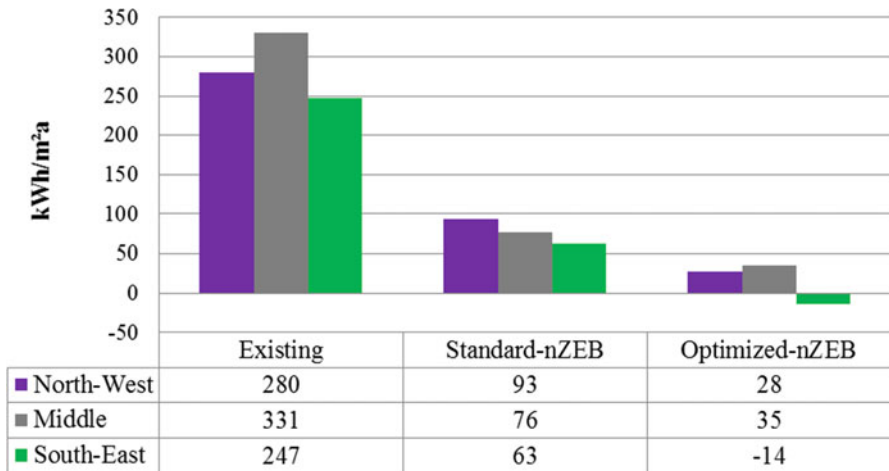
3.5 Comparison of nZEB Scenarios with Existing Condition of Building

The north-west, middle and south-east dwellings in their existing state annually consume $287 \text{ kWh}/(\text{m}^2\text{a})$, $338 \text{ kWh}/(\text{m}^2\text{a})$ and $254 \text{ kWh}/(\text{m}^2\text{a})$ respectively and emit $82.46 \text{ kg}/(\text{m}^2\text{a})$, $97.27 \text{ kg}/(\text{m}^2\text{a})$ and $72.71 \text{ kg}/(\text{m}^2\text{a})$ of carbon dioxide. After the standard nZEB refurbishment, the dwellings' yearly consumption was reduced by 72 % for the north-west, 70 % for the middle and 62 % for the south-east, whereas the corresponding reduction after the optimized nZEB scenario was carried out was 53 %, 66 % and 61 % respectively (Graph 21.6). The CO_2 emission reductions after the simulations was calculated to be 67 % for the north-west, 75 % for the middle and 74 % for the south-east dwelling for the standard nZEB refurbishment and 90, 90 and 105 % respectively for the optimized nZEB refurbishment.

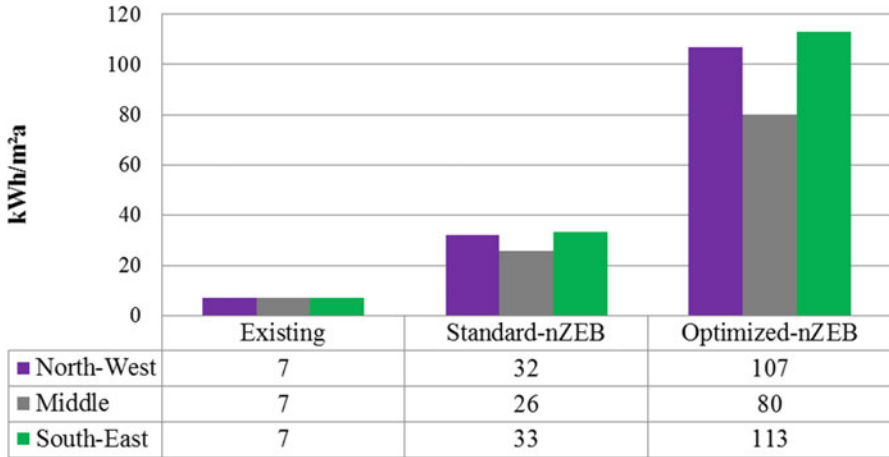
The operational annual costs of the north-west, middle and south-east dwellings in their existing state were € 4704, € 5560 and € 4149 respectively. After the standard nZEB refurbishment the operational costs were reduced to € 1562 for the



Graph 21.5 Energy consumption of dwellings after optimized nZEB refurbishment



Graph 21.6 Comparison of total energy consumption of dwellings



Graph 21.7 Comparison of RES contribution (kWh/m²a)

north-west, € 1276 for the middle and € 1058 for the south-east dwelling, whereas in the optimized nZEB scenario they were reduced to € 470 for north-west and € 588 for the middle dwelling, while for the south-east dwelling, owing to the surplus production of electricity from the PVs, the dwelling has yearly gains of € 235 from supplying electricity to the grid.

Therefore, the payback periods for the standard nZEB scenario are 8 years for the corner dwellings and 4 years for the middle. These were reduced to 5 years for the corner dwellings and 3.5 years for the middle dwelling with the application of the optimized nZEB scenario, which presents significant advantages regarding cost-effectiveness compared with the standard scenario.

Taking into consideration that the payback period will be greater after a loan, since the cost to refurbish terrace family houses into nZEBs exceeds the annual income of the average household [27] and the actual amount of money spent on air conditioning the houses is significantly less [28] than the expenses calculated by the iSBEM-cy tool, leading to an even longer payback period and smaller savings, the lower payback period of the optimized nZEB scenario is even more impactful (Graph 21.7).

4 Conclusions

This study was carried out to determine the overall economic viability of the refurbishment of terrace family houses with respect to achieving nearly zero-energy buildings and to evaluate the effectiveness of the energy-conservation measures related to the upgrading of the energy performance of the envelope,

in terms of energy savings and cost-effectiveness. The results indicate that the refurbishment of three terraced dwellings (representative of existing dwellings of this typology in Cyprus) into nZEBs, as defined by Directive 366/2014, is financially viable, with a payback period of 8 years for the corner dwellings (north-west and south-east) and 4 years for the middle dwelling, when the full sum for the investment is paid immediately upon completion, without the need of a loan.

The payback period will be greater when a loan is made, and the lower initial energy costs of the dwellings, as mentioned, making the standard nZEB refurbishment scenario a less attractive option.

The study leads to the conclusion that the most cost-effective measures for the corner dwellings are to install horizontal overhangs, followed by roof insulation. In contrast, for the middle dwelling, the horizontal overhangs are less cost-effective than the wall insulation owing to the greater wall surface of the dwelling compared with its window surfaces. Furthermore, it was found that when a house already has double glazed windows, their replacement with those having lower U -value does not render it cost-effective, resulting in negligible energy savings.

An alternative refurbishment scenario, which incorporates RESs with a larger PV panel area, results in a shorter – by 3 years – payback period for the corner dwellings and by half a year for the middle one, highlighting the role of PVs in the Mediterranean region. CO₂ emissions were reduced by 90 % for the corner housing unit and by 105 % in the middle house.

The results pointed to the drawbacks of the minimum requirements towards nearly zero-energy houses, as drafted by the Cyprus government, especially the replacement of windows, which is obligatory under the directive. This is a result of the low window U -values (2.25 W/m² K) proposed by the directive, which are the same for all typologies and chronological periods of houses and do not take into consideration the high cost associated with their replacement. Window replacement accounts for up to 36 % of the total investment and does not bring about proportional savings on total energy consumption. In contrast, the installation of shading devices presents both an energy-effective and economically viable choice, although not included in the requirements according to Directive 366/2014.

Therefore, the cost-effectiveness of the different refurbishment measures on the building envelope and the high amounts of energy produced from PV systems must be taken into consideration and redirect the definition of nZEBs in Cyprus to a more flexible and cost-effective choice in order to implement a more feasible option for the refurbishment of old houses.

For methodological reasons associated with the energy classification software used (iSBEM_{cy}), the dwellings were considered independently. For future investigations it would be interesting to study the energy efficiency and cost-effectiveness of the refurbishment measures for the energy improvement of the entire block.

References

1. Economidou M, Atanasiu B, Despret C, Maio J, Nolte I, Rapf O (2011) Europe's buildings under the microscope. A country-by-country review of the energy performance of buildings. Buildings Performance Institute Europe (BPIE), Bruxelles
2. NATO Science Series (2005) Thermal energy storage for sustainable energy consumption. Fundamentals, case studies and design, vol 234, pp Preface–ix
3. European Commission. http://europa.eu/pol/ener/flipbook/el/files/energy_el.pdf
4. Konstantinou T, Knaack U (2013) An approach to integrate energy efficiency upgrade into refurbishment design process, applied in two case study buildings in Northern European Climate. *Energy Build* 59:301–309
5. The Directive 2010/31/EU of the European Parliament and of the Council of 19 May 2010 on the energy performance of buildings (2010) Official J Eur Union 53
6. EU2020 Energy targets. http://ec.europa.eu/europe2020/pdf/themes/16_energy_and_ghg.pdf
7. Ministry of energy, K.Δ.Π. 366/2014. <http://www.mcit.gov.cy/mcit/mcit.nsf/0/Directive366/2014.pdf>. Accessed 22 Mar 2015
8. Marszal AJ, Heiselberg P, Bourrelle JS, Musall E, Voss K, Sartori I, Napolitano A (2011) Zero energy building—a review of definitions and calculation methodologies. *Energy Build* 43 (4):971–979
9. Serghides DK, Georgakis C (2012) The building envelope of mediterranean houses—optimisation of mass and insulation. *J Build Phys* 36(1):83–98
10. Morelli M et al (2012) Energy retrofitting of a typical old Danish multi-family building to a “nearly-zero” energy building based on experiences from a test apartment. *Energy Build* 54 (2012):395–406
11. Adhikari RS et al (2012) Net zero energy buildings: expense or investment? *Energy Procedia* 14:1
12. Konstantinou T, Knaack U (2011) Refurbishment of residential buildings: a design approach to energy-efficiency upgrades. In: *Procedia engineering*, pp 666–675
13. Serghides DK, Saboohi N, Koutra T, Kafatygiotou MC, Markides M (2014) Energy efficient refurbishment of existing buildings: a multiple case study of terraced family housing. In: *Proceeding of WREC 2014*, University of Kingston, London, 3–8 August 2014
14. Article in Greek: Δ.Κ. Σεργίδου, Μ.Α. Μαρκίδου & Μ.Καταφυγιώτου, Κατοικίες Συνεχούς Δόμησης με Σχεδόν Μηδενική Ενεργειακή Κατανάλωση. 10th National conference for renewable energy sources, Thessaloniki, 26–28 November 2014
15. Serghides DK, Al E (2014) Sustainable and low energy buildings: a case study for the Cyprus multi storey residential buildings. *International Congress Energy and the Environment*, 24th Scientific Conference on Energy and the Environment, Opatija, 22–24 October, 2014, pp 211–224
16. Typology of the building stock in Cyprus (2012) Statistical Service of Cyprus. Publication of Census 2011
17. IEE EPISCOPE Cyprus. <http://episcope.eu/building-typology/country/cy/>. Accessed 29 May 2015
18. IEE EPISCOPE project. <http://episcope.eu/index.php?id=97>. Accessed 25 May 2015
19. IEE EPISCOPE typology brochure. http://episcope.eu/fileadmin/tabula/public/docs/brochure/CY_TABULA_TypologyBrochure_CUT.pdf. Accessed 28 May 2015
20. Ministry of Energy, cost optimal tool (software). http://www.mcit.gov.cy/mcit/mcit.nsf/All/Cost_optimal_tool/OpenDocument. Accessed 28 May 2015
21. Ministry of Energy, iSBEM cy tool. <http://www.mcit.gov.cy/mcit/mcit.nsf/All/E074577C58AD9EFCC22575B60047BEA8?OpenDocument>. Accessed 15 May 2015
22. Directive 2002/91/EC of the European Parliament and of the Council of 16 December 2002 on the energy performance of buildings. <http://eur-lex.europa.eu/legal-content/EN/TXT/?uri=CELEX:32002L0091>. Accessed 30 May 2015

23. Data hub for the energy performance of the buildings. http://bpie.eu/uploads/lib/document/attachment/128/BPIE_factsheet_nZEB_definitions_across_Europe.pdf. Accessed 20 May 2015
24. Serghides DK (2009) Optimisation of insulation on mediterranean houses. *ISESCO Sci Technol Vision* 5(8):79–83
25. Ministry of Public Works. [http://www.moi.gov.cy/moi/moi.nsf/all/BBB599BE73734EA8C2257A91003393FC/\\$file/entoli%202-2011.dated%2017.7.2013.pdf?](http://www.moi.gov.cy/moi/moi.nsf/all/BBB599BE73734EA8C2257A91003393FC/$file/entoli%202-2011.dated%2017.7.2013.pdf?) Accessed 30 May 2015
26. Cyprus Electricity Authority, net metering. <https://www.eac.com.cy/EL/EAC/RenewableEnergySources/Documents/netmetering.pdf>. Accessed 20 May 2015
27. Cyprus Statistical Service, population condition. http://www.mof.gov.cy/mof/cystat/statistics.nsf/populationcondition_25main_gr/populationcondition_25main_gr?OpenForm&sub=5&sel=2. Accessed 10 May 2015
28. Cyprus statistical service, household energy consumption. [http://www.mof.gov.cy/mof/cystat/statistics.nsf/All/D548CFD3B755064CC225792000317B59/\\$file/ENERGY_CONSUMP_HH-2009-EL-051011.xls?OpenElement](http://www.mof.gov.cy/mof/cystat/statistics.nsf/All/D548CFD3B755064CC225792000317B59/$file/ENERGY_CONSUMP_HH-2009-EL-051011.xls?OpenElement). Accessed 15 May 2015

Chapter 22

Geo-Climatic Applicability of Direct Evaporative Cooling in Italy

Giacomo Chiesa, Fabio Aquiletti, and Mario Grosso

Abstract This chapter focuses on the climatic applicability of passive direct (downdraught) evaporative cooling (PDEC) techniques in the provincial capital cities of Italy. First, a PDEC potentiality map was produced using a previously developed method based on three variables: wet bulb depression, summer comfort air temperature threshold (25 °C) and cooling degree hours (CDHs). Second, an applicability map was produced by comparing the PDEC potentiality map to the local cooling energy demand. Third, a new method is presented including a calculation of the residual local cooling energy demand, i.e. residual CDH, related to air treatment by direct evaporative cooling. These residual CDH values were calculated considering different step-wise increasing outlet temperatures (WBT; WBT + 1 °C; ...; WBT + 5 °C) as a function of the covered amount of wet bulb depression. Finally, three cities chosen as being representative of their respective Italian climatic macro-zones were selected in order to assess in greater detail the yearly variation of CDH aimed at supporting specific design strategies for ventilative passive cooling solutions.

Keywords Climatic applicability • Direct evaporative cooling • Passive cooling • GIS analysis

Nomenclature

WBT	Wet bulb temperature
DBT	Dry bulb temperature
dWBT	Wet bulb depression
CDH	Cooling degree hours
ext	External
int	Internal
T _{set}	Set-point temperature

G. Chiesa (✉) • F. Aquiletti • M. Grosso
Department of Architecture and Design—DAD, Politecnico di Torino, Viale Mattioli 39,
Turin 10125, Italy
e-mail: giacomo.chiesa@polito.it

$T_{c,a}$	Temperature of comfort for adaptive model
$T_{ext,a}$	External running mean temperature
ϕ	Humidity rate [%]
X	Water vapour in mass unit of dry air [kg/kg]
PDEC	Passive direct (downdraught) evaporative cooling

1 Introduction

Energy consumption for air conditioning is a rising concern in the national energy balances of several countries, influencing the cost of electricity and the need for more power plants [1, 2]; in addition, it spurs increases in CO₂-equivalent emissions, a factor in global warming [3]. As stated by the European Union Directive EPBD 2010/31/EU for nearly zero-energy building and considering future perspectives on net-positive-energy buildings, it is essential to develop and diffuse alternative technologies for cooling based on passive and hybrid solutions. Recent studies report that passive direct evaporative cooling (PDEC) towers could be applied to the majority of European building stocks [4, 5] – more than 70% – and cover from 25 to 85% of the cooling energy load depending on local climatic conditions [4]. Hence, evaporative cooling seems to be a suitable solution for guaranteeing indoor thermal comfort, especially in southern Europe [6].

Recently, several studies have mapped the climatic applicability of PDEC techniques in Europe [6], Spain [4, 6] and China [7] and the suitability of evaporative air conditioning [8]. Following these examples, this chapter aims at analysing the suitability of PDEC techniques in Italy for achieving comfort conditions through the following steps. First, an already consolidated methodology used in [4, 6, 7] is applied to map the performance of PDEC systems as a function of new hourly typical meteorological year (TMY) data recently elaborated by the Italian Thermo-technical Committee (Comitato Termotecnico Italiano) (CTI) in Italian provincial capital cities [9]. This database considers recent climatic variations showing large differences with other climatic sources (ASHRAE and the data collection “Gianni De Giorgio”) [10]. Second, a new method is proposed for evaluating PDEC performance as a function of residual cooling energy demand, expressed by the parameter residual cooling degree hours (CDHs), dependent on varying a PDEC system’s outlet air temperature. This method seems to be more effective in assessing the performance of PDEC systems in temperate climate zones, which are often characterised by a medium-low applicability of PDEC systems. Third, cooling energy demand is estimated for the reference locations against a fixed comfort air temperature threshold value (25 °C). Finally, three cities chosen as being representative of respective different Italian climate macro-zones (Turin for the northern zone, Rome for the central one, and Palermo for the southern one) are analysed in greater detail by studying the yearly distribution of CDHs and the performance of a PDEC system as a function of wet-bulb-depression.

2 Geo-Climatic Potentiality of Passive Direct Evaporative Cooling in Italy

Italy, with a territory lying between 35° and 47° northern latitude, is characterised by a wide range of climatic conditions. These conditions are affected by the presence of the Mediterranean Sea surrounding Italy's boundaries along more than three-quarters of their length as well as by the country's orography: the Alps chain in the north ranging from east to west and the Apennine Mountains crossing Italy from north to south. According to Köppen's classification, Italian climate types include Mediterranean, mild Mediterranean, humid subtropical, suboceanic, humid continental, cold continental and tundra (alpine territories). For this reason, even if the Italian climate could be generally classified as temperate, the applicability of passive and natural cooling techniques presents different potentialities throughout Italy's territory. This chapter analyses the Italian climatic applicability of PDEC systems based on the division of its territory in the provinces; hence there is no direct link to Köppen's classification. Each province is represented by the climate characteristics of its capital city, for which it is possible to use the hourly TMYs produced by CTI (2012–2014) based on directly monitored data. The geo-climatic PDEC applicability in locations other than a provincial capital city can be assessed by interpolating climatic data of the two nearest capital cities, as described in [9].

As reported in [11], the evaporative cooling potential, when long-term local climatic conditions are known and required comfort temperatures from the evaporative system are established, can be estimated using one or more of the following indicators:

- Yearly availability of PDEC cooled air achieving the desired comfort conditions;
- Average monthly temperature of cooling [air for direct evaporative cooling (DEC) and water for indirect cooling];
- Analysis of periods during which PDEC is unavailable, such as periods with high humidity or too hot conditions.

Furthermore, the cooling potential of evaporative cooling systems, without using pretreatment (e.g. dehumidification), is a function of the outdoor wet bulb temperature (WBT), which is the theoretical temperature limit that could be reached with a DEC system, and of the wet bulb temperature depression [dWBT, calculated from the difference between the dry bulb temperature (DBT) and the WBT]. In [11, 12] it is estimated that the outlet temperature from a PDEC system could be approximately 3 °C above the WBT, while in [13] it is suggested that this value be calculated by increasing the ambient WBT by 20–30 % of the dWBT. However, it is possible to use these considerations for estimating outlet temperatures from a PDEC system. Paragraph 3 shows the reduction potential in cooling demand with PDEC.

In this section, the method described in [4, 6, 7] is used. This compares cooling demand, opportunity and potential for using evaporative cooling. This method could be summarised as follows:

- Mapping the potential of PDEC systems ($DBT_{ext} - WBT_{ext}$, which corresponds to the wet bulb depression), the WBT was calculated using [14];
- Mapping the applicability of PDEC for reducing the cooling demand ($DBT_{int} - WBT_{ext}$, where the internal DBT is the comfortable indoor summer temperature, considered to be 25 °C);
- Drawing up a potentiality map of PDEC application, calculated by overlapping the two previous maps;
- Calculating cooling needs using CDHs [7] or the average difference of DBT indoor comfort temperature [5];
- Integrating the previous points in a synthetic map to evaluate the potentiality of PDEC according to cooling needs.

2.1 Potentiality Map of PDEC Application

The geo-climatic, that is site-dependent, potential of PDEC systems for reducing cooling demand in summer (June–August) was represented by a PDEC potentiality map (Fig. 22.1), which illustrates a classification of the average hourly wet bulb depression in Italy by four zones with the boundaries defined in [6] and dividing zone 3 into two subclasses. Figure 22.2 shows a classification of the average hourly difference between the indoor comfort cooling temperature (25 °C) and external WBTs for each Italian provincial capital city (four classes divided as defined in [6]). The Italian dWBT is principally characterised by low and medium values, while the difference between comfort and wet bulb temperatures are medium-high.

Overlapping the PDEC potentiality maps of Figs. 22.1 and 22.2, a potential PDEC applicability map for each reference province is drawn as shown in Fig. 22.3, which represents a range of classes from very low to very high potentiality. The categories of PDEC potentiality are assumed from the literature [6], with some differences as summarised in Table 22.1.

The PDEC potentiality map of Fig. 22.3 shows a prevalence of very low values, especially in northern Italy and near the coast, while low and medium conditions are distributed in the centre and in the south. Both Sardinia and Sicily are characterised by medium-low levels of potentiality.

2.2 Cooling Degree Hours and PDEC Potential

Although the PDEC potentiality map shown in Fig. 22.3 is not related to local cooling energy demand, it is possible to draw an analogous map where the PDEC potential applicability is calculated as a function of CDH based on 25 °C as an

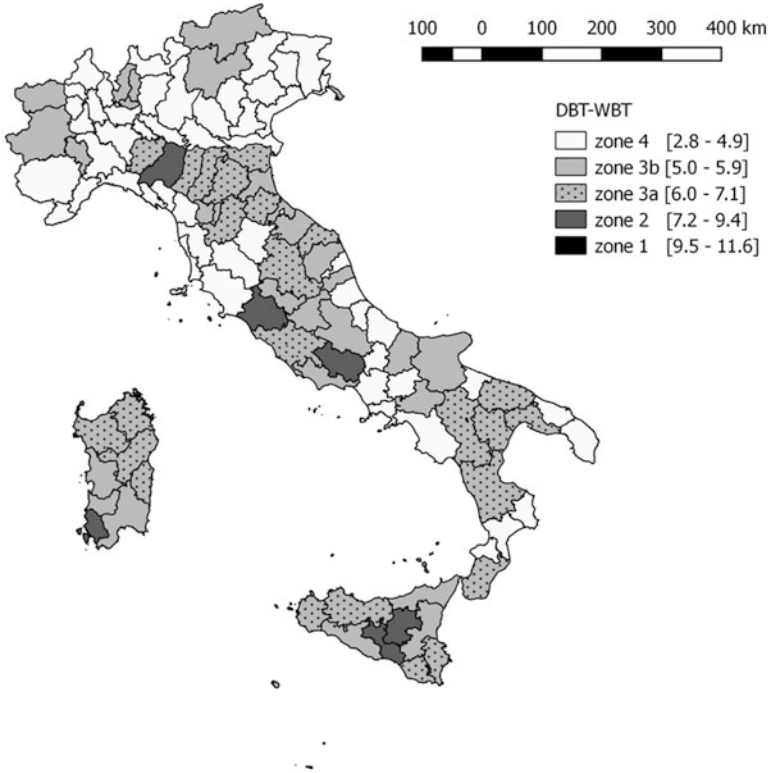


Fig. 22.1 Map of potential applicability zones of PDEC using as indicator the average hourly wet bulb depression

upper comfort limit for indoor air temperature. It is also possible to use the average difference in air temperature between local DBT and the set-point temperature for cooling, as reported in [6]. CDH data are calculated, for each reference location, using the following equation:

$$CDH = \sum (DBT - 25) \quad \text{for positive values.} \quad (22.1)$$

Results are shown in Fig. 22.4 and organised into five classes. Furthermore, Zone 1 (no need for cooling) is divided into two subclasses.

It is possible to assume 1000 CDHs as the minimum threshold for generating a demand for cooling [6]. As shown in Fig. 22.4, only three Italian provincial cities do not reach this limit, while the 33.6 and the 52.8% show respectively a low and medium cooling energy demand.

The potential of PDEC systems could be estimated overlapping the potentiality map of Fig. 22.3 on the CDH map (Fig. 22.4). This resulting new map (Fig. 22.5) uses the classification presented in Table 22.2.

In particular, in the specific Italian conditions, Fig. 22.5 differs from Fig. 22.3 only in a few cases, showing good compatibility between PDEC potentiality and

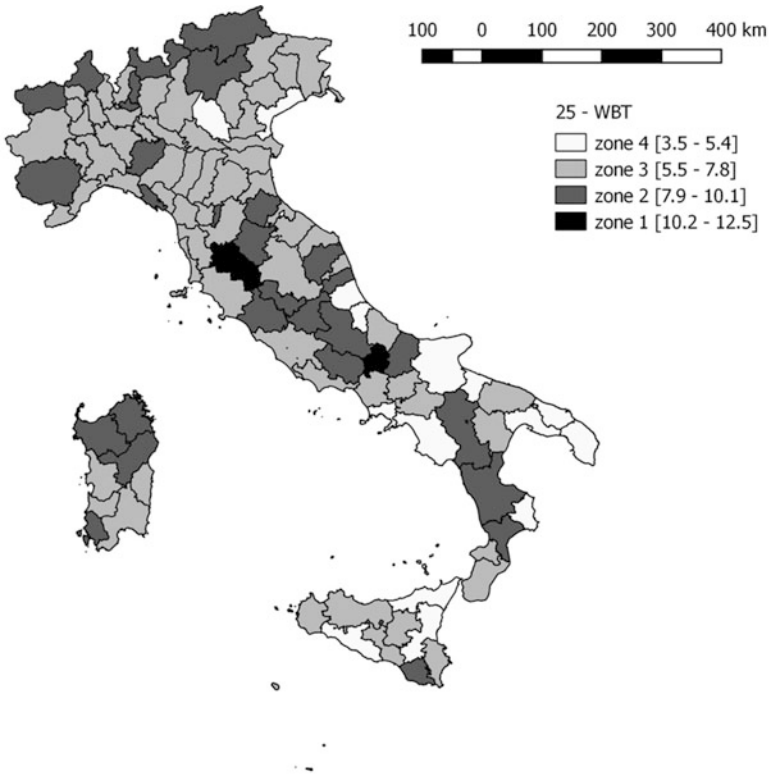


Fig. 22.2 Map of potential applicability zones of PDEC using as indicator the difference between indoor DBT set to 25 °C (as comfort reference) and outdoor WBT

cooling energy demand. To better analyse the geo-climatic applicability of PDEC systems, it is possible to use a new method based on the reduction in CDHs due to PDEC, as described in the following pages.

3 Cooling Energy Demand Reduction from PDEC Systems

3.1 *PDEC Quantitative Potential in Reducing Cooling Demand*

To assess in a quantitative way the PDEC potential in reducing the cooling energy demand in locations with low or medium applicability as shown in Fig. 22.5, the theoretical limit of the outlet air temperature from a PDEC system needs to be calculated. This is the WBT, even if, generally, the outlet value is some degrees above this limit [13, 15]. It is possible to estimate that, after a DEC treatment, the

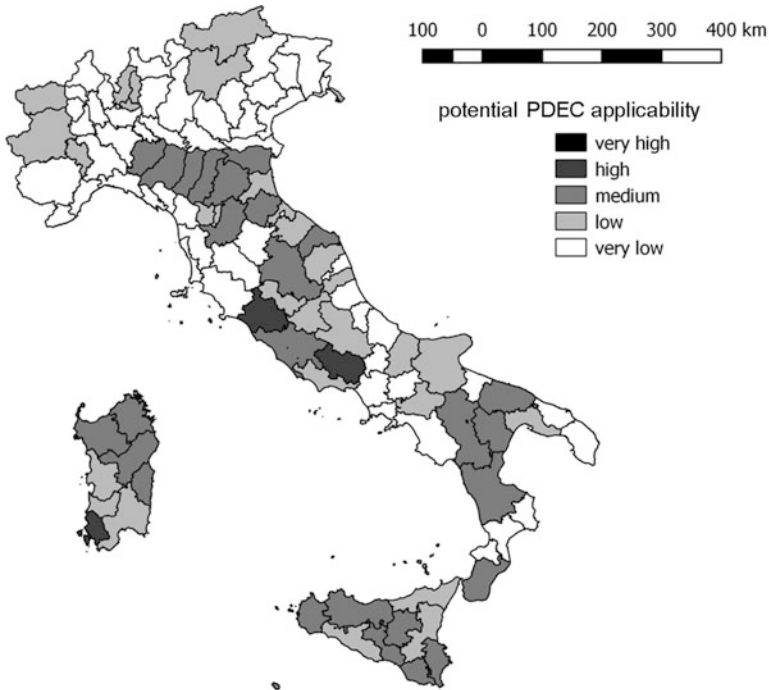


Fig. 22.3 Map of potential PDEC applicability by a classification based on method presented in [6]

Table 22.1 Categories of PDEC potentiality used for Fig. 22.3 (elaborated from [6])

		25-WBT			
		Zone 1 [10.2–12.5]	Zone 2 [7.9–10.1]	Zone 3 [5.5–7.8]	Zone 4 [3.1–5.4]
dWBT	Zone 1 [9.5–11.6]	Very high	Very high	Very high	High
	Zone 2 [7.2–9.4]	High	High	Medium	Medium
	Zone 3a [6.0–7.1]	High	Medium	Medium	Low
	Zone 3b [5.0–5.9]	Medium	Low	Low	Low
	Zone 4 [2.6–4.9]	Very low	Very low	Very low	Very low

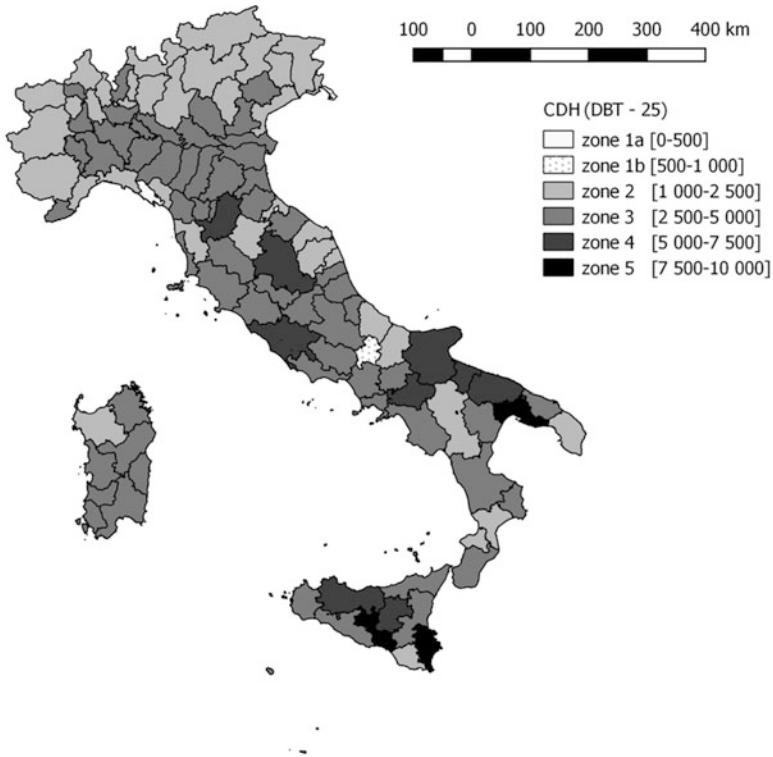


Fig. 22.4 CDH geographical classification for Italian provincial capital cities (TMY database elaborated by CTI) considering a comfort set-point temperature of 25 °C

outlet temperature will be $WBT + n$. In that sense, it is possible to define the residual cooling energy demand of a locality, for $T_{set} = 25$ °C, as the sum for positive values of the hourly difference $WBT + n - 25$, where $dWBT$ is greater than n , and using Eq. (22.1) for other hours. This value could be used to identify the number of CDHs that could not be covered only by the PDEC system. Since this chapter focuses on climatic applicability, no specific building will be taken into account, only the change in residual cooling demand at different values of n . These values could be considered an inverse feasibility of PDEC in reducing cooling demand. In fact, where the residual CDH value for a given n is zero, theoretically no additional cooling is needed. Obviously, this value must be reconsidered when a specific building is taken into account. We defined the n domain as $\{0; 1; 2; 3; 4; 5\}$. For values $n = 3$ (Fig. 22.6) and $n = 5$ (Fig. 22.7) a map of residual CDH₂₅ was produced showing that evaporative cooling is a sufficient technology for meeting the cooling demand in many Italian provincial capital cities. In particular, in Fig. 22.6 only eight provinces show a residual cooling demand that outperforms 1000 CDH, and in any case these values never reach Zone 3. Of course, in those provinces where there is a residual demand in cooling, different techniques must be

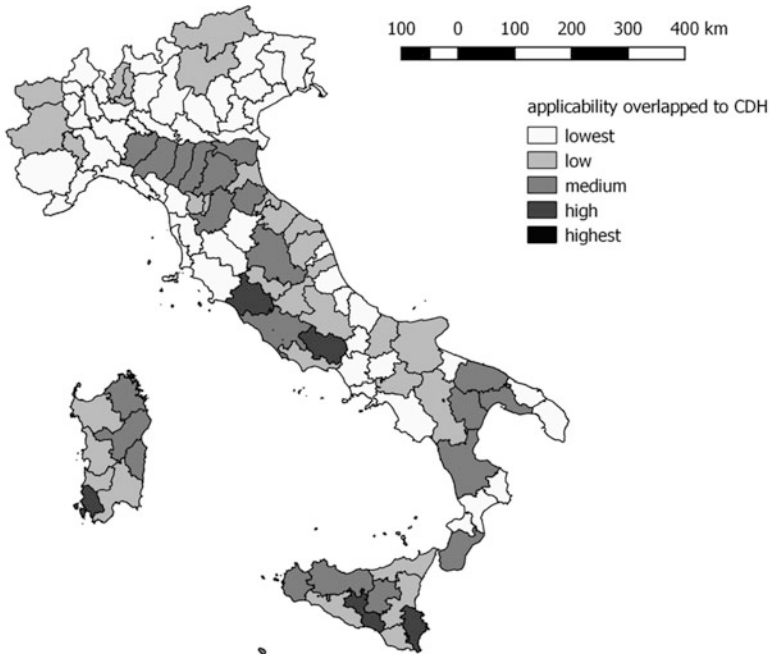


Fig. 22.5 Map of PDEC potentiality zones by overlapping Figs. 22.3 and 22.4

Table 22.2 Matrix of CDH and PDEC potentiality classification used in Fig. 22.5

		CDH				
		[0–1 k]	[1–2.5 k]	[2.5–5 k]	[5–7.5 k]	[7.5–10 k]
Potentiality of intervention	Very high	Lowest	High	Highest	Highest	Highest
	High	Lowest	Medium	High	High	Highest
	Medium	Lowest	Low	Medium	Medium	High
	Low	Lowest	Low	Low	Low	Medium
	Very low	Lowest	Lowest	Lowest	Lowest	Low

considered, even if this calculus is based on a fixed comfort temperature and not on an adaptive situation.

Figure 22.7 illustrates that, even if PDEC systems do not attain a good efficiency (WBT + 5), the cooling demand is reduced in all Italian provincial capital cities. A residual cooling demand is evident in some provinces. A comparison with Fig. 22.2 shows that with low 25-WBT values, PDEC systems are effective only at high performance levels.

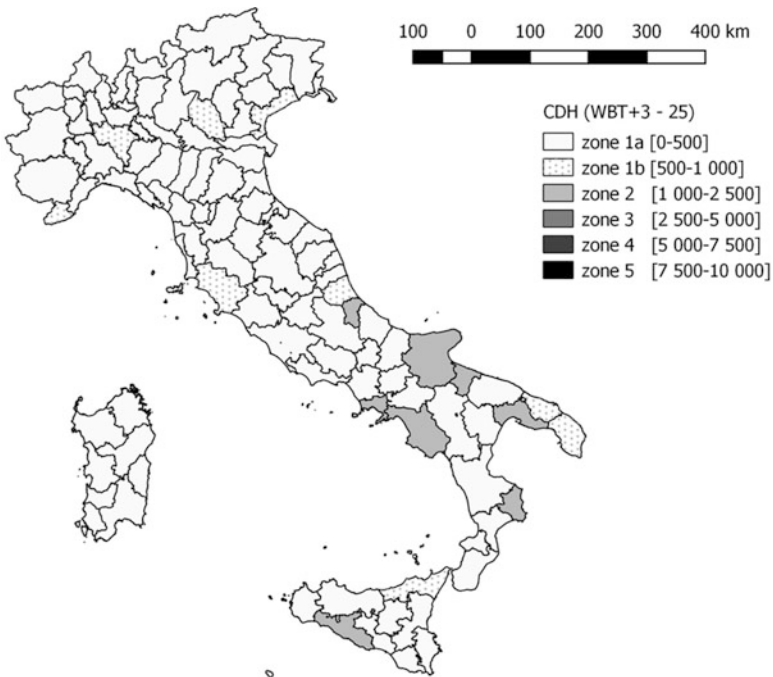


Fig. 22.6 Residual CDHs (comfort set to 25 °C) of Italian provincial capital cities when outlet temperatures from PDEC systems reach WBT+3 (when $dWBT \leq 3$ CDHs are calculated using DBT)

Looking at these figures, it is possible to state that downdraught PDEC systems could represent a very appealing solution for cooling in the Italian climate because of the difference between the CDH values based on DBT and on $WBT + n$. In any case, where the values reported in Fig. 22.2 are low (Zones 3 and 4), a possible residual cooling demand is expected. It is also possible to use a different approach that defines the residual cooling demand as a function of the covered percentage of the wet bulb depression. Nevertheless, this approach is more effective when specific PDEC systems are taken into account [15].

4 Climatic Analysis (Turin, Rome and Palermo)

To analyse in greater detail the Italian climate, three cities were selected (Turin, Rome and Palermo). Their localisations follow the Italian peninsula and represent three different typical climatic conditions. Analyses are based on four main

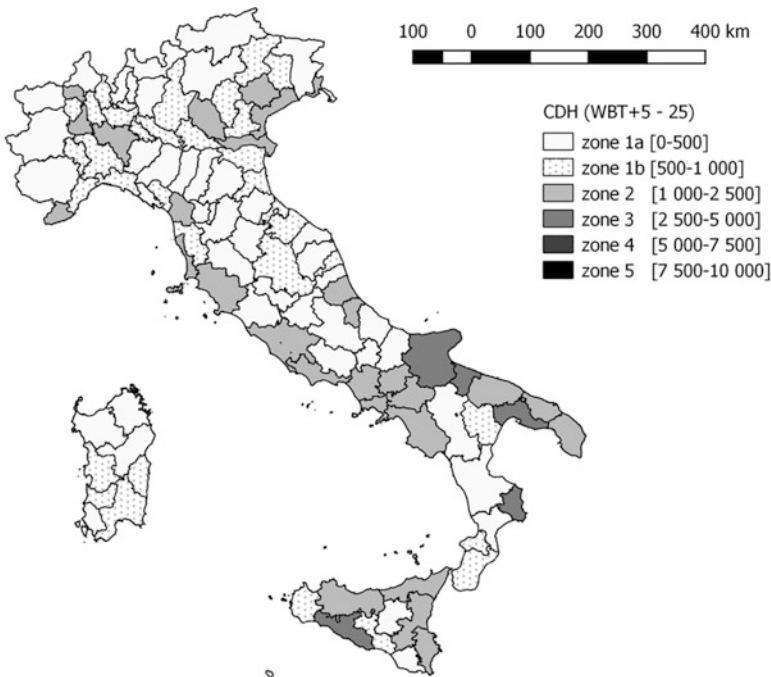


Fig. 22.7 Residual CDHs (comfort set to 25 °C) of Italian provincial capital cities when outlet temperatures from PDEC systems reach WBT+5 (when $dWBT \leq 5$ CDHs are calculated using DBT)

elaborations, described in what follows, which refer to a summer period (1 June–31 August).

Figure 22.8 was used to represent the hourly distribution of required air-temperature degrees for cooling (set point = 25 °C) in relation to the whole number of hours in the considered period. This division helps in analysing the CDH distribution and its hourly consistency. Figure 22.9 divides the percentage of hours in which cooling is and is not required if the comfort condition is set to 25 °C. In this figure different levels of $WBT + n$ are compared (set of n equal to {0;1;2;3;4;5}). The last column is based on the DBT and for this reason corresponds to the benchmark.

Turin is the capital of the Piedmont region; it is classified in Zone 3b in Fig. 22.1 and in Zone 3 in Fig. 22.2. For these reasons it shows a low PDEC applicability in Fig. 22.3, confirmed by overlapping the CDHs (Fig. 22.5). Cooling demand is principally due to a low CDH hourly demand, which affects one third of the summer hours. By using PDEC the cooling requirements can be reduced to only 99 CDHs if the treated air reaches a $WBT + 3$ temperature. This contrasts with the

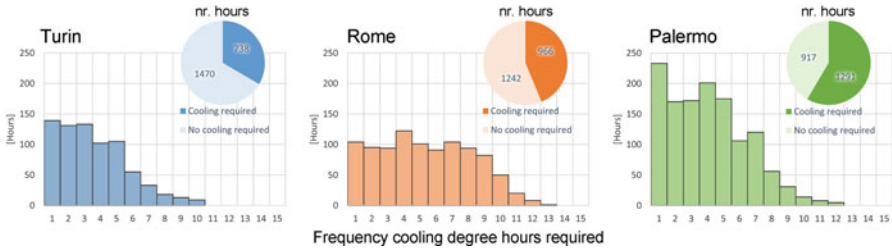


Fig. 22.8 Hourly distribution of required air-temperature degrees for cooling (set point equal to 25 °C) in Turin, Rome and Palermo (June–August)

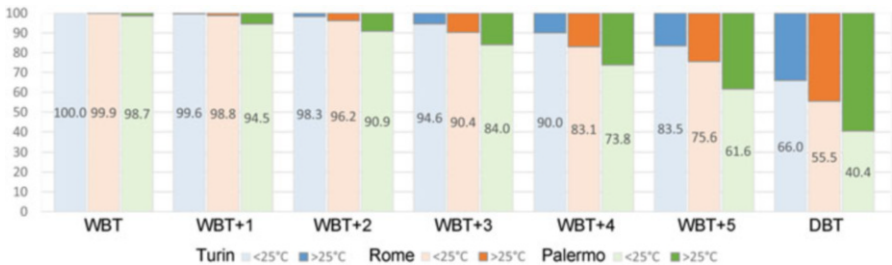


Fig. 22.9 Percentage of hours in which cooling is/is not required (June–August) in Turin, Rome and Palermo comparing the effect of different WBT + n outlet temperatures with benchmark based on DBT (comfort condition set to 25 °C)

traditional CDH at 25 °C that reaches 2433. For this reason, in similar climatic conditions, evaporative cooling can be a good cooling solution.

Rome is the Italian capital; it is classified in Zone 3a in Fig. 22.1 and in Zone 3 in Fig. 22.2. It is characterised by a high CDH value (Fig. 22.4) and a medium applicability of PDEC in both Figs. 22.3 and 22.5. Cooling demand is homogeneous from 1 to 9 °C/h (Fig. 22.8) with a low and medium CDH/h intensity that affects approximately 44 % of summer hours. Considering WBT + 3 temperatures, the residual cooling requirement is 243 CDHs (no cooling demand), but 1082 for WBT + 5. If a psychrometric analysis is considered, only a few hours are not included in the comfort DEC boundary. For these reasons in similar climatic conditions, evaporative cooling can be a good cooling solution, even if PDEC technologies must be correctly designed.

Palermo, the capital of the Sicily region, is classified in Zone 3a in Fig. 22.1 and in Zone 3 in Fig. 22.2. It is in Zone 3 in Fig. 22.4 and is characterised by a medium PDEC applicability (Figs. 22.3 and 22.5). The climate of Palermo seems to be similar to that of Rome, but its cooling demand consistency is characterised by a very high frequency between 1 and 5 °C/h (Fig. 22.8). Cooling is required in 58.5 % of summer hours. DEC results in a good applicability with WBT + 3, but it is not sufficient for WBT + 5. From a psychrometric point of view, several values are not

included in the general comfort DEC boundary, although PDEC solutions could drastically reduce the need for cooling, as illustrated in Fig. 22.9.

5 Discussion and Conclusions

This chapter presented two different methodologies for evaluating the applicability of PDEC techniques. The Italian climate is characterised by medium CDH values, with a high potentiality for passive cooling solutions. Air could represent a good natural heat sink in many situations, as illustrated in [16]. In addition, evaporative cooling represents a good solution for several Italian provinces. Figures 22.6 and 22.7 demonstrate that PDEC solutions are able to meet the climatic cooling demand in the majority of Italian climatic conditions. Direct evaporative cooling can be used to attain a climatic comfort condition at 25 °C, even in those areas where the PDEC applicability is medium (Figs. 22.3 and 22.5). In some climatic conditions, there is a residual cooling demand, as illustrated in Figs. 22.6 and 22.7. In addition, the applicability of PDEC solutions in the three cities analysed in Sect. 4 is effective.

However, the presented analysis is geo-climatic and does not consider actual building conditions. These techniques are effective, both energetically and economically, but there is a lack of legislation, incentives and design tools to promote the use of the techniques.

References

1. Santamouris M (2007) Preface: why passive cooling? In: Santamouris M (ed) *Advances in passive cooling*. Earthscan, London, pp xix–xxxii
2. Unità centrale Studi e strategie dell'ENEA (2013) *Verso un'Italia low carbon: sistema energetico, occupazione e investimenti, Rapporto Energia e Ambiente. Scenari e strategie*, ENEA, Roma
3. European Commission (2010) *How to develop a sustainable energy action plan (SEAP)—guidebook*. Publications Office of the European Union, Luxembourg, p 63
4. Ford B, Schiano-Phan R, Francis E (eds) (2010) *The architecture & engineering of draught cooling*. A design sourcebook. PHDC Press, London
5. Moura R, Ford B (2003) *ALTENER FINAL REPORT. Part 1: market assessment of passive draught evaporative cooling in non-domestic buildings in southern Europe, final report*. ALTENER II project on solar passive heating and cooling. European Commission—DG Research
6. Salmeron JM, Sánchez FJ, Sánchez J, Alvarez S, Molina LJ, Salmeron R (2012) Climatic applicability of draught cooling in Europe. *Arch Sci Rev* 55(4):259–272
7. Xuan H, Ford B (2012) Climatic applicability of draught cooling in China. *Arch Sci Rev* 55(4):273–286. doi:10.1080/00038628.2012.717687
8. Bom GJ, Foster R, Dijkstra E, Tummers M (1999) *Evaporative air-conditioning: applications for environmental friendly cooling*. World Bank Technical Paper No. 421. Energy Series, Washington

9. Comitato Termotecnico Italiano (CTI) (2014) Hourly typical meteorological data for Italian Provincial Capital cities, in accordance with ENEA and Italian Ministry of economic development. <http://shop.cti2000.it/>
10. Chiesa G, Grosso M (2015) The influence of different hourly typical meteorological years on dynamic simulation of buildings. *Energy Procedia* 78:2560–2565
11. Costelloe B, Finn D (2003) Indirect evaporative cooling potential in air-water systems in temperate climates. *Energy Build* 35:573–591
12. Erell E (2007) Evaporative cooling. In: Santamouris M (ed) *Advances in passive cooling*. Earthscan, London, pp 228–261
13. Givoni B (1994) *Passive and low energy cooling of buildings*. Van Nostrand Reinhold, New York
14. Stull R (2011) Wet-bulb temperature from relative humidity and air temperature. *J Appl Meteorol Climatol* 50:2267–2269
15. Chiesa G, Grosso M (2015) Direct evaporative passive cooling of building. A comparison amid simplified simulation models based on experimental data. *Build Environ* 94:263–272. doi:10.1016/j.buildenv.2015.08.014
16. Chiesa G, Grosso M (2015) Geo-climatic applicability of natural ventilative cooling in the Mediterranean area. *Energy Build* 107:376–391. doi:10.1016/j.enbuild.2015.08.043i

Chapter 23

Integrating Deep Offshore Wind with Pumped Hydro Storage in a Central Mediterranean Archipelago's Electricity Generation System



Robert N. Farrugia, Tonio Sant, and Cedric Caruana

Abstract This investigation starts off with a hypothetical deep sea offshore wind turbine array consisting of twenty 5 MW NREL reference wind turbines for offshore deployment. Measure-correlate-predict techniques are utilised to transpose long-term measured wind data from a reference site located at an elevation of just under 220 m above mean sea level to a short-term 80 m wind-monitoring station close to sea level at a coastal location. The extrapolated long-term 80 m level wind speed and direction time series are then used as climatological inputs to a computational fluid dynamics software program that is used to generate wind resources over the extents of the hypothetical 100 MW offshore wind farm zone. Time series of wind speed, wind direction and power production are generated for the array covering a number of years, with the period being analysed here covering the years 2007–2011. Meanwhile, electrical load data on an hourly basis are also assessed in order to enable a wind power/pumped hydroelectric storage to electrical load interfacing exercise. The implications of combining a pumped hydroelectric storage system into the electrical system are assessed. The studies have shown that if the output from the wind farm is set to meet a fixed load threshold on a monthly basis, the surplus wind power can be used to pump water into the storage system. The stored potential energy can then be converted back to electricity by means of a water turbine in instances when wind power falls short of the set threshold. Such a system will

The updated online version of this chapter can be found at https://doi.org/10.1007/978-3-319-30746-6_78

R.N. Farrugia (✉) • T. Sant
Institute for Sustainable Energy, University of Malta, Triq il-Barrakki,
Marsaxlokk MXK 1531, Malta

Department of Mechanical Engineering, University of Malta, Msida MSD 2080, Malta
e-mail: robert.n.farrugia@um.edu.mt; tonio.sant@um.edu.mt

C. Caruana
Department of Industrial Electrical Power Conversion, University of Malta,
Msida MSD 2080, Malta
e-mail: cedric.caruana@um.edu.mt

decouple the renewable energy (RE) supply from the load and, with careful balancing of the stored hydraulic energy against the energy required to reach the threshold, supply a steady contribution to the load over a predetermined period of time. Such a steady contribution is highly desirable in an electrical system as a variable input coming from large-scale wind farms could cause grid imbalance, induce fluctuations and possibly compromise stability. The work has shown that the contribution of a wind farm coupled to a pumped hydroelectric system could contribute primarily to the base load whilst also allowing for green energy generation, facilitate the integration of RE technologies and help achieve part of Malta's RE targets.

Keywords Island • Deep offshore • Wind • Pumped hydroelectric storage

1 Introduction

Located in the central Mediterranean Basin, the Maltese islands have a relatively small land area of 316 km² and a high population density of 1325 persons/km² [1]. The islands' electricity generation infrastructure is presently oil-based, although there are plans to convert to a gas-based infrastructure [2]. Works to connect the islands' currently isolated electricity distribution network to that on mainland Europe by means of a sub-sea interconnector between Malta and Sicily are at an advanced stage [3]. Notwithstanding the islands' reasonable wind resources, the prospects for medium- and large-scale wind projects are challenged by local conditions. The limited size of the islands implies that multiple activities and stakeholders restrict development in an onshore, highly urbanised environment. Whilst a number of sites possessing reasonable wind resources do exist, these are not without their intrinsic barriers of a technical, social, economic or environmental nature. Only a few shallow-water sites and near-shore reefs exist. Although the marine territory is extensive, a plethora of stakeholders and environmental issues makes the development of offshore wind installations using proven technologies challenging [4–10].

The development of deep sea offshore wind turbine systems would extend the horizons as far as the technical potential of wind resources utilisation in the Mediterranean Sea is concerned. Going further offshore would reduce the impacts of the land shadow on wind flow patterns, thereby improving wind farm energy yield. Moreover, the impacts generally associated with near-shore wind projects would be mitigated, enabling much larger projects benefiting from economies of scale to be implemented. The less severe climatic conditions of the Mediterranean Sea are expected to counterbalance the lower wind speeds when compared to offshore sites in northern Europe.

Research at the University of Malta is focusing on the feasibility of offshore wind turbine installations in deeper waters. A recent local study looked into the technicalities and economic feasibility of 20 NREL reference wind turbines rated at 5 MW each [11] and mounted on floating tension leg platform structures located in an area with sea depths of around 200 m off the south-west coast [12].

Whether onshore or offshore, the contribution of large-scale wind power could be hampered in the context of a small electricity system owing to the scale of the wind project, the intermittent nature of the wind resource and demand-side consumer behaviour, amongst other issues. Whilst wind power is non-polluting, it does depend on an unpredictable, site-specific resource, so solutions which decouple supply and demand would enable better energy management. An electrical system will benefit if a wind farm operator can offer a fixed contribution to the generation system because this would facilitate renewable energy (RE) integration, reduce greenhouse gas emissions and help achieve national RE obligations [13]. Wind farm energy yield can be complemented by a contribution from a pumped storage system if the former resource is lacking. Such a system would reduce variability of the RE inputs thus avoiding grid imbalances and instability.

This study looks at several years of wind turbine yield in combination with the electrical load experienced on the Maltese islands and develops a simple model to analyse the prospects of large-scale deep sea offshore wind power coupled to a pumped hydroelectric energy storage system.

2 Methodology

Knowledge on wind resources is an important asset for wind farm performance projections. One solution, short of installing a costly offshore wind monitoring station, is to use mathematical models. In this study, a combination of measure-correlate-predict (MCP) techniques and computational fluid dynamics (CFD) modelling is used to estimate longer-term wind resources and wind turbine energy yield in a deep sea offshore context, with a typical wind resource map being generated (Fig. 23.1).

This study focuses on the same 20 turbine array consisting of 5 MW wind turbines installed well offshore to the south-west of the island of Malta as proposed by Aquilina et al. [12]. The average distance between the middle of the array and the closest landfall is approximately 10 km. Two onshore wind measurement stations are used to generate the wind characteristics at the offshore location. Long-term wind speed and direction records were captured at 10 m above ground level at Wied Rini (Fig. 23.1) high on the southern coastal escarpment [14]. This site serves as a reference site owing to its long-term historical data sets. Meanwhile, shorter-term wind speed and direction records captured at 80 m above the ground from the Malta Resources Authority's Ahrax Point Station [15], which serves as a candidate site. This is located close to sea level, with the overall height of the sensors at around 90 m above the sea surface, which corresponds to the offshore wind turbines' hub height. The time series from the two wind measurement points are correlated over a concurrent 24-calendar-month time frame (November 2009–October 2011) using three MCP methods built into the WindPRO [16] software. The MCP routines used were linear regression, linear regression with speeds in excess of a 2 ms^{-1} threshold and the matrix MCP method. The ensuing wind speed

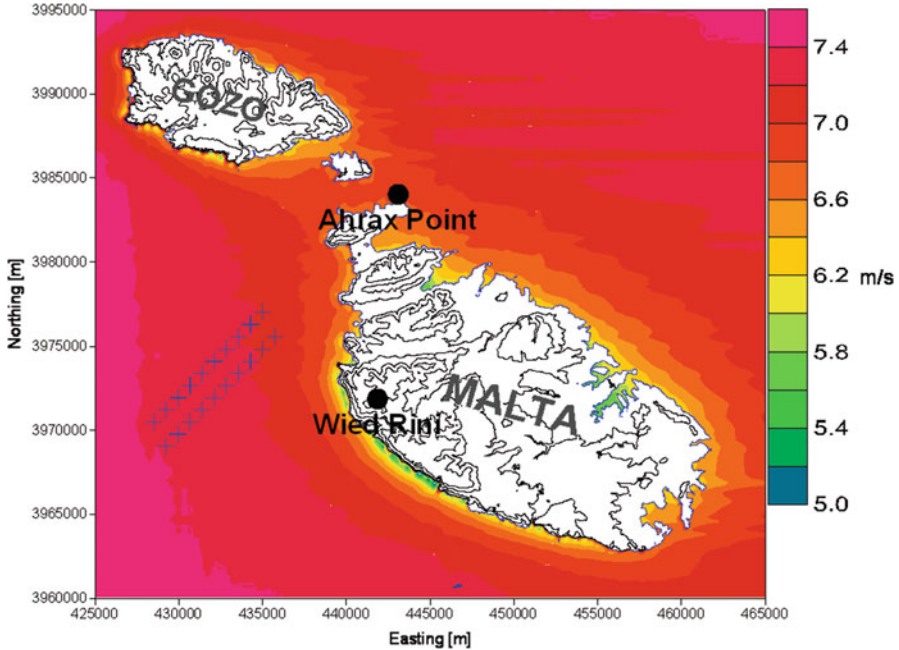


Fig. 23.1 Wind resource map showing average wind speeds extrapolated to a wind turbine hub height of 90 m above the surface and covering the area occupied by the deep sea offshore wind turbine array (blue crosses) to the south-west of the island of Malta

and direction time series at the candidate site spanned over the same duration as the reference site's time frame covering the years 2007–2011. At this point, the CFD software WindSim [17] was used to model wind resources within a macro domain encompassing the whole of the archipelago. The numerical model covering this domain was set with a *Maximum Number of Cells* of four million. The height above the terrain was set at 1500 m, with the number of cells in the *z*-direction increased to 30 from the default values. The boundary layer was set at a height of 500 m, with a speed of 10 m/s set for the top level. A fixed pressure boundary condition was set at the upper limit of the profile. A *Standard k-ε* model was used with the potential temperature set at 291.6 K, which corresponds to an average annual ambient temperature measured over the period 1961–1990 [18]. An air density value of 1.214 kg/m³ was also stipulated. The wind parameter time series generated through the MCPs for the 80 m anemometer at Ahrax Point over the time frame January 2007–December 2011 was used as input to the CFD software's '*Objects*' module so as to calibrate the CFD model against realistic local wind data. This methodology is being used to model wind resources on and in the vicinity of the islands [19]. The 20-wind-turbine array was geo-referenced within the extents of the modelling domain, and wind resources were generated for a height of 90 m above the surface. WindSim has the capability of generating individual and cumulative wind turbine power outputs at the same resolution as that of the climatological time series. In this

case, the methodology was streamlined, and wind turbine power output files were generated using only a matrix MCP method. The turbines' power outputs were then synchronised with the load data for the years 2007–2011. Instances when wind data, and consequently wind farm power output, were not available were removed from the analyses, as were the corresponding load entries. Likewise, in cases where load data were unavailable, the corresponding wind farm yield entries were deleted.

Moretti and Jones [20] recommended that a load fluctuating as a function of time $L(t)$ experienced by a power generation system may be processed in the form of a load duration plot, which is frequently used in the analysis of power generation systems and shows the load against the fraction of time when that load is surpassed. The load duration can be acquired from $L(t)$ directly simply by sorting the records by order of magnitude and plotting them against time when a complete time series is available. In the case of an unscheduled generation plant, such as a wind turbine, the output should be taken as a negative load in the analyses [20]. If hourly wind data are available, it is possible to compute the wind power output $P_W(t)$ for specific wind turbine models, with the resulting net load $L'(t)$ computed using the following equation [20]:

$$L'(t) = L(t) - P_W(t) \quad (23.1)$$

The resulting load duration can then be plotted and compared to the original scenario without a wind contribution, and the impact of the unscheduled generation on the demand may be determined. A load duration plot for the 5 years in question is presented as Fig. 23.2a. A peak load of 434 MW was experienced by the system during 2007. A base load, defined as the minimum load experienced by an electrical system [21], would seem to be 150 MW in the case of Malta, as shown on the right-hand side of the figure. Figure 23.2b shows the total hourly electrical load experienced during the month of January 2007, with the twin peaks experienced during each day shown quite clearly. Also shown is the hypothetical 100 MW wind farm's output during the same month.

3 Modelling a Wind and Pumped Storage System Under Local Conditions

Various authors have assessed different aspects related to the contribution of intermittent renewables to an electrical grid system with pumped energy storage [22–26]. Pumped storage allows a decoupling of supply and demand and is being considered here as a means of mitigating the intermittent nature of wind power.

One of the islands' natural resources is limestone, which is still widely used in the building and construction industries and is extracted in quarries. The artificial voids created by the quarrying operations may be used for various purposes once the operations are discontinued, and saline water open reservoirs for bulk energy

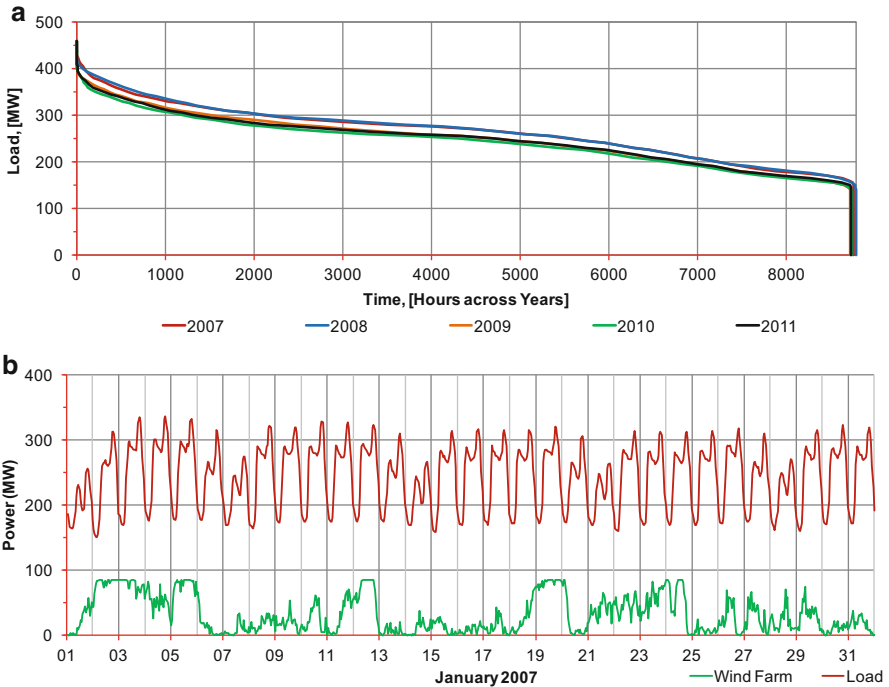


Fig. 23.2 (a) Load duration plots for the years 2007–2011 and (b) plot showing the power output of the 100 MW offshore wind farm compared to the hourly load on the generation system for the month of January 2007

storage could be one such application [27]. This current exercise takes up the idea and strives to numerically match wind farm output in conjunction with pumped storage capabilities to meet a certain percentage of the nation's electrical load. The main question being addressed here is whether wind energy could realistically contribute to a fixed, steady percentage of the base load on a monthly basis. The balance between a wind supply and this fraction of the base load would be retained through the operation of a pumped hydroelectric storage system that dispatches energy when the wind fails to deliver. The output of a 20×5 MW wind turbine deep sea offshore wind farm in time series format and operating under local offshore wind conditions is taken as a basis for the wind energy supply. The pumped hydroelectric storage plant is used as a buffer, employing excess wind energy to drive electric pumps which transport seawater to the elevated, open reservoirs and which then exports hydroelectric electricity when the wind wanes (Figs. 23.3 and 23.4) through water turbines down at sea level. Two complementary operational scenarios are modelled as described in the following sections.

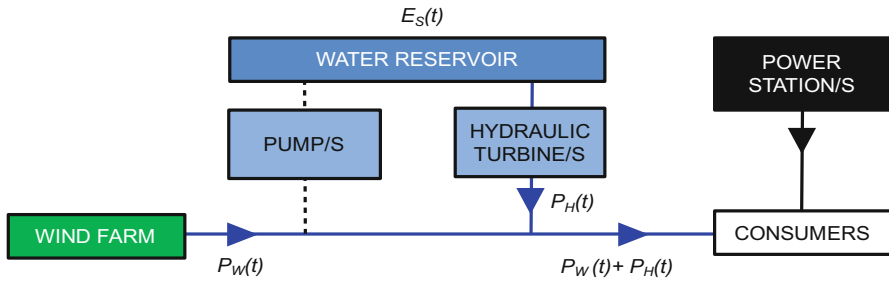


Fig. 23.3 Schematic showing main components of a deep sea offshore wind farm and pumped storage plant in Operational Scenario 1

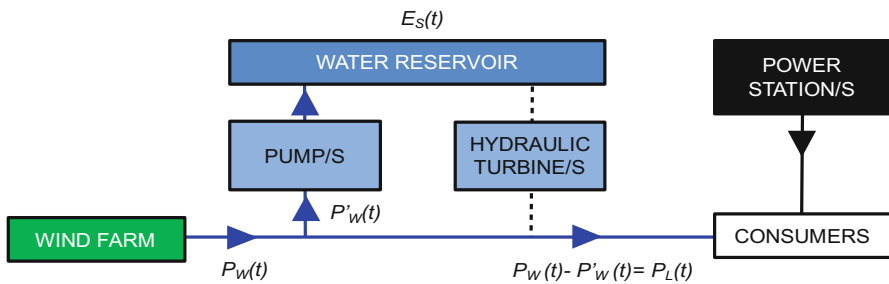


Fig. 23.4 Schematic showing main components of a deep sea offshore wind farm and pumped storage plant in Operational Scenario 2

3.1 Operational Scenario 1

When the wind power output P_W is less than a monthly base load fraction P_L a shortfall, or deficit, will result. The various system power outputs all vary as a function of time t . Equation (23.2) shows that to maintain an output that equals the monthly base load fraction, the wind farm’s constantly changing power output must be complemented by an additional variable quantity, called the shortfall or deficit power P_D such that

$$P_L(t) = P_W(t) + P_D(t) \quad \text{when } P_W < P_L. \tag{23.2}$$

In case where $P_W < P_L$, all the wind power P_W may be fed directly to the grid. In such circumstances, the deficit or shortfall between the wind farm output and the base load fraction P_D will be met by the water turbine power output P_H . Thus, one can also write

$$P_D(t) = P_H(t) \quad \text{when } P_W < P_L. \tag{23.3}$$

Energy shortfalls at times when wind power cannot meet the base load fraction will come from a hydroelectric turbine located close to sea level and driven by water released from the elevated water reservoirs.

3.2 Operational Scenario 2

On occasions when the wind power P_W equals or surpasses the base load fraction P_L (i.e. $P_W \geq P_L$), an amount of wind power P_W that is equal to P_L will be exported to the grid. No deficit will exist between the wind farm output and the base load fraction. Wind power in excess of the base load fraction, P'_W , will be used to pump water from sea level to reservoirs at an elevated location. Thus:

$$P_W(t) - P_L(t) = P'_W(t) \quad \text{when} \quad P_W \geq P_L. \quad (23.4)$$

The excess wind power P'_W may drive the pumps in the pumped storage system so that the available power P_P is

$$P_P(t) = P'_W(t) \cdot \eta_P, \quad (23.5)$$

where η_P is the pumping efficiency.

The power output of the water turbine P_H , as defined in Eq. (23.3), may be computed from

$$P_H(t) = P_P(t) \cdot \eta_H, \quad (23.6)$$

where P_P is the power converted by the pumps and η_H the efficiency of the hydraulic turbines.

It is convenient to work in electrical energy terms (kWh) if hourly or daily assessments are to be conducted. A balancing exercise between the electrical energy available at the water turbine E_H and the quantity required to reach the base load fraction E_D will ensure that the storage system can supply energy when the wind power output is insufficient, that is when $P_W < P_L$ and as long as $E_H \geq E_D$.

Indeed, although a larger storage reservoir would guarantee energy availability, there could be other repercussions of a technical, economic or environmental nature. Having an energy balance between these two energetic quantities alone is also not enough, as the temporal behaviour of the wind, the timing of the hydroelectric power dispatch and the load fluctuations will all dictate the necessary storage characteristics of the system. The net energy between the hydroelectric turbine energy E_H and the deficit in the fraction of base load E_D (which is given a negative sign in order to reflect a deficit when used in the energy balance exercise) can be computed on a temporal basis. Added cumulatively and in chronological order, the energy accounting exercise enables the reservoir energy content E_S

(in Joules) to be determined. The potential energy (PE) stored in the water reservoir may be henceforth found as

$$PE = E_S = m \cdot g \cdot H, \tag{23.7}$$

where m is the mass of water (kg), g the acceleration due to gravity (ms^{-2}) and H the hydraulic head (m). The capacity factor of the storage reservoir is computed as

$$\text{Water storage reservoir capacity factor} = V(t)/V_{\text{Tot}}, \tag{23.8}$$

where $V(t)$ is the instantaneous capacity of the reservoir and V_{Tot} the total capacity of the reservoir, both in cubic meters of water.

4 Results and Discussion

For the purposes of this exercise, the base load was set at 150 MW for every 12-month period under consideration. Being far offshore, the MCP/CFD-generated wind power time series on an hourly basis were downscaled to cater for offshore wind plant availability and other losses and electrical transmission losses between the offshore array and the shore. These two factors were set at 10 and 5% respectively. Pumping efficiency η_P was assumed to be 80%, while the efficiency of the water turbine η_H was set at 90%. The combined pumped hydroelectric generation scheme was assumed to have an overall efficiency of 72%, which is on the conservative side when compared to a round-trip efficiency (kilowatt-hours generated to kilowatt-hours stored) of 78% used by Tuohy and O'Malley [23] for their pumped storage system and other values reported [28].

Figure 23.5 illustrates an energy balance exercise between the energy available at a hydraulic turbine E_H and the energy deficit required to reach the base load

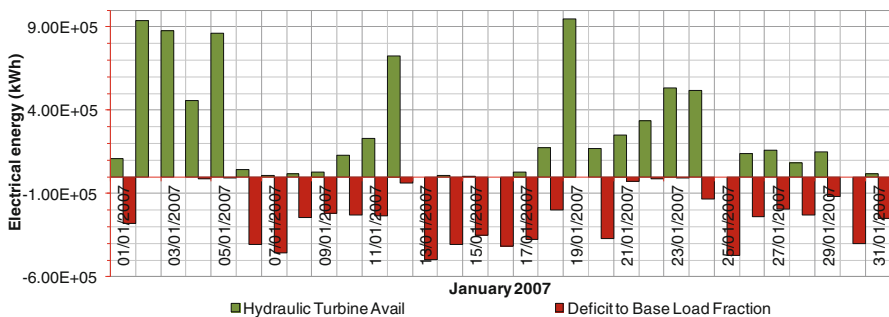


Fig. 23.5 Daily energy balance showing electrical energy available for dispatch at hydraulic turbine E_H and energy required to reach the prescribed monthly fraction of the base load or energy deficit E_D

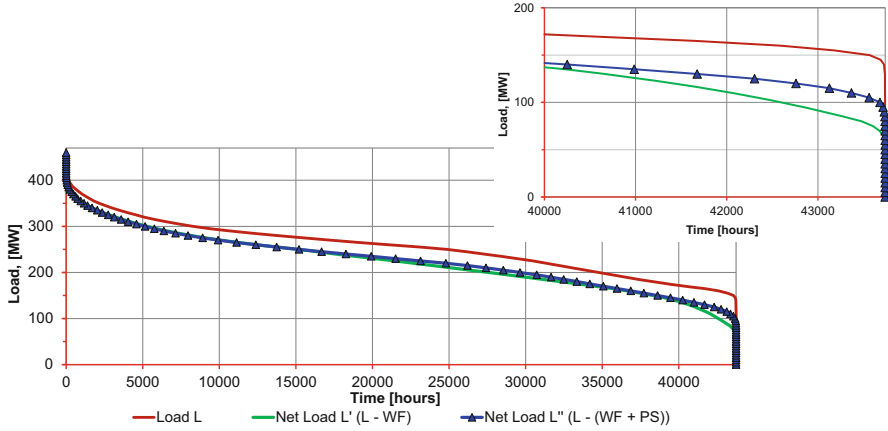


Fig. 23.6 Load duration plots for electrical load L and net load L' for 100 MW deep sea offshore wind farm alone. The net load for the wind farm/pumped storage system is given as L'' . A detailed view of the right end of the plot is also shown. The duration covers the years 2007–2011

fraction E_D for the month of January 2007. The sum of the positive and negative columns should balance out for the month, albeit with a marginal positive availability at the hydraulic turbine side. The energy available at the hydraulic turbine does not and cannot always match the deficit in the base load fraction at a temporal level, so a storage component is required. A number of days of excess wind energy, as shown in the left-hand part of the plot, will have to be stored for use at a later date during the month when the wind wanes and a deficit in the base load fraction is experienced. However, the methodology does not account for time of dispatch of the hydraulic energy because this is considered an electrical control aspect and beyond the scope of this work.

The model was tweaked on a monthly basis with the percentage contributions to the base load fraction being varied in 0.5 % increments to ensure that a net energy balance in favour of electrical energy available at the hydraulic turbine output would always result. This safeguarded against situations where the seawater reservoir would empty completely. It is also worth pointing out that the energy balance straddles across months and years in order to present a more realistic operational scenario.

A load duration plot using the method of Fsadni and Mallia [29] after Moretti and Jones [20] is illustrated in Fig. 23.6 for the cumulative period 2007–2011. The plot shows the load L , the net load L' with only the wind farm contributing to the system and, finally, the net load L'' including the contributions of the combined wind farm and pumped storage system. The largest contribution from the wind component would appear to be in the base load region and, to a lesser extent, within the intermediate load zone. With a pumped storage system coupled to wind power, the contribution is particularly marked in the lower section of the plot, that is as a major contributor to the base load.

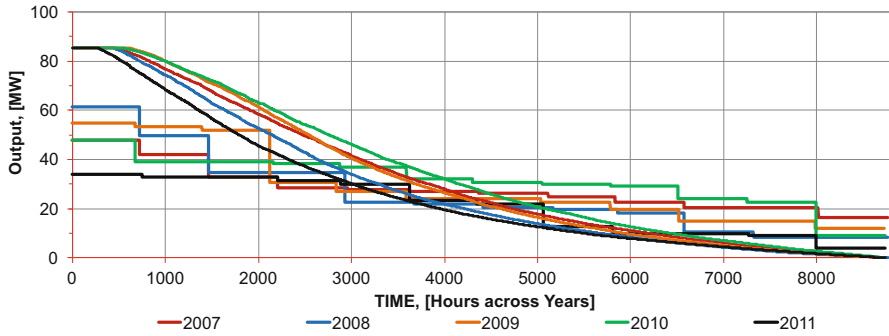


Fig. 23.7 Load duration plots for a wind farm only and for a wind farm/pumped storage system showing the impact of the wind coupled to a pumped storage system as quasi-horizontal stepped lines for the 5 years in question

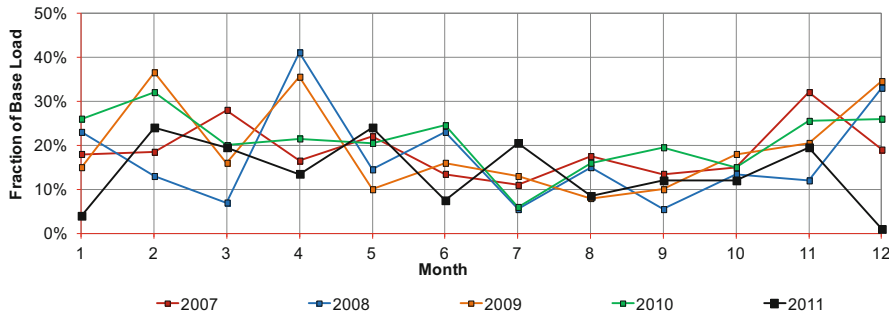


Fig. 23.8 Monthly percentage contribution to base load required to ensure a balance between excess wind power and deficit to base load fraction

Figure 23.7 shows the power output after availability and transmission losses have been deducted for the 5 years in question for a wind farm only. The effects of a wind farm/pumped storage system when contributing to a monthly fraction of the base load are illustrated by the stepped lines in Fig. 23.7. The outputs illustrate that a pumped storage plant will redistribute energy more evenly throughout each year.

Figure 23.8 shows the maximum monthly base load fractions that can be met by the wind farm in a way that allows a marginal net balance in favour of energy availability at the hydraulic turbine.

Assuming that the average hydraulic head H required to pump seawater from sea level up to the seawater reservoirs to be approximately 200 m and that seawater having a density of 1024 kg m^{-3} will be used, one would require varying capacities of reservoir storage, as listed in Table 23.1. Meanwhile, Fig. 23.9 shows time series variations of water storage volumes which will just retain a positive storage balance in the reservoir.

Figure 23.10a shows a plot of the frequency of occurrence against the volume of water stored in the reservoir for the 5 years being assessed. The maximum storage

Table 23.1 Volumes of water required on an annual basis to maintain a positive energy balance in pumped storage system

Year	2007	2008	2009	2010	2011
Volume (thousands m ³)	15,136	34,328	25,423	12,034	37,921

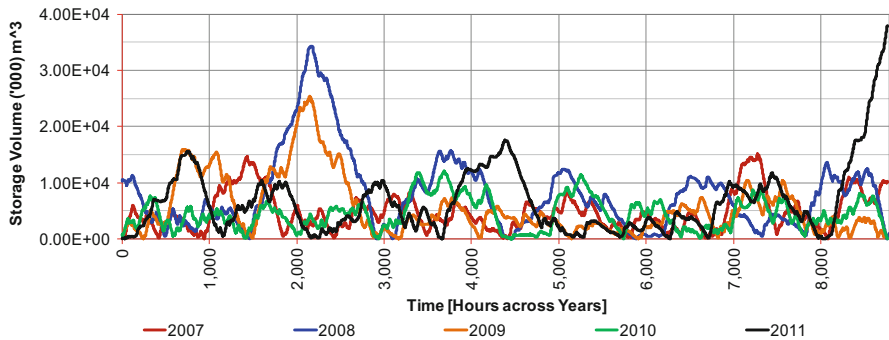


Fig. 23.9 Fluctuations in water volume stored in reservoir required to meet varying demand for years 2007–2011. The peaks indicate the minimum reservoir size required for the duration in question

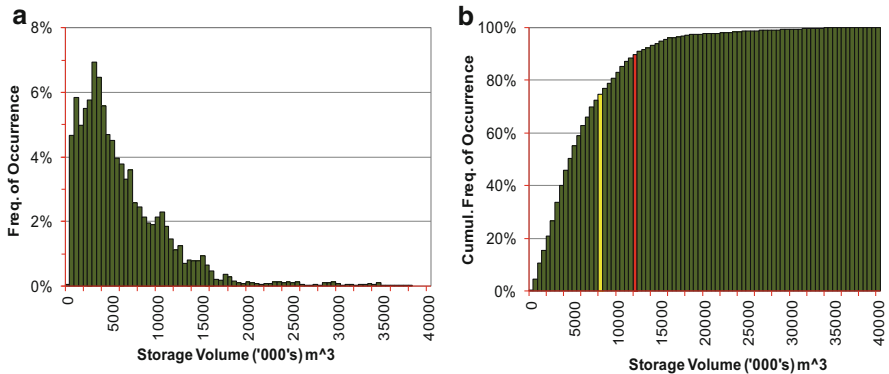


Fig. 23.10 Plots of (a) frequency of occurrence and (b) cumulative frequency against water storage volumes (thousands of cubic meters) computed for the wind farm with pumped storage system for the period 2007–2011. The 75 and 90 % volumes are also highlighted in (b)

capacity required for the system in question would be just over 34.3 million m³. However, as seen in Fig. 23.10b, for 90 % of the time the volume of water stored will be below the 12 million m³ mark and 8 million m³ for 75 % of the time. This raises the issue of the most appropriate water reservoir size. A small reservoir will have a high capacity factor but will then not be capable of retaining sufficient storage volumes over a period of time. In certain instances, exporting the excess wind power could be problematic.

Table 23.2 Average capacity factors achieved for different water reservoir capacities over the 5 year time span

Reservoir volume (thousands m ³)	35,000	30,000	25,000	20,000	15,000	10,000
Average capacity factor (%)	16.8	19.6	23.5	29.4	39.2	58.8

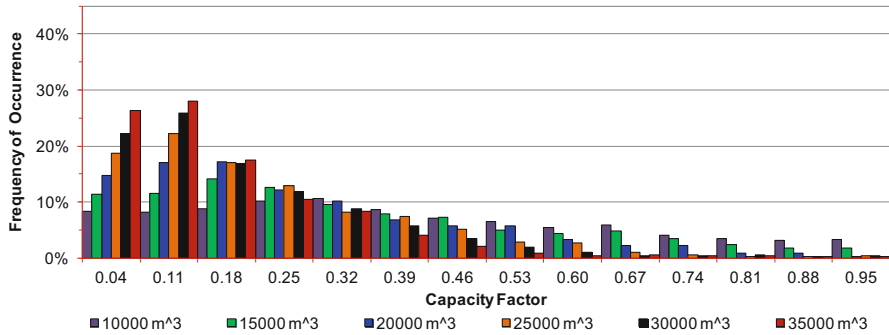


Fig. 23.11 Frequency of occurrence of hourly capacity factors for selected water reservoir storage capacities

Six hypothetical reservoir capacities were assumed starting at 10 million m³ up to 35 million m³ in 5 million m³ increments. The capacity factor, defined as the ratio of the hourly volume to each of the aforementioned set values, was computed for the years under scrutiny. It transpired that decreasing the reservoir capacity increased the average capacity factor (Table 23.2), as expected.

Figure 23.11 shows the frequency of occurrence of hourly capacity factors for selected reservoir capacities. For the lower reservoir volumes, capacity factors in excess of 1.0 will result, implying that such reservoirs would not be capable of absorbing the energy pumped in by the wind-farm-driven pumps. Either the energy will have to be spilled or the wind farm operation stopped, unless other solutions are resorted to. The binned capacity factor values were best described by a probability density function (PDF) determined using a curve fitting process using EasyFitXL [30]; the results are shown in Fig. 23.12. The Weibull distribution was identified as being suitable for representing the histogram data (see fitting results in Fig. 23.11). The Weibull distributions’ PDF $f(x)$ can be expressed in the form

$$f(x) = \frac{\alpha}{\beta} \left(\frac{x}{\beta}\right)^{\alpha-1} \exp\left(-\left(\frac{x}{\beta}\right)^\alpha\right), \tag{23.9}$$

where α is the continuous shape parameter ($\alpha > 0$) and β the continuous scale parameter ($\beta > 0$). The parameters generated through the curve fitting process are listed in Table 23.3.

A recent exercise by Borg [27] estimated the volumes of a conglomeration of quarries on the south-west coastal escarpment at 16.7 million m³, if these are

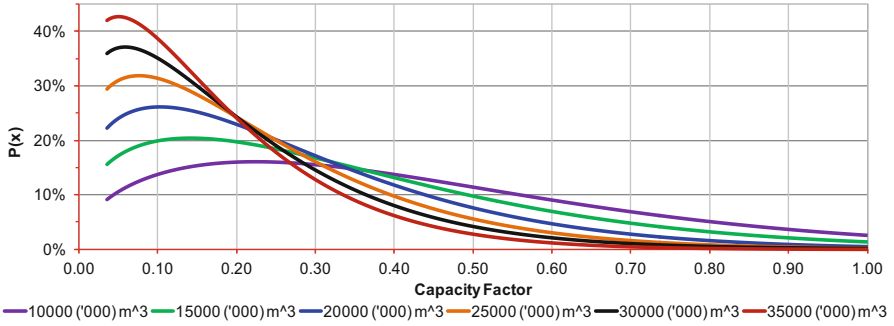


Fig. 23.12 Probability density functions fitted to capacity factors for selected water reservoir storage capacities during the 5 years under investigation

Table 23.3 Parameter values generated for probability density functions using a Weibull distribution

Reservoir volume (thousands m ³)	35,000	30,000	25,000	20,000	15,000	10,000
α	1.2461	1.2501	1.2858	1.3242	1.3542	1.4686
β	0.1835	0.2109	0.2442	0.2967	0.3799	0.4862

assumed to have a maximum depth of 40 m of which only the upper 30 m will be utilised. The quarries in question are slightly less than 250 m above mean sea level, and the horizontal distance between these quarries and the sea is less than 300 m, making the system quite attractive for such a proposal.

5 Conclusions and Recommendations for Future Work

This study has shown that a system consisting of a wind farm coupled to a pumped hydroelectric storage plant can redress the intermittent nature of wind energy and provide a steadier and more manageable energy supply to the Maltese grid. The results demonstrated that wind energy can contribute to the base load and that the combination of wind and a pumped storage system can redistribute excess wind energy to cater for instances when low wind conditions occur and yet ensure a steady electrical energy supply to the grid. Moreover, the study also showed that varying the percentage contribution of the wind farm and pumped storage system to the load allows a balance to be achieved on an hourly and monthly basis.

Future work will focus on the impacts of wind energy/storage system in combination with other renewables such as solar power, which is making increasing contributions to the local electricity system. With grid connection to mainland Europe by means of an interconnector, the possibilities for a wind farm and pumped storage system could be expanded further, allowing both energy export at times of RE oversupply, which has been shown to be highly critical if reservoir sizes are to

be limited, or energy import when rates are preferential, thereby using the hydro-electric system as a buffer store. This allows energy to be redistributed locally at times of peak demand or when time-tiered price tariffs are introduced.

Acknowledgements The authors acknowledge the support of the Malta Resources Authority, Marsa, Malta, for providing wind data from the 80 metre wind monitoring mast at Ahrax Point, Malta, and of Enemalta Corporation, Marsa, Malta, for supplying hourly load data for various years.

The WindPRO software was funded by the project: *Setting up of Mechanical Engineering Computer Modelling and Simulation Laboratory*, part-financed by the European Regional Development Fund (ERDF) - Investing in Competitiveness for a Better Quality of Life, Malta 2007–2013.

References

1. NSO (2014) Census of Population and Housing 2011. National Statistics Office, Valletta, Malta
2. Enemalta Corporation—News and Alerts—Gas Project. <http://www.enemalta.com.mt/index.aspx?cat=3&art=218>
3. Enemalta Corporation—Major Projects—Interconnector. <http://www.enemalta.com.mt/index.aspx?cat=20&art=177>
4. Farrugia RN, Fsadni M, Mallia EA, Yousif C (2006) The renewable energy potential of Malta. In: Proceedings of world renewable energy congress IX, Florence, Italy
5. Farrugia RN, Fsadni M, Mallia EA, Yousif C (2006) Barriers and incentives for the widespread application of renewable energy in Malta. In: Proceedings of world renewable energy congress IX, Florence, Italy
6. Riolo A (2006) Establishing environmentally compatible wind energy potential in Europe—Malta case study. In: EEA expert meeting: “Establishing environmental compatible wind energy potential in Europe”, EEA, Copenhagen, Denmark, 9 November 2006
7. MacDonald M (2005) Strategy for Renewable Electricity Exploitation in Malta. vol. 1. Renewable energy target. Brighton, UK/Malta Resources Authority, Triq Aldo Moro, Marsa, Malta
8. MacDonald M (2009) Feasibility study for increasing renewable energy credentials. Brighton, UK/Malta Resources Authority, Triq Aldo Moro, Marsa, Malta
9. Farrugia RN, Deidun A, Debono G, Mallia EA, Sant T (2010) The potential and constraints of wind farm development at nearshore sites in the Maltese islands. *Wind Eng* 34:51–63
10. Fsadni M, Mallia EA (2011) The potential of wind power generation at Gozo North-offshore. In: ISES Solar World Congress, Kassel, Germany
11. Jonkman J, Butterfield S, Musial W, Scott G (2009) Definition of a 5-MW reference wind turbine for offshore system development. In: National Renewable Energy Laboratory (NREL), Technical report NREL/TP-500-38060, February 2009
12. Aquilina M, Sant T, Farrugia RN (2014) Cost modelling of floating wind farms with upscaled rotors in Maltese waters. In: Proceedings of sustainable energy 2014. In: The ISE annual conference, Qawra, Malta
13. Malta’s National Renewable Energy Action Plan as Required by Article 4(2) of Directive 2009/28/EC, 2010. http://ec.europa.eu/energy/renewables/action_plan_en.htm
14. Farrugia RN, Sant T (2011) Wied Rini II—a five year wind survey at Malta. *Wind Eng* 35:419–432
15. Malta Resources Authority, Triq Aldo Moro, Marsa, Malta
16. WindPRO™ Ver. 2.7 (2008) EMD, Aalborg, Denmark
17. WindSim™ Ver. 5.01.1 (1997–2010) WindSim A/S, Tønsberg, Norway
18. Galdies C (2011) The climate of Malta—statistics, trends and analysis, 1951–2010. National Statistics Office, Valletta, Malta

19. Farrugia RN, Sant T (2013) Mediterranean inshore wind resources: combining MCPs and CFD for marine resources quantification. *Wind Eng* 37:243–256
20. Moretti PM, Jones BW (1982) Analysis method for non-schedulable generation in electrical systems. *Solar Energy* 28:499–508
21. Wildi T (2006) *Electrical machines, drives and power systems*. Sperika Enterprises Ltd., Pearson Education Inc., New Jersey, USA
22. Lindley D (2010) The energy storage problem. *Nature* 463:18
23. Tuohy A, O'Malley M (2011) Pumped storage in systems with very high wind penetration. *Energy Policy* 39:1965–1974
24. Anagnostopoulos JS, Papantonis DE (2008) Simulation and size optimization of a pumped-storage power plant for the recovery of wind-farms rejected energy. *Renew Energy* 33:1685–1694
25. Nyamdash B, Denny E, O'Malley M (2010) The viability of balancing wind generation with large scale energy storage. *Energy Policy* 38:7200–7208
26. Buhagiar D, Sant T (2013) Analysis of a stand-alone hydraulic offshore wind turbine coupled to a pumped water storage facility. In: *Proceedings of sustainable energy 2013: the ISE annual conference*, Qawra, Malta
27. Borg L (2013) Ta' Zuta energy storage—bulk energy storage of 872 GWh—2,829 GWh Yearly
28. Evans A, Strezov V, Evans TJ (2012) Assessment of utility energy storage options for increased renewable energy penetration. *Renew Sustain Energy Rev* 16:4141–4147
29. Fsadni M, Mallia EA (2006) The interaction of wind power generation with electricity demand in the context of a small grid. *Renew Energy* 31:811–819
30. EasyFitXL Ver. 5.5, MathWave Technologies. 3 Dec 2012

Chapter 24

Energy Choice to Support Carbon Dioxide Reduction in Indonesia

Herliyani Suharta, Arnold Soetrisnanto, and Unggul Priyanto

Abstract Greenhouse gas emissions have continued to increase, and economic and population growth continue to be the most important drivers of these increased emissions. The Intergovernmental Panel on Climate Change (IPCC) uses two assessment models that indicate biomass should be a top primary energy source in 2095, while climate change will tend to amplify tree mortality worldwide. The burning of biomass in the twenty-first century will greatly exacerbate global warming and its consequences. This chapter describes the depletion of fossil fuels in Indonesia: oil will vanish within 12.8 years, natural gas within 30.8 years, and good quality coal within 59.8 years. The shrinking energy resources are impacting national energy security. If low-rank coal is burnt for coal-fired power plants, this will affect all efforts to fulfill promises to reduce CO₂ emissions. Nuclear power is proposed as one of the solutions. Government Regulation 79/2014 on the national energy policy is briefly described. The choice is to take or not take this solution. Another choice is to facilitate technology transfer and engage in international collaboration in nuclear power technology.

Keywords CO₂ emission • Fossil fuel depletion • Indonesia • Global nuclear energy policy • Technology transfer

1 Climate Problems as Background

Former US Vice President Al Gore stated: “The warming of the climate system is ‘unequivocal’ and that most of ‘the observed increase’ in global average temperatures since the mid twentieth century is very likely due to ‘the observed increase’ in

H. Suharta (✉)

The Center of Energy Conversion Technology, BPPT, Kawasan PUSPIPTEK, Serpong, Tangerang Selatan 15314, Republic of Indonesia
e-mail: herliyani.suharta@gmail.com

A. Soetrisnanto

National Research Council, Jakarta, Republic of Indonesia

U. Priyanto

The Agency for the Assessment and Application of Technology (BPPT), Jakarta, Indonesia

anthropogenic GHG concentrations” [1, 2]. Total anthropogenic greenhouse gas (GHG) emissions have continued to increase over the period 1970–2010 and reached 49 ± 4.5 GtCO₂ equivalent per year in 2010. Of this, 2 % is flare gases, 6.2 % is N₂O, 16 % is CH₄, 11 % is CO₂ from forestry and others land uses and 65 % is from fossil fuel use and industrial processes. The emissions of CO₂ contributed 78 % of the total GHG emissions. Economic growth, which has risen sharply over this period, together with population growth continued to be the most important drivers of increases in CO₂ emissions [3].

The Copenhagen Accord states that CO₂ concentration in the troposphere must not exceed 450 ppm by 2100 so that the global temperature increase can be kept at 2 °C [4]. This leaves only 50 ppm for the next 87 years of activity [5]. The IPCC Special Report on Carbon Dioxide Capture and Storage from 2007 [6] presents two different integrated assessment models to predict global primary energy use and the corresponding contribution of CO₂ mitigation until 2095 (Fig. 24.1).

Both models indicate biomass as the top primary energy used by humans. However, Craig D. Allen et al. conclude their research finding as follows: ‘climate change tends to amplify tree mortality worldwide, this will increase a risk for forests to shrink and various trees might not grow well’ [7]. The burning of biomass worldwide will steeply raise these risks.

The six rankings of primary energy used in the B2 SSO Message model (Fig. 24.1b) are as follows: biomass (26.26 %), solar and wind (20.86 %), gas-CCS (16.16 %), coal-to-gas substitution (13.47 %), nuclear (9.09 %) and oil (5.78 %). Figure 24.1d shows CO₂ as emitted by renewable energy (36.76 %), CCS (31.62 %), coal-to-gas substitution (16.91 %), conservation and energy efficiency (14.71 %). There are no emissions from nuclear. In 2095, CO₂ emissions will

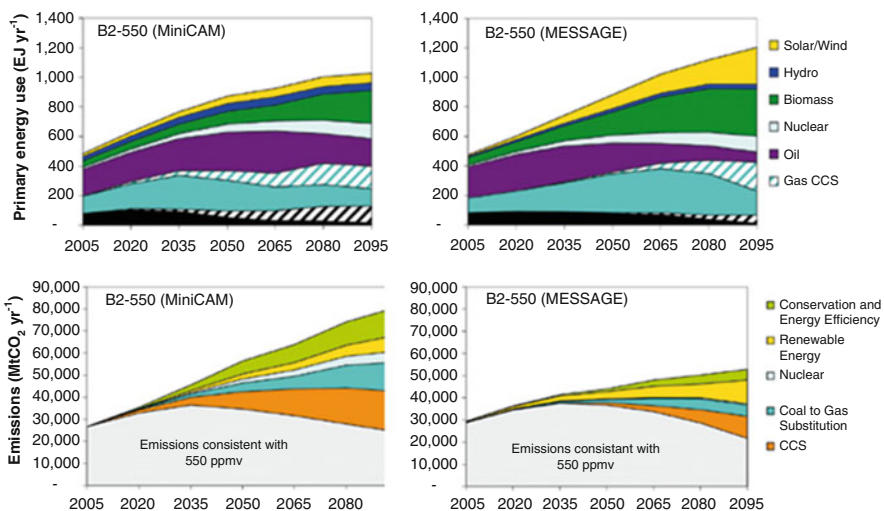


Fig. 24.1 Primary energy in 2095: in MiniCAM model (a; c) and in MESSAGE model (b; d) [6]

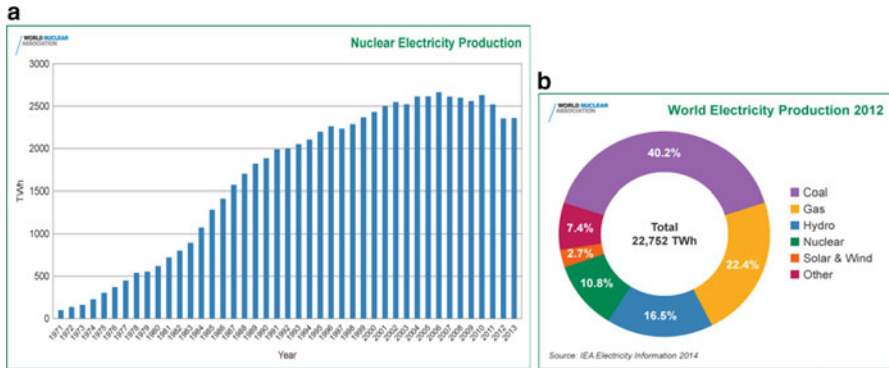


Fig. 24.2 (a) Nuclear electricity production increases continuously and reaches 2700 TWh in 2006, declined to 2350 TWh in 2012. (b) Nuclear power contributes 10.8 % to world electricity production in 2012 [8]

stabilise at 550 ppm. This exceeds Copenhagen Accord targets. Nuclear power, which emits no CO₂, is attracting increasing attention worldwide.

According to the International Atomic Energy Agency (IAEA) [8], 69 nuclear power plants (NPPs) are under construction. They are being built in the following countries: Russia: 9, USA: 5, China: 23, India: 6, South Korea: 4, Pakistan: 2, Slovakia: 2, Turkey: 2, Argentina: 2, Brazil: 1, Finland: 1, Belarus: 1. These 69 NPPs will add to the 439 NPPs that have been installed and are in operation worldwide generating electricity of 2410 TWh in 2015 (Fig. 24.2).

Table 24.1 shows US average levelised cost of various power plants that will be entering service in 2019. Advanced nuclear technology is competing with renewable energy technology [9].

2 Indonesia’s Electricity and Energy Security

Electricity is a priority since it is used to satisfy basic needs: lighting for schools, household needs, communication, entertainment and information technology.

In 2004, Sukma S. Hasibuan [10] projected that by 2020 electricity generation would be 73.56 GW. Of this, coal and diesel power plants will contribute 28.31 GW. The electrification ratio is expected to be 90 %.

Projections made in 2005 for the energy mix scenario in 2025 [11] shows the use of coal at 32.7 %, gas 30.6 %, oil 26.2 %, and new and renewable energy (NRE) at 10.5 %. NRE sources include geothermal at 3.8 %, hydro at 2.4 %, nuclear at 1.993 %, biofuel at 1.335 %, biomass at 0.766 %, microhydro at 0.216 %, wind at 0.028 % and solar energy at 0.020 %. Four NPPs (2 GW each) have been planned to go into operation in 2016, 2017, 2023 and 2024 [12], but still void until 2015. From 2008 to 2012, the installed power generation by the state electricity company

Table 24.1 US average levelised cost for plants entering service in 2019 [9]

US average levelised cost for plants entering service in 2019 (2012 USD/MWh)						
Plant type	Capacity factor (%)	Levelised capital cost	Fixed O&M	Variable O&M (including fuel)	Transmission investment	Total system levelised cost
Conventional coal	85	60.0	4.2	30.3	1.2	95.6
Integrated coal-gasification combined Cycle (IGCC)	85	76.1	6.9	31.7	1.2	115.9
Cycle (IGCC) with CCS	85	97.8	9.8	38.6	1.2	147.4
<i>Natural gas fired</i>						
NG: conventional combined cycle (CCC)	87	14.3	1.7	49.1	1.2	66.3
NG: advanced CC	87	15.7	2.0	45.5	1.2	64.4
NG: advanced CC with CCS	87	30.3	4.2	55.6	1.2	91.3
NG: Conventional combustion turbine	30	40.2	2.8	82.0	3.4	128.4
NG: advanced combustion turbine	30	27.3	2.7	70.3	3.4	103.8
Advanced nuclear	90	71.4	11.8	11.8	1.1	96.1
Geothermal	92	34.2	12.2	0.0	1.4	47.9
Biomass	83	47.4	14.5	39.5	1.2	102.6
Wind ^a	35	64.1	13.0	0.0	3.2	80.3
Wind-offshore ^a	37	175.4	22.8	0.0	5.8	204.1
Solar PV ^{a,b}	25	114.5	11.4	0.0	4.1	130.0
Solar thermal ^a	20	195.0	42.1	0.0	6.0	243.1
Hydro ^a	53	72.0	4.1	6.4	2.0	84.5

^aNon-dispatchable (hydro is dispatchable within a season, but non-dispatchable overall, limited by site and season)

^bCosts are expressed in terms of net AC power available to grid for installed capacity

(PT.PLN) was as follows: 25,593.92 MW in 2008; 25,636.70 MW in 2009; 26,894.98 MW in 2010; 29,268.16 MW in 2011; and 32,901.44 MW in 2012 [13].

Government Regulation 79/2014 on the national energy policy [14] is valid from 2014 until 2050. Pasal 30 says it is a basis to derive a General National Energy Plan (RUEN in Bahasa) and a General National Electricity Plan (RUKN in Bahasa). The target for electricity development is 115 GW (gigawatts) by 2025 and 430 GW by

2050 (see Pasal 8c). This target was derived based on the following assumptions [15]:

- Economic growth will be 6 % per year, and thus energy growth will be about 8–10 %.
- Installed electricity from power plants will be 53 GW (*Note: Draft RUKN 2012–2031 shows 30 GW existing. Additional need in 2015 will be 23 GW, and it is assumed that it will be installed in 2015, to give a total of 53 GW*).
- Accelerated development of 35 GW is expected to finish in 2019. This pace is taken as a benchmark for the rate of Indonesia’s electricity development. To free the lands needed are ongoing, it is expected to finish soon.

Indonesia should be able to develop electricity to as much as $(430 - 53 =) 377$ GW within 35 years. Within 70 years (1945–2015), installed power plant generating capacity was 53 GW (or 26.5 GW/35 years). Based on this history, there will be a need to accelerate electricity development by $(377/26.5=)$ 14.2 times to reach the target level. This is a very high target, especially if nuclear power plant (PLTN in Bahasa) is considered as the last option, or “pilihan terakhir” in Bahasa. This target is set in order to provide 1400 kgs of oil equivalent per capita in 2025, assuming the population in 2025 is 285.7 million, and to provide 3200 kgs of oil equivalent in 2050. This means that the Human Development Index of Indonesia will become 0.74 in 2025 (see yellow line in Fig. 24.3) and increase to 0.86 in 2050 (blue line), the same as Korea, which has 24 NPPs and another 4 under construction. To make this target to become a reality, the primary energy needed will be around 400 MTOE in 2025 and around 1000 MTOE in 2050. However, in 2014, IRES/METI published the following statistics regarding Indonesia’s fossil fuel reserves:

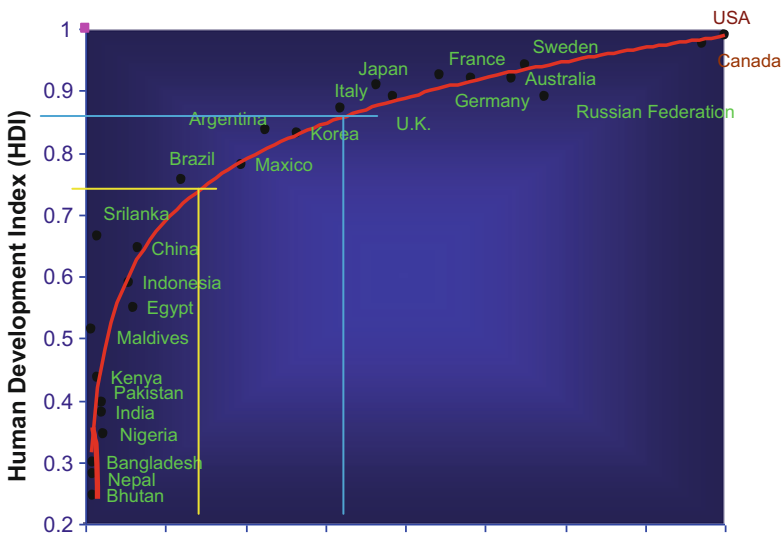


Fig. 24.3 Effect of energy consumption (kgs of oil equivalent) per capita to Human Development Index [16]

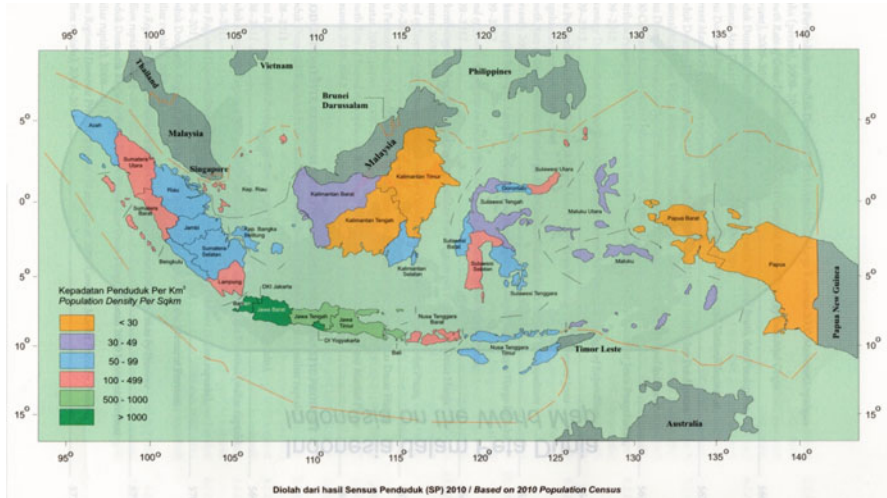


Fig. 24.4 Geographic situation and population density in each province of Indonesia in 2012 [18] (Java-Bali has the densest population)

- Oil reserves will vanish within 12.8 years;
- Natural gas will vanish within 30.8 years;
- Good quality coal will vanish within 59.8 years [17].

PP no 79/2014, Pasal 6 a; Pasal 10 (1) d; Pasal 11 (2) d; Pasal 12 (2) [14] describe efforts to keep strategic reserves intact in order to maintain primary energy provision for the whole country (Fig. 24.4). At the moment, no penalties can be imposed on those who misuse the strategic reserves. It is necessary to add the following conditional phrase under Pasal 24 (2) g: ‘Strategic reserves are not for export.’

Pasal 9 f 1–4 shows the energy mix in the years 2025 and 2050:

- In 2025, NRE will contribute 23 % to the national energy mix, coal 30 %, natural gas 22 % and oil 25 %.
- In 2050, NRE will contribute 31 % to the mix, coal 25 %, natural gas 24 % and oil 20 %.

Owing to its depletion, oil will contribute a very small percentage to the energy mix in 2025, and coal and gas will become major contributors. In 2050, natural gas will have vanished and coal will become the only natural resource left, plus limited renewable implementations. Good quality coal might vanish before 59.8 years as coal will have been used to replace oil/natural gas needs.

This vulnerable situation is not understood well. Most Indonesians think that Indonesia’s energy resources are still abundant. Therefore, efforts to develop new and renewable energy technologies face difficulties related to this public mind-set.

Coal-fired power plants (CFPPs) in Indonesia are designed for good quality coal (bituminous and subbituminous) as intake.

Good quality coal has a heating value of 5000–5500 kcal/kg, and anthracite (the best coal) has a heating value of 6000–7100 kcal/kg, while low-rank coal has a heating value of 2500–4000 kcal/kg. If coal is used to replace oil and gas that have been depleted, or if low-rank coal is used to replace good quality coal needed in all CFPPs, then will affect efforts to fulfil the promise to reduce CO₂ emissions [19]: ‘... Indonesia, of course, faces problems and challenges in our national development: growth, unemployment, poverty, infrastructure building, education and health care. But we have decided and established a National Climate Change Action Plan with the targets of 2020 and 2050. We are devising an energy mix policy including LULUCF (Land Use, Land Use Change, and Forestry) that will reduce our emissions by 26 % by 2020 from BAU (Business As Usual). With international support, we are confident that we can reduce emissions by as much as 41 %. This target is entirely achievable because most of our emissions come from forest related issues, such as forest fires and deforestation ...’

3 Energy Choice and Considerations

In 2014, fossil fuel (oil, natural gas and coal) contributed 42,022 MW electricity (79 %) and NRE contributed 11,330 MW (21 %). Maritje Hutapea has reported on the yearly development of renewable electricity in 2015–2019 (Table 24.2) [20].

Table 24.2 Strategic planning for electricity generation in 2015–2019 [20]

Performance indicator	Unit	2015	2016	2017	2018	2019
(A) <i>Cumulative installed capacity</i>	MW	11,736.20	12,330.80	13,045.80	14,300.70	15,636.20
Installed capacity of geothermal	MW	1440.50	1719.50	2053.00	2741.50	3411.50
Installed capacity of hydro	MW	8.32	8.44	8.56	8.79	9.05
Installed capacity of bioenergy power plant	MW	1.89	2.07	2.29	2.56	2.87
Installed capacity of centralised power plant	MW	76.90	92.10	118.60	180.00	260.60
Installed capacity of wind power plant	MW	5.80	11.20	19.20	30.20	45.40
(B) <i>Biofuel development</i>	Million kl	4.90	9.36	10.20	10.90	11.60
Installed capacity of biodiesel	Million kl	5.53	8.78	9.36	9.95	10.59
Installed capacity of bioethanol	Million kl	0.37	0.58	0.84	0.95	1.01

Note: The Ministry for Energy and Mineral Resources Office (2015), “Strategic Planning for Electricity Generation in 2015–2019”, presented by Maritje Hutapea at *Workshop on Nuclear Power and Small Modular Reactors in Indonesia*, 25 June 2015, Sari Pan Pacific Hotel, Jakarta

Table 24.3 Education in Indonesia [24]

Education	Number
No schooling	5,358,900
Did not complete/have not yet completed primary school	16,108,186
Primary school (passed)	32,411,118
Junior high school	20,222,911
High school (general)	17,248,237
High school (vocational)	9,503,868
Diploma I/II/III/Academy	2,973,663
University	6,981,271
Total	110,808,154

Statistical Yearbook of Indonesia 2013, Table 3.2.7, p. 98.

4 Electricity in Jawa-Bali

Power plants in Java are dominated by CFPPs and gas turbine combined-cycle (GTCC) plants [21]. In 2012, the total installed capacity in Jawa-Bali was 25,782.11 MW or 78.36 % of the total [22]. The electricity produced is $151,922.96 \times 10^3$ MWh. The total electricity produced in Indonesia was $200,317.57 \times 10^3$ MWh [23]. Fossil fuel production in 2012 was as follows:

- Crude oil production was 314.7 Mb/d (million barrel per day) [24];
- Natural gas production was 3174.6 BSCF (billion standard cubic feet);
- Coal production was 386 Mton (million tons).

Java-Bali needs large amounts of fossil fuel products, and these needs will grow as the population grows. On the other hand, some areas in the archipelago have intermittent electricity supply as a result of intermittent fuel supplies. Geographical conditions and storms on the archipelago delay fuel deliveries to some remote islands. Social justice for all Indonesians (Sila number 5 in Pancasila) has not been achieved yet. If Java-Bali has a NPP, this would allow some fossil fuels meant for Java could be distributed to the other islands. However, there is a pro–contra debate on NPP development planning in Java, Indonesia.

5 Education Background of “Pro–Contra” on Nuclear Technology in Indonesia

Among the 244,200,000 inhabitants of Indonesia, on 105,449,254 have attended school (Table 24.3). Only 6,981,272 people, or 2.85 % of the population, have a university degree [24]. The first university degree (S1) requires 4–6 years, the second university degree (S2) requires 1–2 years and the third university degree

(S3) requires another 4–5 years. Thus, the total years of study to get to S3 is around 21–25 years. Those studying nuclear physics need this long study process.

Thus, one asks: how can pro-contra on NPP exist in Indonesia? NPP development in Indonesia lags behind that in India (where 21 NPPs have been installed and are in operation and 6 NPPs are under construction), China (23 installed and operating and 23 under construction), Pakistan (3 installed and operating and 2 under construction), Korea Selatan (24 installed and operated and 4 are under construction) [8].

Specialists with expert knowledge of nuclear physics need to work on many details related to NPP development, from void to become exist, including:

- Preparing all steps needed to design and implement the core science of nuclear physics, selecting an appropriate NPP, designing the cooling system, among others;
- Drawing up a safety plan;
- Doing a risk analysis;
- Designing project plans, scheduling work, operation and project management;
- Administrative tasks;
- Studying the economic viability of the plant, preparing a detailed scope before major financial commitments;
- Preparing innovative manufacturing and networks for production and on-site engineering works.

Experts in nuclear physics are also expected to do a dynamic social research; getting funding from the National Research Council is not possible because their policy is to support research on technology. On the other hand, a small amount of educated people that do not like NPPs and are not in charge of all tasks described previously have presented photos of Chernobyl's victims and natural disasters at the Fukushima Daichi NPP. Studies on NPP [26, 27] have been criticised, even though these efforts are directed to investigate solutions for the critical energy situation in Indonesia. It is inappropriate for experts in nuclear physics must pursue Indonesian to accept NPPs. Should 97 % of the Indonesian population have to be persuaded to order PT.PLN to stop burning coal inside all CFPPs because they emit massive levels of CO₂? 'NPP is the last option', as written in Pasal 11 (3) in PP No. 79/2014, seems inappropriate, especially related to the existence of BATAN (National Nuclear Energy Agency) and BAPETEN (National Nuclear Energy Regulatory Body, which have good human resources. Undang Undang Dasar 1945 Pasal 27 (3); Pasal 28C (1) and (2); Pasal 28I (2); Pasal 30 (1) express the idea that citizens can individually or collectively try to shape a better society.

According to Pasal 33 (2): *'The branches of fossil fuel production that are essential for the country and for the people's life are ruled by the State'*, so 'the last option' in Pasal 11 (3), PP No. 79/2014, shall be decided by the State, 10 years before oil is completely depleted.

Indonesians live alongside nature and absorb its meaning into their soul. Indonesian culture represents human wisdom as expressed in people's behaviours, beliefs, attitudes, values and experiences.

The depletion of fossil fuel reserves is threatening national energy security. When oil is entirely depleted, huge problems will emerge in many places. Huge efforts will have to be made to find solutions before these disasters happen. There is a need to investigate and master NPPs as a solution and prepare for the time when nuclear energy will replace oil and natural gas.

We should not wait until ‘premi pengurusan energi fosil’ as written in Pasal 27 (5) b and Pasal 27(6) in PP no. 79/2014 has run out and the country is financially incapable of finding other solutions. Indonesian wisdom needs to be transformed to provide support for the government’s policy on NPPs to save the nation.

6 A Solution Taken or Not Taken

An IPCC Special Report [6] shows that biomass will become the top primary energy used worldwide until 2095. CO₂ emitted from the burning of wood is equal to CO₂ previously been absorbed along that woody-tree life. In this terminology, biomass combustion is classified as a carbon-neutral process, but the reality is CO₂ in trees will be released into the atmosphere. Private observations have found that young leaves of certain trees could not survive in today’s hot climate; they would shrink, dry out and die (Fig. 24.5). The presence of butterflies, dragon flies and caterpillars has declined. Rich people stay inside buildings with their air conditioning, which releases CO₂ and more if the building designs are not efficient.

Six scenarios for 2100 have been assessed. The probability of maintaining warming below 2 °C over the course of the twenty-first century is as follows: 0 % for CO₂ concentration of 980 ppm; still 0 % (for 770 ppm); 1 % for 700 ppm; 5 % for 630 ppm; 10 % for 560 ppm; 80 % for 440 ppm [28]. WMO and UNEP state that if CO₂ concentrations fall in a range between 485 and 570 ppm, then the sea level will rise by 0.6–2.4 m. Global temperatures will increase by 3.2 to 4 °C [29]. In 2095, CO₂ concentrations will stabilise at 550 ppm. This is scary. The sea level rise will destroy coastal villages along the shore of the Indonesian archipelago.

Humans will be forced to live in a dangerous atmosphere that will become deadly for all living creatures on Earth.



Fig. 24.5 Forest dieback on Bintan Island (Photos by Herliyani Suharta, 14 May 2015)



Fig. 24.6 Resources of radioactive minerals in Indonesia, 2004 [31]

After 20 UNFCCC meetings, humankind still faces difficulties in cutting its energy use. People still need to devote considerable effort to keeping CO₂ concentrations in the atmosphere below 450 ppm by 2100.

‘Energy needs—limited natural resources—CO₂ emissions from human activity—climate change effects “is becoming” a deadly quadrupole problem’, where all the poles end at a dead-end while travelling at different speeds. Comparing the heating values of various fuels (Fig. 24.6, right), a question arises: Instead of burning woody biomass, why not use nuclear technology to produce electricity on a massive scale and produce no CO₂?

7 Appropriate Nuclear Power Plant for Indonesia

Considering Indonesia radioactive sources [31] (Fig. 24.6), West Kalimantan Province, which has uranium deposits and no earthquake history, may be a good candidate for NPP development. Its electricity output can be used to support emerging industrial areas, including manufacturing components of a NPP.

At the moment there are 11 diesel power plants in West Kalimantan Province, and the installed capacity is 449.6 MW [30]. These conditions meet (spasi) the requirements described in Pasal 11 (1) a, c, d, e, PP no. 79/2014. For industry and commercial enterprises, CFPPs and GTCC plants are usually considered, while big hydro and geothermal are site specific. NPP is becoming an appropriate choice. The scale of NPP is important.

The IAEA [32] have identified 28 small-scale reactors designed by companies in the USA, Russia, China, France, IRIS, South Africa, Japan, Canada and South Korea. Small scale reactors seem appropriate for the archipelagic country.

Various small modular reactor (SMR) designs have been assessed and evaluated by BAPETEN to investigate the passive safety features, slower accident progression, smaller source term, multiple modules that would give local manufacturers the

chance to produce components. Other requirements include a compact size and seismic safety; the needs no safety zone are the additional basis in evaluating and investigating a SMR in order to determine whether the selected SMR can be installed close to residential areas so that no excessive transmission grid would be needed.

The energy source (the pellets) should be made such that no radiation is emitted when the pellets disperse. The size of pellets for NPPs is small, much smaller than the size of coal needed for CFPPs. This makes fuel logistics for NPPs more practical. In multiple applications (up to 20 NPPs), the price of a plant's electricity output will be able to compete with CFPPs. The electricity prices from NPPs can be less than USD 0.10/kWh, while the price of electricity from diesel PP will rise to around USD 0.25/kWh [33]. The main point is to start looking for a solution before all fossil fuel resources vanish.

8 Concluding Remarks

Nuclear power technology represents a solution to the problem of increasing global CO₂ emissions. One choice is to apply or not apply this solution. Other choices include helping to facilitate technology transfer and engage in international collaboration in nuclear power technology implementation for countries that need NPP technology. The US government has shown its commitment to slowing global warming. On 14 July 2015, the agreement between Iran and six leading countries (P5 + 1: USA, UK, China, France, Germany, Russia) on a nuclear program for peaceful purposes in Iran has been signed [34]. Some members of the US Congress are skeptical of the agreement, mainly because of regional political issues. Could Indonesia get help in nuclear power technology implementation? If so, this would raise the possibility of an alternative energy solution instead of burning low-rank coal that emits CO₂, burning biomass waste and woody biomass (rain forest) –CO₂ sequestration facilities.

Kusmayanto Kadiman [35] stated the following: ‘Sociopolitical issues will be crucial. Without a formal statement to “Go Nuclear” from the government, nuclear power plants in Indonesia will remain trapped, and a techno-economic assessment will be conducted as an academic exercise only.’ The government should take the lead and step forward carefully to achieve social justice for all people in the Indonesian archipelago in order to reach a higher Human Development Index.

Appendix

Government Regulation No 79/2014 on National Energy Policy (PP no 79/2014 Tentang Kebijakan Energi Nasional or KEN in Bahasa).^[13]

Pasal 4: KEN sebagaimana dimaksud dalam Pasal 2 dan Pasal 3 dilaksanakan untuk periode tahun 2014 s/d tahun 2050.

Pasal 6 a: Sumber Daya Energi tidak dijadikan sebagai komoditas ekspor semata tetapi sebagai modal pembangunan nasional;

c. Ketersediaan Energi dan terpenuhinya kebutuhan Sumber Energi dalam negeri;

Pasal 8

a. tercapainya penyediaan Energi Primer pada tahun 2025 sekitar 400 MTOE (empat ratus million tonnes of oil equivalent) dan pada tahun 2050 sekitar 1.000 MTOE (seribu million tonnes of oil equivalent);

b. tercapainya pemanfaatan energi primer per kapita pada tahun 2025 sekitar 1,4 TOE (satu koma empat tonnes of oil equivalent) dan pada tahun 2050 sekitar 3,2 TOE (tiga koma dua tonnes of oil equivalent);

c. tercapainya penyediaan kapasitas pembangkit listrik pada tahun 2025 sekitar 115 OW (seratus lima belas giga watt) dan pada tahun 2050 sekitar 430 OW (empat ratus tiga puluh giga watt); dan

d. tercapainya pemanfaatan listrik per kapita pada tahun 2025 sekitar 2.500 KWh (dua ribu lima ratus kilo watt hours) dan pada tahun 2050 sekitar 7.000 KWh (tujuh ribu kilo watt hours).

Pasal 9 f: tercapainya bauran Energi Primer yang optimal:

1. pada tahun 2025 peran minyak bumi kurang dari 25% dan pada tahun 2050 menjadi kurang dari 20%;
2. pada tahun 2025 peran batubara minimal 30%, dan pada tahun 2050 minimal 25%; dan
3. pada tahun 2025 peran gas bumi minimal 22% dan pada tahun 2050 minimal 24%.

Pasal 10 (1) d. Ketersediaan Energi untuk kebutuhan nasional dipenuhi dengan: Pengembangan Energi dan Sumber Daya Energi diprioritaskan untuk memenuhi kebutuhan energy dalam negeri

Pasal 11

(1) Prioritas pengembangan Energi dilakukan melalui:

- a. Pengembangan Energi dengan mempertimbangkan keseimbangan keekonomian Energi, keamanan pasokan Energi, dan pelestarian fungsi Lingkungan Hidup;
- b. Pengembangan Energi dengan mengutamakan Sumber Daya Energi setempat;
- c. Pengembangan Energi dan Sumber Daya Energi diprioritaskan untuk memenuhi kebutuhan energy dalam negeri; dan
- d. Pengembangan industri dengan kebutuhan Energi yang tinggi diprioritaskan didaerah yang kaya Sumber Daya Energi.

(2) Untuk mewujudkan keseimbangan keekonomian Energi sebagaimana dimaksud pada ayat (1) huruf a, prioritas pengembangan Energi nasional didasarkan pada prinsip:

- a. Menggunakan batubara sebagai andalan pasokan Energi Nasional.
- b. Ketentuan sebagaimana dimaksud pada ayat (2) dikecualikan bagi Energi nuklir yang dimanfaatkan dengan mempertimbangkan keamanan pasokan Energi nasional dalam skala besar, mengurangi emisi karbon dan tetap mendahulukan potensi Energi Baru dan Energi Terbarukan sesuai nilai keekonomiannya, serta mempertimbangkannya sebagai pilihan terakhir dengan memperhatikan faktor keselamatan secara ketat.

Pasal 12 (2): Pemanfaatan Sumber Daya Energi nasional diutamakan untuk memenuhi kebutuhan Energi dan bahan baku.

Pasal 15 (2) b: Cadangan Penyanga Energi dipergunakan untuk mengatasi kondisi kritis dan darurat energi

Pasal 24 (2) g: Penguatan perkembangan Industri Energi sebagaimana dimaksud pada ayat (1) meliputi:

g. pemberian kesempatan lebih besar kepada perusahaan nasional dalam pengelolaan minyak, gas bumi, dan batubara;

Pasal 27(5)b: Penguatan pendanaan dilaksanakan dengan menerapkan premi pengurangan Energi Fosil untuk pengembangan Energi”.

Pasal 27(6): Premi pengurangan digunakan untuk kegiatan eksplorasi minyak dan gas bumi dan pengembangan Sumber **EBT**, peningkatan kemampuan sumber daya manusia, penelitian dan pengembangan, pembangunan infrastruktur pendukung”

Pasal 30: KEN menjadi dasar dalam penyusunan Rencana Umum Energi Nasional (R U E N) dan Rencana Umum Ketenagalistrikan Nasional (RUKN)

Undang Undang Dasar 1945. Note: * Perubahan II 18 Agustus 2000. ** Perubahan IV 10 Agustus 2002

Pasal 27 (3)*: Setiap warga negara berhak dan wajib ikut serta dalam upaya pembelaan negara.

Pasal 28C*

(1) Setiap orang berhak mengembangkan diri melalui pemenuhan kebutuhan dasarnya, berhak mendapat pendidikan dan memperoleh manfaat dari ilmu pengetahuan dan teknologi, seni dan budaya, demi meningkatkan kualitas hidupnya dan demi kesejahteraan umat manusia.

(2) Setiap orang berhak untuk memajukan dirinya dalam memperjuangkan haknya secara kolektif untuk membangun bangsa, dan negaranya.

Pasal 28I (2)*: Setiap orang berhak bebas dari perlakuan yang bersifat diskriminatif atas dasar apa pun dan berhak mendapatkan perlindungan terhadap perlakuan yang bersifat diskriminatif itu.

Pasal 30 (1)* Tiap-tiap warga negara berhak dan wajib ikut serta dalam usaha pertahanan dan keamanan negara.

Pasal 33 (2):** Cabang-cabang produksi yang penting bagi negara dan yang menguasai hajat hidup orang banyak dikuasai oleh negara. (In English: "the branches of fossil fuel production that are essential for the country and for the people's life are ruled by the State").

References

1. Gore A (2006) An inconvenient truth. Butler and Tanner L. Frome, Great Britain
2. Gore A (2009) Climate change training materials for the Asia Pacific summit participants. Melbourne, June 2009
3. IPCC (2014) Climate change 2014 synthesis report. Summary for policymakers, p. 5. Accessed on June 2015
4. United Nations Climate Change Conference—COP15/MOP5 (2009) Copenhagen accord. [Copenhagen](#), 7–18 December 2009
5. Suharta H et al (2015) Biomass for small power generation in the archipelagic islands of Indonesia host to the World's third largest forest. *ISESCO J Sci Technol* 11(19):76–89
6. IPCC Special Report on Carbon Dioxide Capture and Storage (2007) Fig. 8–4, p 352
7. Allen CD et al (2010) A global overview of drought and heat-induced tree mortality reveals emerging climate change risks for forests. *Forest Ecol Manag* 259:660–684
8. Nuclear power by country, from World Nuclear Association, Wikipedia, the free encyclopedia. Accessed 12 June 2015

9. U.S. Energy Information Administration, Annual Energy Outlook (2014) Early Release December 2013, DOE/EIA-0383ER(2014). Accessed 10 July 2015
10. Hasibuan SS (2004) Arah Kecenderungan Pemakaian Energi. Forum Komunikasi Ketenagalistrikan PT. PLN, 28 September 2003
11. KESDM (2005) Blueprint Pengelolaan Energi Nasional 2005-2025, Lampiran N1: Sasaran Energi Mix Nasional 2025 (scenario optimalisasi). Kementrian Energi dan Sumber Daya Mineral, Jakarta 2005. <http://www.esdm.go.id>
12. KESDM (2005), Blueprint Pengelolaan Energi Nasional 2005-2025, Lampiran P3.1 Road Map in Energi Nuklir 2025. Kementrian Energi dan Sumber Daya Mineral, Jakarta 2005. <http://www.esdm.go.id>
13. Statistical Year Book of Indonesia (2013) BPS, Jakarta, Indonesia, Table 6.2.1, p. 278
14. Peraturan Pemerintah Republik Indonesia Nomor 79 Tahun (2014) Tentang Kebijakan Energi Nasional, declared by President Republic of Indonesia on 17 October 2014
15. SMS communication with Abadi Purnomo, member of National Energy Council (DEN) of Republic of Indonesia on electricity target mentioned in Peraturan Pemerintah Republik Indonesia Nomor 79 Tahun 2014 Tentang Kebijakan Energi Nasional
16. Human Development Index vs Energy Consumption per capita. WREN, UK, September 2003
17. METI/IRES (2014) Hal-hal yang Diperlukan Untuk Pengembangan Energi Terbarukan Dalam Mendukung Ketahanan Energi Nasional. Discussion of METI/IRES with Tim Jokowi-JK, Jakarta on 26 August 2014. Note: IRES is Indonesia Renewable Energy Society; METI (IRES in Bahasa) is Masyarakat Energi Terbarukan Indonesia
18. BPS (2013) Statiscal Yearbook of Indonesia 2013. Badan Pusat Statistik, Jakarta, page after xxviii
19. Susilo Bambang Yudhoyono President of the Republic of Indonesia (2009) Intervention on Climate Change. G-20 Leaders Summit, 25 September 2009, Pittsburgh, at 13:00-working lunch
20. Maritje Hutape, the Director of Energy Conservation in The Misnistry for Energy and Mineral Resources Office (2015) Strategic planning for electricity generation in 2015–2019. In: Presented in workshop on nuclear power and small modular reactors in Indonesia. Sari Pan Pacific Hotel, Jakarta, 25 June 2015
21. Djoko Prasetyo (2013) Some power projects in Java to year 2021 and backbone transmission. In: Presentation on APEC conference on clean, renewable and sustainable use of energy, Bali, Indonesia, September 30–October 2, 2013
22. Statistical Year Book of Indonesia (2013) BPS, Jakarta, Table 6.2.2, p. 279
23. Statistical Year Book of Indonesia (2013) BPS, Jakarta, Table 6.2.3, p. 280
24. Statistical Year Book of Indonesia (2013) BPS, Jakarta, Table 6.1.1, p. 275
25. Statistical Year Book of Indonesia (2013) BPS, Jakarta, Table 3-2-7, p. 89
26. Keraf S (2015) PLTN Pilihan Terachir. Kompas Daily News, 9 June 2015, p. 7
27. Wilardjo L (2015) Surya, Fusi atau Fisi. Kompas Daily News, 15 June 2015, p. 7
28. Schaeffer M, van Vuuren D (2012) Evaluation of IEA 2012 emission scenarios. Climate analitic working paper 2012-1, 8 May 2012
29. WMO and UNEP representative (2013) Characteristic of post-third assessment report stabilization scenarios. In: Presented on APEC conference on clean, renewable and sustainable use of energy, Bali, September 30–October 2, 2013
30. Soetrisnanto A (2015) Deployment of nuclear energy in Indonesia, p. 8. In: Presented in workshop on nuclear power and small modular reactors in Indonesia. Sari Pan Pacific Hotel, Jakarta, 25 June 2015
31. KESDM (2005) Blueprint Pengelolaan Energi Nasional 2005–2025, Lampiran B2 Sumber Daya Radioaktif Indonesia. KESDM is Kementrian Energi dan Sumber Daya Mineral in Jakarta, <http://www.esdm.go.id>
32. IAEA (September 2014) Advances in small modular reactor technology developments. A supplement to: IAEA advanced reactors information system (ARIS). Accessed 30 July 2015
33. Arya Rezavidi (2015) Information on HTMR/HTGR for millist METI/IRES. 1 July 2015
34. AFP/AP/Reuters/CAL (2015) Muncul Keraguan di Kongres AS. Kompas Daily News, 16 July 2015, p. 9
35. Kusmayanto Kadiman (The Minister for Research and Technology of Republic of Indonesia, 2004–2009) Discussion in Millist METI/IRES, Jakarta, 1 July 2015

Chapter 25

A Study of Space Syntax and Sustainable Design in Chinese Vocational Education Parks: Three Case Studies

Qiushi Hao, Benchen Fu, and Teng Fei

Abstract Currently, China has 1334 vocational colleges. This accounts for 62.7 % of all colleges and universities in China. A large portion of vocational colleges is represented by vocational education parks. In China, *vocational education park* refers to a zone that includes multiple vocational educational institutions and their corresponding science parks combined to form a set of teaching, training, research, production, and social services located in one area. Their development is closely tied to city development planning. Because China's vocational education system developed relatively late, there is little past experience with building vocational education parks. As a result, vocational education parks are introspective and self-enclosed with fragmented layouts, dispersed resources, insufficient facilities, and incomplete systems. This phenomenon is becoming increasingly serious. This article is based on research on public space layout expansion for Chinese vocational education parks using urban intensification strategies. The intent is to look at strategies for integrating educational resources, leveraging economies of agglomeration, and continuing development in a compact space by building shared facilities, improving the campus land-use ratio, curbing energy consumption and environmental pollution, containing campus sprawl, and promoting vocational education parks to develop in a healthy, orderly, and sustainable way. This study applies composition analysis techniques to three vocational education park design cases with public space layouts. The study provides a quantitative analysis of the overall and localized degree of space integration and uses these values to perform linear regression analysis. The intensification layout style stands out as a superior approach that establishes a relationship for the composition of public space in a vocational education park. This relationship's decisive influence is explored based on an analysis of the education and administration style of vocational schools. A model and optimization proposal is put forward within a certain scope for the degree of space integration with respect to the jointly coupled factors of space composition, education style, and school administration style. With vocational

Q. Hao (✉) • B. Fu • T. Fei
Department of Architecture, Harbin Institute of Technology,
No. 73, Huanghe Road, Harbin, China
e-mail: haoqiushi@hit.edu.cn

education park public space intensification as a goal and the ability to numerically evaluate data based on degree of integration, vocational education park design evaluation criteria can be established. From now on, the proposed vocational education park public space layout intensification method will provide a scientific and quantitative standard that will ensure a sustainable design strategy for China's characteristic vocational education parks.

Keywords Vocational education park • Sustainability • Spatial synergy • Livability • Accessibility

1 Introduction

By 2016, the number of higher educational institutions in China reached 1335, and vocational educational institutions accounted for 46.9% [1]. However, if many schools are self-enclosed, lower levels of socialization between schools, scattered resources for education, and low building density over a large area will become increasingly common. In the city, sustainable construction, high density, hybridization (space sharing), and the interoperability of vocational education parks have already become important factors in the construction and development of vocational and technical schools. Also, by approaching problems from a novel perspective and planning, integrating resources between schools will lead to an increase in the scale of construction and the optimization of a space's architecture in practice. This core philosophy suggests that collaboration between vocational educational parks can be divided into three levels: (1) space coordination: a campus can achieve high space aggregation efficiency and a manyfold return on section use; (2) economic collaboration: each functional subsystem receives support from other functional subsystems; this produces greater economic value; (3) city collaboration: this can produce an aggregated, radiating, interactive, and synergistic effect on the surrounding city and even become the distinguishing symbol of a city/region.

1.1 Study Objective

This chapter selects three typical vocational education park styles for case studies on layout style [2]. They are classified as shared style (Lanzhou New Area Vocational Education Park), hybrid style (Harbin Vocational Education Park), and dispersed style (Changzhou Vocational Education Park). Their localization, function, and surrounding areas are all similar. The environmental similarities between the selected cases helps to increase this study's legitimacy.

1.2 *Study Perspective*

Each spatial subsystem can receive support from other subsystems; this produces more benefits for the same space [3]. These benefits include sustainability and interoperability. Interoperability in a vocational education park should focus on the spatial synergy between elements [4]. Two elements can have an overall effect on each other or have a multiplier effect on their existing qualities. This not only reflects the amount of integration in a functional space but also includes the space's overall degree of uniformity and coordination of the space's cost constraints, livability, and accessibility. This study presents high-level optimization techniques for construction and integration based around centralization, openness, socialization, and spaces that stimulate innovative thinking.

2 Methodology

This chapter uses three vocational education parks as case studies. Floor area ratio, building density, amount of students, and other specialized factors are analyzed in the selected vocational education parks. In reality, spatial architecture translates into a quantifiable space syntax model [5]. The case studies in this chapter look at the quantity of features and the floor area ratio. They explore spatial synergy in a vocational education park. (This study is aimed at investigating vocational education park campus environments and environmental quality on high-density campuses. It attempts to provide a preliminary summary and a standard of evaluation for campus environmental quality in order to fix an upper limit on the floor area ratio of a vocational education park [6].) Results are determined through software simulation and field analysis. A survey is used to obtain quantifiable data on livability and accessibility from all three of the vocational education parks whose layouts were studied [7]. The space syntax software Depthmap is used to carry out graph analysis; global integration and the correlation between models are calculated. (Integration reflects the number of steps by which two spaces are linked. A high degree of integration is the general goal: a space with higher integration generally has a shallower topological depth [8].) Linear regression analysis is carried out on the three vocational education park layouts, and global and local spatial synergy (livability and accessibility) are used to evaluate and index the system. In addition, architectural drawings and field research are used to analyze problems with feature configuration and spatial organization. This analysis will allow vocational education parks to become optimized and more collaborative.

2.1 Spatial Synergy Analysis

Synergy has two main aspects: livability and accessibility. In the context of space syntax, it acts as the axis for global integration. Local integration is linearly fit along with spatial synergy (R^2) [9].

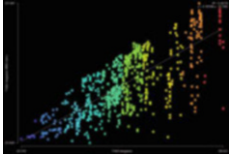
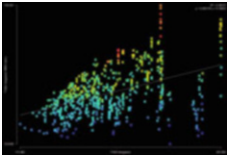
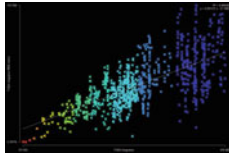
For $R^2 = 0$, there is no relation between global integration and local integration [10]. For $R^2 = 1$, there is a perfect relationship. For $0 < R^2 < 1$, there exists a partial correlation between global and local integration. When $R^2 > 0.7$, an increase in global integration leads to an increase in local integration with an almost linear relationship. R^2 measures the so-called fit between two variables; a better fit means a stronger correlation between global and local integration. From the global and local integration it is possible to infer the global and local synergy. Regarding the global flow of people and the local arrival flow, if $0.3 < R^2 < 0.7$, then there is a moderate linear correlation; global and local integration are certainly related, but further analysis is required to determine the relationship. If $R^2 \leq 0.3$ (a low degree of correlation), global integration cannot help to predict local integration [11]. The spatial synergy is poor, and the tendency is for the global flow of people to be separated from the local flow of arrivals. Through quantitative and qualitative analysis on the results of the software simulation, the relationship between livability (global integration) and accessibility (local integration) is researched for three categories of vocational education park. Based on this complex model of synergy, a system was created to evaluate quotas in a vocational education park (Table 25.1).

First, for the three vocational education parks' global integration and local integration at 800 m, linear fit analysis is performed, and the degree of correlation is determined. As shown in Table 25.2, Harbin Vocational Education Park and Lanzhou New Area Vocational Education Park have a coefficient of determination belonging to the moderate linear correlation category. Changzhou Vocational Education Park has a low linear correlation. Its coefficient of determination is 0.2, which means that the spatial synergy is poor. From these data we need to further analyze the spatial synergy of Harbin Vocational Education Park and Lanzhou New Area Vocational Education Park, namely for livability and accessibility.

Table 25.1 Linear correlation

Coefficient of determination ($0 < R^2 < 1$)	Correlation	State of spatial synergy
$R^2 \leq 0.3$	Low degree of linear correlation	Poor spatial synergy
$0.3 < R^2 \leq 0.7$	Moderate degree of linear correlation	Further study needed to determine spatial synergy
$R^2 > 0.7$	High degree of linear correlation	Excellent spatial synergy

Table 25.2 Spatial synergy analysis of three vocational education parks

	Harbin Vocational Education Park	Changzhou Vocational Education Park	Lanzhou New Area Vocational Education Park
Chart's coefficient of determination			
Local and global integration coefficient of determination at 800 m (R^2)	0.56	0.2	0.47
Relationship	Moderate degree of correlation	Low degree of correlation	Moderate degree of correlation

2.1.1 Livability

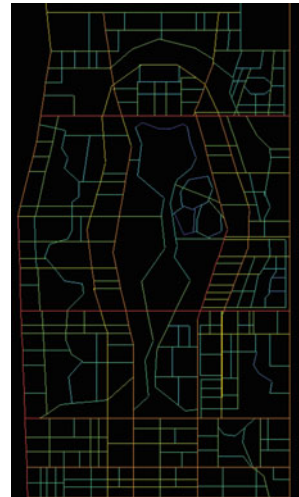
Livability is an important indicator in the evaluation of a vocational education park's spatial synergy. Different spatial architectures form different levels of accessibility and attractiveness in a spatial environment. Through a continuous, regular, distributed, and ordered development, maximization of equality and optimal distribution in a space can be achieved. In the context of space syntax, each indicator of global integration is used as a basis of evaluation.

First, according to each case's functional and spatial architecture, the layout is extracted, summarized, and abstracted into a spatial architecture analysis diagram (Figs. 25.1 and 25.2). Subsequently, using the aforementioned diagram as a map, spatial relationship topologies are generated using Depthmap software. The generated relational data are analyzed as shown in the diagram. In this chapter, the standard deviation and mean of global integration are investigated [12]. Three foreground network indicators for livability are subjected to quantitative analysis [13]. Standard deviation for global integration is a relative concept that measures the degree of dispersion for the distribution of global integration data. It takes into account deviations in global integration data and the mean value for global integration. A smaller standard deviation means smaller variance between data points, and for a large standard deviation the converse is true. The average value for global integration is the expected value of global integration. The foreground network coefficient as a measure of integration stands around 50% [14]. This indicates that more than half of the spaces' accessibilities are relatively good. From this definition it can be shown that the standard deviation value drifts up and down within a range from the average value. The overall average of a space's reachability is represented by the averaged quantized case. The foreground network table shows this value

Fig. 25.1 Harbin
Vocational Education Park
(global integration diagram)



Fig. 25.2 Lanzhou
Vocational Education Park
(global integration diagram)



written above the average. A space with good accessibility is generally well proportioned. Thus, livability can be measured through three relationships, as shown in the chart (Table 25.3).

It was discovered that Harbin Vocational Education Park's average global integration and standard deviation are both lower than those of Lanzhou New Area Vocational Education Park (Table 25.4). The former has a foreground network coefficient of 48.3% and the latter's is 43.5%. Comparing the two reveals that Harbin Vocation Education Park's livability is better than that of Lanzhou New

Table 25.3 Space livability assessment

Global integration (standard deviation)	Global average (integration)	Foreground network coefficient	Space livability assessment
Small	Large	Integration greater than 50 %	Overall livability very good
Large	Large	Integration greater than 50 %	Overall livability poor, but local vitality points could exist
Small	Small	Integration greater than 50 %	Overall livability is very good

Table 25.4 Livability in three vocational education park

	Harbin Vocational Education Park	Lanzhou New Area Vocational Education Park	Changzhou Vocational Education Park
Average global integration	235.2	343.9	186.7
Global integration (standard deviation)	47.7	68.7	35.2
Standard deviation coefficient	0.2	0.19	0.18
Foreground network coefficient (%)	48.3	43.5	44.8
Average topology depth	2690	2942	2674

Area Vocational Education Park. However, although the accessibility in the center is high, there are problems with low accessibility around the periphery.

2.1.2 Accessibility

Campus events have a cost-restricted aspect. If these events exceed some temporal and spatial limit, they cannot occur [15]. If the spatial depth occupies a relatively small area, beneficial economic activities will develop naturally and flourish. The average local integration reflects the distance between one space and each of the immediately surrounding ones. Because of this, the goal is to increase integration as much as possible. It is based on the distance that can be reached by walking 5–10 min. The scope of analysis is to find event efficiency within a radius of 400 to 800 m radius (Table 25.5). If the average distance is more than 400 m between two spaces, walking between the spaces becomes difficult (Figs. 25.3 and 25.4). By continuously testing and adjusting the service radius, two spaces’ local integrations and selectivity will increase by different amounts. Walking 800 m could expand Harbin Vocational Education Park and Lanzhou New Area Vocational Education Park. From comprehensive assessment of the average local

Table 25.5 Accessibility in three vocational education parks

	Harbin Vocational Education Park	Lanzhou New Area Vocational Education Park	Changzhou Vocational Education Park
Total land area (km ²)	0.35	14.5	5
Average topological depth	2690	2942	2647
Average local integration (400 m)	78.26	39.2	37.4
Average local integration (800 m)	133.48	68.5	58.8
Local integration standard deviation	46.8	26.3	35.2
Foreground network coefficient (%)	33.3	45	30.8

Fig. 25.3 Harbin Vocational Education Park [local integration diagram (800 m)]

integration, standard deviation, and foreground network coefficients, it can be observed that the Lanzhou New Area Vocational Education Park has better local integration and pedestrian accessibility. It is able to form a more focused and concentrated spatial organizational relationship.

2.1.3 Effect of Spatial Synergy

Through the foregoing analysis, it can be observed that the overall global space and local space of Harbin Vocational Education Park have relatively poor synergies (Table 25.6). Overall space livability is strong and the spatial organization relationship is very good, but the local space is not able to meet the scale requirements for pedestrians. This is because Harbin Vocational Education Park has a single

Fig. 25.4 Lanzhou Vocational Education Park [local integration diagram (800 m)]



Table 25.6 Spatial synergy evaluation

	Harbin Vocational Education Park	Lanzhou New Area Vocational Education Park	Changzhou Vocational Education Park
Spatial synergy evaluation	Livability: Excellent	Livability: Poor	Livability: Poor
	Accessibility: Poor	Accessibility: Very Good	Accessibility: Poor
	Spatial synergy: Okay	Spatial synergy: Okay	Spatial synergy: Poor

center architecture with strong spatial clustering. This creates high accessibility at the center of the space, but not at the periphery. Therefore, in systems with high integration, area layout and walkability are related features.

A rational partitioning function can cause a category to improve a space’s efficiency. Lanzhou New Area Vocational Education Park’s global livability is slightly less than Harbin’s. Even though its layout architecture is very good, the density is relatively high. Some local areas are formed that have special spatial environments. Furthermore, as park development and evolution continue, their local integration can follow global integration’s increasing trends. This can form healthy relationships between transportation and the flow of people. This is because Lanzhou New Area Vocational Education Park uses a multicenter architecture and multilevel sharing and has integrated features that are distributed organically to improve local spatial accessibility. Changzhou Vocational Education Park is the third case with the worst spatial synergy. On the one hand, the layout is dispersed. However, within the park, intercampus links are poor, which leads to poor livability. Furthermore, Changzhou Vocational Education Park’s academic facilities are arranged entirely on the east side, which reduces pedestrian accessibility. The overall evaluation of its spatial synergy is poor.

2.1.4 Spatial Optimization Recommendations

Because of different organizational features and functional installation differences, there are three styles of spatial synergy in vocational education parks (Fig. 25.5) [16]. These can be used to increase vocational education parks' configurational efficiency and balanced distribution. In addition, they can improve spatial synergy and sustainable development with the goal of optimizing the space [17]. Data were obtained through surveys investigating students' daily lives. In 45 % of schools, academic teaching and technical training were held in technical training rooms (Fig. 25.6). Too much academic teaching functionality creates a waste of spatial resources, which is contrary to the characteristics of a sustainable campus [18].

The following mixed-style vocational education park optimizations are proposed (Fig. 25.7). The foreground network constitutes the primary structure of the park. The top 10 % of ranked integration values will have the best reachability [19]. For optimization planning, 800 m is the maximum recommended mobility radius. With the foreground network as a key factor, increasing configurational efficiency in the technical training area is recommended to form a higher-quality central campus. It is also recommended that more concentrated clusters of practical teaching areas be established according to the spatial characteristics and actual demands of a campus. This will decrease the travel cost, thereby increasing accessibility. Recreational facilities, dormitories, and other functional facilities are optimal at the edge of the network. This increases travel efficiency and space efficiency. Relatively deep spatial depth leads to poor accessibility for a zone, so the surrounding quality should be increased. The spatial architecture should be such that the accessibility and use are fair among different groups of people.

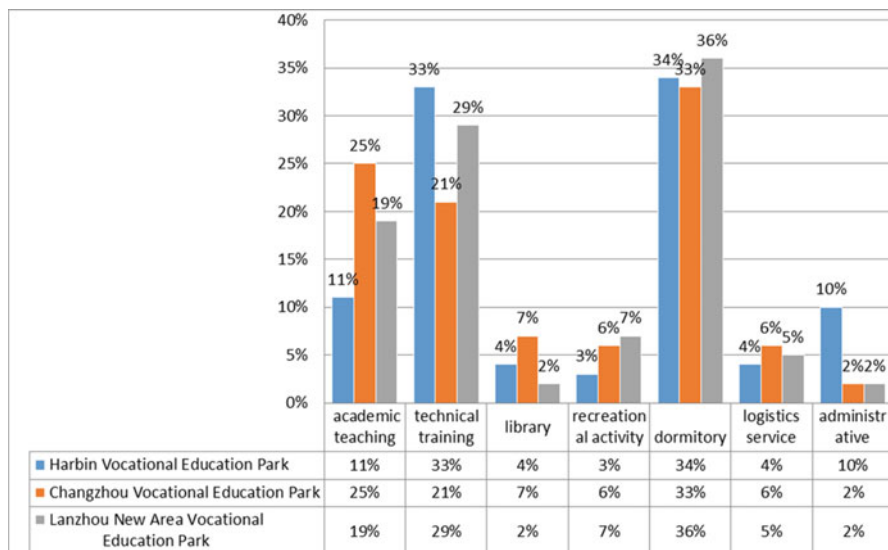


Fig. 25.5 Proportion of function in three vocational education parks

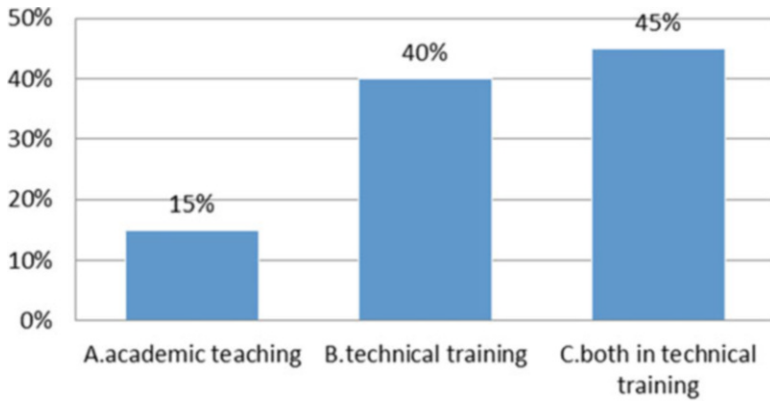


Fig. 25.6 Investigation of students' daily lives

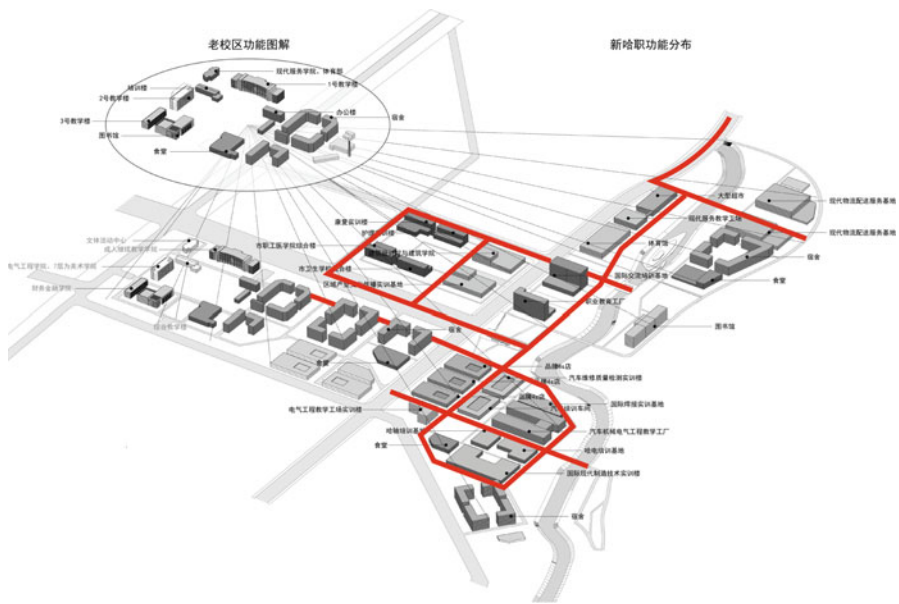


Fig. 25.7 Foreground network of Harbin Vocational Education Park

The following improvements are suggested for shared-style park optimization (Lanzhou New Area Vocational Education Park) [20]. From the city's perspective, Lanzhou New Area Vocational Education Park should adopt educational resources and aggregate, restructure, and develop new methods of utilization. Each campus's teaching, training, and other resources should be used with the intent of space improvement for a potential advantage. In selected spaces that have a topological advantage during construction, it is suggested that they assimilate to each campus's

characteristics to strengthen self-recognition and improve supply and demand efficiency. Planning the layout encourages neighboring teaching facilities to share an organized training area, production area, and teaching area, interlaced with the city's service system. Whenever possible, a campus's production area and community should be integrated. Duplicate facilities should be eliminated. At the same time, the shared link between regions should be emphasized, and park-level and city-level sharing should be established to improve livability.

The following recommendations are made for dispersed style vocational education parks. Changzhou Vocational Education Park has greater complexity and higher uncertainty than the others. Spatial synergy is poor, and there are no relations between the constituent campuses. This vocational education park layout is not recommended.

3 Conclusions and Discussion of Results

This chapter analyzes spatial synergy in vocational education parks based on space syntax. It effectively mixes group analysis and quantitative results for livability and accessibility. It finds a better way to solve spatial organization and synergy problems in a vocational education park. Furthermore, to provide new ways of thinking about layout optimization in a vocational education park's space, it establishes new methods for evaluating spatial synergy. The methods put forward in this study can also be applied generally to other types of campus.

In the future, following the large development of vocational schooling in China, vocational education parks will be used to train high-quality workers and promote sustainable vocational education development. This will enhance China's modern vocational education system and help it to play a more important role. Based on this research, the author puts forward the following ideas and recommendations for the development of spatial synergy in vocational education parks:

1. From an urban planning perspective, vocational education parks should set up close spatial links to the surrounding urban environment. This includes setting up more uniform interfaces, forming a more open network structure, and integrating teaching facilities, factories, and social facilities into one corpus. They should remove single-function and redundant features and instead focus on synergistic ones. This will lead to maximum social and economic benefits.
2. From an interior campus design perspective, full use should be made of a space's livability and accessibility, and spaces should have a synergistic and complementary relationship. Rational allocation of functional categories and plans should be used to improve reachability and guide space optimization regulations. According to the analysis, different teaching space construction and combination methods have a direct impact on campus layout and organization. For example, mixed-model campuses were created brand new for the entire region and set up according to subject type and spatial capacity. Based on the size and capacity of a space, the campus is divided into light and heavy areas.

Simultaneously, to avoid overemphasizing the flexible layout advantages of nonaxial parks, shared buildings should be fully blended, and tight spaces should overlap, to achieve effective space utilization and promotion.

3. From the perspective of the future information age, information technology continues to develop, influencing society as a whole on the psychological and physical levels. The development of network technology and real-time communication software makes different methods of teaching and self-teaching possible. With too large a park size, it would be difficult to allocate campus resources for these new challenges. Future vocational education parks will be fully open and only have spaces for learning. There will be no schools or boundaries between disciplines. Through network technology, any function or information will be achievable remotely. Functional units will be deconstructed, and no distinction will be made between indoor and outdoor. Buildings will transition naturally between each other, and the campus will appear to be more flexible and free.

References

1. Liang H (2009) The study on synergetics development and design of Guangdong vocational and technical college. Huanan University, Guangzhou 186–188
2. Chen W, Chen Y (2013) Lanzhou new district vocational education park design. *Lpaners* 1006-0022(2013)S1-0119-06
3. Wang Z, Wang Y (2015) A study on the structure of vertical space in urban complexes based on synergy theory. *Architect J*
4. Xinlei L (2012) The research of synergetic design for public space of urban complex. Chongqing University, Chongqing 20–126
5. Hillier B (1996) *Space is the machine: a theory of architecture*. Cambridge University Press, Cambridge 50–56
6. Guo B (2013) Research on the architectural planning of training space for Higher Vocational & Technical College in Shaanxi. Xian University of Architecture and Technology, Xian 61–66
7. Zhao X (2013) The research of planning and design of Dalian Vocational Education Park based on practical characteristics. Dalian University of Technology, Dalian 34–38
8. Sheng Q, Yang T, Liu N (2014) Spatial conditions for targeted and optional consumption: a space syntax study on Wangfujing area and three shopping malls. *Architect J*
9. Zheng L, Sun C, Liu L, Wang L (2012) Wandering crowd simulation based on space syntax theory. *Comput Aid Drafting Design Manuf* 22(2):68–73
10. Joao P, Alasdair T (2010) Introduction to UCL depthmap 10. UCL 5–6
11. Nourian G, Rezvani P, Sariyildiz IS (2013) A syntactic design methodology: integrating real-time space syntax analysis in a configurative architectural design process. In: *International space syntax symposium*, Seoul
12. Xia Z, Xu L, Wang P (2014) Pedestrian distribution, space and function in high-rise commercial complex. *Architect J*
13. Dou Q (2009) A space syntax investigation of the changes in residential district planning and design in Beijing. *Architect J*
14. Jin S, Yan A, Zhou L (2014) A study on the spatial distribution of public cultural facilities from the perspective of spatial cognition. *Architect J*

15. Hillier B, Yang T, Turner A (2012) Normalising least angle choice in Depthmap and how it opens up new perspectives on the global and local analysis of city space. *J Space Syntax* 3 (2):155–193
16. Li H (2013) Research on training building space design of higher vocational education. Chongqing University, Chongqing 32–35
17. Cao M (2011) Study on teaching space of engineering course higher vocational-technical college. Xian University of Architecture and Technology, Xian
18. Qu W-J (2011) Practical training space study for engineering vocational technical school. Xian University of Architecture and Technology, Xian 93–102
19. Zhou X, Lu Z (2013) Rereading environmental image in terms of spatial syntax. *Architect J*
20. Wang JS (2010) Characteristics of vocational and technical education in Singapore and its revelation to China. *J Higher Educ Sci Technol*

Chapter 26

Micro-Aeolic in Residential Districts: A Case Study in Sant'Arzenio (South-western Italy)

Dora Francese, Emanuela Adamo, and Shoaib Khanmohammadi

Abstract Renewable energies are sources of energy derived from inexhaustible natural resources. In other words, they are regenerated at the same speed at which they are consumed, and they are freely available. In the new millennium, we find multiple typologies of renewable energies, such as the sun and wind. The latter has undergone tremendous development and evolution owing both to economic and financial incentives and the increased concern with environmental protection. Initially, the integration of wind power into daily life was very difficult because the first power plants were very large, which caused great anxiety around the world – the so-called Not In My Back Yard (NIMBY) problem. For this reason the idea of a wind plant evolved into a softer idea which has brought both change in daily life and the respect for morphology, urbanism and city architecture. In Europe, wind energy has increased in use and quality more than in the USA. Germany and Denmark are the largest producers of wind energy, thanks to the quantity of the available rural spaces but also to effective policies, including permanent government subsidies. In Italy, in contrast, the wind energy boom occurred in the late 1990s. However, the country is reaching the standards of other European countries through widespread installations in Puglia, Sicily and Campania. But so far, we have made reference only to megawatt or multi-megawatt plants which are installed outside urban areas or in sufficiently hilly plains. A micro wind plant is different because it can be installed in an urban setting and inside buildings thanks to the advanced technology and reduced dimensions. A case study of micro wind power in the new scenario is the case proposed here of Sant'Arzenio in Campania. It is a small and uninhabited village which would allow the installation of equipment

D. Francese (✉)
CITTAM, Via Tarsia 31, Naples, Italy
e-mail: francese@unina.it

E. Adamo
Department of Architecture, "Federico II" University, Via Forno Vecchio, Naples, Italy
e-mail: emanuela.adamo@unina.it

S. Khanmohammadi
Department of Mechanical Engineering, Guilan University, Rasht, Iran
e-mail: shoaib.khanmohammadi@gmail.com

because of the open green spaces. The experimental work described here is aimed at promoting the return of citizens to the village.

1 Introduction

The natural evolution of an ancient village is that either it changes with the times and is used for different purposes or it is abandoned, with the ancient walls, buildings and dwellings left to decay. In fact, mainly in the interior parts of Italy, many small medieval towns have been neglected either by local authorities or by the inhabitants' young descendants, who prefer more modern homes in the valleys over the old stone buildings in the hills. These minor historic centres have recently attracted the attention of those interested in restoration, where the first order of business – job creation – has emerged as the main goal of local officials and citizens who are sensitive to cultural heritage.¹ Following the passage of national legislation which put in place restoration plans (Law 457/78), a number of old villages have received rehabilitation and restoration efforts, but rarely have these efforts actually brought cities back to life.

This chapter deals with research carried out between the University of Naples "Federico II", Guilan University (Iran), the Municipality of Sant'Arzenio and the Association GAV,² in which the historic part of Sant'Arzenio, the so-called Borgo Serrone, is a test subject. The centre has in fact been abandoned and needs restoring; a proposal has been put forth to make it an experimental tourist destination and a magnet for young people. Renewable energy systems will be installed following the development and design of special technologies, and an experiment will be carried out to evaluate the noise levels of such systems, in particular wind catchers and aeolic micro-structures.

2 Renewable Energy: Wind

The main objective of the Kyoto Protocol was to reduce temperature rises on Earth as a result of global greenhouse gas emissions, including from Italy, and the use of renewable sources of energy will be required if countries are to achieve this objective.

¹ On these minor historical centres' fate, see Guidoni E., *L'architettura popolare italiana*, La Terza, Bari 1980; Ausiello G., Calvino C., *La tradizione costruttiva mediterranea*, Luciano ed., Napoli 1999; D Francese, *Il benessere negli interventi di recupero edilizio*, Diade, Padova 2002.

² Gruppo Architetti Vallo di diano (Team of Architects of the Diano Valley region).

As is well known, renewable energy sources are the primary sources of almost unlimited energy, with no risk of pollution, unlike with fossil-based fuels. A renewable energy source is commonly called a renewable or alternative.³

The production of clean energy can be based on the following sources:

- Solar radiation, which produces chemical energy, thermal energy and electrical energy;
- Biomass fuel, which is used for feeding power plants for thermal energy and the cogeneration of heat and electricity;
- Marine flooding and waves;
- Meteoric downfall, which produces hydroelectric energy by means of level difference;
- Wind, which produces dynamic and electric energy.

The production of wind energy is based on aeolic plants, which are technological systems employing wind energy in active and passive ways. In particular, on the one hand, passive wind energy systems use the elements constituting the plant with no external action. A typical example is a wind tower, mainly used in construction in the Middle East. On the other hand, active wind energy is derived from external components which produce power to be transformed into energy.

The installation of this latter category of plants strictly depends on wind speed, which provides maximum efficiency for the plant. The tool used to evaluate the proper installation conditions is the anemometer and a flag with a wind direction marker (Fig. 26.1).

The verification of wind intensity is very complex, and outcomes are often unreliable. Therefore, the identification of wind energy capabilities for a particular area is better obtained through data on a long-term basis regarding the direction and

Fig. 26.1 Typical anemometer for catching wind (search <http://www.directindustry.it/prod/vaisala/product-7108-473884.html>)



³ See the definition in *Treccani Dictionary* <http://www.treccani.it/vocabolario/>



Fig. 26.2 Micro-aeolic (*left*) and mega-aeolic (*right*) plants (<http://www.synchronia.com/microeolico-made-in-italy/it3049f>) (<http://www.iltaccoditalia.info/sito/index-a.asp?id=13407>)

speed of the wind with respect to height; in particular, zone morphology affects the wind speed at ground level: the more corrugated the ground is (i.e. slope gradients, trees, buildings), the more obstacles the wind will face and, thus, the more reduced its speed will be.

In addition to the wind analysis, a territorial analysis should be carried out on the diversity in type of houses, historical and artistic assets and landscape values. Therefore, multiple simulations are required to optimize the overall production on yearly basis. In fact, it is important to evaluate the advantages of information on the environment and their impact on the targets.

Following the aforementioned analysis, the type of wind farm shall be selected by subject area. Basically, those systems can be classified as follows: low-power plants up to 20 kW, known as micro-aeolic, and plants with nominal power between 100 kW and 1.5 MW, known as mega-aeolic (Fig. 26.2).

The first category is also called a domestic wind farm since it is usually installed within civil buildings or in urban centres so as to produce sufficient energy to satisfy the need of a single family (two or three persons) or to feed lighting systems in open spaces. This kind of plant is characterized by a reduced height and a small size.

In contrast, mega wind farms are composed of a supporting tower over 100 m high with blades around 12 m in diameter. The blades, which are part of the wind generator and harness the wind, transforming it into kinetic energy, are usually placed at a distance of three to five times the diameter of the blades if the turbines are installed on the same line. Otherwise, if the turbines are installed on the same

row (a typical configuration on wind farms), then the blades are placed at a distance of five to seven times the diameter of the blades.

In addition to the foregoing classification, wind plants can also be categorized into

Horizontal-axis wind turbines,
Vertical-axis wind turbines.

In the case of an historic cultural centre, we believe that the best solution is a plant with a vertical axis because the position of the turbine actually helps to harness all the wind power, especially where there is low pressure.

3 Wind Energy Calculation

Wind energy is the kinetic energy of a stream of airflow with a mass m at a speed V . The calculation of m presents a problem. One way to measure density is to express it in terms of volume: $\rho = m/V$. The volume can be written $V = AL$. Here A is the cross-sectional area perpendicular to the wind stream and L is the horizontal distance. If it is assumed that $L = Vt$, then wind energy (E) can be expressed as

$$E = \frac{1}{2} \rho A V^3 t.$$

If m is the mass of air passing through a wind turbine per unit of time, then the change in momentum is $P = m(V_2 - V_1)$, which is equal to the produced thrust, where V_2 and V_1 are the downstream and upstream speeds far from the rotor. The absorbed power P and the rate of kinetic energy change can be written

$$P = m(V_1 - V_2)\bar{V},$$

$$E_k = \frac{1}{2} m(V_1^2 - V_2^2).$$

The two preceding equations should be equal because the retardation of the wind before the rotor $|V_1 - \bar{V}|$ is equal to the retardation of the wind behind it $|V_2 - \bar{V}|$; in addition, it is assumed that the velocity through the rotor is axial and that the velocity is uniform over the vane area. Then the power exerted by the rotor can be expressed as

$$P = \rho A \bar{V}^2 (V_1 - V_2) = \rho A \left(\frac{V_1 + V_2}{2} \right) (V_1 - V_2),$$

$$P = \rho A \frac{V_1^3}{4} [(1 + \alpha)(1 - \alpha^2)], \quad \alpha = \frac{V_2}{V_1}.$$

Analytical calculations show that for $\alpha = 1/3$, the power P is at its maximum. It can be concluded that when the final wind velocity V_2 is equal to one third of the upstream velocity V_1 , the power is at its maximum. Hence, the maximum power which can be recovered is $\rho AV_1^3(8/27)$ compared with the energy of the original wind, which is $(1/2)\rho AV_1^3$; it may be stated that an ideal wind turbine could recover 16/27 (or 0.593) of the power in the wind.

Wind turbine manufacturers usually provide turbine power curves at different wind speeds. If the power curve of the turbine is not available, the following equation can be used to estimate the power output of a wind turbine:

$$P_{\text{tur}} = \begin{cases} 0 & \text{if } V < V_c, \\ P_{\text{er}} \left(\frac{V^n - V_c^n}{V_r^n - V_c^n} \right) & \text{if } V_c < V < V_r, \\ P_{\text{er}} & \text{if } V_r < V < V_f, \end{cases}$$

where I_{er} is the rated electrical power, V (m/s) is the wind speed, V_c (m/s) is the cut-in wind speed, V_r (m/s) is the rated wind speed, and V_f (m/s) is the cut-off wind speed. Setting $m = 2$ is often sufficiently accurate for the analysis of wind power systems.

4 Case Study: Borgo Serrone-Sant'Arsenio

The research described here is intended demonstrate the application of some of the previously mentioned renewable technologies to a small historic centre in southern Italy.

The first housing cluster is characterized according to its Greek name *serrone*, by the inaccessibility of the place. Between 500 and 700 it had reached its maximum level of development until becoming a unique model and a typical example of a residential dwelling in the whole valley context for its architectural features and for the adopted rural typologies. It is situated in the highest part of the country and today is easily accessible via stone stairways linked by a roadway. The entire archaic urban structure is comprised of a series of houses built over bare rock, whose entrance is characterized by lithic portals. The linear urban conformation develops upward from the lower part to a vertex where a small, ancient, military-residential fortress has existed since 1598. Thanks to its location, the land has an abundance of interesting natural sites and provides a breathtaking panorama, where Vallo di Diano attracts the most attention.⁴

⁴ See the history on <http://www.comune.santarsenio.sa.it/pagina-8.html>

⁵ Degree days are defined and fixed by Italian Law 10/91.

CAPO PALINURO (SA) 185 m. s.l.m. (a.s.l.)											
TEMPERATURE											
MM	Tm	Tx 1d	Tx 2d	Tx 3d	Txm	Tn 1d	Tn 2d	Tn 3d	Tnm	Tx P85-15	Tn P85-15
Gen(Jan)	10.5	13.3	13.4	13.2	13.3	7.8	7.8	7.7	7.8	4.6	5.6
Feb(Feb)	10.2	13.4	13.1	13.4	13.3	7.4	7.1	7.0	7.2	5.0	6.0
Mar(Mar)	11.7	14.0	14.7	16.0	14.9	7.7	8.3	9.4	8.5	5.4	5.6
Apr(Apr)	13.8	16.9	16.6	18.2	17.2	10.3	9.7	11.2	10.4	5.4	4.6
Mag(May)	17.9	20.0	21.4	22.9	21.5	13.0	14.3	15.5	14.3	6.2	5.0
Giu(Jun)	21.7	24.5	25.3	26.6	25.5	17.0	17.7	18.8	17.9	5.0	4.8
Lug(Jul)	24.4	27.6	28.2	29.1	28.3	19.8	20.6	21.2	20.6	3.8	4.2
Ago(Aug)	25.0	29.5	29.1	28.1	28.9	21.8	21.5	20.3	21.2	3.8	4.4
Set(Sep)	22.3	26.9	26.2	24.9	26.0	19.2	18.7	17.6	18.5	4.8	5.2
Ott(Oct)	18.6	23.2	22.4	20.3	21.9	16.4	15.8	13.9	15.3	5.6	6.0
Nov(Nov)	14.4	19.1	17.4	15.7	17.4	12.9	11.4	9.8	11.4	5.2	6.2
Dic(Dec)	11.7	14.8	14.6	13.9	14.4	9.0	9.2	8.6	8.9	4.4	5.6
MM	NgTn ≤ 0	NgTn ≤ -5	NgTx ≥ 25	NgTx ≥ 30	GrGi > 0	GrGi > 5	GrGi 18	Txx	An Tx	Tnn	An Tn
Gen(Jan)	0.3	0.0	0.0	0.0	328	172	233	19.6	1994	-0.8	1985
Feb(Feb)	0.1	0.0	0.0	0.0	288	148	218	23.4	1977	-0.2	1983
Mar(Mar)	0.2	0.0	0.0	0.0	368	211	198	26.2	1994	-0.4	1987
Apr(Apr)	0.0	0.0	0.3	0.0	421	269	129	28.4	1971	3.8	1973
Mag(May)	0.0	0.0	4.3	0.0	565	407	35	33.4	1973	8.0	1992
Giu(Jun)	0.0	0.0	17.9	1.6	651	501	1	36.4	1982	11.4	1976
Lug(Jul)	0.0	0.0	30.2	5.7	766	609	0	38.4	1988	14.6	1978
Ago(Aug)	0.0	0.0	29.9	9.2	772	618	0	37.6	1999	13.4	1977
Set(Sep)	0.0	0.0	21.5	1.4	676	524	2	34.0	1994	9.2	1977
Ott(Oct)	0.0	0.0	4.3	0.0	574	420	24	30.8	1990	6.0	1997
Nov(Nov)	0.0	0.0	0.2	0.0	416	271	107	27.4	1992	2.4	1981
Dic(Dec)	0.0	0.0	0.0	0.0	348	199	190	22.8	1989	0.4	1980

Fig. 26.3 Climate information at clima.meteoam.it

The climatic data gathered from the closest weather station to the village, Palinuro Station, show that the reference climatic zone is zone D ($1440 < DD^* < 2100$). DD (degrees per day)⁵ is a unit used to measure thermal energy requirements. Such data are collected during a conventional heating period and represent the yearly sum of positive or negative difference between the nominal comfort temperature, 20° for Italy, and the daily average external temperature (Fig. 26.3).

As part of the proposed experimental work, the dominant winds were analysed. The following main wind types were recorded in the region:

- Tramontane, coming from the north (Fig. 26.4);
- Scirocco, coming from the south-east (Fig. 26.5).

The micro wind farm penetration in this village is bound with the historical nature of the place. Therefore, a solution was sought that would overcome this obstacle and identify a system which could integrate smoothly with the buildings and create low impacts from visual, social and acoustic perspectives.

After having performed a historical and climatic study of the suburb, some solutions from the points of view of both planning and energy saving were



Fig. 26.4 Tramontane in Borgo Serrone (drawing by Esposito-Orizzonte-Sportiello-Chianese)

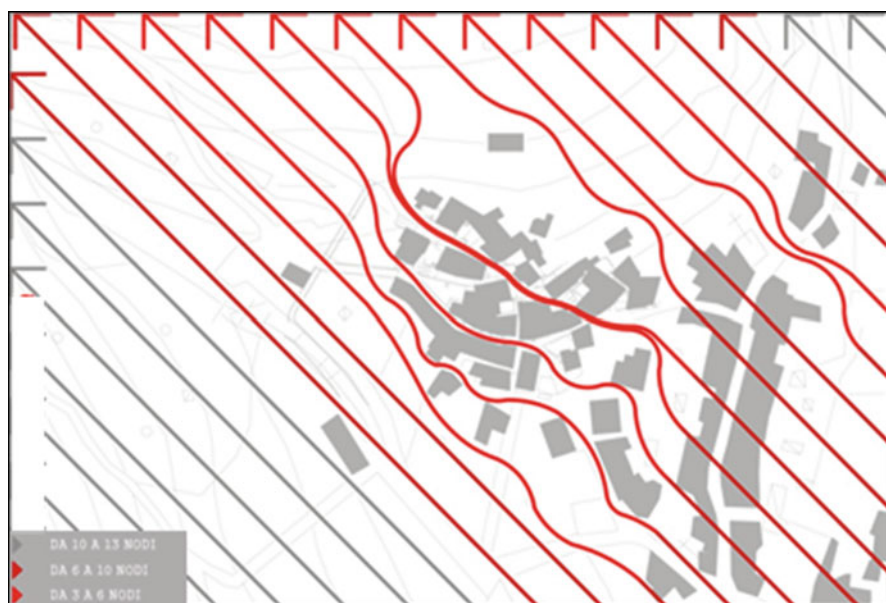


Fig. 26.5 Scirocco in Borgo Serrone (drawing by Esposito-Orizzonte-Sportiello-Chianese)

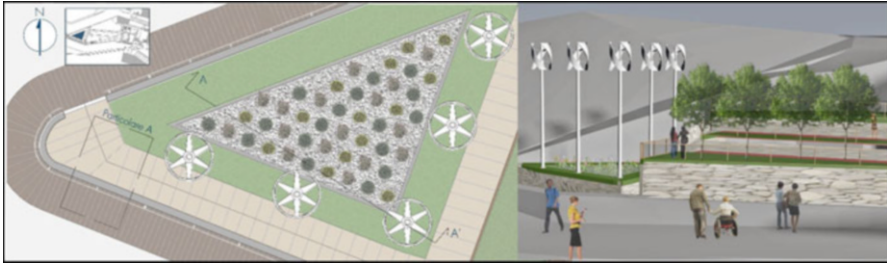


Fig. 26.6 A new micro-aeolic system designed by Arpino-Cerino-Cicchiello-Consalvo

developed. In this specific case, a solution has already been designed in the northern part of the village and selected for a new use destination. The pre-existing plant was integrated with vertical micro-aeolic shovels, which satisfies the environmental requirement of total zero carbon impact (Fig. 26.6).

The first two impacts can be mitigated through integration with the fabrics and by stimulating the population about the needed changes and the methodology. Nevertheless, mitigation of the acoustic impact remains a challenge because, so far, the research has focused on a solution to reduce the noise produced by the large wind generator. In fact, for micro wind plants, the acoustic issue has not yet been properly analysed.

To mitigate this problem and to find a common solution, meaning one that is suitable for both the vertical and horizontal shovel plants, experiments which would ultimately lead to the development of various prototypes will have to be conducted. A comparison of the mitigation levels or the removal of noises coming from the single systems will provide the optimal solution.

References

1. AA. VV (2013) Sistemi eolici. Impianti micro, mini e multi megawatt. Maggioli Editore, Rimini
2. AA. VV (2008) Architettura energetica. Ricerche e proposte per una visione energetica dell'ambiente costruito, Gangemi Editore, Roma
3. Masullo A (2013) Qualità vs. Quantità. Dalla decrescita a una nuova economia. Lit Edizioni, Roma
4. Palumbo M (2012) Architettura produttiva: principi di progettazione ecologica. Maggioli Editore, Rimini
5. Gazzetta ufficiale GU L 130 del 15.5.2002
6. AA. VV Treccani Dictionary. <http://www.treccani.it/vocabolario/>
7. <http://www.comune.santarsenio.sa.it/pagina-8.htm>

Chapter 27

Effect of Shadows on the Performance of Solar Photovoltaic

Hussein A. Kazem, Miqdam T. Chaichan, Ali H. Alwaeli, and Kavish Mani

Abstract This chapter investigates the reduction in photovoltaic (PV) performance due to artificial factors generated by covering each row and column in an array of a solar panel. This covering leads to an overall degradation of the energy produced by that panel. Experiments on the shadow effects of artificial cover, which leads to degraded power generation, were conducted and analyses performed. The obtained results show that the variation in the reduction of PV voltage and power produced from each cell depends on the shadow effect created. Shading causes a decrease in the output of PV, and this chapter's experiments illustrate the extent of that reduction. The difference between shading of cells in series, in parallel, and a combination of series and parallel with respect to time and temperature are also studied. Another factor examined is the artificial thickness of shadows on the surface that is causing the shading.

1 Introduction

As the human population continues to grow, the need for energy, electricity, and water is at an all-time high; energy factories have taken over the world using the best technologies to harvest natural resources. The problem with those natural resources is that most of them are nonrenewable sources; they are depleted. Renewable energy came to be an alternative energy source that could one day replace currently used sources like fossil fuels, that is, oil, coal, and natural gas.

Solar energy is an alternative clean and renewable energy source that could solve the environmental problems facing humanity. Many locations all over the world possess excellent sunshine conditions that make the use of photovoltaic (PV) power generation a viable option. However, PV arrays are affected by temperature, solar

H.A. Kazem (✉) • A.H. Alwaeli • K. Mani
Sohar University, PO Box 44, Sohar PCI 311, Oman
e-mail: H.Kazem@soharuni.edu.om

M.T. Chaichan
University of Technology, Baghdad, Iraq

irradiation, and shading [1, 2]. Shading, whether complete or partial, is caused by clouds, adjacent buildings, towers, or trees; in addition, telephone poles affect cell temperatures and incident solar radiation [3, 4].

Photovoltaic arrays are characterized by the nonlinear instrumental variables (IVs) of PV curves. Stabilizing these curves under variable environmental conditions is a challenging task that becomes more complicated in partial shading conditions when PV arrays do not receive uniform irradiance [5, 6]. Because of the high initial costs of PV systems, the available solar energy must be optimally captured [7]. Although the improvement of PV cell design and fabrication is a crucial issue, the enhancement of the overall performance of PV systems carries the same importance [8].

Shading reduces the power produced by PV arrays and causes a safety hazard [9]. Under partially shaded conditions, the existence of multiple maxima in PV and IV curves makes the PV array characteristics more complicated. The problem in multiple maxima is in the reduction of the PV effectiveness at the maximum power point tracking (MPPT) systems [10]. The drawback of this condition is that it makes it impossible to discriminate between local and global peaks and the output power reduced as a result [11].

Understanding the shading effects on a PV array's performance is crucial because such an understanding can facilitate amelioration of its design and efficiency [12]. Over the years, many researchers studied PV array characteristics and the influence of many design and operating factors [13–15]. However, studying the shadow effect can follow a methodology similar to those mentioned in the literature and can neglect a number of elements. For example, in this chapter, the effect of light intensity is overlooked. The factors discussed in what follows include time, temperature, and open-circuit (OC) voltage. Knowing that time is related to temperature but not having a particular quantity to relate it, two experiments were conducted to study the effect of shading over time and another under a certain temperature regime.

The primary objective was to explore the shading effect on PV cells to determine the degree to which it would degrade and how serious a problem cell shading is. In addition, it is important to understand issues like series, parallel, and series–parallel shading.

2 Experiments and Methodology

The PV cells used in the tests were multicrystalline PV cells. Table 27.1 illustrates the characteristics of the studied PV parameter.

The studied PV parameter is the OC voltage. Moreover, from the studies that were conducted, the following ideas were taken into consideration: PV parameters, effect of time and temperature, and type of material used to cover the PV. The study procedure was to apply the artificial effect and doing the experiments under

Table 27.1 Tested PV cell specifications

Module type	10 (17) P285*350
Peak power	10 W
Open-circuit voltage	22 V
Short circuit current	0.64 A
Peak voltage	17 V
Peak current	0.59 A
Maximum system voltage	600 V

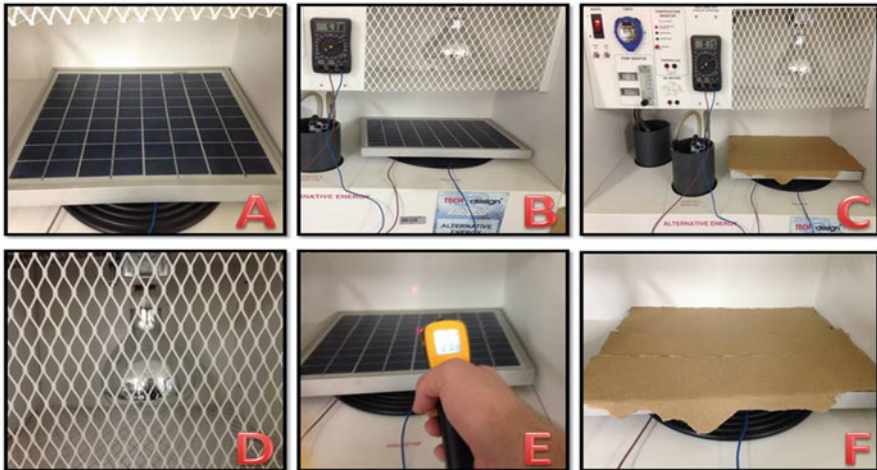


Fig. 27.1 Tools used in experiments: (a) PV, (b) PV location, (c) PV placed and covered entirely with paper boards, (d) light bulb, (e) laser-IR-temperature gun in process, (f) paperboard covering PV

standard testing conditions (STCs). The STCs have a temperature of 25 °C, solar radiation of 1000 W/m², air mass of 1.5, and wind speed of 2 m/s.

The following experiments were conducted:

1. Applying artificial shade on PVs for series, parallel cells, series–parallel shading, and alternative arrays registering the initial value of OC voltage and then waiting 1 min to calculate the value again for the OC voltage.
2. Applying artificial shade on PVs for series, parallel cells, series–parallel shading, and alternative arrays registering the value of the OC voltage when the surface temperature of the PV is 30 °C.

A multimeter was used to calculate the electrical quantity (OC voltage). Also, an infrared (IR) digital temperature meter gun with a laser pointer (surface temperature), artificial light bulb, and pieces of paperboard and, as well as a timer, were used in the experiments. Figure 27.1 shows the elements and tools used in the two experiments.

3 Results and Analysis

Following completion of the two experiments, for test number 1, the following results were obtained (Figs. 27.2, 27.3, and 27.4):

Figure 27.2 shows a clear though insignificant reduction in the value of the PV voltage, from an initial value of 19–17.99 V, which is around 1.01 V. When counting the effect of time, the difference is even smaller, with one covered cell having an open-circuit voltage of $V_{OC} = 18.74$ V, which is 0.26 less than the initial value.

Figure 27.3 shows that shadow on the parallel array combination caused a greater reduction than combinations in series or parallel. The smallest value of OC voltage was 12.53 V after 1 min, compared to 17.81 V, also after 1 min.

Figure 27.4 illustrates that the shadow on individual cells in parallel causes a reduction in output voltage close to the production of cells connected in series. If the time taken for cells in series is about 10 min, while for parallel it is about 4 min, this means that the parallel combination caused a greater reduction than cells in series when exposed for the same amount of time. Comparison of the four cells that are covered in parallel to the other four included in the series reveals that four cells in the series have 0.44 V reductions, while the four cells in parallel have 1.19 V reductions.

Fig. 27.2 Open-circuit voltage measurement for PV cells in series

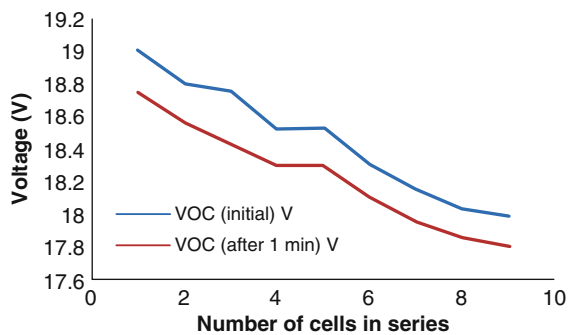


Fig. 27.3 Open-circuit voltage measurements for PV cells in parallel (entire columns)

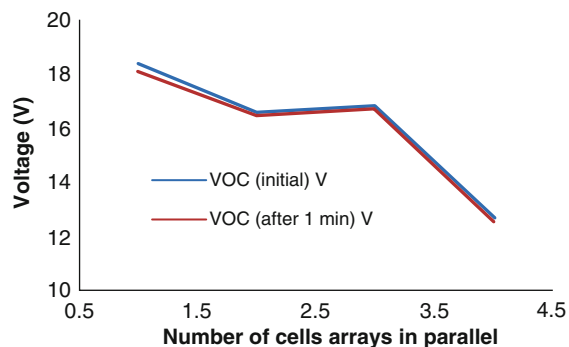


Fig. 27.4 Open-circuit voltage measurements for PV cells in parallel (individual cells)

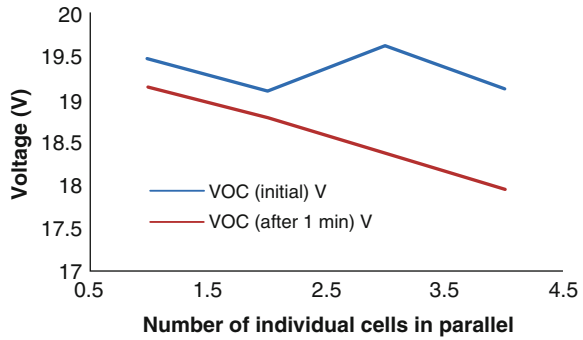


Fig. 27.5 Open-circuit voltage of PV cells in series

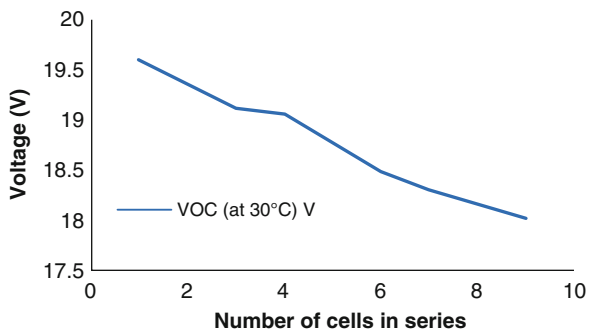
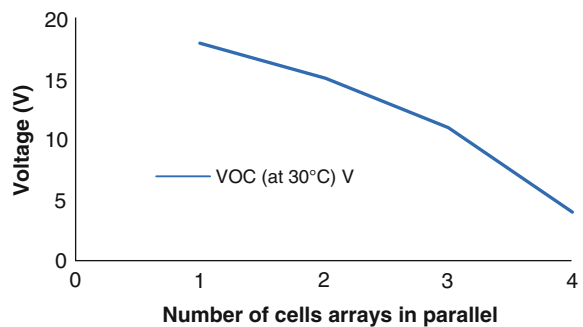


Fig. 27.6 Open-circuit voltage of PV cells in parallel (entire column)



For experiment 2 a different method was used. Instead of recording the time to measure the voltage, a surface temperature of 30 °C was chosen. Once the surface of the PV cell reached 30 °C, the voltage measurement was recorded. Figures 27.5, 27.6, and 27.7 illustrate the results.

Figure 27.5 shows a reduction in the OC voltage of 18.02 when nine cells connected in series are covered. This voltage reduction represents a noticeable decrease, but it is not extremely significant.

Figure 27.6 shows a clear and significant reduction in output voltage when almost all cells are covered (four rows in parallel). It is important to note that the

Fig. 27.7 Open-circuit voltage of PV cells in parallel (individual cells)

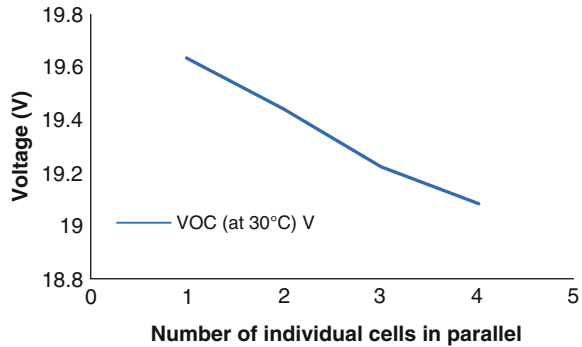
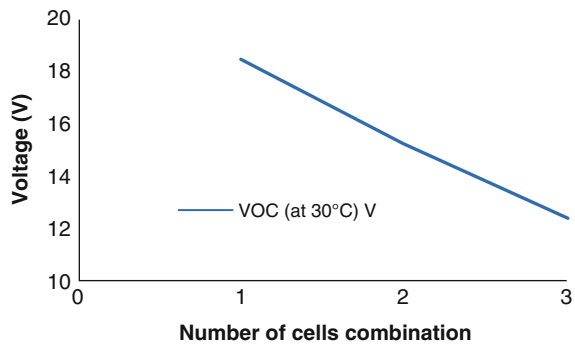


Fig. 27.8 Open-circuit voltage of PV cells in series-parallel combination



small amount of light reaching the cell forced it to produce these 4 V instead of dropping to 0 V.

Figure 27.7 illustrates that the reduction in OC voltage is not significant, but it does exist. It was approximately 0.54 V, which is more than the case with four cells in series, which was approximately 0.52 V.

Figure 27.8 also shows a clear and significant reduction in the output of the PV when four of its cells in series were covered and four of its cells in parallel were included.

4 Conclusion

Shadows covering PV cells do indeed have an adverse impact on PV output voltage; however, the reduction varies depending on how many cells are included and on the cells' combinations. The experimental results show that the largest decrease in output voltage of a multicrystalline PV occurs when parallel combinations of a PV cell are covered by shadows. At the same time, the smallest reduction occurred when the cells involved in series connection.

When nine cells in series were covered, the output dropped to approximately 2 V (with respect to time), but when four arrays of cells in parallel were covered, it fell to almost 6 V. This shows that it is important to compare the effects of shadows in connection with the combinations of cells covered.

References

1. Shaiek Y, Ben Smida M, Sakly A, Mimouni MF (2013) Comparison between conventional methods and GA approach for maximum power point tracking of shaded solar PV generators. *Solar Energy* 90:107–122
2. Tian H, Mancilla-David F, Ellis K, Muljadi E, Jenkins P (2013) Determination of the optimal configuration for a photovoltaic array depending on the shading condition. *Solar Energy* 95:1–12
3. Abdulazeez M, Iskender I (2011) Simulation and experimental study of shading effect on series and parallel connected photovoltaic PV modules. In: Proceedings of the 2011 seventh international conference on electrical and electronics engineering (ELECO), pp 28–32
4. Patel H, Agarwal V (2008) MATLAB-based modeling to study the effects of partial shading on PV array characteristics. *IEEE Trans Energy Conversion* 23(1):302–310
5. Ramaprabh R, Balaji M, Mathur BL (2012) Maximum power point tracking of partially shaded solar PV system using modified Fibonacci search method with fuzzy controller. *Electr Power Energy Syst* 43:754–765
6. Ishaque K, Salam Z, Syafaruddin A (2011) A comprehensive MATLAB simulink PV system simulator with partial shading capability based on two-diode model. *Solar Energy* 85:2217–2227
7. Kuznetsov IA, Greenfield MJ, Mehta YU, Merchan-Merchan W, Salkar G, Saveliev AV (2011) Increasing the solar cell power output by coating with transition metal-oxide nanorods. *Appl Energy* 88:4218–4221
8. Chou CS, Guo MG, Liu KH, Chen YS (2012) Preparation of TiO₂ particles and their applications in the light scattering layer of a dye-sensitized solar cell. *Appl Energy* 92:223–224
9. Masters GM (2004) Renewable and efficient electric power systems. Wiley, Englewood Cliffs
10. Koutroulis E, Kalaitzakis K, Voulgaris NC (2001) Development of a microcontroller-based photovoltaic maximum power point tracking control system. *IEEE Trans Power Electron* 16 (1):46–54
11. Bruendlinger R, Bletterie B, Milde M, Oldenkamp H (2006) Maximum power point tracking performance under partially shaded PV array conditions. In: Proc. 21st EUPVSEC, Germany, pp 2157–2160
12. Koutroulis E, Blaabjerg F (2012) A new technique for tracking the global maximum power point of PV arrays operating under partial-shading conditions. *IEEE J Photovoltaics* 2 (2):184–190
13. Alajmi BN, Ahmed KH, Finney SJ, Williams BW (2011) Fuzzy logic-control approach of a modified hill-climbing method for maximum power point in micro-grid standalone photovoltaic system. *IEEE Trans Power Electron* 26(4):1022–1030
14. Muhammad AK, Saon S, Chee WS (2013) Development of optimum controller based on MPPT for photovoltaic system during shading condition. *Procedia Eng* 53:337–346
15. Ramaprabh R, Mathur B, Murthy M, Madhumitha S (2010) New configuration of solar photovoltaic array to address partial shaded conditions. In: Proceedings of third international conference on emerging trends in engineering and technology, pp 328–333

Chapter 28

Study of Landform-Reconstruction Method Applied to Architectural Forms in Cold Areas

Chen Shuo and Mei Hongyuan

Abstract Since the emergence of the practice of transforming architectural structures into landscapes, the relationship between architecture and the environment has gradually changed from one of binary to multivariate opposition. This chapter introduces topography and field theory in cold-region architectural design and discusses the responses of architectural structures to spaces and landscapes that are influenced by the extreme climate in cold regions through relevant case studies by blanking, simulating, and mixing architectural forms with landforms.

Keywords Landscape architecture • Cold region • Architectural form • Landform reconstruction

1 Design Background of Landscape Architecture of Architectural Form in Cold Areas

The architectural space formed by changes to the land is not the result of current practices. The cave dwelling in the northwest of China and the so-called grotto (Fig. 28.1) architecture in Cappadocia, Turkey, is living space created in a natural setting (Fig. 28.2). Similarly, people in the cold northeast countryside of China still use cellars for the long-term storage of food during the very cold winters (Fig. 28.3). The use and reform of the land seep into people's production and lives and closely correspond to the regional climate and lifestyle. Meanwhile, they subtly influence people's understanding of the land.

The shaping of architectural forms in cold areas is the process of adapting to nature. The average temperature in cold regions is low, hours of sunshine are few, and the winter is snowy, windy, and dusty. Architectural elements, such as high stylobates, small north-facing windows, and sloping roofs, exist in protogenic vernacular architectures in cold areas of China and allow for adaptations to cold climates by using the advantages and avoiding the disadvantages of such regions.

C. Shuo (✉) • M. Hongyuan
Heilongjiang, China

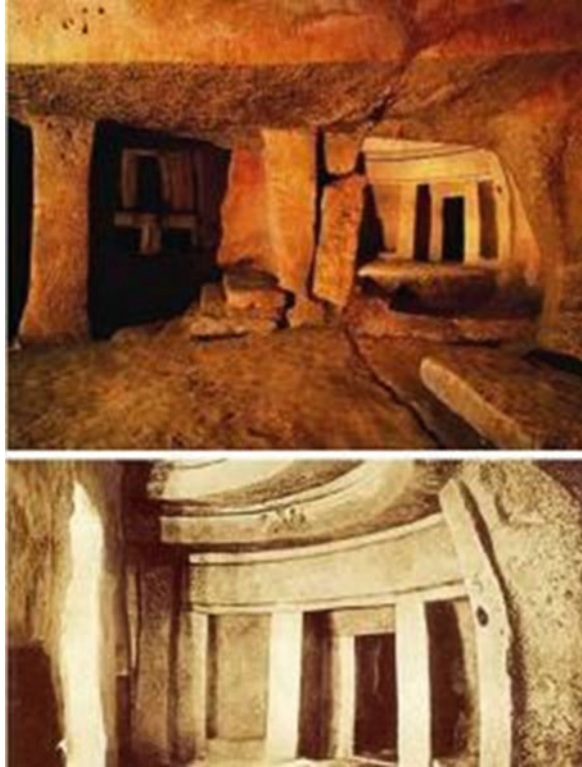


Fig. 28.1 Cave dwelling in mountains



Fig. 28.2 Grotto architecture

As approaches to ecological construction, organic architecture, and regional architecture seek to integrate architectural forms into the terrain of cold region architecture, cold region architecture starts to transform from a closed, monotonous type into a multivariate and open one. Architecture actively responds to the natural

Fig. 28.3 Cellar

environment, as demonstrated, for example, by the introduction of sunlight, the burden of cold wind, and the integration of appropriate technology to preserve heat and conserve energy in buildings [1]. Meanwhile, the expression of regional relations of architecture has been attracting increased attention. The architectures are not limited to the refining and reappearance of history and the mutual excitation among people, architecture and environment gets more attention. Architects emphasize that culture should have continuing vitality. In the treatment of the relationship between architecture and the environment, modern architecture no longer emphasizes simply the façade. However, various approaches to integrating an architectural style with the environment are possible.

As complexity science is incorporated into the field of architecture, design methods have been undergoing unprecedented expansion as structures now have the full-scale openness, noncentrality, and inseparability of complex systems [2]. Architect Greg Lynn overlaid impact factors on architectural structures using digital tools. He has explored extensively architectural skin, space, and so on to transform architectural spaces and entities from ones possessing clarity and singleness of modernism into structured that interlacement and illegibility [3]. His exploration also establishes the theoretical basis for the integrated design of architecture and space. In addition, the introduction of topography not only makes architects focus on construction activities but also is extended and expanded into extensive



Fig. 28.4 Yokohama Wharf, Japan

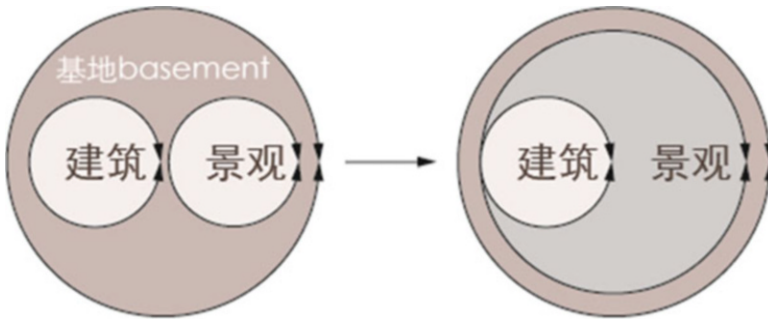


Fig. 28.5 Integration of architectural styles into landscape field (drawing by author)

processes of land reform. The terrain as the matrix of architecture, landscape, and planning constitutes the interrelation of the three. The terrain also promotes the development of landscape architecture of architectural form, for example, the workers of FOA break through the category of typology and replace direct imitation with the abstraction of form and topology of structure. The relation between form and function is more direct and abundant. In the design of Yokohama Wharf in Japan, the problem of a complex streamline is solved and the architectural form is integrated into the complex and volatile environment through the topological operation of the terrain [4] (Fig. 28.4). The existing state of the complex coexistence and flow of substance, personnel, and information and the surrounding architecture is mainly described in “Field Theory” by Stan Allen. It is the basis of form and space and can integrate different elements into a whole. Meanwhile, it respects personality [5]. It is in keeping with “Place Theory” of Norberg Schulz that place must have obvious bounds and boundaries; place is experienced as interior and place, routes and field are the basic schema of positioning. This means that the composition elements of space exist and the space begins to become the real dimension that can detect the existence of the people when these elements are combined. In these theories, architectures no longer occupy the leading role; they are integrated into the field with the matrix of landscape and domain (Fig. 28.5). The objects of study are transformed from architecture entities into the relations among architecture, landscape, sites, behavior, and so on. This change expands the meaning and category of landscape architecture.

2 Reconstruction Method

The reconstruction of land architectural form responds to different environmental contexts with various environmental strategies. The analysis of a profile includes the raised surface of architectural form under the surface, simulated landform above the surface, and the mixed surface among surfaces. These express three strategies of blanking, simulation, and reshaping of the environment (Chart 28.1). In what follows, we will examine the reconstruction method of architectural form in cold areas with cases from the point of view of these three aspects.

2.1 Form Blanking

In cold regions, site design is relatively independent of the architectural space owing to the comparatively closed posture shown by architectures.

Communication between indoor and outdoor spaces in architectures is mainly introduced by windows and courtyards, which has relatively single forms and makes people’s experience of walking limited. Blanking and refactoring of architectural forms retain the continuity of the original environment and reposition the relationship between architectures and sites to extend and regenerate the original environment. They become involved with the earth’s surface based at a minimal level to form a dearchitectural site response. Upheaval and deformation are the common ways of retaining a smooth connection between a building’s outline and its surroundings. Side interfaces of architectures blank in the environment, continue the original texture of sites, and become the extension of sites. On the surface, it seems to change the forms of the underlying surface only, but actually, it results in the activation and reorganization of the whole space of sites.

In the design of a gymnasium newly built in Hellerup Senior High School in Denmark, the gymnasium could only be built in the yard because the multifunctional space and sports facilities were insufficient and the space itself was not large enough. Bjarke Ingels’ design is just like a hill formed naturally by the upheaval of the land. It conceals the volume of the gymnasium under it, which not only meets the functional requirements of a large space but also has no outdoor active space occupying the land. On the contrary, it allows for more activities




Diagram			
Environmental Strategy	Blanking: the minimum intervention	Simulation: the similar aspects and integration	Reshaping: the extension of the field

Chart 28.1 Reconstruction of land architectural form and environmental strategies (drawing by author)

because of the elimination of the land's ups and downs. There are benches and scattered single-person chairs on the board for various activities. At the same time, they change the courtyard, which used to be a space that served as a means of going from one location to one's final destination (Fig. 28.6). In addition, in the Museum for Argo project designed by Not A Number Architects, the same techniques are adopted. The form of the museum is created by a square plane and a hyperbolic wooden roof. The roof is a wavy structure, rising from the land. The design is that of a pented roof and the IMAX theatre inside takes advantage of the two peaks on the roof. An amphitheater is formed making use of the lowest point of the roof touching the land and becomes an active space between functional volumes of major building structures (Fig. 28.7). It conforms to the forms with a natural transition to seats and steps and blurs the bounds of the land and the roof to give people a perception of continuous space.

2.2 *Stimulation of Architectural Form*

The architecture of landform reconstruction makes architectural form become part of the terrain. The architectural form of landform reconstruction and landscape space overlap. This stimulates people's synesthesia faculties by drawing on the participation, experience, and simulation of natural form; meanwhile, landscape boundaries in free form are conducive to revealing the feeling of landscape elements. Japanese architect Kijo Rokkaku proposed making the opinion of nature blend into architectural creations. His buildings try to produce comprehensive sensory communication with people. The architectural form reconstructs stimulative to landform and the complexity of metaphysical nature all provide a direct association of landscape with the stimulation form. It does not simply copy nature but follows the logic of construction and stays close to nature as well.

In the 1990s, starting from the residential area in Rebstock Park, which was designed by Peter Eisenman, the construction industry formed a tendency in landscape architecture to move gradually in a horizontal direction, form a huge mass, and merge the form with the land and urban texture. Buildings simulate the natural landscape in terms of, for example, folds or gradients, which causes the buildings to become better integrated into the natural background. The practice spread inland to artists' studios on the lakeshore, built in Beijing in November 2011, where the lake is to the east of the base and much higher. In the west and south were retaining walls 4–6 m high, and close to the north there was another building. In view of the land characteristics, the designers aimed to develop a project that could integrate with the terrain and make the building a landscape architecture and become part of the lake bund. The boundaries of the roof and façade in the usual sense disappeared, and the building showed an open form like a bank (Fig. 28.8). Although it is a single-story building, the roof and façade are scattered randomly and couch together, which makes the inside space bright and drafty while showing a rich roof shape.

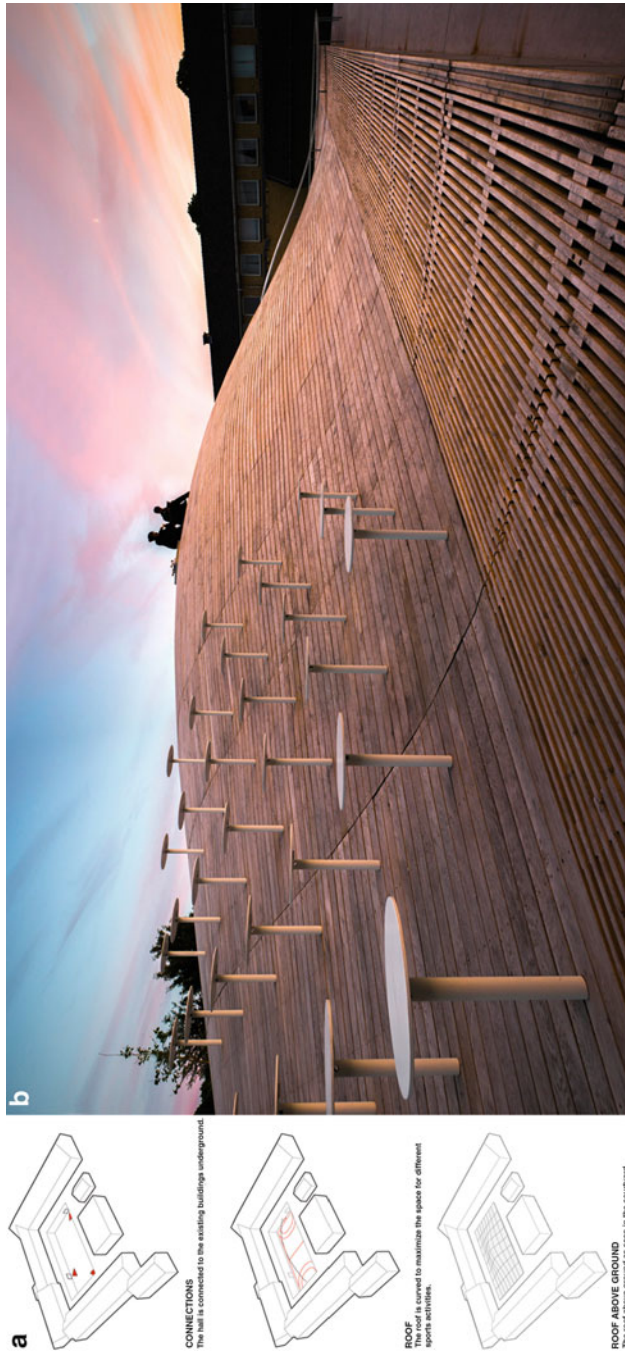


Fig. 28.6 Newly built gymnasium in Hellerup Senior High School in Denmark. (a) Form generation. (b) Arc-shaped board formed by courtyard land upheaval

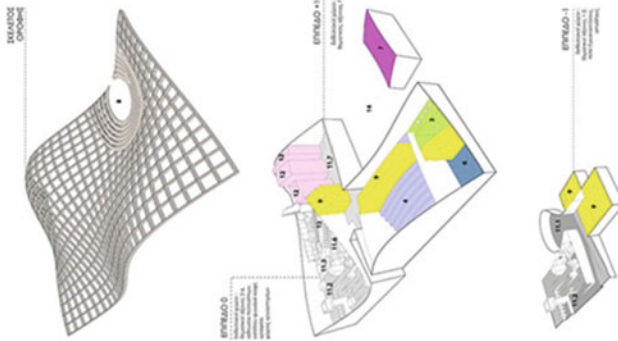
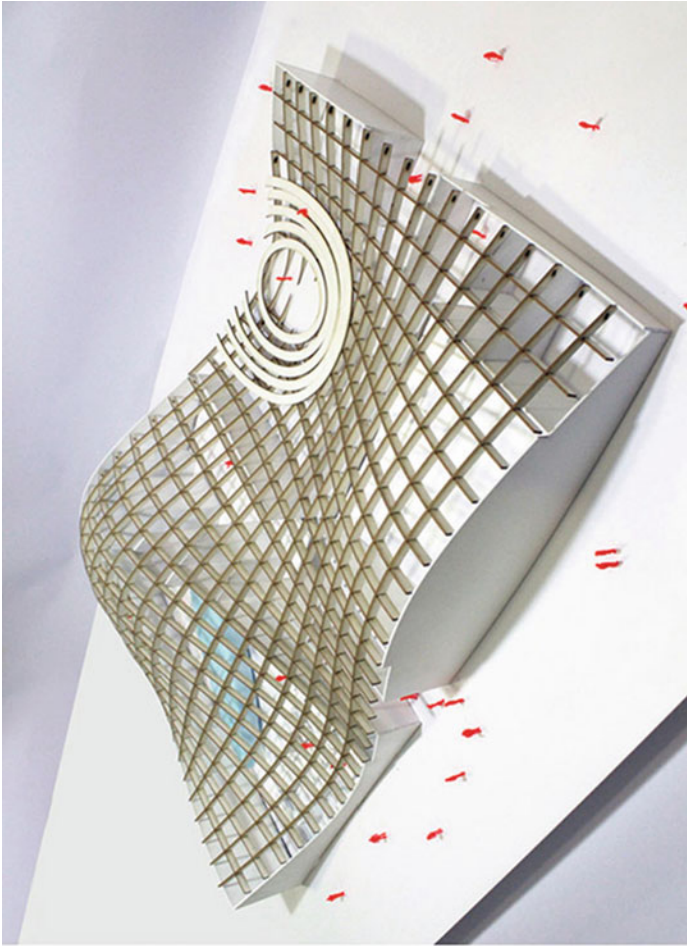


Fig. 28.7 Museum for Argo



Fig. 28.8 Artists' studio on lakeshore. (a) Façade relationship. (b) Aerial view. (c) Interior space

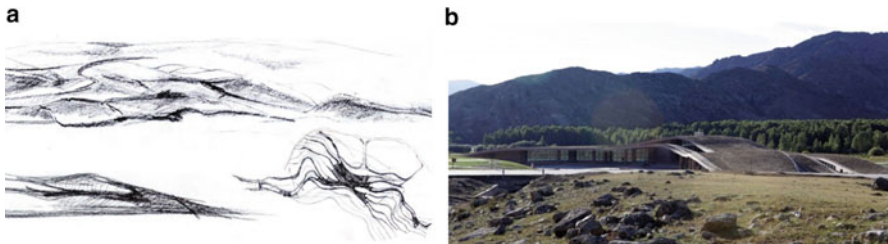


Fig. 28.9 Kокtokay Geological Museum. (a) Concept sketches. (b) Aerial view of outdoor scene

Natural landscape is regarded as the basis of a building at a site dominated by the natural environment. The Kокtokay Geological Museum and Visitor Center located in Kокtokay Geological National Park in Xinjiang, China, mimicks nature, and the architectural form was combined with the changes in surface elevation and integrated the surface morphology abstractly, which entailed blending the building into Mount Altai, the Eerqisi River, and other unique features of the natural surroundings (Fig. 28.9). Architectural form met internal function and construction. The planar curves create a smooth indoor exhibition circuit. A roof system incorporating rainwater collection and green building eliminates the boundary between building and land. It reflects the design intent of Earth folding, expands the sphere of influence for the 4700 m² mass of the building, and blends into the vast natural surrounding landscape.

2.3 *Form Mixture*

In the cold regions at middle and high latitudes, sunlight is an important architectural consideration in construction design since the duration of sunshine in winter is short and the temperature is low. In the design of construction form, consider the overall site design of landform reconstruction and make use of a continuous height changes in building form, combined with cushion space and the efficient absorption and use of sunlight. The methods of twisting and grounding enable the site to receive more sunlight in winter and create a comfortable space for outdoor

activities in winter. At the same time, this approach can also be applied to spatial expansion. An extension of the social space gives a sense of multidimensional expansion and field flow lines and spatial exchanges, spurring more activity. Using nonlinear construction design in the process of mixing surfaces emphasizes the integrity and connectedness between space and shape, breaking the Cartesian spatial system and creating a continuous space by complex mutations or flexible deformation.

For example, for the Youth Activity Center that was built in Teruel, Spain, in 2012, the program made a bold attempt to operate on the surface, placed most of the building underground, and folded the aboveground interface, along with the top, into the building to create a new urban terrain in order to express respect for the historic district (Fig. 28.10). In this way, the coefficient of the building was reduced and formed a communication space like a public square at different levels. A new way to communicate with the city was created by inspiring a variety of flow lines and event spaces with the architectural reconstruction. By mixing the building form and the surface, it drove the spatial vitality of the area. In the nature preserve located in the city of Guadalajara, Mexico, the new museum minimizes and opens urban spaces as much as possible to connect to the ecosystem and makes use of gardens, paths, and landscapes to bring down the barrier between these two important campus buildings (Fig. 28.11). Traditional Spanish houses, a settling tank, and canyons in nature inspired this design. The building form extends from



Fig. 28.10 Youth activity center in Teruel Spain. (a) Sectional relationship. (b) Perspective of main entrance. (c) Rolling roof terrace

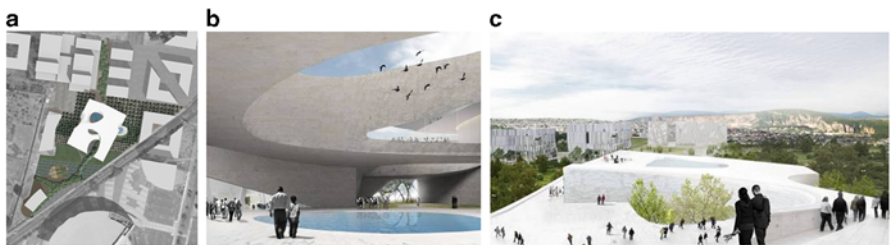


Fig. 28.11 Museum in Guadalajara city. (a) Master plan. (b) Open-air courtyard. (c) Roof terrace

the surface continuously and integrates connections in different directions; a large open-air courtyard and cave-style gardens created natural ventilation and lighting.

3 Conclusion

In cold regions, cold is accompanied by snow. Such a unique natural environment has geographical origins but also gives buildings a more profound sense of shelter. This chapter introduced landform reconstruction against a background of landscape architecture in the design of building forms in cold regions, exploring its intrinsic relevance and noting that building landform reconstruction not only has brought about an integration of architecture, spaces, and landscapes but also deals with a broader perspective on building issues, responses to design requirements from the community, ecology, and communication in the region. These features can enhance public spaces in cold regions, enrich landscapes, and ease the burden of living in a harsh climate. It examined a method of building landform reconstruction from the point of view of three strategies – blanking, simulation, and mixing – and combined the approaches with actual case studies, both domestic and foreign.

References

1. Vaughan J, Ostwald MJ (2010) Using fractal analysis to compare the characteristic complexity of nature and architecture: re-examining the evidence. *Architect Sci Rev* 53:323–332
2. Zhang X (2009) Contemporary architecture complex form design research [D]. Harbin Institute of Technology, pp 36–38
3. Wang L, Lynn G (2006) Digital design research [D]. Southeast University, pp 33–37
4. Im J, Han J (2015) Typological design strategy of FOA's architecture. *J Asian Architect Build Eng* 14(2):443–449
5. Zhao R (2005) From the object scene domain—read Stan Allen “Field status”. *Architects* 2: 85.

Chapter 29

Building-Integrated Renewable Energy Systems, or Rediscovering Forgotten Principles

Ana-Maria Dabija

Abstract The current research and development trend in the construction area is to identify innovation: we discuss innovative materials, principles, and methods.

However, in many cases the innovation lies in the approach, the point of view, not the system or the principle. Such is the case with building technologies, where building components must accommodate the technology and the technology relies on building principles. This is most visible in the building envelope because the envelope is the skin that separates two different hygrothermal environments. The building envelope – in terms of its components and as a whole – must meet the following requirements: *mechanical resistance and stability, fire safety, hygiene, health and the environment, safe use, protection against noise, energy savings, and heat retention.*

Keywords buildings • architecture • renewable energy systems

The current research and development trend in the construction area is to identify innovation: we discuss innovative materials, principles, and methods.

However, in many cases the innovation lies in the approach, the point of view, not the system or the principle. Such is the case with building technologies, where building components must accommodate the technology and the technology relies on building principles. This is most visible in the building envelope because the envelope is the skin that separates two different hygrothermal environments. The building envelope – in terms of its components and as a whole – must meet the following requirements¹: *mechanical resistance and stability, fire safety, hygiene, health and the environment, safe use, protection against noise, energy savings, and heat retention.*

¹According to the Construction Products Directive (Council Directive 89/106/EEC), now replaced by the [Regulation \(EU\) No. 305/2011](#).

A.-M. Dabija (✉)

“Ion Mincu” University of Architecture and Urbanism, Bucharest, Romania

e-mail: am.dabija@uauim.ro

According to the Interpretative Documents Annex I to the directive “*Construction works must be designed and built in such a way that. . .*”² neither the building as a whole nor its components should suffer collapses, deformations, or damage, and its users must be protected against fire, water/snow/hail, and wind; there must be acoustic protection, thermal protection, and protection against heat and bright lights while ensuring appropriate natural light, natural ventilation of the indoor space, and visual communication.

The 305/2011 (EU) regulation adds a new requirement: “*Construction works must be designed, built and demolished in such a way that the use of natural resources is sustainable.*”³ Although this refers to something else (reuse or recyclability, durability, use of environmentally friendly materials), the use of alternative forms of energy as well as design measures that lead to energy saving can be included among measures that lead to durability and environmentally friendly approaches, so that existing (traditional) resources of the planet are preserved. As the integration within the building components of alternative technologies that preserve or produce energy has increased, the building envelope has come to play a new role (not yet a requirement): it saves energy or produces energy.

While the envelope is the “star” of the building in terms of response to most current agents (natural as well as anthropogenic), smart design (architectural but assisted by technology) leads to overall energy savings in a building.

A distinction can be made between systems that produce and systems that save energy: in most cases, *passive* measures, through architectural design, are taken in order to save energy. The production of energy is generally an *active* approach: it takes more than a thermal blanket or a green roof for that.

Architecture is an art; it was defined, by Le Corbusier, as “[. . .] the masterly, correct and magnificent play of masses brought together in light,” but the same renowned architect considered the house “*a machine for living in.*” We can say that architecture is an interdisciplinary art: it brings together specialists from different scientific and professional areas and accomplishes a monumental work of art, on a large scale, for example, the urban scale or landscape (territorial) scale. It is always integrated in a space, in an environment, and it interacts with it. It is always a matter of controversy (fashion and taste), but it always embodies the cultural and economical level of the period in which it was built, the knowledge and the technologies that were used.

The periodic rediscovery of some principles and their reinterpretation from different angles lead to the design of buildings based on these new interpretations. Such buildings are obviously different from the previous ones but, when it comes to the basics, the “discovery” has been . . . discovered before and what is new for us was new 1000 years ago as well. The history of building systems is full of examples of building principles that become “fashionable” once a technical or functional requirement is formulated.

²Interpretative document No. 1: Mechanical resistance and stability.

³Regulation (EU) No. 305/2011.

Sun, wind, water, vegetation, and other aspects are agents that influence buildings as a whole in the present time as well as throughout the history of buildings.

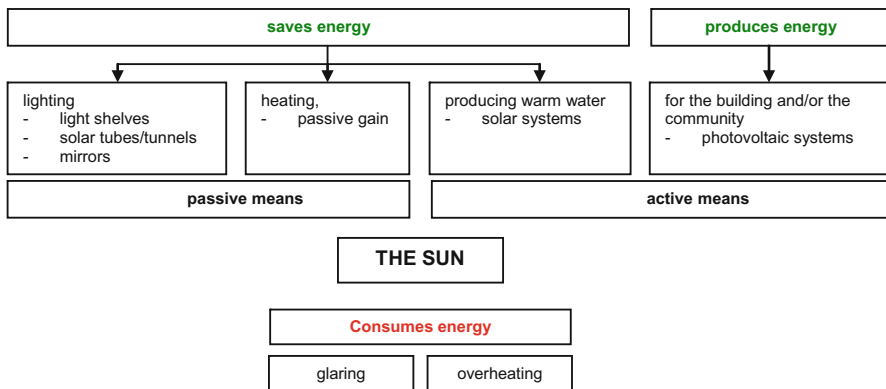
Each of these factors can, however, be a sword that cuts both ways: the sun is a source of energy but it can also be the cause of an overheating space, leading to greater energy use, for example, by air conditioning; the power of the wind has been used for centuries in windmills but it can destroy settlements (hurricanes, tornados); vegetation is a tool for designing buildings with lesser needs for thermal and air conditioning devices and – on the urban scale – can be used to decrease pollution and mitigate the heat-island effect; but, poorly managed, it can lead to moisture and condensation in buildings; phase change materials (PCMs) come with a less spectacular history but with great possibilities for saving energy from air conditioning systems.

1 The Sun

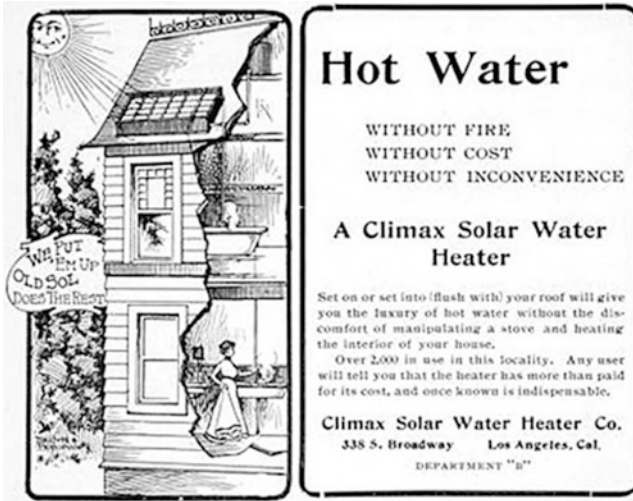
The use of solar *energy* to ensure thermal comfort dates back to antiquity: according to Nicholas Cahill (in *Household and City Organization at Olynthus*), the Greeks had developed by the fifth century BC an urban concept whereby it was possible for each house to have a south-facing façade to ensure maximum warmth provided naturally in winter.

Aristotle notes that northern façades of dwellings were sealed to ensure good protection against winter winds. Socrates is said to have lived in a solar house. According to him, the winter sun that penetrates the south-oriented portico warmed the rooms.

The same principle works today, and the winter sun that penetrates the windows represents a passive (energy) gain, whereas in the summer, the shading devices prevent overheating of the space (which would increase the use of air conditioning).



The use of building-integrated solar panels is not a new idea, either. In 1885 Charles Tellier set on the roof of his house what is reputedly the first solar installation for domestic hot water production. In 1891, Kemp patented a way to combine the old practice of exposing metal tanks to the sun using the scientific principle of the hot box, thereby increasing the tanks' capacity to collect and retain solar heat. It was called a climax solar water heater.⁴



<http://www.greendiary.com/interesting-historic-facts-renewable-energy.html>

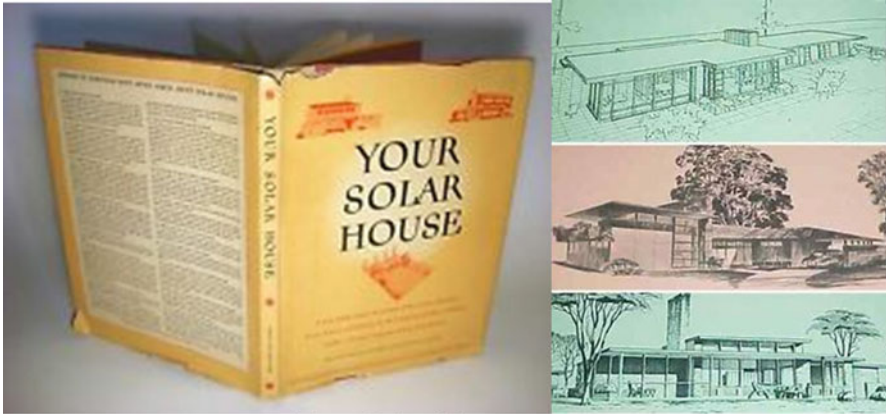
By the end of World War II, the use of building-integrated solar systems seems to have been a common practice; in 1947, a book was published on the topic: *Your Solar House*.⁵

⁴<http://californiasolarcenter.org/history-solarthermal/>

⁵Edited by Maron J. Simon, architectural consultant: Talbot Hamlin, School of Architecture Columbia Univ., technical assistance by Libbey-Owens-Ford Glass Company. A book of practical homes for all parts of the country, by 49 of America's leading architects, containing 49 sets of plans and drawings, together with many suggestions for homebuilders.

It features solar houses located in the following U.S. states: Maine: Ambros E.S. Higgins; Massachusetts: Hugh Stubbins Jr., New York: Edward D. Stoneed; Pennsylvania: Oscar Stonorov and Louis I. Kahn; Virginia: Lawrence Kocher; Indiana: John Lloyd Wright; Illinois: George Fred Keck; Missouri: Harris Armstrong; Washington; Paul Thiry; Oregon: Pietro Belluschi.

Contents: a book of solar houses, local conditions influence costs, sun heats house, insulating windowpane, famous authorities, selected architects, heat and shelter, glassmaking was a secret art, making nature work for man, making homes more livable, interest grows in solar architecture, roof overhangs, seasonal savings, styles in housing for America, answers to questions most often asked about solar houses, New England States, Middle Atlantic states, South Atlantic states, Northeast Central states, West Central states, Southeast Central states, Southwest Central states, Mountain states, Pacific states, list of architects and photos.



Your Solar House cover

Source: ebay

In 1955, Frank Bridgers designed the first office building for Bridgers and Paxton, according to what we would consider today passive design principles. It is said that domestic hot water was produced from the installed solar panels.

The energy crisis of the 1970s led to the reconsideration of energy sources and therefore the rediscovery of the necessity of finding ways to integrate alternative energy source production systems into architecture.

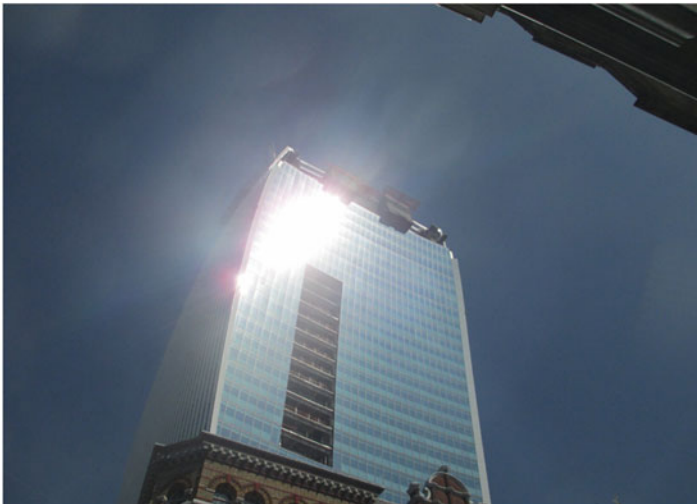
Trombe walls were included in the architectural concept of residential buildings. These systems are not new, either. The first (registered) system belonged to Edward Sylvester Morse and was patented in 1881 as “air heater.” The principle was rediscovered and adapted in the 1960s by Felix Trombe and Jacques Michel.


Accommodating natural light in a building is an architectural approach that leads to passive gains because, by design, natural light is brought into dark spaces by means of architectural elements or specialized construction systems.

Solar light pipes and sun tunnels seem to have been used in ancient Egypt as a means to bring light into dark spaces. The principle of bringing light into dark spaces reappeared around 1850, as patented by Paul Emile Chappuis, using what was called reflectors; they can be seen today in a new interpretation in different buildings and spaces, with the same function: to bring natural light into dark spaces, thus saving energy while creating new characteristics of architectural spaces and images.



Solar tunnels at the Ion Mincu University of Architecture (left)
Photo: personal archive
Solar light pipes, at the Berlin Potsdamer Platz Metro Station (right)
Photo: Dabbelju CC-BY-SA 2.5



The Walkie-Talkie Building, London. Architect Rafael Viñoly
Photo: Mat Brown CC 
<https://www.flickr.com/photos/londonmatt/9681550690/in/photostream/>

Directing light into dark spaces can be accomplished by other means as well, for example, light shelf systems with reflexive surfaces or mirrors.

On the other hand, the principle is a knife that cuts both ways (as happens with everything in life): reflexive surfaces combined with the geometry of (parts of the) the building that focalize the sun's rays. At least once in history the overheating of a surface produced with oriented mirrors set the Roman fleet on fire, led by general Marcellus.⁶ In the recent history of architecture, the geometry of a building that focalizes the sun's rays on the surrounding buildings led to major discomfort for the persons, their belongings, or spaces in the proximity of the "aggressor."^{7,8}

⁶The siege of Syracuse.


⁷<http://www.livescience.com/39371-skyscraper-melts-cars-20-fenchurch.html>: "London's Burning: How a Skyscraper Melts Cars." 3 September 2013 Marc Lallanilla, Assistant Editor: "The building—designed by internationally renowned architect Rafael Viñoly—is a dramatic edifice with curved exterior walls. Built at 20 Fenchurch Street in London's financial center, the 38-story skyscraper is known locally as 'the Walkie-Talkie' for its unusual shape. But that curvilinear shape is exactly what's causing the problem: The south-facing exterior wall is covered in reflective glass, and because it's concave, it focuses the sun's rays onto a small area, not unlike the way a magnifying glass directs sunbeams onto a superhot pinpoint of light".

<http://www.dailymail.co.uk/news/article-2786723/London-skyscraper-Walkie-Talkie-melted-cars-reflecting-sunlight-fitted-shading.html>: Mail Online, 9 October 2014 Gemma Mullin, "The concave design and mirrored glass of 20 Fenchurch Street, which is more commonly known as the Walkie Talkie due to its distinctive shape, had caused the sun to shine powerful, focused rays of light onto the street below."

⁸<http://architecture.about.com/od/ideasapproaches/ss/Controversy-DisneyHall.htm>. "Gehry Responds to Concert Hall Heat," by Jackie Craven:

"Soon after completion of the complex, many people noticed concentrated heat spots, especially as the sun's rays intensified beyond the October opening day. Unconfirmed reports of bystanders roasting hot dogs in the reflected heat quickly became legendary. Blinding glare affected drivers passing the building. Nearby residential buildings noted an increased use (and cost) for air conditioning."



The Austin Disney Concert Hall. Arhitect Frank Gehry
Photo: Jay Sterling Austin CC 
<https://www.flickr.com/photos/11015281@N00/17061987891>



BIPV on the roof of the historic building of the Ion Mincu University of
Architecture and Urbanism,
Bucharest, Romania
Photo courtesy Silviu Gheorghe

Today energy production systems using the sun as a source have become extremely interesting once again, and production technologies have led to an extension of how these systems are integrated into buildings.

The photovoltaic (PV) effect is not new either: By 1838, the 19-year-old teenager Edmond Becquerel had published his comments on the PV phenomenon.

In 1860 Auguste Mouchout built the first solar-energy-driven engine. Albert Einstein published his thesis on the photoelectric phenomenon in 1905 (receiving a Nobel Prize in 1921).

In 1954, Bell Laboratories “stumbled” by chance on the first silicon crystal cell (during an experiment, Bell Labs employees noticed that a silicon rectifier produced more electricity when exposed to the sun).

In 1958 the *Vanguard I* satellite was the first application of PV energy in space.

In 1980 electric cars powered by solar PV modules were produced.

In 1981 a solar-powered airplane crossed the English Channel.

Over the course of these 60 years the evolving technology led to a higher performance of cells (from 4 to 41 %⁹), to a large range of solar cell types (from homogeneous to amorphous), and, therefore, to a broad application field.

Designing a building-integrated PV system involves the use of PV modules that are included in certain parts of the façade or roof.

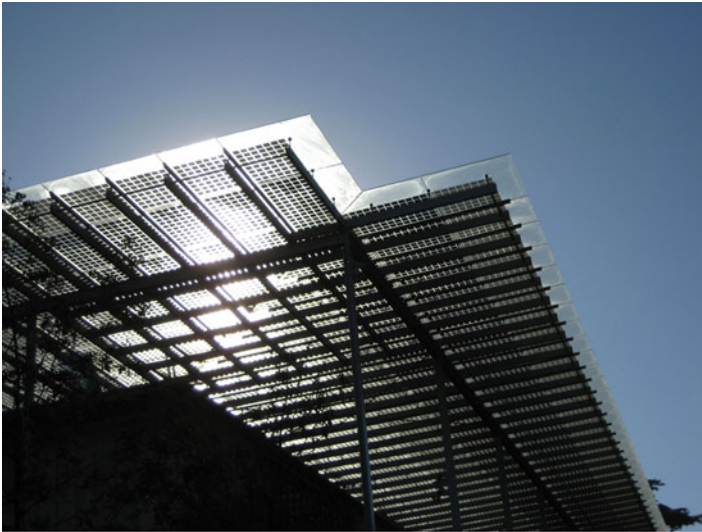

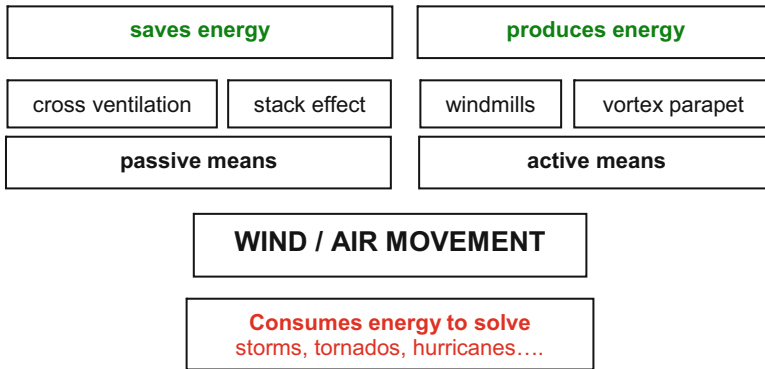


Photo: Kevin Wong, CC 

<https://www.flickr.com/photos/22419112@N08/289434253>

⁹<http://www.pveducation.org/pvc/drom/appendices/solar-cell-efficiency-results2>

At the same time, solar systems have become substitutes for components, particularly for building envelope components, which thus acquire a new function – that of a power generator.



When a building-integrated PV systems, the dimensions, orientation, and shading of the surfaces on which the solar PV panels are installed must be taken into account while meeting volumetric, functional, aesthetic, and legal requirements.

The integration of PV panels is possible for most types of buildings, new or existing, based on an analysis that requires taking into consideration several factors, for example, the urban context, the building style and construction period, the building orientation, the construction system, the impact of the materials, texture, and color of the PV panels in relation to the elements of the existing building and neighborhood, and the thermal and energy requirements of the building that the PV system relates to.

2 Wind and Air Movement


The use of wind power involves a nuanced approach. From wind towers to windmills, passive or active systems save or provide energy while giving specific features to buildings.



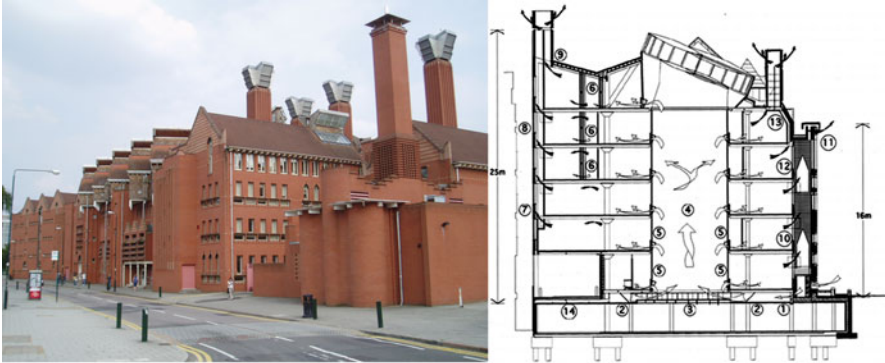
Tower Of Silence, Wind Towers And Ice Chamber, Yazd, Iran
Photo: Julia Maudlin CC 
<https://www.flickr.com/photos/48028519@N05/17153639055>


Wind towers/wind catchers are specific architectural features in North African and Middle Eastern traditional buildings; they are a means to provide ventilation without the use of equipment and so save energy.



Photo: Caroline CC 
<https://www.flickr.com/photos/20466740@N00/9658087851>

Closer to home, chimneys rise to the skies with their specific poetic or idyllic image and with their more mundane (and secondary) role of exhausting air.



De Montfort University, Short and Associates
Photo: Steve Cadman CC . Cross section: courtesy Prof. A.C.Short
<https://www.flickr.com/photos/98115025@N00/47963797>

“Borrowed” from traditional architecture and interpreted using contemporary means, chimneys/wind towers have reappeared in modern cities.



Alexander Building, Punta del Este
Photo: Jimmy Baikovicus CC 
<https://www.flickr.com/photos/7221539@N06/8449720210>

Recently, the possibility of transforming wind power on rooftops into energy has become a preoccupation among technology producers for building integrated energy systems.

Wind turbines have moved to rooftops or façades and have become part of the architectural expression of new buildings.



World Trade Center Bahrain, Atkins Architects

Photo Brian Atkinson CC 

<https://www.flickr.com/photos/23420145@N07/5284923726>



Goat on roof surveying the parking lot

Read Me CC 



<https://www.flickr.com/photos/77379868@N00/583706371>

3 Vegetation

With a special role in increasing the well-being of people, gardens – vertical or horizontal – have accompanied buildings throughout history. From the suspended gardens of Semiramis in ancient Babylon or Viking turf roofs to the rooftop gardens of today, the principles have not changed, though the technology has.



Bad Blumau Arch. Hundertwasser

Enrico Carcasci CC  

<https://www.flickr.com/photos/28458195@N02/3862748756>

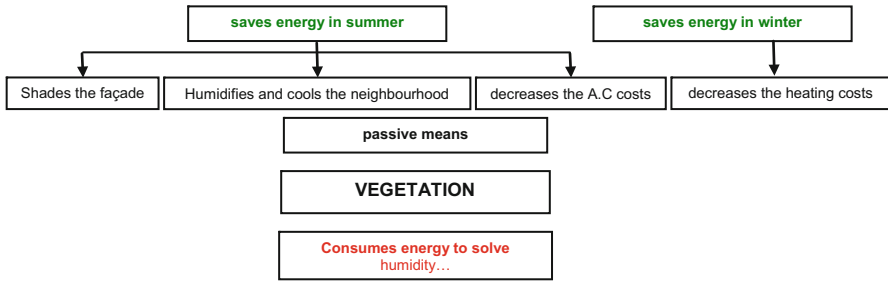


A building covered with ivy, in Bucharest
Photo: Ana-Maria Dabija

The wild vines and ivy that climb freely on façades may induce diseases on buildings that sophisticated living walls and green façades manage to avoid owing to the specific components, details, and building materials.



Musée de Quai Branly Paris.
Arch. Jean Nouvel; Botanist Patrick Blanc
Photo: courtesy Corina and Ioan Lucacel



Sometimes abandoned in history but never entirely forgotten, green assemblies represent means to save energy: less use of air conditioning in summer and better thermal protection in winter (on the top floor). Green roofs and façades better better life conditions in summer for all building inhabitants owing to the humidification and cooling of the air and reduce the costs of purifying air (with regard here only to those aspects where energy is concerned) if the purifiers are properly designed, installed, and maintained.



Bedzed. Arch. Bill Dunster

Photo: Bioregional

<https://www.flickr.com/photos/45856240@N04/10204373696>

4 Phase Change Materials

These materials store and release energy when passing from a physical phase to another. The most common PCM is water: it passes from liquid to solid at 0 °C and from liquid to gas at 100 °C. When ice melts, it releases coolth, thereby contributing to a decrease in the indoor temperature on hot summer days. However, the phenomenon of phase change should happen at around 25–28 °C, which cannot be accomplished by water. The current components of PCMs are salts, some waxes, and other materials that pass from the solid to liquid phase at around 25 °C. The fact that they release what they contained, at the moment of switching from a phase to another, makes them interesting for the construction industry because they release coolth when they become liquid and warmth when they solidify (at night). Research on these materials seems to have been carried out since the 1960s and nowadays has been done on various products (e.g., concrete, plaster, glass) as well as in HVAC systems.

We may say that nowadays we are trying to build in collaboration with nature, and not by defying it. But that is what our predecessors did as well, throughout history, according to the technological development of each period. Technology helps but cannot replace architectural principles. Architecture is for people. Integrating technologies in building gives new expression to existing principles. New technologies cannot replace architecture.

Walter Gropius said it well: “Architecture begins where engineering ends.”

Chapter 30

The Possible Shift Between Heating and Cooling Demand of Buildings Under Climate Change Conditions: Are Some Mitigation Policies Wrongly Understood?

Massimo Palme

Abstract Global warming affects the built environment by changing the environmental conditions under which buildings operate. This change probably means a shift in thermal demand, from a predominant demand for heating to a higher demand for cooling in many climates. For instance, in cold climates global warming seems to be a self-decreasing phenomenon because of lower energy demand in warmer environments. In warmer climates, like the Mediterranean, and in the hottest climates (both humid and arid), global warming must be regarded as one of the main factors (the others are the change in comfort standards and the heat-island effect) in increasing the energy demand to cool buildings. This chapter analyses the environment of various cities, characterised by mild average temperatures and small thermal oscillations, that can be regarded as Mediterranean climate emplacements. Today these cities have more heating than cooling demand but in the future will probably have higher cooling requirements. Results show that by 2050, in most of the considered emplacements, cooling demand will be higher than heating demand and emissions will rise proportionally. Solutions to this problem must be sought in the flexible operation of buildings, and policies should focus on summer-related issues: good natural ventilation, protection from the sun, and internal gain reduction, rather than insulation, air infiltration reduction and solar access.

Keywords Global warming • Climate change mitigation • Building sector energy policy • Natural cooling

M. Palme (✉)
School of Architecture, Catholic University of the North, Antofagasta, Chile
e-mail: mpalme@ucn.cl

1 Introduction

In recent years many cities around the world have experienced heat waves and a generally warmer environment. As a consequence, buildings are shifting from having a predominant heating energy demand to a cooling demand. Depending on the electricity matrix of the country, this cooling demand could cause an increase in the emissions of greenhouse gases. Many countries are making significant efforts to reduce emissions by improving the energy efficiency of the built environment, but policies are normally formulated with *heating* demand reduction in mind. This means more insulation, less infiltration, mechanical ventilation and better efficiency of heating and air-conditioning systems. However, in the future, in many climates, these strategies could prove ineffectual or have a contrary effect to avoid the heat evacuation that warmer environments will need. In Italy, for example, during the first years of operation of buildings' energy certification (introduced to respond to the European Union's EPB Directive of 2002), heating demand was the only parameter considered in obtaining certification (things are fortunately changing in this regard). In Spain, the double system (dynamic simulation or degree-day-based simplified tables) initially generated an excess of good performance certificates obtained by using simplified methods, which are more effective in evaluating heating demand than in calculating cooling need. In Chile and other Latin American countries, building sector energy policies have been introduced in recent years, many times by copying European experiences. However, climates are not always comparable, and even if they are (as in the case of Valparaiso and the central coast of Chile), the first European experiences in terms of energy performance certification have exposed problems of not properly considering cooling performance and not considering climate change as an actor in building performance, not just problems that must be resolved using mitigation strategies. It appears very likely that adaptation to warmer environments will have to be part of the solution for future urban life. Thus, certifications will have to take into account comfort conditions and the energy performance for the entire life cycle of buildings.

2 Methodology

In this chapter, IPCC data are used to simulate the future energy performance of three types of buildings. Future data (2050 and 2080) are obtained using the Climatic Change Weather Files Generator developed by Jentsch et al. [1], and typical meteorological years (TMYs) are obtained from the US Department of Energy. The scenario that was chosen for simulating the future is the A2 IPCC scenario [2]. The A2 scenario describes a heterogeneous world, with slow population increases and differences among regions and social classes. The result is a medium-high emissions scenario. The description of climate in the considered cities using the Strehler classification is as follows:

- Rome's (41°54'N, 12°30'E, 21 m elevation) climate is a typical Mediterranean climate, with temperate winters, warm and humid summers, and large autumns and springs. Seasonal temperature oscillations are moderate, and the day–night fluctuation is not very high. Radiation levels are medium-high, urban density increases the humidity retention effect and a breeze is sometimes present.
- Barcelona's (41°23'N, 2°11'E, 12 m elevation) climate is similar but somewhat hotter in summer and slightly warmer in winter. A breeze is frequently present in summer, helping to cool the urban environment.
- Valparaiso's (33°03'S, 71°37'W, 10 m elevation) climate is also classified as Mediterranean, but it is slightly different from the previous two because of the Pacific Ocean's influence: winter is milder and summer is cooler than in Rome or Barcelona.

The building typologies analysed are as follows:

- Small family houses with external walls made of cement block, insulation and mortar, with a thermal transmittance of 1.77 W/m²K; roof made of metal deck and insulation, transmittance 0.5 W/m²K, 20 % transparency on main façades (simple glass and aluminium, transmittance 5.1 W/m²K).
- Medium-sized apartment blocks with external walls of cement block, insulation and mortar, with a transmittance of 1.77 W/m²K; roofs of mortar, asphalt and insulation with a transmittance of 0.5 W/m²K, 35 % transparency, simple glass with a transmittance of 5.1 W/m²K.
- Tall residential buildings, walls of cement block and insulation with a transmittance of 1.77, roofs of asphalt, insulation and mortar with 0.5 W/m²K, 70 % glazed surface (simple glass and aluminium, transmittance 5.1 W/m²K).

Even if the recommended values for transmittances are different in the three emplacements, the same value is selected to help the resulting comparison between climatic effects. Moreover, the use of higher values of insulation and double glass for windows could only raise the shift between heating and cooling expected as a final result. All buildings have the same occupancy density of 30 m²/person, and the thermostat is set at 18–26 °C over the course of 24 h (Table 30.1).

Simulations were done using Types 56a (multizone building) in the Trnsys tool (version 16). Climatic TMY files are read in Type 109, sky cloudiness is calculated by Type 69b and psychometric variables by Type 33e. The Jentsch method to generate TMY future data uses “shift” and “stretch” modifications for temperature, “stretch” modification for wind speed and global radiation and “shift” for relative humidity and atmospheric pressure. For more detailed information, see the tool manual [3].

Table 30.1 Transmittances and glaze percentage of building typologies

Building	U wall (W/m ² K)	U roof (W/m ² K)	Glazed surface (%)
Family house	1.77	0.5	20
Block	1.77	0.5	35
Tower	1.77	0.5	70

3 Results

Total heating and cooling demands are obtained by simulations for the three building typologies, the three climatic emplacements and considering two orientations: N–S and E–W. Figures 30.1, 30.2 and 30.3 show the heating and cooling demand for the TMY and the modified climates for 2050 and 2080. In the case of the small family house, the total thermal demand decreases in the future simulation for the cases of Rome N–S oriented 2050 and Valparaiso N–S 2050, N–S 2080, W–E 2050 and W–E 2080. However, in all cities and orientations, the shift between cooling and heating energy demand is clear in the 2080 simulation. In the residential block and tall building case studies, results are clearer owing to the less exposed

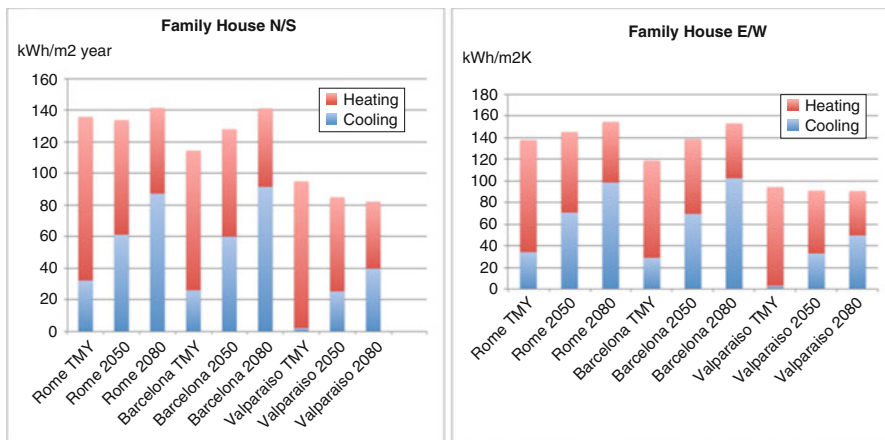


Fig. 30.1 Heating and cooling demand for family house, north–south and east–west oriented

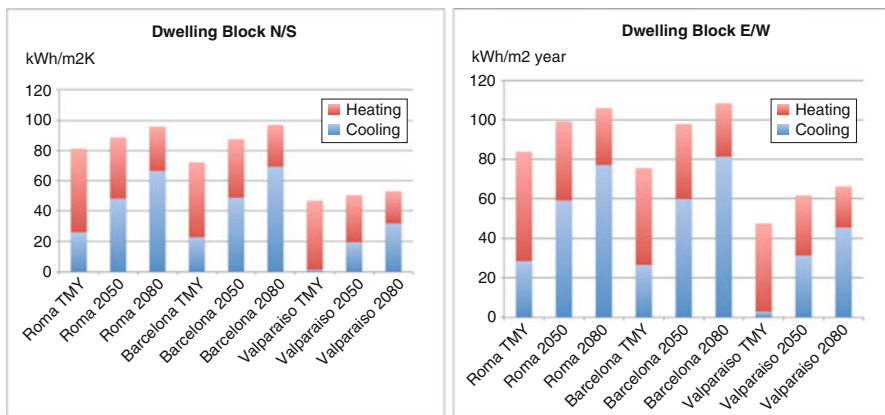


Fig. 30.2 Heating and cooling demand for medium block, north–south and east–west oriented

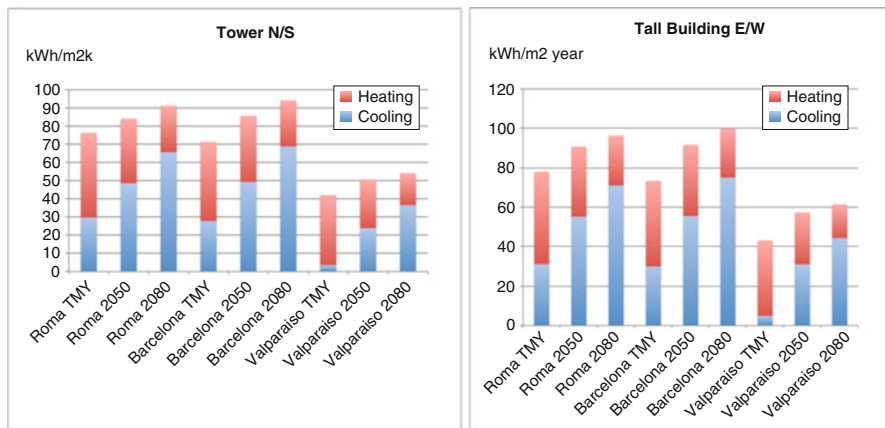


Fig. 30.3 Heating and cooling demand for tall building, north–south and east–west oriented

Table 30.2 Coefficients for calculating emissions (kg CO₂/kWh final energy)

City	Heating coefficient (natural gas)	Cooling coefficient (electricity)
Rome	0.20	0.33
Barcelona	0.20	0.39
Valparaiso	0.20	0.37

surface and greater percentage of glazing in the façade. The results show a higher dependence on orientation, always due to the same factors.

To estimate the relative greenhouse gas emissions, a boiler system is considered for heating and a heat pump is selected for cooling, with respective efficiencies of 0.95 and 3.0. Emissions are obtained using transformation coefficients that depend on the energy matrix and especially on the renewable energy share for electricity production in the countries and regions. In Chile, for example, the renewable contribution to electricity is different in the north and central south because of the presence of two different systems: the Sistema Interconectado del Norte Grande (Great North Interconnected System) (SING) and the Sistema Interconectado Central (Central Interconnected System) (SIC). Valparaiso belongs to the SIC region, which has a 40 % hydroelectric contribution and a 60 % carbon thermoelectric contribution [4]. In the case of Italy and Spain, the energy matrix is more complex, with a total renewable contribution share comparable to the SIC in Chile [5, 6]. The resulting coefficients for all the countries are summarised in Table 30.2.

Table 30.3 summarises the energy demand and the emissions caused by thermal conditioning for average building forms and orientations between the buildings considered in this study.

Table 30.3 Annual final energy consumption and emissions of greenhouse gases

City	TMY energy (kWh/m ²)	2050 energy (kWh/m ²)	2080 energy (kWh/m ²)	TMY emissions (kg CO ₂ /m ²)	2050 emissions (kg CO ₂ /m ²)	2080 emissions (kg CO ₂ /m ²)
Rome	98.9	107.0	114.3	17.8	16.8	16.3
Barcelona	87.7	104.9	115.7	16.3	17.5	17.8
Valparaiso	61.6	66.1	68.0	12.7	11.5	10.7

4 Conclusions

The present work showed the heating and cooling trend for future climatic scenarios in different regions of the world and discussed the appropriate building sector energy policies which should be adopted to address the predicted situation. Warmer environments will cause a shift between heating and cooling in all the considered countries. Total energy demand will increase in all scenarios, except in the case of family houses in Valparaiso, Chile. As a consequence, final energy demand for HVAC will increase by approximately 10 % on average in all the considered countries. Emissions will not increase owing to the 40 % share of electricity generation by renewables in Italy, Spain and in the SIC of Chile. These results reflect the selection of the boiler system for heating. If heating is provided by the same heat pump as cooling, then the change in thermal demand will generate more emissions in the future for all considered scenarios.

Acknowledgement This study is part of the FONDECYT project (11140578) and was sponsored by the Catholic University of the North and by the University of Rome “La Sapienza” Visiting Research Programme.

References

1. Jentsch MF, Bahaj AS, James PAB (2008) Climate change future proofing of buildings—generation and assessment of building simulation weather files. *Energy Build* 40 (12):2148–2168
2. IPCC Special Report (2000) Emissions scenario. IPCC official site <http://www.ipcc.ch>
3. Climatic change weather file generator manual (2009) UKCIP official site <http://www.ukcip.org.uk> or Southampton School of Civil Engineering and the Environment official site <http://www.serg.soton.ac.uk>
4. Chilean Government (2015) Energy Ministry. <http://huelladecarbono.minenergia.cl/sistemas-electricos>
5. Spanish Government (2014) Ministry of industry, energy and tourism. http://www.minetur.gob.es/energia/desarrollo/EficienciaEnergetica/RITE/propuestas/Documents/2014_03_03_Factores_de_emision_CO2_y_Factores_de_paso_Efinal_Eprimaria_V.pdf
6. Italian Government (2013) National information system for environmental protection. <http://www.sinanet.isprambiente.it/it/sia-ispra/serie-storiche-emissioni/fattori-di-emissione-per-la-produzione-ed-il-consumo-di-energia-elettrica-in-italia/view>

Chapter 31

Robustness of Residential Houses in Ecuador in the Face of Global Warming: Prototyping and Simulation Studies in the Amazon, Coastal and Andes Macroclimatic Regions

Massimo Palme and Andrea Lobato

Abstract Ecuador is a small country with high-frequency climatic variability. The principal macroclimatic regions are the Amazon rainforest, with a hot and humid climate; the tropical coast, also with a hot and humid climate; and the highlands, with a tropical mountain climate. The government is working on policies regarding the energy efficiency of all kinds of buildings. In 2011, the Ministry of Urban Development and Housing (MIDUVI), in a design competition called ‘Dwellings for Climate Change’, selected three residential house typologies, one for each macroclimatic emplacement in the country. The winner dwellings were designed considering passive architecture concepts; however, some simulation studies conducted by the National Institute of Energy Efficiency and Renewable Energy in 2014 showed that in many cases the new design proposals have poorer performance than the standard dwelling typically seen in Ecuador for all climatic emplacements. To validate the simulation results, new simulations were conducted using current weather data. The output searched was the total discomfort sensation instead of the thermal demand or energy consumption (heuristic). In addition, global warming was taken into account by simulating future situations in the A2 scenario proposed by the Intergovernmental Panel on Climate Change. Future climate was modelled using the Climate Change World Weather Files Generator developed by the Chartered Institution of Building Services Engineers. Results show that building design in Ecuador is influenced by standards that come from colder countries. This fact leads to generally poor result in terms of natural cooling performance, even in the actual climate. Global warming and urban development, especially in the coastal region, will increase cooling needs, so building design

M. Palme (✉)

Escuela de Arquitectura, Universidad Católica del Norte, Antofagasta, Chile

Instituto Nacional de Eficiencia Energética y Energías Renovables (INER), Quito, Ecuador
e-mail: mpalme@ucn.cl; massimo.palme@iner.gob.ec

A. Lobato

Instituto Nacional de Eficiencia Energética y Energías Renovables (INER), Quito, Ecuador

guidelines for Ecuador will have to be reconsidered and focus in particular on heat evacuation problems instead of heating demand reduction.

Keywords Global warming • Climate change mitigation and adaptation • Social housing • Ecuador

1 Introduction

Ecuador is starting to consider climate change as a priority for the country's development. Recently the Under Secretariat for Climate Change was founded, and many ministries have started to insert related topics in their political agendas. In particular, the Ministry of Urban Development and Housing (MIDUVI) launched in 2011 the competition 'Dwellings for Climate Change' in order to improve the basic residential dwellings that are still being built in all climates of the country. For instance, Ecuador, although it is small, has a unique climatic diversity: in the Andes the climate is tropical mountain, in the Amazon it is tropical wet and in the coastal region it is hot, both arid and humid, depending on the specific location. One of the competition goals was to show the need for different designs for each climate, even for residential dwellings, that must be very inexpensive. The National Institute of Energy Efficiency and Renewable Energy (known by its Spanish acronym INER) is also developing some prototypes for the different climates of Ecuador [1]. In this chapter, a simulation study is conducted to estimate the hours of discomfort (both undercooling and overheating) that residents may feel in the base case (the actual MIDUVI residential house) and in the three prototypes that won the competition. Simulations were conducted for the current climate (typical meteorological year, or TMY) and for the future (2050 and 2080) taking into account the effects of global warming under the Intergovernmental Panel for Climate Change (IPCC) A2 scenario. Since in Ecuador heating and air-conditioning systems are used by only a small part of the population (the wealthy), an analysis was conducted considering naturally ventilated buildings to try to determine the total hours of discomfort during the year.

2 Methodology

In this chapter IPCC data are used to simulate the future energy performance of three types of buildings. Future data (2050 and 2080) are obtained using the Climatic Change Weather Files Generator developed by Jentsch et al. [2] and TMYs are obtained from the meteorological service of Ecuador INHAMI [3]. The selected scenario to simulate the future is the IPCC's A2 scenario. This scenario describes a heterogeneous world, with slow population increases and differences among regions and social classes. The result is a medium-high emissions scenario (Fig. 31.1). A description of the climate of the considered cities, deemed representative of the macroclimates of Ecuador, is as follows:

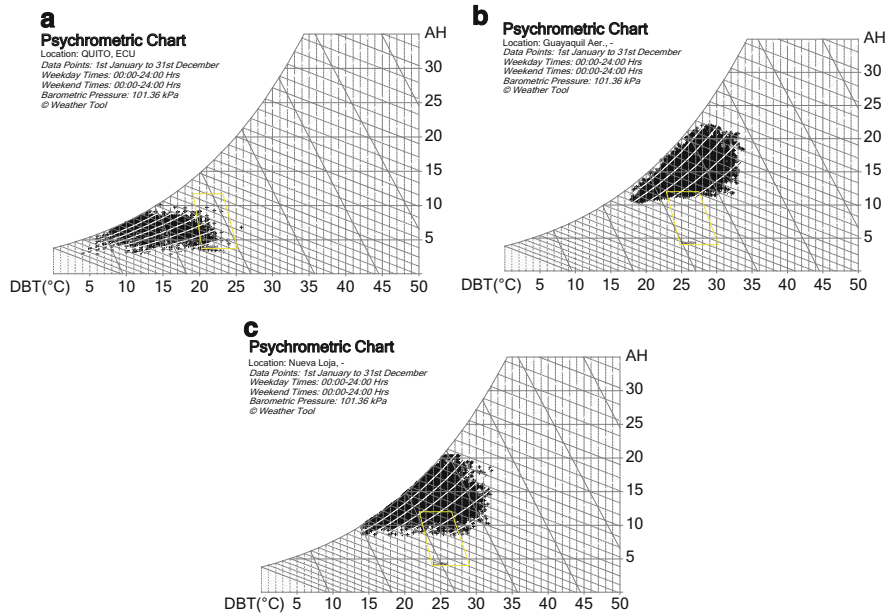


Fig. 31.1 Givoni chart for Quito (a), Guayaquil (b) and Nueva Loja (c)

- The climate of Quito ($0^{\circ}14'S$, $78^{\circ}31'W$ longitude, 2850 m elevation) is tropical mountain, with mild diurnal temperatures and colder nights, in both wet and dry seasons. Radiation levels are high, the urban density increases the heat retention effect and a breeze is sometimes present.
- The climate of Guayaquil ($2^{\circ}11'S$, $79^{\circ}53'W$, 4 m elevation) is hot and wet throughout the year. The ocean breeze, when present, is very important for the natural cooling of buildings. Urbanization affects the temperatures of the city, and in many cases, new constructions along the first costal line block the wind.
- The climate of Nueva Loja ($0^{\circ}5'5''N$, $76^{\circ}52'58''W$, 297 m elevation) is tropical wet, with high humidity and temperatures throughout the year and a night–day oscillation slightly higher than in Guayaquil.

The building typologies analysed are described as follows:

- A MIDUVI house is a small family dwelling with external walls made of cement block having a thermal transmittance of $1.8 \text{ W/m}^2\text{K}$, a metal deck roof with a transmittance of $5.2 \text{ W/m}^2\text{K}$ and 15 % transparency on the main façades (simple glass and aluminium, transmittance $5.1 \text{ W/m}^2\text{K}$).
- The house proposed for the Amazon is a family dwelling with external walls of reeds having a thermal transmittance of $4.5 \text{ W/m}^2\text{K}$, a roof made of polypropylene with a transmittance of $2.7 \text{ W/m}^2\text{K}$ and 10 % glazed surface.
- The house proposed for the mountain region is a more compact house with walls of concrete (transmittance $1.8 \text{ W/m}^2\text{K}$), metal deck roof (transmittance $5.2 \text{ W/m}^2\text{K}$) and 20 % glazed surface.

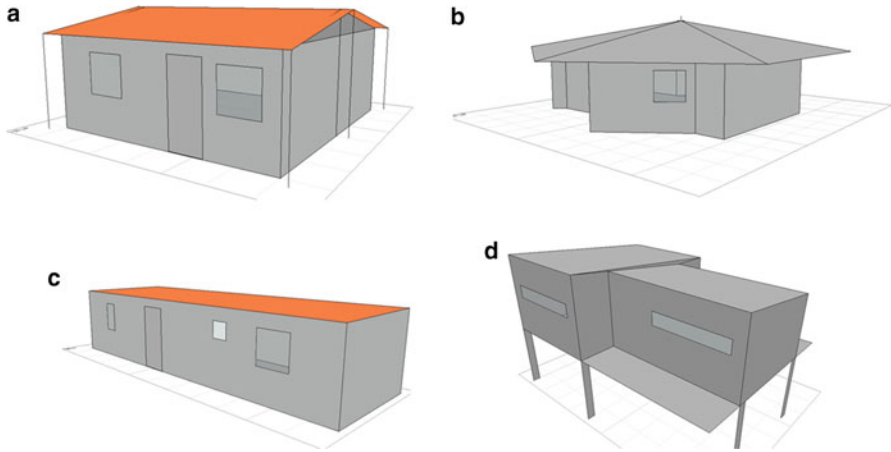


Fig. 31.2 House models for MIDUVI (a), Amazon (b), mountain (c) and coast (d)

Table 31.1 Transmittances and glaze percentage of building typologies

Building	U wall (W/m ² K)	U roof (W/m ² K)	Glazed surface (%)
Mountain	1.8	5.2	20
Amazon	4.5	2.7	10
Coast	3.5	5.2	10
MIDUVI	1.8	5.2	15

- The proposed coastal house is an elevated house with walls of light concrete (transmittance 3.5 W/m²K), steel roof (transmittance 5.2 W/m²K) and 10 % glazed surface.

All houses have the same occupancy density of 10 m²/person for a 24 h period. Figure 31.2 shows the models for the dwellings, and Table 31.1 summarizes the material properties.

Simulations were done using Types 56a (multizone building) in the Trnsys tool (version 16). Climatic TMY files were read in Type 109, sky cloudiness was calculated using Type 69b and psychometric variables by Type 33e. The Jentsch method to generate TMY future data uses ‘shift’ and ‘stretch’ modifications for temperature, ‘stretch’ modification for wind speed and global radiation and ‘shift’ for relative humidity and atmospheric pressure. For more detailed information, see the tool manual [4]. The MIDUVI house was simulated in both main orientations north–south (N–S) and east–west (E–W), whilst the prototypes were simulated using the recommended orientations, N–S for the Guayaquil dwelling and E–W for the one in Quito. Recall that a 0 latitude means that E–W orientations guarantee a solar gain, whilst the N–S orientation has no solar gain throughout the year.

3 Results

Figure 31.3 shows the results in terms of discomfort hours for the MIDUVI house in both orientations and for the new prototypes. Table 31.2 summarizes the discomfort values.

These results confirm the possible impact of climate change on the built environment and the need for a new concept of thermal regulation for the country. Much research is currently being done on this topic for tropical, arid and Mediterranean climates; see for example the work of Palme et al. [5].

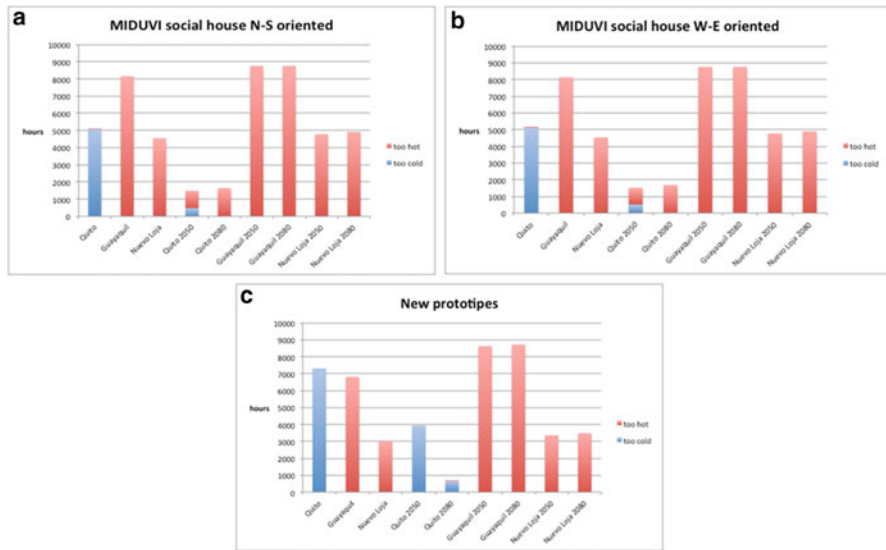


Fig. 31.3 Discomfort hours for MIDUVI house N-S (a), E-W oriented (b) and new prototypes (c)

Table 31.2 Discomfort hours in analysed cases

Case	MIDUVI house N-S		MIDUVI house E-W		New prototypes	
	Too hot (h)	Too cold (h)	Too hot (h)	Too cold (h)	Too hot (h)	Too cold (h)
Quito TMY	41	5071	29	5121	0	7315
Quito 2050	1000	487	1009	511	0	3939
Quito 2080	1640	9	1676	9	8	660
Guayaquil TMY	8161	0	8139	0	6810	0
Guayaquil 2050	8760	0	8760	0	8632	0
Guayaquil 2080	8760	0	8760	0	8724	0
Nuevo Loja TMY	4552	0	4536	0	3024	0
Nuevo Loja 2050	4780	0	4776	0	3352	5
Nuevo Loja 2080	4913	0	4898	0	3480	5

4 Conclusions

The present work showed that new designs for houses are needed in Ecuador. Climate change will affect the performance of buildings; for example in the highlands the MIDUVI house will undergo a shift from heating to cooling demands. In Guayaquil and Nueva Loja, overheating will be the problem and global warming will increase the effect. With respect to the new prototypes, it seems that the different design could reduce the bad performance of the MIDUVI house, but it will not be sufficient. Considering future scenarios, in both hot emplacements (Guayaquil and Nueva Loja), the overheating sensation will be very high. Only the new prototype for the highlands shows significantly better future performance (but not with the current climate) with respect to the MIDUVI house, avoiding overheating. The energy certification of dwellings, under development in Ecuador, will have to focus on heat evacuation in all climates, including the highlands. Going forward, a priority should be to use more simplified calculation methods to estimate the potential to cool buildings naturally. At the urban district level, environmental studies to quantify the contribution of buildings to the heat island effect and its dependence on the urban form are also needed, as in other climates [6]. The blockage of natural breezes in the case of Guayaquil is also a very important topic and should be studied and discussed as soon as possible.

Acknowledgement This study is part of the PROMETEO project ‘Energy Certification of Houses in Ecuador Related to Climatic Observations’ awarded by the government of Ecuador to the main author for the period 2015–2016.

References

1. Lobato A, Vaca D, Rivela B (2014) Coupling multi-criteria analysis and life cycle approach for sustainability assessment of social housing in Ecuador. In: Proceedings of the BauSim 2014, Aachen
2. Jentsch MF, Bahaj AS, James PAB (2008) Climate change future proofing of buildings—generation and assessment of building simulation weather files. *Energy Build* 40 (12):2148–2168
3. IPCC Special Report (2000) Emissions scenario. IPCC official site <http://www.ipcc.ch>
4. Climatic change weather file generator manual (2009) UKCIP official site <http://www.ukcip.org.uk> or Southampton School of Civil Engineering and the Environment official site <http://www.serg.soton.ac.uk>
5. Palme M, Isalgué A, Coch H (2013) Avoiding the possible impact of climate change on the built environment: the importance of the buildings’ energy robustness. *Buildings* 3(1):191–204
6. Palme M, Guerra J (2014) A critical assessment and projection of urban vertical growth in Antofagasta, Chile. *Sustainability* 5(7):2840–2855

Chapter 32

Performance Analysis and Parametric Studies of a Bi-fluid Type Photovoltaic/Thermal (PV/T) Solar Collector in Simultaneous Mode Under Tropical Climate Conditions

Hasila Jarimi, Mohd Nazari Abu Bakar, Mahmud Othman,
and Mahadzir Din

Abstract Performance analysis of a photovoltaic/thermal solar collector with a bi-fluid configuration (air and water) was conducted under real sky conditions in the tropical climate of Perlis, Northern Peninsular Malaysia. In addition to the electricity generated, this type of collector has enabled three different modes of fluid operation: air mode, water mode and simultaneous (bi-fluid) mode. The third mode of fluid of operation is the primary focus in this chapter. This chapter highlights the performance of the collector outdoors, in terms of the experimental and two-dimensional theoretical analysis at steady state. For collector testing under real sky conditions, analyses of the collector for varying sets of mass flow rates under environmental conditions of an average wind speed of 3 m/s and average solar radiation of 700 W/m^2 were conducted. To obtain suitable data, experiments were conducted for each of the mass flow rates on ten different days of testing. For the simultaneous mode, when air flow rate was fixed at 0.0262 kg/s , at a water mass flow rate that varied from 0.0017 to 0.010 kg/s , the electrical efficiency and total thermal efficiency ranged from 8.13 to 8.60% and 44.36 to 47.45% respectively. When the water flow rate was fixed at 0.0066 kg/s , at an air mass flow rate that varied from 0.0092 to 0.0753 kg/s , the efficiencies ranged from 8.10 to 8.56% and 44.06 to 50.37% respectively. Theoretical analysis was then conducted and compared with the experimental analysis by comparing the trend of the curves and using mean absolute percentage error (MAPE) analysis. The curves were found to be in good agreement, and the computed MAPE for the fluids' output temperature was less than 2% . Parametric studies were then conducted to investigate the performance of the collector with the change in air channel depth and performance with the change in collector length. The feasibility of incorporating two different types of working fluid into the same PV/T solar collector was demonstrated based on

H. Jarimi (✉) • M.N.A. Bakar • M. Othman • M. Din
Universiti Teknologi Mara Perlis, Perlis, Malaysia
e-mail: H.Jarimi@gmail.com

the thermal and electrical energy output of the collector under real sky conditions. Therefore, this research will serve as a starting point for further research into a bi-fluid type PV/T solar collector, both experimentally and theoretically.

Keywords Bi-fluid • Photovoltaic thermal (PV/T) • 2-D steady state • Outdoor • Parametric

Nomenclature

A_{PV}	Collector aperture area's subsegment, equal to area of PV module's subsegment (m^2)
C_f	Conversion power factor
C_{pf1}	Specific heat capacity of air
C_{pf2}	Specific heat capacity of water
D_i	Inner pipe diameter
D_o	Outer pipe diameter
f	A general subscript to denote a fluid
f_r	A friction factor in a fluid's channel
G	Global radiation
h	Heat transfer coefficient ($W/m^2 K$)
h_{cvbsf1}	Convection heat transfer coefficient from back surface of Tedlar to air flow ($W/m^2 K$)
h_{cvbsf2}	Convection heat transfer coefficient from back surface of Tedlar to water flow ($W/m^2 K$)
$h_{cvfinf1}$	Convection heat transfer coefficient from surface of a fin to flowing air ($W/m^2 K$)
h_{cvw}	Wind convection heat transfer coefficient ($W/m^2 K$)
h_i	Generalised notation for heat transfer coefficient of linear equations derived from developed energy balance equations for a general heat transfer coefficient i ($W/m^2 K$)
h_{rbsbp}	Radiation heat transfer coefficient between inner surfaces of collector ($W/m^2 K$)
h_{rpvsky}	Radiation heat transfer coefficient from PV cells to sky ($W/m^2 K$)
k_{fin}	Thermal conductivity of fin (W/mK)
k_{f1}	Thermal conductivity of air (W/mK)
k_{f2}	Thermal conductivity of water (W/mK)
k_{PV}	Thermal conductivity of photovoltaic cells (W/mK)
L_{fin}	Length of fin (m)
m	Subsegment for each temperature node
\dot{m}_{f1}	Air mass flow rate (kg/s)
\dot{m}_{f2}	Water mass flow rate (kg/s)
N_{fin}	Total number of fins

$\sum Q_{th,inst}$	Total instantaneous thermal energy produced by solar collector (J)
$\sum Q_{PVT,inst}$	Instantaneous primary energy saving (J)
q	Rate of heat flux (W/m^2)
$q_{uf1,m}$	Rate of heat transfer per unit area for air nodes (W/m)
$q_{uf2,m}$	Rate of heat transfer per unit area for air nodes (W/m)
Re	Reynolds number
S_{PV}	Total rate of solar energy absorbed by solar cells of PV module
S_T	Total energy absorbed by Tedlar
T	Temperature (K)
T_a	Ambient temperature (K)
$T_{bp,m}$	Temperature nodes of surface of back plate (K)
$T_{bs,m}$	Temperature nodes of back surface of Tedlar (K)
T_{bp}	Mean temperature of surface of back plate with fins (K)
T_{bs}	Mean temperature of back surface of Tedlar (K)
T_{PV}	Mean temperature of cell (K)
$T_{f1,m}$	Temperature nodes of air flow in channel (K)
$T_{f2,m}$	Temperature nodes of water flow in copper pipe (K)
$T_{fin,m}$	Mean temperature of fin at subsegment m (K)
$T_{PV,m}$	Temperature nodes of PV cells (at centre of cells) (K)
T_{ref}	Temperature at reference point
T_{sky}	Sky temperature (K)
T_{tin}	Mean inner wall temperature of copper pipe (K)
$U_{t,m}$	Overall top heat loss coefficient for subsegment m
v_{f1}	Maximum velocity of air (m/s)
v_w	Wind speed (m/s)
W	Tube spacing (m)
α_c	Absorptance of PV cells
β_c	PV module packing factor
β_{ref}	Temperature coefficient at reference temperature
δ_{PV}	Thickness of PV module
δ_{si}	Thickness of Si-cells
δ_T	Thickness of Tedlar layer
δ_{EVA}	Thickness of ethylene-vinyl acetate (EVA) layer
δ_{fin}	Fin thickness
$\Delta y_{PV} \Delta x$	Area of subsegment of PV module
Δx	Distance between temperature nodes ($\Delta x = 1$ cm)
ϵ_{sky}	Emissivity of sky
ϵ_g	Emissivity of glass cover
$\gamma_{bsbp,m}$	Area correction factor for heat transfer from back surface of Tedlar to surface of back plate with fins
$\gamma_{bsf1,m}$	Area correction factor for heat transfer from back surface of Tedlar to flowing air

$\gamma_{bsf2,m}$	Area correction factor for heat transfer from back surface of Tedlar to flowing water
$\gamma_{finf1,m}$	Area correction factor for heat transfer from fin surfaces to flowing air
$\gamma_{bpf1,m}$	Area correction factor for heat transfer from surface of back plate with fins to flowing air
$\gamma_{bpa,m}$	Area correction factor for heat transfer from surface of back plate with fins to ambient
τ_g	Transmittance factor of front cover glass of PV module
η	Efficiency
η_c	Electrical efficiency of PV cell
η_{ele}	Electrical efficiency
η_{eth}	Electrical efficiency converted to equivalent thermal efficiency
η_{fin}	Fin efficiency
η_p	Fin effectiveness
η_{Tref}	Electrical efficiency at reference temperature
η_{thf1}	Thermal efficiency of air
η_{thf2}	Thermal efficiency of water
$\sum \eta_{th}$	Total thermal efficiency of solar collector
$\sum \eta_{PVT}$	Primary energy savings or equivalent thermal efficiency
$\sum \eta_{th,inst}$	Instantaneous total thermal efficiency of solar collector

1 Introduction

Theoretical and experimental studies of photovoltaic/thermal (PV/T) solar collectors have been carried out and documented since the mid-1970s. In 1976, Wolf [1] investigated the performance of a combined solar heating and PV electric power generation system for a single family residence in Boston, Massachusetts, USA. In 1979, Florschuetz [2] developed a famous extension of the well-known Hottel-Whillier-Bliss model for thermal analysis of flat-plate collectors to the analysis of combined PV/T collectors. Since then, studies have continued on collector design and performance analysis, including the development of thermal and electrical modelling as well as the influence of various parameters on the overall performance of collectors. To further enhance the technical and economic feasibility of the collector, there is a strong need for continuous research and development (R&D) of this type of technology. Further innovations are required to extend the range of its potential application for further energy optimisation. Until now, collector design has tended to focus on either water or air as the working fluid, implying that the application is limited to either thermal air or water with electricity out of the same PV/T solar collector.

The use of both fluids within the same PV/T collector is intriguing but has not yet been extensively studied. In addition to the electricity generated, this type of collector enables the production of both hot air and water, increasing the total efficiency per unit area as compared to a side-by-side configuration. The use of both fluids (bi-fluid) also leads to a greater range of thermal applications and offers options in which three modes of fluid operation, namely air mode, water mode, and simultaneous mode (air and water), may be produced depending on energy needs and applications. The idea of dual-mode operation of a PV/T solar collector was first introduced by Tripanagnostopoulos [3] at the 17th European PV Solar Conference in Munich [4]. Tripanagnostopoulos [3] proposed three different basic configurations of PV/T dual-mode operations: with the water heat exchanger (WHE) placed directly behind the PV module, placed inside the air channel, and placed on the back plate of the air channel. To test the designed solar collector, experiments were performed with the solar collector. However, to the best of the authors' knowledge, the focus of the current research is the independent mode of fluid operation, such that the mass flow rate of each of the fluid is fixed at 0.02 kg/s. The experimental results indicate that when operated independently, the first design (with WHE placed directly behind the PV module) the electrical efficiency and thermal efficiency of the system are considered satisfactory for the PV component and both water and air respectively.

In 2007, Assoa et al. [4] conducted a study on a PV/T solar collector using both air and water as working fluids. PV cells act as the thermal absorber component for the air heat exchange component, but not for the water heat exchange component. In their study, a two-dimensional (2-D) steady-state analysis is performed. Indoor experimental studies were performed and the results compared with the simulation results and shown to be in good agreement. Several parametric studies were conducted using the validated mathematical model. A significant advantage of this configuration is that high water temperature production is feasible when compared to the conventional hybrid solar collector, without causing undesirable effects on the PV cells. In addition, such a system can also be integrated with solar cooling devices, which is extremely appealing during summertime.

An improved design of a hybrid solar collector integrating both water and air as working fluids, known as a bi-fluid type PV/T solar collector, has been proposed by our research group. The design concept is discussed in detail in Abu Bakar et al. [5]. The researchers further improved the performance of the collector by introducing a low-cost heat transfer enhancement technique via the use of a set of fins parallel to the direction of the air flow, according to Jarimi et al. [6] and as shown in Fig. 32.1. The developed 2-D steady-state mathematical model is briefly discussed in this chapter. Interested readers may refer to Abu Bakar et al. [5] and Jarimi et al. [6] for further details. This chapter focuses on the simultaneous mode of fluid operation, for which the mathematical model was validated against experimental results as performed under the tropical climate conditions of Perlis, Northern Peninsular Malaysia.

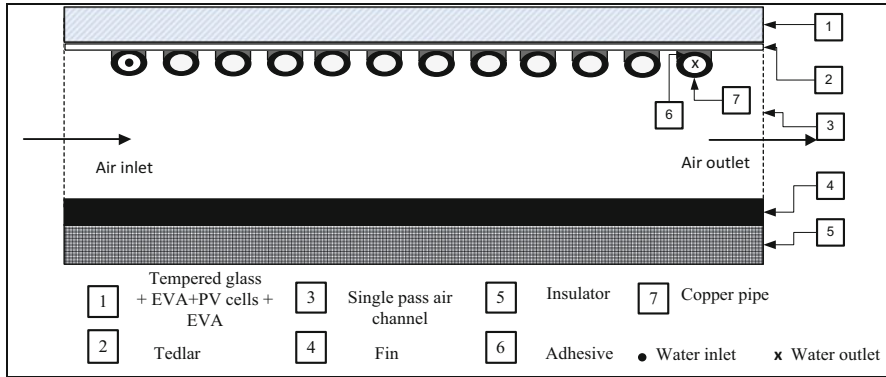


Fig. 32.1 Side-view cross section of designed collector

2 Experimental Method

A non-optimised prototype was fabricated to validate the simulation results from the developed 2-D mathematical model for the collector under study. As shown in Fig. 32.2, to perform the test, outdoor test-rig facilities were set up and fabricated on the rooftop of the Solar Energy Research Lab, UiTM Perlis, Malaysia. In general, the test-rig facilities were comprised of two important sections, namely the air and water heat exchange system and the power-supply and control system. Parameters include inlet and outlet air temperatures, ambient temperature, temperatures at several locations, current, voltage, air and water flow rates, wind velocity and the solar radiation incident on the collector plane. Water was pumped into the collector by an SP737 Tideway-Taiwan electric submersible water pump from the primary water tank. Speed was controlled using a United Automation CSR2-E series power regulator-United Automation, UK. To maintain a constant water temperature, a secondary water tank was used to dispose of the heated water. Before the water entered the collector, the water flow rate was measured using a Blue-White F-440 inline flow meter-USA. Meanwhile, air was pumped into the collector using an air blower consisting of a fan driven by a Siemens 3-phase induction AC motor connected to an AC driver, which controlled the air mass flow rate into the collector.

The air flow rate was measured using an Extech Instruments SDL 350 hot-wire thermo-anemometer. The temperatures of the PV module both at the top and back surfaces, the back plate, and the fluids were measured using K-type thermocouples calibrated prior to collector testing. All thermocouples, as well as the pyranometer, were connected to the channels of Advantech data acquisition modules for data logging via personal computer (PC). The electrical characteristics of the PV module were measured using a VS-6810 tracer-IVT Solar Pte Ltd, Singapore. Thermal readings were recorded at a time interval of 1 s and averaged over the period the system was in steady state. The incorporation of both heat absorbers into the

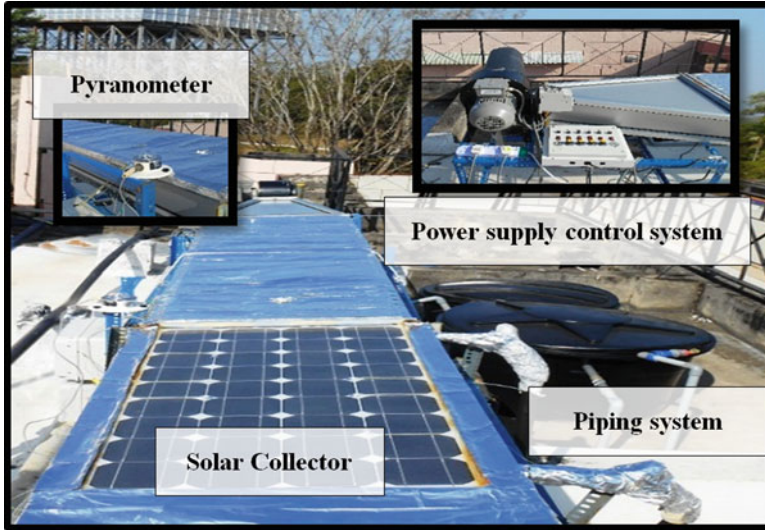


Fig. 32.2 Outdoor test-rig facilities

collector led to a new test-rig design which must be tailored to the dual heat exchange demands. Therefore, the fabrication of the test-rig facilities discussed in this study will serve as a good starting point to further develop experimental research on a bi-fluid type PV/T solar collector.

3 Thermal Model

Temperature nodes were constructed. The energy balance equations were then developed for each temperature node in the x - z plane. To simplify the analysis, the assumptions stated in [5] were employed. Because of the different total PV and back-panel surface areas involved in the heat transfer process, correction factors, γ_s , m , are introduced. For the nodes of the PV module solar cells, the energy balance equation is written as follows:

$$\begin{aligned}
 & \tau_g \alpha_c (PF)G - \tau_g \alpha_c \beta_c (\eta_{ele})G \\
 = & U_{t,m} (T_{PV,m} - T_a) + h_{pvbs,m} (T_{PV,m} - T_{bs,m}) - \frac{k_{PV} \delta_{PV}}{(\Delta x)^2} (T_{PV,m+1} - T_{PV,m}) \\
 & + \frac{k_{PV} \delta_{PV}}{(\Delta x)^2} (T_{PV,m} - T_{PV,m-1}).
 \end{aligned}
 \tag{32.1}$$

For the back surface of the Tedlar nodes, for subsegments without a copper tube, we have

$$\begin{aligned} & h_{\text{Pbs},m}(T_{\text{PV},m} - T_{\text{bs},m}) + \tau_g \alpha_T (1 - \beta_c) G \\ & = h_{\text{cvbsf}1,m} \gamma_{\text{bsf}1,m} (T_{\text{bs},m} - T_{f1,m}) + h_{\text{rbsbp},m} \gamma_{\text{bsbp},m} (T_{\text{bs},m} - T_{\text{bp},m}). \end{aligned} \quad (32.2)$$

For the back surface of the Tedlar nodes, for subsegments with a copper tube, an additional term to account for the heat transferred to the water flow was introduced:

$$\begin{aligned} & h_{\text{pvbs},m}(T_{\text{pv},m} - T_{\text{bs},m}) + \tau_g \alpha_T (1 - \beta_c) G = h_{\text{cvbsf}1,m} \gamma_{\text{bsf}1,m} (T_{\text{bs},m} - T_{f1,m}) \\ & + h_{\text{rbsbp},m} \gamma_{\text{bsbp},m} (T_{\text{bs},m} - T_{\text{bp},m}) h_{\text{cvbsf}2,m} \gamma_{\text{bsf}2,m} (T_{\text{bs},m} - T_{f2,m}). \end{aligned} \quad (32.3)$$

For the back plate nodes, a set of fins was installed on the surface of the back plate. The arrangement of fins on the surface of the back plate was also examined by Tonui and Tripanagnostopoulos [7]. At steady state, the heat convection rate from the fins' surface to the working fluid is equal to the heat conducted to the fin elements. The heat conduction equation may then be expressed as follows:

$$N_{\text{fin}} \left(-k_{\text{fin}} A_{c,\text{fin}} \frac{dT_{\text{fin}}}{dz} \right) = h_{\text{cvfinf}1,m} \gamma_{\text{finf}1,m} (T_{\text{fin},m} - T_{f1,m}). \quad (32.4)$$

In addition, at steady state, the temperature of the fins, $T_{\text{fin},m}$, was also considered equal to the base temperature of the back plate. However, in reality, the temperature of the fin drops along the fin. To take into account this effect, fin effectiveness, η_p , may be included in the heat transfer equation for the back plate nodes. The heat transfer term for the back plate nodes can then be expressed in terms of the back plate temperature $T_{\text{bp},m}$ as follows:

$$\begin{aligned} & h_{\text{rbsbp},m} \gamma_{\text{bsbp},m} (T_{\text{bs},m} - T_{\text{bp},m}) - h_{\text{cvbpf}1,m} \gamma_{\text{bpf}1,m} \eta_p (T_{\text{bp},m} - T_{f1,m}) \\ & = U_{\text{bp},m} \gamma_{\text{bp},m} (T_{\text{bp},m} - T_a), \end{aligned} \quad (32.5)$$

with $\eta_p = 1 - \gamma_{\text{finf}1,m} (1 - \eta_f)$: fin effectiveness, and $\eta_f = \frac{\tanh(m_{\text{fin}} h_{\text{fin}})}{m_{\text{fin}} h_{\text{fin}}}$: fin efficiency.

The following energy balance equation for the air nodes is then obtained:

$$\begin{aligned} & \frac{\dot{m}_{f1} C_{pf1} (T_{f1,m} - T_{f1,m-1})}{(\Delta x \Delta y_{\text{PV}})} = h_{\text{cvbpf}1,m} \gamma_{\text{bpf}1,m} \eta_p (T_{\text{bp},m} - T_{f1,m}) \\ & + h_{\text{cvbsf}1,m} \gamma_{\text{bsf}1,m} (T_{\text{bs},m} - T_{f1,m}). \end{aligned} \quad (32.6)$$

The following energy balance equation for the water nodes is then obtained:

$$\frac{\dot{m}_{f2}C_{pf2}(T_{f2o,m|M} - T_{f2i,m|M})}{(\Delta x \Delta y_{PV})} = \left(h_{cvbsf2,m} \gamma_{bsf2} (T_{bs,m} - T_{f2,m|M}) \right). \quad (32.7)$$

4 PV/T System Yield

Energetic performance or the overall energy gain is the most common performance evaluation method. It is worth emphasising here that even though each energy is evaluated using the first law of thermodynamics with the same standard unit, electric energy and thermal energy are different in nature. Therefore, the combined or overall performance of the collector should be evaluated by carefully taking into consideration the different natures of the energies [8–11]. Additionally, in PVT Roadmap [12], primary energy saving as discussed in detail in Huang et al. [13], was chosen to compute the overall PV/T performance. Therefore, the same type of analysis is used in this study. In Refs. [14, 15], the same form of evaluation was also used. Following the work of Huang et al. [13], the instantaneous primary energy saving, $\sum Q_{PVT,inst}$, may be written as follows:

$$\sum Q_{PVT,inst} = \sum Q_{th,inst} + \frac{P_{ele}}{C_f}. \quad (32.8)$$

Equation (32.8) may also be written

$$\sum Q_{PVT} = \int (\dot{m}_{f1}C_{pf1}(T_{f1o} - T_{f1i}) + \dot{m}_{f2}C_{pf2}(T_{f2o} - T_{f2i}))dt + \frac{\int P_{ele}dt}{C_f}. \quad (32.9)$$

The equation is defined as follows:

The overall equivalent thermal output (energy saving) from a PV/T system = overall thermal energy collected by the collector + overall electrical power output/conversion power factor (C_f).

Therefore, the primary energy-saving efficiency, $\sum \eta_{PVT}$, may be written

$$\sum \eta_{\text{PVT}} = \frac{\int (\dot{m}_{f1} C_{pf1} (T_{f1o} - T_{f1i}) + \dot{m}_{f2} C_{pf2} (T_{f2o} - T_{f2i})) dt}{A_c \times \int G dt} + \left(\frac{\int P_{\text{ele}} dt}{A_c \times \int G dt} \right) \frac{1}{C_f}. \quad (32.10)$$

C_f is known as the power plant conversion factor. It ranges from 0.2 to 0.4 depending on the quality of the coal used [13]. In this study, a value of 0.34 is used, which is the average thermal efficiency of a conventional coal power plant based on the 2008–2012 data as given by Suruhanjaya Tenaga (Energy Commissions) [16].

5 Results and Discussion

5.1 Validation of Mathematical Model

In a theoretical study of a PV/T solar collector, many researchers have emphasised the validation method of the mathematical model developed in their research. As discussed in [7, 8, 17], validation is performed by comparing the results obtained experimentally and theoretically based on the trends shown in the related graphs. In this study, the developed 2-D steady-state analysis was validated against the outdoor experimental data, and the input parameters recorded during the experiment were used in the computer simulation. However, the sky temperature T_{sky} under real sky conditions is typically 5–30 °C lower than the ambient temperature [18]. For theoretical analysis, the input for the sky temperature for outdoor testing was approximated using Eq. (32.11), as proposed by Swinbank [19], which gives a lower value for the sky temperature in comparison to the ambient temperature. The equation is considered suitable and reliable, as used by Abu Bakar and Hj Othman [20], who conducted research on PV/T solar collectors under real sky conditions in Malaysia:

$$T_{\text{sky}} = 0.0552T_a^{1.5}. \quad (32.11)$$

Analysis of the collector for different sets of mass flow rates under environmental conditions with an average wind speed of 3 m/s and average radiation of 700 W/m² was also conducted. To obtain suitable data, experiments were conducted for each of the mass flow rates and involve ten different days of testing. As illustrated in Figs. 32.3 and 32.4, an increase in the mass flow of air at a fixed water flow rate of 0.0066 kg/s and an increase in the water flow rate at a fixed air flow

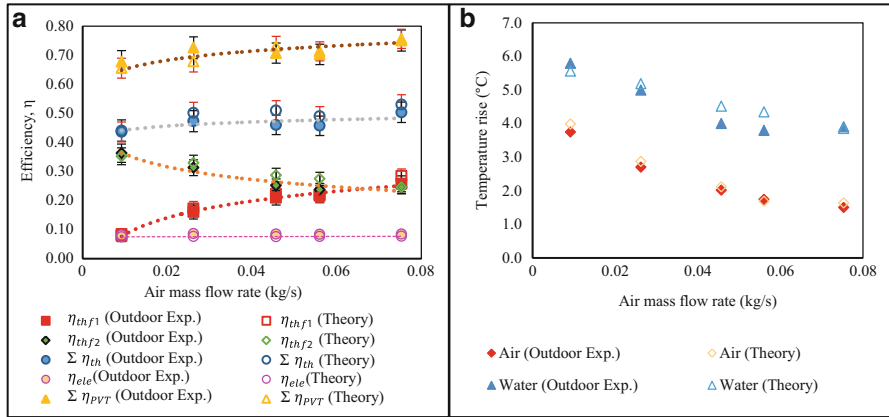


Fig. 32.3 Influence of change in air mass flow rate at fixed water flow rate on (a) average outdoor theoretical and experimental thermal efficiency (η_{thf1} and η_{thf2}), total thermal efficiency ($\Sigma \eta_{th}$) and primary energy-saving efficiency ($\Sigma \eta_{PVT}$) and (b) change in fluid temperature rise [$(T_{f1o} - T_{f1i})$ and $(T_{f2o} - T_{f2i})$] of PV/T solar collector during simultaneous mode at fixed water mass flow rate ($\dot{m}_{f2} = 0.0066$ kg/s, $G = 700$ W/m²)

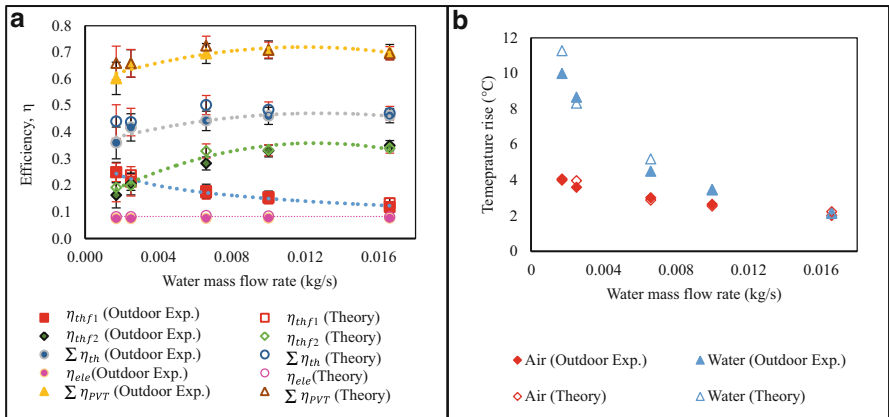


Fig. 32.4 Influence of change in water mass flow rate at fixed water flow rate on (a) average outdoor theoretical and experimental thermal efficiency (η_{thf1} and η_{thf2}), total thermal efficiency ($\Sigma \eta_{th}$), electrical efficiency (η_{ele}) and primary energy saving efficiency ($\Sigma \eta_{PVT}$) and (b) the change in fluid temperature rise [$(T_{f1o} - T_{f1i})$ and $(T_{f2o} - T_{f2i})$] of the PV/T solar collector during simultaneous mode at fixed air mass flow rate ($\dot{m}_{f1} = 0.0262$ kg/s, $G = 700$ W/m²)

rate of 0.0262 kg/s respectively lead to an increase in the total thermal efficiency of the solar collector. As predicted theoretically, as the air mass flow rate increases, the air thermal efficiency, η_{thf1} , increases, but with a decrease in the water thermal efficiency, η_{thf2} . For the simultaneous mode in which the water flow is fixed at

Table 32.1 Calculated mean absolute percentage error

	At fixed air flow rate	At fixed water flow rate
Parameter	MAPE (%)	MAPE (%)
Fluid output temperature (T_{f1o}) and (T_{f2o})	1.41	1.52
Primary energy-saving efficiency ($\sum \eta_{PVT}$)	1.49	4.36

0.0066 kg/s, the ranges of the simulated results are consistent with the recorded results such that, theoretically, the air thermal efficiency, water thermal efficiency, and total thermal efficiency vary from 8.49 to 28.45 %, 35.20 to 24.62 %, and 43.61 to 53.07 % respectively. Meanwhile, experimentally, the computed results vary from 7.79 to 25.74 %, 36.28 to 24.63 %, and 44.06 to 50.37 %. Under conditions with an air flow rate fixed at 0.0262 kg/s, the theoretical air thermal efficiency, water thermal efficiency, and total thermal efficiency varied from 24.91 to 13.32 %, 19.12 to 33.84 % and 44.03 to 47.15 % respectively.

Experimentally, the evaluated air thermal efficiency, water thermal efficiency, and total thermal efficiency were 11.82 to 25.00 %, 16.26 to 34.97 %, and 41.26 to 46.79 % respectively. These consistent values further strengthen the validity of the developed 2-D mathematical model. This is further supported by the computed mean absolute percentage error (MAPE) as low as 1.41 and 1.52 % for the fluids' output temperature at fixed water flow rate and air flow rate condition respectively, as well as a MAPE of 1.49 and 4.36 % for the primary energy-saving efficiency at fixed air and water flow rates respectively, as described in the following table (Table 32.1).

6 Parametric Study

6.1 Performance with Variation in Air Channel Depth

It is crucial to determine the optimum depth of the collector design. In this study, the performance of the collector, with a focus on the simultaneous mode of fluid operation with a change in the air channel depth, was investigated theoretically. At air and water mass flow rates of 0.0262 and 0.0066 kg/s, the change in the thermal efficiency and temperature rise with the variation in the air channel depth are illustrated in Fig. 32.5. Analysis of Fig. 32.5 shows that, for the same air and water mass flow rate, as the depth of the air channel increased, the air thermal efficiency and air output temperature decreased owing to the lower velocity of air flow as a result of the smaller hydraulic diameter of the air channel cross section. In contrast, the water thermal efficiency and change in temperature rise increased with depth. Such conditions were achieved because a decrease in air velocity leads to a lower heat transfer rate by the air flow; therefore, more thermal energy is available for extraction by the water flow. From the curves it may be concluded

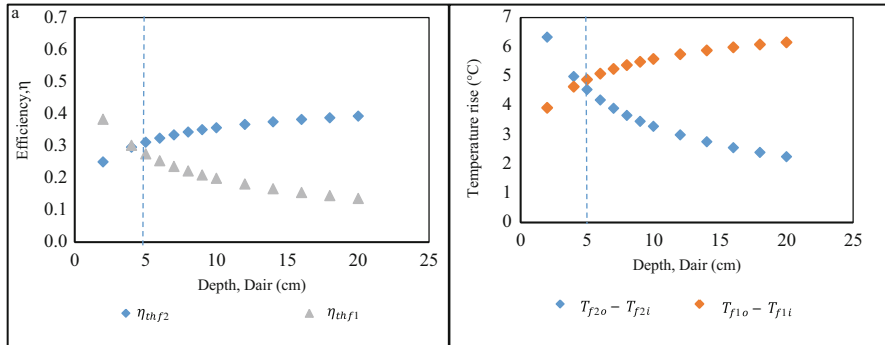


Fig. 32.5 (a) Change in air and water efficiency with channel depth of collector and (b) change in fluid temperature rise with channel depth ($\dot{m}_{f1} = 0.0262$ kg/s, $\dot{m}_{f2} = 0.0066$ kg/s, $G = 700$ W/m²)

that a depth of 0.05 m is the optimum since a further increase in duct depth leads to a lower overall thermal efficiency, lower air thermal efficiency and smaller air temperature rise.

6.2 Performance with Variation in Collector Length

This study devotes some attention to the variation in the fluids' output temperature T_{f1o} and T_{f2o} , the collector total thermal efficiency $\sum \eta_{thf1}$, and the primary energy-saving efficiency $\sum \eta_{PVT}$, with a variation in the length of the collector L_c . Using the validated 2-D steady-state mathematical model, the aforementioned thermal characteristics and electrical performance were simulated against the collector length. It is worth noting that the input parameters, such as the electrical characteristics, the ambient temperature, the fluid inlet temperature, average solar radiation, and sky temperature, were set according to the recorded metrological data of the day of collector testing (14 January 2015). For the existing length, the tube spacing and width of the collector were kept constant, doubling the length of the collector. This means that performance was evaluated at twice 1.183 m and so on. For the simultaneous mode of fluid operation, Fig. 32.6 shows the performance of the collector with variation in its length at a certain hour of the day (i.e. 11:00 a.m., 12:00 p.m., 13:00 p.m., 14:00 p.m. and 15:00 p.m.) of the collector test. The increase in the collector length, as expected, caused an increase in the fluids' output temperature and the mean PV cell temperature. In contrast, the total thermal efficiency and primary energy-saving efficiency are expected to decrease with length. This is because an increase in length leads to an increase in the temperature of the collector's components and therefore the overall heat loss coefficient of the collector. In terms of electrical performance, a decrease in efficiency was observed. This is due to the increase in the mean PV cell temperature

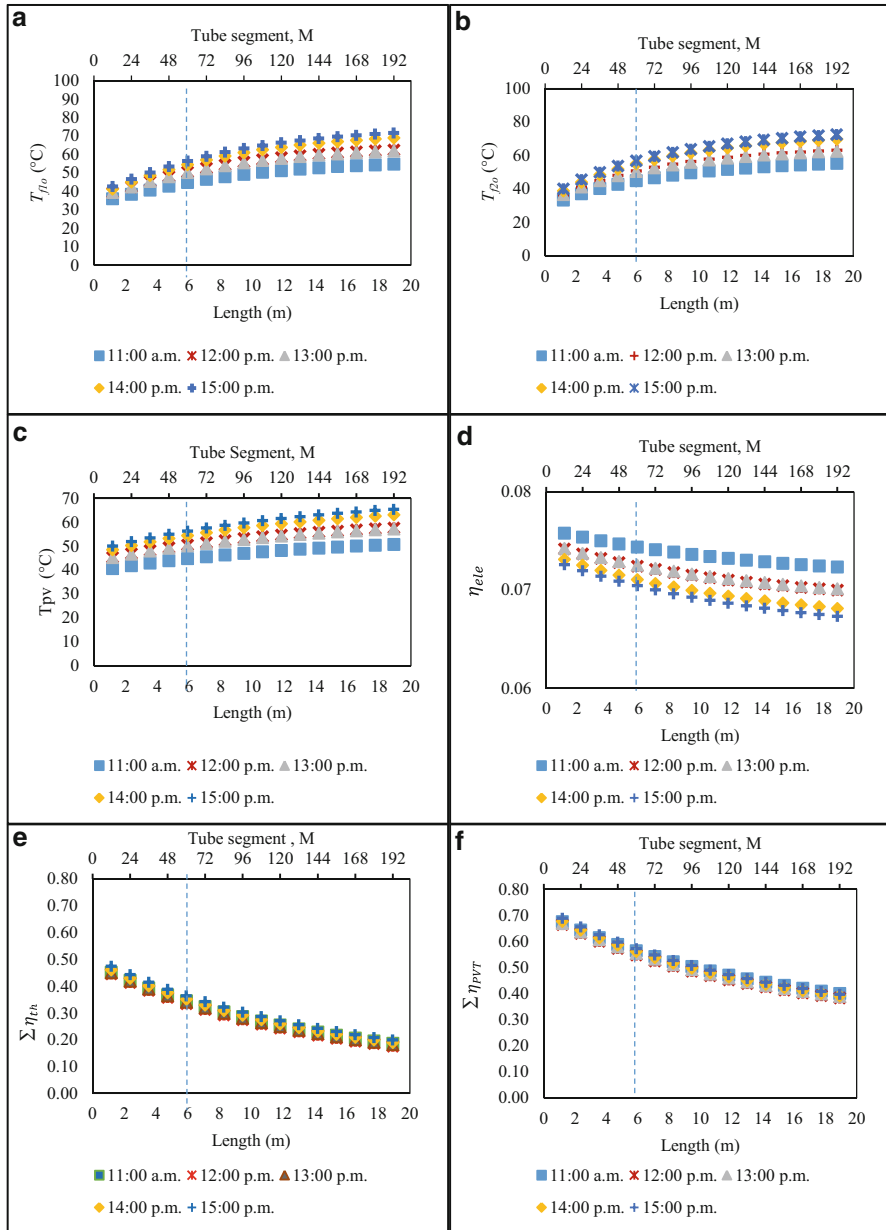


Fig. 32.6 Change in (a) air output temperature, (b) water output temperature, (c) mean temperature of PV cells, (d) electrical efficiency, (e) total thermal efficiency and (f) primary energy-saving efficiency of collector with length during simultaneous mode ($\dot{m}_{f1} = 0.0262$ kg/s, $\dot{m}_{f2} = 0.0066$ kg/s)

as the length of the collector increased. A similar trend of curves and cause was obtained by Sopian et al. [21]. In a study of a PV/T water type solar collector performed by Tiwari and Sodha [22], an increase in the collector length also led to an increase in the fluid output temperature. In their study, temperature output was predicted to nearly plateau starting at a length of 4 m, and hence was considered the optimum length for the designed collector. In this study, based on the plotted curves, the increase in the fluids' output temperature and the decrease in the thermal efficiencies were taken into consideration. When the collectors were arranged in series under the aforementioned ambient conditions, a length of 6 m is considered the optimum length for the whole collector. In addition, the number of tube segments was also included in the figures, so that the relationship between the collector length and the tube segments involved in the study may clearly be seen.

7 Conclusions

On the basis of the experimental and theoretical results as presented earlier, the following conclusions were drawn:

- (a) The developed 2-D steady-state mathematical model was validated for outdoor scenarios, as similar trends of curves were obtained both experimentally and theoretically. Additionally, MAPE analysis gave average values of less than 2% for the fluids' output temperature.
- (b) The developed 2-D steady-state mathematical model was proven useful in simulating the performance of the collector under varying parametric conditions. Optimum depth and length in this study were 0.05 m and 6 m respectively.
- (c) This research will serve as a basis for further research into a bi-fluid type PV/T solar collector. The feasibility of incorporating two different types of working fluids into the same PV/T solar collector was proven based on the thermal and electrical energy output of the collector when it was tested under real sky conditions.

References

1. Wolf M (1976) Performance analyses of combined heating and photovoltaic power systems for residences. *Energy Convers* 16:79–90
2. Florschuetz LW (1979) Extension of the Hottel-Whillier model to the analysis of combined photovoltaic/thermal flat plate collectors. *Sol Energy* 22:361–366
3. Tripanagnostopoulos Y (2007) Aspects and improvements of hybrid photovoltaic/thermal solar energy systems. *Sol Energy* 81:1117–1131
4. Assoa YB, Menezo C, Fraisse G, Yezou R, Brau J (2007) Study of a new concept of photovoltaic–thermal hybrid collector. *Sol Energy* 81:1132–1143

5. Abu Bakar MN, Othman M, Hj Din M, Manaf NA, Jarimi H (2014) Design concept and mathematical model of a bi-fluid photovoltaic/thermal (PV/T) solar collector. *Renew Energy* 67:153–164
6. Jarimi H, Abu Bakar MN, Manaf NA, Othman M, Din M (2013) Mathematical modelling of a finned bi-fluid type photovoltaic/thermal (PV/T) solar collector. In *IEEE Conference on Clean Energy and Technology (CEAT)*, 2013, pp 163–168
7. Tonui JK, Tripanagnostopoulos Y (2007) Air-cooled PV/T solar collectors with low cost performance improvements. *Sol Energy* 81:498–511
8. Chow TT, Pei G, Fong KF, Lin Z, Chan ALS, Ji J (2009) Energy and exergy analysis of photovoltaic–thermal collector with and without glass cover. *Appl Energy* 86:310–316
9. Fujisawa T, Tani T (1997) Annual exergy evaluation on photovoltaic-thermal hybrid collector. *Sol Energy Mater Sol Cells* 47:135–148
10. Joshi AS, Tiwari A (2007) Energy and exergy efficiencies of a hybrid photovoltaic–thermal (PV/T) air collector. *Renew Energy* 32:2223–2241
11. Sarhaddi F, Farahat S, Ajam H, Behzadmehr A (2010) Exergetic performance assessment of a solar photovoltaic thermal (PV/T) air collector. *Energy Build* 42:2184–2199
12. PVT Roadmap (2006) PVT ROADMAP A European guide for the development and market introduction of PV-Thermal technology
13. Huang BJ, Lin TH, Hung WC, Sun FS (2001) Performance evaluation of solar photovoltaic/thermal systems. *Sol Energy* 70:443–448
14. Mishra RK, Tiwari GN (2013) Energy and exergy analysis of hybrid photovoltaic thermal water collector for constant collection temperature mode. *Sol Energy* 90:58–67
15. Fudholi A, Sopian K, Yazdi MH, Ruslan MH, Ibrahim A, Kazem HA (2014) Performance analysis of photovoltaic thermal (PVT) water collectors. *Energy Convers Manag* 78:641–651
16. Suruhanjaya Tenaga (Energy Commissions) (2012) *Industri Pembekalan Elektrik di Malaysia Maklumat dan Prestasi Statistik 2012*. ed. Putrajaya Malaysia: Suruhanjaya Tenaga (Energy Commissions)
17. Othman MY, Yatim B, Sopian K, Abu Bakar MN (2007) Performance studies on a finned double-pass photovoltaic-thermal (PV/T) solar collector. *Desalination* 209:43–49
18. Duffie JA, Beckman WA (2006) *Solar engineering of thermal processes*. Wiley, New York
19. Swinbank WC (1963) Longwave radiation from clear skies. *Q J Roy Meteorol Soc* 89 (381):339–348
20. Abu Bakar MN, Hj Othman MY (2013) *Teknologi pengumpul suria fotovolta terma*. Penerbit Universiti Kebangsaan Malaysia, Malaysia
21. Sopian K, Yigit KS, Liu HT, Kakaç S, Veziroglu TN (1996) Performance analysis of photovoltaic thermal air heaters. *Energy Convers Manag* 37:1657–1670
22. Tiwari A, Sodha MS (2006) Performance evaluation of solar PV/T system: an experimental validation. *Sol Energy* 80:751–759

Chapter 33

Bi-fluid Photovoltaic/Thermal PV/T Solar Collector with Three Modes of Operation: Experimental Validation of a Theoretical Model

Hasila Jarimi, Mohd Nazari Abu Bakar, Mahmud Othman,
and Mahadzir Din

Abstract This chapter discusses theoretical and indoor experimental studies of a bi-fluid type photovoltaic/thermal (PV/T) solar collector. Two-dimensional steady-state analysis was developed and computer simulations were performed using MATLAB. Experiments were conducted for steady-state analysis under the solar simulator at Solar Energy Research Lab UiTM, Perlis, Malaysia, and under real sky conditions of Northern Peninsular Malaysia, to validate the model. The solar collector and the test rig facilities were fabricated to be suitable for mathematical validation purposes in both indoor and outdoor testing. For indoor collector testing, at an average wind speed of 1 m/s and average solar radiation of 700 W/m^2 , the air and water mass flow rate was varied from 0.0074 to 0.09 kg/s and 0.0017 to 0.0265 kg/s respectively. The thermal efficiency increased as the mass flow rate increased. At a mass flow rate of 0.0262 and 0.0066 kg/s for air and water respectively, the thermal efficiency curves tended to plateau, which marked the optimum point of the fluid flow. For the simultaneous mode of fluid operation, testing was conducted with air and water fixed at a flow rate of 0.0262 and 0.0066 kg/s respectively, while the fluids' mass flow rate was varied according to the range used during the independent mode. The range of the computed efficiencies for the simultaneous mode were higher than for the independent mode. In this study, collector outdoor testing was conducted for each mode of operation on a typical day in January in Perlis, Northern Peninsular Malaysia. Based on the outdoor monitoring analysis for simultaneous mode, the performance of the collector was also higher overall than the independent mode. The test was conducted by monitoring the performance of the collector with the air mass flow rate and water mass flow rate fixed at 0.0262 and 0.0066 kg/s respectively. Theoretical analysis was also performed and then validated against the experimental results by a direct comparison of the plotted curves and using mean absolute percentage error (MAPE)

H. Jarimi (✉) • M.N.A. Bakar • M. Othman • M. Din
Universiti Teknologi Mara Perlis, Perlis, Malaysia
e-mail: H.Jarimi@gmail.com

analysis. For the air, water and simultaneous modes, by taking into account both indoor and outdoor collector testing, the theoretical and experimental curves were found to be in good agreement, and the computed MAPE values for the fluids' output temperature were less than 2%. Thus, the two-dimensional mathematical model was proven valid. The PV/T collector designed in this study has a variety of applications because it can be operated in three different modes of fluid operation, and the theoretical model is useful in modelling all three modes without further modification.

Keywords Photovoltaic/thermal • 2D analysis • Bi-fluid • Indoor • Outdoor

Nomenclature

A_{PV}	Collector aperture area's subsegment, which is equal to the area of the PV module's subsegment (m^2)
C_f	Conversion power factor
C_{pf1}	Specific heat capacity of air
C_{pf2}	Specific heat capacity of water
D_i	Inner pipe diameter
D_o	Outer pipe diameter
f	A General subscript to represent a fluid
f_r	A Friction factor in a fluid's channel
G	Global radiation
h	Heat transfer coefficient ($W/m^2 K$)
h_{cvbsf1}	Convection heat transfer coefficient from back surface of Tedlar to air flow ($W/m^2 K$)
h_{cvbsf2}	Convection heat transfer coefficient from back surface of Tedlar to water flow ($W/m^2 K$)
$h_{cvfinf1}$	Convection heat transfer coefficient from surface of a fin to flowing air ($W/m^2 K$)
h_{cvw}	Wind convection heat transfer coefficient ($W/m^2 K$)
h_i	Generalised notation for heat transfer coefficient of linear equations derived from developed energy balance equations for general heat transfer coefficient i ($W/m^2 K$)
h_{rbsbp}	Radiation heat transfer coefficient between inner surfaces of collector ($W/m^2 K$)
h_{rpvsky}	Radiation heat transfer coefficient from PV cells to sky ($W/m^2 K$)
k_{fin}	Thermal conductivity of fin (W/mK)
k_{f1}	Thermal conductivity of air (W/mK)
k_{f2}	Thermal conductivity of water (W/mK)
k_{PV}	Thermal conductivity of photovoltaic cells (W/mK)
L_{fin}	Length of fin (m)

m	Subsegment for each temperature node
\dot{m}_{f1}	Air mass flow rate (kg/s)
\dot{m}_{f2}	Water mass flow rate (kg/s)
N_{fin}	Total number of fins
q	Rate of heat flux (W/m^2)
$q_{uf1,m}$	Rate of heat transfer per unit area for air nodes (W/m)
$q_{uf2,m}$	Rate of heat transfer per unit area for air nodes (W/m)
Re	Reynolds number
S_{PV}	Total rate of solar energy absorbed by solar cells of PV module
S_{T}	Total energy absorbed by Tedlar
T	Temperature (K)
T_a	Ambient temperature (K)
$T_{\text{bp},m}$	Temperature nodes of surface of back plate (K)
$T_{\text{bs},m}$	Temperature nodes of rear surface of Tedlar (K)
T_{bp}	Mean temperature of surface of back plate with fins (K)
T_{bs}	Mean temperature of rear surface of Tedlar (K)
T_{PV}	Mean temperature of cell (K)
$T_{f1,m}$	Temperature nodes of air flow in channel (K)
$T_{f2,m}$	Temperature nodes of water flow in copper pipe (K)
$T_{\text{fin},m}$	Mean temperature of fin at subsegment m (K)
$T_{\text{PV},m}$	Temperature nodes of PV cells (at centre of cells) (K)
T_{ref}	Temperature at reference point
T_{sky}	Sky temperature (K)
T_{tin}	Mean inner wall temperature of copper pipe (K)
$U_{t,m}$	Overall top heat loss coefficient for subsegment m
v_{f1}	Maximum velocity of air (m/s)
v_w	Wind speed (m/s)
W	Tube spacing (m)
α_c	Absorptance of PV cells
β_c	PV module packing factor
β_{ref}	Temperature coefficient at reference temperature
δ_{PV}	Thickness of PV module
δ_{si}	Thickness of Si cells
δ_{T}	Thickness of Tedlar layer
δ_{fin}	Fin thickness
$\Delta y_{\text{PV}} \Delta x$	Area of subsegment of PV module
Δx	Distance between temperature nodes ($\Delta x = 1 \text{ cm}$)
ϵ_{sky}	Emissivity of sky
ϵ_g	Emissivity of glass cover
$\gamma_{\text{bsbp},m}$	Area correction factor for heat transfer from back surface of Tedlar to surface of back plate with fins
$\gamma_{\text{bsf1},m}$	Area correction factor for heat transfer from back surface of Tedlar to flowing air

$\gamma_{bsf2,m}$	Area correction factor for heat transfer from back surface of Tedlar to flowing water
$\gamma_{finf1,m}$	Area correction factor for heat transfer from fin surfaces to flowing air
$\gamma_{bpf1,m}$	Area correction factor for heat transfer from surface of back plate with fins to flowing air
$\gamma_{bpa,m}$	Area correction factor for heat transfer from surface of back plate with fins to ambient
τ_g	Transmittance factor of front cover glass of PV module
τ_{gg}	Transmittance factor due to double glazing (glass covers)
η	Efficiency
η_c	Electrical efficiency of a PV cell
η_{ele}	Electrical efficiency
η_{eth}	Electrical efficiency converted to equivalent thermal efficiency
η_{fin}	Fin efficiency
η_p	Fin effectiveness
η_{Tref}	Electrical efficiency at reference temperature
η_{thf1}	Thermal efficiency of air
η_{thf2}	Thermal efficiency of water
$\sum \eta_{th}$	Total thermal efficiency of solar collector
$\sum \eta_{PVT}$	Primary energy saving or equivalent thermal efficiency
$\sum \eta_{th,inst}$	Instantaneous total thermal efficiency of solar collector

1 Introduction

The research on photovoltaic/thermal (PV/T) solar collectors began as early as mid-1970 and has developed every year since then [1]. The potential of collectors in clean energy utilisation has been a point of focus in studies on the technical feasibility of different solar collector designs that have been carried out by many researchers [1]. The research includes theoretical and experimental analyses of collectors, which commonly focus on a flat plate type using either air or water for the thermal components. At the theoretical level, current research focuses mainly on one-dimensional (1-D) steady-state analysis [2–8], with a few researchers, such as Zondag et al. [2], performing two-dimensional (2-D) and three-dimensional (3-D) analyses of PV/T water type solar collectors; Dehra [9], who carried out a 2-D steady-state analysis of a PV/T air type solar wall collector; and Assoa et al. [10], who performed 2-D steady-state analysis of a bi-fluid type PV/T solar collector.

This chapter discusses the theoretical analysis of a bi-fluid type PV/T solar collector with fins. In comparison to the typical PV/T collector, this type of collector offers more options in which hot air or hot water can be utilised depending on energy needs and applications. In addition, the simultaneous use of both fluids is predicted to further enhance the performance of solar collectors as water will

compensate the low heat capacity of air in extracting unwanted heat from a PV panel. This type of PV/T collector was first introduced by Tripanagnostopoulos [11], followed by Assoa et al. [10]. To date, only the two aforementioned studies have discussed the use of both fluids with the same PV/T collector. An improved design and 2-D steady-state analysis of a PV/T solar collector with a bi-fluid configuration have been presented by the current authors in [12–16]. This chapter further discusses the performance of the collector and the validity of the developed mathematical model when both fluids operate independently and simultaneously. The analysis covers both indoor and outdoor performance under the tropical climate conditions of Perlis in Northern Peninsular Malaysia.

2 Experimental Design

The designed and fabricated collector consists of a PV module, a serpentine copper pipe attached on the back surface of the Tedlar and a single pass air channel as shown in Fig. 33.1. The system works such that air and water will be pumped into and out of the collector to extract the unwanted heat from the PV module and transform it into useful heat according to the energy needs and applications. The use of serpentine-shaped copper pipe has been proven feasible and able to maintain the flow uniformity throughout the pipe [8]. In this design, the pipe is exposed to the air channel and acts as the transverse corrugated surface to the air flow and is called a ‘serpentine-corrugated surface’. The use of additional glazing improves the thermal performance of the collector, but it comes with penalties in the performance of the PV cells [17]. The recorded local ambient temperature at which the collector will be tested can reach as high as 36 °C [18]. Therefore, in this study, the collector will be unglazed because the electricity is the main priority; in addition, we wish to avoid unwanted effects due to the high stagnation temperature. Because of the lower heat

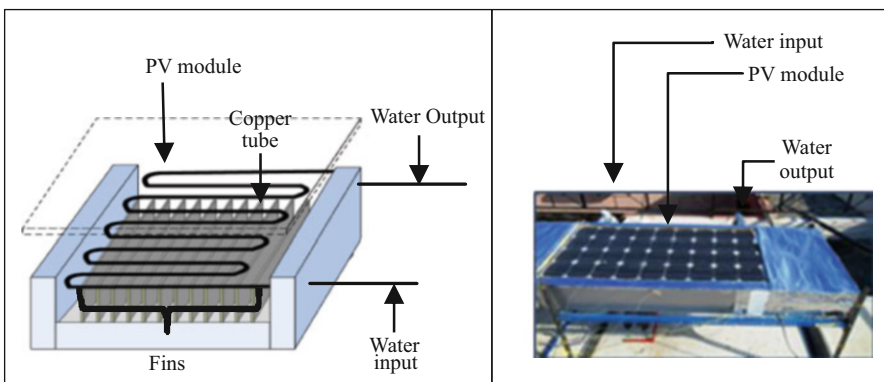


Fig. 33.1 (a) Top cross-sectional view of designed PV/T solar collector and (b) top view of fabricated collector

capacity of air, the emissivity of the copper pipe and the back plate of the air channel is increased by blackening the surfaces. A set of fins parallel to the direction of the air flow was arranged on the surface of the back plate to enhance the heat transfer rate by creating a cross-corrugated configuration [12]. A non-optimised prototype was fabricated to validate the simulation results from the developed 2-D mathematical model for the collector under study.

To perform the test, indoor and outdoor test-rig facilities were set up and fabricated at Solar Energy Research Lab, UiTM, Perlis, Malaysia, and on the rooftop of the lab respectively. In general, the test-rig facilities were comprised of two important sections, the air and water heat exchange system and the power-supply and control system. Meanwhile, for indoor tests, one of the most important components is the solar simulator. Many low-cost solar simulators suitable for solar collector testing have been fabricated worldwide starting as early as 1974 [19, 20]. For indoor testing of the collector, an ideal solar simulator would consist of lamps in which the spectral distribution resembled the spectral distribution of the sunlight. However, because of various economic and physical constraints, this is impossible to achieve [21]. According to several researchers [19–23], following the minimum characteristics or standards as listed in ASHRAE, tungsten halogen lamps may be employed for a solar simulator because they are sufficient and reliable for indoor collector testing. While various types of lamps have been suggested, per the work of Garg et al. [19], Hussain et al. [21], Agrawal et al. [22] and Othman et al. [24], small double-ended linear 500 W quartz-halogen tungsten lamps in the Philips Plusline were used in this study (Halogen lamp—Malaysia; SP737 Tideway—Taiwan; United Automation CSR2-E series power regulator—United Automation, UK; Blue-White F-440 in line flow meter—USA).

Parameters include inlet and outlet air temperatures, ambient temperature, temperatures at several locations, current, voltage, air and water flow rates, wind velocity and the solar radiation incident on the collector plane. Water was pumped into the collector by an SP737 Tideway-Taiwan electric submersible water pump from the primary water tank. Speed was controlled using a United Automation CSR2-E series power regulator-United Automation, UK. To maintain a constant water temperature, a secondary water tank was used to dispose of the heated water. Before water entered the collector, the water flow rate was measured using a Blue-White F-440 inline flow meter-USA. Meanwhile, air was pumped into the collector using an air blower consisting of a fan driven by a Siemens 3-phase induction AC motor connected to an AC driver. The fan was used to control the flow of air flow into the collector. The air flow rate was measured using an Extech Instruments SDL 350 hot-wire thermo-anemometer. The temperatures of the PV module at the top and back surface, back plate and fluids were measured using K-type thermocouples calibrated prior to collector testing. All thermocouples, as well as the pyranometer, were connected to the channels of Advantech data acquisition modules for data logging via personal computer. The electrical characteristics of the PV module for indoor testing were measured using a VS-6810 curve tracer-IVT Solar Pte Ltd, Singapore. Thermal readings were recorded at a time interval of 1 s and averaged over the period the system was in steady state. The incorporation of both heat

exchange systems into the collector leads to a new test-rig design which must be tailored to the dual heat exchange demands. Therefore, the fabrication of the test-rig facilities discussed in this study was a good starting platform to further develop experimental research on a bi-fluid type PV/T solar collector.

3 Theoretical Analysis

A study of a mathematical model of a bi-fluid system during simultaneous mode of fluid operation was carried out by Assoa et al. [10]. However, in this study, the design of the collector is different from that of Assoa et al. [10] in the sense that the water and air heat exchangers are all integrated below the PV module and not alternately.

3.1 Two-Dimensional Steady-State Analysis

Owing to the different total PV and back-panel surface areas involved in the heat transfer process, correction factors, $\gamma_{s,m}$, are introduced. For the nodes of the solar cells of the PV module $T_{PV,m}$, the energy balance equation is written

$$\begin{aligned} \tau_g \alpha_c (\beta_c) G - \tau_g \alpha_c \beta_c (\eta_{ele}) G = U_{t,m} (T_{pv,m} - T_a) + h_{pvbs,m} (T_{pv,m} - T_{bs,m}) \\ - \frac{k_{pv} \delta_{pv}}{(\Delta x)^2} (T_{pv,m+1} - T_{pv,m}) + \frac{k_{pv} \delta_{pv}}{(\Delta x)^2} (T_{pv,m} - T_{pv,m-1}). \end{aligned} \quad (33.1)$$

For the back surface of the Tedlar nodes $T_{bs,m}$, for subsegments with copper tube, an additional term to account for the heat transferred to the water flow is introduced:

$$\begin{aligned} h_{pvbs,m} (T_{pv,m} - T_{bs,m}) + \tau_g \alpha_T (1 - \beta_c) G = h_{cvbsf1,m} \gamma_{bsf1,m} (T_{bs,m} - T_{f1,m}) \\ + h_{rbsbp,m} \gamma_{bsbp,m} (T_{bs,m} - T_{bp,m}) h_{cvbsf2,m} \gamma_{bsf2,m} (T_{bs,m} - T_{f2,m}). \end{aligned} \quad (33.2)$$

For the back plate nodes, a set of fins is installed on the surface of the back plate. At steady state, the maximum heat convection rate from the fins' surface to the working fluid is equal to the heat conducted to the fin elements. The heat conduction equation can then be expressed as

$$N_{fin} \left(-k_{fin} A_{c,fin} \frac{dT_{fin}}{dz} \right) = h_{cvfinf1,m} \gamma_{finf1,m} (T_{fin,m} - T_{f1,m}). \quad (33.3)$$

In addition, at steady state, the temperature of the fins $T_{fin,m}$ is also considered as equal to the base temperature of the back plate. However in reality, the temperature

of the fin drops along the fin. To take this effect into account, fin effectiveness, η_p , must be included in the heat transfer equation for the back plate nodes. The heat transfer term for the back plate nodes can then be expressed in terms of the back plate temperature $T_{bp,m}$ as

$$\begin{aligned} & h_{rbsbp,m}\gamma_{bsbp,m}(T_{bs,m} - T_{bp,m}) - h_{cvbpf1,m}\gamma_{bpf1,m}\eta_p(T_{bp,m} - T_{f1,m}) \\ & = U_{bp,m}\gamma_{bp,m}(T_{bp,m} - T_a). \end{aligned} \quad (33.4)$$

The following energy balance equation for the air nodes is then obtained:

$$\begin{aligned} & \frac{\dot{m}_{f1}C_{pf1}(T_{f1,m} - T_{f1,m-1})}{(\Delta x\Delta y_{pv})} = h_{cvbpf1,m}\gamma_{bpf1,m}\eta_p(T_{bp,m} - T_{f1,m}) \\ & + h_{cvbsf1,m}\gamma_{bsf1,m}(T_{bs,m} - T_{f1,m}). \end{aligned} \quad (33.5)$$

The following energy balance equation for the water nodes is then obtained:

$$\begin{aligned} & \frac{\dot{m}_{f2}C_{pf2}(T_{f2o,m}|_M - T_{f2i,m}|_M)}{(\Delta x\Delta y_{pv})} \\ & = (h_{cvbsf2,m}\gamma_{bsf2}(T_{bs,m} - T_{f2,m}|_M)). \end{aligned} \quad (33.6)$$

3.2 Solution to Equations

Each of the heat transfer mechanisms is associated with its own heat transfer coefficient, which is computed as the heat transfer rate per unit collector surface area. There are various correlations available in the literature to predict the heat transfer coefficients for a developed model. In this study, the thermophysical properties of air and water are assumed to vary with temperature. For a low temperature range, the following correlations, as proposed by Ong [25] and Yaws and Richmond [26], were used to compute the thermophysical properties for air and water respectively. The Nusselt number plays an important role in computing the overall convective heat transfer rate by the fluid flow. Meanwhile, the Reynolds number is important because it determines the flow regime of the fluid flow through the ratio of the inertia forces to the viscous forces in the fluid. Several correlations are available in the literature, including in textbooks on heat transfer, to estimate the Nusselt number for the purpose of computing the convection heat transfer coefficient from the inner wall surfaces to the fluid flow. For the simulation studies carried out in this research, the correlations used in this study were obtained by referring to the available correlations from earlier researchers, as summarised in Table 33.1.

Table 33.1 Previous researchers referring to Nusselt correlations

Type of fluid and surface	Range of Reynolds number (Re)	Ref.	Flow regime
Air; back surface of Tedlar	$Re < 2300$	Manglik and Bergles [29]	Laminar
Air; inner surface of back plate with fins			
Air; back surface of Tedlar	$2300 \leq Re \leq 6000$	Tam and Ghajar [30]	Transition (onset of turbulence)
Air; inner surface of back plate with fins		Gnielinski [31]	
Air; back surface of Tedlar	$6000 < Re \leq 10000$	Lin et al. [32]	Transition (fully turbulent)
Air; inner surface of back plate with fins		Gnielinski [31], with the friction factor f given by Çengel et al. [33]	
Air; back surface of Tedlar	$10,000 < Re \leq 50,000$	Gnielinski [31], with the friction factor f given by Çenge, et al. [33]	Fully developed turbulent
Air; inner surface of back plate with fins			
Water, serpentine copper pipe	$Re < 1000$	Çengel et al. [33]	Laminar
	$1000 < Re \leq 2100$	Tam and Ghajar [30]	
	$2100 < Re \leq 10,000$	Gnielinski [31] with f from Tam and Ghajar [30]	Transition
	$Re \geq 10,000$	Gnielinski [31] with f from Tam and Ghajar [30]	Turbulent

3.3 PV/T System Yield

The energetic performance or the overall energy gain is the common performance evaluation method. It is worth emphasising here that even though each energy is evaluated using the first law of thermodynamics with the same standard unit, electric energy and thermal energy are different in nature. Therefore, the combined or overall performance of the collector should be performed by carefully taking into consideration the different natures of the energies. Following the work by Huang et al. [27], the primary energy-saving efficiency $\sum \eta_{PV/T}$ can be written

$$\sum \eta_{PVT} = \frac{\int (\dot{m}_{f1} C_{pf1} (T_{f1o} - T_{f1i}) + \dot{m}_{f2} C_{pf2} (T_{f2o} - T_{f2i})) dt}{A_{PV} \times \int G dt} + \left(\frac{\int P_{ele} dt}{A_{PV} \times \int G dt} \right) \frac{1}{C_f}. \quad (33.7)$$

C_f is known as the power plant conversion factor. It ranges from 0.2 to 0.4 depending on the quality of the coal used [27]. In this study, a value of 0.34 is used, which is the average thermal efficiency of a conventional coal power plant based on the 2008–2012 data as given by Suruhanjaya Tenaga (Energy Comissions) [28].

4 Results and Discussions

4.1 Indoor

Mass flow rate is an important parameter in the design of PV/T solar collectors [33]. For indoor collector testing, at an average wind speed of 1 m/s and average solar radiation of 700 W/m², the air and water mass flow rates were varied from 0.0074 to 0.09 kg/s and 0.0017 to 0.0265 kg/s respectively. Figure 33.2a, b illustrates the theoretical and experimental analyses of the influence of the variation of the fluids' mass flow rate on the performance of the collector during the air and water modes respectively. Both analyses show the same trend of curves such that the increase in the fluids' mass flow rate results in an increase in the thermal efficiency of the collector and a decrease in the change in temperature rise. This is attributed to the fact that as the mass flow rate increases, the convection heat transfer rate from the inner wall of the air channel and copper pipe to the corresponding working fluids also increases. Therefore, the thermal energy extracted also increases. However, as the mass flow rate increases, the fluids spend less time in the respective channels, and hence the change in the temperature rise decreases. Additionally, Fig. 33.2 also shows that as the mass flow rate continues to increase, the thermal efficiency and the change in temperature rise reach an optimum point and tend to plateau. Figure 33.2a, b indicates that the optimum mass flow rates for air and water are 0.0262 and 0.0066 kg/s respectively. Meanwhile, unlike the thermal efficiency, a marginal increase in the electrical efficiency was observed both theoretically and experimentally. Also included in the data points of the respective curves are the error bars, which represent the absolute errors derived for the thermal, electrical and primary energy-saving efficiency of the collector. The computed absolute errors for the thermal and primary energy-saving efficiency on average vary from 4 to 9 % with respect to the increase

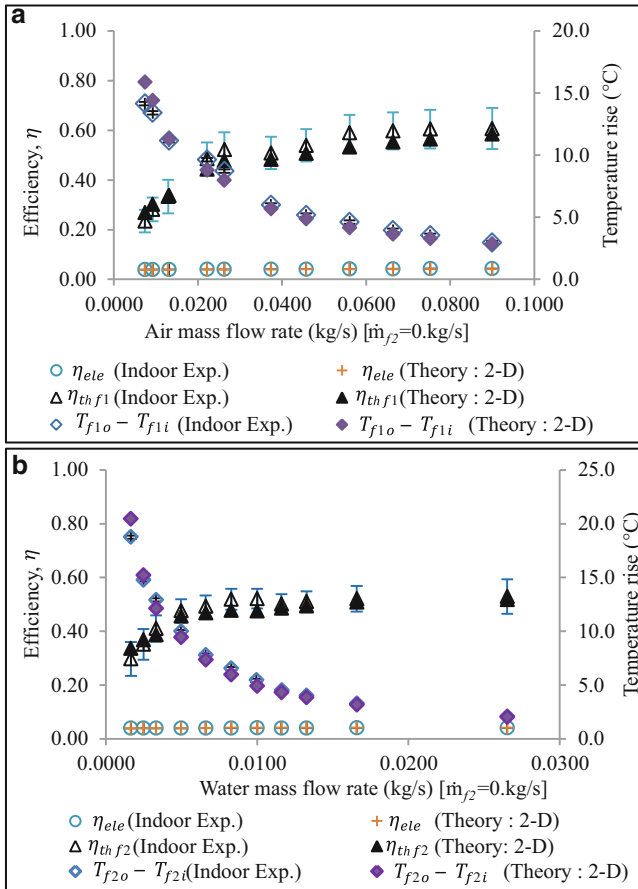


Fig. 33.2 Influence of fluid flow rate on thermal and electrical performance of PV/T solar collector during (a) air mode and (b) water mode for indoor collector testing

in the air mass flow rate. Meanwhile, for the electrical efficiency, the average absolute error is less than 0.2 %. The ranges of the measured and computed values for the change in the air and water temperature rise, i.e. $(T_{f1o} - T_{f1i})$ and $(T_{f2o} - T_{f2i})$ respectively, air and water thermal efficiency (η_{thf1} and η_{thf2}), electrical efficiency (η_{ele}) and total yield of the PV/T system ($\sum \eta_{PV/T}$) for the air mode and water mode are summarised in Table 33.2.

In this study, investigation of the thermal behaviour of each fluid to the collector performance when both fluids are operated simultaneously is interesting in the sense that, even though both of the installed heat absorbers are directly associated to one another, the working fluids are not physically in contact. Also, even though the fluids are not physically in contact, the thermal performance of each working fluid influences that of the others. The testing was conducted with air and water

Table 33.2 Summary of theoretical and experimental results during indoor testing for independent mode of fluid operation

Parameter	PV/T air (air mode)		PV/T water (water mode)	
	Experiment	Theory	Experiment	Theory
T_{f1o} (°C)	47.00–34.66	48.74–34.55	–	–
T_{f2o} (°C)	–	–	50.53–31.66	52.22–31.66
η_{th1}	23.43–59.85 %	26.84–58.5 1 %		
η_{th2}	–	–	29.76–52.95 %	33.63–51.78 %
η_{ete}	3.89–4.33 %	3.77–4.11 %	3.94–4.03 %	3.85–4.08 %
$\sum \eta_{PVT}$	34.87–72.59 %	37.93–70.59 %	41.35–64.79 %	44.96–63.77 %

The range given is with respect to the increase in the fluids' mass flow rate

fixed at flow rates of 0.0262 kg/s and 0.0066 kg/s respectively, while the fluids' mass flow rates were varied according to the range used during independent mode. As can be seen in Fig. 33.3a, theoretically, the mathematical model predicted that the increase in the water flow rate would result in an increase in the water thermal efficiency, but with a decrease in the air thermal efficiency. Meanwhile, when the thermal efficiency was evaluated as a total, the computed thermal efficiency of the water dominated the total thermal efficiency of the system, and the expected total thermal efficiency was therefore higher than the independent mode. The trend of the graphs is explained as follows. When the mass flow rate of one of the fluids increases while the other one remains fixed at a constant mass flow rate, more thermal energy is removed by the fluid with the increased flow rate. Hence, a smaller amount of thermal energy is left to be extracted by the other fluid. This was clearly observed when the water flow rate was fixed. In contrast, as illustrated in Fig. 33.3b, when the air mass flow rate was fixed, the increase in the water mass flow rate had an insignificant effect on the amount of energy extracted by the air flow. These conditions occurred due to the fact that the active convective surface area of the air flow covered the whole back surface area of the PV module, including the outer surface of the copper pipe; meanwhile, for water, its convective surface area is only within the inner wall of the serpentine-shaped copper pipe. The experimental analysis also showed the same trend of the curves as the theoretical analysis. The ranges of the measured and computed parametric values for the simultaneous mode of fluid operation are summarised in Table 33.3.

To further justify the validity of the 2-D steady-state analysis, the simulation results were compared against the experimental results using mean absolute percentage error (MAPE) analysis, as summarised in Table 33.4. The computed errors exist owing to the assumption that the solar radiation of the solar simulator is uniformly distributed across the solar collector, whereas an average spatial uniformity of less than 2 % was measured for each set of solar radiation prior to collector testing. Nevertheless, with respect to the plotted curves and the computed errors, the theoretical and the indoor experimental results are concluded to be in good agreement.

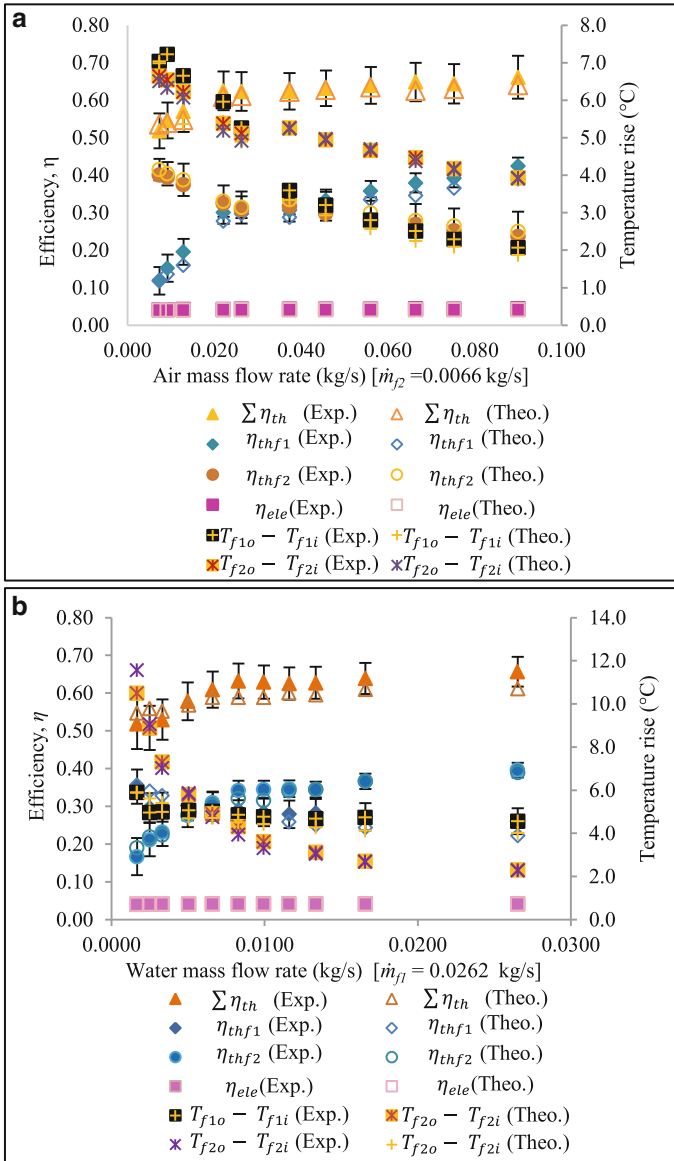


Fig. 33.3 Influence of fluid flow rate on thermal and electrical performance of PV/T solar collector during (a) simultaneous mode at fixed air flow rate condition and (b) water flow rate condition for indoor testing

Table 33.3 Summary of theoretical and experimental results during indoor testing for simultaneous mode of fluid operation

Parameter	Simultaneous mode (fixed air flow rate)		Simultaneous mode (fixed water flow rate)	
	Experiment	Theory	Experiment	Theory
T_{f1o} (°C)	38.10–37.05	38.08–36.35	40.19–34.94	40.13–34.74
T_{f2o} (°C)	42.60–33.30	44.07–33.26	37.64–36.01	37.50–36
η_{thf1}	35.22–26.09 %	35.68–22.22 %	11.83–42.41 %	11.96–39.02 %
η_{thf2}	16.03–39.61 %	19.03–38.97 %	40.04–23.71 %	41.55–25.00 %
$\sum (\eta_{th})$	51.25–65.70 %	54.71–61.20 %	51.87–66.12 %	53.51–64.02 %
η_{ele}	4.13–4.15 %	4.04–4.14 %	4.13–4.37 %	4.05–4.16 %
$\sum (\eta_{PV/T})$	63.39–77.90 %	65.89–72.47 %	64.01–78.98 %	65.42–76.25 %

The range given is with respect to the increase in the fluids’ mass flow rate

Table 33.4 Summary of MAPE values computed against indoor experimental testing

Parameter	Mean absolute percentage error (MAPE) values			
	Air mode (%)	Water mode (%)	Simultaneous mode (fixed air flow rate) (%)	Simultaneous mode (fixed water flow rate) (%)
T_{f1o}	1.34	–	0.93	1.19
T_{f2o}	–	1.31	0.59	0.27
$\sum \eta_{thf}$	6.47	6.03	5.33	2.12
η_{ele}	3.33	1.13	0.97	3.46
$\sum \eta_{EPVT}$	5.10	4.55	4.91	2.27

4.2 Outdoor

The true performance of the collector under real sky conditions still needs to be investigated in order to further justify the validity of the mathematical model. The monitoring period was between 9:30 a.m. and 5:00 p.m. on a typical day in January and February 2015 in Arau Perlis, Malaysia, at a latitude of 6.5224816° N and longitude of 100.2308224°E. Owing to the varying conditions of the environment, following the experimental method conducted by [20], the efficiencies of the PV/T system in a steady-state condition are analysed as per time constant of the collector. The metrological data are illustrated in Fig. 33.4.

As can be seen in Figs. 33.5 and 33.6, outdoor experimental results for all three modes of operation – air, water and simultaneous mode – were compared with the theoretical results. It is concluded that the theoretical results are in good agreement with the experimental analysis such that the trend of the theoretical curves are consistent with the experimental curves. Additionally, the feasibility of the designed PV/T solar collector is proven based on the results obtained from outdoor monitoring analysis. For the air mode, as shown in Fig. 33.5a, the average measured wind speed was 3.21 m/s, and average solar radiation ranged from 426.23 to

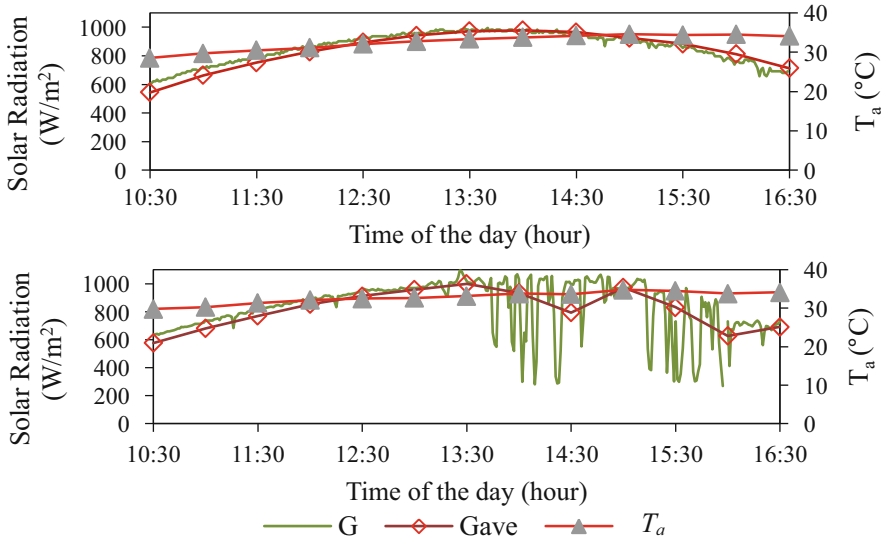


Fig. 33.4 Recorded solar radiation G , average solar radiation G_{ave} and ambient temperature during T_a : (a) air mode (27 January 2015) and (b) water mode (13 January 2015)

977.75 W/m². The evaluated thermal efficiency and electrical efficiency of the collector ranged from 23.63 to 31.96 % and 6.12 to 8.98 %, respectively. Meanwhile for the water mode, as shown in Fig. 33.5b, the measured average wind speed was 3.69 m/s and solar radiation ranged from 460.19 to 1000.13 W/m². The obtained efficiencies varied within a range of 31.15 to 45.41 % and 5.85 to 8.61 % respectively.

Meanwhile, for the simultaneous mode, the metrological data are as shown in Fig. 33.7. The performance of the collector was, overall, higher than in independent mode. The test was conducted by monitoring the performance of the collector with air mass flow rate and water mass flow rate fixed at 0.0262 and 0.0066 kg/s respectively. The average measured wind speed was 3.30 m/s, and the average measured solar radiation ranged from 476 to 1016 W/m². The evaluated electrical efficiency and total thermal efficiency varied between 6.20 and 9.78 % and 43.12 and 47.85 % respectively. The validity of the theoretical model was further strengthened by an evaluation of the MAPE analysis (Table 33.5). It is worth emphasising that computed errors for the electrical efficiency are considered relatively large. Nevertheless, in comparison to the analysis provided in previous studies [35, 36], the computed errors are deemed acceptable. The relatively large MAPE values are attributed to the fact that the electrical characteristics of the PV module respond almost instantaneously to the change in solar radiation. However, the averaging method used corresponds to the thermal time constant of the solar collector. In addition, the product of the effective absorptance–transmittance of the PV/T solar collector, which affects the electrical performance of the collector, was

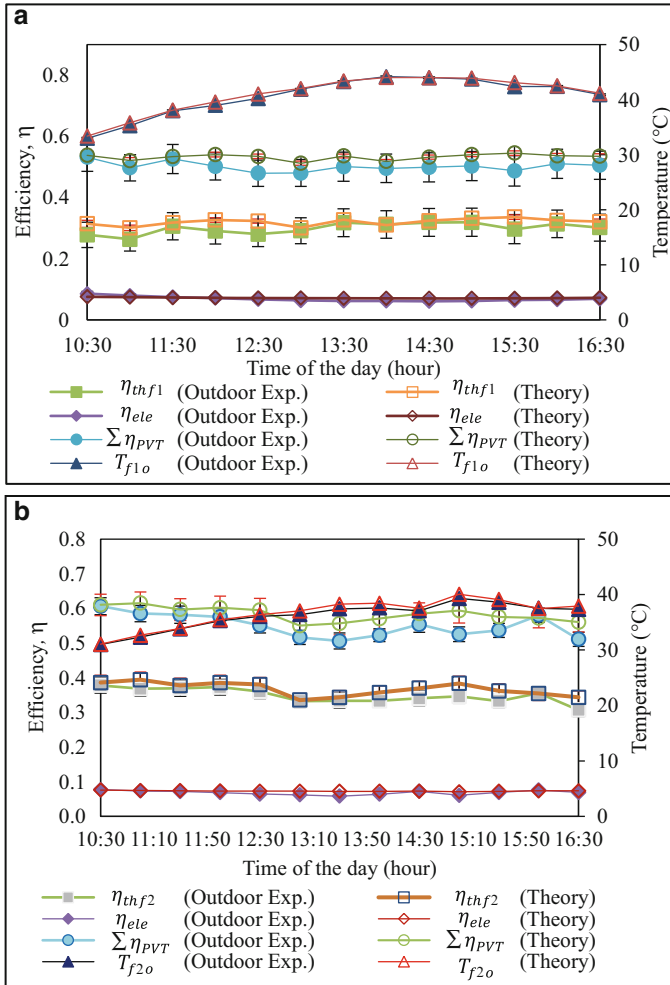


Fig. 33.5 Theoretical and experimental thermal and electrical performance of PV/T solar collector during (a) air mode based on data collected on 27 January 2015 and (b) water mode based on data collected on 13 January 2015 for outdoor collector testing

assumed constant whereas it actually changes during the day owing to the spectral response of the PV cells, which changes owing to changes in the air mass ratio throughout the day. A similar explanation was given by Amori and Taqi Al-Najjar [37]. Nevertheless, such a discrepancy does not affect the fluids' output temperature and its thermal efficiency significantly.

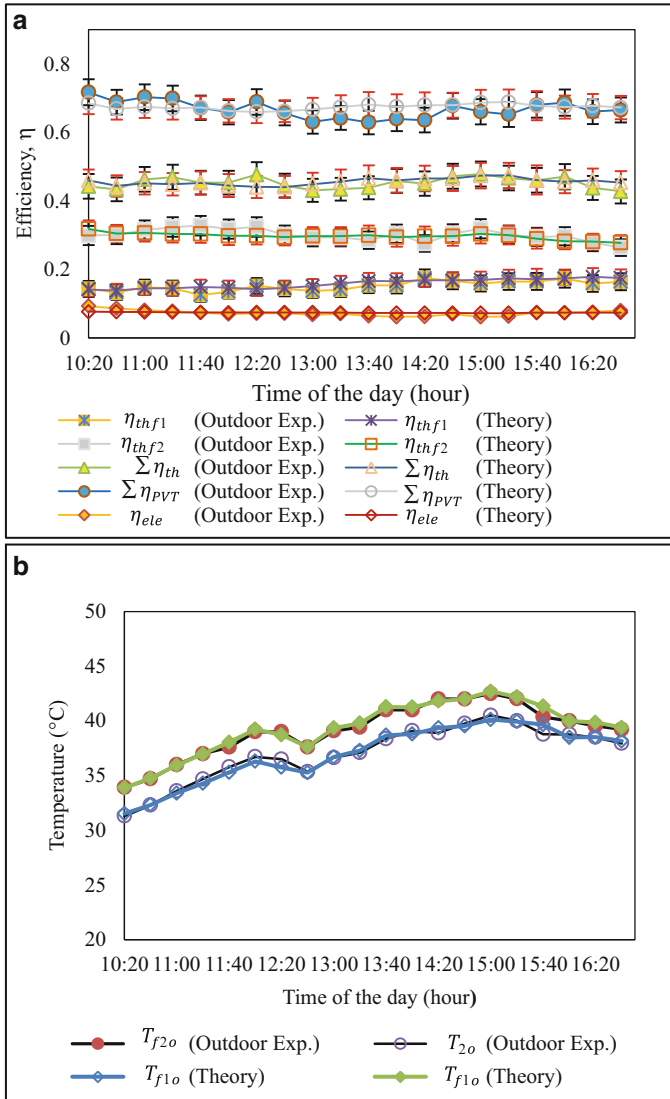


Fig. 33.6 Outdoor experimental and theoretical curves for (a) electrical (η_{ele}), thermal efficiency (η_{thf1} and η_{thf2}), total thermal efficiency ($\sum \eta_{th}$), and primary energy-saving efficiency ($\sum \eta_{PVT}$); and (b) fluid output temperatures (T_{f1o} and T_{f2o}) as per time constant of collector with time of day on 14 January 2015 [$\dot{m}_{f1} = 0.0262$ g/s and $\dot{m}_{f2} = 0.0066$ kg/s]

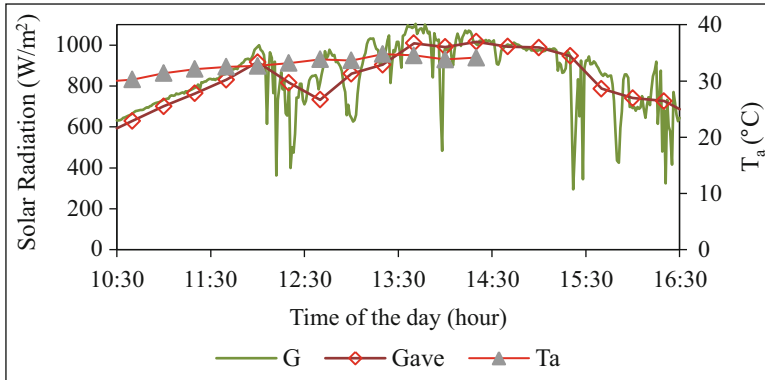


Fig. 33.7 Recorded solar radiation G , average solar radiation G_{ave} and ambient temperature during T_a during simultaneous mode (14 January 2015)

Table 33.5 Summary of MAPE values computed against outdoor experimental testing for $G = 700 \text{ W/m}^2$

Parameter	Mean absolute percentage error (MAPE) values		
	Air mode (%)	Water mode (%)	Simultaneous mode (%)
T_{f1o}	0.80	–	0.43
T_{f2o}	–	1.16	0.67
η_{thf1}	6.33	–	6.51
η_{thf2}	–	5.49	3.98
$\sum \eta_{thf}$	–	–	2.98
η_{ele}	8.94	8.64	8.81
$\sum \eta_{E_{pvt}}$	6.29	6.62	3.62

5 Conclusions

A design of a PV/T solar collector integrating a PV module, a serpentine-shaped copper pipe as the water heat absorber, and a single-pass air channel as the air heat absorber was discussed. To enhance the rate of heat transfer to the air flow, the use of additional fins arranged parallel to the air flow was introduced and a ‘cross-corrugated configuration’ was created. The collector is capable of producing three different modes of fluid operation: air mode, water mode and simultaneous mode. The feasibility of the designed bi-fluid PV/T solar collector was demonstrated based on experimental results obtained indoors and outdoors. A 2-D steady-state finite-difference analysis was conducted and validated for all three modes of fluid operation against indoor and outdoor experimental results. The theoretical model was proven valid since the trend of the theoretical and experimental curves was found to be in good agreement. Additionally, MAPE values computed for the fluids’ output temperature, which is the parameter most discussed by previous researchers, are on average less than 2%, which further strengthens the validity of the mathematical model.

Acknowledgement This work was funded by the Malaysian Fundamental Research Group (FRGS) 600-RMI/ST/FRGS 5/3/Fst (160/2010) and Solar Energy Research Lab, Universiti Teknologi Mara (UiTM), Perlis, Malaysia

References

1. Abdul Hamid S, Yusof Othman M, Sopian K, Zaidi SH (2014) An overview of photovoltaic thermal combination (PV/T combi) technology. *Renew Sustain Energy Rev* 38:212–222
2. Zondag HA, de Vries DW, van Helden WGJ, van Zolingen RJC, van Steenhoven AA (2002) The thermal and electrical yield of a PV-thermal collector. *Sol Energy* 72:113–128
3. Dubey S, Sandhu GS, Tiwari GN (2009) Analytical expression for electrical efficiency of PV/T hybrid air collector. *Appl Energy* 86:697–705
4. Solanki SC, Dubey S, Tiwari A (2009) Indoor simulation and testing of photovoltaic thermal (PV/T) air collectors. *Appl Energy* 86:2421–2428
5. Tiwari A, Sodha MS (2007) Parametric study of various configurations of hybrid PV/thermal air collector: experimental validation of theoretical model. *Sol Energy Mater Sol Cells* 91:17–28
6. Tiwari A, Sodha MS (2006) Performance evaluation of solar PV/T system: an experimental validation. *Sol Energy* 80:751–759
7. Tonui JK, Tripanagnostopoulos Y (2007) Air-cooled PV/T solar collectors with low cost performance improvements. *Sol Energy* 81:498–511
8. Koech RK, Ondieki HO, Tonui JK, Rotich SK (2012) A Steady State Thermal Model For Photovoltaic/Thermal (PV/T) System Under Various Conditions. *Int J Sci Technol Res* 1
9. Dehra H (2009) A two dimensional thermal network model for a photovoltaic solar wall. *Sol Energy* 83:1933–1942
10. Assoa YB, Menezo C, Fraisse G, Yezou R, Brau J (2007) Study of a new concept of photovoltaic–thermal hybrid collector. *Sol Energy* 81:1132–1143
11. Tripanagnostopoulos Y (2007) Aspects and improvements of hybrid photovoltaic/thermal solar energy systems. *Sol Energy* 81:1117–1131
12. Abu Bakar MN, Othman M, Hj Din M, Manaf NA, Jarimi H (2014) Design concept and mathematical model of a bi-fluid photovoltaic/thermal (PV/T) solar collector. *Renew Energy* 67:153–164
13. Manaf NA, Bakar A, Nazari M, Jarimi H, Muhamed S, Othman M (2013) Design of a single-pass bi-fluid Photovoltaic/Thermal (PV/T) solar collector. *Int J Chem Environ Eng* 4
14. Abu Bakar MN, Othman M, Hj Din M, Manaf NA, Jarimi H (2013) Development of an improved photovoltaic/thermal (PV/T) solar collector with bi-fluid configuration. *Int J Chem Environ Eng* 4
15. Jarimi H, Bakar MNA, Othman M, Din MH, Manaf NA (2014) Investigation on the thermal characteristics of a bi-fluid type hybrid solar collector. In *World Renewable Energy Congress 2014*, Kingston, London
16. Jarimi H, Abu Bakar MN, Manaf NA, Othman M, Din M (2013) Mathematical modelling of a finned bi-fluid type photovoltaic/thermal (PV/T) solar collector. In *IEEE Conference on Clean Energy and Technology (CEAT)*, 2013, pp 163–168
17. Chow TT, Pei G, Fong KF, Lin Z, Chan ALS, Ji J (2009) Energy and exergy analysis of photovoltaic–thermal collector with and without glass cover. *Appl Energy* 86:310–316
18. Lawan SM, Abidin WAWZ, Chai WY, Baharun A, Masri T (2013) Reviewing wind speed and energy distribution in Malaysia. *Eur Acad Res* 1:2104–2122
19. Garg HP, Shukla AR, Madhuri I, Agnihotri RC, Chakraverty S (1985) Development of a simple low-cost solar simulator for indoor collector testing. *Appl Energy* 21:43–54

20. Abu Bakar MN, Hj Othman MY (2013) Teknologi pengumpul suria fotovolta terma. Penerbit Universiti Kebangsaan Malaysia, Malaysia
21. Hussain F, Othman MYH, Yatim B, Ruslan H, Sopian K, Anuar Z et al (2011) Fabrication and irradiance mapping of a Low cost solar simulator for indoor testing of solar collector. *J Sol Energy Eng* 133:044502
22. Agrawal S, Tiwari GN, Pandey HD (2012) Indoor experimental analysis of glazed hybrid photovoltaic thermal tiles air collector connected in series. *Energy Build* 53:145–151
23. Fudholi A, Sopian K, Othman MY, Ruslan MH, Bakhtyar B (2013) Energy analysis and improvement potential of finned double-pass solar collector. *Energy Convers Manag* 75:234–240
24. Othman MY, Yatim B, Sopian K, Abu Bakar MN (2007) Performance studies on a finned double-pass photovoltaic-thermal (PV/T) solar collector. *Desalination* 209:43–49
25. Ong KS (1995) Thermal performance of solar air heaters: mathematical model and solution procedure. *Sol Energy* 55:93–109
26. Yaws CL, Richmond PC (2009) Appendix B—thermophysical and transport properties of water. In: Yaws CL (ed) *Thermophysical properties of chemicals and hydrocarbons*. William Andrew Publishing, Norwich, pp 791–799
27. Huang BJ, Lin TH, Hung WC, Sun FS (2001) Performance evaluation of solar photovoltaic/thermal systems. *Sol Energy* 70:443–448
28. Suruhanjaya Tenaga (Energy Commissions) (2012) *Industri Pembekalan Elektrik di Malaysia Maklumat dan Prestasi Statistik 2012*. ed. Putrajaya Malaysia: Suruhanjaya Tenaga (Energy Commissions)
29. Manglik RM, Bergles AE (1995) Heat transfer and pressure drop correlations for the rectangular offset strip fin compact heat exchanger. *Exp Therm Fluid Sci* 10(2):171–180. [http://dx.doi.org/10.1016/0894-1777\(94\)00096-Q](http://dx.doi.org/10.1016/0894-1777(94)00096-Q)
30. Tam LM, Ghajar AJ (2006) Transitional heat transfer in plain horizontal tubes. *Heat Transfer Eng* 27:23–38
31. Gnielinski V (1976) New equations for heat and mass transfer in turbulent pipe and channel flow. *Int Chem Eng* 16:359–368
32. Lin W, Gao W, Liu T (2006) A parametric study on the thermal performance of cross-corrugated solar air collectors. *Appl Therm Eng* 26:1043–1053
33. Çengel YA, Ghajar AJ, Kanoğlu M (2011) *Heat and mass transfer: fundamentals and applications*. McGraw Hill Higher Education, New York
34. Moradi K, Ali Ebadian M, Lin C-X (2013) A review of PV/T technologies: effects of control parameters. *Int J Heat Mass Transf* 64:483–500
35. Joshi AS, Tiwari A, Tiwari GN, Dincer I, Reddy BV (2009) Performance evaluation of a hybrid photovoltaic thermal (PV/T) (glass-to-glass) system. *Int J Therm Sci* 48:154–164
36. Sarhaddi F, Farahat S, Ajam H, Behzadmehr A, Mahdavi Adeli M (2010) An improved thermal and electrical model for a solar photovoltaic thermal (PV/T) air collector. *Appl Energy* 87:2328–2339
37. Amori KE, Taqi Al-Najjar HM (2012) Analysis of thermal and electrical performance of a hybrid (PV/T) air based solar collector for Iraq. *Appl Energy* 98:384–395

Chapter 34

High Quality of Calibration Accuracy for Smart Building Energy-Efficiency Opportunities

G. Mustafaraj

Abstract A well-calibrated model is crucial to accurately represent a building's energy profile. This chapter deals with a building where an underfloor heating system supplied by a geothermal water-to-water heat pump and natural ventilation are the main systems used to maintain comfort conditions. Existing methodologies to establish calibration accuracy are mainly based on whole-building energy consumption comparisons. This research considers whole-building energy consumption with a breakdown of end-use energy consumption. The objective of this work is to develop a two-level calibration methodology which starts with calibration and then continues with the necessary actions for improving building energy efficiency. Finally, the model was simulated to estimate the potential of energy-efficiency improvements. The results of the analysis show that electricity consumption savings and heat released from the heat pump can vary between 20 and 27 % on a monthly basis.

Keywords Calibration • Smart buildings • Energy efficiency • Natural ventilation • Underfloor heating • Water-to-water heat pump • Natural ventilation

1 Introduction

Environmental concerns and the recent increase in energy costs open the door to innovative techniques to reduce energy consumptions. Buildings account for about 40 % of energy consumption in the European Union (EU) [1]. Improvement of their energy performance is a major challenge of the twenty-first century. To this end the new Energy Efficiency Directive was formally adopted by the Council of Ministers

G. Mustafaraj (✉)

International Energy Research Centre IERC, Tyndall Institute, University College of Cork, Cork, Ireland

e-mail: gmustafaraj73@gmail.com

and European Parliament in October 2012. The main objective of the Directive is to promote the improvement of the energy performance of buildings within the EU through cost-effective measures [2]. Hence, this chapter presents a new calibration methodology with the purpose of increasing the accuracy of building energy models as a necessary action before implementing any energy-efficiency measures.

Past research [3–6] dealt mainly with the calibration process without considering any further opportunities for energy savings. Additionally, research on building energy model calibration has been based solely on simple heating, ventilation, and air conditioning (HVAC) systems [e.g. forced ventilation supplied by air-handling units (AHUs)].

The calibration methodology proposed by Raftery et al. [3] recognises the need for systematic evidence-based decision-making to improve reproducibility and reliability in model calibration. Bertagnolio et al. [4] proposed an evidence-based calibration of a simplified dynamic hourly model which uses technical specifications, measurements, sensitivity and uncertainty analysis to predict whole-building energy use. In 2008, the Royal Institute of British Architects (RIBA) and the Chartered Institution of Building Services Engineers (CIBSE) launched CarbonBuzz, a free online platform allowing practices to share and publish building energy consumption data anonymously [7]. It enables designers to compare predicted and actual energy use for their projects, whilst also allowing for comparison against benchmarks and data supplied by other participating practices. In particular, Hamilton et al. [8] compared the predicted and actual electricity consumption in three building sectors: schools, general offices and university buildings. They demonstrated that the measured electricity demands are approximately 60–70 % higher than predicted in both schools and general offices and over 85 % higher than predicted on university campuses. Despite these works, there is a need for further research to develop new calibration methodologies capable of further reducing the gap between predicted and actual energy consumption.

Thus, the contributions presented in this chapter are as follows. First, a novel methodology is presented based on whole-building energy consumption in combination with an end-use energy consumption breakdown.

Second, our calibration methodology considers in a holistic way the complex interactions of the components of HVAC systems that affect the accuracy of the model (e.g. ventilation types and underfloor heating systems). Third, the algorithm developed represents a complete analysis which includes a calibration process and then the required measures to increase energy savings.

This chapter is organised as follows. Section 2 presents the two levels of the calibration methodology and discusses the algorithm. Section 3 gives an overview of the demonstration building and HVAC plants. Section 4 describes the building simulation activity to identify further opportunities of energy savings. Finally, Sect. 5 provides a conclusion with directions for future research works.

2 Overview of Calibration Methodology

In our calibration methodology, input parameters are specified by an analyst and used by energy simulation programs to reproduce a building's thermal processes, while outputs are energy performances simulated by energy simulation programs, given certain input parameters. Two levels of calibration are performed and use a combination of building, system and measurement data.

Building energy models were developed using EnergyPlus version 8.2 [9]. Throughout the calibration process, hourly and monthly EnergyPlus [9] model outputs related to heat pump electricity consumption, heat pump heat released, building total electricity consumption, natural gas and indoor zone temperatures were compared to measured data. The adequacy of this calibration was evaluated against the ASHRAE Guideline 14 [10], which outlines a way to compare model output with sensor data using mean bias error (MBE) and cumulative variation of root-mean-squared error [CV(RMSE)]. ASHRAE Guideline 14 [10] prescribes the acceptable limits for calibration to hourly data as $10\% \leq \text{MBE}_{\text{hourly}} \leq 10\%$ and $\text{CV(RMSE)}_{\text{hourly}} \leq 30\%$, and monthly data as $5\% \leq \text{MBE}_{\text{monthly}} \leq 5\%$ and $\text{CV(RMSE)}_{\text{monthly}} \leq 15\%$. Figure 34.1 shows the procedure for model calibration and identification of energy-savings opportunities and is described as follows.

First level of calibration: The first level corresponds to an 'as-built' model of the installation. This version of the model is based on available as-built data (plans, schemes and nameplate data of main HVAC components) and will be used for screening parameters. The data collected at this stage correspond to the information which can be expected when proceeding to an energy audit/inspection of an installation.

Second level of calibration: The second level involves an intensive use of building energy management system (BEMS) records and the monitoring data collected on site by means of the measurement equipment.

The calibration process during level 2 is a more advanced step which consists of an iterative process to identify the most important parameters. The value of each identified parameter has to be estimated/refined. Various direct or indirect measurement techniques can be used for that purpose (e.g. direct indoor or supply temperature measurement or indirect estimation of operating profiles by means of short-term monitoring of some lighting or appliances consumption measurements).

Finally, the second level of the calibration process also includes parameter estimation. These parameters could be building use related (e.g. occupancy, lighting, appliance) or system operations related (e.g. HVAC thermostat schedules). Earlier research demonstrated that occupancy is one of the important factors in the discrepancies between simulated and measured energy performances [11] because the main end users of energy, such as HVAC systems, lighting and appliances, are influenced by occupancy [12]. Throughout the calibration process, model validation was conducted (on hourly and monthly bases) by comparing model output with real measurements.

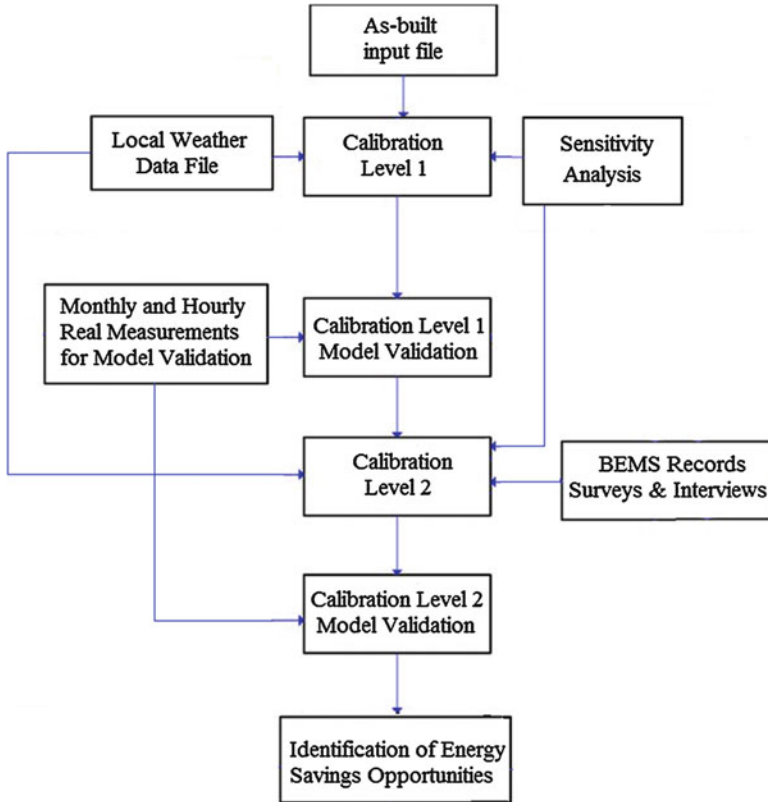


Fig. 34.1 Algorithm for model calibration and energy-saving opportunities

A **sensitivity analysis** was performed throughout the first and second levels as a screening method to rank non-visible parameters based on how the simulated energy consumption would change in response to changes made to each non-visible parameter.

The Morris method [13] was used in our research to identify the influential parameters because it has been proven valid for screening building energy simulation parameters [14]. This method was found to be suitable for application to building energy simulation models by De Wit [14] since it is not dependent on the properties of the model and requires no assumption regarding linearity or correlations between the inputs and outputs of the model. Heiselberg and Brohus [15] also highlighted other advantages of the Morris method. First, the method can handle a large number of parameters and requires a relatively limited amount of simulation runs. Second, the parameters are varied globally within the range and the whole parametric space can be explored without predefining the probability density function of each parameter. Third, the results are easily interpreted and visualized graphically, as prescribed by Morris [13].

To further increase the accuracy of calibration, a local weather data file is used which was built and based on the data collected from an on-site weather station. Finally, identification of energy-saving opportunities is made to further reduce electricity consumed by the water-to-water heat pump.

3 Overview of Building and HVAC Plants

The Environmental Research Institute (ERI) building in Cork is a three-storey 4500 m² research building containing offices, computer laboratories, wet laboratories, a clean room and controlled-temperature rooms. Figure 34.2 shows a 3-D view generated with DesignBuilder [16] using design documents. The geometry of the building model was derived from mechanical ventilation drawings, and DXF files were created from the AutoCAD drawings (DWG).

The building is a reinforced concrete structure providing high levels of thermal mass to allow for natural and mechanical ventilation with night cooling as required. The build-up of the floors, roof, external façades, internal partitions and windows were constructed from as-built structural drawings.

The build-up thermal properties were taken from CIBSE [17] and ASHRAE [18] and are listed as follows:



Fig. 34.2 ERI building 3-D view of design model

- **East and west face:** 250 mm reinforced concrete, 100 mm polystyrene, 25 mm gypsum plaster ($U = 0.258 \text{ W/m}^2\text{K}$);
- **South face:** 10 mm hardwood, 40 mm rockwool, 15 mm plywood ($U = 0.848 \text{ W/m}^2\text{K}$);
- **North face:** 25 mm rockwool, 38 mm air gap, 250 mm cast concrete, 15 mm hardwood ($U = 0.839 \text{ W/m}^2\text{K}$);
- **General flat roof:** 10 mm stone chippings, 20 mm felt/bitumen layer, 75 mm screed, 275 mm polystyrene, 250 mm concrete slab ($U = 0.104 \text{ W/m}^2\text{K}$);
- **Internal partition:** 25 mm gypsum plaster, 50 mm cavity, 50 mm glass fibre quilt, 15 mm plywood, 10 mm gypsum plaster ($U = 0.498 \text{ W/m}^2\text{K}$);
- **Ground floor and first floor slabs:** 250 mm concrete slab, 275 mm polystyrene void former, 75 mm screed ($U = 0.1 \text{ W/m}^2\text{K}$);
- **Lower ground floor slabs:** 750 mm clay, 150 mm stone, 175 mm concrete slab, 50 mm insulation, 75 mm screed ($U = 0.452 \text{ W/m}^2\text{K}$);
- **Glazing north, south, east and west façades:** 4 mm Optifloat/16 mm/4 mm K Glass ($U = 1.7 \text{ W/m}^2\text{K}$).

Apart from smaller areas of the building that occupy the central core of the building space (such as toilet, cold rooms, clean rooms and stores) which are mechanically ventilated by five AHUs, the majority of the building is naturally ventilated.

Figure 34.3 is a schematics overview of the HVAC system. The building is heated by an underfloor heating system that is primarily supplied by a geothermal heat pump which taps into a water supply fed from a culvert running adjacent to a nearby river. The underfloor heating operates at a maximum temperature of 38 °C.

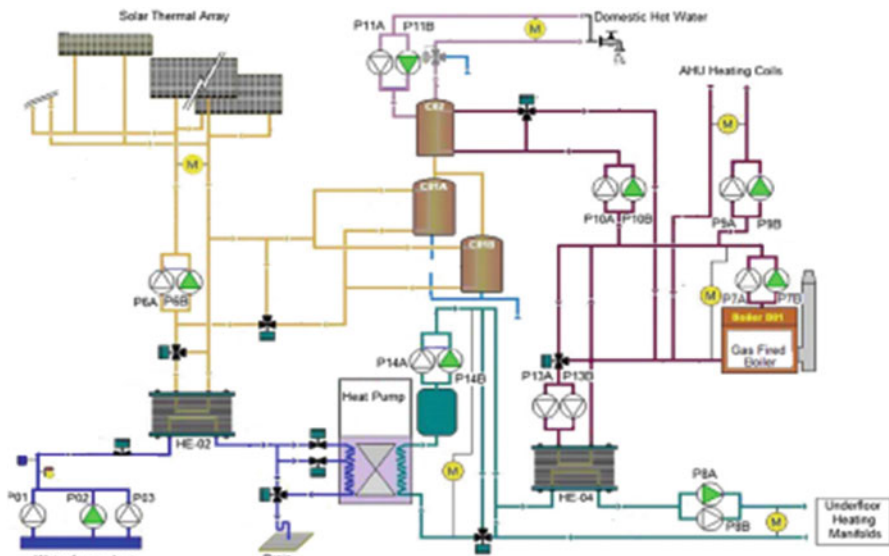


Fig. 34.3 Schematic of HVAC system [11]

Overall, the heat pump (Coefficient of Performance) = 2.4–4.2) meets 80 % of the building's heating requirements, with the balance provided by a condensing gas boiler sized to act as a complete back-up system. The solar thermal collector composed of 28 flat collectors is installed to provide hot water, with the remaining domestic water load provided by a direct gas-fired water heater (Fig. 34.3). It was verified that this heat is only 3–5 % of the heat required by the building.

Consequently, solar panels were included in the EnergyPlus model; however, during the calibration process, no particular attention was given to them.

4 Analysis of Results

The build-up of the floors, roof, external façades, internal partitions and windows of each floor were constructed from as-built structural drawings.

The as-built information was complete and allowed identification of relatively accurate values of envelope component characteristics (e.g. U -values). The selection of the most influential parameters was based on the results of the sensitivity analyses performed in EnergyPlus. Finally, analysis of the results related to model calibration and energy-saving opportunities are presented in Sects. 4.1 and 4.2.

4.1 Calibration

The accuracy of the calibration was evaluated by computing the classical calibration criteria in terms of MBE and CV(RMSE) on an hourly and monthly basis in 2011. During the first level of calibration, fixed values of temperatures were taken from ASHRAE [19] and used as a schedule in Energy Plus. Throughout the first level of the calibration process, the values of MBE and CV(RMSE) on an hourly basis were less than 18.7 % and 36.2 % respectively, while on a monthly basis the value of MBE was less than 8.6 % and for CV(RMSE) it was less than 20.7 %.

In contrast to the first level, during the second level of calibration, the real values of zone temperatures were collected from BEMS at an hourly sampling rate and used in EnergyPlus as the schedule for the temperature.

A comparison between measurements and model output related to the first and second levels of calibration is presented in Figs. 34.4, 34.5, 34.6 and 34.7. An analysis of the results demonstrated improvements in the model prediction as we moved from the first to second level of the calibration process.

In addition, the present research also considered comparisons between simulated and measured data based on hourly data (Figs. 34.8, 34.9 and 34.10).

Finally, after applying the second level of calibration, the values of MBE and CV (RMSE) on an hourly basis were less than 11.4 and 33.5 % respectively, while on a monthly basis the value of MBE was less than 6.1 % and for CV(RMSE) it was less than 16.5 %.

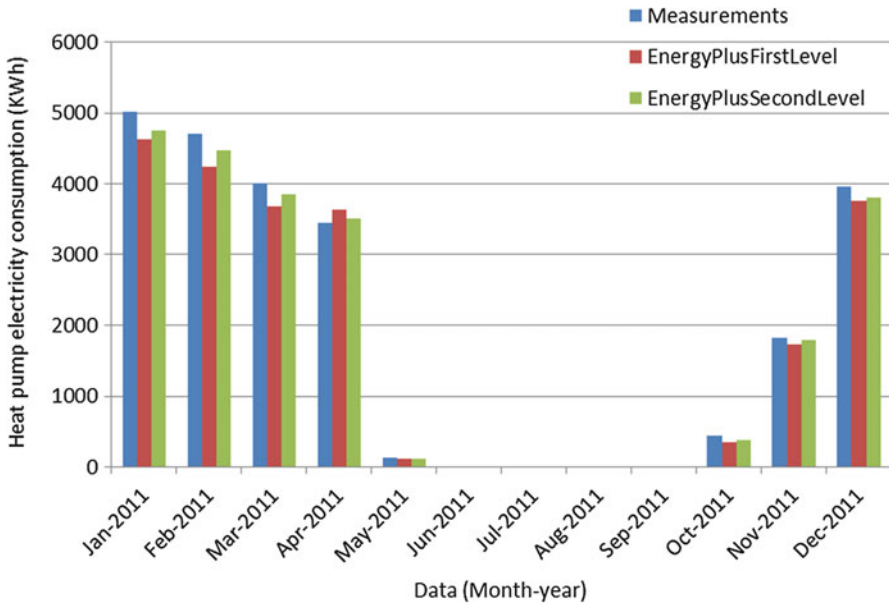
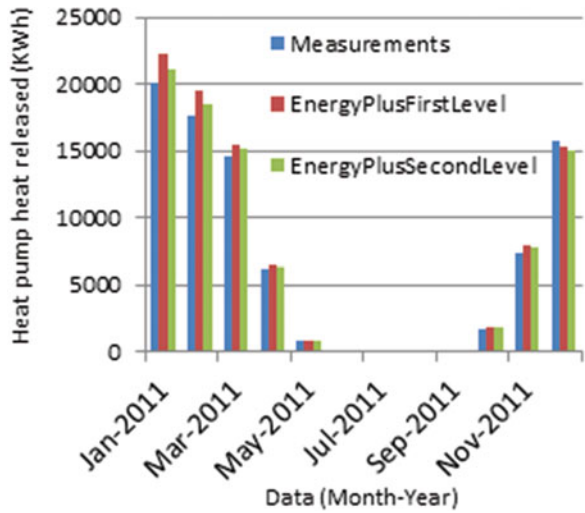


Fig. 34.4 Monthly heat pump electricity usage

Fig. 34.5 Monthly heat pump heat released



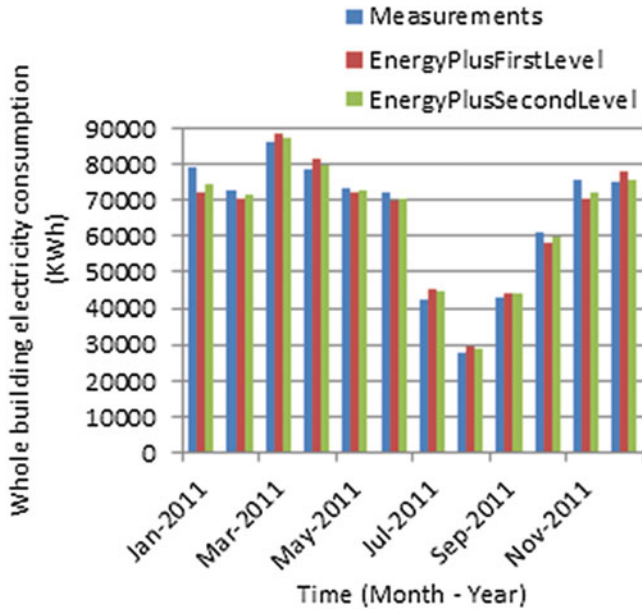


Fig. 34.6 Monthly whole-building electricity usage

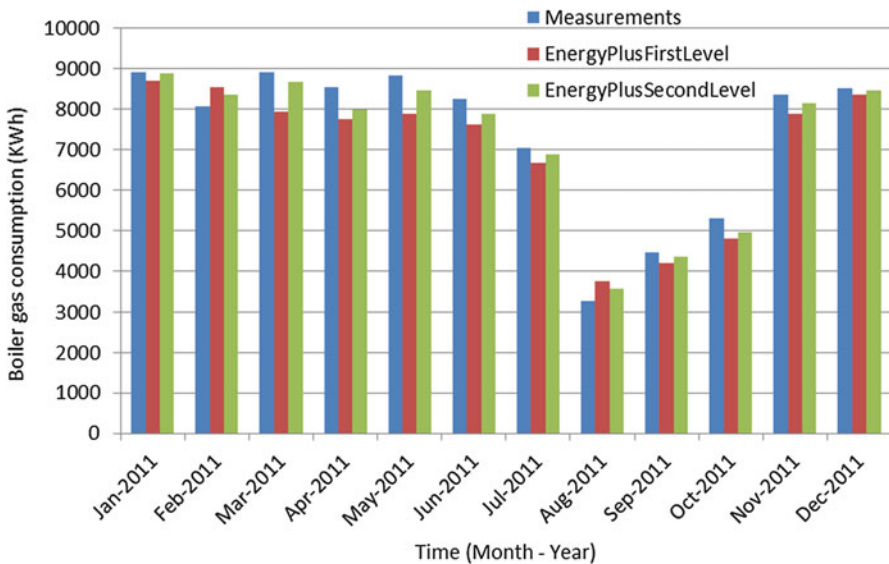


Fig. 34.7 Monthly boiler gas consumption

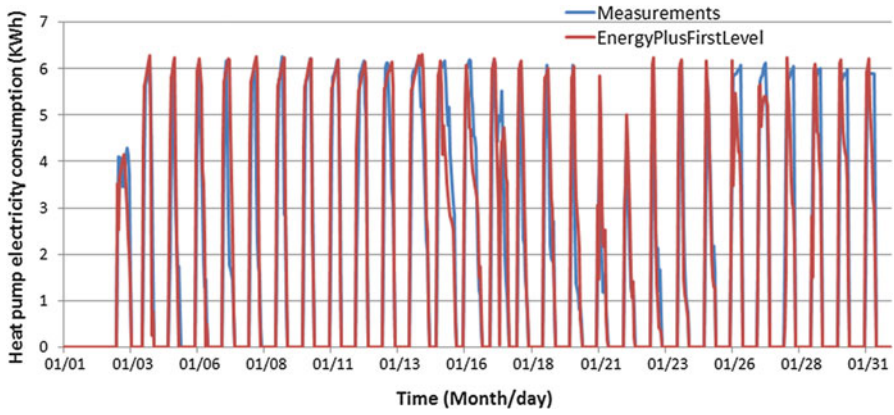


Fig. 34.8 Hourly heat pump electricity consumption

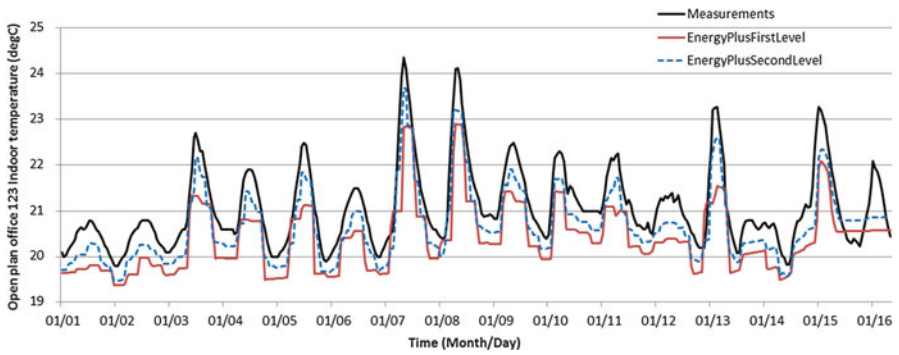


Fig. 34.9 Hourly open office first floor 1.23 indoor temperature comparison – over 2 weeks of data

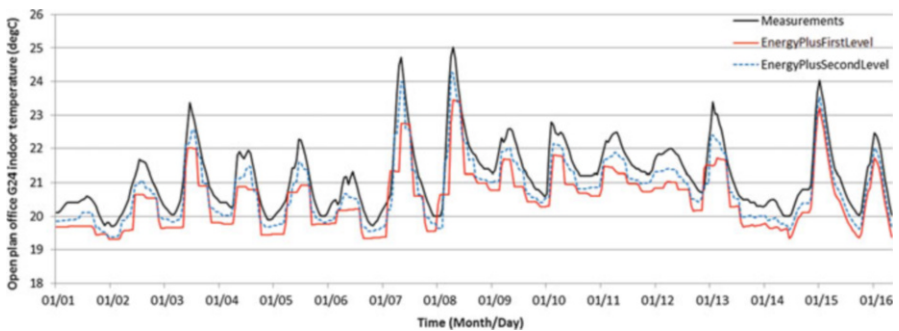


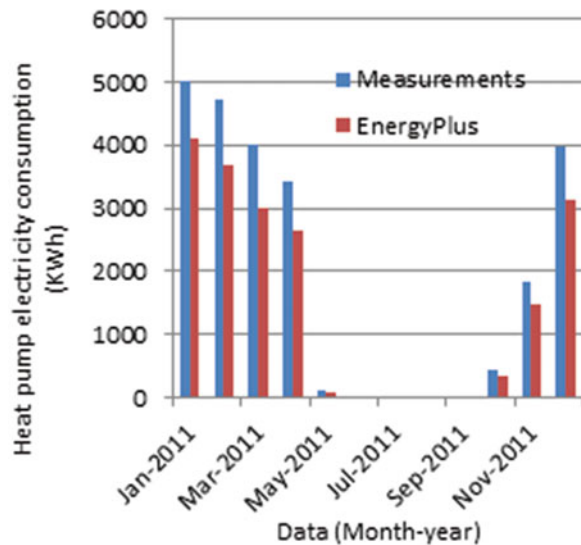
Fig. 34.10 Hourly open office ground floor G24 indoor temperature comparison – over 2 weeks of data

4.2 Energy-Saving Opportunities

Following completion of the calibration process, further reductions in energy consumption could be made by modifying the time schedule of the heat pump. The floor material structure is a concrete base and has a thickness of 70 cm. Therefore, each floor presents a slow thermal response. The time during which the heat pump is turned on can vary between 6 and 12 h and depends on weather conditions. This is managed by the building management system (BMS) technician, who, on the basis of experience and the weather forecast, decides in advance how many hours it will be turned on during the following week. Consequently, the ON/OFF time schedule of the heat pump (which supplies 80 % of the building's heat) is not regulated efficiently because it is not based on real weather condition and the thermal behaviour of the building. Its electricity consumption is higher compared to what is required to provide optimal thermal conditions throughout the building.

Alternatively, the present research analysis used EnergyPlus to turn the heat pump on and off based on the real thermal behaviour of the building and weather conditions given by the weather data file. Results showed that the time required to keep the heat pump on varied from 4 to 8 h at night in order to maintain satisfactory comfort conditions inside the building. Consequently, less time is required compared to that managed by the technician on the BEMS (from 6 to 12 h). Figure 34.11 presents the heat pump's measured and EnergyPlus model output monthly electricity consumption. It was verified that energy savings varied between 20 and 27 % on a monthly basis. Figure 34.12 shows a comparison between measurements and model outputs related to the heat pump's heat released, where from 5 to 10 % less heat is released compared to the measured values.

Fig. 34.11 Monthly heat pump electricity saved



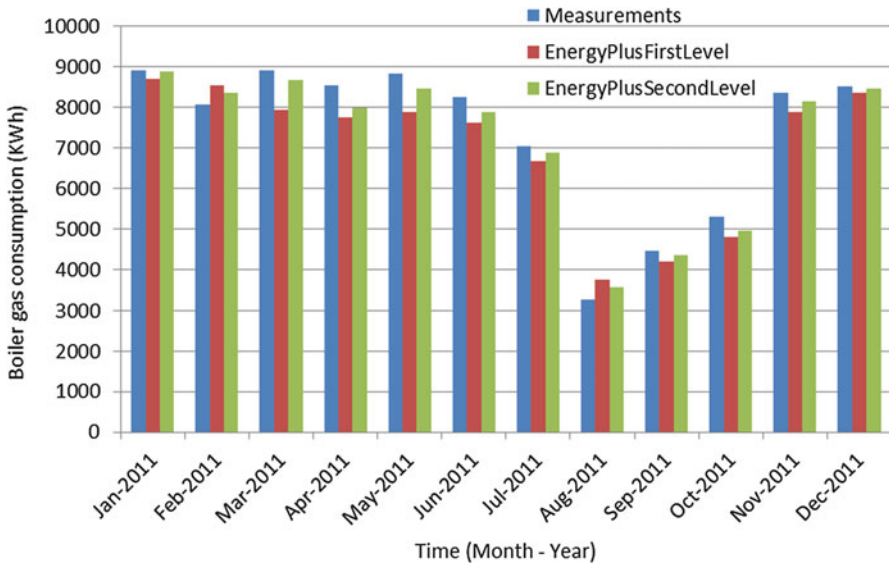


Fig. 34.12 Monthly heat pump heat saved

5 Conclusions and Future Works

This chapter presented a methodology for calibrating the hourly electricity consumption of a water-to-water heat pump. After the second level of the calibration process, the ASHRAE Guideline 14-2002 [10] is almost satisfied except for just a few cases. The second part of this research presented the required actions to improve electricity consumption related to the water-to-water heat pump. The savings from heat pump electricity consumption varied between 20 and 27 % on a monthly basis. Future research and the development of building energy modelling tools will need to focus on improving software capabilities to accept inputs based on accurate/realistic schedules for occupancy, electrical lighting use and equipment use. These inputs are highly variable in actual building use.

There is also lack of sufficient research in developing methods capable of supporting a risk analysis of investment decisions in energy upgrades of buildings, and this could represent an area of future improvement.

References

1. Perez-Lombard L, Ortiz J, Pout C (2008) A review on buildings energy consumption information. *Energy Build* 40:394–398
2. Directive 2010/31/EU of the European Parliament and of the Council. On the energy performance of buildings. Articles 14–16, 19 May 2010

3. Raftery P, Keane M, Costa A (2011) Calibrating whole building energy models: detailed case study using hourly measured data. *Energy Build* 43:3666–3679
4. Bertagnolio S (2012) Evidence based model calibration for efficient building energy services. Ph.D. Thesis, University of Liège
5. Menezes AC, Cripps A, Bouchlaghem D, Buswell R (2012) Predicted vs. actual energy performance of non-domestic buildings: using post-occupancy evaluation data to reduce the performance gap. *Appl Energy* 97:355–364
6. Liu G, Liu M (2012) A rapid calibration procedure and case study for simplified simulation models of commonly used HVAC systems. *Build Environ* 46:409–420
7. CarbonBuzz-website. <http://www.carbonbuzz.org>
8. Hamilton I, Steadman P, Bruhns H (2011) CarbonBuzz—energy data audit, UCL Energy Institute, July 2011
9. EnergyPlus Version 8.2 (2014) U.S. Department of Energy, Energy Efficiency and Renewable Energy, Office of Building Technologies. <http://www.energyplus.gov>
10. ASHRAE guideline 14 (2002) Measurement of energy and demand savings. American Society of Heating, Refrigerating, and Air-Conditioning Engineers, Atlanta, GA
11. Mustafaraj G, Marini D, Costa A, Keane M (2014) Model calibration for building energy efficiency simulation. *Appl Energy* 130:72–85
12. Azar E, Menassa C (2012) A comprehensive analysis of the impact of occupancy parameters in energy simulation of office buildings. *Energy Build* 55:841–853
13. Morris M (1991) Factorial sampling plans for preliminary computational experiments. *Technometrics* 33:161–174
14. De Wit S, Augenbroe G (2002) Analysis of uncertainty in building design evaluations and its implications. *Energy Build* 34:951–958
15. Heiselberg P, Brohus PH (2007) Application of sensitivity analysis in design of sustainable buildings. Proceedings of the international conference on sustainable development in building and environment, Chongqing, China
16. DesignBuilder. www.designbuildersoftware.com
17. CIBSE Guide (2006) A environmental design. The Chartered Institution of Building Services Engineers, London
18. ASHRAE Fundamentals Handbook (2005) Atlanta: American Society of Heating, Refrigerating and Air-Conditioning Engineers, Inc
19. ASHRAE Standard 62.2 (2013) Ventilation and acceptable indoor air quality in low-rise residential buildings

Chapter 35

Liquid and Gas Biofuels from the Catalytic Re-forming of Pyrolysis Bio-Oil in Supercritical Water: Effects of Operating Conditions on the Process

Javier Remón, Pedro Arcelus-Arrillaga, Jesús Arauzo, Lucía García, and Marcos Millan-Agorio

Abstract This work analyses the influence of temperature (310–450 °C), pressure (200–260 bar), catalyst/bio-oil mass ratio (0–0.25 g catalyst/g bio-oil) and reaction time (0–60 min) during the re-forming in sub- and supercritical water of a bio-oil obtained from the fast pyrolysis of pinewood. The original liquid has a 39 wt.% of water and the following elemental composition in dry basis: 54 wt.% C, 3.3 wt.% H, 41.3 wt.% O, 0.8 wt.% N and 0.6 wt.% S. The upgrading experiments were carried out in a batch microbomb reactor employing a co-precipitated Ni–Co/Al–Mg catalyst. Statistical analysis of the re-forming results indicates that the operating conditions and the water regime (sub-/supercritical) have a significant influence on the process. Specifically, the yields to upgraded bio-oil (liquid), gas and solid vary in ranges of 5–90 %, 7–91 % and 3–31 % respectively. The gas phase, having a medium-high lower heating value (2–17 MJ/STP m³), is made up of a mixture of H₂ (9–31 vol.%), CO₂ (41–84 vol.%), CO (1–22 vol.%) and CH₄ (1–45 vol.%). Depending on the operating conditions, the amount of C, H and O (wt.%) in the upgraded bio-oil varies in ranges of 48–74, 4–9 and 13–48 respectively. This represents an increase of up to 42 and 152 % in the proportions of C and H respectively, as well as a decrease of up to 69 % in the proportion of O. The higher heating value (HHV) of the treated bio-oil varies from 20 to 32 MJ/kg, which

J. Remón (✉)

Thermochemical Processes Group (GPT), Aragón Institute for Engineering Research (I3A), Universidad Zaragoza, Mariano Esquillor s/n, E-50018, Zaragoza, Spain

Department of Chemical Engineering, Imperial College London, London SW7 2AZ, UK
e-mail: jrm@unizar.es

P. Arcelus-Arrillaga • M. Millan-Agorio

Department of Chemical Engineering, Imperial College London, London SW7 2AZ, UK

J. Arauzo • L. García

Thermochemical Processes Group (GPT), Aragón Institute for Engineering Research (I3A), Universidad Zaragoza, Mariano Esquillor s/n, E-50018, Zaragoza, Spain

corresponds to an increase of up to 68 % with respect to the HHV of the original bio-oil.

Keywords Bio-oil • Re-forming • Supercritical water • Biofuels

1 Introduction

Dwindling resources and exponential growth in the demand for fossil fuels have motivated researchers to explore alternative energy supplies and technologies to produce both fuels and chemicals [1, 2]. In this context, biomass waste-processing technologies are attracting increasing attention, mainly because biomass is the only renewable source of carbon that can be converted into solid, liquid and gaseous products through different conversion routes [3]. Fast pyrolysis of biomass is one of the thermochemical processes most preferred for the valorisation of biomass. It makes it possible to transform the biomass into a liquid, combustible, easily stored and transported product called bio-oil (typically 50–75 wt.%) with a much higher volume energy density. Bio-oils obtained from the pyrolysis of biomass are dark to brown organic liquids containing the degradation products of cellulose, hemicellulose and lignin. Carbon (C), hydrogen (H) and oxygen (O) are their main constituents, although, depending on the biomass source, small proportions of nitrogen (N) and sulphur (S) are also possible [4]. The chemical composition of these liquids depends on the biomass source as well as the process conditions where the pyrolysis takes place [5]. They normally consist of a complex mixture of many different organic compounds such as aldehydes, ketones, sugars, carboxylic acids and phenols [6].

Bio-oils obtained from the pyrolysis of biomass are a hopeful source of biofuels because they offer several environmental advantages over fossil fuels. They are CO₂/GHG neutral and SO_x emission-free and release more than 50 % lower NO_x than diesel oil during combustion [4, 7, 8]. However, the potential of these liquids as substitutes for petroleum fuels is limited owing to their high viscosity, high water and oxygen contents, low heating value, instability and high acidity [9]. In this sense, sub- and supercritical water as reaction medium is proposed as an interesting process for bio-oil upgrading. Cracking, re-forming and hydrogenation reactions occur thanks to the generation of hydrogen in the same process. In addition, the H₂ solubility limitation can be removed as H₂ and the bio-oil are brought into a single phase with the employment of supercritical water [10]. The properties of water (sub-/supercritical) enable the process to be customised towards the production of liquids or gases depending on the needs of the market, and therefore this technology represents a very promising alternative for bio-oil upgrading. In addition, the hydrogen generated can also be used for the hydrogenation of bio-oil in the same process and the oxygen content of the bio-oil is reduced, which helps to obtain an upgraded bio-oil with better physicochemical properties to be used as a fuel, either alone or mixed with other petroleum-derived fuels.

Given this background, this work studies the valorisation of a fast-pyrolysis bio-oil in sub-/supercritical water to produce gas and liquid biofuels, analysing the influence of the operating conditions on the process.

2 Experimental Procedure

2.1 Bio-Oil Properties

The bio-oil used in this work was supplied by Biomass Technology Group (BTG) in the Netherlands. It was obtained during the pyrolysis of pine sawdust using a rotating cone reactor. The most important properties of the crude bio-oil are summarised in Table 35.1.

2.2 Experimental Re-forming Study

The experiments were planned according to a full factorial design (DOE) with a statistical analysis of the results in order to analyse the effect of temperature (310–450 °C), pressure (200–260 bar), catalyst/bio-oil mass ratio (0–0.25 g catalyst/g bio-oil), reaction time (0–60 min) and all interactions between these operating variables on the process. They were conducted in a stainless steel microbomb batch reactor using a co-precipitated Ni–Co/Al–Mg catalyst. The reaction section, having a volume of 12 mL, is comprised of a 1.27 cm. Swagelok bored-through tee with two ends plugged and connected by means of a 0.64 cm. tube with a wall thickness of 0.18 cm. to a high pressure–high temperature needle valve. A detailed diagram of the reactor is shown in Fig. 35.1. The design and operation of this reactor have been extensively discussed elsewhere [11]. The detailed preparation procedure of the catalyst and its characterisation results can be found in previous communications [12–14].

Table 35.1 Bio-oil characterisation results

Composition		Chemical composition (area %)	
Organics (wt.%)	60.95	Ketones	18.22 ± 0.38
Ashes (wt.%)	<0.001	Carboxylic acids	45.52 ± 2.42
H ₂ O (wt.%)	39.05 ± 0.39	Furans	3.71 ± 0.32
<i>Ultimate analysis (raw basis)</i>		Alcohols	2.22 ± 0.35
C (wt.%)	32.86 ± 0.40	Aldehydes	1.41 ± 0.32
H (wt.%)	6.73 ± 0.16	Phenols	21.35 ± 1.19
O (wt.%) ^a	58.91 ± 0.48	Benzenes	3.86 ± 1.93
N (wt.%)	0.51 ± 0.03	Sugars	1.99 ± 1.14
S (wt.%)	0.99 ± 0.11	Nitrogen compounds	1.72 ± 0.51

Results are presented as mean ± standard deviation

^aDetermined by difference

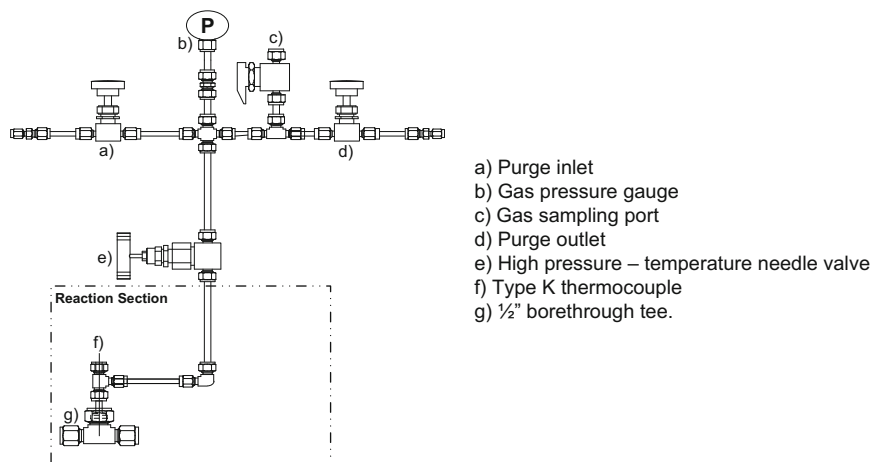


Fig. 35.1 Schematic of batch microbomb reactor

3 Results and Discussion

3.1 Global Results: Yields to Gas, Liquid and Solid Products

The yields to gas, liquid and solid products vary as follows: 7–91 %, 5–90 % and 3–31 % respectively. The statistical analysis of the results indicates that the temperature and catalyst/bio-oil ratio are the operating variables with the greatest effect on the yields to gas, liquid and solid. The reaction time and total pressure of the system have a significant, although weaker, effect on global yields. In addition, significant interactions between variables take place, indicating that the effect of the operating variables on the global yields depends on the other operating conditions.

From the statistical analysis of the results, it was found that an increase in the temperature increased the yields to gas and solid and decreased the yield to liquid. Cracking and re-forming reactions are enhanced with temperature, which favours gas formation from bio-oil, thereby increasing the gas yield and decreasing the liquid yield. An increase in the catalyst/bio-oil ratio results in an increase in the yield to gas and leads to a decrease in the yields to liquid and solid. The presence of catalyst in the process enhances gas formation, increasing the reaction rates of the re-forming and water gas shift reactions. Furthermore, it might inhibit char formation or favour its gasification, which also contributes to a decrease in the yield to solid. An increase in the reaction time results in an increase in the yields to gas and a drop in the yields to liquid. It is believed that the previous is mainly due to the progressive formation of gas from bio-oil with time. Interestingly, the effect of the reaction time on the yield to solid is not significant. This indicates that a large amount of solid (char) might originate from the thermal decomposition of non-volatile species during the heating up of the reactor. This stage occurs

2–3 min prior to the onset of the reaction when immersing the reactor in a sand bath. The effect of the pressure on the global results is weak and strongly influenced by the other operating conditions.

Figure 35.2 displays the effect of the operating variables and most important interactions detected with the ANOVA analysis for the global results. Figure 35.2a, d, g shows the effects of time at 380 °C and 230 bar, in the absence of catalyst and employing a catalyst/bio-oil ratio of 0.25 g/g. The effect of temperature and pressure on global yields is shown and discussed for a reaction time of 30 min. Specifically, Fig. 35.2b, e, h illustrates the effects of temperature and pressure on global yields in the absence of a catalyst for a reaction time of 30 min. These effects are shown for a catalyst/bio-oil ratio of 0.25 g/g in Fig. 35.2c, f, i.

Statistical analysis indicates that an increase in the reaction time increases the yield to gas and drops the yield to liquid, regardless of the other operating conditions. In addition, the re-forming time does not have a significant effect on the solid yield. As an example, the effect of time is shown at the centre of variation in

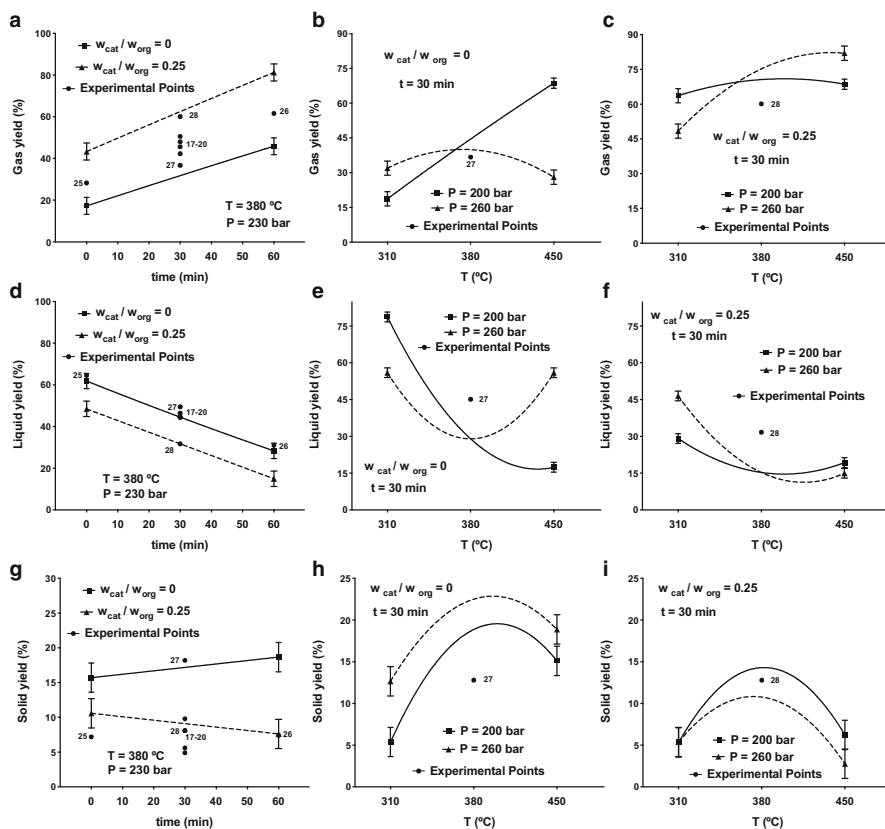


Fig. 35.2 Interaction plots for yields to gas (a–c), liquid (d–f) and solid (g–i). Bars: LSD intervals with 95% confidence

temperature and pressure (380 °C and 230 bar). The effect of temperature on global yields depends on both the pressure and catalyst/bio-oil ratio. In the absence of a catalyst, an increase in temperature from 310 to 450 °C at 200 bar increases the gas yield and cause a drop in the liquid yield. Between 310 and 380 °C the yield to solid increases with temperature, reaching its maximum. A further increase in temperature up to 450 °C slightly decreases the yield to solid. The temperature has a kinetic effect on cracking and re-forming reactions, thereby increasing the formation of gas from bio-oil. In addition, under this pressure, the increase in temperature changes the state of water from subcritical water to vapour at 366 °C. Steam can facilitate the gasification of char, which explains the experimentally observed reduction in the yield to solid. Conversely, at 260 bar an increase in temperature to between 310 and 380 °C slightly increases the yield to gas and causes a dramatic drop in the liquid yield. A further rise in the temperature up to 450 °C leads to a slight decrease in the gas yield and a sharp increase in the yield to liquid. At this pressure, this increase in temperature causes the water to change from a subcritical to supercritical state. Under subcritical conditions an increase in temperature increases gas production from bio-oil. Once supercritical conditions have been reached, cracking and re-forming reactions might be less favoured, thereby increasing and decreasing the yields to gas and liquid respectively. The yield to solid follows the same trend as described for 200 bar, indicating that the presence of supercritical water can partially reduce solid formation or favour its removal.

The effect of pressure also depends on temperature. While an increase in pressure from 200 to 260 bar increases gas formation and decreases the yield to liquid between 310 and 380 °C, it has the opposite effect from 380 to 450 °C. Between 310 and 367 °C water remains under subcritical conditions between 200 and 260 bar, and the pressure has a positive catalytic effect on the process, increasing the reaction rates of cracking and re-forming reactions. Conversely, between 367 and 450 °C the same increment in pressure changes the state of water from steam, where steam re-forming and cracking reactions are favoured, to supercritical water, reducing gas formation and increasing the yield to liquid. The effect of pressure on solid yield is relatively low. In general, an increase in pressure slightly increases the yield to solid, especially between 310 and 380 °C. The physicochemical properties of water changes at temperatures higher than 300 °C, and the solubility of bio-oil in water can be enhanced by pressure, decreasing char formation.

The effect of the presence of a catalyst on global yields can be ascertained from a comparison of Fig. 35.2b and c, e and f, and h and i. It is observed that an increase in the catalyst/bio-oil ratio from 0 to 0.25 g/g increases gas formation, reducing the yield to liquid and solid. Increasing the amount of catalyst in the process enhances re-forming and cracking reactions from bio-oil. In addition, it decreases the solid yield, inhibiting its formation or facilitating its elimination. These figures reveal that in the presence of a catalyst, an increase in the temperature from 310 to 450 °C leads to an increase in the gas yield and to a drop in the liquid yield. However, the effect of the presence of a catalyst depends on temperature and pressure. At 200 bar, an increase in the catalyst/bio-oil ratio produces a higher increase and a lower

decrease in yields to gas and liquid respectively at temperatures lower than 380 than at higher temperatures. Temperature has a positive kinetic effect on gas production; therefore, a positive catalytic effect of a catalyst could be masked as the temperature increases. At high temperatures, where gas production is favoured owing to the presence of steam, the effect of the catalyst becomes insignificant. Conversely, as the pressure increases, the catalyst exerts a greater influence on yields to gas and liquid. A higher increase and decrease in yields to gas and solid respectively take place, notably at temperatures higher than 380 °C. Under these conditions, water is in a supercritical state and gas formation is not favoured. Therefore, the effect of the catalyst is more evident. Solid formation also decreases with an increasing catalyst/bio-oil ratio. This reduction depends on pressure and temperature. At 260 bar, a decrease in solid formation takes place for the whole temperature range, while at 200 bar it takes place at temperatures higher than 380 °C. At low pressure, steam is needed for the gasification of coke, while the sub- and supercritical water conditions achieved with increasing pressure enhances the positive effect of the catalyst.

3.2 Properties of Gas Phase

The gas phase consists of a mixture of H₂ (9–31 vol.%), CO₂ (41–84 vol.), CO (1–22 vol.%) and CH₄ (1–45 vol.%) with a LHV varying from 2 to 18 MJ/m³ STP. Statistical analysis reveals that the temperature and catalyst/bio-oil ratio are the operating variables with the greatest influence on the volumetric composition and the LHV of the gas. One of the main objectives of supercritical water re-forming of bio-oil is to produce a gas with a high H₂ content. Therefore, only the effect of the operating conditions on the concentration of this gas is fully presented and discussed in this work. The effect of reaction time on the relative amount of H₂ in the gas depends on the temperature, pressure and catalyst/bio-oil ratio owing to the existence of significant interactions between these operating variables. Figure 35.3 displays the most important effects and interactions of the operating variables on the proportion of H₂ in the gas. The effect of reaction time is shown in Fig. 35.3a–d. Specifically, Fig. 35.3a, b displays the effect of time as a function of the catalyst/bio-oil ratio at 200 bar at 310 and 450 °C respectively. Figure 35.3c, d illustrates these effects for a pressure of 260 bar.

The evolution over time of the proportion of H₂ in the gas depends on the pressure, temperature and catalyst/bio-oil ratio. At 200 bar the proportion of H₂ shows different trends depending on the temperature and the catalyst/bio-oil ratio. At 310 °C, the proportion of H₂ increases with the progress of the reaction, and an increase in the catalyst/bio-oil ratio increases the concentration of H₂ in the gas. Conversely, at 450 °C, a steady evolution of the proportion of H₂ takes place regardless of the catalyst/bio-oil ratio. At low temperatures high reaction times are needed to increase gas production. In addition, at these temperatures hydrogenation reactions are not kinetically favoured, which leads to a progressive increase in the proportion of H₂ in the gas with time, because H₂ consumption could be

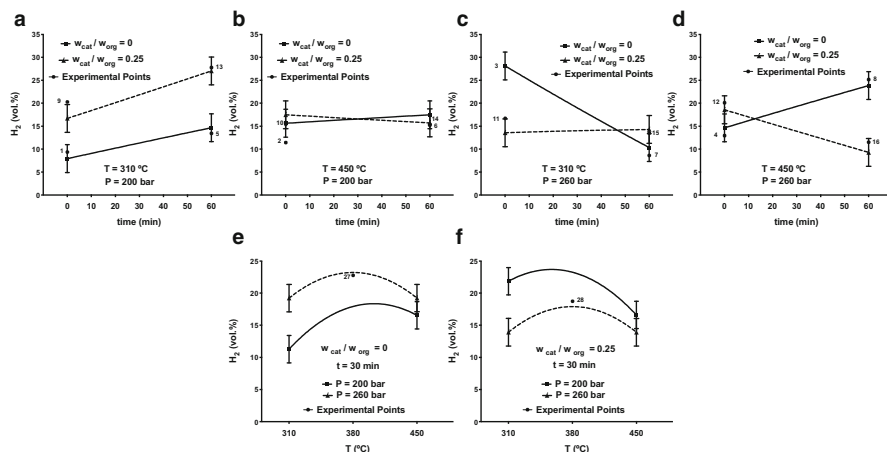


Fig. 35.3 Interaction plots for proportion of H₂ in gas. Bars: LSD intervals with 95 % confidence

lower. Conversely, an increase in the temperature up to 450 °C kinetically enhances cracking, re-forming and hydrogenation reactions. Therefore, hydrogen production and elimination could be compensated, which leads to a steady concentration of H₂ with time. These trends are in accordance with the evolution over time of the concentration of H in the liquid product, which will be discussed further in the analysis of the liquid properties.

At 260 bar a different evolution of the proportion of H₂ with time takes place. This variation also depends on temperature and the catalyst/bio-oil ratio. On the one hand, at 310 °C, the proportion of H₂ in the gas decreases with time in the absence of a catalyst. An increase in the catalyst/bio-oil ratio decreases the proportion of H₂ in the gas, and a steady evolution with time takes place. In the absence of a catalyst, an increase in pressure from 200 to 260 bar promotes gas production, which leads to an initial increase in the proportion of H₂ in the gas. However, as the reaction proceeds, hydrogen could be progressively consumed in the same process. This produces a decrease in the proportion of H₂ in the gas together with an increase in the concentration of H in the liquid phase. An increase in the catalyst/bio-oil ratio enhances bio-oil hydrogenation reactions, thereby decreasing the proportion of H₂ in the gas. This increase in pressure leads to an upsurge in the proportion of H in the liquid, providing evidence for this hypothesis. Under this pressure, a further increase in the temperature up to 450 °C changes the state of water from subcritical to supercritical, which results in a different evolution over time in the proportion of H₂ in the gas. In the absence of a catalyst, an increase in the proportion of H₂ over time takes place. However, an increment in the catalyst/bio-oil ratio up to 0.25 g/g results in a decrease in the proportion of H₂ over time. This increase in temperature increases the proportion of H in the liquid phase, but it develops a steady evolution with time, which can explain the increase in the proportion of H₂ over time in the absence of a catalyst. In addition, a decrease in the proportion of CO occurs, together with an increase in the concentration of CO₂, which suggests a progressive

shift of the WGS reaction with time. CH_4 formation is favoured under these operating conditions, which could be increased in the presence of a catalyst, explaining the decrease observed in the concentration of H_2 .

Figure 35.3e, f displays the effect of temperature, pressure and the catalyst/bio-oil ratio for a reaction time of 30 min. The effect of temperature depends on pressure and the catalyst/bio-oil ratio. In the absence of a catalyst, an increase in the temperature from 310 to 450 °C results in a high proportion of H_2 at 200 bar, while it has a negligible effect at 260 bar. At low pressures, this increase in temperature changes the state of water from subcritical to steam, which favours H_2 production through re-forming and cracking reactions. An increase in the pressure favours the extension of re-forming and cracking reactions, as the partial pressure of the organics inside the reactor increases, increasing the proportion of H_2 in the gas. In addition, at 260 bar, temperature does not influence the proportion of H_2 in the gas. At this pressure, water changes from subcritical to supercritical. This increase in temperature increases cracking and re-forming reactions, but H_2 consumption also increases in supercritical water owing to the higher extension of hydrogenation reactions. An increase in the catalyst/bio-oil ratio up to 0.25 g/g increases the proportion of H_2 at 200 bar between 310 and 380 °C. Conversely, at 260 bar, this increase reduces the proportion of H_2 in the gas for the whole range of temperatures. This indicates that the concentration of H_2 in the gas decreases when water is in a sub- or supercritical state, probably owing to the positive effect the catalyst has on the hydrogenation reaction in the liquid phase.

3.3 Properties of Liquid Phase

The concentrations of C, H and O in the upgraded bio-oil vary as follows: 48–77 wt.%, 4–8 wt.% and 13–48 wt.%. The higher heating value (HHV) of the liquid ranges from 20 to 32 MJ/kg. These results represent a considerable increase in the proportions of C and H and a decrease in the concentration of O (53.91 wt.% C, 3.32 wt.% H and 41.31 wt.% O), together with a substantial increase in the HHV (18.51 MJ/kg) with respect to the original bio-oil. Statistical analysis reveals that the temperature and the catalyst/bio-oil ratio are the operating variables exerting the highest influence on the elemental composition and HHV of the upgraded bio-oils. In general, an increase in the temperature or the catalyst/bio-oil ratio increases the concentrations of C and H and decreases the proportion of O in the liquid. The effects of reaction time and pressure are significant, although they have a lesser influence. In addition, significant interactions between the operating variables take place. The effects of the operating conditions and the most important interactions are displayed in Fig. 35.4. Specifically, Fig. 35.4a, d, g shows the effect of reaction time for catalyst/bio-oil ratios of 0 and 0.25 g/g when a pressure of 200 bar and a temperature of 310 °C are used. Figure 35.4b, e, h displays these effects at 450 °C. Figure 35.4c, f, i shows the effect of temperature and pressure for a catalyst/bio-oil ratio of 0.125 g/g and a reaction time of 30 min.

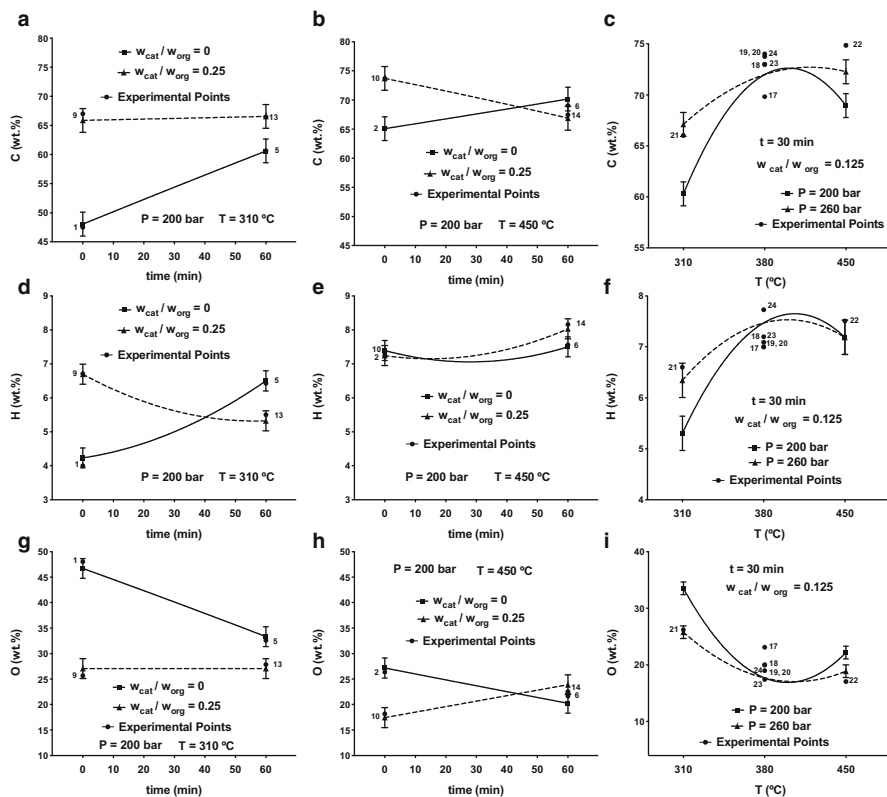


Fig. 35.4 Interaction plots for elemental composition of liquid phase. Bars: LSD intervals with 95% confidence

The effect of reaction time on the elemental composition of the upgraded bio-oil is significant only at pressures under 230 bar. At these pressures the composition of the liquid varies with time. They also display different evolutions depending on the temperature and catalyst/bio-oil ratio. As an example, these trends are represented in Fig. 35.4 for a pressure of 200 bar. When pressures higher than 230 bar are used, a steady evolution for the composition of the liquid takes place. Different trends are found depending on the catalyst/bio-oil ratio and the temperature at 200 bar. In the absence of a catalyst, the proportions of C and H in the liquid increase with time, while the proportion of O decreases. These variations depend on temperature. An increase in the temperature increases the proportions of C and H and decreases the concentration of O in the liquid. In addition, the higher the temperature, the lower the variations over time. In general, an increase in the catalyst/bio-oil ratio causes an increase in the proportions of C and H and a decrease in the concentration of O. When a catalyst/bio-oil ratio of 0.25 g/g is used, the variations in the elemental composition of the liquid with time show two different trends depending on the temperature. At low temperatures (310 °C), the proportion of H decreases with

time, while the concentrations of C and O remain steady. Conversely, at high temperature (450 °C), the proportion of H does not vary, but the concentration of C and O in the liquid drops and increases respectively with time.

The specific effects of temperature, pressure and the catalyst/bio-oil ratio on the elemental composition are discussed for a reaction time of 30 min. In general, an increase in the catalyst/bio-oil ratio has similar effects for the whole range of temperatures and pressures considered. An increase in this ratio increases the proportions of C and H and reduces the concentration of O in the liquid. The presence of a catalyst potentiates cracking and re-forming reactions of light oxygenates, which accounts for this experimental observation. Conversely, important interactions were found for temperature and pressure. Figure 35.4c, f, i shows the effects of the re-forming temperature for pressures of 200 and 260 bar. An increase in the reaction temperature raises the concentrations of C and H and diminishes the proportion of O in the liquid. Cracking and re-forming reactions of light oxygenates present in the bio-oil increase with increasing temperature, which accounts for this variation. An increase in pressure from 200 to 260 bar increases the proportions of C and H and reduces the concentration of O in the liquid.

4 Conclusions

Re-forming of bio-oil in sub- and supercritical water is a promising process for bio-oil upgrading. This process allows the production of gas and an upgraded bio-oil with better physicochemical properties than the original liquid. The gas phase, having a medium-high LHV (2–17 MJ/STP m³), is composed of a mixture of H₂ (9–31 vol.%), CO₂ (41–84 vol.%), CO (1–22 vol.%) and CH₄ (1–45 vol.%). The concentrations of C, H and O (wt.%) in the upgraded bio-oil vary in ranges of 48–74, 4–9 and 13–48 respectively. This represents an increase of up to 42 % and 152 % in the proportion of C and H respectively, as well as a decrease of up to 69 % in the proportion of O with respect to the original bio-oil. The HHV of the treated bio-oil varies from 20 to 32 MJ/kg, which corresponds to an increase of about 68 % with respect to the HHV of the original bio-oil.

Acknowledgement The authors wish to express their gratitude to the Spanish MINECO (projects ENE2010-18985 and ENE2013-41523-R) for providing financial support and the FPI (BES-2011-044856) and mobility (EEBB-I-14-08688) grants awarded to Javier Remón Núñez.

References

1. Bulushev DA, Ross JRH (2011) Catalysis for conversion of biomass to fuels via pyrolysis and gasification: a review. *Catal Today* 171:1–13
2. Escobar JC, Lora ES, Venturini OJ, Yáñez EE, Castillo EF, Almazan O (2009) Biofuels: environment, technology and food security. *Renew Sustain Energy Rev* 13:1275–1287

3. Ayhan D (2008) Biofuels sources, biofuel policy, biofuel economy and global biofuel projections. *Energy Convers Manag* 49:2106–2116
4. Ayalur Chattanathan S, Adhikari S, Abdoulmoumine N (2012) A review on current status of hydrogen production from bio-oil. *Renew Sustain Energy Rev* 16:2366–2372
5. Trane R, Dahl S, Skjøth-Rasmussen MS, Jensen AD (2012) Catalytic steam reforming of bio-oil. *Int J Hydrog Energy* 37:6447–6472
6. Sipilä K, Kuoppala E, Fagernas L, Oasmaa A (1998) Characterization of biomass-based flash pyrolysis oils. *Biomass Bioenergy* 14:103–113
7. Jacobson K, Maheria KC, Kumar DA (2013) Bio-oil valorization: a review. *Renew Sustain Energy Rev* 23:91–106
8. Xiu S, Shahbazi A (2012) Bio-oil production and upgrading research: a review. *Renew Sustain Energy Rev* 16:4406–4414
9. Lu Q, Li W-Z, Zhu X-F (2009) Overview of fuel properties of biomass fast pyrolysis oils. *Energy Convers Manag* 50:1376–1383
10. Fisk CA, Morgan T, Ji Y, Crocker M, Crofcheck C, Lewis SA (2009) Bio-oil upgrading over platinum catalysts using in situ generated hydrogen. *Appl Catal Gen* 358:150–156
11. Pinilla JL, Arcelus-Arrillaga P, Puro H, Millan M (2013) Selective catalytic steam cracking of anthracene using mesoporous Al₂O₃ supported Ni-based catalysts doped with Na, Ca or K. *Appl Catal Gen* 459:17–25
12. Remón J, Broust F, Valette J, Chhiti Y, Alava I, Fernandez-Akarregi AR et al (2014) Production of a hydrogen-rich gas from fast pyrolysis bio-oils: comparison between homogeneous and catalytic steam reforming routes. *Int J Hydrog Energy* 39:171–182
13. Remón J, Broust F, Volle G, García L, Arauzo J (2015) Hydrogen production from pine and poplar bio-oils by catalytic steam reforming. Influence of the bio-oil composition on the process. *Int J Hydrog Energy* 40:5593–5608
14. Remón J, Medrano JA, Bimbela F, García L, Arauzo J (2013) Ni/Al–Mg–O solids modified with Co or Cu for the catalytic steam reforming of bio-oil. *Appl Catal Environ* 132–133:433–444

Chapter 36

Pyrolysis Bio-Oil Upgrading to Renewable Liquid Fuels by Catalytic Hydrocracking: Effect of Operating Conditions on the Process

Javier Remón, Pedro Arcelus-Arrillaga, Jesús Arauzo, Lucía García, and Marcos Millan-Agorio

Abstract This work analyses the influence of operating conditions during the catalytic hydrocracking of a bio-oil obtained from the fast pyrolysis of pinewood. The original liquid has a 39 wt.% of water and the following elemental composition in dry basis: 54 wt.% C, 3.3 wt.% H, 41.3 wt.% O, 0.8 wt.% N and 0.6 wt.% S.

Experiments were carried out in a batch microbomb reactor employing a co-precipitated Ni–Co/Al–Mg catalyst. They were planned according to a full factorial design of experiments with a statistical analysis of the results in order to analyse the effects of temperature (350–450 °C), hydrogen pressure (70–150 bar), catalyst/bio-oil mass ratio (0–0.25 g catalyst/g organics), reaction time (0–60 min) and all interactions between these operating variables on the process. Statistical analysis of the results indicates that the operating conditions have a statistically significant effect on the results. Specifically, the yields to upgraded bio-oil (liquid), gas and solid vary in ranges of 3–97 %, 0–86 % and 3–41 % respectively. Depending on the operating conditions, the amount of C, H and O (wt.%) in the upgraded bio-oil varies in ranges of 50–82, 3.5–8.3 and 9–44 respectively. This represents an increase of up to 52 and 150 % in the proportion of C and H respectively, as well as a decrease of up to 78 % in the proportion of O. The higher heating value of the treated bio-oil varies from 19 to 37 MJ/kg, which is considerably higher than that of the original bio-oil.

Keywords Bio-oil • Hydrocracking • Upgrading • Biofuels

J. Remón (✉)

Thermochemical Processes Group (GPT), Aragón Institute for Engineering Research (I3A), Universidad Zaragoza, Mariano Esquillor s/n, E-50018, Zaragoza, Spain

Department of Chemical Engineering, Imperial College London, London SW7 2AZ, UK
e-mail: jrm@unizar.es

P. Arcelus-Arrillaga • M. Millan-Agorio

Department of Chemical Engineering, Imperial College London, London SW7 2AZ, UK

J. Arauzo • L. García

Thermochemical Processes Group (GPT), Aragón Institute for Engineering Research (I3A), Universidad Zaragoza, Mariano Esquillor s/n, E-50018, Zaragoza, Spain

1 Introduction

The exponential growth in the demand for fossil fuels, which is forecast to double between the years 2000 and 2050 [1, 2], together with declining resources, has led researchers to search for alternative energy supplies and technologies to produce energy, fuels and chemicals from non-conventional and renewable sources. In this context, biomass waste-processing technologies are receiving increasing attention as they meet the difficult challenge of producing energy and fuels through so-called ecologically friendly processes. In addition, biomass is the only renewable source of carbon that can be transformed into solid, liquid and gaseous products through different conversion routes [3].

The thermochemical conversion of biomass is a promising route for the production of chemicals and energy. Among all possible thermochemical processes, fast pyrolysis is one of the most mature and industrially used for biomass conversion. This process allows transforming the biomass into a liquid, combustible, easily stored and transported product called bio-oil, with a typical yield of 50–75 % and having a much higher volume energy density than the original biomass. Bio-oil is a dark to brown organic liquid that consists of the degradation products of cellulose, hemicellulose and lignin [4]. It normally contains a complex mixture of many different organic compounds, such as aldehydes, ketones, sugars, carboxylic acids and phenols [5], whose specific chemical composition depend on the biomass source as well as the process conditions where the pyrolysis takes place [6]. The renewable origin of these liquids, together with their environmental advantages over fossil fuels, makes them a promising source for biofuel production. Bio-oils are CO₂/GHG neutral and SO_x emission-free and release more than 50 % less NO_x than diesel oil during combustion [4, 7, 8]. Unfortunately, the potential of these liquids as substitutes for petroleum fuels is limited owing to their high viscosity, high water and oxygen contents, low heating value, instability and high acidity [9]. This scenario makes the upgrading of bio-oil a fundamental challenge in coming up with a liquid product which can be used as a fuel. Various technologies commonly used in the oil industry, such as hydrotreating and hydrocracking, have been developed and tested for bio-oil upgrading aimed at improving the physicochemical properties of bio-oil.

In this sense, hydrocracking of bio-oil represents a very interesting process for bio-oil upgrading. Hydrogenation and cracking reactions allow the chemical properties of the bio-oil to be improved. This treatment yields a bio-oil with higher C and H contents, decreasing the proportion of O, which is beneficial for increasing the higher heating value (HHV) of the liquid [7]. As a result, hydrocracking produces an upgraded bio-oil with better physicochemical properties than the original feedstock, thereby enabling its use as a fuel, either alone or mixed with other petroleum-derived fuels.

Against this backdrop, this work studies the hydrocracking of a fast-pyrolysis bio-oil to produce an upgraded liquid product with suitable physicochemical properties to be used as fuel, analysing the influence of the operating conditions on the process.

2 Experimental Procedure

2.1 Bio-Oil Properties

The bio-oil used in this work was supplied by Biomass Technology Group (BTG) in the Netherlands. It was obtained during the pyrolysis of pine sawdust using a rotating cone reactor. The most important properties of the crude bio-oil are summarised in Table 36.1.

2.2 Experimental Study

The experiments were planned according to a full factorial design with a statistical analysis of the results in order to analyse the effects of temperature (350–450 °C), hydrogen pressure (70–150 bar), catalyst/bio-oil mass ratio (0–0.25 g catalyst/g bio-oil), reaction time (0–60 min) and all interactions between these operating variables on the process. They were conducted in a stainless-steel microbomb batch reactor using a co-precipitated Ni–Co/Al–Mg catalyst. A diagram of the reactor configuration is shown in Fig. 36.1. The reactor main body was built from a 1.27 cm. Swagelok (Solon, OH, USA) bored-through tee piece with two ends plugged. The other end was connected to a 0.64 cm. tube with a wall thickness of 0.18 cm. that passed through a heat exchanger which maintained a reflux of reactants and products into the reaction zone. The reactor was equipped with a thermocouple which recorded the temperature inside the reactor and a pressure gauge which recorded the pressure in the reactor. The design and operation of this reactor have been extensively discussed elsewhere [10].

Table 36.1 Bio-oil characterisation results

Composition		Chemical composition (area %)	
Organics (wt.%)	60.95	Ketones	18.22 ± 0.38
Ashes (wt.%)	<0.001	Carboxylic acids	45.52 ± 2.42
H ₂ O (wt.%)	39.05 ± 0.39	Furans	3.71 ± 0.32
Ultimate analysis (raw basis)		Alcohols	2.22 ± 0.35
C (wt.%)	32.86 ± 0.40	Aldehydes	1.41 ± 0.32
H (wt.%)	6.73 ± 0.16	Phenols	21.35 ± 1.19
O (wt.%) ^a	58.91 ± 0.48	Benzenes	3.86 ± 1.93
N (wt.%)	0.51 ± 0.03	Sugars	1.99 ± 1.14
S (wt.%)	0.99 ± 0.11	Nitrogen compounds	1.72 ± 0.51

Results are presented as mean ± standard deviation

^aDetermined by difference

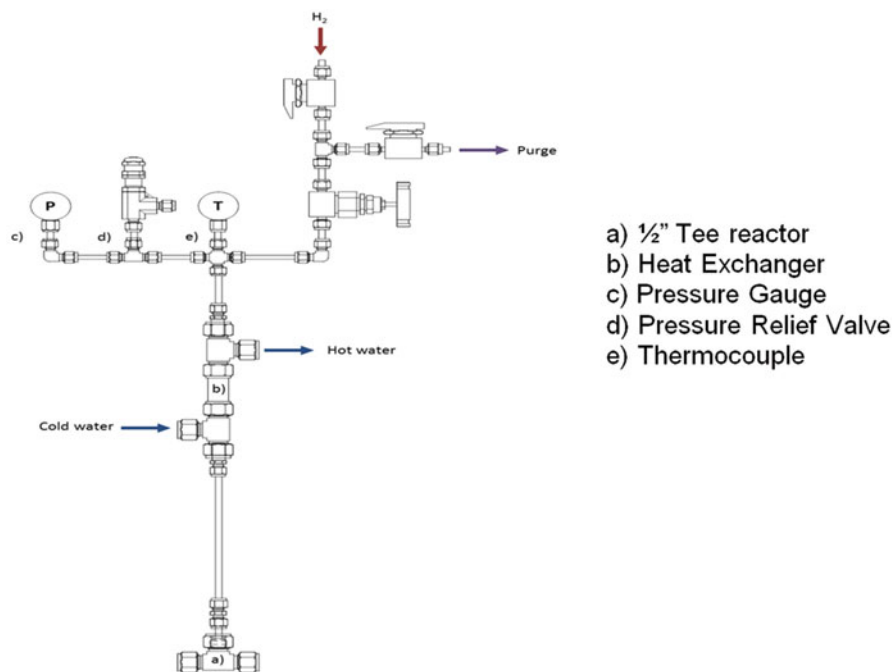


Fig. 36.1 Schematic of batch microbomb reactor

3 Results and Discussion

3.1 Global Results: Yields to Liquid, Gas and Solid Products

The yields to liquid, gas and solid products vary by 3–97 %, 0–86 % and 3–41 % respectively. Statistical analysis of the results indicates that the temperature and reaction time are the operating variables which have the greatest effect on the yield to liquid products. On the other hand, the yields to gas and solid products are highly affected by the temperature and catalyst/bio-oil ratio. The partial pressure of H_2 also exerts a significant effect on global results; however, its effect is less pronounced and mainly related to interactions with the other operating variables. In general, an increase in temperature augments the yields to gas and solid and reduces the yield to liquid. Cracking reactions are intensified with temperature, which enhances gas production from bio-oil. An increase in the catalyst/bio-oil ratio increases the yield to gas and decreases the yield to solid. The presence of a catalyst spurs gas production from bio-oil and helps to prevent the formation of char. An increase in the reaction time enlarges the yield to gas and reduces the yield to liquid because the contact time favours bio-oil cracking reactions to produce gas. Significant interactions between the response variables were found. Figure 36.2 displays

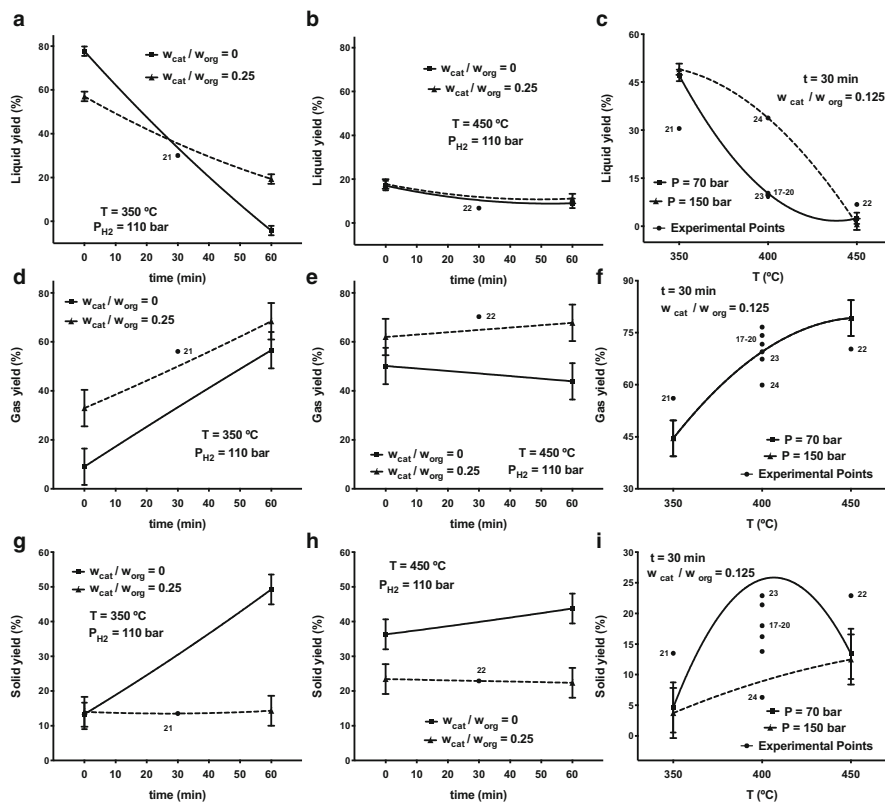


Fig. 36.2 Interaction plots for yields to liquid, gas and solid. Bars: LSD intervals with 95% confidence

the effect of the operating variables and the most important interactions between them on the yields to liquid (upgraded bio-oil), gas and solid.

The effect of the reaction time on global yields depends on the temperature and catalyst/bio-oil ratio. As an example, Fig. 36.2a, d, g shows the effect of reaction time at an intermediate hydrogen partial pressure (110 bar) for catalyst/bio-oil ratios of 0 and 0.25 g/g at 350 °C. Figure 36.2b, e, h displays this effect at a temperature of 450 °C. These figures illustrate how the effect of reaction time is more important at low than at high temperatures. At 350 °C an increase in the reaction time decreases the yield to liquid and increases gas yields. In addition, at this temperature the effect of the catalyst/bio-oil ratio is significant, and sharper variations with time are observed in the absence of a catalyst than when a catalyst/bio-oil ratio of 0.25 g/g is used. In the presence of catalyst, a higher and a lower initial yield to gas and liquid are respectively obtained. This result is the consequence of the intensification of cracking reactions in the presence of a catalyst. These trends make it possible that between 0 and 30 min, an increase in the catalyst/bio-oil ratio from 0 to 0.25 g/g decreases the liquid yield and increases the yield to

gas. Conversely, the liquid yield increases between 30 and 60 min, whereas gas production is not affected. Interestingly, an increase in the solid yield over time occurs in the absence of a catalyst. The use of a catalyst decreases solid production, and a steady evolution for the yield to solid takes place when using a catalyst/bio-oil ratio of 0.25 g/g. This drop in solid production between 30 and 60 min as the catalyst/bio-oil ratio increases accounts for the increase observed in the liquid yield. This seems to indicate that the presence of a catalyst avoids char formation from bio-oil, thereby increasing the yield of liquid.

An increase in the reaction temperature progressively reduces to insignificance the effect of reaction time on global yields. As a result, at 450 °C steady evolutions with time for the yields to liquid, gas and solid take place. At this temperature high and low gas and liquid yields are respectively obtained at the beginning of the reaction. Cracking reactions of bio-oil become intensified with temperature, which dramatically enhances gas production. Therefore, the highest and lowest gas and liquid yields obtained at the end of reactions at 350 °C can be obtained since the start of reactions at 450 °C. This increase in the temperature enhances the kinetics of bio-oil cracking reactions, which experimentally makes insignificant the effect of the catalyst/bio-oil ratio for the yields to gas and liquid. As an exception, a slightly higher yield to gas is obtained with an increase in the catalyst at reaction times higher than 45 min, probably owing to the positive effect exerted by time on gas production. This increase in temperature raises the yield to solid. Furthermore, the effect of the catalyst/bio-oil ratio is significant for this variable, where an increase in the amount of catalyst reduces the solid yield. High temperatures intensify cracking reactions, which can increase the amount of char. However, the presence of a catalyst can positively reduce char formation or facilitate its elimination.

The temperature significantly increases the yield to gas and decreases the yield to liquid. Nevertheless, the effect of temperature on the yield to liquid and solid is dependent on the pressure. Figure 36.2c, f, i shows the interactions between temperature and pressure for the yields to liquid, gas and solid at medium values of the catalyst/bio-oil ratio (0.125 g/g) and reaction time (30 min). An increase in the temperature increases the gas yield regardless of the hydrogen partial pressure. Cracking reactions are enhanced with temperature. Interestingly, this result indicates that the partial pressure of hydrogen does not significantly affect the extension of cracking reactions under the experimental conditions of this study. Conversely, the partial pressure of hydrogen significantly affects the yields to liquid and solid. An increase in the temperature decreases the yield to liquid. The lower the partial pressure of hydrogen, the higher the decrease with temperature of the yield to liquid. As a result, the yield to liquid is negligible at temperatures higher than 400 °C at 70 bar. However, temperatures higher than 450 °C are needed to completely reduce the yield to liquid at 150 bar. An increase in the temperature increases the yield to solid between 350 and 400 °C regardless of the partial pressure of hydrogen. However, high hydrogen pressure contributes to a decrease in solid production, as observed when the hydrogen pressure was increased from 70 to 150 bar. Moreover, when the reaction temperature was increased to 450 °C and the pressure was kept at 150 bar, a slight increase in the yield to solid was

observed. Interestingly, at this temperature, an opposite effect was observed as the solid yield dramatically dropped when the hydrogen pressure was reduced from 150 to 70 bar. At this pressure the increase in temperature helps to char gasification, probably due to the water content of the bio-oil, which leads to a decrease and an increase respectively in the yields to solid and gas.

3.2 *Properties of Liquid Phase*

The concentrations of C, H and O in the upgraded bio-oil vary as follows: 50–82 wt.%, 3.5–8.3 wt.% and 9–44 wt.%. The HHV of the liquid moves from 19 to 37 MJ/kg. These results represent a considerable increase in the proportions of C and H and a decrease in the concentration of O (53.91 wt.% C, 3.32 wt.% H and 41.31 wt.% O), together with a substantial increase in the HHV (18.51 MJ/kg) with respect to the original bio-oil. Statistical analysis reveals that temperature and pressure are the operating variables with the greatest effect on the concentrations of C and O. An increase in temperature increases the proportion of C and drops the relative amount of O in the liquid. The pressure exerts the opposite effect on the concentration of C and O. While an increase in pressure increases the proportion of O, it decreases the concentration of C in the liquid. The catalyst/bio-oil ratio is the operating variable with the greatest effect on the concentration of H. An increase in the amount of catalyst increases the concentration of H, indicating that the catalyst has a positive impact on bio-oil hydrogenation. In addition, significant interactions between these variables and the reaction time are observed.

The effect of the reaction time on the elemental composition of the liquid is dependent on the temperature, pressure and catalyst/bio-oil ratio. Figure 36.3 shows the most important interactions of these variables with time. Specifically, Fig. 36.3a, b displays the effect of the reaction time for the concentration of C as a function of the catalyst/bio-oil ratio at 70 bar and 350 and 450 °C respectively. Figure 36.3c, d shows these effects for a partial pressure of H₂ of 150 bar. Figure 36.3 e–h, i–l displays these effects for the proportions of H and O respectively.

At 70 bar, the effect of the reaction time on the elemental composition of the liquid is only significant at temperatures lower than 370 °C. As an example, the evolution over time is plotted at 350 and 450 °C. At 350 °C, an increase in the reaction time leads to an increase in the proportion of C and a decrease in the concentration of O in the liquid, regardless of the catalyst/bio-oil ratio. Cracking reactions of some bio-oil oxygenated compounds can be enhanced with time, which accounts for this trend. While the proportion of hydrogen in the liquid remains steady over time in the absence of a catalyst, an increase takes place as the amount of catalyst increases since bio-oil can be progressively hydrogenated owing to the presence of the catalyst. At 450 °C, the liquid composition remains steady over time. Furthermore, the liquid phase at 450 °C has the same composition as reached at the end of the experiment (60 min) at 350 °C. Temperature exerts a positive

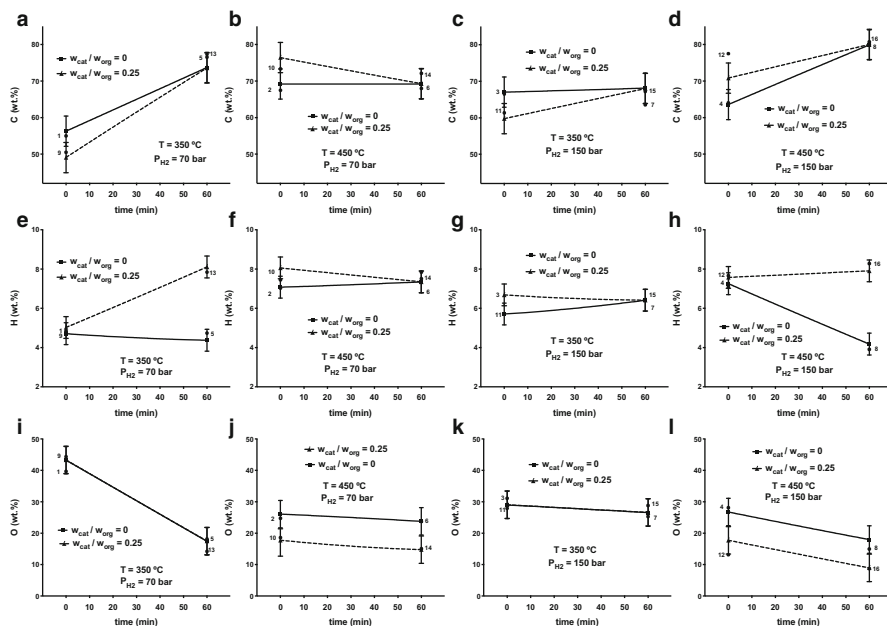


Fig. 36.3 Interaction plots for elemental composition of liquid phase. Bars: LSD intervals with 95 % confidence

kinetic effect on the process. Therefore, lower reaction times are needed at 450 °C than at 350 °C. An increase in the partial pressure up to 150 bar of H₂ does not significantly change the elemental composition of the liquid between 350 and 400 °C. Conversely, at temperatures higher than 400 °C, changes with time are observed. These evolutions with time are represented for a temperature of 450 °C. At 150 bar and 450 °C, an increase in the reaction time raises the proportion of C and diminishes the concentration of O, regardless of the catalyst/bio-oil ratio. The concentration of H in the liquid decreases over time in the absence of a catalyst but remains steady for a catalyst/bio-oil ratio of 0.25 g/g. The presence of the catalyst could favour hydrogen production from bio-oil at high temperatures and pressure by reforming owing to the water content of the bio-oil, which experimentally decreases the proportion of H in the liquid.

The temperature significantly increases the proportion of C and reduces the concentration of O in the liquid. However, the effect of temperature on the yield to liquid and solid depends on the pressure. In addition, different trends with temperature occur for the proportion of H in the liquid when the partial pressure of H₂ is varied. Figure 36.4a, b, c shows the interaction between temperature and pressure for the elemental composition of the liquid phase at medium values of the catalyst/bio-oil ratio (0.125 g/g) and reaction time (30 min).

In general, an increase in the temperature increases the concentration of C and decreases the proportion of O in the bio-oil, as cracking reactions of some bio-oil

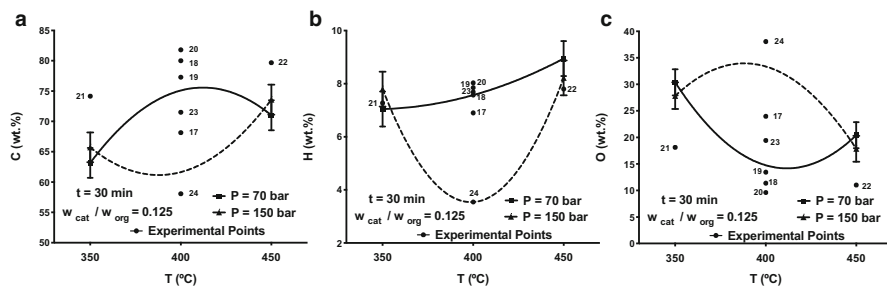


Fig. 36.4 Interaction plots between temperature and pressure for elemental composition of liquid phase. Bars: LSD intervals with 95% confidence

oxygenated compounds can intensify with temperature increases. This evolution depends on the pressure of H_2 . At 70 bar the increase and decrease in the proportions of C and O take place between 350 and 400 °C. A further increase in temperature has a negligible effect on the concentrations of C and O. Bio-oil hydrogenation could intensify between 400 and 450 °C; therefore, an increase in the concentration of H in the liquid takes place. An increase in the pressure of H_2 from 70 to 150 bar decreases the proportions of C and H and increases the concentration of O in the liquid between 370 and 425 °C. This increase in pressure results in a high liquid yield, with an elemental composition similar to that of the original bio-oil. As a result, at 150 bar, an increase in the temperature between 350 and 400 °C does not dramatically change the proportions of C and O in the liquid, but it does sharply decrease the concentration of H. This decrease takes place along with a high decrease in the yield to solid, as described earlier, which suggests that interactions between char and some hydrogenated compounds of the bio-oil might occur. A further increase in the temperature up to 450 °C increases the proportions of C and H and reduces the concentration of O in the liquid. This could be explained by the fact that hydrogenation and cracking reactions might be enhanced thanks to the positive kinetic effect of temperature.

4 Conclusions

Bio-oil hydrocracking represents a promising process for bio-oil upgrading. This process allows the production of an upgraded bio-oil with better physicochemical properties than the original liquid. The amounts of C, H and O (wt.%) in the upgraded bio-oil vary in ranges of 50–82 wt.%, 3.5–8.3 wt.% and 9–44 wt.%, and the HHV goes from 19 to 37 MJ/kg. This represents an increase of up to 42 and 152% in the proportions of C and H respectively, a decrease of up to 78% in the proportion of O and an increase in the HHV of up to 100% with respect to the original bio-oil.

Acknowledgements The authors wish to express their gratitude to the Spanish MINECO (projects ENE2010-18985 and ENE2013-41523-R) for their financial support and the FPI (BES-2011-044856) and mobility (EEBB-I-14-08688) grants awarded to Javier Remón Núñez.

References

1. Bulushev DA, Ross JRH (2011) Catalysis for conversion of biomass to fuels via pyrolysis and gasification: a review. *Catal Today* 171:1–13
2. Escobar JC, Lora ES, Venturini OJ, Yáñez EE, Castillo EF, Almazan O (2009) Biofuels: environment, technology and food security. *Renew Sustain Energy Rev* 13:1275–1287
3. Ayhan D (2008) Biofuels sources, biofuel policy, biofuel economy and global biofuel projections. *Energy Convers Manag* 49:2106–2116
4. Ayalur Chattanathan S, Adhikari S, Abdoulmoumine N (2012) A review on current status of hydrogen production from bio-oil. *Renew Sustain Energy Rev* 16:2366–2372
5. Sipillä K, Kuoppala E, Fagernas L, Oasmaa A (1998) Characterization of biomass-based flash pyrolysis oils. *Biomass Bioenergy* 14:103–113
6. Trane R, Dahl S, Skjøth-Rasmussen MS, Jensen AD (2012) Catalytic steam reforming of bio-oil. *Int J Hydrog Energy* 37:6447–6472
7. Jacobson K, Maheria KC, Kumar Dalai A (2013) Bio-oil valorization: a review. *Renew Sustain Energy Rev* 23:91–106
8. Xiu S, Shahbazi A (2012) Bio-oil production and upgrading research: a review. *Renew Sustain Energy Rev* 16:4406–4414
9. Lu Q, Li W-Z, Zhu X-F (2009) Overview of fuel properties of biomass fast pyrolysis oils. *Energy Convers Manag* 50:1376–1383
10. Puron H, Arcelus-Arillaga P, Chin KK, Pinilla JL, Fidalgo B, Millan M (2014) Kinetic analysis of vacuum residue hydrocracking in early reaction stages. *Fuel* 117:408–414

Chapter 37

Supporting Electromobility in Smart Cities Using Solar Electric Vehicle Charging Stations

J.K. Kaldellis, G. Spyropoulos, and St. Liaros

Abstract Improving energy efficiency in the transportation sector could significantly contribute to limiting environmental degradation and decelerate the depletion of existing fossil-fuel reserves. Effective methods for increasing energy efficiency include the adoption of eco-driving – especially in urban areas – the utilization of more efficient vehicles, and the shift to green public transportation. In any case, to develop a sustainable and efficient transportation strategy in selected cases (e.g., smart cities), the use of so-called clean new technology vehicles should be adopted. The Laboratory of Soft Energy Applications and Environmental Protection (SEALAB) of the Piraeus University of Applied Sciences (formerly TEI of Piraeus) has recently undertaken, within the framework of its innovative activities, the development, construction, and operation of the country’s first stand-alone solar electric vehicle charging station (EVCS), CARPORT, monitoring all energy data and thereby supporting and strengthening the country’s efforts in infrastructure development in the field of electromobility. More specifically, this innovative effort, described in this chapter, aims to accelerate the implementation of a European national electrification action plan through the construction of EVCSs based on photovoltaic generators. The proposed solar EVCS is considered to be one of the most environmentally friendly solutions, capable of supporting the decarbonization of the European transport sector.

Keywords Photovoltaic generators • Green vehicles • Sustainable development • Urban areas

J.K. Kaldellis (✉) • G. Spyropoulos • St. Liaros
Soft Energy Applications and Environmental Protection Laboratory, Piraeus University
of Applied Sciences, P.O. Box 41046, Athens 12201, Greece
e-mail: jkald@teipir.gr

1 Introduction

The continuous dependency of the European Union (EU) on imported fossil fuels (mainly oil and natural gas) and the corresponding environmental degradation, despite the remarkable efforts of the last 30 years, underline the necessity for additional measures, especially in the transportation sector. Actually, the transportation sector absorbs more than 30 % of the EU-28 final energy consumption (Fig. 37.1), while it is responsible for emitting more than 1000 Mtn of carbon dioxide equivalent annually, that is, 20 % of the entire CO₂ production of the EU (Fig. 37.2). Moreover, the road transport sector contributes more than 70 % of the entire transportation sector's CO₂ emissions [1].

The situation is almost identical in Greece, where the transportation sector is the second major final energy consumer (almost 37 %), following that of households and services (Fig. 37.3), being almost exclusively based on motor gasoline (61 %) and diesel fuel (37 %) [1].

Improving energy efficiency in the transportation sector could significantly contribute to limiting environmental degradation and decelerate the depletion of existing fossil-fuel reserves. Effective methods for increasing energy efficiency include the adoption of eco-driving – especially in urban areas – the use of more efficient vehicles, and the shift to green public transportation. In any case, for the development of a sustainable and efficient transportation strategy in selected cases (e.g., smart cities), the use of clean new technology vehicles should be adopted.

The systematic introduction of non-fossil-fueled vehicles and, more specifically, electric vehicles (EVs) may significantly contribute to reducing the concomitant oil consumption and on the limitation of air pollutant emissions, especially in the urban environment. This almost obligatory option has been adopted by most industrial

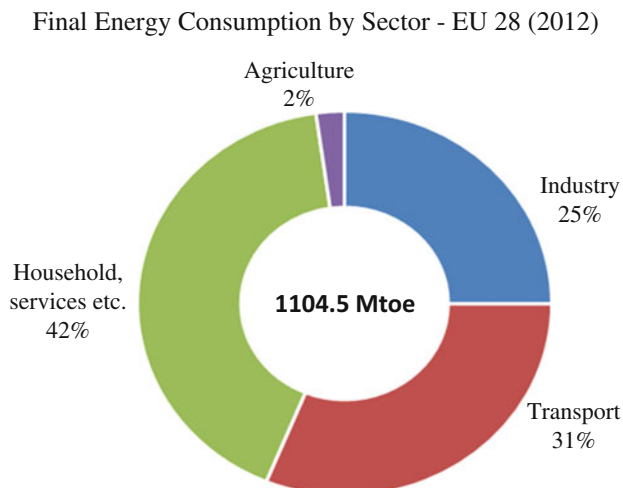


Fig. 37.1 EU final energy consumption analysis for 2012 [1]

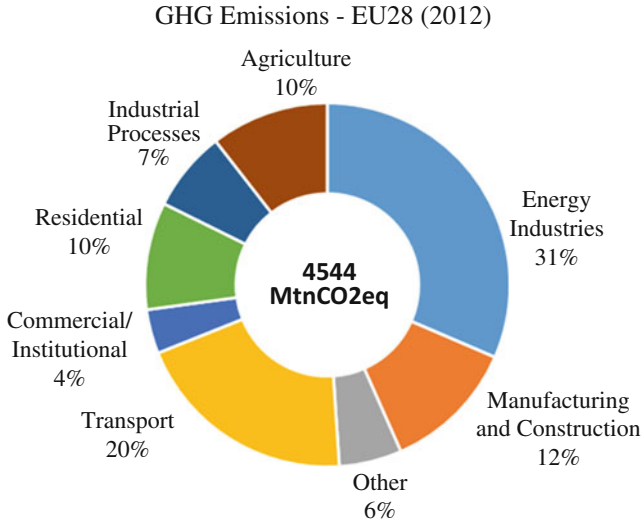


Fig. 37.2 Greenhouse gas emissions analysis by economic activity in EU for 2012 [1]

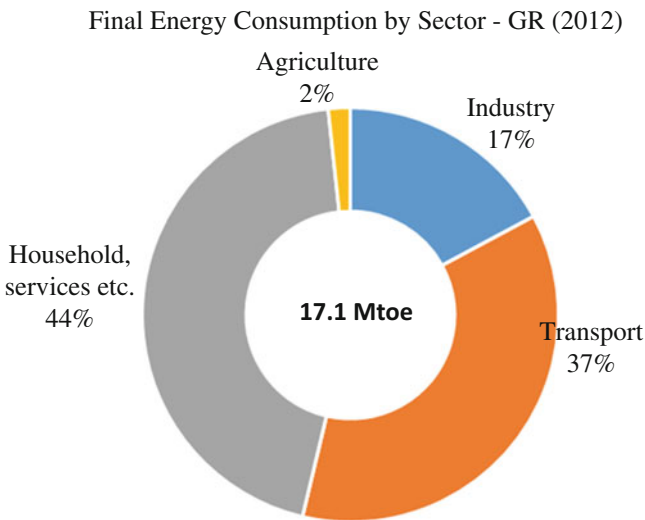


Fig. 37.3 Final energy consumption analysis in Greece for 2012 [1]

countries, including China, which is planning a very aggressive strategy in favor of EVs in the near future [2–5].

According to the available data (Fig. 37.4), more than 700,000 EVs are operating around the world, while in 2014 alone more than 300,000 EVs entered the market (Fig. 37.5) [6]. More specifically, Fig. 37.6 shows annual EV sales volumes increasing significantly from 2013 to 2014 [7]. The most active countries of the

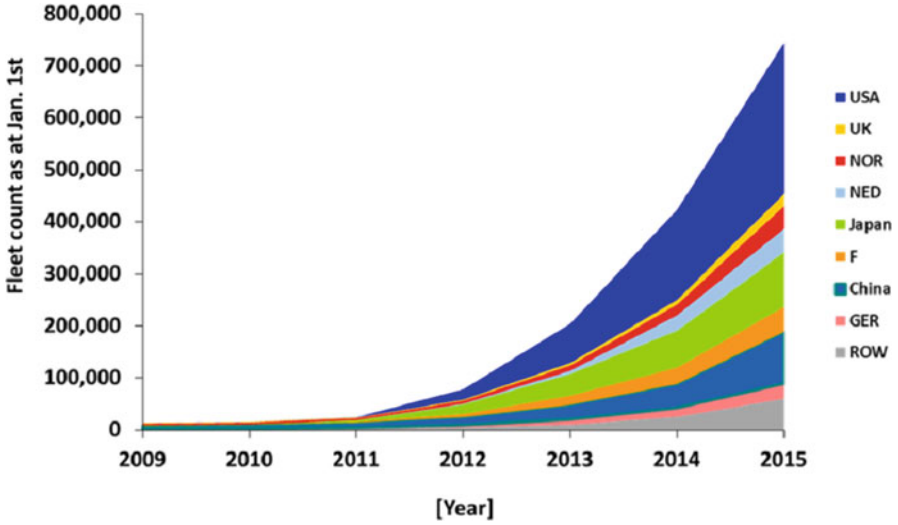


Fig. 37.4 Number of electric vehicles worldwide by 1 January 2015 [6]

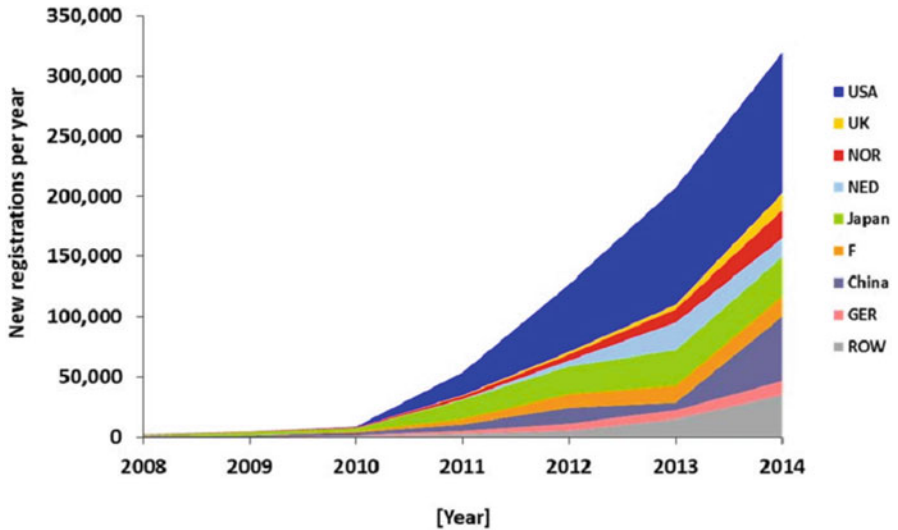


Fig. 37.5 Annual registrations of new electric vehicles during the period 2008–2014 [6]

sector include the USA (with almost 120,000 cars), China (50,000 cars), and Japan, along with several European countries like Norway and Holland. Notable also is the contribution of Germany and France, though it is not commensurate with their economic might.

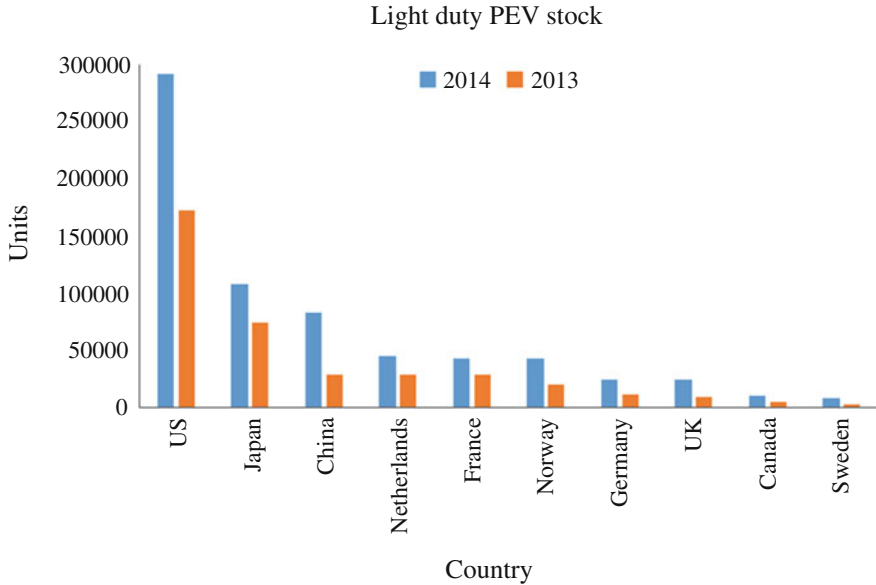


Fig. 37.6 Annual EV sales for major global markets (2013–2014) [7]

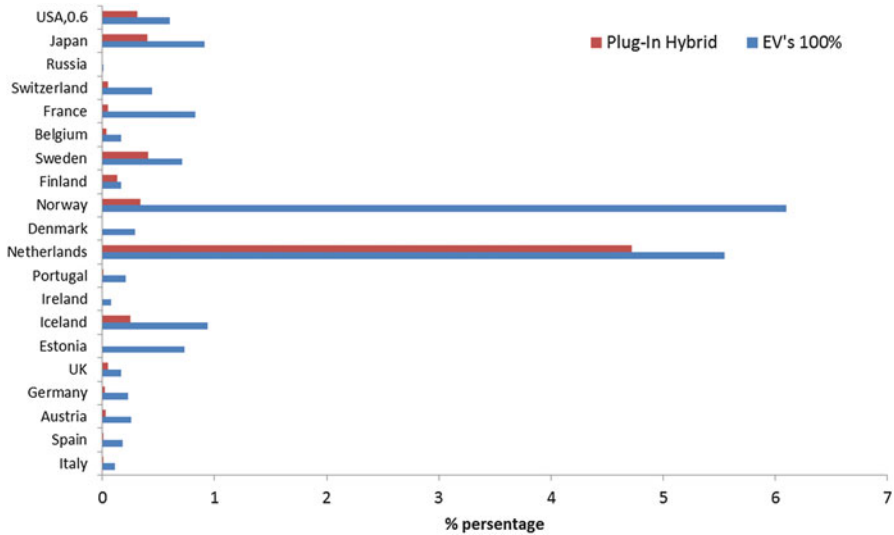


Fig. 37.7 Annual market share of EVs among total new vehicles sales for 2013 [8]

A more detailed inspection of the official data [8] reveals (Fig. 37.7) that the share of EVs in annual new-vehicle sales is remarkably high in Norway and Holland, representing more than 6% of the new-vehicle sales for 2013. More precisely, Norway pays special attention to supporting clean EVs, which

represent the vast majority of the new environmentally friendly vehicles, including plug-in hybrid cars.

Considering this brief presentation of worldwide activities in the area of EVs one may note that the EU plan targets 7.2 million EVs in member countries by 2020. This target is definitely related to an integrated network of electric vehicle charging stations (EVCSs) throughout the EU. More specifically, 13,000 new EVCSs have been planned for Greece in the coming years.

To contribute to and support clean-green transportation activities, the present work investigates the opportunities and any potential problems related to the development of one or more EVCSs. In this context, one may first analyze the environmental performance and the associated cost-related issues of a typical EVCS. Furthermore, special emphasis is placed on supporting the totally green solution of solar-based (powered) EVCSs in comparison with those connected with the electrical grid. For this purpose the main technical characteristics and preliminary performance of an experimental solar-based EVCS created by the Soft Energy Applications and Environmental Protection Laboratory of Piraeus University of Applied Sciences are also included in this chapter.

2 Proposed Solution

To define the main dimensions of a typical EVCS, one should take into account the corresponding energy and power demand, the environmental behavior, and some preliminary cost–benefit estimations.

2.1 Energy Balance of an EVCS: Preliminary Sizing

Based on available data, the specific volume fuel consumption, ε (L/km), of modern private vehicles varies between 6 and 8 L/100 km, while one may expect values even less than 4 L of fuel per 100 km up to 2020. It must be noted that the vast majority of drivers in urban areas and in remote small islands seldom travel more than 50 km/day. The corresponding final energy consumption, E_f , at the vehicle wheels is given as

$$E_f = \varepsilon \cdot Hu_f \cdot \eta_t, \quad (37.1)$$

where Hu_f is the specific calorific heat of the fuel used (kWh/L) and η_t is the total efficiency of the entire power transfer process to the vehicle wheels (including, for example, engine efficiency and gear box loss). Applying Eq. (37.1) one may estimate that the final energy consumption of a modern private vehicle is approximately 10 kWh/100 km or 0.1 kWh/km. In any case, this specific energy consumption may be more than double for vehicles of the previous decade.

The authors believe that values approximating 0.1 kWh/km [well to wheel (WtW)] should be the target for future EVs. It must be noted, though, that taking into account the corresponding losses and self-consumption of the electrical system (e.g., battery losses, electrical generator efficiency), this figure must be increased by at least 50 %. Furthermore, accounting for charging/discharging and other electrical losses, it is expected that WtW consumption will surpass 0.2 kWh/km. Finally, if the required energy is provided by a photovoltaic (PV) generator, via an appropriate charger or EVCS battery bank, then the corresponding consumption may even exceed 0.3 kWh/km, with the most plausible value being 0.25 kWh/km.

In this context, in order for a PV-based EVCS to guarantee the daily autonomy of an EV (assuming 50–100 km/day), the corresponding PV generator's daily production, E_d , should be approximately 12.5 kWh_e, accounting for 50 km, with the value reaching up to 30 kWh_e for 100 km daily autonomy. The energy yield of a PV generator depends on the generator's peak power, P_{\max} , the installation's capacity factor, CF , and the time period under consideration. Thus for a typical day one may write

$$E_d = P_{\max} \cdot CF \cdot \Delta t. \quad (37.2)$$

Applying Eq. (37.2) one may estimate that the PV generator's peak power will vary between 2 and 5 kW_p in the greater Athens (Greece) area (i.e., solar irradiance and ambient temperature). Thus, applying Eq. (37.2) for a typical day in central Greece, one ends up with 15–35 kWh of electricity, which would be able to support directly or via batteries the complete daily energy needs of an EV covering up to 100 km/day.

2.2 Environmental Performance of a PV-Based EVCS

A solar [renewable energy source (RES)]-based EVCS (Fig. 37.8) is, the authors believe, the only almost entirely environmentally benign solution since during its operation it does not burden the environment with any type of air or water pollution. At this point, one should consider the energy embodied in the proposed solution (including the PV panels, the system batteries and electronics, and the balance of system components) [9, 10]. On top of these, one should not disregard the severe problem of battery replacement throughout the operational lifetime of the installation and the batteries' final disposal.

However, the proposed solar EVCS causes no air pollution, which is one of the main problems of the current transportation sector. More precisely, a typical gasoline-/diesel-based private vehicle emits 150–300 g CO₂/km, 1–2 g CO/km, 0.1–0.2 g hydrocarbons (HC)/km, 0.06–0.15 g NO_x/km, and 0.005–0.015 particulate matter (PM/km) [11].

On the other hand, use of the existing electrical grid to support the EV fleet is also related to noticeable levels of air pollution since the electricity generation sector is dominated by fossil-fuel-fired power stations. One important issue is that

Fig. 37.8 Small wind turbine and CARPORT at Piraeus University of Applied Sciences



air pollutants do not appear in EVs' circulation regions (i.e., urban areas) but at the power station sites. Generally speaking, induced air pollution depends strongly on the current electricity generation fuel mix supporting the operation of EVCSs. Theoretically, for countries whose electricity generation is based on RESs the corresponding air pollution is also minimal. However, this is not the case for Greece and most EU member countries. For example, in mainland Greece, more than 40 % of electricity consumption is based on local lignite [12], while for numerous islands of the country electricity production is almost exclusively (almost 90 %) produced by imported diesel and heavy oil [13]. In this context, utilizing some indicative air pollution data [14, 15] and assuming an electricity consumption rate of approximately 0.2 kWh/km, one may arrive at values similar to those in Table 37.1.

Comparing the available data, one may state that in terms of atmospheric pollution, EVs supported by existing electrical grids do not provide the expected environmental benefits, especially on the islands. Furthermore, any environmental advantages of the EVs are highly strongly questionable insofar as the coal-based power stations contribute the majority of the existing fuel mix. This is much more obvious if one takes into account the continuously improving environmental performance of the corresponding internal combustion engines used in road transportation vehicles.

Table 37.1 Comparison of main air pollutant emissions for various private vehicle options in Greece

Air pollutant (g/km)	ICEV ^b	Mainland grid	Island grid	Solar EVCSs ^a
CO ₂	150–300	80–150	120–160	5–10
NO _x	0.06–0.15	0.15–0.25	0.04–0.10	0.00001
HC	0.1–0.2	0	0.05–0.08	0.00002
SO ₂	0	0.2–0.35	n/a	0
PM	0.005–0.015	0.001–0.003	0.005–0.01	0
CO	1–2	0	0.1–0.2	0

^aMainly due to system construction^bInternal Combustion Engine equipped Vehicle (ICEV)

On the other hand, the utilization of solar energy (or any other RES, such as wind energy) to support EVs (Fig. 37.8) is the only environmentally friendly solution that can be integrated on a large scale into both urban and rural areas, minimizing the environmental impacts of the road transportation sector. Obviously, for the commercial application of the proposed solution, a well-organized and reliable network of EVCSs is a prerequisite. In this context, the encouragement of solar-powered EVCSs is currently considered to be the optimum choice toward the decarbonization of the transport sector.

3 Description of a Solar-Based EV Charging Installation

Hitherto, and accounting for available data [16] in Europe, there are more than 15,000 nonresidential slow EVCSs and nearly 1000 fast ones (see also Table 37.2). Unfortunately, one cannot get reliable data about residential charging infrastructures. However, the number of purely PV-based EVCSs is minimal.

The SEALAB of Piraeus University of Applied Sciences (formerly TEI of Piraeus) has recently undertaken, within the framework of its innovative activities, the development, construction (Figs. 37.9 and 37.10), and operation of the country's first standalone solar EVCS, known as CARPORT, monitoring all energy data, thereby supporting development and strengthening the country's efforts in infrastructure development in the field of electromobility.

Essentially, the new CARPORT is a self-funded, stand-alone, and grid-connected solar-based EVCS (Fig. 37.10) developed by researchers at the SEALAB with the contribution of Greek and foreign industrial partners. It is based on a 3 kW_p PV generator (12 × 250 W_p PV panels), equipped with a lead-acid battery storage bank with a nominal capacity of nearly 18 kWh (DOD_{max} = 50 %) and a charger of 5 kW nominal power, providing full (slow) charging in 6 to 8 h.

Table 37.2 Nonresidential charging points installed (approximately) in Europe, end of 2013 [16]

Country	Slow EVCSs	Fast EVCSs
UK	3000	150
France	1700	100
Germany	2800	50
Netherlands	6000	120
Portugal	1000	70
Spain	800	20
Sweden	1000	20
Denmark	3800	120
Norway	1300	90

Fig. 37.9 Proposed solar electric vehicle charging station (CARPORT) at SEALAB of Piraeus University of Applied Sciences: charging point



3.1 Main Installation Cost Parameters of a Solar-Powered EVCS

One of the main drawbacks of similar integrated solar-based EVCSs is the high initial installation costs. More precisely, the initial cost of a single CARPORT able to support one EV on an annual basis (100 km/day), along with a motorbike, ranges between € 12,000 and 20,000. The exact value depends on the peak power of the PV generator, the energy storage capacity, and the operational characteristics of the other major components of the charging station. Obviously, if similar installations



Fig. 37.10 Proposed solar electric vehicle charging station (CARPORT) at SEALAB of Piraeus University of Applied Sciences: general view

were to be mass produced, then the expected initial cost should drop to under € 10,000 and could even approach € 8000 under favorable conditions.

Recently, a net-metering technique was introduced in Greece. With this technique, the solar-based EVCS does not require a large energy storage capacity since energy can be stored in the central electrical grid. If the net-metering solution is adopted, the initial cost (no batteries needed) may be further reduced to values ranging between € 6000 and 8000, and one is not obligated to replace the system batteries every predefined time period. Moreover, if multiple charging points are installed to enable the charging of a larger number of EVs, then the estimated initial installation cost (per charging point) may be less than € 5000.

In the case of the CARPORT developed by SEALAB, the total turnkey cost may even exceed € 25,000, mainly because of the experimental-individual character of the installation and the numerous pieces of used measuring equipment. Actually, the total amount spent will be less than € 4000 (driven primarily by foundation work and auxiliary equipment), without taking into consideration, however, the labor costs of laboratory personnel. This is due to the fact that all the major CARPORT components have been provided (free of charge) by the components' manufacturers in view of the research and demonstrating character of the installation.

It is interesting to note that in the majority of European countries, new EVCS installations are experiencing heavy subsidization [17–19], which in France

approaches 50 % of the initial installation costs. Additionally, in many European countries, the development of EVCSs is undertaken by the state (e.g., UK, Spain), such as in the case of Italy, where the state, with the support of ENEL, Italy's largest power company, has, under the E-Mobility project, installed and is monitoring 400 EV charging points in Milan, Pisa, and Rome.

Applying Eq. (37.2) to the 3 kWp CARPORT, the expected annual energy yield could slightly exceed 5000 kWh_e/year, so the corresponding annual income would vary between € 750 and 1000 per year. Using a simplified cost/benefit analysis, the expected payback period of a commercial PV-based installation is between 10 and 15 years, including regular battery replacement and excluding any initial cost subsidization. This payback period may be drastically reduced if the electricity price is increased (especially in accordance with the operational cost of island local autonomous thermal power stations [13], exceeding in several cases € 0.3/kWh_e) or the initial installation cost is minimized, including direct subsidization [17–19].

4 Conclusions and Proposals

Bearing in mind the firm decision of the EU on sustainable development and energy independence, support for further development of RES-based applications is a decision with respect to goals to be achieved by 2030. Since the transportation sector has by far the lowest RES participation, the significant encouragement of clean EVs is the most promising solution for private road transportation.

However, for the effective support of EVs, the promotion and expansion of an integrated and reliable charging network is necessary. To this end, we propose the adoption of solar-based, instead of simple grid-connected, EVCSs to maximize the environmental benefits and minimize fuel imports. Undeniably, the initial cost required will act as a serious obstacle at present. However, the gradual cost reduction of EVCS components and the economies of scale achieved by installing EVCSs on a massive scale are expected to reduce the initial installation capital by as much as 50 % in the near future. Considering the excellent solar potential of the Mediterranean region and the volatility of oil and gas prices, the proposed solar-based configuration is, in the authors' view, the optimum solution.

More specifically, this innovative effort, as described in this chapter, aims at an accelerated implementation of a European-wide national electrification action plan for the construction of EVCSs based on PV generators. The proposed solar EVCS is one of the most environmentally friendly solutions and is capable of supporting an EV fleet market throughout Europe.

Acknowledgement This study was supported by the European Union and the Greek Ministry of Education through the Excellence II research framework



References

1. EC (2014) EU transport in figures. Publications Office of the European Union, Luxembourg
2. Yao M, Liu H, Feng X (2011) The development of low-carbon vehicles in China. *Energy Policy* 39(9):5457–5464
3. Massiani J (2015) Cost-benefit analysis of policies for the development of electric vehicles in Germany: methods and results. *Transp Policy* 38:19–26
4. Diamond D (2009) The impact of government incentives for hybrid-electric vehicles: evidence from US states. *Energy Policy* 37(3):972–983
5. Jenn A, Azevedo IL, Ferreira P (2013) The impact of federal incentives on the adoption of hybrid electric vehicles in the United States. *Energy Econ* 40:936–942
6. ZSW (2015) ZSW: more than 740,000 cars worldwide powered by electricity. Centre for solar energy and hydrogen research. <http://www.zsw-bw.de/en/support/news/news-detail/mehr-als-740000-autos-weltweit-fahren-mit-strom.html>. Accessed 12 Aug 2015
7. IEA (2015) IEA—International Energy Agency—affordable clean energy for all [iea.org](http://www.iea.org). International Energy Agency. <http://www.iea.org/>. Accessed 18 Aug 2015
8. ABB (2015) ABB group—automation and power technologies, ABB. <http://www.abb.com>. Accessed 18 Aug 2015
9. Kaldellis JK, Zafirakis D, Kondili E (2010) Energy pay-back period analysis of stand-alone photovoltaic systems. *Renew Energy* 35(7):1444–1454
10. Kaldellis JK, Simotas M, Zafirakis D, Kondili E (2009) Optimum autonomous photovoltaic solution for the Greek islands on the basis of energy pay-back analysis. *J Clean Prod* 17(15):1311–1323
11. EC (2014) Road transport: reducing CO₂ emissions from vehicles—European Commission. http://ec.europa.eu/clima/policies/transport/vehicles/index_en.htm. Accessed 26 Apr 2015
12. Kaldellis JK, Zafirakis D, Kondili E (2009) Contribution of lignite in the Greek electricity generation: review and future prospects. *Fuel* 88(3):475–489
13. Kaldellis JK, Zafirakis D (2007) Present situation and future prospects of electricity generation in Aegean Archipelago islands. *Energy Policy* 35(9):4623–4639
14. Kaldellis JK, Kapsali M, Emmanouilidis M (2012) Long-term evaluation of nitrogen oxides and sulphur dioxide emissions from the Greek lignite-based electricity generation sector. *Fresenius Environ Bull* 21(9)
15. Kaldellis JK, Mantelis N, Zafirakis D (2011) Evaluating the ability of Greek power stations to comply with the obligations posed by the second National Allocation Plan concerning carbon dioxide emissions. *Fuel* 90(9):2884–2895
16. ARF (2014) Electric vehicles in Europe: gearing up for a new phase? Amsterdam Roundtable Foundation, Amsterdam
17. Sierzychula W, Bakker S, Maat K, van Wee B (2014) The influence of financial incentives and other socio-economic factors on electric vehicle adoption. *Energy Policy* 68:183–194
18. Bakker S, Jacob Trip J (2013) Policy options to support the adoption of electric vehicles in the urban environment. *Transp Res Part Transp Environ* 25:18–23
19. Cohen N, Naor M (2013) Reducing dependence on oil? How policy entrepreneurs utilize the national security agenda to recruit government support: the case of electric transportation in Israel. *Energy Policy* 56:582–590

Chapter 38

Exploitation of Wave Energy Potential in Aegean Sea: Greece

F. Xanthaki, Chr. Giannaraki, E.F. Zafeiraki, and J.K. Kaldellis

Abstract In recent decades, renewable energy applications have gained significant market share in the global electricity generation sector and in covering the electricity needs of non-interconnected islands. Among the emerging renewable energy technologies, wave energy utilization is indisputably ranked among the energy sources that could resolve the controversial issue of energy demand coverage.

Greece, located in the eastern Mediterranean region (with a special focus on the Aegean archipelago), has almost 16,000 km of coastline, so the exploitation of marine technologies could contribute to the power supply of most islands as well as of the mainland. In this study, an extensive evaluation of the expected wave power in the Aegean Sea is carried out, focusing on selected sea sites where wave buoys have been located. The basic wave parameters (e.g., significant wave height) along with the corresponding wave power are analyzed for selected regions.

Taking into consideration the vast energy potential available in the sea as well as the fact that coastal areas can benefit greatly from the implementation of such energy solutions, the current study emphasizes both the northern and southern parts of the Aegean archipelago where many grid islands not connected to the mainland are dependent on conventional fuels and, more precisely, oil supplies to meet their urgent electricity needs.

Based on the results of this survey, the future prospects of wave energy and the possible implementation of innovative marine technologies could be supported, providing the remote island communities of the Aegean Sea with clean electrical energy at a reasonable cost.

Keywords Significant wave height • Wave power • Buoy stations • Remote islands

F. Xanthaki • C. Giannaraki • E.F. Zafeiraki • J.K. Kaldellis (✉)
Soft Energy Applications and Environmental Protection Laboratory, Piraeus University
of Applied Sciences, P.O. Box 41046, Athens 12201, Greece
e-mail: jkald@teipir.gr

1 Introduction

In recent decades energy demand has seen continuous growth worldwide (long-term average 1.5 to 2.5 %) owing both to increases in world population and the efforts of people (mainly in developing countries) to improve their standard of living. In this context and despite the oil price volatility in the international market, renewable energy applications have gained significant market share in the global electricity generation sector (Fig. 38.1) providing almost 23 % of world electricity demand [1].

However, according to recent information, in several cases the available onshore potential has been exploited extensively (e.g., Denmark and Germany) [2], while at the same time land use for the installation of new renewable energy source (RES) power plants often raises serious opposition from local communities [3]. In this context, the interest in sea-based applications has recently revived, with offshore wind energy comprising the most representative example [4, 5], while at the same time research in the fields of wave and tidal energy generation has encouraged development of new marine technologies.

Greece, located in the eastern Mediterranean region (with a special focus here on the Aegean archipelago), has almost 16,000 km of coastline, so the exploitation of marine technologies could contribute to the power supply of most islands as well as of the mainland. Actually, medium-sized and small remote islands face serious electrification and water shortage problems [6, 7] because their electricity generation is based on outdated internal combustion engines consuming expensive and heavily polluting imported diesel or heavy (mazut) oil. Taking into consideration the remarkable wave potential of these islands [8], wave energy utilization – among the emerging renewable energy technologies – is indisputably ranked among the energy sources that could resolve the controversial issue of energy demand coverage, especially on remote islands.

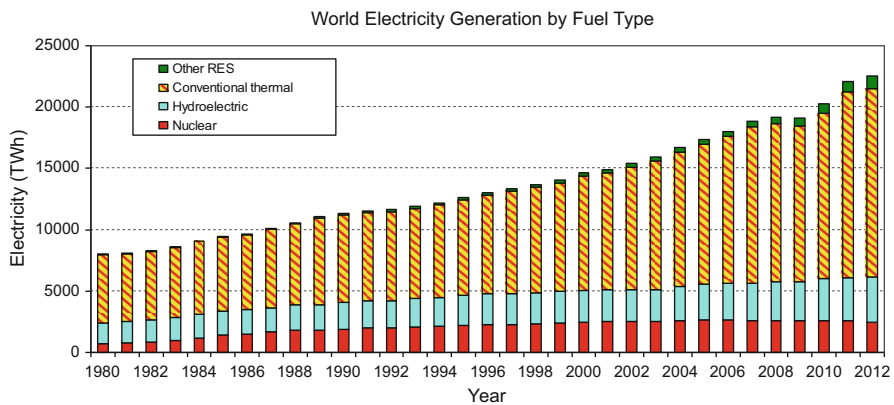


Fig. 38.1 World electricity generation by fuel type

For this purpose, in the present study, an extensive evaluation of the expected wave energy production in the Aegean Sea is carried out, focusing on selected sea sites where wave buoys have been located, so long-term real-world measurements were used. Seasonal monitoring of the basic wave parameters (e.g., significant wave height) along with the corresponding wave power are analyzed for selected regions.

Finally, an integrated energy production calculation model is developed using the wave energy potential parameters and the operational characteristics of existing commercial wave machines. The calculation results, even for enclosed sea cases, are quite encouraging since capacity factor values in a range of 25–35 % may be implemented.

Summarizing and taking into consideration the vast energy potential available in the sea as well as the fact that coastal areas can benefit greatly from the implementation of such energy solutions, the current study emphasizes both the northern and southern parts of the Aegean archipelago, where many grid islands unconnected to the mainland are dependent on conventional fuels and, more precisely, on oil supplies to meet their urgent electricity needs.

2 Wave Energy Opportunities and Barriers

Conventional sources of energy, such as oil, natural gas, and coal, are still the main energy sources used (78.3 %) around the globe, despite the fact that these sources are assumed to be responsible for considerable environmental degradation. For example, more than 30 % of carbon dioxide emissions worldwide are due to the operation of existing power stations. Moreover, taking into account the finite character of fossil-fuel reserves, along with the high levels of SO₂, NO_x, and several other pollutants affecting quality of life, it is imperative to consider carefully the opportunities offered by RES applications.

In this context, the European Union (EU) adopted the well-known 20–20–20 target for 2020, demanding a 20 % reduction in greenhouse gas emissions, 20 % RES penetration in final energy consumption, and 20 % conservation of primary energy. As far as Greece is concerned, an ambitious target of 40 % RES participation in the national electricity consumption has been set. In an attempt to implement these EU targets, special emphasis is placed on the exploitation of wind and solar energy on top of the already mature hydropower technology. However, one of the most promising RESs currently under development is ocean or marine energy. More precisely, according to rough estimates, the tidal potential is approximately 2.5 TW [6], while the near-shore wave potential is estimated at 1.3 TW [7], excluding the deep water wave potential whose economic exploitation is currently under study.

Despite several attempts to develop and test experimental installations, currently there is no industrial-scale wave-based power station in operation anywhere in the world [9]. Of course, there is significant activity surrounding prototypes in several countries, including, for example, the UK, USA, Norway, Portugal, China, Canada,

Table 38.1 Some full-scale WEC prototypes tested in sea [10]

Device	Year of tests	Location	Rated power
AWS	2004	Aguçadoura, Portugal	2 MW
Ceto	2011	Garden Island, Australia	200 kW
Direct drive linear generator	2005	Lysekil, Sweden	10 × 10 kW
EU pilot plant	1999	Pico Island, Azores	400 kW
LIMPET OWC	2000–07	Islay, Scotland	500 kW
Mighty Whale	1998	Nansei Town, Japan	120 kW
OWES	2005–06	Port Kemia, Australia	500 kW
Oyster	2009–11	EMEC, Scotland	300 kW
Pelamis	2004–07	EMEC, Scotland	750 kW
Pelamis	2010–11	EMEC, Scotland	750 kW
PowerBuoy	2009–10	Hawaii, USA	40 kW
PowerBuoy	2011	Invergordon, Scotland	150 kW
WavePlane	2008	Hanstholm, Denmark	100 kW
WaveRoller	2007–08	Peniche, Portugal	2 × 15 kW

and Korea. Table 38.1 [10] presents some full-scale wave energy converter (WEC) prototypes tested in the sea [11]. One of the most interesting attempts to exploit wave energy occurred in 2008: the installation of a set of three 750 kW Pelamis wave energy devices in northern Portugal (located five kilometers off the Agucadoura coast), constituting the first grid-connected wave farm of 2.25 MW in the world. Unfortunately, this project was abandoned owing mainly to financial problems of the partners. Nevertheless, the experience gained is incorporated into the new generation of Pelamis converters to be applied in new projects. Figure 38.2 shows some of the most interesting wave energy applications in Europe [12].

Recently, continued innovation and progress toward commercialization in wave energy have been made. But the industry has also faced some tangible headwinds, particularly for Pelamis Wave Power and Aquamarine Power, two Scottish wave energy firms. Unfortunately, Pelamis faced bankruptcy administration in late 2014 after failing to secure the funding necessary to continue further development of its wave energy converters. The Scottish government stepped forward with plans to continue the work of Pelamis and to retain some of the company's staff under Scottish Wave Energy, funded by the Scottish energy budget. Subsequently, Wave Energy Scotland acquired the intellectual property and physical assets of Pelamis, along with funding of USD 22 million [1].

The main obstacle of both coastal and shoreline installations is the initial installation cost, while for offshore installations, high operation and maintenance costs have been reported. Generally speaking, one may expect significant cost reduction in the near future, especially when mass installation of wave energy converters gets under way.

Finally, as expected, areas with excellent wave potential belong mainly to countries exposed to open seas (e.g., UK, Portugal). In this context, Greek seas, having the highest-quality waves in the eastern Mediterranean region, possess fairly

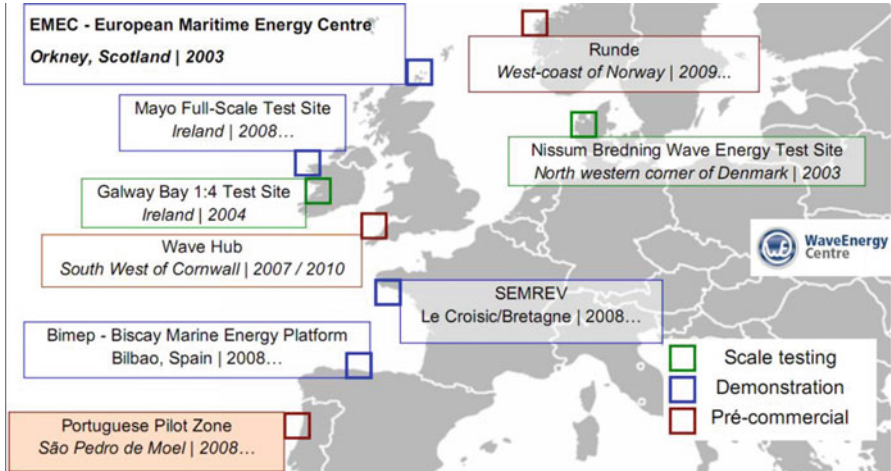


Fig. 38.2 Wave energy trials in European territory, based on [12]

good wave potential [13]. In fact, rough estimates [8, 14] state that the local wave energy potential ranges between 4 and 11 TWh per year, while the corresponding average wave height is around 1 m, although values of up to 6 to 8 m may also be encountered.

3 Wave Energy Potential Analysis

Sea surface wave energy derives from two kinds of water surface motion, vertical and horizontal. Vertical motion defines the height of waves, whereas horizontal motion determines the wave velocity. The entire energy is the sum of the dynamic and kinetic energy of waves. Basic wave characteristics, expressed via four important parameters, are taken into account in wave energy evaluation (Fig. 38.3). These characteristics are the length of the wave, λ , wave height, H (and more precisely the significant wave height, H_s), the wave period, T , and the transmission velocity of the wave, u . Thus, these four parameters are examined to evaluate the site of a potential wave energy exploitation installation along with the wavefront L .

To estimate the wave potential of an area, the types of data that have been commonly used up to now can be divided into three main categories, as follows:

- In situ measurements, which typically provide a temporal average of the main parameters of waves at a specific point or over a relatively small area;
- Satellite remote sensing providing a near-instantaneous average value of the wave parameters over a relatively large area;
- Numerical wave models that provide an estimate of the wave spectrum, which can be assumed as an average over both area and time.

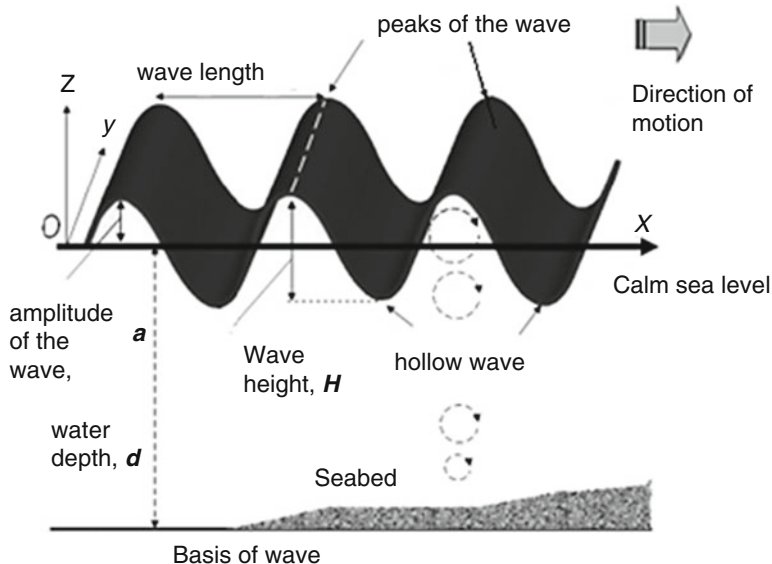


Fig. 38.3 Basic geometric and kinematic description of ripple sizes [23]

In this context the most widely used method adopted (mainly due to a lack of reliable and long-term measurements), especially in the Greek sea, is the application of numerical models (e.g., [15–17]). Recently, the application of satellite data to reproduce the wave potential of selected areas has also been encouraged (e.g., [18, 19]).

However, the present study concentrates on utilizing long-term, in situ measurements obtained by buoys located in certain sea sites in the Aegean Sea and recorded in a database. Therefore, a time series of wave height and period measurements was taken from the Poseidon database of the Hellenic Centre of Marine Research in Greece [20]. These parameters are used to predict the energy yield of a potential wave energy application in selected sea sites of both the northern and southern Aegean Sea. Some of the results related to wave power estimation at these locations are presented in the next section. Indicatively similar wave potential evaluation studies (on the basis of wave buoys) are conducted in the Italian offshore [21] and in the Portuguese near shore [22], also making use of the wave height parameter.

Actually, the present study is based on available data of 4 to 10 years for various sea sites covering the entire region of the Aegean Sea (Fig. 38.4). More precisely, Figs. 38.5, 38.6, 38.7, and 38.8 show wave power time-series estimations based on long-term measurements in four representative sea sites. To this end, two representative areas of the North Aegean were selected, that is, near the Athos peninsula and Lesbos island, respectively and two areas of the South Aegean, that is, the islands of Santorini and Crete. One point that is important to mention is that the data available are not continuous in all regions for the entire 2009–2012 period analyzed here, mainly because of buoy measurement system maintenance problems. However, in

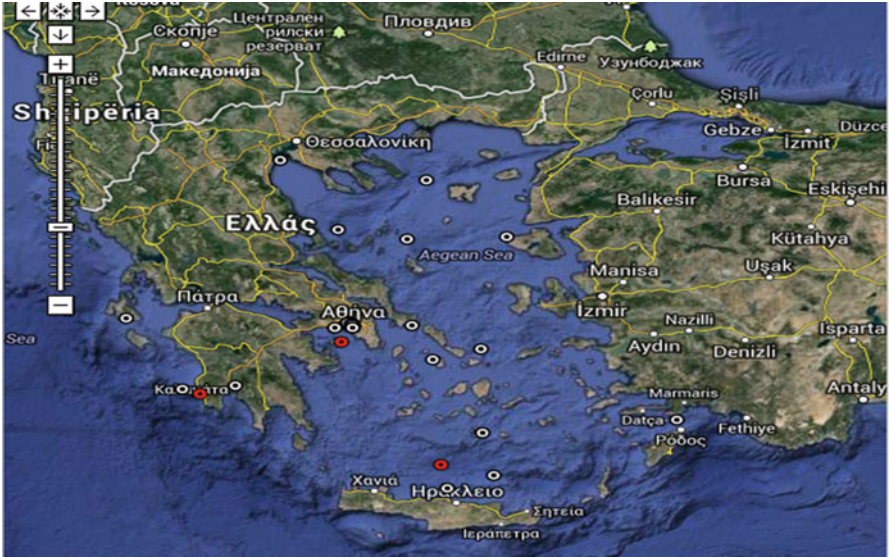


Fig. 38.4 Points where measurement buoy data in Greek seas are available

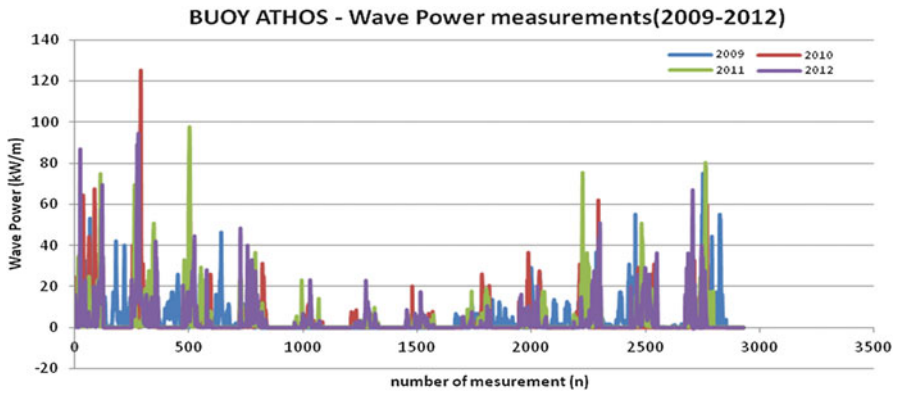


Fig. 38.5 Wave power time series for Athos area (North Aegean) based on buoy measurement

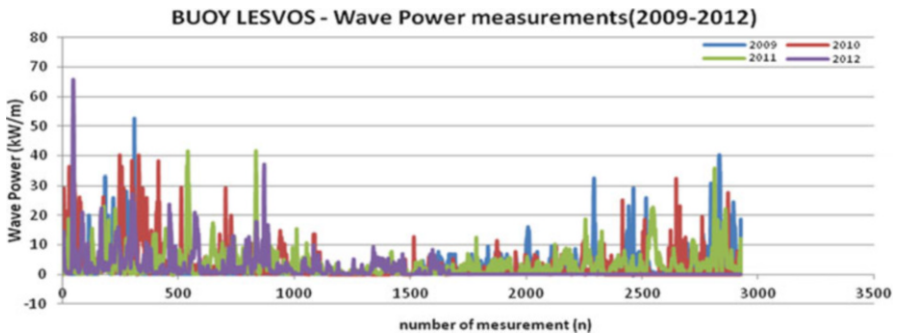


Fig. 38.6 Wave power time series for Lesvos island (North Aegean) based on buoy measurement

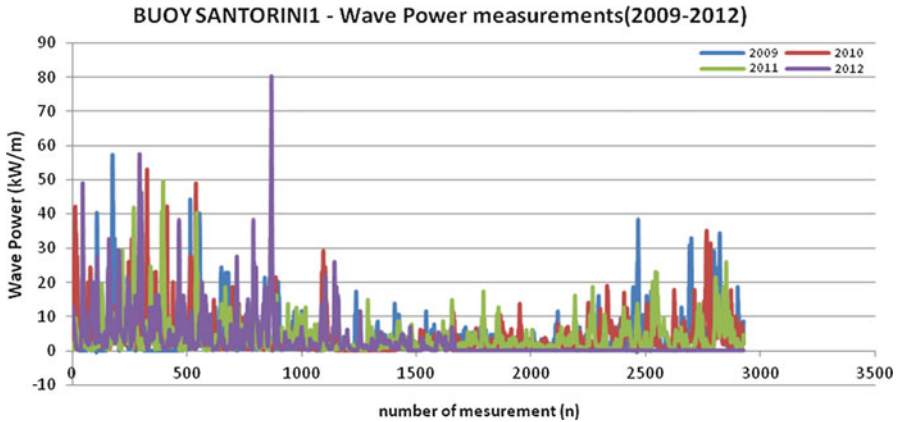


Fig. 38.7 Wave power time series for Santorini island (South Aegean) based on buoy measurement

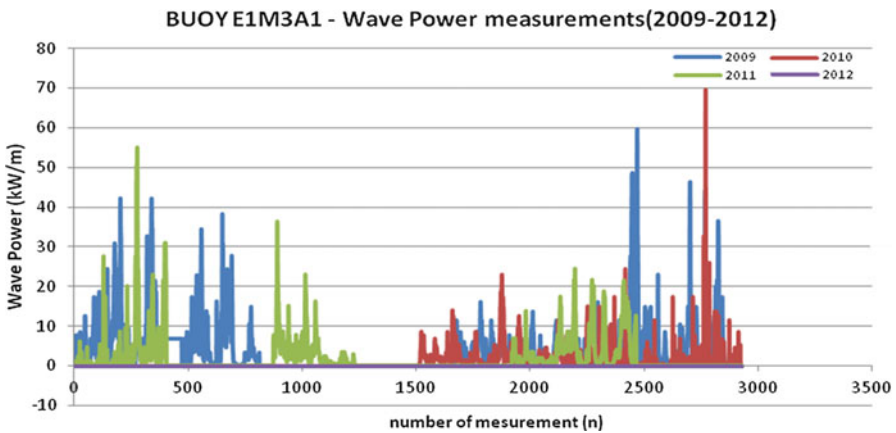


Fig. 38.8 Wave power time series for North Crete area based on buoy measurement

all cases one may detect the same pattern, that is, remarkable wave power in most winter months and some time periods of fair wind potential, mainly during the May–July period.

The last two diagrams (Figs. 38.9 and 38.10) show the combined wave power data for all regions examined and for the entire period (2009–2012) where measurements do exist. According to the data available, excluding the May–July period, the wave potential of all areas examined is quite remarkable, especially for enclosed sea cases.

The results of the wave power values of the present study compare rather favorably with the figures of Wave Atlas [18] and are found to match most of the examined sea sites in the Aegean, excluding some occasional extreme wave events.

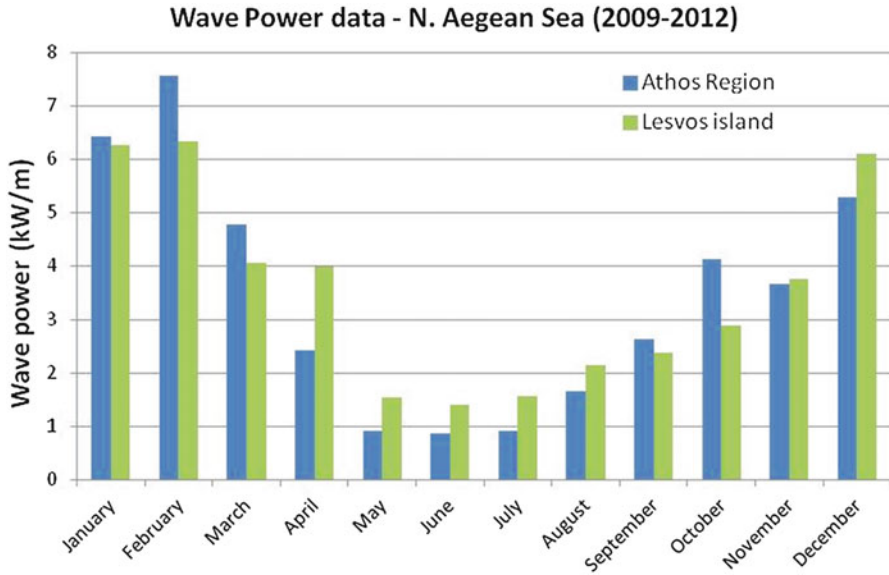


Fig. 38.9 North Aegean Sea wave power data based on long-term measurements

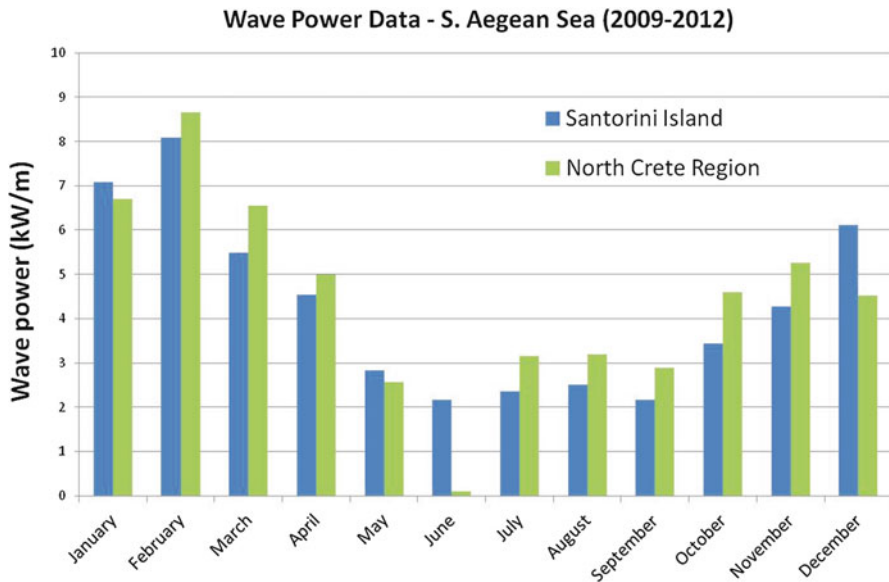


Fig. 38.10 South Aegean Sea wave power data based on long-term measurements

4 Wave Energy Calculation

For the calculation of the energy yield, E , of any wave energy exploitation device for a time interval, Δt , one needs the efficiency of the power generator, η , on top of the available wave energy potential, that is,

$$E = \int_{t_0}^{t_0+\Delta t} P(t) \cdot dt = \xi \cdot L \cdot \int_{t_0}^{t_0+\Delta t} \eta(t) \cdot H_s^2(t) \cdot T_e(t) \cdot dt, \quad (38.1)$$

where H_s is the significant wave height (m), T_e is the wave (energy) period (s^{-1}), and ξ is given for deep-water waves as

$$\xi = \frac{\rho \cdot g^2}{64 \cdot \pi}, \quad (38.2)$$

with ρ being the density of sea water (kg/m^3) and g the gravity acceleration (ms^{-2}). Applying an analysis similar to that adopted for other RES-based power stations [19], one may equivalently write

$$E = CF \cdot P_o \cdot \Delta t = 8760 \cdot CF \cdot P_o = 8760 \cdot \Delta \cdot \omega \cdot P_o, \quad (38.3)$$

with the second relation being valid on an annual basis, that is, $\Delta t = 8760$ h/year, and P_o being the rated power of the wave power device. Moreover, one should take into account that the capacity factor of the installation is the product of the corresponding technical availability, Δ , with the mean power coefficient, ω ; see the last part of Eq. (38.3). More precisely, Δ expresses the hours (%) during the time period Δt that the machines are available (without technical problems or out of operation for service/maintenance) to produce electrical energy without taking into consideration the wave potential availability. On the other hand, ω takes into account the interaction between the local wave potential and the selected wave energy exploitation device.

Recapitulating, for most wave devices the mean power coefficient may be calculated using the machine power curve [$P = P(H_s, T_e)$] and the occurrence matrix probability [$f = f(H_s, T_e)$]. Since the technical availability of similar applications is not well established, it is better at this point to neglect its impact and use the available data to estimate the theoretical value of the capacity factor, that is, assuming $\Delta = 100\%$.

For this purpose, one may use only the *complete measurement years* selected for the areas under investigation. On top of these one needs also the power curve of the wave converter selected for use. For this application the nondimensional power output of the Pelamis wave converter was selected (Table 38.2), expressed on the basis of the wave significant height and energy period (Eq. 38.1). Accordingly, Fig. 38.11 shows the energy-efficiency graph of the Pelamis wave converter

Table 38.2 Pelamis nondimensional power output as a function of (H_s, T_e) based on data by [11]

		Energy Period T_e (s)																
		5	5,5	6	6,5	7	7,5	8	8,5	9	9,5	10	10,5	11	11,5	12	12,5	13
Significant Wave Height $H_{s(m)}$	0,5	idle	idle	idle	idle	idle	idle	idle	idle	idle	idle	idle	idle	idle	idle	idle	idle	idle
	1	idle	3%	4%	5%	5%	5%	5%	5%	5%	4%	4%	3%	3%	3%	idle	idle	idle
	1,5	4%	7%	9%	10%	11%	11%	11%	11%	10%	10%	9%	8%	7%	6%	6%	5%	4%
	2	8%	12%	15%	18%	20%	20%	20%	20%	18%	17%	15%	14%	12%	11%	10%	9%	8%
	2,5	12%	18%	24%	28%	31%	32%	32%	31%	29%	27%	24%	22%	19%	17%	15%	14%	12%
	3	17%	26%	35%	41%	44%	45%	44%	42%	39%	35%	32%	29%	28%	25%	22%	20%	18%
	3,5	x	36%	47%	55%	58%	59%	57%	54%	50%	48%	43%	39%	35%	31%	29%	27%	24%
	4	x	x	62%	67%	72%	73%	71%	67%	63%	57%	51%	49%	45%	40%	36%	32%	28%
	4,5	x	x	73%	85%	86%	86%	84%	79%	78%	70%	63%	58%	51%	47%	45%	40%	35%
	5	x	x	x	99%	97%	97%	94%	89%	89%	81%	74%	69%	63%	56%	49%	46%	44%
	5,5	x	x	x	100%	100%	100%	100%	100%	98%	89%	88%	78%	71%	66%	59%	53%	47%
	6	x	x	x	x	100%	100%	100%	100%	100%	100%	95%	84%	83%	74%	68%	63%	55%
	6,5	x	x	x	x	100%	100%	100%	100%	100%	100%	100%	99%	88%	83%	77%	68%	64%
	7	x	x	x	x	x	100%	100%	100%	100%	100%	100%	100%	100%	90%	82%	78%	70%
	7,5	x	x	x	x	x	x	100%	100%	100%	100%	100%	100%	100%	100%	91%	83%	79%
	8	x	x	x	x	x	x	x	100%	100%	100%	100%	100%	100%	100%	100%	92%	83%

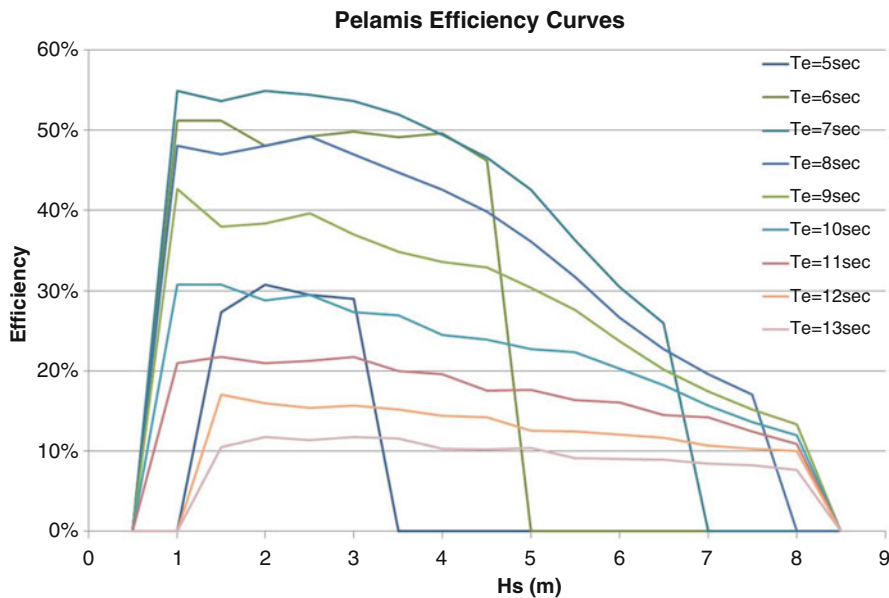


Fig. 38.11 Pelamis wave energy converter efficiency curves

resulting from the operational characteristics of the manufacturer. Using the wave potential data of Figs. 38.5, 38.6, 38.7, and 38.8 and the efficiency values of Fig. 38.11, one may estimate the expected energy yield of similar applications in the selected locations of the Aegean Sea, along with the corresponding capacity factor (or mean power coefficient) time evolution for an entire year (Figs. 38.12, 38.13, 38.14, and 38.15).

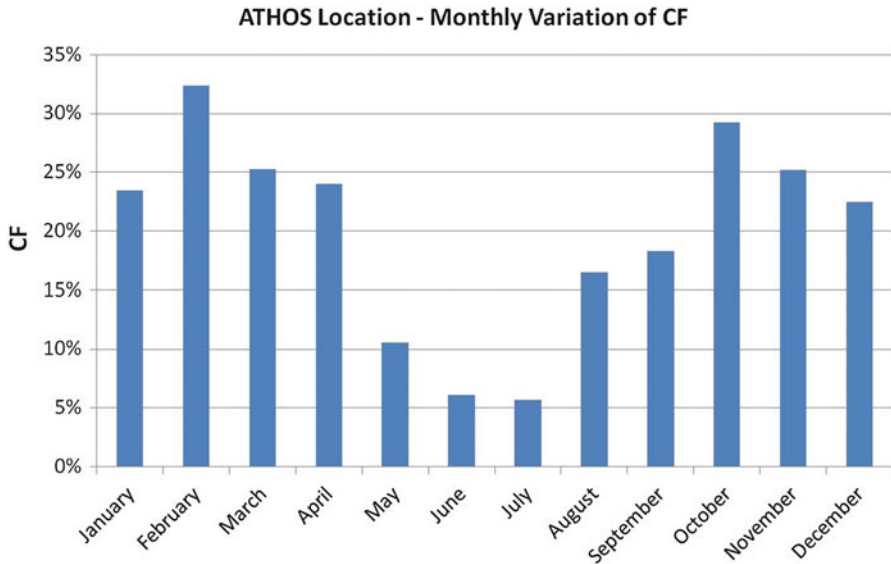


Fig. 38.12 Energy yield (capacity factor) monthly distribution based on application of Pelamis wave energy converter for Athos area

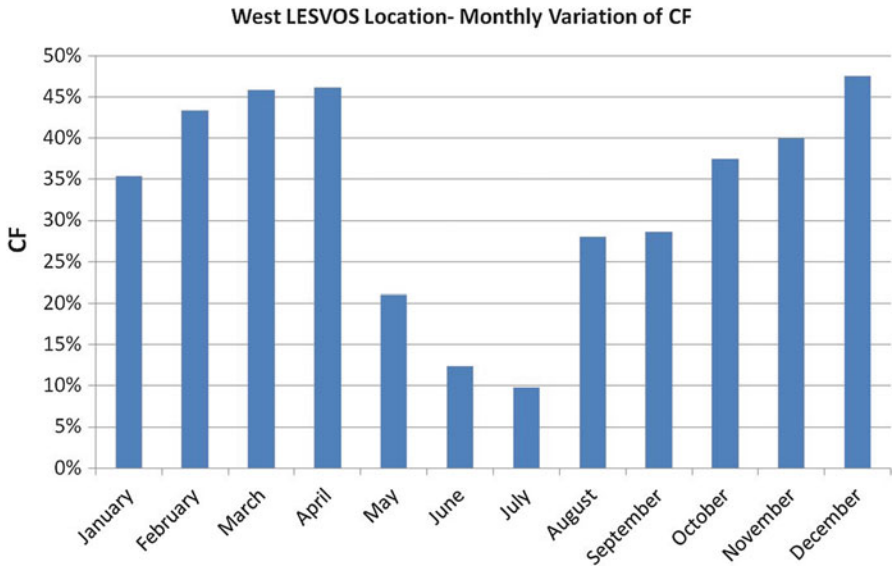


Fig. 38.13 Energy yield (capacity factor) monthly distribution based on application of Pelamis wave energy converter for West Lesvos area

As is obvious, the estimated capacity factor distribution presents a variable profile owing to the almost stochastic character of the available wave potential.

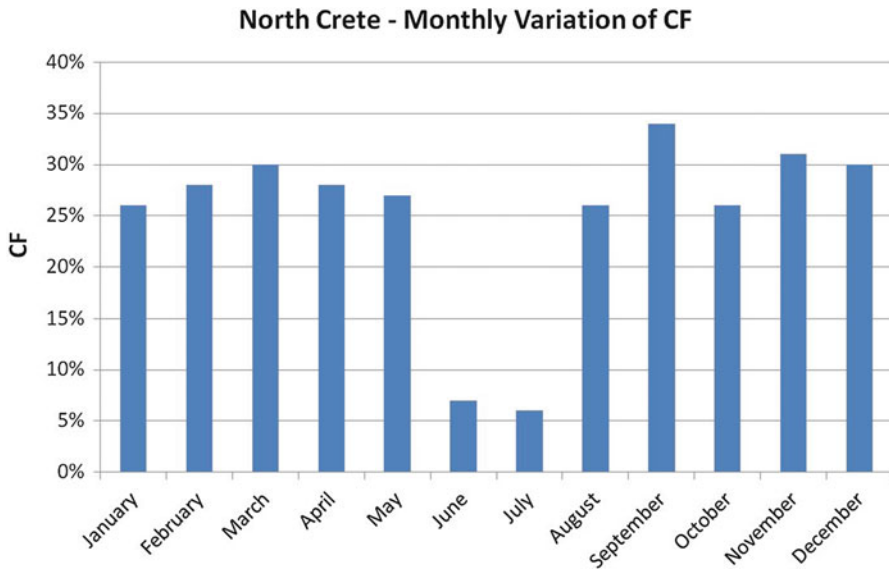


Fig. 38.14 Energy yield (capacity factor) monthly distribution based on application of Pelamis wave energy converter for North Crete area

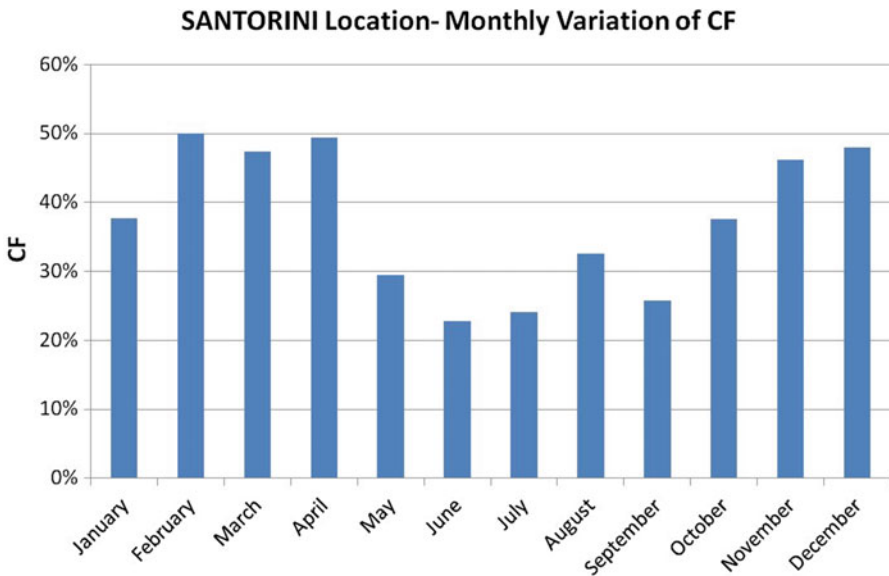


Fig. 38.15 Energy yield (capacity factor) monthly distribution based on application of Pelamis wave energy converter for Santorini Island area

However, in most months of the year, the values implemented are quite high, exceeding 25%. Finally, the expected annual energy yield for all four regions investigated varies between 1800 and 2300 MWh_e using a 750 kW rated power

wind energy converter. Although these values may be affected by the exact value of the technical availability as well as by the continuous technological improvements in the Pelamis wave energy converter, the amount of energy estimated can definitely support the energy needs of the local communities against the utilization of imported oil.

5 Conclusions

Enclosed seas like the Aegean Sea, due to their limited sea distance for waves to develop, do not present the excessive wave heights of open seas. However, the existence of many isolated electrical energy consumers spread over the Aegean archipelago may justify the operation of high-cost installations since the solution up to now has been the operation of oil-based internal combustion engines. On the other hand, the reasonable wave power of the enclosed seas limits the necessity of these sea-based constructions to be characterized by very high mechanical tolerance in order to withstand the great forces due to possible extreme weather conditions appearing in the open sea.

Taking into consideration the special character of the Aegean archipelago, the current study investigates long-term measurements for both the northern and southern parts of the Aegean region focusing on estimating the expected energy yield applying the operational characteristics of the most mature wave energy exploitation device used so far.

Based on the results of this survey, the future prospects of wave energy and the possible implementation of innovative marine technologies could be supported, providing the remote island communities of the Aegean Sea with clean electrical energy at a reasonable cost. Since most wave technologies are not yet mature enough to be economically competitive, the research and development contribution is thought to be critical for their maturation, especially at European levels, where the funding of pilot programs could boost commercial-scale applications.

Acknowledgment This study was supported by the European Union and the Greek Ministry of Education through the bilateral Greek–French collaboration research framework and the NAPOLEON project.



References

1. Renewables (2015) Global status report: renewable energy policy network for the 21st century (REN21)
2. Kaldellis JK, Zafirakis D (2011) The wind energy (r)evolution: a short review of a long history. *Renew Energy* 36(7):1887–1901
3. Kaldellis JK, Kapsali M, Kaldelli E, Katsanou E (2013) Comparing recent views of public attitude on wind energy, photovoltaic and small hydro applications. *Renew Energy* 52:197–208
4. Kaldellis JK, Kapsali M (2013) Shifting towards offshore wind energy recent activity and future development. *Energy Policy* 53:136–148
5. Esteban MD, Diez JJ, López JS, Negro V (2011) Why offshore wind energy? *Renew Energy* 36(2):444–450
6. Egbert GD, Ray RD (2003) Semi-diurnal and diurnal tidal dissipation from TOPEX/Poseidon altimetry. *Geophys Res Lett* 30(17)
7. Wavenet. Results from the work of the European thematic network on wave energy. <http://www.waveenergy.net>
8. Kaldellis JK, Giannaraki Chr (2012) Wave energy potential in enclosed seas: a case study in the south-east Mediterranean sea. In: *Energy Science and Technology*, vole 9: Geothermal and ocean energy. Studium Press, Houston
9. Bahaj AS (2011) Generating electricity from the oceans. *Renew Sustain Energy Rev* 15 (7):3399–3416
10. Stallard T (2012) Economics of ocean energy. In: Sayigh A (ed) *Ocean energy volume of comprehensive renewable energy encyclopedia*, vol 8. Elsevier, Oxford, pp 151–170
11. Heller V (2012) Development of wave devices from initial conception to commercial demonstration. *Compr Renew Energy Encycl* 8:79–110
12. Panagiotopoulos M (2010) Recent technological advancements for exploitation of wave energy, CRES
13. Clement A, McCullen P, Falcao A et al (2002) Wave energy in Europe: current status and perspectives. *Renew Sustain Energy Rev* 6(5):405–431
14. European Ocean Energy Association. <http://www.eu-oea.com/>
15. Christopoulos S (1989) Growth of wind waves—analysis of measurements and predictive mathematical models. Ph.D. Thesis, Aristotle University of Thessaloniki
16. Patelis GB, Kardaras Th (1997) Wave measurements in the Northern Aegean and compared with empirical prediction models. *Hydrographic Service GEN, 5th Hellenic symposium of oceanography and fisheries proceedings*, vol 1
17. Skopeliti A, Tsoulos I, Nakos B, (1995) Development of wave energy atlas in computing environment ARC/INFO. *Chartography laboratory, department of rural and surveying engineering, National University of Athens*
18. Soukissian H, Hatzinaki M, Korres G, Papadopoulos A, Kallos G, Anadranistakis E (2007) *Wind and wave atlas of the Hellenic seas*, Anavyssos, Greece: Hellenic Centre for Marine Research
19. Kaldellis JK, Kapsali M, Giannaraki Chr, Pavlou A (2013) Opportunities for wave energy exploitation in the east Mediterranean region. *Proceedings of the 4th international conference on renewable energy sources and energy efficiency—new challenges*, Nicosia, Cyprus, Jun 6–7, pp 129–138
20. Hellenic Centre for Marine Research. Poseidon database (Athens), c2008-2012. <http://www.poseidon.hcmr.gr/listview.php?id=136>
21. Vicinanza D, Capietti L, Ferrante V, Contestabile P (2011) Estimation of the wave energy in the Italian offshore. *J Coast Res* 64:613–617
22. Rusu E, Soares GC (2009) Numerical modeling to estimate the spatial distribution of the wave energy in the Portuguese nearshore, Unit of Marine Technology and Engineering, Technical University of Lisbon, Portugal
23. Delikaraoglou D, Delikaraoglou S (2010) Searching for wave-energy ‘hot spots’ in the Hellenic seas using satellite altimetry wave data. *Geophys J Roy Astron Soc* 19:70–88

Chapter 39

Energy Performance of a Renovated Multi-Family Building in Sweden

Lina La Fleur, Bahram Moshfegh, and Patrik Rohdin

Abstract Increased attention is being directed towards reducing energy use in buildings, and implementing energy-saving measures when renovating buildings has become of central importance. The aim of this chapter is to study the effects on heat demand of a deep renovation of a Swedish post-war, multi-family building. The studied building was renovated in 2014, and the renovation measures included thermal improvement of the climate envelope and installation of a mechanical supply and exhaust air ventilation system with heat recovery. The effect on heat demand is studied through a whole-building energy simulation, using IDA Indoor Climate and Energy. The IDA model is empirically validated with regard to its ability to predict indoor temperature and energy use. The results indicate a technical potential for a 50.3 % reduction of heat demand from implemented renovation measures, but measured data indicate that actual energy use is around 15 % higher than the technical potential. The reasons for this gap could be overestimated heat recovery efficiency or airing.

1 Introduction

Residential buildings use around 23 % of total energy in the European Union [1]. With increased attention on reducing energy use in buildings, the older part of our housing stock has become a central part in energy-saving measures in the building sector. Buildings usually undergo deep renovation every 40 years, and implemented

L. La Fleur (✉) • P. Rohdin
Division of Energy Systems, Department of Management and Engineering,
Linköping University, Linköping, Sweden
e-mail: lina.la.fleur@liu.se

B. Moshfegh
Division of Energy Systems, Department of Management and Engineering,
Linköping University, Linköping, Sweden

Division of Building, Energy, and Environment Technology, Department of Technology
and Environment, University of Gävle, Gävle, Sweden

solutions will therefore have a long-term effect on the energy use in the residential building sector.

Previous research indicates large energy-saving potential from renovation measures such as thermal improvement of climate envelope and ventilation measures [2–4]. However, many energy-saving measures have seldom shown to be profitable when implemented separately from renovation of buildings [5]. The Building Energy Performance Directive urges the implementation of energy-saving measures when buildings are renovated. Results from studies of deep renovations of Swedish multi-family buildings have shown a potential for a 50 % reduction in energy use [5].

The aim of this study is to evaluate the effects on heat demand from the renovation of a post-war, multi-family building in the city of Linköping, Sweden, and the difference between modelled heat demand and actual demand. The analysis is based on building energy simulations before and after renovation, and the model is empirically validated against measured data.

2 Methodological Approach and Case Description

2.1 Case Description

The studied building is located in Linköping in south-eastern Sweden and owned by a municipal rental company. It was constructed in 1961 and underwent deep renovation in mid-2014. The building is a small multi-family building with 5 stories and 12 apartments, heated with district heating (DH). The original construction was a lightweight concrete (LWC) structure (Table 39.1), with an exhaust air ventilation system with a flow rate of 2590 m³/h. The total transmission and ventilation losses were estimated to be 634.9¹ and 863.3² W/°C respectively.

The thermal quality of the climate envelope was improved (Table 39.1), making the total transmission losses 347.8 W/°C. A mechanical supply and exhaust air ventilation system with heat recovery (efficiency estimated at 70 %) was installed. Mechanical supply air ducts could not be installed on the ground floor, where fresh air is instead supplied via air inlets. The new supply and exhaust air flow is 1537 and 2095 m³/h respectively, giving ventilation losses of 209.5³ W/°C.

¹ Calculated $Q_t = \sum U \cdot A$, where Q_t is the total transmission losses (W/°C), U the overall heat transfer coefficient (W/m²·°C) and A the area (m²).

² Calculated $Q_v = \dot{m} \cdot C_p$, where \dot{m} is the ventilation mass flow (kg/s) and C_p the specific heat capacity of air (J/kg, °C).

³ Calculated $Q_v = (1 - \eta) \cdot \dot{m}_{\text{exhaust}} \cdot C_p$, where η is the heat recovery efficiency, \dot{m}_{exhaust} the exhaust ventilation mass flow (kg/s) and C_p specific heat capacity of air (J/kg, °C).

Table 39.1 Old and new construction

Segment	Area (m ²)	Unrenovated construction	<i>U</i> -value (W/m ² , °C)	Renovated construction	New <i>U</i> -value (W/m ² , °C)
External walls	569.9	250 mm LWC	0.42	250 mm LWC, 100 mm mineral wool	0.19
Windows (including balcony doors)	112.1	3 pane (clear glass)	2.0	3 pane (low emissivity)	1.1
Bathroom windows	5.9	2 pane (clear glass)	2.9	3 pane (low emissivity)	1.1
Doors	3.8	Metal with glazing	2.5	Oak door	0.8
Floor	216.5	200 mm concrete, 100 mm light insulation	0.32	Unchanged	0.32
Roof facing outside	23.1	150 mm concrete, 50 mm cork	0.91	150 mm concrete, 50 mm mineral wool	0.61
Roof towards unheated attic	194.5	50 mm concrete, 120 mm light insulation, 200 mm concrete	0.28	50 mm concrete, 300 mm mineral wool, wood joints	0.12

2.2 Field Measurements

Two reference apartments were used, and data were collected during summer and winter in one unrenovated apartment and during winter in one renovated apartment. Temperature was measured in occupied bedrooms, the kitchen and living room at a height of around 1.2 m using Intab Tiny Tag Plus 2 loggers (accuracy ± 0.35 °C). The concentration of carbon dioxide was measured in the master bedroom using an Intab TinyTag CO₂-logger (accuracy ± 3 %). Data were collected at 5 min intervals. Electricity use in the entire apartment was logged using an EliQ electricity meter. The validation periods were 15 days and chosen to represent the season. The reference apartments were similar in size and located in the same part of the building. Outdoor air temperature and relative humidity were collected on location using Tiny Tag Plus 2 loggers. Wind direction and velocity were logged with an Irox weather capture weather station.

Airtightness of the building climate envelope was measured before and after renovation in accordance with Swedish European Norm EN13829, using Retrotech blower door equipment (flow accuracy ± 5 %) and a Retrotech DM-2 gauge (reading accuracy of ± 1 %).

2.3 Building Energy Simulation

Building energy simulation (BES) offers the possibility of predicting energy use and thermal loads in all sorts of buildings and is commonly used in the planning or

renovation of buildings. BES models include parameters and input data relating to the construction of the building (materials, architectural layout, heating, ventilation and air conditioning design) and the occupancy (use of the building and behaviour) [6]. Whereas data on construction are often known or relatively easy to estimate, occupancy and user behaviour represent one of the larger uncertainties in building energy use and BES.

2.3.1 Model Description

The building was modelled in IDA Indoor Climate and Energy (IDA ICE) version 4.6.2. IDA ICE is a general simulation framework released in 1998 [7] which offers dynamic whole-building simulations. Each apartment was modelled as one zone, except for the reference apartments, where each room was modelled as one zone. Internal gains for whole-year simulation were based on findings from the Sveby programme.⁴ Domestic hot water use was not included in the simulations. Electricity use and CO₂ data were used for construction of equipment and occupancy schedules with 1 h resolution for the reference apartments during validation periods. Electricity use and occupancy were assumed to be equally distributed in the zones since more detailed user patterns are unknown. Indoor air temperature set points were determined using the measured temperature data from the reference apartments. The set point varied from 19.5 to 19.8 °C in the unrenovated reference apartment, and a set point of 20 °C was used for the rest of the building. The set point was 21 °C in all rooms in the renovated reference apartment and the rest of the building. Infiltration rates were based on results from the blower door airtightness measurements.

2.3.2 Climatic Data

Climatic data, including temperature, relative humidity, wind direction and wind speed at 1 h resolution, were collected from the Swedish Hydrological and Meteorological Institute. The STRÅNG⁵ solar radiation model was used for collecting hourly modelled data on direct and global radiation at the building location, and a simplified version of the Reindl model was used for calculating the hourly diffuse fraction. Measured local climatic data were used as climatic input data for the validation periods.

⁴ The Sveby programme is a Swedish national development programme for understanding building energy performance (<http://www.sveby.org/om-sveby/>).

⁵ STRÅNG is a mesoscale model for solar radiation developed by SMHI (the model can be accessed at <http://strang.smhi.se/>).

2.3.3 Model Validation

The inherent complexity of models, simplifications and parameter combinations make it impossible for any method to fully validate a model [6, 8] or for any model to be a perfect representation of reality. Coakley and colleagues [9] highlight that accuracy in predicting energy use is usually the main criterion for model validation, and accuracy of input data or the simulated environment is not assessed. This study empirically validates the model with regard to its accuracy in predicting both monthly heat demand and room air temperature in zones, under realistic conditions, i.e. in an occupied building [6]. Although realistic validation is complex, it offers the possibility of studying model sensitivity to user patterns and occupancy [6]. IDA ICE has been validated several times using both peer-model validation and idealized test cell validation methods, for example in [10].

3 Results and Discussion

3.1 Temperature Distribution in Zones

Figure 39.1 shows the modelled and the measured temperature distribution in four zones in the unrenovated reference apartment during summer. The simulation was performed with and without solar shading (blinds between panes), and the results indicated that adaptive measures had been taken by the occupants to reduce the

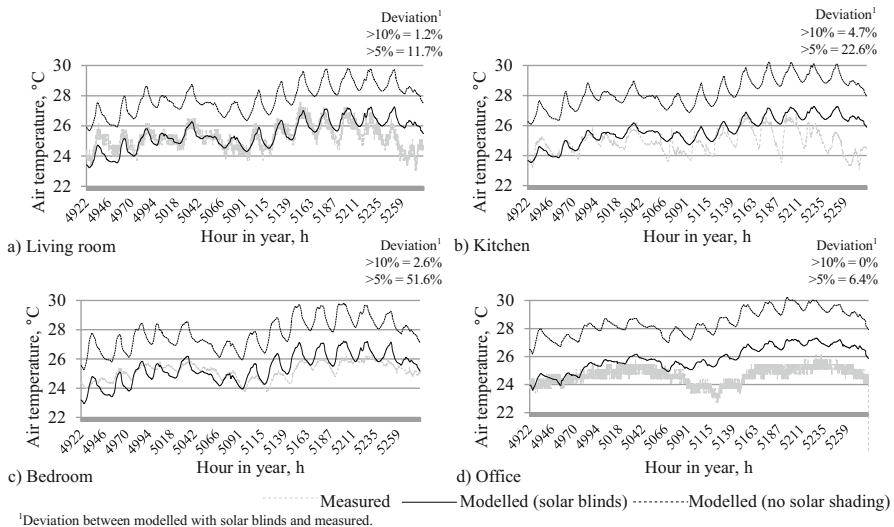


Fig. 39.1 Modelled and measured air temperature in zones between 25 July and 8 August 2013 (unrenovated). Percentage of modelled values with greater than 10 and 5% deviation from measured values can be seen in upper right corner

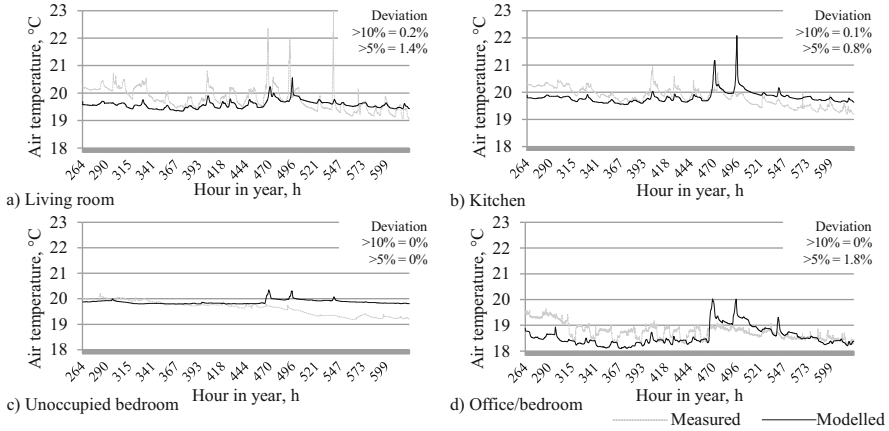


Fig. 39.2 Modelled and measured air temperature in zones between 12 and 26 January 2014 (before renovation). Percentage of modelled values with greater than 10 and 5% deviation from measured values can be seen in *upper right corner*

indoor temperature via solar shading. Modelled peak magnitudes are generally higher than measured data (Fig. 39.1). Other adaptive measures, such as airing, had likely been applied by the occupants.

The model accurately predicts the pattern of indoor air temperature during the winter period, although some differences are seen in peak temperatures. A deviation from measured temperatures of more than 5% occurs in less than 2% of modelled values (Fig. 39.2). Days during hours 470–493 were sunny, and smaller temperature peaks in the measured data could be due to usage of solar shading devices. The difficulty in capturing user behaviour and internal gains is also apparent when comparing modelled and measured temperatures in the office/bedroom between hours 315 and 393. The model shows a lowering of room air temperature, while the measured temperature increases. This could be due to usage of the stationary computer with the door closed, while the doors were modelled open during the day.

Measured air temperatures in the renovated apartment were higher and generally above 21 °C (Fig. 39.3). Although modelled peaks are not as prominent as actual peaks, the pattern is similar and few deviations above 10% occur. The defined schedules seemed to predict usage in a satisfactory way, except in the master bedroom after hour 1459. A lower level of CO₂ was recorded, indicating either airing or changes in occupancy.

3.2 Yearly Heat Demand

The building had a measured yearly heat demand of 101.3 MWh_{DH} in 2013 and the model predicted a yearly heat demand of 99.2 MWh_{DH} with climatic data from the

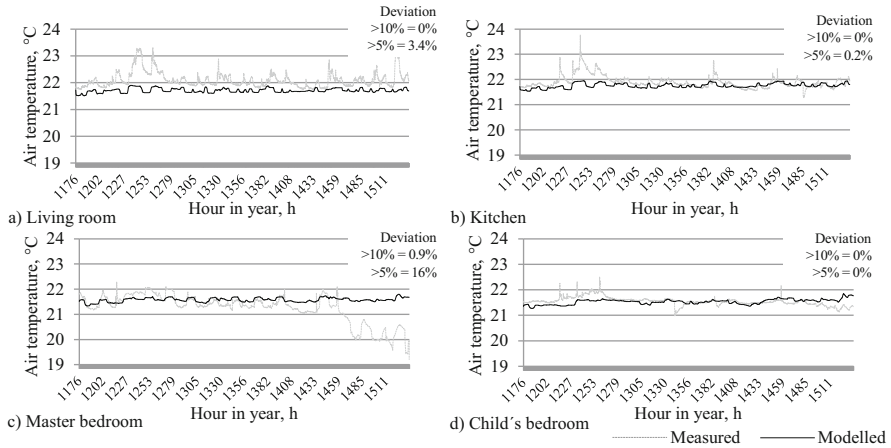


Fig. 39.3 Modelled and measured air temperature in zones between 19 February and 5 March 2015 (post-renovation). Percentage of modelled values with greater than 10 and 5 % deviation from measured values can be seen in *upper right corner*

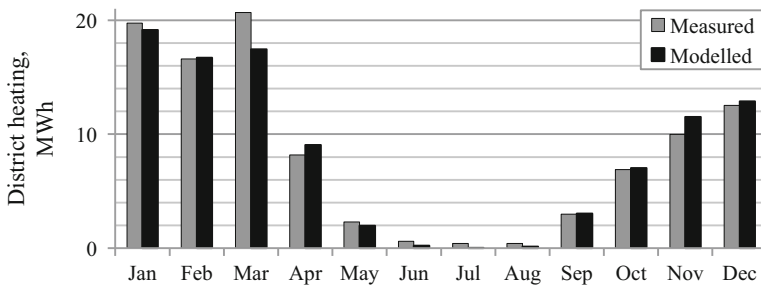


Fig. 39.4 Measures and modelled heat demand during 2013 in unrenovated building

same year, a difference of 2.1 % (Fig. 39.4). An underprediction of heat demand was seen during the coldest months (January and March), while a slight overprediction of heat demand could be seen during the cold and wet months in autumn. The largest difference between modelled and measured heat demand occurred in March and applied user schedules does not seem to entirely match actual use of the building.

The model of the renovated building was compared with the measured DH use between January and April 2015, which amounted to 28.4 MWh_{DH}. The model underpredicted heat demand to 24.1 MWh_{DH}, meaning 15 % less (Fig. 39.5). Since the modelled temperature distribution in the zones corresponded with the measured air temperature, there is little to indicate that the physics of the model was erroneous. Two uncertainties were identified and tested: a lower efficiency of the heat exchanger than expected and more airing than expected. Therefore, two simulations were performed, one with a heat recovery efficiency of 60 % instead

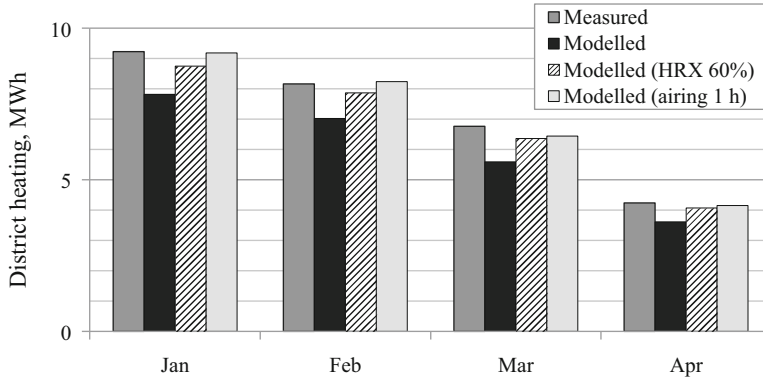


Fig. 39.5 Measured and modelled heat demand, January–April 2015, in renovated building

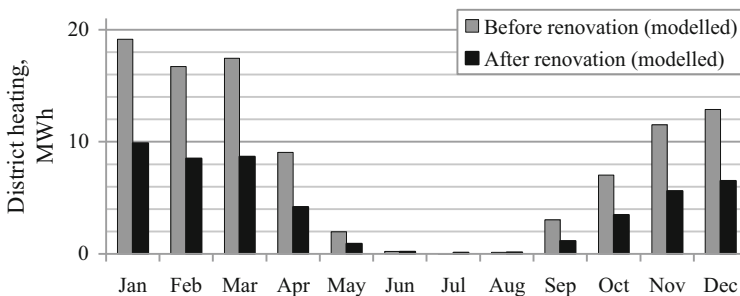


Fig. 39.6 Modelled heat demand in model of building before and after renovation with climatic data from 2013

of 70%, and one with airing by opening of the balcony door for 1 h a day (between 6 and 7 p.m.). Only one parameter was changed during each simulation. Both factors yield a monthly heat demand closer to the measured data (Fig. 39.5).

Comparison of the modelled yearly heat demand in the renovated and unrenovated buildings with climatic data from 2013 revealed that the renovation had a technical potential to reduce yearly heat demand by 50.3% (assuming that none of the uncertainty factors from Fig. 39.5 were applied) (Fig. 39.6). The modelled heat demand corresponded to 99.2 MWh_{DH} before renovation and 49.3 MWh_{DH} after.

4 Conclusions

The validated models were able to predict a realistic simulated environment. The deviation was smaller between modelled and measured temperatures in winter conditions than in summer. The validated model of the building before renovation

predicted a yearly heat demand of 99.2 MWh_{DH}, which is 2.1 % lower than the measured values. The validated model of the renovated building simulated a heat demand of 24.1 MWh_{DH} during the period January–April 2015, which is 15 % lower than actual heat demand. This indicates that some factors affect the final heat demand. Possible reasons for this deviation could be lower efficiency in heat recovery or airing.

5 Further Work

Further analysis will be performed to determine which explanatory variables affect outcome variables most strongly, using for example response surface methodology. A full study will also include electricity for ventilation, as well as a comparison of related CO₂ emissions and primary energy from energy use for heating and ventilation in the building before and after renovation.

Acknowledgement This study was funded by the Swedish Research Council Formas. The authors are grateful to the property owner and occupants for granting access to the building and reference apartments.

References

1. Johansson TB, Patwardhan A, Nakićenović NA, Gomez-Echeverri L (2012) Global energy assessment (GEA). Cambridge University Press, Cambridge
2. Lechtenböhmer S, Schüring A (2010) The potential for large-scale savings from insulating residential buildings in the EU. *Energy Efficiency* 4(2):257–270
3. Galvin R (2010) Thermal upgrades of existing homes in Germany: the building code, subsidies, and economic efficiency. *Energy Build* 42(6):834–844
4. Morelli M, Rønby L, Mikkelsen SE, Minzari MG, Kildemoes T, Tommerup HM (2012) Energy retrofitting of a typical old Danish multi-family building to a “nearly-zero” energy building based on experiences from a test apartment. *Energy Build* 54:395–406
5. Liu L, Moshfegh B, Akander J, Cehlin M (2014) Comprehensive investigation on energy retrofits in eleven multi-family buildings in Sweden. *Energy Build* 84:704–715
6. Ryan EM, Sanquist TF (2012) Validation of building energy modeling tools under idealized and realistic conditions. *Energy Build* 47:375–382
7. Sahlin P, Eriksson L, Grozman P, Johnsson H, Shapovalov A, Vuolle M (2004) Whole-building simulation with symbolic DAE equations and general purpose solvers. *Build Environ* 39(8):949–958
8. Jensen SO (1995) Validation of building energy simulation programs—a methodology. *Energy Build* 22(2):133–144
9. Coakley D, Raftery P, Keane M (2014) A review of methods to match building energy simulation models to measured data. *Renew Sustain Energy Rev* 37:123–141
10. Bring A, Sahlin P, Vuolle M (1999) Models for building indoor climate and energy simulation. In: Report of IEA Task 22: building energy analysis tools, Subtask B: model documentation

Chapter 40

Building Thermal Exergy Analysis

Lorenzo Leoncini and Marta Giulia Baldi

Abstract The energy and environmental impacts due to energy consumption in the building sector are one of the main topics in the global energy field. A building is an energy system that uses energy sources in order to maintain its functionality and to ensure thermal indoor comfort for its occupants. Exergy analysis is a way to assess the impact of an energy system on the environment. This chapter introduces a model able to describe the interaction between a building and its surroundings from an exergetic point of view. The building is considered as a so-called black box, evaluating the exergy of overall energy and matter fluxes that cross the system boundaries. In this way it is possible to evaluate the exergy balance of the system and particularly the destroyed exergy. The exergy destruction percentage can be understood as a building environmental impact indicator. To illustrate the model and its operating suitability, an existing building was analyzed using the transient simulation software Trnsys. The modeling results show that about 95 % of the exergy used from the building is destroyed and that about 5 % is lost (transferred to the surroundings). This means that this building has very high impact. The model can be applied to assess the effectiveness of different building energy retrofit strategies. Through Trnsys modeling some conventional and advanced retrofit strategies, as well as on-site renewable energy utilization, are analyzed. The chapter presents the main analysis results, showing which of these strategies are able to reduce the building's exergy demand and, hence, the building's impact.

Keywords Exergy • Energy retrofit • Building impact • Transient analysis

1 Introduction

The energy and environmental impacts due to energy consumption in the building sector are one of the main topics in the energy field. A building is an energy system that uses energy sources in order to maintain its functionality and to ensure thermal

L. Leoncini (✉) • M.G. Baldi
Department of Industrial Engineering, University of Florence,
via di S. Marta 3, Florence 50139, Italy
e-mail: lorenzo.leoncini@unifi.it; marta.baldi@unifi.it

indoor comfort for its occupants. An exergy analysis is a way to assess the impact of an energy system on the energy sources and the environment [1–3].

Generally, an exergy analysis of an energy system is made to show how the system uses inlet energy to produce a “useful product” (for example, electricity in a power plant). In contrast, a building is designed for thermal indoor comfort, with functionality being the useful product. From this consideration it follows that a building exergy analysis does not necessarily address exergy destruction percentage minimization. Alternatively it could address building exergy demand minimization, as will be discussed in this chapter.

In a previous paper [4] the authors developed a model called the thermal exergy analysis of a building in order to describe the interaction between a building and its surroundings from an exergetic point of view. This model views a building as a black box, taking into account only the flows that cross the system boundaries. The model makes it possible to quantify the exergy inlet and outlet from a building, considering all energy and mass flows, and, hence, to quantify the destroyed exergy. The exergy destruction percentage can be understood as a building impact indicator. In addition, the building exergy demand, normalized with respect to a year of operating time and a square meter of floor area, can be understood as a similar indicator, as explained in [5].

We verified the model reliability under different values of the reference state temperature. This verification [6] revealed that variation in the reference state temperature does not significantly affect the building exergy analysis results. In particular, the exergy magnitude of the sun, fuels and grid electricity are such that, from an overall system point of view, the results are affected marginally by the thermal exergy interaction between a building and its surroundings.

The model can be applied to assess the effectiveness of different building energy retrofit strategies. Through Trnsys modeling some conventional and advanced retrofit strategies, as well as on-site renewable energy utilization, were analyzed. This chapter presents the main analysis results, showing which strategies are able to reduce the exergy destruction percentage, or the building exergy demand, and, hence, the building impact.

2 Building Exergy Analysis in the Literature

In the literature, exergy analysis in the building sector has been mainly applied at the component level rather than at the system level. Lohani and Schmidt present in [7] an energy and exergy study of various heating configurations for a residential building. The fueling devices modeled are a gas-fired condensing boiler, an electric air-source heat pump and an electric ground-source heat pump. The study was carried out splitting the energy chain from the primary sources to the building envelope into subsystems placed in series. For each subsystem were calculated the energy and exergy efficiencies. The analysis results show that most thermodynamic irreversibility happened in the conversion from primary sources to so-called low-temperature thermal energy. Among the fueling devices modeled, the electric ground-source heat pump allowed for the highest overall exergy efficiency.

Yildiz and Güngör describe in [8] a parametric methodology for assessing the exergy efficiency of a generic heating configuration. Through the application to an office building some factors are emphasized that directly affect energy consumption (and the exergy destruction), such as whether the boiler is installed indoors or outdoors, the thermal insulation of the distribution piping, the operating temperature of the fluid, and the temperature difference between the terminal and the room. The resulting overall exergy efficiency is about one order of magnitude smaller than the overall energy efficiency. In agreement with Lohani and Schmidt, Yildiz and Güngör also conclude that most of the thermodynamic irreversibility happens in the conversion from primary sources entering the boiler to low-temperature thermal energy entering the distribution piping.

Hepbasli [9] presents an extensive review of so-called low-exergy heating and cooling configurations. Also Hepbasli, as well as Lohani and Schmidt, splits the energy chain from the primary sources to the building envelope into subsystems placed in series. The calculations are made both under steady-state and transient conditions. Moreover, a comparative review of 20 air-conditioning systems is presented, both from a device-size point of view and a device-efficiency point of view. From this review emerges the suitability of the exergy analysis as a planning tool for air-conditioning systems, considering exergy as a sustainability parameter for the building sector.

Torío et al. [10] propose an exergy vision of renewable energy sources used for fueling building needs, starting from a critical review of the related exergy analysis presented in the literature. The review underlines that exergy analysis methodologies are diverse and sometimes in disagreement with each other. There is no shared characterization of the reference state. Also, there is no commonly shared definition of exergy efficiency; it is variously understood as being “simple” or “rational” or “universal” or “functional.” These considerations lead to an exergy vision based on a distinction between technical boundaries and physical boundaries and between steady-state conditions and transient conditions. The aim of this vision is to define a shared methodological approach in order to make consistent the exergy analysis results.

Systematic studies of exergy analysis applications to whole building systems are reported in the ECBCS Annex 37 [11] and ECBCS Annex 49 [12]. The main topics are respectively low-exergy air-conditioning systems and exergy-efficient buildings and zones.

The Annex 37 study is set up to more levels: at the conceptual level, where exergy is explained as an analysis tool for energy systems; at the experimental level, where the building exergy balance is related to the human body’s exergy balance through comfort indices; at the application level, where many low-temperature heating devices and high-temperature cooling devices are described in order to minimize the thermal difference between a terminal and a room and, hence, to minimize the exergy destruction related to heat exchange.

The Annex 49 study deepens the Annex 37 study, focusing on building exergy analysis methodologies and low-exergy building design strategies. The criteria for the reference state choice and characterization are discussed and formulas for

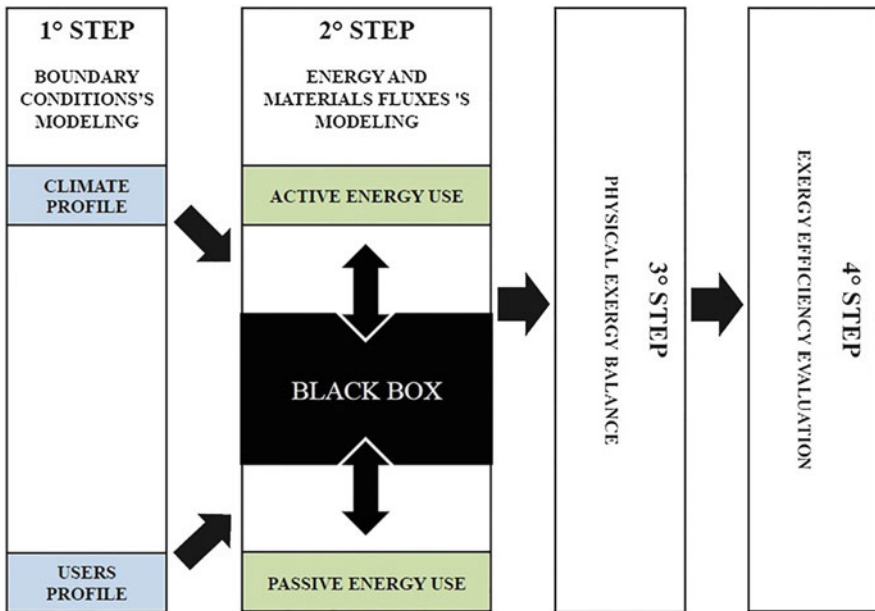
exergy calculations collected. Moreover, some applications of these concepts were presented, both at the building scale and at the district scale.

3 Thermal Exergy Analysis of a Building

We summarize here the main concept of the model in order to allow a better understanding of the computational model described in the following paragraph.

A building is an open thermodynamic system. It exchanges energy and mass flows with its surroundings. Each exchange is characterized by an associated exergy (thermomechanical or chemical) defined with respect to some reference state. The model does not consider the difference in pressure between system and surroundings and the wind kinetic exergy. Consequently, the air potential and kinetic exergy are not calculated.

The flow diagram in Fig. 40.1 illustrates the model concept. The building is treated as a black box: the mass and energy flow inlets are necessary to maintain its functionality and to ensure indoor comfort for the occupants. The model takes into account, for a standard building, the energy and mass flows illustrated in Fig. 40.2.



Active energy use refers to the devices fuelled from energy carriers. Passive energy use refers to the sun radiation incident on the building envelope.

Fig. 40.1 Thermal exergy analysis of a building model concept

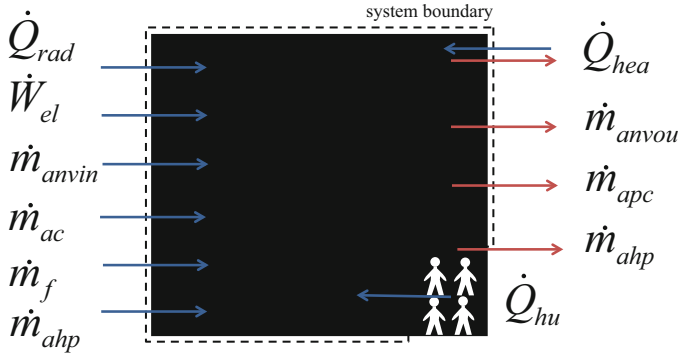


Fig. 40.2 Energy and mass flows considered for a sample building

4 Computational Model of a Sample Building

The sample building is a multiunit linear apartment buildings located in Florence, Italy. It was built in the 1980s, applying the building technologies typical of that time period. The building can be considered as being representative of Italian urban neighborhoods built in the period 1960–1980, mostly composed of multiunit linear apartment buildings. Consequently, this building is suitable for the model aim, which is to present an assessment method applicable to any generic building.

The external walls are composed of reinforced concrete having internal insulation in glasswool, the internal walls are made of plastered brick, the slabs of “predalles” plates, and the windows of a single-layer glaze and an aluminum frame.

The building is equipped with a central heating system, fueled by a gas-fired condensing boiler. Each apartment has a single domestic hot water (DHW) production system, fueled by an electric boiler. Originally the building was devoid of cooling systems. Recently each apartment has been equipped with an air-condensed cooling device, of a split type, which makes it possible to control the indoor temperature year round. The heating set-point temperature is 20 °C, and the cooling set-point temperature is 26 °C. The DHW production temperature is 45 °C.

The building was modeled through the transient simulation software Trnsys [13]. The geometric and thermal properties were drawn using a T3D plugin [14] for SketchUp [15], as shown in Fig. 40.3.

In the Trnsys model, the calculation time step was set at 1 h and the calculation time period at 1 year. The hourly weather data were taken from the test reference year (TRY) for the city of Florence, available from the EnergyPlus database [16].

The user profiles are described using some hourly schedulers taken from a benchmark tool developed by the US Department of Energy [16]. These schedulers feature separately the effects of occupants, lighting, and appliances. These schedulers are also used to describe DHW consumption.



Fig. 40.3 Building drawing in T3D plugin for SketchUp

The core building model is the Trnsys Type 56 (multizone building model, with thermally coupled zones). The model reads and processes the TRN weather data through the Trnsys Type 15-3. Moreover, the model describes the ground thermal properties using Trnsys Type 77.

The following flows, respectively inlet and outlet from the black box, were taken into account:

- Natural gas for the heating system; electricity for the cooling devices, DHW production boilers, lighting, and appliances; supply water to DHW production; air for ventilation, for combustion, and for the condensation of the cooling devices.
- Hot water from DHW consumption; air for ventilation and from the condensation of the cooling devices; products of combustion.

The heat exchange through the building envelope serves as the energy flow inlet and outlet. Moreover, the solar radiation incident on the building envelope (only the absorbed amount) and the energy emitted by the occupants, lighting, and appliances were taken into account.

The exergy of each flow or heat exchange was calculated using the standard formula for exergy analysis.

5 Building Energy Retrofit Configurations

The actual building configuration, called Setting 0, was described in the previous paragraph. In this configuration the the system's annual exergy inflow is 496,323 kWh, and the annual exergy outflow from the system (that is, transferred

to the surroundings) is 22,414 kWh. The ratio between these two indicates that the exergy destruction percentage is around 95 %, and so the building in the actual configuration is very high impact.

Eight different building configurations, called Settings 1 to 8, involving both conventional and advanced energy retrofit strategies, were analyzed using the Trnsys transient model. The purpose of the analysis was to assess which of these strategies would allow for system enhancements, both from a relative point of view, that is, the exergy destruction percentage, and from an absolute point of view, that is, the building exergy demand. The main features of each building configuration are described in what follows:

- Setting 1: application of a thermal insulation to the whole building envelope. The walls' thermal transmittance falls from 0.642 to 0.242 W/m²K, the roof thermal transmittance from 1.427 to 0.250 W/m²K, and the glazing thermal transmittance from 2.83 to 1.4 W/m²K.
- Setting 2: installation of mechanical ventilation systems (one for each apartment) in place of natural ventilation. We implemented a combination of air handler devices (such as heat recovery units and variable-flow-rate fans) and control logics to activate the heat-recovery function in winter and the free cooling function in summer only when suitable for the heating/cooling consumption reduction.
- Setting 3: this configuration is the sum of Settings 1 and 2.
- Setting 4: installation of an electric air-source heat pump that fuels the central heating system, in place of the gas-fired condensing boiler.
- Setting 5: this configuration is the sum of Settings 1 and 4.
- Setting 6: this configuration is the sum of Settings 1, 2, and 4.
- Setting 7: installation on the building roof of solar thermal and photovoltaic devices. The photovoltaic field is fully connected. Instead the solar thermal field is split up into four subfields, for the following reason. The produced thermal energy fuels four semicentralized DHW production systems. These systems are obtained linking the actual individual boilers in four clusters, one for each apartment group connected to the same stairwell. Each system has a solar technical room located on the building roof, equipped with its own water thermal storage and control system. The produced electrical energy fuels the building's needs when consumption is greater than production and is fed to the grid when production is greater than consumption.
- Setting 8: this configuration is the sum of Settings 1, 2, 4, and 7.

The resulting exergy values, both for single flow and for the sum of inlet and outlet flows, for each analyzed building configuration are summarized in Table 40.1.

Table 40.1 Calculation results

Setting	0	1	2	3	4	5	6	7	8
Flow	Exergy (kWh)	Exergy (kWh)	Exergy (kWh)	Exergy (kWh)	Exergy (kWh)	Exergy (kWh)	Exergy (kWh)	Exergy (kWh)	Exergy (kWh)
Natural gas	241,854	134,728	205,928	100,481	0	0	0	251,691	0
Airflow for fuel combustion	0	0	0	0	0	0	0	0	0
Electricity for cooling	7073	7348	3965	3009	7073	7348	3009	4925	2475
Electricity for heating	0	0	0	0	79,049	44,448	33,053	0	33,742
Airflow for chiller condensation	0	0	0	0	0	0	0	0	0
Airflow for heat pump evaporation	0	0	0	0	0	0	0	0	0
Water for DHW use	665	665	665	665	665	665	665	665	665
Electricity for DHW production	83,833	83,833	83,833	83,833	83,833	83,833	83,833	30,682	30,682
Heat flow from people	2309	2309	2309	2309	2309	2309	2309	2309	2309
Electricity for lighting and appliances	62,598	62,598	62,598	62,598	62,598	62,598	62,598	29,273	29,273
Solar radiation	97,558	80,627	97,558	80,627	97,558	80,627	80,627	92,848	76,719
Airflow for ventilation	0	0	0	0	0	0	0	0	0
Heat inflow through building envelope surfaces	432	393	781	841	432	393	841	412	809
<i>Annual amount of exergy inlet</i>	496,323	372,502	457,638	334,364	333,518	282,222	266,936	412,805	243,324
Products of combustion	1374	801	1161	591	0	0	0	1402	0
Airflow necessary from chiller condensation	857	909	426	316	857	909	316	568	258
Airflow from heat pump evaporation	0	0	0	0	2774	1535	1147	0	1176
Water from DHW use	7865	7865	7865	7865	7865	7865	7865	7865	7865
Airflow for ventilation	3390	3472	2527	2746	3390	3472	2746	3363	2699
Heat inflow through building envelope surfaces	8928	4842	8877	4816	8928	4842	4816	9173	4852
<i>Annual amount of exergy outlet</i>	22,414	17,889	20,856	16,335	23,814	18,623	16,891	22,372	16,850
<i>Exergy destruction (%)</i>	95.48	95.20	95.44	95.11	92.86	93.40	93.67	94.58	93.08

6 Results and Discussion

From a relative point of view, that is, considering the aim of exergy destruction percentage reduction, the analysis results show values ranging from 92.86 % in Setting 4 to 95.48 % in Setting 0. The paradox of these results is that whatever energy retrofit strategy leads to an exergy destruction percentage (slight) increase respect to the actual configuration. This configuration, that is, one having the highest energy demand, would seem to be exergetically more suitable. The apparent tradeoff between energy demand and exergy destruction percentage, that is, between energy analysis and exergy analysis, can be overcome by changing perspective from a relative to an absolute one.

We underline that, as mentioned at the beginning of the chapter, a building is not designed to produce something useful but to provide thermal indoor comfort and functionality. So a building exergy analysis will not necessarily address how to reduce the exergy destruction percentage. Alternatively, it could address the building exergy demand reduction.

From an absolute point of view, that is, considering the aim of building exergy demand reduction, the analysis results show that the actual configuration has the maximum exergy requirement. Instead, Setting 8, the one with the lowest energy demand, has the minimum exergy requirement. In this way the alignment between energy analysis and exergy analysis is restored. All building configurations bring exergy savings with respect to the actual configuration. The saving values range from -7.79% (Setting 2) to -50.97% (Setting 8).

The ratio between the Setting 0 inlet exergy and the Setting 8 inlet exergy is around 2:1. The ratio between the Setting 0 outlet exergy and the Setting 8 outlet exergy is around 1.3:1. From these ratios we get the following consideration: energy retrofit strategies affect inlet flow exergy values rather than outlet flow exergy values because the former have high exergy while the latter have low exergy.

On the basis of the analysis, we can look at a building as an intrinsic exergy destroyer. We determined that the main reasons for this quality of being a destroyer lie in the high exergy magnitude of the sun, the fuels, and the grid electricity compared to the low exergy magnitude of the thermal exergy interaction between a building and its surroundings.

To extend the model from the building scale to the district scale we refer to the methodologies presented by Balocco et al. [17] and Balocco and Grazzini [18]. In the first work the extended exergy analysis method is applied to evaluate the sustainability of an urban area. The applied methodology provides a single thermodynamic environmental criterion for the selection of technological alternatives, strategies, and designs that produce lower environmental impacts. In the second work some thermodynamic indicators are introduced that are useful for energy planning in urban areas and for defining the scenarios of integrated low-environmental-impact energy strategies and actions in an urban area.

7 Conclusions

This chapter introduces a model capable of describing the interaction between a building and its surroundings from an exergetic point of view. The building is treated as a black box, evaluating the exergy of overall energy and matter fluxes that cross the system boundaries. In this way it is possible to evaluate the exergy balance of the system and particularly the destroyed exergy. The exergy destruction percentage can be understood as a building environmental impact indicator.

To illustrate the main model concept and its operating suitability, an existing building was analyzed using the transient simulation software Trnsys. The modeling results show that around 95 % of the exergy used in the building is destroyed and that around 5 % is lost (transferred to the surroundings). This means that this building has a very high impact.

However, all the building's retrofit configurations bring exergy savings with respect to the actual configuration. The saving values range from -7.79% (Setting 2) to -50.97% (Setting 8). Looking at the building as an intrinsic exergy destroyer, we conclude that the building energy retrofit can be used to reduce its exergy demand.

In relation to the building design, the exergy approach leads to applying fueling solutions that use a low-exergy energy carrier or to improving the efficiency of the generation devices that use a high-exergy energy carrier. Moreover, the approach leads to a recommendation to install solar photovoltaic or thermal systems in order to take advantage of the electrical or thermal conversion of solar radiation incident on the building envelope. In general, the exergy approach enables building designers to assess their design choices from a perspective of exergy demand minimization, that is, from a perspective of system impact on the environment.

References

1. Romero JC, Linares P (2014) Exergy as a global energy sustainability indicator—a review of the state of the art. *Renew Sustain Energy Rev* 33:427–442
2. Simpson AP, Edwards CF (2011) An exergy-based framework for evaluating environmental impact. *Energy* 36:1442–1459
3. Caliskan H (2015) Novel approaches to exergy and economy based enhanced environmental analyses for energy systems. *Energy Convers Manag* 89:156–161
4. Baldi MG, Leoncini L (2014) Thermal exergy analysis of a building. *Energy Procedia* 62:723–732
5. Leoncini L (2014) Analisi degli scenari energetici europei e sviluppo di un criterio di valutazione exergetica del sistema edificio. PhD Thesis, Università degli Studi di Firenze
6. Baldi MG, Leoncini L (2015) Effect of reference state characteristics on the thermal exergy analysis of a building. *Energy Procedia* 83:177–186
7. Lohani SP, Schmidt D (2010) Comparison of energy and exergy analysis of fossil plant, ground and air source heat pump building heating system. *Renew Energy* 35:1275–1282
8. Yildiz A, Güngör A (2009) Energy and exergy analyses of space heating in buildings. *Appl Energy* 86:1939–1948

9. Hepbasli A (2012) Low exergy (LowEx) heating and cooling systems for sustainable buildings and societies. *Renew Sustain Energy Rev* 16:73–104
10. Torío H, Angelotti A, Schmidt D (2009) Exergy analysis of renewable energy-based climatisation systems for buildings: a critical view. *Energy Build* 41:248–271
11. ECBCS ANNEX 37 (2004) Heating and cooling with focus on increased energy efficiency and improved comfort. Guidebook to IEA ECBCS Annex 37 low exergy systems for heating and cooling of buildings
12. ECBCS ANNEX 49 (2011) Low exergy systems for high-performance buildings and communities—Annex 49 Final Report
13. Transient System Simulation Tool [Internet]. www.tmsys.com
14. Transsolar [Internet]. www.transsolar.com
15. Sketchup [Internet]. www.Sketchup.com
16. Office of Energy Efficiency & Renewable Energy [Internet]. <http://apps1.eere.energy.gov>
17. Balocco C, Papeschi S, Grazzini G, Basosi R (2004) Using exergy to analyze the sustainability of an urban area. *Ecol Econ* 48:231–244
18. Grazzini G, Balocco C (2000) Thermodynamic parameters for energy sustainability of urban areas. *Solar Energy* 69:351–356

Chapter 41

Light and Shadow: Mediterranean Visual Scenes

Judit Lopez-Besora and Helena Coch

Abstract Introducing sustainable criteria in the building sector is a challenge which can be faced using different strategies. The development and integration of renewable energies on different scales is part of the solution, but first the reduction of energy demand in buildings and cities must be taken into account. One of the potentials of the Mediterranean countries is the high radiation availability during most of the year, which can be used in active and passive design strategies. It is considered that urban and architectural design, along with significant knowledge of outdoor luminosity, can contribute to a reduction in the use of energy for lighting in entrance spaces. In this chapter, a field study conducted using different procedures enables an overall definition of the appearance of Mediterranean cities in terms of light, which offers an approach which could be applied to cities and architectural design. The conclusions drawn in this study can lead to design recommendations which integrate the use of shadow, the potential of material properties, and other ways to improve visual adaptation and reduce visual contrast, especially in the entrance of buildings.

Keywords Luminosity • Urban scene • Vision • Mediterranean light

1 Introduction

The need to introduce sustainable criteria in the building sector is currently a hot topic of discussion. Since the first reports warning about global warming, this sector has been one of the most influential because of its economic importance and its potential in energy use reduction. In fact, according to the United Nations Environment Programme [1], the building sector is responsible for more than one third of total energy use and, in most countries, it is the largest source of greenhouse gas emissions. In the European Union (EU), it represents approximately 40 % of final energy consumption.

A big part of this energy will be consumed during the life of a building and will be used mainly for heating, cooling and illumination. In that sense, architecture can

J. Lopez-Besora (✉) • H. Coch
Architecture and Energy, School of Architecture of Barcelona, UPC, Barcelona, Spain
e-mail: juditlb@yahoo.es; helena.coch@upc.edu

benefit from the free energy supplied by the main natural source, the sun. Energy can be provided by active systems, such as photovoltaic or solar panels, or through passive design strategies. One of the most immediate ways is the integration of daylight in buildings. On an urban scale, solar access depends on different aspects: the hours of daylight, the city configuration, the prevailing sky type and illumination on a horizontal surface. These parameters determine the light availability indoors [2], measured by the daylight factor, but also the visual appearance of the city. In this chapter we focus on the latter aspect.

In fact, it is possible to benefit from Mediterranean daylight in different ways depending on the circumstances. First of all, the hours of daylight are very balanced during most of the year. Secondly, the clear blue sky [3] is the most frequent sky type. Apart from this, as the radiation at latitudes from 30 to 45° reaches high values [4], and considering that 48 % of solar radiation lies in the visible part of the spectrum, surfaces shaping a given city are profusely lit. As a convention, it is considered that the illuminance value over a horizontal plane under direct sunlight is about 100,000 lx, but in the case of a vertical one [5], it depends in particular on urban density and the orientation of streets.

The density of an urban tissue is defined by the street section, which is the relation between the width of streets and the height of buildings. It shapes the obstructions and configuration of the urban visual scene, featured by the dimensional relation among three zones: Zone 1, with horizontal surfaces at the bottom (pavements); Zone 2, with vertical elements at the centre (façades); and Zone 3, with the sky vault at the top of the scene. In addition, the orientation determines the exposure to solar radiation in vertical planes, higher in the south and near southern orientations, and absent in the north. Radiation is related to the cosines of the angle between the sun beam and the surface. The luminosity of each zone and the whole scene depends on the geometrical parameters but also on materials and finishes.

The appearance of a city is a key factor in the Mediterranean zone because high levels of irradiation fall on surfaces, bringing about very bright scenes which establish the quality of vision and the indoor adaptation level. In temperate and hot climates, where clear skies predominate most of the year, the quality of vision in entrances depends largely on outdoor visual condition. Paradoxically, the strong flux of Mediterranean light must be compensated by high levels of artificial lighting in entrance spaces owing to the dark adaptation phenomenon. Because the entrance space links the exterior and interior environments, defined by different thermal, acoustic and visual conditions, an adaptation process takes place. In the case of vision, it takes several minutes for the process to complete. As shown by a dark adaptation graph, the cones take from 3 to 7 min on average to adapt, while rod adaptation can last as long as 40 min. The time spent in transitional spaces is not long enough for complete adaptation, but it is possible to improve vision using other strategies. As seen in Fig. 41.1, stretching out time would be a solution, but this is difficult to do. Also, the luminosity of outdoor scenes could be reduced to minimize the difference between both situations. However, the most extended solution takes the opposite approach, which is to increase the interior level of light by means of

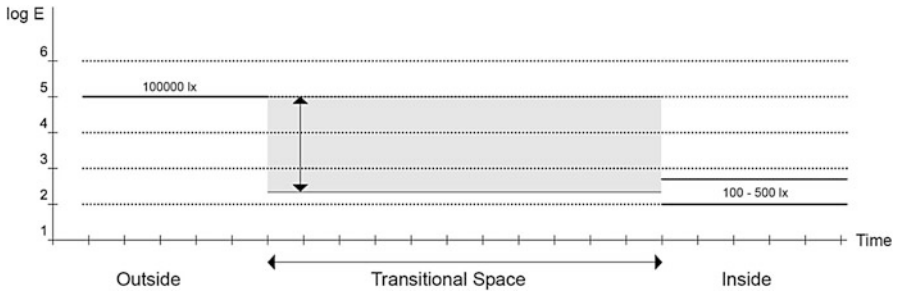


Fig. 41.1 Graph showing a time sequence from outside to inside a building and the $\log E$ during the path; reference illuminance values were taken to define the difference between both situations

more artificial lighting, even though there would be factually no need for an additional contribution of energy.

In this chapter, the definition of luminosity in urban visual scenes is underlined as a means to save energy in connection with lighting in the entrance of buildings. The key points in support of this statement are the potential of entry spaces, the power and distribution of solar light and the luminous analysis of the urban visual scene itself.

2 Methodology

With the aim of determining how bright the different zones in a scene are and comparing them with those from the interior, a series of measurements was taken in real environments in a geographical area next to the city of Tarragona (Spain). The measurements were made during summertime around noon so as to catch the major incidence of sun. During the field work the sky was clear blue. On the exterior, the measured values comprised horizontal and vertical illuminance (E_H , E_V) in sun and shadow points of Zones 1 and 2, as well as horizontal, vertical and sky luminance (L_H , L_V , L_S) in sun and shadow points of Zones 1–3. The total of the points comprised 147 measured values. In the interior, reference luminance and illuminance values from ceiling, walls and pavement were also measured. In this case, 111 points were assessed.

Apart from measurements, three luminance maps were made with HDR picture processing to graphically show the distribution of light within an urban visual scene. The pictures were taken with an 18 mm lens and processed by an online application [6]. The images correspond to a dense city configuration located in the old town of Tarragona and are not coincident with the measured environments.

3 Results and Discussion

The first thing noticed from the luminance maps of a dense urban tissue (Fig. 41.2) is that the distribution of luminosity in the scenes is divided into a dark zone in pavements and façades and a very bright zone in the sky. This is especially so in narrow streets if the direction of the sun beam is different from the main outline. When the sun position changes and it approaches the plot, the vertical and horizontal surfaces are directly flooded with light. It is remarkable that pavements and façades have a predominant position and proportion in the scene and within the visual field [7], while the sky has little presence in streets with this section. However, in more open configurations such as squares, the distribution of plans and luminosity is different, more balanced. In this case, the pavement receives direct light and its luminosity increases, while the façades are partially lit depending on their orientation.

The HDR luminance maps show a distribution of luminosity with indicative values of luminance. But the measurements taken in real environments give more information about the amount of light received and emitted by each surface. According to the illuminance measurements (E_H , E_V), shown in Fig. 41.3, the pavement zone (Zone 1) in sun receives more radiation than façades, as was expected. In addition, the values of E_H are very similar. However, illuminance levels on vertical surfaces (Zone 2) are lower and changeable for every façade orientation. As regard to the shadow points, most of them receive ten times less light than those in the sun. It is also noticed that some environments have shadows with higher illuminance levels than others. This is especially caused by the colour of the environment.

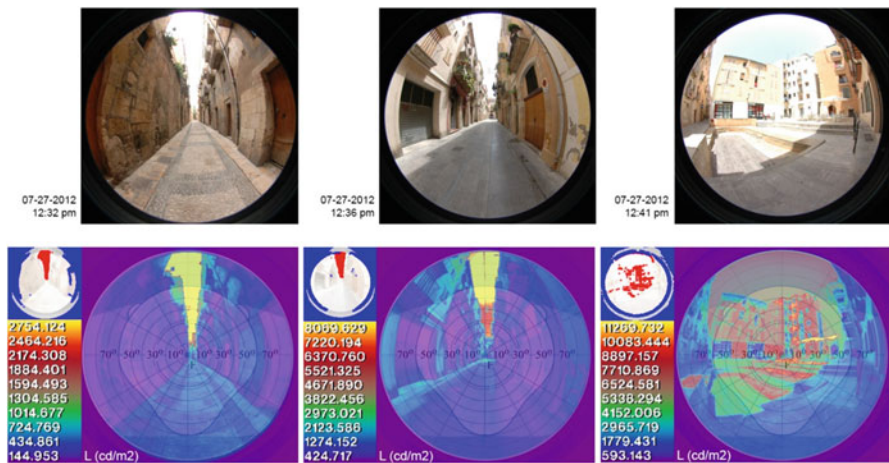


Fig. 41.2 Top: different street images from Tarragona (Spain); below: its corresponding luminance maps

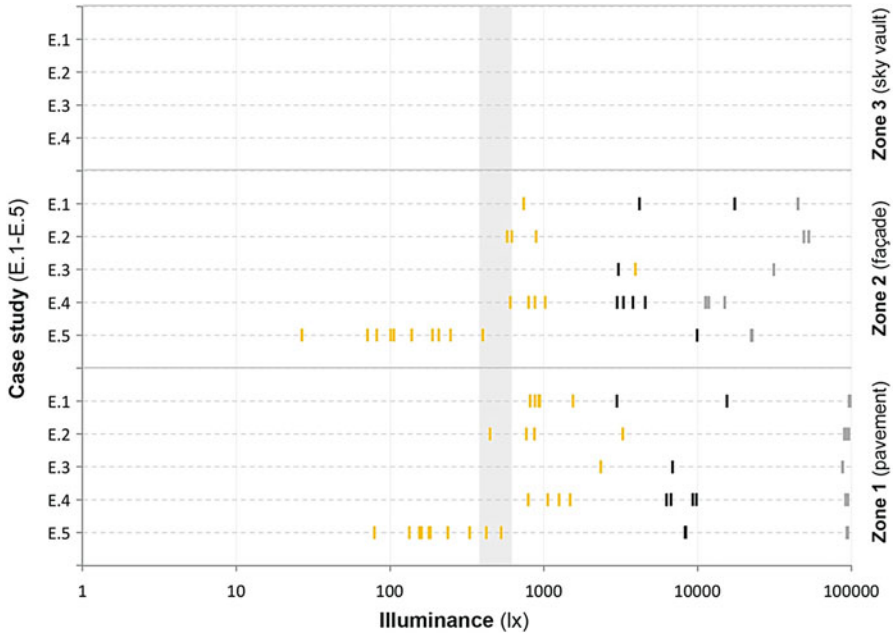


Fig. 41.3 Illuminance values measured in each zone of visual scene for case studies E.1–E.5; *yellow*: measurements taken inside, *black*: measurements taken outside in shade, *grey*: measurements taken outside in sun

The radiation received at a point is perceived as brightness related to different levels of luminance. In Fig. 41.4, the features of each zone can be distinguished. In Zone 1, there is a clear difference between sun and shadow points. As the incidence of light is almost the same for all of them, L_H reflects the material properties of the pavement. The Zone 3 has two groups of L_S : the higher ones correspond to sky luminance in points next to the upper part of the building, while the lower ones represent the shaded surfaces under porches and canopies, also located at the top of the visual scene. While the higher values corresponding to sky are very similar, the shadow points have different values of darkness, depending on the properties of the surrounding surfaces. But the most complex zone is Zone 2. The values of L_V in sun are quite different depending on the properties of materials and the angle of slant. While white façades can reach as high as 17,000 cd/m^2 , the coloured ones do not exceed 3000 cd/m^2 as often. The shadow points remain under 1000 cd/m^2 with some exceptions, depending on the reflectivity of the surrounding surfaces.

As a whole, it can be deduced that, under high radiation conditions, the luminosity at the top and bottom of the visual scene is quite uniform with similar values, even though the pavement is more luminous on average than the sky and its proportion in the scene is greater than of the other zones. The central part of the visual scene, coincident with the most sensitive part of the human visual field [7],

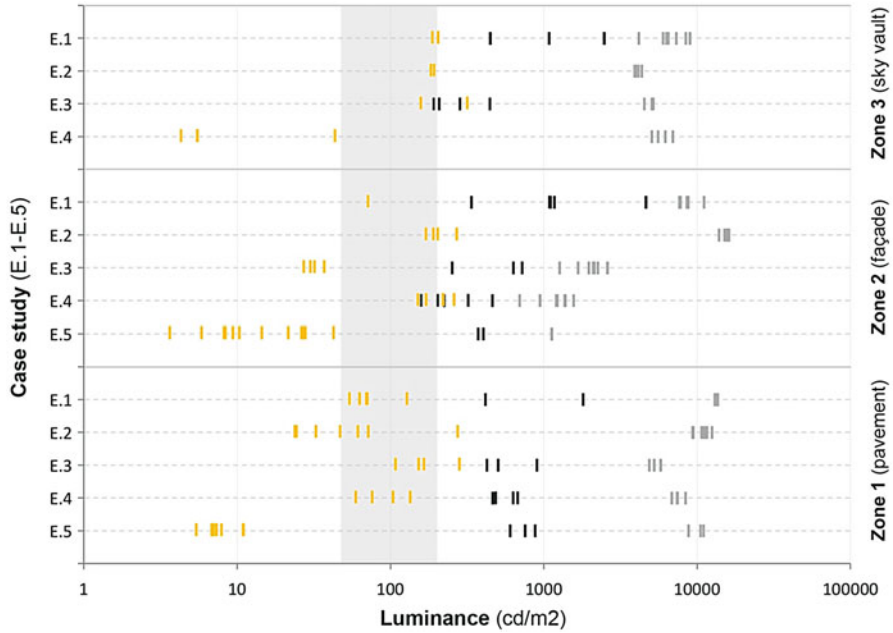


Fig. 41.4 Luminance values measured in each zone of visual scene for case studies E.1–E.5; *yellow*: measurements taken inside, *black*: measurements taken outside in shade, *grey*: measurements taken outside in sun

shows the highest and lowest values of luminance. The amplitude of values turns out to be wider than in the other zones, which signifies that it is a high-contrast zone, with luminosity at shadow points similar to those in the interior and very bright surfaces if the orientation and sun conditions are conducive to that.

If we compare the exterior values with the measurements taken in the entrance spaces, it can be seen that the difference between the outdoor and indoor scenes can be as large as two logarithmic units. Nevertheless, the higher values inside are very similar to the lower values outside. Therefore, it can be deduced that the use of shadow in the immediate surroundings of the building can contribute to minimizing the brightness difference between both situations. According to the dark adaptation graph, if the difference had been more than two logarithmic units, then approximately 10 min would have been required to visually adapt to the situation inside, but if the gap were reduced to the minimum, vision inside would improve considerably.

4 Conclusions

Measurements carried out in real environments offer a generic view of the appearance of Mediterranean cities. In this climate, it is conditioned by the availability of daylight, city configurations and materials used in building surfaces, which are often painted in white. The strong daylight creates very bright surroundings which contrast with interior spaces. Each part of this environment has a different importance in the visual scene, especially pavements and façades, more so than the sky vault or the ceiling. In that sense, the luminosity of pavements and façades determines the quality of vision in the entrance point. In these spaces, much artificial lighting must be provided to compensate dark adaptation, but there are other solutions for reducing energy demand. The design of shade elements just before entrances, which reduce the outdoor luminosity, can improve vision in the interior because luminance values are near those from inside. Although the shade elements can cause a reduction in indoor daylight, this reduction is compensated by better vision using a balanced distribution of light and adequate performance.

But, as was demonstrated by the measurements, shadows have different levels of darkness. In high reflective environments, shadows are even brighter than some coloured façades in the sun. On the other hand, when coloured façades are shaded, there is less contrast between light and shadow. This must be taken into account when designing shade zones.

Apart from this, using local light on pavements and façades contributes to a better perception of space and improves orientation in space. Also, material properties can be used to produce higher values of spatial brightness and prevent dark adaptation. These strategies contribute to optimizing the use of energy for artificial lighting in environments where a natural light source is available most of the time.

References

1. Submission of the United Nations Environment Program (UNEP) (2009) Sustainable building initiative (SBCI) to the ad hoc working group on long-term cooperative action under the convention (AWG-LCA), 24 April 2009
2. Tregenza PR (1995) Mean daylight illuminance in rooms facing sunlit streets. *Build Environ* 30 (1):83–89
3. ISO (2004) 15469:2004 (E)/CIES011/E: 2003. Spatial distribution of daylight—CIE Standard General Sky. ISO, Geneva
4. Baker NV, Fanchiotti A, Steemers K (1993) *Daylighting in architecture: a European reference book*. James & James, London
5. Li HW, Cheung GHW, Cheung KL, Lam NTT (2010) Determination of vertical daylight illuminance under non-overcast sky conditions. *Build Environ* 45:498–508
6. <http://www.jaloxa.eu/webhdr/index.shtml>
7. Panero J, Zelnik M (2007) Las dimensiones humanas en los espacios interiores. Gustavo Gili

Chapter 42

Potential of Solar Electricity for Grid-Connected Systems in Algeria

L. Hassaine and A. Mraoui

Abstract This chapter proposes a photovoltaic (PV) electricity potential for grid-connected systems in Algeria using a solar radiation database and a system model of a PV module and inverter. The solar radiation database is based on the PV Geographic Information System (PVGIS). The database was used to analyze solar energy resources and to determinate the PV potential in Algeria. Climatic parameters (irradiation and temperature) and technological parameters (inverter efficiency) are the most influential parameters for PV production systems. Using the database input data, many calculations were carried out to determine the PV production and identify the influential parameters. Therefore, a map of the PV electricity potential for grid-connected systems in Algeria was developed, and the expected power production for planned PV grid-connected installations was determined.

Keywords Solar potential • Model • Inverted • Grid connected

1 Introduction

It is known worldwide that renewable energy sources have a fundamental role to play in the resolution of energy-related and environmental problems on a global scale. It is also indisputable that the potential of solar energy is far higher than that of any other renewable source. In recent years the use of solar energy has increased significantly, with the growth rate constantly increasing; it is 39% for photovoltaic (PV) [1].

Algeria has great potential regarding the use of solar energy; the received solar energy on horizontal surfaces in the country is approximately 1700 kWh/m²/year in the north and 2263 kWh/m²/year in the south of the country [2, 3]. The use of

L. Hassaine (✉) • A. Mraoui
Centre de Développement des Energies Renouvelables (CDER),
BP 62 Route de l'Observatoire, Bouzaréah, Algiers 16340, Algeria
e-mail: l.hassaine@cderr.dz

PV energy in particular is limited to few applications, such as city street lighting, monitoring stations, and a few telecommunication stations in remote areas. However, the generation of solar electricity from PV will penetrate the energy market, where clear and stable policy commitments have been made. The number of PV installations will undergo significant growth, mainly owing to governments and utility companies that support programs that focus on grid-connected PV systems by producing 40 % of electricity needs in 2020 and export more than 2000 MW of renewable energy by 2020 and more than 10,000 MW in 2030.

Photovoltaic technology is still not fully appreciated in Algeria, one of the main reasons being a lack of understanding of its potential. Without an accurate database and knowledge of the most appropriate locations for renewable energy applications in the country, investment in renewable energy will not be efficient and profitable. It can be made so by creating energy-potential maps. The geographical analysis of the availability of the primary solar energy resource makes it possible to determine the PV electricity potential and improve our knowledge of the potential PV contribution to future energy needs and economic structures. Developing potential maps for a country means creating illustrations revealing the geographical distribution of solar electrical power covering that specific region. A solar PV electrical map demonstrates energy potentials and provides information that is useful for selecting the optimum site selection a solar PV energy system.

Solar insolation data sets are expensive to collect, and few meteorological stations record such data [4]. Approaches used to determine solar radiation over large geographic regions often derive spatial databases of solar radiation using different interpolation techniques (spline functions) [5, 6] or calculate solar irradiance directly from meteorological geostationary satellites [7]. Some solar radiation and climatology databases that extend beyond the national level and offer free online access include the European Solar Radiation Data [8, 9] and NASA's Surface meteorology and Solar Energy (SSE) [10]. Maps for Africa and selected developing countries were created thanks to funding from the European Commission and the United Nations Environment Programme, respectively [11].

The HelioClim database exhibits good performance with a small scattering of data compared to ground measurements (smaller standard deviations) [12, 13]. The results strongly depend on sites and their surrounding terrain configurations [14]. The accuracy of the HelioClim database has been assessed by comparisons with measurements of the World Meteorological Organization (WMO) radiometric network in Europe (55 sites) and Africa (35 sites) for the period 1994–1997. The root-mean-square error of monthly averages of daily irradiation is 600 Wh/m^2 , and the bias is 24 Wh/m^2 [8]. Using 12 ground stations in Africa [15], the measured global horizontal radiation was compared with HelioClim data. The authors found that the surface solar irradiance over the African continent had an average standard deviation of 21 % and a negligible bias [16] and that the HelioClim databases reproduce well the daily solar irradiation at ground level, as well as its day-to-day variations. In North Africa, the root-mean-square deviation is small, approximately 360 Wh/m^2 ; the performances of HelioClim are much better in this region, likely because of the very frequent clear sky conditions [17, 18]; the accuracy of

HelioClim was observed to be very satisfactory for the monthly variations in daily solar irradiation in Sahel sites, while in forest sites the variations in received irradiation do not fit the measurements.

To estimate the solar potential electricity injected into the grid, the performance ratio (PR) factor of a PV system [19] is a crucial parameter for performance evaluation. It summarizes the deviation from standard test conditions (STCs) [20], the various losses due to the equipment of the system (e.g., inverters, cables), and the effect of other external factors (e.g., radiation incidence angle, temperature, soiling). In [21] the PR is calculated using an analytical method. To make this possible, it is necessary to have detailed data on, for example, the solar radiation on the module surface, solar spectrum, incidence angle of radiation, ambient temperature, cell temperature, and inverter operation. For long-term evaluations (typically when annual PV production is considered for investment planning) mean values of the PR can be adopted. Generally, these can vary between 70 and 80 % for PV systems installed in Europe. In [22], a system PR using a typical value for a roof-mounted system with modules from mono- or polycrystalline silicon is considered to be around 0.75. These estimation methods can provide rough results that do not consider the actual characteristics and operating conditions such as modules, temperature coefficient, and ambient temperature.

The aim of this chapter is to provide an analysis of national and regional differences in solar electricity generation from PV systems. We take into account PV systems with flat modules mounted at optimally tilted positions, which maximizes the electrical energy produced. We looked at the generated kilowatt-hours from a typical PV system because this information can be directly used in economic and environmental assessments. Although this analysis focuses on Algeria, the data and maps cover the whole country. We explore annual electricity generation, the potential of PV electricity generation, and the potential of PV electricity injected into the grid taking into account the actual system characteristics, operating conditions, and material parameters (inverter losses).

2 Solar Radiation Resource

Sizing solar energy systems and analyzing the performance of such systems require information on solar radiation at Earth's surface. The measurement of solar radiation flux is made only at meteorological stations. When data are not available, it is necessary to estimate solar radiation fluxes using theoretical models. Many investigations have been carried out to estimate the global solar radiation flux on a horizontal surface [23]. In addition, several meteorological databases are available. These databases can be used to estimate the solar radiation flux at Earth's surface.

In [24], five different meteorological databases were studied – PVGIS, satellite, NASA, Atlas Solar Radiation, and Meteonorm – and they show the annual irradiation on horizontal surfaces for each database. Additionally, the yearly energy PV

production was calculated using TRNSYS, assuming that the PV installation was connected to the grid with no failures.

Also, according to [24], regarding the irradiation on a horizontal surface, nonnegligible differences may be observed between the databases; the minimum value is achieved with PVGIS and the maximum value is given by the NASA database. This difference of 10.6%/year has a direct impact on annual PV production. Thus, it is important for any PV designer to take into account that the choice of one database or another may yield significant differences in the predicted energy output [24].

The PVGIS [25] solar radiation database was used for an assessment of the potential solar electricity generation by PV modules mounted at optimal inclination. The spatial resolution of the resulting grid data layers is $1^\circ \times 1^\circ$. The primary database represents the period 1981–1990 and contains 12 monthly averages and the yearly average of the following climatic parameters:

- Global irradiation on a horizontal surface,
- Diffuse horizontal irradiation,
- Ambient temperature.

The available data are sufficient to simulate the solar energy received by the considered PV grid-connected technology [21] (Fig. 42.1).

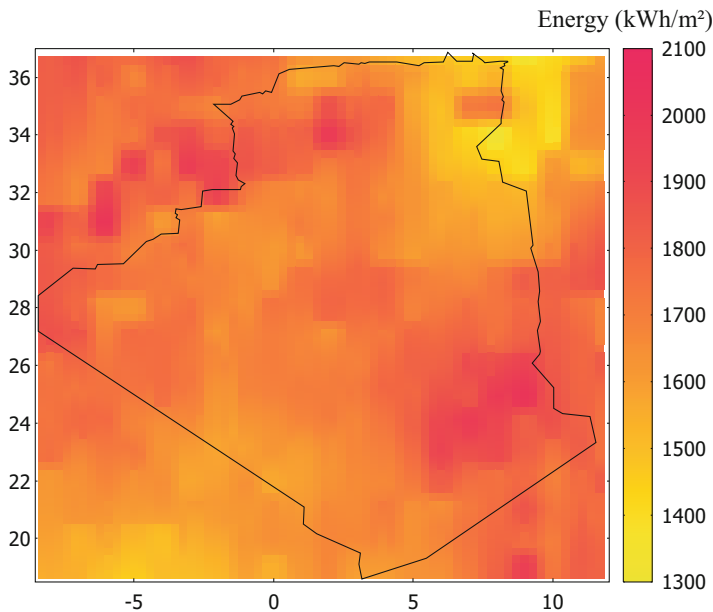


Fig. 42.1 Annual global horizontal irradiation (“JRC’s Institute for Energy and Transport – PVGIS – European Commission,” 2015)

3 Description of Production System

To estimate the PV potential and the PV electricity injected into the grid, different methods can be used [22, 26]. The proposed method is based on a detailed system modeling of a PV module and inverter. Real characteristics, operating conditions, and material parameters (e.g., inverter losses, parasitic losses, shutdowns) are considered.

3.1 Photovoltaic Module

The model used to calculate the PV produced electric power is based on a five-parameter equivalent circuit model, expressed by the equation

$$I = I_L - I_o \left[e^{\frac{V+IR_s}{m}} - 1 \right] - \frac{V + IR_s}{R_{sh}}, \quad (42.1)$$

where $m = N_s n_1 k T_c / q$.

The method proposed in [27] is used; it evaluates the PV system performances and the electric energy produced by the PV generator. With this model it is possible to extrapolate the performance of a PV generator to any condition using information provided by the manufacturer under standard rating conditions (1000 W/m², 25 °C). To extract the reference parameters, the following equations are used:

$$I_{sc,ref} = I_{L,ref} - I_{o,ref} \left[e^{\frac{I_{sc,ref} R_{s,ref}}{m_{ref}}} - 1 \right] - \frac{I_{sc,ref} R_{s,ref}}{R_{sh,ref}}. \quad (42.2)$$

For open-circuit voltage, $I = 0$, $V = V_{oc,ref}$:

$$0 = I_{L,ref} - I_{o,ref} \left[e^{\frac{V_{oc,ref}}{m_{ref}}} - 1 \right] - \frac{V_{oc,ref}}{R_{sh,ref}}. \quad (42.3)$$

At the maximum power point $I = I_{mp,ref}$, $V = V_{mp,ref}$:

$$I_{mp,ref} = I_{L,ref} - I_{o,ref} \left[e^{\frac{V_{mp,ref} + I_{mp,ref} R_{s,ref}}{m_{ref}}} - 1 \right] - \frac{V_{mp,ref} + I_{mp,ref} R_{s,ref}}{R_{sh,ref}}. \quad (42.4)$$

The derivative with respect to power at the maximum power point is zero:

$$\left. \frac{d(IV)}{dV} \right|_{mp} = I_{mp} + V_{mp} \left. \frac{dI}{dV} \right|_{mp} = 0, \quad (42.5)$$

where dI/dV with respect to power at the maximum power point is given by

$$\left. \frac{dI}{dV} \right|_{mp} = \frac{\frac{-I_o}{m} e^{\frac{V_{mp} + I_{mp} R_s}{m}} - \frac{1}{R_{sh}}}{1 + \frac{I_o R_s}{m} e^{\frac{V_{mp} + I_{mp} R_s}{m}} + \frac{R_s}{R_{sh}}}. \quad (42.6)$$

To calculate the parameter in any operating condition, the model equations are as follow:

The modified ideality factor is a linear function of cell temperature:

$$\frac{m}{m_{ref}} = \frac{T_c}{T_{c,ref}}. \quad (42.7)$$

Messenger and Ventre [28] present an equation for the diode theory. For a diode reverse saturation current, I_o , their equation at the new operating temperature is given by

$$\frac{I_o}{I_{o,ref}} = \left[\frac{T_c}{T_{c,ref}} \right]^3 \exp \left[\frac{1}{k} \left(\left. \frac{E_g}{T} \right|_{T_{c,ref}} - \frac{E_g}{T} \right) \right]. \quad (42.8)$$

E_g denotes a small temperature dependence that, for silicon, can be represented as indicated by Eq. (42.9), where

$$E_{g,T_{ref}} = 1.121 \text{ eV}, \quad (42.9)$$

$$\frac{E_g}{E_{g,T_{ref}}} = 1 - 0.0002677(T - T_{ref}). \quad (42.10)$$

The temperature coefficient $\alpha_{I_{sc}}$ is given by the manufacturer, so the light current is

$$I_L = I_{L,ref} + \alpha_{I_{sc}}(T_c - T_{c,ref}). \quad (42.11)$$

A detailed method to calculate the maximum power delivered by a PV panel under any climatic conditions can be found in [27].

3.2 Description of Simulated Solar Photovoltaic System

In this study, a PV panel is considered to be inclined at a fixed angle, and to extract the maximum power delivered by the system, a maximum power point tracking (MPPT) device is used. Thus, for each fixed tilt angle varying from 0 to 90° with a step of 1°, simulations are carried out to calculate the received solar radiation and the produced electrical energy. The characteristics of the used PV module are given in Table 42.1. Single-point MPPT efficiency was considered, having a 90 % DC/DC conversion efficiency.

Table 42.1 Parameters given by the manufacturer used in simulations

Parameter	Value at reference conditions (1000 W/m ² 25 °C)
Short-circuit current	2.91 A
Open-circuit voltage	43.2 V
Current at maximum power	2.8 A
Voltage at maximum power	34 V
Single-panel area	0.898 m ²
Temperature coefficient	0.000451/°C
Generator area	10.776 m ²

3.3 Photovoltaic Generator Production

According to the study reported in [24], the tested panels should deliver a PV power output $\pm 10\%$ under STCs. However, real operating conditions are dynamic owing to temperature, wind speed, and radiation fluctuations. Hence, to compare the real nominal power of the panels, the measured PV power data must be corrected [20] to account for the difference between the real operating conditions and the STCs. The PV output was evaluated, and the real PV performance under quasi-STCs was quantified. Among the experimental data, the power measurements within an irradiance band of 950–1050 W/m² were analyzed for time intervals close to the solar midday (± 2 h) and under clear skies. The power was corrected using the following equation, valid for crystalline silicon panels [29]:

$$P_{\text{mp,corr}} = \frac{P_{\text{mp,measured}}}{1 - 0.0035(T_c - 25) \frac{G_{\text{eff}}}{1000}}, \quad (42.12)$$

where

$P_{\text{mp,corr}}$: corrected power,

$P_{\text{mp,measured}}$: measured power.

The temperature factor can vary between -0.003 and -0.005 ($^{\circ}\text{C}^{-1}$).

4 Inverter Output Power

The inverter model developed in [30] was used to simulate the performance of the PV generator. It was developed using real monitoring of an inverter installed on the *Centre de Développement des Energies Renouvelables* site. This model is based on the empirical performance model inverter presented in [31]. The standard error obtained between measured and modeled inverter efficiency was typically about 0.1 %.

Table 42.2 Values used in performance model inverter

Variable	Value
P_{aco} (W)	2692
P_{dco} (W)	2900
V_{dco} (V)	275.6
P_{so} (W)	25
C_o (W ⁻¹)	-6.67×10^{-5}
C_1 (V ⁻¹)	-0.00296
C_2 (V ⁻¹)	-0.00458
C_3 (V ⁻¹)	0.0255

The AC output power of the inverter, $P_{AC,sim}$, is defined by the following equation:

$$P_{AC,sim} = \left[\left(\frac{P_{aco}}{A-B} \right) - C(A-B) \right] (P_{dc} - B) + C(P_{dc} - B)^2, \quad (42.13)$$

where P_{aco} is the maximum AC output power for the inverter under reference or nominal rating conditions, P_{dc} is the DC power at the inverter input, and parameters A , B , and C are given by the following equations:

$$A = P_{dco}[1 + C_1(V_{DCsim} - V_{dco})], \quad (42.14)$$

$$B = P_{so}[1 + C_2(V_{DCsim} - V_{dco})], \quad (42.15)$$

$$C = C_o[1 + C_3(V_{DCsim} - V_{dco})], \quad (42.16)$$

where V_{DCsim} is the DC voltage at the inverter input, V_{dco} and P_{dco} are respectively the DC voltage and power input at which the AC-power rating is achieved at the reference rating condition, P_{so} is the DC power required at the inverter input to start working properly, and C_1 , C_2 , and C_3 are empirical coefficients to adjust the P_{AC} (P_{DC}) characteristic of the inverter (Table 42.2).

Replacing the $P_{mp, measured}$ (42.13) by $P_{AC,sim}$ the real PV performance connected to the grid $P_{mp, grid}$ can be expressed by

$$P_{mp, grid} = \frac{\left[\left(\frac{P_{aco}}{A-B} \right) - C(A-B) \right] (P_{dc} - B) + C(P_{dc} - B)^2}{1 - 0.0035(T_c - 25) \frac{G_{eff}}{1000}}. \quad (42.17)$$

This equation is used for simulated PV power output for grid-connected systems, which predict to obtain solar electricity map.

5 Estimation of Solar Electricity Potential

The electrical energy produced by a solar cell at any time instant depends on its intrinsic properties and the incoming solar radiation. The algorithm adopted in this work, as described previously, was validated by many works in the field.

PV power generating systems can be divided into independent PV systems and grid-connected PV systems and further subdivided according to the installation environment. Standalone PV systems are called off-grid PV systems. Their applications include rural household power supply, rural central power plants, and power supply for communication, cathodic protection, and lighting. Small and medium-sized standalone PV systems and large systems have been extensively used. Grid-connected PV systems include building-integrated PV systems and terrestrial PV systems. At the scale of the entire interconnected electric power grid, generated electric power must be consumed within milliseconds of being generated. In addition, when the load on the utility grid reaches new peak levels, the system operators must start activating every available generating source.

Figure 42.2 shows the off-grid PV potential of Algeria. The map was obtained by calculating the electricity production of a PV system using the model described earlier. The potential of Algeria varies from 0.46 to 0.62 kWh/m²/day, where the lowest potential is in the northeastern region of the country and the highest potential is in the southeastern region.

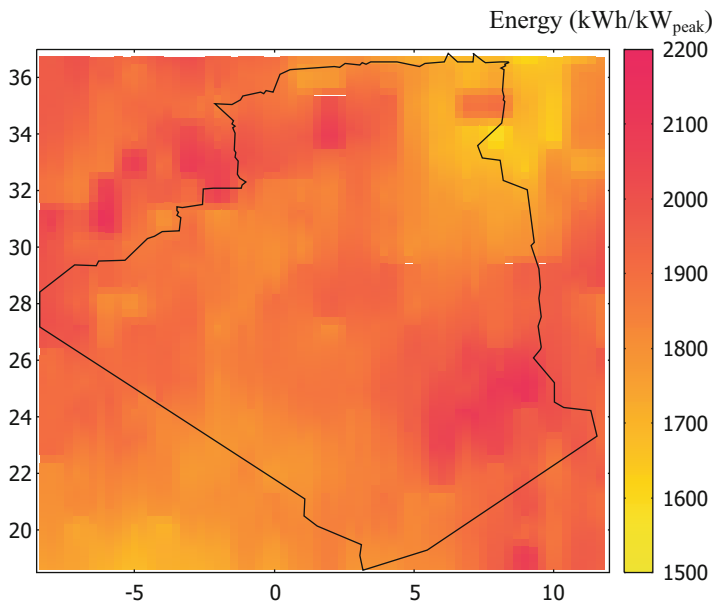


Fig. 42.2 Potential of PV electricity in Algeria

The major elements of a grid-connected PV system do not include storage. The inverter may simply fix the voltage at which the array operates or (more commonly) use a MPPT function to identify the best operating voltage for the array. The inverter operates in phase with the grid (unity power factor) and generally delivers as much power as it can to the electric power grid given the available sunlight and temperature conditions. The inverter acts as a current source; it produces a sinusoidal output current but does not act to regulate its terminal voltage in any way. The utility connection can be made by connection to a circuit breaker on a distribution panel or by a service tap between the distribution panel and the utility meter. Either way, the PV generation reduces the power taken from the utility power grid and may provide a net flow of power to the utility power grid if the interconnection rules permit.

Figure 42.3 represents the potential of grid-connected electrical power. The potential varies from 0.35 to 0.60 kWh/m²/day, with the lowest value in the northeast and the highest in the southeast. The efficiency of the inverter therefore varies from 95 to 75 % depending on the region, mainly influenced by climatic conditions.

Algeria is committed to renewable energy to provide comprehensive and sustainable solutions to environmental challenges and issues of energy conservation related to sources of fossil origin. This strategic choice is motivated by the immense potential of solar energy. This energy is the major focus of a program dedicated to solar PV. The electric power produced by solar energy is expected to reach over 37 % of the national electricity production by 2030.

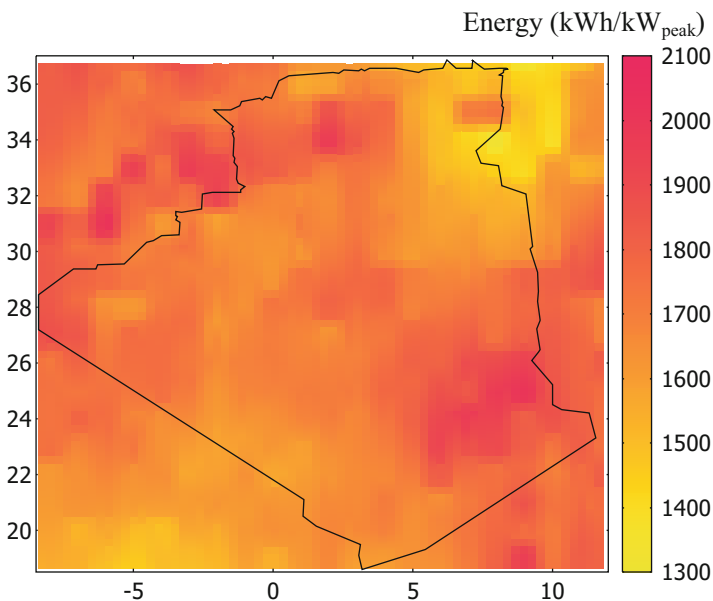


Fig. 42.3 Potential electricity fed to grid in Algeria

Table 42.3 Expected power production by 2021 for planned PV grid-connected projects in Algeria

Site	Latitude	Longitude	Power (MWp)	Area (ha)	Potential (kWh/kW _{peak})	Production (TWh/year)
A. Oussara	35.4	2.9	26	18.57	1755	34.62
Adrar	27.9	-0.3	20	14.29	0.51	26.38
Aflou	34.3	3.3	21	15	1859	29.34
Ain Defla	36.1	2.2	15	10.71	1583	17.93
Aoulef	27	1.1	10	7.14	0.49	12.7
Biskra	34.9	5.7	25	17.86	1480	27.97
Boussaâda	35.2	4.2	25	17.86	1790	33.73
Djelfa	34.7	3.3	20	14.29	1790	27.3
El Bayadh	32.6	1	25	17.86	1652	31.2
Ghardaia	32.6	3.7	20	14.29	1721	26
H. Messaoud	31.7	6.1	23	16.43	1583	27.52
Kabertene	28.4	-0.1	3	2.14	0.51	3.96
Laghouat	33.8	2.9	20	14.29	1859	27.94
Mascara	35.4	0.2	25	17.86	1721	32.31
Medea	36.3	2.8	20	14.29	1687	25.35
M'ghair	33.9	5.9	28	20	1480	31.65
M'sila	35.7	4.5	25	17.86	1618	30.52
Naama	33.2	-0.8	20	14.29	1859	28.01
Ouargla	31.9	5.4	25	17.86	1618	30.8
Oum Bouaghi	35.9	7.1	10	7.14	1480	11.12
Reggane	27	1.1	10	7.14	0.49	12.7
S. Belabbes	35.2	-0.6	25	17.86	1721	32.86
Saida	34.8	0.2	25	17.86	1721	32.31
Setif	36.2	5.4	25	17.86	1549	29.25
Tebessa	35.4	8.1	20	14.29	1721	26.26
Tiaret	34.9	1.6	20	14.29	1859	28.16
Timimoun	29.3	0.2	10	7.14	0.47	12.33
Tissemsilt	35.8	1.9	26	18.57	1583	31.09
Tolga	34.7	5.4	20	14.29	1549	23.64
Touggourt	33.1	6.1	25	17.86	1480	28.09

The Algerian government plans to launch several solar PV projects with a total capacity of approximately 800 MWp by 2020. Other projects with a capacity of 200 MWp/year should be launched during the period 2021–2030. In Table 42.3 power production calculated for planned PV grid-connected projects is summarized.

6 Conclusion

In this work, PV power output for grid-connected systems at different sites in Algeria was determined using Algeria's solar radiation resource, the PV potential, and an inverter output power model; the results obtained provide useful information for the design engineering of PV systems.

The developed maps can be used for the assessment, evaluation, and ranking of sites of PV power plant projects, giving project developers, governments, and other decision makers a well-founded basis for planning and designing the build-out of PV power capacity in Algeria. Maps were created and potential sites for the implementation of large-scale PV power plants identified.

The main conclusion of this study is that there is indeed a huge potential for PV in the country and that the potential sites are principally located in the southern region.

To draw up a roadmap for the implementation of the technology in this country, further studies are necessary; specific sites will have to be assessed in detail, and existing technologies will have to be adapted to local situations.

References

1. Zervos A (2014) Renewables 2014 global status report. In: Renewable energy policy network for the 21st century, Paris
2. Stambouli AB (2011) Promotion of renewable energies in Algeria: strategies and perspectives. *Renew Sustain Energy Rev* 15:1169–1181. doi:[10.1016/j.rser.2010.11.017](https://doi.org/10.1016/j.rser.2010.11.017)
3. Yaiche MR, Bouhanik A, Bekkouche SMA, Malek A, Benouaz T (2014) Revised solar maps of Algeria based on sunshine duration. *Energy Convers Manag* 82:114–123. doi:[10.1016/j.enconman.2014.02.063](https://doi.org/10.1016/j.enconman.2014.02.063)
4. McKenney DW, Pelland S, Poissant Y, Morris R, Hutchinson M, Papadopol P, Lawrence K, Campbell K (2008) Spatial insolation models for photovoltaic energy in Canada. *Sol Energy* 82:1049–1061
5. D'Agostino V, Zelenka A (1992) Supplementing solar radiation network data by co-Kriging with satellite images. *Int J Climatol* 12:749–761
6. Remund J (2008) Quality of Meteornorm Version 6.0. Europe 6
7. Cros S, Albuissou M, Lefevre M, Rigollier C, Wald L (2004) HelioClim: a long-term database on solar radiation for Europe and Africa. In: Eurosun 2004. PSE GmbH, Freiburg, pp 916–920
8. Huld T, Suri M, Dunlop E, Albuissou M, Wald L (2005) Integration of HelioClim-1 database into PV-GIS to estimate solar electricity potential in Africa. In: Proceedings of 20th European photovoltaic solar energy conference
9. SoDa—Free time-series of solar radiation data [WWW Document] (2015) http://www.soda-is.com/eng/services/services_radiation_free_eng.php. Accessed 18 Mar 2015
10. Surface meteorology and Solar Energy [WWW Document] (2015) <https://eosweb.larc.nasa.gov/sse/>. Accessed 18 Mar 2015
11. Nguyen HT, Pearce JM (2010) Estimating potential photovoltaic yield with r. sun and the open source geographical resources analysis support system. *Sol Energy* 84:831–843
12. Wahab MA, El-Metwally M, Hassan R, Lefevre M, Oumbe A, Wald L (2010) Assessing surface solar irradiance and its long-term variations in the northern Africa desert climate using Meteosat images. *Int J Remote Sens* 31:261–280

13. Wahab MA, El-Metwally M, Hassan R, Lefevre M, Oumbe A, Wald L (2009) Assessing surface solar irradiance in Northern Africa desert climate and its long-term variations from Meteosat images. *Int J Remote Sens* 31:261–280
14. Haurant P, Muselli M, Pillot B, Oberti P (2012) Disaggregation of satellite derived irradiance maps: evaluation of the process and application to Corsica. *Sol Energy* 86:3168–3182
15. Ineichen P (2006) Comparison of eight clear sky broadband models against 16 independent data banks. *Sol Energy* 80:468–478. doi:10.1016/j.solener.2005.04.018
16. Wald L, Blanc P, Lefevre M, Gschwind B (2011) The performances of the HelioClim databases in Mozambique. *ISES Solar World Congress 2011:268–275*
17. Blanc P, Gschwind B, Lefèvre M, Wald L (2011) The HelioClim project: surface solar irradiance data for climate applications. *Remote Sens* 3:343–361
18. Njomo D, Wald L (2007) Solar irradiation retrieval in Cameroon from Meteosat satellite imagery using the Heliosat-2 method. *ISESCO Sci Technol Vis* 2:19–24
19. I.E.C. Standard (1998) International Standard IEC 61724: photovoltaic system performance monitoring. Guidelines for measurements, data exchange and analysis. IEC
20. I.E.C. Standard (2007) 60904-3, Photovoltaic devices—part 3: measurement principles for terrestrial photovoltaic (PV) solar devices with reference spectral irradiance data. International Electrotechnical Commission, Geneva
21. Aste N, Del Pero C, Leonforte F, Manfren M (2013) A simplified model for the estimation of energy production of PV systems. *Energy* 59:503–512. doi:10.1016/j.energy.2013.07.004
22. Šúri M, Huld TA, Dunlop ED, Ossenbrink HA (2007) Potential of solar electricity generation in the European Union member states and candidate countries. *Sol Energy* 81:1295–1305
23. Saffaripour MH, Mehrabian MA, Bazatgan H (2013) Predicting solar radiation fluxes for solar energy system applications. *Int. J. Environ. Sci. Technol.* 10:761–768
24. Quesada B, Sánchez C, Cañada J, Royo R, Payá J (2011) Experimental results and simulation with TRNSYS of a 7.2 kWp grid-connected photovoltaic system. *Appl Energy* 88:1772–1783. doi:10.1016/j.apenergy.2010.12.011
25. JRC's Institute for Energy and Transport—PVGIS—European Commission [WWW Document] (2015) <http://re.jrc.ec.europa.eu/pvgis/>. Accessed 18 Mar 2015
26. Gastli A, Charabi Y (2010) Solar electricity prospects in Oman using GIS-based solar radiation maps. *Renew Sustain Energy Rev* 14:790–797. doi:10.1016/j.rser.2009.08.018
27. De Soto W, Klein SA, Beckman WA (2006) Improvement and validation of a model for photovoltaic array performance. *Sol Energy* 80:78–88. doi:10.1016/j.solener.2005.06.010
28. Messenger RA, Ventre J (2010) *Photovoltaic systems engineering*. CRC, Boca Raton
29. Osterwald CR (1986) Translation of device performance measurements to reference conditions. *Sol Cells* 18:269–279
30. Chouder A, Silvestre S, Taghezouit B, Karatepe E (2013) Monitoring, modelling and simulation of PV systems using LabVIEW. *Sol Energy* 91:337–349. doi:10.1016/j.solener.2012.09.016
31. King DL, Gonzalez S, Galbraith GM, Boyson WE (2007) Performance model for grid-connected photovoltaic inverters (No. SAND2007-5036)

Chapter 43

Thermal Energy Recovery System for Upgrading Waste Heat by an Absorption Heat Pump

Yoshinori Itaya

Abstract An innovative absorption heat pump (AHP) system is proposed to increase the temperature from waste heat to a level of 80 °C and to produce hot air over 120 °C for drying or simultaneously generating steam of 100–115 °C. Air is heated up directly by heat exchange in the absorber working in the heating mode of a LiBr/H₂O AHP system. Steam is sequentially produced by heat exchange, with the absorption solution still maintaining a high temperature. An examination was carried out continuously to evaluate the performance of a bench-scale of the AHP. In the proposed AHP, the temperature of hot air at the outlet of the absorber was typically above 120 °C and, steam up to 115 °C was simultaneously generated by recovering the heat of the hot water at 80 °C. The coefficient of performance, defined by the ratio of heat generated to the power consumed for pumps of fluid flow, exceeded 20. It was also found that the fine particle slurry of LiBr crystals is formed stably in the solution under a supersaturation condition when zeolite powder is suspended. Then an almost saturated concentration is maintained as a result of the dissolution of the crystal, even if the solution is diluted by absorption of water vapor in the absorber. The theoretical analysis based on a heat and mass transfer model predicted that the output power of the AHP improved by almost 100 % compared with the conventional solution at concentrations lower than saturation solubility. Measurement of the slurry properties and an experiment on the absorption performance of the slurry were carried out, and the effectiveness of the slurry was confirmed. This chapter reviews a series of works done by the present author.

Keywords Absorption heat pump • Heating mode • Exhaust heat recovery • LiBr crystal slurry • Hot air • Steam

Y. Itaya (✉)

Environmental and Renewable Energy Systems Division, Graduate School of Engineering,
Gifu University, Gifu 501-1193, Japan
e-mail: yitaya@gifu-u.ac.jp

1 Introduction

Several industries exhaust a large amount of thermal energy at temperatures lower than 100 °C. The recovery of such low-grade thermal energy can be a promising candidate to reduce consumption of fossil fuels as well as to mitigate greenhouse gas emissions. An absorption heat pump (AHP) is one useful technology for working in a refrigeration mode by heat without using a compressor [1–4]. An AHP was also recently used to generate steam or raise temperatures by recovering waste heat [5, 6].

A novel steam generation system has been proposed to recover waste hot water at a temperature of 80 °C and to yield steam at temperatures higher than 150 °C using a water-zeolite adsorption heat pump [7]. Performance is evaluated here in a bench-scaled system [8]. This system introduces direct contact of water to zeolite to yield high-temperature compressed steam in a steam-generation step as well as direct drying of zeolite with a hot air stream in a bed to reduce the desorption time as a result of efficient heating in a regeneration step. Then dry air hotter than 120 °C is required to sufficiently regenerate zeolite saturated with water.

The present author and his group proposed a combined system to produce hot air over 120 °C and steam by recovering heat of warm water at 80 °C level. In this work, a lithium bromide/water (LiBr/water) AHP was used, and a bench scale of the AHP equipment was examined to evaluate simultaneous hot air generation over 120 °C and steam yield.

On the other hand, it is known that the performance of an AHP is enhanced if the solution is condensed to a higher concentration. However, too high a concentration of the solution may result in blockage in flow lines of the solution owing to crystallization. Thus the concentration of the solution should be limited at a low level that never yields crystals. In the past several additives were evaluated [9, 10]. Itaya et al. [11, 12] also proposed a method to form a fine-particle slurry of LiBr crystal and evaluated the effectiveness of the slurry to improve absorption performance in a LiBr/water AHP. It was found that the fine-particle slurry of LiBr crystals is formed stably in the solution under supersaturation conditions. Then an almost saturated concentration is maintained when the crystal is dissolved in the solution even if the solution absorbs water vapor in the absorber. The AHP performance was predicted by a theoretical analysis based on a heat and mass transfer model. In addition, an experiment absorbing water vapor in a laboratory scale of batch absorber was carried out.

In this chapter, an outline of a series of these researches is presented to introduce an innovative AHP system for the purpose of conserving energy through the recovery of low-grade waste heat.

2 Absorption Heat Pump System Generating Hot Air and Steam [13, 14]

An AHP system is proposed to recover exhaust heat at a level of 80 °C or heat of warm water heated by solar heaters and to yield simultaneously hot air and steam over 120 °C. This AHP technology is applicable also to systems recovering heating energy for drying and hydrothermal treatment from conventionally exhausted heat. The performance of the AHP system was examined by a bench-scale system.

2.1 Bench-Scale AHP Setup

Figure 43.1 shows an outline of the bench-scale AHP system studied in the present work [13]. Air is heated up directly by heat exchange in the absorber working in the heating mode of a LiBr/H₂O AHP system. The main structure of the present AHP system is composed of evaporators, an absorber, a regenerator, and a condenser. A heat exchanger with spiral type tubes is used in the AHP system. A film of the solution flowing down along the inside wall of the vertical spiral tubes is formed in the absorber to absorb water vapor from the evaporator. In the evaporator, vapor is evaporated on a pure water film flowing on the inside wall of the tubes whose outside wall is heated by hot water flowing at 80 °C among the tube bundle. Then the solution is heated up while flowing down as it gains exothermic dilution heat of the solution and latent heat by water vapor absorption. Air streams in counterflow

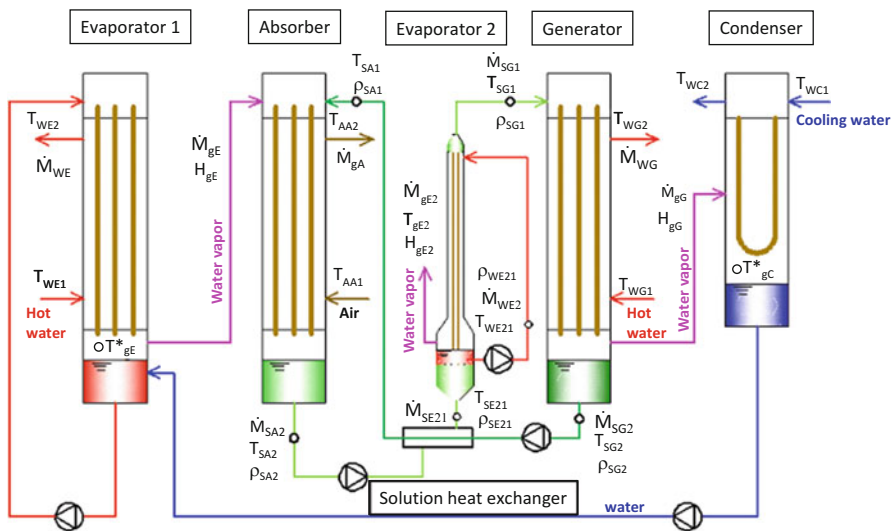
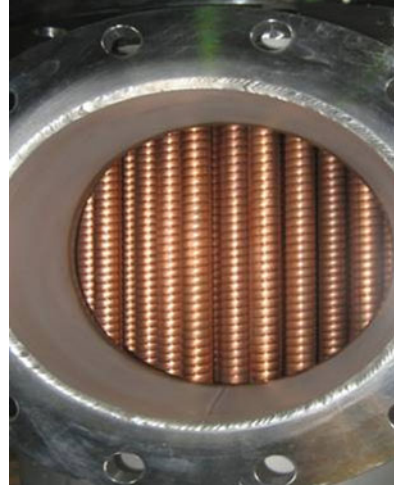


Fig. 43.1 Outline of experimental apparatus

Fig. 43.2 Heat transfer spiral tubes used in absorber



around the tubes in the absorber as seen in Fig. 43.2, and heat exchange takes place to heat up the air through the tubes from the solution. In the generator, the absorbent solution flows down, forming a film on the inside wall of the tubes, and is heated by hot water at 80 °C, which flows around the tubes. The solution is condensed while flowing down by evaporation of water vapor in the generator. The evaporated water vapor transfers into the condenser and is condensed on the surface of the tubes cooled by water fed into the inside. The water in the condenser is returned to the evaporator. An examination is carried out continuously to evaluate the performance of the AHP.

2.2 Performance of Bench-Scale AHP System

Figure 43.3 shows the transient behavior of the outlet temperature of hot air heated in the absorber of the AHP. The mass flow rates of hot water supplied to the evaporator and cooling water to the condenser were fixed at 9.9 and 7.2 kg/s, respectively. Inlet temperatures of the hot water and the cooling water are also drawn in the figure. The outlet temperature of air in the absorber was heated to over 120 °C without significantly affecting the mass flow rate of air fed in the range of 0.08–0.5 kg/s. The air temperature was affected rather by hot water temperature in the evaporator and reached 130 °C when the hot water temperature rose only by 5 °C. An examination was performed on simultaneous hot air heating and steam generation. Figure 43.4 shows the transient temperatures in the absorber and evaporator 2 of the AHP. Hot air of 80 °C at the inlet was heated to 125 °C in the absorber, and saturated steam at 100 °C was simultaneously generated under atmospheric pressure in evaporator 1. When steam generation was regulated at 0.0025 kg/s, the temperature reached 115 °C while the hot air temperature was maintained at 125 °C.

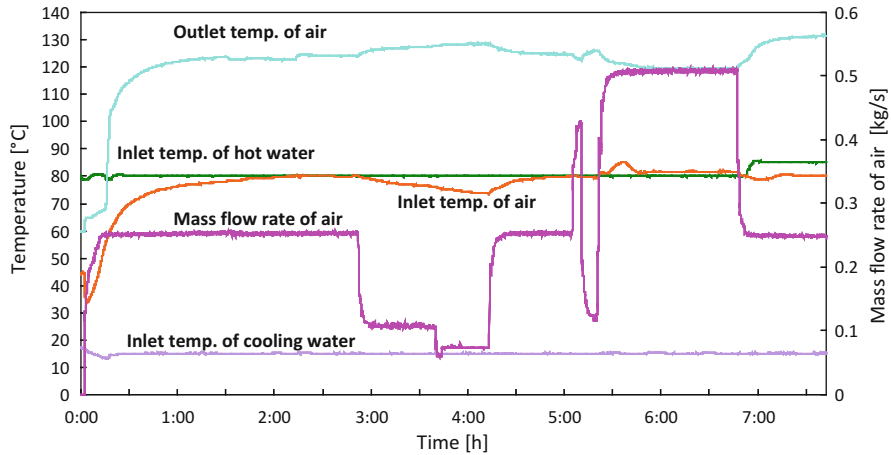


Fig. 43.3 Time behavior of temperature in absorber of AHP (hot water mass flow rate: 9.9 kg/s, cooling water mass flow rate: 7.2 kg/s)

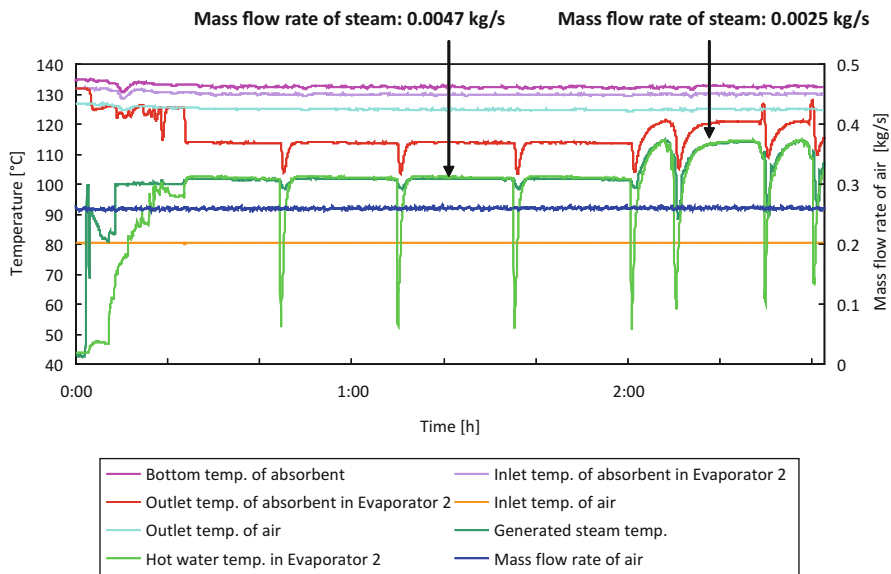


Fig. 43.4 Time behaviors of temperature in absorber and evaporator 2 of AHP (inlet hot water temperature: 80 °C, hot water mass flow rate: 9.9 kg/s; inlet cooling water temperature: 15 °C, cooling water mass flow rate: 7.2 kg/s)

Fig. 43.5 Effect of generated steam temperature on COP (airflow rate: 0.25 kg/s)

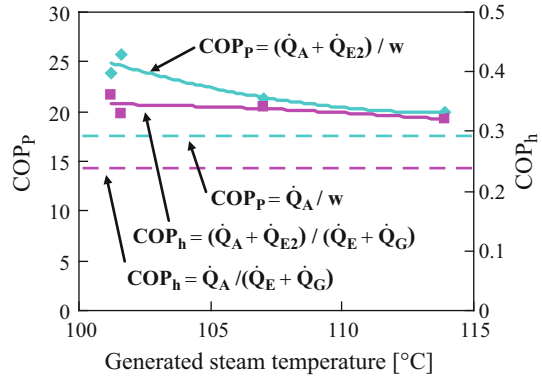


Figure 43.5 shows the influence of steam generation temperature on the coefficient of performance (COP). Two types of COP were defined here:

$$\text{COP}_h = (\dot{Q}_A + \dot{Q}_{E2}) / (\dot{Q}_E + \dot{Q}_G), \quad (43.1)$$

$$\text{COP}_p = (\dot{Q}_A + \dot{Q}_{E2}) / w, \quad (43.2)$$

where w is the pump power for the flow of fluids. Both heat transfer rates are given with reference to the variables in Fig. 43.1:

$$\dot{Q}_A = C_{PA} \dot{M}_{gA} (T_{AA2} - T_{AA1}), \quad (43.3)$$

$$\dot{Q}_E = C_{PW} \dot{M}_{WE} (T_{WE1} - T_{WE2}), \quad (43.4)$$

$$\dot{Q}_{E2} = \dot{M}_{gE2} (H_{gE2} - H_{WE2}), \quad (43.5)$$

$$\dot{Q}_G = C_{PW} \dot{M}_{WC} (T_{WG1} - T_{WG2}). \quad (43.6)$$

COP_h is the heat efficiency to the total input of heat into the system, while COP_p is the coefficient of performance based on the pump power. COP_p for only hot air obtained without steam generation under the same operation condition was 17, while the combination with steam generation resulted in an improved COP_p , over 20, although the magnitude was reduced with an elevation of steam temperature. These results imply that this AHP system may be applicable to air heaters for drying or heating, for example, and steam generators recovering exhaust heat under 80 °C.

3 LiBr Crystal Fine-Particle Slurry for High-Performance AHP [11, 12, 15]

The present author and his group proposed to disperse a fine powder of adsorbent like activated carbon or zeolite into the LiBr/H₂O solution. The adsorbent acts as an adsorber of LiBr in the solution slurry. The amount of equilibrium adsorption of a

soluble component, i.e., lithium bromide here, is dependent on the concentration in the solution. The adsorbed component is desorbed and reduction of the concentration is relaxed even if the solution absorbs water vapor. As a result, the researchers found analytically an improvement of the AHP performance [11]. In this progress, they noticed additionally that the fine-particle slurry of a LiBr crystal could be formed in the solution when the suspension of the solution and the adsorbent powder reached a supersaturation state of the soluble salt [12]. If this phenomenon is applied to the absorbent of LiBr/water AHP, it will make it possible to operate the AHP in as high a concentration as the supersaturation state beyond the solubility of LiBr without causing blockage due to crystal growth. The properties of the LiBr crystal fine-particle slurry were measured, and the effectiveness for improving absorption performance in the LiBr/water AHP is evaluated.

3.1 Preparation of Slurry Samples

The sample of the LiBr solution slurry was prepared by the following procedure. Lithium bromide reagent (purity >99 %) (Sigma-Aldrich, St. Louis, MO) was first dissolved in deionized water. Then the temperature of the solution increased to about 80 °C by the generation of dissolution heat. The solution of 63.4 % LiBr concentration was cooled by stirring after adding and suspending zeolite powder (HSZ-320-NAA, Tosoh Co., Tokyo, Japan) whose weight ratio to the solution was 5.56 %. Fine particles of LiBr crystal began generating in the solution, and slurry was formed (Fig. 43.6a) when the concentration reached a supersaturation state. On the other hand, a large lump of the crystal was grown as seen in Fig. 43.6b, unless any zeolite powder was suspended.

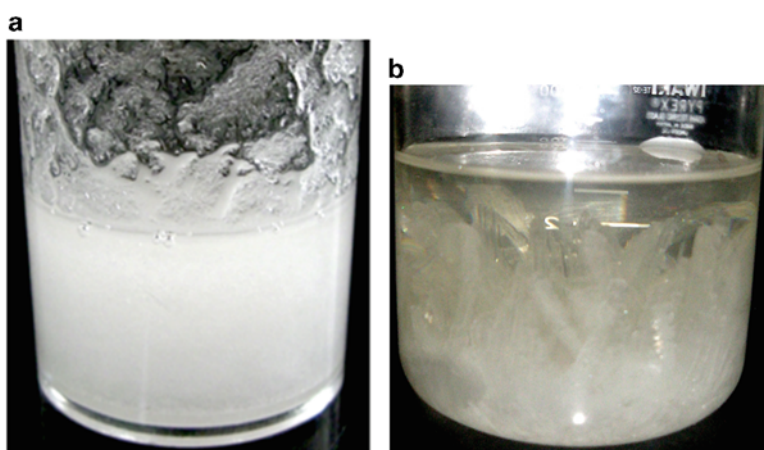


Fig. 43.6 LiBr fine-particle slurry and crystal lump grown in solution. (a) Fine-particle slurry of LiBr. (b) LiBr crystal lump grown

3.2 Measurement of Properties

The particle-size distribution and viscosity were measured as properties of the slurry prepared as described earlier. The size distribution was determined at a temperature of 25 °C by laser diffraction/scattering type of particle size analyzer (LA-920, Horiba, Kyoto, Japan). The viscosity of the slurry was measured using a rotational viscometer (HAAKE, VT550, Thermo Scientific, Yokohama, Japan). The amount of LiBr crystal was varied by controlling the temperature of the slurry.

The particle size distribution of the LiBr crystal in the slurry sample is shown in Fig. 43.7. The solid and dashed lines represent the distribution of the LiBr crystal particles and the zeolite, respectively. The size of the crystal particles was distributed in a range of 10–200 and 2–10 μm for zeolite, and only a small fraction of the crystal particles was observed in the size overlapping with the zeolite. The results seem to suggest that the crystal is generated around particles of zeolite by acting as a seed of nucleus in a supersaturation state. The median size of the crystal particles is estimated to be 7.45 μm , and it is supposed that the crystal grows uniformly around each particle of zeolite whose median size is 7.09 μm . This estimated size was too small to compare with the measurements seen in Fig. 43.7. This means that the coalescence of some particles might occur in the progress of crystal growth or that the crystal could not be grown uniformly in a continuous solid free of any pore or gap. However, the size would be sufficiently small to handle the slurry without causing blockage of the solution stream during the operation.

Figure 43.8 shows the viscosity of the slurry against the amount of LiBr crystal. The viscosities of pure water at 20 °C and LiBr solution of 63.4 % in concentration at 50 °C (free from LiBr crystal) are also compared in the graph. The solution containing no particles was six times as viscous as water, and the

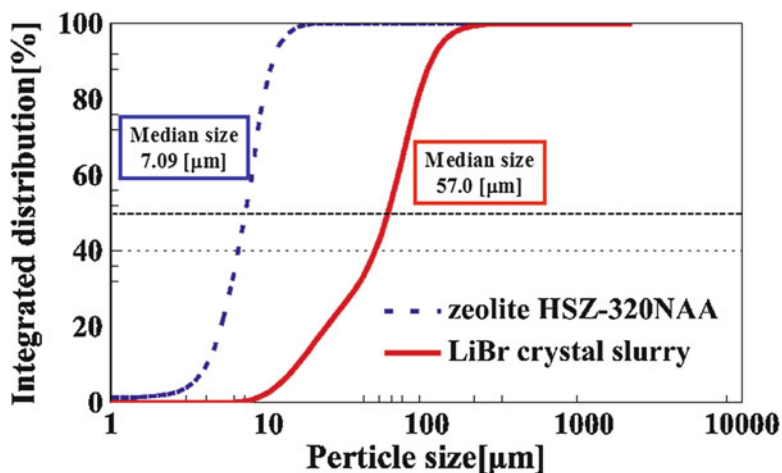


Fig. 43.7 Particle-size distribution of LiBr crystal in slurry and zeolite

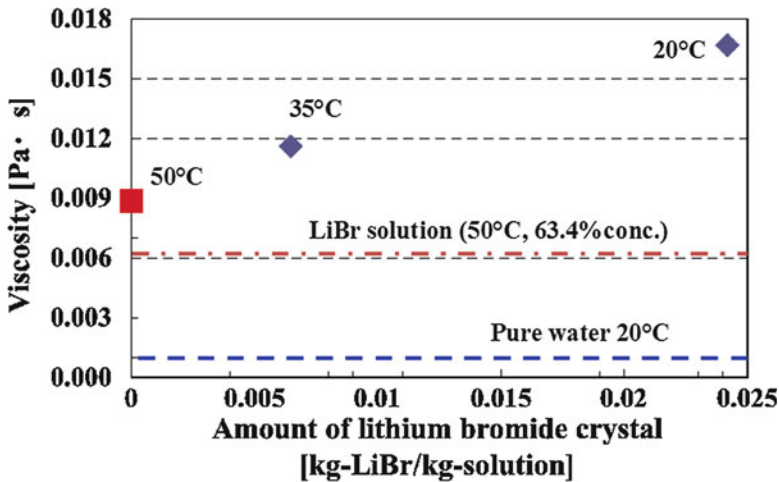


Fig. 43.8 Viscosity of slurry in different contents of LiBr crystal particles

viscosity of the solution was raised additionally 1.5 times owing to the suspension of only the zeolite. When the temperature of the solution containing zeolite drops to 35 and 20 °C, a slurry of LiBr crystal particles is formed and the viscosity increases to almost twice as much at 35 °C and 2.8 times at 20 °C of the original solution with no solid particles. The slurry was confirmed to retain sufficient fluidity in the range of the present level of fine particle contents and temperatures in the slurry.

3.3 Analysis by Modeling on Vapor Absorption Performance in Slurry

An analysis was performed to fundamentally evaluate AHP performance in the case where the fine-particle slurry of LiBr crystal is used as the absorption solution. We considered the case where the slurry flows down in a film on a heat transfer wall cooled by water flowing upward and absorbs water vapor evaporated in an evaporator, as shown by the outline of the model drawn in Fig. 43.9. The slurry was modeled so as to absorb vapor while maintaining a constant concentration in a film flowing down on the heat transfer wall through the test section.

Figure 43.10 shows the absorption rate of water vapor against the surface area of the heat transfer wall in the absorber. The absorption rate is defined by the rate absorbed in the test section from the inlet to the specified surface area. It was assumed that a sufficient LiBr crystal exists in the slurry. The analytical results on the solution/zeolite suspension without crystal particles and the only homogeneous solution are also compared in the figure. The inlet LiBr concentration was set at 64%. The absorption rate in the slurry is almost double that in the homogeneous solution

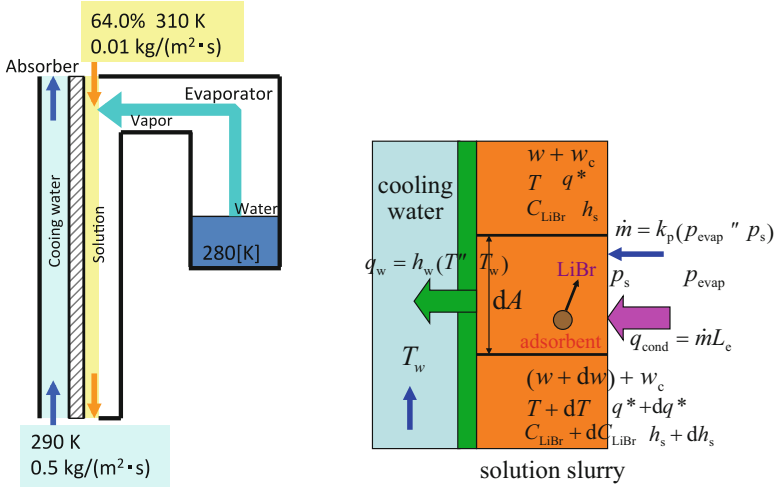
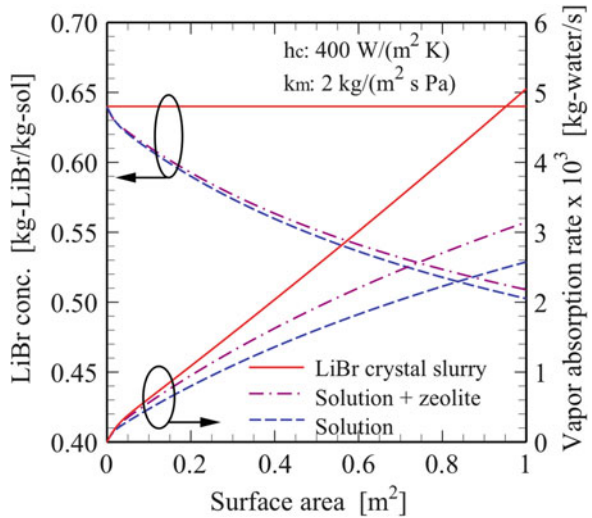


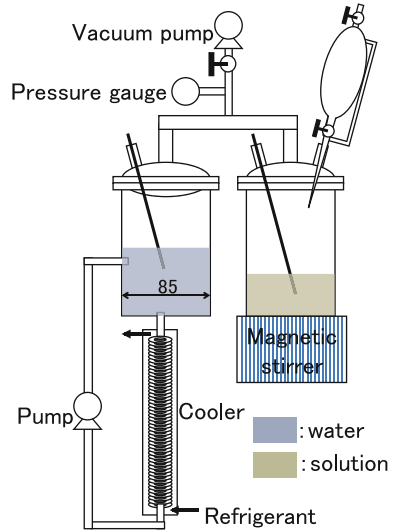
Fig. 43.9 Outlines of absorber in AHP and analytical model

Fig. 43.10 Particle-size distribution of zeolite and LiBr crystal in slurry



with no particles when the surface area of the solution film is 1 m² while that in the solution/zeolite suspension is 20%. The result implies that the performance of the AHP can be greatly enhanced owing to the effect of the excellent hygroscopic power of the solution preserved at high concentration by dissolution of the LiBr crystal if the slurry is used [12].

Fig. 43.11 Experimental setup for evaluation of vapor absorption performance in slurry



3.4 Lab-Scale Examination of Vapor Absorption into Slurry in Absorber

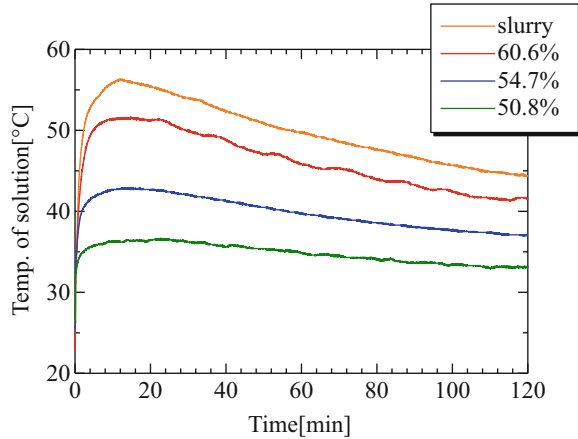
The vapor absorption performance in the slurry and the homogeneous solutions was examined in a lab-scale batch type of experimental setup (Fig. 43.11). The water temperature in the evaporator was maintained constant by circulating water through the cooler. The LiBr slurry was stored in the reservoir preliminarily. The temperature in the absorber was measured as soon as the slurry was transferred to the absorber from the reservoir. The same examination was performed for the samples of the homogeneous solution prepared in different concentrations [15].

Transient temperatures of the solution or the slurry in the absorber are plotted against the time from the beginning of the examination in Fig. 43.12. The rising rate of the temperature in the absorber and the peak temperature become greater at higher concentrations in the solution and reach their maximum in the slurry among the samples examined. The vapor absorption rate in the slurry was estimated from the temperature rising rate to be twice that in the homogeneous solution with 60.6 % concentration.

4 Conclusions

A thermal energy recovery system was proposed to upgrade waste heat by an innovative LiBr/water AHP. The results obtained are summarized as follows:

Fig. 43.12 Transient temperature behavior of solution in absorber



1. The bench scale of the AHP system was shown to heat air to over 120 °C for drying and to yield simultaneously steam at 100 °C from the exhaust heat at temperatures lower than 80 °C.
2. The COP of the system in heat-up mode exceeded 20.
3. Fine particles of LiBr crystal were generated in a supersaturation state beyond solubility if fine powder of zeolite was suspended in the solution.
4. The size of the crystal fine particles in the slurry was distributed in a range of 10–200 μm, and the viscosity of the slurry was 2.8 times of the solution with no particles, that is, maintaining sufficient fluidity.
5. The absorption rate of water vapor in the absorber or the output of the AHP was enhanced significantly up to 100 %, as high as that of the only solution used in the evaluation based on the proposed model.
6. The model was verified by a laboratory-size scale of a vapor absorption experiment, and a comparison was made between the slurry and the homogeneous solution.

Acknowledgment The author acknowledges the support of the New Energy and Industrial Technology Development Organization (NEDO) in Japan for part of this research by the Research and Development Program for Innovative Energy-Efficiency Technology.

References

1. Florides GA, Kalogirou SA, Tassou SA, Wrobel LC (2003) Design and construction of a LiBr-water absorption machine. *Energy Convers Manag* 44:2483–2508
2. Sun DW (1997) Thermodynamic design data and optimum design maps for absorption refrigeration system. *Appl Therm Eng* 17:211–221
3. Herold KE, Radermacher R, Klein SA (1996) Adsorption chillers and heat pumps. CRC, Boca Raton

4. Sencan A, Yakut KA, Kalogirou SA (2000) Exergy analysis of lithium bromide/water absorption systems. *Renew Energy* 30:645–657
5. Grossman G, Childs KW (1983) Computer simulation of a lithium bromide-water absorption heat pump for temperature boosting. *ASHRAE Trans* 89-1:240–248
6. Fujii T (2010) Development activities of low temperature waste heat recovery appliances using absorption heat pumps. In: International symposium on next-generation air conditioning and refrigeration technology, Tokyo, 17–19 Feb 2010
7. Kawakami Y, Abe Y, Ito K, Marumo K, Aoyama T, Tanino M, Nakaso K, Nakagawa T, Itaya Y, Fukai J (2013) Development of bench-scaled adsorption type steam recovery system for generating high temperature steam from hot waste water. In: 2013 AIChE annual meeting, San Francisco, 3–8 Nov 2013
8. Nakaso K, Nakashima K, Tanaka Y, Iwama Y, Fukai J (2013) Study on performance of the novel steam generation system using water-zeolite pair. In: 2013 AIChE annual meeting, San Francisco, 3–8 Nov 2013
9. Donate M, Rodriguez L, De Lucas A, Rodriguez JF (2006) Thermodynamic evaluation of new absorbent mixtures of lithium bromide and organic salts for absorption refrigeration machines. *Int J Refrig* 29:30–35
10. Nakoryakov VE, Grigoryeva NI, Bufetov NS, Dekhtyar RA (2008) Heat and mass transfer intensification at steam absorption by surfactant additives. *Int J Heat Mass Transfer* 51:5175–5181
11. Itaya Y, Ichihashi N, Kobayashi N (2010) Effect of solution/absorbent slurry on absorption heat pump performance. *Kagaku Kogaku Ronbunshu* 36-5:505–511
12. Itaya Y, Ichihashi N, Kobayashi N, Marumo K, Masui T (2013) Enhancement of LiBr-water absorption heat pump performance by supersaturated fine crystal slurry. *Kagaku Kogaku Ronbunshu* 39-1:46–52
13. Marumo K, Kobayashi N, Itaya Y (2014) Development of lithium bromide-water absorption heat pump system for simultaneous production of heated-up air and steam from waste heat. In: Tenth international conference on heat transfer, fluid mechanics and thermodynamics (HEFAT2014), Orlando, 14–26 July 2014
14. Marumo K, Kobayashi N, Nakagawa T, Fukai J, Itaya Y (2016) Lithium bromide/water absorption heat pump for simultaneous production of heated air and steam from waste heat. *J Chem Eng Jpn* 49(3):268–273
15. Itaya Y, Marumo K, Masui T, Nagatani K, Takanao S, Kobayashi N (2016) Formation and vapor absorption characteristics of a LiBr crystal fine-particle slurry. *J Chem Eng Japan*, to be published

Chapter 44

Mathematical Model for System Planning on Campus: A Case Study in Harbin Institute of Technology in China

Rong Guo and Tong Wu

Abstract Addressing the relationship between limited resources and a growing population is a hot issue during the process of urbanization. Effective utilization of rainwater plays a positive role in a low-carbon strategy. The purpose of this study is to present an application of mathematical analytical tools for urban planners in predicting rainwater runoff before constructing. Based on available data and a practical investigation in the study area (Harbin Institute of Technology), this study classifies the area into four parts according to the different runoff coefficients and then evaluates the volume of runoff based on the data of average volume of rainfall and evaporation capacity using mathematical analytical tools. The results show the minimum volume of water reservoirs in a single area. This research will contribute to an understanding of the role played by water resources in low-carbon-precinct buildings in the scientific planning of runoff treatment systems.

Keywords Mathematical analysis • Runoff treatment system • Low-carbon campus

1 Introduction

With the rapid process of industrialization and urbanization in China, population growth and consumption infrastructure upgrades, as well as urban construction, place great pressure on energy resources. With extensive development, land use, and water consumption, the ability to save energy and reduce greenhouse gas emissions is greatly hindered. In the process of urban construction, it is important that cities build green infrastructure reasonably and cost-effectively to become low-carbon cities. As campus water use is the basic unit of water resource

R. Guo (✉) • T. Wu

School of Architecture, Harbin Institute of Technology, No. 66 Xidazhi Street,
Nangang District, Harbin, China
e-mail: hitgr@sina.com

utilization, the effective use of water resources in the process of planning has great significance for the construction of a low-carbon city.

Because of the Harbin Institute of Technology's area and climate, it has a small green area, high building density, and large rainfall surface runoff and faces challenges associated with rainwater collection and utilization. This study took the campus of Harbin Institute of Technology as the research object and investigated water resources, energy, solid carbon, and other aspects of planning that typically have significance for the future development of a campus.

2 Method

2.1 Study Area

The Harbin Institute of Technology campus consists of three parts: the main campus, a science park, and a second campus. The area and population on the main campus are the largest. Therefore, this chapter selects the campus as the research object. As shown in Fig. 44.1, the campus of the Harbin Institute of Technology is located in the western part of Nangang district, Harbin, in north-eastern China. Harbin's natural geographical coordinates are longitude $125^{\circ}42'$ – $130^{\circ}10'$ and latitude $44^{\circ}04'$ – $46^{\circ}40'$. The campus area is 66.79 ha.



Fig. 44.1 location of Harbin Institute of Technology

2.2 *Mathematical Analysis*

Surface runoff is formed after rainfall infiltration and evaporation. The runoff coefficient shows the impact of the entire underlying surface on the rainfall runoff process. Therefore, quantitative analysis is divided into the following steps. First, based on the catchment zone of the study area and different runoff coefficients, a formula is used without consideration for surface runoff evaporation. Then, based on the formula, a calculation is made to determine the evaporation of surface runoff. Finally, based on a certain return period of rainfall intensity calculated in different areas, the minimum capacity of rainwater collection facilities is obtained.

2.2.1 **Catchment Area and Runoff Coefficient**

1. *Catchment area*: According to the terrain and slope direction, and the flow of water potential, the research area is divided into four regions. Figure 44.2 is a schematic diagram of the planning and zoning of the campus runoff process system. Each region is calculated according to the partition of the catchment area of land type, as shown in Table 44.1.
2. *Runoff coefficient*: Referring to the numerical standards given by the “outdoor drainage design specifications” and “building and residential rainwater utilization engineering technology,” the increase in the green area shows an enhancement of the permeability of materials, and the flow coefficient of each subcatchment area on the campus of the Harbin Institute of Technology is shown in Table 44.2.

2.2.2 **Related Hydrological Information**

1. *Rainfall*: According to the relevant data, the average annual rainfall in Harbin is 524.4 mm, the precipitation in the flood season accounts for 77.4 % of the total, in February and October the precipitation is 9.5 % of the total, and in March it is 13.1 % of the total. Table 44.3 summarizes the average annual rainfall in Harbin.
2. *Evaporation*: According to hydrological sector statistics, the city’s average annual evaporation is 504.6 mm, and the maximum value of evaporation occurs in May. After a slow decrease, in February it increases rapidly.

2.2.3 **Calculation of Surface Runoff**

Using the correlation between rainfall and evaporation, the calculation of surface runoff volume can be carried out by combining the relevant variables:

$$V = 0.001 \phi HA$$

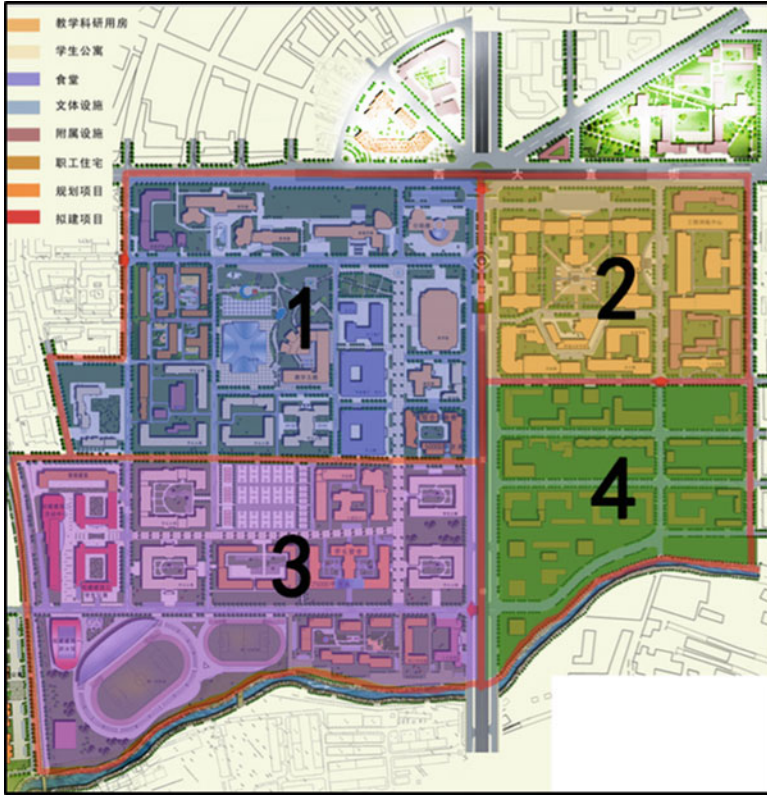


Fig. 44.2 Schematic diagram of planning and zoning of campus runoff process system

Table 44.1 Subcatchment area (m³)

Type	Area				Total
	1	2	3	4	
Architecture	537,975	323,628	421,645	388,652	1,671,900
Road	79,000	61,750	63,780	42,550	247,000
Pavement	798,775	685,700	831,925	598,700	2,915,100
Greenland	481,250	391,470	471,230	501,050	1,845,000
Total	1,897,000	1,462,548	1,788,580	1,530,952	6,679,000

where

V is the total rainwater collection (m³),

ϕ is the runoff coefficient,

H is rainfall (mm),

A is the confluence area.

Table 44.2 Land type and runoff coefficient of Harbin Institute of Technology

Area	Land type	Runoff coefficient
1	Architecture	0.9
	Road	0.5
	Pavement	0.6
	Greenland	0.15
	Water	1
2	Architecture	0.9
	Road	0.5
	Pavement	0.6
	Greenland	0.15
	Water	1
3	Architecture	0.9
	Road	0.5
	Pavement	0.6
	Greenland	0.15
	Water	1
4	Architecture	0.9
	Road	0.5
	Pavement	0.6
	Greenland	0.15
	Water	1

Table 44.3 Average annual rainfall in Harbin

Month	3–5	6–9	10–12	Total
Rainfall	68.5	405.9	50	524.4

If there is no large area of water in the return flow area, the runoff $V' = V$. If there is a large water surface, then $V' = V - V''$ (V'' : volume of evaporation). The formula for water surface evaporation is $V'' = 0.001 A'H'$ (A' : area of water surface, H' : average annual evaporation).

Because there is no water surface in the study area, the evaporation capacity is not calculated. As shown in Table 44.4, the surface runoff in the study area under the average rainfall conditions in different months achieved. According to the preceding formula, the total volume of annual surface runoff volume is about 1,000,000 m³ on the main campus of the Harbin Institute of Technology, and it is more than 40 % of the total rainfall.

2.2.4 Calculation of Minimum Capacity of Rainwater Collection Facilities

To facilitate the utilization of rainwater runoff on the site, the surface runoff should be collected. The use of a rainwater garden approach is adopted to deal with runoff. After part of the rainwater flows into a green space, facilities for the collection and

Table 44.4 Calculation results of surface runoff in various areas (m³)

Area	Month			Total
	3–5	6–9	10–12	
1	38,393	226,834	27,841	293,068
2	29,127	172,094	21,123	222,344
3	46,123	272,513	33,448	352,084
4	17,939	105,996	13,011	136,946
Total	131,582	777,437	95,423	1,004,442

Table 44.5 Minimum capacity of rainwater collection and storage facilities in each catchment area

Area	1	2	3	4	Total
Minimum	4239	3819	6465	1286	15,881

infiltration are utilized. This chapter assumes that all the surface runoff can flow into the storage facilities. Then the capacity of the storage volume equals the runoff volume. The recurrence period and facilities product are positively correlated. Considering the costs, the facilities’ volume cannot be increased without limit. So it is assumed that the return period of a rainstorm is 10 years, and the rainfall duration is 1 h:

$$\text{Rainstorm intensity: } q = 167 A_1(1 + C \log P)/(t + b)n,$$

where

- P is the design return period,
- t is the rainfall duration (min),
- q design storm intensity (mm/min).

A_1 , C , b , and n are constants. According to the outdoor drainage design code, the return period in the Harbin area is 10 years, and the rainfall duration is 1 h, and the rainstorm intensity is 135.62 mm.

According to the formula $V = 0.001 \phi q A$, the minimum capacity of the storage facilities in the four rainwater catchments is achieved, as shown in Table 44.5.

2.3 Results Analysis

A campus runoff treatment system should regard increasing rainfall infiltration volume and groundwater recharge as the planning principle. When the rainfall intensity is greater than the ground infiltration capacity, a series of approaches combining landscape garden design techniques of filtering and purifying processes are adopted, for example, different formats of rain garden (puddles or ponds). If the landscape water capacity reaches saturation again, then the rainwater will overflow

to an artificial lake or river. According to the inner diameter of each watershed total flow calculation results and the site situation, the minimum volume of rainwater-harvesting facilities in this case is 4239, 3891, 6465, and 1286 m³.

3 Planning Strategy for Runoff Treatment System

On the basis of the planning idea and principle, this chapter proposes corresponding planning strategies for the safety and effective utilization of rainwater resources.

3.1 Planning Idea

Based on a quantitative analysis of water resources, this chapter aims to use qualitative and quantitative methods to carry out the plan for a runoff treatment system and to establish a safe, reliable, and low-carbon model campus. It is a new idea to build an economic, environmental, and educative campus.

3.2 Planning Principle

Considering comprehensive campus construction conditions, on the basis of quantitative information on rainwater resources, traditional pipeline and ecological collection and rainfall utilization are combined. The principle behind campus runoff treatment system planning involves the establishment of multilevel partitioning of a runoff processing system. According to the overall layout of the campus and local conditions, drainage areas are reasonably divided so as to achieve safe drainage and rainwater on the campus so that the water can be effectively used, a win-win situation.

From Fig. 44.3, the campus runoff treatment system is divided into a three-ring structure. The outer ring region uses the terrain slope and discharges rainwater into Ma Jiagou River directly. The central ring utilizes a comprehensive collection of ecological grass gullies and rainwater pipes and reuses the collected rainwater; in the heart of the ecological rain collection area, ecological methods of collecting and using rainwater, by roof greening, grassed swales, and sunken green spaces, are adopted.

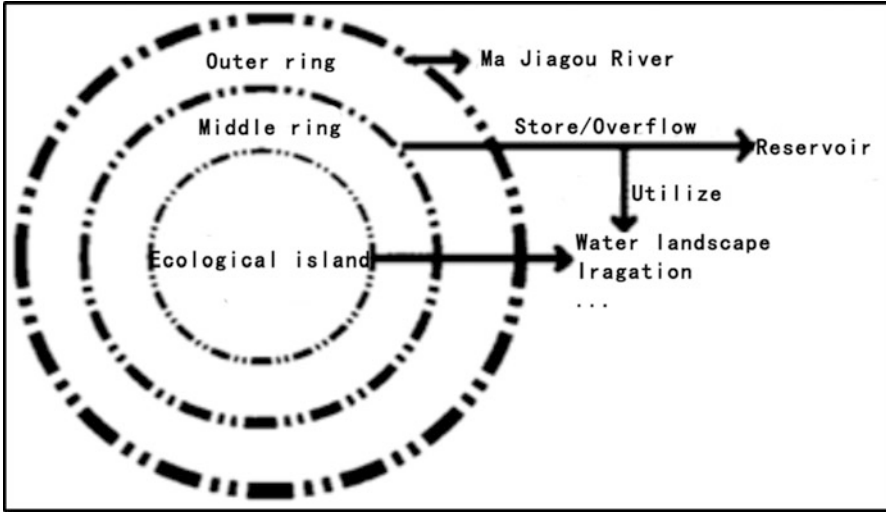


Fig. 44.3 Three-ring structure chart of campus runoff treatment system

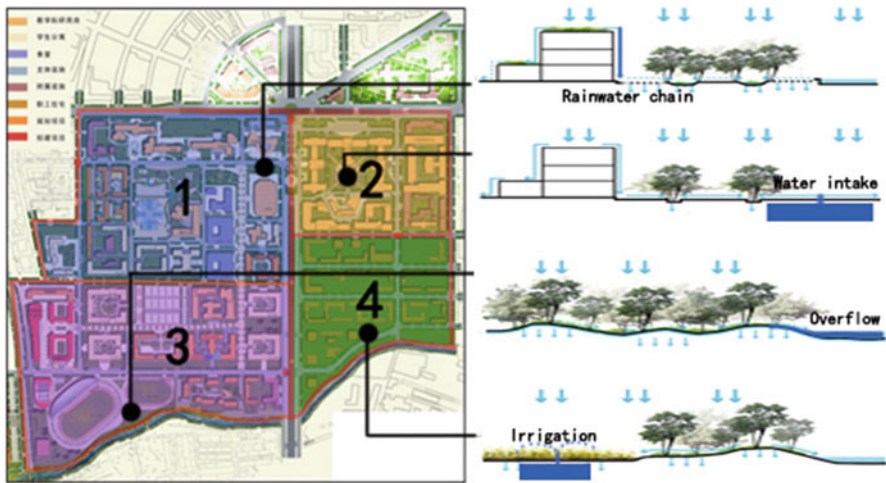


Fig. 44.4 Schematic diagram of campus runoff system plan

3.3 Planning Strategies

Depending on the kind of runoff, the characteristics of the terrain, and the function of a single area, different measures are taken, as shown in Fig. 44.4.

In area 1, because the terrain fluctuation is small, rain is easier to retain, and the existing green space can be utilized well; it is proposed that the existing green space be transformed into a rain garden or ecological grass ditch. The square in front of

the library can be used for rainwater collection, for example, in the form of scaffolding or a rain chain. Thus, a diversified, active space is created while using the area for runoff treatment.

In area 2, rainwater can discharge into the vegetation purification belt by drainage pipe and be transported to an ecological grass ditch. When the ecological capacity of grass ditch water reaches saturation, the water can discharge into the underground reservoir through underground pipes. Finally, overflow that flows back into the vegetation purification belt can form circular purification and storage systems, with intake wells in the reservoir area, at which point the unique characteristics of experiential educative landscape comes into play.

In area 3, runoff is so large that the grass ditch should be set up to absorb and intercept the rain. When the water capacity is saturated, the rainwater flows into the underground reservoir by underground pipe and overflow is transported to the river.

In area 4, rain transported by the drainage pipe is designed to discharge into the vegetation purification zone and ecological grass valley afflux. When the water capacity is saturated, rainwater discharges into the underground reservoir by underground pipe. The reservoir area is designed to be equipped with a wellhead, which can directly irrigate the district green space in a family area, and the reservoir is provided with overflow pipes leading to the river.

4 Conclusion

The concept of a runoff treatment system has become an important one in urban low-carbon construction in China, but most such systems remain at the theoretical level, lacking systematic and in-depth planning. In a sense, the university campus is the epitome of the city; at the same time, social responsibility and the functions of a campus mean that it has a stronger social influence. Therefore, the campus where a runoff treatment planning system is built should be viewed from a broader vantage point, using efficient technical measures combined with geographical conditions, to meet ecological, landscape, security, and service needs. Based on geographic information, scientific calculations, and the economic, environmental, and social benefits of sustainable development, a low-carbon green campus is achievable.

References

1. Lee SY, Maniquiz MC, Kim LH (2012) Appropriate determination method of removal efficiency for nonpoint source best management practices. *Desalin Water Treat* 48(1–3):138–147
2. United Nations (2010) Water resources: long term annual average, environmental indicators water. <http://unstats.un.org/unsd/ENVIRONMENT/waterresources.htm>. Accessed 12 Oct 2010
3. Hasse JE, Lathrop RG (2003) Land resource impact indicators of urban sprawl. *Appl Geogr* 23(2–3):159–175

4. Walsh CJ, Roy AH, Feminella JW, Cottingham PD, Groffman PM, Morgan RP II (2005) The urban stream syndrome: current knowledge and the search for a cure. *J North Am Bentholical Soc* 24(3):706–723
5. Walsh CJ, Fletcher TD, Ladson AR (2009) Retention capacity: a metric to link stream ecology and storm-water management. *J Hydrol Eng* 14:399
6. Wigmosta M, Burges S (1997) An adaptive modeling and monitoring approach to describe the hydrologic behavior of small catchments. *J Hydrol* 202(1–4):48–77

Chapter 45

Urban Sustainable Development in the Mediterranean Area: The Case of Sestri Ponente, Genoa

Katia Perini and Adriano Magliocco

Abstract In November 2014 a green *façade* was built in the Sestri Ponente district in Genoa, Italy, on an office building owned by the Istituto Nazionale di Previdenza Sociale (National Institute of Social Insurance). This area, which is characterized by a relatively high population density, faces important environmental issues related to, for example, air pollution, stormwater management, and the urban heat island effect. The Department of Sciences for Architecture at the University of Genoa (Italy) is conducting monitoring activity to evaluate the effectiveness of the green *façade* with regard to summer cooling, winter heating – in collaboration with Research on the Energy System – air quality improvement, and economic and environmental sustainability. Starting from this first pilot project a question arises: what would be the effect of vegetation at the district scale? This article discusses the potentialities for urban sustainable development of the integration of green infrastructure. Simulations carried out with ENVI-Met software demonstrate the potentialities of different amounts of vegetation for urban heat island mitigation. In addition, the possible stormwater runoff reduction was calculated. Such calculations are based on urban design projects developed for the area to evaluate the possible improvement to environmental quality owing to the integration of green infrastructure.

1 Step One: A Green Façade

In November 2014 the first green *façade* was built in the city of Genoa, Italy, on the south *façade* of an office building owned by the Istituto Nazionale di Previdenza Sociale (National Institute of Social Insurance) (INPS) on Ciro Menotti Street, Sestri Ponente district (Fig. 45.1). The project was developed thanks to a

K. Perini (✉) • A. Magliocco
Dipartimento di Scienze per l'Architettura, Università degli Studi di Genova, Genoa, Italy
e-mail: katia.perini7@gmail.com; magliocc@arch.unige.it



Fig. 45.1 South façade of INPS building in Genoa Sestri Ponente

collaborative effort between the technical director Enrica Cattaneo and the authors of this chapter. This collaboration between INPS and the Department of Sciences for Architecture at the University of Genoa allows for the setup of monitoring activities that involve Research on the Energy System (RSE SpA, GSE group), Regional Environment Protection Agency of Liguria region (ARPA Liguria), and Prof. Marc Otelé of the Delft University of Technology (TU-Delft) regarding air quality, energy performance, and citizens' social perceptions.

The commitment to reduce by 3% per year the energy demand of public buildings (by Law D. Lgs. 102/2014, art. 5) induced INPS Liguria to retrofit some buildings; European funds also made it possible. The Ciro Menotti office building was built in the 1930s with reinforced concrete structure and a light brick envelope (no insulation material). The Sestri Ponente area, which is characterized by a relatively high population density (13,000/km²), faces important environmental issues related to, for example, air pollution, stormwater management, and the urban heat island effect, owing to urban morphology, vehicular traffic, and lack of green spaces. In addition, with the aim of reducing these environmental imbalances, a green *façade* was built, and monitoring activities to qualify the effects of vegetation on air quality improvement and on microclimate are under development.

The benefits of vegetation in urban areas involve a wide range of scales; some have effects only if a large surface in the same area is greened (with clear results on neighbourhoods or cities), whereas others are directly related to the building

microclimate. The benefits on a larger scale are mainly related to improvements in air quality, an increase in biodiversity, and mitigation of the urban heat island effect [1]. Green *façades*, roofs, or a simple placement of trees and shrubs allow for improving the building envelope efficiency, thermal comfort, and visual, aesthetic, and social aspects [2].

As demonstrated by recent studies [3,4], air quality improvements due to vegetation are mainly a result of the absorption of fine dust particles, or particulate matter (PM) and the uptake of gaseous pollutants such as CO₂, NO₂, and SO₂. Carbon dioxide is used by plants for photosynthesis, leading to the creation of oxygen and biomass; in addition, nitrogen and sulphur dioxides are converted into nitrates and sulphates in the plant tissue. The PM, especially the smaller fractions (<10 µm), adhere mainly to the outside of plant parts [3], so vegetation is a perfect anchor for airborne particles at different heights. Dust particles smaller than 2.5 µm are relevant mainly in dense urban areas because they can be inhaled deeply into the respiratory system and cause health issues and damage to human beings [5]. Baik et al. [6] evaluated the positive effects, in terms of air quality improvement, of green roofs by means of a computational fluid dynamics (CFD) model. The results show that vegetation cools the air, improving airflow in urban canyons and allowing a reduction of air pollutants.

Finally, the effects of vegetation in terms of mean radiant and air temperature reduction can be considered [7]. Though trees with wide foliage can provide significant benefits, because of the lack of space in dense urban environments, exploiting building surfaces through the use of green *façades* and roofs can be an interesting strategy.

2 Study Area

Following installation of the green *façade* (Fig. 45.2), the authors considered the possibility of starting a greening process in the area, i.e., finding other possibilities for integrating vegetation. Urban greening should be conceived of as considering different characteristics that make it possible to improve environmental conditions related to air quality, mitigation of the urban heat island effect, and urban environmental aesthetics [8].

The area considered in this study is located in the Sestri Ponente district. This area, which has a relatively high population density, is characterized by a rigid road network with perpendicular paths and by a lack of green areas (Fig. 45.3). The main axis is the aforementioned Ciro Menotti Street, where the green *façade* was installed. The majority of the buildings date back to the late ninth and early tenth centuries. Among the retrofitting measures envisioned, the reconversion of the Sestri Ponente port may be mentioned. This is an industrial port with several defunct buildings and areas, which are not suitable for the current needs of the naval industry.



Fig. 45.2 South façade of INPS building in Genoa Sestri Ponente, June 2015



Fig. 45.3 Area around INPS building in Genoa Sestri Ponente

In 2014 the Piano Urbanistico Comunale (municipality urban plan) was approved. The initiatives expected to be carried out in the area considered are as follows:

- Improvement of the boatyard area, including parts of it into areas more suitable for urban life;
- Requalification of the waterfront and the railroad and train station to favour a connection with the city centre.

3 Vegetation and Urban Regeneration

For the implementation of the Piano Urbanistico and for the improvement of the environmental quality of the district, vegetation can play an important role.

The effects of green areas on microclimate and comfort can be evaluated thanks to the use of environmental modelling. This was conceived with the aim of understanding many current environmental problems; it makes it possible to evaluate the effects of zoning changes (use of territory) on meteorological parameters and on the consequences for quality of life through microclimate models such as ENVI-met is a three-dimensional microclimate model designed to simulate the surface-plant-air interactions in urban environment [7].

ENVI-met models have been used in several studies to evaluate the effects of the characteristics of cities on the microclimate. Krüger et al. [9] observed and estimated relations between urban morphology and changes to microclimate and air quality within a city centre; Fahmy et al. [10] studied the leaf area index (LAI) using an ENVI-met plant database as a platform for a foliage modelling parameter, the leaf area density (LAD). Ali-Toudert and Mayer [11] analyse outdoor thermal comfort on the design of an urban street using the three-dimensional microclimate model made by ENVI-met; they found that vertical profiles and different street orientations have a moderate impact on the air temperature and a strong effect on the heat gained by a human body: the larger the openness of the canyon to the sky, the higher the heat stress. For canyons with a smaller sky view, the orientation is also decisive: east–west (E–W) canyons are the most stressful, and deviating from this orientation ameliorates their thermal conditions. Yang et al. [12] compared field measurements of the thermal behaviour of different types of ground surface and the data obtained with an ENVI-met model. The results show that the ENVI-met model is capable of reasonably modelling the diurnal thermal behaviour of different ground surfaces and their effects on local air temperature and humidity.

An area of approximately 800 m × 800 m was considered in this study. Climatic data recorded within the city centre were used (available to the public on the regions' Web sites: <http://www.cartografiarl.regione.liguria.it/>).

Simulations using the ENVI-met software were carried out for the current situation, highlighting overheating problems in the port area, i.e., where there is no vegetation and all surfaces are artificial (e.g., asphalt roads, concrete) (Fig. 45.4).

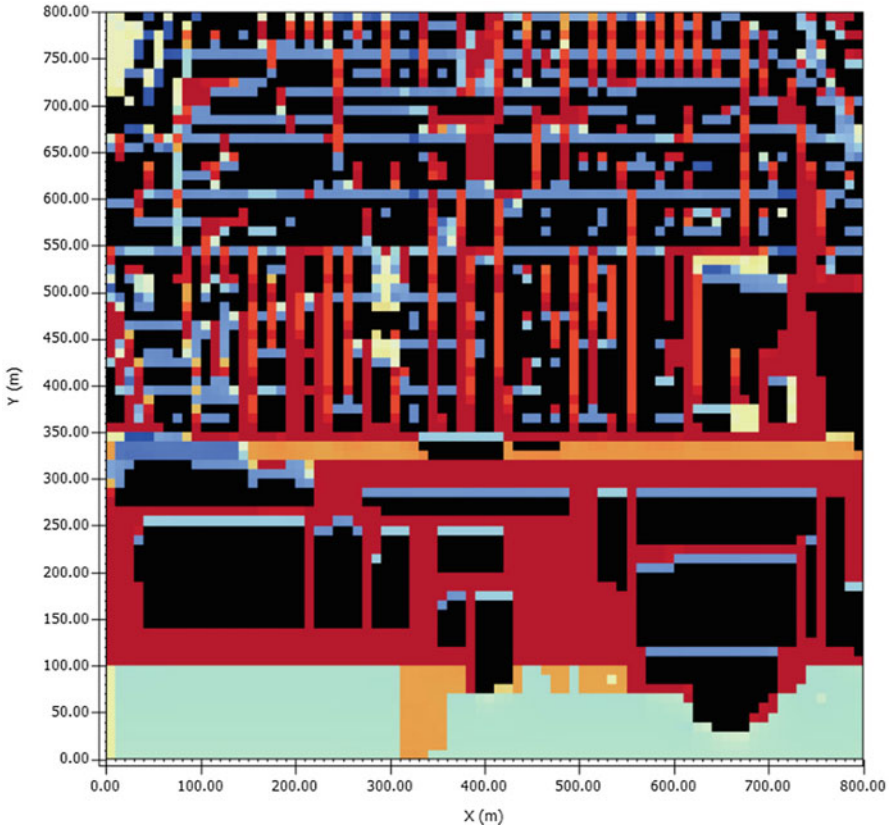


Fig. 45.4 Simulation of superficial temperatures in October, from 22 °C (blue) to 35 °C (red)

In such areas, despite the presence of water, high mean radiant and air temperatures, and PMV¹ values can be recorded, resulting in discomfort for people. For this reason, the area was selected as the site of development of a project for the integration of vegetation, in compliance with the urban plan, designed for the improvement of environmental quality.

¹The predicted mean vote (PMV) is a comfort index defined by Fanger in 1970 and mentioned in ISO 7730:2006 (“Ergonomics of the thermal environment—Analytical determination and interpretation of thermal comfort using calculation of the PMV and PPD indices and local thermal comfort criteria”). PMV takes into account several parameters (e.g., air temperature, mean radiant temperature, wind speed); positive values indicate hot-warm, while negative values cold. According to ISO 7730:2006, PMV values between +0.5 and -0.5 correspond to comfortable thermal conditions.

4 A Master's Thesis for a Retrofitting Project

With the aim of evaluating the effect of greening solutions on the environmental quality of an area, a master's thesis was developed. The requalification strategies assumed include the installation of green roofs and vertical greening systems, green areas on the ground and the replacement of paved surfaces with permeable surfaces.

The design project was based on a gradual implementation strategy, through a step-by-step greening process. The design choices were based on simulation results: situations highlighting the most problematic areas with regard to microclimatic conditions (i.e., western area). Vertical greening systems were assumed to be integrated in the narrowest streets, where trees cannot be planted owing to a lack of space. All flat roofs were assumed to be green with intensive or extensive solutions, considering the type of roof structure.

The plant species chosen, *Citrus aurantium* and *Acer*, tolerate air pollution and atmospheric agents and have basic maintenance needs. In general, the plant species choice plays an important role in restoring ecological imbalances of urban areas since vegetation can provide ecosystem services [13]. For this reason native or naturalized plants should be integrated to allow urban parks to have a key role in improving the environmental quality of a district.

Since most of the area (82 %) is characterized by impervious surfaces (asphalt road and buildings), water management problems often arise, with flooding a consequence (even with just an ordinary storm when the sewer system is overloaded). For this reason, where possible, rain gardens for stormwater runoff reduction [14] are assumed. Green roofs can contribute as well [15] and streets can be converted into permeable surfaces to slow down the flow of water that goes directly through the drainage system into rivers.

To verify the effects of the design choices on mean radiant temperature and air temperature (at 1.6 m from ground level) simulations with ENVI-met software were carried out. Such simulations show a temperature reduction due to vegetation also in the most problematic area (Fig. 45.5).

5 Conclusions

A progressive greening, according to the design project (unfortunately just a teaching simulation), could lead to an improvement in air quality that is currently difficult to quantify. Some other evaluations were done with regard to urban heat island effect mitigation and runoff reduction.

While air temperature cannot be significantly reduced without large trees, the design choices assumed allow for a relevant reduction in mean radiant temperatures, which plays a key role in improving summer comfort conditions (Fig. 45.5).

Considering the final step of the assumed greening process, i.e., when all the roofs are green (115,061 m²) and more than 20,000 m² of asphalt surfaces have

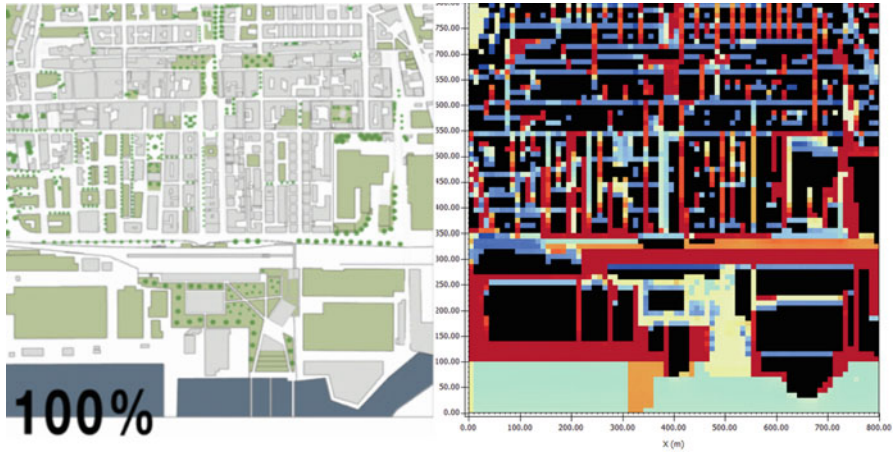


Fig. 45.5 Simulation of superficial temperatures in October with greening project completed

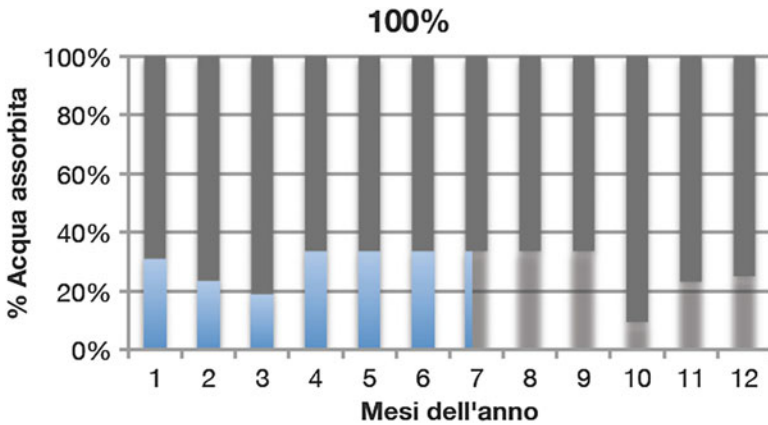


Fig. 45.6 Percentage of rainfall adsorbed with greening project completed

been converted into permeable surfaces, a reduction in stormwater runoff within a range of 10 % (during fall) to 30 % was calculated (Fig. 45.6) depending on the rainfall.

Acknowledgments Master’s students (now graduated architects) Anna Ragosa and Carolina Queirolo are acknowledged. Enrica Cattaneo and Umberto Valle are acknowledged for their fundamental support.

References

1. Köhler M (2008) Green facades—a view back and some visions. *Urban Ecosyst* 11:423–436. doi:[10.1007/s11252-008-0063-x](https://doi.org/10.1007/s11252-008-0063-x)
2. Dunnett N, Kingsbury N (2008) *Planting green roofs and living walls*. Timber Press, Portland
3. Ottelé M, van Bohemen HD, Fraaij ALA (2010) Quantifying the deposition of particulate matter on climber vegetation on living walls. *Ecol Eng* 36:154–162. doi:[10.1016/j.ecoleng.2009.02.007](https://doi.org/10.1016/j.ecoleng.2009.02.007)
4. Sternberg T, Viles H, Cathersides A, Edwards M (2010) Dust particulate absorption by ivy (*Hedera helix* L) on historic walls in urban environments. *Sci Total Environ* 409:162–168. doi:[10.1016/j.scitotenv.2010.09.022](https://doi.org/10.1016/j.scitotenv.2010.09.022)
5. Powe NA, Willis KG (2004) Mortality and morbidity benefits of air pollution (SO₂ and PM₁₀) absorption attributable to woodland in Britain. *J Environ Manage* 70:119–128. doi:[10.1016/j.jenvman.2003.11.003](https://doi.org/10.1016/j.jenvman.2003.11.003)
6. Baik J-J, Kwak K-H, Park S-B, Ryu Y-H (2012) Effects of building roof greening on air quality in street canyons. *Atmos Environ* 61:48–55. doi:[10.1016/j.atmosenv.2012.06.076](https://doi.org/10.1016/j.atmosenv.2012.06.076)
7. Perini K, Magliocco A (2014) Effects of vegetation, urban density, building height, and atmospheric conditions on local temperatures and thermal comfort. *Urban Urban Green* 13:484–494. doi:[10.1016/j.ufug.2014.03.003](https://doi.org/10.1016/j.ufug.2014.03.003)
8. Perini K (2013) *Progettare il verde in città: una strategia per l'architettura sostenibile*. F. Angeli, Milano
9. Krüger EL, Minella FO, Rasia F (2011) Impact of urban geometry on outdoor thermal comfort and air quality from field measurements in Curitiba. *Brazil Build Environ* 46:621–634. doi:[10.1016/j.buildenv.2010.09.006](https://doi.org/10.1016/j.buildenv.2010.09.006)
10. Fahmy M, Sharples S, Yahya M (2010) LAI based trees selection for mid latitude urban developments: a microclimatic study in Cairo. *Egypt Build Environ* 45:345–357. doi:[10.1016/j.buildenv.2009.06.014](https://doi.org/10.1016/j.buildenv.2009.06.014)
11. Ali-Toudert F, Mayer H (2007) Effects of asymmetry, galleries, overhanging *façades* and vegetation on thermal comfort in urban street canyons. *Sol Energy* 81:742–754. doi:[10.1016/j.solener.2006.10.007](https://doi.org/10.1016/j.solener.2006.10.007)
12. Yang X, Zhao L, Bruse M, Meng Q (2013) Evaluation of a microclimate model for predicting the thermal behavior of different ground surfaces. *Build Environ* 60:93–104. doi:[10.1016/j.buildenv.2012.11.008](https://doi.org/10.1016/j.buildenv.2012.11.008)
13. Oberndorfer E, Lundholm J, Bass B, Coffman RR, Doshi H, Dunnett N, Gaffin S, Köhler M, Liu KK, Rowe B (2007) Green roofs as urban ecosystems: ecological structures, functions, and services. *BioScience* 57:823–833
14. Autixier L, Mailhot A, Bolduc S, Madoux-Humery A-S, Galarneau M, Prévost M, Dorner S (2014) Evaluating rain gardens as a method to reduce the impact of sewer overflows in sources of drinking water. *Sci Total Environ* 499:238–247. doi:[10.1016/j.scitotenv.2014.08.030](https://doi.org/10.1016/j.scitotenv.2014.08.030)
15. Fioretti R, Palla A, Lanza LG, Principi P (2010) Green roof energy and water related performance in the Mediterranean climate. *Build Environ* 45:1890–1904. doi:[10.1016/j.buildenv.2010.03.001](https://doi.org/10.1016/j.buildenv.2010.03.001)

Chapter 46

Development of Energy Devices Based on Photovoltaic Panels with Extra Consumer Properties

L. Mikhailov, S. Mikhailova, G. Ismailova, G. Yar-Muhamedova, and S. Sokolov

1 Introduction

The challenge at this time for renewable energy is the low cost of traditional energy resources. Therefore, the economic task of this project is to improve the profitability of devices using renewable energy by giving them additional consumer functions and improving performance in difficult air conditions in the city. Leading countries in the production and use of photovoltaic devices are China, the USA, Japan, and EU member nations. However, the efforts of manufacturers in these countries are focused on the creation of large-scale solar power plants specialized only in the production of electricity. Currently, efforts of well-known companies are under way to make solar cells with a cheaper (10–15 %) average efficiency. Efforts are being made by manufacturers specialized exclusively in the production of electricity to install and operate photovoltaic systems in cities associated with the installation of solar cells on roofs and sun-facing facades of buildings.

The last two decades have seen the study and design of combined photovoltaic solar thermal (PVT) systems [1–8], which should increase the efficiency of solar energy conversion due to trapping and even heat energy, as well as improving the efficiency of PV conversion owing to a decrease in photoconverter temperature. In [9] is a detailed description of the design and calculations for a PVT panels for a city in Sweden. Payback of small power plants with such panels, according to the calculations in [9], is 35 years, even with the high energy costs in Sweden. Despite the disappointingly low margins, large-scale environmental problems require renewable energy sources in the energy circulation and the use of those sources that will provide the greatest return on investment. The cost of energy greatly increases the distance for the transport, so it is necessary to minimize its use.

L. Mikhailov • S. Mikhailova (✉) • G. Ismailova • G. Yar-Muhamedova • S. Sokolov
Physico-Technical Faculty, Al-Farabi Kazakh National University, Almaty, Kazakhstan
e-mail: skysvetik91@mail.ru; guzal_a81@mail.ru

The lowest external costs associated with renewable sources of energy are incurred in the immediate vicinity of the majority of consumers, that is, in cities.

At the same time, because of the increased accident rate of urban energy distribution networks and the rising prices of energy, from year to year the needs and redundancy for energy savings increases, savings that can be achieved by adding to renewable sources to the energy mix. The environment of cities is becoming increasingly worse owing to car exhaust emissions and dust particles that pollute the atmosphere and threaten human health. This situation has prompted a need for active efforts at air purification, making the environment more comfortable for urban dwellers. The elements and components of renewable energy sources can be charged in some of these devices. However, it is hard to imagine that owing to the sharp decline in prices for traditional energy sources, independent urban consumers will demand expensive energy from renewable sources. On the other hand, only with the urban consumers' density is possible to achieve at least some small but steady demand for renewable energy devices. In the structure of residential costs, energy needs account for less than 5%. There is no need to rely on the fact that residential consumers will buy such devices out of a desire to save money on electricity – 1–2% of their electricity budget over the course of 15–20 years following the installation of renewable energy sources (RESs). Therefore, the most attractive way to distribute renewable energy among independent urban consumers is to embed them in home appliances which have market demand. Among the needs to be met by renewable energy devices are those related to health care, comfort at home, reliable and safe consumer devices, aesthetics, and others.

2 Tasks and Possibilities

The scientific and technical task of the project is the construction of modular power units with additional consumer functions. These units will increase the profitability of devices using renewable energy, enhance their relevance for everyday life, and help to address environmental and social problems. Among the functions of such devices are street and house dust collection, room lighting, decoration of façades, additional insulation of buildings, the accumulation of heat and cold in rooms by heat accumulating material and passive heating, and the cooling of rooms by battery-powered air-conditioners.

Important design tasks of the project are, for example, the development of an installation system of solar panels on façades, the assembly of a thermal energy accumulator inside rooms, and the protection of panels from mechanical and abrasive effects. To ensure maximum demand, the devices should have autonomous modules that meet perform their own consumer functions. Users can choose the modules themselves with the necessary functions, such as those related to the elimination of the function of conditioning, dust collecting, or, perhaps, lighting.

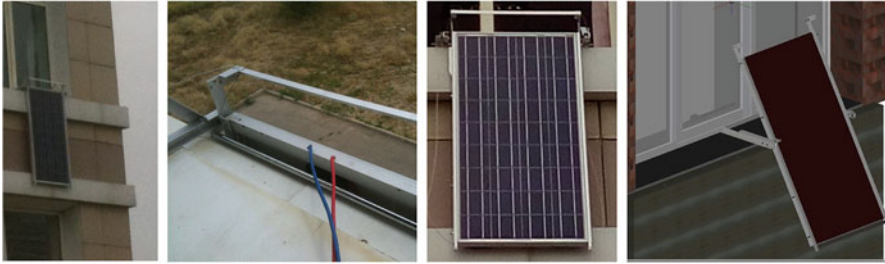


Fig. 46.1 Basic module with solar cell on façade

The basic module is a construction that provides the taking out and fixing of solar panels and connects all modules. The solar panel is framed by duralumin corners that allow sliding on a so-called sled base module and forms grooves for pulling the film. In fact, the base unit is a corner construction fastened to walls and windowsills that fix a solar panel and provides a connection with other modules. Figure 46.1 shows a base module on the Physico-Technikal Faculty façade in Al-Farabi Kazakh National University. The solar panel can move along the guide unit through an open window, first vertically, then turn out the window frame in a horizontal position before being transferred at about 30 degrees and there are closed corners to the into the vertical (parallel to the façade) position.

The device includes several modules providing consumer functions, depending on what the user selects. If you want to collect dust, protect the panel from abrasion, and wash the solar panel using the wiper, you can connect the dust-collecting module. Dust can be collected automatically in the tub, or you can wipe it manually. If the climate is conducive to conditioning, this panel may be “converted” into a PVT module by inserting the heat-receiving part into the solar panel cavity (the inner side). The coolant may be a liquid used in cars—antifreeze. Heat and cold from the solar cell can accumulate into heat sinks, which serve as a heater or cooler of a room.

3 Variants of Use

Of course, the most reasonable use of PV energy, in terms of profitability, is for low-voltage LED lighting fixtures. On the one hand, this is an important consumer function; on the other hand, it makes it possible to smooth out peak electrical loads. In this chapter we look in detail at other features. For instance, ensuring continuous operation of solar panels in all weather conditions will be due to their cleaning from dust, dirt, and snow through the periodic movement of the so-called wiper on the face side of the panel. Also continuous operation will come from reducing the temperature of the panels in active mode as a result of protecting the panels from the

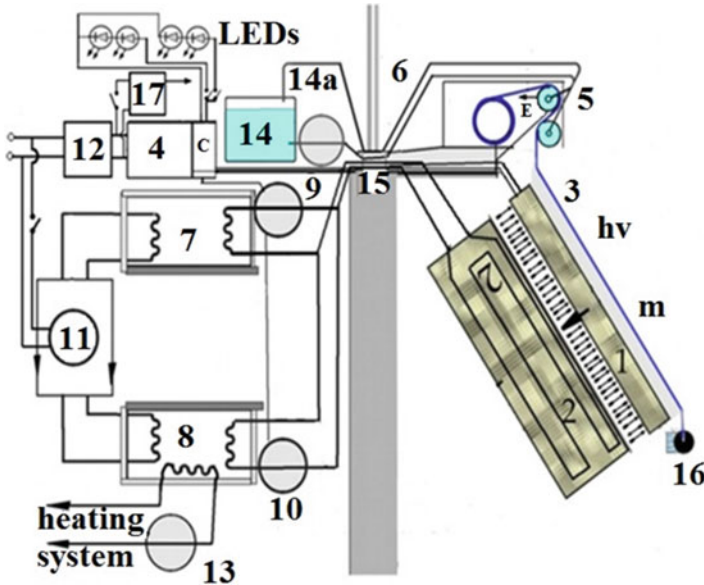


Fig. 46.2 Set of functional modules of the device. 1: solar cell; 2: heat sink and coolant; 3: mobile dust-collecting film; 4: accumulator; 5: unit of electrical charge and washing of film; 6: geared motor; 7, 8: heat and cold sinks with heat exchanger; 9, 10: circulation pumps of heat exchangers; 11: heat pump compressor; 12: uninterruptible power supply; 13: circulating pump to outside with heating system; 14, 14a: liquid sink and circulation pump; 15: pipeline, bracket; 16: light weight and film holder; 17: control module of management

effects of dust and dirt in passive mode. A schematic with a set of functional modules for air conditioning, lighting, and dust collection is shown in Fig. 46.2.

A variant of the functional and structural schematics with a set of modules for the curtain, which controls the solar flux and picks up the dust from the street, is shown in Fig. 46.3.

Lavsan polyester film provides protection against dirt and abrasive effects when the solar panel is not used in the PV or radiator mode. Electrostatic dust collection and washing of the front side panels is done using the same film and electrified wiper. The cleaning liquid is supplied to the system by a circulation pump to film washing tubes, so the dust from the film gets into the liquid reservoir. A spilled portion of the liquid moisturizes the wiper. The lightweight film moves slowly by a motor reducer for a few minutes that make it possible to wipe the film manually with the high voltage switched off. Protection against dirt and abrasive effects and electrostatic dust collection and washing of the front side of the panel by wiper is illustrated in Fig. 46.4.

Using a box 2 with a removable heat circuit. A solar cell can be turned into a PVT module for heat exchange with the environment. In the variant depicted in

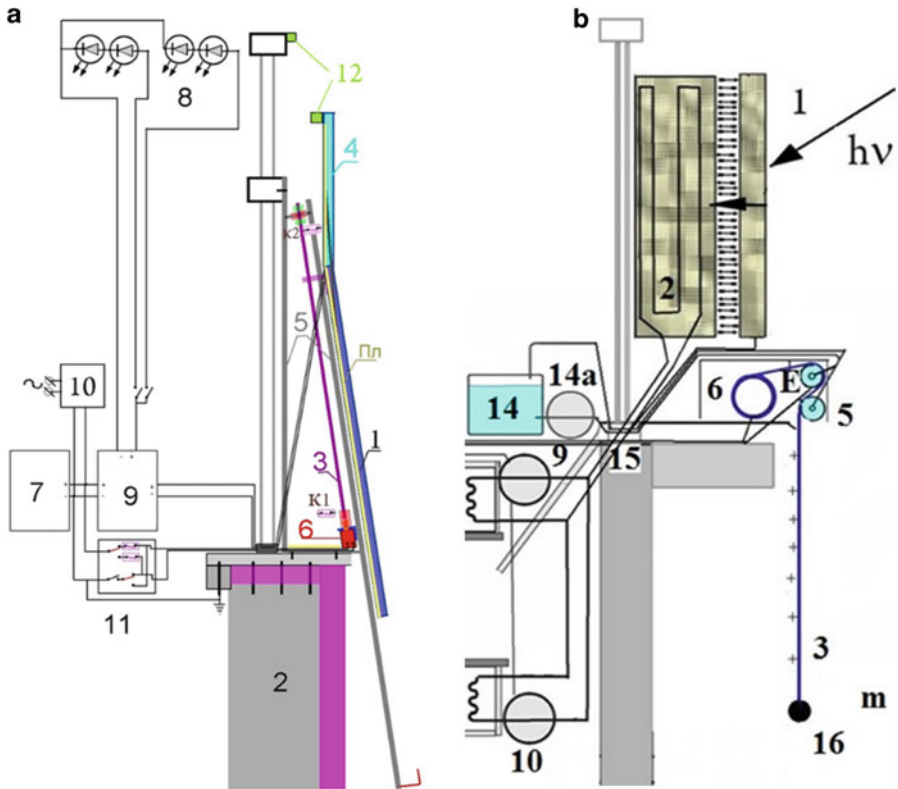


Fig. 46.3 (a, b) Variant of “curtain.” 1: solar cell; 2: heat sink and coolant; 3a: peg; 3b: mobile dust-collecting film; 4: shutter; 5a: corner sled; 5b: unit of electrical charge and washing of film; 6: geared motor; 7: accumulator; 8: LEDs; 9a: controller; 10a: charge; 9b, 10b: circulation pumps of heat exchangers; 11: switchers; 12: rubber damper; 14, 14a: liquid sink and circulation pump

Fig. 46.4, the device can perform as an air conditioner, which additionally heats the room or accumulates heat in heat sink 8. This is possible owing both to the “solar” heat at low air temperatures and to the convective exchange with air at positive temperatures. The film redistributes the heat from the solar panels in such a way that most of it goes to box 2. The lowered film “redistributes” the heat from the solar panels so that most of it goes to cooler 2. At outside temperatures below zero heat from can be moved to cold sink 7, the heat from which is pumped into the heat pump to heat sink 8. Owing to the heat storage, the process of heating and accumulating heat can be separated in time (Fig. 46.5).

The device can work as an air conditioner to cool a room or accumulate cold in cold sink 7. In this case, the process of cooling the room and the process of accumulating cold are separated in time, so the panel play a role as an external radiator air conditioner type “summer,” taking the heat out into the environment (Fig. 46.6).

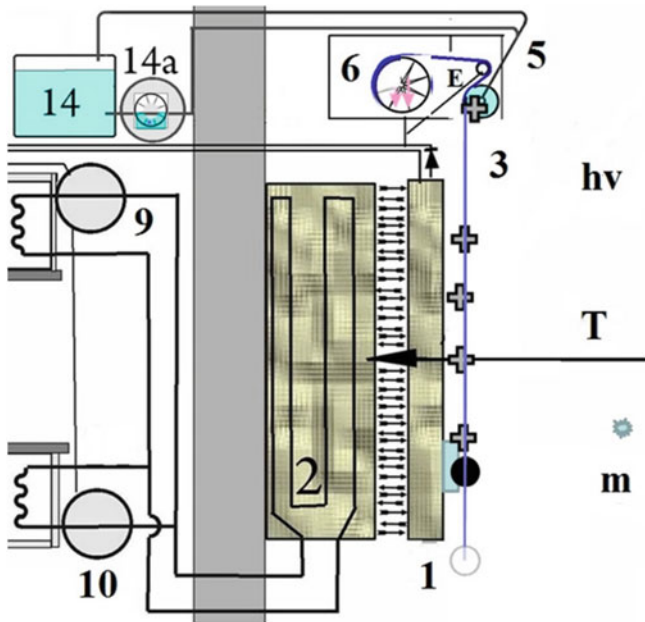


Fig. 46.4 Functional scheme of protection against dirt and electrification mode. 1: solar cell; 3b: mobile dust-collecting film; 5b: unit of electrical charge and washing of film; 6: geared motor; 9b, 10b: circulation pumps of heat exchangers; 14, 14a: liquid sink and circulation pump

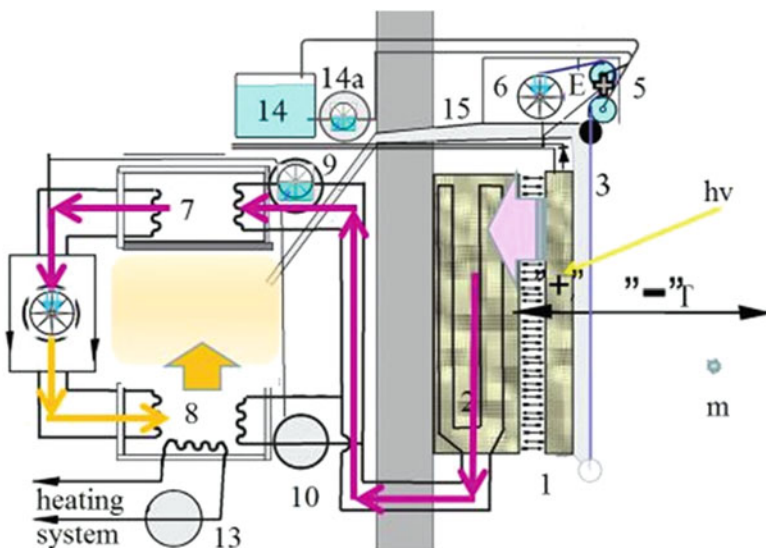


Fig. 46.5 So-called winter-type conditioner. 1: solar cell; 3: mobile dust-collecting film; 5: unit of electrical charge and washing of film; 6: geared motor; 7, 8: heat and cold sinks with heat exchanger; 9, 10: circulation pumps of heat exchangers; 11: heat pump compressor; 13: circulating pump to outside with heating system; 14, 14a: liquid sink and circulation pump; 15: pipeline, bracket

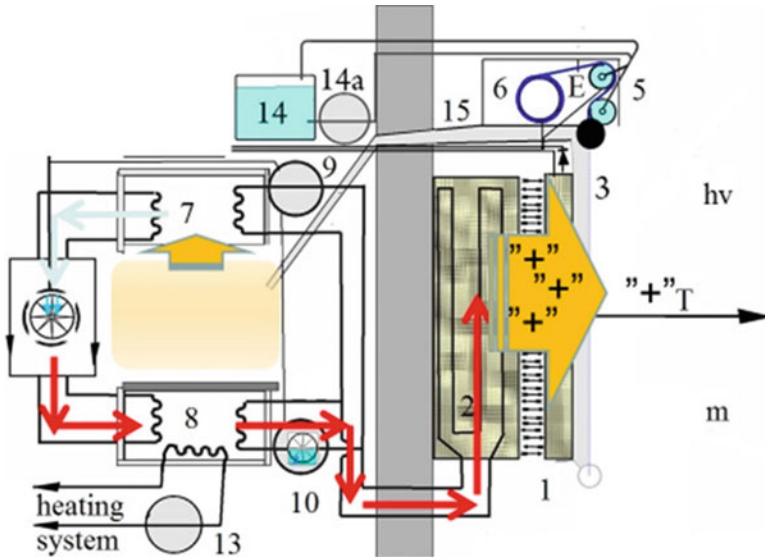


Fig. 46.6 So-called summer-type conditioner. 1: solar cell; 3: mobile dust-collecting film; 5: unit of electrical charge and washing of film; 6: geared motor; 7, 8: heat and cold sinks with heat exchanger; 9, 10: circulation pumps of heat exchangers; 11: heat pump compressor; 13: circulating pump to outside with heating system; 14, 14a: liquid sink and circulation pump; 15: pipeline, bracket

4 Components

The electromechanical part of the device uses inexpensive and common components: low-power refrigerator compressor, low-power 12 V circulation pumps, and gear motor with a 12 V DC motor. A variant with two solar cells with 120 W installation power allows operating with heat power measured in kilowatts, at 200 W PV power, and can be used to clean nearby air (0.5 m/s) from dust with particles more than 10 μm in size and at a speed of 0.1 m³/s (Fig. 46.7).

5 Conclusion

Currently, owing to the low price of traditional energy resources, there are practically no alternatives to the use of cost-effective solar panels and collectors except in home appliances, which are in high demand. The remaining options should be funded. Such devices can be sold as performers of household functions, not only electric energy sources. To increase the profitability of their use, they perform the following functions:

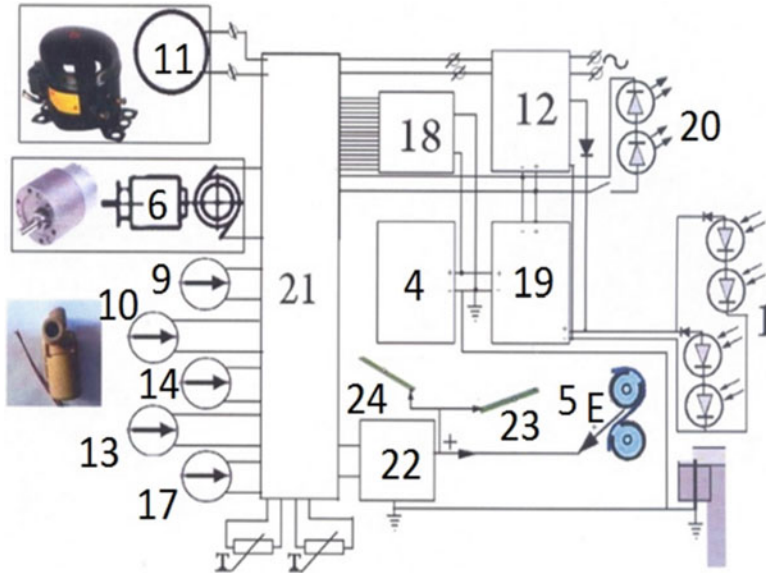


Fig. 46.7 Details and components of device. 1: solar cell; 4: 200 A*hours accumulator; 5: high-voltage electrode for electrifying dust-collecting film; 6: reversing geared motor; 9: circulating pump—radiator of cooling and solar panels; 10: circulation pump storage radiator of heat and solar panels; 11: heat pump compressor; 12: uninterruptible power supply with access to external battery; 13: circulation pump connecting central heating to heat radiator; 14: circulation pump for film washing and solar panel; 17: circulation pump for mixing of crystalline hydrate; 18: switching control unit; 19: battery controller; 20: LED illuminator; 21: switching module; 22: voltage multiplier; 23,24: foil electrodes under dust-collecting radiator drive T-thermistors

- Photovoltaic panels are protected from dirt and dust and their abrasive effects using self-cleaning transparent film;
- Solar panels accumulate electricity;
- They generate heat and cold for emergency rooms;
- Because they are connected to LEDs, as accumulators of energy, they smooth out the load at hours of peak congestion in urban networks when, for example, lights are turned on by consumers;
- They combine the role of thermal collector of solar energy with that of a solar cell;
- They serve as an external heat radiator for the exchange of air with the atmosphere for active heating and cooling systems (cooling the air in a room);
- They combine with central heating and air conditioning the capacity to accumulate heat and cold;
- They collect dust and fumes from car emissions.

Each of these functions can be activated or deactivated at the consumer's discretion without affecting other functions of the device.

References

1. Zhu N (2012) Combination between the solar water heating system and civil architecture. China's international conference for the solar industry, 11–13 Dec 2012
2. Roos F (2012) Design and optimization mounting system for PV power. China's international conference for the solar industry, 11–13 Dec 2012
3. Boonstra C (2012) Towards solar cities: low energy building for a renewable energy future. China's international conference for the solar industry, 11–13 Dec 2012
4. Meytin M (2000) Photovoltaics: materials, technologies and prospects. *Electronics: Science, Technology, Business*, pp 40–46
5. Yudelson J (2008) *Green building through integrated design*. McGraw-Hill, McGraw-Hill's Green Source Series, 21 Oct 2008. ISBN-13: 9780071546010
6. Basnet A (2012) Architectural integration of photovoltaic and solar thermal collector systems into buildings. Master's thesis in sustainable architecture. Norwegian University of Science and Technology Faculty of Architecture and Fine Arts Department of Architectural Design, History and Technology, Trondheim, June 2012
7. Grid connected PV power source of the ICPE's solar park, infrasolar issues, quality, future. The 12th WEC Central & Eastern Europe regional energy forum—FOREN 2014, Bucharest, June 2014. www.icpe.ro
8. Pearce J (2014) Combined photovoltaic solar thermal systems (PVT)—literature review. Michigan Tech's Open Sustainability Technology Lab
9. Kaya M (2013) Thermal and electrical performance evaluation of PV/T collectors in UAE. Master of science thesis EGI 2013:037MSC, KTH School of Industrial Engineering and Management Energy Technology, Stockholm, May 13

Chapter 47

Assessment of Airflows in a School Building with Mechanical Ventilation Using Passive Tracer Gas Method

Jessika Steen Englund, Jan Akander, Mikael Björling,
and Bahram Moshfegh

Abstract The focus of this study is to assess the airflows in a school building built in 1963 in Gävle, Sweden, which is subject to energy conservation measures (ECMs) in a forthcoming renovation. Today, the school building is mainly ventilated by several mechanical ventilation systems, which are controlled by a constant air volume (CAV) strategy. Schedules and presence sensors impose a high operation mode during the day and a low operation mode at night, on weekends and on holidays. The homogeneous tracer gas emission method with passive sampling is used to measure the average local mean age of air (τ) during different operation modes. Temperature, relative humidity and CO₂ concentration are simultaneously measured. The calculated relative uncertainty for the average local mean age of air in every measured point is approx. $\pm 20\%$. The results during low operation mode show an average value of τ of approx. 8.51 h [corresponding to 0.12 air changes per hour (ACH)], where τ in various zones ranges between 2.55 and 16.37 h (indicating 0.06–0.39 ACH), which is related to the unintentional airflow in the school. The results during mixed operation mode show an average value of τ of approx. 4.60 h (0.22 ACH), where τ in various zones ranges between 2.00 and 8.98 h (0.11–0.50 ACH), which is related to both unintentional and intentional airflows in the school. Corridors, basement and attic rooms and entrances have lower τ compared to classrooms, offices and other rooms. High maximums of the CO₂ concentration in some rooms indicate an imbalance in the mechanical ventilation systems. During a regular school week of mixed operation, which includes both high and low

J. Steen Englund (✉) • J. Akander • M. Björling
Division of Building, Energy and Environment Technology, Department of Technology
and Environment, University of Gävle, Gävle 801 76, Sweden
e-mail: jessika.steen.englund@hig.se

B. Moshfegh
Division of Building, Energy and Environment Technology, Department of Technology
and Environment, University of Gävle, Gävle 801 76, Sweden

Division of Energy Systems, Department of Management and Engineering,
Linköping University, Linköping, Sweden

operation modes, it is found that mainly the low operation modes show up in the results. The dynamics of the highly varying airflows in the building cannot be identified using the passive sampling technique.

Keywords Homogeneous tracer gas emission technique • Local mean age of air • Air change rate • Air leakage • School building

1 Introduction

Energy use in the built environment represents almost 40 % of the total energy use in Sweden. Substantial parts of the building stock from the 1950s to 1970s are facing major renovation, which provides excellent opportunities to implement energy conservation measures (ECMs) [1]. School buildings account for around 16 % of Sweden's public buildings. A survey done in 2006 indicated that, on average, schools use 213 kWh/m²/year [2].

Ventilation systems and air leakage often account for a considerable part of the total energy use in buildings. These airflows are often not accurately quantified, which poses problems when predicting the benefits of ECMs. Moreover, airflows may be intentional or unintentional; intentional flows are ventilation rates that correspond to the design of the system, i.e. fulfil the requirements imposed on the system. Unintentional airflows are unwanted ventilation rates owing to air leakage in the building envelope or ventilation systems or are related to the habits of occupants, for example inevitable airflows which arise from passing through entrances or uncontrolled airing. The homogeneous emission technique with passive sampling is an adequate technique to measure the average local mean age of air (τ) in a building. To capture τ during a shorter time period, active pumping can be done. The methods are described in [3] and [4]. The aim of this investigation is to quantify the actual airflows in a school building with mechanical ventilation systems. To assess intentional and unintentional airflows, the homogeneous tracer gas emission method using both passive and active sampling is used. Passive sampling results are presented in this chapter.

2 Case Study: Building Description

The school, which is owned by the municipality of Gävle, includes six buildings which were built in 1961–1963 and have a total heated floor area of 8803 m² with some 430 pupils (ages 6–16 years). The studied building which will undergo ECMs is 4577 m² and has four stories, including basement and attic, and mainly contains offices and lecture rooms for about 150 pupils and 40 staff members (Fig. 47.1).

The average energy use for all six buildings during the period 2012–2014 is 150 kWh/m²/year, a rather good energy performance compared to the Swedish



Fig. 47.1 The studied school building

average of 213 kWh/m^2 annually [2]. This is due to EMCs performed during the last two decades: additional wall insulation in the 1980s, roof insulation and three air handling units with heat recovery unit in the 1990s and adjustment of the HVAC control and regulation system in an energy performance contracting (EPC) project carried out in 2010. The objective of the new ECMs in the forthcoming renovation is to reduce annual energy use by 25 %, that is to 113 kWh/m^2 . Inside, there are four mechanical ventilation systems with heat recovery by rotating heat exchangers. The design flow is $9.8 \text{ m}^3/\text{s}$ (2.36 ACH), when all ventilation systems are running at maximum, provided by 35 kW fan power. Four additional exhaust air fans are located in fume cupboards in four classrooms. The ventilation system is controlled by a constant air volume (CAV) through schedules and presence sensors, which trigger forced ventilation in 21 classrooms on an on/off basis in each room. The other rooms are controlled by regular schedules. The schedules impose high operation mode during the day and low operation mode at night and on weekends and holidays.

3 Method

The homogeneous emission tracer gas method to determine the local mean age of air, using passive and active sampling techniques, is described by Etheridge and Sandberg [5] and in standard operating procedures [3, 4]. In the homogeneous emission technique, a tracer gas is emitted homogeneously and passively at a constant rate within the whole building. The building is divided into multiple zones, where the air is assumed to be fully mixed and the tracer is emitted in



Fig. 47.2 Passive source and sampler

proportion to the volume of each zone. In this study, tracer sources are contained in small metal tubes and the tracer is passively released by diffusion through a narrow capillary core. A thin metal wire blocks part of the opening area in order to adjust the emission rate (Fig. 47.2).

4 Passive Sampling

The diffusive passive sampler is a small glass tube with a well-defined opening area at the top. Sampling occurs through diffusive capture of tracer in an adsorption material (activated carbon) in the tube (Fig. 47.2). The total collected mass of tracer M_p is effectively a time integral of the mass collected in each moment. The average local tracer gas concentration ρ_a [g/m^3] during steady-state conditions is calculated from the amount of tracer M_p [g], the equivalent air sampling rate κ [m^3/h] and the sampling time t [h] according to

$$\rho_a = \frac{M_p}{\kappa \cdot t}. \quad (47.1)$$

The average local tracer gas concentration ρ_a sampled in a specific location is proportional to the local mean age, $\bar{\tau}_p$ [h], of air in the same location. The inverse proportionality factor q_m/V [$\text{g}/(\text{h} \cdot \text{m}^3)$] is the average homogeneous tracer gas emission rate per unit volume in the zone, which gives

$$\bar{\tau}_p = \frac{\rho_a}{q_m/V}. \quad (47.2)$$

The local mean age of air, $\bar{\tau}_p$, is the average time the supply air has spent in the zone before it reaches a specific point p . In the multi-zone representation, point measurements are used to estimate the mean age of air in a completely mixed zone in a larger building, henceforth called τ . The inverse of the local mean age of air is the local air change rate [ACH, h^{-1}].

5 Uncertainties of Local Mean Ages of Air

The average local mean age of air in a measured point has a total uncertainty s according to

$$s = \sqrt{s_{\text{source}}^2 + s_{\text{sampl}}^2 + s_{\text{meas}}^2 + s_{\text{inhom}}^2}. \quad (47.3)$$

The uncertainty of the overall emission rate is denoted by s_{source} , the relative uncertainty connected to the tracer sampling is denoted by s_{sampl} , the relative uncertainty connected to analysis of the samples is denoted by s_{meas} , and the relative uncertainty connected to deviations from the homogeneous tracer emission rate which might occur in single zones is denoted by s_{inhom} .

6 Experimental Setup

6.1 Equipment

A total of 153 passive sources and 98 passive samplers were used during the measuring period. In addition, 18 temperature (T) and relative humidity (RH) loggers (Mitec SatelLite-TH Mitec Instrument, Säffle, Sweden) and five devices of type Rotronic CL11 Rotronic AG, Bassersdorf, Switzerland logging the CO_2 concentration, RH and T every 5 min were used.

6.2 Procedure

In total, five passive measurement series were performed between 22 December 2014 and 2 March 2015. Prior to the first measurements, 18 Mitec TH devices (logging T and RH) and 153 tracer gas sources containing perfluorobenzene were distributed throughout the building; the first floor is as shown in Fig. 47.3. The analysis procedure was to calculate the collected tracer concentration in every

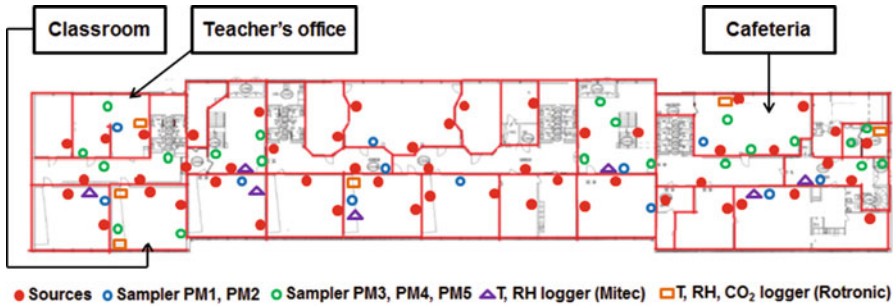


Fig. 47.3 Distribution of tracer sources and samplers on first floor with extra gauges in three selected rooms

sample, according to Eq. (47.1), and establish the average local mean age of air, according to Eq. (47.2). This was made using a dedicated gas chromatograph at the University of Gävle.

The measurement periods were selected to capture different operation modes in the school. Low operation mode refers to periods when no occupants were in the building and the mechanical ventilation was closed (at night and on weekends and holidays). Measurements at low operation aimed to capture unintentional ACH due to leakage. High operation mode refers to periods when occupants were present and the mechanical ventilation systems were running, i.e. during working hours. Mixed operation mode includes both high and low operation modes during an entire 2-week period.

Table 47.1 shows a measurement overview. During the two most extensive measurements, passive measurements (PM) 1 and 2, 39 samplers were distributed throughout all four floors to investigate the average ACH for the whole building. However, some samplers disappeared during PM2. Measurements PM3–PM5 investigate different categories of rooms in more detail and compare several samples in the same room to confirm the reliability of measurements. During PM3–PM5, Rotronic CL11 devices logged CO_2 , T and RH in selected rooms every 5 min.

6.3 Calculated Inaccuracy and Uncertainties

The relative inaccuracy s of the average local mean age of air in every measurement, according to Eq. (47.3), gave a total uncertainty of approximately $\pm 20\%$, within a 95% confidence interval. The relative uncertainty of the sources is approx. 10%, depending on the number of sources in each zone. More sources in a zone gives a lower uncertainty. The relative uncertainty of the samples is calculated to be approx. 14%, and the relative uncertainty of the analysis is approx. 10%. The s_{homog} is set to 0 owing to the assumption of homogeneously emitted tracer and

Table 47.1 Overview of passive measurements

Passive tracer gas measurements					
Measurement series	Number of samplers	Time period	Occupancy presence	Object of investigation	Comments
PM1	39	2 weeks, Dec–Jan	Low operation	Whole building + single zones	All mechanical ventilation was shut off, Christmas holidays
PM2	35	2 weeks, Jan–Feb	Mixed operation	Whole building + single zones	
PM3	8	Approx. 2 weeks, Jan–Feb	Mixed operation	Extra measurements in entrances and corridors	Extra <i>T</i> , RH, CO ₂ measurements simultaneously
PM4	8	Approx. 1.5 week, Feb	Mixed operation	Extra measurements in classrooms, office, café, others	Extra <i>T</i> , RH, CO ₂ measurements simultaneously
PM5	8	Approx. 1.5 week, Feb–Mar	Low/Mixed operation	Extra measurements mainly in offices	Extra <i>T</i> , RH, CO ₂ measurements simultaneously; holiday week for students but personnel were working

fully mixed air conditions in the zones. The accuracy of Mitec SatelLite-TH loggers is $\pm 3\%$ RH and $\pm 0.4^\circ\text{C}$, for relative humidity and temperature respectively. At temperatures of $23 \pm 5^\circ\text{C}$, the Rotronic CL11 has accuracies of $\pm 30\text{ ppm} \pm 5\%$ of the measured CO₂ value, less than 2.5% RH (between 10 and 90% RH) and $\pm 0.3^\circ\text{C}$ on temperature. The detection limit of a 2-week passive measurement period with the present set-up is about 10 ACH.

7 Results and Discussion

Results show that the τ during low operation ranges between 2.55 and 16.37 h (corresponding to 0.39 and 0.06 ACH) during PM1 and during mixed operation between 2.00 and 8.98 h (apparently corresponding to 0.5 and 0.11 ACH) during PM2–5 (Table 47.2). Results are presented in six categories of rooms (A–F) depending on usage and ventilation strategies. The weighted mean of average values for the entire building is 8.51 h (0.12 ACH) during low operation and 4.60 h (apparently 0.22 ACH) during mixed operation. The mixed operation values seem relatively low – especially ACH values.

Table 47.2 Minimum, maximum and average local mean age of air (τ) and average air changes per hour ACH in school building

Measurement results during low and mixed operation	Percentage of total building volume (%)	Low operation, PMI			Mean average ACH [h^{-1}]	Min-Max τ [h]	τ [h]	Mixed operation, PM2–PM5	
		Number of samples	Max-Min average ACH [h^{-1}]	Number of samples				Min-Max τ [h]	τ [h]
A Classrooms	41	16	0.17–0.06	0.08	6.09–16.37	12.58	17	3.71–8.98	5.94
B Administrative and teachers' offices, conference room	10	3(4) ^a	0.11(0.71) ^a –0.08	0.09(0.09) ^a	(1.40) ^a /8.96–12.15	(8.96) ^a /10.77	12	2.00–6.35	4.47
C Other rooms; lunch room, library, cafeteria	8	3	0.19–0.08	0.18	5.14–5.85	5.56	6	2.30–4.06	3.19
D Corridors	17	7	0.42–0.18	0.24	2.55–5.66	4.16	10	2.05–5.09	2.30
E Basement or attic rooms	18	3	0.29–0.15	0.21	3.41–6.65	4.87	3	2.09–5.03	4.50
F Entrances	6	6	0.27–0.23	0.25	3.65–4.44	4.07	11	2.32–3.17	2.69
Whole building	100	38(39) ^a	0.42–0.06	0.12	2.55–16.4	8.51	59	2.00–8.98	4.60

^aRepresent one measuring point in a teacher's office, which is excluded from average τ /ACH for category B and for the calculations for the whole building

As described in Chap. 4, the τ is calculated from the collected mass of tracer during the entire sampling period. An observation obtained during this study is that the calculated τ from the passive sampling mainly represents the time periods with highest concentrations of tracer (the low operation modes), for two reasons. First, owing to the time aspect, low operation modes represent around 70 % of a typical 2-week measuring period. Second, tracer gas concentration during different operation modes varies considerably. During high operation modes, the overall design mechanical ventilation for the entire school reflects ACHs of 2.36 h^{-1} and τ of 0.42 h when all ventilation systems are running. During low operation, the tracer concentration increases in combination with the longer time period in which the sampling occurs. During high operation, tracer concentration in the air decreases during a shorter sampling period. These result in an over time τ that cannot directly be translated into an average ACH value (hence previously termed ‘apparent ACH’). Dynamic flows, i.e. on/off controlled mechanical ventilation system airflows, cannot reliably be assessed with this passive technique alone, as pointed out by Stymne and Boman [6]. The average over time τ represents the local mean age of air, but the inverse of this average does not in general give the average ACH value.

Classrooms represent the largest volume share, about 41 % of the total building volume, and have the oldest air with the highest τ , ranging between 6.09 and 16.37 h during low operation and between 3.71 and 8.98 h during mixed operation. Even if the design ventilation rate in a typical classroom should provide about six ACHs in high operation mode (corresponding to τ equal to 0.17 h), these rooms show a higher τ compared to the other room types. According to staff at the school, classrooms are only occupied about 60 % of the school day, which explains the relatively high τ values during mixed mode. The differences between the classrooms probably depend on differences in class schedules. When the classrooms are unoccupied, doors facing corridors are closed, so the airflows in the corridors have a limited effect on τ in classrooms. Type B rooms (Table 47.2) show lower τ values compared to classrooms. Types D–F (corridors, attic and basement rooms and entrances) show lower τ values compared to other categories. Entrances show lower τ minimums than the classrooms’ τ minimum, during both operation modes, indicating large unintentional airflows caused by air leakage at the entrance doors and people passing through. Large apertures in the external walls of the basement can be one reason for the low τ in category E. Leaky ventilation dampers and ducts might also be an explanation for the high ACH in categories D–F.

Three rooms located on the first floor were selected in order to perform more detailed studies. These studies include multiple passive measurements (PM1, PM2 and PM4), active measurements during night time and investigation of the indoor air quality in terms of the indicators CO_2 concentrations, RH and temperature. Figure 47.4 shows results from PM4. In Fig. 47.5 the maximum and minimum CO_2 concentrations can be seen in the studied rooms. In the classroom, the maximum CO_2 concentration peaked at 640 ppm and has an average τ of 5.81 h. In the school cafeteria, the CO_2 concentration peaks at almost 1700 ppm, far above the ASHRAE standard of 1100 ppm [7], so the ventilation system does not seem to successfully provide good indoor air quality in the cafeteria. In the teachers’ room, the maximum

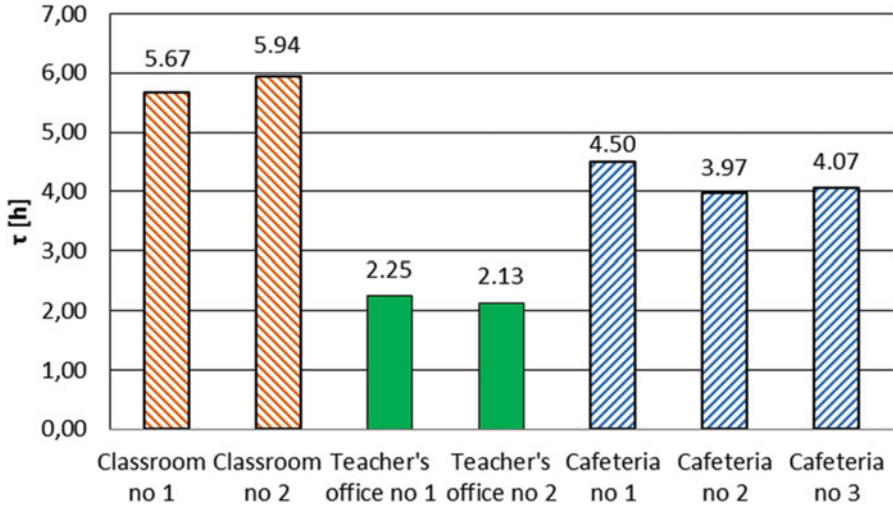


Fig. 47.4 τ in three types of rooms, mixed operation

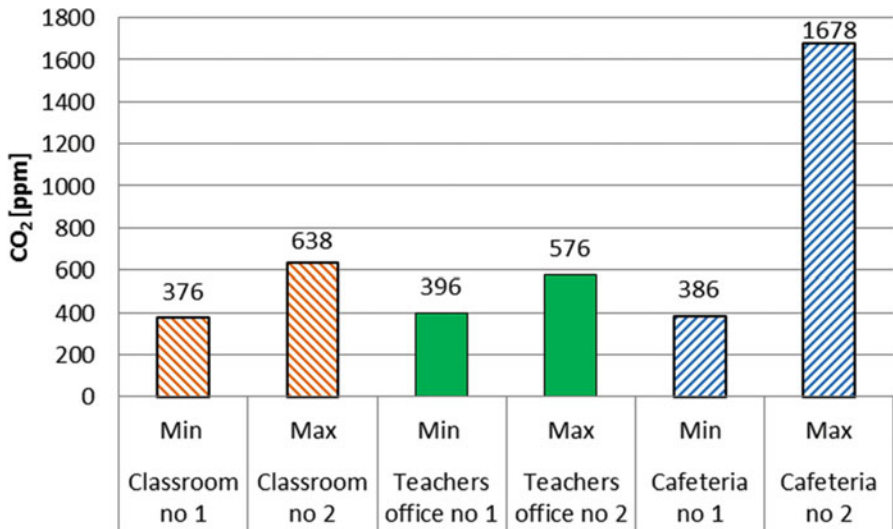


Fig. 47.5 CO₂ minimum and maximum concentrations

CO₂ concentrations never exceed 580 ppm, so the average ACH seems to be very high for this room, where the average τ is 2.19 h. This room is indicated by ^a in Table 47.2.

Figure 47.6 shows the CO₂, temperature and RH in the teachers' room over the course of a week in February. The even temperature distribution over time indicates a high ACH in the room since surplus heat is ventilated away; the same applies to moisture. This confirms the results of a low average τ from passive measurements.

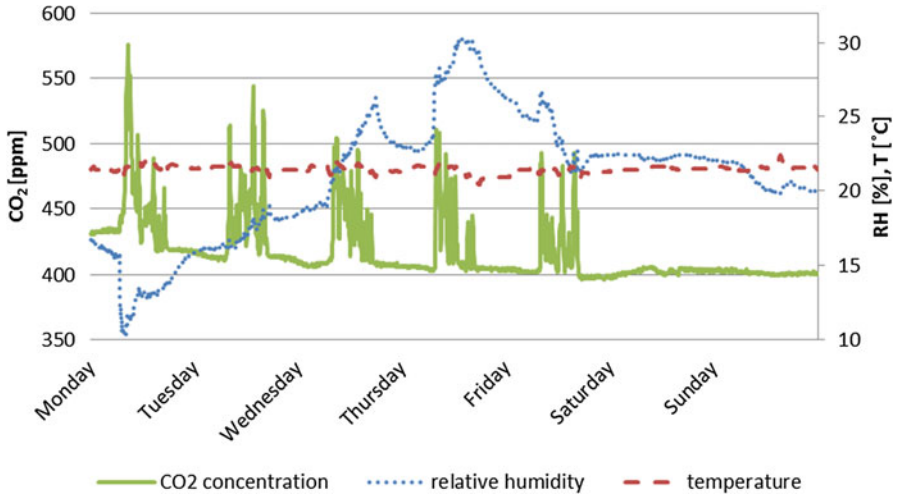


Fig. 47.6 CO₂, temperature and relative humidity in teacher’s office, February 2015

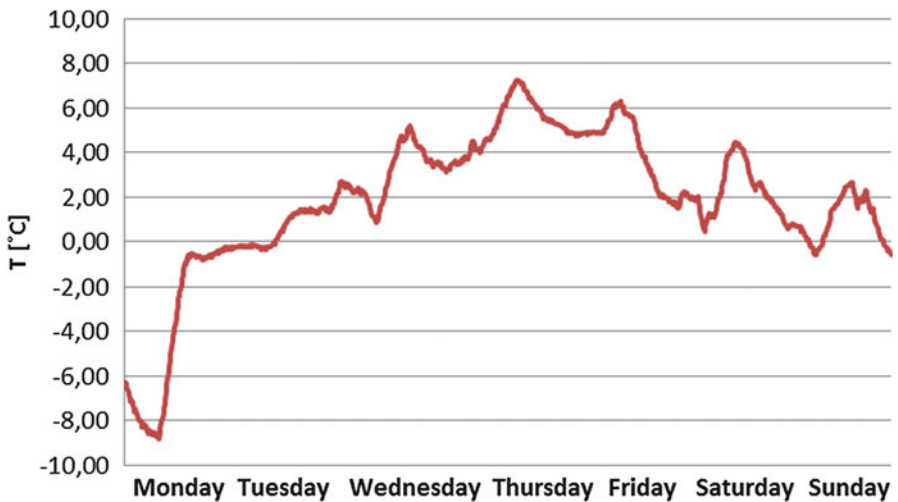


Fig. 47.7 Outdoor temperature, February 2015

Figure 47.7 show the outdoor temperature during the same week in February. The combination of a high ACH and the varying outdoor climate gives intermittent and sometimes low RH, which might influence the indoor air quality. The result from multiple passive sampling and CO₂ measurements in the same rooms indicates that the passive measurements are accurate, and this method shows good repeatability and good correspondence between the various measurements (Fig. 47.4). The ACH discrepancies are less than 7 % between the measurement points in the

same room, with the exception of one measurement point in the cafeteria (number 1 in Fig. 47.4), where the average ACH deviation was around 13 % compared to the other two measuring points. This deviation might depend on the location of the sampler, if it is placed in the vicinity of a supply air terminal.

8 Conclusion

The unknown ACH in the studied school building has been mapped at low operation and mixed operation. The τ in different locations is primarily a result of the amount of tracer collected during the low operation periods. This is because the smaller amount of tracer collected during high operation periods represents only a minor share of the total amount of captured tracer, in comparison with the higher amount of tracer collected during low operation.

Classrooms, administrative offices, teachers' rooms and other common rooms, such as the staff canteen, library and school cafeteria have higher τ values during both low and mixed operation compared to the other room categories – corridors, basement and attic rooms, and entrances. The lowest values of τ during both low and mixed operations were found in entrances, corridors and a basement storage room. Measurements of CO₂ show that today's ventilation systems are not in balance in every room and do not always provide sufficient indoor air quality in all rooms. High unintentional airflows caused by air leakage in entrances, corridors and the basement during low operation can be connected to apertures in external walls of the basement, leakage in the building envelope (especially leaky entrance doors) and leakage in ventilation dampers and ducts and through rotating heat exchangers. The average value of unintentional airflows for the building is 0.12 ACH (τ is 8.51 h) and in the various zones ranges between 0.06 and 0.39 ACH. On average, the estimated total ACH within the building during mixed mode, which accounts for intentional and unintentional airflows, is 0.22 h⁻¹ and in the zones ranges between 0.11 and 0.50 h⁻¹.

The passive tracer gas technique shows promising value when measuring unintentional airflows in low operation modes. However, results from active tracer gas techniques will be compared with results from former passive tests during mixed operation modes to assess high operation airflows since the ACH values obtained by passive sampling is dominated by low operation conditions. In future studies, measured airflows will be used in building energy simulation to diminish the impact of uncertainties in ventilation and infiltration input data. Furthermore, the indoor environmental quality in the school building was investigated through survey studies which are currently being analysed.

Acknowledgement This work was carried out under the auspices of the industrial post-graduate school Reesbe and financed by Gavlefastigheter AB, AB Gavlegårdarna, the Knowledge Foundation (KK-Stiftelsen) and University of Gävle, Sweden.

References

1. Hall T, Vidén S (2005) The million homes programme: a review of the great Swedish planning project. *Plan Perspect* 20(3):301–328
2. Energimyndigheten (2007) *Energianvändning och inomhusmiljö i skolor och förskolor—Förbättrad statistik i lokaler, STIL2* (In Swedish)
3. ISO16000-8:2007. *Indoor air—Part 8: Determination of local mean ages of air in buildings for characterizing ventilation conditions*. Geneva (2007): International Standards for Business, Government and Society
4. Nordtest (1997) *Ventilation: local mean age of air—homogeneous emission techniques*
5. Etheridge D, Sandberg M (1996) *Building ventilation: theory and measurement*, vol 50. Wiley, Chichester
6. Stymne H, Boman CA (1998) Air distribution in an office building as measured with a passive tracer gas technique. In: *Proceedings 17th AIVC-conference, Greece, Vol 1*, pp 379–388
7. ANSI/ASHRAE (2013) *Standard 62.1–2013—Ventilation for Acceptable Indoor Air Quality: ANSI/ASHRAE*

Chapter 48

Energetic and Functional Upgrading of School Buildings

Paolo Giordani, Alessandro Righi, Tiziano Dalla Mora, Mauro Frate, Fabio Peron, and Piercarlo Romagnoni

Abstract In Italy, currently most schools require improvements to energy performance and indoor air quality. On the other hand, school buildings require structural assessment and strong renovation interventions to maintain their service functionality. Moreover, the use of spaces should be reviewed and redesigned to be more compatible with modern educational models, making the schools unique integrated spaces. Each space should have the same dignity and flexibility, meeting anticipated future needs and expectations and offering a positive environment that should support learning, teaching and recreational activities. The national government has recently launched policies and plans to face up to this situation, imposing some guidelines to incentivise the actions of local municipalities. The challenge as well as the aim of this research is to verify the possibility of combining energy retrofits with functional renovations as a unique approach to taking action, exploring the conditions and measures to create synergy. As a case study, school buildings in a medium-sized city, Castelfranco Veneto, in the north-eastern part of Italy were analyzed with the aim of defining a method of intervention on different functional layouts. In a first phase of the work, all 21 schools present in the area were analyzed. Subsequently, three groups of buildings with homogeneous characteristics in terms of age, construction technologies, and shape factors were identified. Finally, a case study for each group was analyzed in detail and a proposal for improvements to the energy efficiency and functionality was presented. In this chapter, one of the case studies is presented.

P. Giordani • A. Righi • T.D. Mora (✉) • M. Frate • F. Peron • P. Romagnoni
Università IUAV di Venezia, Venice, Italy
e-mail: tdallamora@iuav.it

1 Introduction

In present-day Italy school buildings assets are characterised by high levels of energy consumption and inadequate levels of spatial comfort. This research aims to outline a methodology that can be used to assess a series of measures targeted at the improvement of both energetic performances and spatial distribution of this enormous heritage of building stock. In recent years, sustainable policies extensively funded by the Italian government and the European community have facilitated the process, aimed at the improvement of the energetic efficiency of school buildings. However, the rearrangement of their spatial and functional characters has often been left behind.

In March 2013 the Italian Ministry of Education, University, and Research (MIUR) published a document containing guidelines regulating the technical design details of the school building stock [1]. This issue has led to the transformation of school buildings into civic centers, a connection with the urban fabric, where, thanks to a renewed concept of space, frontal lessons are no longer considered the leading model in pedagogy [2, 3].

Indeed, the objective of research in this area has become the creation of a strong synergy between those two aspects of the intervention in order to come up with integrated design solutions – improving both energetic performance of buildings and the quality of space, resulting in a better teaching environment.

2 Methodology

2.1 *Analysis of Existing Stock*

In Italy, the existing school building stock is composed mainly of buildings constructed from the first post-war period to the 1980s. Moreover, historical buildings, built between 1750 and 1900 and readapted for educational activity, represent a smaller part. Therefore, these buildings rarely have the directives of administrative order D.M. 18/12/1975 on school buildings imposed on them [4]. As a whole, the Italian school building stock reveals a generally low level of attention in terms of energy efficiency, low levels of maintenance of different components and finally a not always correct use by users. They do not use the most profitable types of energy, or their production and distribution systems result in low output; energy is not used in the most efficient manner – for example, some buildings are characterised by a high level of heat loss, while other spaces are overheated. In all these scenarios energy use is inefficient, resulting in negative effects on the comfort of users and in the waste of resources.

These buildings are overall characterised by energetically inadequate envelopes and systems, where the comfort and quality of both air and spaces are often at a low level. Moreover, the environmental conditions hamper the learning process and the

work of teachers. To analyse quickly and simply this vast network of buildings, a simplified methodology has been put in place. This technique permits the evaluation of energetic performance with different levels of accuracy.

First, a precise analysis of a sample of buildings must be carried out. This analysis must be accomplished using a database containing information about the age, technology, volume, usage time, spatial distribution and energetic consumption records of buildings.

Second, the buildings are divided into homogeneous groups composed of elements with similar characteristics. The parameters used to accomplish this division are construction period, shape factor and volume of the construction. The construction period identifies the available technology and the materials used, the presence of insulation and the rigidity of the functional layout. The shape factor identifies the shape of the building and serves as a valuable indicator of the level of dispersion of heat through opaque envelopes: buildings with a high shape/volume (S/V) index show greater dispersion through the covering horizontal structure; buildings with a low S/V index show greater dispersion through walls. The volume of construction is also important because it affects the level of energy consumption: the efficiency of improvements grows in proportion to the level of energy consumption of the building. After these considerations, three different groups were selected: historical buildings with low S/V and low volume, non-historical buildings with low S/V and high volume, non-historical buildings with high S/V and low volume. The grouping into homogeneous types of buildings allows for the optimisation of punctual analysis of a specimen of construction aimed at the projection of individual results to all buildings with the same typology.

2.2 *Evaluation of Energetic Performance*

Together with the homogeneous grouping of existing school real estate, it is also necessary to precisely evaluate the energetic performance. Using a simplified evaluation index, it is possible to have an energetic framework of a sample, identifying criticalities and average values for each homogeneous group. The evaluation method employed is the one proposed by the ENEA-Fire methodology [5]. This methodology consists in the estimation of a Normalised Energetic heating Index (IENr). This normalised index takes into account some sensible factors like the amount of hours in which the heating system is turned on and the shape factor (S/V), derived with the ratio of the dispersion area of the construction shell (S) and the relative heated volume (V). The IENr index allows for a first evaluation of the energetic behaviour in the heating season of each building-plant system. This results in an ultimate grouping of the typologies with respect to the level of education: for example, primary school, secondary school and high school. The IENr takes into account actual energy consumption (C), heated volume (V) and the location of the edifice (degree day, GG). It is then normalised through two different

indexes: shape factor (Fe) and the number of hours the heating system is activated (Fh):

$$\text{IENr} = \frac{C \times \text{Fe} \times \text{Fh} \times 1000}{V \times \text{GG}}$$

To ensure the quality of the evaluation, as indicated in the preceding discussion, it is advisable to overestimate the IENr index by 10% so as to take into account eventual areas in which the temperature does not register at a constant 20 °C. Considering both the IENr and the level in the Italian school system, the energetic behaviour of the building-heating system complex is evaluated and grouped into three different classes: good, sufficient and insufficient behaviour.

Following a raw analysis it is possible to analyse in detail the energetic behaviour of a sample of buildings representative of a specific homogeneous class. This analysis is given by the conversion of all information about the constructions into a mathematical model and its energetic simulation in a dynamic regime, calculated using certain software. The mathematical model is created integrating data obtained from previous analysis and other data acquired through the methodology presented in the standard UNI TS 11300 (parts 1 and 2) [6, 7]. The energy analysis of the buildings was performed using the EnergyPlus [8] simulation tool. To improve the quality of the evaluation, the numerical model is calibrated with the data on real consumption.

After the construction and calibration of the numerical model, a direct and precise evaluation is developed towards more advantageous and profitable operations. The results of the various proposed improvements to operations are evaluated through a comparison of performance indices concerning energetic consumption, reduction of emitted CO₂, annual economic savings and time of economic return.

2.3 *Project Proposal*

In accordance with the MIUR guidelines [1], various design proposals were analysed in order to ensure the coexistence of energy-efficiency-improvement measures with the functional improvement. These operations will give new spatiality and new teaching functionalities to buildings. Owing to the low modifiability of the spatial-functional structure of the Italian school building stock, mostly because of their outdated construction, the application of these guidelines has proved to be very difficult; in addition, the guidelines were conceived with new constructions in mind. Various project solutions have been proposed to apply these directives to already existing Italian school buildings (Fig. 48.1). These solutions are not invasive and assure the maximum functional output.

- (a) The action on internal partitions – usually made on the basis of a division between classrooms and hallways – makes it possible in the connection space

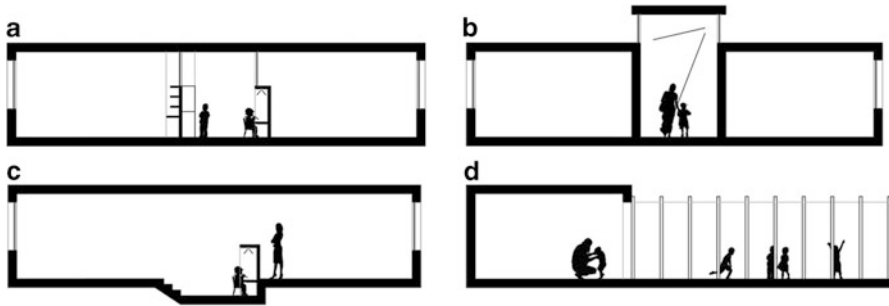


Fig. 48.1 Functional measures schema: (a) on internal partitions, (b) on upper horizontal partitions, (c) on lower horizontal partitions, (d) on external partitions

to define a system of small recesses and spaces for individual study and small student group activities, resulting from the integration of properly equipped walls.

- (b) Operations on upper horizontal partitions are particularly useful as a support to the creation of new teaching spaces since they allow natural light, which promotes well-being, comfort and energy savings in spaces with little lighting, for example, hallways.
- (c) Intervention on lower horizontal partitions, if possible, is extremely effective, especially thanks to the creation of different paving quotas. This action will define diversified spaces in the same space which will assure adequate levels of privacy for specific activities because of visual obstacles.
- (d) Action on the external partitions of buildings is generally applied to buildings with a single floor which open out onto external gardens where possible. Classrooms are designed with the exterior space in mind thanks to the opening of glass panels and pergola systems which serve both as a protection from atmospheric agents and as spaces for outdoor teaching activities.

3 Application

3.1 Case Study: San Andrea Primary School

This section presents an application of the methodology previously described. The case study is a school building property in the municipality of Castelfranco Veneto (TV). The municipality owns 21 school buildings of different levels (e.g. kindergarten, primary and secondary) and aims to develop an intervention strategy targeted at all buildings. The proposed methodology is a tool supporting the Castelfranco Veneto municipality for identifying the most suitable interventions.

The analysed school was identified from the application of the methodology. In fact, 21 schools were analysed in terms of energy performance and then divided into homogeneous groups.

The elementary school San Andrea is a primary school in the village of San Andrea oltre il Muson, located in the south-west of Castelfranco Veneto. The building dates back to the early 1960s and is characterised by a floor above ground and by a small portion on the first floor. The building is constructed of brick masonry without insulation. The pitched roof is made of a slab of masonry covered by a simple blanket of clay roof tiles supported by warping boards and planks of wood. The window frames were replaced in 2007 and are in good condition, but they do not meet the most current standards in terms of energy efficiency. The windows are composed of a metal frame without a thermal break and of a simple double-glazing unit with air. The heating system dates back to the building construction, but in 2007 the old generator was replaced with a condensing boiler of 105 kW which offers good performance, though it is limited by the old system of distribution, control and emission.

Regarding spatiality and space distribution, San Andrea school is an emblematic case and presents characteristics common to the majority of other primary schools built in the 1960s and 1980s. The centrality of the classroom and, therefore, frontal lessons have always been considered the hub of learning.

The school has a functional area of 1236.5 m², of which:

- 259.5 m² (21 %) is used for the classrooms;
- 373.4 m² (30.2 %) is used to support teaching (laboratories, library and gym);
- 319.0 m² (25.8 %) is used as service areas (toilet, kitchen, boiler room); and
- 284.4 m² (23 %) is used as connection spaces (distributive).

A preliminary analysis shows that teaching spaces (the first two items) have an area almost equivalent to the areas of service and connection (last two items). In these terms the design choice has been to carry out a reevaluation of the distributive spaces, which now look like simple corridors which are mostly dark and used only for connection purposes, in order to identify eclectic and multifunctional spaces which can at least partly meet the new functional requirements (see Sect. 1.1.3 of the MIUR guidelines).

3.2 Energetic Improvement Measures

The analysis of the San Andrea school was also supported by an assessment of the dynamic numerical model of the building which was aligned with the actual energy consumption of the school. This allowed us to analyse the energy performance of the building, quantifying the heat loss through the building envelope: 8 % of losses are through glass components, 10 % through walls, 2.5 % through floors, 26.5 % through the coverage (roof), 20 % through infiltration and 33 % from natural ventilation. These data identified two critical issues: dispersion through coverings

Table 48.1 Improvement measures

Measure	Consumption [kWh/a]	Savings [%]	Cost of intervention [€]
Actuality	90,865.25	–	–
Roof insulation	74,856.51	17.62	45,584.26
Wall insulation	80,160.58	11.78	114,750.31
Window replacement	87,803.13	3.37	50,906.35
Heating system generator replacement	87,419.41	3.79	13,645.85
Wall insulation + roof	63,404.14	30.22	154,437.94

and heat loss due to natural ventilation, which, however, is necessary to ensure the correct ventilation of the spaces.

Then improvements more appropriate to the situation were identified and analysed (Table 48.1). The most advantageous strategy identified was to intervene by insulating either the outer walls or covering in order to reduce the energy consumption of the building by 30.22%. Note that in this building, consisting mostly of one floor and with a very high form factor, the single best intervention is to insulate the covering because this results in a reduction in energy consumption of 17.62%. The costs of the intervention were obtained from the official price database of the Veneto region [9].

3.3 *Design for Increasing Functionality*

Following the definition of necessary improvements for energy performance, a design strategy was formulated to improve the use and usability of the space.

Because of the rigidity of the internal structure of the school, it is not possible to make radical changes to the space distribution, but some specific actions could be taken in line with the policy of energy conservation (Fig. 48.2).

The first proposal is to drill the floor ceiling and roof in order to ensure an adequate level of natural lighting and air exchange in the corridor below. The second proposed action is to replace the internal vertical partitions, placed as separators between educational spaces and the hallways, with a system of walls which can accommodate both the side facing the classrooms and laboratories and the side facing the distribution spaces. Storage spaces will be placed near the entrances: in the classrooms for learning materials for the students, in line with the concept of ‘school without a backpack’, and close to the access of the building for materials intended for particular activities. On the sides of these storage spaces, the walls will house in the lower parts a system of recesses for study or individual reading. In the upper parts (above 1.80 m), to ensure adequate visual impediments, some glazed surfaces will be placed between the spaces: in synergy with skylights these must eliminate the feeling of extreme isolation created by the earlier corridor.

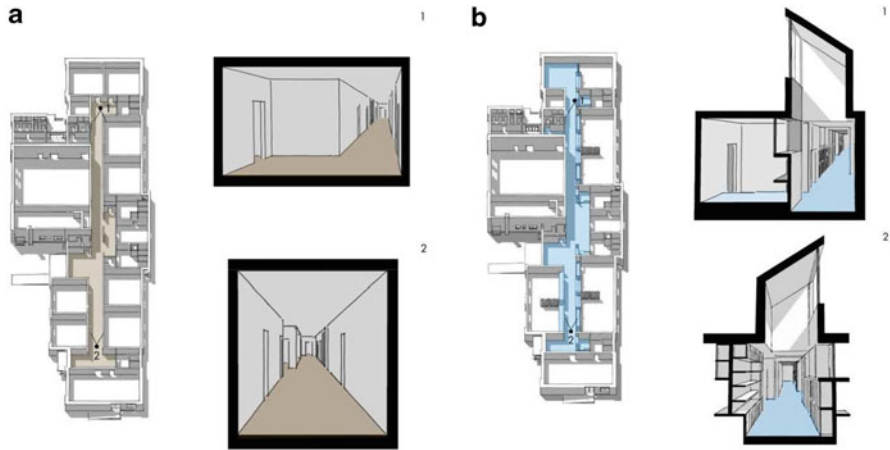


Fig. 48.2 (a) Current situation. (b) Possible intervention of project design

Finally, other spaces obtained from the recess of the corridor near the entrance to the bathrooms have been redefined as informal spaces for relaxing, with the addition of paving and soft seats suitable for this purpose.

4 Results and Discussion

The definition of interventions on various buildings, according to a division into homogeneous groups, allows a more complete view through the identification of parametric costs in $\text{€}/\text{m}^3$ based on detailed metric calculations, which quantify the cost for retrofitting existing school buildings (Table 48.2). Every parametric cost refers to the best intervention among all options in the same category in order to obtain 20% annual savings in energy consumption.

For example, in the S. Andrea case study, 30.22% of annual savings is derived from $110.83 \text{ €}/\text{m}^3$ total parametric cost; the energetic solution combines two interventions – covering insulation (point of greater criticality) and external wall insulation – in order to ensure adequate performance by the elimination of thermal bridges, giving a parametric cost of $42.71 \text{ €}/\text{m}^3$. As regards intervention for increasing functionality, the solution adopted concerns the conversion of the large space of the central connection into a so-called learning street capable of accommodating various educational activities through the use of skylights, movable and furniture and facility, giving a $53.09 \text{ €}/\text{m}^3$ of parametric cost.

The best relation between costs and benefits belongs to the group of nonhistoric buildings with low form factors because the large volumes lead to targeted interventions, mostly by the insulation of walls. With regard to nonhistoric buildings with high form factors, the most efficient intervention is insulation cover. Historic

Table 48.2 Cost-benefit relation

Group of buildings	Energy efficiency parametric cost (€/m ³)	Functional improvement parametric cost (€/m ³)	Total parametric cost (€/m ³)	Annual savings (%)
Historic buildings <i>S/V < 0.70</i>	50.08	42.18	92.26	25.72
Nonhistoric buildings <i>S/V < 0.70</i>	43.53	37.60	81.13	38.25
Nonhistoric buildings <i>S/V > 0.70</i>	43.13	45.68	88.81	35.9
Total	44.54	43.23	87.77	34.9

buildings present a low cost-benefit ratio because the construction technique is outdated, the system net is very rigid and the space is not suitable for school activities. The most significant intervention in these cases appears to be improving the heating system, glazing systems and, sometimes, the lowering of too high ceilings.

5 Conclusions

The values, even if indicative, outline a credible scenario and show how to improve the existing school building stock, and not necessarily requiring high expenditures, but supported in part by incentives – eschewing radical actions which might be more effective but much more expensive and less feasible due to lower investments in the school system.

Several problems have been encountered in the research stages: in the initial data collection period, simulations of the mathematical model, especially the estimated period of natural ventilation inside rooms, and then, during the planning stage, the application of solutions to space-functional distribution into very rigid and not very changeable structures.

The results show the possible interventions on school buildings and their cost-effectiveness, but the main result is the elaboration of an experimental method that offers the best design of rational, sustainable and cost-effective measures to improve the existing buildings, regardless of the geographical context and or type of building analysed.

Research efforts could be directed at studying how this methodology would be replicated on different scales and in different types of existing buildings. For other schools with different uses and different levels (high schools, universities) can be verified by assessing patterns of energy consumption and the proposals of design interventions dedicated instead, in the case of schools in different climate zones, energetic intervention and architectonic design will be based on the setting and

social climate. For other types of buildings, public or private, with different uses (commercial, residential, office), the methodology will be fully adequate, with particular attention paid to the evaluation of energy performance, energy design and functionality.

References

1. Linee Guida MIUR, Norme tecniche quadro edilizia scolastica, 26 Marzo 2013, Italian Ministry of Education, University, and Research (MIUR)
2. Hertzberger H (2007) Space and learning. 010 Publishers, Rotterdam
3. Fisher K (2006) Linking pedagogy and space. Department of Education and Training, Victoria
4. Norme tecniche aggiornate relative all'edilizia scolastica, Decreto Ministeriale 18 Dicembre 1975, Italian Ministry of Education
5. ENEA FIRE Guida per il contenimento della spesa energetica delle scuole, Centro Ricerche Casaccia, Roma, 2004
6. UNI TS 11300-1 (10/2014): Prestazioni energetiche degli edifici, Parte 1. Determinazione del fabbisogno di energia termica dell'edificio per la climatizzazione estiva ed invernale
7. UNI TS 11300-2 (10/2014): Prestazioni energetiche degli edifici, Parte 2. Determinazione del fabbisogno di energia primaria e dei rendimenti per la climatizzazione invernale
8. Strand RK, Crawley DB, Pedersen CO, Liesen RJ, Lawrie LK, Winkelmann FC, Buhl WF, Huang J, Fisher DE (2000) [EnergyPlus: a new-generation energy analysis and load calculation engine for building design](#), Association of Collegiate Schools of Architecture. Proceedings of the ACSA Technology Conference, Cambridge, Massachusetts, 14–17 July 2000
9. Prezziario regionale dei lavori pubblici del Veneto (2013) <http://www.regione.veneto.it/web/lavori-pubblici/prezzario-regionale> (ultima visita marzo 2015)

Chapter 49

Evaluation of Thermal Performance, Environmental Impact, and Cost Effectiveness of an XLam Component for Retrofitting in Existing Buildings

Tiziano Dalla Mora, Alessandro Righi, Fabio Peron,
and Piercarlo Romagnoni

Abstract Renovation and retrofitting of residential buildings is a subject of great concern in Italy: most of the existing building stock is completely inappropriate in terms of structural rigidity in the event of earthquakes and with respect to the objectives of energy efficiency set by European law. This research presents the design of an innovative system of structural reinforcement using cross-laminated timber (CLT) technology based on materials with environmental compatibility: an XLam panel comes attached to a metal structure in the outside or inside layer of the external wall of an existing building; the stratigraphy also includes the insertion of insulation, a net of new systems (hydraulic and thermal), and new window frames. The new component is studied for modularization and standardization to ensure simplicity and speed of installation, low cost of providing, and assembly. The research focuses on aspects related to building physics and sustainability in construction in order to optimize the choice of materials: analyses of performance were conducted and simulations performed on various kinds of insulation materials in order to determine the best possible configuration in terms of thermal performance, environmental impact, and cost effectiveness. The results were verified with the construction of a prototype checked by a thermal test. Finally, with the obtained data the renovation of a case study building with different measures of intervention is verified.

Keywords Italian residential buildings • Structural reinforcement • Energy renovation • CLT technology • Thermal performance • Environmental impact and cost effectiveness

T. Dalla Mora (✉) • A. Righi • F. Peron • P. Romagnoni
Università I.U.A.V. di Venezia, Venice, Italy
e-mail: tdallamora@iuav.it

1 Introduction

In Italy, seismic events in recent years in regions as Molise in 2002, in Abruzzo in 2009, in Emilia Romagna in 2014 have highlighted the total inadequacy of existing buildings during seismic events and consequently the need for action to address this criticality. Moreover, 92 % of the Italian residential stock was built before 2001, but the first legislation to impose technical criteria for anti-seismic construction was enacted in 2003.

This research develops and deepens the application of a particular structural XLam panel connected to existing masonry: wood has excellent characteristics, such as its light weight, mechanical strength, and thermal insulation, and XLam technology has demonstrated a capacity to distribute stress in both the vertical and horizontal directions, even in the presence of openings. An XLam panel shows a great ratio between strength and specific weight compared to other common materials, such as masonry and concrete, and presents a better hard-set and anti-seismic behavior than a wood frame structure.

The proposed technological system is composed as follows: a metal structure is fixed at the slab level or in the existing masonry to provide flexural rigidity and is connected to an XLam panel by a wooden curb that transfers shear stresses coming from the building (Fig. 49.1).

Different kinds of insulating materials have been proposed in order to improve thermal resistance and to optimize the hygrometric behavior of the panel. This study focuses also on the environmental impacts (carbon footprint and embodied energy) of each proposed material, and at the end, the economic feasibility of the materials is evaluated for the proposed combination of layers and products.

The main objective is to identify the best combination to use to meet all benchmarks of the research in terms of reducing energy consumption, lowering CO₂ emissions, and being cost-effective in the case of retrofitting.

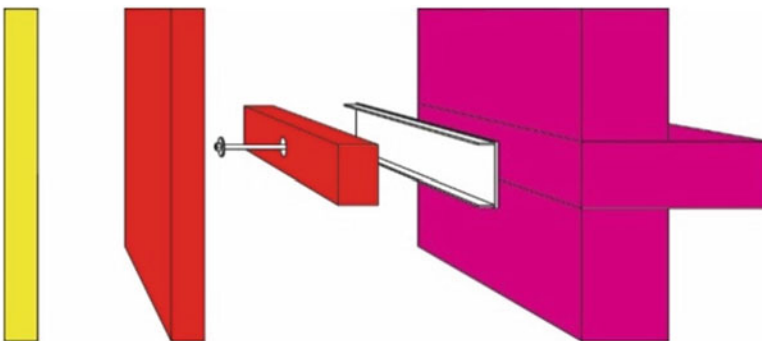


Fig. 49.1 Panel and curb connection to slab level

2 Methodology

The research work was planned and followed a precise strategic line for checking the type of intervention and the performances of the technological component, applying it to a single external wall, and comparing all aspects of the analysis. The first phase saw the construction of a matrix in which elements were selected introducing a code for XLam (K) and insulation [X1 expanded polystyrene (EPS), X2 mineral wool, X3 aerogel] selected from among the best sellers in the market and brick masonry (Ya) to verify the performances with a test in a prototype and with simulations in a real case study; some specific characteristics were identified to carry out the analysis: for example, values of thickness, thermal conductivity, specific heat, steam resistance, environmental impacts by Life Cycle Analysis (LCA), supply, and laying costs.

Then four combinations of different stratigraphies of the various elements were identified; these combinations became the object of all analyses and simulations (Fig. 49.2). Each combination was identified by the real possibility of intervention in the existing masonry building and by adopting the technological system in XLam. The Italian legislation on historic *façade* protection, the level of damage and decay of the building, and the location and condition of the site at the urban level affect the positioning of the panel (see code K in Table 49.1) outside or inside the existing masonry wall and, as a consequence, the internal or external application of insulation (X).

The obtained combinations schema allows to understand what is the more favorable stratification in terms of energy improvement in case of refurbishment in the existing building stock. It is also possible to control the performances of interventions in an existing building.

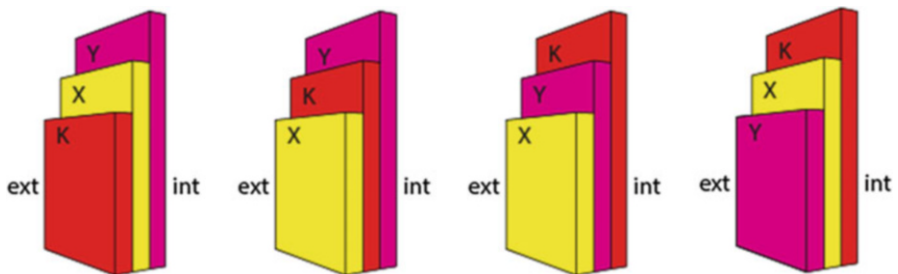


Fig. 49.2 Possible combinations

Table 49.1 Minimum insulation thickness to achieve $U = 0.34 \text{ W/m}^2\text{K}$

Code	Material	Insulation thickness (m) for Ya wall
X3	Expanded polystyrene (EPS)	0.055
X5	Mineral wool	0.068
X6	Aerogel	0.021

This research shows the analysis developed on this new component and its combination of materials: in the first phase by numerical simulation using a mathematical model and then a thermal characterization by testing the materials on a prototype.

3 Simulation and Analysis of Panel

3.1 Thermal Analysis

Because of its fiber orientations and porosity, wood is a poor heat conductor. The thermal conductivity (λ) for wood shows fluctuating values (from 0.10 to 0.20 W/mK) because of the considered wooden species and the invariable content of air and water (and a consequent presence of moisture). The masonry walls instead have different features because the stratigraphy is composed of different materials that differ by age and manufacturing process, and is also influenced by the geographic area and type of construction. However, the thermal property values are obtained from the UNI TS 11300-1 [1] database, which lists the most useful configurations, and the obtained thermal transmittance has a U value between 1.4 and 0.7 W/(m²K).

The proposed insulating materials are different by their origin; they could be of vegetable, mineral, synthetic, or composite origin. The main objective was to identify the thickness of each insulation for the purpose of obtaining the minimum U value of the wall according to current national regulations (Italian Regulation Dlgs. 192/2005 [2], i.e., 0.34 W/m²K for an Italian climate zone E corresponding to the Venice area) and to obtain a thickness value lower than 0.1 m, corresponding to the interspace created by a metal structure for holding up XLam panels. The most important result is that all the proposed insulation allows thicknesses below 0.07 m (Table 49.1). Examples include a selection of masonry with the combination XKY, tested with all types of masonry and selected insulation [3].

3.2 Environmental Impact

The goal was to investigate the impact of the elements in the XLam technological panel. The analysis focused on various insulations selected (Y) to obtain the values of the embodied energy measured in megajoules per kilogram (MJ/kg) (Table 49.2) and to identify those with less impact at equivalent transmittances.

An identical study was also conducted on the brick masonry (X) and on the XLam panel, obtaining a value of 672 MJ. This value is increased by the insertion and the evaluation of insulation materials, provided an absolute value of Embodied Energy ranging between 700 and 1300 MJ.

Table 49.2 Embodied energy values for insulation

Code	Material	Thickness (m)	Specific weight (kg/m ³)	Weight (kg/m ²)	Embodied energy (MJ)	(MJ × kg)
X3	Expanded polystyrene (EPS)	0.10	37.00	4	101.50	386.60
X5	Mineral wool	0.12	100.00	12	16.80	197.65
X6	Aerogel	0.04	120.00	5	53.00	243.18

Table 49.3 Impact categories

Impact category	Measure unit	X3	X5	X6
Human health	DALY	5.21E – 06	2.15E – 05	3.65E – 06
Ecosystem quality	PDF×m ² ×year	3.93E – 01	2.61E + 00	4.39E – 01
Climate change	kg CO ₂ eq	1.12E + 01	1.68E + 01	2.61E + 00
Resources	MJ primary	3.43E + 02	2.23E + 02	2.64E + 02

Table 49.4 IPCC 2007 impacts

Measure unit	X3	X5	X6
kg CO ₂ eq	13.255	17.830	3.370

Subsequent investigations focused on wood panels and insulation for the calculation of the LCA of all materials by software simulations: using the Impact 2002 + v2.11 method, the four impact categories (Table 49.3) and their values were obtained, including the embodied energy expressed in the resource category [7, 8].

Calculation allowed a comparison of the results obtained for embodied energy using the ICE database developed by University of Bath: the results are reliable and comparable this database allows a tolerance of approximately $\pm 30\%$ in respect to Impact 2002+v2.11 method. Finally, a CO₂-equivalent value was derived indicating the extent of the global warming potential (GWP) of greenhouse gases or, rather, the GWP for each selected material (Table 49.4).

A comparison between the production process of packages according to the 2007 Intergovernmental Panel on Climate Change (IPCC) method was analyzed: a 100 % value is attributed on-base percentage to material with a higher CO₂ equivalent and the remaining values were obtained on-base percentage as a consequence. Some materials, such as aerogels and expanded polystyrene, have low impacts since in the first case the material is used in small amounts, while the second one has low harm values in terms of global warming.

3.3 Outcomes on Panel and Simulation on Brick Masonry

With reference to the methodology definition and based on the data of the various analyses, it is possible to put the obtained information in order and to summarize it

for the purpose of configuring the particular base panel and applying it to a case study.

The best combination of existing masonry, XLam panel, and insulation is given in particular by the last variable: in fact, the proposed XLam panel is given by structural calculation, and its characteristics are broadly similar in the actual market; the kind of masonry might change depending on the building, and the selected types of insulation have different properties and performances. The choice was made with an eye toward minimizing heat loss, environmental impacts, and intervention costs (Table 49.5). A further constraint was added in connection with fixing the existing masonry owing to the size of the structure and to the passage of the system net: from the previous analysis it has made that it could take advantage of 10 cm of thickness on the gap in the inner side of the panel in correspondence of structure or exploit the external side with a gap of 10 cm at least for plumping thickness.

The type of insulation that better meets the demands and benchmarks for minimizing thermal, economic, and environmental requirements is aerogel (X6), followed by polyurethane foam EPS (X3) and mineral wool (X5). Aerogel gives the best balance, but it shows significant results only in thermal and impact behavior, even if it is currently cost-prohibitive; polyurethane foam and mineral wool give similar thermal performances, but the former is cheaper because it is more widely sold, and the latter shows a low environmental impact in embodied energy value. This selection was the basis for all further analyses of technology nodes and types of masonry.

After the insulation was chosen and the location decided, the four combinations were verified in order to control the formation of condensation and the heat flow in thermal bridges and to provide data for other areas of research (functional, seismic, structural) or for the design and sizing of the technological element and the architectural and functional conformations for application to residential buildings.

First, a three-dimensional (3-D) model was made from different kinds of masonry, selected from the most frequently encountered in the Italian building stock from 1950. The evaluation of performances allows to determine the best combination of materials depending on the position of the insulation, according to the four combinations explained in the methodology. The result leads to the concept of an external “coat” (KXY), which, in addition to thermally insulate, allows the complete precast of the panel and a fast installation on site, with related economic benefits (Fig. 49.3).

Table 49.5 Outcomes for insulation after thermal, impact, and economic analysis

Code-Material	λ [W/(m K)]	φ (h)	Supply (€/m ³)	Laying (€/m ²)	Embodiment Energy (MJ)	Carbon Footprint (kgCO ₂ eq)
X3—EPS	0.035	19.96	110.00	39.00	386.60	13.255
X5—mineral wool	0.040	19.82	150.00	70.00	197.65	17.83
X6—aerogel	0.013	0.33	430.00	90.00	243.18	3.37

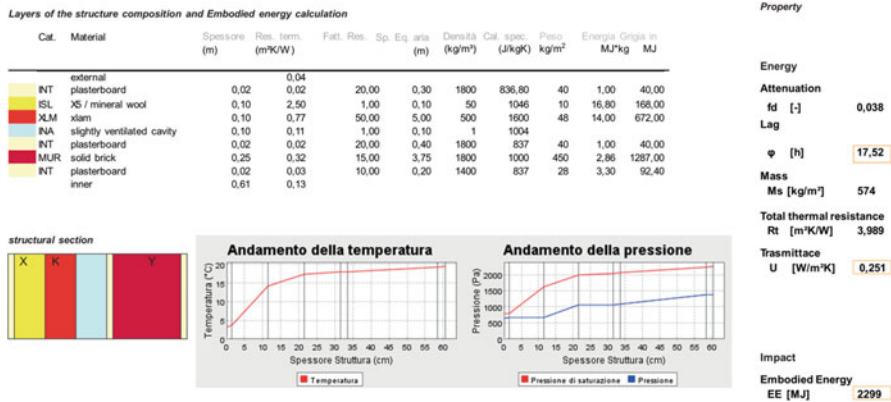


Fig. 49.3 Test on an X5KYa combination

Regarding the intervention on the internal side of the existing masonry, the same orientation as the outside part of the masonry was imposed using a mirrored stratigraphy. The performances of thermal transmittance are improved and to remedy the condensation, two states of vapor barriers were introduced sealing the XLam panel and the insulation package [4–6].

To illustrate the procedure, this chapter presents the results of the selection of three significant elements: XLam panel (K), mineral wool insulation (X5), and plastered masonry on solid brick (Ya). This stratigraphy was chosen because it shows the worst values of temperature and humidity between those obtained with the combinations and with the selected materials, and in addition, it was studied since this type in fact it is the most widespread type of masonry in Italian building stock and it is the same as that of the case study.

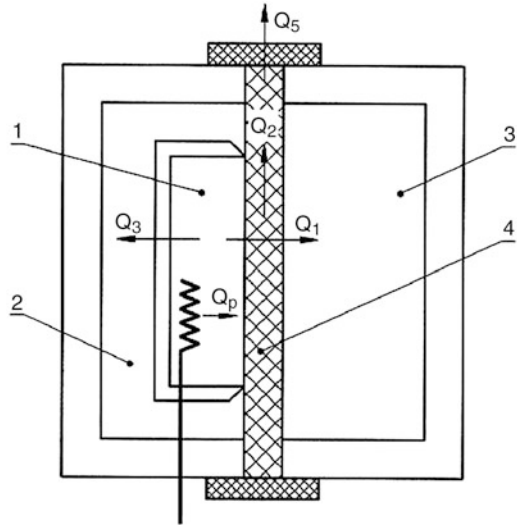
3.4 Characterization and Test on a Prototype Connected to a Brick Masonry

Since the architectural design of the building envelope reflects not only aesthetic concerns but also performance (in particular thermal performance), a hygrothermic test was carried out using a hotbox with a thermal guard (Fig. 49.4) [12–15].

A prototype of the technology was built using an XLam panel (1 × 0.8 × 0.12 m) that was applied to brick masonry and, according to the combination XYK, tests were performed using two types of insulation, mineral wool, and polyurethane foam EPS.

The device allowed the characterization of the thermal behavior of the inhomogeneous structure by calculating, in conditions of steady state, the thermal transmittance (U) and the thermal resistance (R). The measurement equipment was able to maintain a constant temperature difference between the faces of the sample for a

Fig. 49.4 Hotbox schema:
 (1) metering box; (2) hot room with guard;
 (3) cold room; (4) prototype



period of time sufficiently long to permit determination of the stationary state of the thermal flow and, hence, made it possible to perform all the measurements with the required accuracy. The prototype was placed between a hot room ($20\text{ }^{\circ}\text{C}$) and a cold room (at $-5\text{ }^{\circ}\text{C}$); subsequently a metering box was applied where the electrical resistances dissipated a measurable power. Applying a series of thermocouples to the inner and outer surfaces of each stratum of the prototype, the thermal behavior was assessed by measuring the heat flow difference of the temperatures on the walls. In this case the test lasted 3 days to reach the stationarity of the thermal flow, and it returned values of thermal transmittance very similar to those derived from the simulations, with a standard deviation of 0.5 %.

4 Application to Retrofitting: Case Study

The data obtained from analysis of materials and from tests on built components were verified on a case study building requiring energy and seismic refurbishment. It is a multifamily building in Venice from the 1950s, composed of five levels, with an entrance on the ground floor, three levels with six residential units, and warehouses on the last level. The structure is made of reinforced concrete with a masonry envelope made of hollow brick without insulation and single-glazed windows; a high-temperature traditional boiler constitutes the central heating system for heating and domestic hot water (DHW), with radiators as terminals in the individual apartments. The energy performance is therefore very low, but it is similar to that in the majority of existing buildings from that period, so it has serious structural problems with regard to safety and seismic activity (Table 49.6).

Table 49.6 Case study characteristics

Building typology	Multifamily	
Location	Venice	
Climatic zone	E	
Heating degree days	2.345	
Gross volume	1806.71	m ³
Heated area	475.92	m ²
Dispersing area	1068.16	m ²
Glazing area	53.30304	m ²
Floor net height	2.7	m
Footprint area on ground	185	m ²
S/V	0.591	

4.1 Three Possible Scenarios

The aim of the analysis here is to apply the technological system in XLam in such a way as to achieve the minimum requirements of energy performance set by Italian law. With increasing complexity and degree of improvement and investment, three scenarios were created with possible measures in the building in order to compare the results from the point of view of reduction in energy needs, environmental impact, and cost effectiveness (Fig. 49.5).

After the simulation, some considerations are presented (Table 49.7). In case 1, the heating system does not change and the intervention consists of an installation of the technological system in XLam using mineral wool as insulation, as in the X5KYa combination; in addition, all existing windows are replaced with low-energy double-layer windows, in accordance with Italian law. The energy requirement drops to 121.607 kWh/m²a, which is Italian energy class E; the total cost of the intervention is around €150,000,000.

Compared with the previous case, in case 2, the generator is replaced and a condensing boiler is installed, maintaining existing terminals so as not to disrupt the existing situation. Obviously, the energy performance improves and costs increase: energy needs amount to 107,833 kWh/m²a, class D, and the total cost is around €200,000,000.

Finally, case 3 is designed like a standard intervention for improving energy in a multifamily building: in the external envelope windows are replaced with low-emissivity glass and an insulation “coat” of mineral wool is installed. Technology measures consist of the installation of a condensing boiler and a system of solar panels for DHW and photovoltaic panels. With the same overall cost of intervention as case 2, the energy improvement requires 84,400 kWh/m²a, class C, thus reaching the benchmark of 87,975 kWh/m²a as required by Italian law.

The environmental impacts in the proposed interventions are interesting and express the same concepts in thermal analysis: between the traditional intervention of retrofitting and the insertion of the XLam component, the reductions in greenhouse gas emissions are equivalent, and in any case they decrease compared to the existing situation. Moreover, the embodied energy calculation (Table 49.8) of each

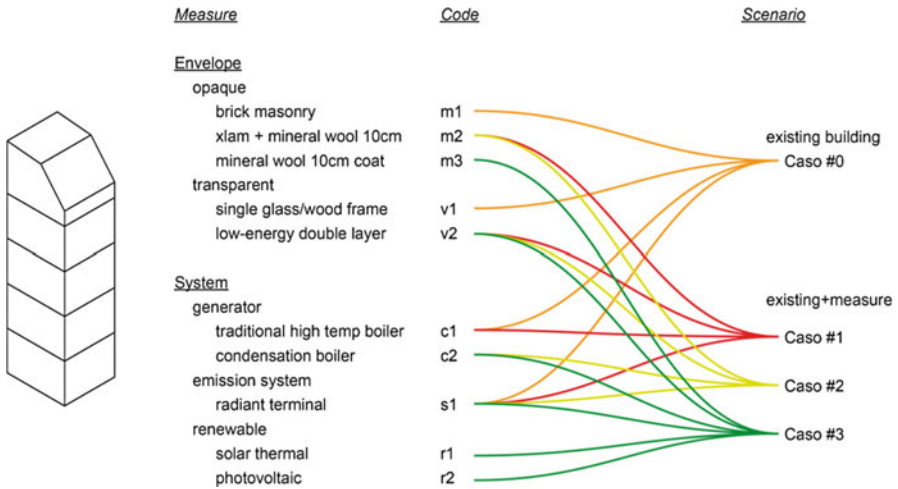


Fig. 49.5 Schema of measures and identification of possible scenario

Table 49.7 Energetic performances

Energy Performances	Measure unit	Case 0	Case 1	Case 2	Case 3
EPi—Total heating need	kWh/m ² a	153.601	83.388	74.359	76.044
EPacs—Total acs need	kWh/m ² a	37.875	38.219	33.475	8.356
Eppl—Global energy need	kWh/m²a	191.476	121.607	107.833	84.400
Energy class		F	E	D	C
CO₂ emissions	kgCO ₂ /m ² a	50.225	31.831	20.745	17.440

intervention on the external envelope shows that the mineral wool coat’s values are four times less than those of the new components, precisely because the last case involves the use of a structural wood panel [9–11].

By comparing the costs and benefits of the interventions, the cost savings in terms of energy needs are significant compared to the current € 8201.62per year: in all three scenarios, the costs are almost halved, with a maximum reduction of 44 % in case 3 due to the renewable energy contribution. Counting the costs, deductions, and actualized savings, the payback time remains very high, about 50–60 years. However, all scenarios would be able to take advantage of national tax relief programs of 65 and 50 %, allowing for writing off the costs of the interventions in 10 years and, consequently, significantly reducing the time for seeing a return on investment – within 30 to 40 years (Table 49.9).

Table 49.8 Embodied energy calculation

Case	Material	Thickness (m)	Specific weight (kg/m ³)	Weight kg/m ²	Embodied energy (MJ)	(MJ × kg)
Case 2	Plasterborad	0.02	2000	40	1.00	40.00
	Mineral wool	0.10	100.00	10	16.80	168.00
	XLam panel	0.10	480	48	14.00	672.00
	Total embodied energy					880.00
Case 3	Plasterborad	0.02	2000	40	1.00	40.00
	Mineral wool	0.10	100.00	10	16.80	168.00
	Total embodied energy					208.00

Table 49.9 Measure cost and time return

Cost and measure	Case 1	Case 2	Case 3
Cost of whole system (XLam + mineral wool) (€)	136,424.00	136,424.00	
Cost of window replacement(€)	13,325.76	13,325.76	
Cost of mineral wool insulation (€)	–	–	42,000.00
Cost of condensation boiler substitution (€)	–	70,000.00	70,000.00
Cost of photovoltaic system (€)	–	–	86,400.00
Cost of solar thermal system (€)	–	–	18,400.00
Total without tax relief (€)	149,749.76	219,749.76	216,800.00
Total with tax relief (€)	97,337.34	142,837.34	127,960.00
Annual cost of energy bills (€)	5208.47	4618.79	3615.09
Time of return on investment without tax relief	–50 years	–61 years	–47 years
Time of return on investment with tax relief	–33 years	–40 years	–28 years

4.2 Outcomes in Different Scenarios

In brief, the XLam system installation gives very good results, improving energy efficiency and safety in the case of seismic events (case 1). However, this technology is very effective and convenient only if it is combined with other measures: in fact, comparing the results of the intervention target for energy efficiency (case 3), the investment is similar, although the reduction in energy needs is considerably higher, but energy bills would still be cut in half. Thus, this new technological system (as in case 2) aims at the seismic and static requalification of Italian buildings and can be drivers of whole-building improvements with regard to energy, aesthetics (*façade* design), and functional measures, reducing the overall costs; in addition, it also brings tax relief.

5 Conclusions

The research presented here has achieved several objectives regarding environmental, economic, and energy issues. The panel with a new technological system makes it possible to achieve good results in terms of the thermal performance of selected insulations, which exceeds the normative standard for efficiency in existing buildings. Furthermore, it is a versatile system because it allows different solutions to reduce size and a heaviness of the technological system (XLam and structure) and different kinds of assembly configurations within and outside of a building according to needs and constraints. The analysis of environmental impacts returns low values due to the use of natural materials (wood, mineral wool), low mass (aerogel), or an optimized production chain (polyurethane).

Thermal tests on the prototype of masonry and XLam proved and validated the simulated values and revealed the behavior of existing masonry subjected to insulation and connected to an XLam panel, producing a null condensation.

The scenarios of the case study demonstrate the economic feasibility and the convenience of the components only if incorporated into a program of general redevelopment and retrofitting of a building.

Further research could be extended to several different scientific areas; with regard to building physics, the analysis of thermal points could be strictly deepened or it could expand the research to various residential typologies in order to obtain output from buildings with different surface/volume index and with different numbers of residential units, in an attempt to attain the objective of an antiseismic building and simultaneously a nearly zero-energy building (NZEB), a building capable of striking a balance between energy consumed and energy produced close to zero.

Therefore, the research presented here has achieved several objectives regarding environmental and energy issues: the proposed technological system allows for different solutions and assembly configurations, designed to reduce the size and weight of insulation materials but always ensuring at least minimum compliance with legal requirements: the combinations with respect to insulation in fact allows for comparable performances and variations according to interventions in existing building typologies.

References

1. UNI TS 11300—Normativa tecnica di riferimento sul risparmio energetico e la certificazione energetica degli edifici
2. D.Lgs.192/2005 e s.m.—Attuazione della direttiva 2002/91/CE relativa al rendimento energetico nell'edilizia
3. UNI EN ISO 6946/2008—Componenti ed elementi per l'edilizia. Resistenza termica e trasmittanza termica. Metodo di calcolo

4. UNI 13788:2003—Prestazione igrotermica dei componenti e degli elementi per edilizia; verifica condensa interstiziale
5. UNI EN ISO 14683/2008—Ponti termici, consente di calcolare il valore della trasmittanza termica lineica Ψ_k ; calcolare i flussi termici attraverso metodi semplificati in corrispondenza alle giunzioni tra elementi di edifici, ma non si applica a ponti termici associati ai telai di porte e finestre o a facciate continue
6. UNI EN ISO 10211/2011—Ponti termici, calcolo flusso termico bidimensionale e tridimensionale
7. ISO 14040—Passaggi per lo sviluppo della procedura del Life Cycle Assessment
8. ISO 14040:2006 Environmental Management—Life Cycle Assessment—Principles and Framework e ISO 14044:2006 Environmental Management—Life Cycle Assessment—Requirements and Guidelines
9. ISO EN 9001—Sistemi qualità—Modello per l'assicurazione della qualità nella progettazione, sviluppo, fabbricazione installazione ed assistenza
10. DI 83/2012 (Art. 11)—Detrazioni per interventi di ristrutturazione e di efficientamento energetico
11. DI 63/2013(Art. 14)—Detrazioni fiscali per interventi di efficienza energetica
12. ASTM C-236 (1993) Standard test method for steady-state thermal performance of building assemblies by means of a guarded hot box
13. ASTM C-1199 (1999) Standard test method for measuring the steady-state thermal transmittance of fenestration systems using hot box methods
14. UNI EN ISO 8990. Determinazione delle proprietà di trasmissione termica in regime stazionario: metodo della doppia camera calibrata e della doppia camera con anello di guardia
15. Zobec M, Colombari M, Peron F, Romagnoni P (2002) Hot box tests for building envelope condensation assessment. Proceedings of the 3rd European conference on energy performance and indoor climate in buildings, Lyon, France, 23–26 October 2002

Chapter 50

Self-Awareness Tool for Renewable Energy Production in Mixed-Use Urban Tissues: *Incubators* European Project for the Mediterranean Region

Luca Caneparo, Federica Bonavero, and Barbara Melis

Abstract Drawing on the *Incubators of Public Spaces* project, funded by JPI *Urban Europe*, this chapter considers the methods and tools used to support individuals', groups', organisations' and enterprises' self-ability to evolve towards grassroots interventions in urban regeneration processes. In particular, the chapter focuses on the assessment of the rational use and sustainable production of energy in mixed-use urban tissues, especially located in the Mediterranean region.

Everywhere in Europe and beyond, the on-going increase in the rational use of energy is changing urban spaces and raising citizens' awareness about energy. In the Mediterranean climate region – characterized by warm to hot, dry summers and mild to cool, wet winters – some strategies have already proven effective and replicable. Moreover, if we take as reference a mixed-use urban tissue, containing dwellings, production buildings, services and open spaces, unexploited synergies between different uses open a number of further opportunities (e.g. the plane roof of a neighbourhood supermarket can easily accommodate photovoltaic panels for the supply of electricity to residential buildings).

In particular, this chapter addresses the topic of renewable energy production potential of a Mediterranean mixed-use urban tissue with regard to its relationships with the local energy demand, with further issues of environmental sustainability (i.e. embodied energy, daylight, transportation energy), and with the role of citizens' self-interest actions. Indeed, the *Incubators* interactive and Web-based platform is designed to provide intuitive feedback about energy balance and cost savings. It provides guidance to tackle path-breaking energy issues on the building, neighbourhood and city scales so as to synergically attain the utmost environmental benefits.

L. Caneparo (✉) • F. Bonavero • B. Melis

Department of Architecture and Design, Politecnico di Torino, Viale Pier Andrea Mattioli, 39–10125, Turin (TO), Italy

e-mail: luca.caneparo@polito.it; federica.bonavero@polito.it; barbara.melis@polito.it

Keywords Sustainable urban neighbourhoods • Energy transition • Web-based energy assessment platform • Self-awareness tool

1 Introduction

The last century has witnessed the mass construction of buildings, often little related to their climatic, cultural and material contexts, with the construction industry primarily delegating the interior comfort of buildings to climatic systems. More, recently, practitioners in the field of architectural design are redesccovering site-specific solutions, which means solutions relating both to the integration of buildings in their surroundings and to the pursuit of energy savings. This trend is confirmed by the European Commission's interest in the cooperative and cohesive development of Europe's regions. The Interreg MED Programme [1] is the reference programme for Mediterranean partner Countries: it is the transnational programme of European Territorial Cooperation that aspires to promote sustainable growth in the Mediterranean area. So far, 155 projects have been programmed with total a budget of more than 250 million euros. This kind of intervention is intended to stimulate a new green economy, fostering a more rational use of material and non-material resources, such as energy and local competence.

Of course, the EU requirements, according to which from 2021 onwards all new buildings must comply with a nearly zero-energy standard, are in the foreground. Therefore, regulation of the energy performance of buildings or, even better, of neighbourhoods is crucial. In particular, it is necessary to investigate whether it is possible to strike a balance between energy consumption and on-site energy production potential, and to take into account the interlacement of urban environments and citizens' behaviours and attitudes with respect to energy issues. The European project *Incubators of Public Spaces*, which Politecnico di Torino is coordinating, aims to improve stakeholders' and citizens' consciousness in urban regeneration projects.

Assuming that many stakeholders and lay people have some degree of environmental goodwill, especially in connection with energy issues, and want to 'do their bit' in the struggle to limit climate change, people are seen as being actively engaged in systems as participants and, as a consequence, able to contribute their considerable knowledge and expertise to those systems.

Goodwill, however, often has good intentions but unpredictable results. To drive these efforts and manage the complexity of urban projects, *Incubators* is working to develop a Web tool. Through this tool, *Incubators* addresses ways to harness the new technological possibilities and integrate them within multilevel planning systems to assist distributed decision-making in the self-organisation of places. The project advances these challenges by linking a unique urban co-creative software to e-participatory engagement applications and crowdfunding tools, involving active co-creation in the placemaking by and for people.

2 Research Objectives

The specific objective of *Incubators* research is to enable all players involved in interventions of urban regeneration – from ordinary citizens to public administrators – to assess their own contributions and the cost-effectiveness of their actions in relation to the benefits obtained. The result will be a tool for a comprehensive and rapid assessment of energy savings and carbon emission reduction (Fig. 50.1).

To reach this goal, the tool must be able to satisfy some performance criteria during the early phases of design:

- To carry out rapid evaluations of the energy consumption of neighbourhood designs and determine the potential for on-site renewable energy production;
- To estimate the cost of intervention;
- To provide a rapid assessment of the concept of a project which will be useful for directing project strategy;
- To engage in the design (or decision) process with private and public stakeholders at the same time;
- To be an open tool accessible to all, in which interested parties in urban development can enter the features of their project and get an assessment of its efficiency;
- To be an intelligible instrument suitable for multi-level competency;
- To be an incremental database about a specific site, useful for sharing information and shortening the data input phase.

When all these requirements are met, the tool will be capable of giving users a complete report on feedback regarding their project proposals. In cases of interventions for energy purposes in urban environments, such as energy plants or energy refurbishment, the *Incubators* tool will assess energy benefits and urban morphological variations concurrently to define an overall judgment about a project.

A very important step in the research has been to identify the dimensions of energy which will be assessed by the *Incubators* tool. In its final version, the Web

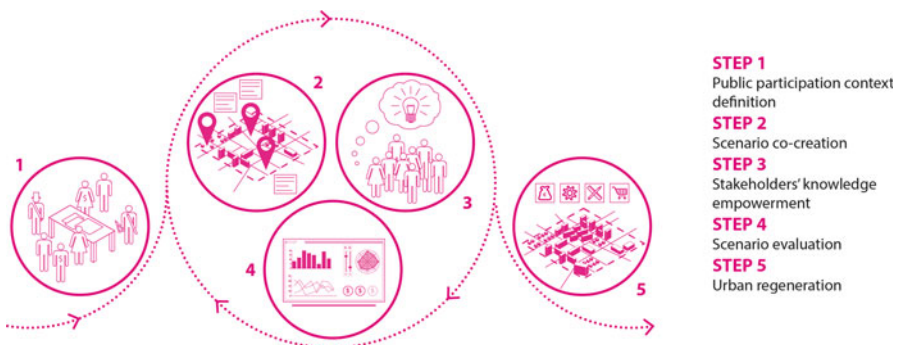


Fig. 50.1 *Incubators* process

tool could be capable of estimating the total energy consumed within a neighbourhood across four energy dimensions: (a) *operational energy*, or the energy consumed in daily operations and maintenance of the neighbourhood; (b) *transportation energy*, or the energy consumed when households travel within and beyond the neighbourhood; (c) *embodied energy*, or the energy used in manufacturing materials or transporting materials to a construction site; (d) *on-site renewable energy production*, which refers to new stocks of energy that could be produced on site; plus the *financial analysis* of costs and savings attributable to an energy-efficient project.

2.1 Framework

Some topics emerge as crucial when this methodology is applied to urban design, to regeneration cases especially. First, the neighbourhood scale is the elementary unit of investigation. At the neighbourhood scale, it is possible to assess the sum and the interlacement of the individuals' actions. In particular, the neighbourhood scale shows better than the building scale the energy balance of urban activities. In fact, the energy dimensions seen earlier are defined at the neighbourhood scale.

Second, social ambitions play a strategic role in urban regeneration, making it essential to put urban stakeholders and their aspirations at the centre of the process and to consider them as agents managing their own practice [2]. However, to do more than just pay lip service to accomplishing this goal, urban stakeholders must also be able to assess their own expectations about both energy and cost aspects, thereby providing informed input. In addition, simple input data management is necessary because, as already stated, non-specialists are also expected to be users as well. Consequently, we are developing a tool that everyone can use to simulate their own projects.

Lastly, the communicative aspects of the tool are very significant. The outputs should be immediately understandable to enable easy comparison of different scenarios. Since we are looking for 'consensus and cooperation rather than strategic action strictly' [3], it is not only a graphic issue, but mostly a skill of summary, without losing the complexity of the real.

3 Tool Development Steps

In furtherance of these objectives, the work is organised on two different levels. One level relates more directly to the design of the tool: its purposes, the features of the neighbourhoods to be assessed and the link between the separated outcomes which pertain to different aspects simulated independently. The other level relates to the usability of the tool, in order to improve users' self-awareness: to this end, we are implementing a Web-based tool, an online platform for both expert users and non-expert users to upload their own projects and simulate them.

3.1 Neighbourhood Simulation Systems

Nowadays several software tools exist to assess sustainability; nevertheless, the majority of them are dedicated to the assessment of energy performances at the building scale, and most of them work only at a detailed stage of the design. More recently, various research projects have addressed simulation at the neighbourhood scale.

To drive actions in urban regeneration, we have investigated both building and neighbourhood scale types of tools to understand how to better formulate the tool for *Incubators*. Platforms from different research groups have been investigated, first to understand the neighbourhood features they are analysing and simulating and, then, to infer examples of simulation workflows.

The selected tools are *Energy Proforma*, *Urban Modeling Interface (UMI)*, *Integrated Environmental Solutions Virtual Environment (IESVE)*, *TOWNScope* and *ArchSim Energy Modeling*. To the best of our knowledge, they represent a good array of tools in this field.

3.2 Main Features of Analysed Tools

The energy dimensions that have emerged from analysing the above mentioned tools are operational energy, transportation energy, embodied energy and on-site renewable energy production. Besides these, two additional features are daylight: given the solar radiation on *façades*, this function computes the interior illumination on an hourly basis; and outdoor comfort: evaluation of human thermal comfort in an urban open space.

Figure 50.2 summarises those dimensions and their frequencies within the analysed tools, at either the neighbourhood or building scale. The dimension of on-site energy production is present only in two tools out of the five considered.

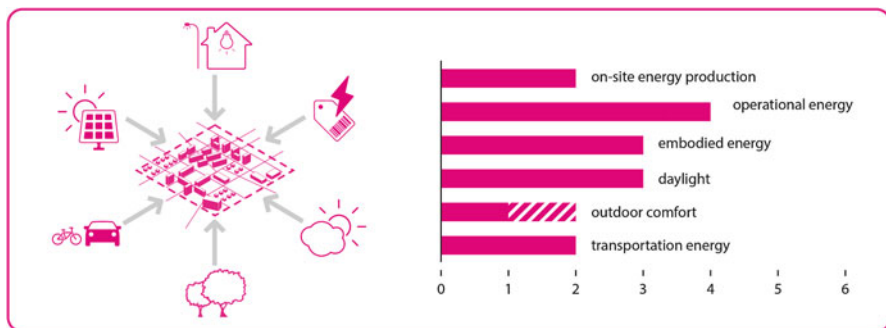


Fig. 50.2 Neighbourhood sustainability dimensions and their frequencies within the investigated tools

Despite that, in recent years, some platforms have been developed specifically to determine the potential of renewable energy available in cities and regions. In the Urban-LEDS Project City on Power [4] information was integrated into an interactive, online spatial decision support system, a tool that helps stakeholders see whether it would be beneficial for them to install renewable energy systems (e.g. a solar panel on the roof of their home).

The most common feature is operational energy, and just one software does not address it; at the neighbourhood scale, it is the energy consumed in daily operations. Sometimes operational energy is calculated using statistical data (*Energy Proforma*); other times it comes from specific data about buildings and neighbourhoods (*UMI*, *IES*, *ArchSIM*), i.e. building geometry, performance of building components, behavioural models, details of heating system, internal gains, air exchanges, weather data, sun gains.

Daylight is quite common too; it is implemented in three tools out of five and is influenced by the orientation of buildings, their shape and spatial relationships, all features which relate to local typologies of buildings and urban tissues, such as blocks in the Mediterranean urban tissues. The embodied energy dimension is as frequent as daylight. The former includes the scope of life cycle analysis (LCA).

Less common features are transportation energy and outdoor comfort. Outdoor comfort is an important parameter; daylight analyses direct and ambient daylight, and is useful to optimise FAR and required hours of direct sunlight during the layout of the site. Apparently assessing outdoor comfort is a difficult task: just one of the investigated tools evaluates it (*TOWNscope* [5]), while efforts are being made to implement it in another one (*UMI* [6]). Nevertheless, some researches about this topic have been done in recent years (i.e. *RUROS: Rediscovering the Urban Realm and Open Spaces* – EU FP5 Project, 2001–2004 [7]).

3.3 Testing

To consider the usability of the *Incubators* tool and its prospective workflow, we ran a simulation with one of the aforementioned tools, *Energy Proforma* developed at the Department of Urban Studies and Planning of the Massachusetts Institute of Technology, Principal Investigators Prof. Dennis Frenchman and Prof. Christopher Zegras, Project Director Arch. Cressica Brazier [8]. *Energy Proforma* is an online platform to provide designers, developers, policymakers and researchers a means to explore and compare relative energy performances among different neighbourhood-scale projects.

Specifically, this test allowed us to assess the platform with the strategies for an eco-neighbourhood in the Mediterranean area, according to the ones identified by Spalla [9]: mixité, density, building refurbishment, accessibility, biodiversity, sustainable mobility, energy efficiency and social cost.

During the simulation study, three major steps have been performed to input project data. The first step consisted in the preparation of a *Trimble SketchUp* 3D

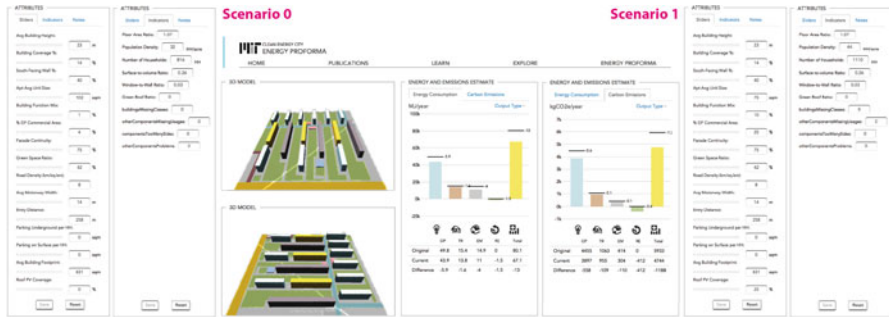


Fig. 50.3 Energy Proforma interactive output display: scenario comparison

model, reducing the geometry of buildings, streets and open spaces to some basic geometrical forms. In the second step, through the *CityGML* plugin menu, specific attributes have been added to the components of the model and saved in XML format. The third step consisted in the upload of the file to the *Energy Proforma* Web page and to the filling of an editable template with specific data for each of the components previously identified.

After completing these steps, energy and emission estimates are calculated and displayed as histograms (centre box of Fig. 50.3). For ease of understanding, an icon is also associated to each energy dimension.

3.4 Case Project

The case project is a social housing neighbourhood in Turin called ‘Quartiere Mirafiori Sud’ that was built by *Gestione Case Lavoratori (Ges.Ca.L.)* in the mid-1960s. The area has a very simple urban design, suitable for simplifying the design process and reducing construction cost and time; the buildings are made of panels of precast reinforced concrete. The result is practical and rather repetitive, although the main problems are the poor energy performance of the buildings, the social uniformity and the aging population. Once the project data are input to the *Energy Proforma* platform – as described earlier – the platform produces estimates about total energy consumption and carbon emissions and displays them through an interactive dashboard (Fig. 50.3).

These values refer to the baseline scenario of the project, called Scenario 0. On the same Web page, it is also possible to change some variables to simulate feasible interventions and to examine their positive or negative effects. By moving the sliders, estimates update dynamically and markers allow appraising the impact of changes at the attributes of the original model. After Scenario 0 has been set up, it becomes quick and easy to obtain Scenarios 1, 2, 3 and so on and examine the variations.

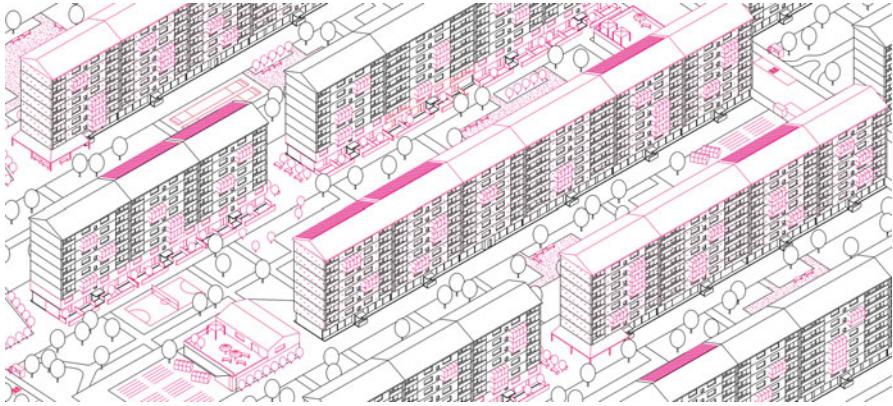


Fig. 50.4 Interventions in Mirafiori Sud case project: insertion of photovoltaic canopies, new facilities, shops, and retrofit of the building envelopes

In the Mirafiori Sud case-project, the following interventions have been simulated: the redesign of open spaces, with systems for on-site production of renewable energy (Fig. 50.4); the split or adaption of large flats, to increase residential density; the insertion of new facilities and shops, to extend the mixité, the retrofit of the building envelopes.

The centre box of Fig. 50.3 shows the outcome of this set of interventions: it is possible to view the evaluation of Scenario 1 in MJ/year or, more interestingly, comparing with the figures of Scenario 0 (the reference values being represented by black lines). The results of the simulation display the reduction of total energy consumption from 80 to 67 MJ/year, the operational energy decreases of 5,9 MJ/year and the embodied energy of 4 MJ/year, the transportation energy gets off of 1,6 MJ/year, on the contrary on-site renewable energy production increases to 1,5 MJ/year.

The integrated simulation of plural energy dimensions in a comprehensive platform allows the users to foresee the overall balance during the design process and to understand the specific contributions to; the information has proven especially useful in the early phases of the master plan.

4 Conclusion

This chapter describes a self-assessment Web tool in which all stakeholders take on a proactive role. It encourages a new form of local environmentalism useful for increasing urban regeneration, with the aim of meeting Europe ‘20-20-20’ targets.

However, the use of an assessment tool is difficult to advance because often it engages the user in a tricky process. Moreover, users do not have a clear idea of their role and potential. To overcome these obstacles, two requirements will be

developed: first, a team of experts will input data that describe a specific neighbourhood (Scenario 0), and then the user will input data pertaining to the specific intervention. Second, the benefits and incentives will be presented as evidence, linked to every user's proposal. Regarding the last strategy, the tool of the *Incubators* project will incorporate a financial analysis, which the considered tools do not consider.

Regarding additional features, it is crucial to decide whether to use statistical data or specific data about buildings and neighbourhoods performances to calculate energy consumption. The final choice will depend on the complexity of the input data phase required and on the reliability of the outcomes. The *Incubators* Web tool provides advance capability for analysing and simulating the designs of neighbourhoods from the early stages of design. Its online accessibility and intuitive interface facilitate an environmentally aware design. The early experimentation outlined in this chapter demonstrated the potential of this tool in cities, and the initial results encourage us to deploy it in further Mediterranean contexts. This will allow us to:

- Perform analyses across different areas and at different scales of time, space and complexity to reduce energy use, CO₂ emissions, and to increase renewables;
- Extend the theoretical foundation to develop an understanding of how technical methods can help to achieve pressing environmental and green energy goals in existing and new cities.

References

1. Interreg MED Programme website, <http://interreg-med.eu/en/home/>
2. Paterson M, Strippel J (2010) My space: governing individuals' carbon emissions. *Environ Plan* 28:341–362
3. Habermas J (1987) Lifeworld and system: a critique of functionalist reason. In: *The theory of communicative action*, vol 2. Beacon, Boston
4. City on Power – EU Project 2012–2014. <http://ispacevm28.researchstudio.at/ittb-torino>
5. TownScope website, <http://townscope.com/>
6. IESVE website. <http://www.iesve.com/>
7. RUROS: EU FP5 Project 2001–2004. <http://alpha.cres.gr/ruros/>
8. Frenchman D, Zegras C (eds) (2013) *Making the clean energy city in China*. MIT, Cambridge
9. Spalla G (ed) (2011) *The sustainable city of the Mediterranean: know the past and the present to build the future*. Allemandi, Torino
10. Energy Proforma website. <http://energyproforma.mit.edu/webtool2S/home>
11. UMI website. <http://urbanmodellinginterface.ning.com/>
12. ArchSim website, <http://archsim.com/>

Chapter 51

Renewable Energy in South of Morocco and Prospects

Hassan Nfaoui and Ali Sayigh

Abstract Morocco imports more than 98 % of its energy. As a result, it has turned its attention to renewable energy, particularly in the southern part of the country, with the objective of increasing renewables' share in the country's energy mix. Southern Morocco has significant solar potential. The annual daily averages of sunshine duration, \bar{n} , range from 6.7 h (Tan Tan) to 8.7 h (Laâyoune), and those of the global irradiation on horizontal surface, \bar{H} , vary between 4.87 kWh/m² (Tan Tan) and 5.54 kWh/m² (Dakhla). The estimated daily direct normal radiation in Laâyoune is 5.55 kWh/m², which means about 3175 h of sunshine per year. Seasonal variations in sunshine, σ , and the clearness index, K_t , for Laâyoune and Dakhla are more regular compared to that in Tan Tan; σ decreases rapidly in summer. This particularity reflects the greater oceanic influence and consequently the presence of a microclimate around Tan Tan, a finding confirmed by the research of J. Buret-Bahraoui. Morocco enjoys an excellent wind potential, particularly in the south. The wind speed annual averages vary between 5.12 m/s at 9 m for Tan Tan and 7.64 m/s at 10 m for Dakhla. The annual frequencies for the class 0 m/s are small for the three considered sites, less than 4 %. A study of wind speed frequency distributions shows that the observed frequencies are well modeled by the Weibull hybrid function. In 2013, wind energy contributed 4.2 % to national electricity production. In 2014, installed wind power in Morocco reached 757.3 MW, with 60 % located in the south. Tarfaya has a 301.3 MW private wind farm. Wind electricity production is estimated at 1.119 GWh/year, making it the largest wind farm in Morocco and Africa; in contrast, Dakhla is not connected to the national grid. Its electricity is supplied by a diesel power plant (37.5 MW). Wind power can contribute to its electrification by coupling it to the diesel plant. Solar thermal power plants constitute an expensive technology and require considerable amounts of water to clean the reflecting mirrors that get very dirty in the desert region, so wind farms are economically and environmentally viable for electricity production

H. Nfaoui (✉)

Solar Energy & Environment Laboratory, Mohammed-V University, Avenue Ibn Battouta,
B.P.1014, Rabat, Morocco
e-mail: nfaoui@fsr.ac.ma

A. Sayigh

WREC, WREN, IEL, PO Box 362, Brighton BN2 1YH, UK

on a large scale in southern Morocco. In addition, compared to solar energy, electricity from wind energy is half as expensive.

Keywords Solar radiation • Wind • Statistics • Weibull hybrid • Potential • Wind farm

1 Introduction

Morocco is a net importer of fossil fuels, which represent over 98 % of its fuel mix. This energy dependence has a negative impact on the state budget in terms of foreign currencies. Moreover, electricity consumption increases annually by 7 %. In 2013, the wind electricity contribution in net electricity consumption in the country reached 5.1 %.

The design, dimensioning, and calculation of the energy balance of a solar system require prior knowledge about the solar energy it receives. Lacking hourly and daily values of bright sunshine n and global radiation on horizontal surface H for assessing the solar potential in southern Morocco, this statistical analysis will be limited to the monthly averages of n and H published by J. Bahraoui-Buret and A. Khtira [1–3].

The assessment of wind potential and the exploitation of wind for electricity production on a large scale in southern Morocco remained limited until the early twenty-first century, despite the existence of wind speed data dating back to 1978 and available at the National Meteorology Direction. A statistical analysis of these data is necessary and important for assessing quantitatively and qualitatively the wind potential available in this region.

In addition to its location in an arid zone, southern Morocco enjoys significant wind potential. This makes the region a favorable area for the installation of wind farms for large-scale electricity production. Then we present an evaluation and prospects of wind farms in southern Morocco.

2 Solar Potential in Southern Morocco

2.1 Sunshine coefficient, σ , and clearness index, K_t

Solar radiation incident on the ground presents a periodic variation linked to variations in the declination, δ , and latitude, φ . To eliminate this variation one generally uses dimensionless coefficients such as the sunshine fraction, $\sigma = n/N$, or the clearness index, $K_t = H/H_{oh}$. The values of σ and K_t then vary only due to climatic fluctuation.

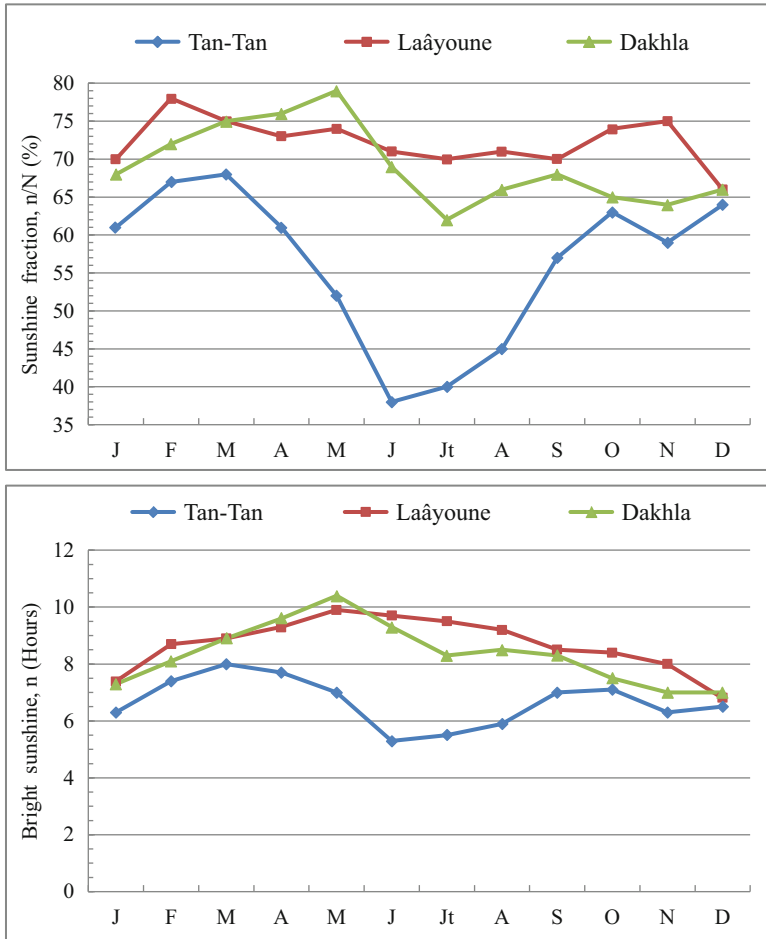


Fig. 51.1 Seasonal variations of sunshine duration, n , and sunshine fraction, σ

2.1.1 Sunshine Fraction, σ

The study of seasonal variations in sunshine duration, n , shows that there is some regularity for Laâyoune and Dakhla, but no regular trend emerges from the seasonal variations in σ . We also find that σ decreases rapidly between May and August in Tan Tan (Fig. 51.1). This particularity, accentuated in summer, denotes a greater oceanic influence and, consequently, the presence of a microclimate around Tan Tan, a finding confirmed by the research of J. Buret-Bahraoui [1, 2].

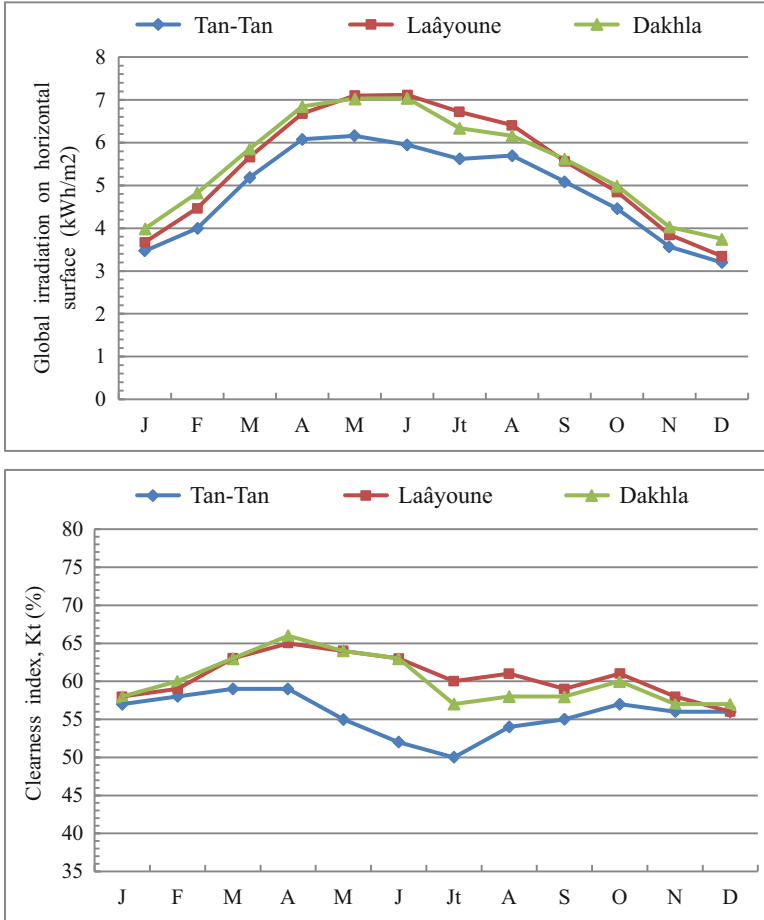


Fig. 51.2 Seasonal variations in global irradiation on horizontal surface H and clearness index K_t ,

2.1.2 Clearness Index, K_t

We note that σ and K_t have similar variations, but the former has a higher variation in amplitude: the effect of atmospheric attenuation and, hence, atmospheric turbidity involves K_t and not σ (Figs. 51.1b and 51.2b).

Note also that the monthly averages of K_t always fall between 55 and 65 % for Laâyoune and Dakhla and between 50 and 60 % for Tan Tan (Table 51.1, Fig. 51.1b). The maximum monthly averages of K_t for the three considered sites occur in April, while the minimum values of K_t occur in December in Laâyoune and Dakhla and July in Tan Tan (Fig. 51.2b).

Table 51.1 Annual averages of n and monthly extreme values of n , H , σ , and K_t for Tan Tan, Laâyoune, and Dakhla, respectively [1–3]

	Mean	Extreme values	
		Maxima	Minima
\bar{n} (heures)	6.7	8.0	5.3
	8.7	9.9	6.8
	8.3	10.4	7.0
\bar{H} (kWh/m ²)	4.87	6.16	3.20
	5.45	7.12	3.35
	5.54	7.04	3.75
$\bar{\sigma}$	0.56	0.68	0.38
	0.72	0.78	0.66
	0.69	0.79	0.62
\bar{K}_t	0.56	0.59	0.50
	0.56	0.65	0.61
	0.60	0.66	0.57

3 Wind Potential in Southern Morocco

3.1 Statistical Characteristics of Wind Speed in Southern Morocco

3.1.1 Annual Average Wind Speed

The annual averages of wind speed for Tan Tan, Laâyoune, and Dakhla are on the order of 5.12 m/s (5.90 ± 0.89 m/s and 7.64 ± 1.15 m/s, respectively) (Table 51.2). Comparison of these averages shows that Dakhla is the windiest site.

Figure 51.3 shows that August and July are the windiest months in Laâyoune and Dakhla, respectively, with monthly averages of 7.67 and 10.12 m/s. November is the least windy month at both sites, with monthly averages of 4.57 and 5.35 m/s. However, for Tan Tan, the seasonal variation is not regular compared to the other sites. Its monthly averages fall between 4 and 6 m/s. For Laâyoune, the maximum speed was 34 m/s in August 1978, while a speed of 27 m/s was obtained for Dakhla in July 1983 (Table 51.2).

3.1.2 Diurnal Variations

Figure 51.4 shows that, in general, for the three considered sites the wind is strong in the afternoon and reaches its maximum at 4:00 p.m. local time; furthermore, it is weak at night. This can be explained by the influence of the sea breeze, a localized circulation pattern characteristic of coastal areas. Knowing this type of variation makes it possible to harmonize the energy generated from wind and the energy needs.

Table 51.2 Annual Weibull Hybrid distribution parameters and annual averages of wind potential [4–9]

Sites	Period of measurements	Average wind speed (m/s)	Maxima (m/s)	Average wind potential (W/m ²)	Annual parameters of Weibull hybrid		Frequency (%) for V = 0 m/s (no wind)
					K	C (m/s)	
Tan Tan	2 years (Nov. 1993–Dec. 1994)	5.12	24	122	2.07	5.43	4
Laâyoune	13 years (Jan. 1978–Dec. 1990)	5.90	27	204	2.47	6.79	2
Dakhla	10 years (Jan. 1980–Dec. 1990)	7.60	34	462	2.32	8.78	2

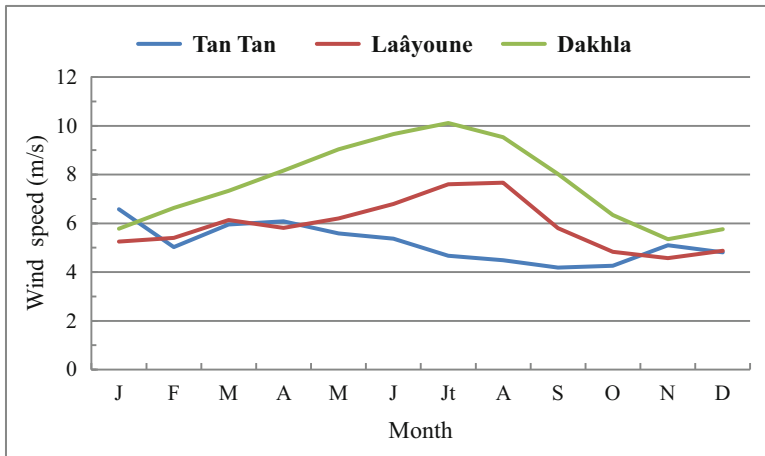


Fig. 51.3 Seasonal variations in wind speed

3.1.3 Frequency Distributions

The annual frequencies for class 0 m/s corresponding to $V = 0$ m/s (no wind) are small for the three considered sites. They are about 2% for Laâyoune and Dakhla and almost 4% for Tan Tan. These figures need to be known when there is a question, for example, of storage sizing for some wind power applications (Fig. 51.5).

Note also that the classes that correspond to wind speeds between 3 and 5 m/s (medium wind) are more important for Tan Tan compared to Laâyoune and Dakhla. Their frequencies are higher than 10%, but their classes corresponding to high

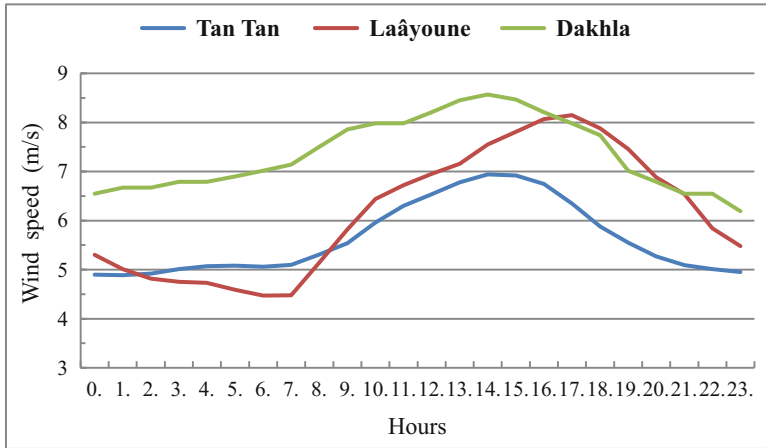


Fig. 51.4 Diurnal variations in wind speed

values of wind speed (strong wind) are not empty compared to Tan Tan. This shows that Laâyoune and Dakhla are windier compared to Tan Tan (Fig. 51.5).

3.1.4 Weibull Hybrid Distributions

Figure 51.5 shows observed distributions and those estimated using the Weibull hybrid function on an annual scale. Note that the observed frequencies are well modeled by the Weibull hybrid function. For Laâyoune and Dakhla, the observed and estimated frequencies are almost the same compared to those for Tan Tan.

3.2 Wind Potential in Southern Morocco

The annual averages of wind potential are calculated for the three considered sites, with $\rho = 1.18 \text{ kg/m}^3$ [4]. Dakhla has the highest potential. It is on the order of 462 W/m^2 , almost double that of Laâyoune and four times that of Tan Tan (Table 51.2, Fig. 51.6).

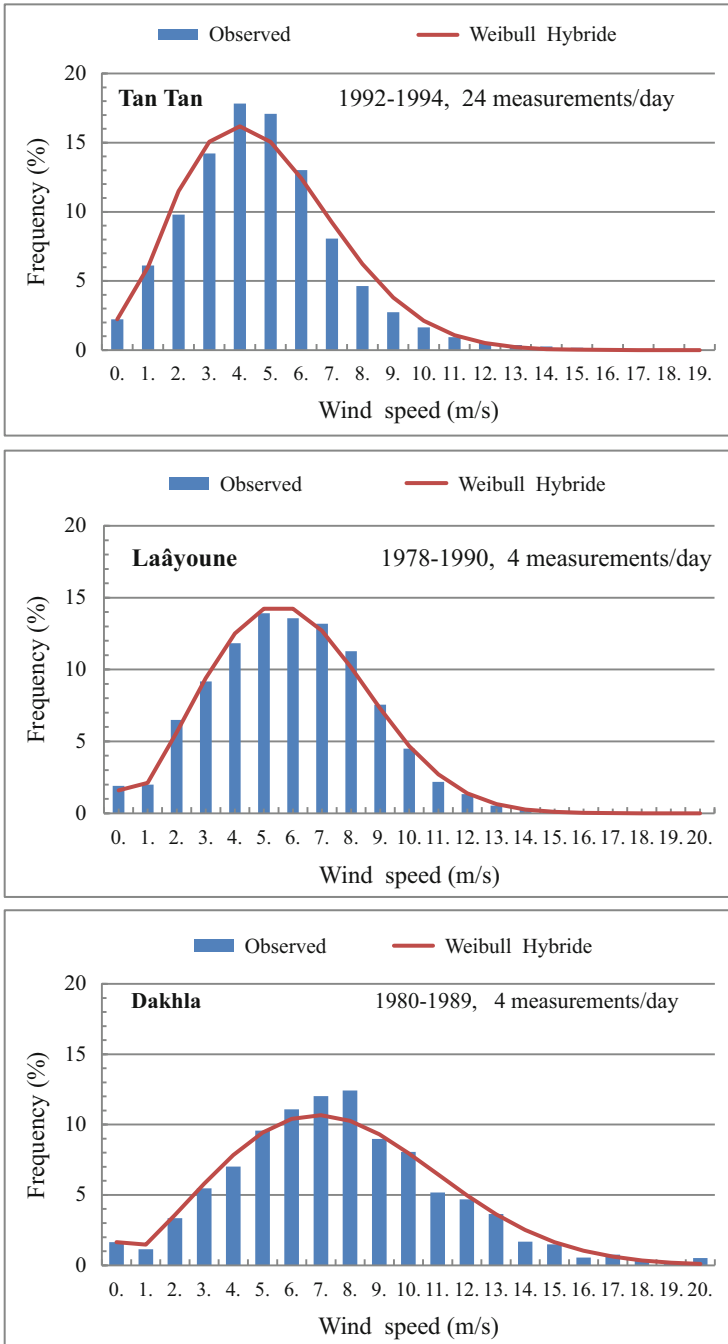


Fig. 51.5 Annual distributions of wind speed

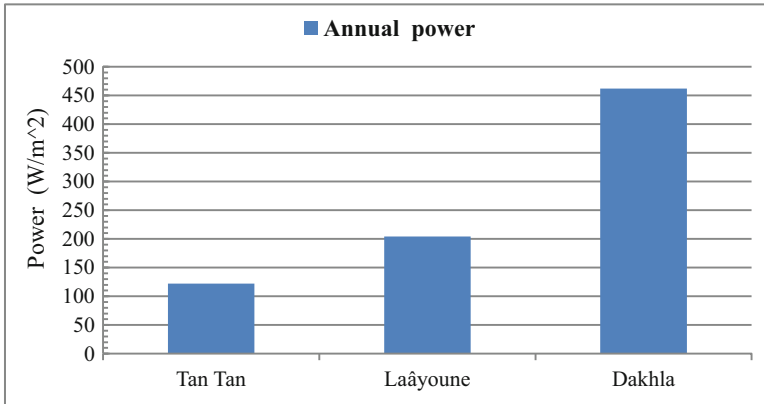


Fig. 51.6 Annual averages of wind potential [8–12]

4 Evaluation and Prospects of Wind Energy in Southern Morocco

4.1 Electricity Sector in Southern Morocco

Major cities in southern Morocco, for example, Tarfaya, Tan Tan, and Laâyoune, are connected to the national grid. On the other hand, Dakhla is electrified by a diesel power plant (37.5 MW). To cope with the significant increase in electricity consumption in the Dakhla region, a new diesel generator with a 16.5 MW capacity is planned for installation by the National Office of Electricity (ONE).

4.2 Wind Energy in Morocco

At the end of 2014, the wind power installed in Morocco amounted to 757.3 MW, with over 60 % being located in southern Morocco (Table 51.3). The wind farm of Al Baida Koudia (Tetouan), 50 MW, was the first wind farm in Morocco; it was installed in 2000. However, the largest wind farm in Morocco and Africa is the Tarfaya wind farm, installed in 2014. Its capacity is 300.1 MW. Table 51.4 shows four other wind farms under development in Morocco with a total capacity of 650 MW. Three of them will be installed in southern Morocco.

Table 51.3 Wind farms installed in Morocco [10–12]

Sites	Number of turbines	Capacity (MW)	Commissioning	Annual production (GWh/án)	Funding	Operator / owner
Koudia Al Baida (Tétouan)		50	2000	226	Banque Européenne d'investissement	CED
Koudia Al Baida (Tétouan)		3.5	2001	12	KfW	ONE
Tétouan		10.2	2005	38	Lafarge Ciments	Lafarge Ciments
		10	2008			
		12	2009			
Tanger		16	2005	0.4		Aliments et Protéines du Nord SARL
Essaouira		60	2007	210	KfW	ONE
Tanger		140	2009 (107 MW)	526.5		
Laâyoune		5	2011	16	Ciments du Maroc	Ciments du Maroc
Akhfenir (Tan Tan)	61	100	2013		Nareva Holding	Nareva Holding
Foum ElOued (Laâyoune)	22	50.6	2013		Nareva Holding	Nareva Holding
Tarfaya	131	300.1	2014 (50 MW)	1084	GDF SUEZ/Nareva Holding	Tarfaya Energy Company (TAREC)
Total		757.3				

Table 51.4 Wind farms under development in Morocco [10–12]

Sites	Capacity (MW)	Wind speed (m/s) at 10 m	Annual production (GWh/an)	Funding	Operator/owner
Akhfenir (Tan Tan)	100			Nareva Holding	Nareva Holding
Tiskrad (Laâyoune)	300	8.45	1000	Nareva Holding	Nareva Holding
Boujdour	100	8.40	385	Nareva Holding	Nareva Holding
Taza	150			EDF-Energies Nouvelles	ONE
Total	650				

4.3 Wind Energy Prospects in Southern Morocco

Increasing the renewable energy share, especially wind power, in southern Morocco in Morocco's electricity production will contribute to the reduction of imports of coal and petroleum products. The installation of wind farms will also participate, on the one hand, in the economic and social development of the region through the involvement of Moroccan firms (e.g., feasibility studies, electrical works, civil works), industrial integration (e.g., parts manufacturing of wind turbines), and the creation of indirect jobs during the construction and direct jobs during the operational phase. On the other hand, wind power generation will contribute to Moroccan energy independence, reduce the consumption of fossil fuels, and, consequently, the economy of foreign currency. Furthermore, wind electricity consumption contributes to environmental protection by reducing CO₂ emissions and greenhouse gases resulting from the use of petroleum products and coal, which will limit the effects of climate change, such as, for example, floods or droughts.

The Dakhla region, which until recently has not been connected to the national grid, is supplied with electric power generated by a power diesel power plant. Thus, wind power can contribute to the electrification of this region by coupling it the diesel plant.

Compared to solar energy, electricity from wind and hydro power are half as expensive. On top of that, installing more wind farms – the goal set by the Moroccan national energy strategy, that is, the wind power share will be 14 % of the national electric mix (14, 580 MW) – is likely to be realized by the end of 2020.

5 Conclusion

Seasonal variations in σ and K_t for Laâyoune and Dakhla are more regular compared to those in Tan Tan. The rapid drop of σ appears to be a notable feature in the summer variation σ , which indicates an increased oceanic influence and, consequently, the presence of a microclimate around Tan Tan site. Southern Morocco has an important solar potential. The annual average daily sunshine varies between 6.7 h (Tan Tan) and 8.7 h (Laâyoune) and global irradiation on horizontal surfaces varies between 4.87 kWh/m² (Tan Tan) and 5.54 kWh/m² (Dakhla).

The statistical characteristics of hourly averages of wind speed for the three considered windiest sites and the most promising ones for wind farm installations were studied on the basis of long-term measurements, especially for Laâyoune (13 years) and Dakhla (10 years). For the three sites, the long-term annual average of wind speed is greater than 5 m/s, a value that allows the wind farms to produce electricity at a rate that is competitive with that generated by thermal or nuclear power plants.

Overall, for the three sites, the wind is strongest in the afternoon, especially in summer, and lower at night. This is due to the influence of the sea breeze. Study of the frequency distribution of wind speed shows that the observed frequencies are well modeled by the Weibull hybrid function.

In 2014, the wind power installed in Morocco reached 757.3 MW, with over 60 % located in the south. In addition, the largest wind farm in Morocco is located in the south. Its capacity is 300 MW and generates 1.084 GWh/year on average, the equivalent of the electricity consumption of Marrakech city. Three other wind farms totaling 500 MW are under development in southern Morocco.

Also contributing to Morocco's energy independence, the electrical energy obtained from the use of renewable energy, particularly wind energy, is a clean energy that contributes to environmental protection from the emission of greenhouse gases.

References

1. Bahraoui-Buret J, Bargach MN, Kaddour ML (1983) Le gisement solaire marocain, Editions SMER
2. Buret-Bahraoui J (1986) Caractéristiques du gisement solaire marocain, Etude spécifique du site de Rabat, Thèse de Doctorat d'Etat, Faculté des Sciences de Rabat
3. Khtira A (1993) Etude spatio-temporelle de l'irradiation solaire globale journalière d'un plan horizontal au Maroc, Doctorat d'Etat, Faculté des Sciences de Rabat
4. Knidiri F, Laaouina A (1986) L'énergie éolienne au Maroc. CDER, Marrakech
5. Enzili M, Nayssa A, Affani F (1995) Le gisement éolien marocain, le Centre Développement des Energies Renouvelables, Marrakech
6. Nfaoui H (2004) Caractéristiques du gisement éolien marocain et optimisation d'un système aérogénérateur/groupe électrogène pour l'électrification des villages isolés, Thèse de Doctorat d'Etat, Faculté des Sciences de Rabat

7. Nfaoui H, Sayigh AAM (2015) Evaluation of renewable energy in the south of Morocco and perspectives. Proc. of Med Green Forum, Florence
8. Enzili M(2008) Renewable energy, energy efficiency in Morocco, situation and prospects, Cairo (Egypt). www.needs-project.org/
9. Nfaoui H, Sayigh AAM (2014) Contribution of renewable energy to energy independence in Morocco: wind energy case. Proc. of World Renewable Energy Congress 2014, London
10. www.mem.gov.ma
11. www.one.gov.ma
12. www.aderee.ma

Chapter 52

Analysis of Energy Performance of a High-Performance Building in a Local Mediterranean Climatic Context

Maria Teresa Lucarelli and Caterina Claudia Musarella

Abstract In recent years in the construction industry, a new energy policy has emerged that, referring to the current European Directive 31/2010/UE, aims to reduce energy consumption through the design of nearly zero-energy buildings (NZEB). However, because this term can have different meanings, it is important to investigate the characteristics of this concept. Thus, this chapter considers as a case study a building defined as a NZEB – Project Botticelli in Mascalucia (Catania, Italy), located in a Mediterranean context. From this analysis we highlight the main strategies used for the design of high-performance buildings, which are similar to Passivhaus strategies, whose criteria, however, identify very selective limits of reference, especially suitable for some climatic contexts. The goal of this investigation is the analysis of these so-called limit values with respect to the specific context of local Mediterranean climates, paying attention to the orientation of buildings through the parameter of solar radiation. The envelope is the element that characterizes the energy efficiency of a building, so it is taken into consideration in the study of external opaque components for the purpose of evaluating energy performance while the building is in use; in this way, it is possible to identify a connection between the “limit” parameters for the design of a high-performance building and the climatic parameters of the context of reference to obtain more complete information about the energy performance of a component.

Keywords Climatic context • Energy • Energy performance • Nearly zero-energy building (NZEB)

M.T. Lucarelli (✉) • C.C. Musarella
dArTe Department, Mediterranean University of Reggio Calabria, Salita Melissari,
89124 Reggio Calabria, Italy
e-mail: matiluc@alice.it; katia.musarella@libero.it

1 General Information

In recent years, the energy sector has been in a transitional phase, and the awareness of the imbalance between natural resources and the growing demand for energy has led to the adoption of new policies that promote the reduction in the consumption of nonrenewable energy sources.

In Europe,¹ energy policy in the building sector refers to the current European Directive 2010/31/UE, confirmed by 2012/27/UE, which aims to reduce energy consumption through the reduction of energy use by introducing the concept of nearly zero-energy building (NZEB), defined as follows:

“... *building high energy performance*” [...] in which “... *energy needs very low or almost zero should be covered in a very significant extent by energy from renewable sources, including energy from renewable sources produced on-site or nearby.*”

The directive leaves to individual nations full freedom to interpret the meaning of NZEB² and to determine the calculation method; the definition is very labile because it does not impose precise limits on energy consumption or some classification. However, the good energy performance of buildings should not be a point of arrival that documents compliance with a rule; it must be a point of departure, a strategic tool – management can support the design choices in view of improvements to the overall energy performance of the building system.

2 Interpretation of the Concept of Nearly Zero-Energy Building

Following the introduction of the concept of NZEB, European Union (EU) member states have tried to find a common definition of *nearly zero-energy building*³; the literature contains various interpretations of the meaning of the letter *N*: *net* or *nearly*, where *net* ZEB indicates an energy demand of zero, whereas *nearly* ZEB

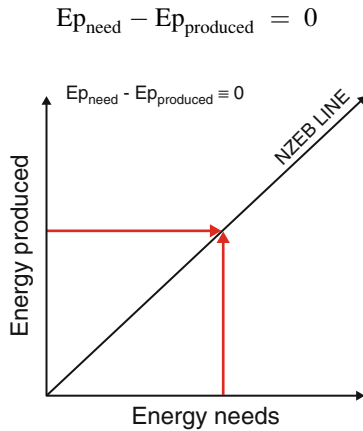
¹Energy policy in the building sector began with European Directive 91/2002/CE, replaced by the current European Directive 31/2010/UE and confirmed by 27/2012/UE.

²The literature contains different definitions of NZEB, but we must also pay attention to the differences found between buildings: *net* energy and *nearly* zero energy buildings. This difference is largely formal in nature, but it is still unclear what meaning should be given to the letter *N* in NZEB (“net” or “nearly”) (interview with Prof. Marco D’Orazio, available at: <http://www.edifici2020.it/nzeb-n-come-net-e-non-near-intervista-a-marco-d-orazio/>).

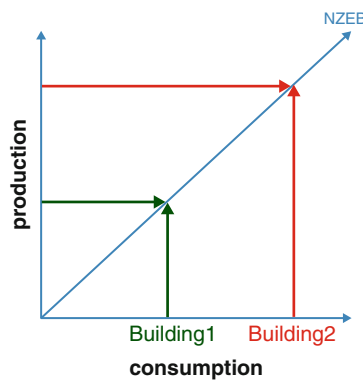
³Project COHERENO and the “Commission report to the European Parliament and the Council” n° 483 from 2013. To make up for the lack of definitions and methodology, a project was developed that is part of the Intelligent Energy Europe project, called COHERENO – “Collaboration for housing NZEB renovation” – which focuses on the elimination of barriers to collaboration by providing guidance on how to collaborate and develop nearly zero-energy buildings. The actors in this project are Austria, Belgium, Germany, the Netherlands, and Norway. The report provides an overview of current definitions of NZEB in the EU and the standards and ratings for existing buildings that can be applied to identify a NZEB.

indicates some level of energy consumption that, while close to zero, allows for country-specific national policy decisions, taking into account the amount of primary energy, expressed as a percentage, from renewable sources.⁴

So, following the general definition provided by European Directive 31/2010, a nearly zero-energy building can be represented as in the following graph, where the y-axis shows the energy requirements of the building and the x-axis its energy production. A building is considered a NZEB when the straight line in the equation is near the axis origin:



Looking at the NZEB line in the graph, it should be noted that the buildings located along that line cannot be considered equally: in fact, a building that consumes and produces 100 turns out to be energetically different from a building that consumes and produces 20. As mentioned previously, one NZEB will be treated as it is close to zero in the consumption of energy.



⁴Kurtnitski J., Allard F., Braham D., Goeders G., Heiselberg P., Jagemar L., Kosonen R., Lebrun J., Mazzarella L., Railio J., Seppänen O., Schmidt M., Virta M., 2011. "How to define nearly net zero Energy buildings nZEB", REHVA Journal, May 2011, p Progress toward Advanced Energy Design Guides (AEDG) and cost-effective net-zero-energy (NZE) buildings.

Under the current and wider debate on NZEB, this chapter draws particular attention to the building envelope, intended as the set of materials constituting the components⁵ with high energy performance; specifically, as an object of investigation, we focus on the external opaque vertical components because they represent elements that characterize the total energy performance of the building, making it possible to analyze different materials interposed between them.

3 Analysis of Case Study

Entering the specific to nearly zero energy buildings was taken like a case study Project Botticelli – Mascalucia House in Catania with the aim of identifying the design strategies used and verifying the energy performance, also done through an analysis of the external opaque vertical components used (Fig. 52.1).

This building was a pilot construction built in 2012 to comply with nearly zero energy defined on the basis of the annual calculated energy consumption,⁶ achieved by applying protocols and Passivhaus CasaClima Gold standards in a Mediterranean climate. A design model of computation in a dynamic regime was adopted that is capable of responding to issues related to climate and management of high summer temperatures. The house is part of the European project “PassREg”⁷ whose partners include the Passivhaus Institut, the Politecnico of Milano (team end-use Efficiency Research Group, eERG-PoliMI), and the energy management office of Sicily and Catania: it was created in order to experiment with a new generation of buildings, nearly zero-energy buildings, as required by European directives. From the design point of view, while maintaining the Passivhaus concept, adjustments were introduced related to Mediterranean climatic factors.

⁵The objectives set by the Italian regulatory and national legislation for NZEB require increasing levels of performance for the components and systems of a building. The objectives are basically of two types: exaggerate performance for static components and promote solutions that make the building envelope a dynamic system, able to adapt to changing external and internal conditions. New thermal insulation products are able to achieve cladding and roofing with thermal transmittance values that are very low, a very important aspect in the renovation of existing buildings, using modest thicknesses of insulation to meet the insulation requirements set by technical regulations. The so-called super insulating materials, the best available materials on the market today, which have thermal conductivity values of around 30 mW/mK, can greatly enhance such benefits: insulating panels with airtel can reach 13 mW/mK, vacuum insulation panels can even reach as high as 7 mW/mK, and similar levels are being targeted by nano-polyurethane foams currently under development (Rapporto Annuale Efficienza Energetica—RAEE 2012).

⁶The information is available in *azero n° 6 “Mediterranea, Passiva, Attiva, Intelligente E Sostenibile”*, 2013, pp. 88–95.

⁷Passive House Regions with Renewable Energies (PassREg). This project aims to promote NZEB across the EU, with the passive house provided, as far as possible from energy innovabili as foundation. The PassREg is a European project and is part of the Intelligent Energy Europe program with 14 partners, 11 countries, and just one objective: Support the regions/provinces/municipalities in the implementation of EU Directive 2010/31 on the energy efficiency of NZEBs.



Fig. 52.1 Botticelli Project. Mascalucia house in Catania. Designers: eng. Carmelo Sapienza arch. Pina Capace arch. Salvo comes

In 2014 the building was certified as CasaClima Gold.⁸

The studied building was analyzed, among others, within a broader framework on NZEB⁹ starting with strategies used in the design phase, as reported in the following table (Table 52.1). The table shows that a NZEB also applies the definition of bioclimatic building and passive house and its strategies, taking advantage of the microclimate of the environment and compensating for minimum energy needs through the use of active systems. However, we must distinguish a passive building from a Passivhaus; a building, in fact, is defined as a Passivhaus if it meets the requirements specified by the Passivhaus Institute.¹⁰

⁸<http://www.agenziacasaclima.it/it/rete-casaclima/la-rete-casaclima/progetto-botticelli/111-25253.html>

⁹Musarella C.C. (2015). *La prestazione energetica nei componenti in fase d'uso rispetto al contesto climatico locale per un edificio ad energia quasi zero*. Phd Thesis Ciclo XXVII, Università Mediterranea di Reggio Calabria, Dipartimento dArTe, Tutor: Prof.ssa Lucarelli; Co-tutor: Prof. M. Milardi, Arch. M. Mandaglio; Referenti Esteri: Prof. A. Tadeu, Prof. N. Simões.

¹⁰The limit values to be met are as follows:

- The annual demand for space heating does not exceed 15 kWh/m²/year, under the Passive House Planning Package (PHPP);
- Depending on local conditions considering the following values:
 - The U of the external opaque components must be less than 0.15 W/m² K;
 - The U of windows and other translucent building components must be less than 0.8 W/(m² K);
 - A constant uniform flow of air through all areas and in all rooms must be ensured (ventilation efficiency);
 - Noise emissions from the ventilation system should be minimal (≤25 dBA).
- Home applications (heating, domestic hot water, and electricity) must not exceed 120 kWh/m²/year total:

(<http://www.zephir.ph/passivhaus.php>).

Table 52.1 Analysis of Botticelli Project. Mascalucia house in Catania (Botticelli Project)

Context analysis	Passive strategies			Active strategies		Energy needs
	Hyper insulation	Solar chimney	Solar screens	Photovoltaic panels	Solar panels	
Altitude: 420 m	X	X	X	X	X	Ep = 43 KWh/m ² /year of which 35.85 KWh/m ² year is generated from renewable sources
Latitude: 37° 35'3.25" N						
Longitude: 15° 1'50.52" E						
Degree day: 1271						
Climatic Zone: C						

The NZEB is proposed, instead, as an evolution of the passive house, because if the building has low energy demands, they can be met by renewable sources, preferably with facilities located on site. However, it is not yet clear whether it is possible to adapt the limit values to all types of climatic contexts; for that reason it was desirable to analyze Project Botticelli considering the energy performance of the envelope, the main element involved in the regulation of the flow of energy as it passes in output relative to the orientation. In fact, for a good design and for the minimization of energy consumption, it is necessary to take into account, in addition to the components' energy performance, the climatic context of reference.

4 Breaking Up of the Case Study

The theme of the component in the building industry has been the object, in recent years, from multiple basic research and applied¹¹ which they have contributed to its evolution through experimentation with new components and materials characterized by high performance. Specifically, the case study will take into account the opaque component perimeter,¹² analyzed previously, and it is broken down than the materials it is made of by checking the energy performance relative to the orientation of the building.

What follows is the breakdown of the opaque perimeter wall of Project Botticelli and the thermal conductivity that identifies the different materials used (Table 52.2).

In this way, we intend to verify the energy performance of the component during the use phase compared to the environmental context, in this case Catania, the site

¹¹Claudi de Saint Mihiel A., Interattività degli involucri edilizi trasparenti e prestazioni di benessere ambientale, in La produzione industrial eco-orientata, a cura di Antonio Passaro, Atti del Convegno Abitare Verde 2007, Luciano Editore, Napoli, 2007.

¹²The opaque component perimeter allows us to analyze the energy behavior of different materials.

Table 52.2 Breaking up of component perimeter opaque

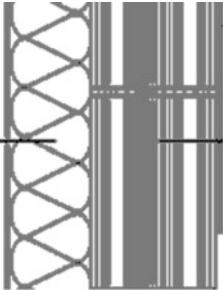
Solution D: opaque component perimeter, Mascalucia house	Number	Layer	Thermal conductivity (W/mK)
	1	Internal plaster in lime by 2 cm	0.9
	2	Brick masonry with pores by 30 cm	0.9
	3	Insulating rock wool by 20 cm	0.038
	4	Plaster exterior clay by 3.3 cm	0.12

Table 52.3 Taken from: UNI 10349—Global solar radiation on vertical surface long exposures to Catania

Orientation	June (MJ/m ²)	December (MJ/m ²)
South	9.1	13.3
SW–SE	14.1	10.5
E–W	17.6	6.2
NW–NE	14.9	2.7
North	10.3	2.3

of the project. Thus, the analysis takes into consideration the parameter of solar radiation (UNI 10349)¹³, that are more specific, as result data, in relation to the exposures in the months of June and December (Table 52.3).

Identified the values of the thermal conductivity of the materials composing the components, and the solar radiation,¹⁴ like the legislation, It is defines a relationship between these in order to determine the energy performance of components relative to the orientation.

In the following table we show the results of the energy performance obtained for the respective components and guidelines (Table 52.4).

Within this context it is deduced that the lower the solar radiation, the greater the ratio between the thermal conductivity of the materials constituting the component and, consequently, the greater the heat transmission. During winter there is an increased need for heat transfer, while during summer extra protection is needed. As shown in Table 52.4, the analyzed component presents interesting performances during summer, especially in long exposures E–W and during the winter in N.W.–N.E.—NORTH. These analyses identify the optimal strategies for improving the energy performance of building components and, consequently, the whole building.

¹³UNI 10349. Norma italiana. Riscaldamento e raffrescamento degli edifici. Dati climatici, 1994.

¹⁴You make, so a conversion from kilowatt hours to megajoules, where 1 KWh = 3.6 MJ, to use a single unit.

Table 52.4 Results of energy performance of opaque perimeter wall

	South summer	South winter	S.W-S.E summer	S.W-S.E winter	E-W summer	E-W winter	N.W-N.E summer	N.W-N.E winter	North summer	North winter
Energetic Performance	0.65	0.45	0.42	0.57	0.34	0.96	0.40	2.21	0.58	2.6

5 Conclusions

The foregoing discussion also makes it possible to understand how the components of a *façade*, analyzed with respect to their stratigraphy, contextualization of climate, and exposure, are crucial for increasing the amount of information obtained regarding their energy performance. In fact, there is a need to develop an innovative interpretation of the same dynamic that makes it possible to have more guidance in developing appropriate strategies to plan buildings that are increasingly designed to be NZEBs. It should be emphasized, however, that to have greater completeness of such information, one should consider other parameters, such as the duration of the energy performance of components along a time axis and the implementation of contextual data, also associated to the possible cost of materials, since the latter are not secondary especially in the case of interventions to recover existing buildings.

References

1. Bollini G (2013) La nuova Direttiva 2012/27/UE sull'efficienza energetica in *azero* n° 06, 6–9
2. Lavagna M, Bonanomi M, De Flumeri C (2012) Edifici a consumo energetico zero. Orientamenti normativi, criteri progettuali ed esempi di Zero Energy e Zero Emission Buildings. Maggioli Editore
3. Lucarelli MT (2010) La gestione sostenibile delle risorse energetiche nei settori dell'edilizia e degli impianti, Ed. C.S.d'A. (Centro Stampa di Ateneo), Reggio Calabria
4. Lucarelli MT, Musarella CC (2014) The optimization of energy performance about a component in relation to climate context, 40th IAHS World Congress on housing—sustainable housing construction, 16–19 December 2014. 40th IAHS World Congress on housing. Sustainable Housing Construction, Funchal, Madeira, Portugal
5. Marszal AJ, Bourrelle JS, Musall E, Heiselberg P, Gustavsen A, Voss K (2010) Net zero energy buildings—calculation methodologies versus national building codes. In: EuroSun Conference, Graz, Austria
6. Milardi M (2012) Il contributo degli Indicatori di Intensità Energetica alle verifiche di ecoefficienza del progetto contemporaneo, *Pluralità Tecnologica*. Papers, designpress ed., Roma, pp 109–122
7. Musall E, Voss K (2012) The passive house concept as suitable basis towards net zero energy buildings. *Passiv Haus Institute*, Hanover, 6 p
8. Rinaldi A (2010) Progettazione ed efficienza energetica. Maggioli Editore
9. Sapienza C (2013) Mediterranea, passiva, attiva, intelligente e sostenibile. In: *azero* n°02, gennaio, p 22–31
10. Sartori I et al (2012) Net zero energy buildings: a consistent definition framework. In: *Energy Buildings*
11. Serra C, Simões N, Tadeu S (2013) Definition of reference buildings for energy performance calculation—Portuguese case. In: *Atti del convegno, Energy for sustainability*, Coimbra
12. Tadeu S, Simões N, Ribeiro J, Gonçalves M, Tadeu A (2013) Energy efficiency measures in portuguese residential buildings dated before 1960: a cost-optimal assessment. In: *Atti del convegno, Energy for sustainability*
13. Torcellini P, Pless S, Deru MD (2006) Zero energy buildings: a critical look at the definition. *ACEEE Summer Study Pacific Grove, California*, 13 p

14. Voss K (2008) What is really new about zero-energy homes? In: 12th International conference on passive houses, Nuremberg, Germany
15. Voss K, Sartori I, Napolitano A, Geier S, Gonzalves H, Hall M, Heiselberg P, Widén J, Candanedo JA, Musall E, Karlsson B, Torcellini P (2010) Load matching and grid interaction of net zero energy buildings. In: EuroSun Conference, Graz, Austria

Chapter 53

Skylight Optimization Design Based on the Interior Ventilation in the Office Building in Cold Region

Tiantian Du and Jianfei Chen

Abstract The severe climate in cold regions imposes strict requirements with respect to building energy savings and challenges indoor environmental comfort levels. The atrium has an important influence on indoor ventilation performance, which is a function of both wind pressure action and thermal pressure action. Specifically, skylights are a significant element for atrium ventilation and their ability to affect atrium ventilation performance and their optimization design strategies need to be studied. This chapter uses Ansys-Airpak ventilation simulation software to explore the skylight's influence on natural ventilation with its three variables: plane position, distribution pattern, and skylight height. Through the simulation, the research leads to three conclusions: (1) skylight outlets should be set on the side behind the wind direction, which is useful for air flow because of the wind pressure; (2) outlets should be set around the skylight uniformly to accelerate the air exchange rate; and (3) the skylight height design should be combined with atrium size and outlet location. Overall, skylights have a significant influence on atrium ventilation performance and should be designed carefully to reduce energy consumption and increase the indoor environmental comfort level.

Keywords Atrium • Natural ventilation • Skylight design • Cold region

1 Introduction

The severe climate in cold regions imposes strict requirements with respect to building energy savings and challenges indoor environmental comfort levels. The high requirements of insulation properties and low window–wall ratio result in poor indoor ventilation [1]. However, atriums have an important effect on indoor ventilation, which is conducted by both wind pressure action and thermal pressure action. Specifically, the skylight is a significant element for atrium ventilation.

T. Du (✉) • J. Chen
School of Architecture, Harbin Institute of Technology, Harbin, China
e-mail: shizhong19892006@163.com

This chapter uses Ansys-Airpak ventilation simulation software to explore its effect on natural ventilation with the skylight's three variables: plane position, distribution pattern, and skylight height [2].

2 Model of Skylight Ventilation

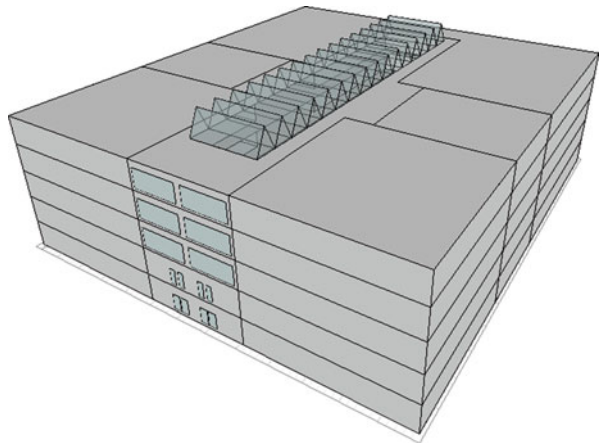
2.1 Model Setting

This chapter chooses a specific building in Harbin, which has the specific characteristics of a cold region [3]. The building has five floors, each 4.35 m high, and the standard layer size is 64×72 m (Fig. 53.1). To simplify the analysis, the model preserves the skylight, atrium, windows on floors 1 and 2 (opening windows 1–8), and the main entrance (opening door), which serves as the main entrance for wind [4]. The size of the atrium is $16 \times 66.2 \times 22.2$ m. The size of the skylight is $11 \times 56 \times 66.2$ m (Fig. 53.2).

2.2 Climate Parameter Setting

The seasons in which natural ventilation is used in office buildings in cold regions are spring and autumn, when the temperature is comfortable and the air-conditioning system is shut down. Based on an analysis of the daily average temperature distribution in Harbin, the exact time period was selected as 16 April–16 June and 16 August–15 October (Fig. 53.3). This chapter takes the worst-case scenario as the study sample, which has the highest temperature during this time period. This is because if the atrium can make use of natural ventilation while

Fig. 53.1 Building model



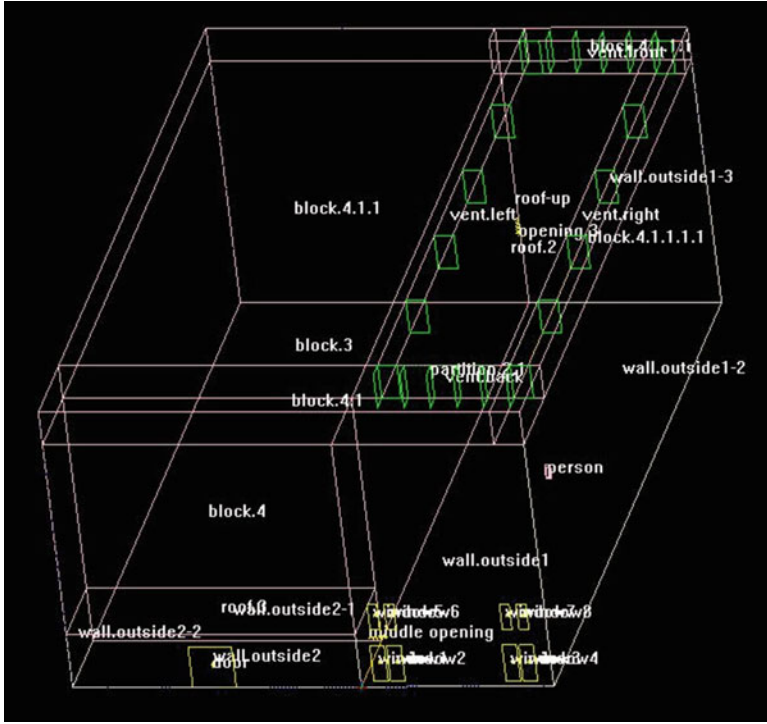


Fig. 53.2 Simulation model

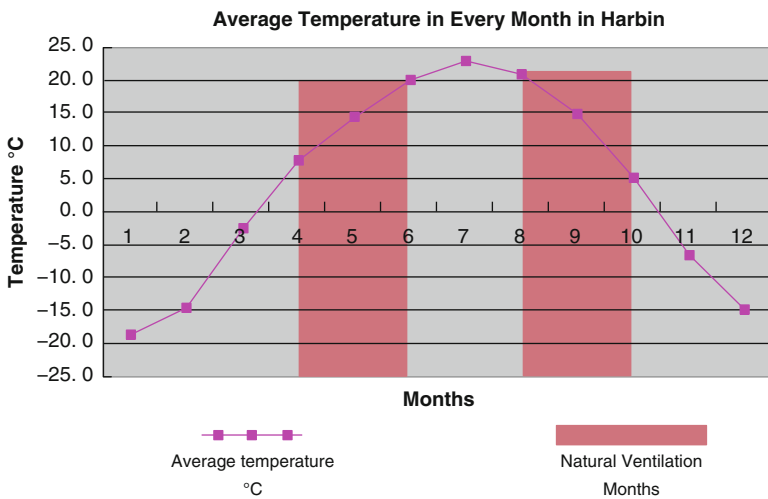


Fig. 53.3 Analysis of natural ventilation months in Harbin

temperatures are at their highest, the other time period can do so as well [5]. Therefore, the simulated wind speed was set at the average value in August – 2.9 m/s with a SW wind direction [3].

3 Simulation Based on Skylight Plane Position

3.1 Simulation Model

The building is simplified as a block of $64 \times 72 \times 22.2$ m, and the skylight is simplified to $11 \times 56 \times 3$ m. The size of testing wind spot outside is set to be $448 \times 704 \times 88.8$ m, at a speed of 2.9 m. The building block is turned by 45° to represent the SW direction (Fig. 53.4).

3.2 Ventilation Results Analysis

According to the simulation of the wind pressure and speed, we can draw the following conclusions (Fig. 53.5):

1. The distribution of the wind pressure on the *façades* is affected by the wind direction. The south and west *façades* have a higher pressure, while the east and north sides have a lower pressure. The southwest corner has a much higher pressure than that in the southeast corner, which can also be seen from the top view.

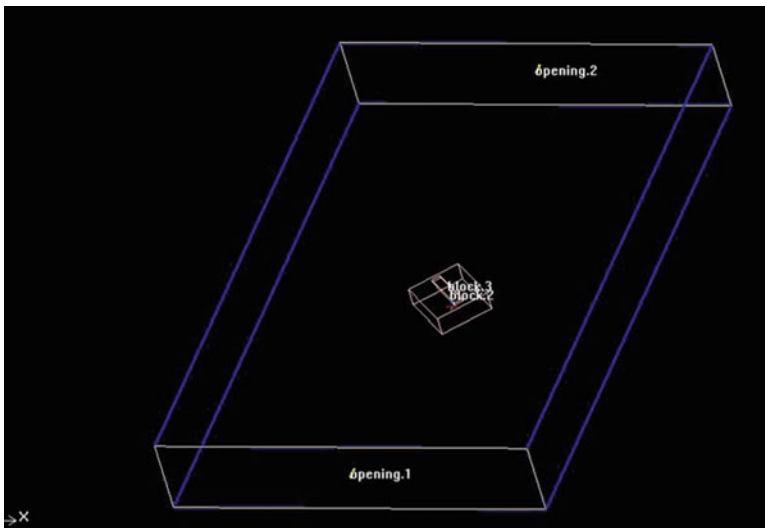


Fig. 53.4 Simulation model of exterior wind

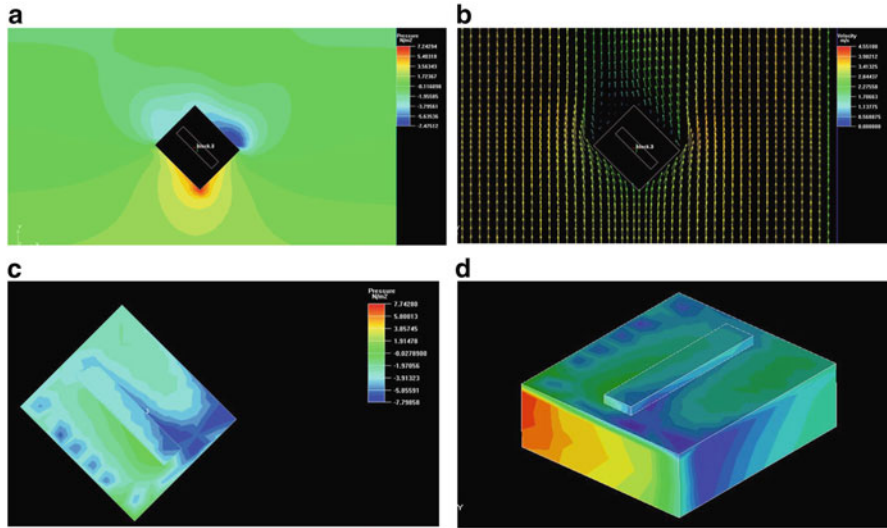


Fig. 53.5 Wind speed and pressure distribution around the façades. (a) Exterior wind pressure distribution. (b) Exterior wind speed distribution. (c) Wind pressure distribution on roof. (d) Building wind pressure distribution

- Recommendations for the skylight position can be made based on the simulation: the inlets of the building should be set at the west and south façades, and the outlets should be set at the east and north sides. In particular, the outlets should be set close to the southeast corner, where the air pressure is higher, to accelerate air exchange.

4 Simulation Based on Skylight Distribution

4.1 Simulation Model

The difference in the combinations between inlets and outlets can affect the indoor wind direction and the uniformity of the wind distribution. Because the inlet is unchangeable, the model is set with outlets having different distribution patterns – east side, northeast sides, and northeast–southwest sides.

4.2 Ventilation Results Analysis

According to the simulation of the wind pressure and speed, and the contrast of the mean age of air and PMV (the predicted mean vote, predicting the average vote

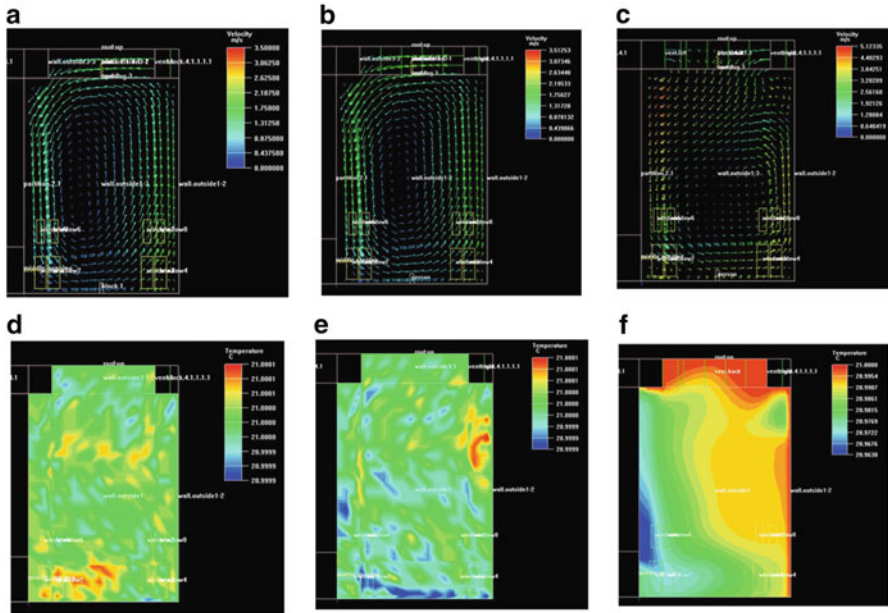


Fig. 53.6 Wind speed and pressure distribution with different outlets. (a) Wind speed of east outlet. (b) Wind speed of northeast outlet. (c) Wind speed of four-sided outlet. (d) Temperature of east outlet. (e) Temperature of northeast outlet. (f) Temperature of four-sided outlet

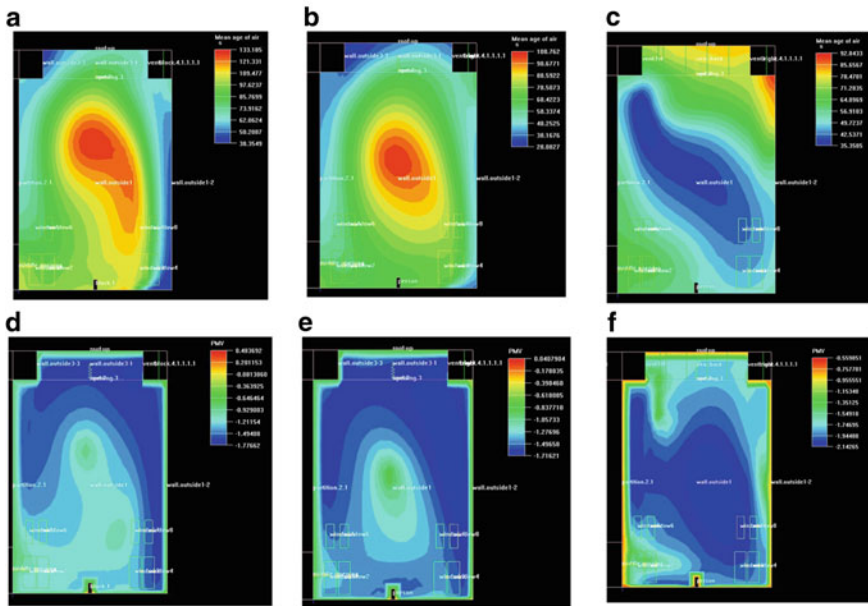


Fig. 53.7 Mean age of air and PMV distribution with different outlets. (a) Mean age of air of east outlet. (b) Mean age of air of northeast outlet. (c) Mean age of air of four-sided outlet. (d) PMV of east outlet. (e) PMV of northeast outlet. (f) PMV of four-sided outlet

of a large group of people on the a seven-point thermal sensation scale), we can draw the following conclusion (Figs. 53.6 and 53.7):

1. An atrium with a four-sided outlet has a higher temperature and wind speed, the temperature is more uniform compared with other sides of the skylight.
2. Based on a comparison with different sections of the atrium, the exterior air flowed inside through the outlet when the depth was 18 m; the interior air flowed outside when the depth was 38 m and 58 m [3].

5 Simulation Based on Skylight Sectional Height

5.1 Simulation Model

A model with four-sided outlets is set with different sectional heights. The ratios between the skylight and atrium heights are 1/5, 1/7, 1/9, and 1/11, which means the skylight sectional heights are 4.4 m, 3.0 m, 2.5 m, and 2.0 m.

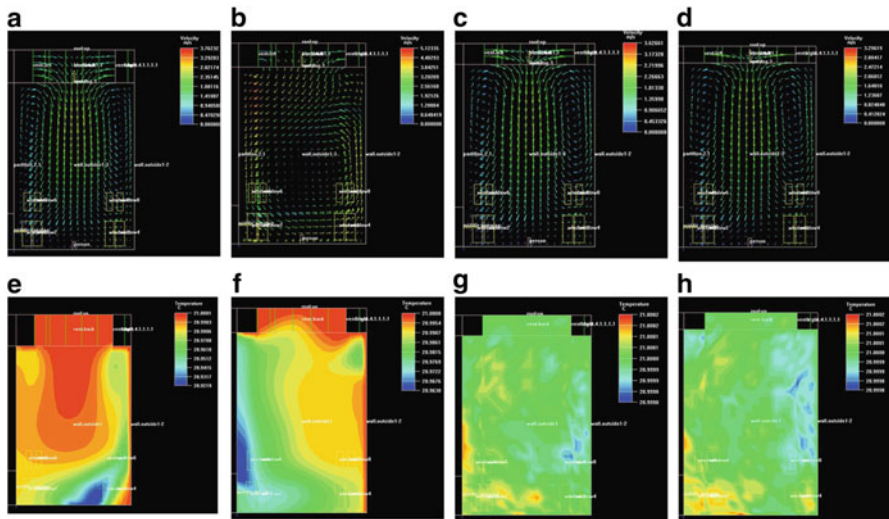


Fig. 53.8 Wind speed and pressure distribution with different sectional heights. (a) $H=4.4$ m wind speed. (b) $H=3$ m wind speed. (c) $H=2.5$ m wind speed. (d) $H=2$ m wind speed. (e) $H=4.4$ m temperature. (f) $H=3$ m temperature. (g) $H=2.5$ m temperature. (h) $H=2$ m temperature

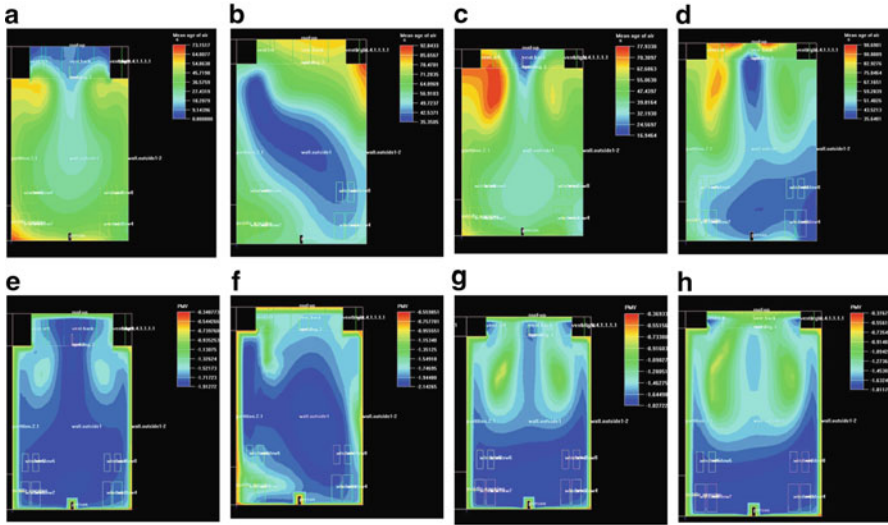


Fig. 53.9 Mean age of air and PMV with different sectional heights. (a) $H = 4.4$ m mean age of air. (b) $H = 3$ m mean age of air. (c) $H = 2.5$ m mean age of air. (d) $H = 2$ m mean age of air. (e) $H = 4.4$ m PMV. (f) $H = 3$ m PMV. (g) $H = 2.5$ m PMV. (h) $H = 2$ m PMV

5.2 Ventilation Results Analysis

According to the simulation of the wind pressure and speed, and the contrast of the mean age of air and PMV, we can draw the following conclusions (Figs. 53.8 and 53.9):

1. As the skylight height increases, the indoor temperature increases. At a height of 3 m, the indoor temperature on the west side is much lower than on the east, while in other cases the temperature distribution is much more symmetrical.
2. At heights of 2 and 2.5 m, the indoor temperature and wind speed are similar, while the temperature at 3 and 4.4 m is much higher.
3. At heights of 2 and 3 m, the atrium has a lower mean air age, which means it takes longer to exchange fresh air.
4. Compared with the PMV figures, the order at which people feel more comfortable at various skylight heights is $2\text{ m} > 2.5\text{ m} > 3\text{ m} > 4.4\text{ m}$.

6 Summary

Through a simulation with three different skylight variables, this chapter explored the effect of skylights on an office building's atrium ventilation. Three conclusions were drawn: (1) skylight outlets should be set on the side behind the wind direction,

which is useful for air flow because of the wind pressure; (2) outlets should be set around skylights uniformly to accelerate the air exchange rate; (3) the skylight height design should take into consideration the atrium size and outlet location. Overall, a skylight has a significant effect on atrium ventilation and should be designed carefully to reduce energy consumption and increase indoor environmental comfort levels.

Acknowledgement This work was sponsored by the Heilongjiang Natural Science Foundation (E201317).

References

1. Yuan MH (2012) Cold region architecture. China Architecture & Building Press, Beijing, pp 3–6
2. Kotani H, Sagara K, Yamanaka T et al (2006) Task ambient air conditioning system with natural ventilation for high rise office building (Part 2: measurement of natural ventilation rate and CFD analysis using measured data). *Balance* 9:3.2–2.7
3. Du Tiantian (2014) Simulation and optimization design study of the cold place office building's atrium skylight. Harbin Institute of Technology, 51–76.
4. Zhou L, Huang H, Shakeri A et al (2005) Indoor environment in an office floor with nozzle diffusers: a CFD simulation. *Proceedings of building simulation conference*, 67–69
5. Hayashi T, Ito K (2012) Coupled simulation of BES-CFD and performance assessment of energy recovery ventilation system for office model. *J Cent South Univ* 3:008

Chapter 54

An Environmental Technological Approach to Architectural Programming for School Facilities

Giacomo Chiesa and Mario Grosso

Abstract This chapter describes synthetically a method integrating functional, technological and environmental aspects of architectural programming for school facilities. This method is based on the analysis of activities and relevant user needs followed by an in-depth assessment of all related functional and environmental aspects usually not considered in current design practices: from the climate response to comfort requirements to the analysis of energy and material flows; from the space–time characteristics of activities to their private/public connotation and interdependency; from the inside/outside interrelationships to the multisensory perception of users. This building programming phase represents a necessary background for the next preliminary architectural composition based on the environmentally sound combination of “virtual” space units through a set of rules aimed at fulfilling the client brief and general sustainability requirements as well as avoiding or, at least, balancing potential conflicts by a tradeoff approach.

Keywords School building • Environmental design • Architectural programming • Site analysis • Building regulations

1 Introduction to Environmental Architectural Programming

Public buildings have a deep symbolic significance, as they rise to the role of spaces available to citizens. This characteristic is particularly strong in buildings at educational institutions representing not only a space of study for the youth but also a place for learning in which citizenship awareness is formed. Today, a new stringent feature is being added to this concept: the need to reach environmental sustainability by complying with the requirement of nearly zero-energy buildings as

G. Chiesa (✉) • M. Grosso

Dipartimento di Architettura e Design, Politecnico di Torino,
Viale Mattioli 39, Torino 10125, Italy

e-mail: giacomo.chiesa@polito.it; mario.grosso@polito.it

established by European Directive EPBD 2010/31/EU for the construction of new public buildings starting from 2018. To achieve this objective, new, or radically refurbished, school buildings will have to be designed taking environmental architectural programming into account whereby educational effectiveness and sustainability will be assessed against a benchmark of much higher quality than the current one.

The difficulties in achieving this goal are several, including, for example, an urgent need for modernizing the majority of existing school buildings, providing them with new functions as well as restoring them from their current state of physical and structural deterioration; the need to integrate aesthetic aspects into environmental and operational features; and, last but not least, the difficulty of finding the necessary project funds.

The aforementioned approach needs to be applied since the earliest design phases and, specifically, the architectural programming phase. Architectural programming is the preliminary design phase dealing with the organization and analysis of information necessary to develop the subsequent design phases in a rational and coherent manner.

Conventional architectural programming deals with general information and standards compliance and is generally based on a prescriptive morphological approach (e.g., quantitative dimensional rules to be followed – minimum area, height, windows area). The subsequent building design phases (configuration of layout, volume, and materials) are carried out in compliance with the standard prescriptions. In contrast, environmental-technological architectural programming includes general information, analysis of activities, needs, and requirements (ANR) according to a performance-driven approach aimed at designing buildings in response to user needs, without confining oneself to any particular shape or dimension, and the definition of indicators as tools for measuring the design performance. When this approach is used, a preliminary phase, before the schematic building design (pre-design), is carried out on space unit layout and technological strategies (virtual configuration) in order to check performance vs. requirements (compliance check).

1.1 Environmental-Technological Architectural Programming

“Activities and environmental systems can be considered as the explanation of human needs and of what they tend to express: they allow for identifying the expected behaviours of users and the relevant requirements based on which designers and producers of technological systems will construct buildings” [1: 115]. The main purpose of the building design process is the realization of projects able to organize the complexity generated by both the user-activity

program and the related responses to the needed framework (UNI 7867/4). In addition, building design must ensure liveability and environmental quality [2–5].

A performance-based design of a building involves the identification of the following items:

- (a) Activities to be performed in the building;
- (b) User needs related to those activities;
- (c) Requirements that spaces and technological systems must have in order to meet user needs;
- (d) Flows that need to be considered, defined as “the movement of persons, goods or materials, in their specific location” [1].

According to Standard UNI 8289: 1981, activities are grouped by affinities of time and space in *environmental units*, and the portion of space in which one or more environmental units are carried out is called a *spatial element*. Environmental units and spatial elements constitute an environmental system. Analogously, the same standards define a *technological system* comprising *technological units*, i.e., a group of compatible functions necessary to fulfill user needs and requirements, and *technical elements*, i.e., building products able to perform the functions of one or more technological units.

The need-requirement system defined by Standard UNI 8289: 1981 is categorized into three main classes: structural (static and dynamic structural safety); operational (usability, management, and integration); context (sociocultural physical) [4]. A subsequent standard – UNI 11277: 2008 – introduced a framework of needs related to the eco-compatibility of a building and the interrelation to the phases of its life-cycle assessment. In addition, Directive CEE n.106/1989 defined six mandatory requirements for construction products to be traded within the European Union states: safety of use; durability; safety against fire; hygiene, health, and environment; protection against noise; energy savings; and heat conservation. A seventh requirement is under development and discussion: sustainability.

In parallel to the typological and topological classification established by the aforementioned UNI standards, the environmental architectural programming approach suggests a modal-dynamic classification to define and analyze activities and relevant needs/requirements. These are classified by modal categories: space–time mode, relational mode, dimensional mode, and physical mode. In the space–time mode, activities are characterized by the time of day and time of year at which they are carried out; their place of execution (external, internal); their “proprioceptive” feature (whether stationary or in motion). The relational mode is related to the privacy level of an activity (individual, group). In the dimensional mode, activities are classified based on the number of people that are involved and the size of the required space. In the physical mode, activities are classified by the material and energy input/output flows involved in the process characterizing their execution.

A synthetic representation of the architectural programming process as a basis for the preliminary design phase according to an environmental/technological approach is shown in Fig. 54.1 [6].

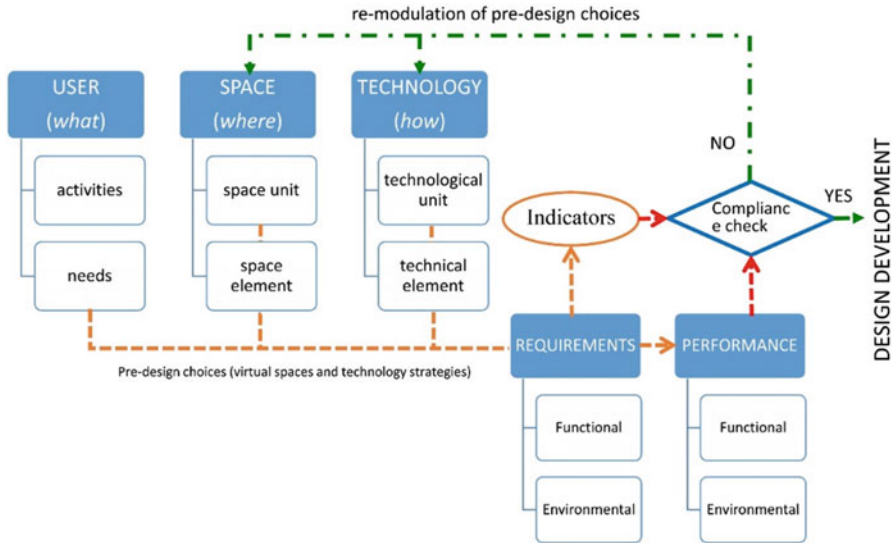


Fig. 54.1 Environmental-technological architectural programming and predesign

2 A Methodological Application: Environmental Architectural Programming for School Buildings

In this paragraph, the environmental architectural programming method described previously is applied to school buildings. As an introductory note, it must be highlighted that the national legislation implemented for this type of building (D.M. 12/18.12.1975) is more specific, from an environmental point of view, than for other types. In fact, it specifies minimum requirements with respect to, for example, space dimensioning and occupation density in relation to different environmental units; airflow rate (air change per hour); and the classroom average daylight factor. In addition, school buildings' design can be based on good practice criteria given by the standard UNI 10339:1995 and shall comply with the national legislation for public buildings regarding execution procedures (D.M. 236/14.1989), elimination of architectural barriers (D.P.R 503/14.07.1996), and fire prevention (D.M. 26.08.1992).

The environmental architectural programming for school buildings is characterized by the following sequence of operations defining:

- A dimensional matrix based on the national standard minimum requirements;
- A matrix of activities according to the modal classification described earlier, and related to functional units, which include activities to be performed for a specified main function;
- A matrix of input/output flows – energy, materials, waste – related to the identified functional units;

- Virtual spaces as tridimensional spatial unit elements related to the identified functional units and characterized by specific dimensions and a virtual envelope;
- A matrix of requirements of the virtual spatial units with relevant envelope characteristics and aggregation rules;
- A hypothesis of localization of the aggregated virtual spatial units on a site-microclimate matrix;
- A template for the compliance check of environmental requirements for technological units and technical elements related to the functional and spatial units.

As an example, the previously described sequence of operations is applied to a junior high school building as follows. Based on the aforementioned Italian legislation, this type of building includes classes of functional units related to the following activities: didactics, group activities and services, complementary activities, physical education, outdoor activities, and residential activities. Didactics includes instructional design, teaching models, assessment practices, human development and curriculum development, and classroom teaching, as well as special activities (art, computer science, linguistics, science, and music). Group activities and services include trips to the library, extracurricular activities, eating in the cafeteria, and hygiene services. Complementary activities include administrative, management, and technical services. Physical education includes activities for physical wellness, sports, and taking care of one's body. Outdoor activities include physical education, sports, and recreational activities. The residential category may include, for example, a room for the janitor.

Taking as an example procedure the class of functional units related to didactic activities, the previously listed sequence of operations is described as follows.

2.1 Dimensional Analysis

A dimensional analysis for the functional and relevant spatial units belonging to the class of didactics activities is to be carried out in relation to the minimum requirements set by the specific Italian legislation as mentioned earlier. The list of functional/spatial units with the minimum requirements in terms of floor area units (m²) per student is shown in Table 54.1. This table also includes empty cells for client brief requirements – which coincide with the law's requirements in the case of a public school building – and for design data with a relevant compliance check.

2.2 Activities Analysis

The activities related to each of the functional units listed in Table 54.1 are classified (Table 54.2) based on the modal approach mentioned earlier, which includes daily and seasonal schedules, location (indoor or outdoor), type of action

Table 54.1 Dimensional matrix: didactic activities

Dimensional analysis		Design				
Definition of spaces		DM 18/12/75 index (12 classrooms, 300 students) [m ² /student]	Client brief requirements	Number of special units	Floor area (m ²)	Index compliance check
Class of functional unit	Functional unit					
Didactic activities	Teaching	Spatial unit	1.8			
	Artwork	Classroom				
	Computer	Special didactic space/class				
	Linguistic					
	Science					
	Music	Musical space/class				
		0.76				
		0.13				

Table 54.2 Analysis of activities. Modal classification of activities for functional units related to didactic activities

Functional unit	Characteristics													Dimensional need					
	Seasonal term						Schedule			Placement		Type of action		Privacy		Group work	Floor area	Height	
	Winter	Spring	Summer	Fall	AM	PM	Nighttime	In	Out	Stationary	Dynamic	Individual							
Teaching	Activity																		
	Speaking	•	•		•	•						•					S	M	N
	Listening	•	•		•	•						•					S	M	N
	Reading	•	•		•	•						•						M	N
Art work	Writing	•	•		•	•						•						M	N
	Watching blackboard	•	•		•	•						•						M	N
	Speaking	•	•		•	•						•					S	M	N
	Listening	•	•		•	•						•					S	M	N
Computer and linguistic	Drawing	•	•		•	•						•						M	N
	Painting	•	•		•	•						•						M	N
	Modelling	•	•		•	•						•						M	N
	Washing instrument	•	•		•	•						•					S	S	N
	Showing	•	•		•	•						•						L	N
	Speaking	•	•		•	•						•					M	M	N
	Listening	•	•		•	•						•					S	M	N
	Reading	•	•		•	•						•					S	M	N
	Writing	•	•		•	•						•						M	N
	Using PC	•	•		•	•						•						M	N
	Watching multi-media board	•	•		•	•						•						M	N
	Watching video	•	•		•	•						•						M	N

(continued)

Table 54.2 (continued)

Functional unit		Characteristics												Dimensional need					
		Seasonal term						Schedule		Placement		Type of action				Privacy			
		Winter	Spring	Summer	Fall	AM	PM	Nighttime	In	Out	Stationary	Dynamic	Individual			Group work	Floor area	Height	
Science	Activity																		
	Speaking	•	•		•	•				•						•		M	N
	Listening	•	•		•	•				•							S	M	N
	Reading	•	•		•	•				•						•		M	N
	Writing	•	•		•	•				•						•		M	N
	Experiment	•	•		•	•				•						•	S	M	N
	Wash instrument	•	•		•	•				•						•	S	S	N
	Watching blackboard	•	•		•	•				•						•		M	N
	Watching multi-media board	•	•		•	•				•						•		M	N
	Music	Speaking	•	•		•	•				•						•	S	M
Listening		•	•		•	•				•							S	M	N
Reading		•	•		•	•				•								M	N
Playing music		•	•		•	•				•						•	S/M	M/L	N
Singing		•	•		•	•				•						•	S/M	M	N
Dancing		•	•		•	•				•					•		S/M	M/L	N
Watching blackboard		•	•		•	•				•						•		M	N
Watching multi-media board		•	•		•	•				•						•		M	N
Watching video		•	•		•	•				•						•		M	N

S small, *N* normal, *M* medium, *M* medium, *H* high, *L* large

(resting or moving), level of privacy (individual or group activity), and qualitative dimensional requirements (floor area and height of spatial unit).

2.3 *Flow Analysis*

Analysis of input/output flows related to activities of the functional units belonging to the class of didactic activities is shown in Table 54.3. This table reports the system analysis of inputs and outputs for each specific activity. The following types of flows are considered: energy, acoustic, materials, emissions to air, water, and ground, and flows impacting indoor air quality (IAQ).

2.4 *Virtual Space Characterization*

Several examples of the application of functional diagrams, mainly related to distribution and communications rather than environmental requirements, can be found in the literature [7–9]. To facilitate the architectural programming process as a predesign tool oriented toward a sustainable approach, a method based on the concept of virtual space is proposed. A virtual space is a parallelepiped volume representing a spatial unit with specific dimensional and modal characteristics and environmental requirements related to the functional unit, as well as the relevant activities with which it is associated. The *façades* of its envelope are compass-oriented and characterized by climate–environmental requirements as well as rules for unit interrelationships and locations on a site (Fig. 54.2a). These *façades* are virtual, i.e., not yet technologically defined.

The environmental requirements of virtual spatial units, as well as their *façades*' characteristics and rules of interrelationship and location, make it possible to aggregate them in an organic manner to determine the basis for designing a sustainable school building. In addition, a correct site-climate analysis is crucial for the completion of the environmental programming process. To this end, a method based on the microclimate matrix that makes it possible to assess the optimal location of activities and related spatial units depending on solar and wind access/protection [2, 3, 10–12] can be used as shown in Fig. 54.2b. An example of virtual spatial characterization for a school building's functional units in relation to various dimensional, relationship, modal, and environmental requirements is shown in Table 54.4.

Table 54.3 Analysis of flows (input and output) for activities related to functional units belonging to class of didactics

Functional unit		Flow analysis: input and output																					
		Energy					Acoustic				Materials			Water and ground emissions				IAQ					
		Input		Output			I/O		Input		Ground	H ₂ O	Vegetation	Inorganic waste	Organic waste	Water output	Airflow rate	Input	Output				
Activity	Electricity	Heating <100 °C	Heating >100 °C	Daylight	Ventilation	Thermal flow <50 °C	Thermal flow >50 °C	Low sound volume	Medium sound volume	Ground	H ₂ O	Vegetation	Inorganic waste	Organic waste	Water output	Airflow rate	Input	CO ₂	Smoke	CO	Radon	VOCs	
Teaching	Speak	•			•	•											•	•					
	Listen				•	•											•	•					
	Read	•			•	•											•	•					
	Write	•			•	•							•				•	•					
	Watch out blackboard	•			•	•											•	•					
	Watch out multimedia board	•			#/no	•											•	•					
Artwork	Speak	•			•	•											•	•					
	Listen				•	•											•	•					
	Draw	•			•	•							•				•	•					
	Paint	•			•	•							•				•	•					
	Mode	•			•	•							•				•	•					
	Wash instrument	•			•	•											•	•					
Computer and linguistic	Exhibit	•			•	•											•	•					
	Speak	•			•	•											•	•					
	Listen				•	•											•	•					
	Read	•			•	•											•	•					
	Write	•			•	•											•	•					
	Use PC	•			#	•											•	•					
Science	Watch out multimedia board	•			#	•											•	•					
	Watch video	•			•	•											•	•					
	Speak	•			•	•											•	•					
	Listen				•	•											•	•					
	Read	•			•	•											•	•					
	Write	•			•	•											•	•					
Experiment	•			•	•											•	•						

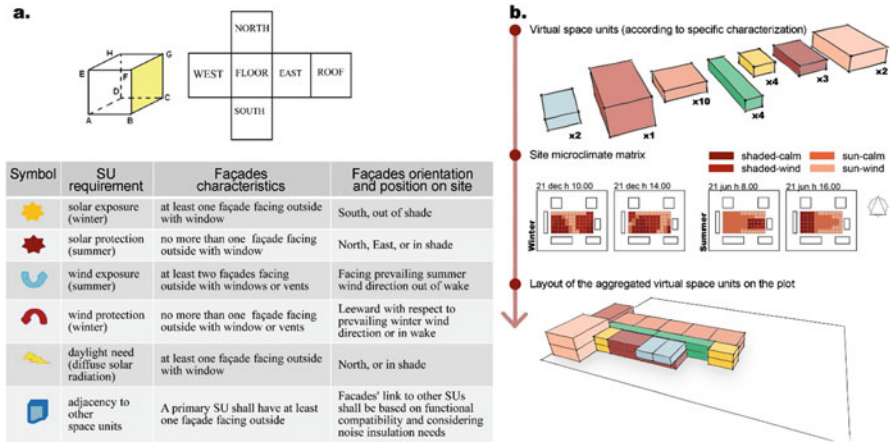


Fig. 54.2 (a) Virtual space unit with its envelope (*above*); example of environmental requirements for virtual spatial units related to a generic functional unit of a school building (*below*); (b) virtual spatial units of a school building related to different functional units and relevant dimensions (*above*); placement of virtual spatial units on a plot according to environmental requirements and a site-microclimate matrix (*below*)

2.5 Environmental-Technological Assessment

The following step of environmental architectural programming is a technological envelope characterization, whereby a virtual space’s *façades* acquire a form associated to technical elements (e.g., windows, walls). This operation is still related to a predesign phase characterized by a list of needs and requirements, as well as their relevant performance check, as shown in Table 54.5 for an example of a technical element (window).

3 Conclusions

This chapter proposes an environmentally related method for architectural programming that is applicable to both retrofit and new construction projects.

The proposed method, through a series of steps comprising activity analysis, requirement definitions, and the compliance assessment of predesign options, can be applied in the earliest design phases to arrive at an environmentally to lead to an environmentally and technologically sustainable final building product. The different proposed tools, including checklists, templates, and matrixes, are based on both qualitative and quantitative evaluations and are flexible, adaptable, and iterative. Their application implies the contribution of an environmental consultant or a designer with environmental knowledge.

Table 54.5 Template for environmental requirements compliance check of a technical element (window) characterizing the technological unit “*façade*” associated to a virtual spatial unit (classroom) belonging to the functional unit “teaching” of a school building

Environmental requirements		Teaching		Spatial unit		
Functional unit		Classroom system	Classroom element	Classroom	Windows	
Needs and requirements		Performance assessment				
Class of needs	Need	Life cycle phase	Class of requirements	Requirement relevance	^a Required performance level	Design performance level
Comfort, hygiene, health	Perceptive, sensorial comfort	Operational phase	Thermal comfort	<i>H</i>	<i>VH</i>	Design performance level
			Visual comfort	<i>H</i>	<i>VH</i>	
Acoustic Comfort	<i>M</i>		<i>VH</i>			
Olfactory comfort	–		–			
Tactile comfort	–		–			
Proprioception comfort	<i>M</i>		<i>H</i>			
Electromagnetic radiation	<i>H</i>		<i>H</i>			
IAQ	<i>H</i>		<i>VH</i>			
Indoor toxicity	<i>VH</i>		<i>VH</i>			
Solar gain for winter heating	<i>H</i>		<i>VH</i>			
Rational use of resources	Rational use of climate and energy resources	Solar control	<i>H</i>	<i>VH</i>	<i>VH</i>	
		Use of natural air movement for cooling	<i>H</i>	<i>VH</i>	<i>VH</i>	
		Air infiltration control in winter	<i>H</i>	<i>VH</i>	<i>VH</i>	

L low, *M* medium, *H* high, *VH* very high

^aFrom regulation and client brief

When functional and environmental components are not taken into account after the preliminary design phases, the possibility that their further integration may result in significant adjustments to the building project with consequent increases, by a proportional factor, in costs and time is very high. The integration of these factors in an advanced design phase, in order to restore the levels of quality of the design, is, in fact, difficult and is often resolved with improper and nonintegrated solutions. Instead, a designer should be able to integrate the various components of the project from the beginning through the necessary tradeoff between aesthetic and functional values.

References

1. Cavaglià G, Ceragioli G, Foti M, Maggi PM, Matteoli L, Ossola F (1975) Industrializzazione per programmi. Strumenti e procedure per la definizione dei sistemi di edilizia abitativa. RDB, Piacenza
2. Grosso M (2008) L'evoluzione della dialettica ambiente/paesaggio e il ruolo della tecnologia dell'architettura. In: Ginelli E (ed) La ricerca a fronte della sfida ambientale. Materiali del III SeminarioOsdotta. Firenze University Press, Firenze
3. Grosso M (2008) Progettazione bioclimatica. In Castelli L (ed) Architettura Sostenibile, utet scienze tecniche, Wolters Kluwers Italia, Milano
4. Grosso M, Peretti G, Piardi S, Scudo G (2005) Progettazione ecocompatibile dell'architettura. Concetti e metodi, strumenti d'analisi e valutazione, esempi applicativi. Sistemi Editoriali/Esselibri, Napoli
5. Scudo G (2007) Prefazione. In: Dessì V (ed) Progettare il comfort urbano, Soluzioni per un'integrazione tra società e territorio. Sistemi Editoriali, Napoli
6. Grosso M, Chiesa G, Nigra M (2015) Architectural and Environmental Compositional Aspect for Technological Innovation in the Built Environment. Heritage and Technology. Mind Knowledge Experience, XIII International Forum Le vie dei Mercanti, Capri, 11–13 Giugno, pp 1572–1581
7. Chiesa G (2010) Biomimetica tecnologia e innovazione per l'architettura. Celid, Torino
8. Ferré et al. (eds) (2005) Verb Conditioning. Architecture Boogazine, Barcelona, Actar
9. Ferré et al. (eds) (2004) Verb Connection. Architecture Boogazine, Barcelona, Actar
10. Brown GZ, Dekay M (2001) Sun, wind & light. Wiley, New York
11. Chiesa G, Grosso M (2015) Accessibilità e qualità ambientale del paesaggio urbano. La matrice microclimatica di sito come strumento di progetto. Ri-Vista 23(1):78–91
12. Grosso M (2011) Il raffrescamento passivo degli edifici, 3rd edn. Maggioli, Rimini

Chapter 55

Green, Smart, Sustainable Building Aspects and Innovations

Abdul Salam Darwish

Abstract Buildings of the future should be designed with features that meet the anticipated challenges of technological, environmental, and societal progress. When increasingly sophisticated communications and control systems are integrated into a building's design, the door is opened to endless innovations; when incorporated into construction procedures, energy consumption is contained and the environment is better protected. Through smart construction, a more comfortable built environment can be created while simultaneously reducing a site's carbon footprint. Green building melds technology and living practices to modify water efficiency and increase energy efficiency. The use of eco-friendly materials and innovative procedures will result in optimized energy performance, extra commissioning measurements and verification, and continual carbon dioxide monitoring. This is essential as LEED and BREEAM schemes are expected to become future requirements of any construction project, large or small. Self-sustaining buildings will be the best solution for meeting the ever-growing technological demand on energy, as well as many countries' stated goals of independence from carbon-based energy sources.

Keywords Green buildings • Smart buildings • Sustainable buildings • Energy efficiency buildings • Building design

1 Introduction

Green building, a term used all over the world, has become synonymous with sustainability. This common connection, however, does not mean that all green building is, in fact, sustainable. Green building is a very important step toward sustainable building and is defined as the practical application of sustainable methods that takes into account not only the building site's environmental conditions but also strives to make the best use of resources throughout the building's phases. These phases include site selection, design, construction, operation,

A.S. Darwish (✉)
Phoenix Renewable Energy Centre, PO Box 470, Manchester M40 0ED, UK
e-mail: darwish@renewableenergycentre.org

maintenance, and demolition. Green building strives not only for sustainability and environmental consideration but also to meet economic needs, including comfort, style, and high performance.

Over the last several decades there has been an increasing awareness of the disparaging connection between traditional economic development and the overexploitation of the world's natural resources. Pollutants and harmful residues from land stripping and the production of building materials are putting the environment under increasing stress. After a century of postindustrial expansion, urban centers now have an acute sense of the impact continual construction wreaks [1]. According to some estimates, the worldwide construction industry consumes about 40 % of total raw materials, at a rate of about three billion tons per year. In the USA alone, buildings account for around 65 % of the total energy consumption and cause 30 % of greenhouse emissions [1]. Since built environments comprise such a large and ever-increasing portion of the world's total greenhouse emissions, and since the majority of those emissions are derived from a building's life cycle, this is obviously the area of urban development where meaningful and long-term change must immediately be implemented. This awareness, and the outcry for the reduction of the impact of human activities, the concept of sustainable development has matured and is defined as "meeting the needs of the current generation without compromising the ability of future generations to meet their own needs" [2].

Smart buildings signify intangible built-up development that utilizes all the latest technological instrumentation and inventions to facilitate modern efforts toward energy-efficient cities and Society with Energy saving awareness and Smart. Mapping out smart buildings requires strategic planning, which relies on many factors. Stakeholders (e.g., local governments, research institutions, grass-roots movements, technology vendors, and property developers) are often driven by conflicting interests [3]. To create better environmental, social, and economic conditions and enhance cities' attractiveness and competitiveness, upgrades to building infrastructures and services must be made. Smart buildings/cities are defined in a multitude of ways, and solutions to building-related issues are proposed without an existing prevalent or universally acknowledged definition of smart building [4, 5]. Many new categories of *city* have entered policy discourse: sustainable cities, green cities, digital cities, smart cities, intelligent cities, information cities, knowledge cities, resilient cities, eco cities, low-carbon cities, livable cities, and combinations thereof [6].

2 Gulf Cooperation Council Energy Situation

Gulf Cooperation Council (GCC) countries, which constitute a major portion of the wealth in the Middle East, face major energy and environmental challenges, as the continuously growing population creates a huge demand for energy. The area is experiencing a high rate of economic growth and modernization. Figure 55.1 shows the annual per capita electricity consumption [7] and demonstrates that GCC

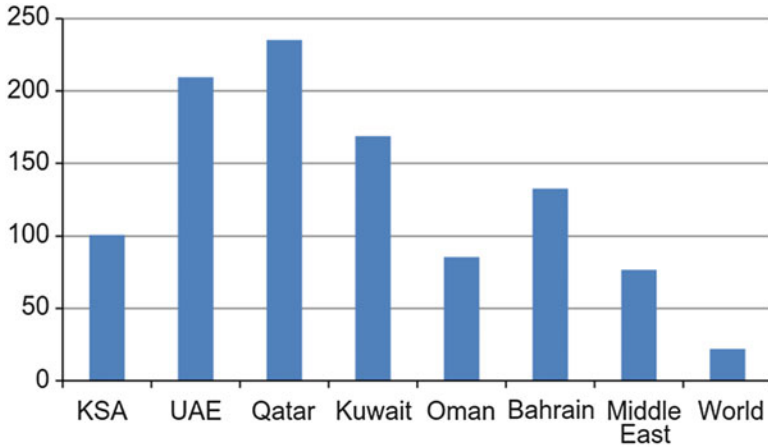


Fig. 55.1 Annual per capita electricity consumption (MW-h) [7]

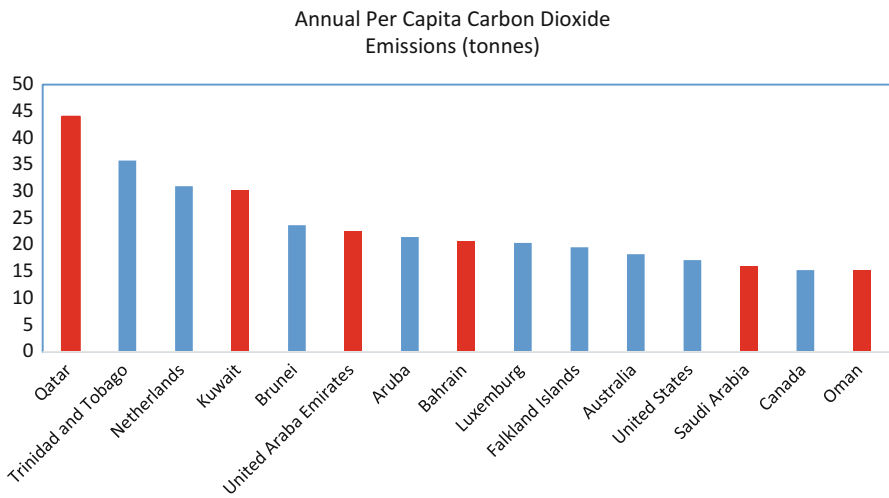
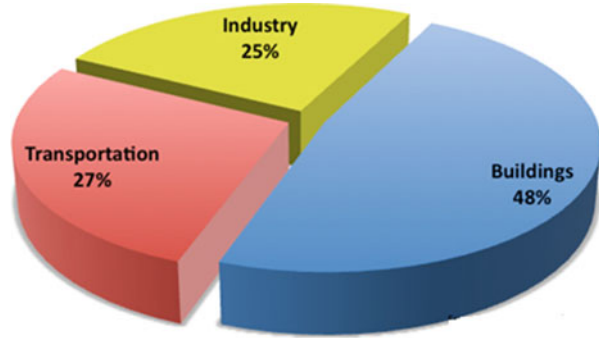


Fig. 55.2 Annual per capita carbon dioxide emissions (tons)

countries have among the highest rates of energy consumption in the world. High energy consumption means high carbon dioxide levels, and so GCC countries also have among the highest levels of CO₂ emissions. Figure 55.2 shows [7] annual per capita carbon dioxide emissions (tons). Qatar, Kuwait, and the United Arab Emirates (UAE) are among the top six countries in the world for CO₂ emissions; Qatar is the global leader.

It is clear that the environmental impact of CO₂ emissions is significant and a grave matter that could lead to future environmental disaster.

Fig. 55.3 Energy consumption sectors



Energy consumed for cooling and heating in buildings is becoming an increasingly serious cause of global warming. Buildings are responsible for 48 % of energy consumption and 45 % of CO₂ emissions within the region. Urbanization has increased the demand for cooling energy and is accelerating the formation of smog. Figure 55.3 shows sectors of energy consumption and illustrates that buildings generate the highest amount of energy consumption [8].

3 Sustainable Buildings: The Right Solution

The benefits of sustainable buildings are as follows:

- Lower life-cycle costs
- Lower insurance fees
- Higher property values
- Higher productivity
- Improved image
- Reduced risks
- Healthier for residents and visitors
- Reduced effects on infrastructure
- Better for the environment and local economy.

The best and most effective way to protect the environment is to use sustainable methods during building construction [9, 10]. It is important that all new construction strike a careful balance between economic, social, and environmental considerations.

Sustainable building innovation creates economic stability, which in turn generates high rates of economic growth and employment. These factors improve project delivery and increase profitability and productivity. Environmental sustainability protects the environment by avoiding pollution, enhancing biodiversity, and developing an eco-friendly transportation system. It also facilitates the management of natural resources by employing technology, education, and forecasting to

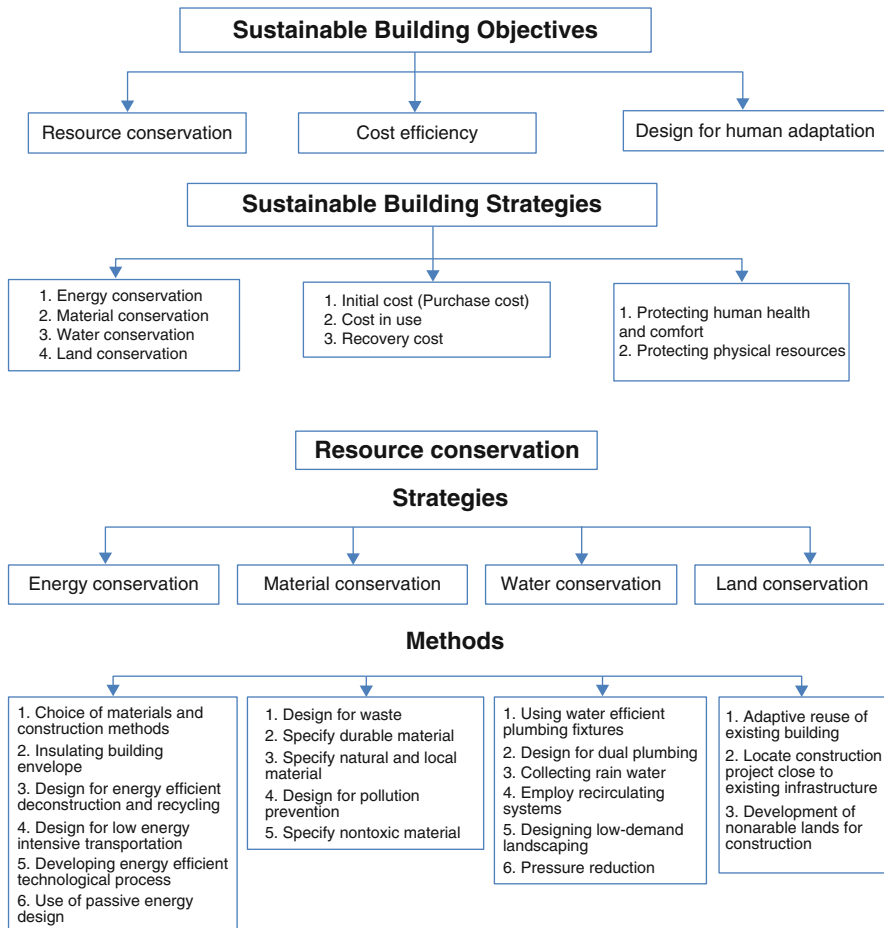


Fig. 55.4 Practical framework for sustainability implementation in building construction, strategies, and methods to achieve resource conservation [11]

improve energy efficiency and ensure the proper utilization of resources. This sustainability is achieved through a social process that recognizes the needs of everyone and creates a partnership with local communities to ensure that everyone’s needs are satisfied [11] (Fig. 55.4).

4 Strategic Energy Technology Plan

A strategic energy technology plan represent the principal decision-making support tool for many countries’ energy policies. It encourages the development and use of low-carbon technologies through the wide dissemination of education and

information technology. It is characterized by specific targets that will be met in a set period of time or by a certain deadline [12].

Countries, both in general and particularly within the GCC area, will need to implement their strategic energy technology plans through the following initiatives:

- Wind initiative
- Solar initiative (i.e., photovoltaic and concentrated solar power)
- Electricity grid initiative
- Carbon capture initiative
- Industrial geothermal initiative
- Transport and storage initiative
- Smart cities and communities initiatives
- Fuel cells and hydrogen initiative
- Wave and tidal initiative.

5 Smart Sustainable Buildings

Smart buildings incorporate all of the latest technological instrumentation and inventions in order to achieve energy efficiency goals and long-term social sustainability. Mapping out a smart building's design requires strategic planning and depends on the actualization of multiple factors. To achieve a perfect combination, smart building construction should not only be smart but also green and intelligent in various design and operation aspects. There are three different approaches to defining intelligent buildings [13].

- Performance-based approach
- Service-based approach
- System-based approach.

The performance-based approach reflects the ways in which the building is performing according to its users' environment and demands and emphasizes the efficient use of resources in a cost-effective manner and in accordance with international standards and measures. The service-based approach considers the quality of services the buildings provide, such as, for example, intelligent functions, communications, or automation. The system-based approach refers to all of the available high-end technology that is embedded within the building's design and construction.

By implementing the right combination and management of these three approaches, an optimal composition of structure, system, service, and management will result in high-efficiency building automation, office automation, communication network systems, safety, and comfort. This combination will satisfy all regulations to fulfill the smart building philosophy (Fig. 55.5) [13].

High-performance building systems and services include the following:

- Heating, ventilation, and air conditioning (HVAC) control

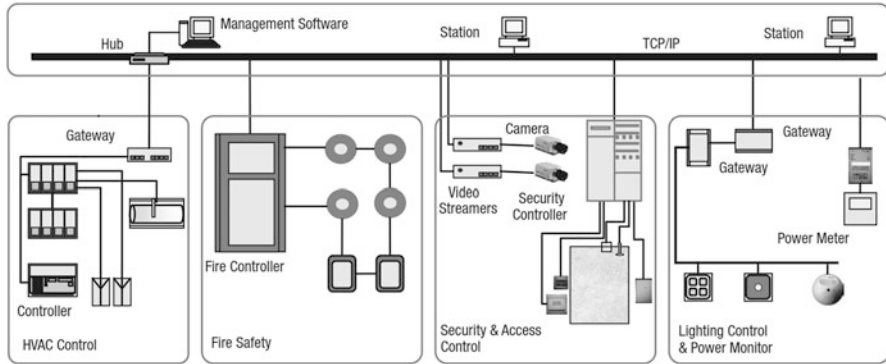


Fig. 55.5 An integrated intelligent building system [14]

- Electrical lighting
- Vertical transport control
- TV and image communications
- Voice and data communications
- Security and access control
- Data and video communications
- Fire alarm control systems
- Integrated building automation systems
- Computerized integrated systems
- Enterprise network integrated systems.

Additionally, smart buildings will need to be capable of integrating into the innovative electrical grid of smart cities so as to be able to fully utilize all potential renewable energy options. This capacity will require computerized power delivery services using the latest two-way communication and control systems for the smart grid, as well as so-called smart meters for commercial and residential buildings.

6 Energy Certification for Smart and Green Buildings

Energy performance evaluations and certifications will positively benefit from so-called intelligent technologies and facilities incorporated into the smart building [11].

- Optimize Energy Performance
Using the building simulation package Energy Cost Budget Method, energy performance is well presented, and therefore points for assessment are earned accordingly.
- Additional Commissioning

This involves an independent commission agent; since a smart building includes the integration of all of the building's systems, the additional commissioning will meet a certification requirement.

- **Measurement and Verification**
Smart metering systems and management system tools that can track actual usage and cost will provide verifications requirements for the monitoring of energy consumption and storage.
- **Carbon Dioxide (CO₂) Monitoring**
Using a smart technology monitoring system, HVAC systems will be adjusted to improve indoor air quality and comfort. Zones and individual spaces will be controlled by integrated monitoring systems.
- **Controllability of Systems: Perimeter and Nonperimeter Spaces**
Lighting, temperature, and ventilation of building spaces are smartly controlled, allowing credits to be awarded for perimeter and nonperimeter spaces.
- **Thermal Comfort: Permanent Monitoring System**
Integrating the temperature and humidity measurement systems into HVAC control systems will automatically provide the desired comfort level. Smart technology will facilitate data collection for systems and occupants. These data will then be used for performance optimization throughout the smart building.
- **Innovation in Design**
As the smart building system introduces many innovative ideas not covered by green building ratings systems, extra rating points are added and granted by the rating system [15].

7 Smart Grid's Impact on Intelligent Buildings and Connected Cities

Reasons to Incorporate a Smart Grid:

1. It is a more reliable type of grid, with fairer pricing and optimum energy use. These qualities make certain locations more attractive places in which to invest.
2. These investments will in turn bring new businesses and consumers to the locations. (This will spur economic growth and create additional customers for utilities.)
3. A generational change is under way; young graduates are very information technology (IT) literate and very aware of the benefits of IT. Their involvement will drive change.
4. A Smart grid reduces power usage at peak hours.
5. It increases grid stability and reliability.
6. It can improve efficiency for energy consumption and data management.
7. It decreases energy costs.
8. It optimizes prices.
9. It empowers customers.

8 Elements of a Smart Energy Building

- Smart lighting system
- Increased daylight appearance
- Onsite electricity generation
- DC grid for DC loads
- Load/generation balancing
- Energy management system
- Electrical and thermal energy storage/buffering
- Energy efficient practices.
 - Active/passive techniques for heating and cooling:
 - Glazing
 - Insulation
 - Shading
 - Construction materials
 - Pricing incentives
 - Low-temperature heating/high-temperature cooling systems
 - High-efficiency heat-recovery ventilation
 - Flexible workspaces (Table 55.1).

9 Building Rating System

The nature of the Middle East's extreme climate, combined with its continuous population growth, has a profound effect on its levels of energy, water, and materials consumption. The concept of smart cities has raised alternatives to traditional building methods. Coupled with green building rating systems, smart cities will lead this building evolution in a sustainable direction. The most important factors for such a rating system are that its implementation must be obligatory and that it must conform with the American LEED and British BREEAM rating systems, though be adaptable to local cultural, environmental, social, historical, and economic contexts.

Countries within the GCC region have used their own modified versions of these systems. For instance, Abu Dhabi of the UAE introduced the Estidama and Pearl Building Rating System in 2007 [16], Qatar introduced the Sustainability Assessment System in 2010 [13], Egypt introduced the Green Pyramid system in 2011, Jordan introduced the Idama system in 2009, and Lebanon introduced the ARZ Building Rating System in 2008 [17].

Table 55.1 The main control and communication systems of a smart building [14]

Control and communication systems	Technology and application
Digital controllers	<ul style="list-style-type: none"> • Computers • Microcomputers • Processors • Digital controllers • Actuators
Building automation systems	<ul style="list-style-type: none"> • Programming and monitoring • Building management functions with automatic processing
Local area networks (LANs)	<ul style="list-style-type: none"> • Wireless technology • LAN technologies
Building automation system communication standards	<ul style="list-style-type: none"> • Integration and interoperability of building automation systems (BAS) • Communication standards for BAS networks • (BACnet) building automation and control networks • (LonWorks) Local operating network • (Modbus) Serial communication protocol • PROFIBUS (process field bus), defined as a standard for field bus communication in automation technology • European installation bus (EIB), defined as a field bus designed to improve electrical installations in homes
Internet technologies	<ul style="list-style-type: none"> • Internet protocols • Internet LAN vs. wide area network (WAN) • Internet technologies at automation level • Internet technologies at management level

10 An Ongoing Case Study in the UAE

A commercial building was considered in Ajman in the UAE taking into account the climate and energy resources in the area. The aim was to create an energy self-sufficient and carbon-neutral green, sustainable, smart building with an extraordinary photovoltaic wall with vertical axis wind turbines and a zero-energy footprint with no grid support. Energy is to be generated using solar and wind technologies that are designed specifically to match the climate and weather conditions over the course of a year. A solar thermal cooling system was selected with an efficient innovative system that matches the building's air-conditioning requirements, with all old conventional systems having been removed. All principles and ideas presented in this chapter were implemented, and an integrated smart control system was designed to fulfill all green building rating requirements. More details will be published in a later report.

11 Conclusion

The Middle East, and specifically the GCC countries, faces considerable energy and environmental challenges that result from its huge energy demands. As GCC countries are able to fund projects and get involved in developing and maintaining better building designs and construction, these countries will reduce their carbon footprints while simultaneously maintaining high rates of economic growth and modernization. Combining smart technology with green buildings results in smart, sustainable, green buildings that can be integrated into smart cities.

References

1. Fakosh U, Ahmed R (2012) The employment of technical development to the direction of high-technology buildings within the framework of sustainable design. *Damascus University Journal of Science and Engineering*, 226–246. <http://www.damascusuniversity.edu.sy/mag/eng/images/stories/229-246.pdf>
2. United Nations (1987) Report of the World Commission on Environment and Development, General Assembly Resolution 42/187, 11 Dec 1987. Accessed 14 Nov 2007
3. Angelidou M (2014) Smart city policies: a spatial approach. *Cities* 41(suppl 1):S3–S11
4. Allwinkle S, Cruickshank P (2011) Creating smarter cities: an overview. *J Urban Technol* 18:1–16
5. Komninos N, Tsarchopoulos P (2012) Towards intelligent Thessaloniki: from an agglomeration of apps to smart districts. *J Knowl Econ* 4:149–168
6. de Jong M, Joss S, Schraven D, Zhan C, Weijnen M (2015) Sustainable–smart–resilient–low carbon–eco–knowledge cities; making sense of a multitude of concepts promoting sustainable urbanization. *J Clean Prod* 109:25–38
7. Asif M (2015) Growth and sustainability trends in the buildings sector in the GCC region with particular reference to the KSA and UAE. *Renew Sustain Energy Rev* 55:1267–1273
8. United Nations Environment Programme (2007) Buildings figure NGS and climate change status, challenges and opportunities. UNEP
9. Abidin NZ (2010) Investigating the awareness and application of sustainable construction concept by Malaysian developers. *Habitat Int* 34:421–426
10. Shen L, Tam V, Tam L, Ji Y (2010) Project feasibility study: the key to successful implementation of sustainable and socially responsible construction management practice. *J Clean Prod* 18:254–259
11. Akadiri PO, Chinyio EA, Olomolaiye PO (2012) Design of a sustainable building: a conceptual framework for implementing sustainability in the building sector. *Buildings* 2(2):126–152
12. Kylili A, Fokaides PA (2015) European smart cities: the role of zero energy buildings. *Sustain Cities Soc* 15:86–95
13. Gulf Operations for Research and Development (2014) Global sustainability assessment system (GSAS). Gulf Operations for Research and Development (GORD), Qatar
14. Wang S (2010) *Intelligent buildings and building automation*. Spon Press, Oxon
15. Galbraith JK (2015) How do smart buildings make a building green? Retrieved from Automated Buildings. <http://www.automatedbuildings.com/news/dec07/articles/sinopoli/071129114606sinopoli.htm>
16. Abu Dhabi Urban Planning Council (2015) Estidama & development review. Abu Dhabi Urban Planning Council. <http://www.estidama.upc.gov.ae/>
17. Attia S (2015) The usability of green building rating systems in hot arid climates. <http://orbi.ulg.ac.be/>; http://orbi.ulg.ac.be/bitstream/2268/164015/1/ID%2312528_Final2.pdf

Chapter 56

Soilless Urban Temporary Agriculture as a Strategy for Brownfield Site Renewal

Leonardo Boganini and Chiara Casazza

Abstract The last few years have witnessed the development of a large number of projects, in the fields of planning and architecture, that aim to integrate food production in urban spaces. This practice goes under the name of Urban Agriculture and it is spreading into many cities because it carries benefits and implications toward urban sustainability (environmental, economic, social and institutional). The paper aims to describe an ongoing research project, Ur.C.A. is an in progress research project, financed by Regione Toscana, and developed by the Interuniversity Centre and the DISPAA Department of the University of Florence, in partnership with two local enterprises: Azienda Agricola Cammelli and Azienda Agricola Artemisia.

Ur.C.A. aims to identify the possibilities and the potential of integrating agriculture in urban settlements, especially in brownfield sites and marginal areas, taking advantage of hydroponic technologies. The integration of agricultural activities in urban areas meets the requirements of consciousness toward food, reducing the gap between production and consumptions, and of alternative sustainable km0 alimentary production chains. Furthermore urban agriculture improves shared public spaces and social and recreational activities.

Brownfield sites and temporary unused areas can be, through urban agriculture, regenerated in terms of space quality, also providing them of new functions and a new role.

The project general objective is to analyze the possibilities of the requalification of the above mentioned urban contexts, through urban agriculture, focusing on legislative and technological feasibility. Ur.C.A. aims to develop an innovative use for brownfield sites that, through the integration of food production, can enhance social innovation, citizens awareness toward environment, health, and diet, social participation, and furthermore can stimulate an urban km0 production and consequently new small scale local economies and green jobs.

Ur.C.A. specific objective is to **identify an innovative hydroponic growth cell system**, suitable for urban contexts in terms of design, technology and sustainability, which would integrate renewable energy resources and rain water collection.

L. Boganini • C. Casazza (✉)

Dipartimento di Architettura DIDA, Centro ABITA, Università degli Studi di Firenze,
Florence, Italy

e-mail: l.boganini@gmail.com; Casazzakia.casazza@gmail.com

The new concepts of growth cell will be especially suitable for urban unused areas: indeed in our towns can be found several spaces that remain temporary, but generally for a long period, unused as “frozen” waiting for new projects to be approved and completed. The Ur.C.A. growth cell, conceived as light, transportable, modular, nearly zero environmentally impacting, and energy efficient, can become a device useful to quickly, but also temporary, requalifying the mentioned areas.

Keywords Urban agriculture • Urban regeneration • Integration • Soilless technologies • Brownfield sites

1 Introduction

The last few years have witnessed the development of a large number of projects in the fields of planning and architecture that aim to integrate food production in urban spaces. This practice goes under the name of urban agriculture¹ [8] and it is spreading to many cities because it carries benefits and implications with respect to urban sustainability (environmental, economic, social, and institutional).

Food production in urban settlements is definitely not a new issue: indeed we can find it in several different periods of history: it is sufficient to mention *les jardins potagers* in France, the Rinascimental Orangeries, the medieval *hortus conclusus*, Howard’s Garden City, Frank Lloyd Wright’s Broadacre City, and the Victory Gardens in the USA during the two world wars (the equivalent of the Italian *orti di guerra*). In recent years the phenomenon has acquired renewed strength and with different characteristics, approaches, forms, expressions, and technologies, showing different spatial and architectonic solutions. Nowadays food production faces different needs than in the past: if previously it almost aimed to satisfy food needs, nowadays it needs to meet the requirements of food security, healthy food access and, in the case of developing countries, it faces the challenges of food deserts, food miles (and consequentially emissions from transport but also preservation and packaging) overcome, sustainability, and alternative food models.

In this last context, which is the one this chapter is concerned with, urban agriculture stands out and is distinguished by its multifunctional features and by the awareness of its role in ecosystem service creation. Indeed it responds to certain shared exigencies and is characterized by specific functions and benefits it brings to urban environments. In particular urban agriculture serves the following functions [6]:

- Creates a short food chain;
- Reduces the distance (physical and psychological) separating consumers and producers;

¹ With the term Urban Agriculture (UA) we can define an “industry” (Luc J.A Mougeot) located within of a town which grows or raises, processes and distributes a diversity of food and non-food products, using mainly human and material resources, inputs and services found in the urban area, and sharing outputs and ecosystem services to the city itself.

- Supports environmental and nutrition education;
- Promotes citizens' participation and inclusion in the food system, city greening and shared green spaces, urban renewal, well-being, health, and job creation through a new urban local food market.

This chapter **will stress the possibilities and the potential of integrating agriculture into the social fabric, especially in transitional areas like brownfield sites and marginal areas, taking advantage of hydroponic technologies** in order to pursue an environmental, architectural, and social renewal and refunctionalization of these urban spaces. The research will focus on the Italian local context, where the research project Urban Con(t)emporary Agriculture (known by its Italian acronym Ur.C.A.) financed by Regione Toscana and developed by the ABITA Interuniversity Centre with the DISPAA Department of the University of Florence, in partnership with local enterprises (Azienda Agricola Cammelli and Campioni Serre) and supported by the Florence municipality public administration interest, is actualizing a pilot project.

2 State of the Art

Urban agriculture is attracting the interest of the scientific community and is becoming a concrete strategy for the city of the future, on two fronts:

- Food: food security, education, health, diet, awareness, sustainable production
- City: urban renewal, sustainability, urban greening, citizen participation, social inclusion

From an overview of the state of the art and from an analysis of national and international case studies we can identify three distinct elements in urban agriculture experiences [2]:

- The kind of spaces that have the potential to host urban agriculture
- Performance and effects on the urban environment
- Growing technologies and devices suitable for urban agriculture integration on different scales depending on available space and performance requirements

Those spaces that have the potential to host urban agriculture projects can be summarized as follows [12]:

- Urban scale: green areas, parks, gardens, pocket spaces, brownfield sites, vacant lots
- Building scale [also called building-integrated agriculture (BIA²): terraces, flat roofs, *façades*, backyard gardens

² Astee, L.Y., Kishnani N.T. (2010) "Building Integrated Agriculture: Utilising Rooftops for Sustainable Food Crop Cultivation in Singapore" *Journal of Green Building*: Spring 2010, Vol. 5, No. 2, pp. 105–113.

Urban agriculture activities can include hobby farming, self-sufficiency, education, therapy, sales of products, community service, urban renewal, nonfood production (e.g., biomass or textiles). Impacts on the urban environment can be illustrated whether from a social, environmental, or economic point of view: it allows urban areas to progress toward being greener with its benefits such as space quality, well-being, urban heat island effect reduction, pollution absorption, good air quality, social inclusion, and safety. Furthermore, urban agriculture, which allows for local short chain production, minimizes agriculture's environmental footprint (in terms of transport and soil consumption), creates jobs, enhances local retail markets, fosters well-being [11], promotes education and health owing to the conscious consumption of food and farming activities, enhances citizen participation in the local governance, and guarantees food self-sufficiency [9].

In terms of growing technologies and devices, it is interesting to note how different technologies have been investigated or adapted (and transferred) from agriculture to architecture [4] in order to make the aforementioned spaces suitable for crop production and to fulfill space and user requirements. Growing technologies and devices can be summarized in the following ways:

- Traditional growing (plants rooting in a soil substrate): in the ground, in vases, raised beds, greenhouses, green roofs, vertical gardens;
- Hydroponics with hydroponic irrigation (plants rooting in a soilless or soil-simulant substrate): greenhouses, growth cells, hydroponic vases, hydroponic towers, vertical farms, vertical gardens, and living walls. These latter are especially suitable in the case of artificial surfaces and when light weight, productivity, and crop protection are required.

Brownfield sites and unused areas can be, through urban agriculture, regenerated in terms of space quality and serve new functions and play new roles. The integration of agricultural activities in these areas meets, on the one hand, the requirements of urban regeneration, by improving shared public spaces and social and recreational activities, and, on the other hand, those of consciousness toward food systems, reducing the gap between production and consumption, and alternative sustainable short chain food production chains [14].

The potential of brownfield site use and renewal for urban agricultural purposes has been developed by some recent projects such as the GrowUp Urban Farms in London, Prinzessinnengarten Community Garden in Berlin, the Jardin Partagés in Paris, the Plant vertical farm in Chicago [3], OrtiDiPinti in Florence, Hayes Valley Farm in San Francisco, and several community gardens in New York City and Detroit.

3 Method

The cities we live in are facing several challenges in their struggle for sustainability. Globalization and industrialization together with the large organized distribution of food products have caused on the one hand a generalized loss of awareness by consumers of food (its quality and its provenance), and the loss of social, cultural,

and educational values connected to it, which have brought other problems such as health and gastrointestinal diseases. On the other hand industrialized agriculture has affected our environment through the exploitation of vast tracts of land, environmental footprint due to transport, food preservation, and the burning of fossil fuels, energy consumption (food preservation), CO₂ emissions (for transport), and chemical pesticides and fertilizers [1].

Recently initiatives aiming to recover awareness of food production and a sustainable food chain, food quality, education, and local products have been spreading, and consumers have become aware of industrial agriculture and food chain unsustainability, demanding consciousness, impact reduction, and traceability. Some government administrations³ [5] are indeed developing the concept of a sustainable urban food system⁴ and enhancing urban food planning strategies.

Furthermore, analyzing the issue from an urban and architectural point of view [13], we can show how our cities are characterized both by a lack of green and shared spaces and by unused or marginal areas and brownfield sites due to bad urban planning or abandoned spaces that remain frozen at the current level of evolution. These blank spaces have become an element of degradation in terms of space quality but also safety and need to be renewed. Usually government administrations consider these spaces for new public projects, but in the meantime, they remain temporarily, but generally for long periods, unused or “frozen” waiting for the projects to be approved and completed.

For example, the city of Florence in its new urban regulations has identified such mentioned spaces as follows:

- ATA: empty lots that will host residential buildings construction
- ATS: empty lots that will host non-residential buildings construction or other urban facilities (parkings, sport fields)

Both these kinds of areas are, as already stated, unused and degraded but might be a resource if they were properly restored and given a new role.

The aforementioned unused or abandoned areas can find new life through **innovative, temporary** urban agricultural use. Indeed, the integration of food production in empty spaces can create a new area of attraction, giving them new functions, and it can enhance social innovation, citizen awareness of the environment, health, and diet, and social participation; furthermore, it can stimulate urban km0 production and consequentially new small-scale local economies and green jobs.

³ Toronto Food Charter or the Portland Food System Strategy.

⁴ The term *urban food system* includes all the activities of the food chain (production, transport, processing, selling, consumption, and waste) and the goal of a sustainable urban food system is to understand and plan their connection with other urban features: transport of food for retail sales, preparation and serving, nutrition education, recreational activities, therapeutic activities, and urban waste management. Therefore, restaurants, retail stores, supermarkets, hospitals, canteens, and schools could talk about the different activities related to food production or be linked in an urban local food system.

Unused areas will therefore host small-scale crop production for local distribution (also involving local cooperatives and enterprises) through high-tech hydroponic greenhouses and shared community vegetable gardens, aiming at self-sufficiency and social inclusion through low-tech (also soilless) raised beds.

A **temporary** use of the aforementioned spaces is a necessary feature: indeed, such areas must not be modified, as they are provisionally unused but waiting for new projects to be developed, and furthermore they are not able to host new construction if not included in a city's regulations. Incidentally, temporary and removable constructions are permitted, especially for public utilities.

The technological feasibility of urban agriculture in the aforementioned contexts relies on the use of innovative off-the-grid greenhouses. These meet the requirements of high productivity, low water consumption, and crop protection. Indeed, they were conceived as being light, transportable, and modular, having near zero environmental impact, and being energy efficient; they can be used to quickly, but also temporarily, restore the kinds of areas mentioned earlier.

The goal of unused areas renovations can be achieved by taking advantage of hydroponic growing methods because they permit a reversible but also sustainable and off-the-grid approach. Furthermore, using hydroponic soilless or soil-simulant growing methods makes it possible to overcome a shortage or lack of cultivable soil, often one of the results of pollution in urban contexts.

The term *hydroponic* describes those cultivation systems that do not use soil as a substratum and that use water as a vehicle to grow nutritive substances. Their management relies on automatic systems, controlling the microclimate, transpiration, irrigation, and the plant nutrition supply.

Cultivation without soil can be classified into two main categories, depending on the substratum:

Fluid Substratum

- Nutrient film technique: film of food plant that flows in intervals
- Aeroponic: plants are cultivated in perforated panels; roots hang under the panel and are sprayed with solutions of food plant.
- Floating: plants are cultivated on floating supports.

Solid Substratum

- Light and static materials like vegetable fiber, mineral wool, and expanded clay are used as support for roots. In both these systems, water is the element that constantly brings nutrients to the plants, making up for the lack of soil that in traditional cultivation stores nutritive elements and serves as a physical support for the plant itself.

The main advantages of the techniques of cultivation without soil are as follows: high productivity in small spaces (the system is 3–10 times more productive than traditional methods in 10–20 times less space and time), product quality improvement thanks to the management system, and water savings (up to 90 % in closed-cycle systems).

4 Results

The previously defined analysis and method are applied to the city of Florence. In this case study we have defined a simple tool that can be useful in identifying the elements, in terms of performance, function, and distribution, needed to realize a temporary urban farming intervention in transitional areas. The tool consists of a series of points and a specific graphic system useful for simplifying the approach to urban farm planning and design.

The main focus is indeed on the design approach, which aims to define the principal criteria useful for both government administrators and designers to improve urban agriculture with a temporary perspective. We can divide the approach to designing new urban agricultural spaces into three areas:

1. Relationship with urban regulations (planning and functional)
2. Analysis of social patterns already present in the area and of its critical points
3. Analysis of technical aspects necessary for crop production and the functional design of the area

Relationship with urban regulations: the regulatory framework

The first analysis, useful for defining a new urban agricultural area, concerns local laws: it is necessary to define the operative framework to understand the possibilities of every specific city. The main categories to check are as follows:

- Urban regulations and specific land-use compatibility with agricultural use, food production, and local selling
- The presence of brownfield sites or unregulated areas
- The presence of transitional areas susceptible to future changes or projects

In the first case it is theoretically possible to create an urban farm that could be used as a food production, distribution, and training center: this is the best possibility, but, unlike some North American cities that adopted specific urban agriculture laws (e.g., San Francisco, Detroit), in the city of Florence no areas have been designated for that. Indeed, inside the urban planning system of the city of Florence, the areas designated for agricultural uses are few and marginal, outside the city limits, and far from the main social scenes.

For the two other cases a temporary design approach and a specific agreement between urban farmers and the municipality are viable and necessary in order to attempt local urban regulations. Indeed the *temporary* feature makes it possible to practice urban agriculture even in areas using land for different (not agricultural) purposes; for example, urban farms will be removed once any expected project is carried out, with the condition of a complete restoration of the space at the end of the agreement.

In the case study (transitional areas) it is possible to distinguish between privately owned and publicly owned lands: in the case of public spaces, the municipality is allowed to temporarily make use of such spaces, while in the case of privately owned spaces, a previous agreement between owners and government

officials is mandatory. In both cases it is necessary to obtain public authorization for temporary buildings and for specific activities (e.g., selling, services). In our case there is a need to use a simple, totally off-the-grid (for example, public water and energy supply networks cannot be used), and very easy-to-assemble system to prepare and design the area.

Analysis of social patterns: new use of public and private space.

The second step is the analysis of the social context: as we have seen, urban agriculture aims to produce food (in particular vegetables) inside the city, with the ultimate goal of developing a new Km0 market. Furthermore, inside this new agricultural system it is possible to identify social values, typical of rural areas, that are helpful in improving social conditions and quality of life.

Through temporary agriculture it is possible to modify the users' spatial perceptions for the purpose of defining a new method to reuse (and revitalize) marginal spaces or, in the case of transitional areas, to speed up the acceptance of new uses. Furthermore, with the involvement of the people, it is possible to use these spaces for temporary educational venues for the purpose of diffusing good practices in terms of sustainable crop production (also using new technologies) and reusing space.

This analysis must concentrate on the following tasks:

- Defining areas inside the city, suitable for urban agriculture, that should be near social points of interest, for example, parks, public squares, hospitals, senior centers, and schools
- Defining the connections between urban agriculture and the other uses or activities already taking place at (or in an area of influence) points of interest/ areas: the scope of the analysis is to define the critical issues
- Comparing this analysis with the regulatory framework

At the end of its analysis (urban regulation and social network) it is necessary to create a city plan where it might be possible to identify those areas that can be used for urban farming and a new services net connecting the main points. Furthermore, it is necessary to identify areas where urban agriculture can help to improve social conditions because it can work as a social buffer while revitalizing marginal areas.

The study must so define the main spaces for urban agriculture, the areas of influence with the main social points, and the transitional spaces already present. This zoning of the city serves to define the main features for the specific context and the benefits it and urban farming projects will be able to bring (Fig. 56.1).

Analysis of technical aspect: function, space, and technology

To optimize the production and connected social value created by temporary urban farming, it is necessary to identify specific activities and their connected spaces.

It is possible to divide spatial typologies into three main and interconnected categories:

- Production space, which is useful for hosting production, improving the creation of new local enterprises focused on vegetable production, and hosting Km0 selling points.

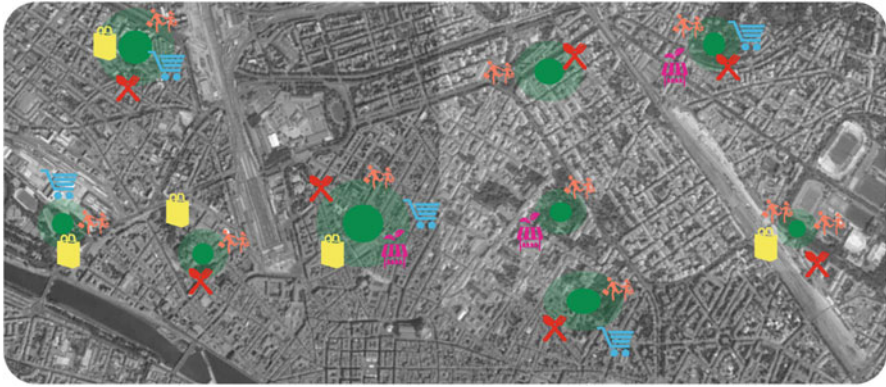


Fig. 56.1 Analysis of social patterns and existing connections in the downtown area of Florence

- Educational spaces and common vegetable gardens, which are useful for improving and divulgating the cultivation of vegetable gardens using specific technologies (like hydroponics) and of sustainable food production.
- Common spaces, useful for improving social connections with the rural world within the city and improving social inclusion and recreation.

This subdivision is helpful in the decision-making phase and in urban farming design, as a function of the main purpose that the area must fulfill: production, social recreation, or education.

The production area is subdivided into several simple spaces: main area, used especially for production; management space, a service zone necessary for the functioning of the production space; core system, which contains the fertigation management system (distribution of water and nutrients) and the climatic condition management system, together with the heating and cooling generator; nursery, where vegetables are kept before the planting phase; entrance and the sale point; packaging area (which connects to the common space) where the products are cleaned and prepared for sale or serving.

The social area aims to improve the connections and interactions among people and rural values: in this case, the simple space serves as a destination point. It is possible to distinguish private vegetable gardens from common vegetable gardens, where users can make use of soilless systems, the compost area, a garden therapy or garden learning area dedicated to the diffusion and application of knowledge, and a didactic area that is open to schools and private gatherings.

The common space is the most flexible one: it can be transformed by designers according to the external context and in concert with the main internal functions. This part of urban farms has the task of creating new connections between the existing social net and the area. In this part one finds the Gruppi d'Acquisto Solidali, or Solidal Buyers Group (GAS) point and all other facilities typically found at main entrances. In the case of GAS, the opportunity a temporary and agricultural use of urban areas it is important in order to allow the diffusion

of those social values related to the practices of Alternative Food Networks, Community Supported Agriculture and Social Buyers Group [10]. All spaces must be dimensioned according to the functions required by every particular place and context.

The building technology used in this type of project is divided into two different groups: the main structure and the production structure. The main structure is composed of all the buildings and all the paths inside the area. The necessity of moving the main structure (assembling and disassembling) requires a light and dry structure, often prefabricated to optimize construction time and costs. In particular, the most delicate parts are the connection with the ground and with the water and electricity networks: in this case, it is necessary to identify systems and strategies to make a zero impact [7]: the use of a photovoltaic system and rainwater reuse are the bases for creating an off-the-grid system. The production technologies are based on hydroponic and soilless systems: the first can be used inside the growth cells and greenhouse; the second, through the use of raised beds, are suitable for social and private areas (Fig. 56.2).

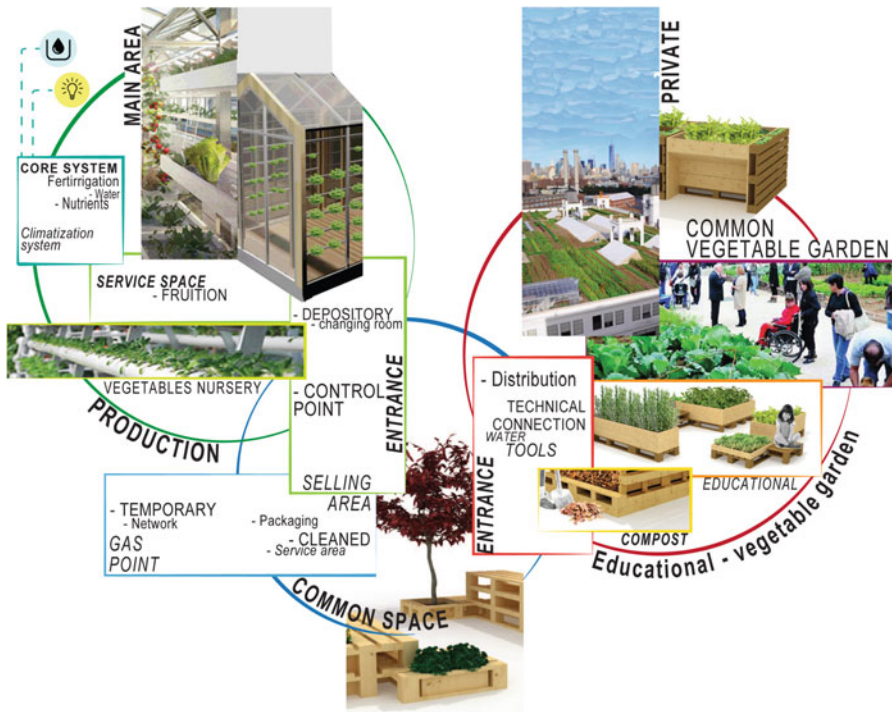


Fig. 56.2 Analysis of technical aspects: connection between space and function

5 Conclusion

Temporary urban agriculture can encourage the reuse and transformation of marginal areas: through their new function it is possible to social cohesion values and to create new enterprises within a city.

The tool that we propose is useful for defining the main areas and criteria (in terms of space and function) to apply urban farming within city limits, with the aim of facilitating, for a given amount of time while these areas await approval for projects, the transition from one land use to another and revitalizing the place and increasing its social value. This new use of urban agriculture requires zero impact and a reversible approach, defining an off-the-grid system useful for producing food and vegetables directly within the city: this can bring a new vision of food distribution and production, in favor of security, health, and new social activities and values.

6 Future Development

The next phase in the development of this research will aim to create the first prototype of a temporary urban farm inside the city of Florence, Italy. With the Ur.C.A. project and the involvement of the city government, we have identified three different areas in which to propose this type of experiment. The research aims to use the same prototype in these zones focusing each time on a different characteristic of urban farming:

- When the focus is on creating new social enterprises in food production and selling, with the involvement of local cooperatives, emphasis will be placed especially on the production area.
- When the focus is on enhancing social participation and inclusion, special attention will be paid to common vegetable garden spaces and the dissemination of rural culture.

Temporary urban farming will be used to redefine a new role for the three aforementioned areas to reduce their local decay and increase their value.

The expected results are manifold: the creation of new a Km0 production and selling point that will include new GAS points, increased use of marginal spaces to reduce social decay, and the diffusion and dissemination of knowledge on hydroponic harvesting systems. This prototype will be carried out also through the development of an off-the-grid system capable of fulfilling all its functions, in terms of energy production and water. The final purpose is to develop a tool dedicated to public administrators and designers that can be useful in decision making on how to integrate urban farming into local regulations.

References

1. Despommier DI (2013) Farming up the city: the rise of urban vertical farm. *Trends Biotechnol* 31(7):388–389
2. Gorgolewski MA, Komisar JU, Narsr JO (2011) Carrot city: creating places for urban agriculture. Monacelli Press, New York, p 240
3. Kaufman JE, Bailkey MA (2000) Farming inside cities: entrepreneurial urban agriculture in the United States, Lincoln Institute of Land Policy Working Paper
4. Palazzo VA (2003) Tecnologie ambientali per l'integrazione di verde agricolo in aree urbane. Tesi di Dottorato, Università degli Studi di Napoli Federico II
5. Pothukuchi KA, Kauffman JE (1999) Placing the food system on the urban agenda: the role of municipal institutions in food systems planning. *Agric Hum Values* 16:212–224
6. Viljoen AN (2005) Continuous productive urban landscapes: designing urban agriculture for sustainable cities. Elsevier Architectural Press, Oxford, p 304
7. Smit J, Nasr J (1992) Urban agriculture for sustainable cities: using wastes and idle land and water bodies as resources. *Environ Urban* 4(2):141–152
8. Mougeot LJA (2000) Urban agriculture: definition, presence, potentials and risks. Thematic paper 1 international conference on growing cities growing food: Urban Agriculture on the Policy Agenda La Habana Cuba, Oct 1999
9. Philips A (2013) Designing urban agriculture: a complete guide to the planning, design, construction, maintenance and management of edible landscapes. Wiley, Hoboken, p 288
10. Butler L, Monorek DM (2002) Urban agriculture and agricultural communities opportunities for common ground. Ames Council on Agriculture Science and Technology
11. Astee LY, Kishnani NT (2010) Building integrated agriculture: utilising rooftops for sustainable food crop cultivation in Singapore. *J Green Build* 5(2):105–113
12. Boganini L, Carta A, Casazza C, Sala MG (2013) The urban agriculture: a classification of possibilities. ICFEEB conference, China
13. Tjeerd Deelstra Herbert Girardet Urban Agriculture and Sustainable cities. In Aesop 2nd European Sustainable Food Planning Conference, Urban Performance Group, University of Brighton
14. Lee-Smith D (2009) Integrating urban agriculture in the urban landscape. In RUAUF Urban Agriculture Magazine 25
15. Lee-Smith D (2009) Carrot city: design for urban agriculture. In RUAUF Urban Agriculture Magazine 22
16. Sommariva E (2012) Agricoltura Urbana strategie per la città dopo la crisi. Atti XV conferenza Nazionale Società Italiana Urbanisti-L'urbanistica che cambia rischi e valori Pescara 10–11 maggio 2012

Chapter 57

Solar Building Systems for the Mediterranean Region: Research Outputs Between Italy and France

Christian Cristofari, Andrea Giachetta, and Chiara Piccardo

Abstract This paper comes from previous investigations carried out by the authors, in France and Italy, and from a cross border cooperation projects based on the joint collaboration between the University of Corsica Pascal Paoli and the University of Genoa. The authors focus on the enhancement of passive solar systems and thermal solar systems, with particular attention to their operation/efficiency and their architectural integration. The exchange between Italian and French experiences, especially between regions with similar climate, can enhance solar building strategies, in accordance with the new European energy standards as well as the Mediterranean climate, the traditional construction technologies and users' needs.

1 Introduction

In the near future, the 'nearly zero-energy' standard imposed by European directives (i.e. 2010/31/EU), will lead the building sector towards a greater use of technology, aimed at maximising both saving energy and producing it from renewable sources.

The use of passive and active solar systems could make a substantial contribution to saving energy, above all in the Mediterranean climatic zone, thanks to the high number of sunlight hours and the mild climate in both winter and summer.

Today, however, energy-efficiency policies for buildings, scientific debate on the subject and technological market solutions seem primarily directed towards the Northern European 'low-energy' building type, considering the Passivhaus standard as the building solution to meet European energy targets. This standard was

C. Cristofari (✉)

University of Corsica Pascal Paoli—IUT UMR CNRS 6134, Corte, France
e-mail: crstofari@univ-corse.fr

A. Giachetta • C. Piccardo

Department of Sciences for Architecture, University of Genoa, Genoa, Italy
e-mail: andreagiachetta@arch.unige.it; chiara.piccardo@arch.unige.it

designed on the basis of the Central European climate in which it originated; it essentially consists of energy conservation measures, with minimum energy exchanges between the outside and inside of a building, being particularly suitable for long and harsh winters. However, the application of the Passivhaus standard to the Mediterranean region is not effective because of the higher cooling demand in summer (if possible, by natural ventilation). Moreover, this standard could meet with resistance from users accustomed to a different management of interior spaces and from professionals because of different traditional construction systems. In addition, Passivhaus technologies could be difficult to manage in terms of architectural integration and landscape impact.

This theme is not sufficiently dealt with in the literature, which instead tries to show how this standard could be applied to the Mediterranean region. This might be happening because, as pointed out by Krainer, ‘in recent years, Passivhaus has become a religious movement’ [1: 393], thus influencing a rather short-sighted attempt to steer policies, European directives and rules of the member states. Krainer highlights the differences between the Passivhaus standard and the bioclimatic approach, where the first tends to alienate people from the natural environment outside their houses, while the second one enhances a strong relationship between inside and outside, in order to obtain advantages in terms of energy, environment, quality of life and health (e.g. a greater amount of natural light, better perception of the passing of time during the day, lower risks of indoor air pollution). Therefore, the bioclimatic approach seems to be more effective than the Passivhaus one, especially in temperate climates (as the Mediterranean climate is), where it may be easily applied. The bioclimatic approach may reduce the ‘artificialisation’ of the microclimatic and environmental conditions of the interiors, according to a broader concept of sustainable design, not limited to the issue of saving energy.

However, this is not only a matter of interpretation of the concept of sustainability as applied to building design, but also a matter of performance. Some studies [2] show that strategies typical of the Passivhaus model, such as mechanical ventilation with heat recovery, are less effective (in terms of energy and comfort) than natural ventilation in temperate maritime climates (this article also refers to the southern coast of England). Moreover, the trend of the diffusion of dry construction systems (again, of northern European origin), which is appropriate to the Passivhaus approach, although of great interest, is not always suitable for the methods typical of traditional Mediterranean constructions (for example in relation to the consistency and the thickness of external walls or the possibility of taking advantage of the thermal mass). There are also significant problems, especially with the retrofitting of existing buildings, in these geographic areas.

Therefore, a reflection on the southern European ‘low-energy building type’ seems necessary, considering technologies suitable to the climate, the natural resources and the traditional construction systems of the Mediterranean region.

Two different research centres are active in this field: the University Institute of Technology (IUT) of Corsica and the Department of Sciences for Architecture (DSA) of the University of Genoa. The two research groups have already collaborated in the cross-border cooperation project ‘Case Mediterranee’ (2010–2012),

funded under the Italy–France Maritime Programme. The relationship between the two groups has strengthened as a result of another project, still in progress, within the same programme, called the Me.R or ‘Mediterraneo in Rete–Mediterranee en Réseau’ (www.mediterraneoinrete.eu). This is a ‘simple project’ of scouting, stimulation and coaching actions for the business development of the cross-border area (2014–2015). The lead partner is the DSA, and the partners are Team s.r.l. (Genoa), Lucense (Lucca), the North Sardinia Industrialists Association (Sassari) and the Chambre de Métiers et de l’Artisanat de la Corse du Sud (Ajaccio). The latter is supported, in France, by the Chambre de Métiers et de l’Artisanat des Alpes Maritimes (Nice) and, for scientific issues, by the IUT.

The project aims to identify and bring together public and private actors (mainly small and medium enterprises) in three sectors (renewable energy, sustainable tourism and biotechnology) through the consultation of stakeholders and the organisation of workshops, focus groups, training and coaching actions for the companies situated in the regions involved (Liguria, Tuscany, Sardinia, Corsica and Provence Alpes Côte d’Azur – the PACA Region). Thus, the new business networks may share know-how, optimise their management, manufacturing and commercial systems and, above all, compete for new funding under the Maritime Programme to develop innovative projects in relation to the identified sectors.

With regard to renewable energy, the collaboration between the research groups of the DSA and the IUT has been decisive and the workshops and the training activities, carried out together, have raised interesting new opportunities for exchanging experiences. Sharing their research outputs, the two groups have identified common interests and the need to develop new building products and design tools, well suited to the local climate, the available resources, the construction methods and user habits in the Mediterranean region. Starting with the Me.R project, the DSA and the IUT are currently working together in this direction, involving organisations and enterprises in innovative projects which take into account recent studies on the implementation of new applications and businesses. The new projects concern the enhancement of passive solar and solar thermal systems, with particular attention paid to their operation and performance and their architectural integration.

2 Studies of Active and Passive Solar Systems in the Mediterranean Region

The use of passive solar systems should be of great interest in both new constructions and retrofitting interventions, especially in relation to the enormous number of post-war period buildings in city suburbs, usually characterised by severe functional and aesthetic disrepair and by high energy demand. In this regard, the DSA has carried out a long campaign of monitoring passive solar systems (in particular, solar greenhouses and Trombe–Michel walls), applied to retrofitted buildings, built around the 1960s in Savona (Liguria) and owned by ARTE, the Regional Territorial

Agency for Building. These buildings, made of reinforced concrete structures cast in situ and double-layer brick walls with no insulation, were retrofitted with the following main interventions on the building envelope: thermal cladding on the *façades*, insufflations of thermal-acoustic cellulose flake insulation in the wall cavities, insulation and waterproofing of the roof and installation of passive solar systems on the southern *façades*.

A winter monitoring campaign (4 December 2013 to 27 January 2014) has, in particular, evaluated the thermal benefits obtained with the solar greenhouse and Trombe–Michel wall systems for the relevant dwellings, while the aim of the summer monitoring campaign was to understand the conditions which could generate overheating in the rooms connected to the passive solar systems and which could provide comfort. The studies also consider several different uses and recognise possible interference deriving from the behaviour of the users in the normal working operations of this technology.

The analysis method used to achieve the aforementioned goals is based on the criteria explained in what follows:

- The reliability and significance of the temperature parameter for a first evaluation of the indoor comfort of the buildings and to illustrate the thermal exchange phenomenon between passive solar systems and the relative space heated by them.
- The necessity of carrying out non-invasive studies which might have caused inconvenience for users and too much expense for the client (ARTE); in this sense, the possibility of installing heat meters near the existing independent heating systems of the concerned building units has been excluded. The fortunate circumstance of having empty lodgings available in one of the tested buildings has allowed the estimation of the real thermal contribution of the solar systems by turning off the heating for the whole survey period (in winter) and obtaining reliable results.
- The integration of various types of instruments: an infrared thermo-graphic camera, eight mini data loggers and a thermo-anemometer.

Two lodgings are directly involved in the tests, denominated A1 and A2 of building A and an interior room, called B1, of building B (Fig. 57.1). All have one south-facing exposed wall where passive solar systems were installed: one greenhouse for lodgings A1 and A2 and two Trombe–Michel walls for B1. Lodging A1 is on the first floor and A2 is on the second; they were chosen because they were empty during the monitoring period. Lodging B2 was occupied; however, the tenant, having understood the purpose of the study, diligently supplied precise time periods in which the heating system was in use.

First, thermo-graphic surveys were conducted inside and outside and primarily highlighted the effectiveness of the insulation solutions of the thermal coat used for the requalification of the buildings under analysis and the decrease in the ‘thermal bridges’ phenomenon in correspondence with the structures in reinforced concrete. These data are obviously important for the evaluation of the performance of passive solar systems; in fact, the application of this type of system in poorly insulated



Fig. 57.1 Building B, one of the monitored buildings, after retrofitting: *left*: Trombe–Michel walls; *right*: solar glasshouses

buildings can be considered of little use because the heat gathered by the collectors is then dispersed in a short time.

During the monitoring campaign, the mini data loggers were placed in the following positions:

- Outside, in the shade, in order to verify the outside temperature at the site (other climatic data were available from the Savona station of the Regional Weather Observatory)
- Inside the passive solar systems (not exposed to direct solar radiations)
- Inside the rooms which were directly connected to the first through adjustable air vents and, in the case of the greenhouse, also by a French window
- In a cellar exposed to the south in building A; the space was not heated or equipped with thermal insulation or, obviously, with passive solar systems

Practically, the situation that emerged, in relation to the course of interior temperatures during the monitored months, is very similar to that which would have been recorded in the premises facing south of the apartments of the same building if the requalification operations had not been completed. This mini data logger was, therefore, used to provide comparison data to appreciate the effect of passive solar systems on heated buildings.

During the winter monitoring campaign, the solar glasshouse and the Trombe–Michel wall systems were set so as to maximise their thermal contribution during the day. In particular, the glasshouses were never shielded by the exterior sun

screen curtains during the whole winter period and their air vents were left open, with some adjustments during the survey; the Tromb -Michel wall had fixed solar shading and its air vents were left open during the survey. The readings of the obtained data have led to several interesting results:

- The passive solar systems demonstrate their efficiency in energy retrofits of existing buildings (if these buildings are adequately thermally insulated). In particular, the use of passive solar systems can take on the heating of the buildings in the Mediterranean climate without harsh winters. In the case study, during the test period which corresponds to the coldest season of the year, even if the recorded temperatures were not particularly rigid and the minimum was 2  C, the passive solar systems applied to the studied buildings demonstrated that they could guarantee comfort range temperatures inside the buildings on sunny days and temperatures which are significantly higher than the external temperature, even on cold and cloudy days. A general trend of rather balanced internal temperatures was recorded, without particular peaks during daylight or drops during the night. For the whole period considered, without the aid of any heating system, lodging A1 (taken as the reference here because the heating system was never turned on) maintained temperatures between 13.3 and 22.40  C (see an example of temperature trend on a significant winter day in Fig. 57.2). This implies that these applied solutions are effectively in a position to guarantee a great decrease in energy consumption for the artificial heating of lodgings.

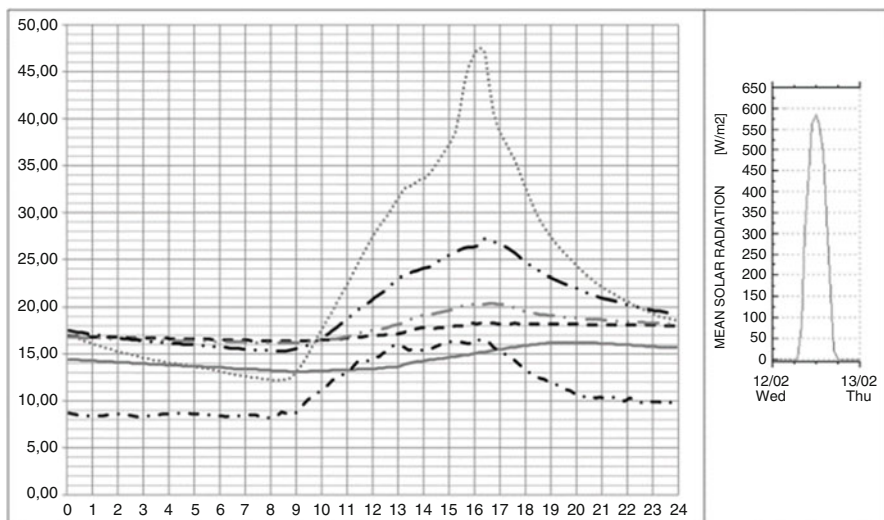


Fig. 57.2 Example diagram showing temperatures recorded by mini data loggers in building A with solar greenhouse on 12 February 2014 (*continuous grey line*: room without passive solar systems; *dash-dot black line*: outside temperature; *dotted grey line*: temperature inside glasshouse; *broken black line*: temperature inside room heated by solar glasshouse; *dash-dot grey line*: temperature inside room heated by solar greenhouse in a semi-direct way; *dash-dot black line*: temperature inside room heated by solar greenhouse in a direct way)

- For an insulated, standard-height room in the Mediterranean climate, to obtain an appreciable convective exchange between the solar greenhouse and the interior of the concerned premises, with a relationship between greenhouse and heated premises volumes of approximately one to two (and a not particularly wide greenhouse able, therefore, to take advantage of the convective motions), a relationship at least higher than 0.4–0.5 % is necessary between the total net area of the wall valves and the air of the separation wall between greenhouse and interior premises. Furthermore, to compensate for the relatively small dimension of the valves, it is useful to leave any windows open during the midday hours (from 10 a.m. to 7 p.m.) on sunny days.

During the summer campaign, we carried out the measurements in lodgings A1 and B1 again. Lodging B1 was occupied by a tenant: this was a limitation, because the indoor thermal conditions were influenced by the tenant's habits. In addition, we could not test extreme situations, which might cause overheating.

The studies of lodging A1, without any tenants, were more interesting. We carried out various measurements with six mini data loggers. We set curtains, wall valves, doors and windows according to different 'layouts' in order to test different situations: overheating, solar shading and reduction, or increase, in air exchanges outside-inside. The results show the different operations of the 'building-solar collector' system.

To reduce the overheating, it was useful to shade and open the windows of the solar collector; moreover, it was also very useful to isolate the greenhouse from the rest of the apartment through the closure devices of the wall valves, even if they reduced airflow. On sunny days, tenants should close the French window and the wall valves that connect the rooms with the greenhouse.

When the windows of the greenhouse are closed and the sunshades are retracted, the maximum temperatures recorded inside the greenhouse were unexpectedly lower than in winter (over 10 °C). In winter, the major sunbeam angle is lower than in summer, so the sunbeams enter more easily below the greenhouse slab and warm the collector for longer. Finally, the summer tests showed that careful management by users could avoid overheating problems.

Starting from the studies conducted in Savona, an interesting degree thesis was carried out (authors: Nicoletta Paladino, Chiara Truffelli, Gio Batta Venturino; tutors: Andrea Giachetta and Chiara Piccardo). As part of this work, additional monitoring campaigns were conducted in Italy on different house types, in weather conditions different from those in Liguria. The studies conducted in the winter season in La Thuile (Aosta) on a single-family detached home, with a two-storey solar greenhouse, have shown the effectiveness of the passive solar system at much lower external temperatures than those recorded in Savona.

Based on the data recorded in Savona and in the other monitoring campaigns, additional studies were carried out to verify whether the most common thermodynamic/energy simulation software for the building design provided similar results. Therefore, the monitored buildings and their solar greenhouses were modelled with the software, setting up their real climatic conditions. We did not expect, of course,

that the simulation outputs would coincide perfectly with the recorded data, but the simulations provided very different results, significantly underestimating the performance of passive solar systems. This also happens because the software is unable to simulate the exchange of heat by convection (normally the most significant exchange in passive solar systems). Some software packages (e.g. Energy Plus) may provide more rigorous simulations, obtaining more realistic data, but their use requires time and specific expertise, which is incompatible with the average design process, especially in the case of buildings of modest size.

Although passive solar systems, when tested, show great potential, the lack of effective simulation software for designers (due to a lack of data, studies and the difficulty in controlling and modelling microclimatic changes) has probably contributed to their limited take-up. For this reason, two possible areas could be investigated in the future: the creation of a new database able to lead to more reliable simulation systems or the design of a new versatile window, adaptive to changing microclimate conditions.

3 Studies of the Architectural Integration of Active and Passive Solar Systems

In this regard, the investigations carried out by the University of Corsica provided some interesting outcomes, such as prototypes of shutters with integrated passive and active solar systems for interior (room-side) convective heat transfer.

The concept of a solar air shutter [3], which is patented and called *volet'air*, produces a low-temperature heat directly from the sun without any other energy supply. The objective is to meet some of the hot air needs for maintaining a healthy ambience in a house. It can be used in the following settings:

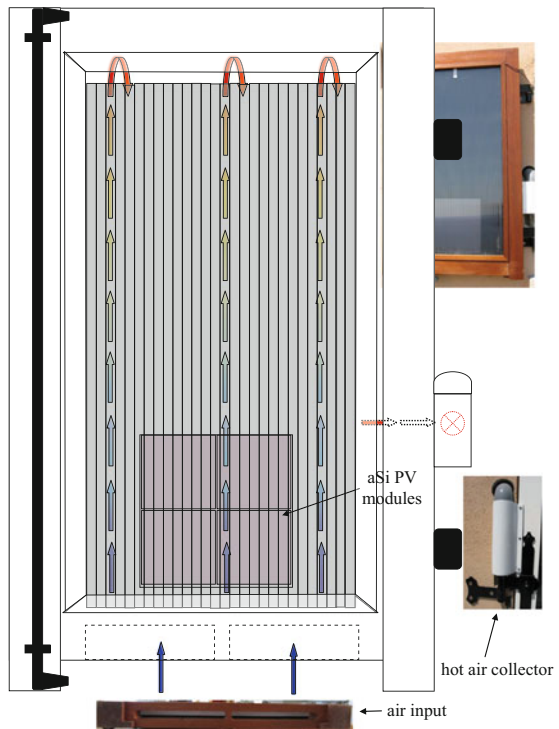
- In a principal residence occupied year round;
- In a secondary residence, which is often unoccupied for long periods throughout the year and for which the thermal balance and ventilation are provided by natural energy exchanges from outdoors to indoors;
- Isolated houses which are not connected to the electrical grid.

The same fluid is used for both ventilation and heat supply. The solar air shutter has the same features as a conventional shutter (Fig. 57.3). The internal area is used as a heat converter, and the frame can be built using various materials (wood, aluminium and PVC). The heat converter is composed of two glazing panels in multi-wall polycarbonate (10 mm depth sheets in twin wall form), specially conceived for outdoor utilisation. The outdoor face is transparent and used as a cover and the indoor face is covered by a black thermal painting and is used as an absorber. a-Si PV modules are integrated in the lower part of the black face and are used to supply the air fan. The shutter runs opened, closed and in intermediate positions thanks to its symmetrical conception. The air enters between two plates

Fig. 57.3 Solar air shutter
volet'air

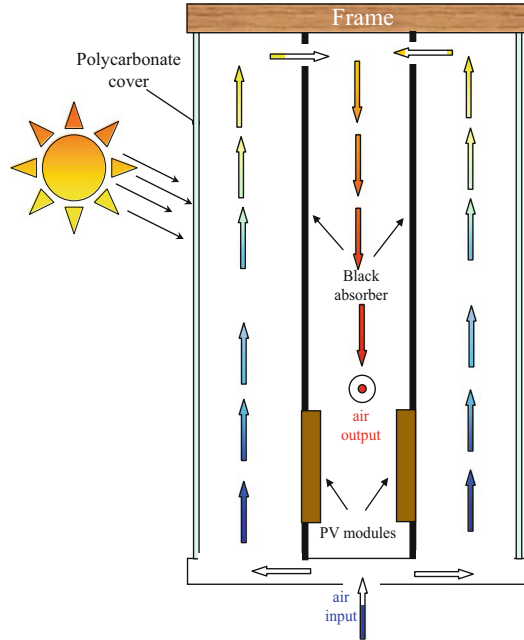


Fig. 57.4 Solar air shutter
volet'air



through two openings under the shutter frame and, having been divided into two parts, runs into the channels to the top, then continues between the two black plates (one of each of the multi-wall polycarbonate glazing panels) when it mixes with the air coming from the other side. Finally, this heated air exits by a collector located on the internal part of the frame where the hinges of the shutter are situated (Fig. 57.4). The air fan is located in the wall of the housing (Fig. 57.5).

Fig. 57.5 Solar air shutter volet'air



Unlike conventional solar collectors, this collector does not use thermal insulation, and this makes it thermally original, inducing a special thermal modelling and energy performance. The more the fluid is heated, the more of it which enters the shutter, which limits the conductive and convective losses with the outdoors, thereby creating a kind of thermal dynamic insulation.

This new concept of solar air collector has the following advantages:

- A new active function is added to the shutter.
- It can produce heat in all positions: open, closed or intermediate.
- The vertical inclination allows it to produce more energy during winter and less during summer.
- It can be sized and produced for all window sizes because each part is made to measure and can be replaced independently when its lifetime limit is reached.
- It can be very easily installed in existing and new houses: the air is introduced into the house by a rotating air collector without costly and bulky air distribution systems.
- The conventional functions of the shutter – sound and thermal insulation and mechanical resistance – are retained.
- It is an autonomous heater because the fan is supplied by the photovoltaic modules and it can be used in remote areas.
- It must be easily removed because the shutter should be cleaned so as to preserve clean air.

The patented solar water collector, H2OSS [4, 5], presents a high degree of building integration with no visual impact from the ground because it is inserted



Fig. 57.6 Patented solar collector H2OSS

into a drainpipe (Fig. 57.6), which maintains the rainwater evacuation role of the drainpipe. It can be used on east-, west- and south-facing walls (the collector being oriented south into the drainpipe). A north-facing wall is excluded owing to important shading effects. The canalisations connecting the house to the heating collector are hidden in the vertical drainpipe. An installation consists of several connected modules. One module is approximately 1 m long and 0.1 m wide (individual houses), and larger modules can be developed for larger buildings. The number of modules depends on the drainpipe length [6]. The structure of the H2OSS solar collector is composed of a glass layer, an air layer, a highly selective absorber and an insulation layer. The cold fluid flows from the tank through the insulated tube and then into the upper tube in thermal contact with the absorber. These systems have also been tested on historical buildings in the research mentioned earlier, the ‘Case Mediterranee’ Maritime European project in connection with refurbishment.

Figure 57.7 shows a historical building composed of four small apartments situated in a Corsican village near the centre of the island. Two integrated solar domestic hot water systems are installed in these apartments. One is integrated into a metal porch roof and one into the gutters. The area of the gutter solar collector and part of the area of the solar metal porch roof are connected to one tank for two apartments (rural tourism houses with a collection area of 1.80 m²). The other part of the solar metal porch roof is connected to another tank for the other apartments (a church rectory with a collection area of 2.02 m², tilted 43°). These apartments are used for different purposes: two of them are for tourists, booked for half the year, while the others are used year round.

An effective application of solar building systems to buildings with historical and architectural value is very important in geographical areas with a rich architectural heritage. Some relevant studies have been conducted within the European project SCORE, which stands for Sustainable Construction in Rural and Fragile Areas for Energy Efficiency (www.scoremed.eu), within the framework of the



Fig. 57.7 Historical building with integrated solar systems

MED Programme (2007–2013). The province of Savona was the lead partner and coordinated 10 partners from 7 different countries: Cyprus, France, Greece, Italy, Portugal, Slovenia and Spain. The DSA has supported the province of Savona as a subcontractor.

The SCORE project aims to promote a sustainable approach to planning and to enhance urban and building requalification, showing how this approach harmonises with the high-quality landscapes of the MED areas. It may also represent an opportunity to reinforce a specific identity of the Mediterranean region, in both coastal and rural areas. These areas are of great interest for their history, culture, landscape and nature, but they are also extremely fragile if we consider the possible impact of human activities and the creation of infrastructures and residential, touristic and production sites, as well as the impact of ports and agricultural activities. Thanks to the SCORE project, the partners have exchanged information about their national policies, regulatory framework and best practices in relation to the common sustainable strategies which aim to produce energy from renewable sources, reduce polluting emissions and protect the environment and health of the population, while dealing with the issue of the architectural integration of technologies and systems. Finally, SCORE records, selects, organises and spreads knowledge about good practices.

The project is intended not only to call attention to well-known sustainable strategies for building design and construction but also to assess the best methods for effective implementation of the aforementioned strategies, with reference to the local regulatory and industry framework (taking into account the need for continuous training of operators and enterprises) and to the building tradition. The exchange between Italian and French experiences, especially between regions

with similar climates, such as Liguria and Corsica, can enhance solar building strategies, in accordance with the new European energy standards as well as with the Mediterranean climate, traditional construction technologies and user needs.

A new regionalism seems to be a promising approach to sustainable architecture. This is important in order to provide effective solutions taking into account the local climate, the building tradition and user habits. This is not a naive regionalism which responds to local issues by adopting the vernacular style of the area; this approach avoids the uncritical acceptance of systems, technologies, products and standards developed in regions with too different climates and resources. Applied research conducted under the aegis of cross-border partnerships, such as those supported by the project Me.R, may be an interesting way to increase local awareness of resources and their sustainable use.

References

1. Krainer A (2008) Passivhaus contra bioclimatic design. *Bauphysik* 30:393–404. doi:[10.1002/bapi.200810051](https://doi.org/10.1002/bapi.200810051)
2. Sassi P (2013) A natural ventilation alternative to the passivhaus standard for a mild maritime climate. *Buildings* 3(1):61–78. doi:[10.3390/buildings3010061](https://doi.org/10.3390/buildings3010061), Directory of Open Access Journals (DOAJ)
3. Canaletti JL, Cristofari C, Notton G (2013) Modelling of the ventilation unit for a stand alone solar collector. *Appl Mech Mater* 330:687–692 (Hindex: 7)
4. Cristofari C (2006) Device for collecting rainwater and solar energy originating from light radiation. Patent n° WO 2006/100395 A1: 28/09/2006
5. Cristofari C, Norvaisien R, Canaletti JL, Notton G (2015) Innovative alternative solar thermal solutions for housing in conservation-area sites listed as national heritage assets. *Energy Build* 89:123–131 (Elsevier IF5 ans: 3.016)
6. Motte F, Notton G, Cristofari C, Canaletti JL (2013) Design and modelling of a new patented thermal solar collector with high building integration. *Appl Energy* 102:631–639 (IF2011: 5,106; IF5 ans: 4,456, Hindex 45)
7. www.mediterraneoinrete.eu
8. www.scoremed.eu

Chapter 58

Spectral Variation of Energy-Efficient Room Lighting

Helmut F.O. Müller

Abstract This research concentrates on advanced lighting systems with increased energy efficiency and improved color effects in relation to human-centric lighting (HCL). HCL includes the visual aspects of color perception like color temperature of light, color rendering, and, last but not least, the aesthetic image of room illumination. In addition, nonvisual effects on the circadian biorhythm, for example, influencing the melatonin hormone level, must be taken into account. Light-emitting diodes (LEDs) have the potential to meet the aforementioned demands of energy efficiency and spectral adaptation if innovative solutions (in contrast to retrofit solutions) are applied. Lighting principles and innovative luminaires are developed for typical office rooms, which allow for variable color temperatures (tunable white) and illuminances, high color rendering indices, decorative and harmonic color compositions, and circadian lighting. Various situations of room illumination are visualized. A prototype luminaire is demonstrated, and characteristics of lighting performance and energy efficiency are given.

Keywords LED lighting • Tunable white • Color image • Circadian effect • Luminaire • Room illumination

1 Introduction

The development of blue Light-emitting diodes (LEDs) with a yellow luminescent substance enabled efficient white lighting systems for indoor and outdoor application. Since 2006 the color quality could be improved by advanced phosphor systems, for example, in the green and red spectral range, allowing color temperatures from warm (2500 K) to daylight white (7000 K) and high color rendering indices (CRIs). The technological development of LED increased the luminous efficacy, now reaching values of 140–150 lm/W in practical applications. But the peak values of different characteristics cannot be combined in one type of LED: The CRI of highly energy-efficient LEDs ranges between 65 and 75, for example,

H.F.O. Müller (✉)

Green Building R&D GmbH, Oberkasseler Str. 6, Düsseldorf D-40545, Germany
e-mail: helmut.mueller@greenbuilding-rd.com

while LEDs with a high CRI ≥ 92 have a luminous efficacy of 85–97 lm/W [1]. Future developments will improve the quality of LEDs in terms of luminous efficacy, color fidelity, and additional visual and nonvisual performances.

New and comprehensive lighting characteristics are developed in addition to the photometric, $V(\lambda)$ -based ones, since LEDs offer a great variety of spectral performances. Especially color quality and nonvisual components are included, focusing on the evaluation of human centric lighting (HCL). Visual aspects of color perception include color temperature of light, color fidelity or rendering (CRI), and, last but not least, color harmony and aesthetic perception of room illumination. In addition, nonvisual effects on the circadian biorhythm, influencing the melatonin hormone level, must be taken into account; it is affected by vertical illumination (on the retina), color temperature, and spatial distribution of luminance. New areas of research are emerging [2], and DIN SPEC 67600 (2013) [3] gives the first design hints for meeting the requirements of biologically effective lighting and HCL.

1.1 Circadian Lighting

The human circadian rhythm shows a 24 h cycle of activity in terms of readiness to work, as can be seen in Fig. 58.1. It is partly influenced by photosensitive ganglion cells in the lower retinal area, which regulate, via the superchiasmatic nucleus, hormone (melatonin) release [4]. Low nighttime activity coincides with high melatonin concentration. But it is possible to suppress melatonin and increase work performance at night (e.g., for shift work) using light in the appropriate way, that is, spectral distribution with a peak in the blue (460 nm), color temperature approximately 8000 K, main direction from front above, and vertical illuminance on the retina ≥ 250 lx. In the daytime melatonin is suppressed and is influenced more by daylight (if available) than by artificial light [1], except in the transition periods of morning and evening.

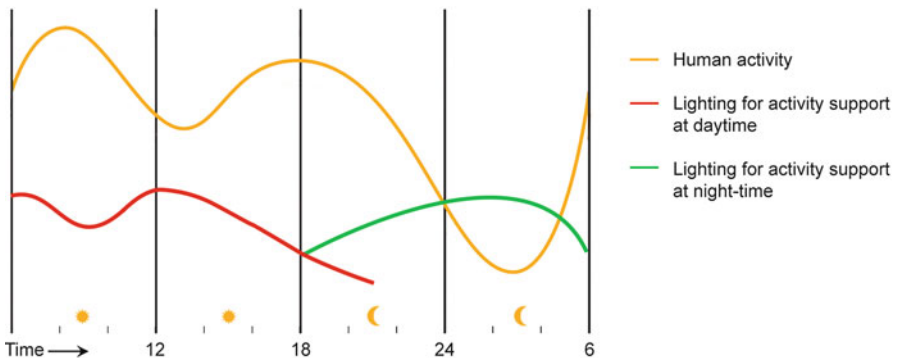


Fig. 58.1 Human activity (readiness to work) in the 24 h cycle [1] and examples of lighting for activity support

Depending on the kind of activity and room occupation (e.g., night-shift work, dwellings, old peoples' homes, schools, offices) dynamic lighting strategies with varying color temperature and illuminance are recommended for the 24 h cycle. Daylighting often is used as a reference for the control of artificial light. The range of characteristics is

- Color temperature: 3300–8000 K;
- Vertical illuminance: 250–1500 lx.

For the spatial distribution of light, large areas with high luminance in the upper visual field are recommended for melanoptical lighting [3]:

- Large area luminaires or luminous ceilings;
- Luminaires with indirect illumination of ceilings and upper wall areas;
- Translucent materials in ceilings or upper wall areas illuminated from behind.

1.2 *Quality of Color Perception*

In conjunction with LED and its spectral variations, increased attention was attracted by various color properties of lighting. Besides color fidelity or rendering, research focused on additional characteristics [2] such as the following:

- Color gamut in relation to color saturation and discrimination;
- Lightness of chromatic objects;
- Color preference and color memory in relation to rooms, objects, or skin, partly in relation to cultural identity;
- Color harmony, especially for combinations of two or more colors.

The CRI, which describes the numerically defined color differences for a set of test color samples under a test and reference light source, is defined in CIE 13.3 (1995) [5] by a set of eight test colors, which can be extended by an additional set of six and additional individual colors. An alternative method for defining CRI is described in CRI2012 [6].

An improvement in CRI can correlate with a significant improvement in other color properties, as shown by experimental development of LED [1].

Concluding the introduction, it can be stated that spectral properties of LED lighting are a main issue in research and development (R&D). The main objectives are to improve the color quality and biological effects of lighting without reducing energy efficiency. Additionally, HCL systems need a dynamic control in terms of illuminance and color temperature over the 24 h cycle. Beyond these requirements, which refer to white light, colorful light effects are an option LED lighting can offer.

2 Methodology and Results

To develop solutions for the required lighting with variable spectral properties, the following approach was taken:

- Literature survey for LED luminaires with spectral variety;
- Design of LED luminaires;
- Architectural integration, lighting design, and simulation;
- Luminaire prototyping;
- Modeling of color harmony.

2.1 LED Luminaires with Spectral Variety

A literature survey revealed that Khan et al. [1, 7] have developed concepts for optimizing LED lighting by hybrid LED luminaires. They used the following principles for their development of white LED lighting with variable color temperatures:

- By mixing the light of a warm white LED (e.g., 2700 K) and a cold white LED (e.g., 6500 K) any color temperature between the two values can be obtained. For this solution it must be accepted that the chromaticity coordinate of the mixed light will not always be on the Planckian locus for white light, that is, the light can have a color fault.
- Better results could be achieved by applying concepts of hybrid-LED luminaires, which consist of one warm white and five color LEDs. CRIs are greater than 90 for CIE–CRI and many additional colors that can occur in museums or shops. Color temperature can be varied from 2700 to 6500 K, and the luminous efficacy can reach values between 90 and 100 lm/W. Specific spectra of the hybrid-LED luminaires must be selected in relation to the lighting task, like in a museum, shop, or office, for example.

2.2 Design of LED Luminaires and Architectural Integration

In this study the task focused on office lighting and was based on developments of transparent LED luminaires with edge-lit light conductors and microstructures [8, 9]. Strips with red, green, blue, and white (RGBW) LED, which are available on the market, are fixed at the edge of a transparent glass pane. The microstructure emits light at a defined angle (approximately 40°) from one surface only. These luminaires, mounted in the upper areas of windows or partitions, can be used for direct lighting of task areas or for indirect lighting of ceilings (Fig. 58.2).



Fig. 58.2 Lighting of an office room. General lighting by transparent LED luminaires integrated into upper area of windows and partitions, light directed toward reflecting ceiling. Task lighting by transparent LED floor lamps. *Left*: Morning; vertical illuminance 1000 lx, daylight white (6000 K). *Right*: Evening; vertical illuminance 300 lx, warm white color temperature (3000 K)

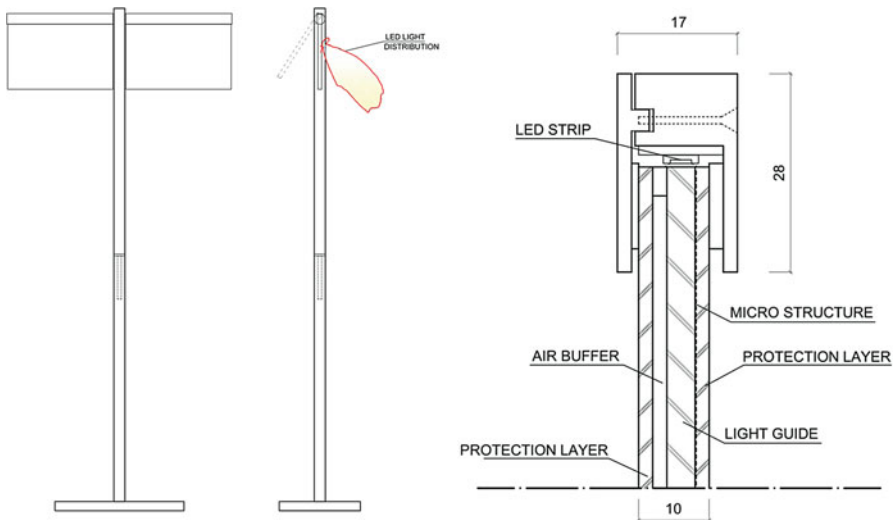


Fig. 58.3 Floor lamp for task lighting. *Left*: Elevation. *Right*: Detail with metal frame, LED strip, and encapsulated light guide

According to the recommendations of DIN SPEC 67600 [3], an indirect illumination of the ceiling was chosen with an adaptation of illuminance and color temperature to the circadian requirements (daylight white in the morning, warm white in the evening). The light simulations were done using the RELUX program.

In addition to general room lighting, a floor lamp was designed for task lighting. Such a light does not constrict one's view because it is transparent and has two lighting elements, which are controlled separately and can be adjusted by rotation in different directions. The RGBW LEDs allow for dynamic variation of illuminance and color temperature as well as chromatic light effects, which can be controlled separately for each lighting element (Fig. 58.3).

2.3 *Luminaire Prototyping*

A prototype of a floor luminaire was developed and designed by Green Building R&D GmbH (Düsseldorf, Germany) and built in cooperation with professional partners. Temicon GmbH (Dortmund, Germany) produced (by UV-embossing technology) samples of the light guide (4 mm PMMA pane) with a microstructure of cylinders (40 μm) on one surface. The LED light is coupled from one edge to the guide [8]. The geometry and distribution of the micro cylinders emit light evenly in one passage through the light guide. Remainders of light reaching the other edges are reflected by metallic layers. To avoid unwanted light emissions by surface interference, the light guide is encapsulated from both sides (Fig. 58.3). An alternative solution with a transparent light guide by Evonic AG (Essen, Germany) emitting light from both surfaces was tested as well (Figs. 58.4 and 58.5). The prototype luminaire was manufactured in cooperation with Patrick Kersten Lichtwerkstatt and Mailänder Lichtdesign (Cologne, Germany).

The characteristics given in Table 58.1 show that the luminous efficacy is high for the W LED and can still be optimized for the RGB LED. The first images of a demonstration and test programme are given in Fig. 58.4.



Fig. 58.4 Prototype of floor luminaire for task lighting with variable flux and color temperature of white light as well as chromatic effect lighting

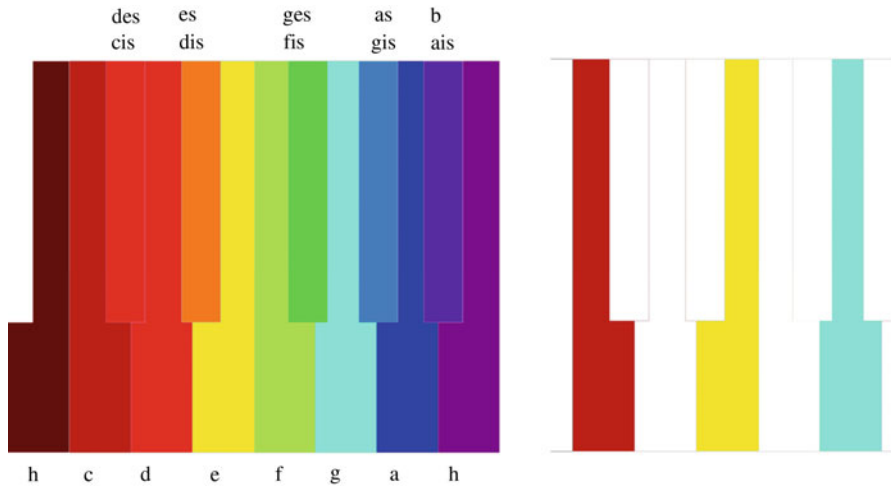


Fig. 58.5 Color effects derived from musical scale. *Left:* Photo of prototype luminaire. *Right:* Simulation of living room with floor luminaires

Table 58.1 Characteristics of prototype luminaire

Luminous flux, max. (two elements 286 × 177 mm)	lm	W	384
		RGB	576
		RGBW	960
Luminous efficacy	lm/W	W	123
		RGB	62
		RGBW	77
Color temperature	K	2800–7000	
Color rendering index (R_a)		70–90	

2.4 Modeling of Color Harmony

Advertisements for RGBW LED sometimes take advantage of the attribute that more than 100 million colors can be generated. But how does one select specific colors of preference from these numerous options? And are there systems of harmony for the combination of colors that can be applied for the individual or general control of colors by LED lighting? LiTG (2015) [10] states that it is very difficult to find an objective and general definition of color harmony, because it depends on many factors like geometry, size, texture, and number and position of colors in space, and this divides the existing studies [11, 12] into two categories:

1. Harmony is generated by colors that are selected systematically from a color circle and presented in rising or falling sequence (according to hue, lightness, and chroma);



Fig. 58.6 *Left:* Piano keyboard with spectral colors defined by octave of visible wavelengths from 390 to 780 nm. *Right:* Example of chromatic harmonies; triad c-e-g

2. Harmony is generated by interrelations of single colors if hue, lightness, or chroma are similar or opposed respectively complementary.

A different system for modeling color harmony is discussed here; it is based on the harmony of the gamut or chromatic scale in music. The relation of color and music has been noted mentioned repeatedly throughout history, for example, by Isaac Newton, who in 1704 proposed in his publication *Opticks* a color circle with seven hues (red, orange, yellow, green, blue, indigo, violet) corresponding to the seven notes of the musical scale. Helmholtz compared wavelengths of color and musical pitch in 1860, and several artists assumed that harmonic color relations had a musical basis. De Maistre, for example, developed a color harmonizing chart.

One octave is defined by doubling the wavelength of the first note. As the visible spectrum of light ranges over an octave at least (360–830 nm, with the limit values fluctuating individually), the musical scale can be transferred and each full or half note be defined by a spectral color. The multiplier for the distance between two half notes equals $^{12}\sqrt{2}$. An example of the resulting 12 spectral colors representing the half notes of an octave is shown by the piano keyboard in Fig. 58.6. Depending on the limits of the visible spectrum, the octave can be shifted slightly, for example, from 380–760 to 390–780 nm, resulting in different colors. As in the musical system, the standard pitch is arbitrary (a^1 in USA 440 Hz, in Austria and Germany 442 Hz, in Switzerland 443 Hz).

The hypothesis that combinations of spectral colors derived from chords of the chromatic scale are perceived harmonically must be investigated by acceptance tests. An example using a combination of three colors transferred from the musical triad c-e-g is shown in Fig. 58.6.

3 Conclusions

Hybrid LED luminaires, for example, with a RGBW LED, offer new options for spectral variety in lighting. Color temperature can be varied from warm to cool white, high CRIs are attained, and a nearly endless variety of color effects is possible through the control of hue, lightness, and chroma. This allows new solutions for lighting design and architecture, for example, edge-lit light guides with microstructures for directional light emission integrated into transparent building components. The applicability of spectral variety for HCL will be supported by validated models for the harmony of color combinations. Luminous efficacy need not be reduced in favor of increased color quality, as values greater than 100 lm/W are feasible using new technical developments.

References

1. Khanh TQ, Bodrogi P, Vinh QT, Winkler H (2015) LED lighting, technology and perception. Wiley, Weinheim
2. LiTG Deutsche Lichttechnische Gesellschaft e.V (2015) Farbqualität: Definition und Anwendungen, Berlin, info@litg.de
3. DIN SPEC 67600 (2013) Biologically effective illumination—design guidelines. Beuth, Berlin
4. Rae MS, Figuera MG, Biermann A, Bullough JD (2010) Circadian light. *J Circadian Rhythms* 8(2):1–10
5. CIE 13.3 (1995) Method of measuring and specifying colour rendering properties of light sources. CIE Central-Bureau, Paris. CIE Publ. 13.2 (2nd edn. corrected reprint), 1974
6. Smet KAG, Schanda J, Whitehead L, Luo MR (2013) CRI2012: a proposal for updating the CIE color rendering index. *Light Res Technol* 45:689–709
7. Khanh TQ, Trinh VQ (2015) LED-systeme mit variablen Spektren. *Licht 1-2/2015*: 72–78
8. Mueller HFO, Sasso F (2014) Energy-efficient lighting by LED. In: Proceedings of WREC XIII, Kingston, 3–8 Aug 2014
9. Tengler F-C, Jakubowski M, Neyer A (2013) High transparent light guiding plate for single-sided light emission. Poster Abstract, (Micro and Nano Engineering) MNE 2013, London
10. Deutsche Lichttechnische Gesellschaft e.V., LiTG (2015) Farbqualität: definition und Anwendungen, Berlin, March 2015
11. Ou L, Chong P, Lou MR, Minchew C (2011) Additivity of colour harmony. *Color Res Appl* 36 (5):355–372
12. Szabo F, Bodrogi P, Schanda J (2010) Experimental modeling of color harmony. *Color Res Appl* 35(1):34–48

Chapter 59

The Housing Retrofit Market in Italy: Constraints and Barriers to Development

Riccardo Pollo

Abstract The construction sector holds great importance for the reduction of energy consumption and for the achievement of goals related to environmental sustainability as stated by European policies. The national energy plan assigns to this sector an important role in curtailing energy consumption. The objectives of the Italian Plan for Energy Efficiency (PAEE) have been surpassed with interventions by owner-occupiers that generate high savings at the same cost, as in the case of the replacement of traditional boilers with condensing boilers and replacement. Many window replacements have been made, with relatively low energy savings but with a quite high amelioration of building maintenance levels. These interventions have been pushed mainly by a favourable policy of tax relief. More difficult is the further achievement of savings through interventions that are more complex and expensive, to be carried out on aged building stock and with a high rate of owner-occupiers. Innovation related to eco-construction is driven by legislation with strict criteria in terms of energy performance. The sector has thus connected a traditional approach to innovation. At the same time the industry has seen the emergence of actors that link supply and demand [designers of system components and building materials, energy service companies (ESCO)]. This chapter examines case studies focusing on the critical issues that have hindered the success of the building retrofit market. The role of construction companies, especially craftsmen, and designers is highlighted and identified as being central in the development of building retrofitting in Italy in terms of both their technical expertise and their closeness to customers.

Keywords Retrofit • Non technical barriers

R. Pollo (✉)

Department of Architecture and Design—DAD, Politecnico di Torino,
Viale Mattioli 39, Torino 10125, Italy
e-mail: riccardo.pollo@polito.it

1 Introduction

As a report published by the Italian Plan for Energy Efficiency states, Italy has reached the intermediate target for reduction in energy consumption and emissions by the 20-20-20 European policy [1].

Nevertheless the building retrofit market in Italy has been characterised mainly by relatively small interventions funded by owner-occupiers and carried out by small firms. The income tax benefit for inhabitants, introduced by law in 2007, was the main factor pushing such interventions. Although for the most part such work has been carried out by residents, private companies also had benefits from these tax incentives.

The main consequences of such a trend are as follows:

- Nationwide significant energy savings;
- Growth in construction sector, mainly among small firms;
- Incentive to innovate for material and component producers, mainly manufacturers of windows, heat generators and insulation materials;
- Reduction in tax fraud by small construction firms.

The mean amount of single retrofit work in 2011 was valued at around €11.700. Most interventions were window replacements and heat generator improvements. Italian tax law includes tax exemptions for work done to reduce heat transfer in parts of building envelopes (roofs as well as external walls). Moreover, the enhancement of a building's energy performance on the whole provides significant tax benefits. Nevertheless, these more complex retrofit interventions were few in number.

In addition to the mechanism of tax benefits, other means can be used to support the housing retrofit market [5]. In particular:

- Capital grants,
- Operating grants,
- Grants or interest rate subsidies,
- Guarantee funds,
- Programs of technical assistance,
- Information activities,
- Local government regulations.

The latter have been particularly developed in many local communities in the form of information service on energy retrofitting and local building rules on energy conservation and retrofitting.

Capital grants are the simplest tools but have limited effectiveness in terms of both the low leverage on other funds and the lost incentive to improve plant management. Also, they do not encourage a good design of interventions, focusing rather on the speed of the presentation of proposals. These actions may be useful when you need to focus on the use of certain technologies, but there is uncertainty with respect to incentives.

Operating grants are related to savings actually achieved in the years following the intervention. The complexities, however, are represented by the difficulty of obtaining reliable parameters to assess the benefits. Constant parameters facilitate the provision of funding, but the risk/reward ratio excessively favors beneficiaries.

The guarantee funds are an important tool for obtaining credit in periods of credit tightening; this requires, however, a sound evaluation of the capacity of the applicant to pay back loans and of the actual proposal. They are suitable under limited technical risk. The most innovative solutions require other tools for experimentation. The use of guarantee funds has been suggested in the case of interventions with relatively long response times as district heating networks or programmes of widespread distributed generation (district heating). Moreover, guarantee funds have the advantage of being revolving. In this way as the loans are repaid, funding can be made available for new loans.

One of the difficulties reported by lenders is to finance individuals who gather more subjects such as condominiums. The risk evaluation of credit in this case becomes very difficult, and so guarantee funds are very helpful. According to European policy, an important role in housing retrofitting would be played by ESCO. Their action can be useful above all for public buildings and for company buildings.

In public buildings the main incentive schemes are:

- The ‘conto termico’, based on the measure of benefits in terms of energy savings during the service life of a building;
- White certificates, which are based on the measurement and certification of energy savings before and following a retrofit.

Both these tools can be managed by ESCOs.

2 The Role of ESCOs

An ESCO is a company that offers energy services which may include implementing energy-efficiency projects (and also renewable energy projects) and in many cases on a turnkey basis. The three main characteristics of an ESCO are as follows:

- ESCOs guarantee energy savings or provision of the same level of energy service at lower cost. A performance guarantee can take several forms. It can revolve around the actual flow of energy savings from a project, stipulate that the energy savings will be sufficient to repay monthly debt service costs or require that the same level of energy service be provided for less money;
- The remuneration of ESCOs is directly tied to the energy savings achieved;
- ESCOs can finance, or assist in arranging financing for, the operation of an energy system by providing a savings guarantee.

Therefore ESCOs accept some degree of risk for the achievement of improved energy efficiency in a user's facility and have their payment for the services delivered based (either in whole or at least in part) on the achievement of those energy-efficiency improvements [2].

A European ESCO market survey points out the difficulties faced by ESCOs in the Italian market: 'Italian energy service providers have always privileged large-project sizes as they are profitable... , and ignored thus large potentials of energy savings in existing smaller properties such as small and medium companies, or households. The sector where most projects have been implemented is the public sector, starting from healthcare. The private sector is presently much less developed, especially in residential homes. Energy efficiency in industry is growing though it is constrained by financial issues. This demand sector consists mainly of small and medium-sized enterprises' [7, 8].

The main issues appear related to low confidence and to some legislative obstacles such as VAT rates which are more favourable in the case of actions carried out directly by private individuals. In Germany, the number of ESCOs is five times than in Italy and the market in 2013 is estimated to be € 3–4 billion about 8 times the Italian market, which has been estimated in 2013 at around €500 million.

3 Best Practices: Germany

The experience of Germany is often cited in the international literature as an example of success in energy retrofitting of buildings. The actions carried out in the last decade by public authorities ranged from credit aimed at upgrading energy efficiency to measures of technical assistance and information of end users and firms.

A recent British study describes the case of the public bank Kreditanstalt für Wiederaufbau (KfW), which implemented a policy of subsidized loans for energy upgrading of existing buildings. An interesting movement has developed in recent decades (i.e. since 1990) to support improvements in the energy performance of buildings. The results are highly significant. Since 2010, KfW has financed the recovery of nine million homes built before 1979, out of a residential building stock of 39.6 million. Between 2006 and 2009, through the programs of KfW, they recovered energetically one million existing buildings and built 400,000 energy-efficient homes, creating 250,000 jobs in construction and industries related to construction such as material and component supplies [4]. The energy efficiency of new buildings has doubled, reducing energy consumption from 120 to 60 kWh/m²/year, while in refurbishments it was reduced to about 80 kWh/m²/year. It is estimated also that every million euros coming from the bank has set in motion nine million euros of private investment with a leverage of 1:10. The three main lines of the German policy are financial support, clearly articulated standards of

reference for the actions of upgrading the energy efficiency of the building stock and stable technical support activities and information.

An important role in the implementation of policies to improve the housing stock's energy efficiency is played by the German environment agency Deutsche Energie-Agentur GmbH (DENA). This body, established by the federal government, KfW, and three other major banking institutions in 2000, aims to implement innovative programmes and campaigns on energy savings. The activity of DENA is divided into five types of actions:

- Communication campaigns to stimulate demand and disseminate information;
- Training of experts in the sector of energy conservation (engineers, architects, artisans and entrepreneurs) through documentation, formation of a database on good practices in different areas (new construction, rehabilitation, rented houses) and the organization of events;
- Improving the transparency of energy standards and certifications (such as the voluntary quality mark 'EPC' for 'Energy Performance Certificate');
- Promotion and development of pilot projects to make clear quality standards and good practices and develop know-how on a regional scale;
- Simplification of methods to improve the reliability of energy recovery operations [7].

DENA has played a crucial role in the promotion of interventions, conducting extensive pilot programmes and setting the standards of operations covered by public agencies at regional and local levels.

On the other hand, Germany has been seen as the champion amongst the European ESCO markets in terms of maturity and the number of stakeholders. Germany remained a frontrunner in this regard during the period 2010–2013, when the German ESCO market was undergoing a slight change of direction towards more private-sector projects, more large international and especially national providers which have a greater geographical scope than ever before and a continued, even increased, role of facilitators (agencies and associations). Moreover the German market continues to grow slowly and is expected to experience further moderate growth until 2020.

4 Problems in Expanding the Retrofit Market

The high initial investment costs often dictate the decisions of small consumers (residential, offices). There is also a frequent lack of awareness of the potential savings and a difficulty of access to incentives. The main obstacles for the market are as follows:

- Restrictions, especially for complex work on whole buildings, on loans from the private sector (banks) due to the complex evaluation and technical validation of interventions;
- Lending procedures, which remain very conservative; there is limited experience and high distrust in financing energy-efficiency projects based on cash flow;
- The financial scale of projects – medium to small size – which does not attract enough interest from large financial institutions;
- A lack of preparation of financial institutions to provide innovative mechanisms;
- Difficulties accessing public funding/taxes dedicated to the development of innovative projects in the public sector, residential and non-residential;
- Difficulties arising from different concerns: the economic benefits and costs of investing compete in different areas. Typically this situation occurs in the tenant–owner [en dash instead of em dash] relationship, where there are owners who could make investments in energy efficiency but derive no direct benefits, just indirect increases in real estate values, while tenants would benefit from lower utility bills but have no interest in investing in properties which are not their own; in addition, they might leave their rentals after a few years before investors recoup their investments;
- A high perception of risk due to the difficulty of knowing the real costs of advanced/innovative technologies, in evaluating unexpected costs and taking into account the considerable fluctuations in energy costs, which affect the return on investment over time;
- The high risk of insolvency in the case of interventions in public and private condominiums [1].

The important role played by rules include the limits described earlier, such as fragmentation at the local level and the difficulties of implementing rules, such as in the case of conducting external verification. The incentive system is not always internally consistent: for example, the white certificate system is in competition with incentives to save energy (called 55 % incentives) but also with those related to building renovations and those for the adoption of solar thermal. Moreover, such a system is not always able to promote the most effective interventions. For example, it privileges simple maintenance, which is not always the best in terms of energy savings achieved considering the amount of money spent. Meanwhile, tax incentives have had the undoubted merit of stimulating an increase in the supply of quality components, which, however, in some cases have reached a state of maturity, from the point of view of diffusion, prices of production and performance. At the same time, the quality of assistance is often inadequate, especially in more complex projects, because of the difficulty associated with proper assessment by clients, showing the important role of information asymmetries in the market of eco-sustainability. Information difficulties are not only between suppliers and user-owners, but also among the many parties involved in the chain: construction firms, designers and manufacturers of materials and components. Among these parties, relationships are often informal, but the difficulties of coordination are relevant in

terms of sharing of information, objectives and tools. An important aspect in this regard is the difficulty of communication between craftsmen and contractors regarding the definition of the optimal solutions of interventions, especially regarding the management and maintenance along the life cycle of the product. As is known, improving building energy efficiency is done by a series of projects both on the building envelope and on heating, ventilation, and air conditioning installations. Nevertheless, use and maintenance can influence very significantly the effectiveness of systems. The relationships between people within the chain and between them require the adoption of contract rules that allow for the improvement in market efficiency. With regard to the issue of the adequacy of technical measures, and in particular for the proper training of installers, especially important for small businesses, it should be emphasized that there are more systematic shortcomings in obtaining information necessary to carry out interventions (e.g. availability of data on the characteristics of buildings and installed products).

5 Some Proposals

These considerations derive some guidance for policies to promote the retrofit market, such as those considered in the construction sector at the local scale, with reference to the issues of interest to the whole (and complex) industry and small construction firms. A first issue concerns the need to put in place measures to reduce the information asymmetry which dominates large parts of this market and which does not allow for the proper recognition of the real potential of interventions to induce a thorough economic assessment by the actors involved on both the demand side and the supply side. Even pursuant to European directives, local authorities are responsible for information and disclosure with regard to energy saving. There have been many experiences which have led to a wide diffusion of the benefits associated with the adoption of innovative solutions, especially in building retrofits, such as information activities carried out by local governments. However, one should not underestimate the use of forms of dissemination targeted along the supply chain by influencing actors representing hubs of relevant decisions: in particular, building managers have an interesting approach to these problems because of their ability to act on a larger share of existing buildings.

In a production chain rather dense players with different roles whose performances are strongly connected must seize opportunities offered by networking to reduce the effects of fragmentation and increase the potential for coordination among actors. The aim can be to offer packages of products/services structured in such a way as to allow for more complex and demanding deals in terms of resources and know-how.

There are two issues that deserve priority consideration with respect to policies along the supply chain. First is joint training for designers, contractors, craftsmen, material suppliers and customers, public and private, in order to create greater sharing of technical and economic characteristics of interventions, evaluation

systems which address alternatives to selecting the most appropriate solutions and identification of critical points in the process of implementing the interventions at different stages/actors. The second aspect concerns the mode of training, which especially for small businesses can be not only traditional but must rely on innovative forms of workshops and result in demonstrators, making it possible to experiment with solutions from the experience of actors in the same chain. The so-called *in vitro* construction experiences can be seen in view of lean production applied to a process of building retrofits, which reproduces the traditional method of operating a local shipyard to stimulate those involved in solutions to relevant issues based on its experience aimed at improving the results with an eye on the final result (customer satisfaction as a means to improve the relationship between the satisfaction of technical requirements and use of environmental resources through interventions).

The improvement process along the supply chain makes it possible to drive the operational process of each operator in the chain, primarily to better use and facilitate economic and contractual procedures and techniques. A codification of the main features of each building in a dossier would allow a significant reduction in transaction costs, due to the extreme variability of the buildings required simply to identify the solutions to implement for maintenance or qualification. This would be a project that would require much time and large-scale implementation but that could be started in a so-called start-up network of existing information in various technical-administrative documents already being produced. It can be seen as a development of information systems in public administration with a view to smart innovation, relying on a system powered by an open decentralization of sources of information (e.g. manufacturers, designers, installers) and to be reused by the same actors.

References

1. PAEE 2014—ENEA (2014) Piano d’Azione Italiano per l’efficienza energetica, luglio 2014
2. JRC (2015) cfr. iet.jrc.ec.europa.eu/energyefficiency/escos. Accessed 19 Aug 2015
3. Bertoldi P et al (2014) Escos market report 2013. European Commission Joint Research Center
4. Schröder M, Ekins P, Power A, Zulauf M, Lowe R (2011) The KfW experience in the reduction of energy use in and CO₂ emissions from buildings: operation, impacts and lessons for the UK. UCL Energy Institute, LSE Housing and Communities, London
5. Di Santo D et al. ENEA (2013) Risorse per incentivare efficienza energetica e fonti rinnovabili—Guida operativa per i decisori della P.A. regionale e locale, Ministero dello Sviluppo Economico—ENEA
6. Ferrero V, Pollo R (2013) Green economy e settore delle costruzioni. In *La Green economy in Piemonte*, Torino, IRES
7. Power A, Zulauf M (2011) Cutting carbon costs: learning from Germany’s energy saving program. London School of Economics, Department of Housing and Communities, London
8. JRC (2014) ESCO MARKET REPORT 2013 cfr. iet.jrc.ec.europa.eu/energy_efficiency/system//tdf/jre-89550_the_european_escos_market_report_2013_online.pdf

Chapter 60

Passive Cooling in Mediterranean Area for a Bioclimatic and Zero Energy Architecture

Fabrizio Tucci*

Abstract Natural and hybrid ventilation systems in Mediterranean climate have huge potential in terms of energy savings and indoor comfort improvement. The main obstacles to more widespread use of such systems lie probably in the difficulties and uncertainties inherent in the design of the systems and in the predictability of actual performance. This chapter describes a methodology for overcoming these problems and presents two case studies that illustrate the process and give an example of the possible results. The design process is articulated through the use of analysis and simulation tools in a progressively more detailed manner. Thus, the general strategies are adapted to the climate and the main building features; site and general building designs depend on the microclimate-specific characteristics; detailed design and system calibration are defined on the basis of internal computational fluid dynamics and subhourly energy simulations. The case studies, two public housing buildings in central Italy, are designed on a high-energy standard, with passive solar systems, natural and hybrid ventilation strategies, high-efficiency heating, ventilation, and air conditioning, and integrated photovoltaic modules. The design process and the estimated performance are illustrated with special regard to ventilation and cooling systems. The buildings are expected to have very low energy consumption and a high quality standard for indoor comfort, showing good potential for these strategies in the Mediterranean climate.

Keywords Natural ventilation • Passive cooling • Energy efficiency • Building simulation

*This contribution is the result of a collaborative effort with Alessudra battisti, the scientific co-principal investigator with me for this experimental research; Maozo cimillo, who carried out the energy-performance simulations; and Filippo calcerno, who did the simulations of fluid-dynamic behaviour.

F. Tucci* (✉)

Department Planning Design Technology, University di Architecture,
Via Flaminie 70-00196, Rome, Italy
e-mail: fabrizio.fucci@uniroma1.it

1 Introduction

With global temperatures rising, a progressively higher frequency of heat waves, and a higher standard of environmental indoor comfort in residential and working environments, European countries saw a dramatic increase in the number of air-conditioning systems installed and related energy consumption [1–3]. From the perspective of nearly zero-energy building, a major importance is assumed by summer energy performance control using low-energy technologies, particularly those using natural ventilation [4].

Technologies and control systems are now available to significantly lower energy demand while maintaining excellent indoor comfort conditions. In the Mediterranean climate, controlled natural or hybrid ventilation is particularly effective in the reduction of energy consumption and in the improvement of indoor air quality (IAQ), even in winter and intermediate seasons [5]. IAQ represents a major problem, especially in new buildings with highly airtight envelopes. Even for energy, beyond a certain limit, it is neither possible nor convenient to reduce consumption by improving the envelope, and it is necessary to use fluid dynamics.

The obstacles to a more extensive use of natural and hybrid ventilation are posed mainly by the extreme variability of conditions, determined by climate, biophysical site characteristics, and building features. For an effective design of devices, general building configurations, and control systems, an innovative approach is needed [6, 7], one that examines in depth the building system through simulation and evaluation methods [8, 9]. This contribution describes a design methodology adopted to address these problems and illustrates a few case studies, built or in the construction phase.

This approach includes a series of progressive steps that move from the site and building analysis for the definition of a general strategy to a detailed verification of airflow in the indoor environment. At different steps, the most updated simulation instruments are used in order to obtain reliable information about both energy consumption and environmental comfort. The case studies pertain to residential building in central Italy, featuring buried earth pipes, ventilation towers, and control systems for wind-driven cross ventilation. All the devices are part of a more comprehensive design strategy, which includes several passive solar systems and tight integration with heating, ventilation, and air conditioning (HVAC) systems. Several physical models were used, such as computational fluid dynamics (CFD) for external ventilation and a detailed analysis of the main internal spaces, dynamic simulations, and air-node networks for internal–external and interzonal ventilation, overall energy performance, and indoor environmental comfort on a yearly basis.

2 Methodology

Given the aforementioned conditions, natural ventilation is approached through a process that involves several progressive steps of analysis and design, as described by the following table. The table includes existing and new buildings, and not all the steps are applicable for both. Furthermore, the analysis–design steps define an iterative process rather than a simple sequence, so normally each stage is repeated more than once (Table 60.1).

Data gathered in the first step make it possible to define the climate type and the overall design strategy, with particular attention to the daily thermal range that above certain thresholds (14 °C in the case studies) allows an excellent application of natural ventilation strategies based on thermal inertia [10]. From these input data, in the second step, a solar analysis is performed by means of simulations to study the optimal placement of passive and active systems and to maximize the solar protection of passive system glazing in summertime. The study proceeds by analyzing the urban microclimate. Airflows between buildings and plant masses, thermal exchanges of heat and vapor between the soil and building *façades*, vegetation hygrothermal and energy exchanges, and mean radiant temperatures are simulated and analyzed using CFD software providing important information for the correct positioning of envelope openings to get the most out of a cross-ventilation strategy. In the third step, once the general building structure is defined, the building energy performance is analyzed through multizonal network simulations that make it possible to tune with a greater level of detail all the passive and

Table 60.1 Methodology

Step	Analysis	Design	Tools
1	General climatic data (temperatures, wind, humidity, and solar radiation)	Selection of natural ventilation strategy and period of usability	Statistical data analysis, simple manual calculations
	General building features (functions, occupancy, internal loads)		
2	Microclimate features (air speed and pressure and solar radiation on building envelope and around it)	Site design (trees and obstructions)	Solar simulations
	Building geometry, envelope, plants, and thermal mass	Building position and orientation, layout, and massing	External CFD simulation
3	Air change needs, thermodynamics, cooling loads, energy demand, and potential for natural ventilation	Building envelope (glazing, opening position, and dimensions)	Node network simulations and thermal simulations (including effects of natural ventilation)
4	Airflow features	Detailed design of openings and internal air paths	Internal CFD simulations
	Internal comfort		

active systems (including, for example, the window-to-wall ratio or the real efficiency of natural ventilation). Finally, airflows within individual apartments are simulated using CFD software to optimize the internal distribution of partitions in order to improve the flow arising from cross ventilation. Other CFD simulations are then run in order to correctly position the inlets and outlets of the ventilation systems and to study their interaction with natural ventilation. Final adjustments are made to reduce turbulence and related discomfort areas in favor of an optimal air washing of the room and to improve the energy performance of natural ventilation.

3 Case Studies

The methodology described earlier was applied in projects involving two apartments buildings in Florence, Italy. Both are multistory public housing constructions that will be built with wooden structures and envelopes. Both are designed on a high energy standard and aim to achieve an A+ class, the highest in the Italian energy certification system. This objective will be pursued through the integration of several energy-saving measures: a superinsulated envelope, the use of passive solar systems, natural and hybrid ventilation strategies, and high-efficiency heating and cooling plants [11].

1. Pegna ex Benelli: This project is located near the airport of Peretola and will serve nonresidential functions on the ground floor and 21 apartments on 3 levels (Fig. 60.1). Each of the three staircases is coupled with a three-level sunspace, and each apartment is provided with its own private sunspace and a Trombe–Michel wall that contributes to the sunspace heating. Fresh air is provided through a system of buried earth pipes that mitigates the external air temperatures during both winter and summer. The apartments are then heated by a

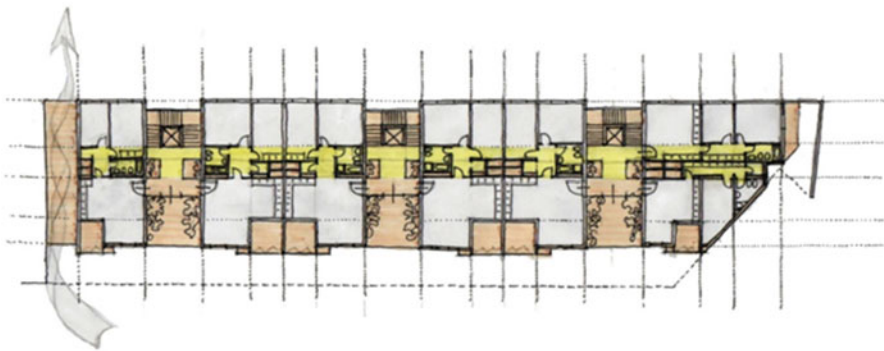


Fig. 60.1 Pegna ex Benelli public housing, plan with apartments (*gray*), distribution (*yellow*), and bioclimatic spaces (*orange*)

radiant ceiling powered by an air-to-air heat pump. In addition, the plan was conceived to allow for natural cross ventilation during intermediate seasons in all of the apartments. During the summer, the common sunspace, in connection with staircases, has openings on opposite *façades* for cross ventilation, and the private sunspaces are fully openable and can turn into open logias.

Passive cooling strategies were planned on the basis of the local climate, with regular ventilation for the deactivation of solar systems and for intermediate conditions in the apartments and with buried earth pipes that make it possible to achieve passive cooling even during the hottest times. In fact, monthly maximum temperatures in Florence are above 26 °C from June to September, and untreated outdoor air would not have been sufficient to ensure acceptable indoor conditions.

The overall energy performance and buried earth pipes were simulated through a dynamic thermal model, using EnergyPlus, while natural ventilation design was facilitated by CFD simulations for both exterior and interior environments. Figures 60.2, 60.3, 60.4, and 60.5 show the progressive deepening of the simulation scope. These studies made it possible to dimensionalize atrium and apartment openings, to detail interior space configurations, and to assess indoor comfort conditions [12].

Furthermore, the studies made available more reliable data for the overall energy simulation, whose main results are presented in Figs. 60.6, 60.7, 60.8, and 60.9. More specifically, the buried earth pipes, with an average length of

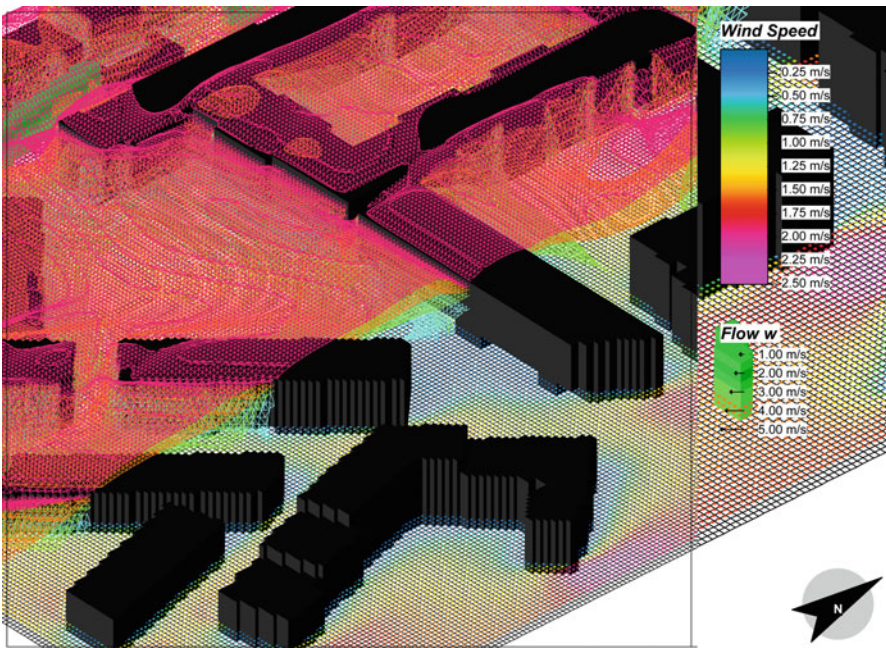


Fig. 60.2 External CFD simulation in typical summer conditions

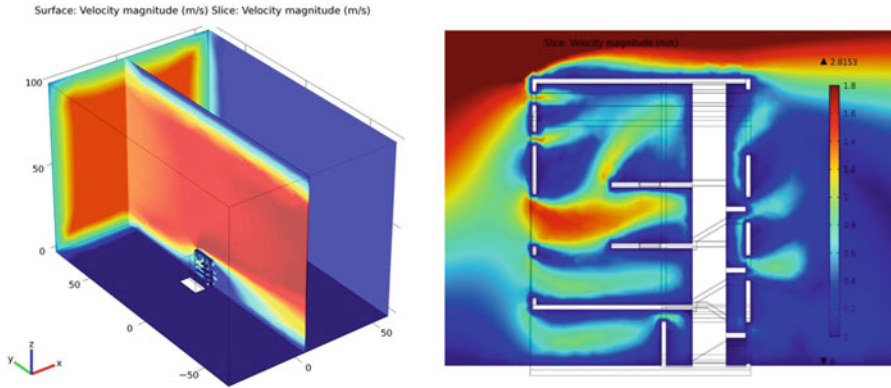


Fig. 60.3 CFD simulation of cross ventilation in one of the atria. Both external and internal environments are included in the same model

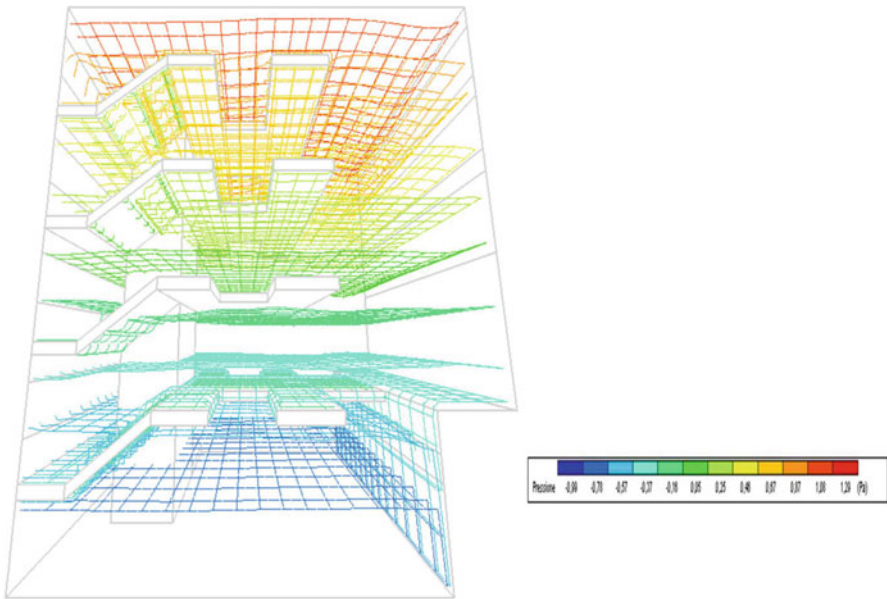


Fig. 60.4 Internal CFD simulation in atrium for buoyancy effects, without wind, in summer conditions. The isosurfaces show the pressure variations due to the stratification of air layers at different temperatures

30 m, provide air at temperatures 1–6 °C lower than the outdoor air, with the best performance during the hottest hours, lowering the cooling demand by 83 % (to 1.5 kW/m²). With the additional contribution of shading devices and cross ventilation, the building can do without air conditioning, with few hours of discomfort throughout the year. According to simulated (Predicted Mean Vote) PMV values, hours within the optimal range (–0.5 to 0.5) account for

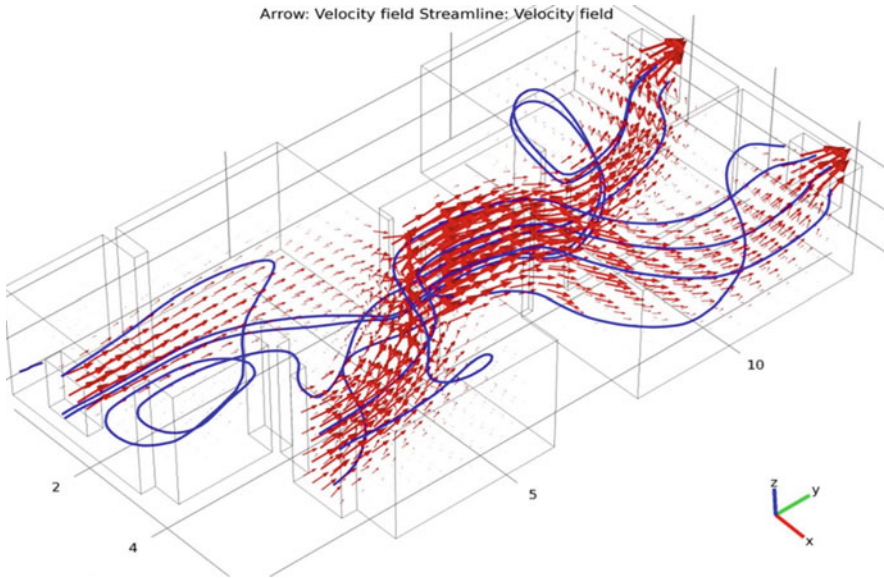


Fig. 60.5 CFD simulation of cross ventilation in one of the apartments. *Lines* and *vectors* show the airflow path and velocity

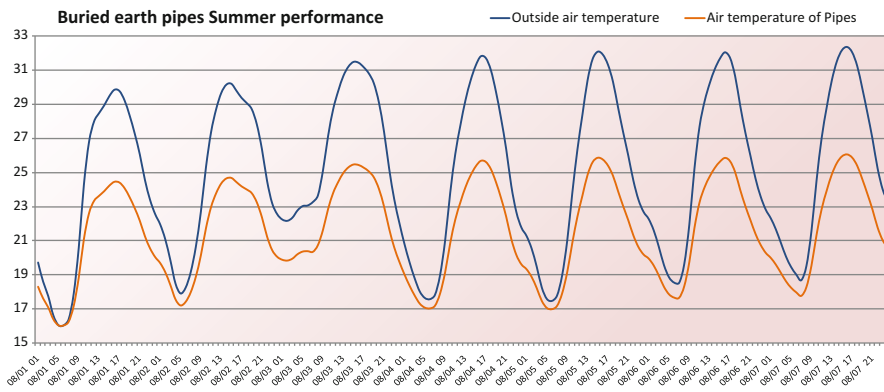


Fig. 60.6 Simulated temperatures of buried earth pipes compared with external air temperatures (blue) in summer conditions

61.96% of total time, whereas hours within the 0.5–1 range and hours above 1 account respectively for 12.53 and 1.2% of total time (Fig. 60.7). Moreover, the simulated indoor comfort with passive systems in the summertime is better than that of the building controlled by traditional air conditioning owing to the good performance during the hottest hours (Fig. 60.8). The effect of passive systems on indoor operative temperature in a free running (without plants) building is illustrated in Fig. 60.9.

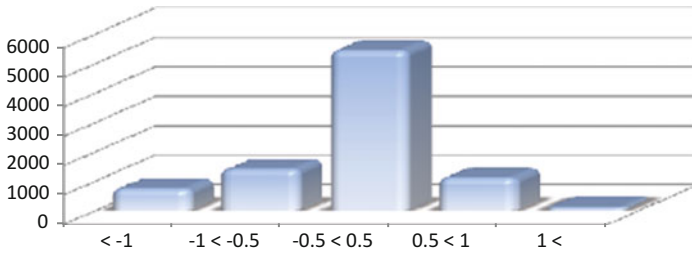


Fig. 60.7 Simulated hourly PMV values throughout the year

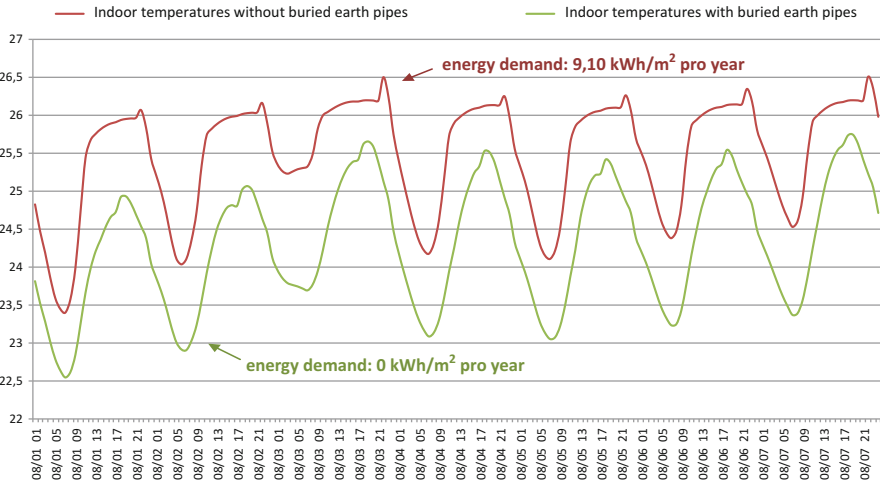


Fig. 60.8 Simulated indoor temperatures with buried earth pipes (and no cooling energy demand) and without them (and a cooling energy demand of 9.10 kWh/m²)

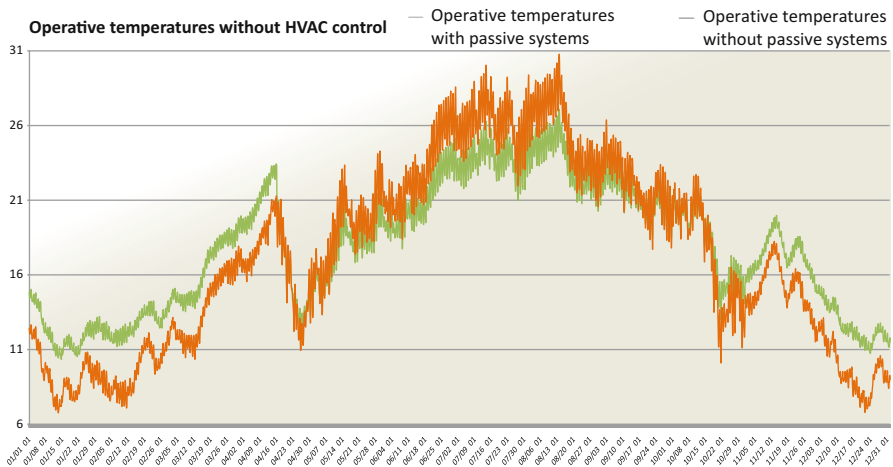


Fig. 60.9 Simulated hourly operative temperatures with (green) and without (orange) passive systems for building without HVAC control



Fig. 60.10 Building plan with passive solar systems. *Yellow*: common six-story sunspaces that provide preheated air for apartments in winter; *orange*: private single-floor sunspaces for each apartment; *orange*: Trombe–Michel walls that support the private sunspaces; *blue*: ventilation tower that distributes air from sunspaces and from underground slab

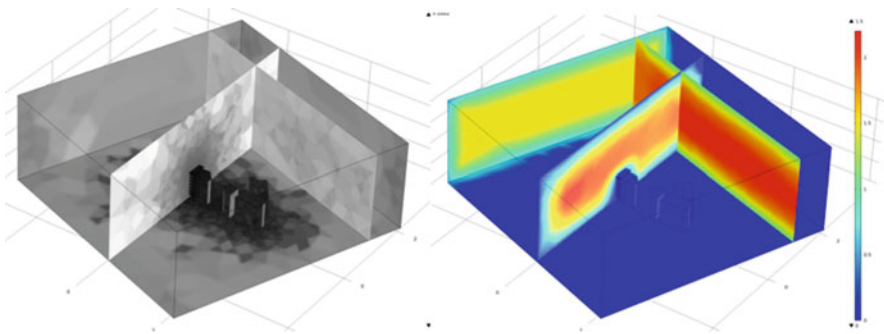


Fig. 60.11 External–internal 3D CFD simulation for cross ventilation in atrium in summer conditions; *left*: mesh resolution variations; *right*: velocity field

2. Torre Agli: This project was planned to replace three obsolete public housing buildings in Florence and provide 84 apartments in 2 six-story buildings with a common underground parking lot on two levels. The buildings incorporate passive systems and high-efficiency plants, similar to the Pegna project (Fig. 60.10). In addition, an experimental solar cooling plant will be installed. Even for this project, natural ventilation was designed using CFD. Figure 60.11 shows one of the simulations that includes both indoor and outdoor environments in the same three-dimensional (3D) CFD model.

When the buried earth pipes are replaced, a hollow space integrated in the underground slab under the parking will be used to cool the air during the summer. The hollow space is divided into separate portions for each distribution tower, proportionally with the volume served by each of them; each portion is configured as a maze, in order to involve all the available surface area in the thermal exchange. The air is taken from outside by vents integrated into the

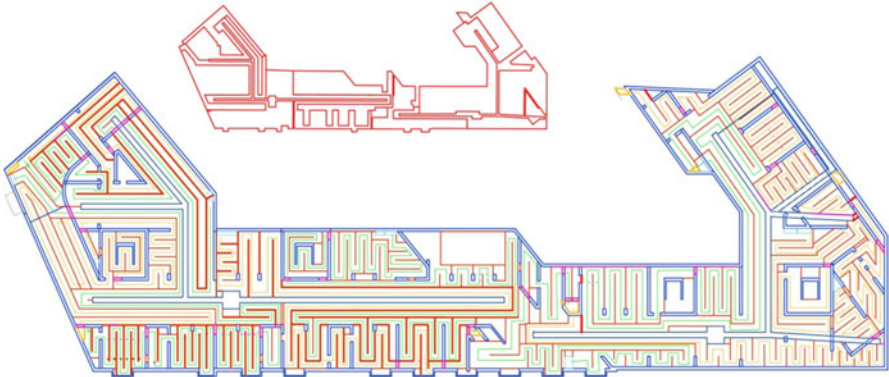


Fig. 60.12 Plan at hollow space level in underground slab

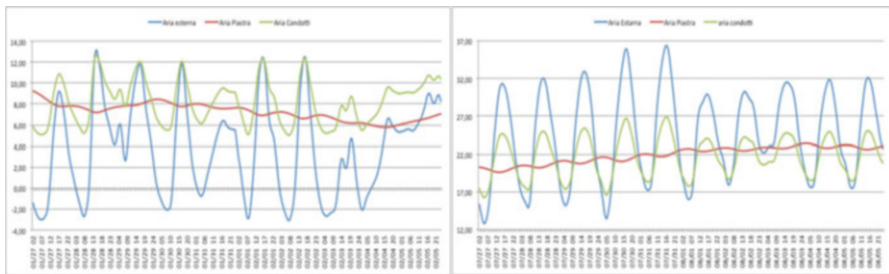


Fig. 60.13 Air temperatures from underground slab during winter (*left*) and summer (*right*)

façades of the building and driven through the distribution tower by fans installed under each of them (Fig. 60.12).

Compared to earth pipes (Fig. 60.13), the performance of this system is more stable in a 24 h period, even though air temperatures tend more toward the daily average, cooling the air during the day and warming it at night, in both summertime and wintertime. For this reason the system will be used only during the summer, when the air is constantly under the comfort threshold in the apartments. The complex of passive cooling measures (cross ventilation, underground slab, and shading systems) is expected to reduce energy demand for cooling by 74 % from 17.3 to 4.1 kWh/m².

4 Conclusions

This chapter describes how it is possible to design an effective natural ventilation system by integrating different analysis methods and tools for each stage of the design process. Moreover, the examples treated illustrate how effective these systems can be in providing high-quality indoor comfort conditions while reducing

energy demand in the Mediterranean climate. The simulation of indoor comfort conditions demonstrates that in many cases it would be possible to completely eliminate the need for mechanical cooling plants, provided the occupants are willing to accept a slightly less controlled and stable condition inside the building and to tolerate few discomfort hours per year during particularly severe climatic conditions. In the examples analyzed in this chapter, the estimated energy savings, based on a comparison of the consumption of the actual building to that of the same buildings without natural ventilation, range from 74 to 100 %.

References

1. Santamouris M (2007) *Advances in passive cooling*. Earthscan, London
2. Kwon O-H, Kim M-H, Choi A-S, Jeong J-W (2013) Energy saving potential of a hybrid ventilation system integrated with heat storage material. *Energy Build* 57:346–353
3. Tucci F (2011) *Efficienza ecologica ed energetica in Architettura*. Environmental and energy efficiency in architecture. Alinea Editrice, Firenze
4. Tucci F (2012). *Atlante dei Sistemi tecnologici per l'Architettura bioclimatica*. Ventilazione naturale negli Edifici/Atlas of technological Systems for bioclimatic Architecture. Natural Building Ventilation. Alinea Editrice, Firenze
5. Grosso M (2011) *Il raffrescamento passivo degli edifici*. Maggioli, Rimini
6. Allard F (1998) *Natural ventilation in buildings: a design handbook*. James & James Ltd, London
7. Mahdavi A, Pröglhöf C (2005) A model-based method for the integration of natural ventilation in indoor climate systems operation. *Proceedings of the Ninth International IBPSA Conference BS 2005 Montréal, Canada 15–18 Aug 2005*
8. Morbitzer C (2003). *Towards the integration of simulation in the building design process*. PhD thesis, Energy System Research Unit, University of Strathclyde
9. Chen Q (2009) Ventilation performance prediction for buildings: a method overview and recent applications. *Build Environ* 44:848–858
10. Givoni B (1998) Effectiveness of mass and night ventilation in lowering the indoor daytime temperatures. Part I: 1993 experimental periods. *Energy Build* 28:25–32. doi:[10.1016/S0378-7788\(97\)00056-X](https://doi.org/10.1016/S0378-7788(97)00056-X)
11. Herzog T, Battisti A, Tucci F (2012) *Sperimentazioni di housing sociale tra efficienza energetico-ambientale e basso costo | Experimentation on Social housing between Energy-environment efficiency and low cost*. *Techné. J Technol Archit Environ* 4:343–354
12. Tucci F (2013) *Efficienza bioclimatico-ambientale per un Housing Sociale a Firenze | Bioclimatic-environmental Efficiency for Social Housing in Florence*. *Il Progetto Sostenibile*, vol 32. gennaio-giugno 2013, pp 40–47

Chapter 61

First-Year Performance of a PV Plant in Jordan Compared to PV Plants in the Region

Ali Hamzeh, Sadiq Hamid, Abbas Sandouk, Zakaria Al-Omari, and Ghada Aldahim

Abstract This chapter presents the first-year (2014) performance analysis of a 276 kW_p grid-connected roof-type solar photovoltaic (PV) plant located at the campus of Al-Ahliyya Amman University (AAU) in Jordan using monitored data. The plant is installed on the 3000 m² roof of the arena building on the university's campus. The array consists of 1176 modules with 2 orientations, 10° and 15°. The PV array is configured in such a way that the system includes 14 panels in parallel with 14 inverters. The plant is equipped with a monitoring system that is connected to the Internet and provides data on a daily basis. The study shows that the actual and estimated specific energy productions are 1639 and 1726 kWh/kW_p/year, respectively. The annual capacity factor and performance ratio are found to be 18.7 and 87.5 %, respectively. The actual energy production is found to be 452,406 kWh/year, whereas the estimated annual energy production is found to be 476,467 kWh, as calculated using the PVsyst v6.32 software. The measured and estimated yields are in close agreement with each other, with a relative error of around 5 %. It is found that the actual yield is at its maximum in July and minimum in January. The analyzed plant is compared to PV plants worldwide, particularly in detail to a PV plant in Syria. The comparison shows that the overall performance of the AAU plant is excellent.

Keywords Photovoltaic plant • Specific system production • Performance ratio • Capacity factor • Jordan, Syria

A. Hamzeh (✉) • S. Hamid • Z. Al-Omari
Faculty of Engineering, Department of Electrical Engineering, Al-Ahliyya Amman University,
Amman, Jordan
e-mail: hamzeh.ali@gmail.com

A. Sandouk • G. Aldahim
FMEE Department of Electrical Engineering, Damascus University, Damascus, Syria

1 Introduction

Al-Ahliyya Amman University (AAU) was established in 1990 as the first private university in Jordan. The university consists mainly of seven buildings, five female dormitories, and cultural foundation forums (Arena); the total built-up area of the university campus is 72,868 m². The average specific electrical energy consumption of the university is around 4.5 kWh/m²/month. The annual electricity consumption is about 4 GWh [1]. The electrical use breakdown is shown in Fig. 61.1.

To reduce its electricity bill, AAU decided to install a solar photovoltaic (PV) plant with a capacity of 276 kWp on the roof of the Arena building, which has an area of 3000 m² (Fig. 61.2).

Following the design stage, and after receiving confirmation of the university's presidency, the installation of the system started and continued for around 10 days. After installing the system it was examined by Jordanian Electric Power Company, which released the necessary approvals to connect the system to the grid. This chapter presents measured system data for the year 2014 and a performance analysis of these data with the aim of showing whether this project is promising and inspires confidence for the university to install additional PV plants. Moreover, the plant's behavior is compared with that of other plants in the region and worldwide.

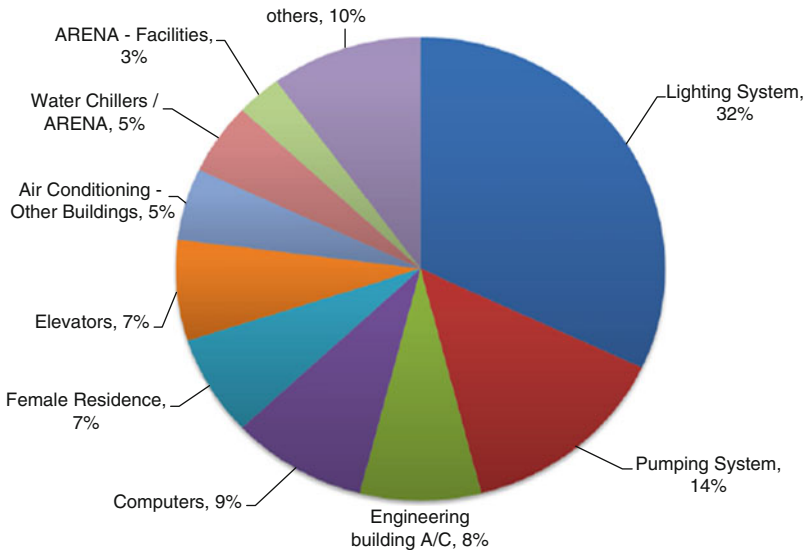


Fig. 61.1 Electrical use breakdown of AAU [1]



Fig. 61.2 PV plant on roof of cultural foundation forums building (ARENA) in AAU, Amman, Jordan

2 Technical Description of System

The PV system is located in the As-Sarw area (between Amman and As-salt city), Jordan, at a latitude of $+32.05$ ($32^{\circ}03'00''N$) and longitude of $+35.72$ ($35^{\circ}43'12''E$). The module that was used is ET-P660235WW/ET-P660235WB with its data shown in Table 61.1. The array comprises 1176 modules configured as 14 subarrays. Each subarray consists of four strings with 21 modules connected in series for each string. The system is equipped with 14 subarray identical inverters SUN2000-20KTL from Huawei Technologies with technical specifications as shown in Table 61.2. The array orientation is fixed at two orientations: mixed tilt/azimuth of $15^{\circ}/0^{\circ}$ and $10^{\circ}/0^{\circ}$. The plant is equipped with a monitoring system connected to the Internet and provides daily data that can be followed on the Web [2]. Figure 61.3 shows a schematic layout of the PV plant.

3 Actual and Estimated Energy Production

According to the monitored plant data from 1 January to 31 December 2014, the actual energy production was 452,506 kWh/year, with a specific final yield (Y_f) of 1639 kWh/kWp. The minimum value was 16,898 kWh in January, while the highest value was 55,821 kWh in July (Fig. 61.4). The PV plant is simulated by the program PVsyst v6.32. The simulation results show that the expected energy fed into the grid was found to be 476,467, with a specific final yield of 1726 kWh/kWp, which is in

Table 61.1 Module data under standard test conditions

Model type	ET-P660235WW, ET-P660235WB
Cells per module	60
Cell type and dimension	Poly 156 × 156 mm
Pmax	235 W
Module efficiency	14.44 %
Power tolerance	2 %
Vmp	29.83 V
Imp	7.88 A
Voc	37.08 V
Isc	8.5 A
Maximum system voltage	DC 1000 V
NOCT	45.3 °C
Voltage coefficient	-0.34 %/°C
Current coefficient	0.04 %/°C
Power coefficient	-0.44 %/°C

Table 61.2 Inverter specifications

Maximum efficiency	98.5 %
European efficiency	98.20 %
Maximum DC input	22.5 kW
Maximum input voltage	1000 V
Maximum input current per MPPT	18 A
Operating voltage range	250–850 V
MPP voltage range	480–800 V
Rated input voltage	620 V
Number of MPP trackers	3

MPPT Maximum Power Point Tracker; *MPP* Maximum Power Point

good agreement with actual measurements, with a relative deviation of around 5 %. It is obvious from Fig. 61.4 that the actual values exceed the estimated values from April to August. In 2014, the PV plant saved approximately 331 tons of CO₂, which would have been emitted by a crude oil fired thermal power plant generating the same amount of electricity.

The measurement and estimation (simulation) of PV energy production is a fundamental issue in PV system engineering. Measurement and monitoring is generally simpler than estimation, which is dependent on weather. Monitoring and estimation of PV can be used for various purposes, for example, to conduct a financial analysis. Whatever the goal, the processes and methods are critical to the technical and financial viability of PV technology and its integration into the utility grid. Simulation of PV systems differs from monitoring. The input may be either measured or calculated. The output is not measured; it is calculated. Simulation is a two-part process entailing the use of a set of input parameters and a model or transfer function of the physical plant used to calculate the performance of a PV system [3].

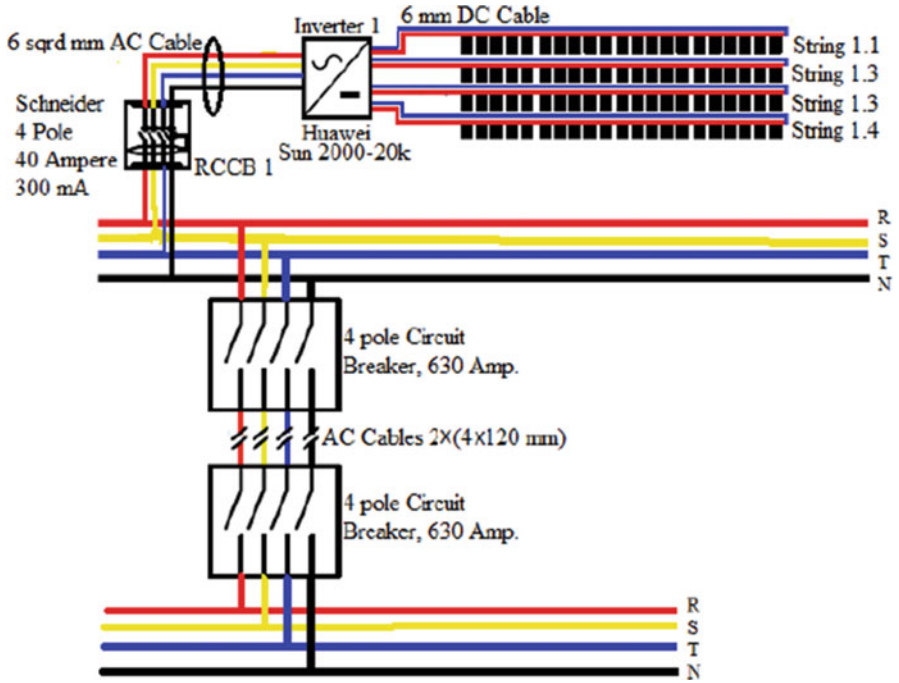


Fig. 61.3 Layout of one subarray of the AAU PV plant

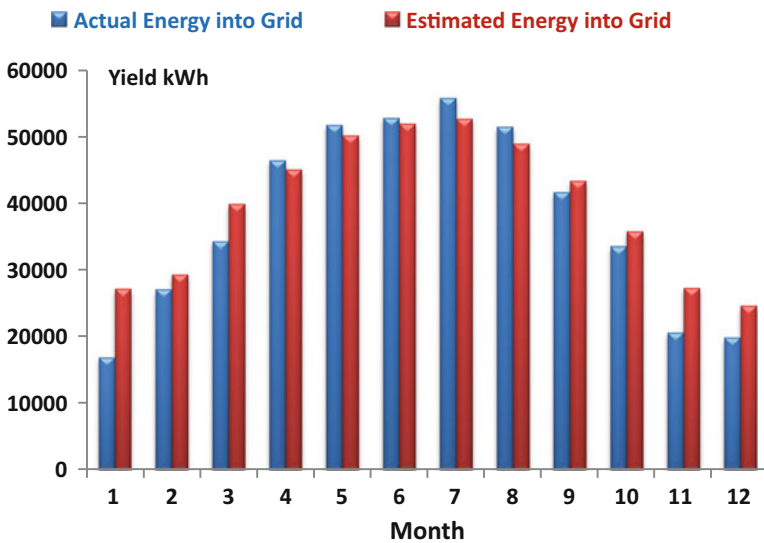


Fig. 61.4 Measured and estimated energy production for January–December 2014

4 Performance Ratio

4.1 Definition

One of the key evaluation criteria of the PV system is the performance ratio (PR) of a grid-connected PV plant. The PR is an indicator of the effectiveness of the plant in transforming the solar energy captured by PV arrays into AC energy delivered to the utility grid. The PR is defined for a period of time (usually a month or a year) as the ratio of the measured generated AC energy fed into the point of common coupling (PCC) to the potential array output DC energy under standard test conditions. The calculation of annual and monthly PR percentage can be performed by Eqs. (61.1) and (61.2), respectively [4–6]:

$$\text{Annual PR}\% = \frac{\text{Measured Energy at PCC} \left[\frac{\text{kWh}}{\text{year}} \right]}{\text{Insolation} \left[\frac{\text{kWh}}{\text{m}^2 \cdot \text{day}} \right] * \text{active array area} [\text{m}^2] * 365 * \eta_{\text{module}}} * 100, \quad (61.1)$$

$$\begin{aligned} \text{Monthly PR}\% \\ = \frac{\text{Measured Energy at PCC} \left[\frac{\text{kWh}}{\text{Month}} \right]}{\text{Insolation} \left[\frac{\text{kWh}}{\text{m}^2 \cdot \text{day}} \right] * \text{active array area} [\text{m}^2] * \text{month days} * \eta_{\text{module}}} * 100. \end{aligned} \quad (61.2)$$

4.2 Performance Ratio Calculation:

- Active array area (Area of module cells) = $0.156 * 0.156 * 60 * 1176$
= 1717.148 m².
- The solar data of a plant's location are assumed to be those of Amman and is adopted from NASA's Surface Meteorology and Solar Energy satellite included in the database of the PVsyst v6.32 software. Based on horizontal values, the global monthly average insolation in the collector plane is computed using the PVsyst v6.32 software; the results are represented in Fig. 61.5. The yearly average global insolation in the collector plane is 5.71 kWh/m² day.

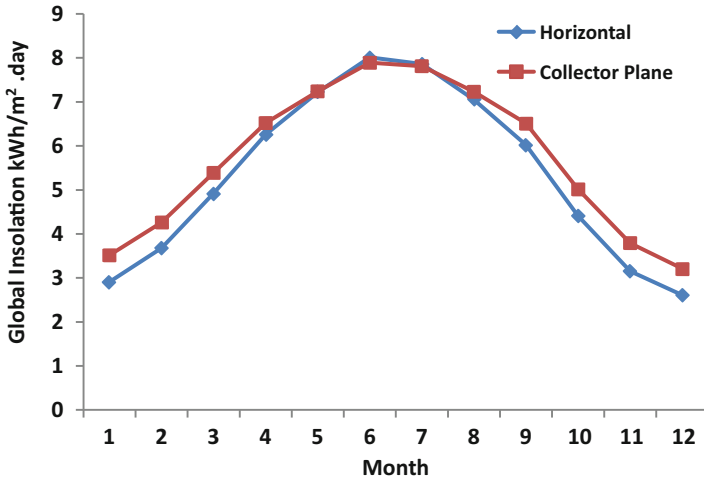


Fig. 61.5 Global monthly average insolation at AAU

The plant annual PR is calculated using Eq. (61.1):

$$\begin{aligned} \text{Actual annual PR}\% &= \frac{452405.92}{5.71 \cdot 1717.148 \cdot 365 \cdot 0.1444} \cdot 100 = \frac{452405.92}{516777.854} \cdot 100 \\ &= 87.544 \%. \end{aligned}$$

In modern solar PV plants, the performance ratio should typically be around 80 % in the starting year. According to the National Renewable Energy Laboratory (NREL) (Golden, CO), the standard performance ratio for a new PV system is around 77 %, and over time the PR will degrade [7]. Thus, the PR value of over 87 % for the new university PV system shows the excellent quality of the system. The PR value indeed evaluates the total losses of the system, less than 13 % for our system. These losses account for, among things, mismatched modules, differences in ambient conditions, dirty collectors, inverter efficiency, wiring losses, system availability, diodes, and connections.

It is a good practice to calculate the monthly PRs in order to be aware of the losses that occur each month, which can help in deciding on measures to reduce them. The calculation process is illustrated by an example for March 2014:

$$\begin{aligned} \text{PR}\% \text{ for March} &= \frac{34251}{5.39 \cdot 1717.148 \cdot 31 \cdot 0.1444} \cdot 100 = \frac{34251}{41431.04} \cdot 100 \\ &= 82.67 \%. \end{aligned}$$

The results are shown graphically in Fig. 61.6.

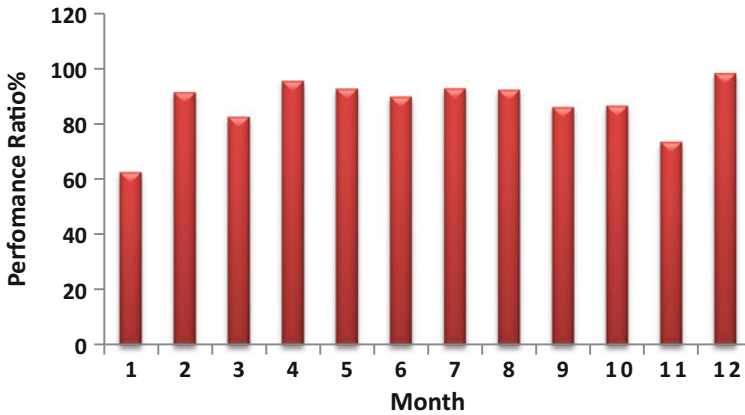


Fig. 61.6 Monthly performance ratios, January–December 2014

It is obvious from Fig. 61.6 that the PR is at its minimum in January (62.45 %), at its maximum in December (98.40 %), and over 90 % for more than 6 months. The performance ratio for the whole year is found to be 87.544 %, as calculated earlier.

4.3 Performance Ratio Levels Worldwide [8]

Many studies have been conducted [9–12] to analyze the performance of PV systems installed in different countries at different times. An increasing trend of the annual PR values has been observed over the years (Table 61.3). The average PR values increased from about 65 % in the 1990s to over 80 % in the 2000s. Compared to average PR levels for PV plants worldwide, the AAU plant is among those plants with the best PR.

5 Capacity Factor

5.1 Definition

The other key parameter for evaluating PV plants is the capacity factor (CF). The CF of a power plant is the ratio of its actual generated energy over a period of time to its potential output if it could operate at full nameplate capacity. The main difference between the PR and CF is that the CF ignores environmental conditions affecting the plant, while the PR accounts for these conditions. The CF may be, however, a value that serves as a comparison criterion for evaluating power stations with different fuels. Renewable power plants or conventional power plants with

Table 61.3 Performance ratio values for reported PV systems worldwide [8]

Installation time	Country	PR range	Mean PR
1990s	Germany	0.38–0.88	0.67
2000s	France	0.52–0.96	0.76
2000s	Belgium	0.52–0.93	0.78
2000s	Taiwan	<0.3 to >0.9	0.74
2000s	Germany	0.70–0.90	0.84

Table 61.4 Average capacity factor for various power plants in UK

Type	Average CF (2007–2012) (%)
Nuclear	62
Combined cycle	57
Coal-fired	45
Hydroelectric	34
Wind	28
PV	9

high fuel costs that are usually operating at peak load periods have relatively low capacity factors. Table 61.4 shows average CFs for different power plants in the UK [13].

According to the NREL, the CF of PV plants over a year is calculated as follows:

$$\text{Annual CF\% (according to NREL)} = \frac{\text{Actual produced kWh}}{\text{DC rated power} \times 8760} \times 100, \tag{61.3}$$

$$\begin{aligned} \text{Monthly CF\% (according to NREL)} \\ = \frac{\text{Actual produced kWh/month}}{\text{DC rated power} \times 24 \times \text{month days}} \times 100. \end{aligned} \tag{61.4}$$

5.2 Calculation of AAU Plant Capacity Factor

The annual capacity factor of AAU plant is calculated using Eq. (61.3):

$$\text{CF\% of AAU plant} = \frac{452405.92 \text{ kWh}}{276 \text{ kW} \times 8760} \times 100 = \mathbf{18.7 \%}.$$

Monthly CFs are calculated and represented graphically in Fig. 61.7, which shows that the CF is at its minimum in January (8.23 %) and at its maximum in July (27.18 %). The average CF for the entire year is 18.7 %. According to [13], the CFs of evaluated PV plants in the USA and UK are as follows:

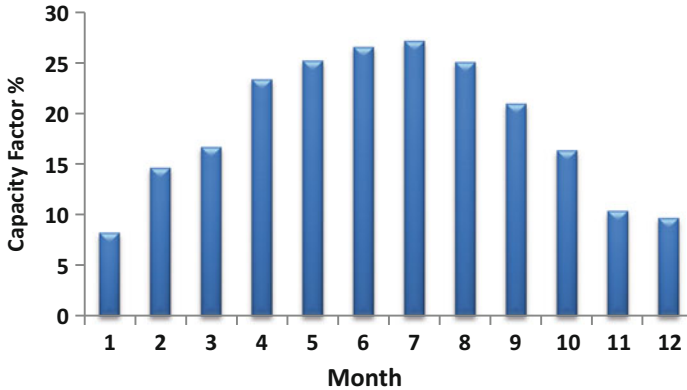


Fig. 61.7 Monthly CFs for AAU plant

PV solar in Massachusetts 13–15 %, PV solar in Arizona 19 %, PV solar in UK 8.6 %. The annual CF of a PV plant in Egypt is 18.12 % [14]. Compared to the CF values in some countries, our plant possesses a very high CF, which again indicates excellent performance.

6 Effect of Ambient Temperature on Power Output of Array and Inverter

Cell temperatures change not only as a result of variations in ambient temperatures but also because of insolation changes on the cells. Manufacturers often provide a parameter called nominal operating cell temperature (NOCT), which can be used for considering the changes in cell performance with temperature. The NOCT is the cell temperature in a module under the following conditions: ambient temperature of 20 °C, solar irradiance of 0.8 kW/m², and wind speed of 1 m/s. To account for other ambient conditions, the following expression may be used [15]:

$$T_{\text{cell}} = T_{\text{amb}} + \frac{\text{NOCT} - 20^{\circ}}{0.8} * S, \quad (61.5)$$

where T_{cell} is the cell temperature (°C), T_{amb} is the ambient temperature (°C), and S is the actual solar irradiance (kW/m²).

The approximate calculation of the power output of the array (P_{DC}) and power output of inverters (P_{AC}) can be carried out as follows.

- From given monthly average ambient temperatures, the average T_{cell} is determined for each month using Eq. (61.5):

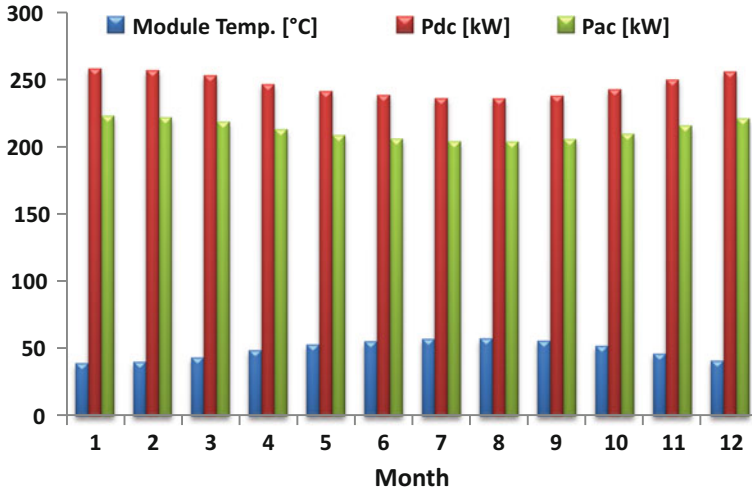


Fig. 61.8 Module temperature effect on power output of PV array (P_{DC}) and inverter (P_{AC})

$$P_{DC} = 276[1 - 0.0044(T_{cell} - 25)]kW, \tag{61.6}$$

$$P_{AC} = \eta_{conversion} * P_{DC} \text{ kW}. \tag{61.7}$$

The results are shown in Fig. 61.8.

As can be seen in Fig. 61.8, when cells heat up and, consequently, the cell temperature increases, both maximum DC power available and AC output power decrease. The minimum value occurs in August with 14.5 % less than rated power, and the maximum is found to be in January with a 6.4 % rated power drop. Given this significant variation in performance as the cell temperature changes, it should be quite apparent that the temperature needs to be included in any estimate of array performance.

7 AAU PV Plant Versus a Syrian PV Plant

To compare the quality of our plant with PV plants in the region, a grid-connected PV system in Syria is briefly analyzed and compared to the AAU PV plant. The considered Syrian PV plant is a grid-connected plant operating since 9 November 2010. It is installed in Damascus on the roof of one of the Electricity Ministry buildings. The PV array consists of 45 modules with a rated power of 90 W each. The module made in Syria has an efficiency of 13.56 % and 36 cells connected in series. The cell area is 156.25 cm². The array orientation is fixed at a tilt angle of 35°. Based on the measured solar insolation on a horizontal surface in Damascus

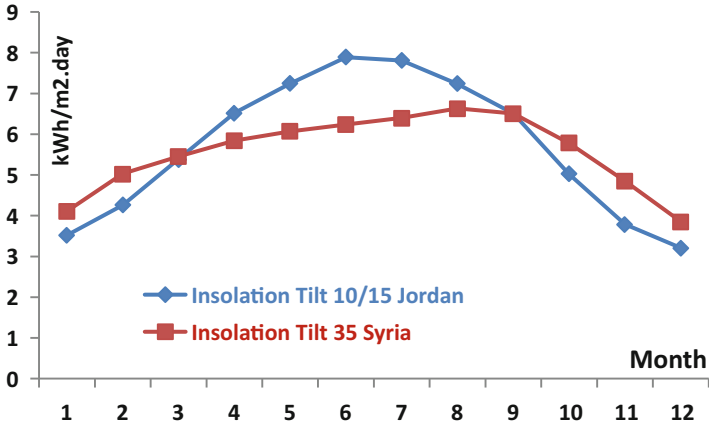


Fig. 61.9 Insolation on tilted array for Damascus and Amman

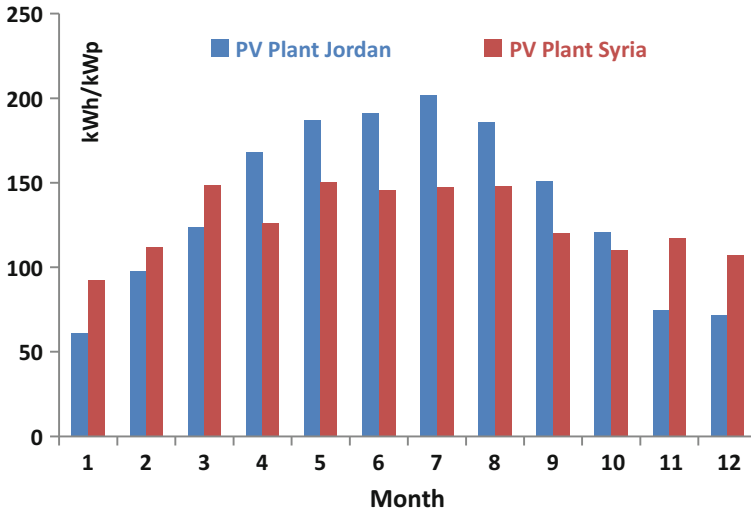


Fig. 61.10 Comparison between the two plants in terms of specific final yield

[16], the monthly values on the tilted collector are computed and represented in Fig. 61.9, along with the insolation in Amman as well. The yearly average insolation in Damascus is 5.56 kWh/m²/day, whereas that value is 5.71 in Amman.

According to the measured data of the Syrian PV plant [17], the energy production in 2013 (the third year of operation) was 6177 kWh and the specific yield was 1525 kWh/kWp, which is less than the specific yield of our Jordanian plant by around 7%. The lowest specific yield was found to be in January (92.59 kWh/kWp), while the highest value was in May (150.12 kWh/kWp). The specific yield of the Syrian plant exceeds that of the Jordanian plant in November and winter months (Fig. 61.10). This result is due to the higher array tilt angle (35°) of the Syrian plant compared to the 10° to 15° of the Jordanian plant.

Table 61.5 Comparison results in terms of main parameters

	Yearly insolation (kWh/m ² /day)	Specific final yield (kWh/kWp)	PR%	CF%
PV plant Jordan	5.71	1639	87.5	18.7
PV plant Syria	5.56	1525	88.2	17.4

The annual PR of the Syrian plant is 88.2 %, which is slightly greater than the PR of the Jordanian plant (87.5 %). It is calculated using Eq. (61.1):

$$\begin{aligned} \text{Actual annual PR}\% &= \frac{6177}{5.56 \times 36 \times 0.0156 \times 45 \times 365 \times 0.1365} * 100 = \frac{6177}{7000.675} * 100 \\ &= 88.2 \%. \end{aligned}$$

The CF of the Syrian plant is 17.4 %, which is less than the CF of the Jordanian plant by around 7 %. It is calculated using Eq. (61.3):

$$\text{CF}\% \text{ of Syrian plant} = \frac{6177 \text{ kWh}}{4.05 \text{ kW} \times 8760} * 100 = \mathbf{17.4} \%$$

The comparison results are summarized in Table 61.5.

8 Conclusions

A performance analysis of the 276 kWp grid-connected PV plant at AAU in Jordan was carried out in terms of main performance criteria such as specific final yield (Y_f), performance ratio (PR%), and capacity factor (CF%). The values of Y_f, PR, and CF were found to be 1639 kWh/kWp, 87.5 %, and 18.7 %, respectively. The plant was simulated using the program PVsyst v6.32. The estimated energy injected into the grid was found to be in good agreement with the actual energy production, with a relative deviation of around 5 %. A comparison of these values with evaluation parameters of reported PV plants in some countries revealed that our plant is among the best. A relatively extended comparison was conducted with a grid-connected PV plant in the region (Syria), which was briefly analyzed, and showed that the performance of both plants is approximately similar. Thus, the overall performance of the AAU PV plant was found to be excellent during the first year of operation, and the studied PV system represents a successful project in Jordan and in the region, which will help to justify installing more plants at the university and elsewhere.

References

1. EcoSol (2014) Complete energy solutions—practical case study. Presentation conducted at Al-Ahliyya Amman University
2. <http://www.spirea.de/solarlog-aau-arena/>
3. James M Bing (2015) Application note predicting and monitoring PV energy production. ECI Publication No Cu0207. www.leonardo-energy.org, Jan 2015
4. SMA Solar Technology AG, Performance ratio, Technical information Perfratio-UEN100810. <http://files.sma.de/dl/7680/Perfratio-UEN100810.pdf>
5. Cristian P, Chioncel, Ladislau Augustinov, et al. (2009) Performance ratio of a photovoltaic plant. Bulletin of Engineering, Copyright © University Politehnica Timisoara/Fascicule 2/April–June/Tome II, pp 555–58
6. Ebenezer NyarkoKumi, Abeeku Brew-Hammond. Design and analysis of a 1MW grid-connected solar PV system in Ghana. African Technology Policy Studies Network, ATPS 2013 ATPS Working Paper No. 78
7. Ralf Muenster, National Semiconductor. Watts matter: maintaining the performance ratio of PV systems. <http://www.solarindustrymag.com/>
8. Jahn U, Nasse W (2004) Operational performance of grid connected PV systems on buildings in Germany. Prog Photovolt Res Appl 12(6):441–448
9. Leloux J, Narvarte L, Trebosc D (2012) Review of the performance of residential PV systems in France. Renew Sustain Energy Rev 16(2):1369–1376
10. Leloux J, Narvarte L, Trebosc D (2012) Review of the performance of residential PV systems in Belgium. Renew Sustain Energy Rev 16(1):178–184
11. Huang HS, Jao JC, Yen KL, Tsai CT (2011) Performance and availability analyses of PV generation systems in Taiwan. World Academy of Science, Engineering and Technology, vol 54
12. Reich NH, Mueller B, Armbruster A, van Sark WGJHM, Kiefer K, Reise C (2012) Performance ratio revisited: is PR > 90% realistic? Prog Photovolt Res Appl 20(6):717–726
13. CHROISIS Sustainable Solutions (2012) Whitepaper on PR vs. CUF. <http://chrosis.de/wp-content/uploads/2012/12/PR-vs-CUF-WP.pdf>
14. Elhodeiby AS, Metwally HMB, Farahat MA (2011) Performance analysis of 3.6 kw rooftop grid connected photovoltaic system in egypt. International Conference on Energy Systems and Technologies (ICEST 2011), Cairo, 11–14 March 2011
15. Masters GM (2004) Renewable and efficient electric power systems, Stanford University, Wiley
16. Al-Mohamad A (2004) Global, direct and diffuse solar-radiation in Syria. Appl Energy 79:191–200, www.elsevier.com/locate/apenergy
17. Private communication with National Energy Research Center (NERC), Syria

Chapter 62

Gauging the Effectiveness of a Resource Management Awareness Campaign on a Central Mediterranean Island

Paul Refalo, Robert N. Farrugia, Luciano Mulè Stagno, Charles Yousif, Tonio Sant, Nora Jakkel, Anthony Zammit, and Joseph Portelli

Abstract The ‘Reduce and Save’ campaign aimed to promote environmental sustainability awareness on the island of Gozo. Gozo forms part of the central Mediterranean Maltese Archipelago and has been earmarked to become an eco-island through the implementation of a local sustainable development strategy by 2020. The campaign falls under the umbrella of a wider-ranging initiative known as the eco-Gozo project, under the auspices of the Ministry for Gozo. The Reduce and Save campaign consisted of the identification and training of personnel capable of conducting a number of home visits in an attempt to reach as many Gozitan households as possible. The home visits made by these personnel consisted of 30-min information sessions on energy, waste and water management aspects, the distribution of informational printed matter and the filling in of a questionnaire to enable data compilation on specific topics. This chapter assesses the results generated by the questionnaire in conjunction with other information sources. Analyses of questionnaire responses revealed that a favourable disposition towards renewable energy (RE) technologies and energy-saving and water-conservation measures already existed amongst Gozitan households. Data on RE installations and energy-saving ventures for the islands are compiled by national entities such as the National Statistics Office and the Malta Resources Authority. These and other sources are assessed in order to gauge the effects, if any, of the Reduce and Save campaign. Any impacts on the behavioural patterns of Gozitans following the campaign are assessed by comparing specific indicators for the island with similar information for the main island of Malta. While the results help to consolidate the information compiled, they also enable the refinement of the training and dissemination methodologies utilised as a means of tailoring a similar, albeit larger-scale,

P. Refalo • R.N. Farrugia (✉) • L. Mulè Stagno • C. Yousif • T. Sant • N. Jakkel
Institute for Sustainable Energy, Triq il-Barrakki, Marsaxlokk MXK1531, Malta
e-mail: robert.n.farrugia@um.edu.mt

A. Zammit • J. Portelli
Ministry for Gozo, Pjazza San Frangisk, Victoria VCT 1335, Gozo, Malta

campaign for the main island of Malta. Similar exercises aiming to increase awareness on environmental sustainability can also be replicated for other islands or communities.

Keywords Sustainability • Environment • Gozo • Malta • Energy • Water • Waste

1 Introduction

Malta, Gozo and Comino together make up the Maltese Archipelago. The islands, which are located in the Central Mediterranean basin and form part of the European Union, are small in size, with a total land area of 316 km², and heavily populated. The island of Gozo has around 31,000 inhabitants and an area of 67 km². Increasing environmental concerns have seen a number of initiatives aimed at improving energy efficiency and sustainability on the islands. The particular characteristics of the islands make them especially suited for case studies such as the eco-Gozo project [1], which aims to transform the smaller island of Gozo into an ecological island. The project, which is run by the Ministry for Gozo [2], consists of a number of sustainability-related initiatives, one of which was the Reduce and Save campaign. The ministry engaged the Institute for Sustainable Energy of the University of Malta [3] to manage this campaign. Courses were designed and delivered to a group of trainers, who were then assigned to visit as many Gozitan households as possible. The house calls were structured to consist of thirty-minute information sessions during which the trainers advised and discussed energy and environmental issues with residents and distributed informational printed material, such as brochures, which were prepared specifically for the initiative. Time was allocated during the home visit to fill in a questionnaire on sustainability issues and practices. Further information on this part of the initiative may be obtained in [4].

2 Method

The home visits commenced at the beginning of 2012, with the Reduce and Save campaign lasting a full 12 months. During this period, 8828 households were visited out of the 15,636 targeted. There are 25,070 houses on Gozo, with 11,630 which are permanently occupied, 7444 used seasonally and 5996 completely vacant [5]. A total of 15,636 Gozo dwellings were identified through the Electoral Register [6], identifying the owners of the households. The other 9434 households are either secondary dwellings or belong to persons who live permanently in Malta and would not be listed in the Gozitan register. The questionnaire, which was the primary tool used for data capture, yielded a number of interesting and positive results on the perceptions and habits of Gozitans concerning energy- and environment-related issues. Although this was in itself a positive outcome, the scope of the Reduce and

Save campaign was expected to have wider and longer-term impacts on the island of Gozo. This study investigates whether these goals were attained and whether they rendered longer-lasting benefits as part of the eco-Gozo vision.

Coincidentally, a national census had also been conducted by the National Statistics Office in November 2011 [5], just before the start of the Reduce and Save campaign, enabling the comparison of key indicators related to dwellings on both Malta and Gozo. Data on renewable energy (RE) installations and energy-saving ventures are also collected by the Malta Resources Authority [7]. This chapter shall take into consideration these different national sources to gauge the impact on the behavioural changes, if any, undergone in Gozitan households over the duration of and following the campaign.

3 Results and Discussion

3.1 *Energy-Efficiency Measures*

In recent years, the Maltese government has promoted a number of energy-efficiency and energy-saving measures. The most noteworthy are the following [7]:

- Compact fluorescent lamps (CFLs) were supplied to all households; the number of lamps supplied was related to the number of persons residing in each dwelling and amounted to almost 1 million bulbs;
- White goods (or whiteware) rated at Class A or better enjoyed a rebate of 15.25 % for a limited time;
- Roof insulation and double glazing in dwellings were supported by a grant of 15.25 % up to a maximum grant of € 1000. This grant is ongoing.

Of the energy-saving measures, the CFL initiative was widely implemented as the lamps were distributed free of charge, and the removal and replacement of inefficient light bulbs is an easy and straightforward process. As for appliances, results from the questionnaires compiled in this project [4] show that 62 % of all Gozo households had, at some time or other during the 5 years leading up to 2011, purchased one or more energy-efficient appliances.

Electricity generation reached a peak during 2007, with 2.3 million MWh on record [8]. The years 2009 and 2010 witnessed a reduction in electricity consumption in the Maltese Islands, after which the demand increased once again in 2011 and 2012. During 2012 solar photovoltaic (PV) installations contributed some 0.6 % to the overall electricity generation figure in the Maltese Islands [8].

Figure 62.1 shows the percentage change in electricity consumption when comparing the year 2012 to the previous year in the domestic and residential sectors [9]. A domestic meter is installed in a dwelling with a registered number of persons residing in it. By contrast, a residential meter is installed in a building, or part of it, in which persons do not reside permanently. A residential meter, for example, would be

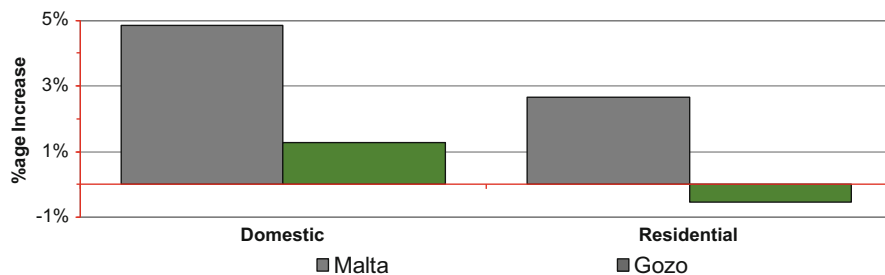


Fig. 62.1 Relative change in electricity consumption comparing years 2011 and 2012 in domestic and residential sectors

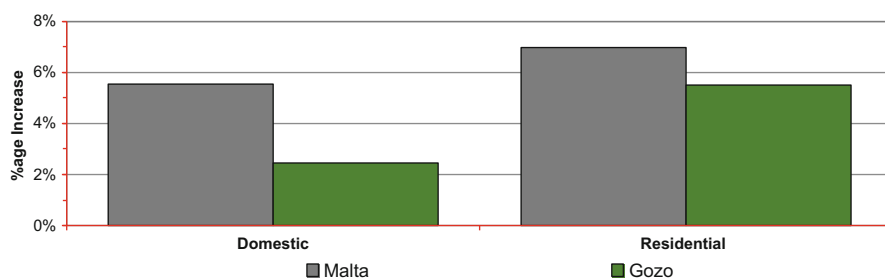


Fig. 62.2 Relative change in water consumption comparing years 2011 and 2012 in domestic and residential sectors

Table 62.1 Percentage change between 2011 and 2012 figures for electricity and water services in combined domestic and residential sectors

Service	Malta (%)	Gozo (%)
Electricity	+3.0	-0.2
Water	+6.8	+5.0

installed in the common areas of a block of apartments and in seasonally used dwellings. In the case of the main island of Malta, electricity consumption increased in both sectors. It is interesting to note that in the case of Gozo, the rate of change was lower in both the domestic and residential parts. Additionally there was a comparative decrease in residential sector consumption registered during the year when the Reduce and Save campaign was under way.

Figure 62.2 shows the change in water consumption for the same two sectors. It is interesting to note that water consumption increased on both islands, although the change on Gozo was lower (Table 62.1). One should keep in mind that the residential sector data are significantly affected by factors such as an increase in the influx of tourists or more holiday goers to one or both islands. Tourists spent 7.6% more nights on Gozo compared to the previous year [10]. However, the electricity used in the residential sector still saw a decrease.

The method of building construction and the materials used also contribute significantly to the energy performance of local dwellings. A number of measures could be implemented in new buildings, although older, already-existing houses will have to retrofit changes to components which are part of the building fabric. Simple measures to improve the energy performance rating of buildings consist in the use of shading materials to protect a building's flat roofs and side walls from direct solar radiation. The same applies to behavioural aspects of residents, such as switching lights off when rooms are unoccupied, reducing/increasing temperatures on air-conditioning units in winter/summer and opening doors and windows during hot summer months to lower indoor temperatures. Figure 62.3 shows the percentage of Gozitan households which applied the various energy efficiency measures to their homes. Natural night ventilation and air-conditioning unit temperature regulation were observed, with 79 and 35 % of respondents implementing these energy-saving measures.

Grants supporting roof insulation had a more limited uptake at the time of the home visits. Figure 62.4 shows the number of households benefitting from the grant in place for this measure [11]. The number of applications filed for financial support for roof insulation increased appreciably from 2012, a trend which could be indicative of the positive effects of the Reduce and Save campaign.

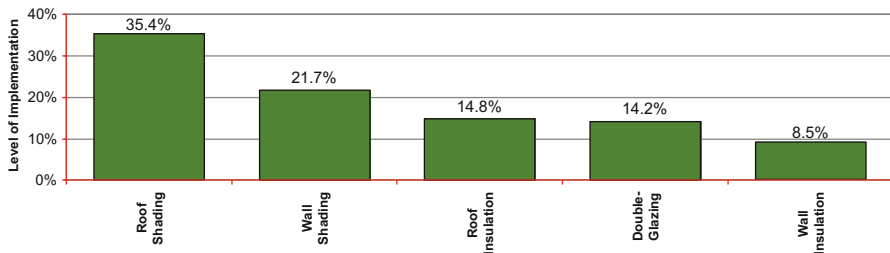


Fig. 62.3 Sustainable measures implemented in building fabric of Gozitan households at time of compilation of Reduce and Save campaign questionnaires

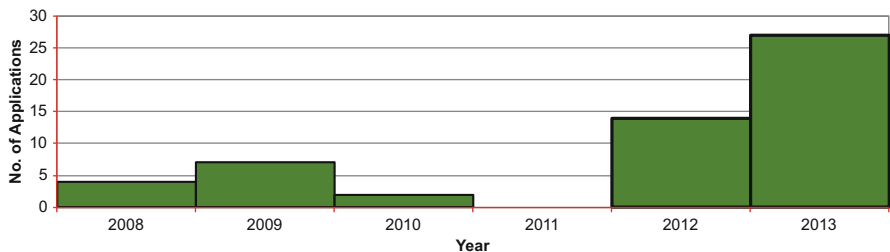


Fig. 62.4 Roof insulation implementation in Gozo for the period 2008–2013. The latter years following the Reduce and Save campaign are emphasized to show the possible effects of the Reduce and Save campaign home visits

The reported results indicate that the Reduce and Save campaign could have had an impact on the perceptions of Gozo homeowners, with data sources for the years immediately preceding, during and immediately following the campaign showing reductions in consumption and improvements in sustainable energy practices.

3.2 Solar Energy as a Sustainable Energy Option

The Maltese Islands enjoy a typical Mediterranean climate with hot summers and cooler winters [12]. The islands have amongst the best solar radiation levels in the EU Mediterranean states [13]. The main RE technologies installed in buildings have been solar water heaters (SWHs) and PV systems. In recent years, efforts to implement solar technologies have been spearheaded by specific grants offered by the government of Malta. The following sections examine the influence the Reduce and Save campaign had on homeowners as far as the installation of solar technologies is concerned.

3.2.1 Solar Water Heating Systems

SWHs have been installed in the Maltese Islands since the 1960s. These installations were set up by cost- and environmentally conscious individuals on their own personal initiative. More recently, the installation of such systems has been supported by a series of fiscal grants that generally compensate a percentage of the system's capital investment up to a maximum percentage or capping value. The 2005 Census of Population and Housing [14] and the later 2011 census [5] both showed that the island of Gozo had a higher number of SWHs installed per capita. Figure 62.5 shows the number of SWH systems installed per household for both islands in the period 2009–2012. It is evident that more systems were installed on Gozo. The trends indicate that there has been no significant increase in installation figures during 2012, and this could be due to a number of reasons:

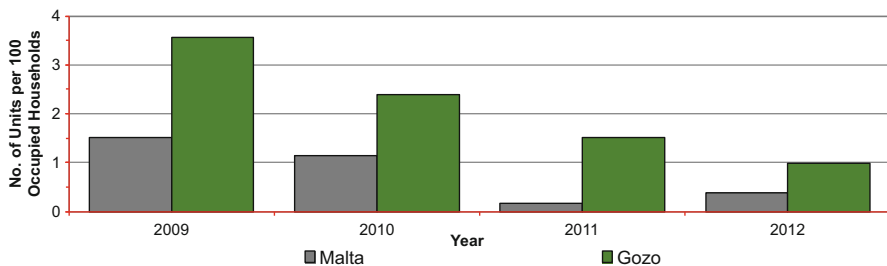


Fig. 62.5 Number of SWH systems installed per 100 households

- The grants for PV systems were more attractive than for SWH systems;
- The price of solar heating systems remained stable, whilst that of PV systems has dropped significantly over the years;
- Hot water is not needed throughout the year;
- PV electricity is more attractive than SWHs because electricity can be used for more applications;
- It is simpler to install PV than SWH systems because the latter require a certain degree of retrofitting in existing dwellings, both in terms of plumbing and related additional expenses, such as replacing tiles and the difficulty many encounter in not finding an exact match to the floor and wall tiles already installed in their bathrooms;
- PV systems can be used to export electrical energy for a price, whilst hot water is only used in-house;
- In Malta, 60.8 % of the dwelling stock comprises apartments and ground-floor maisonettes, which would typically not have access to rooftops. This value is much greater than the number of similar dwellings on Gozo, which is 28.2 % [5].

One should keep in mind that, notwithstanding the relevance of these observations, SWH systems still offer distinct advantages over solar PV:

- A SWH system requires a smaller footprint to produce the same amount of energy as that produced by a PV system;
- The cost of energy produced by a SWH is lower than for a PV system, provided that the solar heater is extensively used;
- SWHs can store energy, thereby reducing the peak loads on the power stations. This is particularly true in the evenings, when many residents use electric water boilers for domestic hot water needs. Notwithstanding this, the consumer has no particular interest in safeguarding this important feature, and the grants on solar heaters give no extra weighting to the energy storage capability of solar heaters.

3.2.2 Solar Photovoltaic Systems

In the case of PV systems, the fiscal incentives have been stronger than for SWHs, resulting in higher penetration levels of this technology. PV systems enjoyed a 50 % grant on capital costs, capped at a maximum of € 3000, in 2011. The installation of PV systems on the island of Gozo increased steadily between 2009 and 2012, as illustrated in Fig. 62.6, which shows the number of PV systems per 100 households. Over the 3-year period, installed PV systems increased substantially on the smaller island of Gozo, particularly during 2012 [15].

Figure 62.7 shows the percentage increase in the number of installations on an inter-year comparison basis, with 2012 showing an increase in the number of systems when the Reduce and Save campaign was in full swing. These trends could be attributed to the fact that there might be a higher level of awareness on Gozo or that the islanders enjoyed a higher feed-in tariff for PV-generated electricity than Maltese residents (Gozo residents enjoyed a feed-in tariff of € 0.28/kWh

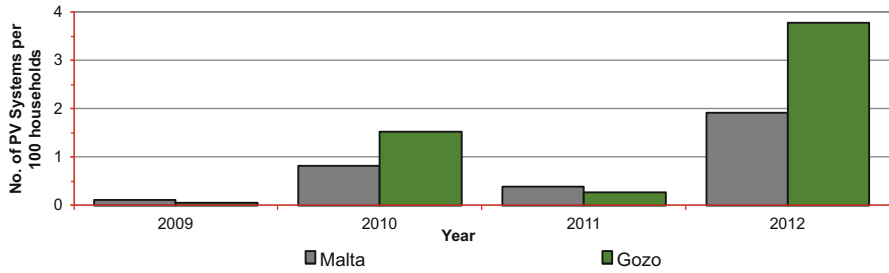


Fig. 62.6 Number of PV systems (per 100 households) on Malta and Gozo

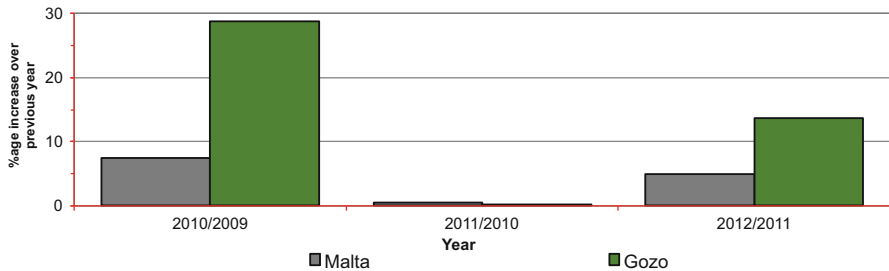


Fig. 62.7 Percentage increase in number of PV system installations on a yearly basis for Malta and Gozo

compared to the € 0.25/kWh for systems installed in Malta). Other aspects, such as the different and changing grant systems put in place over the years, could also have had an influence on these trends. The smaller number of installations in 2011 could be explained by the change in the grant which occurred in 2010. By September 2010, the funds allotted for PV systems had been fully used [16], and another grant which was issued in February 2011 was discontinued [17]. Another 2011 grant was kicked-off only in July of that year and was limited to 2000 households [18]. The grants had to be taken up within 10 days of initiating the call [19].

The fact that the process to have a PV system approved and installed is affected by a time lag of a few months might suggest that one might need to wait for additional data to become available in order to determine which factors are driving this technology on the island of Gozo.

3.3 Reducing, Reusing and Recycling Domestic Waste

Efforts to instil environmental awareness in citizens across the islands have been ongoing for a number of years, spearheaded by the local agency WasteServ (Malta) Ltd [20]. Waste collection on a door-to-door basis takes on a number of forms; for example, the Black Bag scheme captures mixed waste from homes and commercial

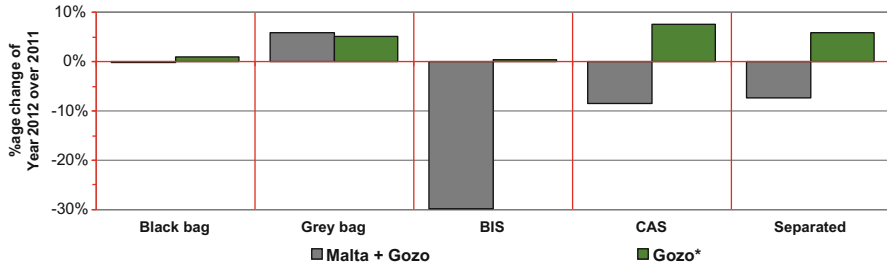


Fig. 62.8 Percentage change in waste collection tools for Malta and Gozo in a preliminary inter-annual comparison

enterprises, while the Grey (or Green) Bag scheme takes place on specific days and targets the collection of recyclable materials (paper/cardboard, metal, plastic) from households. The static Bring-in Sites (BIS) set up in different localities enable the separate disposal of paper, plastic, metal and glass items while Civic Amenity Sites (CASs) serve as hubs and offer regional facilities, where large items such as household furnishings, electrical/electronic appliances, automobile tyres and domestic hazardous waste may be disposed of. Free bulky refuse collection services also exist for both households and industry [20]. Waste collection has also seen private firms enter the waste management system in recent years.

The eco-Gozo project also targeted sustainable waste management as part of the Reduce and Save campaign. Analysis of data from the years immediately before and during the campaign shows (Fig. 62.8) that in the case of Malta, there was a reduction in various modes of waste collection. This could have been partly due to the entry of one or more private contractors in the provision of waste management services, and therefore the data in hand do not cover the full range of data for Gozo. The figures for Gozo* refer to collected waste taken for treatment at WasteServ facilities. It is worth remarking that in the case of waste recycling, an increase implies an improvement, although the possibility of increasing waste quantities could also be the case [11].

As far as Gozo is concerned, the increase in the level of Grey/Green Bag tonnage collected between the years 2011 and 2012 is very similar to the increase achieved on both islands (Malta and Gozo) together. There was a marginal increase in quantity in the case of the BIS waste on Gozo. CAS saw an increase in use of 7.6% on Gozo; however, the waste collected from all the CASs around both islands saw a decrease of 8.5%. Once again, one could argue that the increases could be due to more waste being generated. When comparing 2011 and 2012, there was a reduction of 7.4% in the amount of separated (Grey Bag, BIS, CAS) waste on the islands. However, on Gozo, this amount increased by 5.9% over the same period [11, 21, 22]. This might be an indication that the Reduce and Save campaign has improved the waste management practices in Gozo.

4 Conclusions and Recommendations for Future Work

This preliminary investigation into the efficacy of an island-wide knowledge transfer exercise aimed at instilling environmental awareness on energy, water and waste management has shown that residents on the island of Gozo already had pre-conceived perceptions of these issues and had implemented reasonable measures to introduce sustainable practices into their lifestyles at the time of the home visits.

Interventions such as roof and wall shading and roof and wall insulation were amongst the measures being implemented to improve the performance of buildings. Energy-saving practices, including natural night-time ventilation during the hot summer months and user intervention to control air-conditioning systems, were also being used. Residents were aware of the benefits of energy-saving appliances, with 62% of respondents having replaced their old appliances with energy-efficient versions.

The new and additional knowledge imparted by the Reduce and Save campaign could be discerned in a number of key indicators, which augur positively. These are as follows:

- Reductions in electricity and water consumption at the domestic and residential levels,
- Increase in the number of dwellings opting for roof insulation,
- Increase in the number of PV systems installed on Gozo,
- Increase in the waste management system's recycling components.

On the other hand, there seems to be a drop in the number of SWHs being installed, although the drivers of this trend seem to be more complex and beyond the immediate goals of this study.

These preliminary findings should form the basis of future work in the field. Further studies on the effectiveness of the Reduce and Save campaign could take place in the near future when more recent data become available. One way of scientifically determining whether the Reduce and Save campaign was effective and whether lifestyles and practices on the island of Gozo are becoming more sustainable would be to select a sample of households which were targeted in the original campaign for a second round of fact-finding meetings. This would help confirm whether these preliminary indicators were sending the right message.

Similar initiatives should be undertaken occasionally to keep the population abreast of the more recent developments and to retain the impetus of the knowledge transfer process from educators, scientists and experts to the general society. The eco-Gozo project and the Reduce and Save campaign should serve as showpieces for similar environmental awareness and sustainability dissemination methodologies aiming to increase awareness on environmental sustainability for islands or communities.

Acknowledgements The authors acknowledge the support of the staff at the Ministry for Gozo and the University of Malta. The authors also thank Ing. Marco Cremona, Prof Paul Pace, Ms Jeannette Fiott and other WasteServ personnel for their contributions to the 'Train the Trainers' exercise and for their support to the Reduce and Save initiative. The authors additionally extend

their gratitude to Mr George Said from the National Statistics Office for his help and suggestions. Last but not least, the authors acknowledge the important role played by the trainers in completing the tedious and time-consuming house visits.

References

1. EcoGozo web page. http://www.ecogozo.com/index.php?option=com_content&view=article&id=102&Itemid=36&lang=en
2. Ministry for Gozo, Pjazza San Frangisk, Victoria, Gozo. <https://mgoz.gov.mt/en/Pages/Home.aspx>
3. Institute for Sustainable Energy, University of Malta, Triq il-Barrakki, Marsaxlokk MXK1531, Malta
4. Refalo P, Mule' Stagno L, Farrugia RN, Yousif C, Sant T, Jakkell N, Zammit A, Portelli J (2014) The 'reduce and save' campaign: an island-wide resource management awareness initiative. In: World Renewable Energy Congress (WREC) XIII, London, United Kingdom
5. NSO (2014) Census of population and housing 2011. National Statistics Office, Valletta, Malta
6. Electoral Register—15 Apr 2011, Department of Information, Government of Malta, Valletta, Malta, 15 Apr 2011
7. Malta Resources Authority, Triq Aldo Moro, Marsa, Malta
8. Energy consumption in Malta: 2003-2012. National Statistics Office, Lascaris, Valletta, Malta, Tech. Rep. 193/2013, 9 Oct 2013
9. National Statistics Office, Lascaris, Valletta, Malta
10. Collective Accommodation Establishments (2013) http://www.nso.gov.mt/statdoc/document_view.aspx?id=3812&allEditions=true. Accessed Dec 2013
11. Private Communication (2014) National Statistics Office, Valletta, Malta, 27 Mar 2014
12. Galdies C (2011) The climate of Malta—statistics, trends and analysis, 1951-2010. National Statistics Office, Valletta, Malta
13. Oña Quecedo G, Yousif C, Bilbao Santos J (2010) Comparison of solar radiation in Marsaxlokk, Malta and Valladolid, Spain. In: World Renewable Energy Congress, Abu Dhabi, United Arab Emirates, 25–30 Sept, 2010, p 1515
14. NSO (2006) Census of population and housing 2005. National Office of Statistics, Lascaris, Valletta, Malta
15. Malta Resources Authority (2013) The uptake of photovoltaic systems in the Maltese residential sector. Malta Resources Authority, Marsa
16. Grech S (2010) The Times of Malta—no further subsidies on PV panels this year. TMI, 7 Sept 2010
17. The Times of Malta (2010) Photovoltaic panels scheme stopped prematurely—new scheme to be launched in June. ToM
18. The Malta Independent (2011) 2,000 families to benefit from latest PV panel scheme, 24 June 2011
19. Malta Government Gazette No. 18,773. No. 617—Malta Resources Authority—grant for the purchase of photovoltaic systems in the domestic sector—Call 2011/PV/1. p 8764
20. WasteServ Malta Ltd., Marsascala, Malta
21. Private Communication, WasteServ Malta Ltd., Marsascala, Malta
22. National Statistics Office (2012) Solid waste management in Malta. National Statistics Office, Valletta, Malta

Chapter 63

The 'Reduce and Save' Project: An Island-Wide Resource Management Awareness Initiative

Paul Refalo, Luciano Mulè Stagno, Robert N. Farrugia, Charles Yousif, Tonio Sant, Nora Jakkel, Anthony Zammit, and Joseph Portelli

Abstract The Republic of Malta is an archipelago composed of three inhabited islands – Malta, Gozo and Comino. The main island of Malta has one of the highest population densities in the world, at 1566 inhabitants/km², and is the largest island, with an area of 246 km². Gozo has about 31,000 inhabitants and an area of 67 km², while Comino is much smaller and has fewer than 10 inhabitants and a hotel. In 2008, the government of Malta, through the Ministry for Gozo, embarked on a programme with the aim of transforming Gozo into an eco-island. This initiative was called the eco-Gozo Project – a Local Sustainable Development Strategy for an Island and Its Community. As part of this undertaking, the ministry commissioned the Institute for Sustainable Energy at the University of Malta to conduct an educational campaign named 'Reduce and Save'. The aim of this campaign was to design and deliver information sessions on water and energy conservation, renewable energy and waste management in every household in Gozo. The main objectives of this initiative were to increase awareness and disseminate eco-friendly information with the aim of improving the quality of life and levels of sustainability on the island. The methodology consisted of training courses, examination of the trainers, the island-wide house-call programme, the approach used during the visits themselves and the results compiled through a specific questionnaire. These actions all served to couple an educational campaign focusing on sustainability and environment-related issues with a data-gathering exercise in an island community. The results showed a favourable opinion on renewable energy and energy-saving and water-conservation measures and gave a snapshot of the renewable energy installations (such as solar water heaters and photovoltaic systems), energy-saving measures (such as roof insulation and double glazing) and water-saving measures (such as recycling of grey water and the use of rainwater catchment in dwellings'

P. Refalo • L. Mulè Stagno • R.N. Farrugia (✉) • C. Yousif • T. Sant • N. Jakkel
Institute for Sustainable Energy, Triq il-Barrakki, Marsaxlokk MXK1531, Malta
e-mail: robert.n.farrugia@um.edu.mt

A. Zammit • J. Portelli
EcoGozo Regional Development Directorate, Ministry for Gozo, Pjazza San Franġisk, Victoria
VCT 1335, Gozo, Malta

existing water cisterns) at the time of the home visits. In the context of the development of a local, community-based sustainable development strategy, this initiative was instrumental in empowering and engaging the population at a time when this wide-ranging community project was being launched.

Keywords Sustainability • Citizen empowerment and engagement • Malta • Gozo • Energy • Water • Waste

1 Introduction

The Republic of Malta is located in the Central Mediterranean Basin and consists of three inhabited islands: Malta, Gozo and Comino (Fig. 63.1). The main island, Malta, is the largest and most densely populated, with an area of 246 km² and a population of over 386,000, while Gozo and Comino had 31,375 inhabitants in 2011 [1]. Gozo has a land area of 67 km², while Comino measures 3.5 km² and is virtually unpopulated. The Maltese Islands have a binding target to reach 10 % of primary energy consumption from renewable energy sources by 2020, according to the European Union (EU) Renewable Energy Directive [2]. Another important target is to reach a 20 % improvement in energy efficiency, as stipulated by the Energy Efficiency Directive [2, 3]. In 2008, the government of Malta, through the Ministry for Gozo [4], embarked on a programme with the aim of transforming

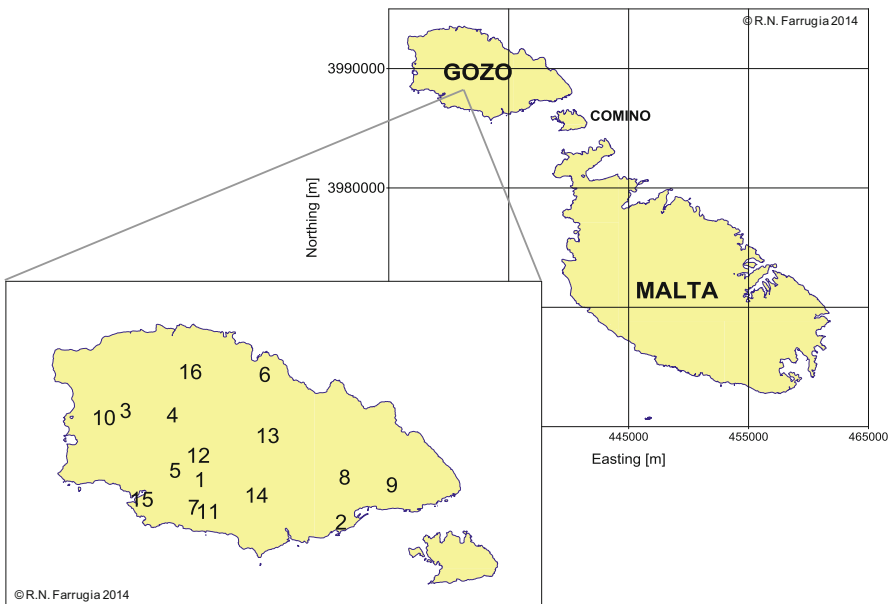


Fig. 63.1 Schematics showing Maltese archipelago and island of Gozo with locations of main towns/villages on the island (Table 63.1)

Gozo into an eco-island. This initiative was called the eco-Gozo Project – a Local Sustainable Development Strategy for the Island and Its Community [5]. The eco-Gozo strategy focuses on four main pillars: *'to bring together the environmental challenges on the island, the economic aspirations of its people, the development of society and the preservation of its cultural identity'* [6]. As part of this undertaking, the Ministry for Gozo commissioned the Institute for Sustainable Energy at the University of Malta [7] to design a campaign called Reduce and Save. The aim was to design and conduct outreach visits of 30-min informational sessions to every household on the island as a means of increasing awareness and disseminating eco-friendly information, with the aim of improving the quality of life of people and helping them improve levels of sustainability in their lifestyles. This chapter will assess the results collected during the Reduce and Save campaign.

2 Methodology

The Reduce and Save campaign consisted of a number of phases, starting with a public call for trainers. The trainers were expected to have a sound knowledge of science, engineering or architectural streams with a minimum level of education at the advanced level in associated subjects. The next step was the 'train the trainers' phase, which started in November 2011. The trainers were given over 40 h of training by experts on principles and theory of sustainability, the use of renewable energy, energy conservation, water conservation and waste resource management as applicable at a domestic level. The training also included modules on communication skills, as the sessions with the residents were envisioned to be interactive, with the trainer taking cues from observations within the household and through dialogue with the interviewees. The trainers were also provided with information on the eco-Gozo initiative, the rationale behind it and progress achieved until then. The training course was followed by an oral examination, with each trainer first being asked to lead a mock home visit followed by a question-and-answer session, testing the prospective trainer's ability to respond to typical questions that a homeowner might ask. A short questionnaire and an information leaflet with tips related to energy, water and waste management were also prepared for distribution during the home visits [8].

The following phase involved home visits. There are 25,070 houses in Gozo, of which 11,630 are permanently occupied, 7444 used seasonally and 5996 completely vacant [1]. A total of 15,636 Gozo dwellings were identified through the Electoral Register [9], identifying the owners of the households. The other 9434 households are either secondary dwellings or belong to persons who live permanently in Malta and would not be listed in the Gozitan register.

House visits were scheduled in a logical manner – first according to locality and then down to the street level. Prior to commencement of the programme of visits within a town or village, a notice to all households was mailed through the ministry, informing them of the project, its scope and the planned visit they had to receive.

Trainers were provided with official identification cards to allow homeowners to identify them as authorised representatives of the Reduce and Save campaign.

The visits to households were launched in January 2012, and by the end of the campaign, which lasted just over 12 months, almost 9000 home visits had been made. In cases where homeowners were not available at the time of the visit, a second attempt was made. Failing this, a note with the trainer's contact details was posted, allowing homeowners to set another appointment, if they so wished. There were only a few instances when a visit was declined.

Generally, a visit would last about half an hour, during which the information leaflet was handed out and discussions on the sustainable actions in everyday life were held. Towards the end of the visit, time was allocated for filling in the questionnaire. The aim of the questionnaire was to capture a snapshot of the environment and energy-related lifestyles and perceptions. The questionnaire also included a variety of questions on renewable energy and energy-saving measures at home, on water use and on quality-of-life issues related to the environment. Over 7000 questionnaires were filled in. In cases where homeowners requested further information, they were encouraged to contact the Institute for Sustainable Energy at the University of Malta for further technical or specialised support. In total, 8828 house visits were successfully concluded by the trainers, as shown in Table 63.1. This translates into a success rate of 57 % when considering the number of attempted house calls or 76 % if only occupied dwellings (11,630) are taken as the baseline.

One of the least successful localities in terms of successful house visits concluded was Marsalforn, a seaside hamlet forming part of the village of Żebbuġ. The majority (38 %) of the seasonal households in Gozo are found in this popular seaside summer resort.

Given the initial success of the project, the Ministry for Gozo and the Institute for Sustainable Energy took action, so that the campaign was subsequently extended to reach out to small businesses on the island. In all, a further 891 visits to businesses were made. Classification of this business category was made according to the business type and size. This classification included restaurants, coffee shops and bars as well as small retail outlets. A 65 % success rate was achieved in the case of this extension to the project. A large number of outlets were in the vicinity of the island's main town, Victoria, which is the main administrative and commercial hub servicing both locals and visitors to the island of Gozo.

3 Results and Discussion

3.1 Overview of Questionnaire Responses

The questionnaire was envisaged to capture a snapshot of Gozitans' aspirations, perceptions and actions on a number of sustainability-related issues. Questions addressed renewable energy installations, such as solar water heaters (SWHs) and

Table 63.1 Table showing number of house calls made with success rate as a percentage of total number of visits

Locality number	Locality	Population	Number of attempted house visits	Number of occupied dwellings	Number of successful visits	Success rate on attempted visits (%)	Success rate on occupied dwellings (%)
4	Ghasri	431	224	165	149	67	90
2	Ghajnsielem	2645	1293	963	855	66	89
9	Qala	1811	941	692	601	64	87
7/15	Munxar	1068	707	401	345	49	86
3	Gharb	1196	682	447	355	52	79
13	Xaghra	3968	2106	1458	1135	54	78
8	Nadur	3973	1860	1521	1146	62	75
10	San Lawrenz	610	297	222	167	56	75
12	Victoria	6252	2895	2240	1670	58	75
11	Sannat	1837	776	637	473	61	74
1	Fontana	882	413	330	232	56	70
14	Xewkija	3143	1326	1147	794	60	69
16/6	Żebbuġ	1841	1224	798	530	43	66
5	Ker-em	1718	892	609	376	42	62
	Total	31,375	15,636	11,630	8828	57	76

Fig. 63.2 Actions perceived to improve quality of life in line with eco-Gozo concept

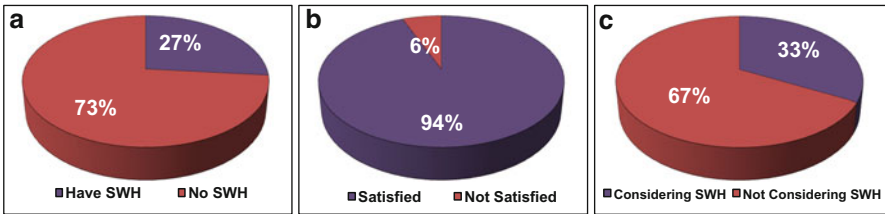
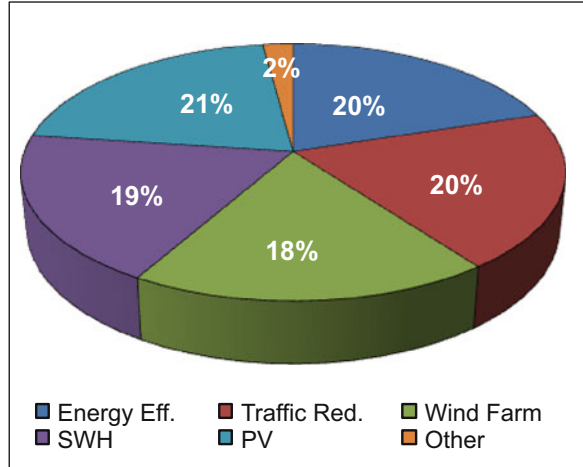


Fig. 63.3 Questionnaire results for solar water heating systems in Gozo. Respondents were asked whether they (a) own a SWH, (b) are satisfied with their SWH, (c) consider installing a SWH

photovoltaic (PV) systems, energy-saving measures (e.g. roof insulation and double glazing) and water-saving measures (such as recycling grey water and using rainwater catchments in dwellings’ water cisterns).

The first question asked about what measures were perceived to be most in line with achieving the eco-Gozo vision. Respondents were asked to state which actions contributed most to this ideal. The installation of PV systems, energy efficiency, traffic reduction, installation of SWHs and the development of an offshore wind farm were seen as the most important initiatives that could be undertaken – and in this order of importance (Fig. 63.2).

Other questions focused on the presence and effectiveness of SWH systems in Gozitan households. Traditionally, local dwellings use electrical resistance hot water boilers with storage for their domestic daily hot water requirements, with a typical efficiency of 75%. SWH systems were installed in 27% of respondent homes (Fig. 63.3a), and the majority of these were satisfied with the system’s performance (Fig. 63.3b). Of those not having such a system, 33% were in favour of installing a SWH at some point in the future (Fig. 63.3c). The average estimated energy generation of a solar heater is 1650 kWh_{thermal}.

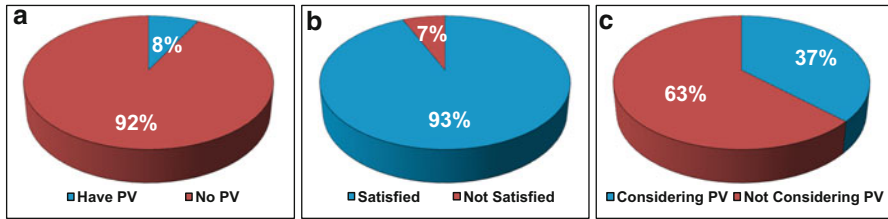


Fig. 63.4 Questionnaire results for photovoltaic systems in Gozo. Respondents were asked whether they (a) own a PV system, (b) are satisfied with their PV system, (c) consider installing a PV system

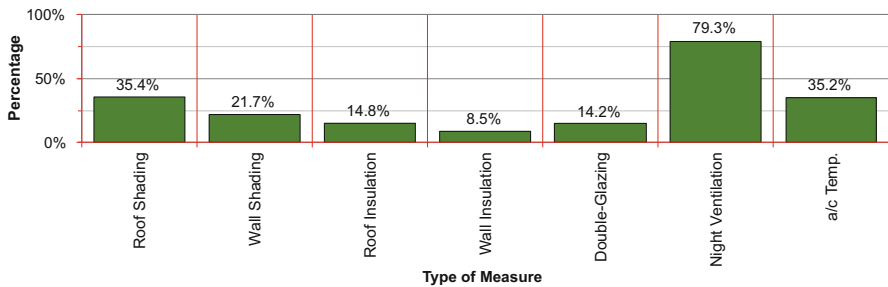


Fig. 63.5 Energy-saving and energy-efficient measures implemented in Gozitan households

PV systems have penetrated the Gozo market to a lesser degree when compared to SWHs, with only 8 % of respondents having the former system installed at the time of the visits. Many interviewees were satisfied with their system’s performance. A marginally higher number of respondents would consider the installation of a PV system in the future (Fig. 63.4a–c). The average size of a residential PV system was calculated to be around 2 kWp, which corresponds to an annual electrical energy output of around 3200 kWh/year [10].

Construction methods used in contemporary dwellings could contribute significantly to energy efficiency in the domestic sector. A number of measures could be designed and implemented in new buildings, although older, already existing houses will have to retrofit improvements to the building fabric. Residents’ behaviour will also affect a building’s energy performance. Figure 63.5 shows the various measures that Gozitan households were implementing at the time of the house calls. Night-time natural ventilation – particularly during the hot summer season – is seen as the most frequently implemented measure, with roof and wall shading, as well as air-conditioner thermostatic control, coming in as the next most frequently implemented measures.

Another question delved into whether Gozitan families had purchased energy-efficient appliances during the preceding 5 years, with about 62 % of the respondents answering in the affirmative.

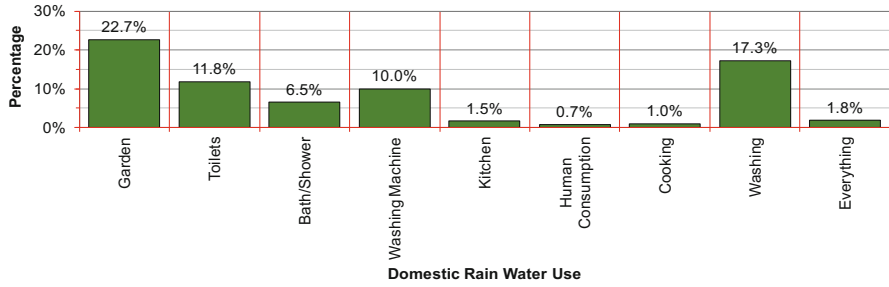


Fig. 63.6 Rainwater catchment in wells is utilised for different tasks at domestic level

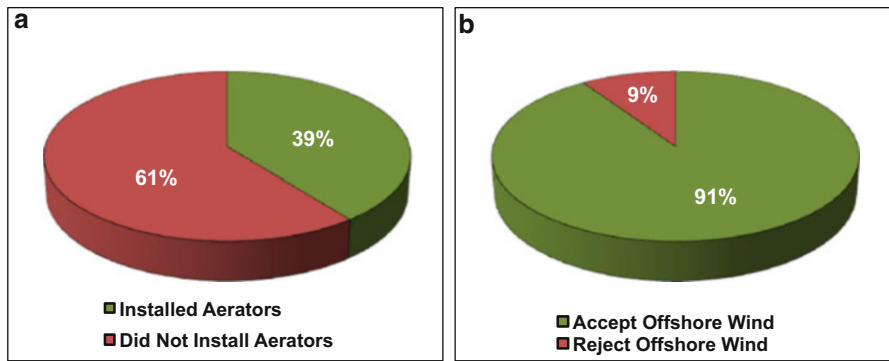


Fig. 63.7 Pie charts showing (a) number of households that installed aerators on water faucets and (b) response to acceptability of offshore wind farm off the coast

Water-conservation awareness was addressed in another set of questions. As far as potable water is concerned, 79% of respondents use bottled mineral water, followed by 14% consuming water produced by domestic small reverse osmosis (RO) units. Only 7% claimed to be using mains water, rainwater stored in wells or filtered mains water. The high use of bottled water gives rise to waste generation in the form of plastic bottles. Building regulations make it mandatory for every home to have a rainwater reservoir [11]. However, only 28% of respondents had a well or a cistern for rainwater catchment in place. This is quite low considering that buildings in the Maltese Islands have flat roofs and that rainwater may be conveyed and stored in wells within premises. Those having cisterns used the water for a variety of domestic tasks, with a minority extending use of this water to personal hygiene or consumption (Fig. 63.6). This latter use is not particularly recommended because there is no guarantee that the water is safe for such purposes, unless the water is subjected to frequent testing for quality and sanitation.

In a bid to increase the rational use of water and engage the population, the Ministry for Gozo had previously distributed free water aeration kits to be fitted to kitchen faucets to encourage water conservation. Figure 63.7 shows that the majority of homeowners did not install these gadgets. One of the reasons reported to the trainers was that the aerator reduced the water pressure at the outlet.

Another question addressed wind energy systems, with a total of 91% of respondents in favour of offshore wind farms, regardless of whether or not this would be visible from the shore (Fig. 63.7b). In a densely populated archipelago, such a result is quite interesting.

4 Conclusions and Recommendations

The Reduce and Save project served as a combined educational campaign, an initiative to empower and engage the community in the development of a local sustainable development strategy and a fact-finding initiative in an island scenario. The project structure enabled a small core of experts in the fields of energy, waste, water conservation and sustainability to extend and convey knowledge to the wider population through the training of a team of trainers. The methodology used, consisting of the selection and training of the trainers, the structuring of the house calls with the preparation of informational material and the data-gathering component in the form of the questionnaires were critical components necessary to render the project effective.

From the questions and additional comments submitted by respondents, a general outline of public perceptions and the islanders' receptiveness to certain initiatives may be drawn up. Residents on the island of Gozo appear to be receptive to an increase in the use of renewable energy technologies. This is quite understandable considering that Gozitans were given, for a limited time, preferential feed-in tariffs (€0.28/kWh) when compared to their Maltese counterparts (€0.25/kWh), although this in itself might not be the only reason. A complementary study [12] was undertaken to gauge the effectiveness of the Reduce and Save campaign's home visits by comparing trends based on different national information sources in the energy, waste and water sectors. This analysis strove to see whether the campaign had an impact on Gozitan households in comparison with the main island of Malta.

As for the customer satisfaction aspect, solar systems should be installed according to best practices because their correct operation will instil confidence and serve as showcases for further market penetration. On a similar note, the potential for energy efficiency in households is only partly tapped, and new schemes are required to encourage people to replace appliances with high-efficiency products, which are often more expensive but cost-effective in the long-term.

Grey water management is another area worthy of attention, particularly in the residential and tourist sectors. The construction of cisterns in dwellings and the promotion of rainwater catchments in public areas are also highly commendable. The Ministry for Gozo has already embarked on this initiative together with other stakeholders under the Alter Aqua Initiative [11]. Moreover, since 2010, the eco-Gozo Regional Development Directorate has embarked on an ongoing valley cleaning campaign in order to increase the rainwater harvesting potential, which to date has increased by more than 50,000 m³ of water.

Given that Gozo is around 35 km from the main power station, located in the south of Malta, it is sensible to save electricity and as far as possible generate it on the island of Gozo itself. This will reduce losses due to electrical power transmission, thereby also reducing CO₂ emissions at the point of generation. The attractiveness of an offshore wind farm off the coast is worthy of further consideration, as the population seems amenable to such a development.

Most importantly, this project highlighted the fact that the population is keen to participate in and contribute towards the achievement of the eco-island ideal being pursued for their island through the eco-Gozo project. Moreover, it proved to be a very effective way to increase awareness among the population and to empower and engage citizens on a personal level to partake directly in the achievement of higher standards of sustainability for their island through the eco-Gozo venture.

Acknowledgements The authors would like to acknowledge the support of the staff at the Ministry for Gozo and the University of Malta. The authors would also like to thank Ing. Marco Cremona, Prof. Paul Pace, Ms Jeannette Fiott and other WasteServ personnel for their contributions to the ‘Train the Trainers’ exercise and for their support to the Reduce and Save initiative. Last but not least, the authors acknowledge the important role played by the trainers in completing the tedious and time-consuming house visits.

References

1. NSO (2014) Census of population and housing 2011. National Statistics Office, Valletta, Malta
2. Ministry for Resources and Rural Affairs (MRRRA), Floriana, Malta (2010) Malta’s national renewable energy action plan as required by Article 4(2) of Directive 2009/28/EC
3. Malta indicative national energy efficiency target for 2020 in accordance with Article 3 of Directive 2012/27/EU, Apr 2013
4. Ministry for Gozo, Pjazza San Frangisk, Victoria, Gozo. <https://mgoz.gov.mt/en/Pages/Home.aspx>
5. Eco-Gozo (2009) A better Gozo: proposed action 2010–2012. Ministry for Gozo, Pjazza San Frangisk, Victoria, Gozo
6. EcoGozo web page. http://www.ecogozo.com/index.php?option=com_content&view=article&id=102&Itemid=36&lang=en
7. Institute for Sustainable Energy, University of Malta, Triq il-Barrakki, Marsaxlokk MXK1531, Malta
8. Ministry for Gozo, Pjazza San Frangisk, Victoria, Gozo. Naqqas u Ffranka—promotion of sustainable energy, water and waste management practices in Gozitan households
9. Electoral Register—15 April 2011, Department of Information, Government of Malta, Valletta, Malta, 15 Apr 2011
10. Malta Resources Authority (2013) The uptake of photovoltaic systems in the Maltese residential sector. Malta Resources Authority, Marsa
11. Services Division, Building Regulations Office, Malta. Document F—technical guidance on conservation of fuel, energy and natural resources (minimum requirements on the energy performance of buildings regulations 2006)
12. Refalo P, Farrugia RN, Stagno LM, Yousif C, Sant T, Jakkal N, Zammit A, Portelli J (2014) Gauging the effectiveness of a resource management awareness campaign on a central Mediterranean island. In: World Renewable Energy Congress (WREC), London, UK

Chapter 64

Heat and Light Intensity Influence on (I–V) Characterization of Cu₂S Film/p-Si Heterojunction

M. Saadeldin, M.M. El-Nahass, and K. Sawaby

Abstract Cuprous sulphide was deposited on p-type silicon substrate by thermal evaporation techniques, to form a Cu₂S film/p-Si heterojunction, and deposited on glass to measure the thermoelectric power. The thickness of the Cu₂S film is $d = 113$ nm, the structure of the Cu₂S thin film was investigated by X-ray diffraction. Surface morphology and grain size were obtained by transmission electron microscopy. The thermoelectric power of the Cu₂S thin film was obtained and the Seebeck effect was positive, which refers to a p-type semiconductor. Current–voltage (I–V) characteristics in the dark at temperatures ranging from 393 to 373 K were investigated. I–V characteristics in illuminance at light intensities from 1400 to 22,000 lx were investigated by changing the distance between the light source and the sample.

Keywords I–V characteristics of Cu₂S film/p-Si • Thermal evaporation

1 Introduction

Recent investigations have attracted considerable interest in Cu₂S thin films because of their extensive potential applications in solar cells, photothermal conversions of solar energy as solar absorber coating, electroconductive coatings, solar control coatings, microwave shielding coatings and sensors [1, 2]. They have also been used in air-glass tubular solar collectors as absorber coatings in photodetector and photovoltaic applications. Cu₂S thin films are efficiently used in solid junction solar cells that have many applications as direct conversion devices. Cu₂S is known to be an excellent heterojunction partner with CdS. Much attention has been focused on thin-film CdS/Cu₂S heterojunctions owing

M. Saadeldin (✉) • K. Sawaby
Physics Department, Faculty of Science, Cairo University, Giza 12613, Egypt
e-mail: msaadeldin@hotmail.com

M.M. El-Nahass
Physics Department, Faculty of Education, Ain-Shams University, Cairo 11757, Egypt

to their great promise as a low-cost solar power converter because of their high efficiency with improved stability [3]. Si/Cu₂S heterojunctions used as a photo-detectors cuprous sulphide exist in several crystallographic and stoichiometric forms including chalcocite (Cu₂S, orthorhombic), djurleite (Cu_{1.96}S, orthorhombic), digenite (Cu_{1.8}S, orthorhombic), anilite (Cu_{1.75}S, orthorhombic) and covellite (CuS, hexagonal). Cu₂S thin films have been prepared using various deposition techniques, such as chemiplating, solid-state reaction, sputtering, spray pyrolysis, flash evaporation, a photochemical method and a vacuum evaporation method. Copper sulphide has been investigated both in bulk and thin-film form with regard to its.

1.1 Thin-Film Preparation

The cuprous sulphide powder used in this research was obtained from Sigma-Aldrich Corp. (St. Louis, MO), with a purity of 99.99%. Thin films of Cu₂S were deposited onto p-Si single-crystal and glass substrates by a conventional thermal evaporation technique, using a high vacuum coating unit (Edwards, E306 A). The films were deposited from a molybdenum evaporator boat containing Cu₂S powder in a vacuum at 10⁻⁵ Pa. The deposition rate was controlled at 2.5 nm s⁻¹ using a quartz crystal thickness monitor (FTM, Edwards). The thickness of the film was 113 nm.

2 Results and Discussion

2.1 Structural Properties

2.1.1 X-Ray Diffraction Investigation

The structural properties of both powder and thin film were investigated using an X-ray diffraction (XRD) technique. A Philips X-ray diffractometer (X'Pert model) was used for measurements, with monochromatic Cu K α , operated at 40 kV and 25 mA). The XRD patterns for Cu₂S in powder form and as-deposited Cu₂S film on glass substrate are shown in Fig. 64.1.

In Fig. 64.1, the XRD pattern shows that both the powder of Cu₂S and the thin film have a polycrystalline form. By indexing the peaks, Cu₂S is defined as an orthorhombic crystal system with a lattice parameter [$a = 11.82 \text{ \AA}$, $b = 27.05 \text{ \AA}$, $c = 13.43 \text{ \AA}$] from a card number (ICCD Card Number 09-0328). The value of the crystallite size was calculated using the Scherrer equation [4]

$$D = \frac{0.9\lambda}{B \cos \theta},$$

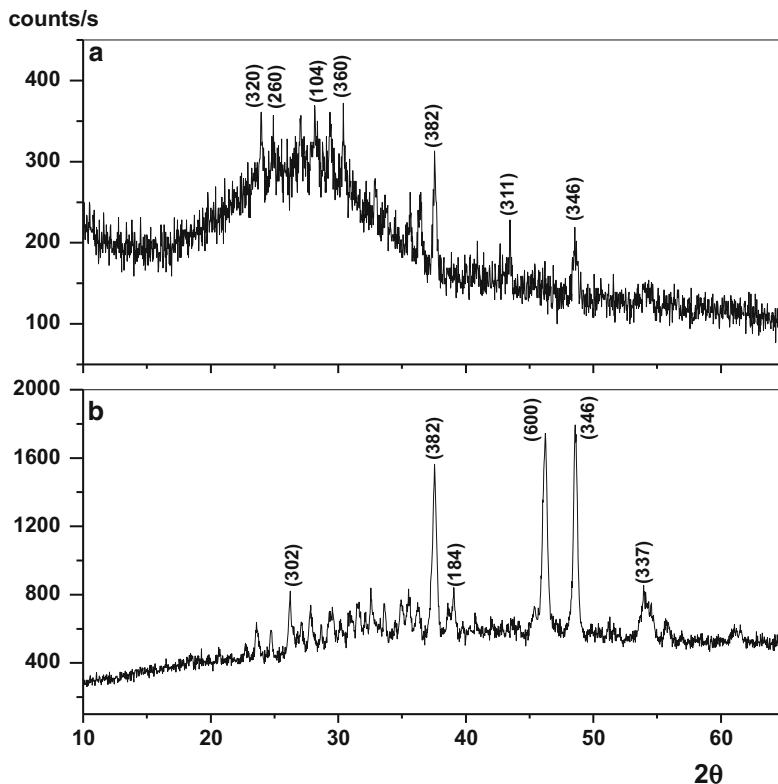


Fig. 64.1 XRD pattern: (a) Cu₂S powder, (b) deposited Cu₂S film

Table 64.1 Dependence of crystallite size on thickness of as-deposited Cu₂S

Film thickness (nm)	125	200	260	335	400
Crystallite size (nm)	28	85	120	190	245

The d planes, the Bragg, s angle, and hkl are shown in Table 64.2.

where $\lambda = 1.54 \text{ \AA}$ for Cu $K\alpha$, B is full width at half maximum, and θ is Bragg's angle. Table 64.1 shows that the crystallite size increases with increasing film thickness.

2.1.2 Transmission Electron Microscopy Microanalysis

A transmission electron micrograph for a deposited Cu₂S thin film with thickness 113 nm is shown in Fig. 64.2. This figure illustrates a nano-crystalline structure with an average grain size of 43 nm. The surface morphology is homogeneous.

Table 64.2 Presentation of analysis of XRD by calculating d spacing and hkl at different θ

d -Space	3.7139	3.5731	3.2990	3.1617	3.0387	2.9398	2.7193	2.5177	2.4659	2.393
2θ	23.9	24.89	27	28.2	29.36	30.37	32.78	35.6	36.4	37.5
HkIl	320	260	153	104	342	360	362	451	460	382

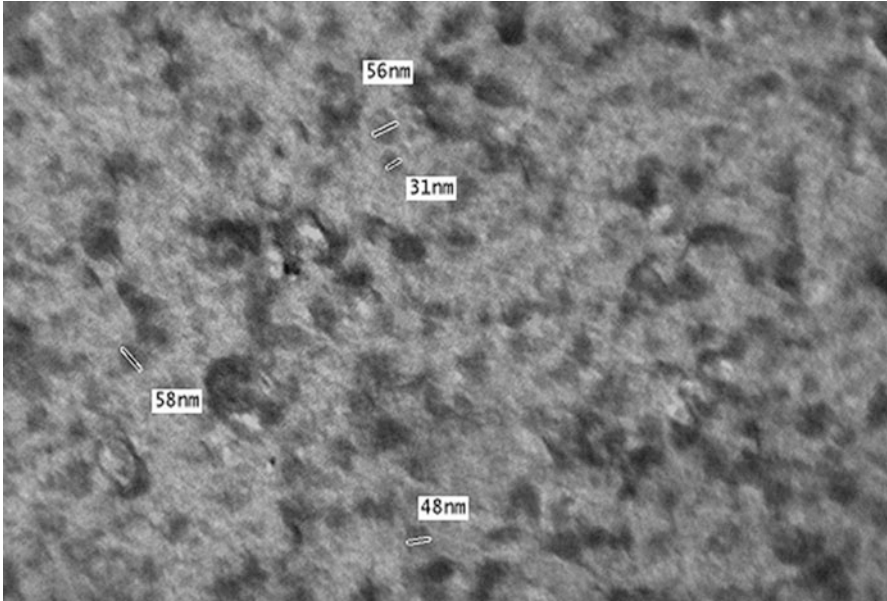


Fig. 64.2 Transmission electron microscope images of Cu₂S film

Atomic-force microscopy (AFM) measurements were performed in a $5 \times 5 \mu\text{m}$ scan area as shown in Fig. 64.3a, b. The AFM technique provides a direct observation of the surface morphology of the prepared film. The two-dimensional (2D) and three-dimensional (3D) AFM images of the Cu₂S film are shown in the figure. The film exhibits nanoparticles with an average size of around 44 nm.

The mean radius and roughness of the particles have been measured using a computer program. The as-deposited film has a comparatively smoother surface. Both the mean radius and roughness of the film particles increase with annealing temperature, as observed in Table 64.3

2.2 Thermoelectric Powers

The thermoelectric power of a Cu₂S thin film with a thickness of 419 nm has been studied. Figure 64.4 shows the temperature dependence of the thermoelectric power (S) of an as-deposited film.

It was found that S is always positive, indicating the p-type nature of Cu₂S films. The temperature dependence of S in the case of p-type semiconductors is given by [5]

$$S = \frac{k_B}{e} \left(A + \frac{\Delta E_S}{k_B T} \right), \quad (64.1)$$

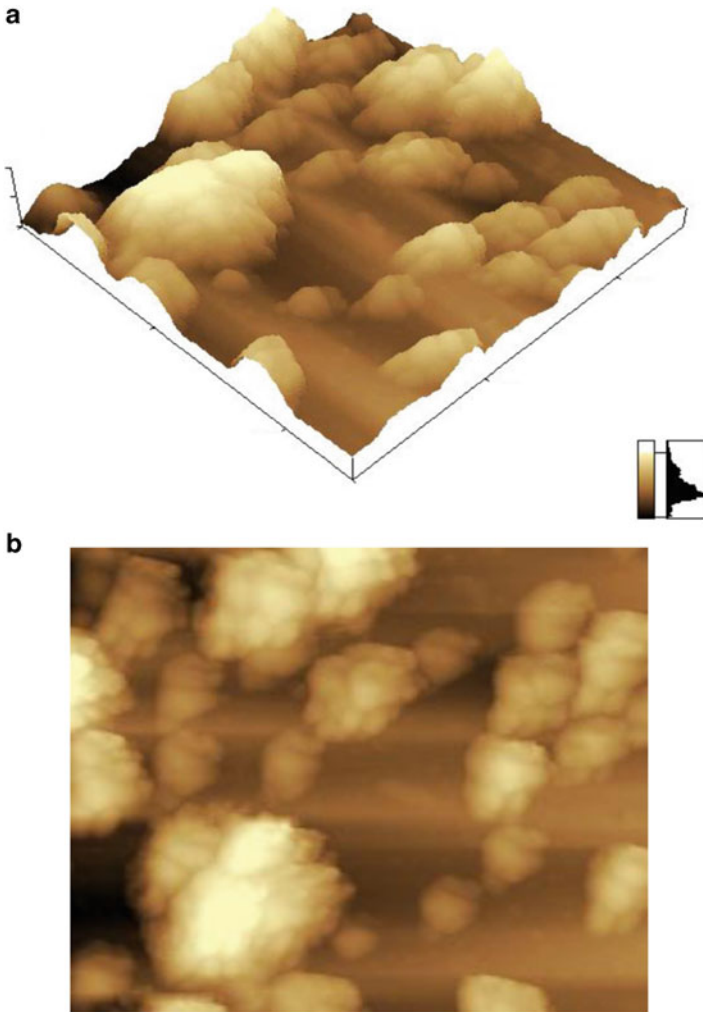


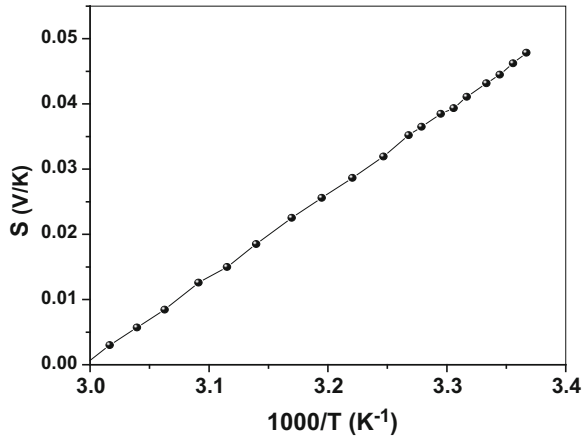
Fig. 64.3

Table 64.3 Calculation of mean radius and roughness of as-deposited and annealed films

Cu ₂ S film	Mean radius μm	Mean roughness μm
As-deposited	0.107	1.58
Annealed	0.125	1.8

where ΔE_S is the activation energy of the thermoelectric power, e is the electronic charge, and A is a constant depending on the nature of the scattering process. From Fig. 64.4, the slope of the straight line yields ΔE_S and the intercept on the S -axis at $I/T = 0$ yields A .

Fig. 64.4 Variation of Seebeck coefficient, S , with $1000/T$ thin films with different thicknesses



2.3 Characteristic in the Dark at Different Temperature

The I–V characteristic of a Cu_2S thin film/p-Si single crystal at different temperatures ranging from 303 to 373 K make it possible to determine specific parameters of the junction such as the diode quality factor (n), the rectification ratio (RR), the series resistance (R_s), and the barrier height at the junction interface (Φ) [6]. The dark I–V characteristics are extremely useful in identifying the transport mechanism's operating conduction. The I–V characteristics of a Cu_2S thin film with a thickness of 113 nm deposited on a p-Si single crystal at different temperatures are illustrated in Fig. 64.5. The device clearly exhibits the rectification behaviour in dark, which is enhanced by increasing the temperature. The curves exhibit diode-like behaviour [7]. With the forward direction to the positive potential on Si. This behaviour can be understood by the formation of an n–p heterojunction, namely the barrier at the interface limits forward and reverse carrier flow across the junction, where the built-in potential could be developed. The experimentally measured characteristics of a non-ideal diode often present a more complex behaviour than the ideal that the summation of two exponential expressions is frequently used to model [8]:

$$I = I_{01}[(\exp e(V - IR_s/n_1k_B T) - 1) + I_{02}[\exp e(V - IR_s/n_2k_B T) - 1] + (V - IR_s/R_{sh}), \quad (64.2)$$

where I_{01} and I_{02} are the reverse saturation currents, n_1 and n_2 are the diode quality factor, and R_s and R_{sh} are the series resistance and the shunt resistance, respectively. The calculated values of I_{01} , I_{02} , n_1 , and n_2 are shown in Table 64.4.

Fig. 64.5 Forward current semi-logarithms of Cu₂S film/p-Si heterojunction at different temperatures with voltage

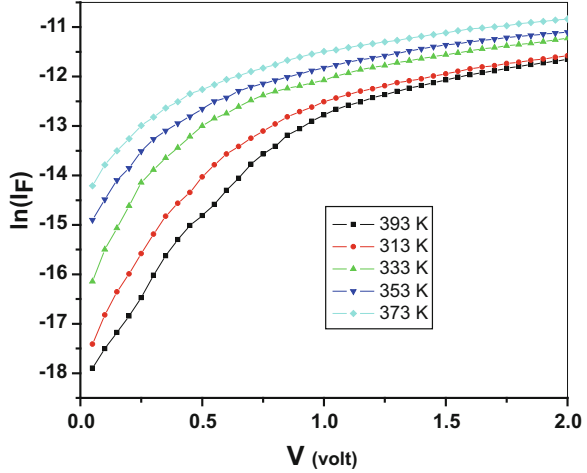


Table 64.4 Calculated values of I_{01} , I_{02} , n_1 , and n_2

kT/q	I_{01}	I_{02}	n_1	n_2
0.033	1.3×10^{-8}	3.4×10^{-7}	3.9	14.8
0.026	2×10^{-8}	6.8×10^{-7}	4.5	23.9
0.028	8.3×10^{-8}	1.85×10^{-6}	4.6	30
0.030	3×10^{-7}	2.5×10^{-6}	5.8	31
0.032	6.2×10^{-7}	3.7×10^{-6}	6.5	33

2.4 Junction Parameters

Figure 64.5 shows a semi-logarithmic plot of the forward current of a Cu₂S film/p-Si heterojunction at different temperatures with voltage. It shows a linear exponential increase in the forward current with applied voltage for the junction. In the reverse biasing, the current also increases non-linearly at low temperatures. The device has a photovoltaic effect.

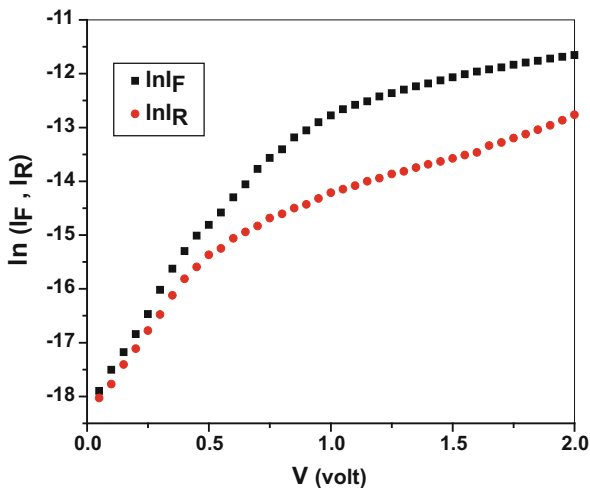
2.4.1 Rectification Ratio

The rectification ratio (RR) is defined as the ratio of the forward current to the reverse current at a certain value of the applied voltage:

$$RR = I_F/I_R. \tag{64.3}$$

The calculated RR at 1 V for the investigated device was found to be 4.3 at room temperature (Fig. 64.6).

Fig. 64.6 Forward and reverse current semi-logarithms of Cu₂S film/p-Si heterojunction at room temperature with voltage



2.4.2 Series Resistance

The series resistance R_s (material resistance and contact resistance in the junction) is an important parameter in improving a cell. Its value can be calculated from the slope of the linear part of the voltage difference against the current, obtained from Fig. 64.7 by drawing the semi-logarithmic forward current against the applied voltage at room temperature for the Cu₂S film/p-Si heterojunction [9].

The obtained value of the R_s was 104 K Ω .

2.5 Conduction Mechanism of p-Cu₂S Film/p-Si Single-Crystal Heterojunction

2.5.1 Temperature Dependence of I–V Characteristic

The temperature dependence of the $I_F - V$ characteristic was measured in order to investigate the current transport mechanism. The forward $I_F - V$ characteristics were first fitted to the standard diode equation:

$$I_F = I_{01} \exp(qV/n_1 k_B T) + I_{02} \exp(qV/n_2 k_B T), \quad (64.4)$$

where I_0 is the saturation current and n is the quality factor. The semi-logarithmic plots of the forward current voltage characteristics of p-Cu₂S film/p-Si single-crystal heterojunction at different temperatures ranging from 303 to 373 K are shown in Fig. 64.7. The forward characteristics can be divided into two regions, so there is a different conduction mechanism. At low voltage characteristic $V \leq 0.25$ V the forward bias current increases exponentially with voltage. The forward $I_F - V$

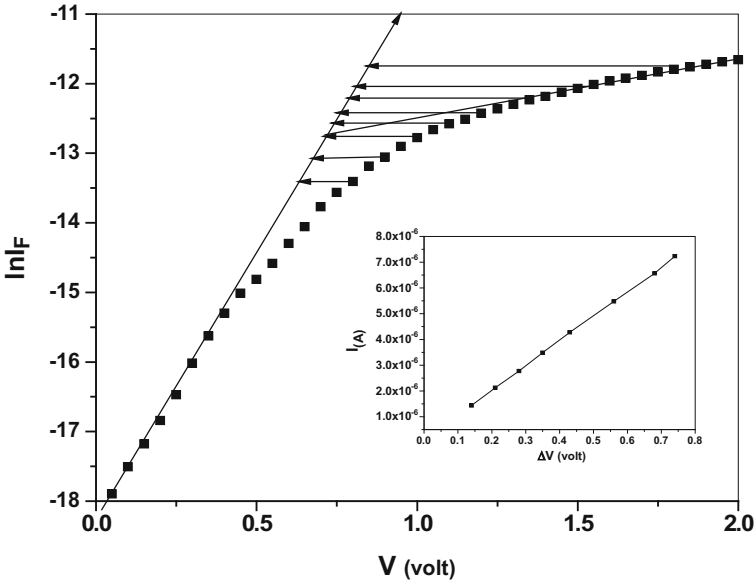


Fig. 64.7 Semi-logarithms of forward current against voltage at room temperature. The figure inside is the voltage difference against current

characteristics were first fitted to the standard diode equation (64.4), where I_0 can be obtained by extrapolation of the linear $\ln I_F - V$ portion to the $\ln I_F$ axis at zero voltage and n can be evaluated from the slope of the linear fit region. The values of n are higher than unity; this may be attributed to either a recombination of free carriers in the depletion region or an increase in the diffusion current. The quality factor is almost found to be variable at different temperatures, as in the upper table. The behaviour is in accordance with thermionic emission [10]. To confirm that the thermionic emission is the operating mechanism, more analysis must be carried out. According to the thermionic emission the saturation current I_0 is given by

$$I_0 = CT^2 \text{EXP}(-\Phi/kT), \tag{64.5}$$

$$\ln(I_0/T^2) = \ln C + (-\Phi/kT), \tag{64.6}$$

where Φ is the barrier height, and C is a constant. The plot of the logarithms of (I_0/T^2) against $1000/T$ supports the thermionic emission mechanism. From Fig. 64.8 the barrier height Φ is 0.48 eV.

2.5.2 Temperature Dependence of $I_R - V$ Characteristic

The typical dark reverse $I_R - V$ characteristics at different temperatures are shown in Fig. 64.8. The reverse current shows a dependence on the voltage. This is

Fig. 64.8 Semi-logarithms of (I_0/T^2) against $1000/T$

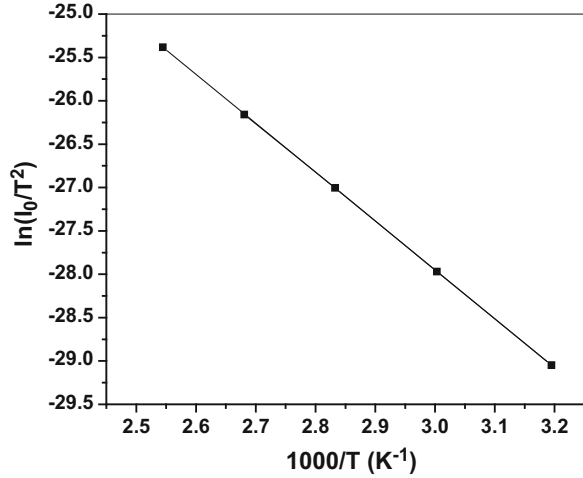
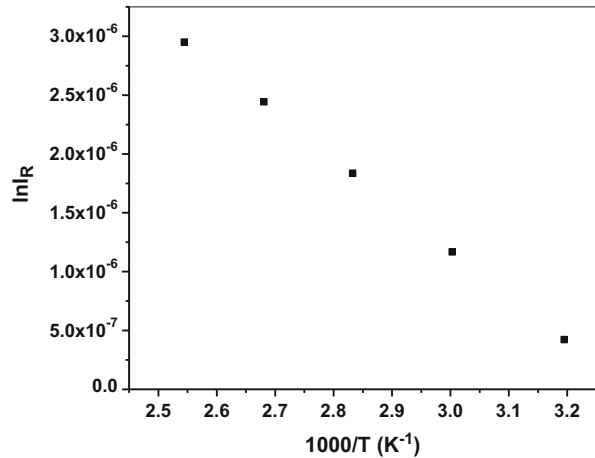


Fig. 64.9 Semi-logarithms of reverse current against $1000/T$ at $V = 0.2$ V



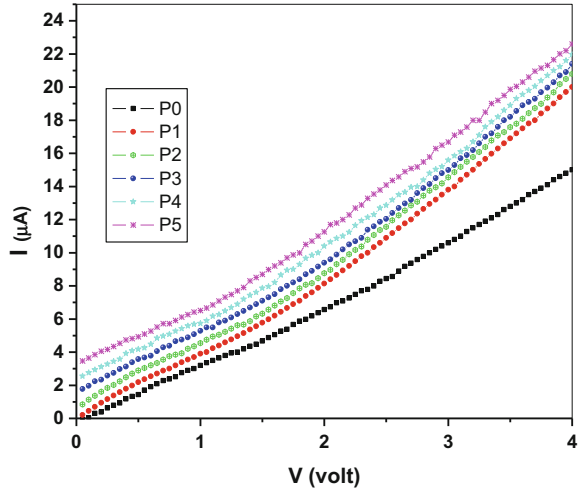
predicted by thermionic emission, which leads to the assumption that the nearly flat reverse I–V characteristic could be fit over a wide range of voltages, assuming that the generation and recombination of carriers in the Si substrate are the dominant source of the reverse current. Thus the reverse current due to the generation and recombination of carriers in the depletion region becomes

$$I_R = C \exp(-\Delta E_r/k_B T), \tag{64.7}$$

where ΔE_r is the carrier activation energy.

The dependence of $\ln(I_R)$ on $1000/T$ is shown in Fig. 64.9. The activation energy was determined from the slope of the straight line, which was equal to $\Delta_r = 0.335$ eV.

Fig. 64.10 Photocurrent against applied voltage at different light intensities



2.6 Influence of Light Intensity on I–V Characteristic of Cu₂S Film/p-Si Heterojunction

Cuprous sulphide materials (Cu₂S) are sense for heat and light. The I–V characteristic increases by increasing the temperature and the light intensity [11]. The source of light distanced to the heterojunction, by the change the distance between the source and the junction the light intensity change from 1400 to 22,000 lx.

Figure 64.10 shows the variation in the photocurrent with the light intensity at different voltages [12]. The variation in the photocurrent with the illumination intensity is shown in Fig. The photocurrent increases with as the illumination intensity increases. This indicates that illumination increases the production of electron–hole pairs. The photocurrent in the reverse direction is strongly increased by photo-illumination. This suggests that the Cu₂S/p-Si diode is a photodiode.

2.7 Dark C–V Measurements at Room Temperature at 1 MHz

The $C^{-2} - V$ plot on the voltage axis is shown in Fig. 64.11. From the following equation

$$\frac{1}{C^2} = \frac{2}{qN_c K_s \epsilon_0 A^2} (V_{bi} - V)$$

Fig. 64.11 $C^{-2} - V$ plot

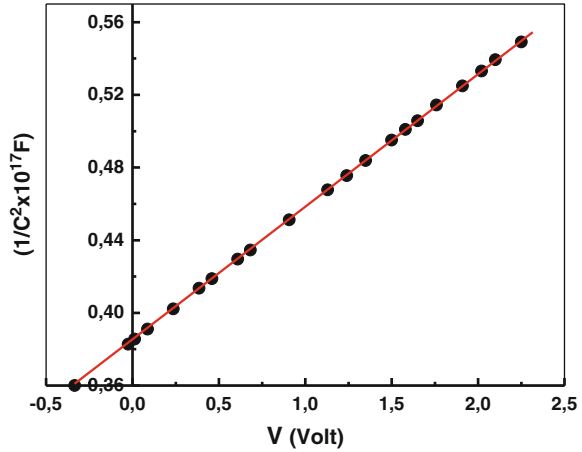
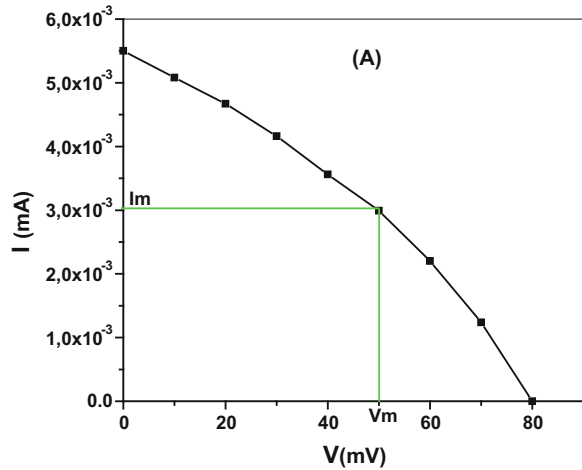


Fig. 64.12 I-V characteristics under illumination



where V_b is the built-in voltage from the extrapolation of the $C^{-2} - V$ plot to the voltage axis, V is the reverse voltage, A is the area of the diode, N_i is related to the slope of the $C^{-2} - V$ curve, and K_s and ϵ'_0 are the dielectric permittivity.

From Fig. 64.11 the following values are calculated: $V_b = 0.25$ V, $C_0 = 1.6$ pf, $N = 1.75 \times 10^{13} \text{ m}^{-3}$, and the depletion width is 3.24×10^{-4} cm. I-V characteristics under illumination are shown in Fig. 64.12. The values of the cell performance are calculated as follows: $I_{sc} = 5.5 \mu\text{m}$, $V_{oc} = 0.8$ Mv, $I_m = 3 \mu\text{m}$, $V_m = 0.5$ Mv, $FF = 0.34$, and the efficiency is 2.4. The low value of the fill factor and the efficiency may be due to the higher series resistance.

3 Conclusion

X-ray diffraction of Cu_2S indicated that Cu_2S is of a semi-amorphous and polycrystalline nature and is an orthorhombic crystal system. Scanning electron microscopy of an as-deposited Cu_2S thin film showed a uniform formation of the film and clearly indicated the formation of a microcrystalline structure. The I–V characteristics in the dark at different temperatures (303–373 K) revealed that the junction behaved like a diode. Capacitance measurements yielded a carrier concentration ($N = 1.73 \times 10^{13} \text{ cm}^{-3}$) and built-in voltage ($V_b = 0.25 \text{ eV}$). The photovoltaic characterization of {Au/ Cu_2S film/p-Si/Al} was investigated, and the efficiency of the cell was $\eta = 2.4\%$.

Photo responses showed that the high broad peak maximum at around 492 nm may have been due to the absorbance band of Cu_2S ($E_g \sim 2.3 \text{ eV}$). The present Cu_2S film/p-Si heterojunction showed acceptable sensitivity for the detection of light.

References

1. Ali HAM, Soliman HS, Saadeldin M, Sawaby K (2014) *Mater Sci Semicond Process* 18:141–145
2. Saadeldin M, Soliman HS, Ali HAM, Sawaby K (2014) *Chin Phys B* 23(4)
3. Bagul SV, Chavhan SD, Sharma R (2007) *J Phys Chem Solids* 68:1623–1629
4. Shide MS, Ahirrao PB, Patil IJ, Patil RS (2012) *Ind J Pure Appl Phys* 50: 657–660
5. El Nahass MM, El Barry AMA (2007) *Ind J Pure Appl Phys* 45: 465–475
6. Ashour A (2006) *J Optoelectron Adv Mater* 8(4): 1447–1451. Aug 2006
7. Mott NF, Davis EA (1979) *Electronic processes in non-crystalline materials*. Clarendon, Oxford
8. Ashery A, Metwally HS, Terra FS, El-Shazly AA (2001) *Ind J Pure Appl Phys*, 39: 450
9. El-Nahass MM, Zeyada HM, Aziz MS, El-Ghamaz NA (2005) *Solid State Electron* 49:1314
10. Song DY, Zhao J, Wang A, Widenborg P, Chin W, Aberle AG (2001) *Proc. 17th Euro. photovoltaic solar energy conference*, WIP, Munich, p 1865
11. Ashour A, Ramadan AA, Abd EL-Hady K, Akl AAS (2005) *J Optoelectron Adv Mater* 7 (3):1493
12. Rastogi AC, Salkalachen S, Bhide VG (1978) *Electrical conduction and transition in vacuum deposited Cu_2S films*. *Thin solid films* 52:1–10
13. Yahiya KZ, Yasmeen ZD, Ahmed SD (2007) *Eng Technol* 25(2)
14. Dhar S, Chakrabarti S (1997) *Prosperities of chemically deposited Cu_2S films on porous silicon*. *J Appl Phys* 82:655–657

Chapter 65

Using Renewable Energy to Process Seaweed

A. Kamaruddin, Aep Saepul Uyun, Herman Noer Rahman, Eri Suherman, and Salnida Y. Lumbessi

Abstract The main focus of this study is on the development of Seriwé hamlet. The hamlet is located in southeastern East Lombok Regency, where 370 households earn their livelihoods by cultivating seaweed. After harvesting, the seaweed is usually dried using direct sunshine, where the seaweed is spread out on mats and frequently mixed with sand and other foreign materials. This may take 2 to 3 days or even weeks if the weather is bad. The dried seaweed is then sold to traders at a fixed price without further processing owing to a lack of processing facilities. The aim of this study was to develop a way to change this traditional method of drying using an improved hybrid solar–wind dryer that is clean and hygienic. Cash flow analysis of the hybrid solar–wind dryer demonstrates the benefits of using it when it is leased. After drying, seaweed is processed in a newly built processing building, where ten units of processing facilities are provided. The processing of seaweed uses clean water supplied from a desalination facility powered by solar photovoltaics and wind energy. The processed seaweed is expected to enjoy robust demand. This study also presents a socioeconomic analysis of Seriwé hamlet that includes the impact of the project on the welfare of the Seriwé community.

Keywords Seaweed • Processing • Hybrid solar–wind dryer • Energy consumption • Socioeconomic study

1 Introduction

Seriwé hamlet is located about 100 km from the capital city of Mataram of the Indonesian province of West Nusa Tenggara, a 2 h drive in a four-wheel vehicle. The hamlet is able to grow seaweed and produces about 10 tons of wet seaweed/month. Around 391 households earn their living by growing seaweed. The most

A. Kamaruddin (✉) • A.S. Uyun • H.N. Rahman • E. Suherman
Graduate School/Renewable Energy, DarmaPersada University, Jl Radin Inten II,
Pondok Kelapa, East Jakarta 13450, Indonesia
e-mail: Kamaruddinabd@gmail.com

S.Y. Lumbessi
Faculty of Fisheries, Mataram University, Jl. Majapahit No. 62, Mataram, Indonesia

popular variety of seaweed grown in the area are of the species *cottonii* (*Kappaphycus alvarezii*), which have been cultivated for more than 10 years. Initially, people were trained in seaweed cultivation through government assistance. Now all individuals own one to two long lines (25 × 50 m, dimension of long line) where they grow seedlings on their own. It takes 45 to 60 days to harvest seaweed for a total possible yield of 6.4 to 8 tons wet seaweed/long line or 800–1000 kg dried seaweed at 45% wet basis, with five harvests/year. Usually people dry seaweed for around 3 days in direct sun to reduce the moisture to 45 % wb. Collectors then may come directly to the hamlet to buy the sundried seaweed at an average price of Rp 5500/kg dry seaweed without consideration for the standard quality. Some farmers are already obligated to sell to the collector at an arbitrary price set by the collector [1]. The seaweed production potential is 50 tons/month for *cottonii* and 25 tons/month of *Eucheuma spinosum* species.

Seriwe hamlet also has the potential to harness renewable energy, such as oar and wind energy. The solar insolation varies between 4 and 6 kWh.m²/day, and the average clearness of the sky is 40–60 %. The wind velocity varies between 3.2 and 5.8 m/s. Considering these potentials, it was recommended that a hybrid solar–wind dryer be built having a transparent structure with 8 × 16 m floor space and 3 m height (Fig. 65.1). The figure shows the interior of the hybrid solar–wind dryer, where four racks are covered with a fishing net. It is expected that the drying capacity will be 800 kg wet seaweed, and their moisture content could be reduced to 35 % wb within 1–2 days.

After drying, the seaweed is processed in a processing building (Fig. 65.2), where ten units of processing facilities will be provided. The final product is in the form of local cake and chip and fine powders. The building's dimensions are 19.5 × 8 m and 4.5 m high. After drying, the seaweed is processed further into local cake or pharmaceutical base material to further increase its value added. Figure 65.2 shows the processing building.



Fig. 65.1 External view (left) and interior of hybrid solar–wind dryer showing racks covered with fishing net



Fig. 65.2 Processing building

2 Socioeconomic Conditions of Seriwé Hamlet

2.1 *Input/Output Table*

A survey was conducted in Seriwé hamlet to collect data relevant for the construction of an input/output (I/O) table. Table 65.1 shows the leading economic sectors of the hamlet. With this knowledge a strategy can be devised to improve economic conditions. Table 65.1 shows the results of the constructed I/O table for Seriwé hamlet showing that seaweed production is the leading economic sector, followed by fisheries. Therefore, it was decided to make an investment in developing the knowledge required to increase the value added of the seaweed sector by establishing a small processing center (SPC) comprised of a hybrid solar–wind dryer and a processing building. From Table 65.1 we see that the current gross domestic product of Seriwé hamlet is Rp 5,196,516,000, which can be determined by subtracting the final demand from import [2].

2.2 *LEAP Analysis*

A Long-range Energy Alternatives Planning System (LEAP) analysis was conducted to determine the hamlet’s potential future energy needs [2] (Table 65.2).

Table 65.1 I/O table of Serive hamlet (transaction in million rupees)

Sector	Intermediate demand	Final demand	Total demand	Import	Total output	Supply
1. Seaweed	3910.00	6881.60	10,791.60	1742.73	9048.88	10,791.60
	71.40 %	63.33 %	66.04 %	30.74 %	84.78 %	66.04 %
2. Fisheries	0.00	777.60	777.60	0.00	777.60	777.60
	0.00 %	7.16 %	4.76 %	0.00 %	7.29 %	4.76 %
3. Corn	6.93	33.37	40.30	4.00	36.30	40.30
	0.13 %	0.31 %	0.25 %	0.07 %	0.34 %	0.25 %
4. Commerce	1179.00	2404.80	3583.80	3066.00	517.80	3583.80
	21.53 %	22.13 %	21.93 %	54.08 %	4.85 %	21.93 %
5. Transport	196.00	0.00	196.00	6.00	190.00	196.00
	3.58 %	0.00 %	1.20 %	0.11 %	1.78 %	1.20 %
6. Energy	184.45	0.00	184.45	850.20	(665.75)	184.45
	3.37 %	0.00 %	1.13 %	15.00 %	-6.24 %	1.13 %
Total	5476.38	10,865.44	16,341.83	5668.93	10,672.90	16,341.83
	100.00 %	100.00 %	100.00 %	100.00 %	100.00 %	100.00 %

Table 65.2 Results of LEAP analysis

Year	Household (in Barrel of Oil Equivalent)			
	Transportation	Cooking	Lighting	Total
2012	434.7	657.9	150.4	1243
2013	440.3	666.5	152.4	1259.2
2014	446	675.2	154.4	1275.6
2015	451.8	683.9	156.4	1292.1
2016	457.7	692.8	158.4	1308.9
2017	463.7	701.8	160.5	1326
2018	469.7	711	162.6	1343.3
2019	475.8	720.2	164.7	1360.7
2020	482	729.6	166.8	1378.4

Figure 65.3 shows the trend of energy consumption among Serive households to 2020. It shows that cooking accounts for the largest demand for energy, followed by transportation and lighting. It does not include the impact of energy demand by SPCs.

3 Seaweed Drying Test

A drying test was conducted for 21 h continuously to determine the drying constant. Figure 65.4 shows the drying curve, while Fig. 65.5 shows the conditions of the drying test under solar irradiation and the resulting chamber temperature. It was found that the drying curve followed closely the thin layer drying model:

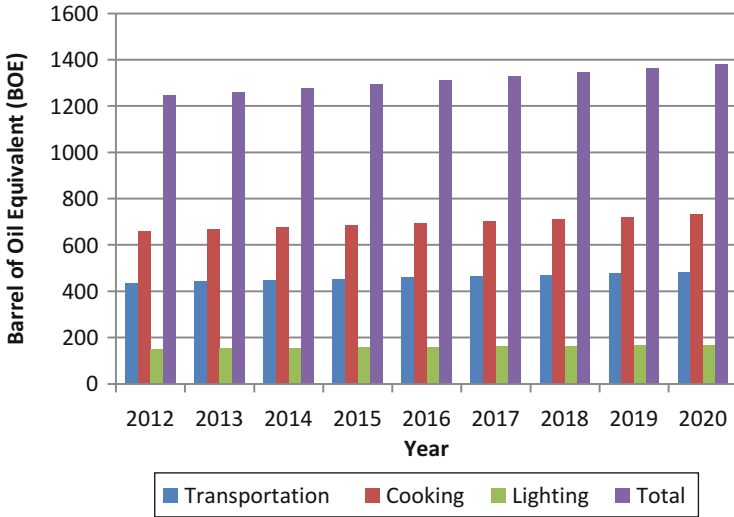


Fig. 65.3 Household energy demand

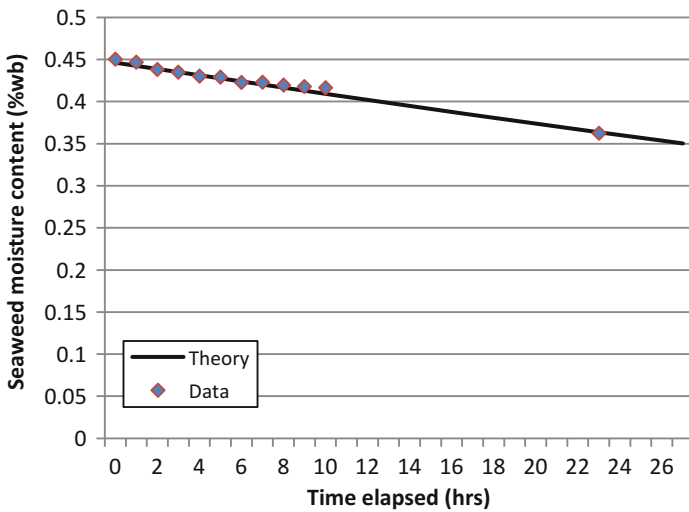
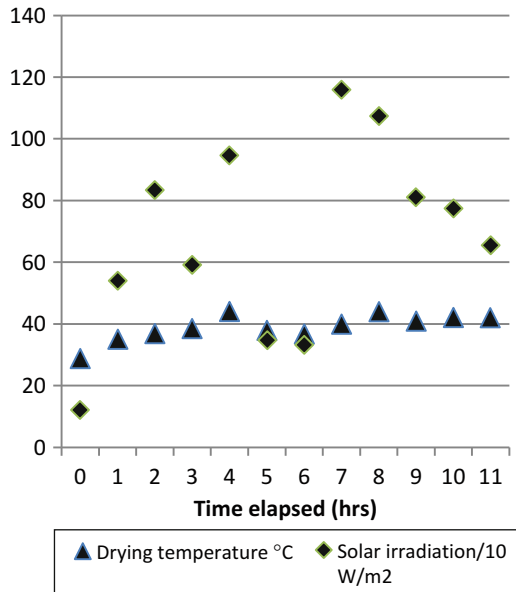


Fig. 65.4 Comparison of data and theory

$$\frac{M - Me}{Mo - Me} = \text{Exp}(-0.017t),$$

where M is the moisture content of the seaweed (%db), Me is the equilibrium moisture content (%db), Mo is the initial moisture content (%db), t is the time (h), and the coefficient 0.017 is the drying constant (1/h). Using this model one can calculate the time required for seaweed to attain 35 % wb, which in this case was 28 h or 2 days if drying is done during the day only.

Fig. 65.5 Solar irradiation and chamber temperature



4 Cash Flow from Using Hybrid Solar–Wind Dryer

The drying process can be carried out using the hybrid solar–wind dryer shown in Fig. 65.1. If the dryer is leased, the resulting cash flow will be as given in Tables 65.3 and 65.4. Shown here is the case where the hybrid solar–wind dryer is leased, with costs varying between Rp 1200 and 1450/kg wet seaweed. Table 65.4 shows that leasing the dryer at a cost of Rp 1200/kg results in a 4-year payback time, with a return on investment (ROI) of 23.2% and a net present value (NPV) of Rp 228,751,000.

Table 65.5 shows the variation in payback and ROI for the four different leasing costs. Here, leasing for Rp 1200/kg to Rp 1450/kg yielded a payback time of 3–4 years with the ROI varying between 23.2 and 43.7% and NPV varying between Rp 228,751,796.81 and Rp 740,923,710.

Table 65.3 Data for cash flow from using hybrid solar–wind dryer

Data	Quantity (Rp)
Price of dryer	80,000,000.00
Load (wet seaweed)-kg	800.00
Price of dried seaweed (at 35 % wb)	8000.00
Recovery (%)	0.69
Salary of owner (Rp/year)	10,500,000.00
Working days (days/year)	180.00
Labor (Rp/year)	30,937,500.00
Cost of electricity (Rp/year)	2,585,952.00
Drying time (days)	2.00
Operation and maintenance-Rp/year	2,250,000.00
Depreciation (Rp/year)	8,000,000.00
Total production cost (Rp/year)	134,273,452.00

5 Conclusions

Seriwe hamlet is capable of growing seaweed and renewable energy sources such as solar and wind energy. These resources could be developed to support the economic development of the hamlet. The use the facilities presented here may help improve and increase the value added of seaweed, which could bring benefits and to the community.

Table 65.4 Cash flow analysis of hybrid solar-wind dryer

Year	Revenue/investment	Production cost (Rp/year)	Interest rate (12%/an)	Income (Rp)	Cummulative (Rp)	ROI Calculation	ROI	NPV (Rp)
0	117.74		0.12		(117.74)	(117.74)	0.232	(117.74)
1	86.40	37.74	14.13	34.54	(83.20)	(67.53)		(74.29)
2	86.40	37.74	14.13	34.54	(48.66)	(32.06)		(38.80)
3	86.40	37.74	14.13	34.54	(14.13)	(7.56)		(10.06)
4	86.40	37.74	14.13	34.54	20.41	8.86		12.97
5	86.40	37.74		48.66	69.07	24.34		39.19
6	86.40	37.74		48.66	117.74	33.67		59.65
7	86.40	37.74		48.66	166.40	38.63		75.27
8	86.40	37.74		48.66	215.06	40.52		86.86
9	86.40	37.74		48.66	263.73	40.33		95.10
10	86.40	37.74		48.66	312.39	38.78		100.58
						0.24		228.75

Table 65.5 Variation in leasing cost

Leasing cost (Rp/kg)	Pay back (years)	ROI	NPV (Rp)
1450.00	3.00	0.437	740,923,710.26
1400.00	3.00	0.402	643,148,009.06
1300.00	3.00	0.330	461,157,141.92
1200.00	4.00	0.23	228,751,796.81

Acknowledgement The authors thank Mitsui & Co. Ltd. for its support under Environment Fund K14-0705 and the Directorate General of Higher Education for its support through the MP3EI research project grant 261/SP2H/ditlitlabmas/V/2012.

References

1. Kamaruddin A, Uyun AS, Rahman HN, dan Eri Suherman (2012) Penerapan Teknologi Berbasis Sumber Energi Terbarukan Setempat Dalam Rangka Pembangunan Sektor Perikanan, (Applications of renewable energy sources for the development of fisheries sector). Final report of MP3EI
2. Kamaruddin A, Setiawan AA, Uyun AS, Rahman HN, EriSuherman, Jombrik, Sukardi (2013) Development of proper economic modeling for improving the Indonesian energy strategy in selected Indonesian villages. Support for Economic Analysis Development in Indonesia (SEADI)-A USAID project grant

Chapter 66

New Environmentally Friendly Chlorine-Free Solar-Grade Silicon Production Technologies

Sergey Karabanov, Victor Yasevich, Dmitriy Suvorov, Evgeniy Slivkin, and Andrey Karabanov

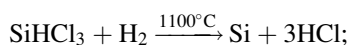
Abstract One of the major lines of solar energy development is the creation of environmentally friendly, wasteless, and cheap solar-grade silicon production technologies. Currently the main silicon production technologies are based on a reduction of silicon hydrogen chloride compounds: trichlorosilane, tetrachlorosilane, and monosilane. These technologies use environmentally dangerous and nonfireproof compounds in quantity. Such production levels can be profitable only in large volumes (more than 1000 tons per year). This chapter examines the research results of methods of silicon purification by extraction from a solid phase and plasma-chemical purification of metallurgical-grade silicon from impurities to the solar-grade level.

Keywords Silicon • Silicon purification • PV technology • Extraction from a solid phase • Plasma

1 Introduction

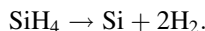
Currently the main solar-grade silicon production industrial technologies are as follows [1]:

- Siemens process and its modifications (e.g., Schmid silicon), based on the reduction of silicon from trichlorosilane (SiHCl_3):



- Union Carbide process (UCP):
This process is based on the reduction of silicon from silane:

S. Karabanov (✉) • V. Yasevich • D. Suvorov • E. Slivkin • A. Karabanov
Ryazan State Radio Engineering University, Ryazan, Russia
e-mail: pvs.solar@gmail.com



The process requires many purification operations, more than the Siemens process.

– Fluidized bed reactor (FBR) process:

This process also uses SiH_4 , but compared with the UCP, silicon deposition and silicon granule production happen differently.

The main disadvantage of the aforementioned technologies is that they require the application of trichlorosilane (SiHCl_3) or silane (SiH_4): explosive, toxic liquids.

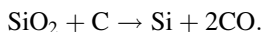
At the same time, works on the development of new, chlorine-free, solar-grade silicon production technologies are being carried out.

1. Elkem Solar Silicon (ESS) Production Process [2]

This process is based on metallurgical-grade silicon purification and consists of five independent processes combined together: metallurgical-grade silicon production, slag treatment, leaching, solidification, posttreatment. The ESS process consumes four times less power than the Siemens process.

2. Solar-grade silicon production of highly purified quartz [1]

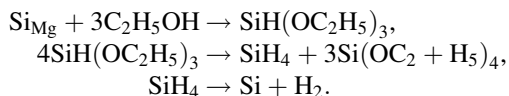
This technology is based on the direct carbothermal reduction of silicon from SiO_2 :



Highly purified pyrocarbon obtained by the plasma method is used as reductant.

The method provides cost savings of power inputs.

3. Solar-grade silicon production with the use of ethanol instead of TCS [1], the so-called alkosilane purification method. The technology is based on ethanol usage:



The authors believe that the technology makes it possible to reduce the cost of solar-grade silicon and is considered to be an environmentally friendly process. There are a number of other technological approaches to chlorine-free, solar-grade silicon production. This chapter presents the results of research on the creation of chlorine-free technologies for solar-grade silicon production: silicon purification by the method of extraction from a solid phase, and plasma-chemical purification of metallurgical-grade silicon.

2 Method of Silicon Purification by Extraction from a Solid Phase

This chapter analyzes silicon prototypes obtained by extraction from a solid phase and compares data from the mathematical modeling of the process of purifying upgraded metallurgical-grade silicon to solar-grade silicon by extraction from a solid phase. In the calculations the diffusion of the basic impurities determining the quality of solar-grade silicon (boron, phosphorus, aluminum, carbon, iron, and copper) is considered.

3 Mathematical and Numerical Model of Impurity Extraction from Silicon Particles

The mathematical modeling is carried out for the parameter calculation of the technological purification process when acceptable time and purification efficiencies are achieved. The mathematical model of impurity diffusion is based on an approximation of the spherical geometry of silicon particles.

The particles' impurity diffusion is expressed by Eq. (66.1):

$$\frac{\partial}{\partial t} n(r, t) = D(T) \left[\frac{\partial^2}{\partial r^2} n(r, t) + \frac{2}{r} \frac{\partial}{\partial r} n(r, t) \right], \quad (66.1)$$

with the boundary conditions

$\frac{\partial}{\partial r} n(0, t) = 0$ in the particle center,
 $n(R, t) = n_{\text{extr}}(t)$ on its surface, where

$$n_{\text{extr}}(t) = n_{0\text{extr}} + \frac{V_{\text{Si}}}{V_{\text{Ext}} + V_{\text{Si}}} \frac{3}{R^3} \int_0^R n(r, t) \cdot r^2 dr,$$

and with the initial condition

$$n(r, 0) = n_0,$$

$$n_{\text{extr}}(0) = n_{0\text{extr}},$$

where $n(r, t)$ is the silicon impurity concentration, $n_{\text{extr}}(t)$ the impurity concentration in the extractant, r the radial coordinate, t time, $D(T)$ the diffusion coefficient, T temperature, R the particle radius, n_0 the silicon initial impurity concentration, $n_{0\text{extr}}$ the initial impurity concentration in the extractant, V_{Si} the silicon volume, and V_{extr} the extractant volume.

The peculiarity of this model is that it makes it possible to take into account the impurity concentration time change in the extractant. This allows for greatly increasing the calculation accuracy and reliability of the silicon purification process.

The numerical model is presented as a system of finite-difference equations. The impurity concentration increment at each i th time pitch is described by the following expression:

$$\Delta n_{i,j} = \Delta t \cdot D \left[\frac{n_{i,j+1} - 2n_{i,j} + n_{i,j-1}}{\Delta r^2} + \frac{2}{r_j} \left(\frac{n_{i,j+1} - n_{i,j-1}}{2\Delta r} \right) \right], \quad (66.2)$$

where Δt is the time pitch, D the diffusion coefficient, r the spatial value, and Δr the spatial pitch.

In the calculations, the diffusion of the basic impurities defining solar-grade silicon quality – boron, phosphorous, aluminum, carbon, iron, and copper – is considered. The data on the impurity diffusion coefficients were taken from Refs. [3, 4].

4 Modeling Results

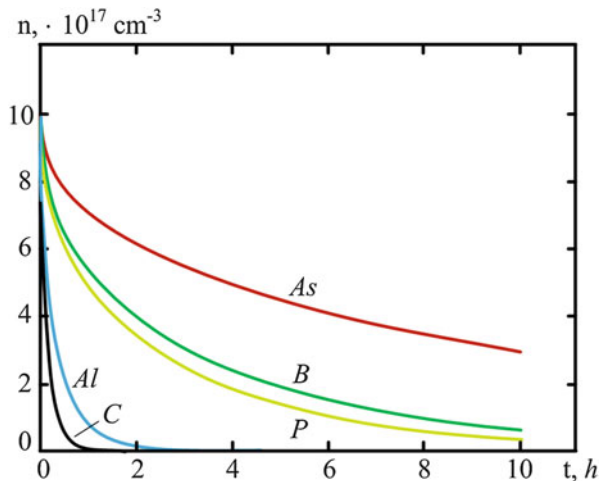
4.1 Numerical Experiment Conditions

To calculate the extraction from silicon particles, the following conditions of the numerical experiment were selected: operating temperature range: 1200–1395 °C, particle diameter: 10–60 μm , initial impurity concentration: 10^{18} cm^{-3} , impurity concentration in extractant: $5 \times 10^{13} \text{ cm}^{-3}$. The upper boundary of the selected temperature range actually corresponds to the melting temperature of silicon; the lower boundary was selected taking into account the condition of completing the purification process in an acceptable amount of time. The particle diameter range corresponds to the dimensions of the particle produced upon grinding the silicon using ball mills. The initial impurity concentration corresponds to the impurity concentration on the level of tens of parts per million (prerefining metallurgical-grade silicon). The impurity concentration in the extractant is selected taking into account that the purification-grade condition of less than 1 ppm was met.

4.2 Numerical Experimental Results

Figure 66.1 shows a diagram of the average impurity concentration reduction. At a constant temperature and particle diameter, the purification rate depends on the diffusion coefficient, whose value is defined by the impurity type.

Fig. 66.1 Time change of average impurity concentration in silicon particles in purification conditions: $D = 20 \mu\text{m}$, $T = 1300 \text{ }^\circ\text{C}$



The diagram shows that at a temperature of 1300 °C and diameter of 20 μm, the phosphorus content decreases by more than ten times during 10 h of processing. On the basis of numerical experimental data, the possibility of extracting impurities from a solid phase for the purification of preliminarily refined metallurgical-grade silicon is shown [5]. The obtained calculation data were used when it was decided to optimize the silicon purification modes on a pilot plant and confirmed experimentally.

5 Purification of Silicon by the Extraction Method and Experimentation

Figure 66.2a, b shows the purification process steps.

5.1 Extractant Preparation

The extractant was prepared. First, the extractant was dehydrated in air by heating it stepwise. During the first stage most of the water was removed from the extractant at a temperature of 110 °C until it was transformed into a solid substance. Then crystal water was removed at a temperature of 250 °C. Dehydrated extractant was broken in particles of 0.5–1 mm. Then the extractant was mixed with silicon powder and placed in a graphite crucible.

The graphite crucible with the extractant–silicon powder mixture was placed on the crucible’s holder. The installation chamber (Fig. 66.3) was closed and pumped

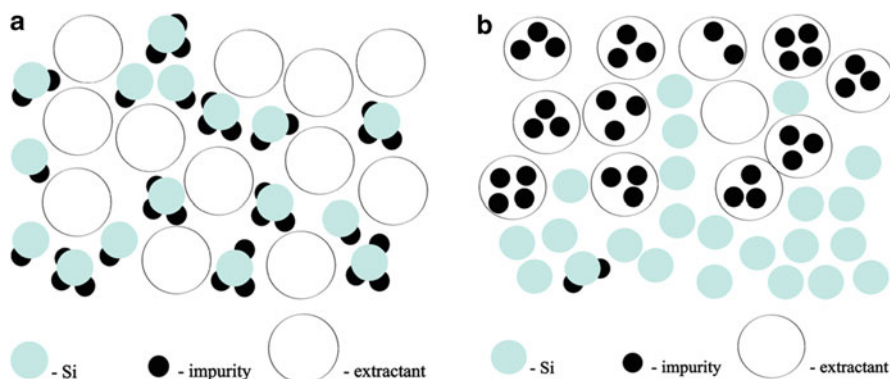
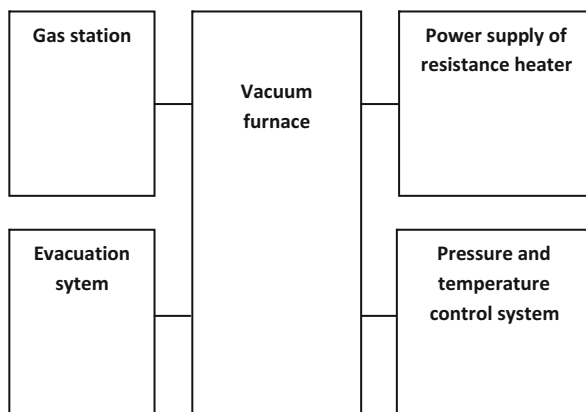


Fig. 66.2 Silicon purification process by extraction from a solid phase (a) before extraction (b) after extraction

Fig. 66.3 Installation functional diagram for silicon processing by extraction from a solid phase



out to a pressure of 2×10^{-2} mmHg. Then argon was supplied to the chamber, and the chamber was washed with argon within 15 min. The evacuation valve was closed, and an excess argon pressure in the chamber of 2 atm was created. The crucible temperature increased smoothly up to the extractant melting temperature and remained constant within 30 min for removal of residual water. The crucible temperature increased up to 1200 °C. The crucible with the extractant was kept at this temperature for no less than 4 h. Upon termination of the process, heating of the crucible was switched off and the crucible was cooled down within 2 h. When the crucible was cool, the chamber was depressurized and the crucible removed. To separate silicon from the extractant, the crucible was placed in a vessel with distilled water and boiled to complete the reagent dissolution. Then, to completely purify the silicon from the residual extractant, the silicon powder was exposed to vacuum melting at a pressure of 5×10^{-6} mmHg in a graphite crucible in a furnace by microwave heating.

Table 66.1 Impurities in source silicon

Impurity	Content, ppm	Content, ppm (a)	Content, ppm (b)
Al	80	0.3	1
B	10	1	5
P	50	30	40
F	6	0.4	0.7
Fe	30	<0.1	<0.1
As	0.2	<0.3	<0.3
Cr	20	<0.1	<0.1

Impurities in silicon at silicon–extractant ratio of 1:2 (a)

Impurities in silicon at silicon–extractant ratio of 1:4 (b)

Processing of the silicon powder was carried out at various ratios of silicon to extractant, at temperatures and processing times according to the described technology. In particular, silicon processing in the extractant was carried out at a ratio of 1:1 for 4 h at a temperature of 1200 °C.

Table 66.1 shows the results of the impurity analysis in the source silicon. Silicon processing in the extractant at a silicon–extractant ratio of 1:2 within 4.5 h at a temperature of 1300 °C makes it possible to reduce considerably the impurity concentration. In particular, the content of boron was reduced by ten times (Table 66.1a). Silicon processing at a silicon–extractant ratio of 1:4 for no less than 4 h at a temperature of 1000 °C shows a considerable reduction in the concentration of impurities, in particular boron (Table 66.1b).

The analysis of the experiments shows that for effective silicon purification it is necessary to increase considerably the extractant–silicon ratio to carry out processing at the highest temperature and longest time. In this regard, silicon was processed in extractant at a silicon–extractant ratio of 1:10, processing temperature of 1350 °C within 6 h. As a result of such processing, the content of boron decreased to 0.1 ppm. The produced silicon was melted in vacuum and subjected to direct crystallization twice according to Czochralski’s method. Ultimately, silicon with a content of the basic substance of 99.9999 % was produced.

Thus:

1. The mathematical model of silicon purification process from the impurities by the method of extraction from a solid phase being in the fine-dispersed state was designed. The model is based on the approximation of spherical geometry of silicon particles, and it takes into account the diffusion of the major impurities defining the solar-grade silicon quality: B, P, Al, Cu, Fe, As.
2. Using the model the impurity concentration distributions along the particles axial profile at various time points, dynamics of changes of average impurity concentration in time have been obtained.
3. On the basis of simulation data the requirements for the technological purification mode have been determined.
4. A few silicon samples processed by the method of extraction from a solid phase under various purification conditions have been obtained.

5. It is established that the maximum efficiency is reached at the temperatures, close to melting silicon temperatures (about 1350 °C) and the process time of more than 4 h.
6. The prototypes were analyzed on spark-gap mass spectrometer and raster electronic microscope with energy-dispersive attachment- microanalyzer. The analysis of results showed the efficiency of the use of impurity extraction from a solid phase for purification of preliminary refined metallurgical-grade silicon into solar-grade silicon in industry.

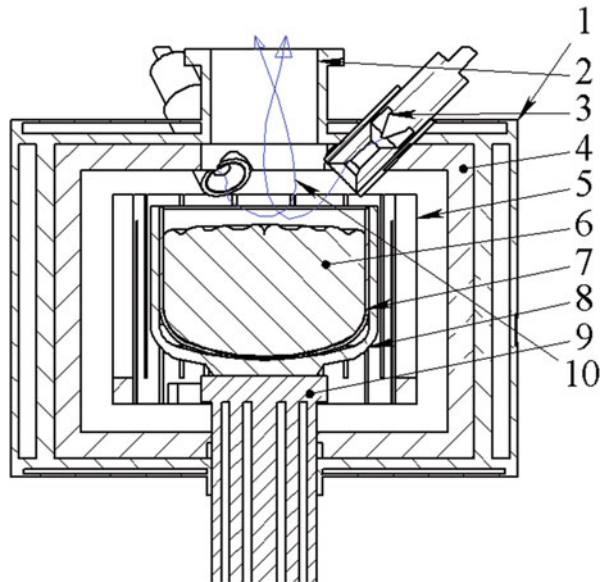
6 The Method of Plasma-Chemical Purification of Metallurgical-Grade Silicon

This chapter presents a method of plasma-chemical purification of metallurgical-grade silicon to the solar-grade level.

1. An experimental purification unit is developed and produced.
2. The technology of metallurgical-grade silicon plasma-chemical purification is developed.

The silicon purification device (Fig. 66.4) consists of a steel chamber with water-cooled walls (1), a cylindrical quartz crucible (7), a graphite support for quartz crucible installation (8), and an elevator for vertical displacement of the support and crucible (9). The crucible, the support, the elevator, and the graphite heater (5) with power supply and temperature monitoring system are widely used in the design of

Fig. 66.4 Silicon purification device



units for silicon crystal growing and are chosen on the basis of cost and availability. The chamber walls (1) have graphite felt thermal screens (4). In the top part of the chamber (1) are three two-mode jet plasmatrons (3) operating in the mode of 50–80 A pilot DC arc using dry argon and 100–200 A primary AC arc as plasma-forming gas or using a mixture of dry argon and water vapors as plasma-forming gas. The plasmatron anodes (3) have a system for supplying water to the plasma-forming channel. In the center of the top part of the chamber is located an opening for pumping gases (2).

The device works as follows. Metallurgical-grade silicon (6) is loaded in the crucible (7). The crucible is loaded taking into account the densest filling and taking into account that after melting the melt mirror level must be below the top edge of the quartz crucible by 20–30 mm; thus the crucible elevator (9) is in the fully down position. Then the chamber (1) is closed and the gases are degasified up to a pressure of 0.1–1.0 Torr through an opening (2).

Warming up and melting of the loaded silicon is carried out by the graphite heater (5). The vacuum chamber walls are equipped with a layer of high-efficiency thermal insulation made of graphite felt (4) for a minimal decrease in thermal losses. In the process of silicon melting its level in the crucible decreases. After the last bit of silicon is melted, the graphite heater temperature stabilizes at 1500 °C. The use of a standard cylindrical quartz crucible, a graphite heater, support, elevator, and thermal insulation makes it possible to obtain and maintain a silicon melt at minimal cost.

Then dry argon is supplied in the plasmatrons (3) and the DC electric arc is struck. The arc current for each of the three plasmatrons is 50–80 A. For each plasmatron a low-power DC power supply with falling volt-ampere characteristic and arc ignition system is needed. Thus, full galvanic separation of the plasmatron anodes and cathodes from the chamber, supply line, and each other is carried out. A contracted jet of warmed-up ionized gas at a temperature of 4000–6000 °C moves in the low-density medium at high speed. Thus, jets (10) from the three plasmatrons cross in the center of the surface of the melt; for this purpose the crucible is raised by the elevator. The gas reflected from the surface of the melt is degassed through an opening (2) at high speed. The cylindrical form of the crucible and arrangement of the plasmatrons at an acute angle to the surface of the melt facilitates achieving the optimum path of the plasma jet from the plasmatrons [6–9].

Table 66.2 shows the test results of silicon samples after plasma-chemical purification:

Processing parameters for result 1: current: 50 A, total processing time: 20 min, dry argon pressure: 600–1000 Pa;

Processing parameters for result 2: current: 70 A, total processing time: 60 min, dry argon pressure: 600–1000 Pa;

Processing parameters for result 3: current: 70 A, total processing time: 60 min, humidified argon pressure: 600–1000 Pa;

Table 66.2 Test results for determining full impurity composition of multicrystalline silicon ingot samples obtained in experiment with different technological processing parameters

Sample description	Element content in sample, ppm (1 ppm = 0.0001 %)						Solar-grade silicon wafer
	Raw silicon KP-00	Result 1	Result 2	Result 3	Result 4	Result 5	
Li	5	0.001	0.001	<0.001	<0.001	<0.001	<0.001
Be	0.001	0.001	0.001	<0.001	<0.001	<0.001	<0.001
B	20	3	2	10	5	0.1	0.09
F	0.3	0.4	0.4	<0.001	1	1	1
Na	0.6	0.01	0.01	<0.001	<0.001	0.01	0.01
Mg	70	0.5	0.01	<0.001	<0.001	0.01	0.01
Al	5000	600	500	60	2	0.08	0.08
P	30	20	20	6	2	0.01	0.01
S	2	0.1	0.1	2	<0.1	<0.1	<0.1
Cl	4	1	0.6	0.3	<0.1	0.2	0.2
K	0.01	0.01	0.01	0.2	<0.01	<0.01	<0.01
Ca	3000	200	200	3	0.05	0.5	0.5
Sc	0.01	0.01	0.01	<0.01	<0.01	<0.01	<0.01
Ti	1000	80	500	7	<0.01	<0.01	<0.01
V	200	0.01	0.01	<0.01	<0.01	<0.01	<0.01
Cr	20	0.2	1	0.2	<0.01	<0.01	<0.01
Mn	200	2	20	4	<0.01	<0.01	<0.01

Processing parameters for result 4: current: 70 A; total processing time: 120 min; dry argon: 60 min, pressure: 600–1000 Pa, humidified argon: 60 min, pressure: 600–1000 Pa;

Processing parameters for result 5: dry argon current: 70 A, processing time: 24 h, pressure: 600–1000 Pa; humidified argon current: 70 A, processing time: 24 h, pressure: 600–1000 Pa; cooling: 48 h, total processing time: 96 h.

The silicon plasma-chemical purification method has a number of fundamental advantages:

- Absence of harmful and toxic substances in the production process;
- The possibility of combining the purification process with melt-oriented crystallization, which greatly reduces the cost of produced solar-grade silicon;
- Possibility of scalable production;
- Low power consumption in silicon production (22–25 kWh/kg).

The obtained data show that the method of plasma-chemical purification of metallurgical-grade silicon makes it possible to reach solar-grade silicon purification. This method allows for the creation of a power- and resource-saving, environmentally friendly, and wasteless industrial production technology for solar-grade silicon using metallurgical-grade silicon as raw material.

References

1. www.Silicontimes.Com/ru/production
2. <http://Injapan.no.bizdelegation-day2/files/2012/10/10-ulset-Elkem.pdf>
3. Beke DL (1998) Diffusion in semiconductors and non-metallic solids. Springer, Berlin, p 257
4. Luque A, Hegedus S (2003) Handbook of photovoltaic science and engineering. Wiley, West Sussex, p 1164
5. Karabanov S, Suvorov D, Sazhin B, Slivkin E (2011) Silicon purification by the method of extraction from solid phase. Bulletin of Ryazan State Radio Engineering University, No. 1 (Issue 35), ISSN: 1995-4565, Ryazan
6. Karabanov S, Dshkhunyan V, Yasevich V, Hoshino M (2010) Method for manufacturing ingots of polycrystalline silicon. Patent 2465201 RU, 13 Dec 2010
7. Karabanov S, Dshkhunyan V, Yasevich V (2010) Method for purification of metallurgical-grade silicon by moisturized AC plasma in vacuum. Patent 2465202 RU, 17 Nov 2010
8. Karabanov S, Dshkhunyan V, Yasevich V, Hoshino M (2011) Method for refinement of metallurgical-grade silicon. Patent 2465200 RU, 14 Feb 2011
9. Karabanov S, Dshkhunyan V, Yasevich V, Hoshino M (2010) Method for refinement of metallurgical-grade silicon with dry argon plasma with water injection on the surface of melted silicon with subsequent directional crystallization. Patent 2465199 RU, 17 Nov 2010

Chapter 67

Some Physical Properties of Pure and Fluorine-Doped Tin Oxide Films Used as Transparent Conducting Oxide

Kamil M. Yousif and Sayran A. Abdulgafar

Abstract For architectural use, coated window glass can be categorized into two classes: low-emissivity (E) window glass and solar control window films. Low-E glass serves a thermal insulation function. The application of low-E glass to buildings will significantly reduce energy consumption, mainly during cold seasons. Solar control films are designed to absorb or reflect incident solar radiation in order to diminish solar heat gains through glass. The application of selective coatings, i.e., low-E coating in glazings, allows for a more efficient management of heating and cooling loads of a building. Low-E coatings include many transparent conductors (TCs). TCs have a wide variety of uses. One of the applications of TCs is their use as low-emissivity windows in buildings. Another example is where the front surfaces of solar cells are covered with transparent electrodes. TCs' ability to reflect thermal infrared heat is exploited to produce energy-conserving windows. Therefore, TCs can contribute to energy savings and can be considered important eco-materials for a sustainable energy future. This chapter includes an investigation of some of the physical properties of pure and fluorine-doped tin oxide thin films, which are TCs. Thin films were prepared on borosilicate glass slides by the spray pyrolysis technique. The optical energy gap was calculated for pure SnO₂ films. The structure of specimens was studied by the X-ray diffraction technique. The mechanical durability of doped tin oxide thin films is related to hardness. Vickers hardness and microhardness techniques were used to investigate the hardness of tin oxide thin films. We conclude that tin oxide thin films are harder than glass substrates.

Keywords Energy conserving windows • Low emissivity windows • Spray pyrolysis • Vickers hardness and microhardness

K.M. Yousif (✉)

Department of Environmental Science, Faculty of Science, Zakho University,
Zakho, Kurdistan Region, Iraq
e-mail: kamy22002@yahoo.co.uk

S.A. Abdulgafar

Department of Physics, Faculty of Science, Dohuk University, Dohuk, Kurdistan Region, Iraq

1 Introduction

In recent years, there has been growing interest in the application of transparent conducting oxide (TCO) films in a variety of optoelectronic devices and in the field of energy conversion materials, such as solar cells, fuel cells, and lithium batteries, as well as in environment-related fields (e.g., gas sensors that detect gases such as H₂, SO₂, CO, and others).

Tin oxide thin films are one type of transparent conductor (TC). They are transparent to visible light, and their ability to reflect thermal infrared light is exploited to make energy-conserving windows. In addition, they can be used as low-emissivity windows in buildings [1, 2]. Hence, they may be considered an eco-material for sustainable energy future.

Tin dioxide (SnO₂) is an important oxide material that combines high optical transparency in the visible light spectrum and low electrical resistance [3, 4]. SnO₂-coated architectural windows allow light but not heat to transmit in and out of buildings [5, 6]. The aforementioned physical properties are valuable in a number of applications in many fields, such as solar cells, electrode materials, light-emitting diodes, and gas sensors [7–14].

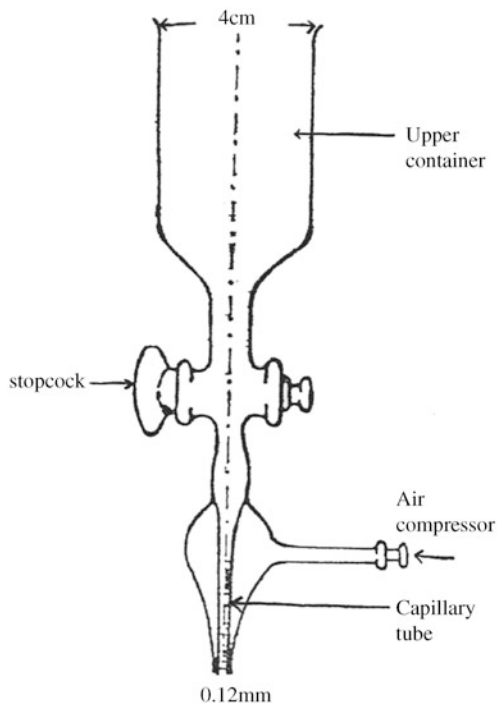
Either doped or nondoped tin oxide thin films can be fabricated using a number of techniques, such as chemical vapor deposition (CVD) [15, 16], sputtering [17], sol–gel [18], dip coating techniques [19], and spray pyrolysis [20–22].

One of the present authors, Yousif (2008) [23], has already reported the preparation and characterization of pure and doped SnO₂ by spray pyrolysis using stannous chloride (SnCl₂). In the present work, the structure of the specimens was studied by X-ray diffraction (XRD). In addition, we investigated some of the physical properties of pure and doped SnO₂ layers deposited by the chemical spray pyrolysis method using SnCl₄. These properties included the optical and mechanical hardness of pure and doped SnO₂.

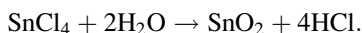
2 Experimental Technique

The pyrolytic spray technique is not expensive and is well suited for large-scale applications. A suitable design of the spray nozzle is given in Fig. 67.1. The capillary is surrounded by a bubble tube through which air is compressed by a small compressor [24]. The cleaned substrates were heated uniformly on a hot plate up to 450 °C, and the temperature of the sample surface was measured by a thermocouple probe. Pure SnO₂ layers were deposited by spray pyrolysis on microscopic glass slides (25.4 × 76.2 × 1 mm) used as substrates. The solution contained SnCl₄: H₂O: CH₃CH₂OH: HCl in the ratio of 0.29: 0.38: 0.30: 0.015. To deposit uniform films, the distance between spray nozzle and substrate was maintained at 33 cm and the spray rate was approx. 15 cm³/min. Various

Fig. 67.1 Spray nozzle



thicknesses of pure SnO_2 thin films were prepared [24]. The basic reaction during production of the film was



For fluorine doping, NH_4F dissolved to the starting solution and the amount of NH_4F was varied from 2 to 8 wt%. The transmittance for SnO_2 samples was measured using a SPECORD 200 UV/Vis double-beam spectrophotometer with a wavelength range of 190–1100 nm. The XRD pattern of the layers was investigated using $\text{Cu K}\alpha$ radiation, $\lambda = 1.54 \text{ \AA}$.

The Vickers hardness (VH) values of specimens (nondoped tin oxide thin films, doped tin oxide thin films, and glass substrates) were measured at room temperature using the VH test. The surface was subjected to a standard pressure for a standard length of time by means of a pyramid-shaped diamond. The diagonals of the Vickers indents were measured using an optical microscope attached to the equipment, and the hardness was calculated using the standard equation for the Vickers geometry,

$$\text{HV} = 1.8544F/d^2, \quad (67.1)$$

where HV is the Vickers hardness number (VHN) in kg/mm^2 , F is the normal load (kilogram-force - kgf), and d is the average diagonal length of the indentation (mm). Five indents were taken for each sample under identical loading conditions. An average value of each specimen was calculated and subjected to statistical analysis. The microhardness (MH) values of the same specimen were measured with a microhardness tester (Clemex-CMT) using a Vickers diamond tip under a kilogram-force of $50 \times 10^{-3} \text{ kg} \times g$ (in N), where $g = 9.806 \text{ m}\cdot\text{s}^{-2}$ (standard gravity). The period of indentation load was 15 s. The MH was determined using the preceding formula.

3 Results and Discussion

3.1 Transmittance and Absorption Coefficient

The transmittance (TR) of the films decreases with increasing film thickness (Fig. 67.2). The films are doped with NH_4F for a different fluorine doping concentration of 2 to 8 wt%. The color of the nondoped tin oxide thin film was white, which turns colorless on doping 8 wt% of NH_4F . The TR values of the films have been plotted as a function of wavelength for different fluorine doping concentrations (Fig. 67.3). From the figure it is clear that these films have high TR in the visible range and very low or zero TR in the UV region. The TR of the films increases with increasing NH_4F concentration. Fluorine-doped tin dioxide (FTO), in which fluorine atoms replace the oxygen sites in the lattice, increases the density of electron distribution on the surface of SnO_2 nanocrystals, creating free electrons to promote higher conductivity [23] for the samples, and this may lead to increases in the TR in the visible range. This increase in the TR with increasing fluorine concentration is in good agreement with earlier reports [6–8]. The optical energy gap is an essential parameter needed to design many semiconductor devices, such as photovoltaic cells. The semiconductor bandgap was determined by analyzing the optical data using the expression for the absorption coefficient (AB) and photon energy ($h\nu$) with the following relation [8]:

$$\text{AB} = A_0(h\nu - E_g)^n, \quad (67.2)$$

where A_0 is a constant for a given semiconductor, E_g is the energy gap, and $h\nu$ is the photon energy. For allowed transitions, n is equal to 1/2 and for forbidden transitions it is 3/2 [1]. The AB at various wavelengths was calculated from the transmission spectra and from AB values greater than 10^4 ($\text{AB} > 10^4 \text{ cm}^{-1}$) at the fundamental absorption. Therefore, we can conclude that the electron transition is a direct transition. The value of the optical energy gap, E_g , was calculated. It is approx. 2.25 eV. This value is very close to the results obtained by other researchers

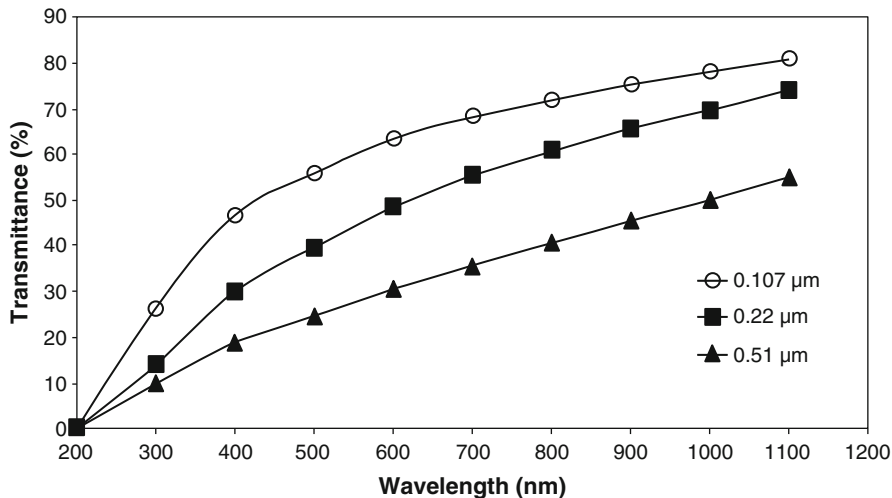


Fig. 67.2 Transmittance of spectra of pure SnO₂ thin films as a function of wavelength for different thicknesses

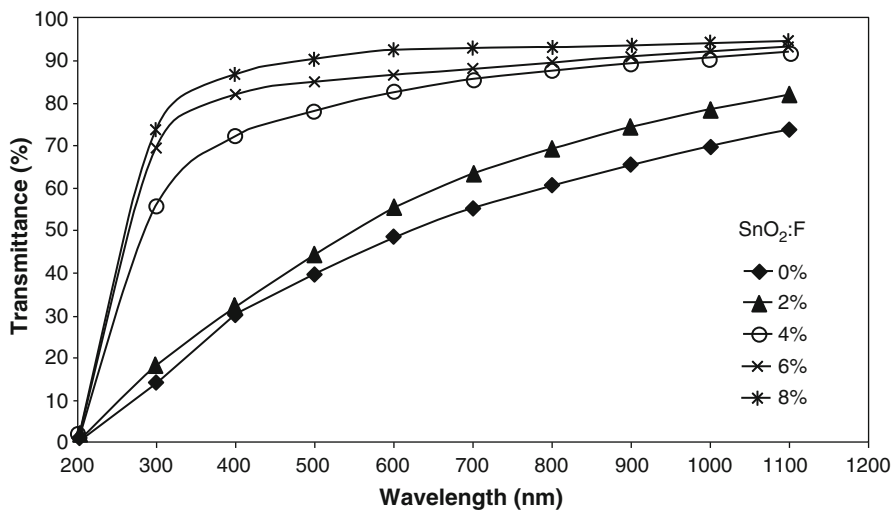


Fig. 67.3 Transmittance spectra of SnO₂: F thin films as a function of wavelength for different fluorine doping concentrations (wt%)

for pure SnO₂ films which having amorphous structure [3], but it is less than that films has a polycrystalline nature deposited on glass slides at 400 °C.

3.2 *X-Ray Diffraction*

The examination of the samples by XRD confirmed that the structure of pure and doped SnO₂ was amorphous. All films deposited by the spray method at a substrate temperature of around 300 °C are amorphous, but films deposited at higher temperatures become polycrystalline.

3.3 *Results of Mechanical Hardness*

Hardness is the mechanical behavior representing material resistance. It covers several properties: resistance to deformation, resistance to friction, and abrasion [25, 26]. In Vickers hardness - VH and Knoop hardness, the hardness number is determined by the load over the surface area of the indentation, not the area normal to the force, and is therefore not pressure. When concerned with coatings and surface properties, it is important to investigate the properties of friction and wear processes, which are related to macroindentation. Although the quantitative Vickers numbers are in the same sequence as Mohs's scale of hardness, certain textures or aggregate forms may hinder or prevent a true hardness determination. For this reason the Mohs scale of hardness is not suitable for accurately gauging the hardness of industrial materials; a more precise measure is to be found in the Vickers hardness - VH and Knoop hardness. The mechanical durability of TCs is related to the hardness of the crystals from which they are formed [2]. The Average Vickers Hardness (AVH) obtained for glass substrates is ~ 5.70 Gpa. The AVH for nondoped tin oxide thin films is ~5.80 Gpa, while the AVH for doped tin oxide is ~5.83 Gpa.

Where materials have a fine microstructure and are multiphase, nonhomogeneous, or prone to cracking, macrohardness measurements will be highly variable and will not identify individual surface features. It is here that micro- or nanohardness measurements are appropriate. In the present study, the average values of microhardness (AMH) for nondoped tin oxide thin films was 4.65 GPa. The AMH for doped tin oxide thin films was 4.70 GPa, while the AMH for the glass substrates was 4.6 GPa. It is seen that tin oxides are harder than glass substrates. Gordon (2000) [2] reported that the hardness values for glass and tin oxide are 5 and 6, respectively (using the Mohs scale). We believe that the deposition condition, heat treatment, and structure of the film play an important role in determining the hardness of the film. For example, Tseng et al. (2011) [27] reported that the microhardness for annealed fluorine-doped tin oxide thin films was less than that of unannealed films.

4 Conclusions

The spray pyrolysis technique was employed to prepare low-cost pure and fluorine-doped tin oxide thin films. The optical transmittance increased with increases in the fluorine concentration to a maximum of 94 % at 1100 nm (8 wt% of NH_4F). The high transmittance made these films suitable for window materials in solar panels. The absorption coefficient values for the specimens was ($AB > 10^4 \text{ cm}^{-1}$) at the fundamental absorption. The electron transition was direct. The AMH for nondoped tin oxide thin films was 4.65 GPa, while that for doped tin oxide thin films was 4.70 GPa. We conclude that tin oxides are harder than glass substrates.

References

1. Zhao H, Kiwi J, Pulgarin C (2013) Oxygen distribution of F-doped tin oxide films coated on float glass along depth before and after heat treatment. *Int J Appl Glass Sci* 4(3):242–247
2. Gordon RG (2000) Criteria for choosing transparent conductors. *MRS Bull/August*. 52–57
3. Batzill M, Diebold U (2005) The surface and materials science of tin oxide. *Prog Surf Sci* 79:47–154
4. Elangovan E, Ramamurthi K (2005) A study on low cost-high conducting fluorine and antimony-doped tin oxide thin films. *Appl Surf Sci* 249(2):183–196
5. Finley JJ (1999) Heat treatment and bending of low-E glass. *Thin Solid Films* 351:264–273
6. Aukkaravittayapun S, Wongtida N, Kasewatin T, Charojrochkul S, Unnanon K, Chindaodom P (2006) Large scale F-doped SnO_2 coating on glass by spray pyrolysis. *Thin Solid Films* 496:117–120
7. Boiadjiev SI, Dobrikov GH, Rassovska MM (2007) Preparation and properties of RF sputtered indium–tin oxide thin films for applications as heat mirrors in photothermal solar energy conversion. *Thin Solid Films* 515:8465–8468
8. Wu S, Yuan S, Shi L, Zhao Y, Fang J (2010) Preparation, characterization and electrical properties of fluorine-doped tin dioxide nanocrystals. *J Colloid Interface Sci* 346:12–16
9. Hou LR, Yuan CZ, Peng Y (2007) Synthesis and photocatalytic property of $\text{SnO}_2/\text{TiO}_2$ nanotubes composites. *J Hazard Mater* 139:310–315
10. Groult H, Nakajima T (eds) (2005) Fluorinated materials for energy conversion. Elsevier, Oxford
11. Manavizadeh N, Akbari Boroumand F, Al-Soleimani E, Raissi F, Bagherzadeh S, Khodayari A, Rasouli MA (2009) Influence of substrates on the structural and morphological properties of RF sputtered ITO thin films for photovoltaic application. *Thin Solid Films* 517:2324–2327
12. Sheel DW, Yates HM, Evans P, Dagkaldiran U, Gordijn A, Finger F, Remes Z, Vanecek M (2009) Atmospheric pressure chemical vapour deposition of F doped SnO_2 for optimum performance solar cells. *Thin Solid Films* 517:3061
13. Delahoy AE, Guo S (2011) Chapter 17: Transparent conducting oxides for photovoltaics. In: Luque A, Hegedus S (eds) *Handbook of photovoltaic science and engineering*, 2nd edn. Wiley, Chichester, pp 716–796
14. Karl S, Kundoo S. Synthesis and characterization of pure and F-doped tin-oxide nanoparticles by sol-gel methods. *Intr J Sci Res*
15. Kwoka M, Ottaviano L, Passacantando M, Santucci S, Szuber J (2006) XPS depth profiling studies of L-CVD SnO_2 thin films. *Appl Surf Sci* 252:7730–7733

16. Rajaram P, Goswami YC, Rajagopalan S, Gupta VK (2002) Optical and structural properties of SnO₂ films grown by a low-cost CVD technique. *Mater Lett* 54:158–163
17. Huang JL, Pan Y, Chang JY, Yau S (2004) Annealing effects on properties of antimony tin oxide thin films deposited by RF reactive magnetron sputtering. *Surf Coat Technol* 184:188–193
18. Wu S, Yuan S, Shi L, Zhao Y, Fang J (2010) Preparation, characterization and electrical properties of fluorine-doped tin dioxide nano-crystals. *J Colloid Interface Sci* 346:12–16
19. Hammad TM, Hejazy NK (2011) Structural electrical and optical properties of ATO thin films fabricated by dip coating method. *Int Nano Lett* 1(2):123–128
20. Ikhmayies SJ (2014) Optical parameters of SnO₂: F thin films prepared by the spray pyrolysis technique. In: A Sayigh (Ed) World Renewable Energy Congress, WREC XIII, Kingston University 3–8 Aug 2014
21. Oshima M, Yoshino K (2012) Thickness dependence of structure and optical characteristics in fluorine-doped SnO₂ films grown by spray pyrolysis method. *Jpn J Appl Phys* 51(12R)
22. Ramaiah KS, Raja VS (2006) Structural and electrical properties of fluorine doped tin oxide films prepared by spray-pyrolysis technique. *Appl Surf Sci* 253:1451–1458
23. Yousif KM (2008) Physical properties of tin oxide thin films doped with fluorine for renewable energy applications. Fluorine doped tin oxide films prepared by spray-pyrolysis technique. Published in World Renewable Energy Congress, 19–25 Jul 2008, Glasgow, Scotland
24. Abdulgafar SA (2006) Preparation and characterization of some selective coatings for solar energy applications. MSc thesis College of Science, University of Duhok, Iraq
25. Jonsson B, Hogmark S (1984) Hardness measurements of thin films. *Thin Solid Films* 114:257
26. Chicot D, Lesage J (1995) Absolute hardness of films and coatings. *Thin Solid Films* 254:123
27. Tseng S-F, Hsiao W-T, Chiang D, Huang K-C, Chou C-P (2011) Mechanical and optoelectric properties of post-annealed fluorine-doped tin oxide films by ultraviolet laser irradiation. *Appl Surf Sci* 257(16):7204–7209

Chapter 68

Socioeconomic, Environmental, and Social Impacts of a Concentrated Solar Power Energy Project in Northern Chile

Irene Rodríguez, Natalia Caldés, Alberto Garrido, Cristina De La Rúa, and Yolanda Lechón

Abstract Concentrated solar power deployment could play an important role in the sustainable development strategy of Chile, the country with the highest solar potential in the world. In this regard, besides electricity generation costs, it is also important to assess the socioeconomic, environmental, and social implications of energy investment projects. To shed some light on this issue, this chapter contributes to the existing body of knowledge by conducting a sustainability assessment of the installation, operation, and maintenance of a 110 MW concentrated solar power tower plant in Chile. Using an input–output methodology based on plant cost data, this chapter estimates the direct and indirect socioeconomic and environmental effects of the project in terms of economic activity, job creation, energy consumption, and CO₂ emissions. Additionally, using the Social Hotspots Database, a preliminary social risk analysis in those economic sectors most stimulated by the project in terms of employment is performed. Assuming domestic provision of all goods and services, results show that the associated total socioeconomic impacts over the lifetime of the plant would amount to US \$3124 million, a multiplier effect of 2.2, and a ratio of indirect per direct job creation of 1.21. Additionally, results also show that direct and indirect economic activities required by the project would generate 64.36 g CO₂/kWh. Finally, a social assessment indicates the existence of a high unemployment risk in those sectors most stimulated; therefore the project could decrease these unemployment risks.

Keywords Input–output analysis • Sustainability impact assessment • Concentrated solar power • Chile

I. Rodríguez (✉) • N. Caldés • C. De La Rúa • Y. Lechón
Energy Systems Analysis Unit, Energy Department, CIEMAT (Centro de Investigaciones Energéticas, Medioambientales y Tecnológicas), Madrid, Spain
e-mail: irene.rodriguez@ciemat.es; <http://www.ciemat.es>

A. Garrido
CEIGRAM Research Centre for the Management of Agricultural and Environmental Risks,
Universidad Politécnica de Madrid, Madrid, Spain

1 Introduction

Over the course of history, energy has been an essential driver in the development of civilizations [1]. At the same time, the energy sector is one of the largest consumers of natural resources and responsible for greenhouse gas (GHG) emissions. In this sense, a sustainable approach that considers the harmony between economy, society, and environment must be put in place [2].

One way to reduce GHG emissions worldwide is to progressively replace fossil-fuel technologies with renewable ones. The country with the highest solar energy potential is Chile, in particular the Atacama Desert in Northern Chile [3]. The need to promote a wide portfolio of renewable energy technologies in Chile is critical owing to the seasonality of its large hydropower energy and its large dependency on fossil fuels, mostly imported [4]. The Chilean Energy Commission notes that 82 % of the electricity of the Northern Chile Electric System (SING) comes from coal resources [5].

For this reason, the Chilean government introduced in 2008 the Non-Conventional Renewable Energy Law 20.257 (excluding hydropower), which consists in increasing renewable energy production to 10 % of the total energy mix by 2024 [6]. This law was renewed in 2013 (Law 20/25) by increasing the renewable energy target to 20 % in 2025 [7]. Moreover, in 2014 the “Energy 2050” program was launched, which established a long-term vision in the Chilean energy system to 2050. It consists of four steps [8]: energy agenda (end of 2014), roadmap to 2050 (first semester 2015), long-term energy policy (end of 2015), and dissemination (first semester 2016).

In Chile, because of its outstanding solar resource, concentrated solar power (CSP) is one of the most promising renewable energy technologies. Compared to other technologies, the main advantage of CSP is its storage capacity [9]. The capacity factor of CSP plants increases with energy storage systems, ranging from around 20 % without storage system, to 40 % with 6 h of storage, to 60 % with more than 12 h of storage [10].

At the same time, compared to other renewable energy technologies, its main disadvantage is its higher cost [11]. However, recent research indicates that its levelized cost of energy (LCOE) will experience a considerable decrease over the period 2010–2030 and a slower but continuous rate between 2030 and 2050 [12]. It is expected that the main LCOE reduction will come from the solar field (15–16 %) by improving economies of scale, low values of turbine power output (33–78 MWe), and very high thermal energy storage systems (14–16 h) [11]. According to various studies, as a result of these improvements, a 25–30 % reduction in the LCOE is expected. Also, it is important to consider that LCOE also depends on plant location, decreasing in countries with the highest solar irradiation [12]. The most suitable Chilean region in terms of solar irradiation is Antofagasta Region II, within the Atacama Desert. Antofagasta has great energy demands, mainly from the mining sector, which in 2012 represented 61.1 % of the regional gross domestic product (GDP) [13].

Thus, given the large energy consumption of the mining sector, the huge solar potential, and the expected cost reduction of the technology, CSP is likely to play a key role in the energy mix and contribute to the decarbonization efforts of the country. In this connection, the present chapter conducts a sustainability assessment of the flagship CSP project in Antofagasta, “Cerro Dominador,” applying an input–output (I-O) framework and making use of the Social Hotspots Database (SHDB).

2 Methodology

The I-O methodology analyzes the response of economic sectors to an increase in the demand for goods and services generated by a project [14]. This methodology was first developed in 1936 by Wassily Leontief [15]. Nowadays, it is a robust and widely used tool, including in the energy sector [16].

I-O analysis is based on I-O tables (IOTs), which display the intersectoral relations among the economic sectors of a country. From IOTs it is possible to obtain the technical coefficients that indicate the consumption that one sector requires from another to produce a single monetary unit’s worth of some good or service [Eq. (68.1)] [17]:

$$a_{ij} = x_{ij}/X_j, \quad (68.1)$$

where x_{ij} is the amount of product that sector j requires from sector i to generate its final product X , and a_{ij} is the amount of product that sector j requires from sector i to produce one unit of product of j .

Additionally, IOTs display the added value of each sector and the final consumption of private and public sectors [18]. Equation (68.2) shows the final production calculation, which accounts for both direct and indirect effects in the economy. Direct effects refer to those produced by the increase in the demand of those sectors that directly provide goods and services required for the construction, operation, and maintenance of plants, whereas indirect effects are those produced by the effect that this new investment has on new flows of purchases and sales among sectors [19]:

$$X = (I - A)^{-1}Y, \quad (68.2)$$

where X is the final product, A is the technical coefficient matrix, Y is the final consumption demand, and $(I - A)^{-1}$ is the Leontief inverse matrix, which quantifies the direct and indirect requirements to satisfy a certain final demand.

Because of the interdependency among economic sectors, the development of any project involves widespread stimulus of various sectors in the economy. Such an effect is the so-called multiplier effect and indicates how much the total income of a country increases for every monetary unit invested in a project. The multiplier effect is the ratio between total effects (direct and indirect effects) and direct

effects [20]. Moreover, the methodology makes it possible to estimate the induced effects that account for the economic effects generated by the expenditures of workers involved on a project [21].

An extension of this methodology consists in assessing other types of effects – such as job creation and CO₂ emissions – per unit of output for each economic sector. The estimation of such effects is shown by Eq. (68.3) [21]:

$$\Delta X * Z_i = (I - A)^{-1} * \Delta Y * Z_i, \quad (68.3)$$

where ΔX is the total (direct and indirect) increase in goods and services, $(I - A)^{-1}$ is the Leontief inverse matrix, ΔY is the final demand, and Z_i is the environmental or socioeconomic vector, which indicates, for example, the employment, emissions, or energy consumption per unit of production for each sector included in IOTs.

One of the advantages of the methodology is that IOTs are usually available from national statistics databases. However, the methodology also faces some limitations: production capacity is assumed to be unlimited, it does not account for the possibility of storage, and, finally, no informal transactions in the economy are accounted for. Also, IOTs are only published and updated every few years, which prevents a given analysis from considering some relevant changes in the economy (e.g., technological improvements) [17].

With respect to social impacts, the SHDB is used to identify the main social risks in those sectors that are more affected by a project in terms of employment. The SHDB differentiates social risks into five different impact categories¹ in a specific economic sector in a specific country [22]. Moreover, the SHDB makes it possible to assess the risk of themes and subthemes within a social impact category. The different degrees of social risk are classified as very high, high, medium, and low. Finally, the so-called Social Hotspot Index (SHI) compares, in a quantitative way, the different social risks among sectors and countries. The index formation is based on the transformation of qualitative data into quantitative data of the risk of each social theme. The final SHI of each impact category results from the addition of all social risks of all social themes within an impact category [Eq. (68.4)]. A SHI close to 100 means that there exist high or very high social risks within an impact category [23]

$$SHI_{cat} = \sum (R_{avg} * W_T) / \sum (R_{max} * W_T) \quad (68.4)$$

where SHI_{cat} is the index of the social risk of each impact category, subscript T is the social theme, n is the number of themes within an impact category, R_{avg} is the average risk of each social theme, R_{max} is the maximum risk of each theme, and W_T is the weight assigned to each social theme.

¹The categories are *labor rights and decent work, healthy and safety, human rights, governance, and community infrastructure*.

The principal advantage of the SHDB is that it allows one to consider only the most common socioeconomic impacts (like employment) but also other social impacts not usually accounted for (e.g., human rights, labor rights, cultural aspects) [23].

3 Data and Assumptions

The principal assumptions considered in this work are as follows: (1) all project components are manufactured domestically (no-import assumption); (2) plant construction takes 1 year; (3) the lifetime of the plant in the operation and maintenance (O&M) phase is 30 years; (4) no additional energy fuel (e.g., natural gas) is used; and (5) the electricity demand of the plant is met by the Chilean electricity system (without self-consumption).

Table 68.1 shows the principal characteristics of the Cerro Dominador project based on the CSP World Database [37] and Ref. [24, 25].

3.1 *Direct, Indirect, and Induced Economic Effects; Employment Vector Data Source*

The direct and indirect economic effects were calculated based on the Chilean IOT and investment and O&M cost data from other plants.

The Chilean IOT was obtained from the Organization for Economic Co-operation and Development (OECD) statistical database [26]. The IOT

Table 68.1 Principal characteristics of Cerro Dominador plant

Owner	Abengoa
Location	Maria Elena, Antofagasta
Status	Under construction
Operation start date	June 2018
Power	110 MW
On-peak capacity factor	94.5 %
Energy in a year	910,602 MWh
Lifetime energy generation	27,318 GWh
Land area	1400 ha
Technology	Central receiver
Number of heliostats	10,600
Storage hours	17.5
Type of storage	Sodium and potassium molten salts
Type of cooling system	Dry
Investment cost	US \$1300 M
Use of electricity	Supply to SING

reference year is 2003; it contains 37 economic sectors, and the monetary unit is million Chilean pesos, which, for this work, were converted into US million dollars (US \$M)

The investment costs were estimated based on the cost data of a 17 MW Spanish plant [19] and were extrapolated to a 100 MW plant with 15 storage hours [27]. The case study investment cost breakdown is described as follows: 37 % solar field, 14 % tower, 6 % storage system, 12 % power block, 1 % land, 8 % engineering and insurances, 6 % construction, 6 % financial costs, 5 % balance of plant, and 5 % other expenses.

The total investment cost assumed is US \$1338 M, which is similar to that in the environmental impact statement (US \$1300 M) [24]. A cost reduction of 12 % was assumed by 2015 according to the International Renewable Energy Agency (IRENA) [10].

O&M cost estimations were determined based on an extensive literature review. The annual O&M cost of a 100 MW plant with 9 h of storage was estimated at US \$6,500,000/year [28]. Based on this reference and an O&M cost breakdown [27], it was assumed that the O&M cost without personnel costs for this case study would amount to US \$4,877,704/year. The discount rate considered for the current conversion of future prices is 5 % [19]. The O&M breakdown in this case study is described below based on Ref. [27]: 31 % solar field and storage system, 20 % financial costs, 25 % personnel costs, 14 % power block, and 10 % variable costs. Table 68.2 displays all the plant costs assigned to the various sectors of the Chilean IOT in both investment and O&M phases based on the Spanish plant [19].

For the assessment of the induced effects, personnel cost data, their propensity to consume, and the distribution of household expenditures were considered. The personnel cost assumption is US \$1,622,296/year based on Refs. [27] and [28]. The propensity to consume considered for Chile is 0.67 [29]. The Chilean household expenditure distribution in percentage terms across economic sectors in 2003 can be consulted in Ref. [30]. Regarding employment, Table 68.3 shows the total employment data by sector in Chile in 2003 from the Chilean National Statistics Institute (INE) [31].

To overcome the data gap between the nine economic sectors for which the Chilean INE provides employment data and the 37 sectors of the IOT, the employment vector of Brazil from the World IO Database (WIOD) [32] was considered, except with respect to the agricultural, mining, and construction sectors, which do not need any desegregation.

3.2 Environmental Vector Data Source

With regard to energy consumption, most data come from the Chilean National Emissions Inventory (NEI) [33]. For the disaggregation of all 37 sectors of the IOT, the National Energy Balance (BNE) from the National Energy Commission (CNE)

Table 68.2 Costs assigned to each economic sector of Chilean IOT in both investment and O&M phases

IOT sector	Investment phase		O&M phase	
	Percentage to sector (%)	US \$1000	Percentage to sector (%)	US \$/year
8-Chemicals	6.6	99,694	4	195,108
9-Plastics	1.5	22,395	1	48,777
10-Nonmetallic minerals	27.7	421,495	6	292,662
11-Basic metals	4.3	65,885	–	–
12-Fabricated metals	19.5	296,698	–	–
13-Machinery and equipment	9.1	138,533	1	48,777
14-Office and computer machinery	–	–	3	146,331
15-Electrical machinery	11.0	167,121	2	97,554
21-Electricity, gas, and water	0.1	1512	10	487,770
22-Construction	6.7	101,579		
26-Postal and telecommunication services	–	–	15	731,656
27-Finance and insurance	5.4	82,041	25	1,219,426
28-Real estate activities	0.1	1787	–	–
29-Machinery and equipment rental	0.1	1100	4	195,108
30-Computer activities	0.1	962	4	195,108
31-Research and development	0.1	962	2	97,554
32-Other business activities	7.7	117,322	22	1,073,095
35-Health and social work	0.1	1650	1	48,777
Total cost	100	1,520,736	100	4,877,704
With 12 % cost reduction	100	1,338,248	–	–

Table 68.3 Disaggregation by economic sector (%) of total Chilean employment in 2003

Economic sector	Percentage of total employment (%)
Mining and quarrying	1.4
Agriculture, fishing, hunting	13.7
Industry	14.2
Electricity, water, gas	0.4
Construction	8.0
Trade	19.5
Transport and communications	8.4
Financial services	8.2
Community and social services	26.3
Total	100.0

Table 68.4 Proportion of total Chilean energy consumption and CO₂ emissions among economic sectors in 2003

Economic sector	Percentage of total energy consumption (%)	Percentage of total CO ₂ emissions (%)
Energy industry	31.3	30.7
Manufacturing, construction, and mining	22.1	23.6
Transport	37.6	37.7
Fishing	0.8	0.8
Public, residential, and commercial	8.2	7.2
Total	100.0	100.0

of Chile in 2003 was consulted [34], except for the fishing and transport sectors, for which the NEI has exclusive data.

Finally, because of the large contribution of fossil fuels to the Chilean energy mix, the distribution of the CO₂ emission vector among IOT economic sectors is based on the energy consumption vector. Table 68.4 shows the distribution of energy consumption and CO₂ emissions among economic sectors from the official Chilean NEI.

4 Results and Discussion

The results in terms of impacts throughout the whole lifetime of a plant are presented in what follows, with distinctions between socioeconomic, environmental, and social direct effects (DEs) and indirect effects (IEs) in both investment and O&M phases.

4.1 Socioeconomic Impacts: Direct, Indirect, and Induced Economic Effects and Employment Effects

Figure 68.1 shows the total direct, indirect, and induced economic effects (in millions of US dollars, US \$M) on each economic sector² generated by the project. The total effect that the solar plant would generate over the course of its lifetime in the Chilean economy is US \$3124 M, of which US \$1407 M is direct effects, US \$1683 M is indirect effects, and US \$34 M is induced effects. The

²The complete economic sector titles can be found in Appendix 1 (United Nations database).

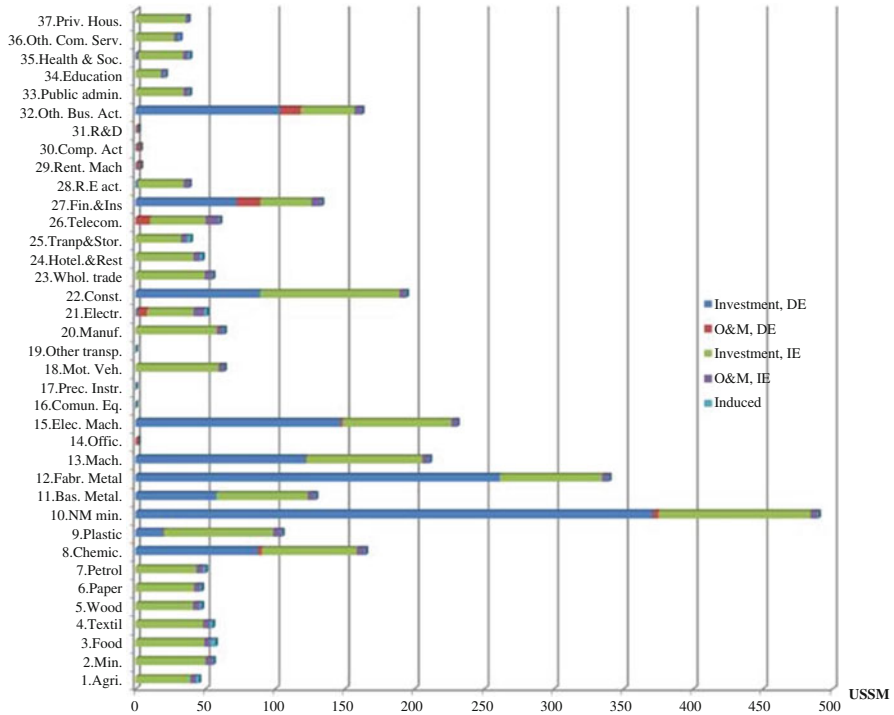


Fig. 68.1 Direct (DE), indirect (IE), and induced economic effects (in millions of US dollars) over lifetime of plant in both investment and O&M phases by economic sector

multiplier effect would be 2.19, indicating that for each dollar invested in the project, US \$2.19 would be generated in the economy as a whole.³

Regarding direct effects, the main sector that would be affected in the investment phase is sector 10, Other nonmetallic minerals. This fact is due mainly to the heliostats and the tower, which are the most expensive components of the plant. The second most benefited sector is sector 12, Fabricated metals, followed by sector 8, Chemicals, sector 13, Machinery, and sector 15, Electrical machinery. Other stimulated sectors would be sector 22, Construction, sector 27, Financial intermediation, and sector 32, Other business activities.

In the O&M phase, the largest stimulated sectors would be sector 27, Financial intermediation, and sector 32, Other business activities, followed by sector 21, Electricity, gas, and water supply, and sector 26, Postal and telecommunications services. Regarding indirect effects in both phases, the most affected sectors would be sector 10, Nonmetallic minerals, sector 12, Fabricated metals, sector 11, Basic

³ Comparing these results with the economic effects of the 17 MW Spanish plant, the total effect is €2230 M, with a multiplier effect of 2.3 [19].

metals, sector 13, Machinery, sector 15, Electrical machinery, and sector 22, Construction.⁴

The induced effect⁵ would be US \$33.4 M, with US \$15.4 M being direct effects and US \$18 M indirect effect. In this case, the most affected sectors would be sector 3, Food products, beverages and tobacco, and sector 25, Transport and storage, because of the large Chilean household expenditure in these sectors.

Referring to employment, the plant would create 134,949 new jobs in the whole lifetime of the plant, with 61,063 being direct jobs and 73,887 being indirect jobs. The ratio between indirect jobs over direct jobs would be 1.21, which, taking into consideration the labor force of the country, is consistent with similar results from the literature [35]. Figure 68.2 shows the total direct and indirect full-time 1 year of employment (in thousands of employees) generated over the whole lifetime of the project in both investment and O&M phases by economic sector.

The sector⁶ with the largest direct job creation in the investment phase would be sector 15, Electrical machinery and apparatus, owing to the large contribution of this sector to the power block (80%). Other sectors that would be affected, but to a lesser extent, are sector 10, Nonmetallic minerals, sector 11, Basic metals, sector 12, Fabricated metals, sector 13, Machinery and equipment, sector 22, Construction, and sector 32, Other business activities (mainly engineering jobs). Regarding direct jobs in the O&M phase, the most stimulated sectors would be sector 32, Other business activities, mainly related to engineering jobs, and sector 26, Postal and telecommunications services.

The highest indirect employment would also be in sector 15, Electrical machinery and apparatus. To a small extent, other sectors, like sector 1, Agriculture, or sector 4, Textile products, would also be stimulated owing to their relevance in the labor force of the country.⁷

It is important to note that if imports were taken into account, domestic stimulus, both in terms of economic growth and employment creation, would have been smaller because some of the components (such as the receptor or the generator) are currently made in certain specific countries and their manufacture on a domestic scale is not expected, at least in the short term [35]. Nevertheless, it is expected that even when considering such imports, a remarkable amount of stimulus in the domestic economy and job creation would take place (both directly and indirectly). This would lead to a diversification of business activities and contribute to the

⁴The sectors that do not result indirectly stimulated are those which do not have data in the original IOT.

⁵The induced effect is only estimated in the O&M phase due to personnel cost data lack associated to the investment phase.

⁶Sectors that do not appear in figures is due to the insignificance of results

⁷Some desegregation like “industry” was performed with the employment vector of Brazil because of a lack of data for Chile, and because labor productivity in Brazil in 2003 was smaller (World Bank database) [36], the employment results in some industrial sectors in Chile could be overestimated.

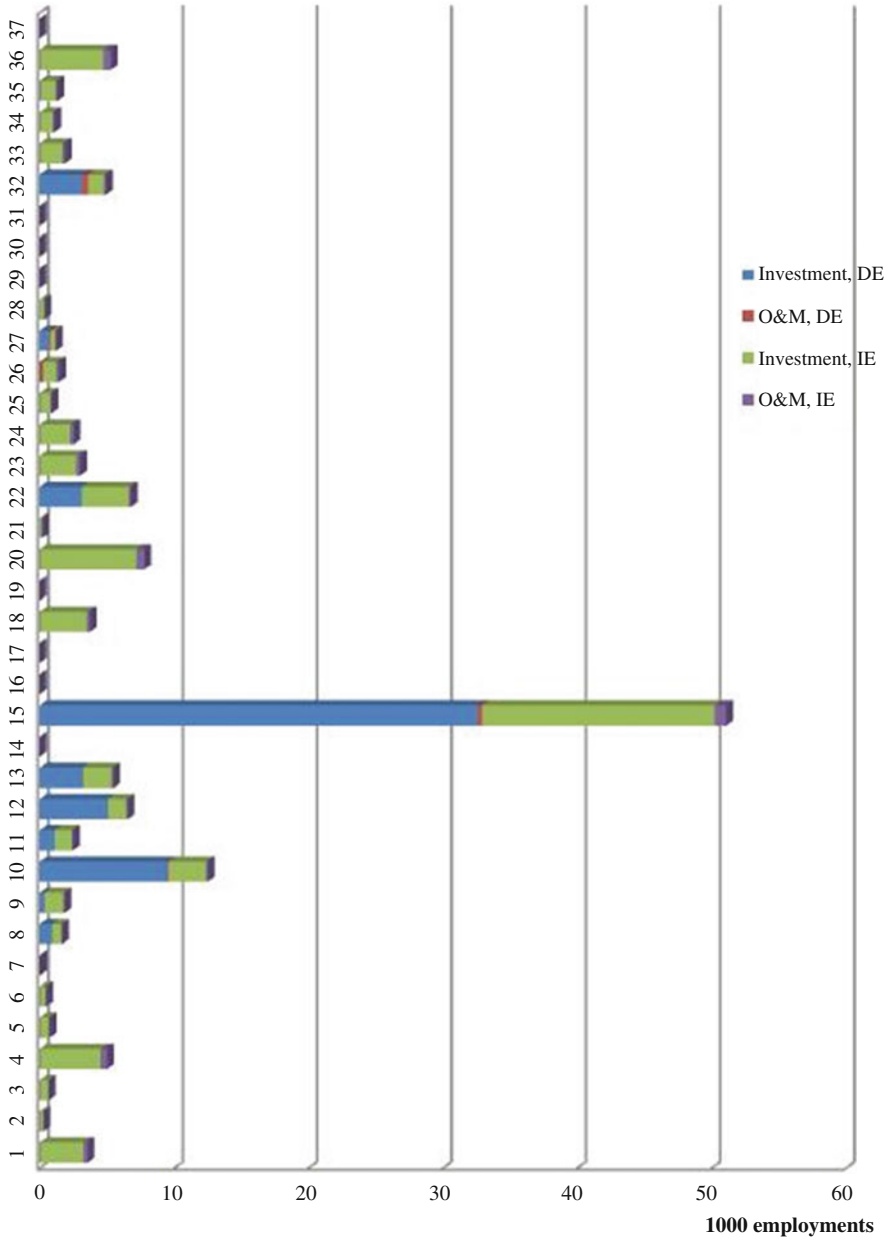


Fig. 68.2 Direct (DE) and indirect (IE) employment in (thousands of jobs) over lifetime of plant in both investment and O&M phases by economic sector

decoupling of Chile’s GDP from some key sectors, such as mining, which is particularly dominant in the northern part of the country.

4.2 *Environmental Impacts: Energy Consumption and CO₂ Emissions*

Figure 68.3 shows the direct and indirect energy consumption in thousands of terajoules (TJ) over the whole lifetime of the plant in both investment and O&M phases by sector. The energy consumption throughout the lifetime of the project would be 12,243 TJ, with 5225 TJ being direct consumption and 6989 TJ being indirect consumption.

In the investment phase, the largest consumption would come from sectors 10, Nonmetallic minerals, and 11, Basic metals, due to the huge amount of energy they require for their production. In the O&M phase, the most affected sector would be sector 21, Electricity, gas and water supply.

Indirect energy consumption in the investment phase would mostly come from sectors 11 and 21, Basic metals and Electricity, gas and water supply, respectively, followed by sector 6, Paper products, sector 8, Coke, refined petroleum products and nuclear fuel, sector 25, Transport and storage, and sector 37, Private households with employed people. In the O&M phase, the most affected sectors would be the most energy-intensive sectors: 11, 21, and 25, Basic metals, Electricity, gas and water supply, and Transport and storage, respectively.

Regarding CO₂ emissions, the project would generate over its lifetime 1759 Gg CO₂, with 1007 being direct emissions and 753 indirect emissions. The amount of emissions per kilowatt hour⁸ would be 64.36 g CO₂/kWh.⁹ Figure 68.4 shows the direct and indirect CO₂ emissions in hundreds of gigagrams over the lifetime of the plant in both investment and O&M phases by economic sector.

Sectors with the highest direct emissions in the investment phase would be sectors 10 and 11, Nonmetallic minerals and Basic metals, respectively, owing to their large energy consumption based on the fossil-fuel-intensive energy mix in Chile. To a lesser extent, sectors 12, Fabricated metals, and 15, Electrical machinery, would also produce considerable amounts of emissions. In the O&M phase, the emissions would mainly come from sector 21, Electricity, gas and water supply. The main sectors that contribute to indirect emissions coincide with those of direct emissions, plus sector 25, Transport and storage, and sector 37, Private households.

Based on these results, it would be advisable to pay attention to these sectors and try to implement specific measures (e.g., renovation of obsolete components, technologies with CO₂ sequestration) and formulate policies aimed at improving their energy efficiency and reducing CO₂ emissions.

⁸ It is assumed that the plant would produce 27,300 GWh in the whole life time.

⁹ Some comparisons for this result have been done: 60.1 g CO₂/kWh from a 50 MW parabolic trough plant without natural gas consumption [17]; 60 g CO₂ eq./kWh [37] and 48 g CO₂ eq./kWh [38] from a solar tower plant.

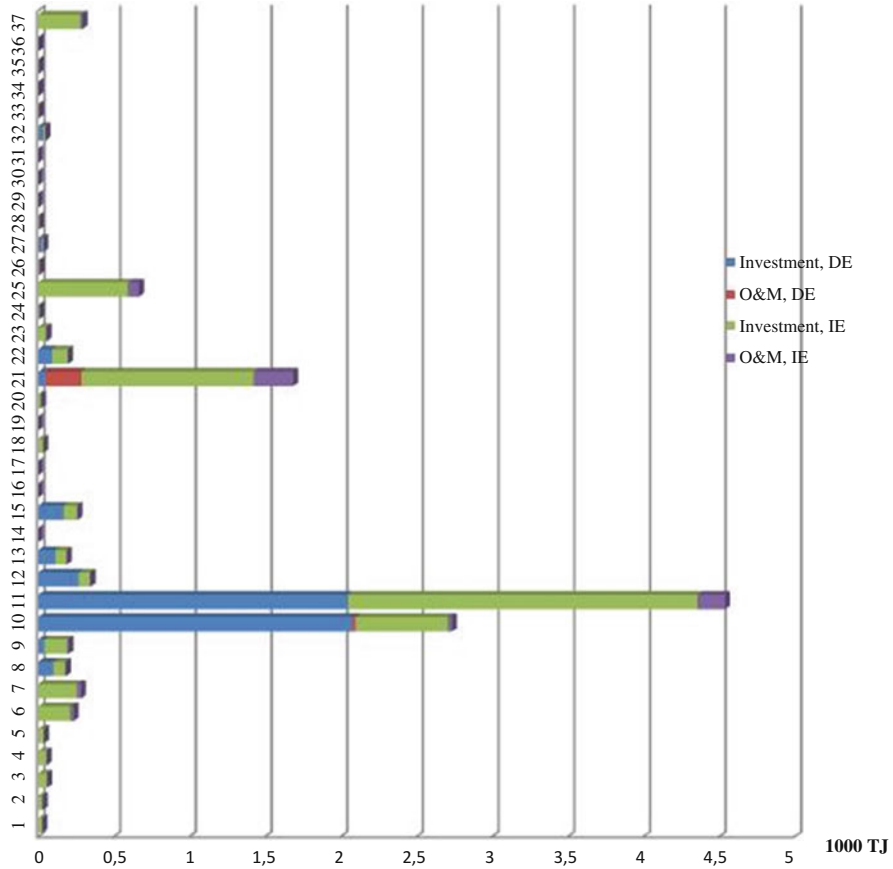


Fig. 68.3 Direct (DE) and indirect (IE) energy consumption (in thousands of terajoules) over lifetime of plant in both investment and O&M phases by economic sector

4.3 Social Impacts

A social risk analysis is performed in those sectors that show the largest total job creation as a result of the project. These sectors are sector 22, Construction, sector 15, Machinery and electric equipments, sector 20, Manufacturing, sector 12, Fabricated metals, and sector 10, Nonmetallic mineral products.¹⁰

The SHI for these sectors has a value of 60.81, except in the construction sector, which shows a higher value ($SHI_{const} = 67.5$). In Fig. 68.5 it is possible to compare

¹⁰The corresponding sectors in the SHDB are Construction, Machinery and equipment n.e.c., Manufactures n.e.c., Metal products, and Mineral products n.e.c.

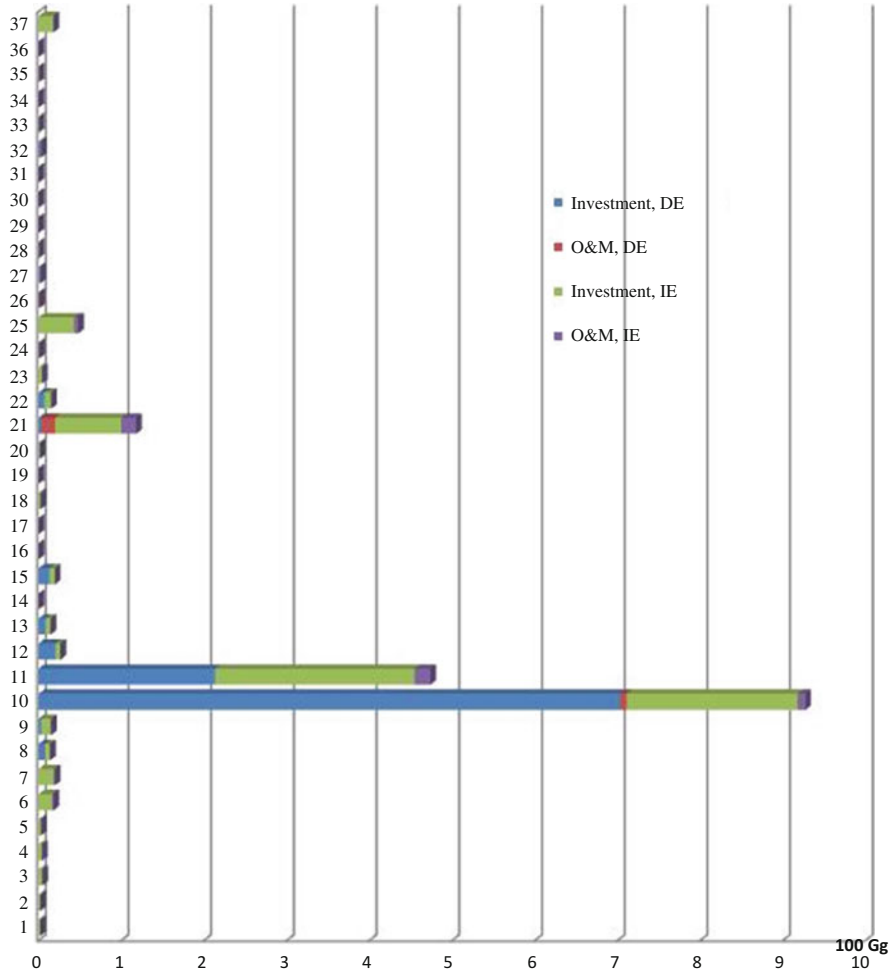


Fig. 68.4 Direct (DE) and indirect (IE) CO₂ emissions (in hundreds of gigagrams) over lifetime of plant in both investment and O&M phases by economic sector

this sector’s value within different countries, in which the SHI in the construction sector in Chile is lower compared to some other Latin American countries and even Spain, but higher compared to Norway. Also, results differ among the different impact categories.

The higher SHI value of the Chilean construction sector compared to all other Chilean sectors mentioned earlier comes from the labor rights and human rights categories. Within the labor rights category, the breakdown in each social theme¹¹

¹¹ There are more social themes within the impact category *Labor rights and decent work*, but they are not explained because of a lack of data in the SHDB.

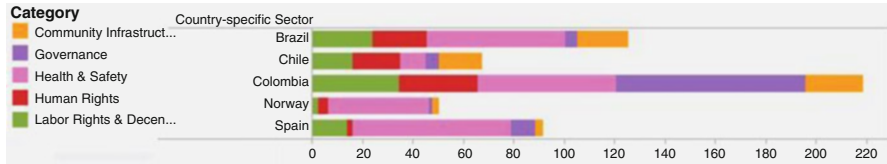


Fig. 68.5 Comparison of SHI in construction sector and its different impact categories among different countries (Brazil, Chile, Colombia, Norway, and Spain)

is 5 % forced labor, 19 % freedom of association, 13 % labor laws, 19 % migrants workers, 5 % poverty, and 39 % unemployment.

In this way, the most important risk in the construction sector in Chile is unemployment, with a risk value classification of very high. This is consistent with some results from the Employment and Unemployment Survey in Santiago de Chile, which indicated that the construction sector had the highest unemployment rate (10.4 %) in March 2014, double the nationwide average unemployment rate (5.7 %) [39]. Additionally, the unemployment risk is also high in the remaining sectors, with a high risk value according to the SHDB.

In this sense, job creation as a result of the Cerro Dominador project could contribute to the decreased unemployment risks, especially in the construction sector as its very high risk value. This sector could be particularly relevant for the Chilean economy since it is among the sectors that are most responsible for economic revitalization in the short and medium term. This is because it is a highly labour-intensive sector, mainly local labor force, mainly local, which, at the same time, stimulates demand in various other sectors, both directly and indirectly [40].

Local job creation and other livelihood effects as a result of CSP deployment in other areas of the world have been demonstrated and assessed [41]. In particular, the results of this research in the Ouarzazate area (Morocco) indicate that more than 1500 new jobs were created in Morocco, of which 700 were generated locally in the Ouarzazate area. In addition to these jobs, other social effects were assessed, such as the reinforcement of familial bonds in connection with migratory flows and new sources of income, as well as the creation of new infrastructures. However, this research also indicates that official entities like ministries should support local industries and promote skill development and research and development (R&D) in order to increase the competitiveness of the sector and increase productivity among the whole supply chain necessary for the project. Finally, despite all the advantages, the principal concerns of the studied population in Ouarzazate were related to water needs for the operation and maintenance of the plant in such an arid region, the small local population, emergent industrial development, and issues related to nontransparency and an absence of local population participation in decision making [41]. Such findings could be of great relevance for Chile since the local population might encounter similar opportunities and challenges.

5 Conclusions

Based on CSP cost data and the Chilean IOT, in this chapter a sustainability impact assessment of a CSP project in Chile was conducted in terms of economic stimulus, job creation, energy consumption, CO₂ emissions, and the existence of social risks in the country. Under a 100 % local content assumption, the economic sectors most benefited by the project would be nonmetallic minerals and fabricated metals. In addition to these sectors, the project would stimulate (both directly and indirectly) other domestic sectors like construction. In terms of employment creation, the most stimulated sector would be the one related to machinery and electrical equipment. Other sectors with large job creation figures would be nonmetallic minerals, fabricated metals, and construction. With regard to environmental impacts, those sectors with the largest energy consumption and CO₂ emissions would be nonmetallic minerals and basic metals.

Finally, social risk assessment indicated that high unemployment was the most relevant social risk in those sectors most affected socioeconomically by the project. Therefore, the project would lead to social benefits. Results also indicated that other social risks (e.g., child labor) would also have to be monitored.

To conclude, this chapter has shown that CSP technology could play a relevant role as a driver of economic stimulus and diversification of the Chilean economy and generate new employment opportunities, with a significant potential to revitalize the local economy. Additionally, the large solar potential, together with the environmental benefits of a renewable technology, indicates that CSP could be a promising technology in Chile in the short to medium term, specifically in regions with high solar irradiation like the Atacama Desert. Consequently, supporting policies that account for such positive externalities should be put in place to foster the deployment of this technology in Chile.

Acknowledgments This work was funded by a grant from CIEMAT for the training of research personnel.

Appendix 1: Description of Chilean IOT (United Nations) [42]

Sector 1: Agriculture, hunting, forestry, and fishing

Sector 2: Mining and quarrying

Sector 3: Food products, beverages, and tobacco

Sector 4: Textiles, textile products, leather, and footwear

Sector 5: Wood and products of wood and cork

Sector 6: Pulp, paper, paper products; printing and publishing

Sector 7: Coke, refined petroleum products and nuclear fuel

Sector 8: Chemicals and chemical products

Sector 9: Rubber and plastic products

Sector 10: Other nonmetallic mineral products
 Sector 11: Basic metals
 Sector 12: Fabricated metal products except machinery and equipment
 Sector 13: Machinery and equipment n.e.c.
 Sector 14: Office, accounting, and computing machinery
 Sector 15: Electrical machinery and apparatus n.e.c.
 Sector 16: Radio, television, and communication equipment
 Sector 17: Medical, precision, and optical instruments
 Sector 18: Motor vehicles, trailers, and semi-trailers
 Sector 19: Other transport equipment
 Sector 20: Manufacturing n.e.c.; recycling
 Sector 21: Electricity, gas, and water supply
 Sector 22: Construction
 Sector 23: Wholesale and retail trade; repairs
 Sector 24: Hotels and restaurants
 Sector 25: Transport and storage
 Sector 26: Postal and telecommunication services
 Sector 27: Finance and insurance
 Sector 28: Real estate activities
 Sector 29: Renting of machinery and equipment
 Sector 30: Computer and related activities
 Sector 31: Research and development
 Sector 32: Other business activities
 Sector 33: Public administration and defence; compulsory social security
 Sector 34: Education
 Sector 35: Health and social work
 Sector 36: Other community, social, and personal services
 Sector 37: Private households with employed persons

References

1. Kammen DM, Dove MR (1997) The virtues of mundane science. *Environ Sci Policy Sustain Dev* 39(6):10–41
2. World Commission on Environment and Development (1987) Our common future (the Brundtland report). *Med Confl Surviv* 4(1):300
3. Seminario Iberoamericano de Energías Renovables (2009) Las energías renovables en América Latina: Chile [Internet]. <http://es.slideshare.net/CanalEndesa/las-energias-renovables-en-amrica-latina-chile>. Accessed 29 Apr 2015
4. Larraín T, Escobar R (2012) Net energy analysis for concentrated solar power plants in northern Chile. *Renew Energy* 41:123–133, <http://dx.doi.org/10.1016/j.renene.2011.10.015>
5. Comisión Nacional de Energía (2013) Electricidad—Generación Bruta SING en 2013 [Internet]. <http://www.cne.cl/estadisticas/energia/electricidad>. Accessed 30 Jun 2015
6. Ministerio de Energía (2008) Ley 20.257: Modificaciones a la ley general de servicios eléctricos respecto de la generación de energía eléctrica con fuentes de energías renovables no convencionales. 2008(7681):7681.

7. Ministerio de Energía (2013) Gobierno promulga Ley 20/25 y anuncia entrada en vigencia de Ley de Concesiones. [Internet]. <http://www.minenergia.cl/ministerio/noticias/generales/gobierno-promulga-ley-20-25-y-anuncia.html>. Accessed 30 Jun 2015
8. Ministerio de Energía (2014) Energía 2050—Proceso Participativo Política Energética—Ministerio de Energía—Gobierno de Chile. [Internet]. <http://www.energia2050.cl/programa>. Accessed 30 Jun 2015
9. CSPToday (2012) Guía de Internacionalización de la CSP
10. Hoffschmidt B, Alexopoulos S, Rau C, Sattler J, Anthrakidis A, Boura C et al (2012) Concentrating solar power. *Compr Renew Energy* 3(2):595–636, <http://dx.doi.org/10.1016/B978-0-08-087872-0.00319-X>
11. Avila-Marin AL, Fernandez-Reche J, Tellez FM (2013) Evaluation of the potential of central receiver solar power plants: configuration, optimization and trends. *Appl Energy* 112:274–288, <http://dx.doi.org/10.1016/j.apenergy.2013.05.049>
12. Hernández-Moro J, Martínez-Duart JM (2013) Analytical model for solar PV and CSP electricity costs: present LCOE values and their future evolution. *Renew Sustain Energy Rev* 20:119–132
13. Banco Central de Chile (2012) Base de Datos Estadísticos—Precio Interior Bruto Regional por Sectores Económicos en 2012 [Internet]. <http://si3.bcentral.cl/Siete/secure/cuadros/arboles.aspx>. Accessed 30 Jun 2015
14. Ten Raa T (2006) *The economics of input-output analysis* [Internet]. Cambridge: Cambridge University Press. <http://ebooks.cambridge.org/ebook.jsf?bid=CBO9780511610783>. Accessed 30 Jun 2015
15. Leontief W (1936) Quantitative input and output relations in the economic systems of the United States [Internet]. http://www.jstor.org/stable/1927837?seq=1#page_scan_tab_contents. Accessed 30 Jun 2015
16. Linares P, Leal J, Sáez R (1996) Evaluación de las externalidades de la biomasa para producción eléctrica [Internet]. <http://bddoc.csic.es:8080/detalles.html?id=113934&bd=ICYT&tabla=docu>. Accessed 30 Jun 2015
17. De la Rúa Lope C (2009) Desarrollo de la herramienta integrada “análisis de ciclo de vida—Input Output análisis para España y aplicación a tecnologías energéticas avanzadas.” Planta
18. Tarancón MÁ (2003) Técnicas de Análisis Económico Input-Output
19. Caldés N, Varela M, Santamaría M, Sáez R (2009) Economic impact of solar thermal electricity deployment in Spain. *Energy Policy* 37(5):1628–1636
20. Holland D, Cooke SC (1992) Sources of structural change in the Washington economy. *Ann Reg Sci* 26(2):155–170, <http://link.springer.com/10.1007/BF02116367>. Accessed 30 Jun 2015
21. Caldés Gómez N, Lechón Pérez Y (2010) Análisis de externalidades de las energías renovables [Internet]. *Tratado de energías renovables*. Editorial Aranzadi. pp 951–1004. <http://dialnet.unirioja.es/servlet/articulo?codigo=3187593>. Accessed 30 Jun 2015
22. Social Hotspot Database [Internet]. <http://socialhotspot.org/>. Accessed 30 Jun 2015
23. GreenDelta (2013) SOCIAL HOTSPOT DATABASE introductory user tutorial
24. ABENGOA (2013) Declaración de Impacto Ambiental de Cerro Dominador [Internet]. <http://es.slideshare.net/VctorA1/adenda-n-1plantasolarcerrodominador>. Accessed 30 Jun 2015
25. CSP World (2015) CSP World Map|CSP World [Internet]. <http://www.cspworld.org/cspworldmap>. Accessed 30 Jun 2015
26. Organization for Economic Cooperation and Development (2015) Trade, input-output tables [Internet]. <http://www.oecd.org/trade/input-outputtables.htm>. Accessed 30 Jun 2015
27. Fichtner (2010) Assessment of technology options for development of concentrating solar power in South Africa, December
28. Kolb G, Ho C, Mancini T, Gary J (2011) Power tower technology roadmap and cost reduction plan. SAND2011-2419, Sandia ... [Internet]. (April):38. <http://prod.sandia.gov/techlib/access-control.cgi/2011/112419.pdf>
29. De Gregorio J (1998) Comportamiento de los agentes económicos

30. Chile Central Bank (2009) Clasificación del gasto en consumo final de los hogares e instituciones privadas sin fines de lucro por finalidad, periodo 2003–2007
31. Instituto Nacional de Estadística (2014) Series Empalmadas Diciembre-Febrero 1986 a Diciembre-Febrero 2010—Base Censo 2002|Instituto Nacional de Estadísticas|INE 2014 [Internet]. http://www.ine.cl/canales/chile_estadistico/mercado_del_trabajo/empleo/series_estadisticas/nuevas_empalmadas/series_fecha.php. Accessed 30 Jun 2015
32. World Input Output Database (2015) WIOD data [Internet]. http://www.wiod.org/new_site/database/seas.htm. Accessed 30 Jun 2015
33. Poch ambiental and Deuman (2008) Inventario nacional de emisiones de gases de efecto invernadero
34. Ministerio de Energía (2003) Balance Nacional de Energía 2003 [Internet]. http://antiguo.minenergia.cl/minwww/opencms/14_portal_informacion/06_Estadisticas/Balances_Energ.html. Accessed 30 Jun 2015
35. Dii (2011) The economic impacts of desert power: socio-economic aspects of an EUMENA renewable energy transition
36. World Bank Database (2015) Indicators|Data [Internet]. <http://data.worldbank.org/indicator>. Accessed 30 Jun 2015
37. Lenzen M (1999) Greenhouse gas analysis of solar-thermal electricity generation. *Solar Energy* 65(6):353–368
38. Norton B, Eames PC, Lo SN (1998) Full-energy-chain analysis of greenhouse gas emissions for solar thermal electric power generation systems. *Renew Energy* 15(1–4):131–136
39. Centro de Microdatos del Departamento de Economía de la Universidad de Chile (2014) Encuesta de Ocupación y Desocupación en el Gran Santiago: Informe Trimestral de Empleo Marzo 2014
40. Solimano A, Meller P (1983) Desempleo en Chile: interpretación y políticas económicas alternativas
41. CSPToday (2015) Five things you need to know about community buy-in in Morocco. CSP Today [Internet]. <http://social.csptoday.com/markets/five-things-you-need-know-about-community-buy-morocco>. Accessed 30 Jun 2015
42. United Nations Database (2015) United Nations Statistics Division—Classifications Registry [Internet]. <http://unstats.un.org/unsd/cr/registry/regcs.asp?Cl=17&Lg=1&Co=23>. Accessed 30 Jun 2015

Chapter 69

Learning Sustainability from Arab Gulf Vernacular Architecture

Khaled A. Al-Sallal

Abstract This chapter describes an approach that helps to understand the complex relationship between environmental and sociocultural factors and how to learn/derive sustainable design guidelines from vernacular architecture. The method identifies at the outset that vernacular architecture is a result of both cultural and environmental influences. It describes a set of factors that belong to two different categories, sociocultural and environmental, and that have had impact on generating the vernacular architecture of the Arab Gulf. Then it focuses on analyzing selected architectural elements based on the influencing factors. It presents a matrix that illustrates the function of each element and the complex relationship between each element and the factors that affect it. To understand these complex relationships, another matrix was devised to analyze the interactions between these elements under the relevant factors. The outcomes can be used to develop rules of thumb for sustainable design.

Keywords Architecture • Cooling • Desert • Design • Passive • Sustainable • Vernacular

1 Introduction

Several scholars have considered settlements as an outcome of environmental and sociocultural factors. The studies by Rapoport [1–3] noted that a house cannot be considered in isolation; it is part of a larger system of settings (i.e., a settlement) in which the house exists and hence must be considered as part of the settlement. Numerous examples from various places throughout the world support this argument. Oliver [4, 5] has provided extensive evidence in support of this idea that is shared by many well-known scholars from around the world, who have established a valuable collection of vernacular building traditions spanning the entire globe, including locations in the Arabian Peninsula, such as Yemen, Saudi Arabia, Oman, and Bahrain.

K.A. Al-Sallal (✉)
UAE University, P.O. Box 15551, Al-Ain, United Arab Emirates
e-mail: k.sallal@uaeu.ac.ae

In the United Arab Emirates (UAE), some studies have relied on the documentation and categorization of traditional design elements (e.g., Dubai Municipality 1997). Other studies have gone into more depth to show the human and environmental values reflected in vernacular settlements. El Aswad [6] offered an insightful analysis of the spatial structure of a modern vernacular settlement in Al-Ain, UAE, through a careful reading of people's habits and lifestyles and by tying this into a larger cultural framework. Dostal [7] explored the traditional architecture of Ras Al Khaimah with a specific emphasis on various house types as they relate to different climatic conditions (winter and summer).

In a different climatic zone not far from the Gulf, yet sharing a very similar sociocultural background, Yemen has a very distinctive vernacular architecture. The vernacular tower architecture of the historical city of Sana'a followed certain conventions that were well known and practiced by its inhabitants. These conventions grew out of long-term experiences developed over the lifetime of the city to satisfy human sociocultural needs and to meet the requirements of climate and environment. Because the city's inhabitants abided by these conventions, a consistent architectural language arose that gave a very unique identity to Sana'a architecture and preserved it for a long time. Al-Oulfi [8] provided a historical background in which the Yemeni architecture was compared and related to other architectures in the Arab region and in the world. Lewcock [9] described the old city of Sana'a and its architecture, including the tower houses. Other studies have focused on environmental factors and how they are related to human factors [10–16].

2 Theoretical Framework and Methodology

This study emphasizes the environmental component of architecture with a specific focus on the extent to which vernacular architecture is able to respond to climatic conditions. Furthermore, the cultural aspect defined here as a way of life of the people constitutes another component in the theoretical framework. The recognition that tradition/heritage is a living and continuing process of change is incorporated into the model, and the term is specified further to include both traditional vernacular (Bastakiy'ya-Dubai and Al'Marija-Sharjah, for example) and modern vernacular (housing neighborhoods built by the government and modified by its inhabitants and rural settlements). The model also attempts to move away from the temptation to copy traditional elements by extracting principles/lessons from traditional buildings and settlements (relationships among buildings), which could then be reapplied in contemporary housing projects utilizing modern technologies and processes. Furthermore, the study hopes to make a contribution to the large body of knowledge on this topic, thereby furnishing data that could further aid in the development of theory on the relationship/interaction between people and the built environment, thereby furthering our understanding of these processes (Fig. 69.1).

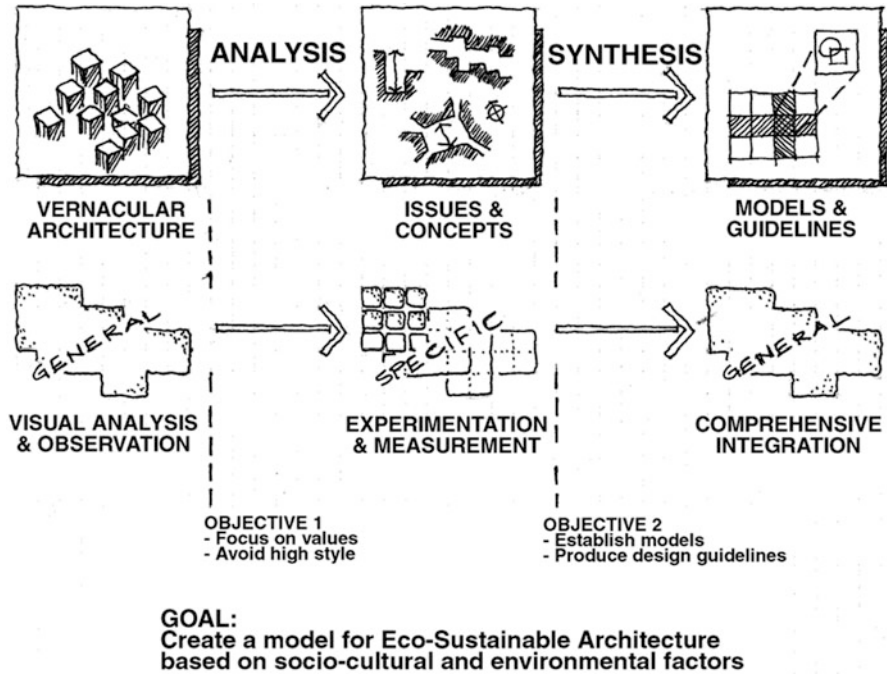


Fig. 69.1 Theoretical framework of study

To achieve the study objectives, the research utilizes a photographic survey, a library search, thematic map analysis, three-dimensional computer modeling, and energy simulation to achieve the targeted results in each of the research phases as follows:

- Phase 1. Fieldwork exploratory visual survey and office work analysis of the city map to determine the physical features of interest to the research;
- Phase 2. Three-dimensional computer modeling and energy simulation to analyze selected prototypes that are common in the region;
- Phase 3. Comprehensive environmental and sociocultural analysis of results; this phase will investigate the critical relationship between environmental and sociocultural factors to observe any conflicting or matching points in design; it will describe the results by illustrating them graphically in matrix format.

3 Urban and Architectural Context

Many vernacular settlements in the Arabian Peninsula were generated as a result of trading purposes and hence developed on the old caravan paths used for trading. An example of this type is the city of Muscat; Muscat dates back to the first century AD

when it was a concealed harbor from where frankincense was transported to Greece, Rome, and the Mediterranean. Dubai developed as a result of fishing and pearl diving activities. Other inland settlements were established mainly as centers of power of old civilizations and a place for royals; an example of this type is the city of Sana'a in Yemen. This study focuses on settlements that existed in the Arabian Gulf area.

The desert architecture in the Middle East and North Africa was basically the result of three main factors: the hot dry or humid climate, sociocultural life, and locally available construction methods and materials. Generally this type of architecture is characterized as having a high-density plan where buildings were close to each other or attached, penetrated by narrow alleys (called *Sikka* in the local dialect) that were shaded for most of the day (Fig. 69.2). These alleys are oriented either to promote sea breezes in coastal settlements or to limit dusty winds in inland settlements. The compact planning plays a vital role in traditional desert settlements. Some of the benefits can be outlined as follows:

- The interiors of the buildings are protected by almost blank walls with very small openings, which helps to provide shading and control heat, dust, and sand.
- The streets are narrow and winding; therefore, there is less tendency for wind velocity to increase as a result of tunneling effects.
- Public spaces, such as market squares, are well sheltered from the impact of desert winds by adjoining houses and high walls.

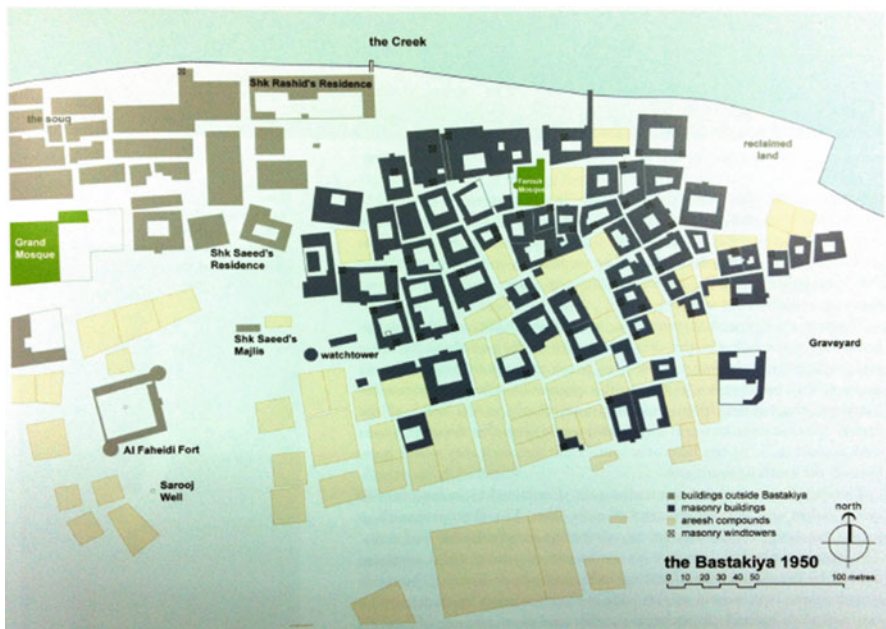


Fig. 69.2 Plan of Bastakiya area in Dubai

In coastal settlements, such as the Al-Bastakiyah district in Dubai or Al Murijah in Sharjah, the alleys mostly ran from north to south and ended at the sea, permitting the prevailing north winds to pass through. Another important feature in this architecture is the use of wind towers that helped to passively cool the occupants. The wind towers of these vernacular houses gave the only variation in height to the outline of the district and thus created a more interesting and beautiful skyline. So-called introvert-plan houses comprising a series of rooms built around a central courtyard, open to the sky, are the configuration of residential buildings in this area. This plan satisfies social conditions and in particular privacy for the various elements of extended families; in addition, it is a flexible space that can be adapted to the changing requirements of an extended family. This configuration agreed with Islamic teachings advocating a separation between public and private life (with the latter turning its back on the street). The house or *bait* is the basic element in desert settlements and is turned in upon itself as it opens onto the private courtyard, known as a *hawsh*. The majority of people in the Arab Gulf region lived in houses built of date-palm products. Other materials used to construct houses were stones in the mountains' areas and mud bricks in the oases. The richer ruling families and merchants built their houses of coral stone, mud bricks, and imported mangrove wood [17].

The courtyard acts as a center of home life (Fig. 69.3). In this configuration, the family, especially the woman, can enjoy complete privacy, while at the same time the house is open to relatives, friends, and neighbors who may wish to come in to the men's reception room (*majles*). The external walls represent a powerful physical barrier between the interior and the exterior. From the outside the walls of the



Fig. 69.3 View of a courtyard – a traditional house in Sharjah

house rise up high with bare surfaces, rough and massive, that contrast sharply with the interior, where arches and screens achieve an intricate pattern of light and shade. The courtyard also acts as a wind-generating tool in the house, the hot air ascending and cooler air replacing it from the surrounding rooms. This movement creates constant air circulation in the house and provides a pleasant living microclimate for the inhabitants.

There is a need to understand how the traditional architecture succeeded in maintaining a balance between environmental influences and sociocultural needs and why modern houses failed to do so. Learning from the past by exploring design-oriented guidelines from traditional architecture is necessary to reveal proven design methods that could serve as the basis for creating sustainable communities.

4 Analysis and Discussion

4.1 Effect of Culture

Traditional settlements are flanked by alleys that run in different directions to connect between houses and public buildings, such as the mosque or the market (Suq), and between residential districts. In the intersection of these alleys, one can find social squares (Fig. 69.4c, d) connected to the public areas, especially the mosques and *suq*. The width of the main alleys should permit activities to be performed comfortably, such as walking and transporting goods to the market, and accommodate other public facilities. The social square is directly connected to the mosque that is needed for daily prayers as well as to support certain social events, such as celebrations, feasts, and weddings. Location, size, shape, and shape proportion of the outdoor space are the design parameters that determine its adequacy for supporting certain functions. Hence, the space of a social square should permit gatherings of many people, usually males, to celebrate religious feasts and social ceremonies.

As the alley runs through residential units, it becomes narrow and more private, serving only a limited number of houses. Since the activities of the main alley and the social square are public, the privacy of the entrances and ground floor openings of the houses located around the square should be maintained. This is an effect of the outdoor space function on building form. Thus a concern for privacy was reflected in the physical form of the buildings in a number of ways:

The position of doors opening onto streets: a main door, usually visible from the street and having an elaborate porch, is used by men and guests, while another, secondary, door, much smaller in size and hidden from strangers, is used by women.

Minimum use of windows facing the street: only reception rooms on the first floor have large low-level windows onto the street. Higher up the building, rooms are more private and windows do not face the streets; openings are screened with *mashrabiya*s to provide privacy and permit air circulation.

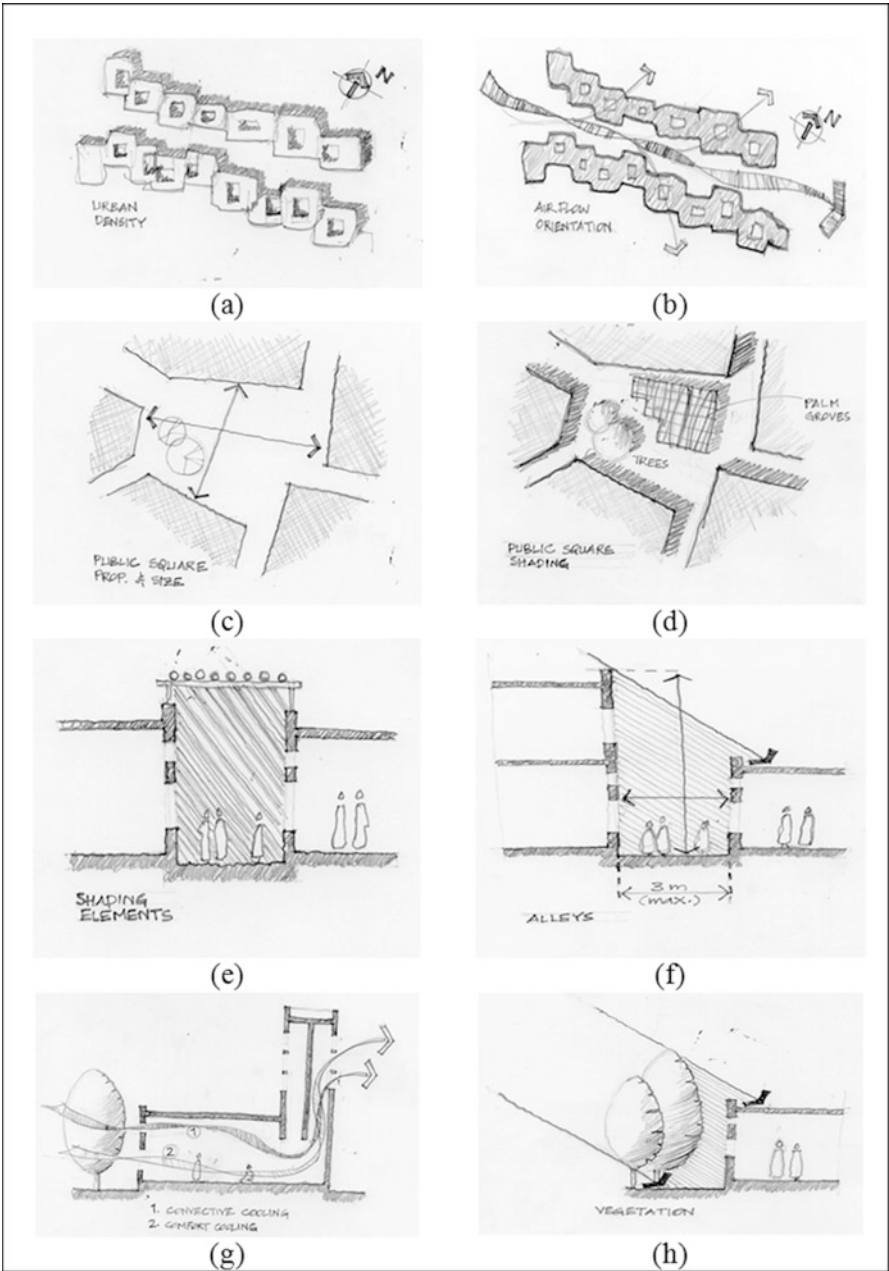


Fig. 69.4 Sketches showing some design concepts in vernacular architecture of Arab Gulf: (a) compact planning where buildings were close to each other or attached, penetrated by narrow alleys; (b) alleys were oriented to promote sea breezes and to limit dusty winds; (c) size and space proportion of social squares promoted solar shading and social activities; (d) shading of social squares by vegetation or light structures made of palm groves; (e) shading of sikka by palm groves; (f) buildings heights were increased while alleys were made more narrow ($h/w = 2:1-1:1$) to promote shading; (g) wind towers assisted by windows open to courtyards helped to provide comfort cooling for people and cool building structure by convective ventilation; (h) sun shading and evaporative cooling provided by vegetation in courtyards

Restricted building heights: usually rooms in vernacular houses were added in stages to respond to growth in family size; according to the social structure the extended family lived under one roof. These traditional buildings and the way they expand follow certain conventions developed by their inhabitants throughout history. Examples of these conventions are as follows:

- Buildings should be no more than two floors high.
- The terraces of neighboring buildings should be at the same height so that no house can overlook another.
- No window should open onto another family's or person's private space etc.

4.2 *Effects of Climate*

Solar shading: The vernacular settlements in the Gulf were compactly organized to maximize solar shading and keep the extreme solar radiation away from buildings' structures and occupants. This was achieved through the following means (Fig. 69.4a–f)

- Form–space proportion: The ratio of form to space increased the density of the built area;
- Size of alleys: Alleys were narrow, not exceeding 3 m;
- Building height and alley width proportion: Buildings heights were increased while alleys were made more narrow ($h/w = 2:1-1:1$);
- Public social squares: The size and shape proportion of public squares promoted solar shading by the surrounding buildings and vegetation;
- Covered alleys: Alleys in public zones, such as in the market, were shaded by palm groves.

At the architectural scale, several methods were used to provide shading. These are as follows:

- The courtyard maximized shading with its walls and vegetation for most daytime hours.
- Solid air-puller walls (*masqat*) provided total shading.
- Traditional windows provided total shading with their wooden shutters.

Airflow: The main alleys in the coastal settlements in the Gulf ran in the north–south direction (Fig. 69.4a). This helped the desirable north and northwest breezes to infiltrate into the main city building masses. Houses were oriented to capture the pleasant sea breezes. This is an effective traditional design solution at the urban scale, which promotes passive cooling effects through the following methods:

- Convective cooling of building structures by dissipating heat from the building mass,
- Cooling by ventilation for building occupants by dissipating heat from their bodies,
- Reduction of the effect of excessive humidity by stirring air currents.

At the architectural scale, several methods were used to provide passive cooling:

- Courtyards provided convective cooling by acting as a wind-generating tool in houses, where hot air ascends and cooler air replaces it from the surrounding rooms. This promoted evaporative cooling by the use of vegetation, lowering the air temperature;
- Wind towers helped to passively cool private spaces in traditional houses by four triangular vertical tunnels that attracted air from all directions and increased its speed (Fig. 69.4g);
- Air-puller walls allowed airflow to circulate through rooms, removing hot air through convective cooling, while maintaining the privacy of the indoor space.

4.3 Relationships Between Factors

The factors that formed the vernacular settlements of the Gulf can be divided into two groups: *sociocultural* and *environmental* factors. The *privacy* of the house occupants, their *safety*, and *sociability* with the outside world and within the house are examples of important cultural requirements that have a great impact on the architecture of vernacular settlements. *Solar access/shading* and *ventilation* are examples of environmental factors that played significant roles in forming the climatic-responsive architecture of these settlements. To respond to the influence of these factors, numerous innovative architectural solutions were developed, such as compact building organization, courtyards, windows, air pullers, and wind towers. These features gave the architecture of the Gulf a unique identity and attractive character.

The way the vernacular architecture responded to the needs of the sociocultural and environmental factors by innovative concepts has been investigated and described. Tables 69.1 and 69.2 below provide matrices that illustrate how some traditional design concepts (or elements), such as courtyards, air-puller walls, windows, and wind towers, responded to environmental and cultural factors. This matrices can be a useful tool not only to carry out the function of each architectural element but also to understand the complex relationship between each architectural element and the factors that influence its design and operation.

To understand these complex relationships, another matrix was also devised (Table 69.3). It helps to analyze the binary relationship between any two factors regardless, of category (i.e., sociocultural or environmental). Three types of relations have been identified: *agreement* (A), *disagreement* (D), and *no relation* (N). For example, courtyards with vegetation provide shading and passive cooling for most of the daytime hours while maintaining the privacy of the family inside. Therefore, in the courtyard case, there is a high degree of agreement between privacy and shading and between privacy and passive cooling. In contrast, in the case of air-puller walls, there is a high degree of agreement between passive cooling and privacy, while there is a disagreement relation between cooling

Table 69.1 Traditional design concepts’ response to environmental factors

Environmental factor	Courtyard	Air-puller wall	Windows	Wind tower
Shading	Courtyard maximizes shading with walls and vegetation for most daytime hours	Solid air-puller walls provide total shading	Provided using wooden shutters	Overshadows roofs and other structures of house
Passive cooling	Comfort ventilation: courtyard acts as wind generator in house; hot air ascends and cooler air replaces it from surrounding rooms. Evaporative cooling: vegetation creates an evaporative cooling effect that lowers air temperature and increases humidity	Allows airflow to circulate through rooms, removing hot air through convective cooling while maintaining privacy of indoor space	Windows promote airflow with assistance of courtyard by acting as inlet openings during day or outlet openings at night	Wind towers help to passively cool private spaces in traditional houses with four triangular vertical tunnels that draw in air from all directions and speed it up

(or privacy) and sociability. This is because this kind of system promotes cooling by ventilation while maintaining the privacy of inner rooms by solid walls. These solid walls prevent any opportunity for sociability. This is a good example of matching between two factors (i.e., passive cooling and privacy) at the expense of a third one (i.e., sociability). The location of windows is determined according to the level of privacy required for each space. For example, windows in private rooms open out onto the courtyard to maintain privacy, while windows of the men’s reception are open to public alleys, which can promote sociability. Therefore, in the window case, sometimes there is disagreement between passive cooling and privacy. The occupants must choose between closing windows using shutters for complete privacy or opening them to create airflow for ventilation.

5 Conclusion

This study proposes a model that helps explore abstract concepts from traditional environments and present methods to reapply them in contemporary architecture. It depends mainly on abstracting complex architectural environments into more simplified, yet more comprehensive and meaningful, relationships. It helps in

Table 69.2 Traditional design concepts’ response to sociocultural factors

Sociocultural factor	Courtyard	Air-puller walls	Windows	Wind tower
Privacy	Provides totally enclosed space that maintains privacy of house, especially for women	Provide high visual and acoustic privacy for indoor spaces	Privacy is provided with wooden shutters; location of windows on ground floors open onto courtyard; those opening to public spaces are located on upper floors	Wind towers help maintain privacy of indoor spaces requiring circulating airflow
Safety	Provides safe and pleasant enclosed space for children and helps parents watch children in courtyard from surrounding spaces or from <i>liwan</i> (i.e., shaded outdoor space surrounding courtyard)	Provide greater safety than windows because they are totally closed and cannot be penetrated, but meet requirements for ventilation	Provided by use of steel bars and wooden shutters	Triangular tunnels of wind towers are usually open in summer and closed in winter with wooden shutters; the shutters and narrow design of the openings helps to guarantee safety of house
Sociability and visual connection	Serves as center of home social life; its introverted design provides visual connection to <i>liwan</i> and other rooms to shaded and planted areas	Used for most private rooms and hence do not improve sociability	Low-level windows (usually a small number and used only for men’s reception) provided limited visual connection with outside	Wind tower room is most appropriate room for family or female gatherings in summer

fostering an understanding of the complex relationships between environmental and sociocultural factors in a more visual depiction and design-oriented approach while keeping them coherent. The sociocultural and environmental impacts on four settings from the vernacular architecture of the Gulf are analyzed. The study provides two matrices that illustrate how some traditional design concepts (or elements) responded to environmental and cultural factors. These matrices can be used as a useful tool not only for fulfilling the function of each architectural element but also for realizing the complex relationship between each architectural element and the factors that influence its design and operation. To understand the interactions between elements, another matrix is developed. It helps analyze the binary relationship between any two factors based on three types of agreement/conflict relations. It is believed that the same model could also be applied to analyze other architectural settings or comparing design alternatives.

Table 69.3 Analysis of level of agreement between environmental and sociocultural factors

Analysis of level of agreement between environmental and sociocultural factors	
Courtyard	Air puller
Wind tower	Traditional window
<p> Agreement Disagreement No relation </p>	

References

1. Rapoport A (1969) *House, form and culture*. Prentice Hall, Engelwood Cliffs
2. Rapoport A (1983) Development, culture change and supportive design. *Habitat Int* 7 (5/6):249–268
3. Rapoport A (1999) A framework for studying vernacular design. *J Archit Plann Res* 16 (1):52–64
4. Oliver P (1987) *Dwellings: the house across the world*. University of Texas Press, Austin
5. Oliver P (ed) (1997) *Encyclopedia of vernacular architecture in the world*. Cambridge University Press, London
6. El Aswad S (1996) *The folk house: an anthropological study of folk architecture and traditional culture of the Emirates Society*. The United Arab Emirates University, Department of Sociology, Al Ain
7. Dostal W (1983) *The traditional architecture of Ras Al-Khaimah (North)*. Reichert, Wiesbaden
8. Al-Oulfi M (2000) *Characteristics of Yemeni architecture: forms and directions of development*, unpublished PhD Thesis, Shanghai Tongji University, China
9. Lewcock R (1986) *The old walled city of Sana'a*. Paris: UNESCO
10. Al-Sallal KA (1993) The role of indigenous fenestration to reduce energy requirements in the Sana'a house. In: *Solar energy: research and applications—proceedings of fourth Arab international solar energy conference*, vol 2. Royal Scientific Society, Amman, pp 875–888
11. Al-Sallal KA (1996a) Traditional methods in new forms: insight to achieve energy conservation in the modern Sana'a house. In: Sayigh A (ed) *Proceedings of the World Renewable Energy Congress*, Denver, CO, vol 3, pp 1438–1441
12. Al-Sallal KA (1996b) Solar access/shading and building form: geometrical study of the traditional housing cluster in Sana'a. In: Sayigh A (ed) *Proceedings of the World Renewable Energy Congress*, Denver, CO, vol 3, pp. 331–334
13. Al-Sallal KA (2004) *Sana'a: transformation of the old city and the impacts of the modern era*. In: Elsheshtawy Y (ed) *Planning Middle Eastern cities: an urban kaleidoscope in a globalizing world*. Routledge, London
14. Al-Sallal KA (2013) Vernacular tower architecture of Sana'a: theory and method for deriving sustainable design guidelines. In: Sayigh A (ed) *Sustainability, energy and architecture: case studies in realizing green buildings*. Elsevier, Amsterdam
15. Al-Sallal KA, Cook J (1992) Sana'a historical windows: integration between comfort and aesthetics. In: Burley S, Arden ME (eds) *Proceedings of 17th national passive conference of American Solar Energy Society*, American Solar Energy Society, Boulder, vol 17, pp 197–202
16. Al-Sallal KA (2001) The balanced synthesis of form and space in the vernacular house of Sana'a: bioclimatic and functional analysis. *Archit Sci Rev* 44(4):419–428
17. Kay S, Zandi D (1991) *Architectural heritage of the gulf*. Motivate Publishing, Dubai

Chapter 70

Transparent Conducting Oxides for Solar Cell Applications

Shadia J. Ikhmayies

Abstract Transparent conducting oxides (TCOs) are wide bandgap semiconductors ($E_g \geq 3.1$ eV) whose properties strongly depend on stoichiometric deviations, such as oxygen deficiency, and on the nature and quantity of impurities trapped in the host lattice. Examples of TCOs include tin oxide (SnO_2), indium tin oxide (In_2O_3), and zinc oxide (ZnO). The best-known application of TCOs in solar cells is their use as fore contacts. High-efficiency CdTe solar cells are generally grown in a superstrate configuration, where the CdTe/CdS stacks are deposited on TCO-coated glass substrates. Another development is an application of a TCO as a back electrical contact on CdTe, leading to bifacial CdTe solar cells, which can be illuminated from one or both sides.

In this chapter, a review of the properties of TCOs of potential use in solar cells was performed, with a focus on tin oxide and zinc oxide thin films. This focus is due to the fact that these two compounds in thin film forms are technologically important materials in photovoltaic cells. The electrical, optical, structural, compositional, and morphological properties of both of these compounds are discussed.

Keywords Transparent conducting oxides • Solar cells • Fore contacts • Tin oxide • Zinc oxide

1 Introduction

Transparent conducting oxides (TCOs) are wide bandgap semiconductors ($E_g \geq 3.1$ eV) that have high transmission of light in the visible and near-infrared regions, high reflectance in the infrared region, and high electrical conductivity [1]. Because of these properties, TCO materials have been used in a wide range of applications in science and technology, including solar cells [2], heat-reflecting mirrors [3], antireflection coatings [4], and a variety of electro-optical devices such as flat panel display devices [5, 6]. The properties of TCOs strongly depend on the

S.J. Ikhmayies (✉)

Faculty of Science, Physics Department, Al Isra University, Amman 11622, Jordan

e-mail: shadia_ikhmayies@yahoo.com

stoichiometric deviation and on the nature and quantity of impurities trapped in the host lattice [7].

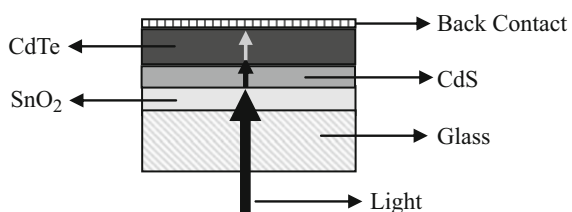
TCOs include undoped and fluorine-doped tin oxide (SnO_2 and $\text{SnO}_2:\text{F}$), indium oxide (In_2O_3), indium tin oxide (ITO), and undoped and doped zinc oxide (ZnO). To combine and stabilize the properties of TCO films, an alternative strategy is proposed in the literature whereby TCO materials are fabricated based on multicomponent oxides, which consist of a combination of binary or ternary compounds such as $\text{In}_2\text{O}_3\text{-ZrO}_2$, $\text{TiO}_2:\text{ZrO}_2$, ZnO-SnO_2 , $\text{In}_2\text{O}_3\text{-Sc}_2\text{O}_3$, and $\text{ZnO-V}_2\text{O}_5$.

TCO thin films can be prepared using a variety of methods such as chemical vapor deposition (CVD), sputtering, sol-gel process, and spray pyrolysis (SP). Sputtering and evaporation processes often prove to be too expensive for some industrial applications. Chemical spraying offers a competitive alternative for the mass production of these coatings. SP presents some noticeable advantages, such as the possibility of varying film properties by changing the composition of the starting solution (through the introduction of dopants and changing the film microstructure) and its low cost when large-scale production is needed [8].

In solar cells TCO have several uses, where they can be used as fore contacts in thin-film solar cells such as the superstrate configuration of CdS/CdTe . The layers for superstrate cells are grown on TCO-coated glass substrates. The TCO allows light to enter the device while maintaining electrical contact with the cell. To be used as a fore contact in such solar cells, TCOs must have n-type conductivity. Figure 70.1 shows a schematic of a thin film $\text{SnO}_2/\text{CdS}/\text{CdTe}$ solar cell, where SnO_2 is used as a fore contact. A second application of TCOs in solar cells is that they can be used as back electrical contacts on CdTe , leading to bifacial CdTe solar cells, which can be illuminated from one or both sides. A third application is to use TCOs as a buffer layer. To obtain Cd-free solar cells, TCOs can be used instead of CdS in thin-film solar cells, such as CuInS_2 thin-film solar cells.

This chapter presents a review of TCOs prepared in our lab for use in solar cells. Thin films of SnO_2 , $\text{SnO}_2:\text{F}$, ZnO , and $\text{ZnO}:\text{Al}$ were prepared and characterized by X-ray diffraction (XRD), scanning electron microscopy (SEM), current-voltage ($I\text{-}V$) characteristics, and transmittance spectroscopy. SnO_2 was prepared by thermal evaporation, and the others were prepared by the SP technique. The structural, optical, and electrical properties of the films are also discussed.

Fig. 70.1 Schematic of superstrate configuration of $\text{SnO}_2/\text{CdS}/\text{CdTe}$ thin-film solar cell. Note: Drawing is not to scale



2 Undoped Tin Oxide Thin Films

Undoped tin oxide (SnO_2) films were prepared by thermal evaporation at ambient temperature [9, 10]. The films are amorphous, nanocrystalline, or partially polycrystalline. But these films have high transmittance and smooth surfaces, and they show interference maxima and minima. They need chemical heat treatment to be suitable for use in thin-film solar cells.

3 Fluorine-Doped Tin Oxide Thin Films

Fluorine-doped tin oxide ($\text{SnO}_2:\text{F}$) thin films were prepared using the SP technique on glass substrates [11–15]. XRD diffractograms of the films are shown in Fig. 70.2, where the films are polycrystalline and show the tetragonal rutile structure of SnO_2 . Miller indices are indicated on the diffractograms for each diffraction peak. As seen in Fig. 70.2, there are greater crystallization and orientation of crystal growth in the case of the higher substrate temperature.

The morphology of the same films was observed by SEM (Fig. 70.3). The micrographs confirm that the films are polycrystalline. The films appear fully covered with material, and the film prepared at the higher substrate temperature shows larger grains, consistent with the XRD diffractograms in Fig. 70.1. The grain size was estimated by the SEM for a random set of grains, and the numbers are displayed in each micrograph.

The electrical properties of these films were recorded at room temperature by measuring the I–V characteristics at room temperature. Figure 70.4 shows the I–V plots for three films prepared at different substrate temperatures – 380, 450, and 480 °C. From such measurements the resistivities of the order of 10^{-3} to 10^{-1} Ω cm were obtained for films with different thicknesses.

Transmittance measurements were recorded at room temperature in the wavelength range 290–1100 nm (Fig. 70.5). The maximum transmittance of the films is

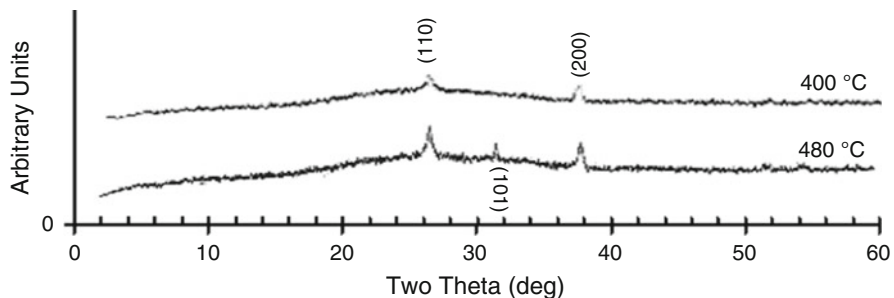


Fig. 70.2 X-ray diffractograms for $\text{SnO}_2:\text{F}$ thin films prepared using SP technique at different substrate temperatures. (a) $T_s = 400$ °C. (b) $T_s = 480$ °C

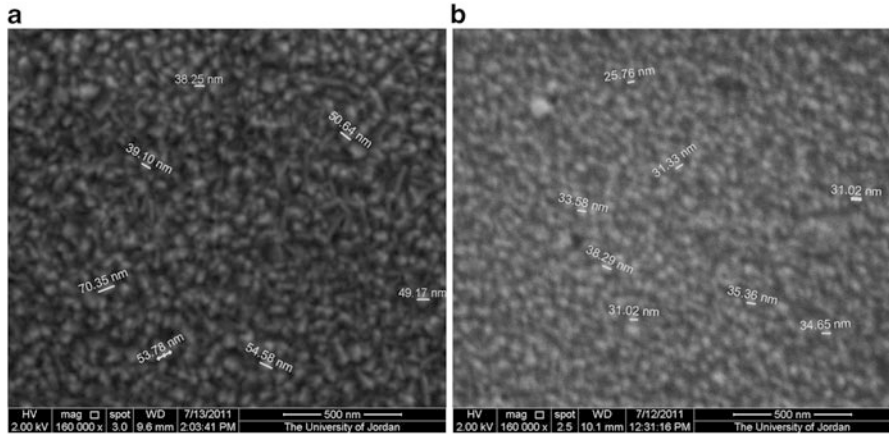
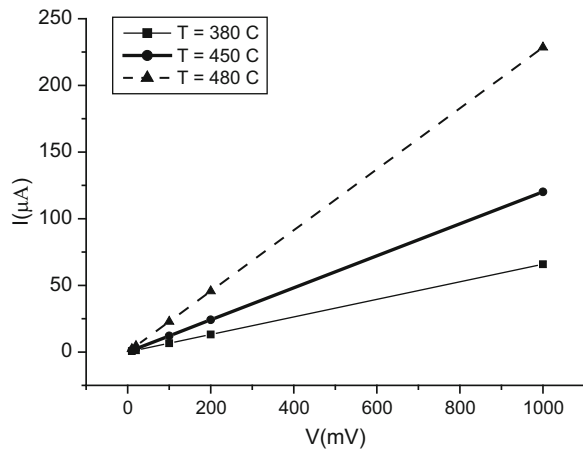


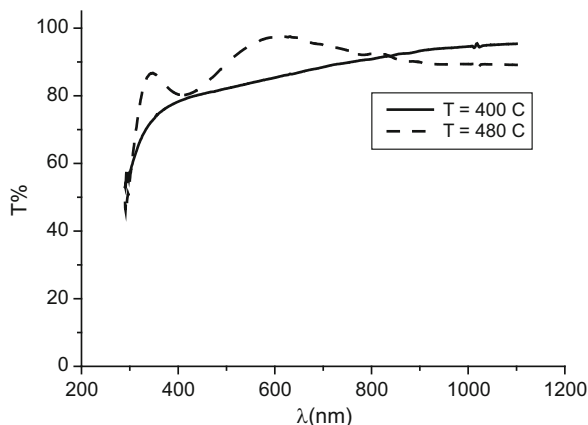
Fig. 70.3 SEM images of SnO₂:F films prepared using SP technique at different substrate temperatures. (a) T_s = 400 °C. (b) T_s = 480 °C

Fig. 70.4 I–V plots for SnO₂:F thin films prepared at different substrate temperatures



as high as 95 and 97.5 % for films prepared at 400 and 480 °C, respectively. Films prepared at higher deposition temperatures have a higher transmittance, especially in the visible region. Also, these films show interference peaks. Transmittance data were used to estimate the absorption coefficient α and to deduce the bandgap energy of the films. This was done by assuming a direct transition and plotting $(\alpha h\nu)^2$ against the photon's energy $h\nu$; the optical bandgap energy was deduced from the linear fits of the linear portions of curves, and it was found that $E_g(400\text{ °C}) = 3.468 \pm 0.052\text{ eV}$, $E_g(480\text{ °C}) = 3.325 \pm 0.012\text{ eV}$.

Fig. 70.5 Transmittance of $\text{SnO}_2:\text{F}$ films prepared at different substrate temperatures. (a) $T_s = 400^\circ\text{C}$. (b) $T_s = 480^\circ\text{C}$



4 Undoped and Aluminum-Doped Zinc Oxide Films on Glass Substrates

The films were prepared by the SP technique on glass substrates at 450°C [16–19]. Figure 70.6 displays the XRD diffractogram of one of the films, where there is no difference between the diffractograms of the undoped and Al-doped films. As seen in the figure, the film is polycrystalline with a wurtzite (hexagonal) structure, where Miller indices of the diffraction peaks are displayed on the diffractogram. Figure 70.7 depicts a SEM image of one of the ZnO films prepared at 450°C . The film is fully covered with material and polycrystalline, in accordance with the XRD diffractogram shown in Fig. 70.6. The electrical properties of the films were measured at room temperature by recording the I–V plots shown in Fig. 70.8 for the undoped and Al-doped ZnO films. From such plots, the resistivity of ZnO thin films was found to be around $133\ \Omega\ \text{cm}$ and that of ZnO:Al around $90\ \Omega\ \text{cm}$. Figure 70.9 displays the optical transmittance of undoped and Al-doped ZnO thin films measured at room temperature. Both the doped and undoped films have high transmittance, with maximum values of 84.2 and 92.0% for the undoped and Al-doped films, respectively. This high transmittance is good for the use of the films as fore contacts in thin-film solar cells.

5 Undoped Zinc Oxide Thin Films on Aluminum Substrates

The films were prepared by the SP technique on aluminum substrates at 350°C . Figure 70.10 depicts the XRD diffractogram of two films of different thicknesses. The films are polycrystalline and show a wurtzite (hexagonal structure); the thicker film shows a larger intensity of the diffraction peaks. Also, Miller indices of the

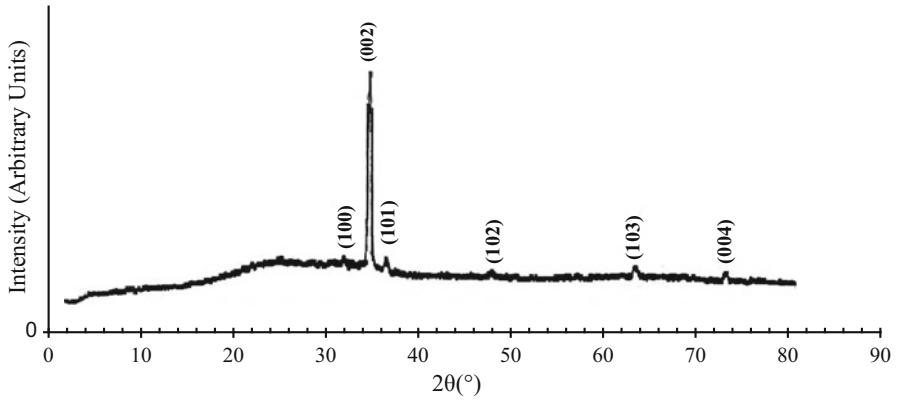


Fig. 70.6 X-ray diffractogram of one of the as-deposited ZnO thin films

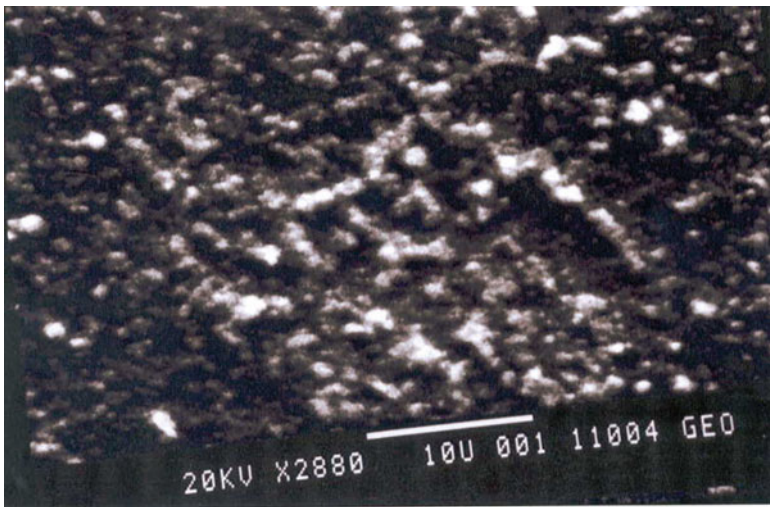


Fig. 70.7 SEM micrograph of ZnO film prepared at 450 °C

Fig. 70.8 I-V plots of ZnO and ZnO:Al thin films prepared using SP technique at 450 °C

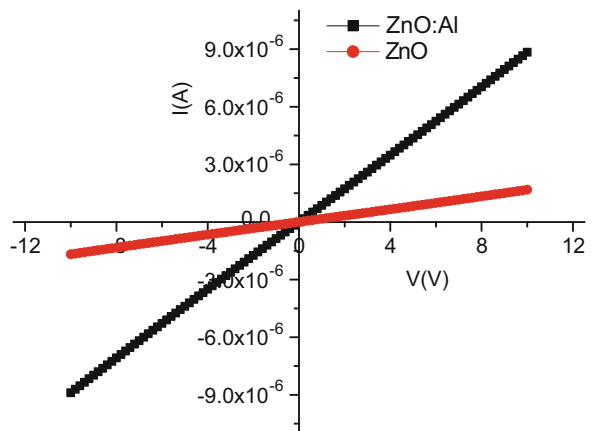


Fig. 70.9 Transmittance of ZnO and ZnO:Al films prepared using SP technique at 450 °C

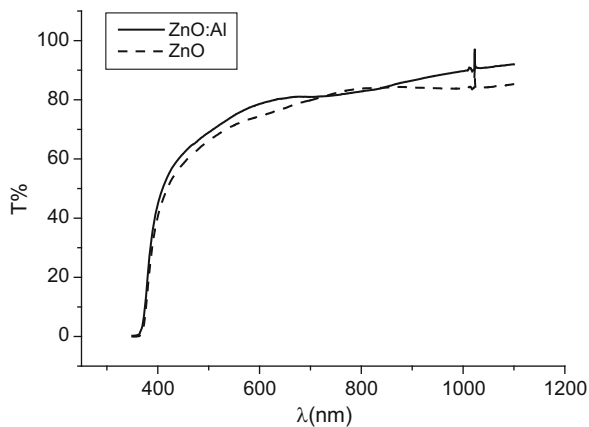
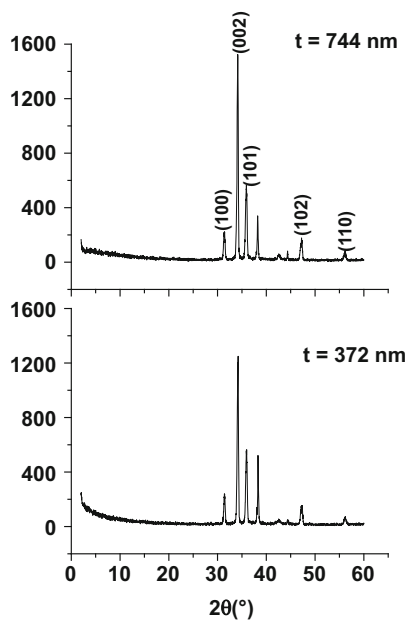


Fig. 70.10 XRD diffractograms of ZnO thin films of different thicknesses on aluminum substrates



diffraction peaks are displayed on the diffractograms. Figure 70.11 displays the SEM micrographs of the same films, and the films appear polycrystalline, with grains in the form of rods of hexagonal cross sections, and the thicker film shows larger grains.

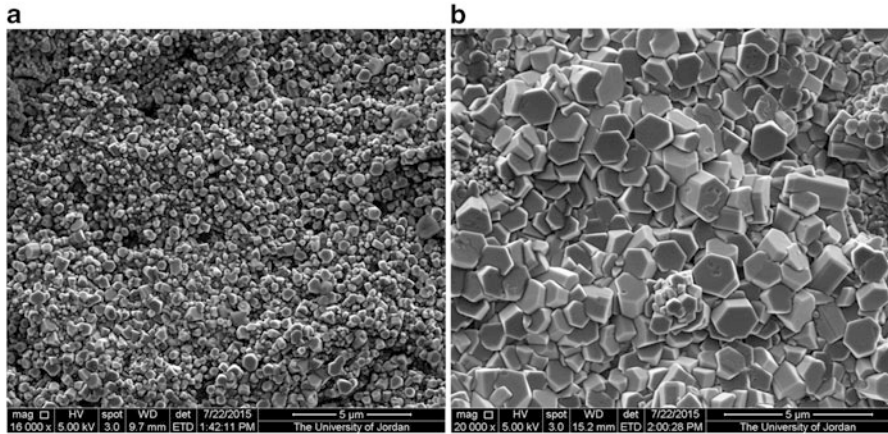


Fig. 70.11 SEM images of ZnO thin films of different thicknesses on Al substrates. (a) 372 nm. (b) 744 nm

6 Conclusions

TCOs are important materials that have many electro-optical applications. In thin-film solar cells they can be used as fore contacts, back contacts in bifacial cells, and as buffer layers. High-quality TCOs, such as doped and undoped SnO_2 and ZnO, were produced using the SP technique, which is a low-cost method. These TCOs can be used for solar cell applications.

References

1. Riveros R, Romero E, Gordillo G (2006) Synthesis and characterization of highly transparent and conductive $\text{SnO}_2\text{:F}$ and $\text{In}_2\text{O}_3\text{:Sn}$ thin films deposited by spray pyrolysis. *Braz J Phys* 36 (3):1042–1045
2. Ferekides CS, Mamazza R, Balasubramanian U, Morel DL (2005) $\text{Cd}_{1-x}\text{Zn}_x\text{Te}$ thin films and junctions. *Thin Solid Films* 480–481:471–476
3. Chopra KL, Dass SR (1983) *Thin film solar cells*. Plenum Press, New York
4. Hartnagel HL, Dawar AL, Jain AK, Jagadish C (1995) *Semiconducting transparent thin films*. Institute of Physics, Philadelphia
5. Costellamo JE (1992) *Handbook of display technology*. Academic, New York
6. Ishibashi S, Higuchi Y, Ota Y, Nakamura K (1990) Low resistivity indium-tin oxide transparent conductive films. I. Effect of introducing H_2O gas or H_2 gas during direct current magnetron sputtering. *J Vac Sci Technol A* 8:1399–1402
7. Lee SU, Boo J-H, Hong B (2011) Structural, electrical, and optical properties of $\text{SnO}_2\text{:Sb}$ films prepared on flexible substrate at room temperature. *Jpn J Appl Phys* 50:01AB10
8. Yadav AA, Masumbara EU, Moholkar AV, Neumann-Spallart M, Rajpure KY, Bhosale CH (2009) Electrical, structural and optical properties of $\text{SnO}_2\text{:F}$ thin films: effect of the substrate temperature. *J Alloys Compd* 488:350–355

9. Ikhmayies SJ, Ahmad-Bitar RN (2013) An Investigation of the bandgap and Urbach tail of vacuum-evaporated SnO₂ thin films. *Renew Energy* 49:143–146
10. Ikhmayies JS (2012) Properties of amorphous SnO₂ thin films prepared by thermal evaporation. *Int J Mater Chem* 2(4):173–177
11. Ikhmayies SJ, Ahmad-Bitar RN (2008) Effect of processing on the electrical properties of spray-deposited SnO₂:F thin films. *Am J Appl Sci* 5(6):672–677
12. Ikhmayies SJ, Ahmad-Bitar RN (2008) The effects of post-treatments on the photovoltaic properties of spray-deposited SnO₂:F thin films. *Appl Surf Sci* 255:2627–2631
13. Ikhmayies SJ, Ahmad-Bitar RN (2009) Effect of the substrate temperature on the electrical and structural properties of spray-deposited SnO₂:F thin films. *Mater Sci Semicond Process* 12(3):122–125
14. Ikhmayies SJ, Ahmad-Bitar RN (2011) An investigation of the bandgap and Urbach tail of spray-deposited SnO₂:F thin films. *Phys Scr* 84:055801 (7pp)
15. Ikhmayies SJ, Ahmad-Bitar RN (2012) Using HF rather than NH₄F as doping source for spray-deposited SnO₂:F thin films. *J Central South Univ* 19:791–796
16. Ikhmayies SJ, Abu El-Haija NM, Ahmad-Bitar RN (2014) A comparison between different ohmic contacts for ZnO thin films. *J Semicond* 36(3): 033005-1-6
17. Ikhmayies SJ, Abu El-Haija NM, Ahmad-Bitar RN (2010) Characterization of undoped spray-deposited ZnO thin films of photovoltaic applications. *Fluid Dyn Mater Process* 6(2):165–178
18. Ikhmayies SJ, Abu El-Haija NM, Ahmad-Bitar RN (2010) The influence of annealing in nitrogen atmosphere on the electrical, optical and structural properties of spray-deposited ZnO thin films. *Fluid Dyn Mater Process* 6(2):219–232
19. Ikhmayies SJ, Abu El-Haija NM, Ahmad-Bitar RN (2010) Electrical and optical properties of ZnO:Al thin film prepared by the spray pyrolysis technique. *Phys Scripta* 81(1): art. no. 015703

Chapter 71

Solar-Driven Cold Storage Units to Reduce Food Waste

Sraisth

Abstract This chapter presents the current situation of food wastage around the globe by comparing developed and developing countries. The research further focuses on India, presenting the state of food wastage and briefly discussing cold storage facilities and problems faced by the cold chain sector. Sustainable off-grid solar cooling technology measures that can be used for cold storage are briefly described. Finally, the chapter discusses how solar cooling technology could be distributed across India to reduce food wastage and, consequently, how that would benefit society and the environment.

Keywords Food wastage • Cold storage • Solar cooling • System • Off-grid solar systems

Abbreviations

AFP	Advanced flat plate collector
AusAID	Australian Agency for International Development
CPC	Compound parabolic collector
CSIRO	Commonwealth Scientific and Industrial Research Organization
ETC	Evacuated tube collector
FAO	Food and Agriculture Organization of the United Nations
FPC	Flat plate collector
MOFPI	Ministry of Food Processing Industries
PTC	Parabolic trough concentrator
TERI	The Energy and Resource Institute

Sraisth (✉)

Global Production Engineering in Solar Technology, TU Berlin, Pascalstrasse 8-9, Berlin 10587, Germany

e-mail: sraisth@gmail.com

1 Introduction

Food wastage is a global concern, and the waste occurs at every step of the food chain, such as during production, harvesting and processing, as well as on the consumer end. The food waste that will be discussed in this chapter is focused on post-harvest losses. The increasing world population is a concern in terms of energy and food demand. The production and supply of food must increase but accessibility to good, healthy food for every human being is challenged by food wastage. According to Surange [1], food production is growing at a rate of 14–15 % to support increasing populations, but there are no data about reducing food wastage.

India also plays a significant role in food wastage, wasting almost 25–30 % of its food production in post-harvest losses [2]. These data illustrate the level of food wastage in India and how its cold storage sector is performing; in addition, they raise the issue of what measures the government could implement to prevent losses and improve the cold chain industry.

Many articles and papers have been written regarding solar cooling/refrigeration systems, mainly focusing on new researches in solar cooling technology, different methods of achieving cooling and many other topics. Similarly, many articles address cold storage conditions and measures to improve them. There are no research papers or information linking solar-technology-based cooling systems to the reduction of food wastage and improvements in the cold chain industry.

The aim of this chapter is to present the possibility of using solar cooling/refrigeration systems for the cold storage of fruits, vegetables, cereals and other foods, as well as other measures the Indian government could implement to improve the cold chain sector and incorporate it into the solar cooling/refrigeration systems and collectively help to reduce food waste. There are many direct and indirect benefits of reducing food waste for both society and the environment; these are briefly explained in the final section of this paper.

2 Food Waste

According to Wilmoth [3], director of the United Nations (UN) Population Division, the world's population will hit approximately 9.7 billion in 2050, which is 33 % more than the current population. The demand for food will increase by 60 % in 2050, as estimated by Alexandratos and Bruinsma [4], but this presents a challenge in terms of global food wastage; Fox and Fimeche [5] estimate that approximately 30–50 % of total global food production is wasted every year and this food loss is equivalent to 6–10 % of human-generated greenhouse gas emissions [6]. The researchers also stated that in the past 30 years just 5 % of research investments have focused on food waste reduction; the rest is devoted to food

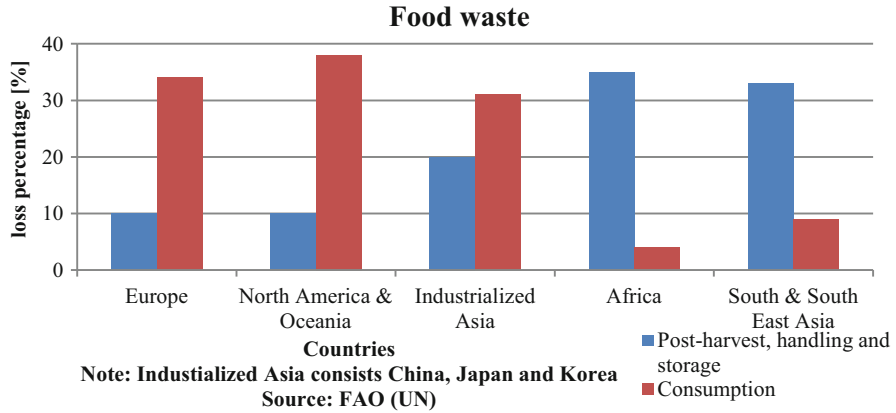


Fig. 71.1 Comparison of food wastage in developed and developing countries

production. But the current situation calls for more investment in food waste prevention to reduce post-harvest losses. Lack of food availability is not the only result of food wastage; food wastage increases investments in waste management and increased greenhouse gas emissions. A large portion of the losses is from postharvest losses, for which developing or poor countries have inadequate infrastructure and transportation, while losses from developed countries mostly occur at the consumption stage [6]. This is also supported by an FAO study [7], as shown in Fig. 71.1. This food wastage has consequences for the environment, such as increasing our carbon and water footprints and requiring the expansion of landfills for decomposing waste.

2.1 Food Wastage in India

India is the second largest producer of fruits and vegetables in the world. A large portion of this food is wasted or damaged due to a lack of storage and transportation. According to Emerson Climate Technologies [8], India produces 250 million tonnes of food yearly, and out of that, 25–30 % is wasted in post-harvest losses [2], which is a very huge amount to serve a few countries across the world. Out of the total fruits and vegetables production, 18 % go to waste at a value of €2 billion euro, also 6 % cereals and 2–4 % of meats production go to waste [8]. This leads to less amount of quality food which leads to high prices and also pillaging. A reason for all are mainly due to lack of adequate high quality cold storage facilities, lack of refrigerated transport, availability of power supply, and others like the cost of investment and operating expenses in the cold chain [8].

3 Cold Storage Facilities in India

According to Emerson Climate Technologies [8], India has 6300 cold storage facilities with an installed capacity of 30.11 million metric tonnes covering only 10–11 % of the total food produced; to prevent food wastage, this capacity must be doubled. Thus, around € 7 billion need to be invested in cold storage infrastructure by 2015–2016 to keep up with the increasing demand for fruits and vegetables. The main cause of less number of cold storage units, which causes widespread suffering among India's rural population because of the frequent power cuts, apparently from increasing demand, which leads to high energy costs, resulting in further investment costs and operating expenses required for the cold chain industry. Another factor in this depreciation of cold storage is the gradual increase in real estate prices since cold storage facilities require land [8]. According to the Ministry of Food Processing Industries in India [9], 96 % of cold storage occurs in the private sector, and there are major inefficiencies associated with cold storage facilities, because most such facilities are for single food items like potatoes and they are not evenly distributed across India, as the southern and eastern parts of the country lack sufficient cold storage facilities [8].

4 Measures

The idea for reducing food waste is to install off-grid solar systems which would benefit farmers because they would be able to store their products as soon as they are harvested without wasting time on transport and without have to leave the harvested crops out in the open. Almost all cold storage is used by large farmers, but small farmers can also store their crops or directly sell them to storage unit owners. According to the Census of India [10], there are 638,596 villages in the country, and 70 % of the population is devoted to farming, so it represents a huge market.

4.1 Solar-Driven Cooling Systems

There are two main stand-alone systems which can be used to store food easily, namely solar thermal and solar photovoltaic (PV) cooling systems. India has good solar potential, having average sun peak hours (SPH) of 5.21 kWh/m²/day, and in some places this number reaches approx. 7 SPH in certain months [11]. Thus, installing PV systems producing electricity to power refrigeration systems with good battery systems could be useful in food storage. Solar collectors producing thermal energy for cooling can also be divided into categories of adsorption, absorption and desiccant systems [12]. Here the cooling systems which can be beneficial to cold storage systems will be briefly described.

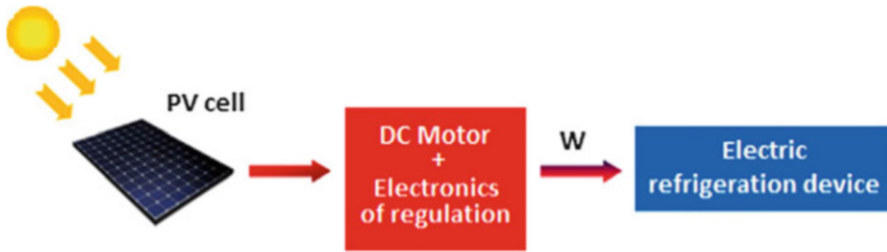


Fig. 71.2 Schematic diagram of PV-driven conventional vapor compression refrigeration cycle

4.1.1 Photovoltaic Cooling Systems

In this system the electricity generated using PV modules is directly fed into the DC motor which runs the compressor; also, using a vapour pressure cycle, a cooling effect is created, as shown in Fig. 71.2 [13]. If the refrigeration system is running on AC, then an inverter needs to be installed. Installing more PV modules than is required by the capacity is helpful for such stand-alone systems since the excess energy can be stored in the batteries and utilized in bad weather conditions and at night. Presently, hundreds of companies produce different solar modules with different levels of power, made of crystalline (mono or poly) silicon, amorphous silicon (thin film) and many other technologies like cadmium telluride (CdTe) or chalcopyrite organic solar modules. However, solar panels can be selected taking into consideration cold storage capacity, comparing different values of voltage, current and efficiencies with respect to the area and technology of the modules.

4.1.2 Solar Thermal Cooling Systems

According to Allouhii et al. [13], the output temperature of acceptable thermal collectors like FPC, AFP, CPC, ETC and PTC is the required driven temperature for solar cooling cycles and have 70–80% efficiency even at the high driving temperature of 90 °C. This cooling system is also subdivided into two other methods of refrigeration system, namely sorption refrigeration and thermo-mechanical refrigeration [13]. Since a thermo-mechanical system is a much larger refrigeration system than a sorption refrigeration system, for off-grid storage only sorption systems will be considered and discussed further.

A solar sorption cycle requires thermal power which is generated by thermal collectors, and the refrigeration effect is produced by physical and chemical reactions between the sorbent and the sorbate; an example of such a system is shown in Fig. 71.3 [13]. There are two main types: absorption and adsorption refrigeration systems. Common substances used for absorption systems are water (H₂O) and ammonia (NH₃) (refrigerant), or H₂O (refrigerant) and lithium bromide (LiBr), and for adsorption systems common substances are silica gel water, zeolite water, activated carbon-NH₃ and NH₃ salts with alkaline compounds [13].

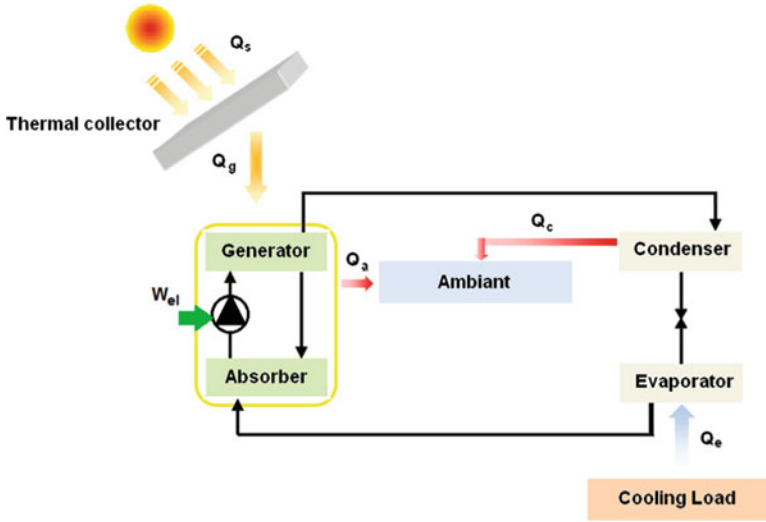


Fig. 71.3 Schematic diagram of solar thermal heat-driven sorption refrigeration cycle

Table 71.1 Comparison between absorption and adsorption refrigeration systems

Thermal process	Advantage	Disadvantage
Absorption system (Market: 82%)	Operates silently	High installation costs and large installation area for continuous systems
	High reliability	Quite complicated system requiring advanced knowledge for maintenance
	Easy implementation	High heat release to ambient air
	Low-temperature heat supply	
	COP = 0.5–7.3	
Adsorption system	Low maintenance costs	Poor thermal conductivity of adsorbent
	No moving parts	Very sensitive to low temperatures at night
	Low heat source temperatures	Low COP
		Bulky machine

Adsorption systems have a very high payback period – 37.7 years – compared to absorption systems, which have a payback period of 5.8 years, so the latter was preferred over the former. Table 71.1 [13] also shows some differences between the two systems and why mostly absorption systems are preferable.

The PV and absorption system had better energy-saving potential compared to other systems. Economically and environmentally speaking, an absorption system is better than a PV system. An absorption system has low coefficient of performance (COP) but high efficiency, whereas a PV system has low efficiency but higher COP when coupled with motors. Ultimately, there is little difference in

overall efficiency of both systems. Therefore, only these two systems were described for their high reliability and easy implementation. Research on these storage units revealed that some small companies in India, namely Ecozen Solutions, Cold Star, Promethean and Coolify, were working on PV cooling systems [14].

4.2 Solar Storage Unit Distribution Across India

A solar-driven cold storage system can be distributed across India using technology suitable for particular fruits and vegetables while considering their availability around the country. The distribution of cold storage is uneven in India, and most of cold storage facilities (47 %) are located in northern India [1]. Narula and Mann [15] reported that most of the cold storage is near cities and marketplaces, but it should be near farms. Installation near farms would help in reducing the time from harvest to storage and, hence, reduce wastage due to transport and handling. Also, farmers can utilize cold storage for excess production to prevent price fluctuations on the market and provide food during the off-season, helping to reduce waste at marketplaces due to excess food and less demand.

There are different crops, fruits and vegetables, and to preserve them, different cold storage temperature conditions are required. Thus, foods which require temperatures above 0 °C, like mango, potato, banana and many others, can be stored using an absorption system (H₂O–LiBr), and for foods requiring temperatures below or near 0 °C, like apple, cabbage and green peas, use a NH₃–H₂O absorption system [12, 16]. Table 71.2 [16, 17] shows examples of fruits and vegetables which can be stored according to the storage temperature required. The reason for choosing these commodities is their different temperature requirements; other foods can be easily covered in those ranges.

North and North-east India lack cold storage, so for apples which are produced in North India can use the kind of absorption system shown in Table 71.2. Pineapples,

Table 71.2 Fruit and vegetable storage temperatures and recommended solar cooling absorption system

Fruits and vegetables	Storage temperature (°C)	Storage life	Recommended solar cooling system
Apple	0–2	2–8 months	NH ₃ –H ₂ O
Banana (ripe)	13–16	7–28 days	H ₂ O–LiBr
Mango	10–13	20–24 days	H ₂ O–LiBr
Oranges	0–5	1–2 months	NH ₃ –H ₂ O
Cabbage	0–2	5–6 months	NH ₃ –H ₂ O
Green peas	0–2	7–10 days	NH ₃ –H ₂ O
Potatoes	7–10	2–5 months	H ₂ O–LiBr
Beans, green	4–7	7–10 days	H ₂ O–LiBr

which require 10–13 °C for storage, are produced mostly in the North-East and can be preserved using a H₂O–LiBr absorption system. In India, almost all fruits and vegetables are produced just about everywhere; the difference is the production volume, so both PV and absorption cooling systems can be easily utilized. All meat, fish and poultry require storage temperatures of around –18 °C or below for 6–12 months or more to preserve them [18], so systems running on PV and a NH₃–H₂O absorption system will be suitable for preserving them. India has a long coastline, so most marine foods come from the southern and eastern coasts of the country, and irradiation is also suitable in those parts; for example West Bengal has an average irradiation of 4.78 kWh/m²/day and the level in Andhra Pradesh is 5.02 kWh/m²/day [11]. So both a PV system and a NH₃–H₂O absorption system are reliable in those regions.

4.3 *Government Measures and Investment Potential*

Several measures have been taken by the Indian government to improve the cold chain in the country. MOFPI, the government of India [9], have enacted various policies and schemes and given financial support to build a robust cold chain sector.

- Custom duties are just 5 % on imported refrigeration machinery and parts; there is no excise duty.
- An autonomous registration society, the National Centre for Cold Chain Development, was established to work in close collaboration with industry and other private stakeholders to promote and develop an integrated cold chain sector in India.
- Central sector schemes have been implemented to provide integrated infrastructure facilities and enable the linking of producer groups to processors and the market through a well-equipped supply chain.
- A centrally sponsored scheme was created under the National Mission on Food Processing to set up processing and preservation facilities at the village level.
- Make in India, the government’s new initiative programme to encourage manufacturers, under a food processing, foreign direct investment (FDI) sector policy, permits 100 % FDI in the automatic route for most food products and 24 % FDI for items reserved for micro and small enterprises [19].

The national food processing policy aims to increase the level of food processing to 25 % in 2025 as compared to the present 10–12 % [19]. Fortunately, the Indian government has started investing in this area and has developed and implemented the first off-grid 15 kW biomass–solar hybrid cold storage model for 25 tonnes of food in the 15 kW system, which has a cooling capacity of 4.27 TR (tonnes of refrigeration) in Bankipur and Rehaspur, Uttar Pradesh, India; the project was installed by TERI and CSIRO with the support of AusAID [15].

This is just one biomass hybrid project; it covers just one village, meaning that, considering there are 638,596 in the country, that leaves 638,595 more villages to

cover, and that's without considering farms. To reduce food wastage, 61.13 million metric tonnes more of cold storage facility is required [8], and each village will require approximately 100 tonnes of cold storage. Investment at a level of around € 670,000 is needed to store 6000 tonnes of food, so for one village, € 11,111 in investment is needed, excluding land costs, since land costs vary across the country. Thus, in total, there is a market of at least € 7 billion in India [8]. PV systems cost around € 1300 for 1000Wp, including electrical components. For 100 tonnes of cold storage capacity, an efficient system would need another € 20,000 investment. Thus, approximately € 30,000 of investment opportunity is available for each village, and for absorption systems it will cost less than PV systems because absorption systems are cooling systems and so entail no extra costs for refrigeration, just collector costs and installation. Overall, to cover each village and meet cold storage targets, there is an investment potential of almost € 19 billion in solar cooling systems to raise the level of cold storage availability from 10 % of food products to 100 % percent, which would contribute towards a sustainable future and improved climate.

5 Conclusion

Implementing solar stand-alone cooling systems would have several positive impacts on economic development, society and the environment.

- First, it would improve life in villages with no or poor grid connection, which would also facilitate a more even distribution of a cold chain sector around the country and help villages increase their quality of life and access to electricity.
- It would benefit farmers, who could sell their food at better prices, without having to worry about tending to crops if there is a system in place which is run by storage unit owners (or the village community), and the latter could sell food in markets at reasonable prices (considering maintenance and transportation), as the maximum investment would be only at the initial stage of system installation. Hence, food prices would go even lower than present prices because there would be no wastage.
- Collectively, all these benefits would lead to high productivity and good quality of food. It would also eliminate middlemen, who deceive farmers and earn money illegally.
- Only 55 % of villages are connected to the grid, which at any rate provides only a 6 h supply of electricity a day [15]. Because of this, the government and private firms are not investing in cold storage near farms, but off-grid systems can attract both government and private firms and benefit their business.
- Globally, greenhouse gas emissions in India due to food wastage rank third, after the USA and China [7]. Thus, installing solar-driven cooling systems would help reduce the carbon footprint.

- Reduced food wastage would be accompanied by positive impacts on water usage, landfills for waste decomposition, regulation of food productivity and, consequently, land required for irrigation to meet elevated demand for food due to population increases [7].

The solar off-grid cooling system is a new concept, and there is considerable scope for improving such systems, which can be utilized for the preservation of food on farms. Presently most PV modules available on the market have 15–20 % efficiencies, but researchers continue to improve the technology, reaching ever greater efficiencies; for example, recently the greatest efficiency achieved is 46 % by Fraunhofer Institute for Solar Energy Systems ISE in Freiburg, Germany, in collaboration with Soitec and CEA-Leti, France, for multi-junction solar cells [20]. Thus, in future, improved efficiency modules will be produced, which will reduce constraints on area requirements and will help to develop a stand-alone cold storage market. Food is essential to life, and its wastage has consequences which can be addressed using measures described herein which would affect farmers, society, enterprises, government and, most importantly, the climate in a positive way. These measures can have a substantial impact in terms of fighting global warming and providing a sense of food security across the globe.

References

1. Surange A (2013) Cold chain development in India—modernization of the infrastructure of cold storage perishables. ACR Project Consultants, Pune
2. Sinha V (2014) Alternate energy options for strengthening energy efficiency for cold storage. National Centre for Cold-chain Development (NCCD), Delhi
3. Wilmoth JR (2015) World population likely to surpass 11 billion in 2100. American Statistical Association NEWS, Seattle
4. Alexandratos N, Bruinsma J (2012) World agriculture towards 2030/2050: the 2012 revision. Working paper no. 12-03. Rome: FAO
5. Fox T, Fimeche C (2013) Global food waste not, want not. Institution of Mechanical Engineers, London
6. Aulakh J, Regmi A (2013) Post-harvest food losses estimation-development of consistent technology. FAO, Washington
7. FAO (2013) Food wastage footprint impacts on natural resources. Food and Agriculture Organizations of the United Nations (FAO), Rome
8. Emerson Climate Technologies (2013) The food wastage & cold storage infrastructure relationship in India; developing realistic solutions. Emerson, Pune
9. Ministry of Food Processing Industries, Government of India (2014) Government support & initiative to build a robust cold chain. National Centre for Cold-chain Development (NCCD), Ministry of Agriculture, Government of India, New Delhi
10. Census of India (2001) Number of villages. http://censusindia.gov.in/Census_Data_2001/Census_data_finder/A_Series/Number_of_Village.htm. Accessed Mar 2015
11. Synergy Enviro Engineers (2015) Synergy Enviro Engineers. http://www.synergyenviron.com/tools/solar_insolation.asp?loc=India. Accessed Mar 2015
12. Ziegler I (2015) Thermally driven cooling. TU Berlin, Berlin

13. Allouhii A et al (2015) Solar driven cooling systems: an updated review. *Renew Sustain Energy Rev* 44:160–172
14. Adarsh VS (2014) Farmers turn to start-ups like Ecozen and ColdStar for cold storage solutions. *Economic Times*, 22 Nov 2014, p 1
15. Narula A, Mann L (2014) Arrived cold storage solutions for villages. *Akshay Urja* 7(5):10–15
16. McGregor BM (1989) *Tropical products transport handbook*. Agriculture handbook no. 668, 2nd edn. U.S. Department of Agriculture, Washington, p 148
17. Cornell Cooperative Extension (2015) *Storage guidelines for fruits & vegetable*. Cornell, Chemung County
18. Cano-Muñoz G (1991) *Manual on meat cold store operation and management*. Food and Agriculture Organization (FAO) of UN, Rome
19. Make in India (2014) *Make in India*. <http://makeinindia.com/sector/food-processing/>. Accessed Aug 2015
20. Fraunhofer ISE (2014) New world record for solar cell efficiency at 46%. Fraunhofer ISE, Freiburg

Chapter 72

An Adaptive Thermal Comfort Model for the Romanian Climate

Ioana Udrea, Cristiana Croitoru, Ilinca Nastase, Ruxandra Crutescu, and Viorel Badescu

Abstract Human thermal comfort (HTC) embraces two major approaches, Fanger or classical theory and an adaptive one. Adaptive HTC equations make up parts of the worldwide recognized thermal comfort standards. The balance between thermal comfort and energy saving is held by the adaptive approach of thermal comfort. The use of adaptive HTC equations in the evaluation of existing buildings and in the design of new buildings has led to an important decrease in energy consumption and a minimization of building maintenance costs.

The adaptive HTC equations found in international comfort standards are determined from specific databases. New adaptive HTC equations are being developed worldwide for specific climatic regions. The aim of this chapter is to find a HTC equation for Romania's climate (Köppen climate type D – temperate continental climate) that is similar to the EN 15251 adaptive HTC equation. To this end, a field survey was conducted between 2013 and 2014 in several naturally ventilated buildings (buildings at two prominent universities in Bucharest – a passive office building and a residential house) in Romania. Comfort parameters were measured, and comfort questionnaires were distributed to occupants.

Keywords Adaptive human thermal comfort • Temperate continental climate • Energy saving • EN 15251

I. Udrea (✉) • V. Badescu
ASC-Romania, 9 Stefan Marinescu Street, Bucharest 060121, Romania

Faculty of Mechanical Engineering and Mechatronics, Thermodynamics Department,
Polytechnic University of Bucharest, Spl. Independentei 313, Bucharest 060042, Romania
e-mail: ioana.udrea@asc-ro.com; badescu@theta.termo.pub.ro

C. Croitoru • I. Nastase
Building Services Department, Technical University of Civil Engineering in Bucharest,
66 Avenue Pache Protopopescu, Bucharest 020396, Romania
e-mail: cristianaverona@yahoo.com; ilince.nastase@gmail.com

R. Crutescu
Faculty of Architecture, Spiru Haret University, Bucharest, Romania
e-mail: pasivhausoffice@gmail.com

1 Introduction

Thermal comfort theory embraces two major approaches, the Fanger model, known as the classical model, and the adaptive model. The Fanger model considers that human thermal comfort (HTC) depends on indoor climate parameters. However, people have a natural tendency to adapt to changes in indoor thermal environments. This natural tendency is quantified by the adaptive thermal comfort (ATC) theory. It relates the indoor acceptable temperature to outdoor temperature [1]. The ATC approach is based on field studies, which means gathering data on indoor and outdoor thermal climate while simultaneously obtaining responses of subjects in real buildings. The classical thermal comfort theory differs by considering climate-control chamber parameters. Determining acceptable indoor temperature is important, not only for thermal comfort assessment but also for the building energy consumption minimization and its sustainability. Clearly, the ATC model modifies the heating period downward if the temperature set points of the cooling and heating equipment are chosen according to the acceptable thermal comfort limits previously determined using ATC theory.

Current comfort standards that implement adaptive models are ASHRAE Standard 55 [2] and EN 15215 [3]. These standards offer thermal comfort equations that relate indoor acceptable operative temperature to mean outdoor air temperature, and they are established for a specific climate database.

The development of the adaptive theory took a long time, both for obtaining a database as large as possible and in terms of determining the statistical method of analysis and obtaining results. De Dear realized the assembly, cleaning and standardization of the database, with financial support from ASHRAE Inc. The entire database, and details about the projects that generated it, can be found on the Web site of the Architecture University of Sydney [4]. With it was made ASHRAE RP-884, which shows the connection between the average operative indoor temperature and the outdoor effective temperature [5]. Of the adaptive theory pioneers we mention those who received special acknowledgement from de Dear and Brager in RP-884 [1], i.e. Andris Auliciems, Fergus Nicol and Michael Humphreys. Because ACT was too presented in a very technically scientific way, the standard has been changed for practical applications used for the assessment and design of buildings [6], and the work of de Dear and Brager was included in ASHRAE Standard 55 for the first time in 2004.

In Europe, based on data obtained from the EU project Smart Controls and Thermal Comfort (SCATs) [7], a specific ATC algorithm was determined for this zone [8]. A relationship between indoor comfort and outdoor temperature was developed for free-running buildings (this category includes besides naturally ventilated buildings, mechanically ventilated ones but where no energy is being used either for cooling or for heating at the time of the survey).

A review on HTC, especially on ATC, can be found in [9]. It presents a classification of ATC equations according to climate (Köppen–Geiger system), location and building type (mechanically conditioned, free running, or mixed

mode). Of the studies conducted in the last 3 years we may mention [10], where the authors formulate new ATC equations using the statistical meta-analysis database of ASHRAE RP-884 [1]. These equations are applicable in naturally ventilated buildings in hot-humid, hot-dry, and moderate climates. The data are sorted into three climate groups using the world map of the Köppen-Geiger climate classification. The authors, Toe and Hubota, analyze the variation of the ATC equations depending on the type of mediation applied to the outside air temperature. In [11] a procedure is presented for developing an adaptive comfort model for Southeast Asia. A meta-analysis, composed of a large number of dates obtained from a field survey conducted in this region, was used. The adaptive comfort model obtained is applicable to the hot-humid climate of Southeast Asia in naturally ventilated buildings. In [12] a thermal comfort field study is conducted in office buildings in two cities in India for 7 months. The authors develops an adaptive thermal equation using the EN 15251 method. The paper concludes that serious attention must be given to environmental and thermal adaptation in buildings in India, where energy consumption in buildings is increasing rapidly. An attempt to find the best fit among available comfort equations for predicting occupant comfort in the tropical climatic regions of India was made by Mishra and Ramgopal in [13]. The results showed that the comfort equation developed from the EN15251 method is suitable for predicting comfort in naturally ventilated buildings in India.

The ATC in Romania's climate (Köppen climate type D – temperate continental climate) is poorly studied, and no thermal comfort equation specific to it could be found. The climate of the country has a specific feature: low temperature in winter and high temperature in summer [14]. The aim of this paper is to formulate a thermal comfort equation, following the method in the EN 15251 model, in Romania's climate.

2 Method and Procedure

2.1 Building Presentation

The experimental data presented in this work were collected from measurement campaigns carried out in six different unconditioned buildings. AMVIC (Fig. 72.1a) is a passive office building, located in Bragadiru, a small town situated 10 km south of Bucharest, Romania. The building has a ground floor and four levels and opened in February 2009 [15]. Another construction is the building of the Faculty of Building Services of the Technical University of Civil Engineering in Bucharest (UTCB) (Fig. 72.1b). The building was constructed at the end of the nineteenth century and was renovated and consolidated in 2003 [16]. Next is the building of the Polytechnic University of Bucharest, Faculty of Mechanical Engineering and Mechatronics. It was built in the 1970s, and the windows were changed around 2008. The others buildings are the Laboratory Building of UTCB, the rectorship building of Polytechnic University of Bucharest, and a residential



Fig. 72.1 Photos of two buildings: (a) AMVIC office building; (b) Faculty of Building Services of Technical University of Civil Engineering in Bucharest (UTCB)

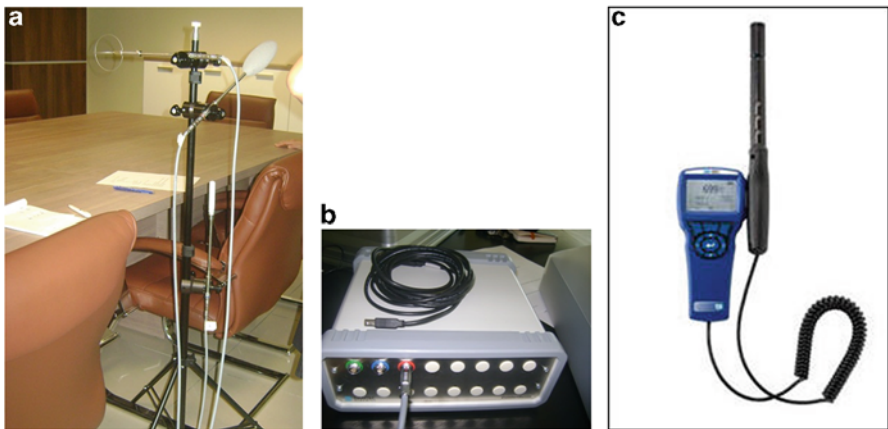


Fig. 72.2 Measurement devices: (a) ComfortSense set up on its stand inside AMVIC building; (b) ComfortSense main frame; (c) IAQ-Calc 7545 indoor air quality meter

building situated on the west side of Bucharest. Of these buildings, a total of 22 classrooms or complete floors were studied.

2.2 Measurement Surveys

The thermal comfort parameters were evaluated mainly using the ComfortSense device from Dantec Dynamics, a Nova Instruments Company, located in Denmark. It is a measurement system based on the ISO 7730 international standard (Fig. 72.2a) and consists of a mainframe with a built-in A/D converter and USB 2.0 interface (Fig. 72.2b). A computer may be connected to the mainframe and the measurement probes positioned on the system stand. The operator can

communicate with the entire setup at the same time from the PC. The measurement is set up using a PC and application software. The measured and processed parameters resulting from the measurements were the operative temperature, relative humidity, temperature, velocity, turbulence intensity, draught rate, predicted mean vote, predicted percentage of dissatisfied, and mean radiant temperature. Another device, the TSI IAQ-Calc 7545 indoor air quality meter (Fig. 72.2c), was used where ComfortSense was not available.

Measurements were undertaken between July 2013 and October 2014 on 42 different days. In the office building, the measurement procedure consisted of replacing the chair of some workstations with the measurement station. In the university building one or two measurement were taken in each classroom.

2.3 *Questionnaire on Thermal Comfort*

The field study presented here included questionnaire surveys and simultaneous measurements of the environmental variables in relation to thermal comfort. A total of 765 questionnaires were filled out in this survey. It took on average approximately 2–3 min to fill out the questionnaire. An important information requested on questionnaire was the assessment of thermal sensation, where the subjects had to chose an option on the ASHRAE 7-point rating scale. In the office building, we tried to give a questionnaire to a worker at each workplace where measurements were taken. In classrooms, the questionnaires were given to anyone who was present.

2.4 *Calculation Method According to EN 15251*

Over time, Humphreys carried out several studies to analyze the HTC indexes and concluded that the more complex the index, the lower the correlation with a subjective sensation. For the EN 15251 method he proposed a simple index: the operative temperature. According to [17], the neutral or comfort temperature is the operative temperature at which either the average person will be thermally neutral or at which the largest proportion of a group of people will be comfortable.

In the EN 15251 method [17], to estimate the neutral temperature for a small sample or for a single comfort vote, a single standard value can be used for the regression coefficient. This value is called the Griffiths constant. In Eq. (72.1), T_{comf} is the neutral or comfort temperature, C is the comfort vote on the ASHRAE scale, G is the Griffiths constant, and T_g is the global temperature (which measures the operative temperature):

$$T_{\text{comf}} = T_g - C/G. \quad (72.1)$$

According to Nicol and Humphreys [17], “the value of the Griffiths constant can be estimated from comfort studies and represents the maximum rate of change of comfort vote with temperature when no adaptation to temperature changes takes place and measurement errors are excluded.” Griffiths [18] recommended a constant of 0.33 for thermal comfort studies, de Dear [1] found for ASHRAE RP-884 database a value of 0.5 for the Griffiths constant, and Nicol and Humphreys [17] analyzed the database of the SCATs project and observed two proper values for the Griffiths constant, 0.4 and 0.5. Humphreys et al. explained in [19] that the difference between the constant found in 1975 and present constants is due to the fact that the old surveys were conducted over more protracted periods, and the coefficient therefore was reduced because of adaptation during the survey period. Finding the Griffiths constant is a difficult process that requires a large database for a meta-analysis. For example, in [11], the authors analyzed a database of 5176 sets of observations recorded in the hot and humid climate specific to Southeast Asia. They followed the method used by Humphreys et al. [19] to predict the regression slope (Griffiths constant), but they were unsuccessful with the method because in their database the correlation was very weak and the low correlation failed to reach statistical significance. For this study we chose a value of 0.5 for the Griffiths constant, a value that is suitable for the European climate according to [17].

Comfort temperature values were obtained for all comfort votes and corresponding operative temperatures, according to Eq. (72.1). For each comfort vote the exponentially weighted running mean outdoor temperature was calculated using the mean temperatures for the last 7 days, Eq. (72.2) [17]:

$$T_{\text{rm}} = (T_{\text{od-1}} + 0.8T_{\text{od-2}} + 0.6T_{\text{od-3}} + 0.5T_{\text{od-4}} + 0.4T_{\text{od-5}} + 0.3T_{\text{od-6}} + 0.2T_{\text{od-7}}) \cdot 3/8. \quad (72.2)$$

Each point, representing a neutral temperature derived from a single comfort vote, was plotted against T_{rm} , and this resulted in a scatterplot (Fig. 72.3). The resulting relationship between neutral temperature and outdoor temperature is given by Eq. (72.3) and represents the regression line for all points of the graph in Fig. 72.3. Equation (72.3) represents the seeking ATC equation, the equation specific to Romania’s climate:

$$T_{\text{comf}} = 0.325 \cdot T_{\text{rm}} + 18.47. \quad (72.3)$$

We also wanted to determine the category of acceptability in accordance with the EN 15251 method. The method consider that people who record a comfort vote of “slightly cool”, “neutral” or “slightly warm” on the ASHRAE Scale, feel comfortable. The parameter T_{diff} is introduced in Eq. (72.4) as the difference between the measured indoor operative temperature (taken as the measured global temperature T_g) and the neutral temperature T_{comf} , calculated as in Eq. (72.1):

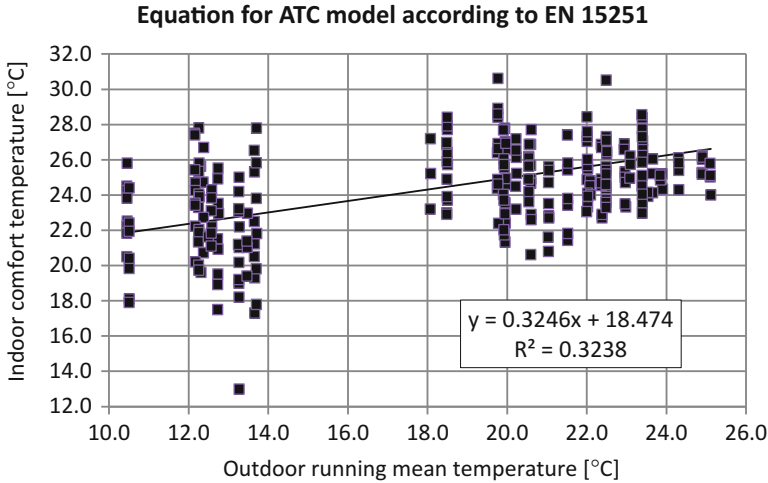


Fig. 72.3 Scatterplot of neutral temperature against running mean outdoor temperature

Table 72.1 People who recorded comfort/discomfort for category of difference T_{diff} , for the studied database and for the database used in EN 15251

Difference (K)	±2	±3	±4
Total number of people	506	632	788
People who record comfort	453	560	674
People who record comfort (%)	89.53	88.61	85.53
People who record discomfort (%)	10.47	11.39	14.47
People who record discomfort EN situation (%)	10	25	35

$$T_{diff} = T_g - T_{comf}. \tag{72.4}$$

T_{diff} was calculated for all the records in the database. Then the database was filtered so that only votes included into the T_{diff} interval remained. This was done for intervals corresponding to the EN 15251 category of acceptability ±2, ±3, ±4 K. For all intervals the proportion of people who recorded comfort was computed. The results are presented in Table 72.1.

A significant difference is observed between the percentage of people who recorded discomfort in our study and those in the European project. It is difficult to conclude that, on average, the discomfort degree is lower in our country than the average in European countries studied in the SCATs project for the free-running buildings. This could be the result of the lower number of votes recorded in our study or the uneven distribution of the votes in the studied period. Thus, we represented the acceptability category for limits situated at ±2, ±3, and ±4 K from the ATC equation, as in EN 15251 (Fig. 72.4).

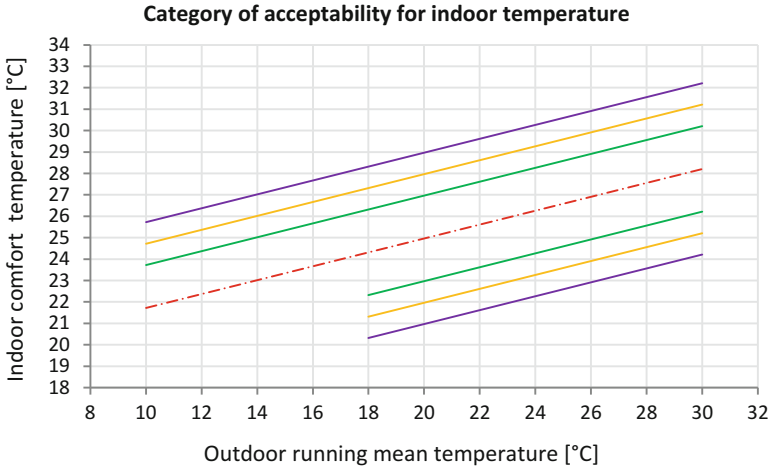


Fig. 72.4 Category of acceptability for operative temperature, situated at ± 2 (green line), ± 3 (yellow line), and ± 4 (violet line) degree distance from the ATC equation (dashed red line)

Table 72.2 ATC equations and specific climatic zone

Author (year)	Equation	Climate type/countries
SCATs project (2000) [3]; model included in EN 15251	$T_{\text{comf}} = 0.33T_{\text{rm}} + 18.8$	Southwestern European climate/France, Greece, Portugal, Sweden, UK
ASHRAE RP-884 (1997) [1]; model included in ASHRAE 55	$T_{\text{operative}} = 0.31 \times T_{\text{outdoor}} + 17.8$	Worldwide
Toe and Hubota (2013) [10]	$T_{\text{neutop}} = 0.33T_{\text{outrm}} + 17.4$	Moderate climate; data from RP-884 ASHRAE database

3 Results and Discussion

We wanted to compare the ATC equation obtained in this study with the equations of the standards related to ATC and especially with equations for a climate like Romania’s. For this purpose we created Table 72.2, which shows the ATC equations of the standards EN 15251 and ASHRAE 55 and one ATC equation for the moderate climate. The last climate can be compared with a temperate continental climate, like Romania’s. This is the equation of Toe and Hubota [10] for a mild climate; it was obtained by sorting the ASHRAE RP-884 database for specific climate types. The slope of this equation is 0.33, which is close to the slope in our study, 0.325. The intercept of Toe and Hubota’s equation is 17.4, which is closer to 17.8, the value of the ASHRAE intercept. This is normal because the two projects used the same data. In our case, the intercept was 18.47, which is closer to the SCATs project slope, which is specific to Europe.

4 Conclusions

The purpose of this chapter was to develop an ATC equation specific to Romania's climate, according to the method given by standard EN 15251. We used the data recorded in six free-running buildings located in Bucharest and Bragadiru. The chosen value for the Griffiths constant was 0.5, and for the exponentially weighted running mean outdoor temperature we used the mean temperatures for the last 7 days. We obtained the equation and then plotted the acceptability category limits on a graph. We discussed the limits of our study. Finally, we compared the obtained equation with other ATC equations obtained for the specific climate.

For future work it will be useful to enlarge the database with measurements obtained throughout Romania and with a uniform distribution for the entire period of the study.

Acknowledgements Part of this work was funded by the Sectoral Operational Programme Human Resources Development 2007–2013 of the Ministry of European Funds through the Financial Agreement POSDRU/159/1.5/S/138963.

References

1. de Dear RJ, Brager GS, Cooper D (1997) Ashrae rp-884; Developing and adaptive model of thermal comfort and preference. Technical report. The American Society of Heating, Refrigeration and Air-Conditioning Engineers, Inc., and Environmental Analytics, editor, Atlanta
2. ASHRAE Standard 55-2010 (2010) Thermal environmental conditions for human occupancy. ASHRAE, Atlanta, GA
3. EN 15251:2007 (2007) Indoor environmental input parameters for design and assessment of energy performance of buildings addressing indoor air quality, thermal environment, lighting and acoustics. Brussels: CEN (European Committee for Standardization)
4. de Dear RJ (2010) A global database of thermal comfort field experiments. ASHRAE Trans 104(1), © 2002–2014 The University of Sydney. Last updated 14 Jan 2010. http://sydney.edu.au/architecture/staff/homepage/richard_de_dear/index.shtml. Accessed 9 Oct 2014
5. de Dear R, Brager G (1998) Developing and adaptive model of thermal comfort and preference. ASHRAE Trans 104(1)
6. de Dear RJ, Brager GS (2002) Thermal comfort in naturally ventilated buildings: revisions to ASHRAE Standard 55. *Energy Build*, 34(6), 549–561
7. Wilson M, Solomon J, Wilkins P, Jacobs A, Nicol F (2000) Final report of SCATs task 1, instrumentaion. Oxford Brookes University. <http://www.learn.londonmet.ac.uk/portofolio/1996-1998/scats/index.shtml>
8. Nicol JF, Humphreys MA (2002) Adaptive thermal comfort and sustainable thermal standards for buildings. *Energy Build* 34(6):563–572
9. Mishra AK, Ramgopal M (2013) Field studies on human thermal comfort—an overview. *Build Environ* 64:94–106
10. Toe DHC, Hubota T (2013) Development of an adaptive thermal comfort equation for naturally ventilated buildings in hot-humid climates using ASHRAE RP-884 database. *Front Archit Res* 2:278–291
11. Nguyen AT, Singh MK, Reiter S (2012) An adaptive thermal comfort model for hot humid South-East Asia. *Build Environ* 56:291–300

12. Indraganti M, Ooka R, Rijal HB (2013) Field investigation of comfort temperature in Indian office buildings: a case of Chennai and Hyderabad. *Build Environ* 65:195–214
13. Mishra AH, Ramgopal M (2015) An adaptive thermal comfort model for the tropical climatic regions of India (Köppen climate type A). *Build Environ* 85:134–143
14. Rotar N (2014) Teza de doctorat (PhD Thesis): Contributii la studiul modificarii performantelor cladirilor pasive in conditiile climatului sud-est european (România), UPB, Fac. Inginerie Mecanica si Mecatronica
15. Hera D, Drughean L, Ilie A, Crutescu R (2008) Climatizarea unei case pasive cu functiune mixta, a XV-a Conferinta; Confort, Eficienta, Conservarea energiei si Protectia mediului, 26–27 noiembrie 2008
16. Udrea I, Croitoru C, Nastase I, Dogeanu A, Badescu V (2014) Thermal comfort analyses in naturally ventilated buildings, mathematical modelling in civil engineering. *Sci J* 10(3):64–70, ISSN 2066-6926, On-line ISSN:2066-6934
17. Nicol JF, Humphreys M (2010) Derivation of the adaptive equations for thermal comfort in free-running buildings in European standard EN 15251. *Build Environ* 45:11–17
18. Griffiths I (1990) Thermal comfort studies in buildings with passive solar features, field studies. Report of the Commission of the European Community, ENS35 090, UK
19. Humphreys MA, Nicol JF, Raja IA (2007) Field studies of indoor thermal comfort and the progress of the adaptive approach. *Adv Build Energy Res* 1(1):55–88. doi:[10.1080/17512549.2007.9687269](https://doi.org/10.1080/17512549.2007.9687269)

Chapter 73

A Whole-Building, Integrated Approach for Designing a High-Performance, Net-Zero-Energy and Net-Zero-Water Building

Richard V. Piacentini

Abstract The Center for Sustainable Landscapes (CSL) at Phipps Conservatory and Botanical Gardens is a 2,262 m² educational, research, and administrative services facility set on an 11,736 m² site. Performing 70% more efficiently than a typical building and achieving an energy use intensity of 18 (2.98 kWh/m²/year), it operates at net-positive energy and captures and treats all of its sanitary and storm water. It is the world's first building to attain Living Building Challenge, LEED Platinum, Four Stars Sustainable SITES, and WELL Platinum certifications.

The CSL is the result of a whole-building, integrated, outside-in, passive-first design process guided by ecological planning principles. Two years of bimonthly design charrettes brought together team members involved in every phase of the project to capitalize on collective wisdom, shorten feedback loops, augment system synergies, minimize compromises and costs, and exceed net-zero-energy and net-zero-water performance.

Operations are enhanced by collaborating with the University of Pittsburgh and Carnegie Mellon University on original research in the CSL related to building performance. Both Universities receive real-time data from thousands of control points from the building automation and water reuse systems. Engaging staff with feedback from this research allows Phipps to continually improve the CSL's performance.

Keywords Energy • High performance green buildings • Integrative design • LEED • Living Building Challenge • Net-positive energy • Net-zero energy • Net-zero water

R.V. Piacentini (✉)
Phipps Conservatory and Botanical Gardens, Pittsburgh, PA, USA
e-mail: rpiacentini@phipps.conservatory.org



Denmarsh Photography, Inc.

1 Design and Process

In January 2013 Phipps Conservatory and Botanical Gardens began to operate the Center for Sustainable Landscapes (CSL), a 2262-m² educational, research, and administrative services facility set on an 11,736-m² site. It is the world's first building project to simultaneously attain [Living Building Challenge](#), [LEED Platinum](#), [Four Stars Sustainable SITES](#), and [WELL Platinum](#) certifications.

A critical component to achieving net-zero-energy and net-zero-water performance was the initiation of a facilitated integrative design process (IDP) from the outset. Integrative design (ID) is “a discovery process that optimizes the interrelationships between all the elements and entities that are directly and indirectly associated with building projects in the service of efficient and effective use of resources” [1] and a process for designing all building systems concurrently, rather than sequentially, to ensure that they work in harmony [2].

There are many benefits to following an IDP, including increased building performance, greater environmental benefits, savings in money and time, optimization of systems, a shortened construction document phase, and a reduced number of change orders [1]. Early initiation of an ID approach can positively impact a project's budget and schedule by reducing the time spent on design and construction [3–5] as well as increasing building efficiency and lower life-cycle costs [6].

Phipps Conservatory is located in the state of Pennsylvania in the northeastern USA. It opened in 1893 and was run by the City of Pittsburgh until 1993, when management was assumed by a nonprofit organization. In 1999 Phipps embarked on a three-phase expansion plan, resulting in the construction of the CSL.

Key features of the CSL include a 2262 m² building on an 11,736 m² site, a former brownfield. The building is 70 % more efficient than a typical building in the USA and operates at an energy use intensity (EUI) of 18 (2.98 kWh/m²/year). This is accomplished with the use of a 125 kW photovoltaic array, a 10 kW vertical axis wind turbine, and fourteen 150-m-deep geothermal wells.

The CSL was designed to meet the Living Building Challenge (LBC), the most rigorous green building standard in the world today. The LBC sets performance criteria in seven areas: place, water, energy, health and happiness, materials, equity, and beauty. In addition, projects must demonstrate that they simultaneously meet net-zero energy and net-zero water over a 1-year operating period. There are currently 190 projects worldwide pursuing LBC certification.

Phipps pursued a whole-building, ID approach with a goal of creating harmony between all living and technical systems. This approach resulted in 2 years of bimonthly design charrettes involving architects, designers, landscape architects, engineers, energy and lighting experts, modelers, academics, contractors, estimators, staff, and community members. The IDP optimizes the relationships between all systems continuously throughout the design phase to maximize synergy and efficiency and eliminate compromises. The following description of the IDP used at Phipps is based on the charrettes led by CSL project team members John Boecker and Marcus Sheffer and the paper “Understanding Integrative Design in LEED v4” [7]

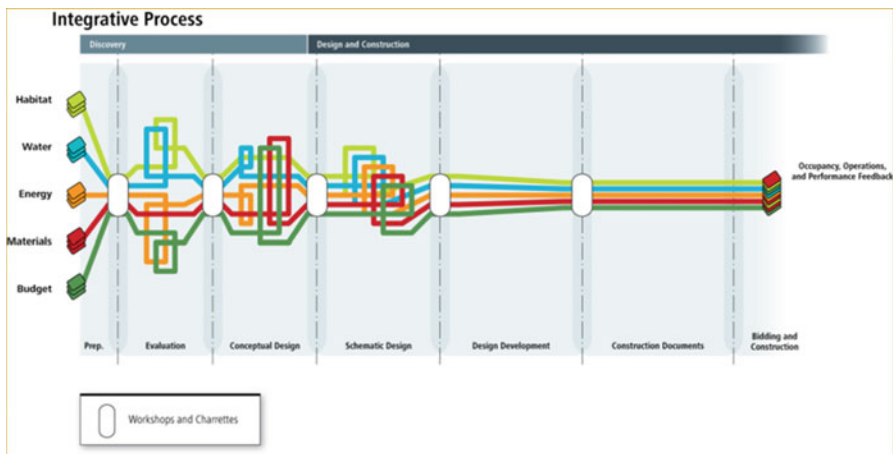


Image credit: 7group

The IDP starts with a discovery phase in which the team is brought together to question assumptions, align around goals, and discover solutions together. A

touchtone exercise was used to identify core values and primary objectives for the project. This was followed by goal setting related to aspirations, budget, schedule, program, and quality and performance expectations. This critical phase ensured that everyone was aligned around the same goals and priorities before moving on to the next phase.

The next part of the discovery phase focused on energy and water systems. Background data and research were gathered to develop a robust understanding of site conditions; benchmarks against other buildings were established, and a model of expected energy loads was developed; and expected water needs and treatment needs were defined.

Performance targets were then set to assess both the energy and water strategies. These were used to determine the best combination of passive and active energy strategies that would result in the most energy-efficient and cost-effective building before design began. Factors assessed for strategic implementation included site conditions, building massing and orientation, building envelope, lighting levels, thermal comfort ranges, plug and process loads, and program and operational hours. Water strategies were devised based on indoor and outdoor water use demand, sanitary water treatment, stormwater management, and the potential use of captured nonpotable water.

The IDP allowed for the team to develop and review various design strategies together. After building orientation on the site was determined, extensive modeling took place to estimate performance against targets and goals. Models were established to assess daylighting strategies, natural ventilation, and thermal comfort. In the case of the CSL, a number of different passive energy-saving strategies were reviewed, including minimizing glazing on the west side of the building, using sunshades to block summer sun, and placing sun shelves to reflect natural light deep into the office space. Additional strategies assessed by the team included the use of natural ventilation to minimize the need for air conditioning, the elimination of both mechanical heating and cooling systems for the atrium, the use of open office architecture to allow for maximum penetration of natural light and ventilation throughout the space, and equipment choices such as the use of laptop computers instead of desktops to save energy.

Having a cohesive team made it possible to adapt to changes during construction. For example, originally all the vertical walls in the atrium were to be made of poured-in-place concrete to provide thermal massing. After construction delays required a switch to drywall, the team discovered a new type of phase change material and was able to pull together quickly to assess and install sheets of it behind all the vertical surfaces in the atrium to restore thermal massing benefits.

Modeling also helped when determining the most cost-effective and efficient ways to generate energy. After comparing a number of different combinations, the best solution was determined to be 125 kW of photovoltaic panels, a 10 kW vertical axis wind turbine, and fourteen 150-m-deep geothermal wells.

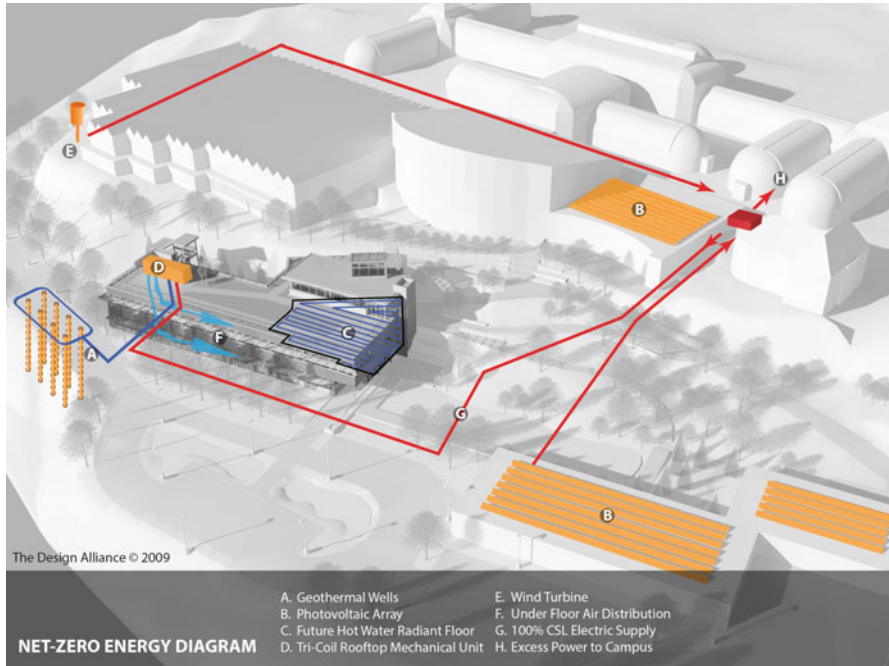


Image credit: The Design Alliance

2 Performance

All the stormwater from the lower 11,736-m² site is managed on site through a series of strategies that includes a green roof, five rain gardens, a lagoon, permeable asphalt paving, and 302,833 L of underground water storage.

All sanitary water is managed on site. Water from toilets and sinks is sent to a settling tank. Liquid from the tank is then pumped through two constructed wetlands where plants and microbes clean the water. The water then passes through four underground sand filters before being sent to a storage tank. Water in the tank is passed through an ultraviolet light to kill any pathogens before being sent to flush the toilets again. Any excess treated water is stored in two 45,424 L repurposed fuel tanks until it can be sent through the wetlands again, where it is subject to evapotranspiration. In the future, excess water from these tanks will be sent to six solar distillers to make distilled water that can be used for watering plants in the greenhouses.

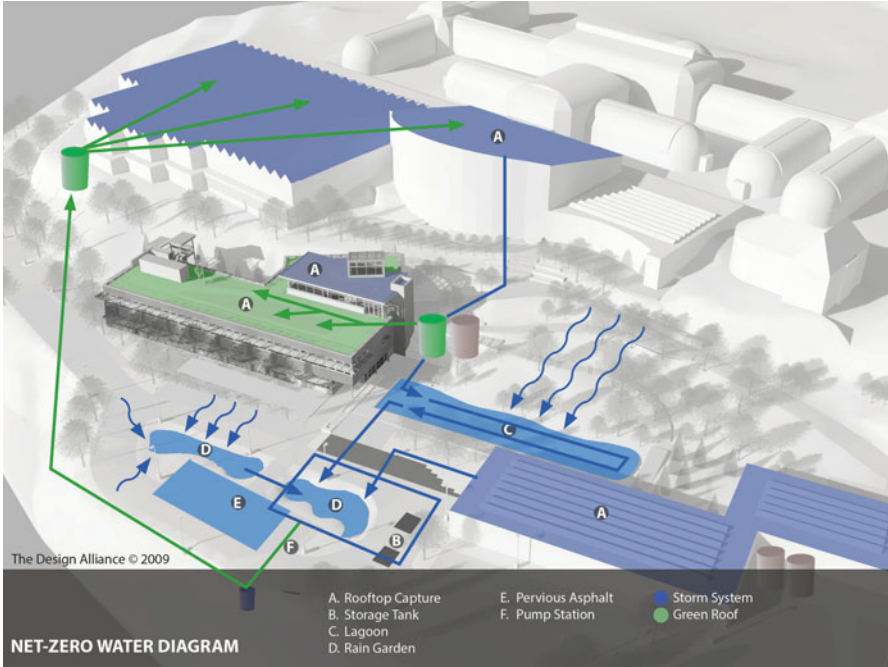


Image credit: The Design Alliance

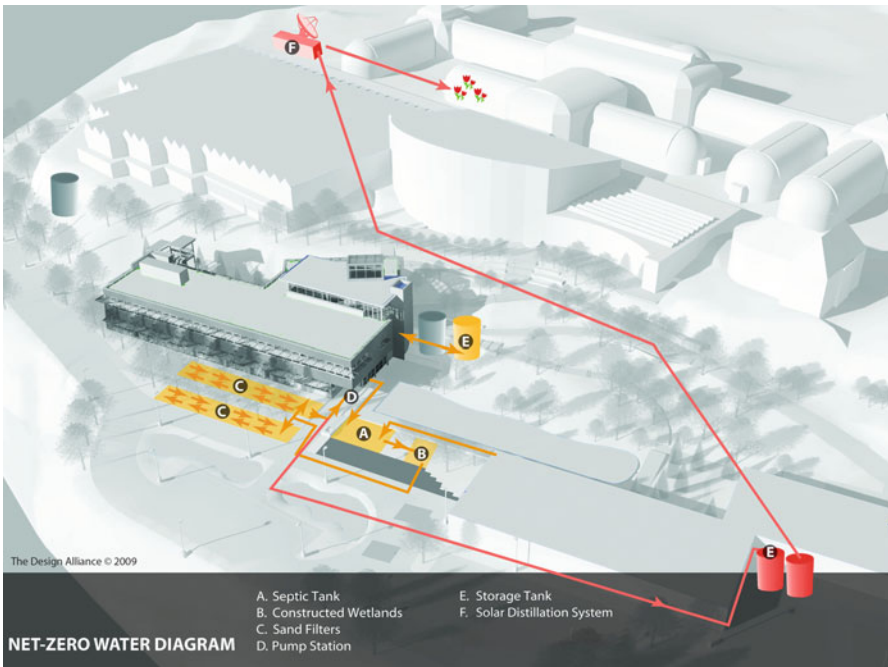


Image credit: The Design Alliance

The building is performing significantly better than standard office buildings for both energy and water use, and potable water requirements are drastically reduced by the treatment and reuse of sanitary water for flushing toilets.

The initial performance target for energy was for the building to consume 117,623 kWh of energy per year. During the first year the building consumed 129,876 kWh; however, actual production of 134,958 kWh exceeded actual use by 5082 kWh.

Comparison to Baseline Buildings

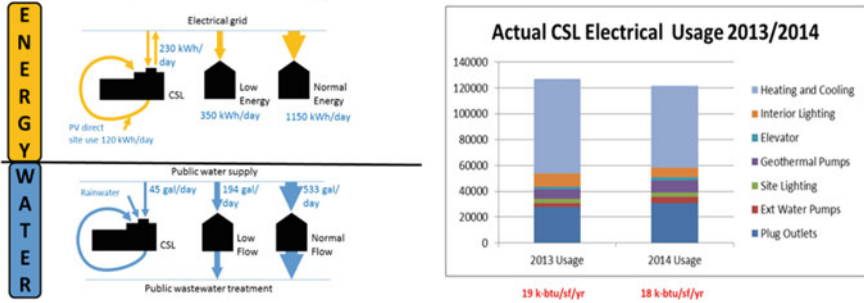


Image credits: Left: Collinge, W.O.; Anderson, N.E.; Thiel, C.L.; Hasik, V.; Landis, A. E.; and Bilec, M.M. Right: Jason Wirick

Continuous monitoring and refining led to a reduction in EUI from 19 (3.15 kWh/m²/year) to 18 (2.98 kWh/m²/year).

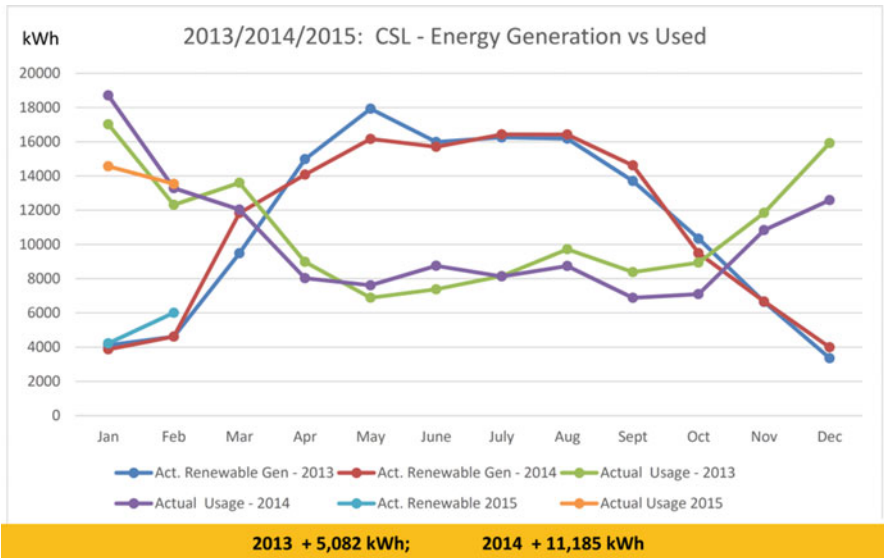


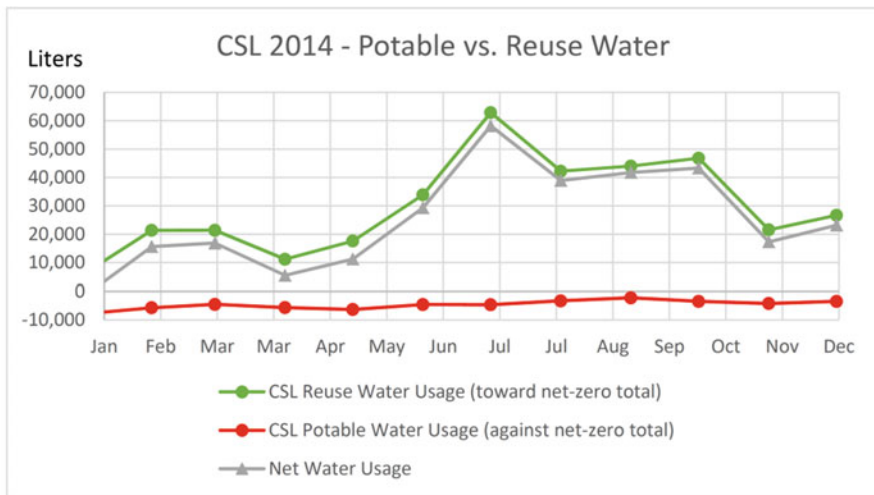
Image credit: Jason Wirick

Continuous monitoring and refining led to an increase in net-positive energy. In 2014 net energy production increased to 11,185 kWh for the year.

Phipps continues to work with researchers from Carnegie Mellon University and the University of Pittsburgh, conducting original research on building performance. Thousands of data points from data loggers and sensors in the building continuously provide real-time data to researchers at both universities. Original research published or in-prep includes the following:

- Occupant behavior and schedule modeling for building energy simulation through office appliance power consumption data mining [8];
- An online platform to automate the LEED energy performance evaluation and submission process [9];
- EnergyPlus model-based predictive control within design–build–operate energy information modeling infrastructure (*Journal of Building Performance Simulation*) [10];
- Dynamic LCA of a zero-energy and zero-water building and implications at the community scale [11].

Not only have these studies contributed to the research and knowledge base for high-performance green buildings, but they have also provided valuable feedback to Phipps, which has allowed us to engage staff in improving the performance of the building.



2014 + 298,600 liters of treated sanitary reused rather than potable water

Image credit: Jason Wirick

Other research is being conducted on the green roof and rain gardens. Sensors in these spaces monitor rainfall, light, temperature, relative humidity, wind speed, water storage in soil, soil temperature, water storage over soil, and water quality (electrical conductivity and pore water analysis). Green roof drainage is measured directly using a pan lysimeter. The CSL manages 10,220,607 L of rainwater each year.

The green roof captures between 80.3 and 89.3 % of rainfall and has significantly helped moderate the rooftop temperature of the building.

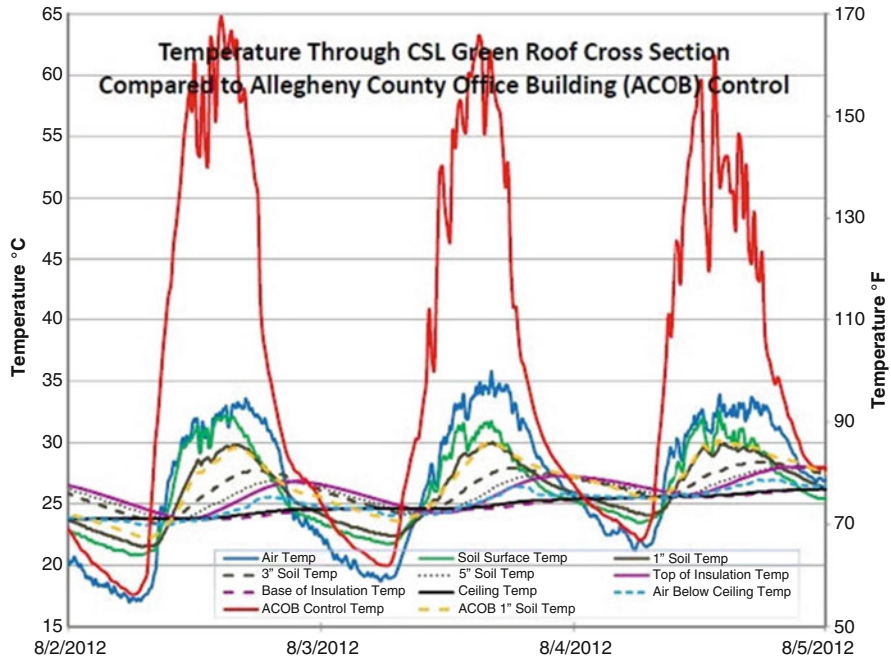


Image credit: John Buck at Civil and Environmental Consultants

CSL staff occupants are provided with sensors that allow them to see how much energy they are consuming at their desks in real time and how changes they make in the way they do things affect building energy use. They can also record their degree of comfort in the building directly on their laptop computers. These data also help us in refining building performance.

3 Conclusion

A whole-building ID approach is essential to the development of high-performance, net-zero-energy, net-zero-water buildings. Engaging the entire project team around a common set of goals at the outset is key. Regular engagement and modeling of

proposed systems early in the design phase aids in the discovery of the most cost-effective and efficient solutions. After construction, extensive commissioning, ongoing monitoring and fine tuning, and occupant engagement can result in further improvements in performance and overall energy and water use.

Acknowledgements Chris Minnerly, The Design Alliance; John Boecker and Marcus Sheffer, 7group; Alan Traugott, CJL Engineering; José Almiñana, Andropogon Associates; John Buck, Civil and Environmental Consultants; Emily Kalnicky, PhD., Joe Reed, and Jason Wirick, Phipps Conservatory and Botanical Gardens.

References

1. 7group, Reed B (2009) The integrative design guide to green buildings: redefining the practice of sustainability, vol 43. Wiley, Hoboken
2. Cross JE, Barr S, Putnam R, Dunbar B, Plaut J (2015) The social network of integrative design. Institute for the Built Environment, Colorado State University, Fort Collins
3. The American Institute of Architects (AIA) California Council (2007) Integrated project delivery: a guide. The American Institute of Architects California Council, Washington
4. Gotthelf H, Ozbek M, Guggemos A (2013) Potential efficiency gains from early involvement of steel fabricators and erectors: lessons learned from the NREL research support facility project. *Int J Constr Educ Res* 9(2):147–160
5. Leicht RM, Molenaar KR, Messner JI, Franz BW, Esmaeili B (2015) Maximizing success in integrated projects: an owner's guide. Version 0.9, May. <http://bim.psu.edu/delivery>
6. NREL, Research Support Facility (RSF) Workshop (2011) Summary of review panel findings. National Renewable Energy Lab, Editor. U.S. Department of Energy
7. Boecker J. (2014) Understanding integrative design in LEED v4. *Syntheegrative Thinking*, #3-2014. Retrieved from <http://www.sevengroup.com/r-publications/syntheegrative-thinking/>
8. Zhao J, Lasternas B, Lam KP, Yun R, Loftness V (2014) Occupant behavior and schedule modeling for building energy simulation through office appliance power consumption data mining. *Energy Build* 82:341–355
9. Zhao J, Lam KP, Biswas T, Wang H (2015) An online platform to automate LEED energy performance evaluation and submission process. *Constr Innov* 15(3):313–332
10. Zhao J, Lam KP, Erik Ydstie B, Karaguzel OT (2014) EnergyPlus model-based predictive control within design–build–operate energy information modelling infrastructure. *J Build Perform Simul* 8(3):1–14. doi:10.1080/19401493.2014.891656
11. Collinge WO, Anderson NE, Thiel CL, Hasik V, Landis AE, Bilec MM (2015) Dynamic LCA of a zero energy and water building and implications at the community scale. *ISIE*

Links

<https://phippscsl.org>

<https://youtube.com/watch?v=0qk4hbNEWdQ>

Chapter 74

Dynamic Simulation for Increasing the Efficiency of Solar Cooling Systems in Northern Latitudes

Peteris Shipkovs, Janis Shipkovs, Andrejs Snegirjovs, Galina Kashkarova, Kristina Lebedeva, and Lana Migla

Abstract Latvia lies on the eastern shores of the Baltic Sea at 57°00'N latitude. In Latvia, cooling is required about 1500 k.h degree hour (at an indoor temperature of 21 °C). This chapter presents the optimization of a solar cooling system in Latvia using the model of a solar cooling system which was created by a dynamic simulation program. The model is similar to the existing real solar cooling system installed at the Institute of Physical Energetics. The precision of the model was tested by comparing it with real equipment. Simulations were carried out using metrological data from different European countries. Simulation results, the dependency of the heat carrier average temperature and the ratio of energy from a pump to the system were collected and analysed. Different element locations of the solar cooling system were compared in two models. The annual cool production of the solar cooling system was defined.

Keywords Solar energy use • Solar cooling system • Thermal-driven chiller

1 Introduction

The modelling of a solar cooling system was performed using a dynamic simulation program. The model is similar to the existing real solar cooling system at the Institute of Physical Energetics. The precision of the model was tested by comparing it with real equipment. In the model, the location of the inflow, outflow and return lines of pumps was changed.

P. Shipkovs (✉) • G. Kashkarova • K. Lebedeva • L. Migla
Institute of Physical Energetics, Aizkraukles 21, Riga LV-1006, Latvia
e-mail: shipkovs@edi.lv

J. Shipkovs • A. Snegirjovs
Institute of Physical Energetics, Aizkraukles 21, Riga LV-1006, Latvia
Riga Technical University, Kaļķu iela 1, Rīga LV-1658, Latvia
e-mail: shipkovs@edi.lv

Simulations were carried out using metrological data from different European countries. In this way, the variation range was determined for the impact of pump placement effect on solar cooling systems in different climatic conditions to assess the possibility of using the model in other EU countries.

The PolySun simulation program was used for system simulations. The base model was adapted to the model with low-power heat-driven adsorption cooling. The adsorption chiller's nominal power is 8 kW and maximum cooling capacity is 11 kW. Heat was used for thermally driven chilling; this heat was mainly derived from a solar thermal system. In this case, a solar thermal system with thermal power of 15 kW at $\Delta T = 70$ K was used [1]. A 1 m³ accumulation tank with an 8 kW electric heater was included in the solar thermal system. The cooling system was designed in such a way as to provide around 80 % of the maximum cooling power. A cold water buffer was used for peak alignment. A wet cooling tower with 21 kW of nominal power was used for heat rejection. Excess heat from the solar thermal system was redirected to hot water preparation. Hot water consumption was designed according to the solar thermal system's monthly maximum productivity in the non-cooling season.

2 Methods and Results

It has been demonstrated that the most rapid development due to improvements and installations of solar cooling systems has been achieved in the European region. That is why this study mainly discusses the results of that region. The results of different European regions were analysed through the base model simulation of the given system. Following evaluation of the obtained results, Spain (SR: southern region) was taken as the reference location where maximum productivity is necessary. Latvia (NR: northern region) was chosen as the location of minimum productivity with a relative necessity for cooling.

Simulation results show that cold yield with the given solar cooling system ranges from 1.5 MWh/a in NR to 3.7 MWh/a in SR. The working time of the thermally driven chiller ranges from 410 h/a in NR to 970 h/a in SR. The cold yield in the given study includes the rejected heat from indoors. Heat rejection demand has been adapted to space-heating in a certain climate in the cooling season. The study is aimed at household and office space cooling, so the cooling demand of the technical process was not included in this model.

The aforementioned cold production with a thermally driven chiller mainly consumes heat. The heat supplied in the generator ranges from 3.6 MWh/a in NR to 10.3 MWh/a in SR. Recooling heat with a wet recooling tower ranges from 5.1 MWh/a in NR to 14 MWh/a in SR. Both water and electricity are used while the wet recooling tower is operating. Electricity was mainly consumed for the operation of the fan, ranging from 0.25 MWh/a in NR to 0.6 MWh/a in SR for a given level of heat rejection. The thermal efficiency of the wet cooling tower ranges from 16.9 % in NR to 22.6 % in SR. In at the same time turn, for 1 MWh heat rejection with the

wet cooling tower, from 0.043 MWh in SR to 0.050 MWh in NR of electricity is consumed for the operation of the fan.

Solar cooling systems have six closed circuits:

Solar collector circuit – between solar collectors and hot accumulation tank

Driving heat circuit – between hot accumulation tank and thermal driving chiller

Recooling circuit – between thermally driven chiller and cooling tower

Chilled water circuit – between thermally driven chiller and cold accumulation tank

Hot water circuit – between hot accumulation tank and hot water accumulation tank

Cooling distribution circuit

Each circuit has its own pump, which can be separately controlled by certain programs from a common control unit. Each pump consumes electricity and creates potential energy – pressure and kinetic energy – flow. In addition, heat losses are released during pump operation. Part of the heat losses go to the environment, mostly indoors, and the other part of the heat losses is transferred to the heat carrier. Kinetic energy combines with heat losses to the heat carrier to create the total energy to the system from pumps. The total energy input to the system ranges from 7 to 31 % of the consumed electricity in the solar cooling loops. The ratio depends on the operating parameters, including the temperature of the heat carrier to which that energy is transferred [2].

As can be seen from Fig. 74.1, the percentage of energy that is transferred to the heat carrier from the consumed electricity is inversely proportional to the temperature of the heat carrier which flows through the pumps. The main reason is that the potential increase raises the heat flow from the pump components to the heat carrier. This potential is directly proportional to the temperature difference, meaning that the heat flow amount increases with the decrease in the heat carrier temperature at the inlet of the pump.

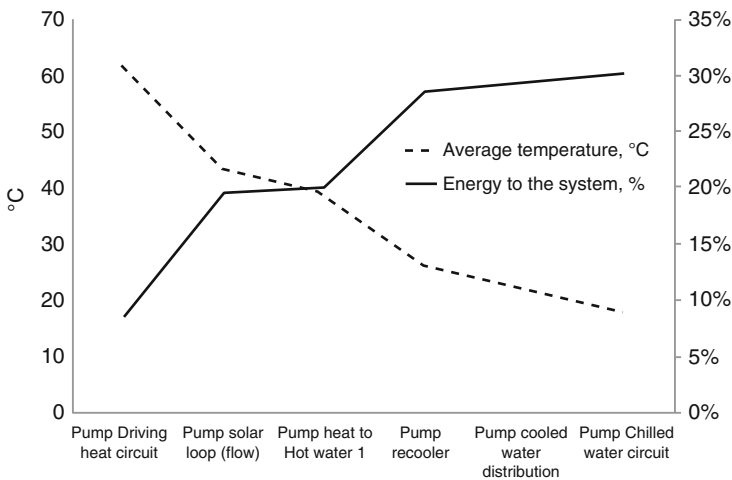


Fig. 74.1 Dependency of heat carrier average temperature and ratio of energy from pump to system

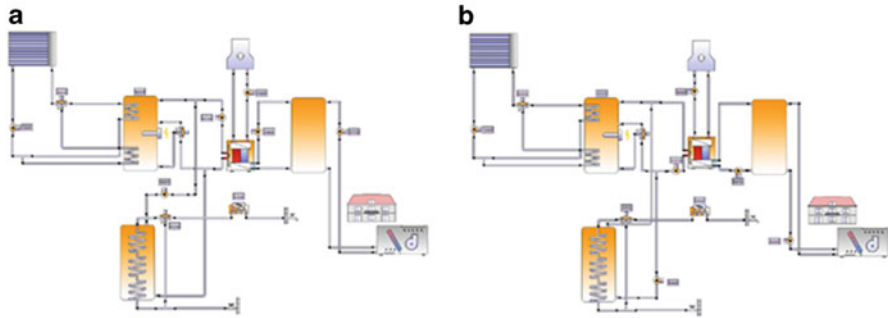


Fig. 74.2 Principal scheme of Options A and B

The yield of the solar cooling elements (such as the solar collector, heat-driven adsorption chiller, cooling tower and heat exchangers) depends on the intake amount of heat. Therefore, the pump location before or after the specified element of the given system affects the element yield. In the present study, the location of pumps will be changed at the flow return line of circuits in to correct the solar cooling model during operation [3]. Other parameters remain unchanged. Mainly two models are compared (Fig. 74.2). The yields of the overall solar cooling system and its elements will be evaluated in the results section.

The temperature of the heat carrier increases owing to the supplied thermal energy. The effectiveness of the heat-driven chiller, cooling tower, indoor fan coil and heat exchanger depends on the temperature difference between the heat carrier temperature and the second environment – fluid, outdoor or indoor air. The energy transferred from the pump to the heat carrier is eventually fully converted to heat. It in turn will positively impact the solar thermal cooling elements.

The pump location is not changed in the solar collector loop because the pump might overheat. This is extremely important when the pump is located close to the solar collectors and overheated, or even gaseous, antifreeze or glycol could enter the pump and cause thermal damage. As can be seen from Table 74.1, the maximum temperature in the annual experiment reached 124 °C, and this temperature could go even higher in a solar collector circuit. The maximum temperatures of the technical water circuit are close to the boiling temperature and are observed in a hot circuit and a hot water circuit [4].

Initially, the thermal energy from the solar thermal system passes through a driving heat circuit. Installing the pump before the thermally driven chiller is a more efficient solution in this circuit. The nominal driving temperature in the circuit is 55–95 °C. Actually, the working average temperature is close to 60–63 °C. The pump operates from 4.7 % in NR to 11 % of year time in SR. The pump in this circuit consumes from 8 kWh/a in NR to 19.5 kWh/a in SR. The given pump transfers from 8.5 to 13 % of the energy from electricity consumption to the heat carrier, or from 1 kWh/a in NR to 2.5 in SR.

In a chilled water circuit it is also useful to put the pump before the thermal driven chiller; in this case recently cooled coolant is not heated. The nominal operating temperature in the circuit is 6–20 °C, whilst the actual average operating

Table 74.1 Temperatures in circuits of solar cooling system

	Northern region			Southern region		
	Flow average temperature	Return average temperature	Maximum temperature	Flow average temperature	Return average temperature	Maximum temperature
Pump at chilled water circuit	17.8	17.9	28.9	21.9	22	38
Pump at cold water distribution	21.2	21.9	29	26.4	26.9	38
Pump at driving heat circuit	61.6	58.3	98.6	61.7	58.7	96.9
Pump at recoolor	26.2	25.4	41.2	26.8	26	42.5
Pump at solar loop	43	61.2	122.1	58.2	76	124.5
Pump at heat to hot water	40.5	39	99.7	61.8	60.1	99.8

Table 74.2 Pump energy flows

a						
	Option A			Option B		
	Electricity consumption	Energy to system	Heat loss	Electricity consumption	Energy to system	Heat loss
Northern region	kWh					
Pump at chilled water circuit	8.3	2.5	5.8	8.3	2.5	5.8
Pump at cold water distribution	29.1	8.5	20.6	29.1	8.6	20.6
Pump at driving heat circuit	8.2	0.7	7.5	8.2	0.9	7.3
Pump at recooling	20.7	5.9	14.8	20.7	5.9	14.8
Pump at solar loop	39	7.6	31.4	38.9	7.5	31.4
Pump at heat to hot water	37.9	7.6	30.4	38.1	7.7	30.5
b						
	Option A			Option B		
	Electricity consumption	Energy to system	Heat loss	Electricity consumption	Energy to system	Heat loss
Southern region	kWh					
Pump at chilled water circuit	19.4	5.5	13.9	19.4	5.5	13.9
Pump at cold water distribution	69.1	19.7	49.3	69.1	19.8	49.3
Pump at driving heat circuit	19.3	2.3	17	19.2	2.5	16.7
Pump at recooling	48.6	13.8	34.8	48.5	13.9	34.7
Pump at solar loop	47.6	7.6	40	47.6	7.6	40
Pump at heat to hot water	22.5	1.5	21	23.1	1.7	21.5

temperature is around 17.8–22 °C. From 8.3 kWh/a in NR to 19.4 kWh/a in SR is used for pump operation. From 28.4 to 30.1 % of the energy from the spent electricity is transferred to the heat carrier, corresponding to 2.5 kWh/a in SR and 5.5 kWh/a in NR.

The generated heat of the thermally driven chiller plus the heat from indoors are rejected through the recooling tower. It is useful to place the pump in the heat recooling circuit before the recooling tower. The nominal operating temperature in the circuit is 22–37 °C, and the actual temperature is about 26–26.8 °C. The pump consumes from 20.7 kWh/a in NR the 48.6 kWh in SR.

The longest operating pump is the one in the hot water circuit and the operation time is up to 73.4 % per annum. Taking into account that the temperature of the heat carrier loop is given as being high enough, during operation of this pump, 37.9 kWh/a of electricity is consumed, and 20.2 % of this energy, or 7.6 kWh/a, is transferred to the system. Temperature data described previously and the rest of the circuit are shown in Table 74.2a, b. We can conclude that correct positioning of

the pumps makes it possible to efficiently use an additional 25 kWh/a in NR to 43 kWh/a in SR.

Looking at the component yields of the solar cooling system of Options A and B, the effects of pump positioning can be observed. If the pump is placed in an ideal-case scenario (Option A) compared to the worst-case scenario (Option B), the additional loaded heat transferred to the thermally driven chiller is from 5.4 kWh/a in NR to 11.7 kWh/a in SR. In this case, the adsorption chiller works 0.6–1.3 h more and produces more cold, from 3.2 kWh/a in NR up to 4.4 kWh/a in SR, which constitutes 0.15 and 0.11 % of the total annual yield. Accordingly, the recooling tower rejects 0.8–1.2 kWh/a more heat. The additional heat and total required quantity of electricity are reduced by up to 0.24 % per year, or 5.1 kWh in NR. It should also be mentioned that the more preferred systems use in the ideal scenario a decreased amount of heat from solar collectors, about 0.21 % of 28 kWh/a in NR. This does not affect the overall positive impact.

3 Conclusions

Solar cooling is topical and profitable in the Baltic Sea region countries. It is important to underline that solar cooling allows not only effective use of solar collectors but also significantly reduces fossil fuel use for cooling. Solar cooling makes it possible to provide comfortable conditions in the workplace, ensuring that keeping indoor temperatures in line with health standards will remain very topical in our country as well as in neighbouring countries.

Annual cool production of solar cooling systems is up to 230 kWh for every kWp of adsorption chiller nominal power; 560 kWh of thermal energy is used for this purpose and 89 % of this energy is produced by solar collectors. Of the total solar thermal energy produced, 29 % is spent in the adsorption cooling process, 60 % is used for hot water preparation, and the rest is heat losses.

Generally, auxiliary heat demand for adsorption chillers requires only 0.6 % of the total energy demand in the cooling season; the rest is provided by solar thermal system heat production. Using an average of 0.92 parts of heat energy and 0.08 parts of electricity, it is possible to chill 0.38 parts of the heat.

Electricity is mostly consumed for fan cooling towers in the solar cooling process, and it constitutes 82 % of the total electricity consumption for the solar cooling process during the year. Pumps are the next major consumer of electricity; they account for 16.6 % of the total electricity consumption in the cooling season. A thermally driven chiller consumes only 2.9 kWh/a or makes up 0.9 % of total electricity consumption.

Acknowledgment This work was supported by the ESF “Attraction of Human Resources to Science (2nd round)” project “Development of the innovative technologies for the accumulation and production of heating and cooling” number 2013/0064/1DP/1.1.1.2.0/13/APIA/VIAA/050.

References

1. Shipkovs P, Snegirjovs A, Kashkarova G, Lebedeva K, Migla L (2014) Solar cooling in high latitudes conditions. In: EuroSun2014, international conference on solar energy and buildings annual conference, 6 p
2. Shipkovs P, Kashkarova G, Lebedeva K (2009) Solar energy use for sustainable development. In: Proceedings of 29th ISES biennial solar world congress 2009, South Africa, pp 1881–1887
3. Shipkovs P, Vasiļevska L, Lebedeva K, Pankars M, Snegirjovs A (2010) Modeling of solar heating systems in Latvia. In: Proceedings of 10th REHVA world congress on sustainable energy use in buildings. CLIMA 2010. Turkey, Antalya, 8 p
4. Shipkovs P, Snegirjovs A, Kashkarova G, Shipkovs J (2014) Energy Procedia. In: 2013 I.E. solar world congress, vol 57, pp 2629–2635

Chapter 75

Investigation of Urban Microclimate Parameters of City Square in Harbin



Hong Jin, Peng Cui, and Meng Huang

Abstract This chapter aims to address the characteristics of urban microclimate that affect building energy performance and implementation of renewable energy technologies. An experimental campaign was designed to investigate microclimatic parameters, including air and surface temperature, direct and diffuse solar irradiation levels on both horizontal and vertical surfaces, wind speed, and direction in a city square in Harbin, China. The outcomes of this research reveal that the climatic parameters are significantly influenced by the attributes of urban textures, which highlight the need for both providing microclimatic information and using it in a building's design stages. This research provides valuable microclimatic information for a city square in Harbin. According to the outcomes of this research, a feasibility study for the implementation of renewable energy technologies and the thermal/energy performance assessment of buildings needs to be conducted using microclimatic information rather than meteorological weather data that are collected mostly from nonurban environments.

Keywords Microclimatic parameters · City square · Energy consumption simulation

1 Introduction

Open spaces in cities take a large variety of forms and surface characteristics. The microclimate of these spaces is influenced by several parameters such as urban geometry, vegetation, water levels, and surface properties. Inappropriate

The original version of this chapter was revised. The correction to this chapter is available at https://doi.org/10.1007/978-3-319-30746-6_77

H. Jin · P. Cui (✉) · M. Huang
Heilongjiang Cold Architectural Science Key Laboratory, School of Architecture, Harbin
Institute of Technology, Harbin, China
e-mail: 14b334004@hit.edu.cn

uses of these parameters contribute to the harshness of the environment and make temperatures in the urban environment higher than in the suburbs. This phenomenon is called the urban heat island UHI [1]. The dominant causes of UHI identified so far include heat trapping by urban geometry, properties of urban surfaces, changes in vegetation cover, and human-caused (anthropogenic) heat input.

In the open literature, issues related to microclimate are addressed through numerical simulations and experiments. Many studies have involved the simulation of urban microclimates [2–9]. In terms of experimental studies, most are reported mainly in the context of air circulation and temperature distribution within urban street canyons [10–12]. In these studies, the geometric characteristics of the general urban layout are idealized as infinite parallel walls of a street canyon with an emphasis on pedestrian comfort, pollutant dispersion, and natural ventilation. Santamouris et al. [10] studied the thermal characteristics in a deep ($H/W = 2.5$) pedestrian canyon with a northwest–southeast (NW–SE) axis, under hot weather conditions, in Athens, Greece. A surface temperature difference of up to $19\text{ }^{\circ}\text{C}$ was observed between opposite building walls. The air temperature difference near the two opposing facades varied by up to $4.5\text{ }^{\circ}\text{C}$ due to the impact of convection heat transfer from adjacent wall surfaces. Niachou et al. [11] reported an experimental study of a typical street canyon ($H/W = 1.7$) orientated in an east-southeast–west-northwest (ESE-WNW) direction in Athens, Greece, again under hot weather conditions. The measured surface temperature difference across the street reached almost $30\text{ }^{\circ}\text{C}$, and this caused overheating at lower air levels. Georgakis and Santamouris carried out detailed experiments in a deep canyon in Athens during the summer period to evaluate the potential of natural ventilation in the urban environment and to better understand the airflow and thermal phenomena in deep urban canyons on climatic variables [13–15].

To see how the city square could be made sustainable and reduce the energy consumption of the surrounding buildings, this chapter presents the analysis of microclimatic conditions in an urban square of Harbin, China. A number of field measurements were carried out during summer 2015 and winter 2014 aimed at an investigation of the microclimatic parameters that affect thermal conditions in the city's square. This study focuses on an experimental investigation of the wind characteristics (speed and direction) and thermal profile (air temperature distribution) of an area composed of several building blocks in the city center. The data analysis presented here emphasizes the differences observed within the square, in different city squares, and a comparison of the microclimatic parameters in the urban scale for the area shows the increased energy needs of the surrounding buildings during the winter period.

2 Experimental Setup

The experimental measurements were made in summer 2014 in Harbin (126.63 E and 45.75 N). Harbin is a typical city in a severe, cold region among China's climate zones. The measuring site is displayed in Fig. 75.1. It is a mixture of residential buildings and a shopping mall. Naturally, there is a square enclosed by roads, and there is also lawn area within the square and trees along some roads. Four separate roads are identified to monitor microclimatic variables and the building and road surface temperatures.

The square is 230 m long by 188 m wide; the left side of the square is a shopping mall, while the right side is a continuous row of attached buildings, including a newly built museum. The main land surface condition is concrete, tile lawn, and asphalt, as shown in Fig. 75.1.

2.1 Measurement Parameters and Instruments

The microclimatic variables were measured at eight locations with different land surface conditions. These weather stations are labeled WS1 to WS8. Weather station 1 (WS1) was located in a tree area, WS2 in the middle of the square, WS3 in an

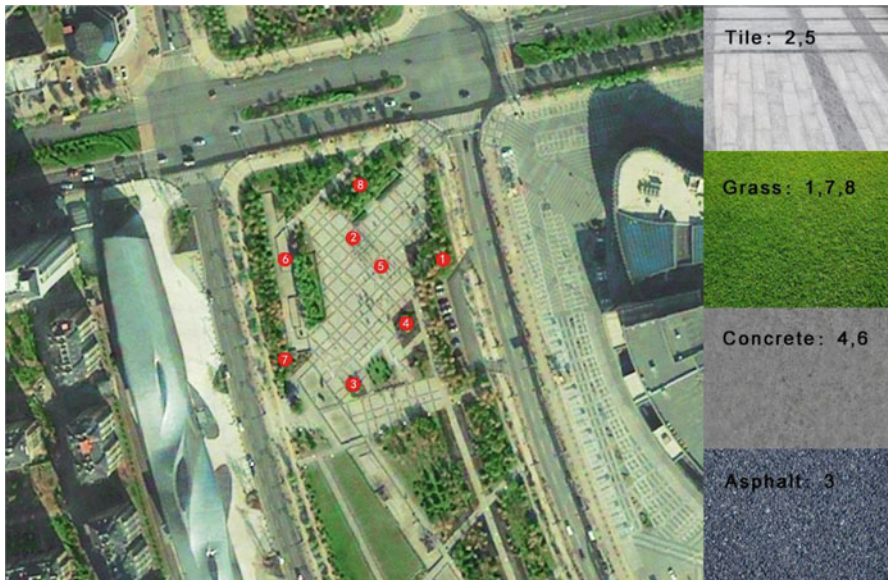


Fig. 75.1 Field measurement site of Chunshui Square, Harbin

asphalt area, WS4 in grass, WS5 in the middle of the square, WS6 near a pond, WS7 among trees along the street, WS8 was in a wooded area. Besides, WS9 was the official Harbin urban climate center weather station which was set in suburb area. Finally, the air temperature was also measured at a height of 1.5 m by the HOBO (UX100-011) temperature sensor mounted on a tripod. In addition, surface temperatures were measured at each 0.2 m height of the tripod, and the test weather station was set as shown in Fig. 75.2. Table 75.1 summarizes the measured variables, the instruments, and the observation arrangements. Air temperature and relative humidity data were collected by the HOBO data logger, which was mounted in a radiation shield.

Based on long-term observations, the typical summer day experienced an average temperature above 22 °C, and the typical winter day had an average temperature below -20 °C. Based on a previous study, fairly clear and calm days were selected, and rainy and cloudy days were excluded for regression analysis. A criterion of bell-shaped hourly solar radiation and air temperature profiles was proposed to exclude cloudy days. The following criteria were proposed to select typical summer days:

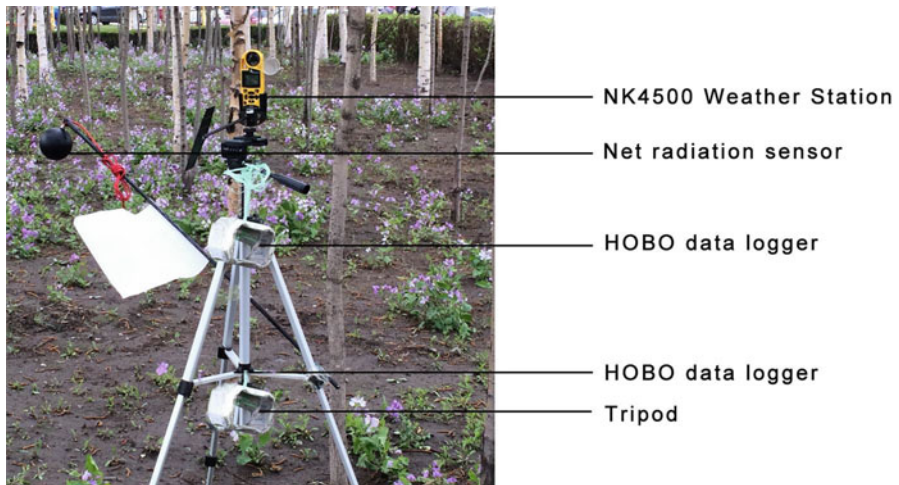


Fig. 75.2 Sensors for surface temperature, wind velocity and net radiation. (The measurement of air temperature/relative humidity in 0.2 m and 1.5 m above the surface)

Table 75.1 Measured variables, instruments, and observation arrangements

Variable	Sensor type	Accuracy	Sample
Ta, RH	HOBO pro v2 data logger	±0.2 °C, ±2.5% (RH)	1 min
Ts	Thermal infrared imager	±2 °C (-40–120 °C)	2 min
Net radiation	Net radiation sensor	±10% for 12 h totals	1 min
Wind velocity	NK4500 weather station	0.4–60.0 m/s	4 Hz

daily maximum solar radiation exceeding 800 W/m^2 , daily average temperature exceeding $22 \text{ }^\circ\text{C}$, no rain, daily average wind speed under 3 m/s , and both hourly temperature and hourly solar radiation showing bell-shape profiles.

Our main analysis tool in developing the climatic maps was the Geographical Information System (GIS), a technology that can be used to view and analyze data from a geographic perspective. GIS links location and information layers to reveal how they interrelate.

3 Data Analysis

3.1 Surface Temperature and Air Temperature

Figure 75.3 shows the air temperature at 1.5 m at the different measurement stations and the range of deviation between weather and measurement stations. Figure 75.4 shows the air temperature at 0.2 m at the different measurement stations.

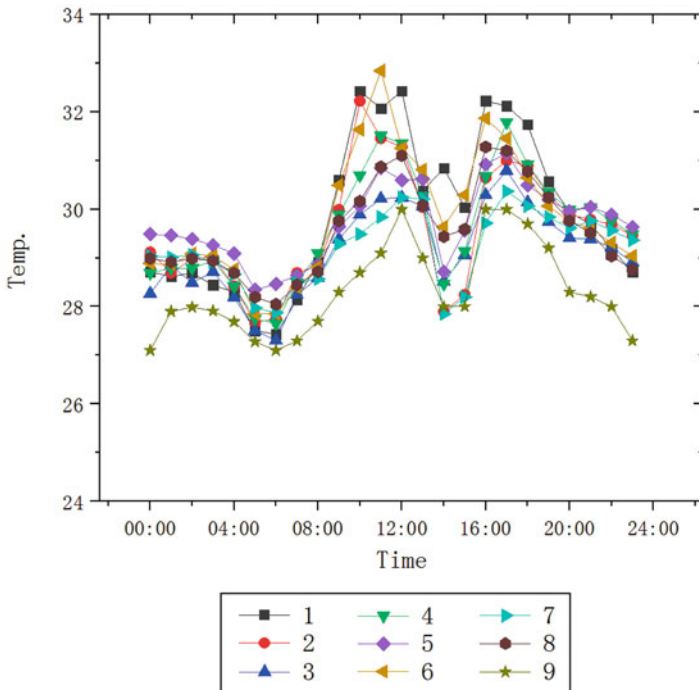


Fig. 75.3 Range of deviation between weather and measurement stations

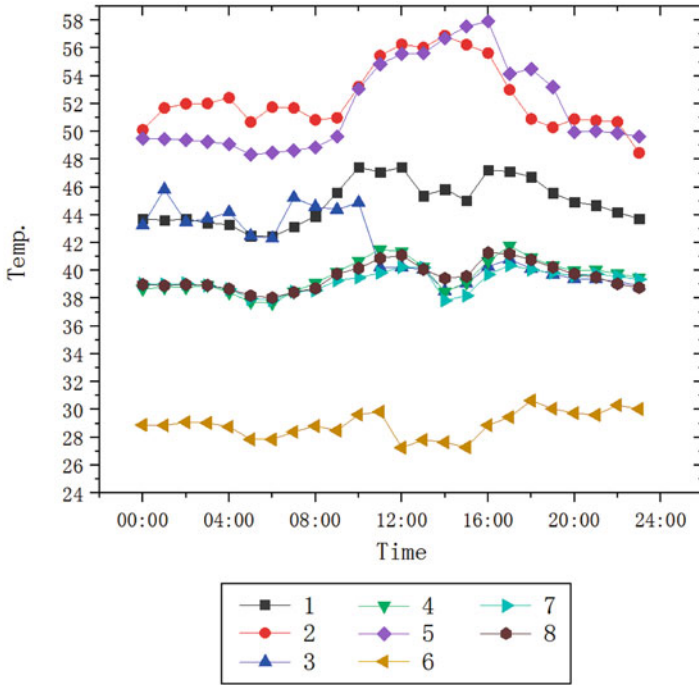


Fig. 75.4 Temperature at 0.2 m at measurement stations

It can be seen that the temperature of each measurement point was distinct (Fig. 75.3). Even for the small-area squares, the largest temperature difference in the daytime could reach 2.7 °C. The highest temperature was 32.7 °C at point 6, while the lowest one was 30 °C at point 3. By comparing these readings with the data set in the suburban district, it was found that the temperatures of each measuring point were significantly higher than those for the areas without buildings and paved with rigid materials, which is obviously due to the heat island effect.

Besides, in the night the changing trend of the temperatures for the underlying surface is nearly the same with those for the air temperatures. The temperature difference was relatively small. For the day time, due to the underlying environment and the increasing extend, the temperatures of measuring points in the area paved with rigid materials was larger than those for other measuring points in the day time.

The local microclimate was affected, for example, by the nearby building density, green plot ratio (GnPR), underlying surface type, and SVF (sky view factor). This study mainly focuses on the change in the microclimate in the small urban squares. The temperature change at 0.2 m above the ground is shown in Fig. 75.4. Owing to the different underlying surface, the temperature difference was large, which even reached 30 °C. The temperatures of each measuring point remained unchanged at

night. After 8 a.m., as the sunlight increased, the temperature of each measuring point increased. After 4 p.m., the temperature decreased and tended to stabilize. It is worth noting that the temperature at point 6 at night was higher than that during the day. This was because point 6 was located near a water body, which has a high heat capacity. The water body absorbed the heat in the daytime and released the heat in the nighttime. However, a comparison of the data at a height of 1.5 m revealed that the near-water-surface temperatures were lower than those of the human body. Therefore, the location of the water body could only lower the temperature near the Earth's surface, which obviously would not lower the air temperature at the height of human beings.

The temperatures of the square centers at points 2 and 5 observed a normal distribution, which increased with sunlight intensity. The temperature differences of points 1 and 8 were rather limited, which was mainly due to the blocking of sunlight irradiation by the bushy leaves of green plants in the summer. In addition, a temperature difference of 2 °C was observed between points 1 and 8 due to distinct SVF values, even though the two points were located in groves. The temperature at point 6 was the most stable and the lowest one. This was mainly because point 6 was located at a platform on the water surface and the water body had a higher heat capacity, leading to the absorption of more heat from sunlight irradiation.

The temperatures at heights of 0.2 and 1.5 m were virtually unrelated. Especially when the underlying environment was distinct, the temperatures at the two heights were significantly different. This was mainly because the rigid pavement would absorb the sunlight, leading to an increase in temperatures at the Earth's surface. However, the temperatures at the measured points at the two heights were nearly the same when the SVF values were rather high. This was mainly due to the fact that the trees prevented sunlight from being absorbed by the underlying surface. Note that, due to the air flow and more balanced heat distribution, the trend in temperature change at 1.5 m height was significantly different from that at the Earth's surface. It is obvious from Fig. 75.4 that the temperature change was more evident when the underlying material was tile than for grass, pitch, and water.

3.2 *Soil Temperature and Soil Heat Flux*

Figure 75.5 illustrates the different ground type surface temperature at measurement stations.

From Fig. 75.5, it was found that the temperatures at different heights significantly differed from those reported by the meteorological station. Moreover, the temperature change trends for distinct underlying materials were extremely different.

For underlying grass, the temperatures reflected a decreasing trend during the time period 0:00–7:00 a.m. At 5:00 a.m., the near-earth-surface temperature reached its lowest point, 29.7 °C. Temperatures at a height of 1.5 m were rather stable. They started to increase at 5:00 a.m. and reached their maximum of 32.6 °C at 12:00 a.m. and then started to decrease. The temperatures started to increase again starting at

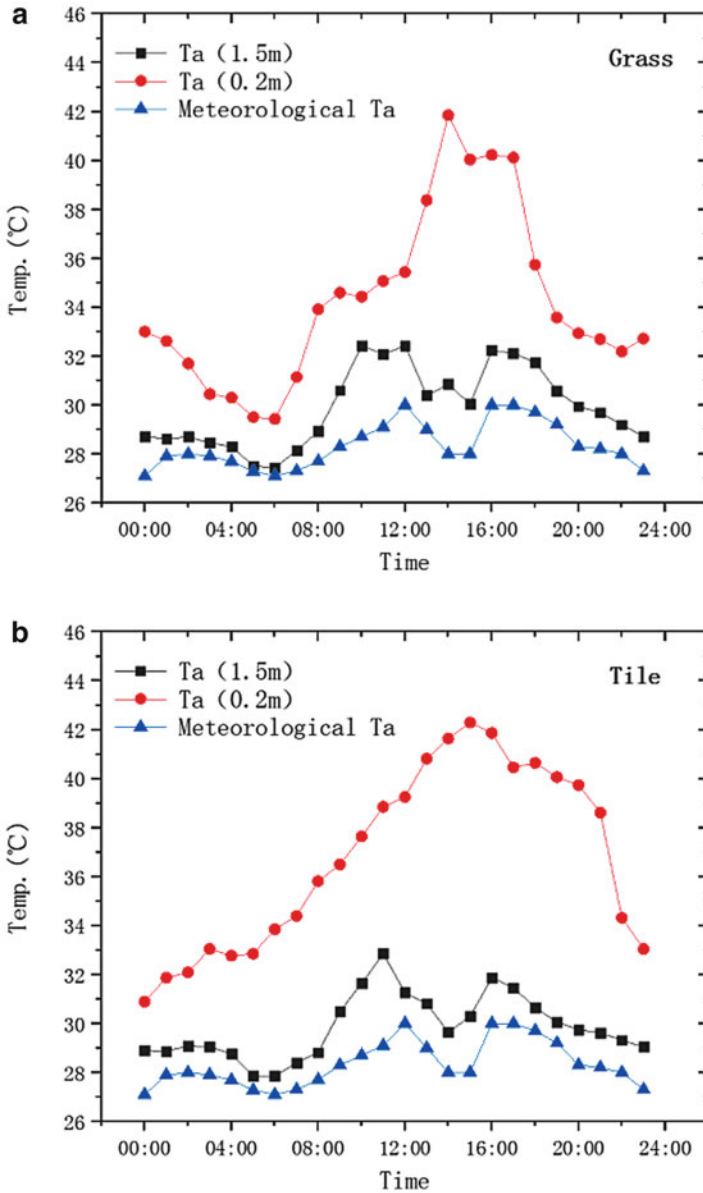


Fig. 75.5 Ground surface temperature at measurement stations. (a) The temperature variation of different height on grass underlying (b) The temperature variation of different height on tile underlying (c) The temperature variation of different height on concrete underlying (d) The temperature variation of different height on asphalt underlying

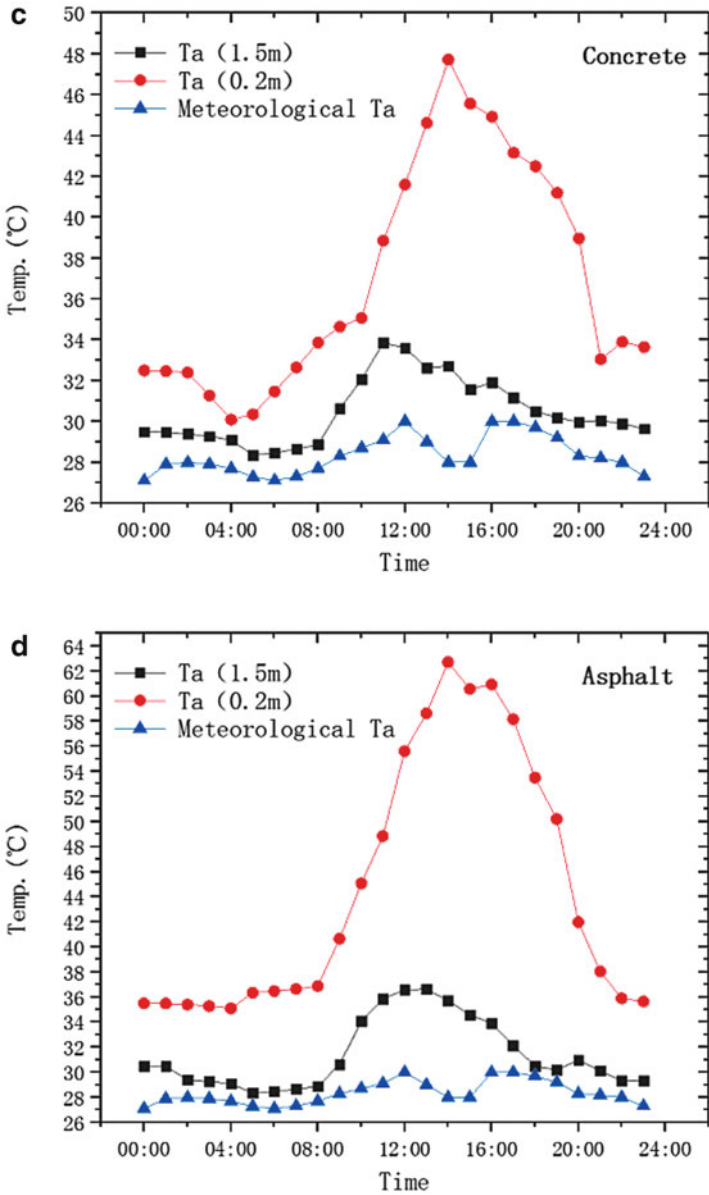


Fig. 75.5 (continued)

4:00 p.m. till 5:00 p.m. and then decreased. It is worth noting that, when the near-Earth-surface temperature reached its maximum, temperatures at 1.5 m decreased. This was because when the sunlight intensity hit its peak, the elevated near-Earth-surface temperature would lead to the evaporation of water from the grass, reducing the air temperature. The contrast of air temperatures with reference ones showed that at night the average temperature of the urban square experienced a difference of 0.7 °C over that of the suburban area. In the daytime, the largest temperature difference was 2.3 °C at 10:00 a.m.

When the underlying material was tile, the temperatures near the Earth's surface followed a normal distribution. The lowest temperature near the Earth's surface was 30.7 °C at midnight. Subsequently, temperatures underwent a linear increase, reaching a maximum of 42.4 °C at 4:00 p.m. and starting a gradual decrease.

It is notable that the air temperature change trend when the underlying material was tile at the height of a human being was basically the same as that when the underlying material was grass, both of which tended to decrease at 2:00 p.m. This was because as the underlying tile in the measured square, white tile was chosen. When the sunlight's intensity hit its peak, some of the heat was reflected away. Meanwhile, a greater wind speed also removed some of the heat.

When the underlying material was concrete, temperatures near the Earth's surface and at a human height both followed a normal distribution. In addition, the increasing trend of the temperatures near the Earth's surface was sluggish. The lowest temperature near the Earth's surface was 30.1 °C at 4:00 a.m. Then the temperature increased linearly and reached its maximum of 48.2 °C at 2:00 p.m. and then gradually decreased. Temperatures at 1.5 m were stable at night and started to increase gradually at 8:00 a.m., reaching their maximum at 33.7 °C at 11:00 a.m., then gradually decreased.

As with underlying concrete, for asphalt the temperatures near the Earth's surface and at a human height followed a normal distribution. The lowest temperature near the Earth's surface was 34.1 °C at 4:00 a.m. Then the temperature increased linearly, reaching its maximum of 62.2 °C at 2:00 p.m., then gradually decreased. Temperatures at 1.5 m were stable at night. They started to increase gradually at 8:00 a.m. and reached their maximum of 35.7 °C at 12:00 a.m. and then gradually decreased. Similarly, the increasing trend of temperatures near the Earth's surface was sluggish.

The foregoing analysis shows that for different underlying materials, temperatures at the same time differed. Air temperatures were not in a linear relationship with those near the Earth's surface, which was the result of the comprehensive effect of the factors of wind speed, humidity, sunlight irradiation intensity, and so on.

3.3 Spatial Distribution of Air Temperature and Humidity

It is generally accepted that the distinct effects of different ground types on the air above the ground are more evident under weather conditions of clear skies and light wind. Figure 75.6 shows the specific temperature at 1.5 m above ground at 2:00 p.m. on July 14, and Fig. 75.7 shows the specific humidity at 1.5 m above ground at the same time. The graph is calculated using GIS.

It can be seen from Fig. 75.6 that the temperature at point 3 was the highest and those at points 1 and 8 in the woods were the lowest. The measured temperatures had a positive relation to SVF values. For the same SVF, the type of underlying decided the change in temperature. The largest temperature difference was 2.3 °C.

Obviously, green land effectively decreased air temperatures, while the water body had no significant effect on them. Figure 75.7 shows the distribution of the humidity of the measured squares. The humidity was high for green lands and water bodies and low for the open space in the square. The largest humidity difference reached 18%, which would affect the comfort level of the human body. Notably, humidity near the water bodies was lower than that near the woods. This was mainly because the wind transported away the water vapor that evaporated from the water body. As for the thick woods, the wind speed was relatively low, so humidity there was high.

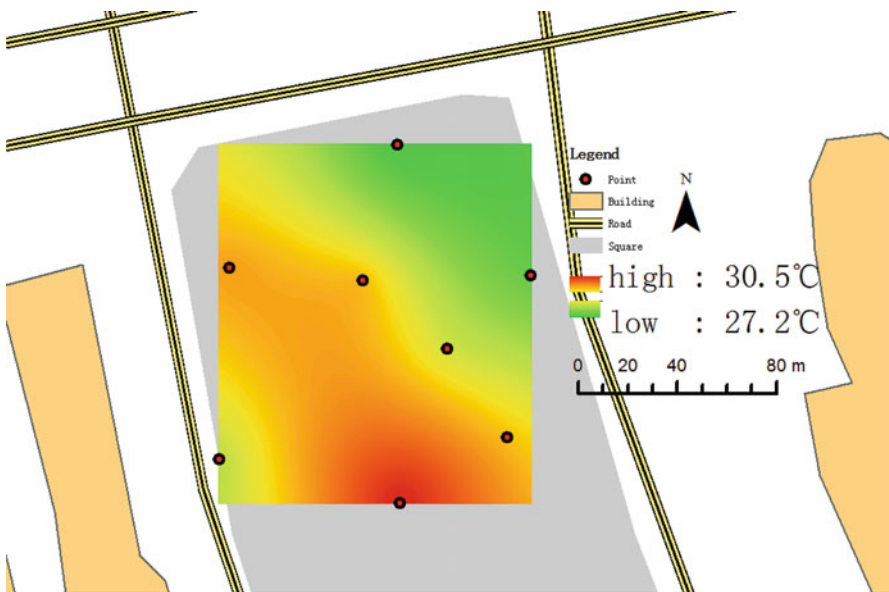


Fig. 75.6 Ground surface specific temperature at 1.5 m above ground (July 14, 2014, 2:00 p.m.)

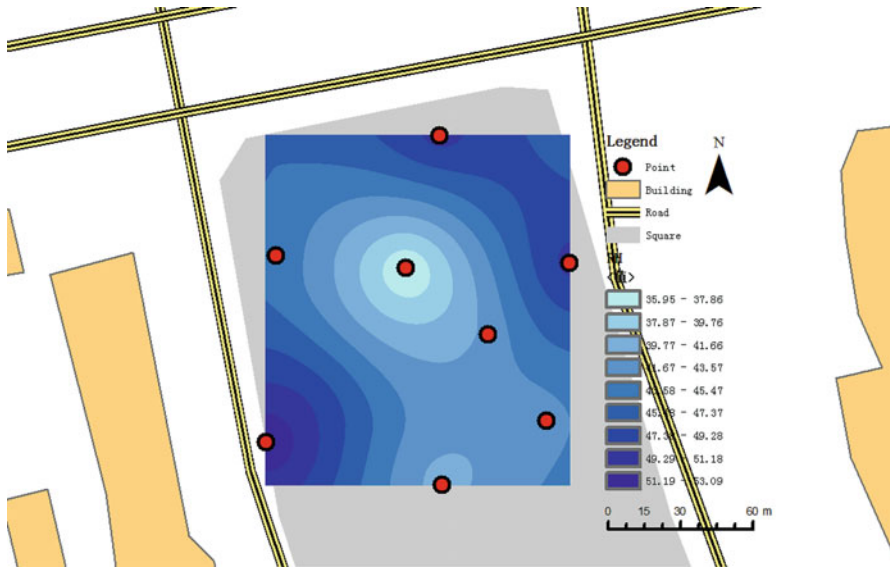


Fig. 75.7 Ground surface specific humidity at 1.5 m above ground (July 14, 2014 2:00 p.m.)

Therefore, in terms of comfort level, squares should not be too large. Moreover, more trees should be planted in the square in the direction of the leading wind to deflect the heat to create a pleasant microclimate environment.

3.4 Wind Spatial Distribution

Within the urban square, as these climatic variables are the outcome of the interaction between the buildings and the background regional weather conditions, they vary from location to location. To compare the windiness of different urban locations, a derived variable of “wind run” is calculated at the observation points of the weather stations from WS1 to WS8. Wind run is the measurement of the “amount” of wind passing the station during a given period of time, expressed in “kilometers of wind.” WeatherLink is software that records measurements of weather stations and calculates wind run by multiplying the average wind speed for each archive record by an archive interval of 5 min. Wind run value takes into account any wind direction. Figure 75.8 presents a comparison of the daily wind run at 1.5 m height within the test site, for a period of 1 week from July 14 to 18, 2014. They are calculated for different locations of the weather stations: WS1–WS8. The variation of wind run with height is investigated by monitoring the wind speed and direction at a weather-station trailer-mast height of 1.5 m.

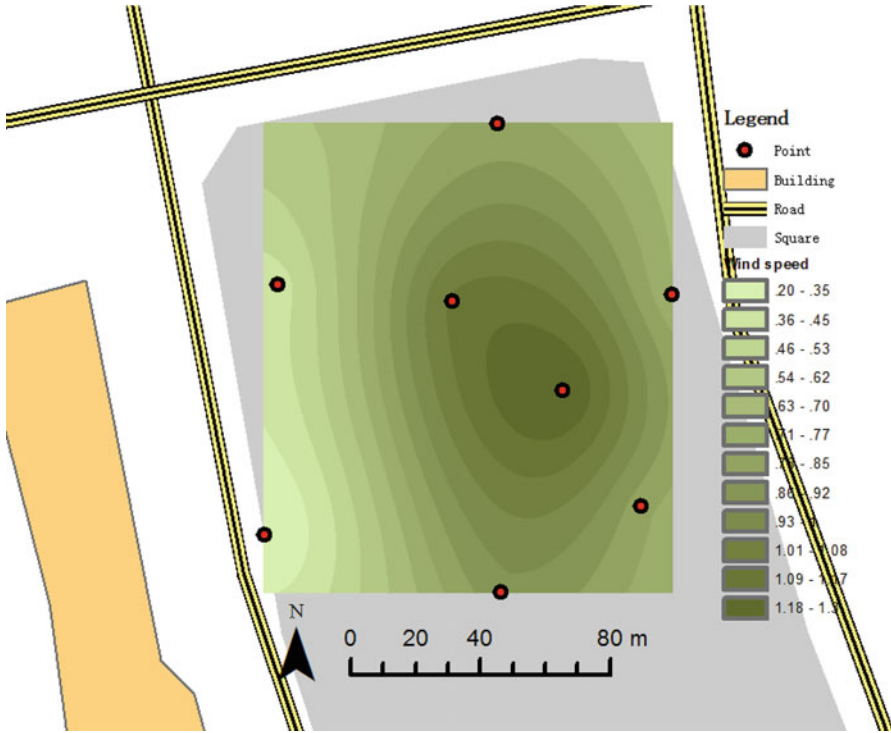


Fig. 75.8 Windiness of measurement site from July 14 to 18, 2014

As shown in Fig. 75.8, the wind speeds for each measurement point were completely different. The highest wind speed was 1.5 m/s, measured at points 2 and 5. This was because there was nothing to block the wind in the center of the square, and in addition the main wind direction was southeast, where no trees were located, leading to high wind speeds. In a hot summer, the wind moves the heat out of the square, and the wind reached high speeds there. A low wind speed improved the comfort level in the square.

4 Conclusion

In this chapter, an experimental study of microclimates in an urban square in Harbin, China, is presented. The field measurements consisted of air temperature, wind speed, global solar radiation, and surface temperatures of building walls and the ground. The main conclusions can be summarized as follows:

1. The layout and configurations of buildings cause variations in the microclimate from one location to another;
2. Evapotranspiration effects from vegetation can help cool down the ambient air temperature;
3. The surrounding high-rise buildings block direct solar radiation, but at the same time may decrease wind permeability. The combined effect should be considered on a case-by-case;
4. The wind potential in an urban area is significantly reduced due to the sheltering effects, but urban texture still plays a role.

The outcomes of this study reveal that the microclimatic parameters are significantly influenced by the contribution of urban textures. Consequently, the temperatures in an urban area are distinct from the meteorological weather data due to the distinct underlying surfaces. This underlines the need for a radical change with respect to considering microclimatic information in urban planning and assessing building thermal and energy performance. In addition, the variation in wind speed, solar radiation, and temperature in the studied urban area in Harbin provides an exemplary case to demonstrate the importance of considering microclimatic parameters in feasibility studies for the implementation of renewable energy technologies at both the design and policymaking levels.

Acknowledgments This research was supported by the National Natural Science Foundation of China (Project 51438005).

References

1. Oke TR (1987) *Boundary layer climates*, 2nd edn. Routledge, London
2. Graves H, Watkins R, Littlefair P, Westbury P (2001) *Cooling buildings in London: overcoming the heat island*. Building research establishment. Construction Research Communications, London
3. Elnahas MM, Williamson TJ (1997) An improvement of the CTTC model for predicting urban air temperatures. *Energy Build* 25:41–49
4. Bozonnet E, Belarbi R, Allard F (2005) Modelling solar effects on the heat and mass transfer in a street canyon, a simplified approach. *Sol Energy* 79:10–24
5. De la Flor FS, Domínguez SA (2004) Modelling microclimate in urban environments and assessing its influence on the performance of surrounding buildings. *Energy Build* 36:403–413
6. Williamson TJ, Erell E (2001) Thermal performance simulation and the urban microclimate: measurements and prediction. In: *Proceedings of IBPSA conference*
7. Yao R, Luo Q, Li B (2011) A simplified mathematical model for urban microclimate simulation. *Build Environ* 46:253–265
8. Li XX, Liu CH, Leung DYC, Lam KM (2006) Recent progress in CFD modelling of wind field and pollutant transport in street canyons. *Atmos Environ* 40:5640–5658
9. Erell E, Williamson T (2006) Comments on the correct specification of the analytical CTTC model for predicting the urban canopy layer temperature. *Energy Build* 38:1015–1021
10. Santamouris M, Papanikolaou N, Koronakis I, Livada I, Asimakopoulos D (1999) Thermal and air flow characteristics in a deep pedestrian canyon under hot weather conditions. *Atmos Environ* 33:4503–4521

11. Niachou K, Livada I, Santamouris M (2008) Experimental study of temperature and airflow distribution inside an urban street canyon during hot summer weather conditions—part I: air and surface temperatures. *Build Environ* 43:1383–1392
12. Bourbia F, Awbi HB (2004) Building cluster and shading in urban canyon for hot dry climate: part I: air and surface temperature measurements. *Renew Energy* 29:249–262
13. Georgakis C, Santamouris M (2006) Experimental investigation of air flow and temperature distribution in deep urban canyons for natural ventilation purposes. *Energy Build* 38:367–376
14. Kolokotroni M, Davies M, Croxford B, Bhuiyan S, Mavrogianni A (2010) A validated methodology for the prediction of heating and cooling energy demand for buildings within the urban heat island: case-study of London. *Sol Energy* 84:2246–2255
15. Radhia H, Fikryb F, Sharples S (2013) Impacts of urbanisation on the thermal behaviour of new built up environments: a scoping study of the urban heat island in Bahrain. *Landsc Urban Plann* 113:47–61

Retraction Note to: Chapter 6 Green Buildings and Renewable Energy Application Based on Life Cycle Performance Costing



Wim Zeiler, Anna Vanderveen, Wim Maassen, and Rik Maaijen

**Erratum to: Chapter 6 in: A. Sayigh (ed.),
Mediterranean Green Buildings & Renewable Energy,
https://doi.org/10.1007/978-3-319-30746-6_6**

The authors are retracting this chapter *Green Buildings and Renewable Energy Application Based on Life Cycle Performance Costing* because Anna Vanderveen, Wim Maassen and Rik Maaijen did not agree to be included as authors and were not aware of the submission and publication of this chapter.

The online version of the original chapter can be found at
https://doi.org/10.1007/978-3-319-30746-6_6

© Springer International Publishing Switzerland 2018
A. Sayigh (ed.), *Mediterranean Green Buildings & Renewable Energy*,
https://doi.org/10.1007/978-3-319-30746-6_76

E1

Correction to: Investigation of Urban Microclimate Parameters of City Square in Harbin



Hong Jin, Peng Cui, and Meng Huang

Correction to:
Chapter 75 in: A. Sayigh (ed.),
Mediterranean Green Buildings & Renewable Energy,
https://doi.org/10.1007/978-3-319-30746-6_75

The authors required to revise their chapter after original publication, description statement as below

Description of Amendment

Some peers read our paper and contacted us to point out a few questionable problems. After considering these problems carefully, we re-examined this paper and found data to be incomplete, leading to debatable conclusions. Moreover, the analysis details for the data needed to be amended. To avoid misleading the readers, we carefully revised the data and analysis and made necessary adjustments to the conclusions.

There were two main problems in the original paper. Firstly, eight points were measured while one key measuring point was neglected. Secondly, the software we used for contrastive analysis was Envimet. When we used this software recently, we found some discrepancy. Besides, the setting of the boundary conditions directly affected the simulated results. We therefore deleted the data obtained using Envimet. As replacement, we used the data obtained during the actual experiment period. The specific amendments are listed below:

The updated online version of this chapter can be found at
https://doi.org/10.1007/978-3-319-30746-6_75

1. For Fig. 75.1, the types of underlying surface were added, making the content easily understood.
2. The content of Sect. 2.1 was reorganized. The content related to the software Envimet was deleted. The actual measured data were further interpreted.
3. Figures 75.3 and 75.4 were replotted. The missed points were added. Additional data and content were further interpreted.
4. Section 3.2 was rewritten. The content related to the software Envimet was deleted. The actual measured data were used for the analysis.
5. In Sects. 3.2 and 3.4, the wrong figures were replaced. Actual measured data were used to replace the data obtained by the software.

In addition, the main structure, introduction, and main conclusions were not adjusted. Only the software-related content was amended. Besides, some missing data were added.

Correction to: Integrating Deep Offshore Wind with Pumped Hydro Storage in a Central Mediterranean Archipelago's Electricity Generation System



Robert N. Farrugia, Tonio Sant, and Cedric Caruana

Correction to:
Chapter 23 in: A. Sayigh (ed.), *Mediterranean Green Buildings & Renewable Energy*,
https://doi.org/10.1007/978-3-319-30746-6_23

The original version of the chapter was inadvertently published without incorporating the author's corrections to the acknowledgement section. The acknowledgement section has now been corrected.

The updated online version of this chapter can be found at
https://doi.org/10.1007/978-3-319-30746-6_23

© Springer International Publishing Switzerland 2020
A. Sayigh (ed.), *Mediterranean Green Buildings & Renewable Energy*,
https://doi.org/10.1007/978-3-319-30746-6_78

C1